PROCEEDINGS

THA 2019

INTERNATIONAL CONFERENCE ON

"Water Management and Climate Change towards Asia's Water-Energy-Food Nexus and SDGs"

Swissôtel Bangkok Ratchada
Bangkok, Thailand
23-25 January 2019

THA 2019

INTERNATIONAL CONFERENCE ON

"Water Management and Climate Change towards Asia's Water-Energy-Food Nexus and SDGs"

Swissôtel Bangkok Ratchada

Bangkok, Thailand

23-25 January 2019

CONTACT INFORMATION AND DETAILS:

Contact address:
Contact Person: **Dr. Supattra Visessri, Dr. Sucharit Koontanakulvong**
Water Resources System Research Unit
Room 203, Bldg. 2 Faculty of Engineering,
Chulalongkorn University , Bangkok
Tel: +66-81-694-6680, +66-81-646-9750, +66-2-218-6426
Fax: +66-2-218-6425
Email: supattrav@hotmail.com, sucharit.k@chula.ac.th
For more detailed information you are more than welcome to visit our website:
http://www.watercu.eng.chula.ac.th
http://aseanacademicnetwork.com

CONTENT

CONTENT (con't)

CONTENT (con't)

CONTENT (con't)

CONTENT (con't)

Session D Disaster Management/Groundwater Management

Guested Paper

CONTENT (con't)

CONTENT (con't)

CONTENT (con't)

Preface

The THA 2019 International Conference on “Water Management and Climate Change towards Asia's Water-Energy-Food Nexus and SDGs” was organized from January 23rd to 25th, 2019 at Swissôtel Le Concorde, Bangkok. The event was organized by Chulalongkorn University, in association with 8 national and 9 international collaborative agencies. The 8 national co-organizers are the Thai Hydrologist Association (THA), Kasetsart University (KU) Kamphaengsaen Campus, Asian Institute of Technology (AIT), Royal Irrigation Department (RID), Department of Water Resources (DWR), Department of Groundwater Resources (DGR), Thailand Research Fund (TRF), and Office of the National Water Resources (ONWR). The 9 international collaborative agencies include Kyoto University, National Taiwan University (NTU), National Chen Kung University (NCKU), Department of Hydraulic and Ocean Engineering National Cheng Kung University, Korea Water Resources Association (KWRA), The International Society of Paddy and Water Environment Engineering (PAWEE), International Water Resources Research Institute (IWRRI), Japan Society of Hydrology and Water Resources, and Japan-ASEAN Science, Technology and Innovation Platform (JASTIP). The main objective of the THA 2019 was to provide a platform for researchers, scientists, practitioners, and policy makers to share and present new advances, research findings, perspectives, and experiences in disaster, irrigation and water management. Special attentions were given to developing certain skills or competence, or general upgrading of capacity for climate change adaptation, participatory water management, disaster and environmental management, sustainable development in irrigation and drainage, WEF Nexus, and Sustainable Development Goals (SDGs). The conference brought together leading researchers, engineers, scientists, and officials in the domain of interest from around the world.

The THA 2019 international conference was successful according to the main objective of serving as the public assembly. Welcome speech of the THA 2019 international conference was given by Assoc.Prof.Dr.Supot Teachavorasinskun, Dean of Faculty of Engineering, Chulalongkorn University, on behalf of Prof. Dr. Bundhit Eua-arporn, President of Chulalongkorn University. The opening remarks was given by Air Chief Marshal Chalit Pukbhasuk, the Privy Council of Thailand. At this conference we had three keynote speakers, 377 Thai participants, 142 foreign participants from 17 countries including Australia, Cambodia, China, Germany, India, Indonesia, Japan, Korea, Lao PDR, Malaysia, Myanmar, Philippines, Singapore, Taiwan, United Kingdom, United Arab Emirates, and Vietnam. The three keynote presentations given by distinguished speakers who were invited to participate in the conference emphasized the implementation of the 2030 agenda for sustainable development in cities of Asia and the Pacific, importance of the Water-Food-Energy-Security Nexus in Asia-Pacific, and Water-Energy-Food Nexus: Current Status and Challenges in

Thailand. There were 21 invited paper and 83 selected papers to present under 4 subthemes. In detail 37 papers on Climate Change and Uncertainty in Hydrology and Meteorology, 1 paper on Participatory Management for Water and Irrigation Project, 11 papers on Emerging Digital Technologies in Water Management and Environment Towards Nexus and SDGs, and 34 papers on Disaster Management and Groundwater Management.

The first subtheme on Climate Change and Uncertainty in Hydrology and Meteorology covers the topic of climatic and rainfall change including climate change adaptation. In hydrology and meteorology, the topic covers a broad range of areas such as storm prediction, river flow, sedimentation, and drainage. Some research papers discuss about the impact of climate change on flooding, reservoir management, ocean wave, and water quality.

The second subtheme on Participatory Management for Water and Irrigation Project covers participatory management experiences shared by presenters from many countries and water use efficiency for crop and water-energy-food nexus.

The third subtheme on Emerging Digital Technologies in Water Management and Environment Towards Nexus and SDGs covers many issues of water-energy-food nexus and SDGs. The technologies on urban water supply, application of irrigation, water quality management, downscale of rainfall prediction, and water footprint were discussed.

The last subtheme on Disaster Management and Groundwater Management covers many issues about policy on disaster management, assessment of extreme events including flood, drought and landslide. In addition to groundwater issue, the papers cover groundwater modeling, assessment of groundwater under climate change, groundwater yield estimation, effect of land use change on groundwater, etc.

Apart from the presentations based on the above-mentioned themes, the ASEAN Academic Networking in Water & Disaster Management and Climate Change was organized in parallel to the THA 2019 international conference. The aim of the ASEAN Academic networking was to encourage further collaboration in research, to exchange knowledge and technology pertaining to disaster warning, management and recovery and to suggest appropriate policies that correspond to the increased severity of the climate change and natural disasters as well as the interconnection among WEF Nexus. The ASEAN Academic networking was divided into four sessions including country report, academic presentations, roundtable discussion, and technical training. There were 19 invited presentations from ASEAN countries; 10 of which were for the country report and the other 9 were for the academic sessions. Suggestion, recommendations, opportunities for further research direction

and collaboration were discussed among ASEAN representatives and also shared from the views of invited speakers from China and Japan.

The exhibition at the THA 2019 International Conference consisted of 23 booths from governmental agencies and public and private companies. Applications, models, tools and technologies were displayed at the booths..

At the end of the THA 2019 International Conference, the Bangkok Statement 2019 was announced by Asst. Prof. Dr. Anurak Sriariyawat, Head of the Department of Water Resources Engineering, Chulalongkorn University. The closing remarks were given by Assoc. Prof. Dr. Sucharit Koontanakulvong, Chairman of THA2019 Working Committee.

Major outputs obtained from the THA 2019 can be summarized below:

- Knowledge dissemination and exchange from the presentations. At this conference and workshops we had 3 keynote speakers, 377 Thai participants, 142 foreign participants from 17 countries: Australia, Cambodia, China, Germany, India, Indonesia, Japan, Korea, Lao PDR, Malaysia, Myanmar, Philippines, Singapore, Taiwan, United Kingdom, United Arab Emirates, and Vietnam, 21 invited papers, 83 technical papers participated.
- Formal announcement of Bangkok Statement 2019 for collaboration in the ASEAN Academic Networking in Water & Disaster Management and Climate Change.
- A technical training on “Nexus” and “Downscaled MRI-GCM data applications”
- Poster exhibition displaying water-related technologies, products and services from governmental agencies, universities, research institutions and private companies

Major outcomes are listed below:

- Creating an opportunity for being a coordinator in research and education regarding Water & Disaster Management and Climate Change which has already started.
- Presenting technologies and water management in Thailand to ASEAN and other countries outside ASEAN.
- Strengthening collaboration among ASEAN countries in the area of water and climate change and bringing it towards WEF Nexus and SDGs.

This document presents main conclusions from the THA 2019 International Conference on “Water Management and Climate Change towards Asia's Water-Energy-Food Nexus and SDGs”. Related materials that will be issued separately are the THA 2019

proceedings, a book titled “Water Management and Climate Change towards Asia's Water-Energy-Food Nexus and SDGs”, and the Special Issue of THA 2019 in Engineering Journal (EJ) (http://www.engj.org/index.php/ej/; ISSN: 0125-8281), Faculty of Engineering, Chulalongkorn University and Hydrological Research Letters (HRL), Japan Society of Hydrology and Water Resources (http://www.hrljournal.org; ISSN: 1882-3416).

Lastly, we would like to take this opportunity to express our sincere gratitude to all participants for their contributions and support that driving the THA 2019 International Conference toward the desired objectives and achievement.

Dr. Supattra Visessri
Dr. Sucharit Koontanakulvong
Editors of THA 2019 Proceedings

Organization committee

Advisory Committee:

1	Prof. Dr. Bundhit Eua-arporn	President of Chulalongkorn University
2	Assoc. Prof. Dr. ChongrakWatcharinrat	Acting President of Kasetsart University
3	Dr. Eden Y Woon	President of Asian Institute of Technology
4	Dr. Thongplew Kongjun	Director General of Royal Irrigation Department
5	Mr. Suwat Piampaijai	Director General of Department of Water Resources
6	Miss Jongjit Niranathmateekul	Director General of Department of Groundwater Resources
7	Dr. Subin Pinkayan	President of Thai Hydrologist Association
8	Prof. Suthipun Jitpimolmard, M.D.	Director General of Thailand Research Fund
9	Dr. Somkiat Prajamwong	Secretary General of Office of the National Water Resources
10	Prof. Dr. Yasuto TACHIKAWA	Kyoto University, Japan
11	Prof. Dr. Wei Cheng Lo	NCKU, Taiwan

Organizing Chair:

1	Prof. Dr. Supot Teachavorasinskun	Dean of Engineering Faculty, Chulalongkorn University

Organizing Co-Chair:

2	Dr. Damrong Sripraram	Dean of Engineering Faculty, Kasetsart University
3	Assc.Prof. Dr. Chanathip Pharino	Director of Public Wellbeing Division, Thailand Research Fund

Technical Committee:

1	Assoc. Prof. Dr. Bancha Kwanyuen	Kasetsart University
2	Dr. Tosiyuki Nakaegawa	Meteorological Research Institute, Japan
3	Professor. Yasuto Tachikawa	Kyoto University, Kyoto, Japan
4	Dr. Kazuaki Yorozu	Kyoto University, Kyoto, Japan
5	Assoc. Prof. Takahiro Sayama	Kyoto University, Kyoto, Japan

Organization committee (con't)

Technical Committee:

6	Dr. Patinya Hanittinan	Kyoto University, Kyoto, Japan
7	Prof. Shigenobu Tanaka	Kyoto University, Kyoto, Japan
8	Prof. Tetsuya Sumi	Kyoto University, Kyoto, Japan
9	Prof. Tomoharu Hori	Kyoto University, Kyoto, Japan
10	Prof. Dr. Oki Taikan	Tokyo University, Japan
11	Prof. Dr. Takao Masumoto	Akita Prefectural University, Japan
12	Prof. Dr. Makoto Taniguchi	Research Institute for Humanity and Nature (RIHN), Japan
13	Associate Professor, Dr. Kiguchi Masashi,	Institute of Industrial Science, the University of Tokyo, Japan
14	Assistant Professor, Dr. Noda Keigo	Gifu University, Japan
15	Associate Professor, Dr. Tebakari Taichi	Toyama Prefectural University, Japan
16	Professor. Lo, WeiCheng	National Cheng Kung University, Taiwan
17	Prof. Wu, Jianhong	National Cheng Kung University, Taiwan
18	Dr. Wu, Meng-Hsuan	National Cheng Kung University, Taiwan
19	Mr. Huang, Chi-Htsung	National Cheng Kung University, Taiwan
20	Ms. Chen Li-Chen	National Cheng Kung University, Taiwan
21	Prof. Dr. Ming-Daw Su	National Taiwan University, Taiwan
22	Professor C.H. Fan	National Taiwan University, Taiwan
23	Prof. K.S. Cheng	National Taiwan University, Taiwan
24	Professor Y.P. Lin	National Taiwan University, Taiwan
25	Professor M.C. Hu	National Taiwan University, Taiwan
26	Professor Y.L. Yeh	National Taiwan University, Taiwan
27	Dr. Seungsoo Lee	APEC Climate Center (APCC), Republic of Korea
28	Prof. Dr. Yeonsu Kim	K-water, Republic of Korea
29	Prof. Dr. Wansik Yu	K-water, Republic of Korea

Organization committee (con't)

Technical Committee:

30	Prof. Dr. Joo-Cheol Kim	K-water, Republic of Korea
31	Prof. Dr. Kwansue Jung	Chungnam National University, Republic of Korea
32	Prof. Dr. Mikyoung Choi	Chungnam National University, Republic of Korea
33	Prof. Dr. Hyunuk An	Chungnam National University, Republic of Korea
34	Prof. Dr. Chang-lae Jang,	Korea National University of Transport, Republic of Korea
35	Prof. Dr. Jun Kyung Soo	Sungkyunkwan University, Republic of Korea
36	Prof. Dr. Joo-Heon Lee	Joongbu University, Republic of Korea
37	Assoc. Prof. Dr. Yongwon Seo	Yeungnam University, Gyeongsan, Republic of Korea
38	Prof. Dr. Wen Chen	Chinese Academy of Sciences, China
39	Prof. Dr.Yangbo Chen	Sun Yat-sen University, China
40	Prof. Dr. LIU Hui Zhi	Institute of Atmospheric Physics, China
41	Prof. Dr. Lin WANG	Institute of Atmospheric Physics, China
42	Prof. Dr. Chenghai Wang	Lanzhou University, China
43	Prof. Dr. Song YANG	SunYat-sen University, China
44	Prof. Dr. Alan Milano	Mindanao State University, Philippines
45	Prof. Dr. Muhammad Syahril Badri Kusuma	Institut Teknologi Bandung, Indonesia
46	Prof. Ignas Sutapa	Indonesian Institute of Sciences, Indonesia
47	Prof. Dr. Vuong Bui Tran	Vietnam National University, Viet Nam
48	Prof. Dr. Lawrence Surendra	University of Mysore, INDIA
49	Dr. Andrew Dansie	UNSW Global Water Institute, Australia
50	Prof. Dr. Kala Vairavamoorthy	Iteso Welfare Association (IWA), UK
51	Dr. Jiramate Changklom	Imperial College London, UK
52	Dr. Sachin Shan	USGS_Texas, USA

Organization committee (con’t)

Technical Committee:

53	Dr. Priyantha Ranjan Sarukkalige	Curtin University, Australia
54	Asst. Prof. Dr. Somchai Donjadee	Kasetsart University
55	Asst. Prof. Dr. Nitirach Sanguanduan	Kasetsart University
56	Assoc. Prof. Dr. Chaisri Suksaroj	Kasetsart University
57	Asst. Prof. Dr. Wisuwat Taesombat	Kasetsart University
58	Assoc. Prof. Dr. Adichai Pornpromin	Kasetsart University
59	Assoc. Prof. Dr. Surachai Lipiwattanakarn	Kasetsart University
60	Asst. Prof. Dr. Jirawat Kanasut	Kasetsart University
61	Asst. Prof. Dr. Napaporn Piamsa-nga	Kasetsart University
62	Dr. Songsak Bhaddraravudthichai	Kasetsart University
63	Asst. Prof. Dr. Jerasorn Santisirisomboon	Ramkhamheang University
64	Assoc. Prof .Dr. Usa Humphries	King Mongkut's University of Technology Thonburi, Thailand
65	Assoc. Prof. Amnat Chidthaisong	King Mongkut's University of Technology Thonburi, Thailand
66	Asst.Prof. Dr. Chaiwat Ekkawatpanit	King Mongkut's University of Technology Thonburi, Thailand
67	Asst.Prof. Dr.Duangrudee Kositgittiwong	King Mongkut's University of Technology Thonburi, Thailand
68	Dr. Prem Rangsiwanichpong	King Mongkut's University of Technology Thonburi, Thailand
69	Assoc. Prof. Dr.Uma Seeboonruang	King Mongkut's Institute of Technology Ladkrabang, Thailand
70	Dr. Chanyut Kalakan	Burapha University, Thailand
71	Dr. Srisunee Wuthiwongyothin	Burapha University, Thailand
72	Assoc.Prof. Dr.Sombat Chuenchooklin	Naresuan University, Thailand
73	Dr. Tipaporn Homdee	Nakhon Phanom University, Thailand
74	Assoc. Prof. Dr. Sacha Sethabutra	Srinakharinwirot University, Thailand

Organization committee (con't)

Technical Committee:

75	Dr. Phayom Saraphirom	Khon Kaen University, Thailand
76	Assoc. Prof. Dr. Sucharit Koontanakulvong	Chulalongkorn University, Thailand
77	Asst. Prof. Dr. Anurak Sriariyawat	Chulalongkorn University, Thailand
78	Asst. Prof. Dr. Aksara Putthividhya	Chulalongkorn University, Thailand
79	Assoc. Prof. Dr. Tuantan Kitpaisalsakul	Chulalongkorn University, Thailand
80	Dr. Piyatida Ruangrassamee	Chulalongkorn University, Thailand
81	Dr. Pongsak Suttinon	Chulalongkorn University, Thailand
82	Dr. Supattra Visessri	Chulalongkorn University, Thailand
83	Dr. Patama Singhruck	Chulalongkorn University, Thailand
84	Dr. Somkiat Apipattanavis	Office of the National Water Resources, Thailand
85	Dr. Atsamon Limsakul	Department of Environmental Quality Promotion, Thailand
86	Dr. Oranuj Lophensi	Department of Groundwater Resources, Thailand
87	Dr. Aranya Fuangswasdi	Department of Groundwater Resources, Thailand
88	Dr. Sukrit Kirtsaeng	Thai Meteorological Department, Thailand
89	Dr. Piyaman Srisomporn	Hydro and Agro Informatics Institute, Thailand
90	Dr. Surajate Boonya-aroonnet	Hydro and Agro Informatics Institute, Thailand

Working Committee:

1	Assoc. Prof. Dr. Sucharit Koontanakulvong	Chulalongkorn University
2	Dr. Supattra Visessri	Chulalongkorn University
3	Dr. Jutithep Vongphet	Kasetsart University
4	Dr. Ketvara Sittichok	Kasetsart University
5	Mr. Somkiat Kitsuwanakul	Thai Hydrologist Association

Website and Information System:

1	Miss Daunpen Punayangkool	Chulalongkorn University
2	Miss Chanyanut Nantipatwong	Chulalongkorn University

Organization committee (con’t)

Website and Information System:

3	Miss Napaporn Noppakhun	Chulalongkorn University
4	Miss Wichuta Hemsatien	Chulalongkorn University
5	Miss Marayart Petcharat	Thai Hydrologist Association

Conference Organizing Institutes

Chulalongkorn University (CU), Thailand

Thai Hydrologist Association, Thailand

Faculty of Engineering at Kamphaengsaen, Kasetsart University (KU), Thailand

Asian Institute of Technology, Thailand

Royal Irrigation Department (RID), Thailand

Conference Organizing Institutes (con't)

General of Department of Water Resources (DWR),Thailand

Department of Groundwater Resources, Thailand

Thailand Research Fund,Thailand

Office of the National Water Resources, Thailand

Collaborative agencies

Kyoto University, Japan

National Taiwan University, Taiwan

National Cheng Kung University (NCKU), Taiwan

Department of Hydraulic and Ocean Engineering, National Cheng Kung University (NCKU), Taiwan

Korea Water Resources Association, Republic of Korea

Collaborative agencies (con't)

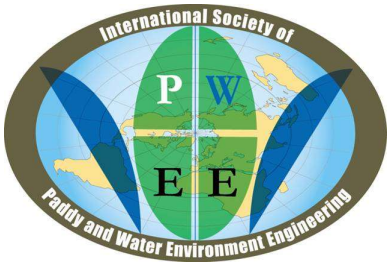

International Society of Paddy and Water Environment Engineering (PAWEES)

International Water Resources Research Institute, Republic of Korea

Japan Society of Hydrology andWater Resources, Japan

Japan-ASEAN Science, Technology and Innovation Platform (JASTIP)

AIMS AND SCOPE

The objective is to provide a platform for researchers, scientists, practitioners, and policy makers to share and present new advances, research findings, perspectives, and experiences in Disaster, Irrigation and Water Management towards W-E-F Nexus. Special attentions will be given to developing certain skills or competence, or general upgrading of performance ability for climate change adaptation, participatory water management disaster and environmental management, and sustainable development in irrigation and drainage in the monsoon Asia.The conference will bring together leading researchers, engineers, scientists, and officials in the domain of interest from around the world

The conference will bring together leading researchers, engineers, scientists, and officials in the domain of interest from around the world topics of the conference are:

A. **Climate Change and Uncertainty in Hydrology and Meteorology**
B. **Participatory Management and Technologies for Water and IrrigationProjects**
C. **Emerging-Digital Technologies in Water Management and Environment Towards Nexus (WEF) and SDGs (Big Data, IOT)**
D. **Disaster Management/ Groundwater Management**

The presentation contents can be highlighted as follows:

Session A Climate Change and Uncertainty in Hydrology and Meteorology

The session started with the research results of downscaling research based on the Multi-Model Simulations of SEACLID/CORDEX Southeast Asia. The climate change data had been utilized to study impact on weather prediction, design wave, river discharge, landslide risk, reservoir operation. The studies on satellite rainfall estimate, extreme rainfall, urban flood, spatial heterogeneity and trans-boundary pollution were presented and lastly, the change of water budget in the seasonal tropical forest was presented for discussion.

Session B Participatory Management for Water and Irrigation Project

The session started with question on principles and methods of PIM in Action from Japanese experiences. The study on improving crop water use with efficient irrigation technologies was presented and discussed with the negotiation process and institutionalization in the participatory water management. The water use efficiency is discussed with the Water-Food Nexus approach.

Session C Emerging-Digital Technologies in Water Management and Environment Towards Nexus (WEF) and SDGs (Big Data, IOT)

WEF Nexus in practices were introduced to achieve sustainable resources security with proposed indicators under a DPSIR framework. New concept on Water Footprint for quantifying impact on rice production was reviewed and criticized. Lastly the concept of smart urban water systems – in practice was introduced for discussion.

Session D Disaster Management/Groundwater Management

The session started with the introduction of policies and technical works on river management for disaster risk reduction under climate change and the research on extreme flood frequency analysis and risk curve development under a changing climate was also presented. The assessment of the climate change impacts of groundwater abstraction was presented with various studies on groundwater parameter estimation under various situations. The discussion evaluation of near-real-time satellite-based rainfalls and research on Input-Output analysis of water deficits were presented for discussion.

Publication Opportunities

Journal Publication

Selected manuscripts from THA2019 proceedings will be recommended to be published in the Engineering Journal (EJ) : International Journal ISSN 0125-8281 (indexed with ESCI (Web of Science), Scopus, IET Inspec, Index Copernicus, DOAJ, and TCI: http://www.engj.org.)

Conference Proceedings

The full papers after correction will be published in the Conference Proceedings.

(selected/related full papers will also be published in book titled "Water Management and Climate Change towards Asia'sWater-Energy-Food Nexus and SDGs" after peer review.)

Introduction Speech

(1) Dear Air Chief Marshal Chalit Pukpasuk, the Privy Council of Thailand; President of Chulalongkorn University; the chairman of the THA2019 International Conference on Water Management and Climate Change towards Asia's Water-Energy-Food Nexus and SDGs; delegates from United Nations Economic and Social Commission for Asia and the Pacific (UN-ESCAP), Pacific Water Research Centre, Canada and Office of the National Water Resources (ONWR), Thailand, management from water institutions, faculties from universities in ASEAN and in neighboring region and all honorable participants. I would like to report on the background of the THA2019 International Conference as follows:

(2) The THA conference series was initiated in 2015 by the Faculty of Engineering, Chulalongkorn University to address water management and climate change issues which has drawn interest from a large number of researchers over the world. In the THA2015, ASEAN Academic Network was formed and subsequently led to the establishment of a UNESCO Chair on Water, Disaster Management and Climate Change at Chulalongkorn University.

Two years later in 2017 when Chulalongkorn University celebrated 100th anniversary of its founding, the THA2017 International Conference on Water Management and Climate Change Towards Asia's Water-Energy-Food Nexus was organized to fulfill Chulalongkorn University's mission to be the "Pillar of the Kingdom".

Following on the success of the THA2015 and THA2017, the THA2019 International Conference on Water Management and Climate Change towards Asia's Water-Energy-Food Nexus and SDGs is organized as the third of the THA conference series. The main objective of the conference is to provide a platform for researchers, scientists, practitioners, and policy makers to share and present new advances, research findings, perspectives, and experiences in climate change, irrigation, emerging technologies, disaster management, and SDGs.

The conference consists mainly of four parts including oral presentation, poster exhibition, workshops and technical visit. The presentations are categorized into four main themes including 1) Climate Change and Uncertainty in Hydrology and Meteorology, 2) Participatory Management for Water and Irrigation Project, 3) Emerging Digital Technologies in Water Management and Environment Towards Nexus and SDGs, 4) Disaster Management and Groundwater Management. Two workshops of Nexus and Downscaled GCM applications on the last day of the conference are newly introduced this year. The ASEAN Academic Networking is also a part of every THA conference series dedicating to the promotion of collaboration in research and education in ASEAN.

(3) Chulalongkorn University, in association with 8 national co-organizers and 9 international collaborative agencies has worked closely together to organize the THA2019 International Conference from 23rd to 25th January 2019. The 8 national co-organizers are the Thai Hydrologist Association (THA Hydro), Kasetsart University (KU) Kamphaengsaen Campus, Asian Institute of Technology (AIT), Royal Irrigation Department (RID), Department of Water Resources (DWR), Department of Groundwater Resources (DGR), Thailand Research Fund (TRF), and Office of the National Water Resources (ONWR).

(4) The THA2019 is highlighted by 3 keynote speakers including: first, Ms.Natasha Wehmer, Sustainable Urban Development Section, Environment and Development Division, United Nations Economic and Social Commission for Asia and the Pacific (UN-ESCAP); second, Prof. Zafar Adeel, Pacific Water Research Centre, Canada; and third, Dr. Somkiat Prajamwong, Office of the National Water Resources (ONWR), Thailand. There are 21 invited session speakers.

(5) The THA2019 is expected to contribute to improved scientific understanding of climate change, NEXUS and SDGs from the presentations given by scholars and experts from several countries in different regions of the world and from the hands-on workshops. The THA2019 is also a forum for creating academic network for future collaboration.

(6) Next, I would like to invite Prof. Dr. Supot Teachavorasinskun, Dean of Faculty of Engineering and on behalf of the President of Chulalongkorn University to make a welcome speech for the THA2019 International Conference.

Welcome Speech

Prof.Dr.Supot Teachavorasinskun

Dean of Faculty of Engineering, Chulalongkorn University

On behalf of Prof. Dr. Bundhit Eua-arporn, President of Chulalongkorn University

(1) Dear Air Chief Marshal Chalit Pukpasuk, the Privy Council of Thailand; co-organizing agencies; collaborative agencies; esteemed delegates and management from water institutions, and all honorable guests, on behalf of the President of Chulalongkorn University, I, Prof. Dr. Supot Teachavorasinskun, Dean of Faculty of Engineering, Chulalongkorn University would like to convey to all of you participating in the THA2019 conference my heartfelt welcome. It's my privilege and pleasure on behalf of Chulalongkorn University to welcome you today to the THA 2019 International Conference on Water Management and Climate Change towards Asia's Water-Energy-Food Nexus and SDGs. We are delighted to have participants from many countries to participate this conference. That many of you have traveled long distances to be here serves as a reminder to us all how important water is.

(2) Water is crucial natural resource. It is one of the basic needs of living organisms and the fundamental factors for economic and social development. Water management is a complex issue. Imbalance between limited water supply and increasing demand due to rapid population and economic growth has been a conventional issue for water and disaster management. A contemporary issue associated with climate change and uncertainty makes water management in present day more challenging than in the past. Natural disasters such as floods, typhoons, earthquakes, tsunamis, and volcanic eruptions commonly occurring in the Southeast Asia region have been intensified due to more severe climate variation and climate change.

(3) Chulalongkorn University realized the importance of academic collaboration on addressing the water management and climate change issues, the THA conference was therefore initiated with an aim to serve as a public forum to promote continuous coordination and strengthen collaboration among academics, researchers, policy makers, and government executives in ASEAN countries to address more challenging water issue due to changing environment and to put forward research findings into operation. In 2015 the first THA conference on Climate Change and Water & Environment Management in Monsoon Asia and the UNESCO Chair in Water, Disaster Management and Climate Change were launched. The second THA conference in 2017 focused on Water Management and Climate Change Towards Asia's Water-Energy-Food Nexus.

(4) The theme of the THA2019 conference is designed to match with on-going global trend. The THA2019 covers not only water management and climate change but also Water-Energy-Food Nexus and SDGs. The THA2019 pays particular attention to developing the skills and ability to address the

problems of water and disaster management, participatory management, environmental management and sustainable development goals.

(5) As a co-organizer, I hope that we will receive contributions from all participants through the presentations and discussion which are vital important for developing effective and practical measures against climate change. As noted in this conference, "Toward together" we can create better environment for all.

Opening Speech

Air Chief Marshal Chalit Pukpasuk

The Privy Council of Thailand

(1) Good morning Ladies and Gentlemen, Dear Distinguished delegates, I am pleased to welcome you to the THA 2019 International Conference on Water Management and Climate Change Towards Asia's Water-Energy-Food Nexus and the ASEAN Academic workshop which are organized by Chulalongkorn University, in association with 8 national and 9 international collaborative agencies. It is high time that such an event took place to address emerging issues regarding climate change and water management and to foster research contributions. The list of registration reveals the diversity of participants from many countries around the world. As we are now in Thailand, I would like to take this opportunity to share with you the philosphy of water management in Thailand that are applied to the royal projects and able to support SDGs.

His Majesty the late King Bhumibol Adulyadej, the Symbolic "Father of Water Resources Management", recognized the importance of water, as he constantly reminded the public that "Water is life" as it is a basic necessity of life. His speech delivered at Chitralada Palace on 17th March 1986 was "...We must realize the importance of water. We need it to drink, for daily use and for agriculture. Where there is water, there is life. If there is water, we can survive. If there is no electricity, we can still survive. However, if there is no water but there is electricity, we will perish..."

(2) Water is central to all aspects of life and is the core of sustainable development. Despite its fundamental role across all sectors, water is all too often managed in a fragmented manner. The lack or excess of water is not simply an issue for innovative technology and science to address. It could affect social equity and justice. Water management in the recent decade is particularly challenging due to a number of factors such as competing demands on water arising from population growth and socio-economic development, extreme weather conditions, high natural variability and fluctuation in water demand and supply.

(3) To address water management issues, knowledge exchange, technology transfer and collaborations in research are much needed. We all can help to move our community towards sustainability by focusing our research efforts around the 2030 Agenda for Sustainable Development Goals and attempting to explore better solutions for water-related problems specifically the impacts of climate change, disaster and other pressing challenges on Asia's water-energy-food nexus.

(4) The philosophy of Sufficiency Economy conceived by His Majesty the late King Bhumibol Adulyadej can be considered as a solution for sustainability as it fits well with the SDGs. The philosophy of "Sufficiency Economy" or "The Middle Path" is to develop the ability to take

appropriate conduct to create a balanced and stable development under changing environment. Sufficiency refers to three components including moderation, reasonableness and self-immunity. Moderation is reflected in the sense of not too much or not too little. Reasonableness means that all choices made should be justified by ethics, law justice, and social norms. Self-immunity is also known as resilience against the risks which arise from internal and external changes. His Majesty the late King Bhumibol Adulyadej's legacy, the Philosophy of Sufficiency Economy, is believed to help societies around the world deliver on the SDGs as it has been proven to be useful in Thailand.

(5) The THA2019 provides a valuable opportunity for scientists, researchers, policy planners and decision-makers to discuss and share knowledge and experiences to seek for cutting-edge solutions for water management for our region and our world. I would like to thank both local and international participants attending this conference. I wish the THA2019 great success in advancing water-related research mission and I hope you have a fruitful discussion and rewarding experience in the THA2019. The THA conference series is expected to continue playing an important role in facilitating technical knowledge dissemination and networking in the future.

(6) Now it is time to declare the THA2019 international conference officially open and hope that the conference will proceed towards the objectives set. Thank you and enjoy your stay in Thailand.

Session A

Climate Change and Uncertainty in Hydrology and Meteorology

Guested Paper

Changes of the precipitation and the Monsoon Transitional Zone in East Asia: past and future

Wen CHEN[1], Jin-Ling PIAO[1], Wen ZHOU[2], Hans-F. GRAF[1], Lin WANG[1], Joong-Bae AHN[3], and Alexander POGORELTSEV[4]

Abstract

The monsoon transitional zone (MTZ) in East Asia is the transitional belt between humid and arid regionsand is characterized bysharp climate and biome gradients. Thisbelt is considered to be "interface fragile" to natural disastersand climate changes.However, significant attention is not given to the variationof the MTZ in East Asia. Thus, there is an urgent need to address the precipitation variation and the associated MTZ changes, especially during rainy season.

A decadal change of summer rainfall in the MTZ of East Asia is observed around 1999. This decadal change is characterized by an abrupt decrease of summer rainfall of about 18% of the climatological average amount leading to prolonged drought in the region. Three different drought indices, the standardized precipitation index, the standardized precipitation evapotranspiration index, and the self-calibrating Palmer Drought Severity Index, present pronounced climate anomalies during 1999-2007, indicating dramatic drought exacerbation in the region after the late 1990s. This decadal change in the summer rainfall may be attributable to a wave-like teleconnection pattern from Western Europe to Asia. A set of model sensitivity experiments suggests that the summer warming sea surface temperature in North Atlantic could induce this teleconnection pattern over Eurasia,resulting in recent drought in the MTZ region.

With the CMIP5 simulation results, a focused and detailed survey of MTZ has been conducted. Inthe historical period, the MTZ experienced coastward migration with increasing aridity throughoutMTZ. Furthermore, precipitation fluctuation mainly contributes to interannual variability of MTZ whereas potential evaporation behavior dominates its long-term trends. In global warming scenario period, there will be continuing southeastward displacement for the front edge but the opposite northwestward movement is projected forthe rear one, as a consequence of significant drying trendsin the humid zone together with regime shifts towards humid conditions in the arid zone. Moreover, interannual variability of MTZ is expected to become stronger, resulting in more frequent occurrences ofextreme swings. Finally, it is noted that uncertainty arising from climate models dominates in the MTZ than dispersedemission scenarios, in contrast to the situation in humidand arid zones.

[1]Institute of Atmospheric Physics, Chinese Academy of Sciences, Beijing, China
[2]School of Energy and Environment, City University of Hong Kong, Hong Kong
[3]Department of Atmospheric Sciences, Pusan National University, Pusan, Korea
[4]Russian State Hydrometeorological University, St. Petersburg, Russia

Future change analysis of extreme floods using large ensemble climate simulation data

Yasuto TACHIKAWA*

Abstract

Future change analysis of extreme floods in Japan using large ensemble climate simulation data is discussed. At first, a change of the magnitudes of probable largest-class floods caused by a historical typhoon is analyzed using typhoon track ensemble simulations combined with a pseudo-global warming experiment. Then, to estimate a change of probability distributions of extreme rainfall and floods, simulated river discharge using "Database for Policy Decision-Making for Future Climate Change, d4PDF" is analyzed. The d4PDF consists of large ensemble members of climate simulations for the 60-years historical simulations with 50 ensemble members and 60-years future simulations with 90 ensemble members. The magnitude of a largest-class floods equivalent to a 900-years flood is also analyzed. The study basins are the Ara River basin (2940km^2) in the Tokyo metropolitan area, the Shonai River basin (1010km^2) in the Nagoya area, and the Yodo River basin (8240km^2) in the Osaka and Kyoto area in Japan. The results reveal the clear increase of the magnitude of extreme rainfall and floods.

*Department of Civil and Earth Resources Engineering, Kyoto University, Japan
tachikawa@hywr.kuciv.kyoto-u.ac.jp

Dynamic decision support systems based on Nash bargaining solution for water resources management in a reservoir-river basin

Lai Sai Hin*, Mehdi Zomorodian, Mehran Homayounfar

Abstract

Langat River Basin is a strategic catchment in Malaysia, providing water for important demand points including Kuala Lumpur, Klang Valley, Putrajaya, and Cyberjaya. However, the growth of demand, along with recent drought events has warned decision-makers about the reliability and vulnerability of the current water resources system. In this study, two dynamic models based on Nash Bargaining Solution (NBS) were developed to deal with conflict situations. In the first model, a continuous dynamic game model for water allocation in a reservoir system considering the randomness in both reservoir inflow and the rest of the network flow was developed. The second model combined a simulation-optimization modeling method based on coupled System Dynamics (SD) and Game Theory (GT). This model benefits from SD advantages in capturing dynamic behaviors of a system and existing feedback loops between system components during simulation. In order to identify the efficiency of the proposed methods, a case study was carried out at Langat river basin in Malaysia. Based on various reliability indices (Relibility, Resilience and vulnerability) calculated from results obtained, both models are capable of tackling conflict issues in water allocation under situations of water scarcity. The calibrated model was used to simulate for five different managerial scenarios between 2014-2035, and compared against their overall sustainability index (SI) and satisfaction level (SL). The results obtained from analyses showed that supply-oriented policies are temporary solutions, while combining demand and non-revenue water management can secure sustainable development for a more extended period in Langat River Basin.

Keywords *Water shortage, Water Resources Management, Decision support system, System Dynamics, Game Theory, Nash Bargaining Solution*

Technical Paper

Assessment of Runoff Sensitivity to Changes in Precipitation at the Indochina Region

Patinya Hanittinan

Abstract

Reliable assessment of runoff is a key for the prediction and management of freshwater resources. Therefore, hydroclimate forcing datasets, e.g., precipitation and total runoff (ROF) using the output from the multiple-realization, single-model ensemble named "d4PDF", were obtained in this study. Due to lack of direct observation of the ROF, we first evaluated the validity of the present-climate d4PDF precipitation using the Taylor diagram. The model was able to reproduce the extreme indices with a respectable performance regarding pattern correlations (0.6-0.9) and the centered-pattern RMSE (0.5-1). Finally, the runoff sensitivities, which are the relative change in ROF due to the change in various precipitation indices, were discussed. The results showed that the elasticity of runoff to precipitation is greater than unity for 83-95% of land grid cells during annual and wet-season time scale, indicated a faster response of the ROF under changing climate.

Keywords *d4PDF, runoff generation, extreme indices*

Irrigated Water Management under Climate Change Scenario Using Water Evaluation and Planning Model in Stung Sreng basin, Cambodia

Ratboren Chan[1], Oeurng Chantha[1,a,*], Marith Mong[1] and GuekLeang Hak[1]

Abstract Stung Srengbasin is the most potential one to extract water for both domestic used and agricultural sector; however, this basin encounters the management problem that can cause water scarcity. WEAP model was applied in this basin to determine the situation of irrigation water requirement under climate change scenario. The current and future streamflow were generated from SWAT model. As a result, the reference scenario defines irrigated demand from 2018 to 2030, and it is founded that the water demand is 679 MCM and unmet demand is around 95 MCM. There are only 2 irrigation schemes among 51 schemes that require most water demand which is around 150 to 200 MCM. Furthermore, the scarcity of water will occur mostly in November and December around 35 to 60 MCM. Based on the annual increase scenario, the irrigated area in dry season increases every year by 5% until 2030. The result showed that water demand in this scenario is 684.483 MCM. It means the irrigation demand will have risen around 5.5 MCM by 2030. The scarcity of water in dry season does not occur. For climate change scenario which selected from climate model: GISS-E2-R-CC, the result illustrates that the trend of water and unmet demand are going to increase slightly for both RCP 2.6 and 8.5 compared to annual increase scenario. The peak of water demand in dry season is in March and November; on the contrary, for the lowest demand was in May and June. In addition, the most scarcity of water in this scenario is in November and December.

Keyword *WEAP model, Water demand, unmet demand and climate change scenario*

[1]Faculty of Hydrology and Water Resources Engineering,
Institute of Technology of Cambodia,
Phnom Penh, Cambodia.

[a]chantha@itc.edu.kh

Introduction

The abundant of water resources plays a vital role in developing national economic in many sectors. The management of the abundant of water resources must be deeply concerned and to be used in many sectors, including agricultural, manufacturing, energy, inland navigation, tourism, environmental protection, water supply, sanitation and domestic used; therefore,there are many developers who built some water resources modeling for studying about assessment and planning on water resources sector, such as Soil and Water Assessment Tool (SWAT) and Water Evaluation and Planning (WEAP) model, to prevent the issue of scarcity of water. The capacity of SWAT model can simulate streamflow in the past and future under various conditions. For example, the study, which is about hydrologic simulation of the little Washita river experimental watershed using SWAT, was used to evaluate the capabilities of SWAT to predict streamflow under varying climatic conditions. Eight years of precipitation and streamflow data were used to calibrate parameters in the model, and 15 years of data was used for model validation. Test results showed that once the model was calibrated for wet climatic conditions, it performed well in forecasting streamflow responses over wet, average, and dry climatic conditions selected for model validation (Van Liew and Garbrecht, 2003). After getting streamflow data from SWAT model, WEAP model can be applied for estimating water demand management under various conditions too. A research paper mentions about Simulation of water resources management scenarios in western Algeria watersheds using WEAP model. The model is applied to evaluate and analyze the existing balance and expected future water resources management scenarios by taking into account the different operating policies and factors that may affect the demand until 2030. The results showed that neither domestic demand nor agricultural demand met the basis year 2006. The results also pointed out that domestic demand can be satisfied for the considerable scenarios (Hamlat et al., 2013). In Cambodia, water resources play role as the main factor for economic growth that is related to many sectors such as agricultural, water supply and sanitation, industrial, fisheries and tourism; meanwhile, Cambodia can also face a water shortage due to the lack of management technical and the impact of climate change. Thus, WEAP model application is applicable

in the case study of Cambodia to identify the situation of water requirement and planning the future management work, for instance, the Assessment of Irrigated Water Allocation in the Stung ChreyBak Catchment of Tonle sap Lake Basin using the WEAP model by (MONG et al.). This research aims to apply WEAP model to define the situation of supply water for irrigation schemes under the diverse scenarios. By the reason above, this study intentionally focuses on irrigated water management under climate scenario using water evaluation and planning model (WEAP) at Stung Sreng River basin, Tonle Sap Basin. The current baseline and future streamflow simulating from SWAT model will be used for this study in order to achieve the two main objectives which are to (1) estimate the irrigation water demand and unmet demand in each irrigation schemes under present and future under effect of climate change and (2) evaluate the different situation of irrigation water requirement under climate scenario RCP2.6 and RCP8.5.

Methodology

A. Study area

The Stung Sreng River Basin was considered as the study area which is located at the northwest of Cambodia as shown in Figure 1. Understandably, it is a tributary within the third largest river basin of Tonle Sap Great Lake, lower Mekong River Basin. The river basin area is totally 9 986 km^2 and is covered by three provinces, including Banteay Meanchey, Oddar Meanchey, and Siem Reap province. There are around 51 irrigation schemes which equal nearly 53 000 ha of land.

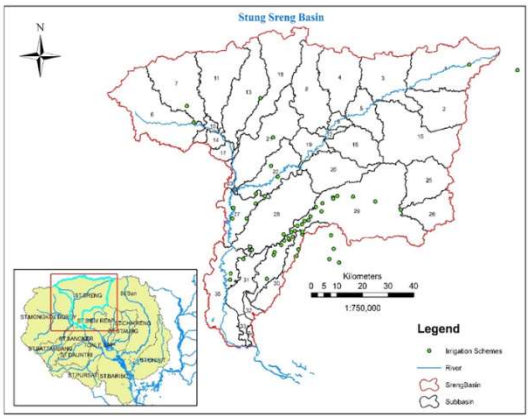

Fig. 1. Map of Stung Sreng Catchment

B. Generality of WEAP model

The Water Evaluation and Planning (WEAP) model was developed by the Stockholm Environment Institute (SEI). It provides a comprehensive, flexible and user-friendly framework for policy analysis. It operates at a monthly step on the basic principle of water balance accounting. The user represents the system in terms of its various sources of supply (e.g. rivers, groundwater, and reservoirs), withdrawals, water demands, and ecosystem requirements. The result of the model was calculated as water demand in each irrigation scheme and amount of water shortage in the scheme.

C. Stream flow in Stung Sreng Basin

The streamflow in Stung Sreng catchment was divided into 35 sub-basins that was generated from Soil and Water Assessment Tool (SWAT) mode. The observed daily streamflow from 1994 to 2013 recorded by the Department of Hydrology and River Works of Ministry of Water resources and Meteorology in Stung Sreng basin at Kralanh station was used to compare between the simulated and measured discharge based on Model analysis calibration and validation of SWAT-CUP. The average of monthly streamflow from SWAT was regarded as an input data of Water Evaluation and Planning model (WEAP) in Current Account (2018), and Reference Scenario and Annual Increase Scenario (2017 to 2069). The future stream is projected to change due to the alteration in climate data. By adjusting the change factor in basin parameters of climate data, including temperature, humidity, solar radiation and precipitation, that was downscaled by MRC into SWAT model to simulate the future change of streamflow under climate change scenario.

D. Cropping pattern

Water balance calculations in this study are considered two cropping patterns distributed in a year round: wet season rice and dry season rice. Cropping patterns for the season rice crops are based on the assumption that the transplanting method is used as the prevailing and dominant farming practice. This method produces a higher unit yield of rice than the direct sowing method (CDRI, 2015).

Table I Selected Cropping pattern

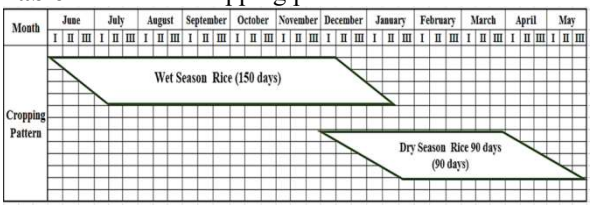

E. Irrigation water requirement

Irrigation water requirements (IWR) of each crop for each diversion unit were estimated based on a cropping calendar as shown in the following equation:

$$IWR = (ET_0 \times Kc + PR + Lp - ER) / IE \ , \qquad (1)$$

Where:

- IWR: Irrigation water requirement for diversion unit
- ETo: Reference evapotranspiration
- Kc: Crop coefficient
- PR: Percolation rate (in case of paddy)
- Lp: Land preparation requirement
- ER: Effective rainfall
- IE: Irrigation efficiency

The irrigation water requirement for climate change scenario will be used the same formula by adjusting the values of future temperature and precipitation and those values were adjusted by Mekong River Commission (MRC, 2015). The future Reference Evapotranspiration and Effective Rainfall will be calculated as the formula below:

$$ET_0 = P \times (0.46 T_{mean} + 8), \quad (2)$$

$$ER = 0.8 \times R \, (0.5 \le R \le 80 \, mm), \quad (3)$$

F. Describtion of climate model

Climate models are the primary tools available for investigating the response of the climate system to various forcing, for making climate predictions on seasonal to decadal time scales and for making projections of future climate over the coming century. The system of models is driven by climate change scenarios that represent a range of plausible future climate changes as projected by global climate model (GCM) simulations available at the initiation of the interdisciplinary study. For comparing the river discharge change based on climate change scenarios, the climate change model of three institutes, namely Geophysical Fluid Dynamics Laboratory (GFDL) (R30 version) (Manabe et al., 1992). Goddard Institute for Space Studies (GISS) (Hansen et al., 1984) and Institute Pierre-Simon Laplace (IPSL) (Sperber et al., 2013).

Climate change model, namely GISS was used in order to reach the objectives in this study. The new version of the GISS climate model used for CMIP5/ACCMIP simulations is called ModelE2. The new E2 version of the GISS climate model was run with fully interactive reactive chemical constituents in simulations for the Coupled Model Intercomparison Project 5th phase (Taylor et al., 2012) and the Atmospheric Chemistry and Climate Model Intercomparison Project) (Lamarque et al., 2012). This version is a complete rewrite of previous models incorporating numerous improvements in basic physics, the stratospheric circulation, and forcing fields (Schmidt et al., 2006). Notable changes include the following: the model top is now above the stratopause, the number of vertical layers has increased, a new cloud microphysical scheme is used, vegetation biophysics now incorporates a sensitivity to humidity, atmospheric turbulence is calculated over the whole column, and new land snow and lake schemes are introduced. The performance of the model using three configurations with different horizontal and vertical resolutions is compared to quality-controlled in situ data, remotely sensed and reanalysis products. Overall, significant improvements over previous models are seen, particularly in upper-atmosphere temperatures and winds, cloud heights, precipitation, and sea level pressure (Schmidt et al., 2006).

G. Representative concentration parthways (RCPs)

The four RCPs are consistent with certain socio-economic assumptions. These will later be replaced by the Shared Socio-economic Pathways which will provide flexible descriptions of possible futures within each RCP (Bjørnæs, 2013). But there only two RCPs will selected to apply with climate model GISS-E2.

RCP 2.6 (low emission of CO2): radiative forcing reaches 3.1 W/m2 before it returns to 2.6 W/m2 by 2100. In order to reach such forcing levels, ambitious greenhouse gas emissions reductions would be required over time.

RCP 8.5 (high emission of CO2): Increasing greenhouse gas emissions that lead to high greenhouse gas concentrations over time.

H. Definiting of demand management scenarios

This demand management scenario creates three different scenarios: reference, annul increase of irrigation area and supply management scenario, and climate change scenario. The assumptions are presented as below:

Table II Scenarios assumption

Scenarios	Description
Reference	What if "question and key assumptions" The reference scenario will evaluate the reported irrigated area against the stream flow of the catchment, and then identify the water demand and unmet demand in each irrigation scheme.
Annual increase of irrigation area	This scenario assumes that the irrigated area in dry season will increase by 5% percent per year over the period from 2019-2030 (CDRI, 2011).
Climate change scenario, GISS-E2-R-CC: RCP2.6: low emissions RCP8.5: High emissions	The impact of climate change on local hydrological regime, mainly streamflow by producing an extended duration of drought in dry season and high intensity of rainfall in wet season.

I. Overal flowchart

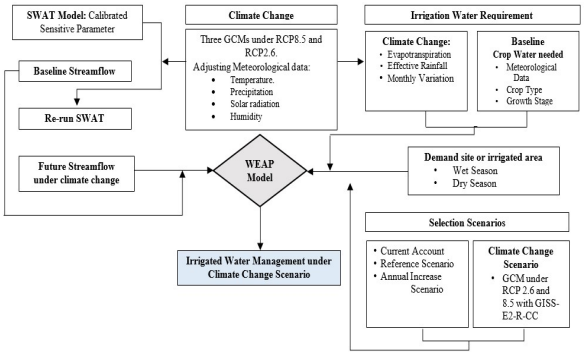

Fig. 2. Overall flowchart

Result and discussions

A. Current account

Irrigation water demand in the current account is calculated based on the irrigated area of 52 600 ha. The monthly variation in irrigation water demand was estimated based on the rice crop factor and the pattern of farmer's rice crop cultivation. The current account of irrigation demand in 2018 is about 679 million cubic meters per annum. As the result, because of the area of this irrigation scheme which is huge comparing to other schemes area, there are two reservoirs, Plang and Slaeng Spean that need a lot of irrigation demand, which are 191.36 and 151.28 MCM, respectively.

B. Reference scenarios

The reference scenario calculates the irrigation water demand from 2019 to 2030s at 679 million cubic meters per annum. As a result, the irrigation water demand in Stung Sreng Basin in dry season is low if comparing with wet season. The most water demand during dry season is in December at 93.930 MCM. On the other hand, the most irrigation water demand in wet season is in July and November at 110.168 and 172.471 million cubic meters per annum, respectively. Nevertheless, the total amount of unmet demand that occurs in this basin is 94.265 MCM, the irrigationscheme that mostly met the scarcity water is Kralanh irrigation scheme at 30.966 and 18.475 MCM in both November and December, respectively. Furthermore, there have no unmet demands in dry season because most of irrigation scheme in this basin does not activate.

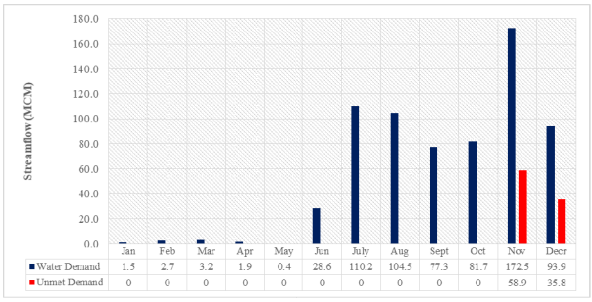

Fig. 3. Monthly variation of water demand and unmet demand

According to result shown above, in dry season the water demand for rice growing plant is low. It is due to the limited of activities in each demand site. It meant that there are very little farmer will grow rice in dry season. Meanwhile, in rainy season, the requirement of water is needed as shown in fig 3, but the amount of both water and unmet demand are shown higher in November and December. Base on the selected cropping pattern in this study, we know that the dry season rice will start at late of November so that is the reason why the water demand is high due to the needed of water for support dry growing or also the scarcity of water occurs because November is the end of rainy season. The amount of rainfall is less and tend to entry dry season while the water is needed.

C. Annual increase in irrigated area scenario

Annual increase in irrigation demand assumes that the command of dry season rice is increased annually by 5 percent. The command area in 2018 is 52 600 ha, whose irrigated area in dry season is 691 ha and it will go up 5% over the period of 2019 to 2030. The total command area in 2030 is approximately 53 100 ha.

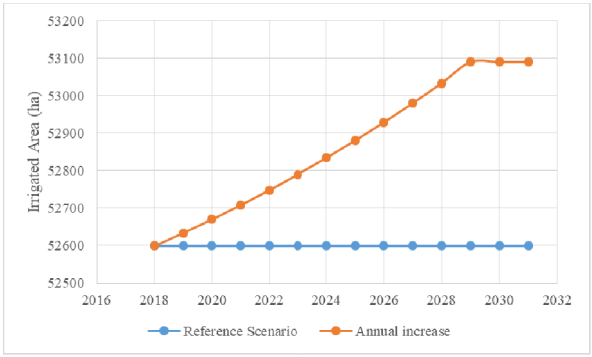

Fig. 4. Trend of increase in dry irrigated area

In the reference scenario, water demand is 678.35 MCM from 2018 to 2060s. The annual increase of irrigation area will be a steady increase in irrigation demand from 678.85 MCM in 2019 to 985.36 MCM in 2070s. This study was assumed that the irrigated area would remain stable from 2030 to 2070; hence, the annual irrigation would stay constant at 772.59 MCM until the end of study timeframe.

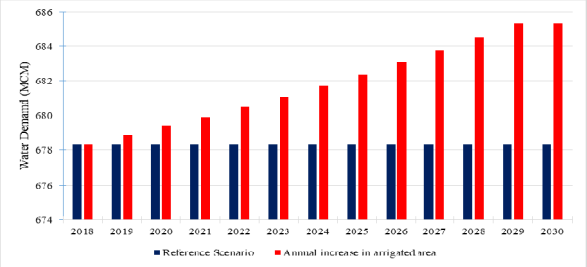

Fig. 5. Comparison of water demand between reference and annual increase scenario

Moreover, the scarcity water in each irrigation scheme is happened only in November and December around 94.63 MCM per annum. The trend of unmet demand in annual increase scenario climbed moderately to nearly 100 MCM per annum.

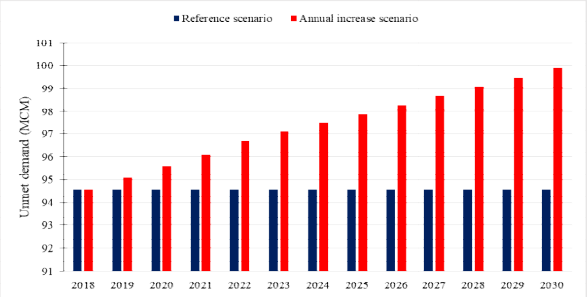

Fig. 6. Comparison of unmet demand between reference and annual increase scenario

D. Climate change scenarios

The future streamflow under climate change scenario was generated using weather generator downscaled by Mekong River Commission (MRC) and input in SWAT model to simulated future streamflow in each tributary. This study was selected GISS model, one of three climate change by three institution. In GISS model, we select two different RCP to input, including RCP 2.6 and 8.5 for 2030 and 2060.

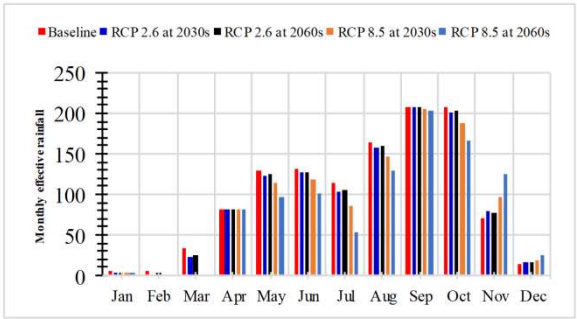

Fig. 7. Comparison between simulated and observed streamflow under GISS model, RCP 2.5 and 8.5

- GISS-E2-R-CC in 2030s

The water demand in this scenario indicates the different trends between annual increase scenario and both RCPs. On November, the monthly water demand in this month is relatively high compared to other months in both scenarios while in May is the lowest water demand.

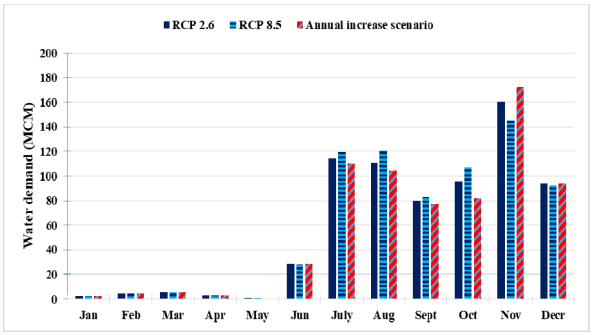

Fig. 8. Monthly variation of water demand in each scenario at 2030s

Otherwise, for the scarcity of water, the monthly unmet demand in this month is high in November and December compared to other months in both scenarios. The graph demonstrates that the scarcity of water mostly occurs in rainy season.

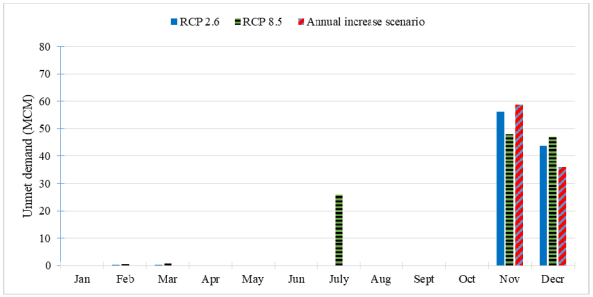

Fig. 9. Monthly variation of unmet demand in each scenario at 2060s

- GISS-E2-R-CC in 2060s

In 2060s scenario, the values of each scenario are quite different from climate change scenario in 2030s, if considering on the monthly trend, yet the results show the same as the previous scenarios for both water demand and unmet demand. For the water demand, in November, the monthly water demand in this month is high compared to other months in both scenarios while in May is the lowest water demand. In contrast, the monthly unmet demand in this month is high in November and December compared to other months in both scenarios.

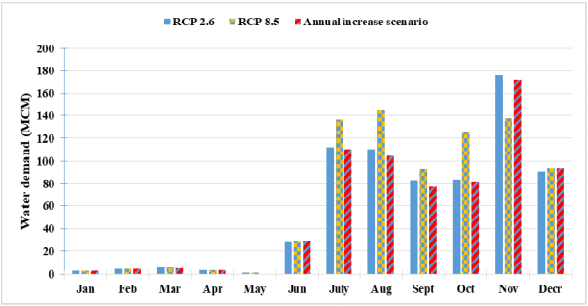

Fig. 10. Monthly variation of water demand in each scenario at 2060s

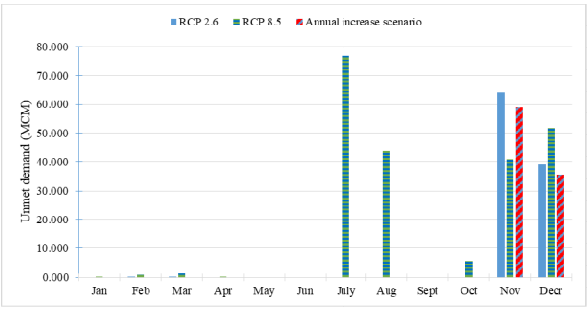

Fig. 11. Monthly variation of water demand in each scenario at 2060s

To sum up in this part, focus on unmet demand that shown in each graphs above, the reason why in future scenarios the quantity of unmet demand are shown more in July, August and October and the amount of water is high than reference scenario because of the change in rainfall distribution due to climate change as shown in Fig 7. Due to the climate is changed, it will effected on the monthly streamflow in each river. In figure 7 show that the quantity of discharge in future scenarios are mostly lower that baseline flow.

Conclusions

To sum up, this study is attempted to apply WEAP model application to identify the situation of irrigation requirement in Stung Sreng Catchment in different scenarios, including scenario of increase in irrigated area and climate change under global circulation model. The results from the model have shown that in current account, the irrigation water demand to support irrigated area of almost 53 000 ha is about 678 MCM per year. For the reference scenario, it illustrates the water demand and unmet demand in this area from 2019 to 2030. The results have also demonstrated the water demand is 679 MCM and unmet demand is around 95 MCM. In addition, the annual increase scenario identifies the water demand and unmet demand situation when the irrigated area in dry season constantly increase 5% per year until 2030. The water demand in this scenario will be 684.483 MCM at 2030. It implies that irrigation demand increases roughly 5.5 MCM and the scarcity of water is around 100 MCM. For climate change scenario selected from climate model: GISS-E2-R-CC, the result reveals that the trend of water and unmet demand are going to increase gradually for both RCP 2.6 and 8.5 compared to annual increase scenario. The peak of water demand in dry season is in March and November. In contrast, for the lowest demand was in May and June. Additionally, the most scarcity of water in this scenario is in November and December.

References

[1] Bjørnæs, C., 2013. A guide to Representative Concentration Pathways. CICERO. Center for International Climate and Environmental Research.

[2] CDRI, 2015. CLIMATE CHANGE AND WATER GOVERNANCE IN CAMBODIA, Challenge and Perspectives for Water Security and Climate Change in Selected Catchments, Cambodia.

[3] CDRI. 2015. CLIMATE CHANGE AND WATER GOVERNANCE IN CAMBODIA, Challenge and Perspectives for Water Security and Climate Change in Selected Catchments, Cambodia.

[4] Hansen, J., Lacis, A., Rind, D., Russell, G., Stone, P., Fung, I., Ruedy, R., Lerner, J., 1984. Climate sensitivity: Analysis of feedback mechanisms. Climate processes and climate sensitivity, 130-163.

[5] Hamlat, A., Errih, M., Guidoum, A., 2013. Simulation of water resources management scenarios in western Algeria watersheds using WEAP model. Arabian Journal of Geosciences, 6(7), 2225-2236.

[6] Lamarque, J.-F., Shindell, D., Josse, B., Young, P., Cionni, I., Eyring, V., Bergmann, D., Cameron-Smith, P., Collins, W., Doherty, R., 2012. The Atmospheric Chemistry and Climate Model Intercomparison Project (ACCMIP): overview and description of models, simulations and climate diagnostics. Model Dev. Discuss, 5, 2445-2502.

[7] Manabe, S., Spelman, M., Stouffer, R., 1992. Transient responses of a coupled oceanatmosphere model to gradual changes of atmospheric CO2. Part II: Seasonal response. Journal of Climate, 5(2), 105-126.

[8] MOE. 2002. Cambodia's Initial National Communication under the United Nations Framework Convention on Climate Change. (Phnom Penh: MOE).

[9] MONG, M., OEURNG, C., LY, S., Techno-Science Research Journal.

[10] MRC. 2015. Pilot Stung Sreng River Basin Plan, Ministry of Water Resources and Meteorology, Cambodia.

[11] Phalla, C., Paradis, S., 2011. Use of hydrological knowledge and community

participation for improving decision-making on irrigation water allocation: CDRI.

[12] Schmidt, G. A., Ruedy, R., Hansen, J. E., Aleinov, I., Bell, N., Bauer, M., Bauer, S., Cairns, B., Canuto, V., Cheng, Y., 2006. Present-day atmospheric simulations using GISS ModelE: Comparison to in situ, satellite, and reanalysis data. Journal of Climate, 19(2), 153-192.

[13] Sperber, K., Annamalai, H., Kang, I.-S., Kitoh, A., Moise, A., Turner, A., Wang, B., Zhou, T., 2013. The Asian summer monsoon: an intercomparison of CMIP5 vs. CMIP3 simulations of the late 20th century. Climate Dynamics, 41(9-10), 2711-2744.

[14] Taylor, K. E., Stouffer, R. J., Meehl, G. A., 2012. An overview of CMIP5 and the experiment design. Bulletin of the American Meteorological Society, 93(4), 485-498.

[15] Van Liew, M. W., Garbrecht, J., 2003. Hydrologic simulation of the little Washita river experimental watershed using SWAT 1. JAWRA Journal of the American Water Resources Association, 39(2), 413-426.

FUTURE CLIMATE PROJECTIONS WITH A HIGH HORIZONTAL RESOLUTION GLOBAL CLIMATE MODEL FOR IMPACT ASSESSMENTS IN WATER SECTORS IN SOUTHEAST ASIA

Tosiyuki NAKAEGAWA[1,a,*]

Abstract Future climate scenarios for impact assessments for the entire world have been provided with a Meteorological Research Institute (MRI) global climate model (GCM) with high horizontal resolution of 20 km (MRI-AGCM) under a research program, Integrated Climate Change Projection in Japan. Reliable impact assessments requires a precise physical-based model for each sector. Such a model often requires its high-horizontal-resolution forcing data such as meteorological variables, land cover, soil types, and river cross section. Therefore, we have provided the data of future climate scenarios for impact assessments for foreign impact assessment researchers and investigated impact assessments on water resources with collaboration with impact assessment researchers. First, we evaluated a present-day climate simulation in Southeast Asia with MRI-AGCM against observations and obtained good reproducibility of the present-day climates. Indeed, future changes in surface air temperature extreme indices are projected to increase in the entire Southeast Asia, but future changes in precipitation extreme indices is projected to vary with area even within Southeast Asia. Five day rainfall totals is projected to increase in more than half of land area of Southeast Asia with high confidence and to decrease in spotty areas scattered in Southeast Asia with less confidence. We also assessed water resources in Chao Phraya River in a late 21st century under SRES A1B and obtained a peak of river discharge at Nakhon Sawan located in the central region in September, a delay of one month after the maximum monthly mean precipitation.

Keywords *future climate, impact assessment, water resources, global, Southeast Asia, global climate model*

This study is conducted under a research program, Theme C: Integrated Climate Change Projection in the Program for Risk Information on Climate Change: TOUGOU-C supported by MEXT, Japan

[1]The Japan Meteorological Business Support Center and Meteorological Research Institute, Japan Meteorological Agency
Tsukuba, Japan
[a]tnakaega@mri-jma.go.jp

Introduction

Future climate projections are essential for impact assessments on each sector of industries for infrastructure designs, and decision making against the impacts. We developed a Meteorological Research Institute (MRI) global climate model (GCM) with high horizontal resolution of 20 km (MRI-AGCM) under a research program, Integrated Climate Change Projection in Japan to precisely project future climate changes. Due to high horizontal resolution, the projections are being used for impact assessments of future climates on many sectors of industries, especially on water sectors.

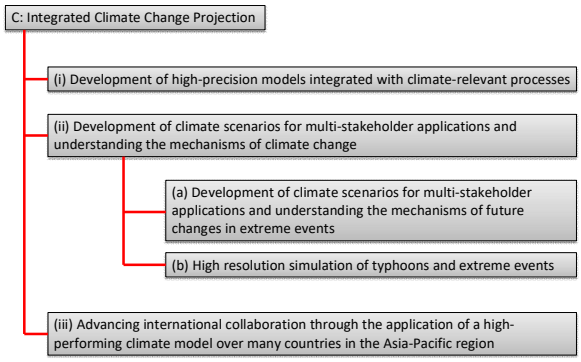

Fig. 1.. Structure of Integrated Climate Change Projection in the Program for Risk Information on Climate Change: TOUGOU-C. Courtesy of Dr. Takayabu (PI: MRI)

We have participated in a research program, the future climate projections under a research program the Program for Risk Information on Climate Change (TOUGOU) and studied future climate projections in Theme C: Integrated Climate Change Projection in the Program for Risk Information on Climate Change: TOUGOU-C. TOUGOU-C is composed of 3 components (Fig.1). This overview reported some good practices about impact assessments of climate changes on water sectors with future climate projections with the MRI-AGCM by using climatic indices.

Model, Experiment Setups, and Methods

A. Model

The MRI-AGCM used in this study has been developed based on an operational global weather forecast model in Japan Meteorological Agency. MRI-AGCM is atmospheric model with a land-surface bio hydrological model. Semi-Lagrangian scheme is used in the dynamical core to allow stable and fast numerical integration which is impossible in a conventional Eulerian scheme. Convection scheme used here is Yoshimura scheme [2]. Shortwave radiation scheme is developed by Shibata and Uchiyama (1992) [3], longwave radiation scheme is developed by Shibata and Aoki (1989) [4], and land-surface bio hydrology: MJ-SiB: SiB with 4 soil-layers and 3 snow-layers. Mellor & Yamada (1974,1982) level-2 closure model is used as planetary boundary later scheme. The horizontal resolution is TL959 or about 20-km grid spacing with 60 vertical layers. Another version of MRI-AGCM with middle horizontal resolution of TL319 or about 55-km grid spacing is also used to quantify uncertainty in future climate projections to allow multiple experiment setups since MRI-AGCM with 55-km grid spacing runs more than 10 times faster than MRI-AGCM with 20-km grid spacing. We perform regional dynamical downscaling with a Non-Hydrostatic Regional Climate Model (NHRCM) for Japan region from MRI-AGCM outputs, while visiting scholars do so for their own country's region.

B. Experiment setups

MRI-AGCM with 20-km grid spacing is atmospheric GCM and sea surface temperatures (SSTs) must be prescribed in all experiments. For the present-day climate simulation, observed SSTs are used. For future climate simulation, SSTs are obtained as the CMIP5 multi-model ensemble mean.

We performed future climate projections with a variety of experiment setups in order to estimate uncertainty in future climate projections with 60-km grid spacing version of MRI-AGCM due to computer efficiency/resources although a fast supercomputer the Earth Simulator is available for these simulations. First we used four different future projected SSTs to quantify the effect of the uncertainties in projected SSTs on the future climate projections. The projected SSTs are developed by performing a cluster analysis of future SSTs projected by CMIP5 multi model ensemble. Second, we used three different convection schemes to quantify the uncertainty in subgrid-scale cumulus parameterization. Therefore, we performed twelve simulations with different experiment setups.

We performed future climate projections under SRE SA1B, RCP 8.5 scenario and currently performed those under RCP 2.6 Time-slice experiments shown in Fig. 2. is chosen due to high computer burdens. In this overview, we used future climate projections under SRES A1B and RCP 8.5. We defined the present-day climate as a period from 1979 to 2003, and the future climate as a period from 2075 to 2099.

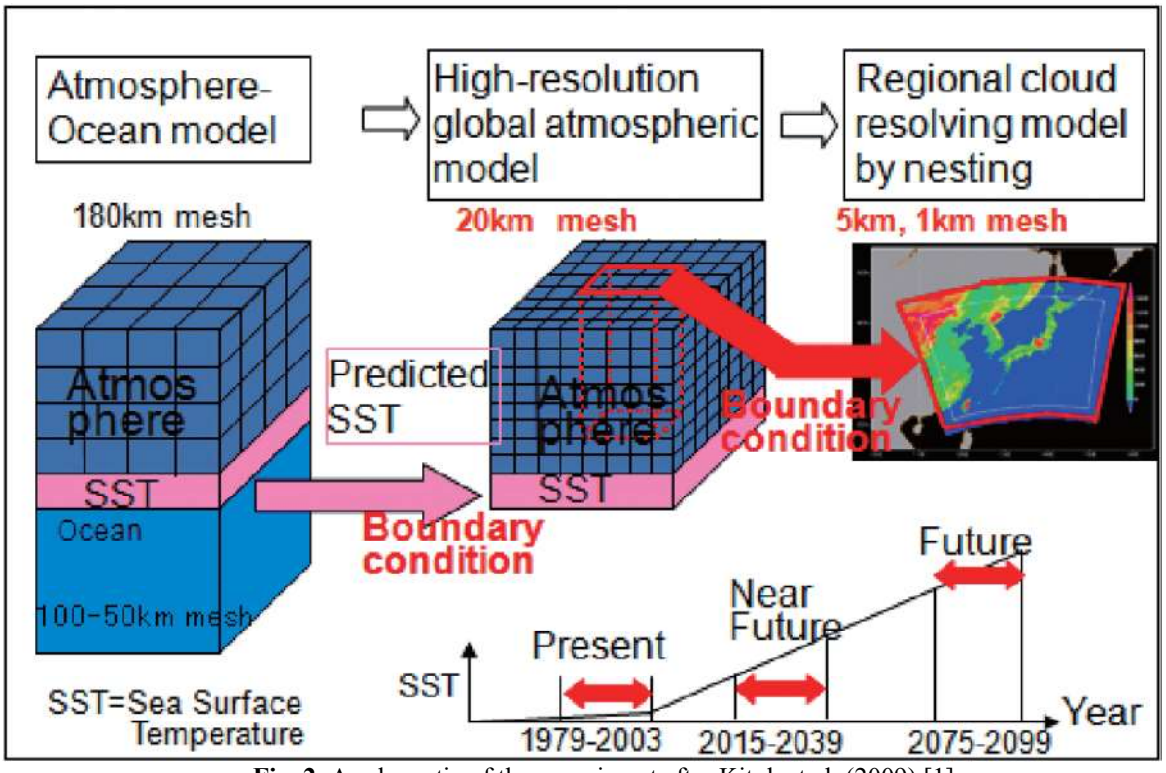

Fig. 2. A schematic of the experiment after Kitoh et al. (2009) [1]

C. Analysis method

We analyze future changes in the annual maximum 5-day rainfall total (Rx5d) and consecutive dry days (CDD) since these climatic extreme indices represent water excess and water scarcity as a meteorological forcing. In this analysis we defined dry day as day when the daily rainfall amount is equal to or greater than 0.1 mm/day and the count of the CDD do not exceed a calendar year.

Although we performed ensemble climate simulations with 60-km grid spacing with different convection schemes, we present the results with ensemble climate simulations with 20-km grid spacing with the Yoshimura scheme.

Evaluation of Present-Day Climate Simulation

First, we evaluate the climatological mean annual, June-July-August, and December-January-February precipitation against the observations. Overall capability of presipitation simulated in MRI-AGCM is reasonable and better than CMIP5 AOGCMs primarily due to use of the present-day observed SST and high horizontal resolution.

We compared Rx5d of the present-day climate simulations with that of observations. The large-scale distribution of Rx5d is well captured in the present-day climate simulations with MRI-AGCM. However, the absolute values in some regions are over- and underestimated (figure not shown). These differences between the simulation and the observations is due to horizontal resolution, representation of convection, and others since a GCM is tuned so that global-scale model's simulation with proper physics is optimized.

Capability of CDD similar to Rx5d is obtained; good geographical distributions of CDD but with over- and underestimations in some regions.

These results allow us to further analyze the future changes in Rx5d and CDD.

Results

A. Rx5d.

Figure 3 shows future changes in annual maximum 5-day rainfall total (Rx5d) in Southeast Asia. Most of the land areas has significant increases in Rx5d in ensemble mean (Fig. 3.a). It means that water excess or flood in the future climate often occurs and become larger in magnitude than those in the present-day climate. The increase exceed 60 mm/5-days in some areas such as the Malaysia and Miramar, suggesting distinct increase in flood damages.

However, the mainland of Thailand, Vietnam, and the Luzon Island do not so. These areas are located between 10ºN –20ºN and adjacent to a northern part of the South China Sea. This insignificant changes are consistent among the eachmember of the 4 experiments (Fig. 3c to 3f). One possible reason is a large difference among the projected SST used for each member of the 4 experiments. No consistent changes are seen in these areas.

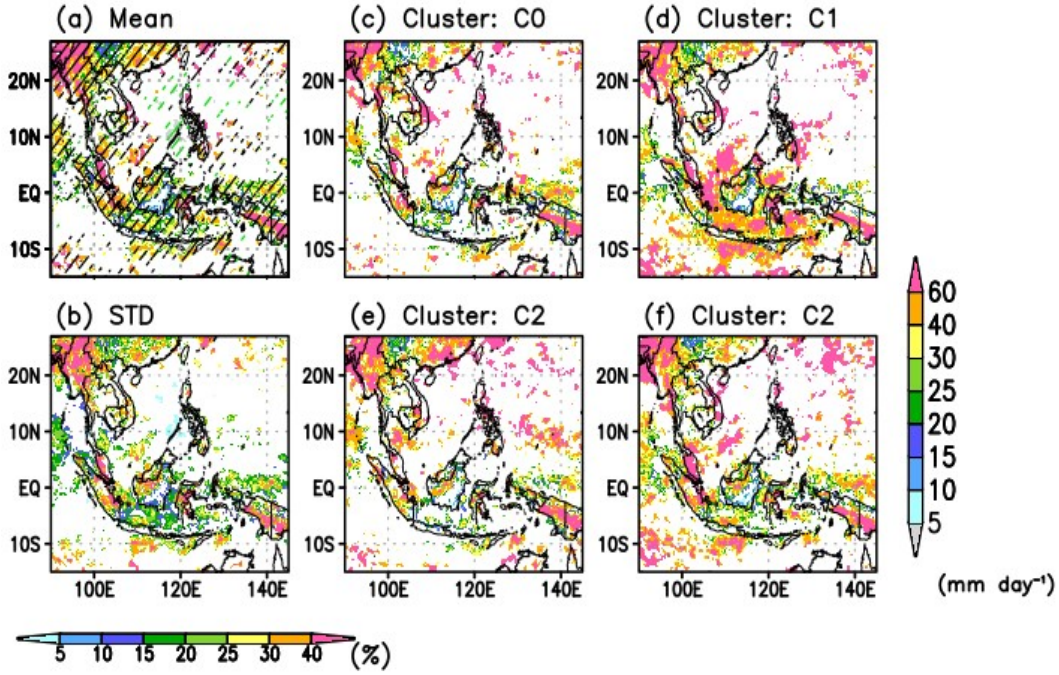

Fig. 3. Future changes in annual maximum 5-day rainfall total (Rx5d) in Southeast Asia. (a) ensemble mean of the 4 experiments with 4 different projected SSTs, (b) standard deviation of the ensemble members of the 4 different experiments with 4 different projected SSTs, (c) to (f) each of the 4 experiments with different projected SSTs. Colored areas denotes statistically significant change at 95% level while hatched areas denote consistent changes among the 4 different experiments.

Most of the oceans in Southeast Asia except for in the Thai Bay, the Java Sea, and others have insignificant changes. However, consistent changes are seen n some of these ocean areas.

B. CDD

Figure 4 shows future changes in annual maximum consecutive dry days (CDD) in Southeast Asia. Statistically significant changes are not seen in most of the land areas except for scattered spotty areas. However, the Malay Peninsula and the Sumatra Island show the significant increase in CDD in the future climate with high consistency. This result suggest that water scarcity or drought may reduce in the future climate. CDD only represent information about the annual maximum of dry days but does not that of monthly to seasonal mean rainfall total. Both should be considered for a good practices in water sector.

C. River discharges in Chao Phraya River

As an example of impact assessments of climate changes on the water sector using MRI-AGCM, Chao Phraya River is taken up[5]. Projections of river discharges at Nakhon Sawan located in the central region of the Chao Phraya River in the future climate is performed using outputs from MRI-AGCM and a river routing model, Global River-flow model using TRIP or GRiVET [6]. The inputs to GRiVET from MRI-AGCM are summation of surface and subsurface runoff computed in one-dimensional land-surface model, hereafter referred to as total runoff.

River discharge at Nakhon Sawan is projected to reach the peak in September in the future climate, a delay of one month after the maximum monthly mean precipitation.

Concluding Summary

Future climate changes with MRI-AGCM with 20-km grid spacing are investigated in this overview. Five day rainfall totals (Rx5d) is projected to increase in more than half of land area of Southeast Asia with high confidence and to decrease in spotty areas scattered in Southeast Asia with less confidence. Consecutive dry days (CDD) is projected to increase in small spotty areas confined except for the Malay Peninsula and the Sumatra Island.

Water resources in Chao Phraya River in a late 21st century under SRES A1B are projected and the following result is obtained: a peak of river discharge at Nakhon Sawan located in the central region in September, a delay of one month after the maximum monthly mean precipitation.

We demonstrated future impact of climate changes on the river discharges using total runoff of MRI-AGCM. Instead of using total runoff, surface meteorological forcings such as radiations, surface air temperature, and precipitation, one can perform hydrological simulations with a land-surface modeland a river routing model.

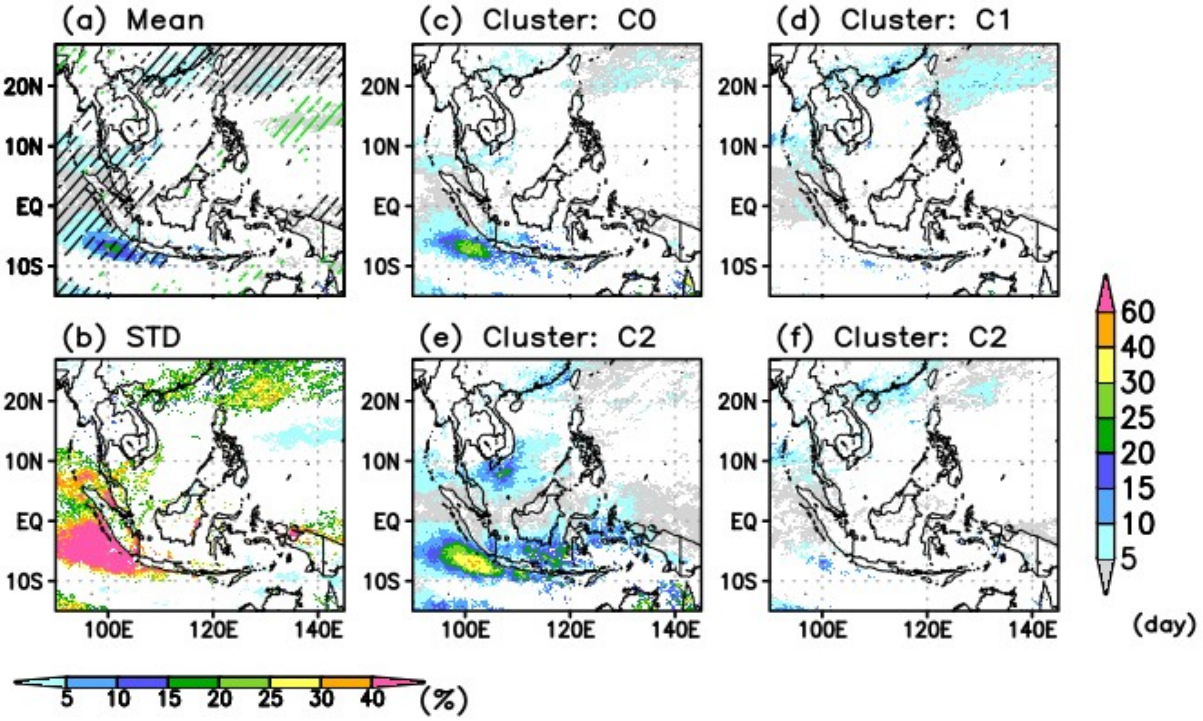

Fig. 4. Same as in Fig. 3 but for consecutive dry days.

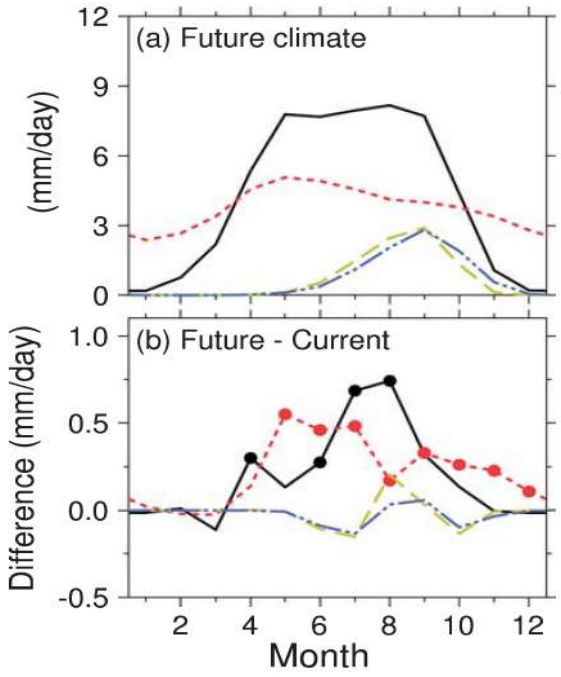

Fig 5. Climatological monthly mean hydrological variables at Nakhon Sawan in the late 21st century using the 20-km mesh MRI-AGCM. Black solid, red dashed, green centered and blue cutting-planed lines denote precipitation, evaporation, total runoff, and river discharge, respectively. Circles denote statistically significant change (P < 5%) compared to the present-day values. (a): The amount of the projected future climate, (b): The changing amount of the projected future climate.
After Champathong et al. (2013) [5].

We have already performed future climate projections under RCP 8.5 and have been performing those under RCP2.6, will be available. The former is already available on request and the latter will be so.

Most hydrological and water resources scientists often request outputs with more high resolution than 20 km. Regional-scale dynamical downscaling may answer this questions. We have already done the dynamical downscaling with 5-km grid spacing over the entire Thailand and will be available very soon.

Acknowledgment

The author thanks all the participants of Theme C: Integrated Climate Change Projection in the Program for Risk Information on Climate Change: TOUGOU-C. Without their effort, he cannot prepare this overview.

References

[1] Kitoh, A., Ose, T., Kurihara, K., Kusunoki, S., and Sugi, M. Projection of changes in future weather extremes using super-high-resolution global and regional atmospheric models in the KAKUSHIN Program: Results of preliminary experiments. Hydrological Research Letters, 3, 49-53, 2009.

[2] Yoshimura, H., R. Mizuta, and H. Murakami, A spectral cumulus parameterization scheme interpolating between two convective updrafts with semi-lagrangian calculation of transport by compensatory subsidence. Mon. Wea. Rev., 143, 597-621, doi:10.1175/MWR-D-14-00068.1, 2015.

[3] Shibata, K. and T. Aoki, An infrared radiative scheme for the numerical models of weather and climate. J. Geophys. Res., 94, 14923-14943, 1989.

[4] Shibata, K. and A. Uchiyama, Accuracy of the delta-four-stream approximation in inhomogeneous scattering atmospheres. J. Meteor. Soc. Japan, 70, 1097-1109, 1992.

[5] Champathong, A. D. Komori, M. Kiguchi, T. Sukkhapunnapan, T. Nakaegawa, and T. Oki. Future projection of mean river discharge climatology forthe Chao Phraya River basin. Hydrological Research Letters, 7, 36-41. doi: 10.3178/hrl.7.36, 2013.

[6] Nakaegawa, T. and M. Hosaka, 2008. Effects of calibrated current speeds and groundwater scheme in a global river-flow model on river discharge and terrestrial water storage, Hydrological Research Letters, 2, 18-21.

Assessment of runoff generation using the Simple Biosphere Model including Urban Canopy for upper Chao Phraya River Basin, Thailand

Teerawat RAM-INDRA

Abstract Upper Chao Phraya river basin is consisting of four river basins: Ping, Wong, Yom, and Nan which play an essential role essential water to the central part of Thailand. Each sub-basin has a variety of topography from mountainous area to flat plain. It is usually difficult for field measurement with complex terrain to directly measure the land and atmosphere interaction. The land surface model (LSM) is an alternative way to provide that information. In this study, the runoff simulated by a land surface model named Simple Biosphere Model including Urban Canopy (SiBUC) for the regional scale of the upper Chao Phraya River Basin. The forcing data are gathering from observation, reanalysis, and satellite estimation. A kinematic wave routing model was applied for the runoff product and analyzed at representative discharge observation stations for the upper Chao Phraya river basin. The validation is needed to test the performance of the model in the study area. The result could provide more understanding of the characteristic of runoff in the upper Chao Phraya river basin and should serve as the reference runoff generation data in the future research.

Keywords *Land surface model, Upper Chao Phraya River basin, Runoff generation*

Introduction

A Global Circulation Model (GCM) is one of the most reliable tools and widely used for research on climate change and related fields including its impact on the hydrologic cycle. Though GCM has a good agreement with observation data in many necessary parameters in large scale [1], there still have uncertainties in climate predictions for three sources: internal variability, model uncertainty and scenario uncertainty [2]. Bias correction techniques could be a way to reduce uncertainty in GCMs output. Several studies have developed bias correction methods to adjust GCM outputs. However, due to the north of Thailand sub-basin scale has a variety of topography from the mountainous area in the northern part to flat plain in the southern region. It is usually difficult for field measurement with complex terrain to directly measure the land and atmosphere interaction. To provide those data, land surface model is another way. Although, the land surface model need to evaluate their performance before entrusting the result from the simulation.

This paper presents the evaluation process of land surface model name SiBUC over the upper part of Chao Phraya River Basin, Thailand by feeding the runoff generation to the flow routing model and compare to the river discharge observation data at five representative point for each sub-basin and the joint position of Chao Phraya River.

Study Area

This study was performed on the fourtributaries of Chao Phraya River in Thailand, Ping River Basin, Wang River Basin, Yom River Basin, and Nan River Basin. The river flows through the northern part of Thailand to the southern part and meets at the middle of the country. The size of the basin are around 34,500 km^2, 10,800 km^2, 24,000 km^2, and 34,700 km^2 respectively. Figure 1 shows the river channel in upper Chao Phraya and points of evaluation for each tributary, and all the tributary joins together. The observation stations for each basin are select; Ping river: inflow to Bhumibol Dam, Wang river: W.3A stations, Yom river: Y.14, Nan river: inflow to Sirikit Dam, and C.2.

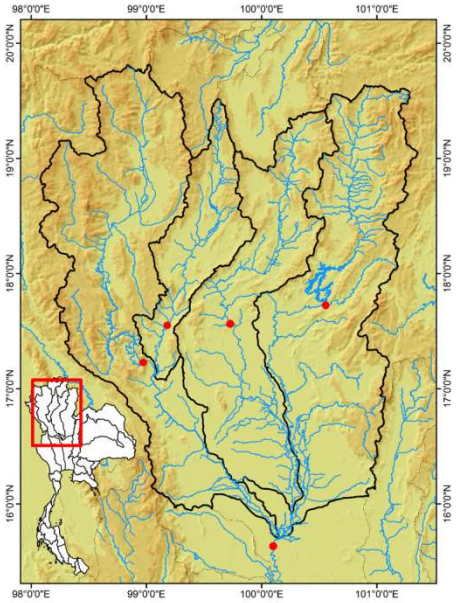

Fig. 1. upper Chao Phraya basin and river discharge observation stations (red dot) used in the study

Hydrologic Model

A. Land surface model

This study is utilized land surface process model to produce runoff generation. The land surface process model proposed by Tanaka [9] namely Simple Biosphere including Urban Canopy (SiBUC) developed from Simple Biosphere [10] with modify in [11] to more cooperate with cropping pattern in southeast region were used in the study. The SiBUC are using mosaic parameterization approach to include each land-use patch of the grid element to the atmosphere. The models are incorporated with three sub-models (green area, urban are and water body) to describe each grid cell. The average surface fluxes for each grid are from averaging the surface fluxes based on each land-use weighted by its sectional area. SiBUC is using Richards' equation for soil moisture store in three sub-soil layer and Darcy's law to expressed vertical exchanges between soil layers.

B. Flow routing model

The runoff generations are feed to a distributed flow routing model; 1K- FRM to simulate the river discharge. The models are based on one-dimensional kinematic wave develop in Hydrology and Water Resources Research Laboratory, at Kyoto University. The runoff generations are routed to the downstream according to the topography data. The model and program for preparing topography input can be obtained from 1K-FRM website (http://hywr.kuciv.kyoto-u.ac.jp/products/1K-DHM/1K-DHM.html).

$$\frac{\partial A}{\partial t} + \frac{\partial Q}{\partial x} = q_L \tag{1}$$

$$Q = \alpha A^m,\ \alpha = \frac{\sqrt{\sin\theta}}{n},\ m = \frac{5}{3} \tag{2}$$

The continuity equation is defined in (1). Where; t is time; x is space coordinate; A is flow cross-section area; Q is flow rate; q_L is lateral flow per unit length from the side of the main flow or can determine as rainfall intensity or runoff generation give vertically to the slope. Equation (2) are derived simplify momentum equation with Manning equation to rout the water. Where n is manning coefficient; θ is channel gradient.

C. Simulation setting

The cell size of SiBUC model are set into 10 km with aggregate all the input surface data include of land use, soil data, and vegetation data to the model resolution while the methodological data are utilized as same as an original resolution of JRA-55. The simulation periods start from 1 January 1991 to 31 December 2010 total of 20 years.

As the output runoff generate, they were used as input to flow routing model, 1K-FRM at 1 km spatial resolution. The simulation is set to the natural condition of the entire study area that means no dam structure includedand all replication in one, without dividing the watershed area.

Data

A. Forcing data

SiBUC needs seven components meteorological data to drive the model: precipitation, air temperature, specific humidity, surface pressure, wind speed, downward shortwave radiation, and downward longwave radiation. In this study, precipitation data were obtained from observation stations of Royal Irrigation Department, Thailand (RID) and Thailand Meteorological Department, Thailand (TMD) across the study area and using interpolation technique called inverse distance weighting to make a spatial precipitation dataset. Other data are gathering from the product of the Japanese 55-year reanalysis (JRA-55) [3] propose by Japan Meteorological Agency (JMA). The JRA-55 systems are configuration of data sources, quality control, data selection for observations, data assimilation system and forecast model. The spatial resolution of JRA-55 is TL319L60 or corresponding to a grid interval of 60 km.

B. Land use

The land use data are based on MODIS land use [4, 5]. These data sets are WGS 1984 coordinate system reprojected product of Global Mosaics of the standard MODIS land use data product (MCD12Q1) in the IGBP Land Use Type Classification at a spatial resolution of 10 km. Each cell class is modified to match on the land survey data from the Land Development Department, Thailand (LDD) on the category of an urban area, cropland and irrigation area.

C. Elevation and slope

The elevation data used in the study are obtained from Hydrological data and maps based on SHuttle Elevation Derivatives at multiple Scales (HydroSHEDS) with also used to create the slope data. The HydroSHEDS is derived primarily from elevation data of the Shuttle Radar Topography Mission (SRTM) at 90 km spatial resolution.

D. Soil data and vegetation data

The soil texture data are calculated from soil physical properties from Digital Soil Map of the World (DSMW) [6] using criteria of twelve major soil texture classifications defined by the USDA [7]. DSMW is a digitized version of the FAO-UNESCO Soil Map of the World produced in the paper version. For other soil data such as soil depth and root depth are obtain from ECOCLIMAP [5]. ECOCLIMAP is included with an ecosystem classification and a coherent set of land surface parameters database at 1 km resolution developed by Centre National de RecherchesMétéorologiques, France (CNRM-GAME). The vegetation parameters used in this study are extracting from MCD15A3H V006 [8] which are combined fraction of Photosynthetically Active Radiation (FPAR), and Leaf Area Index (LAI) datasets at a 4-day time interval and 500 m spatial resolution. The data were aggregated into 12-day interval to clear out the missing data.

Result

A. Runoff production

The SiBUC are given the result of runoff generation. It can compare to precipitation in term of runoff ratio to explain how much precipitation becomes runoff by calculating annual runoff divide by annual precipitation. On the other hand, they can also show how much the precipitation is lost through the evapotranspiration process. Figure 3 shows the annual average runoff ratio of the study area from 1991 - 2010. The ratios vary from 0.1 to 0.9 based on the land use tile. Most of the high value of the ratio is located in the urban area that considerate as impermeable pavement which does not allow the evaporation of soil moisture by the model. Still, the overall precipitation excludes the urban area are only around 20% to 30% are become runoff.

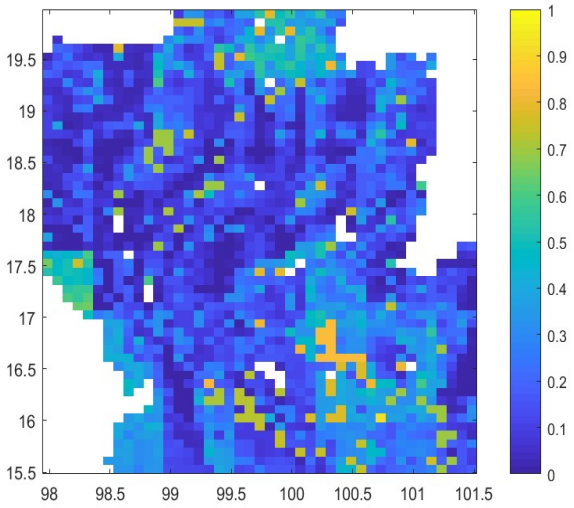

Fig. 2. runoff ratio

B. Monthly discharge

Monthly average discharge for 20 years is shown in Figure 4 for representative observation discharge point of 4 tributary and C.2 station. The simulation condition of the flow routing model for C.2 station did not include the dam in the upstream. So, the river discharge cannot directly compare and can assume that one of the reasons for causing the highly overestimates from the simulation. Hence, the explanations below will not be considerate with the C.2 station.

The result shows the hydrograph are followed the pattern of the observation data with some miss estimation on inflow to Bhumibol Dam, W.3A, and Y.14. For inflow to Sirikit Dam, they see a substantial underestimate between simulate result and observation for the entire period. The average observation flow in dry season for each river is 22%, 18%, 13% and 17% for inflow to Bhumibol Dam, W.3A, Y.14, and inflow to Sirikit Dam. When compared with the average flow in wet season while the simulation result of average flow in dry season to wet season is 21%, 13%, 17%, and 32% respectively. When comparing the average flow of simulation with observation in wet season, the difference is -12%, -24%, 33%, and 149% respectively. The negative percentage represents overestimate by simulate and positive are represent the underestimation. From this result also show a large underestimate value for inflow to Sirikit Dam that requires further analysis to understand the cause of huge amount of error.

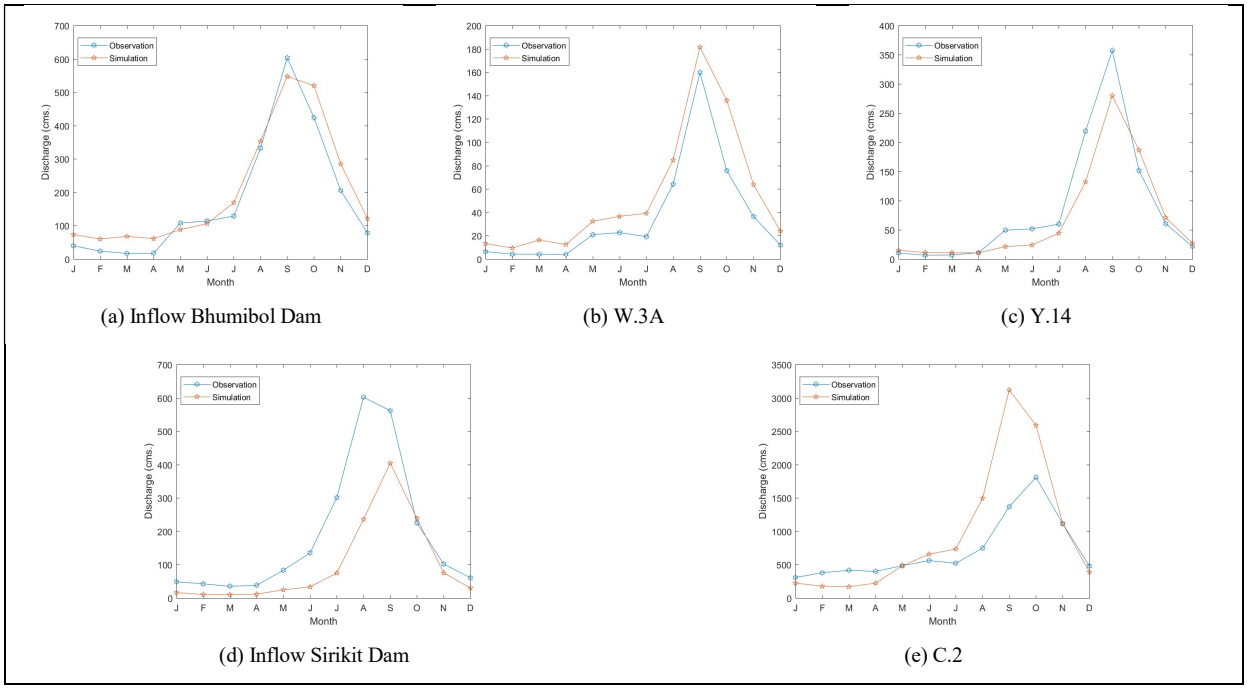

(a) Inflow Bhumibol Dam (b) W.3A (c) Y.14

(d) Inflow Sirikit Dam (e) C.2

Fig. 3. Monthly average discharge from 1991-2010.

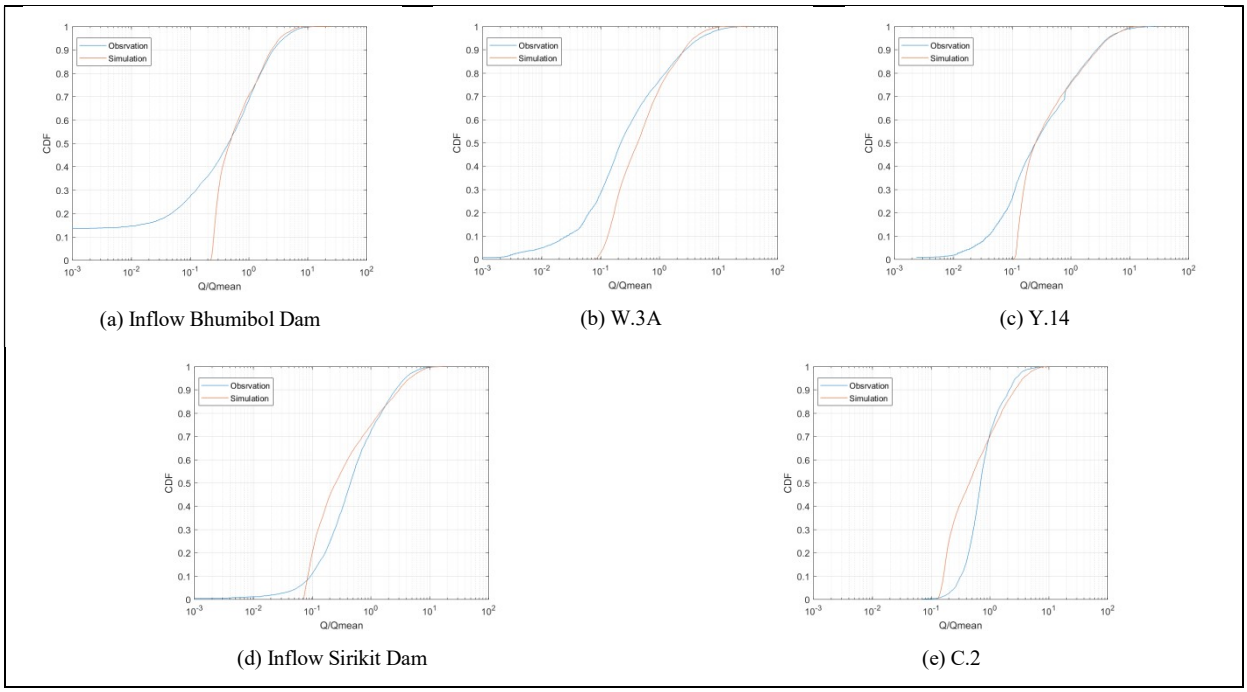

(a) Inflow Bhumibol Dam (b) W.3A (c) Y.14

(d) Inflow Sirikit Dam (e) C.2

Fig. 4. Cumulative distribution transformation for daily discharge from 1991-2010

C. Daily discharge

Figure 4 is present cumulative distribution function (CDF) of daily discharge for 20 years. The CDF has illustratedthe probability that discharge events are less or equal to a specified value based on the normalized of daily discharge for all representation observation stations. The value of normalizing daily discharge can describe the high discharge are more than 1 ($Q/Q_{mean}> 1$) and for low discharge are less than 1 ($Q/Q_{mean}< 1$).

With large difference in high and low flow rates in the upper Chao Phraya River basin. We expect a good estimation for extreme value to give the accurate data for study relate to high and low value of discharge in the future. The daily result show most of the stations have clear overestimate in the frequency of low discharge. On the other hand, the frequency of high discharge is somewhat overestimated when considering inflow BB and W.3A, slightly underestimate for inflow for SK and seem to good match at Y.14.

Concluding Summary

This paper present the performance of land surface model: SiBUC on upper Chao Phraya River Basin that includes 4 major tributaries: Ping, Wang, Yom, and Nan. Since the total runoff data are difficult to obtain by measurement in the real field; the river discharge is used to evaluate instead of runoff generated by the model. Discharge observation data of each river basin are used to representative comparison point for each sub-basin.

The result seems to perform well for monthly scale for inflow BB, W.3A, and Y.14 but still large underestimate for inflow SK. In the daily scale, the simulated performance for high and low discharge still found difficult to capture. From this result, the model is needed to focus on particular sub-basins to adjust the model parameter to improve the performance and can generate runoff more accurate. The runoff generation data from this study will provide as near reference runoff data and use for the future study.

Since this study does not include large dame in the simulation, we cannot directly compare the simulation result to the observation data. Hence, the significant difference can be assumed that it affects the dam structure which comes to two solutions for the future work. First, neutralize the river by removing the effect of Bhumibol dam and Sirikit dam as in [12] using the water balance equation and dam inflow data, dam outflow data. Second, include the dam operation function into the flow routing model.

Acknowledgment

The authors are grateful to the Royal Irrigation Department, Thailand, the Thai Meteorological Department, The Electricity Generating Authority of Thailand, and the Land Development Department, Thailand for provision of observation and survey data.

References

[1] Raisanen, J. 2007. How reliable are climate models? Tellus. 59A, 2-29.

[2] Hawkins, E., and R. Sutton. 2009. The Potential to Narrow Uncertainty in Regional Climate Predictions, B. Am. Meteorol. Soc., 90, 1095–1107.

[3] Ebita, A., et al. 2011. The Japanese 55-year Reanalysis "JRA-55": an interim report, SOLA, 7, 149-152.

[4] Channan, S., K. Collins, and W. R. Emanuel. 2014. Global mosaics of the standard MODIS land cover type data. University of Maryland and the Pacific Northwest National Laboratory, College Park, Maryland, USA.

[5] Friedl, M.A., et al. 2010. MODIS Collection 5 global land cover: Algorithm refinements and characterization of new datasets, 2001-2012, Collection 5.1 IGBP Land Cover, Boston University, Boston, MA, USA.

[6] FAO-Unesco, 1977. Soil map of the world.

[7] Soil Science Division Staff. 2017. Soil survey manual. C. Ditzler, K. Scheffe, and H.C. Monger (eds.). USDA Handbook 18. Government Printing Office, Washington, D.C.

[8] Myneni, R., Y. Knyazikhin, and T. Park. MCD15A3H MODIS/Terra+Aqua Leaf Area Index/FPAR 4-day L4 Global 500m SIN Grid V006. 2015, distributed by NASA EOSDIS Land Processes DAAC, https://doi.org/10.5067/MODIS/MCD15A3H.006.

[9] Tanaka, K. 2005. Development of the new land surface scheme SiBUC commonly applicable to basin water management and numerical weather prediction model. Doctoral thesis, Kyoto University.

[10] Sellers, P., Y. Mintz, Y. E. A. Sud, and A. Dalcher. 1986. A simple biospheremodel (SiB) for use within general circulation models. Journal of theAtmospheric Sciences, 43(6), 505–531.

[11] Yorozu, K. and Y. Tachikawa. 2015. The effect on river discharge estimation by considering an interaction between land surface process and river routing process, Proc. IAHS, 369, 81-86, https://doi.org/10.5194/piahs-369-81-2015.

[12] Kotsuki, S., and K.Tanaka. 2013. Uncertainties of precipitation products and their impacts on runoff estimates through hydrological land surface simulation in Southeast Asia, Hydrological Research Letters, 2013, Volume 7, Issue 4, Pages 79-84, https://doi.org/10.3178/hrl.7.79.

Investigating the effect of initial soil moisture on river discharge using pseudo-discharge data generated by a distributed hydrologic model

Kazuaki Yorozu[1], Yutaka Ichikawa[1] and Yasuto Tachikawa[1]

Abstract The initial condition of soil moisture for river discharge simulation is neglected for river planning or management. In this study, the effect of initial soil moisture on river discharge was investigated. The target of this study was the upper part of Bhumibol dam catchment in Thailand. Throughout statistical correlation test for JRA-55 atmospheric reanalysis data and CHIRPS satellite-based rainfall data, it was assumed that monthly atmospheric fields in rainy season didn't have significant autocorrelation. Therefore, a log-term atmospheric data was generated by recombining atmospheric data between August and September. And then, a long-term pseudo-discharge data was generated utilizing a distributed hydrologic model using recombination atmospheric data. Annual maximum daily river discharge from a pseudo-discharge data was evaluated by comparing the river discharge data generated by original atmospheric data and a distributed hydrologic model. It was found that significant difference was not detected with 10% level between a CDF from the former data and that from the latter data. Annual maximum daily river discharge from a pseudo-discharge data could be categorized into two groups. First one was the data using same rainfall, another one was the data using same initial soil moisture. Analyzing each data, it was estimated that the effect of rainfall on river discharge was 718 cubic meter per second and the effect of initial soil moisture was 127 cubic meter per second.

Keywords *river discharge, soil moisture, distributed hydrologic model*

[1]Graduate school of Engineering
Kyoto University
Kyoto, Japan

Introduction

For river planning and basin water resources management, it is necessary to determine the design water level which has long term return period. In general, observation record is shorter than that. Therefore, pseudo-discharge data is generated much enough to determine design level. There are many methods for generating pseudo-discharge data. The typical one is to prepare various spatial and temporal patterns of rainfall and calculate discharge by them utilizing rainfall-runoff simulation model. In this method, it is assumed that the initial condition has no impact on that peak discharge. However, some papers mentioned that initial soil moisture may affect flood [1] [2].

For considering the effect of initial soil moisture on discharge explicitly, it is better to utilize a distributed hydrologic model. Yorozu and Tachikawa have developed a distributed hydrologic model which consists of land surface model SiBUC and flow routing model 1K-FRM [3]. In their model, runoff is calculated according to soil moisture content which is updated based on the diurnal cycle of atmospheric condition. In this sense, a distributed hydrologic model must be utilized for much longer period to consider soil moisture impact on discharge.

In previous study, some method has been developed for generating pseudo-discharge data of Bhumibol dam inflow utilizing a distributed hydrologic model [4]. In that study, numerous atmospheric data was created by recombining both atmospheric reanalysis data and satellite based observed rainfall data as a data could be happened in actual situation. And then, Bhumibol dam inflow was calculated utilizing a distributed hydrologic model by those data. Unfortunately, in that paper, the effect of initial soil moisture on discharge wasn't analyzed well because of precipitation data accuracy. Therefore, the objective of this paper is to investigate the effect of initial soil moisture on discharge updating preparation of precipitation data on previous paper.

Methodology

A. Target catchment

In this study, Bhumibol dam inflow is set as target discharge for analyzing the effect of initial soil moisture. Bhumibol dam is one of the biggest dam in

Thailand and located in upper part of Ping river basin, northern east part of Thailand. To simulate Bhumibol dam inflow, upper part of Bhumibol dam is a target catchment of this study.

B. Distributed Hydrologic Model

Yorozu and Tachikawa [3] have developed a distributed hydrologic model which consists of land surface model SiBUC and flow routing model 1K-FRM. A land surface model SiBUC is originally from the Simple Biosphere model. SiBUC uses a mosaic approach to incorporate the effects of land surface heterogeneity on land surface fluxes. A flow routing model 1K-FRM is based on one-dimensional kinematic wave theory (http://hywr.kuciv.kyoto-u.ac.jp/products/1K-DHM/1K-DHM.html).

SiBUC provides surface and sub-surface runoff, and irrigation water withdrawal with 1K-FRM as lateral inflow. On the other hand, 1K-FRM provides the river discharge rate as the irrigation water source for the irrigation scheme in SiBUC.

This distributed hydrologic model was tested for 2011 Thailand large flood. As a result, simulated peak inflow is 3410 m^3 s^{-1}, which error is 57 m^3 s^{-1} (1.7%), and peak timing is same as observation. The Nash-Sutcliffe coefficient for daily inflow is 0.79. Those result could conclude our model has enough ability to reproduce flood discharge.

C. Generating Atmospheric Data

In this study, JRA-55 atmospheric reanalysis data [5] and CHIRPS (Climate Hazards Group InfraRed Precipitation with Station data) [6] rainfall data are utilized for implementing a distributed hydrologic model. Yorozu et al. [4] checked whether monthly atmospheric data have auto-correlation with one-month time-lag on upper part of Bhumibol dam catchment. Through their analysis, they concluded atmospheric data between August and September could be assumed to be not related. Then, numerous atmospheric data ware generated by recombining atmospheric data between August and September.

D. Simulation

Following previous study [4], two kinds of simulations were carried out in this study. One of the simulations is done by actual time series of atmospheric data. Another is done by recombined atmospheric data. Hereafter, the former one is called as CONT simulation and the latter one is called as RECOM simulation.

In previous study, monthly precipitation amount by JRA-55 was corrected by that by CHIRPS. In this study, daily precipitation amount by JRA-55 was corrected for more precise analysis. The CONT simulation covers from 1983 to 2016, total 34 years. According to the previous study, time series of atmospheric data was recombined between August and September. For example, atmospheric data from January to August in 1983 was combined with atmospheric data from September to December in 1985. This means that the combination of data from January to August is 34 years and the combination of data from September to December is also 34 years. Then, the RECOM simulation consists of 1156 years which means 34 years multiplied by 34 years. While the RECOM simulation actually includes the CONT simulation, all the simulation data is analyzed as it is because this paper doesn't focus on comparison of them.

Each 1156 years result in RECOM simulation can be divided two groups. One is different atmospheric data after September is used but same atmospheric data before August. Another one is vice versa. The first group is expected to show the impact of rainfall pattern on discharge because there is same soil moisture at the end of August but different rainfall pattern after September. The second group is the result by using different atmospheric data before August is used but same atmospheric data after September. This group is expected to show the impact of soil moisture before flood event on discharge because there is different soil moisture at the end of August but same rainfall pattern after September which usually causes flood in upper part of Bhumibol dam catchment.

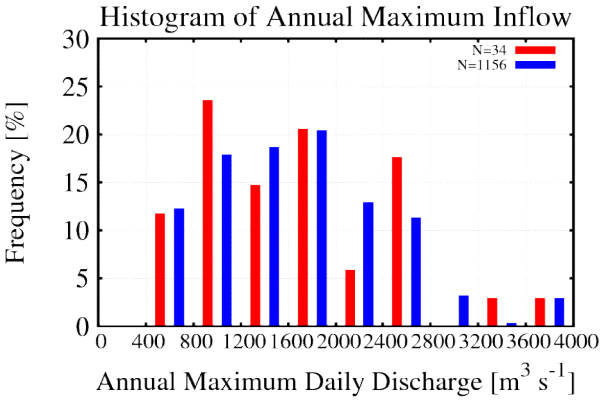

Fig. 1. Histogram of annual maximum inflow estimated by CONT simulation (red) and RECOM simulation (blue).

Results

A. Annual Maximum Daily Discharge

A distributed hydrologic model carried out for 34 years in case of CONT simulation which uses actual time series of atmospheric data and for 1156 years in case of RECOM simulation which uses recombined atmospheric data. Therefore, 34 of annual maximum daily discharge can be derived from the result of CONT simulation and 1156 of that from RECOM simulation.

The histogram of annual maximum daily discharge for both simulations is shown in Fig. 1. In that figure, red bar shows the histogram by CONT simulation and blue bar shows that by RECOM simulation. It can be seen that both histograms look similar. Two sample Kolmogorov-Smirnov test, generally utilized, was implemented for identifying the difference of those distributions. As a result, null hypothesis, which is that populations of both data follow different distributions, was rejected with 10% significant level. It concluded that the difference between the distribution of annual maximum daily discharge for CONT simulation and that by RECOM simulation is not detected. It is assumed that the annual maximum daily discharge by RECOM simulation is reasonable.

Then, let's focusing on maximum value of annual maximum daily discharge in each simulation. In CONT simulation, maximum value is 3676 m^3 s^{-1}. However, maximum value in RECOM simulation is 4002 m^3 s^{-1}. This difference may be caused by the difference of soil moisture at the end of August.

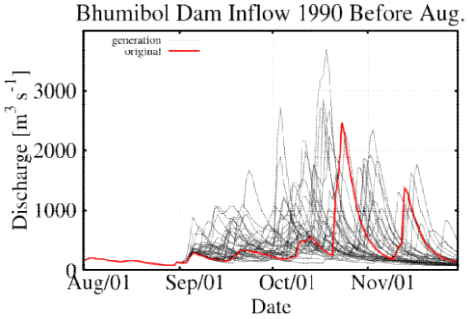

Fig. 2. Hydrographs for Bhumibol dam inflow by CONT simulation in 1990 (red) and RECOM simulation in which atmospheric data in 1990 is used from January to August (grey).

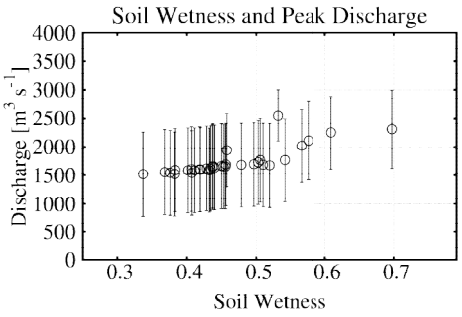

Fig. 3. Averaged annual maximum daily discharge (circle) and standard deviation (bar) by RECOM simulation in which same atmospheric data is used from January to August. Horizontal axis is catchment averaged soil moisture at the end of August.

B. Effect of Rainfall Pattern

It is possible to investigate the effect of rainfall pattern on discharge analyzing result which was used different atmospheric data after September and same atmospheric data before August. Because there is same soil moisture at the end of August but different rainfall pattern after September. Fig. 2 shows hydrographs in which atmospheric data in 1990 is used from January to August because this case shows highest variation of annual maximum river discharge. From that figure, it can be seen that there is no different time series of discharge until the end of August because atmospheric data is same and different

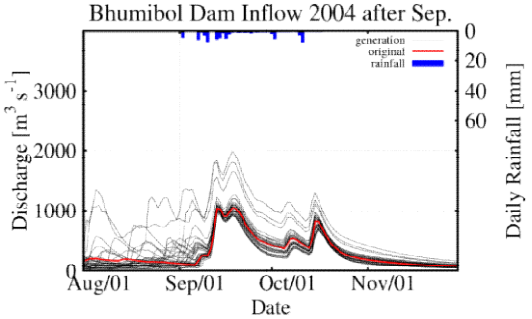

Fig. 4. Hydrographs for Bhumibol dam inflow by CONT simulation in 2004 (red) and RECOM simulation in which atmospheric data in 2004 is used from September to December (grey). The blue bar is hyetograph in 2004.

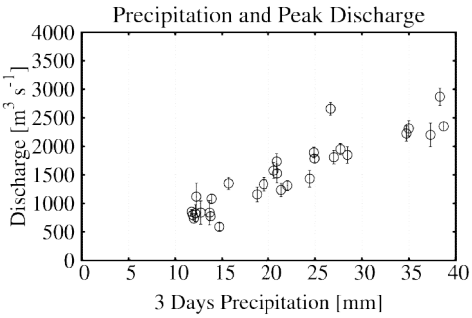

Fig. 5. Averaged annual maximum daily discharge (circle) and standard deviation (bar) by RECOM simulation in which same atmospheric data is used from September to December. Horizontal axis is catchment averaged three days rainfall after September.

pattern after September because atmospheric data is different among simulations.

Annual maximum daily discharge is 2467 m^3 s^{-1} by CONT simulation. On the other hand, in RECOM simulation maximum value of annual maximum daily discharge is 3696 m^3 s^{-1}, minimum value is 623 m^3 s^{-1}, average value is 1662 m^3 s^{-1} and standard deviation is 743 m^3 s^{-1}. This result shows that simulated peak discharge could vary about 45%, maximum case is 5.9-fold, if there is difference of rainfall pattern.

Fig. 3 shows the relationship between soil moisture and annual maximum daily discharge. In that figure, for RECOM simulation in which same

atmospheric data is used from January to August, averaged annual maximum daily discharge is shown as circle and standard deviation is shown by bar. From that figure, it can be seen that positive relation between soil moisture at the end of August and averaged annual maximum daily discharge. The standard deviation, which is indicated by bar in that figure, could be assumed to show the effect of rainfall pattern on discharge estimation. From the result, it is calculated by 718 m^3 s^{-1}

C. Effect of Initial Soil Moisture

It is possible to investigate the effect of soil moisture before flood event on discharge analyzing result which was used different atmospheric data before August and same atmospheric data after September. Because there is different soil moisture at the end of August but same rainfall pattern after September which usually causes flood in upper part of Bhumibol dam catchment. Fig. 4 shows hydrographs in which atmospheric data in 2004 is used from September to December and hyetograph in 2004 because this case shows highest variation of annual maximum river discharge. From that figure, it can be seen that there is different time series of discharge until early September because atmospheric data is different and similar pattern after rainfall event in early September because atmospheric data is same among simulations.

Annual maximum daily discharge is 1053 m^3 s^{-1} by CONT simulation. On the other hand, in RECOM simulation maximum value of annual maximum daily discharge is 1982 m^3 s^{-1}, minimum value is 931 m^3 s^{-1}, average value is 1117 m^3 s^{-1} and standard deviation is 237 m^3 s^{-1}. This result shows that simulated peak discharge could vary about 21%, maximum case is 2.1-fold, if there is difference of soil moisture at the end of August.

Fig. 5 shows the relationship between maximum three days rainfall after September and annual maximum daily discharge. In that figure, for RECOM simulation in which same atmospheric data is used from September to December, averaged annual maximum daily discharge is shown as circle and standard deviation is shown by bar. From that figure, it can be seen that positive relation between three days rainfall after September and averaged annual maximum daily discharge. The standard deviation could be assumed to show the effect of soil moisture before flood event on discharge estimation. From the result, it is calculated by 127 m^3 s^{-1}which is one third of the effect of rainfall pattern on discharge.

Concluding Summary

Following precious study [4], numerous atmospheric data was generated by recombining atmospheric data and huge amount of pseudo-discharge data was created utilizing a distributed hydrologic model for the upper part of Bhumibol dam catchment. By using generated pseudo-discharge data, the effect of rainfall pattern on discharge and that of initial soil moisture on discharge were analyzed. As a result, the former one is calculated by 718 m^3 s^{-1} and the latter one is calculated by 127 m^3 s^{-1}. From this study, it is seemed that the effect of initial soil moisture on discharge is not negligible.

References

[1] M. G. Grillakis, A. G. Koutroulis, J. Komma, I. K. Tsanisa, W. Wagner, and G. Blöschl, "Initial soil moisture effects on flash flood generation - A comparison between basins of contrasting hydro-climatic conditions," *J. Hydrol.*, vol. 541, pp. 206-217, 2016.

[2] R. Sakazume, M. Ryo, and O. Saavedra, "Consideration of antecedent soil moisture for predicting flood characteristics," *Journal of Japan Society of Civil Engineers, Ser. B1 (Hydraulic Engineering)*, vol.71, pp.I 97–I 102, 2013 (in Japanese).

[3] K. Yorozu, and Y. Tachikawa, "The effect on river discharge estimation by considering an interaction between land surface process and river routing process," *Proc. of the International Association of Hydrological Sciences*, vol.369, pp.81-86, 2015.

[4] K. Yorozu, N. Kurosaki, Y. Ichikawa, S. Kim, and Y. Tachikawa, "A study on long-term river discharge data generation by distributed hydrologic model and recombination atmospheric data," *Journal of Japan Society of Civil Engineers, Ser. B1 (Hydraulic Engineering)*, vol.74, pp.I_127-I_132, 2018 (in Japanese).

[5] S. Kobayashi, Y. Ota, Y. Harada, A. Ebita, M. Moriya, H. Onoda, K. Onogi, H. Kamahori, C. Kobayashi, H. Endo, K. Miyaoka, and K. Takahashi, "The JRA-55 Reanalysis: General specifications and basic characteristics," *J. Meteor. Soc. Japan*, vol. 93, pp. 5-48, 2015.

[6] C. Funk, P. Peterson, M. Landsfeld, D. Pedreros, J. Verdin, S. Shukla, G. Husak, J. Rowland, L. Harrison, A. Hoell, and J. Michaelsen, "The climate hazards infrared precipitation with stations—a new environmental record for monitoring extremes," *Scientific Data*, vol. 2, 150066, 2015.

Overview of Dynamical Downscaling of Climate Simulations over Southeast Asia in MRI

Hidetaka Sasaki[1], Toshiyuki Nakaegawa[2], Sujittra Ratjiranukool[3], Patama Singhruck[4], Waranyu Wongseree[5], Faye Cruz[6], Ngai Sheau Tieh[7] and Truong Ba Kien[8]

Abstract Several researchers are invited to MRI in order to conduct collaborative researches between the institutes in Southeast Asia and MRI every year. The experiments of dynamical down scaling have been conducted by using the Non-hydrostatic Regional Climate Model (NHRCM) in each country. NHRCM is derived from the non-hydrostatic model used operationally for weather forecasting by the Japan Meteorological Agency. NHRCM has high performance for reproducing the Japanese climate and the calculation results are used for many official reports published by Japanese Ministries. However, the reproducibility of the NHRCM varies from country to country. In this study, NHRCM is used to dynamically downscale climate projections from the 20 km resolution MRI Atmospheric General Circulation Model (MRI-AGCM3.2) over Southeast Asia at very high resolution (from 2 to 5km) for the present climate (1981-2000) and far-future climate (2080-2099) under the RCP 8.5 scenario.

Keywords *regional climate model*

[1]Atmospheric Environment & Applied Meteorology Research Department
MRI
Tsukuba, Japan
[2]Climate Research Department
MRI
Tsukuba, Japan
[3]Department of Physics and Material Science,
Faculty of Science
ChiangmaiUniversity
Chiangmai, Thailand
[4]Department of Marine Science, Faculty of Science
Chulalongkorn University
Bangkok, Thailand
[5]Department of Electrical and Computer Engineering, Faculty of Engineering
King Mongkut's University of Technology North Bangkok
Bangkok, Thailand
[6]Manila Observatory
Ateneo de Manila University
Quezon, Philippines
[7]Climate and Ocean Analysis Laboratory, Faculty of Science and Technology
UniversitiKebangsaan Malaysia
Selangor, Malaysia
[8]Tropical Meteorology and Storm Division
Vietnam Institute of Meteorology, Hydrology and Climate change
Hanoi, Vietnam

Introduction

Non-hydrostatic Regional Climate Model (NHRCM) was developed by Sasaki, H., K. Kurihara, I. Takayabu and T. Uchiyama [1] based on NHM which had been used for weather forecast operationally in Japan. Sasaki, H., A. Murata, M. Hanafusa, M. Oh'izumi, and K. Kurihara [2] showed that NHRCM had high performance for reproducing the present climate and has been used by government services for assessing the impact due to global warming in Japan. NHRCM has been also applying to other regions (e.g., Kieu-Thi, X., H. VU-Thanh, T. Nguyen-Minh, D. Le, L. Nguyen-Minh, I. Takayabu, H.Sasaki, and A. Kitoh [3], Cruz, F. T., H. Sasaki, and G. T. Narisma [4], and Cruz, F. T, and H. Sasaki [5]). The reproducibility varies from region to region. Meteorological Research Institute (MRI) has invited many researchers from all over the world, especially from Southeast Asian countries to conduct collaborative research for reproducing the present climate and projecting the future one around their countries.

Reproducibility in present climate

NHRCM simulations have been done over a domain (321x411 grid points) with a grid spacing of 5 km (NHRCM05) which covered Thailand. Boundary conditions for NHRCM05 were derived from MRI-AGCM with 20-km horizontal resolution. Time-slice simulation for baseline and future period is from 1980 to 2000 and from 2079 to 2099, respectively. Parameterization schemes, for example, the Kain-Fritsch scheme for cumulus convection (Kain, J.S., and J.M. Fritsch [6]) and Mellor-Yamada for turbulence closure models (Mellor, G. L., and T. Yamada [7]), were applied in NHRCM05 simulation.

The climatological simulated precipitations were compared to gridded observation, APHRODITE with 0.25° resolution and 11 stations from Thai Meteorological Department (TMD). Figure 1. shows seasonal change of precipitation from TMD, APHRODITE, NHRCM05. NHRCM05 generally underestimates precipitation all month in the northern

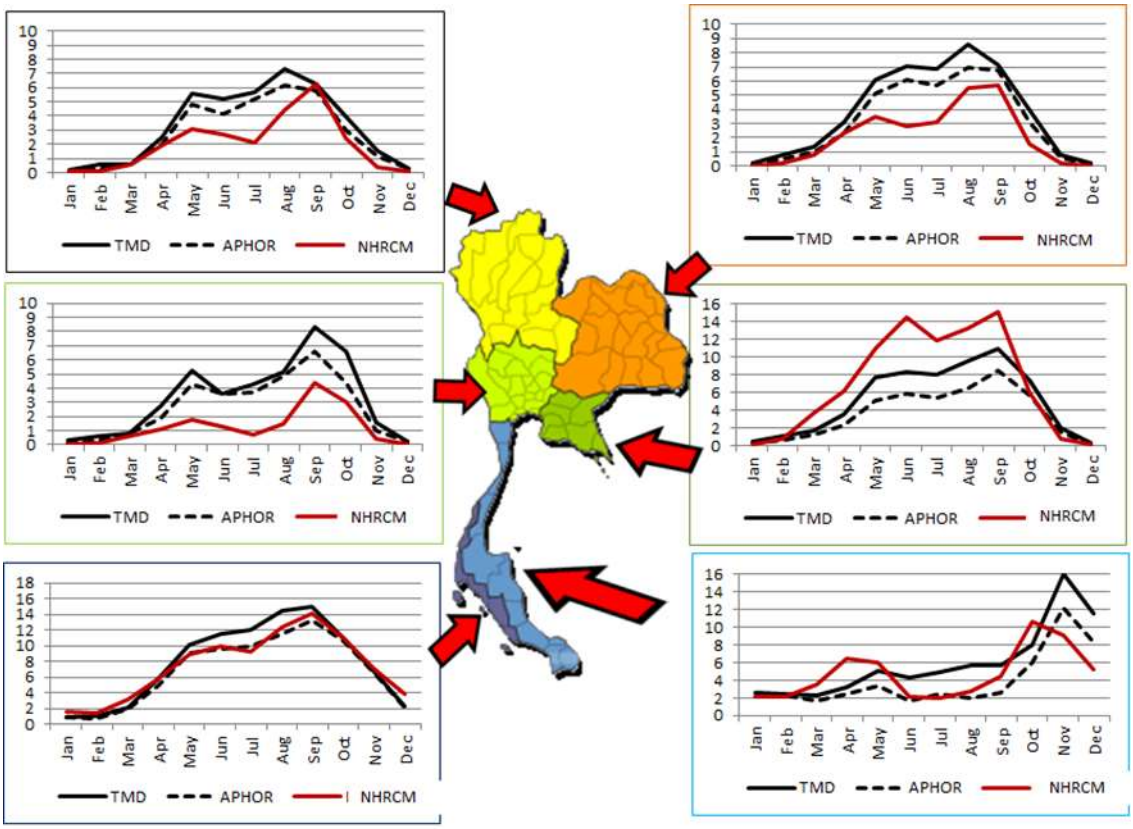

Fig. 1 Seasonal change of precipitation in Thailand. Black solid line, black broken line and red line indicate TMD, APHRODITE, NHRCM05, respectively.

part of Thailand. The precipitation amount in NHRCM05 is rather underestimated in western region and overestimated in eastern region in central part of Thailand. NHRCM05 well reproduced over southern Thailand west coast. The phase of rainfall peak is somewhat shifted over southern Thailand east coast.

Coordinated Reginal Climate Downscaling Experiment in Southeast Asia (CORDEX-SEA) designated 5 valuable areas in Southeast Asia region. Mekong river basin is designated as valuable area in Thailand. Future climate change projection was conducted by using 2km grid spacing NHRCM in that area. Figure 2 shows the seasonal change of precipitation averaged over calculation domain in NHRCM and APHRODITE. NHRCM02 is somewhat underestimated in rainy season. Its amount is about from 70% to 80% of APHRODITE. On the other hand, NHRCM02 overestimates the precipitation in dry season. The precipitation amount about twice in December. However, the absolute value of the difference is small. The NHRCM02 almost well reproduce the seasonal change of precipitation amount.

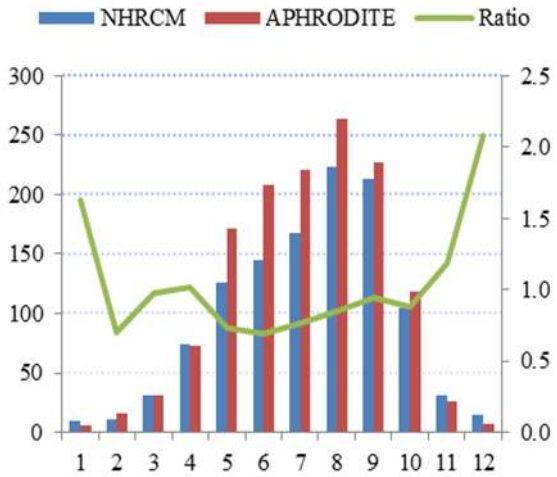

Fig. 2 Seasonal change of precipitation in Mekong river basin. Blue and red bars indicate NHRCM02 and APHRODITE, respectively.

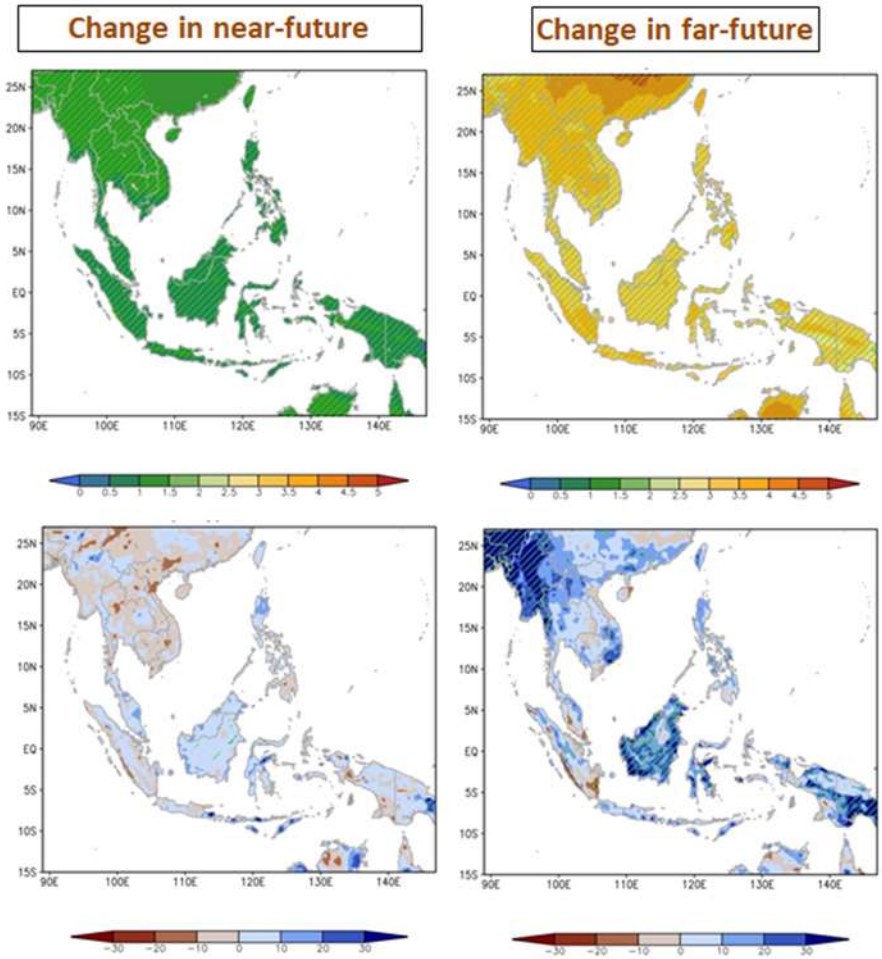

Fig. 3 Temperature (upper panels) and precipitation (lower panels) change in near (left panels) and far future (right panels). Hatched areas show the significant levels are 99% or higher in temperature and 95% or higher in precipitation.

Future projection of climate change

A. Southeast Asia

Future climate projections for Southeast Asian region at 25 km resolution were generated using NHRCM to dynamically downscale the climate projections from the 60 km resolution MRI Atmospheric General Circulation Model (MRI-AGCM3.2). Twenty-year simulations have been done for the present climate (1981-2000), and for the far-future climate (2080-2099). For the future climate, the four Representative Concentration Pathways (RCP) scenarios (RCP 2.6, RCP 4.5, RCP 6.0 and RCP 8.5) have been considered to provide a range of possible values of future changes. A simulation was also performed for the near-future (2020-2039) under the RCP 8.5 scenario.

Figure 3 shows distribution map of temperature and precipitation change in near and far future. Under the RCP 8.5 scenario, the projected warming is significantly up to about 1.5 °C in the near-future and 4 °C in the far-future over the region. Precipitation is projected to increase less than 10% in most of the area but not significant in near future. On the other hand, NHRCM projected that precipitation increases significantly in many areas in far future.

B. Vietnam

The calculation domain has 301 × 461 grids covering the area from 7.0°N to 25.5°N, 97.8°E to 112.0°E with the 5 km resolution. The NHRCM was carried out the simulation for the baseline period of 1981- 2000 and far future period of 2079-2099 with MRI-AGCM20/RCP8.5 driven data.

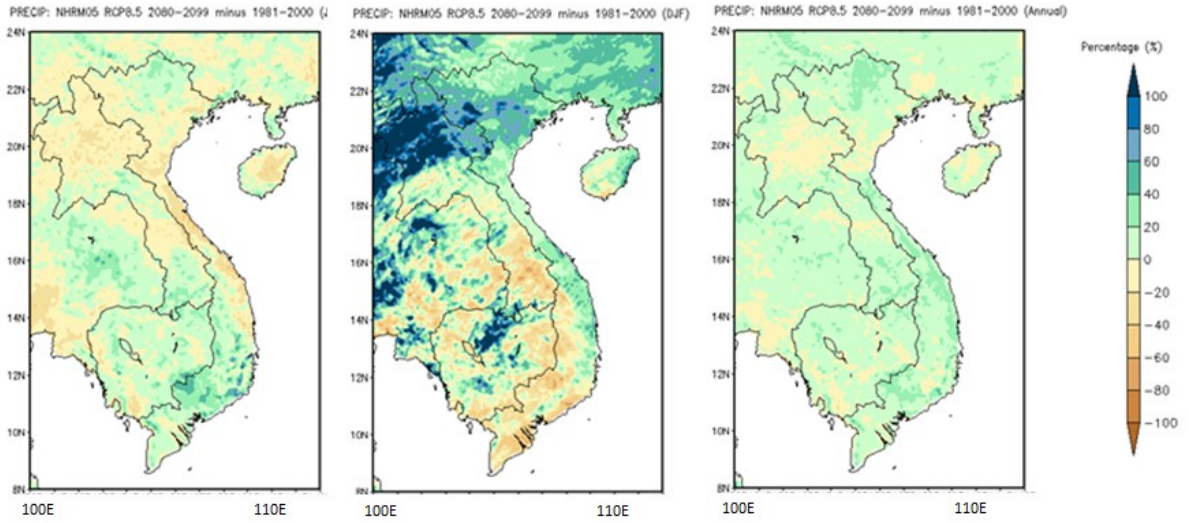

Fig. 4 The difference of precipitation amount between future (2080-2099) and baseline (1981-2000) in summer (left), winter (center) and annual (right) over Vietnam with RCP8.5 scenario.

Table 1 List of climate change scenario made by NHRCM around Southeast Asia

Country	Grid spacing	Domain	Scenario	Depository
Thailand	5km	Thailand	P and RCP 8.5	MRI
	2km	Mekong River	P and RCP 8.5	MRI
	2km	Nan and Yom River	P and RCP 8.5	MRI
Indonesia	5km	Batang Hari River	P	MRI
Philippines	25km	SE Asia	P + perfect boundary	Manila Obs.
			RCP 2.6, 4.5, 6.0, 8.5	
	5km	Philippines	P and RCP 8.5	Manila Obs.
	5km	Philippines	P and RCP 8.5	calculating
	2km	Mindanao	P and RCP 8.5	calculating
Vietnam	20km	Vietnam	P and RCP 8.5	Hanoi Univ.
	5km	Vietnam	P	closed
	5km	Vietnam	P and RCP8.5	MRI
Malaysia	5km	Malaysia	P and RCP8.5	MRI
			P:present	

Figure 4 shows precipitation increases slightly over most of Vietnam in the annual mean, except in North Central, few parts of Central Highlands where the variations are small, or even show minor decreases. The summer precipitation is projected to decreases in the Central region of Vietnam on the lee side of the mountains, with the southwest flow (summer monsoon). However, the projected precipitation is increased in the Northern mountain, Central Highlands and. Finally, the winter rainfall tends to decrease in the Northern, Central region of Vietnam on the lee side of the mountains, with the northeast flow (winter monsoon).

Concluding Summary

Many researchers have been invited to MRI from all over the world especially from Southeast Asia to project future climate change due to global warming by using NHRCM. They have made many climate change scenarios by using various kind of grid spacing NHRCM over various region in Southeast Asia by using several kinds of RCP scenario. Table 1 is a list of climate change scenario made by NHRCM. It is desirable that the data sets are widely used for impact assessment research and adaptation measures.

Acknowledgment

This work was conducted under the TOUGOU Program of the Ministry of Education, Culture,Sports, Science and Technology (MEXT) of Japan.

References

[1] Sasaki, H., K. Kurihara, I. Takayabu and T. Uchiyama, 2008: Preliminary experiments of reproducing the present climate using the non-hydrostatic regional climate model, SOLA, 4, 25-28, doi: 10.2151/sola.2008-007.

[2] Sasaki, H., A. Murata, M. Hanafusa, M. Oh'izumi, and K. Kurihara, 2011: Reproducibility of present climate in a non-hydrostatic regional climate model nested within an atmosphere general circulation model. SOLA, 7, 173-176, doi: 10.2151/sola.2011-044.

[3] Kieu-Thi, X., H. VU-Thanh, T. Nguyen-Minh, D. Le, L. Nguyen-Minh, I. Takayabu, H.Sasaki, and A. Kitoh, 2016: Rainfall and Tropical Cyclone Activity over Vietnam Simulated and Projected by the Non-Hydrostatic Regional Climate Moel - NHRCM. Journal of the Meteorological Society of Japan, 94A, 135-150.

[4] Cruz, F. T., H. Sasaki, and G. T. Narisma, 2016: Assessing the sensitivity of the Non-hydrostatic Regional Climate Model to Boundary Conditions and Convective Schemes over the Philippines. Journal of the Meteorological Society of Japan, 94, 165-179.

[5] Cruz, F. T, and H. Sasaki, 2017: Simulation of present climate over Southeast Asia using the Non-Hydrostatic Regional Climate Model. SOLA, 13, 13-18.

[6] Kain, J.S., and J.M. Fritsch, 1990: A One-Dimensiona lEntraining/Detraining Plume Model and Its Application in Convective Parameterization. J. Atmos. Sci., 47, 2784–2802

[7] Mellor, G. L., and T. Yamada, 1974: A Hierarchy of Turbulence Closure Models for Planetary Boundary Layers. J. Atmos. Sci., 31, 1791–1806.

Calibration, Validation and Uncertainty Analysis of SWAT Model for predicting reservoir inflow in Umiam Watershed, Meghalaya

Jeffrey Denzil K. Marak[1], Arup Kumar Sarma[1] and Rajib Kumar Bhattacharjya[1]

Abstract The prediction of inflow to a reservoir is of utmost importance for the optimal operation of the reservoir. Umiam watershed is of great significance to the Meghalaya State of India as it serves five major reservoirs for generation of hydropower. The objective of this study is to calibrate and validate the Soil and Water Assessment Tool (SWAT) model for Umiam watershed in Meghalaya, India for predicting reservoir inflow and to quantify the uncertainties. The SWAT model was configured for Umiam basin and the calibration, validation and uncertainty analysis of the model was carried out using SUFI-2 algorithm. The model was calibrated using the reservoir inflow data obtained from mass balance calculation for the period 1979 – 1995 and validated for the period 1996-2000 on monthly basis. The sensitivity analysis shows that the parameters such as Curve Number, Groundwater Delay Time, Groundwater Revap Coefficient, Saturated hydraulic conductivity, Baseflow Alpha Factor, HRU Slope, Soil Evaporation Compensation Factor, Available water capacity of the soil are very sensitive ($p < 0.05$). The streamflow simulated by the model showed a good correlation with the observed data with R2 values of 0.96 and 0.86 for calibration and validation periods respectively. From this study, it can be concluded that SWAT model can be used to predict reservoir inflow in Umiam Watershed.

Keywords *Sensitivity, Uncertainty, SWAT-CUP*

[1]Department of Civil Engineering
Indian Institute of Technology
Guwahati, India
jeffreymarak@iitg.ac.in

Introduction

Hydrologic models serves as an important tool for quantifying inflows to reservoirs and thus help in planning and management of water-use in a catchment [1], [2]. However, natural processes are difficult to predict using simple mathematical equations and thus, there is always some uncertainty associated with hydrological models [3]. Before a hydrological model is considered satisfactory for decision-making process, its uncertainties emerging from model structure, parameters and input data, needs to be analysed and quantified [4].

SWAT is amongst the most widely used public domain hydrologic models for watershed scale studies and has been applied world wide [5]–[7]. K. C. Abbaspour et al., (2015) applied SWAT model on a continental scale for Europe to study hydrology and water quality. SWAT was used by Gosain et al. (2006) for studying impact of climate change in 12 major river basins in India. On a smaller scale, Pandey et al., (2017) employed SWAT model for Armur watershed in Godavari river basin, India, which had an area of 20,319 hectares. SWAT model has large number of parameters which makes manual calibration of parameters in SWAT model a tidious task. Therefore, SWAT-CUP (Calibration and Uncertainty Program) was ensued to facilitate automatic calibration of SWAT parameters and carry out uncertainty analysis [10].

Umiam Stage 1 reservoir in Meghalaya serves five cascading hydropower stations in the area. Thus, it is important to have a hydrologic model that is capable of simulating its inflow. The calibrated model can be used to predict reservoir inflow taking into account changes in climatic conditions and will help the authorities in management of reservoir water. In this study, we use SUFI-2 (Sequential Uncertainty Fitting) algorithm in SWAT-CUP to evaluate the applicability of SWAT model in Umiam Watershed and to analyse the uncertainties.

Study Area

The Umiam River flows from Sawlad village, south of Shillong and flows through Shillong City till it reaches Umiam Stage 1 reservoir. The watershed area is located between the longitudes 91.67 and 91.95 and latitudes 25.45 to 25.67, at a distance of 15 km to the North of Shillong. The watershed has an area of

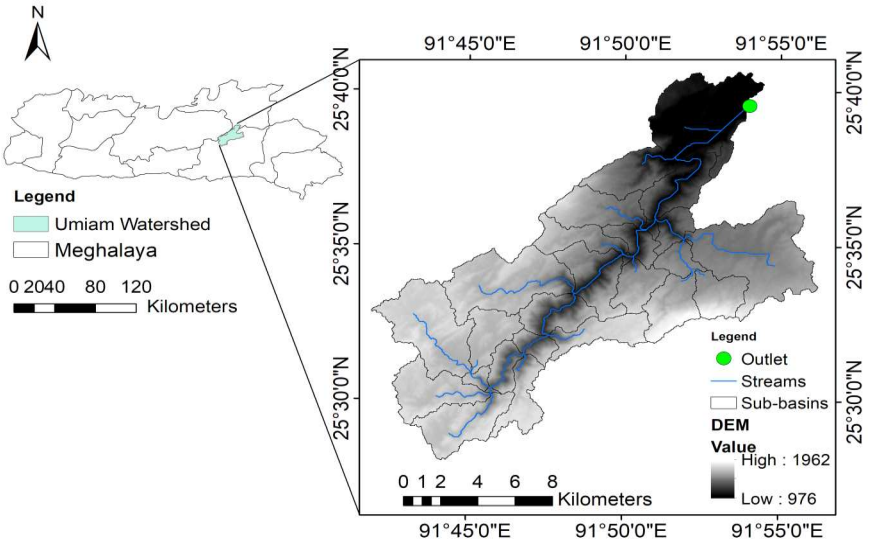

Fig. 1 Map showing Umiam Watershed and its topographic features

218.4 Km^2. Elevation ranges from 1962 m in the upstream region to 976 m near the reservoir.

The area experiences heavy rains during monsoon and cold winters. The minimum temperatures ranges from 13.95°C to 16.70°C in winter and maximum temperature varies from 22.08°C to 26.47°C in summer. The watershed receives annual average rainfall of 3385 mm.

Data

SWAT requires topographic, pedologic, landuse and land cover, and meteorological data for model building and simulations. In this study, the SRTM DEM of 30 m is used for watershed delineation and creating reaches in ArcSWAT interface. The soil map was extracted from Harmonized World Soil Database (HWSD), as defined in FAO-UNESCO Soil Map of the World. Land use and land cover (LULC) data of 500 m resolution was obtained from USGS Land Cover Institute website [11]. The daily precipitation and temperature data are derived from gridded dataset prepared by Indian Meteorological Department (IMD). The data for otherparameters like humidity, solar radiation and wind are simulated using the inbuilt weather generator in SWAT due to unavailability of data. The monthly inflow data of Umiam Stage 1 reservoir were collected from Meghalaya Power Generation Corporation Limited (MePGCL), Shillong.

Methodology

A. Watershed configuration

Watershed delineation is done using automatic watershed delineator in ArcSWAT. 31 sub-basins are formed after delineation. Next input is soil and vegetation cover information which is crucial in the water movement process and forms an important input for hydrologic simulation [16], [17]. We reclassified LULC raster into 9 classes according to SWAT LULC code. There are two soil types in the study area according to FAO data i.e. Ao74-2b-3646 and Ao75-2b-3647,both belonging to dominant

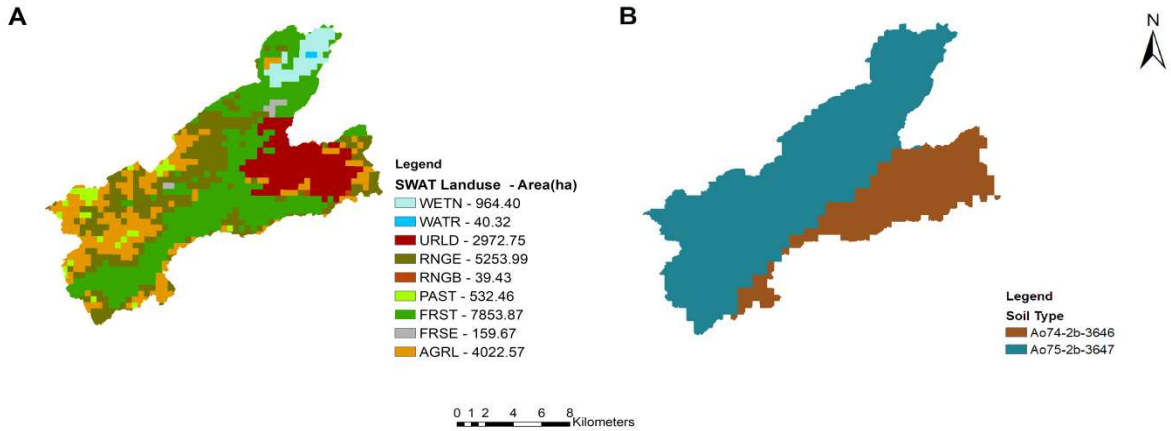

Fig. 2. Land Use and Land Cover Map (A) and Soil Map (B) of Umiam Watershed

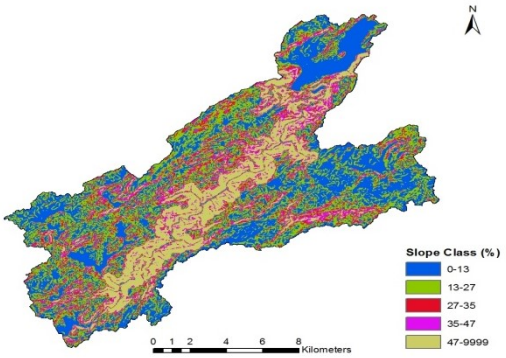

Fig. 3. Slope Map of Umiam Watershed

soil group called OrthicAcrisols. Five slope classes are defined based on slope map of the area (Fig. 3). Based on the LULC, soil and slope combinations, 258 Hydrologic Response Units (HRU) are formed.

B. Sensitivity Analysis

SWAT model simulates complex hydrological processes and therefore has over 200 hydrological parameters. A sensitivity analysis is carried out to distinguish the most sensitive parameters that influence the model output in the study area. Based on the sensitivity analysis, we can reduce the number of parameters to be used for calibration by eliminating the less sensitive parameters [18]. The sensitive parameters represent the most important processes in the study area. Arnold et al., (2012) categorized the parameters from 64 studies based on the processes they represent. In this study, we select 15 parameters based on literature for sensitivity analysis which influence hydrology and streamflow. Sensitivity analysis was done using all at a time sensitivity method.

C. Model Calibration, Validation and Uncertainty Analysis

The model calibration, validation, and uncertainty analysis are done using SUFI-2[12] algorithm in SWAT-CUP program [13]. In the SUFI-2 algorithm, all the uncertainties associated with the model such as parameter, conceptual, model and input uncertainty are accounted by parameter ranges. The parameters are sampled using the Latin Hypercube sampling method and uncertainties are propagated and reflected in the 95 percent prediction uncertainty (95PPU) band of SUFI-2 output. Initially, SUFI-2 assumes a wider range of 95PPU to include observed data under that range. This bracketing of observed data by 95PPU is measured by an index called p-factor which ranges from 0 to 1 (where 1 signifies complete bracketing of observed data within 95PPU region). The SUFI-2 algorithm gradually reduces the uncertainty range to acceptable range called r-factor. Smaller r-factor indicates better calibration performance. The iteration is continued until the 2.5th percentile and 97th percentile brackets most of the observed data under a specified objective function, which is R2 in this case.

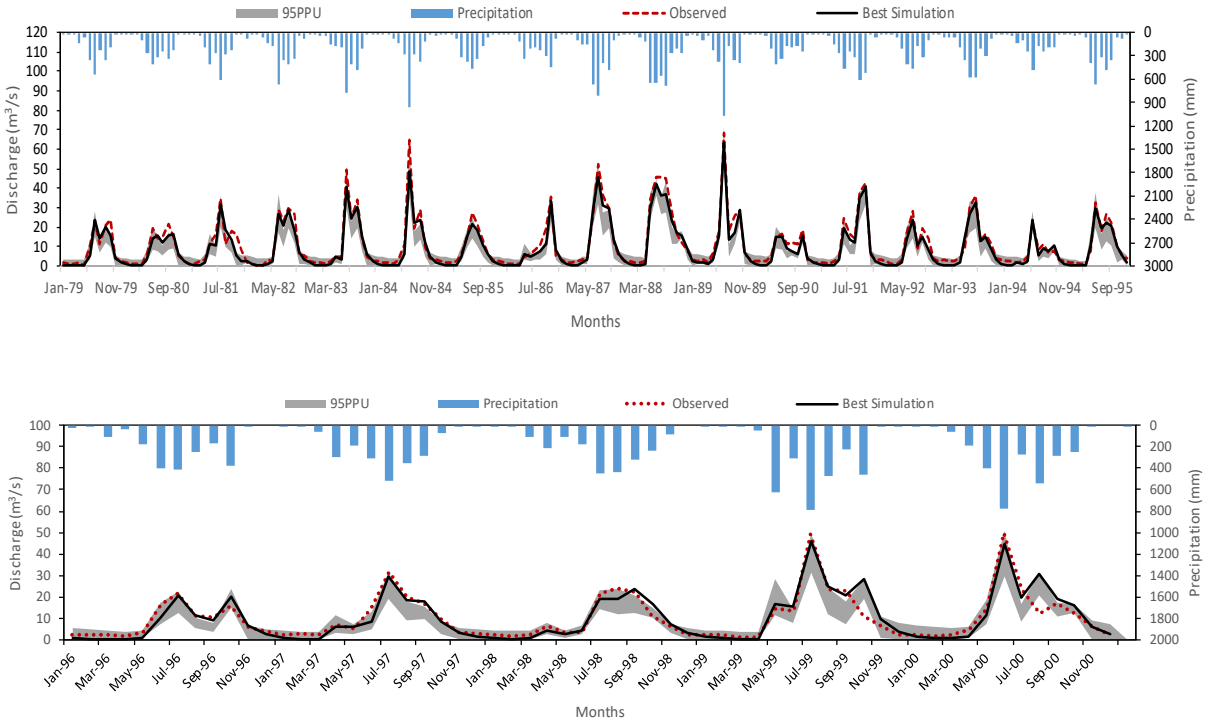

Fig. 4. 95PPU (shaded region) from SUFI-2 output. Calibration period at the top and validation period at the bottom.

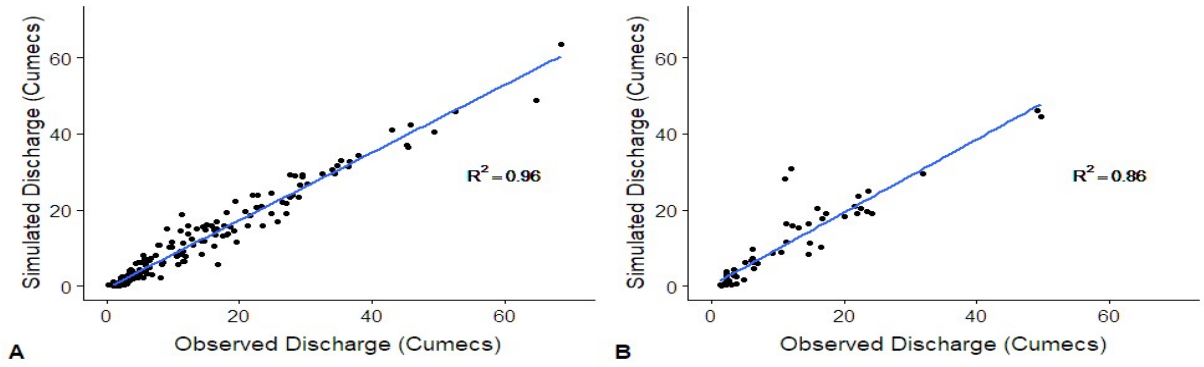

Fig. 5. Scatter plot of Observed vs. Simulated flow during Calibration (A) and Validation (B)

The SWAT model is run for 22 years, from 1974 to 1995. A warm-up period of 5 years is used thus, the effective period of simulation started in 1979. Validation is done for the period 1996 to 2000 using monthly observed flow data. For each iteration, 500 simulations are carried out and after each iteration, parameter values are replaced by new values suggested by SWAT-CUP. A total of 4 iterations lead to satisfactory model performance and no further improvement was observed in the objective function i.e. R^2

Results and Discussion

A. Sensitivity Analysis

The sensitivity of parameters is determined based on p-value and t-statistic given by global sensitivity test in SWAT-CUP. The sensitivity analysis revealed that the most sensitive parameters are CN2, GW_Delay, GW_Revap, SOL_K, ALPHA_BF, HRU_SLP, ESCO and SOL_AWC. These parameters can be said to represent the rainfall-runoff process in the watershed. Most of the sensitive parameters mentioned above are found to be sensitive in several other studies [14]–[17].

B. Calibration and Validation

The model is calibrated using monthly flow data for 17 years (1979-1995) and validated for 5 years (1996-2000) (Fig. 4). The calibrated parameter ranges are shown in Table 1. The prefix R and V before the parameter names in Table 1 signifies relative change and replacement methods of altering the parameter values respectively [13]. The model shows very good performance in the calibration period, with slight under-prediction. From Fig. 4, it can be observed that most of the peak flows are underpredicted by SWAT. Large uncertainty can be seen in the baseflow region. The reason for inefficient baseflow simulation may be due to the inability of SWAT to accurately simulate groundwater flow [18]. The p-factor value (0.81) and r-factor (0.5) are under

Table 1 Calibrated Parameter ranges

Sl. No	Parameter	Description of Parameter	Lower and Upper Bounds	Fitted Value	Sensitivity Rank
1.	R__CN2.mgt	SCS runoff curve number	-0.20 to 0.20	0.034	1
2.	V__GWQMN.gw	Threshold depth of water in the shallow aquifer required for return flow to occur (mm)	0 to 25	21.37	15
3.	V__GW_REVAP.gw	Groundwater "revap" coefficient	0.02 to 0.2	0.073	3
4.	V__REVAPMN.gw	Threshold depth of water in the shallow aquifer for "revap" to occur (mm)	0 to 10	9.79	12
5.	V__ESCO.hru	Soil evaporation compensation factor	0.8 to 1	0.85	7
6.	V__EPCO.hru	Plant uptake compensation factor	0.8 to 1	0.87	10
7.	R__OV_N.hru	Manning's "n" value for overland flow	-0.2 to 0.2	0.066	14
8.	V__ALPHA_BF.gw	Baseflow alpha factor (days)	0 to 1	0.725	5
9.	V__GW_DELAY.gw	Groundwater delay (days)	30 to 450	40	2
10.	R__SOL_AWC(..).sol	Available water capacity of the soil layer (mm H2O /mm soil)	0.2 to 0.4	0.08	8
11.	R__SURLAG.bsn	Surface runoff lag time (days)	-0.3 to 0.2	0.12	11
12.	R__RCHRG_DP.gw	Deep aquifer percolation fraction	-0.2 to 0.2	0.14	13
13.	R__CH_K2.rte	Effective hydraulic conductivity in main channel alluvium (mm/hr)	-0.2 to 0.2	0.19	9
14.	R__SOL_K(..).sol	Saturated hydraulic conductivity (mm/h)	-0.8 to 0.8	0.136	4
15.	R__HRU_SLP.hru	Average slope steepness (m/m)	0 to 0.2	0.089	6

acceptable range recommended by K C Abbaspour et al., (2015b). The highest observed average monthly inflow during the calibration period was in July 1989 (68.41 cumecs) followed by July 1984 (64.77 cumecs). The corresponding flows simulated by SWAT were 63.59 cumecs and 48.71 cumecs respectively.

The model set up after a calibration process, needs to be evaluated by a validation process in order to test the performance of the model to a different input dataset. The calibrated model with optimum parameter values is validated for the period 1996 – 2000. During the validation period, the R2 and NSE were slightly lower than in the calibration period, whereas, p-factor and r factor increased to 0.88 and 0.66 respectively. In the validation period, highest inflow occurred in July 2000 (49.58 cumecs) against SWAT simulated flow of 44.55 cumecs. The performance statistics of the model is given in Table 2.

Table 2 Model performance

Performance Index	Calibration	Validation
R^2	0.96	0.86
NSE	0.94	0.85
PBIAS	15	1.6
p-factor	0.81	0.88
r-factor	0.50	0.66

Conclusions

The SWAT model was successfully calibrated and validated for Umiam watershed. The sensitivity and uncertainty analysis was also carried out for Umiam watershed using SUFI-2 scheme in SWAT-CUP. The sensitivity analysis was done for the 15 hydrological parameters, out of which the most sensitive parameters are CN2, GW_DELAY, GW_REVAP, SOL_K, REVAPMN, ALPHA_BF, HRU_SLP, ESCO, and SOL_AWC. The observed and simulated discharge shows good conformity during the calibration and validation periods. This shows that the parameters used in the simulations are able to mimic the hydrological processes taking place in the Umiam watershed. SWAT could simulate peak flows very well in the Umiam watershed while it has some limitations in simulating baseflows accurately. The model showed promising results in this study indicating that SWAT model and SWAT-CUP can be used to predict reservoir inflows and climate change study. Future studies may address the effect of landuse and climate change on streamflow in Umiam watershed.

Acknowledgment

We would like to thank the Meghalaya Power Generation Corporation Limited (MePGCL) for providing the hydrological data.

References

[1] R. Quilbé, A. N. Rousseau, J.-S. Moquet, S. Savary, S. Ricard, and M. S. Garbouj, "Hydrological responses of a watershed to historical land use evolution and future land use scenarios under climate change conditions," *Hydrol. Earth Syst. Sci. Discuss.*, vol. 12, pp. 101–110, 2008.

[2] P. Vallam, X. S. Qin, and J. J. Yu, "ScienceDirect Uncertainty Quantification of Hydrologic Model," 2014.

[3] B. Uniyal, M. K. Jha, and A. K. Verma, "Parameter identification and uncertainty analysis for simulating streamflow in a river basin of Eastern India," *Hydrol. Process.*, vol. 29, no. 17, pp. 3744–3766, 2015.

[4] C. Fu, A. L. James, and H. Yao, "Investigations of uncertainty in SWAT hydrologic simulations: A case study of a Canadian Shield catchment," *Hydrol. Process.*, vol. 29, no. 18, pp. 4000–4017, 2015.

[5] Y. Grusson, F. Anctil, S. Sauvage, and J. M. S. Pérez, "Testing the SWAT model with gridded weather data of different spatial resolutions," *Water (Switzerland)*, vol. 9, no. 1, pp. 1–16, 2017.

[6] J. G. Arnold and N. Fohrer, "SWAT2000: Current capabilities and research opportunities in applied watershed modelling," *Hydrol. Process.*, vol. 19, no. 3, pp. 563–572, 2005.

[7] Y. Zhang, J. Xia, T. Liang, and Q. Shao, "Impact of water projects on river flow regimes and water quality in Huai River Basin," *Water Resour. Manag.*, vol. 24, no. 5, pp. 889–908, 2010.

[8] K. C. Abbaspour, E. Rouholahnejad, S. Vaghefi, R. Srinivasan, H. Yang, and B. Kløve, "A continental-scale hydrology and water quality model for Europe: Calibration and uncertainty of a high-resolution large-scale SWAT model," *J. Hydrol.*, vol. 524, pp. 733–752, 2015.

[9] B. K. Pandey, A. K. Gosain, G. Paul, and D. Khare, "Climate change impact assessment on hydrology of a small watershed using semi-distributed model," *Appl. Water Sci.*, vol. 7, no. 4, pp. 2029–2041, 2017.

[10] K. C. Abbaspour, "SWAT - CUP SWAT Calibration and Uncertainty Programs," p. 100, 2015.

[11] P. D. Broxton, X. Zeng, D. Sulla-Menashe, and P. A. Troch, "A global land cover climatology using MODIS data," *J. Appl. Meteorol. Climatol.*, vol. 53, no. 6, pp. 1593–1605, 2014.

[12] K. C. Abbaspour, C. A. Johnson, and M. T. van Genuchten, "Estimating Uncertain Flow and Transport Parameters Using a Sequential Uncertainty Fitting Procedure," *Vadose Zo. J.*, vol. 3, no. 4, p. 1340, 2004.

[13] K. Abbaspour, "SWAT-Calibration and uncertainty programs (CUP)," *Neprashtechnology.Ca*, 2015.
[14] B. a Tolson and C. a Shoemaker, "Watershed Modeling of the Cannonsville Basin using SWAT2000: Model Development , Calibration and Validation for the Prediction of Flow , Sediment and Phosphorus Transport to the Cannonsville Reservoir," *Water Resour.*, no. February, p. 159, 2004.
[15] A. Stehr, P. Debels, F. Romero, and H. Alcayaga, "Hydrological modelling with SWAT under conditions of limited data availability: Evaluation of results from a Chilean case study," *Hydrol. Sci. J.*, vol. 53, no. 3, pp. 588–601, 2008.
[16] J. Schuol, K. C. Abbaspour, R. Srinivasan, and H. Yang, "Estimation of freshwater availability in the West African sub-continent using the SWAT hydrologic model," *J. Hydrol.*, vol. 352, no. 1–2, pp. 30–49, 2008.
[17] K. Smarzy, Ń. S. K. A. Abcdef, and Z. M. Ad, "Calibration and validation of SWAT model for estimating water balance and nitrogen losses in a small agricultural watershed in central Poland," 2016.
[18] R. Rostamian *et al.*, "Application of a SWAT model for estimating runoff and sediment in two mountainous basins in central Iran of a SWAT model for estimating runoff and sediment in two mountainous basins in central Iran Application of a SWAT model for estimating runoff and sediment in two mountainous basins in central Iran," *Hydrol. Sci. Sci. Hydrol.*, vol. 53, no. 5, p. 53, 2008.

A STUDY ON BIAS CORRECTION METHOD FOR RUNOFF GENERATION DATA BASED ON REFERENCE DATA CREATED BY LAND SURFACE MODEL

YUSUKE MIZUSHIMA[1,a], KAZUAKI YOROZU[1,b], YUTAKA ICHIKAWA[1,c] and YASUTO TACHIKAWA[1,d]

Abstract Climate change has a great influence on hydrologiccycle and water resources. General Circulation Model (GCM) is generally used for assessing the impact on natural disasters such as floods and draughts due to climate change. To improve the reliability of future climate prediction by GCM, it is effective to correct the bias of that output. From the viewpoint of water management, bias correction for runoff generation data is required. In this study, bias correction was performed for the MRI-AGCM3.2S 3-hourly runoff generation data from 1982 to 2001, by applying Quantile-Quantile Mapping (QQM) method. The target area was Oyodo river basin in Kyushu Island, Japan. Due to an unavailability of runoff generation observation, land surface model SiBUC was utilized for creating reference runoff generation data by using meteorological data such as APHRO_JP precipitation data and JRA-55 reanalysis data. The effect of the bias correction was evaluated by calculating the river discharge utilizing river routing model, 1K-FRM. As a result, the simulated river discharge using bias-corrected runoff generation data showed an improvement compared with that using the original one. However, it was found thatthe simulated river discharge using bias-corrected runoff was overestimated compared with that using reference data especially on high flood events. Therefore, QQM method was independently applied for high runoff generation data and low data by setting threshold values for reference data and original data, respectively. The overestimation result was improved by this advanced approach.

Keywords *Climate change, Bias correction, Runoff generation data*

[1]Department of Civil and Earth Resources Engineering, Kyoto University
Kyoto, Japan

[a]mizushima.yusuke.88e@st.kyoto-u.ac.jp
[b]yorozu@hywr.kuciv.kyoto-u.ac.jp
[c]ichikawa@hywr.kuciv.kyoto-u.ac.jp
[d]tachikawa@hywr.kuciv.kyoto-u.ac.jp

Introduction

Climate change has a great influence on hydrologic cycle and water resources. General Circulation Model (GCM) is generally used for assessing the impact on natural disasters such as floods and draughts due to climate change.To improve the reliability of future climate prediction by GCM, it is effective to correct the bias of that output.However, compared with bias correction for precipitation and temperature, there are few studies on bias correction related to river discharge.

Bias correction method for the MRI-AGCM3.2S 3-hourly runoff generation data using reference data created by land surface model SiBUC was initially proposed by Duong[1]. Bias correction to runoff generation data showed an improvement in river discharge simulations. However,in bias correction of runoff generation data, Duong pointed out further works needed to be done, for example, considering their temporal distribution pattern.

Based on these backgrounds, the purpose of this study is to revise bias correction method for runoff generation data and simulate river discharge more precisely.In this study, bias correction was performed for the MRI-AGCM3.2S 3-hourly runoff generation by followingDuong's study and the effect of bias correction was evaluated by simulating river discharge utilizing flow routing model 1K-FRM.

Methodology

Observational datasets are needed to apply bias correction method to GCM runoff generation data. However, runoff generation observation cannot be available. Instead,in this study,reference data is created by land surface modeland it is used as pseudo-observation. In addition, the effect of bias correction is not evaluated with runoff itself but with simulated river discharge by corrected runoff. Based on these matters, the flow of this study is shown in Fig. 1.The MRI-AGCM 3.2S 3-hourly runoff generation data is used as GCM runoff generation data. Quantile-Quantile Mapping (QQM) method was selected as the bias correction method by following Duong's study.Then, the river discharges are simulated by using original GCM runoff generation data, reference data from land surface model SiBUC and bias-corrected runoff generation data. Duration curves are drawn by 3

kinds of river discharge.The simulated river discharge using bias-corrected runoff generation data is validated referred to that using reference data.

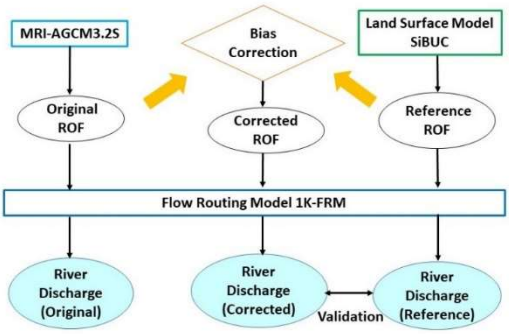

Fig. 1 The flow of this study

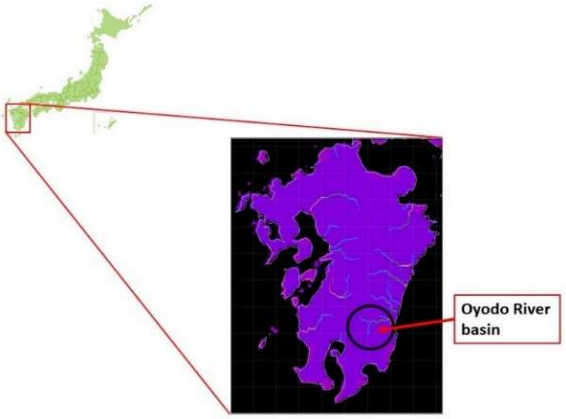

Fig. 2 The study area- Oyodo River basin

Simulation Design

A. Study Area

The target area in this study is Oyodo river basin in Kyushu Island, Japan. Fig. 2 shows the location of Oyodo river basin.Oyodo River is a first-class river flowing from Kagoshima prefecture to Miyazaki prefecture. The total length of Oyodo River is about 107 km and the catchment area is about 2230 km^2.

B. Flow Routing Model 1K-FRM

1K-FRM is a flow routing model based on kinematic wave theory. It was developed by Hydrology and Water Resources Research Laboratory of Kyoto University[2].1K-FRM calculates river discharges with each unit, slope unit and river unit.Different Manning roughness coefficients are set in each unit.The kinematic wave model is applied to all units and runoff is routed according to the flow direction information.The spatial resolution of this model is 30 seconds (1-km).The basic form of the kinematic wave flow equation is:

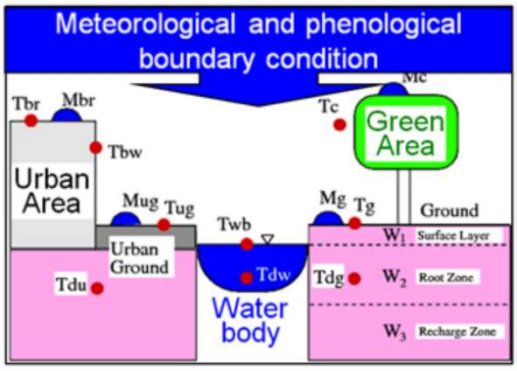

Fig. 3 Schematic image of SiBUC model

$$\frac{\partial A}{\partial t}+\frac{\partial Q}{\partial x}=q_{\mathrm{L}}(x,t) \tag{1}$$

$$Q=\alpha A^{m},\alpha=\frac{\sqrt{i_0}}{n}\left(\frac{1}{B}\right)^{m-1},m=\frac{5}{3} \tag{2}$$

where,$A(x,t)$ is the flow cross-sectional area,$Q(x,t)$is the flow discharge, $q_{\mathrm{L}}(x,t)$ is the lateral inflow per unit length, $i_0$is the slope, n is the Manning roughness coefficient, and B is the width of the flow. Equation (1) is the continuity equation. It is derived from the principle of mass conservation within a control volume. Equation (2) is derived from Manning's laws which are flow resistance laws of open channel uniform flow.

C. Land Surface Model SiBUC

The land surface model Simple Biosphere including Urban Canopy was developed by Tanaka [3] in Disaster Prevention Research Institute in Kyoto University. SiBUC model uses mosaic approach, which couples independently each land-use patch of the grid element to the atmosphere, to incorporate all kind of land-use to land surface scheme.

In SiBUC model, each land surface grid is classified into three land use categories, urban area, water body, and green area.Fig. 3 shows the schematic image of surface elements in SiBUC model.

The fractions of these land-use categories are fixed for each grid cell in SiBUC model. And surface fluxes are obtained by averaging the surface fluxes over each land-use weighted by its fractional area.In this study, the spatial resolution is the same as that of the MRI-AGCM 3.2S (20-km).

Fig. 4 shows the schematic image of water budget in the green area model of SiBUC and Table. 1 shows the variables used in the model. Soil is expressed by three layers and the governing equations for the three soil moistures are based on Richards' equation with forcing terms of evapotranspiration (E_s,$E_{dc,1}$,$E_{dc,2}$) and infiltration (P_1). Equation (3) to (5) is the governing equations to soil moisture of three layers.

$$\frac{\mathrm{d}W_1}{\mathrm{dt}}=\frac{1}{\theta_s D_1}\left[P_1-Q_{1,2}-\frac{1}{\rho_w}\left(E_s+E_{dc,1}\right)\right] \tag{3}$$

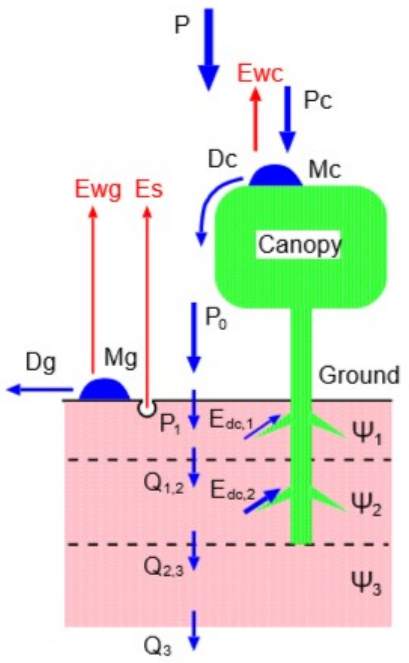

Fig. 4 Schematic image of water budget in the green area model of SiBUC

$$\frac{dW_2}{dt} = \frac{1}{\theta_s D_2}\left[Q_{1,2} - Q_{2,3} - \frac{E_{dc,2}}{\rho_w}\right] \quad (4)$$

$$\frac{dW_3}{dt} = \frac{1}{\theta_s D_3}\left[Q_{2,3} - Q_3\right] \quad (5)$$

In this model, after precipitation reaches the ground, some of the water infiltrates through the soil following Darcy's law and the rest becomes surface runoff. Sub-surface runoff is calculated from the third layer of the soil. Runoff generation is the total sum of surface runoff and sub-surface runoff. It is used as input into flow routing model 1K-FRM.

D. Data

1) GCM Runoff Generation Data

GCM data used for this study is 3-hourly runoff generation data from the super-high resolution (20-km) atmospheric general circulation model MRI-AGCM3.2S. It is one of the latest atmospheric GCMs based on a model jointly developed by the Japan Meteorological Agency (JMA) and the Meteorological Research Institute (MRI) [4]. The MRI-AGCM provides data for three climate experiments: present climate experiment (1979-2008), near future climate experiment (2015-2044), and future climate experiment (2075-2104). The data used for future projection were based on the Special Report on Emissions Scenarios (SRES) A1B scenario. In this study, only the output of present climate experiment is used.

2) Meteorological Data

The meteorological data to force land surface model SiBUC includes seven components: precipitation, air temperature, specific humidity, surface pressure, wind speed, long wave radiation and short wave radiation.

In this study, the product of the Japanese 55-year reanalysis (JRA-55) project was utilized to use as inputs to SiBUC. The Japanese 55-year Reanalysis (JRA-55) is the second reanalysisproject conducted by Japan Meteorological Agency (JMA)

Table. 1 List of variables used in the green area model of SiBUC

Symbol	Definition	Units
W_i	soil moisture stores	-
D_i	root depth	M
θ_s	soil water content at saturation	-
ρ_w	water density	kg m^{-3}
E_s	direct evaporation of water from the surface soil layer	kg m^{-2} s^{-1}
$E_{dc,i}$	abstraction of soil moisture by transpiration	kg m^{-2} s^{-1}
P_1	infiltration into the upper soil layer	ms^{-1} ms^{-1} ms^{-1}
$Q_{i,i+1}$	flow between soil layer	
Q_3	gravitational drainage from recharge layer	

using more sophisticated Data Assimilation system based on the operational system as of December 2009, and newly prepared past observations [5].

However, JRA-55 precipitation and surface radiation data are forecast data, not reanalysis data. Therefore, other data sources are considered to use as substitution.

For precipitation data, the Asian Precipitation - Highly-Resolved Observational Data Integration Towards. Evaluation of Water Resources (APHRODITE's Water Resources) project was selected. APHRODITE's Water Resources project was conducted by the Research Institute for Human and Nature (RIHN) and the Meteorological Research Institute (MRI/JMA) from 2006 to develop state-of-the-art daily precipitation datasets on high-resolution grids covering the whole of Asia [6]. In this study, precipitation data to force land surface model for Kyushu area was extracted from the APHRO_JP V1207 [7] dataset with spatial resolution of 0.05 degree. Temporal resolution of APHRO_JP precipitation data is daily.

And the Surface Radiation Budget (SRB) dataset was used as long wave radiation and short wave radiation.Surface Radiation budget (SRB) dataset is produced and achieved by the NASA Langley Research Center Atmospheric Sciences Data Center (NASA/GEWEX). It is produced on a 1

degreex1 degree global grid using satellite-derived cloud parameters and ozone fields, reanalysis meteorology, and a few other ancillary datasets. The SRB dataset contains 3-hourly long wave and short wave radiative fluxes.

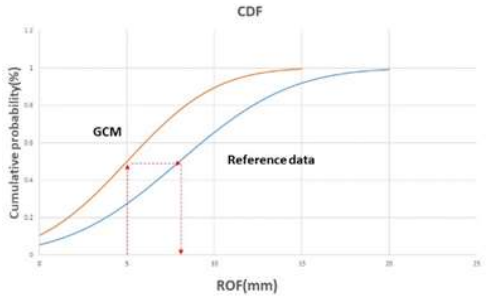

Fig. 5 Schematic representation of QQM method

Bias Correction For GCM Runoff Generation Data

A. Application of Quantile-Quantile Mapping(QQM) Method

To correct biases in GCM runoff generation data, quantile-quantile mapping (QQM) bias correction method was selected. The bias correction based on QQM method has been widely used to correct outputs of climate models.Teutschbein and Seibert [8]compared the various bias correction methods and showed that the QQM method is more effective than the other methods.

In QQM method, GCM outputs and observations are sorted to construct cumulative distribution functions (CDFs). These CDFs are used to define the quantiles of simulated values and observations. Then, GCM simulated values are substituted with those of the identical quantile from the observational dataset. Fig.5 shows the schematic representation of QQM method.

In this study, runoff data simulated by SiBUC model were used as reference data to correct the MRI-AGCM3.2S runoff generation data. The effect of bias correction is evaluated by simulating river discharge using flow routing model 1K-FRM.

B. Results

Fig.6-a shows the duration curves of 20 years from 1982 to 2001 at Kashiwada station in Oyodo River basin. The red line indicatesthe simulated river discharge using original GCM runoff generation data, the blue line indicates that using reference data and the black line indicates the observational river discharge. It can be seen that the simulated river discharge using reference data is closer to the observation in the high peak discharge(larger than 100 m^3s^{-1}) compared with that using original GCM outputs. Therefore, land surface model SiBUC is considered to reproduce runoff better than the MRI-AGCM3.2S. In addition, theriver discharge simulated using bias-corrected runoff generation data showed an improvement compared with that simulated using original one. However, shown in Fig.6-b whose horizontal axis is logarithm, there were also a problem that the river discharge simulated using bias-corrected runoff generation was overestimated in high peak discharge as compared with that using reference data.

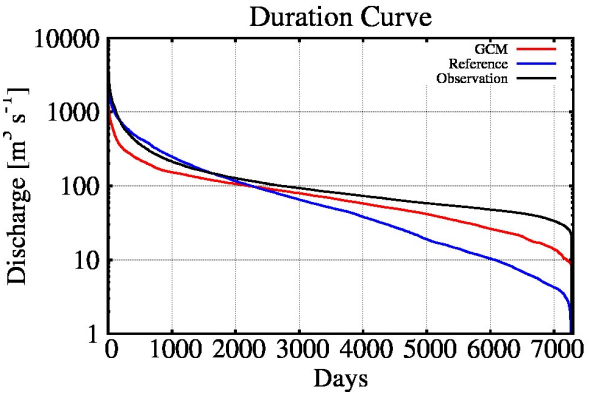

Fig. 6-a Duration curves of 20 years at Kashiwada, Oyodo River basin(vertical axis islogarithm)

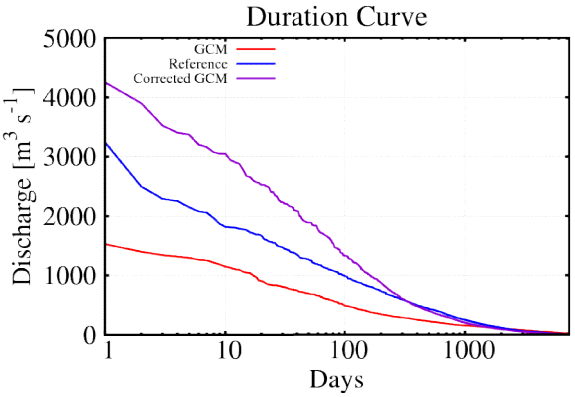

Fig. 6-b Duration Curves of 20 years at Kashiwada, Oyodo River basin (horizontal axis is logarithm)

Fig. 7 shows a histogram of two kinds of runoff generation data, GCM outputs and reference data, in July for 20 years. The red bar indicates the result of GCM and the blue one indicates that of reference data. Shown in Fig. 7, the frequency of high runoff amount is higher in reference data than that in GCM outputs.Therefore, the runoff of reference data which is assumed to be dominated by surface runoff can be substituted with the runoff of original GCM outputs which is assumed to be dominated by sub-surface runoff. Fig. 8 shows the time series of runoff generation data in original GCM outputs and bias-corrected data. The red line indicates the result of original GCM outputs and the purple one indicates that of bias-corrected data.Both lines show high runoff value on July 8th, but relatively large value can be seen continuously in bias-corrected data after the flooding event while relatively low value can be seen in original GCM data after that. As shown in Fig. 8, relatively

large values that contribute to flooding may appear continuously. It is occurred due to the difference of frequency distributions between original GCM data and reference data.This is considered to be one of the causes of overestimation in simulating river discharge.

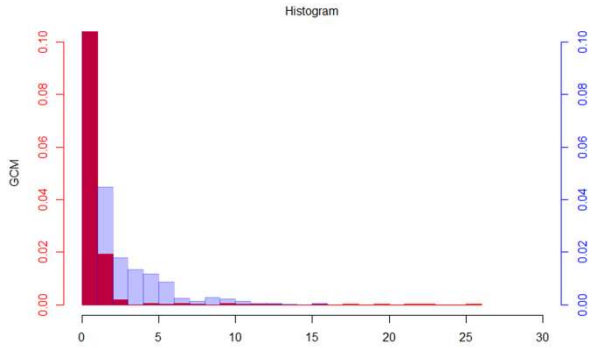

Fig. 7 Histogram of runoff generation data in GCM outputs and reference data in July for 20 years

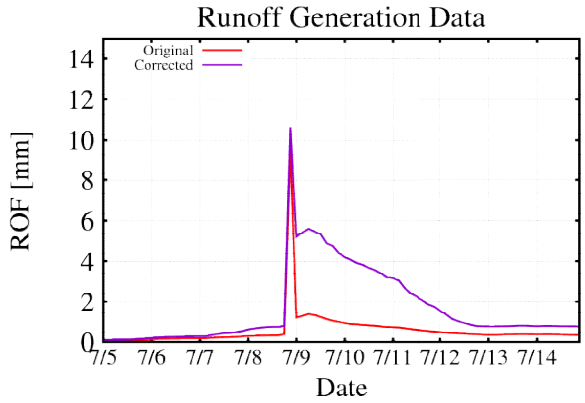

Fig. 8 Time series of runoff generation data in original GCM outputs and bias-corrected data

Revision Of Bias Correction

A. Grouping QQM method

In order to improve the overestimation, a revision of bias correction was considered to be effective. The purpose of this revision is to reduce the frequency of high runoff generation data that contribute to flooding after bias correction and to improve the overestimation of river discharge.

The frequency of high runoff amount is higher in reference data than that in GCM outputs and after bias correction, relatively large values that contribute to flooding may appear continuously and it may cause overestimation in simulating river discharge. Therefore, it is considered to be needed to reduce the frequency of high runoff amount in bias-corrected runoff generation data for improving overestimation results. In consideration of the difference in frequency distribution in the two kinds of data, a threshold is set for each data and divides each data into high runoff generation data contributing toflooding and low runoff generation data not contributing to flooding.Threshold values are set for reference data and original data, respectively.In this study, the number of datawhich is larger than the threshold value in original datasets is set to be smaller than the number which is larger than the threshold value in reference datasets. As shown in Table. 2, twokinds of threshold patterns were applied in this study.QQM method was applied for high runoff generation data and low data independently. This method is called grouping QQM method.

Table. 2 Pattern of threshold value

	Threshold value of original GCM outputs	Threshold value of reference data
Pattern1	Applying 5% value from largest on each month of each cell	Applying 10% value from largest on each month of each cell
Pattern2	Applying 2.5% value from largest on each month of each cell	Applying 10% value from largest on each month of each cell

B. Results

Fig.9 shows time series of 4 kinds of runoff generation data. The red line indicates the result of original GCM outputs, the purple one indicates that of simple QQM method, light blue one indicates that of pattern1, pink one indicates that of pattern2. By applying grouping QQM method, itcan be possible toreduce the amount of runoff generation data at the time of flooding, compared with simple QQM method.

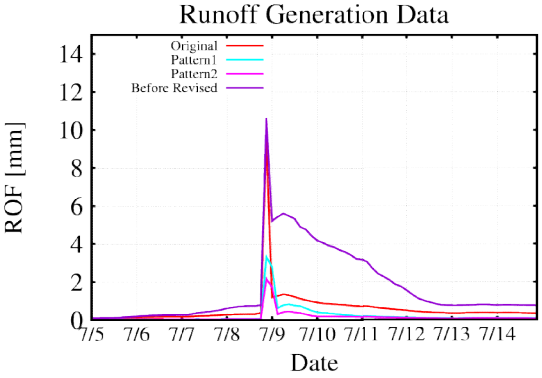

Fig. 9 The effect of bias correction on runoff generation data

Fig. 10 shows the duration curvesof 20 years from 1982 to 2001 at Kashiwada station in Oyodo River basin in 5 kinds of simulated river discharge.In addition to the colors of Fig. 9, the blue line indicates the result of reference data. In the high peak discharge, all the two patterns could reduce river discharge compared with before revision. In Pattern 1, the results that are closer to reference data were obtained. Therefore, they showed an improvement in simulating river discharge by applying grouping QQM method.

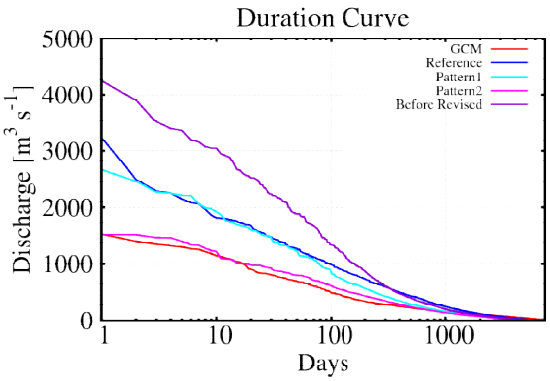

Fig. 10 The effect of bias correction on river discharge

Conclusions

Bias correction was performed for the MRI-AGCM3.2S 3-hourly runoff generation based on reference data created by land surface model SiBUC and the effect of bias correction was evaluated by simulating river discharge utilizing flow routing model 1K-FRM. Bias correction applying the QQM method is effective by creating reference data of runoff generation data. However, it was found that the river discharge simulated using bias-corrected runoff was overestimated compared with that using reference data especially on high flood events. Therefore, the QQM method was revised by setting threshold values for runoff generation data. By this revision, overestimation of river discharge isimproved and river discharge is simulated more precisely.

As the improvement of the land surface model progresses and the reproducibility of reference data improves, it can be expected that more reliable bias correction is performed.

References

[1] D. D. Toan, "Assessment of river discharge changes in the Indochina Peninsula region under a changing climate," Doctoral dissertation, Kyoto University, 2014.

[2] Hydrology and water resources laboratory, Kyoto University,http://hywr.kuciv.kyoto-u.ac.jp/products/1K-DHM/1K-DHM.html,access 2018/10/24.

[3] K. Tanaka, "Development of the new land surface scheme SiBUC commonly applicapble to basin water management and numerical weather prediction model," Doctoral dissertation, Kyoto University, 2005.

[4] R. Mizuta, H. Yoshimura, H. Murakami, M. Matsueda, H. Endo,T. Ose, K. Kamiguchi, M. Hosaka, M. Sugi, S. Yukimoto, S.Kusunoki, and A. Kitoh, "Climate Simulations Using MRI-AGCM3.2 with 20-km Grid,"Journal of the Meteorological Society of Japan, vol.90A, pp.233-258, 2012.

[5] S. Kobayashi, Y. Ota, Y. Harada, A. Ebita, M. Moriya, H. Onoda, K. Onogi, H. Kamahori, C. Kobayashi, H. Endo, K. Miyaoka, and K. Takahashi, "The JRA-55 Reanalysis: General specifications and basic characteristics," Journal of the Meteorological Society of Japan, vol. 93, pp. 5-48, 2015.

[6] A. Yatagai, K. Kamiguchi, O. Arakawa, A. Hamada, N. Yasutomi and A. Kitoh,"APHRODITE: Constructing a Long-term Daily Gridded Precipitation Dataset for Asia based on a Dense Network of Rain Gauge," Bulletin of American Meteorological Society, vol. 93, pp. 1401-1415, 2012.

[7] K. Kamiguchi, O. Arakawa, A. Kitoh, A. Yatagai, A. Hamada and N. Yasutomi,"Development of APHRO_JP, the first Japanese high-resolution daily precipitation product for more than 100 years,"Hydrological Research Letters, vol. 4, pp. 60-64, 2010.

[8] C. Teutschbein, and J. Seibert, "Bias correction of regional climate model simulations forhydrological climate-change impact studies: Review and evaluation of different methods,"Journal of Hydrology, vol. 456-457, pp.12-29,2012.

Comparison of physics-based and data-driven models for streamflow simulation of the Mekong river

Giha Lee[1,a], Daeup Lee[1,a], Yonghun Jung[2,a] and Tae-Woong Kim[3,b]

AbstractIn recent, the hydrological regime of the Mekong River is changing drastically due to climate change and haphazard watershed development including dam construction. Information of hydrologic feature like streamflow of the Mekong River are required for water disaster prevention and sustainable water resources development in the river sharing countries. In this study, runoff simulations at the Kratie station of the lower Mekong River are performed using SWAT (Soil and Water Assessment Tool), a physics-based hydrologic model, and LSTM (Long Short-Term Memory), a data-driven deep learning algorithm. The SWAT model was set up based on globally-available database (topography: HydroSHED, landuse: GLCF-MODIS, soil: FAO-Soil map, rainfall: APHRODITE, etc) and then simulated daily discharge from 2003 to 2007. The LSTM was built using deep learning open-source library TensorFlow and the deep-layer neural networks of the LSTM were trained based merely on daily water level data of 10 upper stations of the Kratie during two periods: 2000~2002 and 2008~2014. Then, LSTM simulated daily discharge for 2003~2007 as in SWAT model. The simulation results show that Nash-Sutcliffe Efficiency (NSE) of each model were calculated at 0.9(SWAT) and 0.99(LSTM), respectively. In order to simply simulate hydrological time series of ungauged large watersheds, data-driven model like the LSTM method is more applicable than the physics-based hydrological model having complexity due to various database pressure because it is able to memorize the preceding time series sequences and reflect them to prediction

Keywords *LSTM, Mekong River, SWAT*

[1]Dept. of Construction & Disaster Prevention Eng., Kyungpook National University
Sangju, Korea
[2]Dept. of Construction & Disaster Prevention Eng., Kyungpook National University
Sangju, Korea
[3]Dept. of Civil and Environmental Eng.,
Hanyang University
Ansan, Korea

[a]leegiha@knu.ac.kr
[b]twkim72@hanyang.ac.kr

Introduction

In recent, the hydrological regime of the Mekong River is changing drastically due to climate change and haphazard watershed development including dam construction. Information of hydrologic feature like streamflow of the Mekong River are required for water disaster prevention and sustainable water resources development in the river sharing countries. In this study, runoff simulations at the Kratie station (Cambodia) of the lower Mekong River are performed using SWAT (Soil and Water Assessment Tool), a physics-based hydrologic model, and LSTM (Long Short-Term Memory), a data-driven deep learning algorithm.

Methdology

A. SWAT

The Soil & Water Assessment Tool (https://swat.tamu.edu/)is a small watershed to river basin-scale model used to simulate the quality and quantity of surface and ground water and predict the environmental impact of land use, land management practices, and climate change. SWAT is widely used in assessing soil erosion prevention and control, non-point source pollution control and regional management in watersheds. SWAT is a continuous time model that operates on a daily time step at basin scale. SWAT uses a two-level disaggregation scheme; a preliminary sub-basin identification is carried out based on topographic criteria, followed by further discretization using land use and soil type considerations. Areas with the same soil type and land use form a Hydrologic Response Unit (HRU), a basic computational unit assumed to be homogeneous in hydrologic response to land cover change. The SWAT is used as a basic tool for Mekong river hydrologic simulations in the Mekong River Commission [3], [4], [5].

B. LSTM

Long Short-Term Memory, an evolution of RNN, was introduced by Hochreiter and Schmidhuber [1] to address problems of the aforementioned drawbacks of the RNN vanishing gradient by adding additional interactions. LSTMs are a special kind of RNN, capable of learning long-term dependencies and remembering information for extended periods of time

as a default. According to Olah [2], the LSTM model is organized in the form of a chain structure. However, the repeating module has a different structure. Instead of a single neural network like standard RNN, it hasfour interacting layers with a unique method of communication.

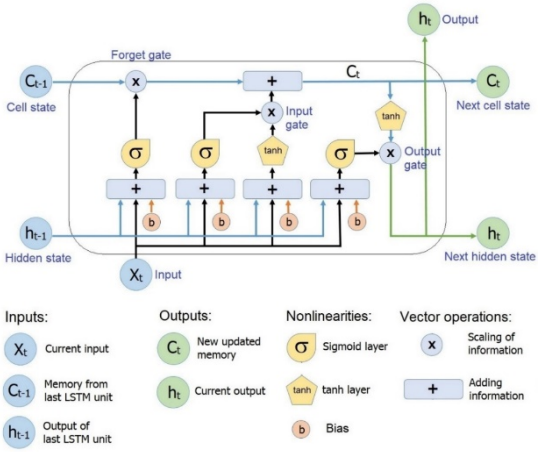

Fig. 1 The structure of LSTM neural network

The structure of the LSTM neural network is shown in Fig. 1.

A typical LSTM network is comprised of memory blocks called cells. Two states are being transferred to the next cell, the cell state, and the hidden state.The cell state is the main chain of data flow,which allows the data to flow forward essentially unchanged.However, some linear transformations may occur. The data can be added to or removed from the cell state via sigmoid gates. A gate is similar to a layer or a series of matrix operations, which contain different individual weights. LSTMs are designed to avoid the long-term dependency problem because it uses gates to control the memorizing process.

C. Lower Mekong River

The Mekong River is a nationally shared river originating from the uppermost reaches of China and passing through the Mekong Delta of the most downstream Vietnam. The watershed covers about 10 times (795,000 km^2) of South Korea with an annual average flow of about 15,000m^3/s. Fig. 2 shows the location of the main water level stations in the lower Mekong region (excluding upstream in China), and Table 1 shows the watershed area and runoff. As shown in Table 1, the annual average flow rate at the Kratie site is about 90% of the Mekong River main stream.

Table 1. Mean annual discharge at main water level stations

Station Name		Catchment area (km^2)	Mean annual discharge (m^3 /s)	As % total Mekong
1	Chiang Saen	189,000	2,700	18
2	Luang Prabang	268,000	3,900	26
3	Chiang Khan	292,000	4,200	28
4	Vientiane	299,000	4,400	29
5	NongKhai	302,000	4,500	30
6	Nakhon Phanom	373,000	7,100	47
7	Mukdahan	391,000	7,600	51
8	Pakse	545,000	9,700	65
9	Stung Treng	635,000	13,100	87
10	Kratie	646,000	13,200	88
Basin Total		795,000	15,000	100

Fig. 2 Main water stations of the Mekong River

Applications

The SWATmodel was set up based on globally-available database(topography: HydroSHED, landuse: GLCF-MODIS, soil: FAO-Soil map, rainfall: APHRODITE, etc.) and then simulated daily discharge from 2003 to 2007. The data from 2000 to 2002 were used for model parameter optimization by SWAT-SUP, automatic calibration tool. The LSTM was built using deep learning open-source library TensorFlow (https://www.tensorflow.org) and the deep-layer neural networks of the LSTM were trained based merely on daily water level data of 10 upper stations of the Kratie during two periods: 2000 ~ 2002 and

2008 ~ 2014. Fig. 3 shows the water level time series of the stations for LSTM application. Then, LSTM simulated daily discharge for 2003 ~ 2007 as in SWAT model.

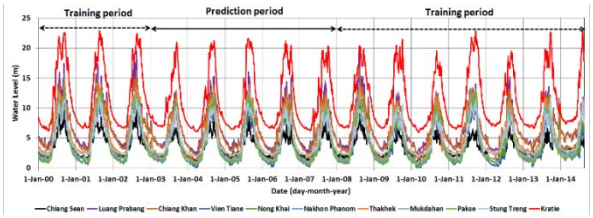

Fig. 3 Data sets for LSTM training and prediction (water level time series)

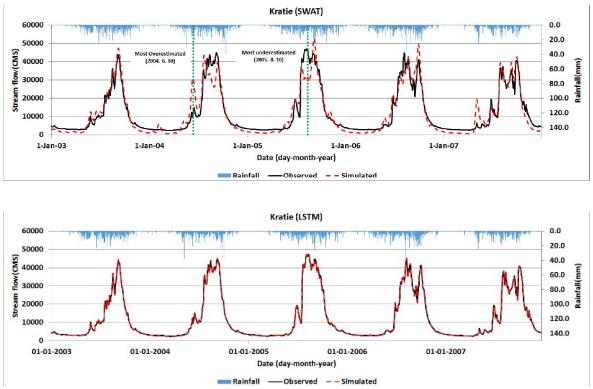

Fig. 4 Comparison of hydrographs between SWAT and LSTM

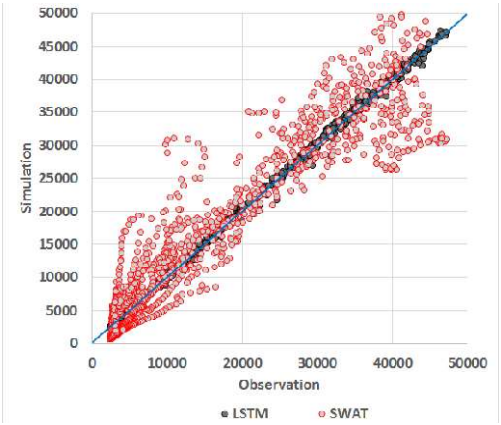

Fig. 5 Stream flow scatter plots of the two models

Results & Discussion

To evaluate the performance of two models, NSE(Nash-Sutcliffle Efficiency) and RMSE(Root Mean Square Error)were used.

$$NSE = \left(1 - \frac{\sum_{i=1}^{n} (O_i - P_i)^2}{\sum_{i=1}^{n} (O_i - \overline{O}_i)^2} \right) * 100 \qquad (1)$$

$$RMSE = \sqrt{\frac{1}{n} \sum_{i=1}^{n} (O_i - P_i)^2} \qquad (2)$$

Here, O_i and P_i are observed discharges and simulated discharge at time t, respectively; $\overline{O}$is the mean of observed discharge; n is the total number of observations.

The results of the quantitative evaluation of the accuracy of the SWAT model were as follows: RMSE: 3941.71 ㎥/s, NSE: 0.9. The SWAT simulation results were overestimated or underestimated for the simulation period. On the other hand, the LSTM model showed a very good agreement of hydrograph: NSE: 0.99 and RMSE: 330 ㎥/s. The LSTM model provides very stable flow simulation results regardless of flow magnitude.

A variety of physical rainfall-runoff models have already been developed for the nonlinear nature of runoff analysis. When sufficient physical data and parameter correction are assured, these models have been proven to be very usefulfor simulation of rainfall-runoff and spatial hydrological variability However, the complexity of such a physical model may cause uncertainty problems in model structure, grid scale, and parameters, and may be limited by data construction and simulation time. Therefore, the LSTM model, which memorizes the preceding information in the time series prediction at a specific time steps and reflects it to the prediction,can be used as a complementary means.

Acknowledgment

This research was supported by International Hydrologic Program funded by Ministry of Environment in Korea.

References

[1] Hochreiter, S., Schmidhuber, J. Long short-term memory. *Neural Comput.*, *9*, 1735-1780, **1997**.

[2] Olah, C. Understanding LSTM networks. In *http://colah.github.io/posts/ 2015-08-Understanding-LSTMs/*, **2015**.

[3] Shrestha, B., Babel, M. S., Maskey, S., Griensven, A. V., Uhlenbrook, S., Green, A., and Akkharath, I. Impact of climate change on sediment yield in the Mekong River basin: a case study of the Nam Ou basin, Lao PDR.*Hydrology and Earth System Sciences*, Vol. 17, No. 1, 1-20, **2013.**

[4] Vilaysane, B., Takara, K., Luo, P., Akkharath, I., and Duan, W. Hydrological stream flow modelling for calibration and uncertainty analysis using SWAT model in the Xedone river basin, Lao PDR. *Procedia Environmental Sciences*, Vol. 28, 380-390, **2015**.

[5] Vu, M. T., Raghavan, S. V., and Liong, S. Y. SWAT use of gridded observations for simulating runoff - A Vietnam river basin study. *Hydrology and Earth System Sciences*, Vol. 16, No. 8, 2801-2811, **2012**.

Characteristics of River Discharge Simulation Using NHRCM 5km Output by a Distributed Hydrologic Model in Thailand

AuliaFebianda Anwar Tinumbang[1], Kazuaki Yorozu[1], Yutaka Ichikawa[1] and YasutoTachikawa[1]

Abstract A river discharge estimation using a detailed projection of climate data and hydrologic model is important to make a basin-level assessment including climate change impact. Recently, a result of a first version of NHRCM 5km-spatial resolution is available for Thailand area, provided by JMA/MRI. The objective of this research is to evaluate river discharge simulated by using the NHRCM 5km output. Before the river discharge simulation is performed, a 20-years-mean NHRCM 5km rainfall was verified with APRHODITE observation data. It was found that NHRCM 5km rainfall was underestimated in the most of Thailand region. However, some area in the northern region, which almost corresponds to Bhumibol dam catchment, was overestimated, particularly in the rainy season. Hence, it showed a better accuracy. After that, the river discharge was simulated using NHRCM 5km output as forcing data by a coupled of a land surface model SiBUC and a flow routing model 1K-FRM. The simulated river discharge was evaluated with the observed inflow data. The 20-years-mean monthly river discharge showed an overestimated result during rainy season. This is consistent with the rainfall analysis, but only the total amount of rainfall could not explain the reason of overestimation. The analysis of heavy rainfall day (more than 20 mm/day) showed a large number of events during rainy season, which might be the reason of overestimated river discharge.

Keywords *NHRCM 5km, distributed hydrologic model, river discharge*

[1]Department of Civil and Earth ResourcesEngineering
Graduate school of Engineering, Kyoto University
Kyoto, Japan

Introduction

The impact of global warming for the future water resources is attracting widespread interests for scientists, policymakers, engineers, etc. In order to predict the changes and impact of global warming, particularly for regional level assessment, the output of high-resolution global climate model (GCM) is generally used. In the recent years, many researchers already developed regional climate model (RCM) with a fine grid-spacing. For example, Sasaki *et al*. [1] developed a Non-hydrostatic Regional Climate Model (NHRCM) with 5km spatial resolution. This model performance was tested in Japan applying multiple nesting method. The outer boundary was an output from Atmospheric General Circulation Model 20km and the inner boundary was created by NHRCM15km. It showed the annual mean surface temperature and precipitation had a good agreement with observed data. This fine resolution model also had a better reproducibility of the local features, such as it could reproduce a heavy precipitation events which could not be obtained from the results of GCM. In this study, we utilized the output of NHRCM 5km which was applied for Thailand region and conducted a river discharge simulation by using a distributed hydrologic model. The objective of this research is to evaluate the NHRCM 5km output data from river discharge view point.

Methodology

A. NHRCM 5km output data

The Non-hydrostatic Regional Climate Model (NHRCM) with 5km spatial-resolution is developed in Japan Meteorological Agency Meteorological Research Institute by Sasaki *et al*. [1]. The outer boundary condition for NHRCM 5km for Thailand region is obtained from the result of the NHRCM with 25km spatial resolution nested within present climate simulation using MRI-AGCM version 3.2H with grid spacing of 60km [2]. The product of NHRCM 5km consists of 20 years data for the current climate (1980 – 1999) and future climate (2080 – 2099) under SRES A1B. However, only the result of current climate data is used in this study. For each year, the simulation starts from April to May in the following year (in total 14 months). The first two months data are discarded because it is assumed as model spin up simulation.

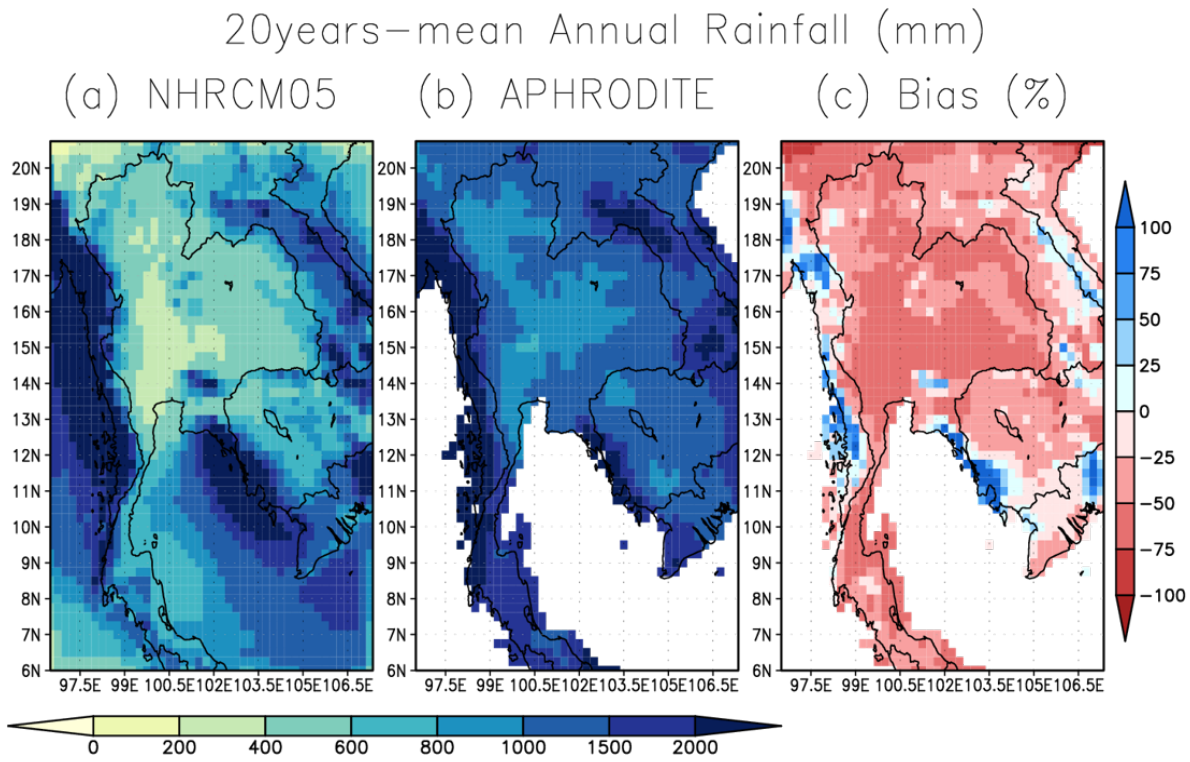

Fig. 1. 20-years-mean (1980 – 1999) annual rainfall (unit: mm) of (a) NHRCM 5km, (b) APHRODITE, and (c) bias (unit: %) of NHRCM 5km
rainfall relative to APHRODITE. Red color represents underestimated value of NHRCM 5km while blue color is overestimated result.

B. Observed rainfall and inflow discharge data

In this research, the observed rainfall data that is used for evaluation of NHRCM 5km rainfall output data is obtained from Asian Precipitation – Highly-Resolved Observation Data Integration towards Evaluation of water resources(APHRODITE) [3] with 0.25° spatial-resolution. In addition, the observed inflow data with daily records in Bhumibol Dam is acquired from the Electricity Generating Authority of Thailand (EGAT).

C. Distributed hydrologic model

A distributed hydrologic model, which is a coupled of land surface model SiBUC (Simple Biosphere including Urban Canopy) and a flow-routing model 1K-FRM [4] is used for conducting a river discharge simulation. SiBUC [5] is a land surface model which implements a mosaic scheme that can consider a mixture of land use, paddy field, and irrigation system in the model. 1K-FRM [6] is a distributed flow routing model, developed based on one-dimensional kinematic wave theory to conduct a river discharge simulation. The forcing data used for SiBUC model is obtained from NHRCM 5km output rainfall, surface pressure, humidity, short-wave radiation and long-wave radiation in downward direction, wind speed, and air temperature. The SiBUC model is used with a spatial resolution of 3 minutes and temporal resolution of 1-hour. 1K-FRM is utilized with 1-km spatial resolution and the output with 1-hour temporal resolution. The runoff output from SiBUC model is given to 1K-FRM to conduct a river discharge simulation. This model was tested for 2011 Thailand big flood and showed good performance for simulating river discharge [7].

Result and Discussion

A. Characteristics of NHRCM 5km rainfall output data

The reproducibility of NHRCM 5km rainfall for Thailand region was analyzed by comparing with APHRODITE observation data. First, the NHRCM 5km rainfall was aggregated from the original resolution to 0.25° resolution, which corresponds to APHRODITE grid spacing. The 20-years-mean annual rainfall was calculated for both NHRCM 5km and APHRODITE data.

The calculated result of 20-years-mean annual rainfall of NHRCM 5km and APRHODITE are shown in Figure 1(a) and 1(b), respectively. The result of NHRCM 5km rainfall shows that the amount of rainfall in the central part of Thailand is lower than northern part, and the southern part of Thailand is the highest. The APHRODITE observed rainfall also shows the similar trend. Therefore, it can be said that

the NHRCM5km rainfall output could catch the spatial distribution of the observed rainfall.

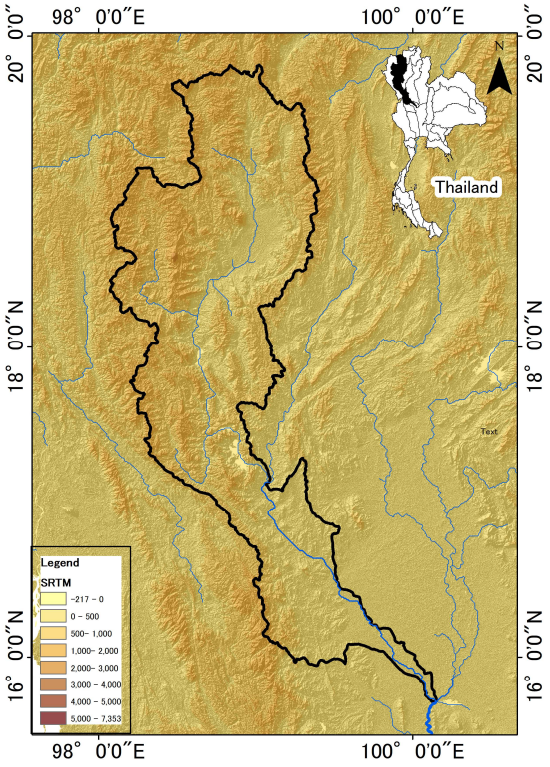

Fig. 2. Ping River Basin. Red circle shows Bhumibol Dam location.

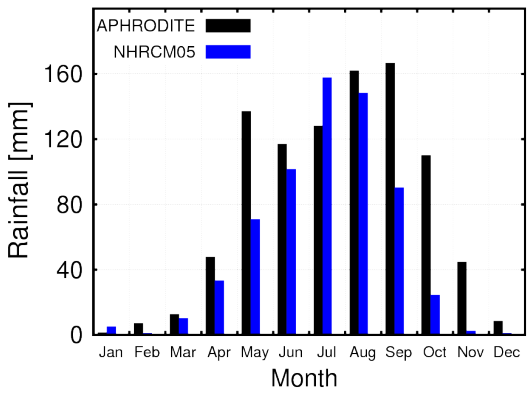

Fig. 3. 20-years-mean basin average rainfall in the Bhumibol Dam catchment. Black color shows APHRODITE rainfall and blue color shows NHRCM 5km rainfall.

However, the absolute value of NHRCM 5km is mostly underestimated in all over the region. This result is clearly shown from the calculation of 20-years-mean bias in the Fig. 1(c). The bias of NHRCM 5km is calculated in (1),

$$B = (R_n - R_a) / R_a \quad (1)$$

with B is bias, R_n is NHRCM 5km rainfall, and R_a is APHRODITE rainfall. Although, it can be seen that there is an overestimation result in some region in the upper part (shown in black circle) and in the eastern part of Thailand. The bias in these regions is comparatively smaller than other regions. Based on this result, the upper region in Thailand, which almost corresponds to Bhumibol Dam catchment, was selected for river discharge simulation.

Bhumibol Dam catchment is located in 98–99.5°E, 17–19.9°S. It is located in the upper part of Ping River Basin (Fig. 2), with the area is about 26,400 km^2. The result of 20-years-mean basin average rainfall for NHRCM 5km and APHRODITE in the upper part of Bhumibol Dam catchment is shown in Fig. 3. From this result, the total amount of rainfall is overall underestimated and thatin June, July, and August (JJA) shows a better accuracy compared to other months. And then, the NHRCM 5km rainfall produces the peak of rainy season on July, while the observed peak rainy season is on September.

B. Characteristics of NHRCM 5km river discharge

To conduct a river discharge simulation, first, the forcing data from the NHRCM 5km output was aggregated from the original grid spacing into 0.05°(or 3-minute resolution) grid size. Then, the forcing data was given into SiBUC model to calculate the runoff. After that, the river discharge was calculated by 1K-FRM using the runoff output.

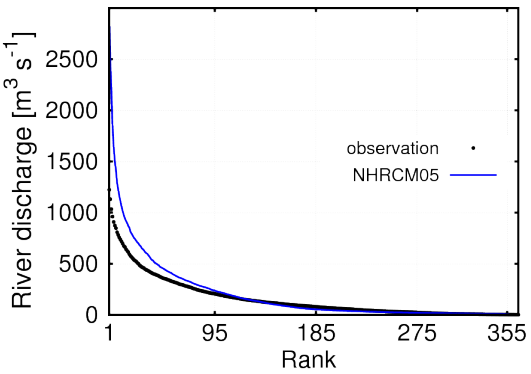

Fig. 4. Flow Duration Curve of 20-years-mean river discharge. Black dots show the observed inflow in Bhumibol Dam and blue line shows the simulated result using NHRCM 5km forcing data.

The simulated river discharge is obtained for daily discharge for 20-years period. The daily river discharge for a year is sorted from the highest to the lowest to draw a Flow Duration Curve (FDC). In total, there are 20-FDCs for river discharge simulation during 1980 – 1999. Then, 20-years-mean FDC was calculated for both simulated river discharge and the observed inflow in Bhumibol Dam. The result isshown in Fig. 4. The first quartile (95th day) represents a high-flow discharge, 2nd quartile (185th day) is a normal-flow discharge, 3rd quartile (275th day) is a low-flow discharge, and 4th quartile is a drought-flow discharge.

The high-flow discharge is about 15% overestimated by NHRCM 5km, while the normal-flow, low-flow and drought-flow, the simulated discharge is well compared with the observed data.

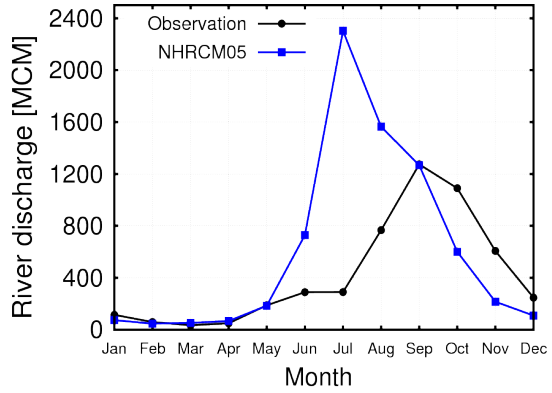

Fig. 5. 20-years-mean monthly river discharge. Black color shows the observed inflow in Bhumibol Dam and blue color shows the simulated result using NHRCM 5km forcing data.

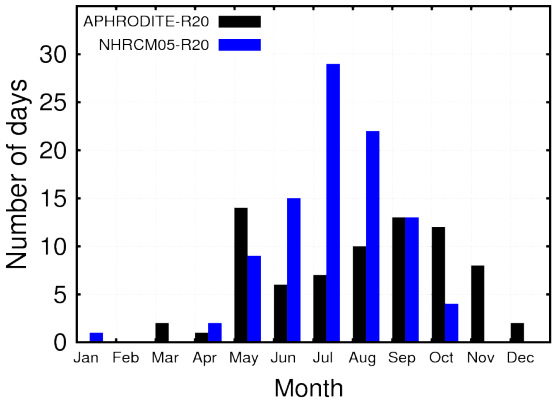

Fig. 6. Number of heavy rainfall days (more than 20 mm day-1) during 1980 - 1999. Black color shows APHRODITE rainfall and blue color shows NHRCM 5km rainfall.

Fig. 5 shows the result of 20-years-mean monthly river discharge of NHRCM 5km and observed inflow. The peak discharge simulated from NHRCM 5km was produced much earlier compared to the observed inflow. This might be explained by earlier peak of the basin average of NHRCM 5km rainfall. The simulated monthly river discharge is particularly overestimated during JJA period. Therefore, only the total monthly rainfall could not explain the reason of overestimated simulated river discharge.

The number of heavy rainfall days (more than 20 mm day^{-1}) during 1980 – 1999 is shown in Fig. 6. In this result, the short-term heavy rainfall of NHRCM 5km shows a larger number of events compared to the observed APHRODITE rainfall, particularly in JJA period. From this result, it is thought that more frequent short-term heavy rainfall events from NHRCM 5km output might be one of the causes of the overestimated river discharge of NHRCM 5km. However, the hydrological model itself might also have some influence on this overestimated result. Therefore, the parameter settings or the model structure itself should also be examined to see its effect on the river discharge estimation.

Conclusions

In this research, the first version of NHRCM 5km output data was evaluated. Before the river discharge is simulated, the 20-years-mean NHRCM 5km rainfall was compared with APRHRODITE data, as a reference data. The bias calculation shows that most of NHRCM 5km rainfall was underestimated in most of Thailand region, except in Bhumibol dam catchment. The basin average rainfall for upper part of Bhumibol Dam catchment showed a comparatively smaller bias during JJA period compared to other months. While the river discharge simulation showed an overestimated result particularly during JJA period. The NHRCM 5km rainfall had more frequent events of heavy rainfall days (more than 20mm/day) which might be one of the causes to produce extreme simulated flood discharge.

Acknowledgment

We would like to express our deep gratitude for Dr. Patama who provided and simulated the NHRCM 5km data used in this research under supervision of Dr. Hidetaka Sasaki from JMA/MRI. This study has been supported by TOUGOU Program (Integrated Climate Model Advanced Research Program) 2017-2021 Theme-C supported by MEXT.

References

[1] H. Sasaki, A. Murata, M. Hanafusa, M. Oh'izumi, and K. Kurihara, "Reproducibility of present climate in a non-hydrostatic regional climate model nested within an atmosphere general circulation model," SOLA, vol. 7, pp.173-176, 2011.

[2] R. Mizuta, H. Yoshimura, H. Murakami, M. Msatsueda, H. Endo, T. Ose, K. Kamiguchi, M. Hosaka, M. Sugi, S. Yukimoto, S. Kusunoki, and A. Kitoh, "Climate simulations using MRI-AGCM with 20-km grid," J. Meteor. Soc. Jpn., vol. 90A, pp. 235-260, 2012.

[3] A. Yatagai, K. Kamiguchi, O. Arakawa, A. Hamada, N. Yasutomi, and A. Kitoh, "APHRODITE: Constructing a Long-term Daily Gridded Precipitation Dataset for Asia based on a Dense Network of Rain Gauges," Bull. Am. Meteorol. Soc.,vol, 93, pp. 1401-1415, 2012.

[4] K. Yorozu, and Y. Tachikawa, "The effect on river discharge estimation by considering an interaction between land surface process and river

routing process," Proc. IAHS, vol. 369, pp. 81-86, 2015.

[5] K. Tanaka, "Development of the new land surface scheme SiBUC commonly applicable to basin water management and numerical weather prediction model," PhD thesis, Kyoto University, Japan, 2005.

[6] Hydrology and Water Resources Research Laboratory, "1K-FRM/1K-DHM," http://hywr.kuciv.kyoto-u.ac.jp/products/1K-DHM/1K-DHM. html, last access 2018/10/27.

[7] K. Yorozu, N. Kurosaki, Y. Ichikawa, S. Kim, and Y. Tachikawa, "Astudy on long-term river discharge data generationbydistributed hydrologicmodelandrecombinationatmosphericdata," Journal of Japan Society of Civil Engineers, Ser. B1 (Hydraulic Engineering), vol.74, pp. I_127-I_132, 2018 (in Japanese).

A NEW APPROACH OF RAINFALL FREQUENCY ANALYSIS USING EVENT-MAXIMUM RAINFALLS

Ke-Sheng Cheng[1,a] and Bo-Yu Chen[1,b]

Abstract Frequency analysis is a crucial step in hydrological engineering design. By estimating the probability distribution of annual maximum rainfalls of a specific duration, the exceedance probability and average recurrence interval, i.e., return period, of certain rainfall depths can be calculated. Annual maximum series (AMS) is most widely used for rainfall frequency analysis. By choosing the maximum rainfall in each year and regarding each year as a "block", the distribution of annual maximum rainfalls could be approximated by the Generalized Extreme Value (GEV) distribution, according to the Extremal Type Theorem. However, two concerns may arise when using AMS. AMS of specific durations were selected without considering rainfall events and thus AMS may be composed of rainfalls of two or more separated storm events, particularly for AMS of longer durations. As the result, frequency analysis using AMS tends to overestimate rainfall depth. However, in reality, such AMS rainfall amounts might not result in severe flooding since flood flow of the first storm could have receded before the beginning of the second storm. The second concern is the assumption of annual maximum rainfall distribution. According to the Extremal Type Theorem, the block size (number of events in each year) should be the same for AMS to be approximated be the GEV distribution. This is obviously not the case in the real world. The annual number of storm occurrences is not a constant, so the GEV approximation of AMS rainfalls is not theoretically granted. Therefore, we propose an event-maximum-rainfalls (EMR) based approach for frequency analysis. For any given design duration, we firstly extracted event-maximum-rainfalls of individual storm events by considering the minimum inter-event time of different storm categories including Meiyu, typhoons, convective storms, and winter frontal rainfalls. Annual counts of storm events and event-maximum rainfalls were modeled by the Poisson distribution and Pearson Type III distribution, respectively. For each storm category, a storm-type-specific mixture distribution of annual maximum rainfalls was then derived. Finally, the cumulative distribution function of the over-all (considering all storm types) annual maximum rainfalls was obtained from the storm-type-specific mixture distributions. Stochastic simulation was conducted to demonstrate the proposed EMR-based approach. The EMR-based approach is superior to the traditional AMS-based approach in terms of the biasedness and mean squared error. The EMR-based approach is particularly useful in situations of short record length and outlier presence.

Keywords *Event-maximum series, annual-maximum series, frequency analysis*

[1]Dept. of Bioenvironmental Systems Engineering
National Taiwan University
Taipei, Taiwan

[a]rslab@ntu.edu.tw
[b]r06h41003@g.ntu.edu.tw

Introduction

generalized extreme value(GEV) distribution is widely used in frequency analysis.[1][2][4] The AMS method samples maximum rainfall in each year and estimate the underlying distribution of annual maximum rainfalls (AMRs). Then design rainfalls of specific exceedance probabilities (or return periods) are determined.

The AMS method is straightforward and easy to implement, however, it selects the largest total rainfall depths of individual years without considering rainfall events. As a result, AMRs may consist of rainfalls from two or more rainfall events. Moreover, the AMS method selects only the highest rainfall in each year, resulting in waste of information. In Taiwan, there are more than 300 automated rainfall stations with 20 – 30 year hourly rainfall records. Such rainfall data have not been used for AMRs rainfall frequency analysis due to short record lengths.

Another concern about the AMS method arises when using the GEV distribution for AMRs. According to extremal type theorem, if there exists constant sequence $\{a_n>0\}$ and $\{b_n\}$ such that the distribution of n^{th} order statistic(among n samples) would converge to a non-degenerate distribution G as n approcimate infinity, then G is a member of the GEV family[3]:

$$G(z) = \exp\{-[1+\xi(\frac{z-\mu}{\sigma})]^{-1/\xi}\} \quad (1)$$

with

$$1+\xi\left(\frac{z-\mu}{\sigma}\right) > 0, -\infty < \mu < \infty, \sigma > 0, -\infty < \xi < \infty$$

AMS method uses GEV approximation by regarding each year as a "block" with n rainfall samples and annual maximum rainfall is the n^{th} order statistic. However, the approximation is only valid when the sample size *n* is large. Also, the annual count of events

varies each year, making the AMRs not suitable for GEV distribution. In addition to the AMS method, partial duration series (PDS) method is another frequently used method in frequency analysis.[2][7][9][10] The method includes the well-known peak over threshold (POT) method which uses the generalized Pareto distribution(GPD) for design rainfall estimation. The method separate rainfall record into independent events by setting a threshold value and ignore values below the threshold. PDS method could preserve more samples than AMS method. The challenge for PDS method is the choice of the threshold value. To maintain the independence between rainfall events, the threshold value should not be too low while the higher the threshold is, the more data may loss. There's no absolute criterion to select the threshold, so the PDS method is not as popular as AMS method.

To preserve as many data as possible and to avoid the dilemma of deciding threshold, [6] used minimium inter-event time as criterion to separate independent rainfall event and use the generalized Poisson and GPD for frequency analysis. The result showed that the estimation from the event-based method is lower than the traditional approach and is more appropriate for hydraulics design. In this paper, we proposed a new event-maximum-rainfalls (EMR) based approach for frequency analysis. The method separate rainfall record into different types of independent events and estimate the underlying AMR distribution.

Method

Let n be the number of typhoon events in each year and $\{X_1 \ldots X_n\}$ be the rainfall depth of typhoon that are independent and identically distributed with distribution F_X. Then, the AMR of typhoon and its distribution can be obtained by order statistic:

$$Y = \max\{X_1, X_2, \ldots\ldots, X_{n-1}X_n\}$$

$$F_Y(y) = F_X(y)^n$$

Since the number of typhoon events in each year is not constant, it may be assumed to follow poisson distribution with parameter λ [5], then the AMR distribution of typhoon can be written as:

$$F_Y(y) = = \sum_{n=0}^{\infty} P(n;\lambda) * F_X(y)^n$$

$$= \sum_{n=0}^{\infty} \frac{e^{-\lambda}\lambda^n}{n!} * F_X(y)^n \quad = e^{-\lambda[1-F_X(y)]} \qquad (2)$$

In Taiwan, rainfall events could be classified into four types - typhoon, convective storm, mei-yu and frontal rain, so the true AMR is the maximum value among these different types of AMR. Let Z be the True AMR, Y_1, Y_2, Y_3, Y_4 are the AMR correspond to typhoon, convective storm, mei-yu and frontal rain, then since all rainfall events are independent, the distribution of Z is:

$$F_Z(z) = F_{Y_1}(y_1) * F_{Y_2}(y_2) * F_{Y_3}(y_3) * F_{Y_4}(y_4)$$

$$= e^{-\lambda_1[1-F_{x_1}(z)]-\lambda_2[1-F_{x_2}(z)]-\lambda_3[1-F_{x_3}(z)]-\lambda_4[1-F_{x_4}(z)]}$$

Which is the true distribution of AMR used in EMR-based frequency analysis.

Simulation Study

To compare the EMR based approach with traditional AMS based approach, we use Monte Carlo simulation to simulate 44 years rainfall records of typhoon and mei-yu from poisson and gamma distribution. Then the L-moment method is used for parameter estimation in both methods to estimate return level with corresponding return period. Finally, bias and mean square error(MSE) are calculated to evaluate these methods.

After deciding record length N=44 years and given parameters of poisson and gamma distribution(Table I), the steps of each simulation run are as follow:

In each year i,

(1) Generate event number n_{i1} and n_{i2} of typhoon and mei-yu events from corresponding poisson distribution.

(2) Generate n_{i1} typhoon rainfall $\{X_{i,1}, \ldots, X_{i,n_{i1}}\}$ of typhoon and n_{i2}mei-yu rainfall depth $\{Y_{i,1}, \ldots, Y_{i,n_{i2}}\}$ from corresponding gamma distribution.

(3) Let $a_i = \max\{X_{i,1}, \ldots, X_{i,n_{i1}}, Y_{i,1}, \ldots, Y_{i,n_{i2}}\}$ be the i^{th}element of annual maximum rainfall series.

(4) Repeat (1)-(3) N times to obtain EMR series and AMS series.

(5) Conduct event-based frequency analysis and AMS frequency analysis. Gamma distribution is used to estimate rainfall distribution in EMR method while GEV distribution and Pearson type III distribution(PTIII) are used for AMS estimation.

Return levels correspond to return period 5, 10, 25, 50, 100, 200 years are calculated.The total simulation run is set to 1000 and the return levels from EMR and AMS are compared to theorecical values in Table II to calculate bias and MSE. Results are shown in Fig 1.

Clearly, the AMS-GEV method has the largest bias and MSE while EMR approach has the smallest. As return period increases, the bias and MSE of three approach increase since the cumulative distribution function become flatter in the tail of the distribution and small bias in parameter estimation would cause larger bias in quantile estimation comparing to smaller return period. The poor performance of AMS-GEV approach may due to small and non-constant sample size in each year causing the distribution unable to converge, and thus unstable parameter estimation with larger bias in each

simulation run. Changing the record length from 44 years to 20 years would result in similar bias and larger MSE with similar trend. Indicating that for short record length, the EMR approach is still more suitable for estimation.

Real Data Analysis and Discussion

We choose three rain gauge stations in northern, central and southern part of Taiwan to compare frequency analysis result of two methods. L-moment method is used for parameter estimation and the L-momnet ration diagram with acceptance region is used for goodness of fit test.[8] Both EMR and AMS methods used PTIII distribution for rainfall distribution. Rainfall records are first separated into different types of independent storm events using minumum inter-event time and season (Table III). Since AMS is mostly consists of typhoon, mei-yu and convective storm, we would use these three types of storm in EMR frequency analysis.
The design durations are 1, 2, 3, 6, 12, 24, 48, 72 hours and the return periods are 5, 10, 25, 50, 100, 200 years. The estimated return levels are shown in table IV .

Table I. parameter settings for simulation study

	Gamma-scale	Gamma-shape	Poisson-λ
Typhoon	141.19,	1.34	2.09
Mei-yu	53.87	0.68	11.45

Table II. Theoretical Values of return level with corresponding return period

Return period	5	10	25	50	100	200
Theoretical value	352	459	596	698	799	899

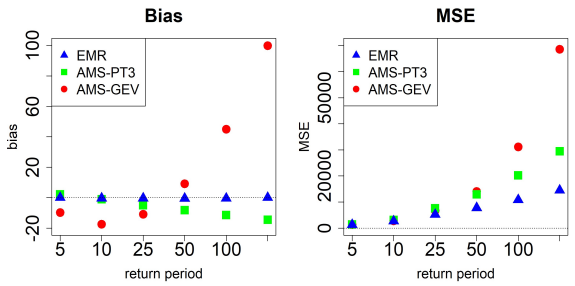

Fig. 1 Bias and MSE of Return level of EMR and AMS frequency analysis

The estimation of AMS method is higher than the one from EMR method in all design durations, this difference is due to the way AMS method selects samples. AMS method does not consider rainfall events, thus when using moving window to search annual maximum rainfall, the selected sample may consists of two or more rainfall events. Most hydrologic and hydraulic design assume the rainfall comes from single event, so the estimation from AMS method would cause overestimation. The effect is more apparent in the difference between 48-hour and 72-hr return, in EMR method, the return level has little difference while in AMS method the difference is obvious. In Taiwan, there are only a few rainfall events lasting longer than 3 days, so when using 72-hour design duration, most selected rainfall events actually having durations close to 48-hour and the estimated return level is similar to the 48-hour result. On the other hand, AMS method could select more than one event, so the return level in higher duration would tempt to be overestimated

By removing the largest value in EMR/AMR series and calculate the return level again (Table V), it is possible to compare how sensitive both methods are to their sample (or outlier). Result shows that the AMS result changes much more than the EMR result. Due to the small sample size, AMS method is more unstable than EMR method. When confronting an extreme rainfall event in the rainfall record, AMS is easier to be influenced and to have larger estimation.

Table III. Event Number of each types of storm and record length of three stations

station	Convective storm	Meiyu	Typhoon	Record length
01B030(WuDuh ,North)	260	230	147	32
01F680(TBK,central)	355	300	70	42
467480(Chiayi, South)	754	504	92	44

Table IV. Return Level estimated from EMR method and AMS-PTIII method

	Annual Maximum Rainfall					
Dur\yr	5	10	25	50	100	200
1	83.06	110.38	150.09	181.82	214.52	247.94
2	118.26	168.88	248.67	315.09	384.97	457.4
3	148.47	209.78	301.89	376.75	454.59	534.63
6	217.61	302.27	422.15	516.56	613.12	711.29
12	300.45	409.39	557.82	672.17	787.72	904.18
24	389.03	514.85	680.73	806.01	931.17	1056.24
48	460.45	599.99	781.77	918.03	1053.5	1188.53
72	495.21	639.63	827.06	967.21	1106.4	1244.89
	Event Maximum Rainfall					
1	81	93	108	119	130	141
2	121	139	163	180	197	214
3	146	170	199	221	243	264
6	204	244	295	332	370	407
12	288	355	441	504	566	628
24	378	476	600	692	783	872
48	430	544	690	797	903	1008
72	431	545	691	798	904	1009

Conclusions

We propose a new approach for rainfall frequency analysis using event-maximum-rainfalls. Simulation study shows that the EMR method has better performance over traditional AMS approach in terms of biasedness and mean square error. Having

more samples than AMS method, estimation from EMR method is more stable for both short and long record length. In real data analysis, effect of sample size and outlier to both methods were discussed. The result shows that EMR method is preferred to avoid overestimation and to reduce bias.

Table V. Return Level estimated from EMR method and AMS-PTIII method after removing largest value

	Annual Maximum Rainfall					
Dur\yr	5	10	25	50	100	200
1	76.02	89.75	107.54	120.83	134.03	147.15
2	108.78	132.03	163.77	188.24	213	237.95
3	135.31	167.3	210.33	243.24	276.35	309.61
6	198.03	250.83	320.32	372.75	425.09	477.37
12	276.25	353.83	454.43	529.62	604.26	678.5
24	363.77	463.9	591.9	686.68	780.26	872.93
48	434.81	552.01	701.46	811.94	920.91	1028.73
72	470.4	595.59	755.55	873.96	990.85	1106.59
	Event Maximum Rainfall					
1	77	89	104	116	127	138
2	114	132	155	172	189	205
3	138	161	191	213	234	256
6	195	236	288	327	366	404
12	280	350	438	502	565	627
24	371	472	599	691	782	872
48	422	540	687	796	902	1008
72	423	541	689	797	903	1009

References

[1] Al Mamoon, A, Rahman, A, 2017, "Selection of the best fit probability distribution in rainfall frequency analysis for Qatar"", Natural hazards , 2017, Vol.86(1), p.281-296

[2] Chin, RJ, Lai, SH, Chang, KB, Jaafar, WZW & Othman, F, 2018, "Statistical Analysis Towards Improvement of Design Rainfall: Case Study of Peninsular Malaysia", Iranian journal of science and technology. Transactions of civil engineering. , 2018, Vol.42(2), p.121-131

[3] Coles, S. An introduction to statistical modeling of extreme values. Springer, 2001.

[4] Deka, S, Borah, M, Kakaty, SC, 2011, "Statistical analysis of annual maximum rainfall in North-East India: an application of LH-moments", Theoretical and applied climatology , 2011, Vol.104(1-2), p.111-122

[5] Haight, F. A., 1967, Handbook of the Poisson Distribution. John Wiley & Sons, New York.

[6] Jun, C.H., Qin, X., Tung, Y.K. & Michele, C.D., 2017, "Storm event-based frequency analysis method", 2017, Hydrology Research (2017) 49 (3): 700-710.

[7] S. Beguerı´a, 2005, "Uncertainties in partial duration series modelling of extremes related to the choice of the threshold value", Journal of Hydrology 303 (2005) 215–230

[8] Wu, Y.C., Liou, J.J., Su, Y.F. & Cheng, K.S., "Establishing acceptance regions for L-moments based goodness-of-fit tests for the Pearson type III distribution", 2012, Stoch Environ Res Risk Assess (2012) 26: 873

[9] W. Zucchini & P. T. Adamson, 1989, "Bootstrap confidence intervals for design storms from exceedance series", Hydrological Sciences Journal, 34:1, 41-48.

[10] Zhou, ZZ, Liu, SG, Hu, Y, Liang, YY, Lin, HJ, Guo, YP, 2017, "Analysis of precipitation extremes in the Taihu Basin of China based on the regional L-moment method", Hydrology Research, 2017, Vol.48(2), p.468-479

SEASONAL STREAMFLOW FORECASTS BASED ON PHYSICAL-BASED MODEL FOR CHAO PHRAYA RIVER BASIN IN THAILAND

Wongnarin Kompor[1,a], Natsuki Yoshida[1,b], Sayaka Yoshikawa[1,c], Shinjiro Kanae[1,d]

Abstract Seasonal forecasts of river flow are crucial for river management in Thailand. The forecasted data can support a water manager to operate the reservoir more effective. The current status of seasonal climate forecast studies shows the evidence that the ability of a forecast will lower during the spring season (February to May), which called spring predictability barrier (SPB). However, there is still no evidence on how much of effect from lower forecast skill during spring in seasonal forecast data to seasonal streamflow forecast. Thus, this study aims to verify the effect of SPB on a streamflow forecast. This study presents the development of a seasonal streamflow forecast dealing with a physical model-based system to produce probabilistic seasonal streamflow forecasts in Chao Phraya river basin. The hydrological model, The H08 model, is forced with the observed meteorological dataset (1981-2004) to verify the model accuracy. The hindcast is simulated using the bias-corrected output of a seasonal rainfall forecast provided by the previousstudy.The current study, the ability to forecast is compared with observed river discharge and simulated river discharge from the H08 model. Last, we verify the accuracy of seasonal streamflow forecast due to the effect of SPB. Overall, results show that the hindcast simulation in August and November have better agreement with observed river discharge and simulated river discharge than prediction during spring (February to May). The accuracy during the effect of SPB is dramatically dropping when compared to other period. This study recommends that the prediction during spring should be improved in the hydrological model and seasonal climate prediction.

Keywords *Seasonal Streamflow Forecasts, Spring Predictability Barrier, Seasonal Rainfall Forecasts, Hydrological Model*

[1]Department of civil engineering
Tokyo Institute of Technology
Tokyo, Japan

[a]kompor.w.aa@m.titech.ac.jp
[b]yoshida.n.al@m.titech.ac.jp.
[c]yoshikawa.s.ad@m.titech.ac.jp
[d]kanae@cv.titech.ac.jp

Introduction

A seasonal predictionis needed for effective water resource management such as flood protection and mitigation. At seasonal predictions scale (up to 6-monthlead-time) are beneficial to water management in terms of timely enough for reservoir operation. Water manager needs to make a decision on reservoir operation especially during the end of the dry season to wet season such as Chao Phraya River Basin (CPRB) that located in Thailand. However, there was an issue on the low accuracy of seasonal prediction for climate variables on spring, which is so-called "spring predictability barrier (SPB)", is identified critical issue for seasonal prediction in global scale [1].

Recent studies on streamflow forecast have the ability to forecast up to 6 to 7 month ahead [2]. The hydrological model is forcing with a range of probability in seasonal climate forecast which known as ensemble streamflow prediction (ESP) method. Previous studies have indicated that the accuracy of seasonal hydrological prediction was related to seasonal climate prediction data and watershed initial moisture condition [3] that lower skills in prediction.Wood et al. found that the largest predictability at seasonal scales are during winter where snowmelt raises soil moisture to generate runoff and streamflow is relatively slow. The smallest predictability found at the end of a climatologically dry period and preceding a wetter one that nearly all forecasts skill derives from the skill of seasonal climate prediction [4]. However, none of the previousstudies mention the effect of SPB on hydrological forecasts. The SPB defined as the low predictability during the spring (February to May). The cause of SPB has not yet been fully understood, and various hypotheses have been still discussed to explain this phenomenon [5]. In addition, during spring (February to May) is the initial prediction time before the wet season (such as Thailand) that could help water management be more effective.

Thus, the objective of this study aims toclarify the effect of SPB, which have the evidence in a global scale, to the predictability of river discharge in CPRB and evaluate the accuracy of seasonal streamflow forecasts on each initial prediction day.

Data and Methodology

A. Experiment setting

The process to study in this paper as followed

1) Simulate river discharge bythe hydrological model (the H08 model) using observed meteorological datafrom 1981 to 2004
2) Downscale seasonal rainfall prediction (Preprocessing).
3) Simulate river discharge by the H08 model using downscale seasonal rainfall prediction from 1982 to 2004
4) The river discharge results from step 3 were bias-corrected with observed river discharge (Post processing)
5) The river discharge results from step 1, step 3 and step 4 were compared with observed river discharge.

B. Study Area

CPRB (Fig.1), which red color indicates the high elevation and green color indicates the low elevation, is located in Thailand with a large area about 158,000 km² (30% of land area). CPRB can divide into two parts 1) Upper part and 2) Lower part. Lower part starts from NakornSawan. The lower part of CPRB flows through the central plain from NakornSawan passing Bangkok toward the Gulf of Thailand. There are two large-scale reservoirs affect to CPRB 1) Bhumibol reservoir located in Ping river and 2) Sirikit reservoir in Nan river. The observation point to represent the runoff for CPRB located in NakhonSawan city, hereafter C2 point.Fig.2 shows river discharge and rainfall in CPRB.The blue line shows the observed river discharge while the black line shows the observed river discharge excluded the effect of the reservoir, hereafter Naturalized observed river discharge. During May to October is a wet season and during November to April is dry season in this basin. The streamflow in CPRB mostlyaffected by rainfall during the wet season and like most river basin in Southeast Asia region that during winter season has no snow.

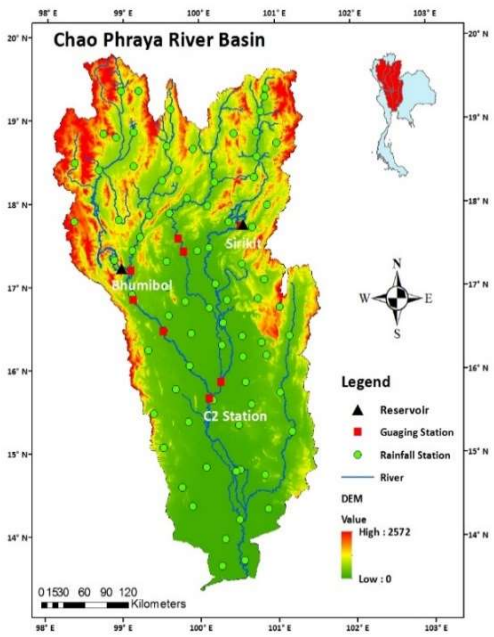

Fig. 1. CPRB and observation C2 point station

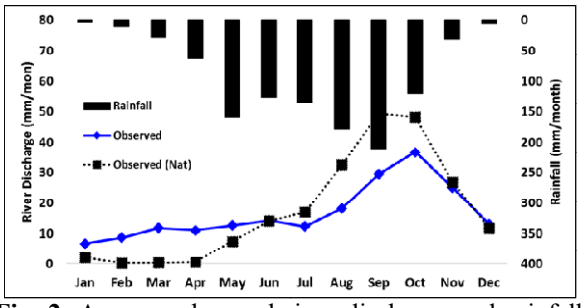

Fig. 2. Average observed river discharge and rainfall in CPRB

C. Hydrological model

A fully distributed model,the H08 model, have developed for well-organized in CPRB. Previous studies also have reproduced well in CPRB [6]. The detail of the H08 model, a distributed global water resource model, can follow in Hanasaki et al.(2008a) [7]. In this study, land surface and river modules from the H08 modelwere used. The setting of the land surface model (initial hydrological condition) and river model parameters in the H08 model followeda previous study [8]. The soil water balance was expressed as equation (1) as follow:Punctuate equations with commas or periods when they are part of a sentence, as in

$$\frac{dW}{dt} = Rainf + Q_{sm} - E - Q_s - Q_{sb} \qquad (1)$$

where W is soil water content, *Rainf* is the rainfall, Q_{sm} is the snowmelt rate, E is evaporation, Q_s is a surface runoff and Q_{sb} is the subsurface runoff. The total runoff (Q_{tot}) shown in equation (2) as follows:

$$Q_{tot}=Q_s+Q_{sb} \quad (2)$$

Where Q_s is the surface runoff generated when soil water content (W) exceeds the capacity of soil water (W_f=0.15×SD), where SD is soil depth, as shown in equation (3).

$$Q_{sb}=\frac{W_f}{\tau\times 86400}\left(\frac{W}{W_f}\right)^{\gamma} \quad (3)$$

where τ and γ are two shape parameters for subsurface flow generation.

H08 was run from 1981 to 2004 which runs on a domain from 97º E to 102º E and from 13º N to 20º N. There are two simulations were carried out in this study. First, the H08 model was forced by observed meteorological dataset for calibrate model. Furthermore, details, 1981 was simulated for a spin up the initial hydrological states such as soil moisture and discharge (exclude snow since no snow in this area). Second, theH08 model was driven by seasonal rainfall prediction to validate the prediction simulation. In prediction simulation, the H08 model was forced by observed meteorological data except for rainfall data while seasonal rainfall prediction used as input.

D. Data

The observation data used to compare the results of river discharge from the H08 model. There are two types of input data in this study 1) meteorological forcing data and 2) seasonal rainfall prediction. Meteorological forcing data used for calibrating the H08 model and bias-corrected prediction data. Seasonal rainfall prediction data used to validate the seasonal prediction.

1) Observed data

The observed rainfall data and observed river discharge data were used to compare the results from the H08 model in this study. Theobserved rainfall datafrom 1981 to 2004 in daily scale received from "Meteorological Department of Thailand" and "Royal Irrigation Department (RID)". The observed river discharge data at C2 station on monthly scale received from RID during 1981 to 2004. The naturalize observed river discharge (black dot line in Fig. 2) is the observed river discharge exclude the effect of the reservoir as followed from a previous study [7].

2) Meteorological forcing data

Kotsuki et al. provided a set of gridded meteorological data for CPRB, hereafter "K10" data, from 1981 to 2004 [9]. K10 is analyzed from ground observation, which ranges from 97º E to 102º E and from 13 º N to 20 º N that cover the CPRB's area. The spatial resolution of K10 data is 5 minute gridded (1/12 degree). K10 provided seven parameters as input data; 1) surface air temperature (K, 3-hourly), 2) specific humidity (kg/kg, daily), 3) surface air pressure (Pa, 3-hourly), 4) wind speed (m/s, hourly), 5) shortwave radiation (W/m², 3-hourly), 6) longwave radiation (W/m², 3-hourly), and 7) rainfall (kg/m²s¹, daily). The accuracy of rainfall from K10 data compared with ground observed station shows a good agreement in Fig. 3. However, rainfall from K10 trends to underestimate when compared with observed rainfall station that leads to underestimating in simulated river discharge when using K10 as input data.

3) Seasonal rainfall prediction

The seasonal rainfall prediction data from a previous study [10]were used in this study for two reasons. First reason, this seasonal data easy to access for utilizing. The second reason, they mentioned that their predicting system is less affected by SPB. Another reason is this seasonal rainfall prediction have been focusing on Thailand's meteorology. The available data period range from 1979 to 2011 but this study used 1982 to 2004 to simulate the river discharge from 1982 to 2004.

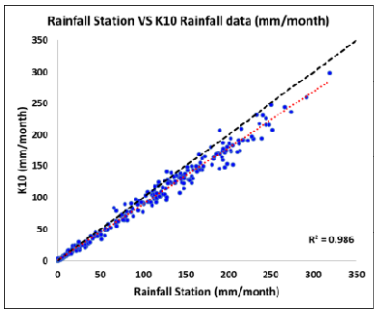

Fig. 3. Comparison between observed rainfall and K10 rainfall datain CPRB
The seasonal

The seasonal rainfall data provided in monthly time scale with four cases about an initial day on the 1st day for prediction, 1) February 2) May 3)August and 4) November. The ability for prediction is six months ahead. As for other seasonal prediction, this seasonal data studied based on ensemble prediction systemand provide an anomaly with a reference period between 1961 and 2000.The reason for making a prediction set (or ensemble) instead of producing a single prediction because this prediction set aims to give an indication of the range of possible future states of the atmosphere. The output from this study provided eight ensembles, which difference initial condition, rainfall data. The ensemble with the different initial condition can show the range of possibilities in prediction. In this study, a seasonal rainfall prediction in anomaly was combined with Asian Precipitation Highly Resolved Observational Data Integration Towards the Evaluation of Water Resource (APHRODITE) data [11] to generate total rainfall prediction data. Seasonal rainfall prediction data was regridded with spline interpolation from 1x1º latitude and longitude grid to a 5x5 minute grid resolution. Fig. 4 shows the accuracy of raw seasonal prediction data for each initial month.

Black lines show the accuracy of K10 data compared with the observed station in CPRB. Each initial month has six monthslead-time and eight-ensemble member. Overall,the accuracy of seasonal rainfall prediction is significantly lower especially during February as shown in Fig. 4a and Fig. 4d.

4) Preprocessing and postprocessing

Preprocessing and postprocessing are common in seasonal streamflow forecast, which discussed in the previous study, by taking bias correction technique to both meteorological seasonal forecasts in preprocessing and seasonal streamflow forecast in postprocessing process to remove the systematic bias of both hydrological model and climate variables [2]. This study was applied the simplest and most popular which called linear scaling method. The linear scaling method will be applied by a grid-to-grid monthly correction in this study. Linear scaling (LS), shown in equation (4), corrects the mean of the predictions based on the difference between observed (using K10 as reference data) and prediction means.

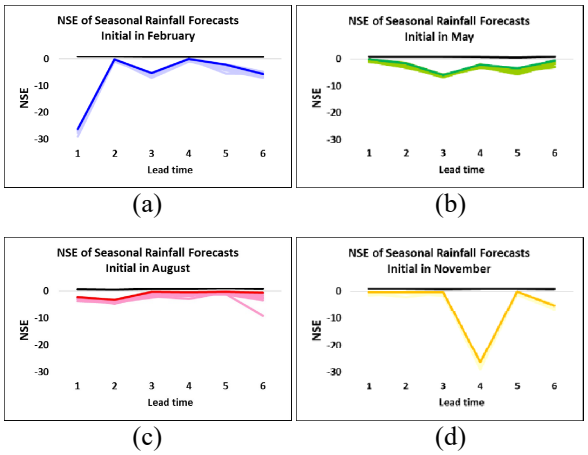

Fig. 4. The accuracy of raw seasonal rainfall prediction for each initial month (a) February (b) May (c) August and (d) November as initial month

$$P_{cor,d,i,j} = P_{sim,d,i,j} \times \frac{\sum_{j=1981}^{2004} P_{obs,d,i,j}}{\sum_{j=1981}^{2004} P_{sim,d,i,j}} \qquad (4)$$

where P_{cor} is bias-corrected rainfall prediction or river discharge, P_{sim} is rainfall prediction or simulated river discharge, P_{obs} is observed rainfall or river discharge, $i$is monthly for bias correction,j is year (1981 to 2004), and d is daily for each month.

Results and Discussion

A. Model calibration

H08 was driven by K10 data to simulated river discharge from 1981 to 2004. Fig. 5 shows the simulate river discharge results. The simulated results compared with observed river discharge and observed naturalize observed data (exclude the effect of the reservoir) at C2 station. From Fig. 5, the simulation (red line) and naturalize observed data (blue line) shows a good agreement with a high accuracy index (0.88 in NSE, 0.88 in R^2 and 4.79 mm/month in RMSE). Although, river discharge during wet season (peak) trends to underestimate with naturalizing observed data due to K10 rainfall data trends to underestimate the ground observed station. However, simulated river discharge is overestimated at some period such as 1994. The accuracy of each month simulation was discussed as shown in Fig. 6 (black line)

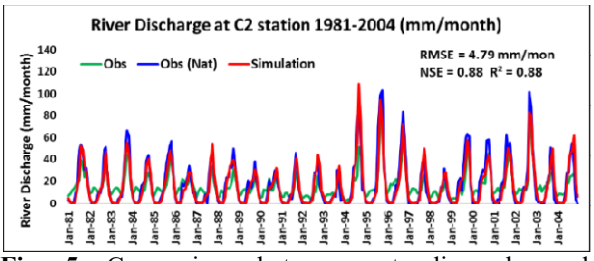

Fig. 5. Comparison between naturalize observed (blue), simulated river discharge (red) and observed river discharge (green) in monthly scale

B. Preprocessing

Bias correction by linear scaling used for remove systematic bias for seasonal rainfall prediction using K10 as reference data from 1981 to 2004. Fig. 6 shows the result of preprocessing for each initial month from first lead month until a seventh lead month.Overall predictability was improved after bias corrected seasonal rainfall prediction data especially February and November as an initial month. The smallest predictability on February (first lead month of the initial month in February and fourth lead month of the initial month in November) were improved the accuracy. The significant predictabilityis November and February as an initial prediction. The smallest predictability is May which beginning of the wetseason in Thailand. The accuracy of mean ensembles member trend to higher accuracy for first-month lead-time and slowlylower accuracy for longer lead-time except for initial month at August. The lower accuracy inAugust might come from difficulty in peak prediction on the wet season (normally August is the highest rainfall intensity in CPRB).

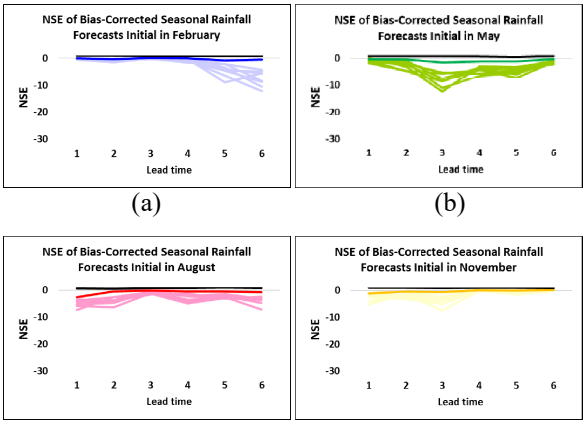

Fig. 6. The accuracy of bias-corrected seasonal rainfall prediction for each initial month (a) February (b) May (c) August and (d) November as initial month

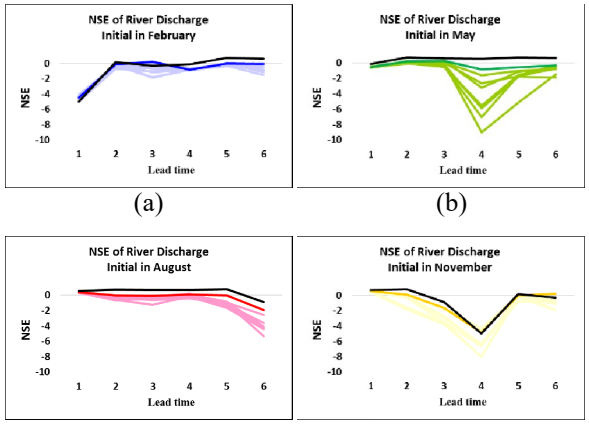

Fig. 7. The accuracy of river discharge prediction for each initial month (a) February (b) May (c) August and (d) November as initial month

C. River discharge prediction

After successfully bias correction of seasonal rainfall prediction in preprocessing section. The H08 model was simulated the river discharge by bias-corrected seasonal rainfall. The discharge by bias-corrected seasonal rainfall was compared the results with the gauge station at C2. Fig. 7 shows the accuracy ofriver discharge prediction.The black line shows the accuracy of river discharge simulation using K10 as input data.The results illustrate that the smallest accuracy is in February which both K10 and seasonal rainfall prediction as input data. The reason for low accuracy during February might come from the hydrological model. Soil moisture during January to April found to be low in a hydrologicalmodel that makes hydrological model hardly generate the runoff and streamflow in this case. The smallest predictability found in May as an initial month because seasonal rainfall prediction from Fig. 6 found lower in accuracy especially third-monthlead-time that lead to lower accuracy in fourth lead-month prediction in Fig. 7b. However, it is difficult to see how much difference between the accuracy of river discharge simulation using K10 as input data and seasonal rainfall data. Thus, Fig. 8 shows the difference NSE. Blue, green, red and yellow color indicates mean different the accuracy of river discharge between K10 and seasonal rainfall prediction as input data to The H08 model. Light color in Fig. 8 represents the difference accuracy of river discharge simulation for each ensemble member. The significant differencesfound in May as an initial month. This large difference generated from the low accuracy of seasonal rainfall prediction during peak period (August to September).

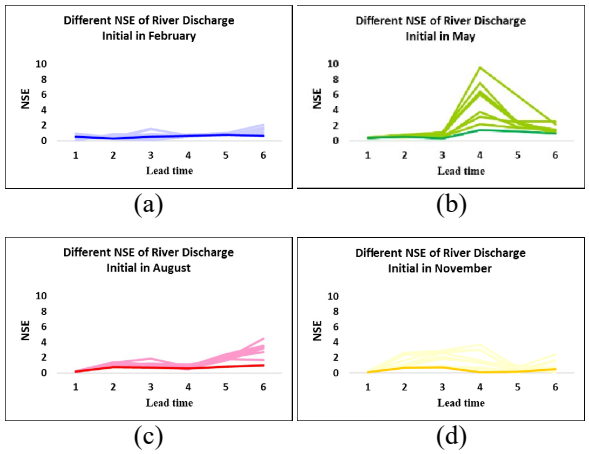

Fig. 8. Difference accuracy of river discharge prediction between K10 and seasonal rainfall prediction as input data to H08 mode for each initial month (a) February (b) May (c) August and (d) November as initial month

D. Postprocessing

River discharge simulation from the previous section was bias-corrected with observed river discharge in this section.Bias correction by linear scaling removes monthly discharge bias for C2 station. The results of river discharge simulation from postprocessing were shown in Fig. 9. Fig. 9 is the river discharge simulation from each initial month for prediction with 1 to 3 long lead-time. The accuracy of runoff prediction was indicated by r-coefficient, RMSE and NSE as shown in Fig. 9.The horizontal axis in Fig. 9 indicates the monthly time step of the results ranges from 1982 to 2004. The vertical axis indicates river discharge in mm/month unit. River discharge prediction for the next 1 to 3 months is more accuracy than river discharge prediction for the next 4 to 6 months. Overall accuracy performance shows an agreement. However, peak river discharge at some period (ex. 1995) was lower than observed river discharge. The overall accuracy of each initial month

for prediction shows in Fig. 10. Fig. 10 shows the accuracy using NSE as accuracy index. Blue, green, red and yellow color shows the accuracy of mean ensemble river discharge from eight ensembles. The results show that the overall accuracy increase after bias-corrected river discharge simulation especially the initial month for prediction at February and November.But the accuracy of May as initial month trends to increase at the 1st to 3rd lead-month before gradually lower the accuracy due to bias correction by linear scaling. The reason that the accuracy of May as an initial month on the 4th lead month drops was due to linear scaling method cannot remove bias for peak river discharge. In another word, linear scaling by remove bias using mean difference cannot remove bias for the peak. The most predictability found in August and November as the initial month that slowly lower accuracy when time pass. The output of each initial month illustrate in hydrograph is shown in Fig. 11. Initial month in each graph has a range only six months for each year such as Fig. 11a shows the output of river discharge from February to July range from 1982 to 2004, Fig. 11b shows the output of river discharge from May to October for each year. The most predictability is November as an initialmonth;second most predictability is August as an initial month while the less predictability is May as an initial month.

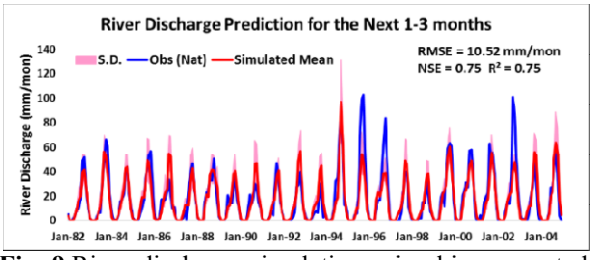

Fig. 9. River discharge simulation using bias-corrected rainfall prediction of 1 to 3 months lead time as input data from 1982 to 2004.

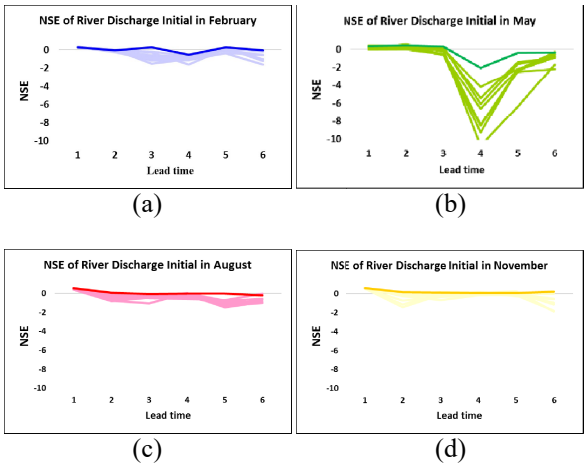

Fig. 10. The accuracy of river discharge simulation using bias-corrected rainfall as input after postprocessing (a) February (b) May (c) August and (d) November as an initial month for prediction

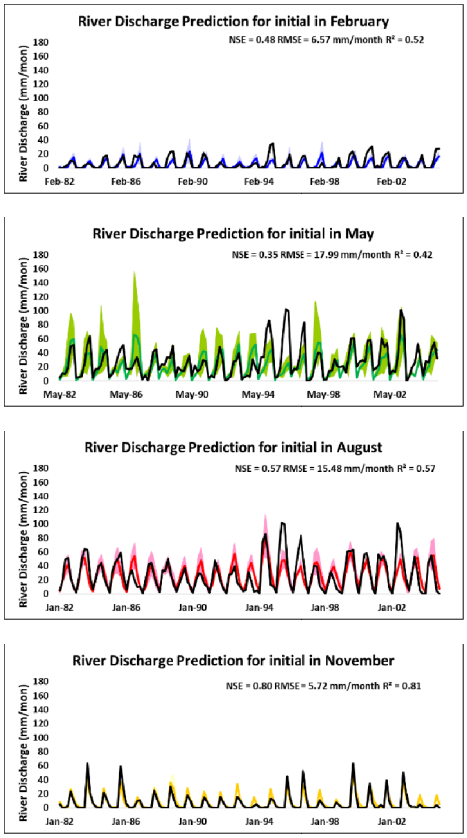

Fig. 11. River discharge simulation for each initial month

Conclusions

In this study, we found that river discharge prediction based on a hydrological model using bias-corrected seasonal rainfall prediction by linear scaling methodcan predict the monthly river discharge in CPRB with acceptable accuracy as r coefficient, RMSE and NSE index shown in Fig. 9. The results ofthe accuracy of the next 1 to 3 months in river discharge prediction were better in accuracy than river discharge prediction for the next 4 to 6 months. We found that the effect of SPB on rainfall prediction shows less predictability on May that effected on lower river discharge prediction skills during spring, which initial day for prediction is the first day of February and May. On the other hand, the river discharge prediction skills were shown better results for the initial day for prediction of first August and November due to rainfall prediction are better in accuracy. Thus, its conclusion that the river discharge prediction from the hydrological model for the initial day for prediction in August and November are better than prediction in February and May. We also found that bias between observed river discharge and simulated river discharge arise from the H08 model and rainfall prediction. Therefore, a study of prediction rainfall and SPB is important for river discharge prediction especially during the transitional time (end of dry season to wet season).Future study on rainfall prediction can be developed to compare the river

discharge prediction skills by current dynamical seasonal rainfall prediction. Together with the hydrological model developing and rainfall prediction will give a lot of benefit for water management in Thailand.

Appendix

Nash-Sutcliffe model efficiency coefficient (NSE) used to indicate the accuracy (predictive power) between observed data and simulated data of hydrological model. NSE can range from -∞ to 1 which an efficiency of 1 means perfect match between simulated discharge and observed data. NSE equals to 0 indicates that the model predictions are accurate as the mean of observed data where below 0 means the observed mean is better predictor than the model. The equation of NSE shows as equation (5).

$$NSE = 1 - \frac{\sum_{t=1}^{T}(Q_m^t - Q_o^t)^2}{\sum_{t=1}^{T}(Q_o^t - \overline{Q_o})^2} \quad (5)$$

where Q_m^t is model data, Q_o^t is observed data and $\overline{Q_o}$ is average value of observed data.

References

[1] Jin, E.K., Kinter, J.L., Wang, B., Park, C.K., Kang, I.S., Kirtman, B.P., Kug, J.S., Kumar, A., Luo, J.J., Schemm, J., Shukla, J., Yamagata, T.: Current Status of ENSO Prediction Skill in Coupled Ocean-Atmosphere Models. Clim. Dyn., Vol. 31, pp.647-664, 2008

[2] Greuell, W., Franssen, W., Biemans, H. and Hutjes, R. Seasonal streamflow forecasts for Europe – Part I: Hindcast verification with pseudo- and real observations. Hydrology and Earth System Sciences, 22(6), pp.3453-3472, 2018.

[3] Crochemore, L., Ramos, M., Pappenberger F.: Bias Correcting Precipitation Forecasts to Improve the Skill of Seasonal Streamflow Forecasts. Hydrol. Earth Syst. Sci., Vol. 20, pp.3601-3618, 2016

[4] Wood, A.W., Hopson, T., Newman, A., Brekke, L., Arnold, J., Clark, M.: Quantifying Streamflow Forecast Skill Elasticity to Initial Condition and Climate Prediction Skill. J Hy-drometeorol. Vol. 17, pp. 651-668, 2016

[5] Duan, W., Wei, C.: The 'Spring Predictability Barrier' for ENSO Predictions and its Possible Mechanism: Results from a Fully Coupled Model, *Int. J. Climatol.*, Vol. 33, pp.1280-1292, 2013

[6] Mateo, C., Hanasaki, N., Komori, D., Tanaka, K., Kiguchi, M., Champathong, A., Sukhapunnaphan, T., Yamazaki, D.,and Oki, T. Assessing the impacts of reservoir operation to floodplain inundation by combining hydrological, reservoir management, and hydrodynamic models. Water Resources Research, 50(9), pp.7245-7266, 2014.

[7] Hanasaki, N., Kanae, S., Oki, T., Masuda, K., Motoya, K., Shirakawa, N., Shen, Y., Tanaka, K.: An integrated model for the assessment of global water resources – Part 1: Model description and input meteorological forcing,Hydrol. Earth Syst. Sci., Vol. 12, pp. 1007–1025, 2008

[8] Hanasaki, N., Mateo, C., Saito., Y. : H08 Manual User's Edition Supplement 1: Regional Application -Case Study of the Chao Phraya River, 43 pp, National Institute for Environmental Studies, Tsukuba, Japan., 2012

[9] Kotsuki, S., Tanaka, K., Kojiri, T., Hamaguchi, T.: The water budget analysis with land surface model in Chao Phraya River basin, 23rd annual conference, JSHWR, pp. 44-45, 2010

[10] Imada, Y., Tatebe, H., Ishii, M., Chikamoto, Y., Mori, M., Arai, M., Watanabe, M., Kimoto, M. : Predictability of Two Types of El Niño Assessed Using an Extended Seasonal Prediction System by MIROC. Mon Weather Rev. Vol. 143, pp. 4597-4617, 2015

[11] Yatagai, A., Arakawa, O., Kamiguchi, K., Kawamoto, H. : A 44-Year Daily Gridded Precipitation Dataset for Asia. Sola. Vol. 5, pp. 3-6, 2009

CHARACTERISTICS OF GRIDDED RAINFALL DATA FOR THAILAND FROM 1981–2017

SHOJUN ARAI[1,a], KAZUYA URAYAMA[2,b], TAICHI TEBAKARI[2,c] and BOONLERT ARCHVARAHUPROK[3]

Abstract

We used a spatially interpolated gridded dataset produced by the Thai Meteorological Department (TMD) to explore long-term rainfall trends. We placed data from 1981–2017 into a 0.5° grid using the Kriging method. Long-term trends in maximum daily and monthly rainfall, and total annual rainfall, were analyzed using the nonparametric Mann–Kendall test. Chumphon, Lamphun, Nakhon, Sawan, and Buriram provinces exhibited significant positive trends in the annual maximum daily rainfall ($p<0.05$, $p<0.01$). The coastal area of Chachoengsao Province exhibited a significant negative trend ($p<0.05$). January rainfall showed a negative trend throughout Thailand. Annual rainfall showed a positive trend in many regions, especially in northern, northeastern, and southern areas. The eastern region exhibited a negative trend but statistical significance was not attained. The 10-, 30-, 50-, and 100-year daily rainfall probabilities were estimated using the Generalized Extreme Value method. The eastern side of the southern region exhibited remarkably high rainfall.

Keywords *Generalized extreme value distribution, Mann–Kendall test, rainfall, Thailand*

[1]Graduate school of Environmental Engineering
Toyama Prefectural University
Imizu, Toyama, Japan
[2]Department of Environmental and Civil Engineering
Toyama Prefectural University
Imizu, Toyama, Japan
[3]Thai Meteorological Department
Bangkok, Thailand

[a]t857001@st.pu-toyama.ac.jp
[b]t517009@st.pu-toyama.ac.jp
[c]tebakari@pu-toyama.ac.jp

Calibrating LAI Parameter with Remote Sensing Data for SIMRIW-RS in Thailand

Mongkol RAKSAPATCHARAWONG[1], Watcharee VEERAKACHEN[1], Peerapon PROMPITAKPORN[1], Chinnapoj WONGSRIPISANT[1], Koki HOMMA[2], Masayasu MAKI[3] and Kazuo OKI[4]

Abstract Rice is a major industrial crop in Thailand and has been cultivated country-wide. An ability to estimate rice production on a regional scale is therefore imperative for adaptation plan to climate change. For example, agricultural zoning can be adopted to optimize among locale characteristics, farmer practices, water resources, and expected yields. Recently, a crop simulation model called SIMRIW-RS has been validated for rice yield estimation, based on calibration of field parameter, namely accurate LAI values in early growing period. This paper presents a calibration of SIMRIW-RSand a methodology to incorporate remote sensing data products (NDVI and EVI2) into SIMRIW-RS by means of estimated LAI parameter. Based on data collected from rainfed paddy field in Nongchok District, Northeast-Bangkok during 2017-2018, our results show that the model calibrated with LAIestimated by NDVI can simulate LAI values for the entire crop with RMSE less than 1.0, and consequently achieve simulated yield with mean percentage error (MPE) around 2%. In addition, SIMRIW-RS also shows to be insensitive to pixel size when data from drone is upscaled to be ten times larger, which makes it compatible with medium- to high-resolution satellite images.This work concludes that SIMRIW-RS can be adapt to Thai rice, and NDVI product from remote sensing data in early stage can be used to provide field-to-field variations for SIMRIW-RS to work on a regional scale.

Keywords *crop simulation model; EVI2; LAI; NDVI; remote sensing, rice yield estimation*

[1]Chulabhorn Satellite Receiving Station,
Faculty of Engineering
Kasetsart University
Bangkok 10900, Thailand
[2]Graduate School of Agricultural Science
Tohoku University
Sendai, 981-8555, Japan
[3]Faculty of Engineering
Tohoku Institute of Technology
Sendai, 982-8577, Japan
[4]Institute of Industrial Science
The University of Tokyo
Tokyo, 153-8505, Japan

This work is supported by Japan International Cooperation Agency (JICA) under the Advancing co-design of integrated strategies with adaptation to climate change in Thailand (ADAP-T) Project.

Introduction

World's demand for rice in the last decade has been increasing [1], around 1.46% annually, from 447.2 million tons (MT) in 2009/10 to 509.5 MT in 2018/19. A study based on CERES Rice Model [2] reveals that climate change plays an important role on rice production; a deficit of precipitation 1 mm/day can reduce rice yield by 133kg/ha and a 1^{o}C of temperature rise can reduce the yield by 300kg/ha. These numbers may significantly affect Thailand as a world major rice production and exporter. According to the 1961–2015 World bank's historical data, Thailand's average precipitation and temperature changes in 2015 are –0.58 mm/day and 0.82^{o}C, respectively [3]. To put these numbers into perspective, average rice yield could be reduced by 12.75% [4].

Since rice is cultivated country-wide, occupying half of the arable areas at 9.2 million hectares and involving 16 million farmers [5], the Royal Thai government has put great efforts to stabilize the socioeconomic of rice production. Since the past, government subsidy in various forms (pricing subsidy is the most common) have been implemented but their effectiveness is still questionable. The government does not have good tools to facilitate their schemes, especially to report the current and expected status of paddy field and rice yield. Remote sensing techniques has been used to develop a rice acreage monitoring platform by GISTDA and is currently operational on a website http://rice.gistda.or.th/ricefield.This service updates the paddy field area of Thailand every two weeks; however, it does not provide rice yield information. Concurrently, the Office of Agricultural Economics (OAE) jointly developed a technique called "crop cutting" with Japan International Cooperation Agency (JICA)'s experts to estimate the yield from multiple sample plots. This data is used to estimate the total yield by multiplying it with the paddy field area estimated from remote sensing. While this technique can satisfy the need for yield information to be displayed on geographic information system (GIS), it is expensive and time-consuming to achieve good accuracy. Moreover, it can only "estimate" based on current data but cannot "predict" the yield in advance which is becoming more importance to deal with climate change impacts as well as rice production stability.

Crop simulation is a mathematical model used for studying crop growth and yield based on specific conditions defined by set of input scenarios. Typical inputs are climate data, crop data, soil data, and field and irrigation management data. By preparing future climate data as input, the model can predict crop growth and yield for a desired crop calendar in advance, hence, farmers can have valuable information for appropriate actions in response to climate change. Similarly, the government can have an overall picture of rice crop production to make decision and setup measures such that the adverse impacts are minimized. Wide range of crop simulation models are presently available, DSSAT [6] is among the famous ones that requires many input parameters while CropSyst, WOFOST, and SPAC are reported to be rather complicated for end users [7]. AquaCrop [8], developed by the Food and Agriculture Organization (FAO), is considered more user-friendly in terms of input requirements and simulation settings. The model has been successfully tested and widely adopted for major crops in many countries [9,10]. Since AquaCrop does not support direct inputs from remote sensing products, its usage is limited to farm-scale where a set of input parameters represents a homogeneous farmland. Recent study in Thailand [11] shows how AquaCrop can take canopy cover (CC) as an input derived from NDVI product based on HJ-1A/B satellite images, achieving simulated yield with R^2=0.88. This promising result suggests that a combination of crop model and remote sensing products can be used to evaluate rice production in a regional scale. However, its calibration process requires significant amount of 28 satellite images which may not be practical for model deployment in different regions.

SIMRIW-RS [12] is a rice crop simulation model that incorporates weather data, farm management, field parameters, cultivar parameters, while utilizing remote sensing information to optimize the model parameters. The authors mentioned that the Leaf Area Index (LAI) and LAI growth rate values correspond to soil fertility and water stress of the field. The model can calculate LAI values, establish a soil fertility map, and simulate rice growth and productions, even though climate data and farming management information (e.g., fertilizer, cultivar, and plating date) are not entirely available. However, at least 2 calibrations at early growing periods, with an estimated LAI from remote sensing data are required [13] to achieve good accuracy. If applied to a similar group of paddy fields in the same periods, SIMRIW-RS may require minimal remote sensing satellite images for calibration and, thus, is more practical to put into operations. On the other hand, it is also applicable for "big farm strategy" where remote sensing data from drone is possible.

This work presents a calibration procedure for SIMRIW-RS based on actual LAI from an experimental field in Bangkok and estimated LAI from multispectral images from drone. Our results show that SIMRIW-RS can achieve simulated LAI with RMSE at 0.95 and simulated yield with mean percentage error (MPE) at –2.07%. The rest of the paper is organized as follow. Section 2 elaborates material and methods. Section 3 provides results and discussion. Section 4 concludes this work.

Material and Method

A. Experimental Field

The experimental field is a 6.88-hectare paddy field located at Nongchok district in Bangkok (13.936121,100.86953). The rice cultivar is RD–41 (100–day cycle) and RD–57 (110–day cycle). Fifty sample plots ($1x1m^2$) were selected throughout the field (evenly distributed by the field periphery as shown in Fig.1) for ground data collections including LAI, aboveground biomass, and multispectral image from drone. Table 1 shows field survey schedules in 2017 and 2018. Equipment used in this study is GPS Garmin Colorado 300, LAI-2200 Plant Canopy Analyzer, DJI Phantom 3 advanced with Parrot Sequoia multispectral camera, and a grain moisture meter.

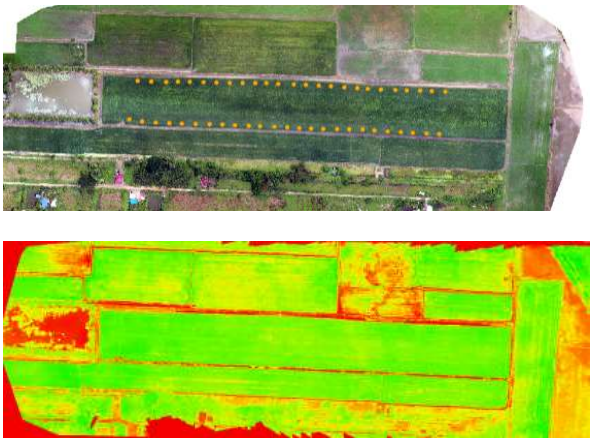

Fig. 1. The experimental field (upper) Orthorectified image and sample plot locations shown in orange dots, (lower) NDVI product (values increase from red to green colors)

Table 1. Field survey dates and average lai values

No.	2017			2018		
	Date	*DAP*[a]	*Average LAI*	*Date*	*DAP*	*Average LAI*
1	01/06	37	2.78	16/05	21	0.83
2	09/06	45	4.06	30/05	35	2.79
3	16/06	52	4.47	07/06	43	3.94
4	23/06	59	4.58	20/06	56	4.54
5	30/06	66	6.00	29/06	65	4.67
6	07/07	73	6.42	09/07	75	4.70
7	27/07	93	3.41	01/08	98	4.36
8	01/08	98	–			–

[a]DAP stands for Day After Planting

B. Field Data

- Leaf Area Index (LAI) is defined as one-sided green leaf area per unit ground surface area. It is used to characterize plant canopies. SIMWIW-RS calculates this value based on its initial value of field and cultivar parameters. It then simulates the aboveground dry matter and the yield based on this simulated LAI. Calibration of this value with actual LAI from the field can help optimizing the model's parameters and improve its accuracy. This study collected LAI values from 50 plots for the entire crop season in year 2017 and 2018. Actual LAI values are averaged to indicate therice growing periodand is shown as average LAI in Table 1.
- Normalized Difference Vegetation Index (NDVI) and 2-band Enhanced Vegetation Index (EVI2) are typical data products from remote sensing data. NDVI is used to identify vegetation and its condition of the area and is defined as

$$NDVI = \frac{NIR - Red}{NIR + Red} \quad (1)$$

where NIR and Red are the spectral reflectance measurements in the red (visible) and near-infrared bands, respectively. The possible values are in ±1 interval. Highervalues indicate better vegetation conditions in the vegetative regions.

- EVI2 is a variation of EVI when the blue band is not available. It is designed to enhance vegetation signal sensitivity in high biomass area and is more responsive to canopy variations than NDVI. It is defined as

$$EVI2 = 2.5 * \frac{NIR - Red}{NIR + 2.4 * Red + 1} \quad (2)$$

To apply SIMRIW-RS at regional scale while retaining field-to-field variation, remote sensing data can be used in lieu of actual LAI for model calibration.The calibration using Normalized Backscattering Coefficient from COSMO-SkyMed (SAR) data to estimate LAI values was proposed in [13] and successfully achieved simulated yield at 3.5% error in Vientiane, Laos PDR. Similarly, this work attempts to find the relationship between NDVI/EVI2 versus actual LAI values and evaluates if both remote sensing data products can be used to estimate LAI for model calibration. Actual LAI values in 2018 were used for regression whereas LAI values in 2017 were used for performance evaluation. On each field survey, remote sensing data were collected using Parrot Sequoia multispectral and CCD cameras installed on DJI Phantom 3 advanced with 10cm ground sample distance (GSD) or 10cm/pixel. Therefore, each plot contains 10x10 pixels, its corresponding NDVI/EVI2 indices are an average value from 100 pixels in the plot.

Fig. 2. Field survey activities.

- Weather data are mandatory inputs for SIMRIW-RS to calculate relevant parameters and to simulate rice growth conditions. A nearby weather station transfer data automatically to our server at Chulabhorn Satellite Receiving Station (CSRS). Received data are processed into a daily data format, which are accumulated rainfall (mm/day), average temperature (Celsius/day), daytime (hours/day), and solar radiation (W/m^2/day).
- Yield data were collected on each plot for a total of 50 plots by reaping the rice plant within circular area of 1m^2, threshing rice and carefully separating the grain, drying the grain by sunlight until its moisture content is < 20%, and weighting the grain and stump and finally record the values.

C. Experimental Setup

There are two issues to be investigated in this work, to find a suitable growing period to estimate LAI values from EVI2/NDVI for model calibration; and to evaluate the effects of resizing data pixel from 10x10cm^2 to 1x1m^2. The latter is to understand the results when satellite data is to be applied to the model in the future. As mentioned in [13], at least two calibrations of LAI in early growing period are essential to achieve accurate simulated LAI and yield from SIMWIR-RS. Therefore, the experimental steps are designed as follow.

- In response to early growing period criteria, only data from the 1st, 2nd, and 3rd field surveys were used to find relationship between actual LAI and EVI2/NDVI from drone images. The regression performance is evaluated in terms of RMSE on another data sets.
- Use the regression formulas and NDVI/EVI2 products to estimate LAI values to calibrate SIMRIW-RS, based on the following timing strategies. Method I: use NDVI/EVI2 from the 1st and 2nd field surveys, Method II: use NDVI/EVI2 from the 2nd and 3rd field

surveys, and Method III: use NDVI/EVI2 from the 1st and 3rd field surveys.

- Let SIMRIW-RS generate simulated LAI and simulated yield and evaluate RMSE of the simulated LAI with the 4th, 5th, and 6th field survey and evaluate MPE of the simulated yield with the actual yield.
- Determine which method performs the best in terms of RMSE and MPE indices.
- Resizing pixel size from 10x10cm^2 to 1x1m^{2}using standard software and repeat the experiment steps.

Results and Discussion

A. Estimating LAI from Remote Sensing Data

Field data collected in 2018were used for regression between actual LAI values and NDVI/EVI2 products. Both linear and nonlinear regressions were performed to maximize a coefficient of determination, R^2, and were compared based on RMSE evaluated by data collected in 2017. Figure 3 clearly states that nonlinear regressions outperform linear regressions for both indices. Especially for NDVI, R^2 value from exponential regression improves significantly (R^2=0.8923) because NDVI tends to saturate at LAI value greater than 3.0. We estimated LAI using EVI2/NDVI from field data collected in 2017, and calculated RMSE based on actual LAI for performance comparison purpose. Table 2 summarizes regression characteristics and RMSE performance. Linear regressions were chosen as they provide lower RMSE.

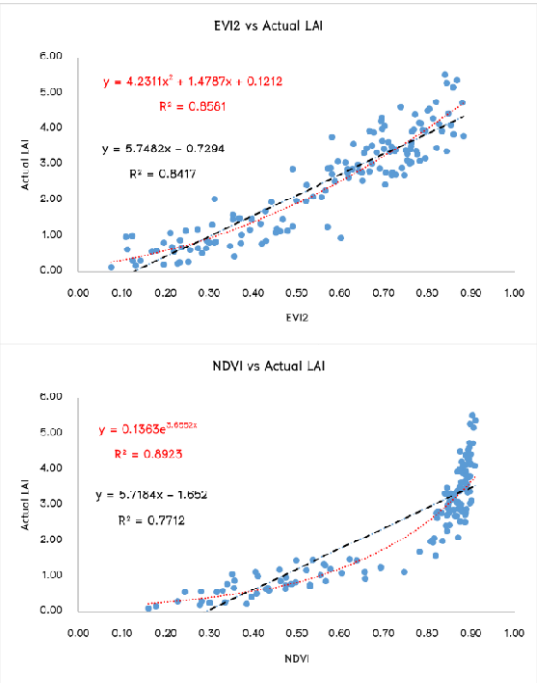

Fig. 3. Linear and nonlinear regressions between (top) actual LAI versus EVI2 and (bottom) actual LAI versus NDVI at early growing stage.

Table 2. Performance comparison between linear and nonlinear regressions based on EVI2/NDVI products

	Linear Regression	Nonlinear Regression
EVI2	$LAI = 5.7482 * EVI2 - 0.7294$ $R^2 = 0.8417, RMSE = 1.205$	$LAI = 4.2311 * EVI2^2 + 1.4787 * EVI2 + 0.8581$ $R^2 = 0.8581, RMSE = 1.276$
NDVI	$LAI = 5.7184 * NDVI - 1.652$ $R^2 = 0.7712, RMSE = 1.376$	$LAI = 0.1363 * e^{3.6552*NDVI}$ $R^2 = 0.8923, RMSE = 1.587$

B. Evaluating Rice Growing Period for SIMRIW-RS Calibration

To achieve good simulation results, SIMRIW-RS shall be calibrated with LAI values from the field or from remote sensing data in early growing period. Previous discussion has shown how to estimate LAI from EVI2/NDVI products. Here, we investigate the growing period that determines suitable times to estimate LAI values. It is worth noting that, from this point on, only field survey data in 2017 were used because its corresponding yield data was ready. Method–I, –II, and –III correspond to DAP equals to 37/45 days, 45/52 days, and 37/52 days, respectively. For a given method, LAI is estimated by EVI2 and NDVI products as inputs to SIMRIW-RS to simulate LAI and finally the rice yield values. Since each pixel is 10x10cm^2, all the values of 100 pixels are average on each plot for a total of 50 plots. The RMSE of simulated LAI compared to actual LAIfor all methods, at later growing period—59/66/73 days, are stacked up as shown in **Error! Reference source not found.**. Both EVI2 and NDVI calibrations exhibit similar RMSE pattern but NDVI, particularly based on Method–I, seems to achieve lower RMSE on most plots. Similarly, NDVI with Method–I show the lowest MPE for simulated yields. These performance indices are summarized in **Error! Reference source not found.**. (Best results are shown in bold.) Method–Ithat uses 37/45 days estimation of LAI are recommended because they represent low dispersion region of the trend lines (actual LAI is less than 2.0) as shown in **Error! Reference source not found.**. By the same token, Method–III is too late to provide good estimation of LAI at 52 days.

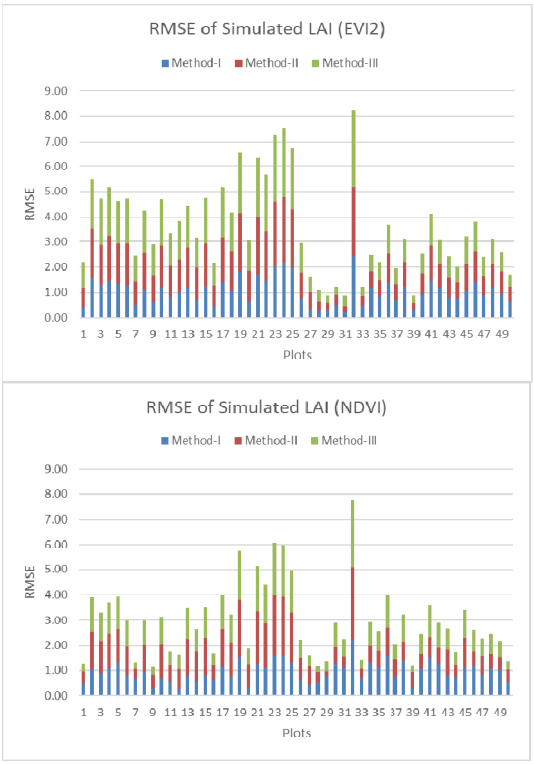

Fig. 4. RMSE of simulated LAI, calibrated with (top) EVI2 and (bottom) NDVI.

C. Resizing pixel size of drone image

To apply SIMRIW-RS in a reginal scale, remote sensing from satellite is inevitable. While coverage is key advantage to satellite image, spatial resolution is its drawback especially for a sub-meter images because they are expensive and scarce. Nevertheless, satellite data resources at resolution 5–10 meters are becoming mainstream and some are freely available (such as data from CBERS–04 and Sentinel–2 satellites). As a result, we aim to quantify how SIMRIW-RS responses to medium- to high-resolution satellite images. By upscaling the pixel size hundred times larger (at 1x1m^2) and repeating the experiment. The results are shown in **Error! Reference source not found.** and the difference is shown to be minimal. While Method–III exhibits lowest difference, it is not a choice. Method–I based on NDVI calibration is achieving the lowest RMSE and MPE at 0.93 and –2.25, respectively.

Table 3 Performance of EVI2 and NDVI calibrations on simulated LAI and simulated yield.

Product	Mode	Method	Pixel Sizes		Diff.
			10x10cm^2	*1x1m^2*	
EVI2	RMSE (LAI)	I	1.06	1.05	0.02
		II	1.22	1.26	–0.03
		III	1.29	1.30	–0.01
	MPE (Yield)	I	–6.17	–7.31	1.14
		II	–10.27	–11.55	1.27
		III	–11.52	–12.26	0.74
NDVI	RMSE (LAI)	I	***0.95***	***0.93***	0.02
		II	1.04	1.05	0.00
		III	0.97	0.96	0.01
	MPE (Yield)	I	***–2.07***	***–2.25***	0.18
		II	–9.68	–9.92	0.23
		III	–6.32	–6.32	0.00

Conclusions

In this study, the calibration procedure of SIMRIW-RS using field data and images from drone are investigated in Thailand. SIMRIW-RS can simulate rice growth and yield based on soil fertility in terms of simulated LAI values. However, the simulated values based on initial conditions may not reflect field-to-field variations correctly, so it needs calibration from external sources. Remote sensing data products, EVI2 and LAI, are shown to have a good relationship with actual LAI from the field with R^2 = 0.8417 and 0.7712. Our study shows that we can use them to estimate LAI values to calibrate SIMRIW-RS at early growing period (37/45 days) which NDVI is superior in terms of RMSE (for simulated LAI) and MPE (for simulated yield) at 0.95 and –2.07, respectively. As remote sensing data form satellite will enable SIMRIW-RS to apply on a regional scale, we therefore repeat the experiment on upscaled data pixels (ten times larger) and still obtaining very similar results. We conclude that SIMRIW-RS is potentially compatible with commonly available satellite data and our further performance investigation is underway.

Acknowledgment

This research was supported by "Advancing Co-design of Integrated Strategies with Adaptation to Climate Change in Thailand (ADAP-T)" supported by the Science and Technology Research Partnership for Sustainable Development (SATREPS), JST-JICA. The authors thank ADAP-T office for their long-term support on the LAI-2200 Plant Canopy Analyzer. The assistance from local farmers is also appreciated. Finally, the data processing done by GIS staffs at CSRS is well received. Their perseverance is truly an asset.

References

[1] FAO Departments and Offices, "World Food Situation," Food and Agriculture Organization, 5 July 2018. [Online]. Available: http://www.fao.org/worldfoodsituation/csdb/en/. [Accessed 21 August 2018].

[2] S. A. Saseendran, K. Singh, L. S. Rathore, S. V. Singh and S. K. Sinha, "Effects of Climate Change on Rice Production in the Tropical Humid Climate of Kerala, India," Climatic Change, no. 44, pp. 495-514, 2000.

[3] "Climate Change Knowledge Portal for Development Practitioners and Policy Makers," The World Bank Group, [Online]. Available: http://sdwebx.worldbank.org/climateportal/index.cfm?page=downscaled_data_download&menu=historical [Accessed on 15 October 2018].

[4] USDA Foreign Agricultural Services, "Thailand Grain and Feed Annual 2017," U.S. Department of Agriculture,15 March 2017. [Online], Available: https://gain.fas.usda.gov/Recent%20GAIN%20Publications/Grain%20and%20Feed%20Annual_Bangkok_Thailand_3-16-2017.pdf [Accessed on 15 October 2018].

[5] "The Rice Mountain". The Economist. 2013-08-10. Retrieved on 30 September 2016.

[6] M. Dias, C. Navaratne, K. Weerasinghe, R. Hettiarachchib, "Application of DSSAT crop simulation model to identify the changes of rice growth and yield in Nilwala river basin for mid-centuries under changing climatic conditions," Procedia Food Sci., no. 6, pp. 159–163, 2016.

[7] Zhang, W.; Liu, W.; Xue, Q.; Chen, J.; Han, X. Evaluation of the AquaCrop model for Simulation Yield Response of winter Wheat toWater on the Southern Loess Plateau of China. In Water Science & Technology; IWA Publishing: London, UK, 2013; p. 822.

[8] "AquaCrop," Food and Agriculture Organization,[Online]. Available: http://www.fao.org/aquacrop. [Accessed 21 August 2018].

[9] Rallo, Giovanni & Agnese, Carmelo & Mario, Minacapilli & Provenzano, Giuseppe, "Assessing AQUACROP water atress function to evaluate the transpiration reductions of olive mature tree," Italian Journal of Agrometeorology. no. 17, pp. 21-28, 2012.

[10] GE Greaves, Y-M. Wang,"Assessment of FAO AquaCrop Model for Simulating Maize Growth and Productivity under Deficit Irrigation in a Tropical Environment," Water.,no. 8(12):557, 2016.

[11] K. Prathumchai, M. Nagai, NK. Tripathi, N. Sasaki, "Forecasting Transplanted Rice Yield at the Farm Scale Using Moderate-Resolution Satellite Imagery and the AquaCrop Model: A Case Study of a Rice Seed Production Community in Thailand," ISPRS International Journal of Geo-Information, no. 7(2):73, 2018.

[12] K. Homma, M. Maki and Y. Hirooka, "Development of a rice simulation model for remote sensing (SIMRIW-RS)," Journal of Agricultural and Meteorology, no. 73(1), pp. 9-15, 2017.

[13] M. Maki, K. Sekiguchi, K. Homma, Y. Hirooka, K. Oki, "Estimation of rice yield by SIMRIW-RS, a model that integrates remote sensing data into a crop growth model," Journal of Agricultural Meteorology, no. 73(1), pp. 2-8, 2017.

Implementation of Nays2DFlood Modeling for Integrated Floodplain/StromwaterManagement : Case Study in Sukhumvit Area, Bangkok, Thailand

Sanit Wongsa[1,a,*], Napaporn Piamsa-nga[2,b], Varameth Vichiensan[3,c] and Shinichiro Nakamura[4,d]

Abstract Flooding in urban areas is an inevitable problem for many cities in the world. In Thailand, Bangkok has serious problems related to urban flooding. The situation was highlighted in October 2018, when residences experienced ankle to knee-deep flood water on the streets. Daily activities in parts of the city were nearly paralyzed and heavy traffic jams occurred due to stagnant water on the streets. The study has depended on a combined approach of physically based modeling and GIS. The architecture of the software consists of 3 functions: pre-processor, post-processor, and solver. Nays2DFlood is a flood flow analysis solver that relies on unsteady 2-dimensional plane flow simulation using boundary-fitted coordinates1 as the general curvilinear coordinates. The urban drainage is structured by Nays2DFlood software for the basis of two networks, one simulating the two-dimension free-surface flow over the streets and one for the pumping/canal/pipe system. The interaction between street and pumping/canal/pipe system is modeled in a simple way. In 2017, ADAP-T project carried out a pilot study about urban flooding and adaptation modeling for Sukhumvit area, Bangkok Metropolitan. This study is performed as an extension and improvement of pilot study in terms of analyzing drainage system on effect of flood hazard, vulnerability, risk map and adaptation under the issue of climate change in Sukhumvit area, Bangkok, together with suggestion of alleviation scenarios to relieve flood problems.

Keywords *urban flooding; climate change adaptation, iRIC software*

[1]Dept. Civil Technology Education, FIET
King Mongkut's University of Technology Thonburi
Bangkok, Thailand
[2]Dept. Water Resources Engineering
Kasetsart University
Bangkok, Thailand
[3]Dept. Civil Engineering
Kasetsart University
Bangkok, Thailand
[4]Dept. Civil Engineering
Nagoya University
Nagoya, Japan

[a]sanit.won@kmutt.ac.th
[b]fengnpr@ku.ac.th
[c]fengvmv@ku.ac.th
[d]shinichiro@civil.nagoya-u.ac.jp

Introduction

Bangkok Metropolitan Administration (BMA) has experienced water logging for the last few years. Even a little rain may cause severe problems for certain city areas, which are inundated for several days. The water depth in some areas may be as much as 20-50 cm, which creates large infrastructure problems for the city and huge economical losses in production together with large damages of existing traffic system, infrastructures, properties and goods. The BMA is protected from river flooding by an encircling embankment. Most of the time during the monsoon season, the water level in the Chao Phraya River remains about 2-3 m higher than the water level inside the city area, consequently the city drainage depends very much on the water levels of the peripheral river systems. The situation becomes worse when monsoon runoff generated from short duration and high intensity rainfall combines with high water level in river system. The main causes of floods in BMA can be classified into two types. The first one results from high water level of Chao Phraya River, canals system and the other caused by heavy rainfall. Thailand Great Flood in 2011 were caused by 5 tropical storms, resulting heavy rainfall occurred in upper and mid-Chao Phraya River Basin and the built-up areas of the city. The severe water logging in October 23, 2018 was originated from local high intensity rainfall, insufficient drainage capacity and garbage clogged the drainage system (*Fig. 1*)

Fig. 1. Flooded in Bangkok: originated from local high intensity rainfall. (https://www.google.com/search?q=ขยะน้ำท่วมกรุงเทพ).

Description of the System

The BMA has been struggling to divert floodwater out of the city because its water drainage system was developed mainly for handling localised flooding caused by heavy rainfall, not massive flood water from the upstream areas.

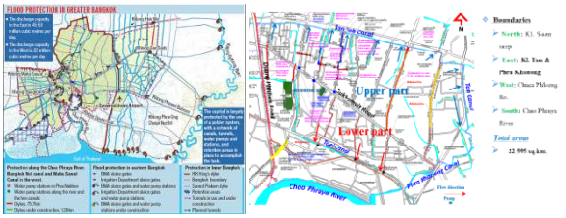

Fig. 2. Bangkok's and Area-13 water drainage system (Department of Drainage and Sewerage: DDS).

BMA invested heavily in its water drainage infrastructure after 1983 when major flooded hit the city. Since then, canals and tunnels have been dug, retention ponds designated, and pump stations constructed to help drain the flood water. The water drainage system is based on a polder system, where dykes are built around the city, and floodwaters are directed to the sea by pumps, water drainage canals and tunnels (*Fig. 2*). Polder systems have been developed mainly in inner Bangkok, the western side of the city, and the eastern side. In inner Bangkok, a large polder has major roads and railways cutting through the Ramkhamhaeng and Phetchaburi areas, acting as its main dykes. The polder is divided into more than 20 sub-polders where drainage canals and tunnels and pumps help drain water out from the protected areas inside them. On the eastern side, His Majesty the King's dyke (RAMA IX), which runs north to south, and around 20 retention ponds help retain up to 6 MCM of flood water before it is pumped out and drained to the sea at the Gulf of Thailand. Giant tunnels have also been installed to help speed drainage. The western side has a network of dykes along the Chao Phraya, Mahasawas and Bangkok Noi canals preventing flooding from flowing into the protected areas inside the dykes. This study focus on water management in Area-13 (Sukhumvit-North sub-polder), which includes the most important commercial areas of BMA, hence most of areas are impervious. Collected storm water from each sub-catchment is drained by sewer pipes/canals to SaenSaep, Ton and PhraKanong canals and finally it is drained to main river system by pumps and canals at the basin in front of the sluice gate.

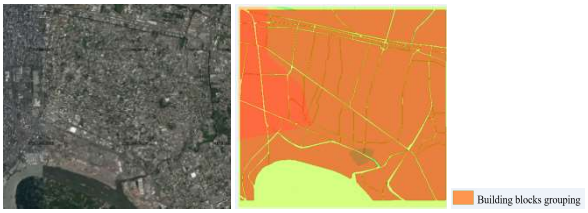

Fig. 3. DEM with canals, roads and sewer system in Area-13 (Sukhumvit-North sub-polder).

DEM represents land elevation data, which are crucial for estimating storage volume of surface flooding. In addition, result presentation in form of flood inundation map are performed based on application of iRIC Software, ArcGIS and Google Earth. Hence, the quality of the output depends on the quality of the DEM. Available DEM from pilot project was 30 m resolution from Land Development Department (LDD), which is too rough for urban flooding analysis as the dimension of typical features in the city are around 5-20 m. By using DEM 30 m resolution, which cannot cover significant details in study area, it may lead to inaccurate results. Establishing new DEM with the resolution of 5 m, which yield sufficient accuracy is performed based on the application of iRIC software. For simulating real-life situation of urban flooding, the major canals, roads, pumps and sewer system where floods occur are included in the DEM (*Fig. 3*).

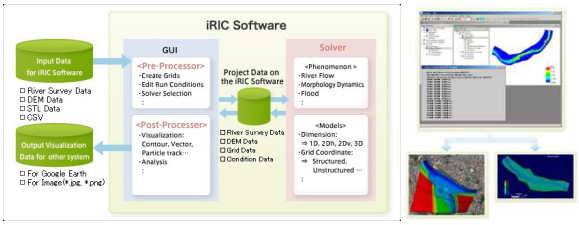

Fig. 4. The architecture of aiRIC software (http://i-ric.org/en/).

iRIC Software and Model Setup

A. iRIC Software

The iRIC software is public domain interface for calculating flow, sediment transport and morphodynamics in rivers and other geophysical flows. This interface is completely free to any users and includes 13 models ranging from simple one-dimensional models through three-dimensional models. The Nays2DFlood, which is one of the models enclosed in the iRIC system, is a flood flow solver developed by iRIC [1]. Tools for creating these systems are supplied in iRIC webpage [2], [3]. This model can be used in a general, non-orthogonal coordinate system with adaptable grid. The architecture of aiRIC software consists of 3 functions: pre-processor, post-processor, and solver. (*Fig. 4*). Pre-processor is for creating calculation lattices and setting calculation conditions, hydrologic conditions,

calculation methods. Calculation lattices can be created from survey data such as river survey data and DEM data. Post-processor is for visualization and analysis of calculation results. Visualization of calculation results can be used for purposes such as creation of vector, contour, and other diagrams, as well as creation of graphs. Nays2DFlood is a flood flow analysis solver that relies on unsteady 2-dimensional plane flow simulation using boundary-fitted coordinates1 as the general curvilinear coordinates.

The model employs time stepping with a choice of differencing schemes for advection of momentum, including the upwind scheme and the CIP (Cubic Interpolated Pseudo-Particle) scheme [4]. The water surface elevation is calculated using a successive relaxation technique. In order to consider the effects of roads and buildings on flood analysis, the governing equations of previous Nays2DFlood have been modified to express effects of obstructions by building and road against two-dimensional water flow. In numerical model, the governing equations for a two-dimensional plane flow field are written in a general, non-orthogonal coordinate system. However, we can rewrite the continuity and *x*-*y* momentum equations here in an orthogonal coordinate system for simplicity, and can be written as following [5], [6],

$$\frac{\partial h}{\partial t} + \frac{\partial \gamma_x hu}{\partial x} + \frac{\partial \gamma_y hv}{\partial y} = q_{in/out} \quad (1)$$

$$\gamma_v \frac{\partial uh}{\partial t} + \frac{\partial \gamma_x hu^2}{\partial x} + \frac{\partial \gamma_y huv}{\partial y} = -\gamma_v hg \frac{\partial H}{\partial x} - \frac{\tau_x}{\rho} - hR_x \quad (2)$$

$$\gamma_v \frac{\partial vh}{\partial t} + \frac{\partial \gamma_x hu}{\partial x} + \frac{\partial \gamma_y hv^2}{\partial y} = -\gamma_v hg \frac{\partial H}{\partial y} - \frac{\tau_y}{\rho} - hR_y \quad (3)$$

where, h is water depth, u and v are velocities, g is gravitational acceleration, H is water level, $q_{in/out}$ is the rate of water entering or leaving ground surface per unit area, including the excess rainfall, the upstream catchments inflows, the influent and effluent of sewer networks, and the overland flow drained by hydraulic facilities, τ_x and τ_y are bed shear stress, ρ is water density, *x*, *y* and *t* are direction and time, respectively. A building might occupy a significant, but not full, area within a computational grid, which has similar or slightly higher size than the building scale. Neither the ground elevation nor the roof elevation is appropriate to interpret the condition. γ_x, γ_y and γ_v are the parameters for indicative of the effects of buildings against two-dimensional flow, which can be expressed as following,

$$\frac{\tau_x}{\rho} = c_f u\sqrt{u^2 + v^2} \quad (4)$$

$$\frac{\tau_y}{\rho} = c_f v\sqrt{u^2 + v^2} \quad (5)$$

$$hR_x = \frac{h}{2} C_d{}'(1 - \gamma_x) u\sqrt{u^2 + v^2} \quad (6)$$

$$hR_y = \frac{h}{2} C_d{}'(1 - \gamma_y) v\sqrt{u^2 + v^2} \quad (7)$$

$$C_f = \frac{g\gamma_v {n_m}^2}{h^{1/3}} \quad (8)$$

where, C_f is a drag coefficient of shear stress, n_m is Manning's roughness parameter and $C_d{}'$ is drag the ratio of a drag coefficient to typical length of building in a calculation grid.

There are consisting of 4 steps for numerical model simulation. First, the calculation grids are created from DEM data are used to create a grid and to determine the attributes of each node or cell by interpolating relevant values. Second, the calculation parameters were set to the model. The conditions of study are based on real parameters. Third, model is simulating in a small time step. Finally, the numerical results are visualized to graphic animation.

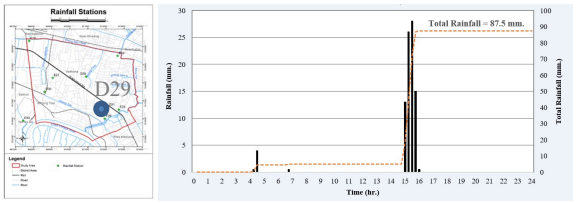

Fig. 5. Location and rainfall of D29 rain gauge station in October 23, 2018.

B. Model Setup

For model simulation, grid size 5m x 5m with totaling of 177,141 grids were adopted, with time step and manning's roughness parameter are Δt= 0.05s and n_m = 0.03, respectively. Geographic data are used to create a grid and to determine the attributes of each node or cell by interpolating from DEM data. For model simulation, rainfall at station D29 (Bangkok: DDS), and water level at pond/canal were adopted for input data and initial conditions, respectively. The 15 minute interval rainfall data recorded at D29 automatic rain gauge stations, extremes event during October 23, 2018, with totaling 87.5 mm are utilized to study the characteristic features of urban flood in Bangkok. Temporal changes in the short duration (less than 60 minutes), with total rainfall was 93 mm (*Fig. 5*).

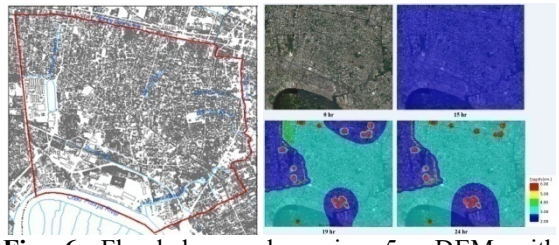

Fig. 6. Flooded area by using 5m DEM without building.

Fig. 7. Flooded area by using 15m DEM with grouping building block.

Fig.6 shows the flood depth extent and location, which obtained from the simulation of the iRIC model by using only topography without building block, road/street and pumping station. The simulated flooding depths have been traced for several selected locations along with the available real flood marks to provide a general idea on how the simulated flood depths deviate from the real data. However, overall flood depth, areas and flow direction tends to underestimate the water depths. It was found that the differences are larger for flooded areas. For simulation with building block, it took a lot of computation times, since there are many small building blocks in computation domains. *Fig. 7* shows simulated results by grouping DEM from 5 m to 15 m and building blocks, which gives with better estimation, and more robust. It was found that the model flooded areas are similar to observe in Area-13. Therefore, DEM 15 m with grouping building blocks have been adopted in this study. The optimal value needs certain runs to tune and it differs from case to case [7].

Results and Discussion

A. Simulation of October 23, 2018 Flooding (present scenario)

All consisting conditions of major canals, roads, pumps and sewer system have been included in the model. Then, the model has been properly calibrated for the surface roughness and runoff coefficient. It was found that manning's roughness n_m = 0.03 and runoff coefficient C= 0.8 have been used in entire simulation domain. Good matching of model results and observed data ensures that the model was able to reproduce the actual flooding situation. Overall flood duration and areas at 4 selected locations ((1) AokMontri, (2) Ekamai, (3) Phrompong and (4) Khlong Toei) are identical. But, flood depth are 4-6 cm, tends to underestimate the water depths slightly. The differences are larger at the main road, due to the different levels of traffic surface with walkways and garbage clogged the road drainage, which smaller grid sizes are required (*Fig. 9-10*).

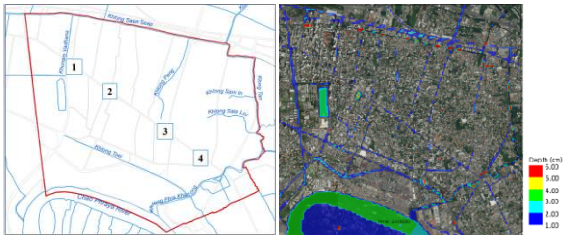

Fig. 8. Maximum flooded area in Area-13. (Present scenario).

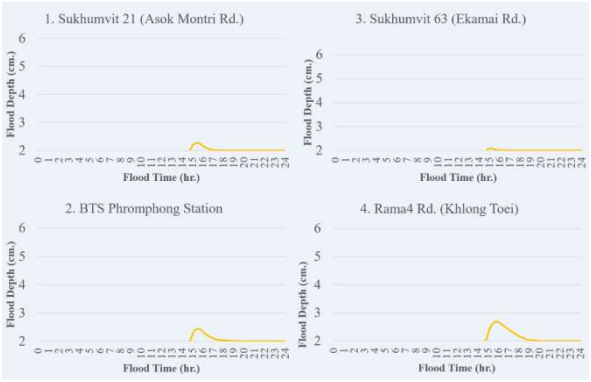

Fig. 9. Time series flood depth at several selected locations (Present scenario)

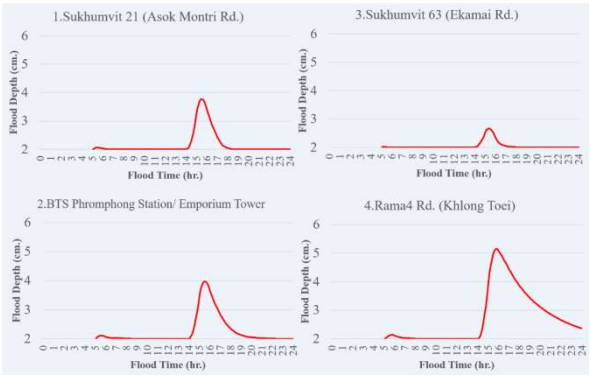

Fig. 10. Time series flood depth at several selected locations (Climate Change Scenario).

B. Simulation of Climate Change Scenario

A number of future climate projections indicate a likelihood of increased magnitude and frequency of hydrological extremes. An attempt was made to identify the possible alleviation scenarios for the climate change. The drainage infrastructures in an urban area are usually designed based on the rainfall depth calculated employing statistical analyses of observed precipitation data. The rainfall depths are calculated from the historic rainfall time series without considering climate change impact. So, the designing of storm water management infrastructure based on design storm considering the assumption of non-stationary climate will not be able to manage extreme events in future climate. Changes in extreme rainfall events will have a significant implication on the design of storm water management infrastructures. This study assessed the potential impact of changed rainfall

extreme on drainage systems in the BMA Area-13 sub-polder. The design storms for the study area were re-calculated from observed rainfall data and employing as time series rainfall input for the study area in present infrastructure scenario.

This study used the series of annual maximum rainfall at 15, 30 mins 1, 2, 3, 6, 12 and 24 hrs of rainfall durations from 2000-2015 about 60 stations. We used the Gumbel Distribution Method for calculated all IDF curves. A design storm can be represented by a value of rainfall depths or intensity (presented by IDF curves) or by a design hyetograph specifying the time distribution of rainfall during a storm, and return period were calculated for historic observations at station [8].

It was found that overall flood depths, duration and areas are increased from present condition more than 1.5 - 2.0 times in Area-13 (Sukhumvit-North sub-polder) areas. For flood depths in Sukhumvit21 (AsokMontri Rd.) and Khlong Toei (Rama 4 Rd.) are increased from 0.025 – 0.040 m to 0.04 – 0.06m, due to an insufficient drainage capacity of sewer and pumping systems (*Fig. 10*). The results show an increase in design storm depths under projected climatic change scenarios that suggest an update of current standard for designing is needed. A concept of applying real time control and increasing pump capacity real time/ remote control and to improve the drainage capacity locally may be used as a tool to reduce flooding. *Fig. 8* to *10* depict the generated heavy rainfall flood based on water depth for Area-13, BMA, Thailand. The condition of the improvement of present condition has a significant role on generated flood water depth and extents area. However, land-use development (urbanization) increases impervious areas and generated considerable impacts on drainage system. Rainfall events with higher intensity of climate change scenario lead to higher runoff and flood water depth. Therefore, this contributes to enlargement of the area of flood and hazard classes. Eventually, increase of development magnitude leads to boost the river flood from the main Chao Phraya and the peripheral river systems. During flood event, flood flow exceeds the river banks and overflows into the sub-polder (protection area), in this case, the characteristics of floodplain topography affects on the flood distribution.

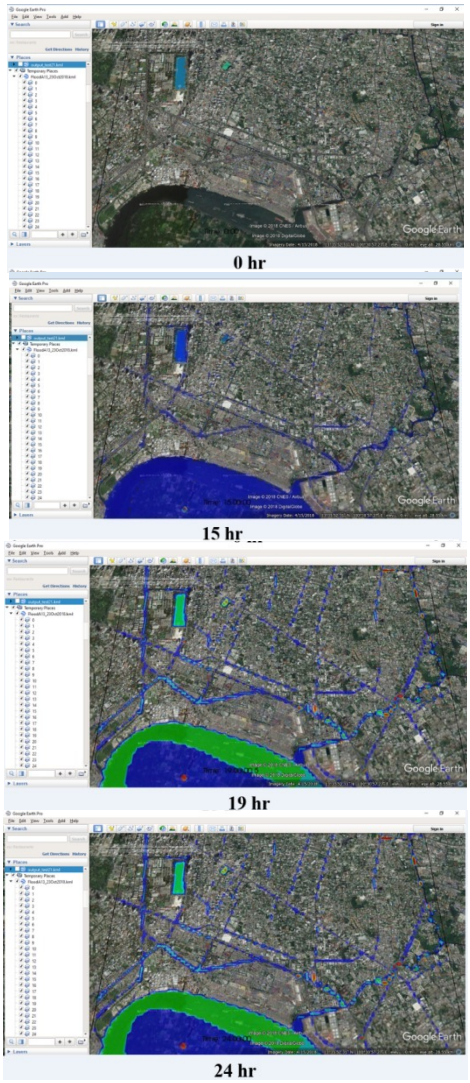

Fig. 11. Visualization of calculation results to Google earth.

C. Output Results to Graphics and Animation

For visualization and analysis of calculation results of iRIC software. The visualization of calculation results can be used for purposes such as creation of vector, contour, and other diagrams, as well as, creation of graphs. Furthermore, visualization results can be output to file in graphic formats such as JPG, or output to Google Earth and ArcGIS.

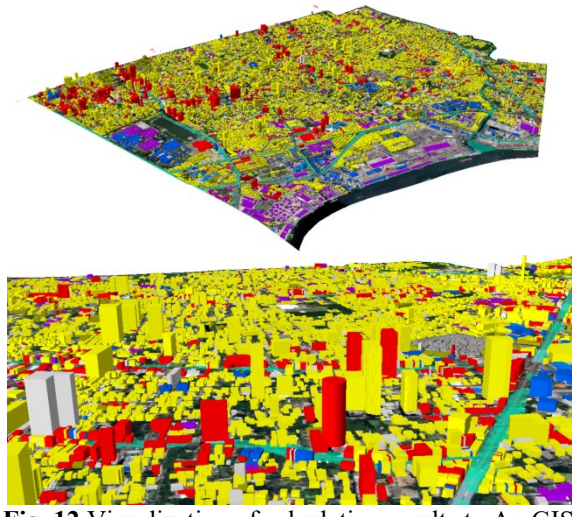

Fig. 12. Visualization of calculation results to ArcGIS.

Conclusions

The study of urban flooding in Area-13 (Sukhumvit-North sub-polder), BMA, Thailand by using iRIC software for the basis of two networks, one simulating the two-dimension free-surface flow over the streets and one for the pumping/canal/pipe system. This study explored the potential simulation for 2 scenarios; (1) present condition, and (2) future impact of climate change. The results show that improved the drainage capacity locally, such as, sewer and pumping systems can reduce present flood condition. For projected climatic change scenarios, it was found that overall flood depths, duration and areas are increased 150-200%. Overall, the urban storm water management infrastructures designed based on current climate condition will not be able to cope with the increased design storm depth under future climate condition, an update of current standard for designing is needed. The findings of this study would encourage municipalities and other stakeholders for considering climate change impact in planning and designing of storm water management infrastructures to ensure that they will work effectively in future. A concept of applying real time control and increasing pump capacity real time/ remote control and to improve the drainage capacity locally may be used as a tool to reduce flooding.

Acknowledgment

This research was supported by "Advancing Co-design of Integrated Strategies with Adaptation to Climate Change in Thailand (ADAP-T)" supported by the Science and Technology Research Partnership for Sustainable Development (SATREPS), JST-JICA. We are also indebted to Department of Drainage and Sewerage (DDS: BMA) and Ms. Komkong T. (RA) for providing some fields and calculation data.

References

[1] http://i-ric.org/en/introduction.
[2] Wongsa, S. (2013) 2011 Thailand Flood, Journal of Disaster Research, 8(3):380-385.
[3] Wongsa, S. (2015) Experiment and Simulation on Earthen Embankment Breach, Journal Geoscience and Environment Protection, 3:59-65. (http://dx.doi.org/10.4236/gep.2015.310010).
[4] Yabe, T., Ishikawa, T., Kadota, Y., and Ikeda, F. (1990) A Multidimensional Cubic-Interpolated Pseudoparticle (CIP) Method without time splitting technique for hyperbolic equations, Journal of the Physical Society of Japan, 59(7), 2301-2304.
[5] McMillan, H. K., and Brasington, J. (2007) "Reduced complexity strategies for modelling urban floodplain inundation." Geomorphology, 90(3-4), 226-243.
[6] Miura, S., Kawamura, I., Kimura, I., and Miura, A. (2011) Study on inundation flow analysis method in densely populated urban area on alluvial fan, Journal of Hydr. Eng. JSCE. 67(4): 979-984.
[7] Wongsa, S., Vichiensan, V., Piamsa-nga, N., and Nakamura, S. (2018) Study on inundation flow analysis method in densely populated urban area on alluvial fan, Journal of Hydr. Eng. JSCE. 67(4): 979-984.
[8] Narktap, S. and Piamsa-nga, N. (2018) Urban Flooding and Adaptation to Climate Change in Sukhumvit Area, Bangkok, Thailand, UDM2018, Palermo, Italy.
[9] M. Young, The Technical Writer's Handbook. Mill Valley, CA: University Science, 1989.

Impact of Heavy Rainfall Cause by Climate Change on Urban Area in Bangkok, Thailand

Thidarat Komkong[1,a,*] and Sanit Wongsa[1,b]

Abstract This paper describes benchmark testing of two-dimensional (2D) hydraulic models (Nays2D Flood) in terms of their ability to simulate surface flows in a densely urbanized area. The model are applied to a 22.595 km2 urban catchment within the city of Whattana – Klongtoey Districts. The purpose of this research is to study the capacity of current drainage system by Nays2D Flood. It is used to simulate a flood event that occurred at this site on 16th May, 2017, There was rain 90 millimeters within 3 hours which caused flooding in some area. And adapted to simulate under heavy rainfall cause by climate change. An identical numerical grid describing the underlying topography is constructed for model, using a DEM (Digital Elevation Model) from Land Development Department (LDD) and grouping building in study area. Procedure is commencing by studying existing drainage system, The calibration of parameter which effect on simulation model such as, a runoff coefficient = 0.35, a coefficient of Manning's n = 0.02. The result show that the terrain data available from DEM systems are sufficiently accurate and resolved for simulating urban flows. The existing drainage system could not achieve the design rainfall. Case of present, flooding in Asokmontri Sukhumvit and Rama 4 road, depth of flood 15-20 centimeters, and duration about 1-3 hours. Under projected climatic change scenarios, the results of flood depths, duration and areas are increased from present condition more than 1.0 - 3.0 times in the study area.

Keywords *heavy rainfall; climate change; urban area*

[1]Dept. Civil Technology Education, FIET
King Mongkut's University of Technology Thonburi
Bangkok, Thailand

[a]tkthidarat@gmail.com
[b]sanit.won@kmutt.ac.th

Introduction

Floods occur on a more frequent base than ever before. Due to climate change weather patterns change and rain intensity increases. Climate change also influences rainfall events. This causes increasing rainfall to flood more often. The increasing amount of rain is problematic especially in urban areas, which drainage system can often not handle this large amount in a short time.

Bangkok area is urbanization near coast and land below mean sea level, so a little rain may cause severe problems for certain city areas. When floods occur they create a great disturbance in the daily life. Roads can get blocked, people can't go to school or work. The economic damage is high but the number of casualties is usually very low, because the nature of the flood. The water slowly rises, when the city is on flat terrain the flow speed is low and rise is relatively slow.

With the current rate of climate change these extreme situation will occur more often in the future. The increasing rain intensity will cause city drainage system will not be able to handle the large amount of water. This will lead to more floods. This threat will become major in the future but one thing that does not change is the location of these urban areas in these dangerous areas. It is estimated that the population is still growing rapidly in urban areas, which will cause that an increasing number of people will be at risk in the future.

Data Preparation and Semulation

A. Data Preparation

Nays2D Flood is a 2-dimensional, flood flow simulation modeling for simulating. We implemented the Digital Elevation Model (DEM) form Land Development Department (LDD) 5 m resolution but it is not coverage the study area. So we interpolated the DEM data by Arc GIS and then we converted the DEM data to point and calculated coordinates X,Y (Fig. 1). And then we edited elevation of DEM in the main canals (SaenSeap, Tan, and PhraKhanong) and Chao Phraya River by use water level from Department of Drainage and Sewerage (Fig. 2). When we modified the DEM data from Arc GIS, we prepared the DEM to .tpo file for Nays2D Flood model.

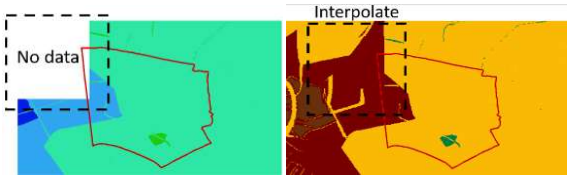

Fig. 1. The DEM data (left) Original DEM data, (right) Interpolate DEM data.

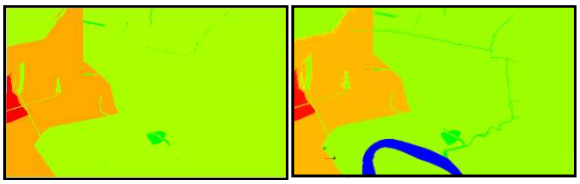

Fig. 2. The DEM interpolate (left) DEM without canal and river, (right) modified DEM to have main canals and river

We made building block grouping by Arc GIS from building blocks data with aerial photo scale 1:4,000 from Department of City Planning Bangkok Metropolitan Administration (CPD). For the background image we used an image obtained from CPD too (Fig. 3).

Fig. 3. Grouping building blocks Preparation (left) Aerial photo, (middle) Building blocks, (right) Building blocks grouping

For model calibration and study the characteristic features of urban flood in study area. We used the 15 minute interval rainfall data from automatic rain gauge stations with the maximum rainfall in the study area. On 16thMay,2017, we used rainfall data recorded at D29, with the maximum rainfall 25.5 mm and the total rainfall 93 mm (Fig. 4).

And validation by another heavy rainfall event. We used rainfall data recorded on 14thOctober, 2017 at E40 station, with the maximum rainfall 32 mm and the total rainfall 162 mm (Fig. 5).

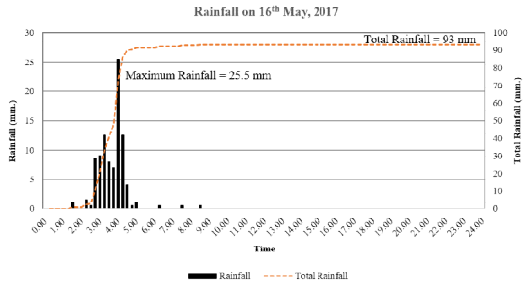

Fig. 4. Rainfall of rain gauge station on 16th May, 2017.

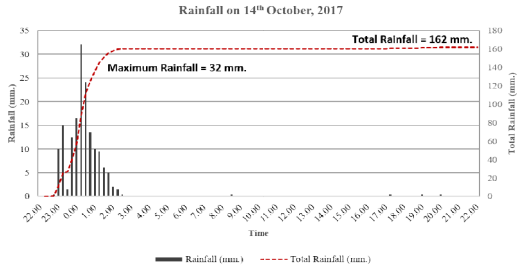

Fig. 5. Rainfall of rain gauge station on 14thOctober, 2017.

For the calibration of flood duration and areas at 4 locations was 1) AsokMontri, 2) Phrompong, 3) Ekamai and 4) Khlong Toei. We checked with flood reports from DDS and News from websites were available the data for validated of simulations for both of events.

Urban pluvial flood models for each pilot location and further testing of these the improved rainfall estimates and forecasts resulting from Gumbel Distribution Method for calculate all IDF curves. We used the series of annual maximum rainfall at 15, 30 mins 1, 2, 3, 6, 12 and 24 hrs of rainfall durations about 60 stations. Design storm depths associated with duration of 15 minutes for 16 years (2000 – 2015) and return period were calculated for historic observations at stations [1]

For sewers and pumps we used the information from DDS and we were setting the discharge and position by Nays2D Flood model (Fig. 6).

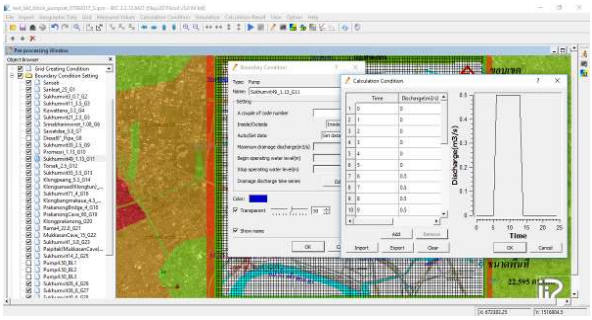

Fig. 6. iRIC Nays2D flood-solver window: Setting pumps and sewers data.

B. Model Setup

The Nays2DFlood, which is one of the models enclosed in the iRIC system, is a flood flow solver developed by iRIC [2]. Tools for creating these systems are supplied in iRIC webpage [3], [4]. For model simulation, analyzed area 42.25 km^2 grid size 5 m, 10 m and 15 m with totaling of 1,442,401, 423,801 and 177,141 grids were adopted.

This study used time step Δt = 0.05s manning's roughness n_m = 0.02 and runoff coefficient C = 0.8. The model were calibrated by a heavy rainfall event occurred on 16th May, 2017 and validated by another heavy rainfall on 14th October, 2017.

For the analysis of impact, we used the flood simulation result on 16thMay, 2017 compared with the result of heavy rainfall cause by climate change. The overall workflow of flood simulation is show in Fig. 7.

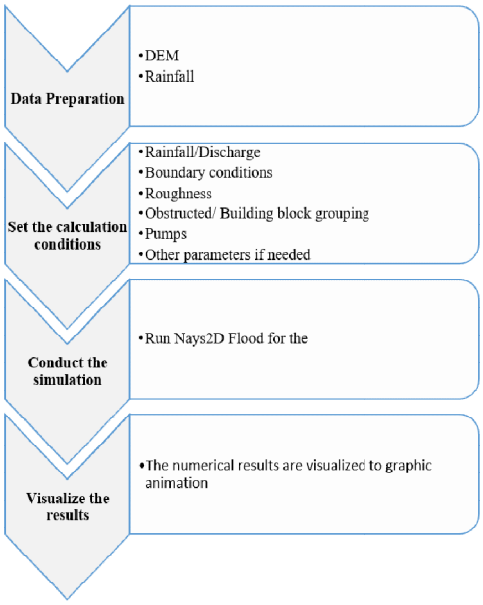

Fig. 7. Procedure for operating the Nays2D Flood solver with iRIC.

C. Model Equations

The model employs time stepping with a choice of differencing schemes for advection of momentum, including the upwind scheme and the CIP (Cubic Interpolated Pseudo-Particle) scheme [4]. The water surface elevation is calculated using a successive relaxation technique. In order to consider the effects of roads and buildings on flood analysis, the governing equations of previous Nays2DFlood have been modified to express effects of obstructions by building and road against two-dimensional water flow. In numerical model, the governing equations for a two-dimensional plane flow field are written in a general, non-orthogonal coordinate system. However, we can rewrite the continuity and *x*-*y* momentum equations here in an orthogonal coordinate system for simplicity, and can be written as following [5], [6],

$$\frac{\partial h}{\partial t} + \frac{\partial \gamma_x hu}{\partial x} + \frac{\partial \gamma_y hv}{\partial y} = q_{in/out} \quad (1)$$

$$\gamma_v \frac{\partial uh}{\partial t} + \frac{\partial \gamma_x hu^2}{\partial x} + \frac{\partial \gamma_y hu}{\partial y} = -\gamma_v hg \frac{\partial H}{\partial x} - \frac{\tau_x}{\rho} - hR_x \quad (2)$$

$$\gamma_v \frac{\partial v}{\partial t} + \frac{\partial \gamma_x huv}{\partial x} + \frac{\partial \gamma_y hv^2}{\partial y} = -\gamma_v hg \frac{\partial H}{\partial y} - \frac{\tau_y}{\rho} - hR_y \quad (3)$$

Where equation (1) is continuity equation and equation (2) and (3) are equation of motion for *x* and *y* directions. *h* is water depth, *t* is time, *u* and *v* are velocities in *x* and *y* directions, *g* is gravity accretion, *H* is water level,$\tau_x$$\tau_xand\tau_y$are bed shear stress in *x*and*y* directions, p is water density,γ_x, $\gamma_y$and$\gamma_v$are the parameters for indicative of the effects of buildings against 2D flow.

$$\frac{\tau_x}{\rho} = c_f u\sqrt{u^2+v^2} \quad (4)$$

$$\frac{\tau_y}{\rho} = c_f v\sqrt{u^2+v^2} \quad (5)$$

$$hR_x = \frac{h}{2} C_d{}'(1-\gamma_x)u\sqrt{u^2+v^2} \quad (6)$$

$$hR_y = \frac{h}{2} C_d{}'(1-\gamma_y)v\sqrt{u^2+v^2} \quad (7)$$

$$C_f = \frac{g\gamma_v n_m{}^2}{h^{1/3}} \quad (8)$$

where,$C_f$is a drag coefficient of shear stress, n_m is Manning's roughness parameter and$C_d{}'$is drag the ratio of a drag coefficient to typical length of building in a calculation grid.

Result and Discussion

A. Model Calibration and Validation

Model calibration and sensitivity analysis are undertaken for the 16thMay, 2017event to obtain the optimal set of parameter values for the study area. The first heavy rainfall eventfor calibration lasted for 2.5 hours, the peak rainfall intensity reached 25.5 mm and the precipitation accumulation for the 24 hours with 93 mm.

For the flood on 16thMay, 2017, the simulation of the event agrees well with the observation. The model predicted peak flood depth is about 0.201 to 0.205 m is in agreement with the observed value from the flood event on this day at the 4 points for calibration (Fig. 8).

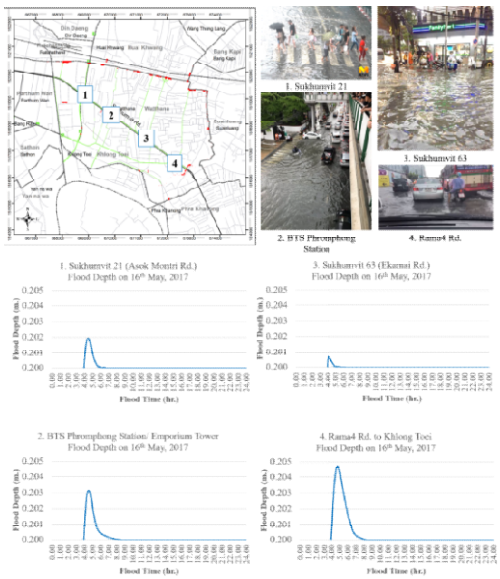

Fig. 8. Time series flood depth on 16thMay, 2017. (calibration)

For the best simulation, we perform the result to the difference of computational grid size with 5 m, 10 m, and 15 m. For the grid size we considered from the wide of canals and roads/streets in the study area (5 to 15 m).

Table I. shows calculation time and the result of each run. The calculation time for the simulation using 5 m grid size is 5 times longer than 15 m grid size and 4 times longer than 10 m grid size simulation.

Inthis example, considering the balance of resolutions of the computation time and the inundation depth, we adopted a grid of 15 m. It is important to carry out such a sensitivity analysis in advance.

Table I. Compare the simulation results with grid size 5 m, 10 m, and 15 m

Study area	**22.595 km^2 (Wattana-Khlong Toei District)**		
Analyzed area	**42.25 km^2 (6.5 km x 6.5 km)**		
Data	**Grid size**		
	15 m	***10 m***	***5 m***
Totaling of grids	177,141	423,801	1,442,401
Simulation Time	About 7 hr	About 9 hr	About 35 hr
Flood Depth	Close to the real situation	More than the real situation	More than the real situation
Flood Area	Close to the real situation	Close to the real situation	Close to the real situation
Flood Duration	Close to the real situation	More than the real situation	More than the real situation

To avoid the potential problem of model overfitting, the optimal set of parameters identified in the model calibration and sensitivity analysis for the heavy rainfall event on 16thMay, 2017 is used to simulate the inundation processes of another heavy rainfall event on 14thOctober, 2017.

The second heavy rainfall event for validation lasted for 3 hr, the peak rainfall intensity reached 32 mm and the precipitation accumulation for the 24 hours with 162 mm.

For the flood on 14thOctober, 2017, the simulation of the event agrees well with the observation. The model predicted peak flood depth is about 0.202 to 0.222 m is in agreement with the observed value from the flood event on this day (Fig. 9).

For the flood depth and flood time of the inundation processes simulated by the established iRIC model for both of heavy rain fall events. The depth and duration of flood at point 4 (Khlong Toei) are longer than at point 1 (AsokMontri),2 (Phrompong)and 3 (Ekamai) both of the simulations due to the elevations at point 4 lower than point 1, 2 and 3. If the value of rainfall are increased, the flood depth and flood durations are increased too.

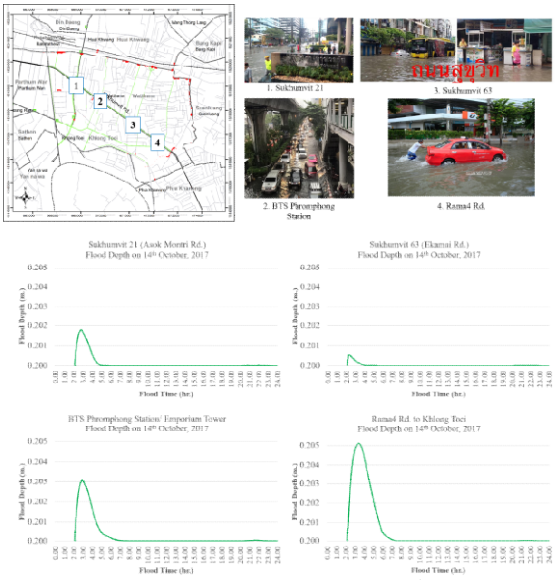

Fig. 9. Time series flood depth on 14thOctober, 2017. (validation)

The overall patterns of flood depth and duration in the two simulations agree well with observations.

B. Simulation Under Heavy Rainfall Event Cause by Climate Change.

The study about climate projection indicates that a likelihood of increased magnitude and frequency of hydrological extremes. Changes in extreme rainfall events will have a significant implication flood on the urban area. This study assessed the potential impact of rainfall from calculation rainfall extreme by climate change on study area.

The rainfall were calculated from the series of annual maximum rainfall at 15, 30 mins 1, 2, 3, 6, 12 and 24 hrs of rainfall durations from 2000-2015 about 60 stations and used the Gumbel Distribution Method for calculate all IDF curves. A design storm can be represented by a value of rainfall depths or intensity (presented by IDF curves) or by a design hyetograph specifying the time distribution of rainfall during a storm. Design storm depths associated with duration of 15 minutes for 16 years (2000-2015) and return period were calculated for historic observations at station [1]

The results above show that the model works well for the heavy rainfall events in urban area. After that we simulated under heavy rainfall event cause by climate change for analyzed the impact the flood on study area.

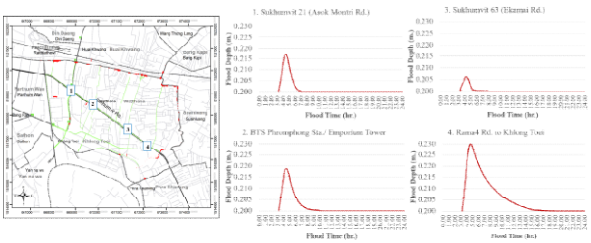

Fig. 10. Time series flood depth predict under heavy rain event cause by climate change.

The Fig. 10 shows flood depth and flood time of the result from simulation under heavy rainfall event cause by climate change. For all of point, the inundated flood depths and flood durations from heavy rainfall event cause by climate change are more than the flooded in present.

C. Impact of Flood on Study Area

For the analysis of impact, we used the flood simulation result on 16thMay, 2017 compared with the result of heavy rainfall cause by climate change.

All of 4 points with 1) AsokMontri, 2) Phrompong, 3) Ekamai and 4) Khlong Toei from the result of heavy rainfall cause by climate change have flood depth and duration more than the present scenario, especially at Khlong Toei that flood depth high to 0.23 m and flood duration more than 15 hr ,due to this point have low terrain (Fig. 11).

It was found that overall flood depths, duration and areas are increased from present condition about 1.0 - 3.0 times. For flood depths are increased from 0.201 – 0.205 m to 0.206 – 0.230 m, flood durations are increased from 1.00 – 3.30 hr to 3.30 – 15.30 hr, due to an insufficient drainage capacity of sewer and pumping systems (Table II.).

Table II. Flood Depth and Flood Duration

Point	Flood depth (m)			Flood duration (hr)		
	Present	*Climate change*	*Δ*	*Present*	*Climate change*	*Δ*
1	0.202	0.217	0.015	2.30	3.30	1.00
2	0.203	0.219	0.016	3.00	7.00	4.00
3	0.201	0.206	0.005	1.00	3.30	2.30
4	0.205	0.230	0.025	3.30	15.30	12.00
Avg.	0.203	0.218	0.015	2.30	7.30	5.00

The Table III. shows flood area and flood volume are increased from present condition about 1.0 times. For flood area are increased from 709,000 m^2 to 729,000 m^2, flood volume are increased from 143,927 m^3 to 158,922 m^3 , due to the rainfall are increased from present and capacity of sewer and pumping systems still the present condition.

Table III. Flood area and Flood Volume

Flood area			Flood Volume		
Present	*Climate change*	*Δ*	*Present*	*Climate change*	*Δ*
(m^2)	*(m^2)*	*(m^2)*	*(m^3)*	*(m3)*	*(m3)*
709,000	729,000	20,000	143,927	158,922	14,995

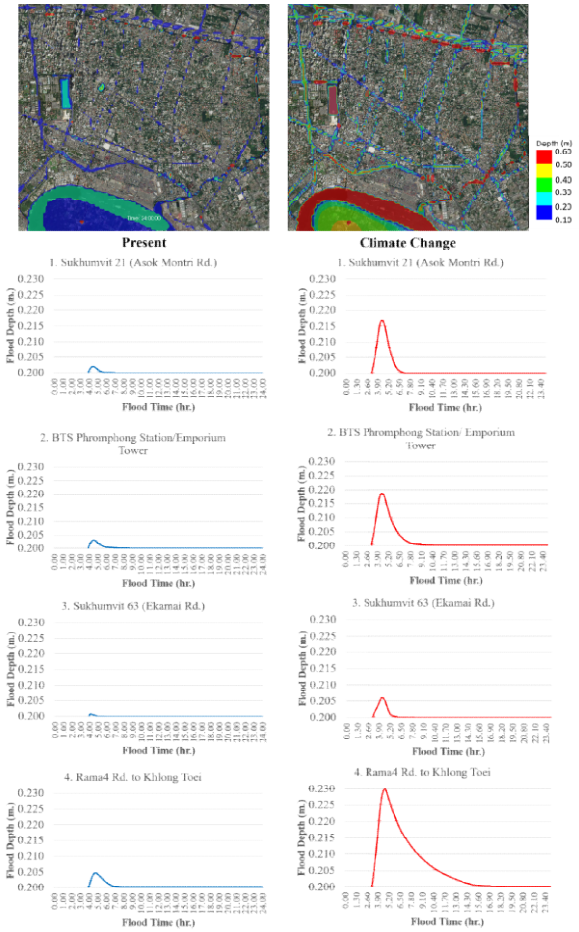

Fig. 11. Compare the flooded present with predict under havy rain event cause by climate change.

Conclusions

The model is tested in a 22.595 km2 urban catchment, the downtown of Bangkok district, Thailand. While common flooding events in a natural watershed inundate large areas and last for hours and days, urban flooding event usually occur in a small or even tiny subcatchment and on discrete sites with lower elevation due to natural topology or civil engineering projects. The urban flooding events normally last for tens of minutes or hours.

The results above show that the i-RIC model could simulate for heavy rainfall events in urban area well. According to the above comparison, the result of simulation under climate change can be seen that depth and duration of flooded increased more than 1.0 to 3.0 times

The study area is one of the frequently flooded spots. It is located at a main avenue in the downtown area, and the flooding often causes serious traffic jam.

So, we should study

1) The evaluation principle for hazard/risk of flood to transport and traffic for avoid or implement mitigation measures from flood in study area.
2) The impact of flood on build-up area, infrastructure, and economic in study area.
3) The method to retention the water from flood for reused in the study area.
4) The planning and designing of storm water management infrastructures for work effectively in future under climate change.

Acknowledgment

This research was supported by "Advancing Co-design of Integrated Strategies with Adaptation to Climate Change in Thailand (ADAP-T)" supported by the Science and Technology Research Partnership for Sustainable Development (SATREPS), JST-JICA. And the Department of Drainage and Sewerage (DDS: BMA) for supporting and providing the data and Asst. Prof. Dr. SanitWongsa for advice and supporting.

References

[1] Narktap S. and Piamsa-nga N., The High-Resolution Analysis of Intensity-Duration-Frequency Curves for Bangkok Metropolitan Area, NCCE23, 2018 , pp.380-385.
[2] http://i-ric.org/en/introduction..
[3] Wongsa, S. (2013) 2011 Thailand Flood, Journal of Disaster Research, 8(3):380-385.
[4] Wongsa, S. (2015) Experiment and Simulation on Earthen Embankment Breach, Journal Geoscience and Environment Protection, 3:59-65. (http://dx.doi.org/10.4236/gep.2015.310010).
[5] Yabe, T., Ishikawa, T., Kadota, Y., and Ikeda, F. (1990) A Multidimensional Cubic-Interpolated Pseudoparticle (CIP) Method without time splitting technique for hyperbolic equations, Journal of the Physical Society of Japan, 59(7), 2301-2304.
[6] McMillan, H. K., and Brasington, J. (2007) "Reduced complexity strategies for modelling urban floodplain inundation." Geomorphology, 90(3-4), 226-243.
[7] Miura, S., Kawamura, I., Kimura, I., and Miura, A. (2011) Study on inundation flow analysis method in densely populated urban area on alluvial fan, Journal of Hydr. Eng. JSCE. 67(4): 979-984.

EFFECT OF CLIMATE CHANGE ON WATER MANAGEMENT IN LOWER CHAO PHRAYA RIVER

Sanit Wongsa[1,a,*] and Sunaree Sueathung[1,b]

Abstract Climate change causes serious risks to the well-being of nature and people all over the world. Within the estuaries, sea water can be the important controls of water level, salinity and coastal erosion. The objective of this study is to evaluate the effect of climate and sea level changes on water management in lower part of Chao Phraya River, by using MIKE11 model. The study covered the area from Chao Phraya Dam (barrage), Chai Nat Province to the river estuary at the Gulf of Thailand, SamutPrakan Province. The model was divided into two parts, hydrodynamic (HD) module and advection-dispersion (AD) module. Calibration of each part was done by adjusting its important coefficients. It was observed that the Manning's coefficient (n) and coefficient dispersion of mass were in the range of 0.025-0.040 and 800-1,600 m2/s, respectively. The results of comparison between models and observation data revealed order of forecasting error (R2) in the range of 0.70-0.99 for water level and 0.73-0.86 for salinity. For model application, the RCP2.6 and 8.5 scenario from IPCC report were simulated, sea water level rising in were 0.76 and 1.06 m (in the year of 2100), respectively. Maximum salinity at Samlae Station were 0.63-0.67 g/l, the value of 0.25 g/l exceeding standard and the pointed tip of salinity was at Ko rain sub-district, Ayutthaya Province. Results of this study can be used as guidelines for the management of water resources and agriculture of the Chao Phraya River Basin.

Keywords *global warming;sea water level change; Chao Phraya river;mike11 model*

[1]Dept. Civil Technology Education, FIET
King Mongkut's University of Technology Thonburi
Bangkok, Thailand

[a]sanit.won@kmutt.ac.th
[b]kungsunaree@hotmail.co.th

Introduction

Climate change has been observed have local and global effects. Most of the effects were negative. The notable phenomena effected by extreme weather events, are heavy rains, heat waves, and draught. Climate change causes serious risks to the well-being of nature and people all over the world. Within the estuaries, sea water can be the important controls of water level, salinity and coastal erosion. Although the precise effect of climate change on estuaries dynamics and its processes in the alluvial river system is still not clear, there seems to be no doubt that it influences sea water level and salinity intrusion. Recently, numerical modelling has been shown to answer some of these problems. A number of works have used numerical models attempting to simulate river catchment hydrological processes of rainfall-runoff, sediment transport, salinity intrusion and coastal erosion processes as well as to study the impact of climate change. In addition, the numerical model has been applied to predict hill slopes and river channels ([1], [2], [3], [4], [5]). Thus, it is clear that the numerical models appear to have considerable potential as tools for investigating hydrodynamic, sediment transport and water quality over long period simulation. [6] have predicted that sea water level affected rice production in Mekong Delta, Vietnam, during the flood season. However, there are a few application studies in Thailand. [7], [8], [9], [10], [11] have exploited MIKE11 model to predict sea level affecting salinity intrusion and agricultural production in Tha Chin, Mae Klong and Chao Phraya rivers. Metropolitan Waterworks Authority (MWA) reported that salinity intrusion, raw water supply and agriculturalproductivity in Chao Phraya River was affected by climate change.

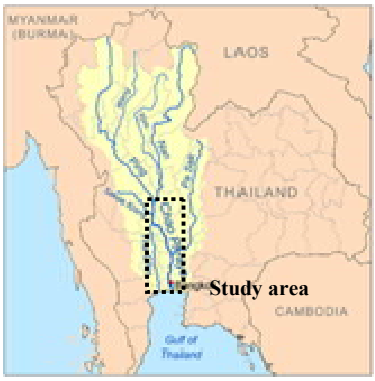

Fig. 1. Study area of the Lower Chao Phraya River.

This paper addresses these issues by using a proposed MIKE11 numerical modelling to simulate the effects on sea water level change and salinity intrusion. Performance of the numerical model was applied to simulate flow events in 2100, which are water level change and salinity intrusion on agricultural and raw water supply in the Lower Chao Phraya River, Thailand. (*Fig. 1*)

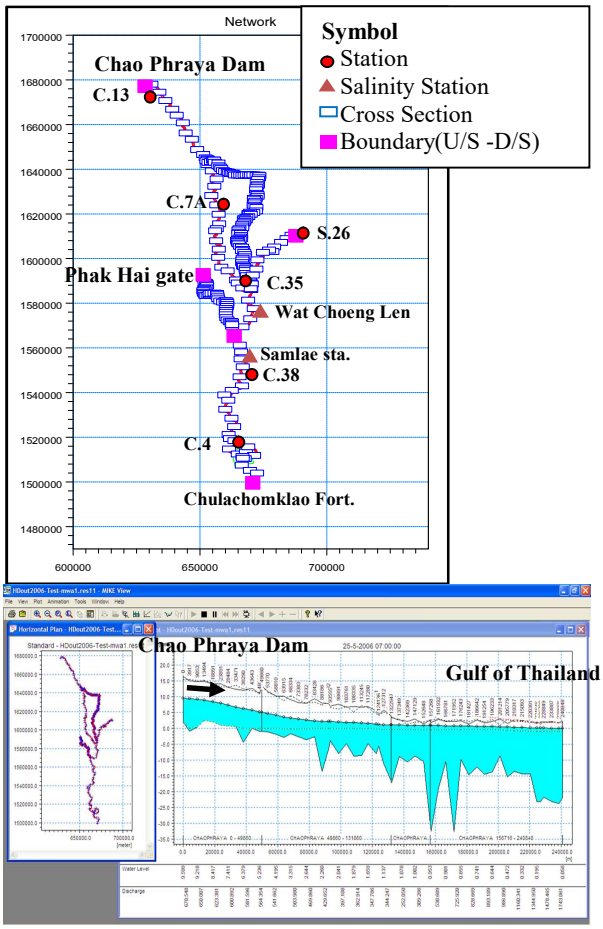

Fig. 2. Model setup

Description of the System

Chao Phraya River is the most important and largest river flowing fromNakhonSawan Province to estuary at the Gulf of Thailand in SamutPrakan Province, located at central part of Thailand. The climate of the Chao Phraya River has a tropical wet and dry or savanna climate, which generates wet and dry seasons of more or less equal length. The monsoon season is usually from May until late September and/or early October. In the wet season, averagely 1-2 tropical depressions occur over much of the area from August to October of the year. The average annual discharge is 718 m^3/s and rainfall varied between 1,122 to 1,511 mm, depending on monsoon direction and elevation.

The proposed model was applied to Lower Chao Phraya River catchment. Chao Phraya River is the most important and largest river flowing from Chai Nat Province to estuary at the Gulf of Thailand in SamutPrakan Province, located at central part of Thailand. Cities along the Chao Phraya include Chai Nat, Singburi, Ang Thong, Ayutthaya, Pathum Thani, Nonthaburi, Bangkok and SamutPrakan, listing from north to south.

However, some parts of the catchment continue to suffer from drought problems due to the uneven distribution of rainfall. Some areas experience both flooding and drought conditions in a single year, due to temporal and spatial uncertainties in the monthly rainfall or the poor management of the conveyance infrastructure. The Chao Phraya River also imports water from Mae Klong River (right bank) and Pasak River (left bank) to boost water supply, which can also multiply the risk of flooding in the downstream and Bangkok metropolitan areas. The common practice in Thailand is to manage the risks after considering which areas are likely to be vulnerable to either flood or drought. Failure to manage risk by addressing one aspect at a time can lead to adverse results. Therefore, climate change and an association with managing flood and drought risks are new challenge in Thailand and becoming increasingly important.

MIKE11 Software and Model Setup

A. MIKE11 Software

The MIKE11 model has been used. This numerical model simulates water flow and salinity as a consequence of low flow conditions. The shallow water equation was used for simulation of 1-D unsteady water flow and transportation of mass was used for salinity. To modelling the river network of the Lower Chao Phraya, a digital elevation map (DEM) was applied. The model input data were cross-section, flow discharge, water level, side flow and salinity. The MIKE11 program, 6-points Abbott's finite difference scheme was used to solve governing equations, consisting of separate modules each representing a different procedure in calculation process. A first module calculated hydrodynamics of river flow (HD module), and the next module of transportation of mass (salinity intrusion; AD module). To assess the influence of the water flow and salinity impacts on climate change of the Lower Chao Phraya River catchment, the MIKE11 model has been used. This numerical model simulates water flow and salinity as a consequence of low flow conditions. The shallow-water equation for one-dimensional unsteady flow can be expressed as following,

Continuity equation:

$$\frac{\partial Q}{\partial x}+\frac{\partial A}{\partial t}=q \qquad (1)$$

Momentum equation:

$$\frac{\partial Q}{\partial t}+\frac{\partial\left(\alpha\frac{Q^2}{A}\right)}{\partial x}+gA\frac{\partial h}{\partial x}+\frac{gQ|Q|}{M^2AR^{4/3}}=0 \qquad (2)$$

where, Q = flow discharge (m^3/s), A = flow section area (m^2), q = side flow discharge (m^2/s), h = flow depth (m), R = hydraulic radius (m), g = acceleration (m/s^2),α= momentum correction factor, M = Strickler's Number (M = 1/n; n = Manning's roughness coefficient), x and t = flow direction and time, respectively.

For transportation of mass, such as, salinity can be obtained from,

Advection-Dispersion equation:

$$\frac{\partial AC}{\partial t}+\frac{\partial QC}{\partial x}-\frac{\partial}{\partial x}\left(AD\frac{\partial C}{\partial x}\right)=-AKC+qC_2 \quad (3)$$

where, C = salinity concentration (mass/volume), D = dispersion coefficient (m^2/s), K = consumption rate (s^{-1}) and C_2 = Source/Sink Concentration (mass/volume).

B. Model Setup

To modeling the river network of the Lower Chao Phraya, a digital elevation map (DEM) has been used. The model input data were cross-section, flow discharge, water level, side flow and salinity. The MIKE11 program, 6-points Abbott's finite difference scheme was used to solve governing equations, consisting of separate modules each representing a different procedure in calculation process. A first module calculated hydrodynamics of river flow (HD module), and the next module of transportation of mass (salinity intrusion; AD module). The model setup of plan view and longitudinal profile of the Lower Chao Phraya are shown in *Fig. 2*.

C. Field measurements

Field measurements have been carried out at the mouth of the Chao Phraya River in Thailand. The study was conducted at the field level, saline water and temperature by using handheld multi-parameter instrument. The measurement was done between May - September, 2018 at different intervals (*Fig.3*).

Fig. 3. Chao Phraya River Field measurements.

Results and Discussion

The Lower Chao Phraya River was used for calibration and verification of the proposed model. The calibration and validation have focused on the applicability of water flow and salinity intrusion by using flow conditions in the year of 2010 and 2012, respectively. Performance of the foregoing numerical model was applied to simulate scenario from IPCC SRES[12], consisting of RCP2.6 and RCP8.5, the predicted global average sea level rising from 1990 to 2100 for the SRES scenarios by using GCMs. RCP2.6 and RCP8.5are consistent with a wide range of possible changes in future anthropogenic greenhousegasemissions, andaim to represent their atmospheric concentrations. For model simulation, flow discharge at station C.13 (Chao Phraya Dam) and water level at Chao Phraya River Estuary (Marine Department) were adopted for upstream and downstream boundaries. Before the water flow and salinity calculation was carried out, the model was run to provide the steady state of necessary flow variables.

A. Model Calibration

The comparison of time series of measured and simulated water surface level and salinity at two major gauge stations in 2010 and Manning's roughness coefficient (n) are shown in *Fig.* 4-5. Good agreement between the simulated and measured hydrographs for the low flow events was achieved by considering side flow and pumps in the areas. The coefficient of determinant (R^2) and Index of agreement (IA) have been used as the main criteria to judge whether the data fitted between measurement and simulation. The comparison model was followed by adjusting important coefficient for two parts. The study results, manning (n), global dispersion factor, global exponent and K_{mix} were in the range of 0.03, 800-1,600 m^2/s, 0.1-1.0 and 800-1,600, respectively. The results of comparison between models and observation data revealed order of forecasting error, R^2 and IA were in the range of 0.76-0.99, 0.77-0.98 for water level and 0.73-0.76, 0.76-0.82 for salinity. These indicate well fitted between measured data and this proposed model.

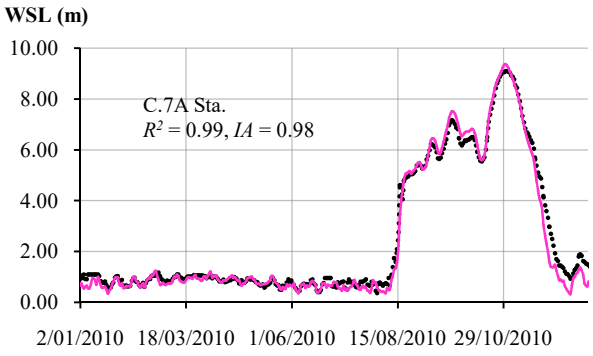

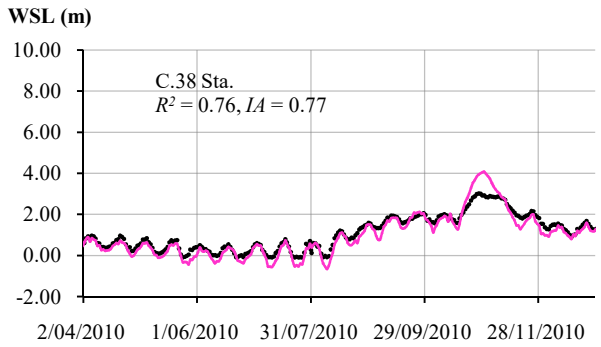

Fig. 4. Comparison of time series of stage hydrograph between simulated results (smoothed-line) and measured data (dotted) at the major gauge stations (model calibration).

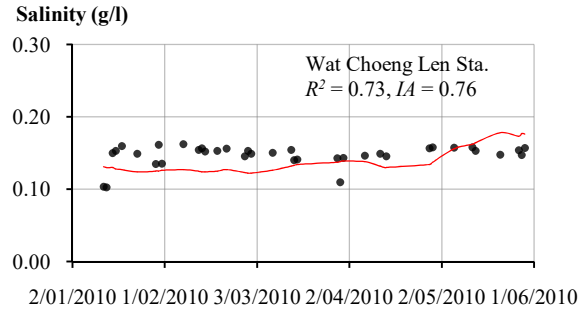

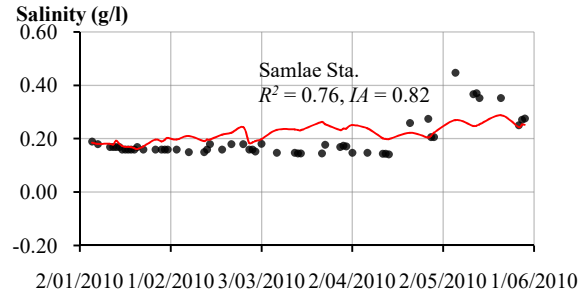

Fig. 5. Comparison of time series of salinity between simulated results (smoothed-line) and measured data (dotted) at the major gauge stations (model calibration).

B. Model Verification

The comparison of time series of measured and simulated water surface level and salinity at two major gauge stations in 2012 are shown in *Fig.* 5-6. Good agreement between the simulated and measured water surface level was achieved by considering side flow and pumps in the areas. It was observed that the values of R^2 and IA for two major gauge stations in verification period were between 0.93-0.94, 0.97-0.98 for water level and 0.71-0.91, 0.72-0.87 for salinity, indicating well fitted between measured data and this proposed model. Good performance of simulated results was observed in both water flow and salinity intrusion characteristics, therefore, indicating that model simulation is reasonable. (*Fig.*6-7).

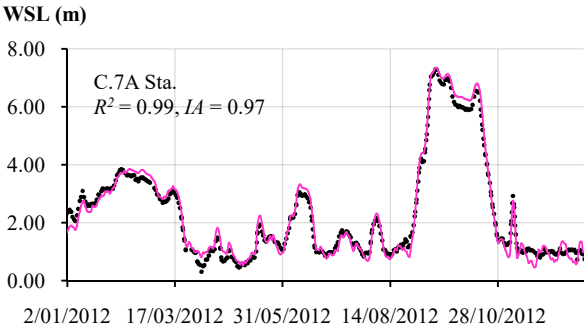

Fig. 6. Comparison of time series of stage hydrograph between simulated results (smoothed-line) and measured data (dotted) at the major gauge stations (model verification).

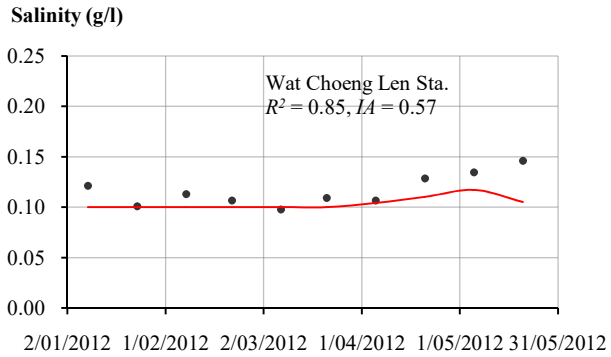

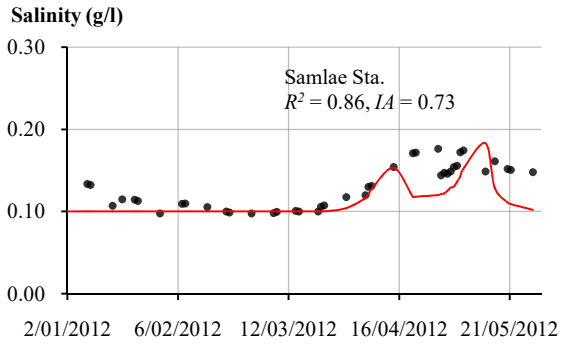

Fig. 7. Comparison of time series of salinity between simulated results (smoothed-line) and measured data (dotted) at the major gauge stations (model verification).

C. Model Application

For model application, a scenario RCP2.6 and RCP8.5 from IPCC report were simulated, sea water level rising in was 0.40 and 0.70 m in the year of 2100. The comparison of time series of measured and simulated flow discharge at the major gauge stations are shown in Fig. 7-8. It was found that sea water level at the Chao Phraya estuary had rising and be taking tendency to intrusion of sea water level. Salinity was shown to be in the same tendency. For IPCC SRES in the year of 2100, sea water level rising in RCP2.6 and RCP8.5 scenario was 0.40 and 0.70 m, and salinity values and intrusion distant were in the range of 0.38-0.45 g/l and 142.0-157.0 km (from Chao Phraya Dam), and salinity at Samlae Station were 0.29-0.37 g/l. The value of 0.25 g/l exceeding standard and the pointed tip of salinity was at Bang Sai District, Ayutthaya Province. The worst case scenario, a constant value of salinity of 30 g/l was adopted at the Gulf of Thailand. It was found that salinity at Samlae Station was 0.63-0.67 g/l, the value of 0.25 g/l was at Pratuchai Sub-district, Ayutthaya Province, 133.0 km from Chao Phraya Dam. We could also observe these effects gained a more conspicuous large against higher sea water level rising (*Fig.* 8-9).

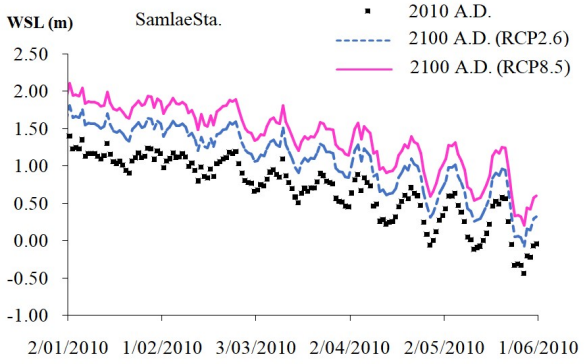

Fig. 8. Water Level in the year of 2100 (IPCC AR5), with 0.40 m and 0.70 m sea water level rising in RCP2.6 and RCP8.5 scenario

However, Metropolitan Waterworks Authority (MWA, 2011) reported that climate change affected salinity intrusion and raw water supply in Lower Chao Phraya River. The observed effects demonstrated that Samlae Pumping Station will not be available when salinity is over 0.25 and/or 0.50 g/l, and water supply shortage. The mitigation plan has suggested that the diversion from Mae Klong River and construction of new pump station for short-term and long-term, respectively. The proposed locations of a new raw water pump station along the Chao Phraya River from Ayutthaya to Singburi Province. It was found that the most suitable sites when evaluation by multi-criteria analysis (MCA) is the proposed site at Klong Pongpheng, Ayutthaya Province.

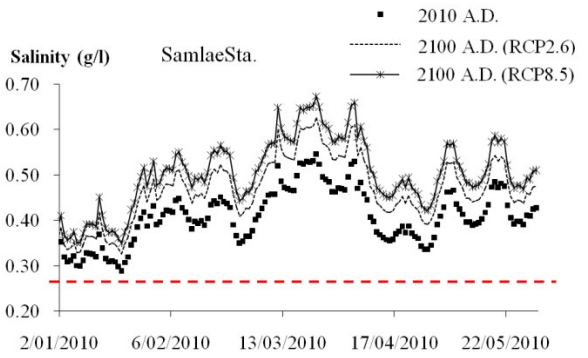

Fig. 9. Salinity in the year of 2100 (IPCC SRES), with 0.40 m and 0.70 m sea water level rising in RCP2.6 and RCP8.5 scenario and salinity 30 g/l at downstream (Gulf of Thailand).

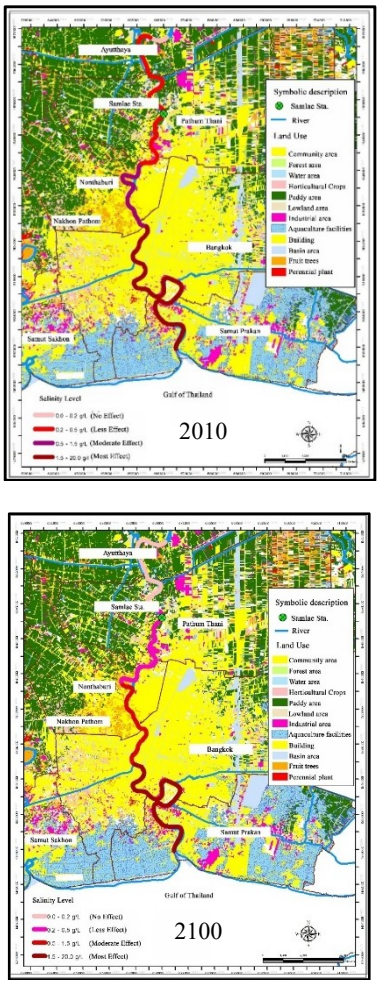

Fig. 10. Salinity profile in the year of 2010 and 2100 (IPCC SRES).

For impact analysis on the urban and agricultural areas, it was found that in the Lower Chao Phraya River sea water level change will affected the water supply in urban, and agricultural areas. Salinity level less than 0.2 g/l was not impacted; it can use irrigation for any planting. Salinity level from 0.2 had little impact, while salinity level from 0.5, and salinity level more than 1.5 g/l were highly impacted (*Fig.* 10). For agricultural sectors, the value of 0.20 g/l

exceeding standard and the pointed tip of salinity was at Ban Mai District, Ayutthaya Province (123 km. from Chao Phraya Dam).

Conclusions

In this study, the MIKE11 model was exploited to simulate the effects of climate and sea level changes on the raw water supply of MWA and agricultural areas in the lower part of Chao Phraya River in the year 2100. The study covered the area from Chao Phraya Dam, Chai Nat Province to the Gulf of Thailand at SamutPrakan Province. IPCC SRES predicted that in the year 2100, sea water level rising in RCP8.5 scenario was 0.70 m. Based on this information, the simulation showed that salinity at Samlae will be exceeded 0.25 g/l. Therefore, it suggested to add pump station at Samlae to site at Klong Pongpheng, borderline of Ayutthaya and Ang Thong Province. This will help to balance level of salinity in river not over 0.25 g/l. For agricultural sectors, the value of 0.20 g/l exceeding standard and the pointed tip of salinity was at Ban Mai District, Ayutthaya Province (123 km. from Chao Phraya Dam). Results obtained from this study will give guideline in raw water resources management for water supply and agricultural in Chao Phraya River Basin.

Acknowledgment

This research was supported by the Biodiversity-Based Economy Development Office (BEDO). We are also indebted to Royal Irrigation Department (RID), Harbor Department (HD) and Hydro and Agro Informatics Institute (HAII) for providing data.

References

[1] DHI Water and Environment. MIKE11: A modeling system for rivers and channels - User Guide, Denmark, 2000.
[2] M.J. Kirby, "Modelling some influences of soil erosion, landslides and valley gradient on drainage density and hollow development". Catena Supplement, vol. 10, pp. 1-11, 1987.
[3] Metropolitan Waterworks Authority. "Potential and solution for raw water crisis: Final report", Bangkok, 2011.
[4] R., Wassmann, N.X. Hein, C.T. Hoanh, and T.P. Tuong, "Sea level affecting Vietnamese Mekong Delta: water elevation in the flood season and implications for rice production", Climate Change 66: 89-107, 2004.
[5] J.M. Wicks, and J.C. Bathurst, "SHESED: A physical based, distributed erosion and sediment yield component for the SHE hydrological modelling system", J. Hydrology, vol. 175, pp. 213-238, 1996.
[6] S. Wongsa, and Y. Shimizu, "Modelling artificial channel and landuse changes and their impact on floods and sediment yield to the Ishikari basin."Hydrological processes vol.18, pp. 1837-1852, 2004.
[7] S. Wongsa, "Distributed model for catchment scale simulation of runoff and sediment transport", Ph.D. Thesis, Hokkaido University, Japan, 2004.
[8] S. Wongsa, and C. Ekkawatapanit, "Effect of sea water level change on the management in the Lower Thachin River", report for ESS Program, King Mongkut's University of Technology Thonburi, Thailand, 2009.
[9] S. Wongsa, C. Ekkawatapanit, and K. Treerittiwitaya, "Effect of sea water level change on the management in the Lower Thachin River", Proc. the International Symposium on Coastal Zones and Climate Change: Assessing the Impacts and Developing Adaptation Strategies, 2010.
[10] S. Wongsa, and P. Kamolsin, and K. Inkliang "Effect of Sea Water Level Change on the Estuaries Management in the Lower Thachin and Mae Klong Rivers", Proc. of GMSTEC 2010: International Conference for a Sustain-able Greater Mekong Subregion, 2010.
[11] IPCC, http://www.grida.no/publications/other/ipcc_tar/?src=/climate/ipcc_tar/wg1/412.htm
[12] S. Wongsa "Impact of Climate Change on Water Resources Management in the Lower Chao Phraya Basin, Thailand", J. Geoscience and Environment Protection, vol.3, no.10, pp.53-58, 2015.

Estimating Probability Distribution of Benefit from Flood Control Projects

Keita Kobayashi[1,a,*]

Abstract Frequencies of severe flood events are expected to increase due to a changing climate. Therefore, it becomes more and more important to implement suitable flood defenses based on quantitative benefit analysis of flood control projects such as dam construction and embankment. In general, the benefit from flood control projects is defined as the sum of expected value of annual reduced damage cost over the evaluation years, considering discount rate of each year. Since flooding is low-frequency events especially in highly protected areas, it is highly uncertain whether actual reduced damage cost is distributed around its expected value, i.e. benefit calculated from the expected value does not necessarily occur frequently. The probability distribution of reduced damage cost would provide more comprehensive information for decision making. This study redefined benefit from a flood control project as a reduced damage cost, which is actually a random variable, and developed its probability distribution by applying an extreme rainfall generation method. Then, we demonstrated the presented method under several scenarios of dam construction projects. The estimated probability distribution was skewed leftwards, and had a long tail. It reveals large variability of reduced damage cost. From the probability distribution, we can extract several statistics in addition to the expected value, which provide more information to discuss the characteristics of actual reduced damage cost by flood control projects.

Keywords *benefit from flood control projects, probability distribution, uncertainty*

[1]Kyoto University

[a]kobayashi.keita.55e@st,kyoto-u.ac.jp

Introduction

It is concerned that frequencies of intense rainfall events will increase due to climate change. To implement adaptation measures against the expected severe flood events, countermeasures should be taken, and fundamental measures are constructing flood defenses such as embankment and dam. In Japan, cost-benefit analysis is utilized from 1997 to evaluate the efficiency of public works, where benefit corresponds to reduced inundation damage cost by installing flood defenses, and the efficiency of flood control projects are measured by comparing it with the cost for construction and maintenance. According to the manual issued by the Ministry of Land, Infrastructure, and Transport (hereinafter called "MLIT") [1], the benefit from flood control projects is defined as the sum of the expected value of annual reduced damage cost over the evaluation years, considering discount rate of each year.

Theoretically, annual reduced damage cost is actually a random variable; accordingly, the sum of annual reduced damage cost is also random variable. Therefore, the benefit defined above is equivalent to the expected value of the sum of annual reduced damage cost over the evaluation years when neglecting discount rate. According to central limit theorem, actual reduced damage cost is normally distributed around the benefit calculated from the expected value when evaluation period is long enough. However, this is not guaranteed for an actual evaluation period due to the low frequency of flooding. In other words, it is highly uncertain whether actual reduced damage cost is distributed around its expected value, i.e. benefit calculated from the expected value does not necessarily occur frequently. These facts show that the above deterministic approach to decision making of flood control projects based on cost-benefit analysis includes the uncertainty of the probabilistic characteristics of reduced damage cost. If we can estimate the probability distribution of reduced damage gained over evaluation period, we can get more comprehensive information from the distribution in addition to the expected value, e.g. the probability with which actual reduced damage cost becomes larger than expected value. These will help advanced decision making of flood control projects based on multiple criteria.

In a literature, several uncertainties for benefit calculation have been discussed, e.g. the uncertainty of risk evaluation process including flood

frequency analysis [3] and risk premium. For example, in the field of urban planning, it is discussed that willingness to pay becomes higher than the expected value of reduced damage cost because of risk aversion [4]. Risk premium is induced from the probability distribution of reduced damage cost; therefore, estimating the probability distribution of benefit is important to explicitly incorporate the idea of risk premium into in the process of decision making for disaster prevention investment.

On the other hand, recent studies have developed methods for estimating a flood risk curve, i.e. the probability distribution of annual maximum inundation damage cost, considering influential factors of risk evaluation such as rainfall time-space distribution and/or hydrograph variations [2], [5]. For instance, Tanaka et.al. [5] showed that considering the rainfall time-space distribution makes it possible to enhance the accuracy of evaluating flood disaster risk. This study demonstrates the derivation of the probability distribution of *T*-year cumulative reduced-damage cost by generating huge number of rainfall events in consideration of rainfall time-space distribution.

From these backgrounds, the purpose of this study is estimating the distribution of *T*-year cumulative reduced damage which is defined as sum of annual reduced damage cost over *T*years, and quantifying the probability with which we can actually benefit from flood control projects. The study area is Yodo River basin (8,240km^2) and several construction scenarios of the existing dams in the Kizu River basin (Takayama Dam, Murou Dam, Shorenji Dam, Hinachi Dam, Nunome Dam) are evaluated. For each project, we estimate the probability distribution of *T*-year cumulative reduced damage cost at conjunction area of three tributaries, Kizu River, Uji River, and Katsura River, and analyze its stochastic characteristics. The impact of design of projects and evaluation period on the estimated distribution is also examined.

Basic Concept of Estimating Probability Distribution of TYearcumulative Reduced Damage Cost

According to the manual of cost-benefit analysis issued by MLIT [1], benefit of flood defenses over T years $B(T)$ is defined as

$$B(T) = \sum_{t=1}^{T} \frac{b}{(1+r)^{t-1}}, \quad (1)$$

where b is expected value of annual reduced damage; r is discount rate; and T is evaluation period. Denoting annual flooding damage before and after flood control investment as D_a and D_b, respectively, b is defined with annual reduced damage $D_{\mathrm{R}} = D_b - D_a$ as

$$b = \mathrm{E}[D_{\mathrm{R}}] = \mathrm{E}[D_{\mathrm{b}}] - \mathrm{E}[D_{\mathrm{a}}]. \quad (2)$$

On the other hand, we define T-year cumulative reduced damage cost $D_{\mathrm{R,all}}(T)$ as follows.

$$D_{\mathrm{R,all}}(T) = D_{\mathrm{b,all}}(T) - D_{\mathrm{a,all}}(T) \quad (3)$$

where $D_{\mathrm{b,all}}(T)$ and $D_{\mathrm{a,all}}(T)$ are cumulative damage cost before and after investment, and denoted as

$$D_{\mathrm{b,all}}(T) = \sum_{t=1}^{T} D_{\mathrm{b},t}\ , D_{\mathrm{a,all}}(T) = \sum_{t=1}^{T} D_{\mathrm{a},t}, \quad (4)$$

respectively, where $D_{\mathrm{b},t}$ and $D_{\mathrm{a},t}$ are flooding damage costs of year t before and after flood control investment. In this study, we estimate probability distribution of T-year cumulative reduced damage cost $D_{\mathrm{R,all}}(T)$ defined in (3). In addition, we investigate impact of evaluation period T length on the probability distribution of $D_{\mathrm{R,all}}(T)$. Note that expected value of T-year cumulative reduced damage cost is obtained from (1) and (4), and we can confirm that benefit $B(T)$ used in the manual [1] corresponds to the mean value of $D_{\mathrm{R,all}}(T)$ when neglecting discount rate, i.e.

$$\mathrm{E}\left[D_{\mathrm{R,all}}(T)\right] = \mathrm{E}[D_{\mathrm{b,all}}(T)] - \mathrm{E}[D_{\mathrm{a,all}}(T)]$$

$$= \sum_{t=1}^{T} \mathrm{E}\left[D_{\mathrm{b},t} - D_{\mathrm{a},t}\right] = \sum_{t=1}^{T} \mathrm{E}\left[D_{\mathrm{R},t}\right] = \sum_{t=1}^{T} b, \quad (5)$$

where $D_{\mathrm{R},t}$ is reduced damage cost of year t.

Methodology of Estimating Probability Distribution

In this research, we take a Monte Carlo approach to obtain enough number of samples of T-year cumulative reduced damage cost, by generating enormous number of extreme rainfall events. Assume rainfall events follow the following three assumptions which were used by Tanaka et.al. [5].

Assumption 1. When rainfall occurs, possible rainfall pattern is limited to the N patterns. Pattern ξ_i $(i = 1,2,\dots,N)$ occurs with probability p_i. Denote rainfall duration time of pattern ξ_i asd_i.

Assumption 2. Basin averaged total rainfall r_{a}follows the conditional cumulative distribution function (CDF) $G_{R_{\mathrm{a}}|D}(r_{\mathrm{a}}|d_i)$given d_i.

Assumption 3. Annual number of occurrences of rainfall events follows the Poisson distribution with occurrence ratio ofμ_{a}.

Define$r(x,y,t)$ as rainfall intensity at a location (x,y) and time t, and rainfall pattern ξ_i is defined as

$$r(x,y,t) = r_{\mathrm{a}}\xi(x,y,t),\ (x,y) \in A, 0 \le t \le d, \quad (6)$$

where A is the targeted watershed. $\xi(x,y,t)$ is normalized to satisfy the following equation:

$$\iint_A \left(\int_0^d \xi(x,y,t)dt\right)dxdy = S, \qquad (7)$$

where S means the catchment area of targeted watershed. Rainfall duration time d is defined as follows.

$$d = \sup\{t|\xi(x,y,t) > 0,\ \exists(x,y) \in A, t > 0\} \qquad (8)$$

Definingthe starting time of rainfall as 0, d indicates the maximum time until which rainfall lasts at a certain point in the watershed.

Following these assumptions, we generate immense samples of T-year cumulative reduced damage cost, following the steps shown below.

Step 1. Generate the annual number of occurrencesof rainfall events n from the Poisson distribution

Step 2. Prepare N past rainfall events and extract rainfall patterns $\xi_i(x,y,t)$ normalized by total rainfall amount. Note that $t$satisfies inequality, $0 \le t \le d_i, (x,y) \in A$ where d_i is the rainfall duration time of pattern $\xi_i(x,y,t)$; $A$is the catchment area. Generate one pattern with the probability $1/N$, i.e. randomly.

Step 3. By following Step 2, the conditional CDF$G_{R_a|D}(r_a|d_i)$ corresponding with the generated rainfall pattern $\xi_i(x,y,t)$is determined. Generate total rainfall amount$r_a$from the conditional CDF$G_{R_a|D}(r_a|d_i)$. From the obtained total rainfall amount r_a and its spatiotemporal pattern $\xi_i(x,y,t)$, one rainfall event is determined

Step 4. Running a rainfall-runoff model and an inundation model, calculate damage costs with/without investment, D_b and D_a, f. Then, calculate the reduced damage cost for the generated rainfall event.

Step 5. Repeating Steps 2 to 4 for n times, sum reduced damage costs of each rainfall events and obtain one sample of annual reduced damage costD_R.

Step 6. Repeating Steps 1 to 5 for T times, sum annual reduced damage and get one sample of T-year cumulative reduced damage cost$D_{R,all}(T)$. In this research, discount rate was eliminated to focus the discussion on probabilistic characteristics of reduced damage cost.

Step 7. Repeat Step6 for M times and estimate the probability distribution of T-year cumulative reduced damage cost from the many samples of$D_{R,all}(T)$.

Application to the Dam Construction Projects

A. Rainfall generation and Damage cost calculation

The above presented method was applied to four different scenarios of dam construction projects for five actual dams along the Kizu River (TakayamaDam, MurouDam, ShorenjiDam, HinachiDam, NunomeDam), whose locations are displayed in fig. 1. According to Tanaka et.al. [6], when flood beyond design level occurs, the river overflows around the three tributaries' conjunction area, and the overtopping probability of downstream Yodo River becomes very low. Hence we analyze the effect of dams from the reduced damage cost at three tributaries' conjunction area indicated by the red colored box in fig.1. In the flood simulation, we do not consider dyke breach, and only consider damage from overtopping.

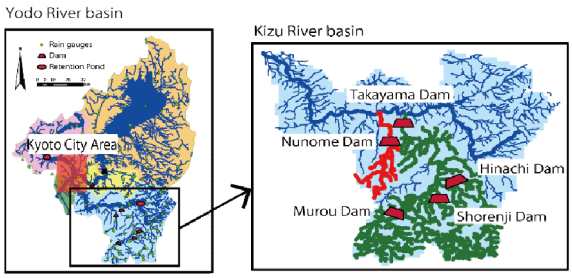

Fig. 1. Figure of Yodo River basin.

We used the conditional CDF of basin-averaged rainfall on duration $G_{R_a|D}(r_a|d_i)$ on the Yodo River basin and rainfall-runoff/inundation models estimated/constructed by Tanaka. et al. [6] as follows. Rain gauge data for 35 years (1980 to 2014) at 156 stations were used in analysis. They extracted spatiotemporal rainfall patterns of the 1,317 rainfall events observed over 35 years, i.e. $N = 1{,}317$. From the basin-averaged rainfall and duration time of the 1,317 rainfall events over 35 years, they estimated the conditional probability distribution of one basin-averaged rainfall on duration time. One rainfall event is defined as a series of rainfall events without dry period longer than 5 hours. In order to estimate conditional probability distribution, the generalized Pareto distribution and two-variable exponential distribution were fitted to the marginal distribution of basin-averaged rainfall $G_{R_a}(r_a)$ and rainfall duration time$G_D(d)$, respectively. Their correlation structure $C(G_{R_a}(r_a), G_D(d))$ was modelled by using the normal copula. According to the Theorem of Sklar[7], this notation indicates the simultaneous distribution$G_{R_a,D}(r_a, d)$. Finally, the conditional cumulative distribution was obtained as

$$G_{R_a|D}(r_a|d) = \frac{1}{g_D(d)}\frac{\partial}{\partial d}G_{R_a,D}(r_a, d). \qquad (9)$$

As a rainfall-runoff model used was 1K-DHM [8], a distributed rainfall runoff model based on a kinematic wave flow approximation. 1K-DHM calculates the slope runoff and river routing at each cell at around 1km (30 sec) resolution over a two dimensional domain. Slope runoff is simulated with the continuity and momentum equations of the

kinematic wave theory, considering saturated and unsaturated subsurface flows and surface flow with the following discharge-storage relation.

$$q = \begin{cases} v_c d_c \left(\frac{h}{d_c}\right)^{\beta} & (0 \le h \le d_c) \\ v_c d_c + v_a (h - d_c) & (d_c \le h \le d_a) \\ \alpha (h - d_c)^m + v_a (h - d_c) + v_c d_c & (d_a \le h) \end{cases} \quad (10)$$

where, q is the slope runoff discharge per unit width; h is the water depth; d_a and d_c are the water depth corresponding to the maximum water content of saturated and unsaturated soil layers, respectively; v_a and v_c are the water velocity of saturated and unsaturated soil layers, respectively; $\alpha = n/\sqrt{\sin\theta}$; n is the roughness coefficient; and θ is the slope gradient. River flow is simulated with a kinematic wave model. All dams in Yodo basin are modeled in accordance with their operation rules, and rainfall-runoff before/after a project is represented by excluding/including the corresponding dam models.

Overflow inundation over the floodplain was modelled with one dimensional local inertial equation for river routing and two dimensional one for floodplain simulation. One dimensional local inertial equation is denoted as

$$\frac{\partial A}{\partial t} + \frac{\partial Q}{\partial x} = 0, \quad (11)$$

$$\frac{\partial Q}{\partial t} + gA\frac{\partial (h+z)}{\partial x} + gn^2 \frac{Q|Q|}{R^{4/3}A} = 0, \quad (12)$$

where t is the time; x is the location in the downstream direction; A is the cross-sectional area; Q is the discharge; z is the elevation; g is the gravity acceleration; n is the roughness coefficient; and R is the hydraulic radius. Neglecting the advective term of the Saint-Venant equation, high speed arithmetic operation is realized with the same level of accuracy as the diffusion equation. Damage cost is calculated for house, households, and office depreciable/stock assets, by multiplying exposed asset at each cell of the inundation model by damage ratio which is a function of maximum flood depth. The function is defined in the manual of MLIT [1].

In accordance with MLIT's manual [1], evaluation period T was set as 50 years.. When disaggregating a rainfall event into to basin-averaged cumulative rainfall and its spatiotemporal pattern as in this study, it is obvious that flood damage cost monotonically increases with basin-averaged rainfall for a fixed rainfall pattern; therefore, we have developed a relation between cumulative rainfall and resulting flood damage cost for all the rainfall patterns before Monte Carlo simulation, then in Step 4 to calculate flood damage cost, flood damage cost for the generated rainfall event was calculated by linearly interpolating the relation for the generated rainfall pattern, instead of running rainfall-runoff/inundation models for all the generated events. Repeating the calculation of T-year cumulative reduced damage cost for $M = 100{,}000$ times, we estimated the probability distribution of the benefit of each scenario.

B. Trial Calculation Results of 50 years total reduced damage cost.

Among the five dams, we first set project J: there is no dam on the Kizu River and construct Takayama Dam on the basin. Figure 2 shows the histogram of simulated T-year cumulative reduced damage cost. Red line indicates the expected value. JPY is converted to USD at a rate of 100 yen per dollar. Obviously, the distribution is skewed leftwards with a long tail. The probability with which the benefit is equal to or over the expected value is about 10-20%, and one with which benefit is obtained is about 55%. On the other hand, extremely large benefit values much larger than the median value occurs with a certain probability. These indicated that the expected value integrated different types of benefit and made it difficult to grasp the whole characteristic of the benefit of the project. By estimating the distribution of reduced damage cost as fig.2, more detailed information as demonstrated above becomes available, which is expected to support more rational decision making.

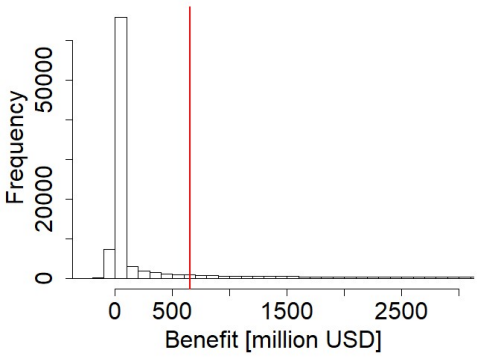

Fig. 2. Histgram of 50-years cumulative reduced damage cost of the project constructing Takayam Dam. Red line indicates expected value.

Differences of Probability Distribution between Projects

Among the five target dams, the Takayama Dam has the largest flood storage capacity. As shown in fig.1, among the other four dams, Nunome Dam is located on a different tributary river. To examine the impact of the location of dams on the estimated probability distribution, we split the construction project of the four dams into projects K, and project L: Project K first constructs three dams except for the Nunome Dam (Shorenji Dam, Murou Dam, and Hinachi Dam), and Project L then constructs the Nunome dam. Table.1 shows the statistics of three projects (J, K, L) gained from their probability distribution of 50-year cumulative reduced damage

cost. Comparing with Projects K and L, Project L shows lower skewness and higher probability of getting more befit equal to or more than expected value, and the occurrence of benefit.

As shown in fig.1, in the Project K, Takayama Dam is already constructed in the same tributary, so dams constructed in Project K can mitigate damage only for flood causing inflow volume over the storage capacity of Takayama Dam. On the other hand, the Project L constructs Nunome Dam in the tributary where no dam has been constructed before; thusNunome dam more frequently shows flood control effect than dams installed by Project K. Accordingly, Project L is expected to benefit the target area more frequently than Project K. As shown in Table.1, difference between the expected value of Projects K and L is about 26%. On the other hand, the probability with which the benefit equal to or more than its expected value by Project L is 230% larger than Project K, indicating that using other statistics provided different characteristics of projects from the expected value .

Relation Between Probability Distribution and Central Limit Theorem

When evaluation period *T* is large enough, probability distribution of *T*-year cumulative reduced damage cost theoretically converges to normal distribution, so reduced damage cost is assumed to distribute around its expected value. Figure.4 shows the variation of histogram of Project J when changing the evaluation period from 50 years to 1,000 years. For comparison of distribution characteristics, cumulative reduced damage cost was converged to annual

Table I. Benefit statsitics of each project

Project	J	K	L
Expected value	655	197	157
Standard variarion	2240	804	355
Skewness	38.3	5.44	2.92
Probability with which benefit becomes larger than expected value	0.18	0.10	0.23
Occurrence probability of benefit	0.55	0.30	0.74

mean value by dividing evaluation year *T*. We can confirm that probability distribution of reduced damage cost skewed leftwards and have a long tail in limited evaluation period of 50 years, but the distribution approaches bilaterally symmetrical and the probability we can actually get benefit equal to or more than the expected value increases as the evaluation period becomes larger. This indicated that the general evaluation period of 50 years are not quite enough to represent the annual reduced damage cost by its expected value.

Conclusions

In the present benefit evaluation method, benefit is represented as the expected value of cumulative reduced damage in evaluation period. However, flooding is a low-frequency event, especially in highly protected areas; thus,it is highly uncertain whether actual reduced damage cost is distributed around its expected value. In this research, in order to quantify stochastic characteristics of benefit, we developed an estimation method of *T*-year cumulative reduced damage cost probability distribution, and applied the method to several scenarios of flood control projects on the Kizu River.

By estimating probability distribution of *T*-year cumulative reduced damage cost, we can get more statistics as well as mean value, and reveal the characteristics of each project. Following findings were obtained in this study:

1. In all the four projects, probability distribution skewed leftwards, and the probability with which we can actually obtain the benefit equal to or more than the expected value is about 10-20%. On the other hand, extremely large benefit values is expected with a certain probability. In the process of averaging reduced damage cost,
2. The expected value of benefit and other statistics such as the probability with which benefit is obtained show different characteristics depending on projects
3. When we set longer evaluation period, 1000 years, distribution of cumulative reduced damage approaches normal distribution, and benefit wasevenly distributed around its expected value, compared with offsetting evaluation period to 50 years. This indicated that *T*-year cumulative reduced damage cost was distorted because the evaluation period was not long enough to represent the expected value as the benefit due to low frequency of flooding.

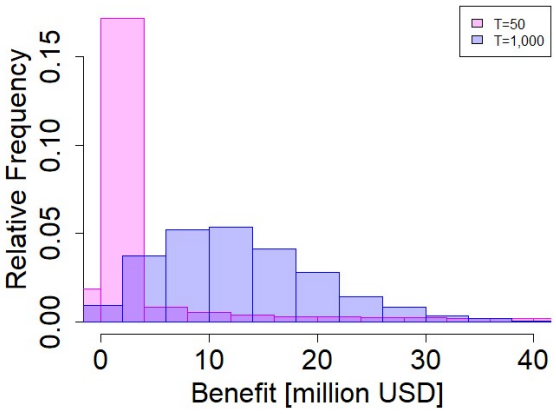

Fig. 3. Histgram of 50 and 1,000 years cumulative reduced damage cost of the project

This study proposed an idea to estimate the probability distribution of *T*-year cumulative reduced damage cost for providing information about various statistics of reduced damage cost and making more rational decision making. We will discuss how to incorporate this idea into the actual decision making process for advanced decision making process of flood control projects.

Acknowledgment

This study was supported by Kansai Energy Recycling Foundation.

References

[1] The flood control economic survey manual (draft) pp. 15-62, 2005.
[2] Apel, H., Thicken, A. H., Merz. B. and Blöschl, G. "A probabilistic modelling system for assessing flood risks", Nature Hazards," Vol. 38, No. 1-2, pp. 79-100, 2006
[3] Falter, D., Schröter, K., Dung, N. V., Vorogushyn, S., Kreibich, H., Hundecha, Y Apel, H., Merz, B. "Spatially coherent flood risk assessment based on longterm continuous simulation with a coupled model chain. Journal of Hydrology, Vol. 524, pp. 182-193 2015.
[4] Yokomatsu, M., Kobayashi, K. "Economic benefit of physical risk reduction by disaster prevention investment", No. 660/Ⅳ-49, pp.111-123, 2000.
[5] Tanaka, T., Tachikawa, Y., Ichikawa Y., Yorozu, K. "A flood risk curve development using conditional probability distribution of rainfall on duration", Journal of JSCE B1 (Hydraulic Engineering), Vol. 72, No. 4, I_1219-I_1224, 2016.
[6] Tanaka, T., Ichikawa, Y., Yorozu, K., Tachikawa, Y. "Development of a probablistic flood damage map and its application to benefit analysis of land raising", Journal of JSCEJournal of JSCEB1 (Hydraulic Engineering), Vol. 72, No. 4, I_1477-I_1482, 2018.
[7] Nelsen, R., 2006. An Introduction to Copulas. Springer, New York.
[8] Tachikawa, Y., Tanaka, T.: 1K-DHM/1K-FRM, http://hywr.kuciv.kyoto-u.ac.jp/products/1k-DHM/1k-DHM.html

Climate change impact on rainfall pattern in Bangkok Metropolitan region

Shotiros Protong[1,a]

Abstract The extreme rainfall trends in Thailand frequently occurred during the past decades. The climate change problems have caused extreme monsoons and tropical cyclones, with heavier rainfall leading to floods and inundations in cities. This research will focus on the comparison of rainfall pattern maps, between both the observed rainfall (1980 – 2017) and the modelled rainfall (2006 – 2050), are supported on Arc GIS software version 10.3. Average observed rainfall data are recorded by the Thailand Meteorological Department (TMD) during the 1980-2017 period. Metropolitan region consists of Nakhon Pathom, Pathum Thani, Nonthaburi, SamutPrakan and SamutSakhon provinces. Rainfall pattern is described by interpolation using the rain stations covering eighteen provinces of the central part of Thailand namely, Bangkok, Nakhon Pathom, Nonthaburi, Pathum Thani, SamutPrakan, SamutSongkhram, SamutSakhon, Uthai Thani, Nakhon Sawan, Ang Thong, Phra Nakhon Si Ayutthaya, Kanchanaburi, Ratchaburi, Chai Nat, Lopburi, Saraburi, Sing Buri and SuphanBuri. The interpolation is used for this case because there are only six rain stations in Bangkok Metropolitan region. The achievement of interpolation which is a part of Arc GIS 10.3, is used to estimate the rainfall values. In general, the rainfall values are usually high in the rainy season (mid-May to October), but this approach calculates the wet days all through the year, due to the probability of flood and inundation corresponding to heavy rainfall not only in the rainy season but also in other seasons. The rainfall values should be calculated for the rainfall intensity (defined as mm of rainfall per twenty-four hours) for the natural disaster analysis. To address the research objective, knowledge and study result in rainfall pattern impact due to climate change show in terms of the rainfall intensity classification. It leads to investigate the disaster risk, vulnerability and adaptation plans for water resources management in the future.

Keywords *rainfall intensity, observed rainfall, modelled rainfall and Arc GIS 10.3*

[1]Department of Water Resources

[a]shotirosprotong@yahoo.com

Introduction

Bangkok Metropolitan has been known as the fast growing economy of Thailand, it contributed the national Gross Domestic Product (GDP) and the government budget as well as population growth continuously increased and also high population density. Flood and drainage problem occurred frequently and severely in Bangkok Metropolitan not only rainy season, but also in other seasons. Flood also affects the infrastructure and the transportation system was disrupted, causing drainage system problem in lowland areas. In Thailand, there are three climate seasons a year, which are the dry season, the rainy season and the winter season. In general, during the middle of February until the middle of May, it is the dry season, lasting three months. In February, the north of Thailand is covered by high pressure from China. Then, it is weakened because of warm air and fog remaining in some areas, thus leading to cool to cold weather in north-eastern and northern parts. In March and April, a hot low-pressure cell influences the northern part, moreover, the southeast and the south winds may lie over the north as the result of hot weather in some areas, causing widespread thunder showers and hot weather on some days. In the dry season, the average maximum temperature is around 35 – 40°C (TMD, 2011).

The history of during the 21st century, the greenhouse gases and aerosols were rapidly released into the atmosphere causing warmer weather and increasing monsoon rainfall. The thermodynamic forcing leads to accumulated precipitation in South Asia as the atmospheric moisture content is higher over the Indian Ocean. Over the second half of the twentieth century, the change of monsoon rainfall has been related to increased greenhouse gases and aerosol concentrations leading to the prediction modelled monsoon under equilibrium. The climate simulation of the 21st century RCP scenario is to provide evaluation of global climate change and respond in the region scale in different climate model. In future simulation, it depends on how climate model reproduces the preindustrial, historical and current circumstances, processes and sensitivities. The intensity of rainfall over the western part of the North Pacific and the center is widely increased (Turner et al., 2012). The trend of rainfall decreased to moderate rainfall, while the increased intensity of monsoon rainfall under the model projection remains high. The overall annual rainfall is relatively low, while daily rainfall changes

are quite high during the Asian monsoon. This study conducts to analyse rainfall pattern under different modelled future emissions of greenhouse gases in Assessment Report 5 (AR5) in emission scenario RCP 8.5. The RCP8.5 describes both assumptions about high population and relatively slow income growth with modest rates of technological change and energy intensity improvements, leading to high energy demand and GHG emissions in the long term for absence of climate change policies (Riahi, 2011). Eventually, rainfall intensity will be evaluated under scenario simulation RCP 8.5 in Bangkok Metropolitan from 2018 to 2050

Description of study sites

Bangkok Metropolitan is located in the central part of Thailand, between latitude 13o 95' and 13o 50' north and between longitude 100o 90' and 100o 32' east. It is bordered by SuphanBuri and Phra Nakhon Si Ayutthaya provinces in the north and, to the east of the Bangkok Metropolitan, by Nakhon Nayok and Chachoengsao provinces, while in the south, it is bordered by the Gulf of Thailand and in the west, by Ratchaburi province (TMD, 2007). Bangkok Metropolitan 2 region is cover Bangkok and five adjacent provinces: Nakhon Pathom, Pathum Thani, Nonthaburi, SamutPrakan and SamutSakhon. Bangkok Metropolitan region has a total area of about 7,762 km2 (TMD, 2011). The study area consists of the following location (Fig 1.):

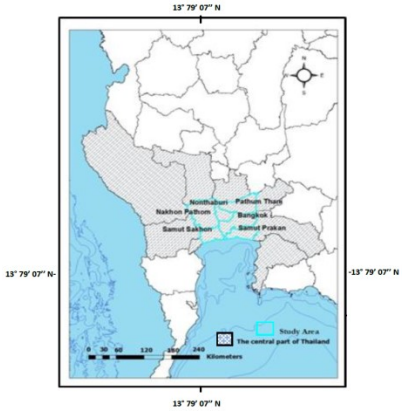

Fig. 1. Location of Bangkok Metropolitan consists of Bangkok and five surrounding provinces: Nakhon Pathom, Pathum Thani, Nonthaburi, SamutPrakan and SamutSakhon.

Methodology

1. Rainfall values analysis

The rainfall calculation was a consideration of both daily rainfall and three-hourly rainfall (Fig. 2). Both daily rainfall and three-hourly rainfall during 1981-2010 are used to calculate the standard hours of daily rainfall. Three hourly data observed rainfall values obtained at the times: 1am, 4 am, 7am, 10am, 1pm, 4pm, 7pm and 10pm (Thai Meteorological Department) and are used to calculate three-hourly rainfall rates for the seventeen rain stations covering eighteen provinces: Bangkok, Nakhon Pathom, Nonthaburi, Pathum Thani, SamutPrakan, SamutSongkhram, Nakhon Sawan, Ang Thong, Phra Nakhon Si Ayutthaya, Kanchanaburi, Ratchaburi, Chai Nat, Lopburi, Saraburi, Sing Buri and SuphanBuri. In terms of extreme rainfall indices, a wet day is defined as a day that has a rainfall amount greater than or equal to 1 mm (Maijandee et al., 2014). Figure 2 shows the processing steps in the rain analysis.

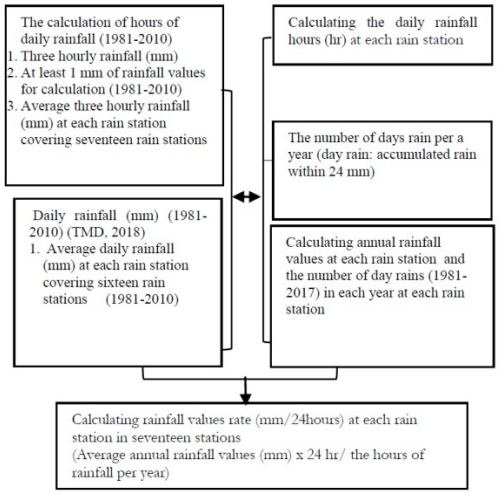

Fig. 2. Methodology of rainfall intensity calculation

2. The future simulation

The General Circulation Model (GCM) explains the relationship between the rising greenhouse gasses and climate conditions at a global and regional scale. But the GCM cannot extend to explain climate change conditions in the local scale, as it displays at coarse a spatial resolution. Therefore, the simulation of the Regional Climate Model (RCM) is necessary to assess the impact of climate change at the local scale.

The Southeast Asia Regional Climate Downscaling (SEACLID) was established as a collaborative project in regional climate downscaling from various countries within the Southeast Asia region. SEACLID aims to downscale a number of CMIP5 GCMs for the Southeast Asia region through task-sharing basis among the institutions and countries involved. The products would be the high-resolution climate change scenarios (25 km x 25 km) for the Southeast Asia region (SEACLID, 2018). For climate change in Thailand, the high-resolution of simulation scenarios are the basic requirement for climate change impact, vulnerability and risk assessment to study at local and regional scales. The precipitation input is needed to predict for future climate, was used to assess the simulation scenario of future change for latitude 13o 56′ and 15o 66′ north and between longitude 99o 29′ and 101o 40′ east. During the 2006 to

2017 period, the comparison between observed and modelled annual rainfall is presented for calibration.

Over the baseline period 2006 to 2017, for seventeen central rain stations covering eighteen provinces, there are four rain stations in Bangkok, two rain stations in Lop Buri, SuphanBuri, Kanchanaburi, one rain station in Samutprakan, Pathum Thani, Nakhon Pathom, Ratchaburi, Chai Nat, Si Ayuttaya and Nakhon Sawan respectively. The average of observed annual rainfall volumes and the annual modelled rainfall volumes arecompared covering seventeen rain stations. The comparison between observed and modelled rainfall presented approximately 2.20% - 15.3% difference from 2006 to 2017 respectively.

Results and Discussion

1. Observed rainfall calculation

The average observed rainfall values between 1981 and 2017 were calculated, covering eighteen provinces: Bangkok, Nakhon Pathom, Nonthaburi, Pathum Thani, SamutPrakan, SamutSongkhram, SamutSakhon, Uthai Thani, Nakhon Sawan, Ang Thong, Phra Nakhon Si Ayutthaya, Kanchanaburi, Ratchaburi, Chai Nat, Lopburi, Saraburi, Sing Buri and SuphanBuri. This spatial scale was selected as the downscaling of the SEACLID covered all eighteen provinces, including the study site (Figure 1). The average annual rainfall values werecalculated in mm/24 hours for accumulated rainfall within 24 hours, i.e. the wet time period, according to the natural disaster analysis. Thus, average three-hourly rainfall from 1981 to 2010 were used to calculate the standard of days rain per year for rain stations covering eighteen provinces. The days-rain per year and annual rainfall were used to calculate rainfall in mm/24 hours as in Table 1.

The interpolation of rainfall intensity values in seventeen rain stations covering the eighteen provinces for spatial analysis. Then, the interpolation map is presented with rainfall values (mm/24 hours) covering the eighteen provinces. This result is divided into two parts. The first part describes the intense rainfall distribution map for the observed rainfall in Bangkok metropolitan regions, calculating rainfall values from 1980 to 2017. The second part, the intense rainfall distribution map in the future simulation during 2017-2050 will be forecast by SEACLID. Finally, the comparison of rainfall patterns, between both the observed rainfall present-day and the modelled rainfall, are described by maps.

As a result of the spatial rainfall intensity distribution, the rainfall amount (mm/24 hours) in the Bangkok Metropolitan region was less than other regions in the central part from 1980 to 2017. The average observed rainfall values between 1980 and 2017 were calculated, covering six provinces: Bangkok, Nakhon Pathom, Pathum Thani, Nonthaburi, SamutPrakan and SamutSakhon provinces. The average annual rainfall values were calculated in mm/24 hours for disaster analysis because this unit will show accumulated rainfall within 24 hours, i.e. the wet time period. There was a large rainfall intensity amount in the northern of central part, from around 90 -130 mm/24 hours during 1980 – 2017 period. The rainfall patterns slightly increase in Bangkok Metropolitan regions from 1980–1990, 1991–2000, 2001–2010, and 2011–2017 respectively as shown in Fig. 3 – Fig 6.

Rainfall values (1980-2017)	Bangkok	Ayutthaya	Nakhon Sawan	Chai Nat	Pathum Thani	RatchaBuri	Lopburi	SamutPrakan	Kanchanaburi	Nakhon Pathom	SuphanBuri
Average annual rainfall	1,499.2	1,131.4	1,309	1,127.1	1,239.8	1,098.6	1,113.5	989.6	1,412.7	1,010.0	1,027.5
Days rain per a year	21	8	13	9	10	9	13	18	18	9	14
Average rainfall (mm/24 hours)	71.4	141.4	100.7	125.2	124.0	122.1	85.6	55.0	78.5	112.2	73.4

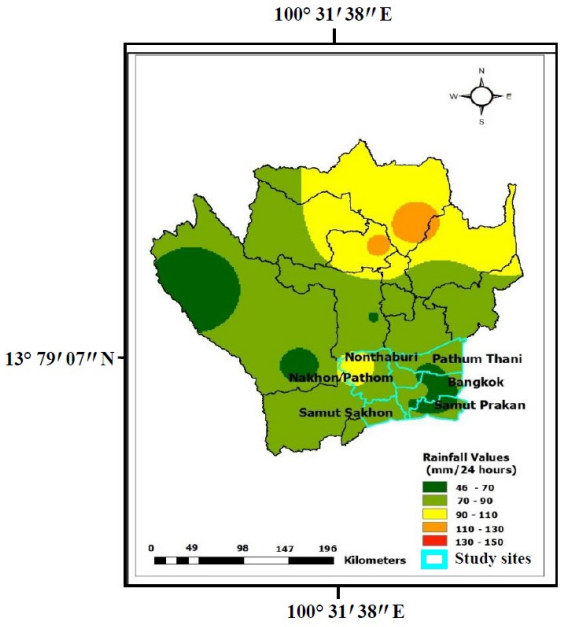

Fig. 3. The interpolated map covering eighteen provincesfrom 1981 to 1990 and the rainfall values focusing on Bangkok Metropolitan region

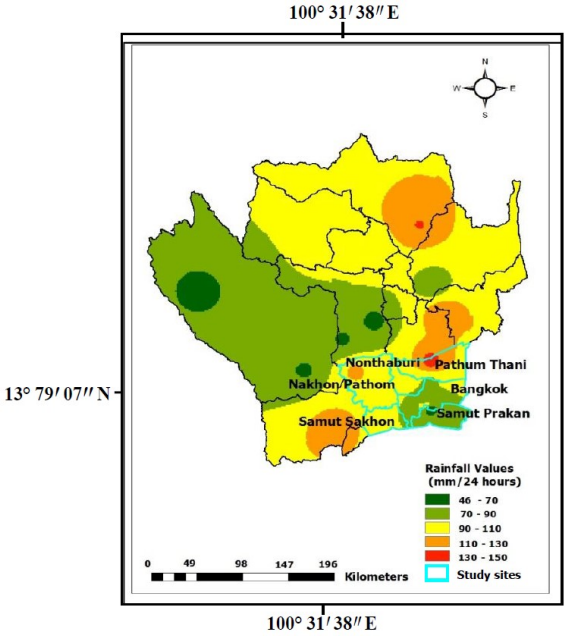

Fig. 5. The interpolated map covering eighteen provinces from 2001 to 2010 and the rainfall values focusing on Bangkok Metropolitan region

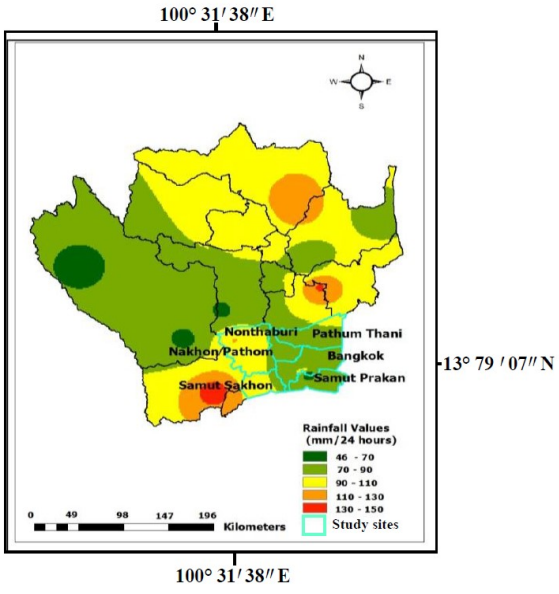

Fig. 4. The interpolated map covering eighteen provinces from 1991 to 2000 and the rainfall values focusing on Bangkok Metropolitan region

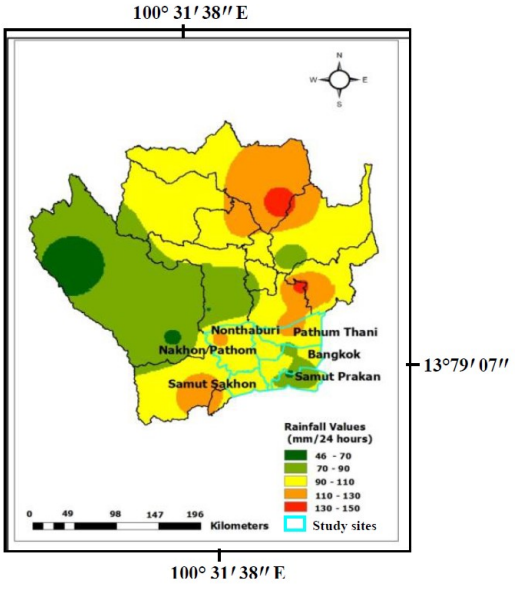

Fig. 6. The interpolated map covering eighteen provinces from 2011 to 2017 and the rainfall values focusing on Bangkok Metropolitan region

The rainfall values analysis focused on Bangkok Metropolitan region, the strongly intense rainfall present in six provinces: Bangkok, Pathum Thani, SamutSakhon: 46-90 mm/24 hours, Nonthaburi, SamutSakhon are 70-90 mm/24 hours and between 70 - 110 mm/24 hours in Nonthaburi from 1981 to 1990, while Bangkok, SamutSakhon and SamutSakhon: 70-110 mm/24 hours, between 90 - 130 mm/24 hours in Nakhon Pathom, Nonthaburi and Pathum Thani from 2000 to 2017 respectively. The trend of rainfall pattern slightly increased from 1981 to 2017.

2. Rainfall pattern in the simulation scenario at local scale: downscaling

The prediction of daily rainfall is obtained by SEACLID from 2018 to 2050 under simulation scenario RCP 8.5, which is only 365 days per year. In this study, the precipitation data is downscaled from latitude 13°56′ and 56°66′ north and between longitude 99°29′ and 101°40′ east, which is the central part of Thailand. The average three-hourly rainfall totals from 1981 to 2010 are used to calculate the standard of days of rain per year for each rain station covering six provinces. The days of rain per year and annual rainfall were used to calculate rainfall in mm/24 hours as in Table 1. The modelled rainfall intensity values will be averaged by the interpolation approach and represented by the rainfall intensity rate on the map as show in Fig 7 - Fig 9.

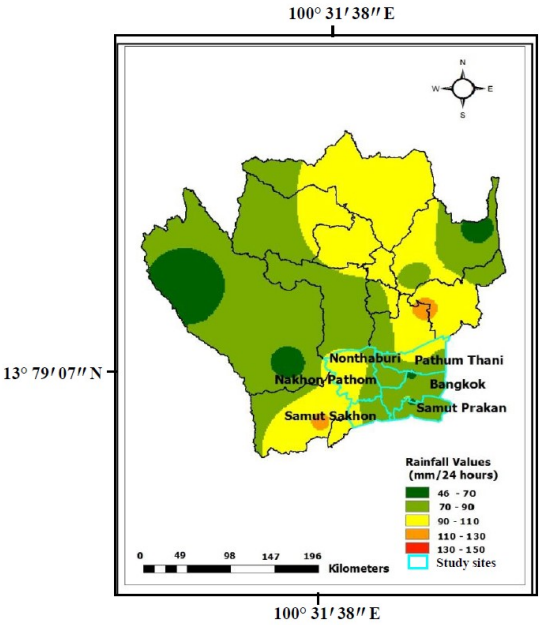

Fig. 7. The interpolated map covering eighteen provincesfrom 2018 to 2027 and the rainfall values focusing onBangkok Metropolitan region

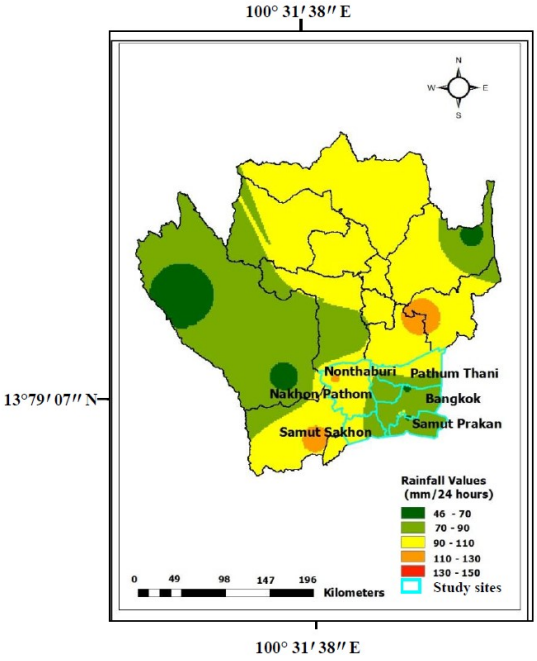

Fig. 8. The interpolated map covering eighteen provincesfrom 2028 to 2037 and the rainfall values focusing onBangkok Metropolitan region

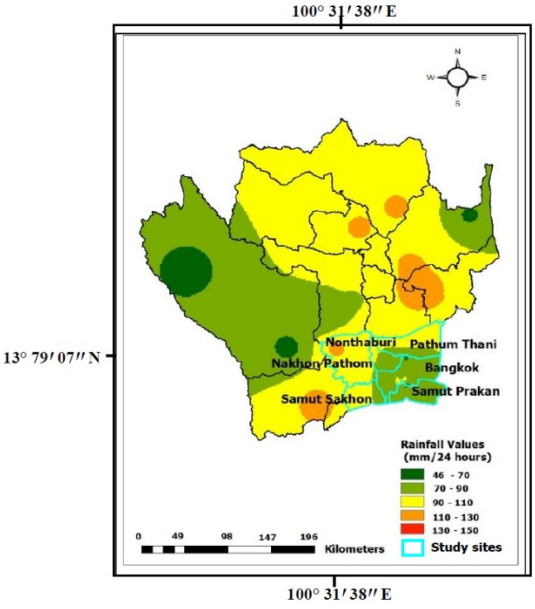

Fig. 9. The interpolated map covering eighteen provincesfrom 2037 to 2050 and the rainfall values focusing onBangkok Metropolitan region

The rainfall values analysis focused on Bangkok Metropolitan region, the strongly intense rainfall present in six provinces: Bangkok, Nonthaburi, SamutPrakan: 70-90 mm/24 hours, Pathum Thani SamutSakhon and Nakhon Pathom are 70-110 mm/24 hours from 2018 to 2027, while Bangkok and SamutPrakan: 70-90 mm/24 hours, between 90 - 130 mm/24 hours in Nonthaburi and Pathum Thani, and 90 and 130 mm/24 hours in SamutSakhon and Nakhon Pathom from 2037 to 2050 respectively. The trend of rainfall pattern slightly increased from 2018 to 2050.

3. The comparison of observed and modelled rainfall intensity in Bangkok Metropolitan region

Bangkok Metropolitan region is focused on the urban areas because population growth population density increased continuously in city. Therefore, rainfall values should be calculated for the rainfall intensity (defined as mm of rainfall per twenty-four hours) for the disaster analysis such as flood and drainage in city. The trend of both observed and modelled rainfall intensity from 1981 to 2050 slightly increases: most areas of Bangkok are 40 – 90 mm/24 hours from 1981 to 2017 and 70 - 90 mm/24 hours from 2018 to 2050. During 1981 to 2017 period, the increasing of rainfall intensity leaded to rainfall pattern areas. The observed rainfall intensity (mm/24 hours) increased from 40 – 70, 70 – 90, 90 – 110 in Bangkok respectively (Fig 7 – Fig 8). In terms of modeled rainfall intensity (mm/24 hours), the increasing of both observed and modelled rainfall intensity also leaded to bigger impact of rainfall pattern areas in Pathum Thani and Nakhon Pathom provinces from 1981 to 2050 (Fig 3 – Fig 9).

Finally, both observed and modelled rainfall pattern areas are almost in the same direction however the trend of rainfall intensity increase gradually from 1981 to 2050.

Turner (2012) observed change in rainfall has been responding to anthropogenic activity over the decades in the twentieth century. The result of aerosol concentration and greenhouse gases have increased and linked with human activity. By the end of the twenty-first century, these phenomena will lead to increased rainfall. The IPCC (2012) insists that extreme weather conditions rapidly growing in the future will lead to changed rainfall, both in intensity and seasonality.

Acknowledgement

I would like to say thank for Thai Meteorological Department(TMD) and Ramkhamhaeng University (RU) to give me a secondary data. Thanks to Department of Water Resources to support me for this public paper.

Reference

[16] DWR (2018) (Department of Water Resources) The political boundary data base in Thailand.
[17] Houghton, J. (2009) Global Warming. New York: Cambridge University Press. pp 139-140.
[18] Maijandee, S., Kreasuwun, J., Komonjinda, S., Promnopas, W. (2014) Effects of Climate Change on Future Extreme Rainfall Indices over Thailand. Global NEST, 16, 306-315.
[19] Riahi, K., Rao, S., Krey, V. et al. Climatic Change (2011) 109: 33. https://doi.org/10.1007/s10584-011-0149-y.
[20] SEACLID, (The Southeast Asia Regional Climate Downscaling) (2017) Preparation of Climate Change Scenarios for Climate Change Impact Assessment in Thailand Southeast Asia Regional Thai Centre.
[21] TMD (2011) (Thai Meteorological Department) [On-line]. Available at: http://www.tmd.go.th/info/info.php (Accessed on 25.10. 2018)
[22] TMD (2018) (Thai Meteorological Department) The rainfall and rain stations data base in Thailand.
[23] Turner, Andrew, G., and Hariharasubramanian Annamalai, Climate change and the South Asian summer monsoon. Nature Climate Change 2.8 (2012): 587-595.

Prospect of Discharge at Daecheong and Yongdam Dam Watershed under Future Greenhouse Gas Scenarios using SWAT Model

Seon Hui Noh[1,a], Kwansue, Jung[1,b] and Jinhyeog Park[1,c]

Abstract

In this study, the future expected discharges is analyzed at Daecheong and Yongdam Dam Watershed under Future Greenhouse Gas Scenarios based on RCM with 1 km spatial resolutions from Korea Meteorological Agency(KMA). HadGEM2-AO, which is the climate change prediction model that KMA recently introduced is used for this study. Geum river watershed area is 9,914.013㎢ and there are two dams, one of dam is Daecheong Dam completed in 1980, the other dam is Yongdam Dam completed in 2001. The runoff is simulated using the ArcSWAT model from 1988 to 2010. The simulation is in good agreement with measured data at the Yongdam Dam and Daecheong Dam showing R^2 of 92.25% and 95.40% respectively. Using the average discharge from 2001 to 2010 as a baseline, the simulated annual average discharge increased by approximately 47.76% and 36.52% under the RCP4.5 scenario and RCP8.5 scenario respectively for the from 2011 to 2100.

Keywords *SWAT, Discharge, Climate Change, RCP Scenario, HadGEM2-AO*

[1]Department of Civil Engineering
Chungnam National University
Daejeon, Korea

[a]tjsgml2022@hanmail.net
[b]ksjung@cnu.ac.kr
[c]park5103@kwater.or.kr

Uncertainty in Runoff Estimation for a Catchment of the Tha Chin River's Upper Plain in Chai Nat Province, Thailand

Sombat Chuenchooklin[1,a], Udomporn Pangnakorn[2,b] and Puripus Soonthornnonda[3,b]

Abstract Runoff production to the upstream of the HuaiKhot Wang Man diversion canal with a catchment of the HuaiKhunKaew watershed in the upper part of the Tha Chin Basin was studied in 2006 – 2013. The soil and water assessment tool (SWAT) and the hydrological modeling system (HMS) using on the Climate Forecast System Reanalysis (CFSR) were applied to the simulation of the daily outflow. The results of both SWAT and HMS fitted to the observed data at the outlet during the calibration in 2010-2012 in the basis of monthly mean outflow according to the Nash and Sutcliffe efficiency (NSE), correlation (R^2), and the root mean square error (RSME) were 0.62 and 0.18, 0.66 and 0.46, and 14.3 and 18.1 m^3/s, respectively. These models show they are applicable enough for further efficient water management in the downstream area.

Keywords *streamflow estimation, PUB, SWAT, HMS, CSFR*

[1]Assoc. Prof.: Department of Civil Engineering, Faculty of Engineering, Naresuan University, Phitsanulok, 65000, Thailand
[2]Assoc. Prof.: Department of Agricultural Sciences, Faculty of Agriculture Natural Resource and Environment, Naresuan University, Phitsanulok, 65000, Thailand
[3]Lecturer: Department of Civil Engineering, Faculty of Engineering, Naresuan University, Phitsanulok, 65000, Thailand

[a]sombatc@nu.ac.th

Introduction

The small to the medium watershed is usually a lack of hydrological data collection, which may consider as the Prediction in Ungauged Basin (PUB) [1]. The way of obtaining the quantity of surface flow by some modeling has been widely used such as the Hydrologic Modeling System (HMS) [2]. It is the rainfall-runoff model that user can apply with any transform method, loss rate, and base-flow methods in the component of the basin model manager. HMS components include meteorological, control specifications, time-series-paired or grid data manager, that can compute surface runoff, return flow, reservoir, diversion, source & sink, flow, reach routing, and etc. The production from HMS is the hydrograph for specific sub-basin and reach, that can be directly inputted to the worldwide 1 or 2-dimensional hydrodynamic model of the River Analysis System (RAS) [3]. The Soil and Water Assessment Tool (SWAT) [4], is a physical base or river basin scale model developed to quantify the impact of land management practices on water, sediment and agricultural chemical yields in large, complex watersheds with varying soils, land use, and management conditions over long periods of time. SWAT components include weather, surface runoff, return flow, percolation, evapotranspiration, losses, pond, crop growth and irrigation, groundwater flow, reach routing, and etc. Both HMS and SWAT production are the hydrograph for every sub-basin and in the river reaches as surface runoff model. RAS is designed to perform one and two-dimensional hydraulic calculations for a full network of natural and constructed channels with the graphical user interface (GUI). The system contains several hydraulic design features that can be invoked once the basic water surface profiles are computed. Recently, the Japanese distributed hydrological model such as the Integrated Flood Analysis System (IFAS) developed by PWRI [5], which can be applied to the larger watershed. However, IFAS has taken long simulation time than others in comparing the result of the watershed.

Inefficient water resource management for the challenging of the flood and drought problems in the small to a medium watershed in Thailand was reported. The managing of the diversion channel seemed to be difficulty operated because of uncertainty streamflow runoff caused by the fluctuation of upstream runoff with none of any properly water storage systems as poor water management [6, 7]. The challenging of

surface water problems in NongMamong district, Chai Nat province, Thailand had proposed to study. It included a diversion channel: HuaiKhot – Wang Man canal to convey part of a flood from upstream and store in the proposed retention ponds [8]. Thus, this study aims to analyze the daily streamflow discharge produced from the upstream watershed of the HuaiKhot - Wang Man diversion channel in the NongMamong district using both HMS and SWAT as the comparative testing of the sensitivity from both models while compared to the observed data at an outlet of the basin.

Material and Method

A. Study Area

The study area: HuaiKhunKaew watershed locates in the upper part of the Tha Chin Basin, that situates between the southern part of the Sakae Krang river basin and the upper plain of the Tha Chin river basin in Uthai Thani and Chai Nat provinces, Thailand. The HuaiKhunKaew is a major stream and flows directly from west to east of the study area. The HuaiKhot is the largest tributary stream with sub-watershed meets the lower plain of the HuaiKhunKaew stream. The overall drainage area watershed is approx.1,066 km^2 measured at the hydrological observation station at C.51 from the Royal Irrigation Department (RID). An existing diversion channel: HuaiKhot - Wang Man conveys the water flow from the HuaiKhot sub-basin in Ban Rain district, Uthai Thani province to NongMamong district in Chai Nat province. with the flow rate of 10 m^3/s [9]. The study area showed in Fig. 1.

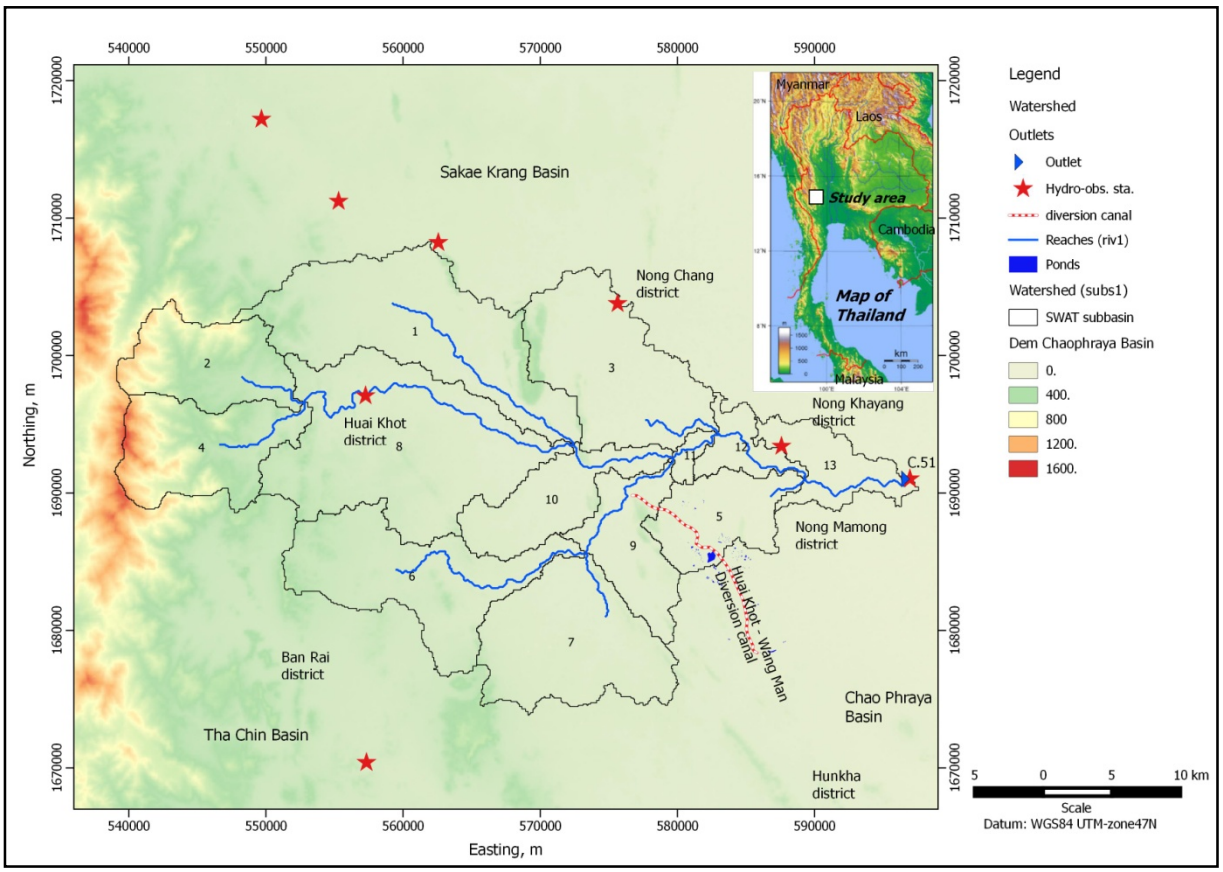

Fig. 1. Location of the study area located in the upper plain of the Tha Chin's river: HuaiKhunKaew watershed and its 13 sub-basins, stream networks, outlet, observed station, altitude (DEM 30m), and the HuaiKhot – Wang Man diversion canal in NongMamong district, Chai Nat province

B. Models Application

The current study applied the SWAT as for the hydrological study and water balance using global soils map, land-use maps, and the Climate Forecast System Reanalysis (CFSR) from global weather data. In this study, SWAT was modeled using an open source geographic information system platform calling the Quantum GIS (QGIS) interface as QSWAT [10]. The comparative study applied HMS as for the calculation daily river outflow from each sub-basin using CSFR.

The first model applied by using SRTM-DEM [11] in the QSWAT as for the watershed delineation. There were 13 sub-basins included stream networks, and topographic slope, as well as the global

land uses and soils maps via SWAT editor [12]. The full hydrological response unit (HRU) contained 6 land-use groups i.e. paddy field and upland crops (CRIR), other uplands (CRWO), mixed forest (FODB), forest (FOEB), grassland (SAVA), shrub tree (SHRB). Each HRUs contained soil, land-use, curve number (CN), soil-loss, and etc. These data resulted in sub-basin parameters that should be calibrated in order to ensure that the simulated result from the model fit to the observed data. These data were applied to HRUs in each sub-basin showed in Fig. 2.

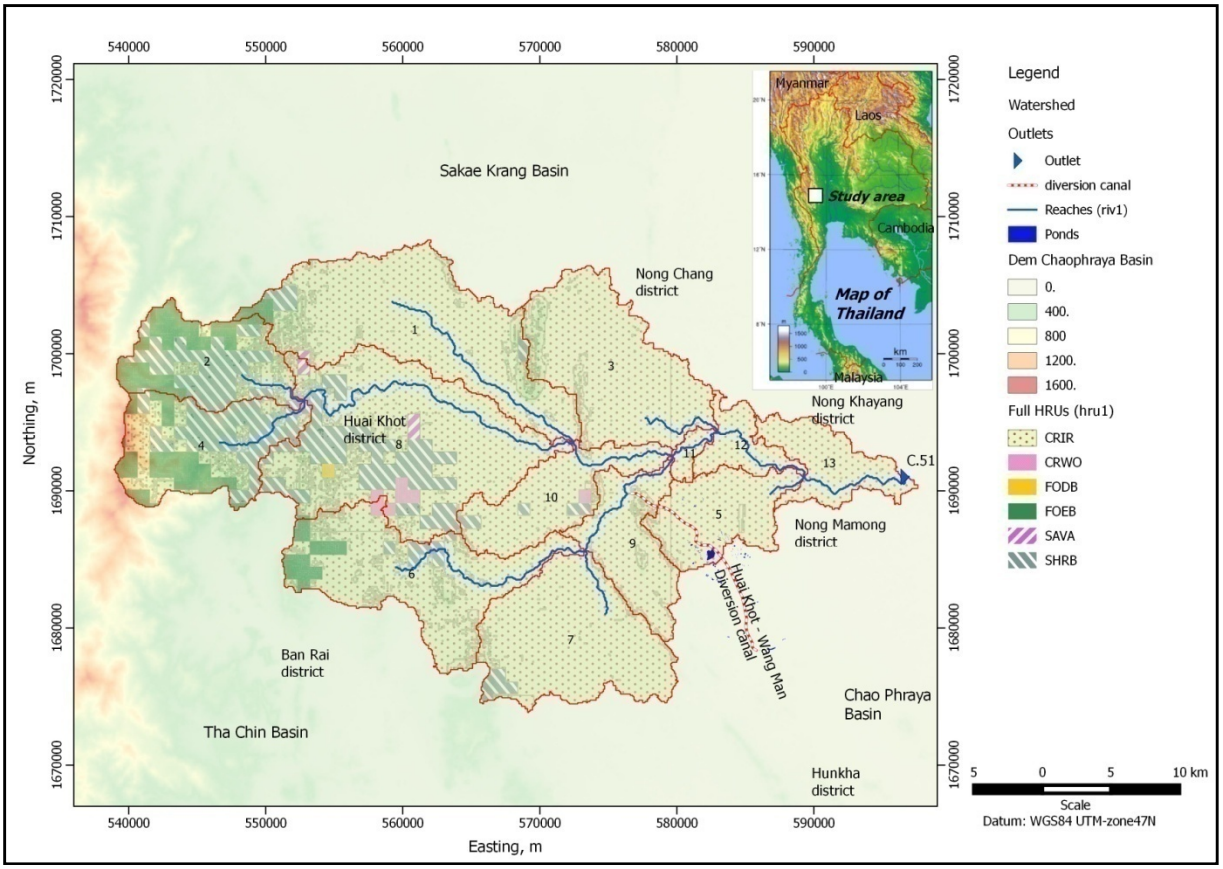

Fig. 2. The full 6- HRUs grouping resulted by using the global land use classes and soil types overlaying on the existing topographic map

The HMS modeled by overlaying with existing streamflow layouts layer. It included 6 sub-basins with each area of 408, 82, 282, 58, 112, and 123 km^2, respectively. In addition, the stream reaches and junctions were modeled as shown in Fig. 3. The basin parameters based on given the initial loss, constant loss late, and transformation by the Clark unit hydrograph.

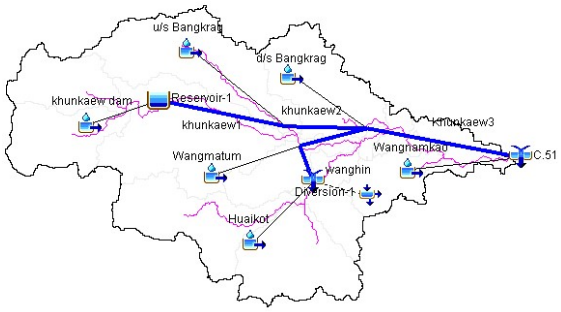

Fig. 3. The location of sub-basins, stream reaches, junctions, and outflow of was modeled for the HuaiKhunKaew based on the HMS.

C. Rainfall Data

The CSFR data had proved that it could be reliably applied to watershed modeling across a variety of hydro-climate regimes and watersheds with a good stream flow predictions particular for PUB [12]. CSFR data with 6 grid points in the basin were applied to both models and using the interpolation method as aerial rainfall based on Thiessen polygon and fitted to the observed data in 2007 – 2013 [11].

D. Model Sensitivity

The Nash and Sutcliffe efficiency (NSE) model [12], and the root mean square error (RSME) were used to test the model sensitivity while compared to the observed data particular with daily river flow discharge. NSE is computed as follows:

$$\mathrm{NSE} = 1 - \left[\frac{\sum_{i=1}^{n}\left(Y_i^{obs} - Y_i^{sim}\right)^2}{\sum_{i=1}^{n}\left(Y_i^{obs} - Ymean\right)^2}\right] \qquad (1)$$

where Y_i^{obs} is the ithobservation for the constituent being evaluated, Y_i^{sim} is the ith simulated value of the constituent being evaluated, Y^{mean} is the mean of observed data for the constituent being evaluated, and n is the total number of observations. NSE ranges between $-\infty$ and 1.0 (1 inclusive), with NSE = 1 being the optimal value. Values between 0.0 and 1.0 are generally viewed as acceptable levels of performance, whereas values <0.0 indicates that the mean observed value is a better predictor than the simulated values, which indicates unacceptable performance.

The root mean square error (RSME) is computed as follows:

$$\text{RSME} = \sqrt{\frac{\sum_{i=1}^{n}(Y_i^{obs} - Y_i^{sim})^2}{n}} \qquad (2)$$

RSME incorporates the benefits of error between simulated result and observed data.

The simulated production of daily and monthly streamflow in each reach was compared to the observed data based on the correlation (R^2).

Results

The results of both HMS and SWAT models based on daily outflow discharge in 2010-2012 were plotted to the observation data at C.51 and CSFR from global rainfall as shown in Fig. 4.

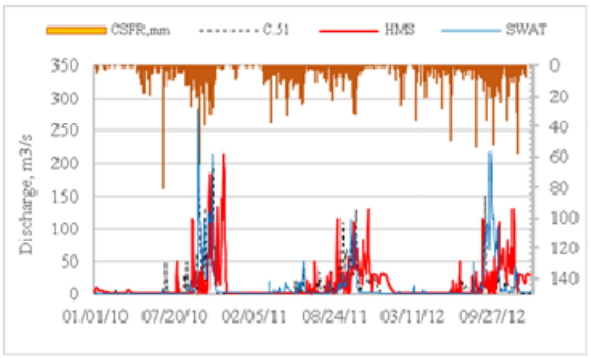

Fig. 4. Comparison of daily simulated and observed flow for SWAT and HMS outlet at C.51 during the model calibration in 2010-2012

The above results from SWAT showed that it incorporated to the calibrated parameters with the most effect by the average basin curve number (CN) of 61.6 and correlation fitted to the observation data with R^2 of 0.51, NSE of 0.42, and RSME of 22.68 m^3/s. However, the results from HMS was fair with R^2 of 0.09, NSE of -0.58, and RSME of 31.07 m^3/s, respectively. Instead of using daily calibration, the monthly basis of both simulated and observed from both models was applied to this study and the result from both HMS and SWAT outflow hydrographs were compared to the observed data at C.51 and CSFR global rainfall as shown in Fig. 5.

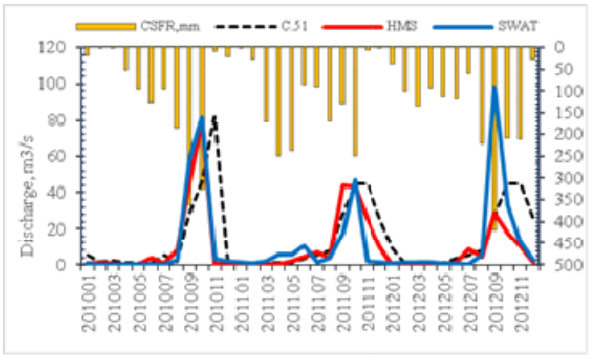

Fig. 5. Comparison of monthly simulated and observed flow for SWAT and HMS outlet at C.51 during the model calibration in 2010-2012

The results of both SWAT and HMS fitted to the observation data with NSE of 0.62 and 0.18, R^2 of 0.66 and 0.46, RSME 14.28 and 18.13 m^3/s, respectively. Those calibration results were good enough for the model validation. Table 1 showed the model sensitivity during the calibration in 2010-2012 of both SWAT and HMS models.

Table I. Comparative of model sensitivity during the calibration of both HMS and SWAT in 2010-2012

No.	Monthly calibration in 2010-2012		
	Model sensitivity	***HMS***	***SWAT***
1	RMSE (m^3/s)	18.13	14.28
2	NSE	0.18	0.62
3	R^2	0.46	0.66

Table 2, Fig. 6, and Fig. 7 showed model sensitivity during the verification in 2013 of both SWAT and HMS models. The results also fitted to the observation data with NSE of 0.71 and 0.46, R^2 of 0.76 and 0.58, RSME 9.73 and 13.25 m^3/s, respectively.

Table II. Comparison of model sensitivity during the validation stages between HMS and SWAT in 2013

No.	Monthly validation in 2013		
	Model sensitivity	***HMS***	***SWAT***
1	RMSE (m^3/s)	13.25	9.73
2	NSE	0.46	0.71
3	R^2	0.58	0.76

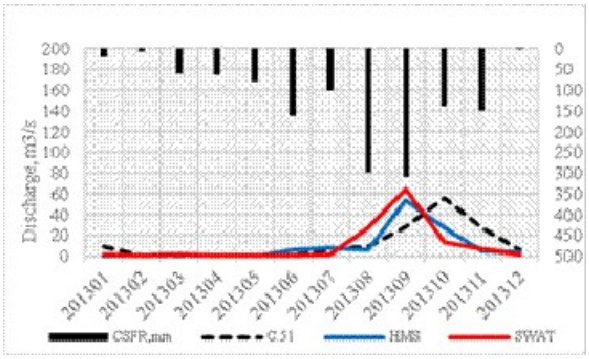

Fig. 6. Comparison of monthly simulated and observed flow for SWAT and HMS outlet at C.51 during the model validation in 2013

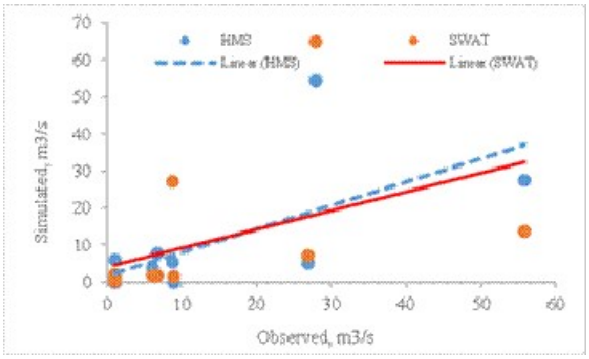

Fig. 7. Correlation of monthly simulation discharge and observation at C.51during the model verification from both SWAT and HMS in 2013

Discussion

The results of runoff production to the outlet of the HuaiKhunKaew watershed using both SWAT and HMS models in 2010 – 2013 showed the difference in model sensitivity of both during calibration and verification in 2010-2012 and 2013, respectively. The SWAT model seems to be very applicable and results are realized to the observed data. However, the complication of the calibration parameters of SWAT is more difficult than HMS with less parameter. The CFSR is the most convenient for applying in both models. The inspection on sensitivity should be carried out and compared to ground-based observation data.

Conclusions and Recommendation

Both models of SWAT and HMS can be applied for an efficient downstream canal management such the HuaiKhot - Wang Man diversion canal as well as the managing of the regulated structures by given the amount of inflow discharge to the canal from the model based on existing basin parameters. Recently, much global rainfall models produce the forecasted rainfall for coming 1 or 2 weeks. The amount of streamflow entering the gate can be estimated using either HMS or SWAT.

Acknowledgment

The authors would like to express our gratitude and thank the Thailand Research Fund (TRF) for funding research the subject "The Development of Supporting Mechanisms for Budget Planning of Water Resources and Agriculture based on the Application of Information Technological Linkages (ITLs) in Chai Nat Province". We also thank the Governor of Chai Nat Province and their related local agencies including the Provincial Land Development, Agriculture, NongMamong Municipal, Regional Irrigation Office XII included Chai Nat Irrigation Office. Finally, we would like to thank Naresuan University (NU) to support the research.

References

[1] G. Blöschl, "Predictions in ungauged basins – where do we stand?", Proceedings of the International Association of Hydrological Sciences, Copernicus Publications, 373, 57-60, 2016, retrieved from http://www.proc-iahs.net/373/57/2016/.

[2] US Army Corps of Engineers (USACE), "Hydrological Modeling System HEC-HMS", 2017, retrieved from http://www.hec.usace.army.mil/.

[3] J. G. Arnold, and N. Fohrer, "SWAT2000: Current Capabilities and US Army Corps of Engineers, "HEC-RAS's User Manual", 2016, retrieved from http://www.hec.usace.army.mil/.

[4] Research Opportunities", Applied Watershed Modeling. Hydrological Process, 19, 563-572, 2005, retrieved from http://dx.doi.org/10.1002/hyp.5611.

[5] Public Works Research Institute (PWRI), "Integrated Flood Analysis Systems: IFAS Version 1.2 User's Manual", 2017, retrieved from http://www.icharm.pwri.go.jp/research/ifas/.

[6] S. Hungspreug, W. Khao-uppatum, and S. Thanopanuwat, "Operational Flood Forecasting for Chao Phraya River Basin. Proceedings of the International Conference on The Chao Phraya Delta: Historical Development, Dynamics and Challenges of Thailand's Rice Bowl", Kasetsart University, Bangkok, 12-15 December 2000.

[7] Japan International Cooperation Agency (JICA), "The Study on Integrated Plan for Flood Mitigation in Chao Phraya River Basin. Summary and Main Report", Royal Irrigation Department Kingdom of Thailand, 1999.

[8] Thailand Research Fund (TRF), Final Report: The Development of Supporting Mechanisms for Budget Planning of Water Resources and Agriculture based on the Application of Information Technological Linkages (ITLs) in Chainat Province, Water Resource Research Center of Naresuan University, 2018.

[9] Royal Irrigation Department (RID), "Reconnaissance Study of the Huai Khot - Wang Man Diversion Canal Systems and Regulating Structures in Ban Rai and Nong Mamong Districts", Prepared by the Engineering Branch of Regional Irrigation Office 12 Chai Nat (in Thai and unpublished), 2015.

[10] Y. Dile, R. Srinivasan, and C. George, "QGIS Interface for SWAT (QSWAT version 1.5)", 2018, https://swat.tamu.edu/.

[11] D. R. Fuka, M. T. Walter, C. MacAlister, A. T. Degaetano, T. S. Steenhuis, Z. M. Easton, "Using the Climate Forecast System Reanalysis as weather input data for watershed models", Hydrological Processes, 2013, Published online in Wiley Online Library, DOI: 10.1002/hyp.10073.

[12] J. E. Nash, and J. V. Sutcliffe, "River flow forecasting through conceptual models: Part 1. A discussion of principles", Journal of Hydrology, 10 (3), p282-290, 1970.

A Study on the Hydraulics Estimate of Tamsui river under Climate Change

Chih-Tsung Huang[1], Meng-Hsuan Wu[1], Wei-Cheng Lo[1] and Chen-Min Kuo[1]

Abstract This study aims to discuss the influence of A1B(CMIP3) and RCP8.5(CMIP5) climate change scenarios on flood analyses. Urban flood disasters have become a serious problem for city and river management worldwide, especially under the changing climate. This research discusses the influences of rainfall, discharge and flood stage in Tamsui River under different climate change scenarios. The downscaling rainfall data of CMIP3 and CMIP5 are provided by TCCIP (The Taiwan Climate Change Projection and Information Platform Project) and are used for frequency analysis to generate the 2-day max rainfall of a 200-year return period. Then, the 200-year 2-day max discharges of each section of Tamsui River are calculated using the unit hydrograph method. The 200-year 2-day discharges were used as inputs into the HEC-RAS hydraulic model to calculate flood stage. The results showed that compared to the A1B(CMIP3) scenario, the RCP8.5(CMIP5) scenario shows a 1%~5% increase in rainfall, 4%~6% increase in discharge, and 1%~3% increase in flood stage.

Keywords *climate change, HEC-RAS, flood stage*

[1]Department of Hydraulic and Ocean Engineering
National Chen Kung University
Tainan, Taiwan

Introduction

Due to the impact of climate change, the frequency of extreme rainfall events has been increased significantly [1]. Many countries already have awareness of the impacts of climate change. The Intergovernmental Panel on Climate Change (IPCC) had published several assessment reports in 1990, 1995, 2001, 2007 and 2014 respectively. The climate data form Fourth Assessment Report (AR4) on 2007 used the Coupled Model Intercomparison Project Phase 3 (CMIP3), the latest one Fifth Assessment Report (AR5) in 2014 was based on Coupled Model Intercomparison Project Phase 5 (CMIP5). According to Taylor et al. [2], whether in AR4 or AR5, the intensity and frequency of extreme rainfall events increase in the middle and low latitude regions. Kitch et al. [3] used the climate data form RCP4.5 and RCP8.5 scenarios of AR5 to analysis the global rainfall change. The result showed that the heavy rainfall in South Asia significantly increased.

This study aims to discuss the difference of rainfall between the AR4 and AR5 of IPCC. The A1B (CMIP3) scenario of AR4 and the RCP8.5(CMIP5) scenario of AR5 were selected respectively. The A1B (CMIP3) scenario assumes that global population peaks in mid-century and declines thereafter. The RCP8.5 (CMIP5) scenario was indicated by the radiative forcing in the year 2100 relative to 1750 greater than 8.5 watts per square meter. It means greenhouse gases are highly discharged, and there is no measure to reduce greenhouse gases in countries around the world. Based on these two scenarios, we discuss the influences of rainfall, discharge and flood stage in Tamsui River under different climate change scenarios.

Research Methodology

This study aims to quantify the effects of climate change in the Tamsui River, the flowchart is shown in Fig. 1. The first, the precipitation and rainfall distribution of A1B and RCP8.5 climate change scenarios were analyzed. The second, the result of rainfall analysis was applied to analysis of rainfall-runoff. Finally, the difference of flood stage and discharge along the Tamsui River Basin between this two scenarios were evaluated.

A. Study Area

The Tamsui River Basin is located in northern Taiwan, shown as Fig. 2. The main stream is 158.7 km and the catchment area is 2,726 km^2. It is not only the third longest and largest river in Taiwan but also the most important river in northern Taiwan. The population in the Tamsui River Basin is about 8 million, more than 30% of the national population. The Tamsui River Basin includes the Tamsui River main stream, Dahan River, Xindain River, and Keelung River. The terrain is more elevated (3529m) in the north and lower in the south (0m).

According to the statistics of Central Weather Bureau of Taiwan, the annual average precipitation of the Tamsui River Basin is about 2,119 mm [4]. Most of the precipitation events were mainly caused by typhoons and monsoon rains. These events brought adequate water for the reservoirs.However, if the precipitation exceeds the load of the hydraulic structures, it will cause an incalculable loss to the downstream.

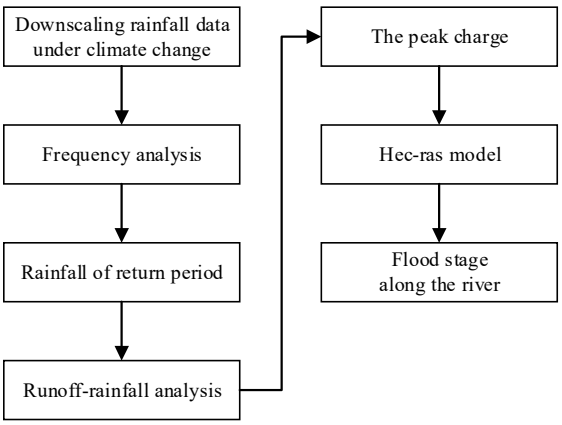

Fig. 1. Flowchart of the evaluation of the influence of climate change on river flow and flood stage

B. Rainfall Analysis

The general circulation model (GCM) is the main tool for simulating climate change conditions in the future [5]. But the resolution of GCM is approximately 200 to 500 km. It is necessary to downscale the GCM data fordischarge and flood stage simulation.

The downscaling rainfall data of A1B(CMIP3) and RCP8.5(CMIP5) climate change scenarios during the near future (2020~2039) used in this study produced by Taiwan Climate Change Projection and Information Platform (TCCIP). After the rainfall data produced by TCCIP was used for frequency analysis, we can get the rainfall of return period of the chosen rainfall station in Tamsui River Basin.

C. Runoff-Rainfall

In order to calculate the discharge of each river section in Tamsui River Basin, this study used the unit hydrograph published by the Water Resources Planning Institute, Water Resources Agency, Taiwan for rainfall-runoff analysis [6]. For infiltration, it was calculated using the U.S. Soil Conservation Service Curve Number (SCS CN) method. The SCS CN method is as follows:

$$P_e = \frac{(P-0.2S)^2}{P+0.8S} \quad (1)$$

$$S = 25.4\left(\frac{1000}{CN} - 10\right) \quad (2)$$

where, P_e is the rainfall excess in mm, P is the rainfall depth in mm, S is the potential maximum retention, CN is the SCS curve number, which can be determined by soil type, soil infiltration capability, forest coverage and land use. The lower the curve number, the more permeable the soil is. The curve number of each region of the Tamsui River Basin was shown in Fig. 3.

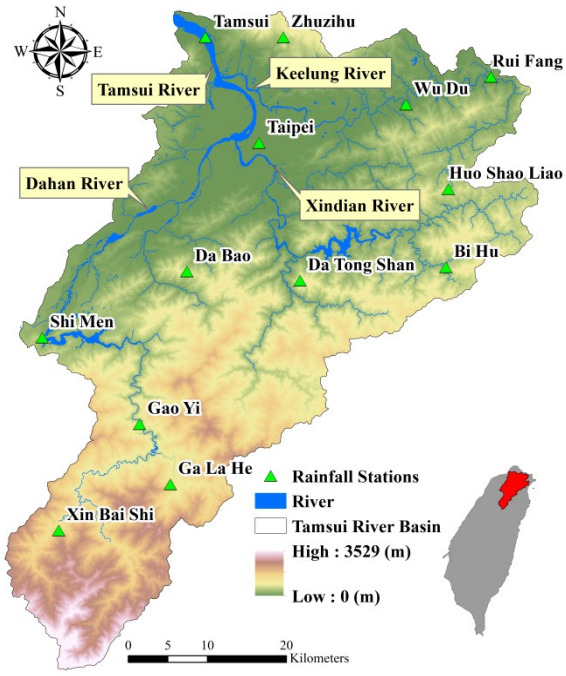

Fig. 2. Tamsui River Basin

D. Hydraulic Analysis

Based on above analysis results, the difference of flood stage and discharge along the Tamsui River Basin between this two scenarios was calculated. This study used the Hydrologic Engineering Center's River Analysis System (HEC-RAS) model developed by the Hydrologic Engineering

Center, U.S. Army Corps of Engineers to calculate the hydraulic conditions. The HEC-RAS model is dependent on finite difference solutions of 1-D Saint-Venant equations [7]. The governing equations are as follows:

$$\frac{\partial A}{\partial t}+\frac{\partial Q}{\partial x}=0 \quad (3)$$

$$\frac{\partial Q}{\partial t}+\frac{\partial\left(Q^2/A\right)}{\partial x}+gA\left(\frac{\partial H}{\partial x}+S_f\right)=0 \quad (4)$$

where, A is cross section area normal to the flow, Q is discharge, g is gravity acceleration, H is elevation of the water surface, S_f is longitudinal boundary friction slope.

The setting of HEC-RAS model and the required geologic data, such as river cross section (measured in 2011), hydraulic structures and Manning's roughness coefficient (0.03 to 0.065) are provided by the projects of the Tenth River Management Office, Water Resources Agency, Taiwan.

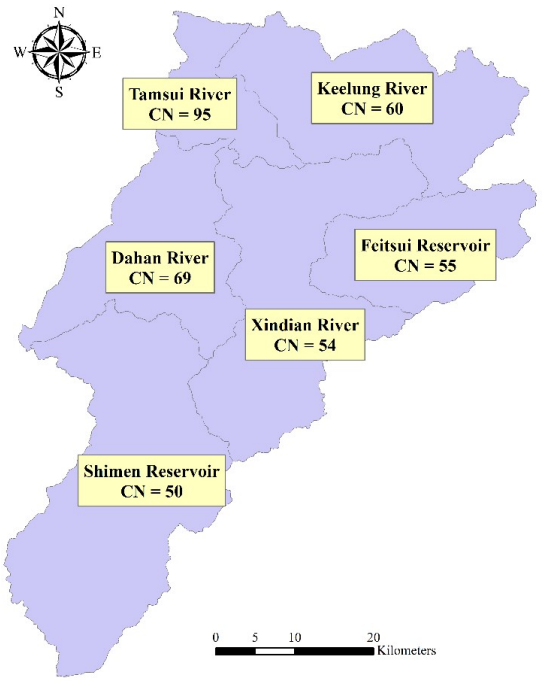

Fig. 3.CN number in each region of the Tamsui River Basin

AnalysisResult

A. Rainfall

According to the results of rainfall analysis, the rainfall of a 200-year return period in the Tamsui River Basin under different climate change scenarios was shown in Table I. The results showed that compared to A1B(CMIP3) scenario, the RCP8.5(CMIP5) scenario shows a 1%~5% increase in rainfall. The largest increase in the 1-day rainfall is Taipei Rainfall Station (4.3%), and the largest increase in the 2-day rainfall in Tamsui Rainfall Station (4.8%).

B. Discharge and Flood Stage

After analyzing the change ratio of rainfall between this two scenarios, this study used the analysis results to assess the impact of the change on existing flood control structures. Therefore, the 200-year 2-day rainfall of this two scenarios were selected for hydraulic analysis. The first, the rainfall excess was calculated by SCS CN method. Then, the peak discharges of each river sections were calculated by the unit hydrograph, the results were shown in Table II. The results showed that compared to A1B(CMIP3) scenario, the RCP8.5(CMIP5) scenario shows a 4%~6% increase in discharge. The largest increase in the peak discharge is Keelung River(5.6%).

The peak discharges of the 200-yr 2-day were used as inputs into the HEC-RAS hydraulic model to calculate flood stage along the Tamsui River Basin. The simulation results are shown in Fig. 4 to Fig. 7. The results showed that compared to A1B(CMIP3) scenario, the RCP8.5(CMIP5) scenario shows a 1%~3% increase in flood stage.

Table I. The rainfall of the 200-year return period in the Tamsui River Basin under climate change

Rainfall Station	A1B(CMIP3)		RCP8.5(CMIP5)		Changing Ratios	
	1 Day	*2 Day*	*1 Day*	*2 Day*	*1 Day*	*2 Day*
Tamsui	494	772	510	809	3.2%	4.8%
Taipei	583	858	608	893	4.3%	4.1%
Zhuzihu	1,409	1,871	1,450	1,933	2.9%	3.3%
Bi Hu	905	1,368	922	1,386	1.9%	1.3%
Huo Shao Liao	1,006	1,663	1,028	1,730	2.2%	4.0%
Da Bao	549	1,025	567	1,068	3.3%	4.2%
Rui Fang	655	867	666	868	1.7%	0.1%
Da Tong Shan	647	1,180	662	1,211	2.3%	2.6%
Wu Do	1,078	1,909	1,120	1,981	3.9%	3.8%
Shi Men	652	1,001	662	1,026	1.5%	2.5%
Gao Yi	912	1,489	930	1,531	2.0%	2.8%
Ga La He	558	1,261	573	1,299	2.7%	3.0%
Xin Bai Shi	1,301	2,739	1,344	2,809	3.3%	2.6%

[a.] unit: mm

Table II. The peak discharge of the 200-year 2-day return period in the river section of the Tamsui River Basin under climate change

River Section	A1B(CMIP3)	RCP8.5(CMIP5)	Changing Ratios
Tamsui River	26,652	27,904	4.70%
Dahan River	14,084	14,709	4.44%
Xindian River	12,244	12,722	3.90%
Keelung River	5,707	6,024	5.55%

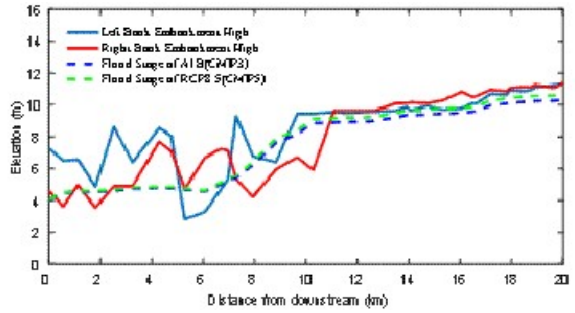

Fig. 4. The flood stage of the 200-year 2-day return period in Tamsui River

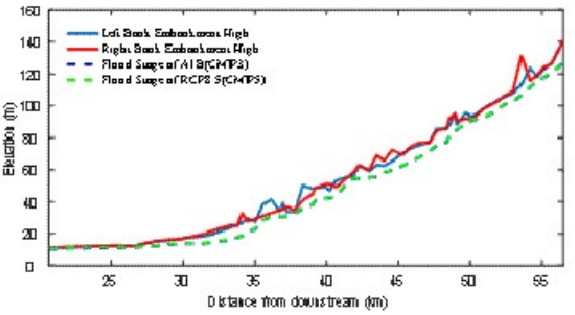

Fig. 5. The flood stage of the 200-year 2-day return period in Dahan River

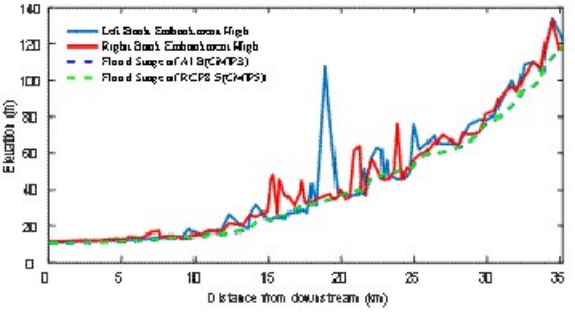

Fig. 6. The flood stage of the 200-year 2-day return period in Xindian River

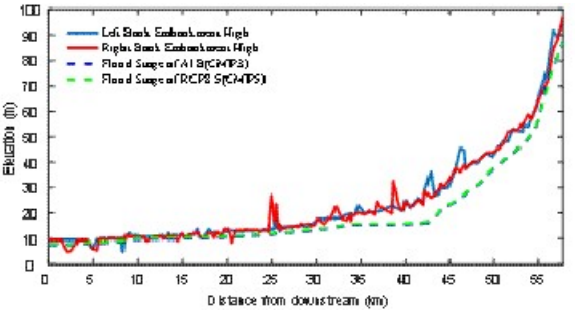

Fig. 7. The flood stage of the 200-year 2-day return period in Keelung River

Conclusions

This study used downscaling rainfall data produced by the TCCIP for river hydraulic simulation. The simulation results showed that compared to the A1B(CMIP3) scenario, the RCP8.5(CMIP5) scenario shows a 1%~5% increase in rainfall, 4%~6% increase in discharge, and 1%~3% increase in flood stage. It showed that the flood control flood control structures will face greater challenges in the near future under climate change.

Acknowledgment

This study is funded by the Water Resources Agency, Ministry of Economic Affairs, Taiwan (grant numbers MOEAWRA1060408).

References

[1] IPCC, "Climate Change 2014: Synthesis Report," 2014.
[2] Taylor, K. E., Stouffer, R. J., Mehl, G. A., "An overview of CMIP5 and the experiment design," Bulletin of the American Meteorological Society, 93(4), pp. 485-498, April 2012.
[3] Kitoh, A., Endo, H., "Changes in precipitaion extremes projected by a 20-km mesh global atmospheric model," Weather and Climate Extremes, 11, pp. 41-52, March 2016.
[4] The 10th River Management Office, Water Resources Agency, Ministry of Economic Affairs, "Investigation of Current Status in Tamsui River System," 2017.
[5] Hsiao-Ping Wei, Keh-Chia Yeh, Jun-Jih Liou, Yung-Ming Chen and Chao-Tzuen Cheng, "Estimating the Risk of River Flow under Climate Change in the Tsengwen River Basin," Water, 8(3), 2016..
[6] Water Resources Planning Institute, Water Resources Agency, Ministry of Economic Affairs, "Hydrology Analysis of Tamsui River," 2015.
[7] US Army Corps of Engineers Hydrologic Engineering Center, "HEC-RAS 5.0, Hydraulic Reference Manual," 2016.

Optimal reservoir operations under inflow scenarios in Nam Ngum River basin using Mixed-Integer Nonlinear Programming

Bounhome Kimmany[1,a], Supattra Visessri[1,b,*] and Piyatida Ruangrassamee[1,c]

Abstract Optimal reservoir operation is crucial, especially for large multipurpose reservoirs. The reservoir operation is complex and challenging subject to increasing water demands, variable reservoir inflow, and climate uncertainties. Nam Ngum 1 (NN1) is one of the key hydropower plants in the energy sector in Laos. This research aims to maximize the hydropower production under the impact of different reservoir inflow scenarios (observed inflow and inflow forecasting from time series model). Two time series models including Autoregressive (AR) and Autoregressive Integrated Moving Average (ARIMA) with different orders and parameters were used to simulate inflow. The simulated inflow obtained from the time series models was compared with the observed inflow. The best candidate model for each time series process was selected based on Akaike Information Criterion (AIC). ARIMA (2,1,3) was selected for monthly reservoir inflow simulation due to its ability to capture better low flow and high flow characteristics of the system. The NN1 reservoir operation optimization was formulated using Mixed Integer Non-linear Programming (MINLP) technique. The total annual and monthly power productions from optimization model under different inflow scenarios were analyzed. With optimized operation suggested by the model, the annual hydropower production can be increased 12.25% under observed inflow scenario and 2.22 % under simulated inflow scenario. The methodology for optimal operation demonstrated in this study can be used as a guideline for determining water release under different inflow scenarios in the Nam Ngum River basin and can be extended further for modelling multiple multipurpose reservoirs as a single system.

Keywords *Optimal reservoir operation, Inflow forecasting, Time series model, ARIMA, MINLP technique*

[1]Department of Water Resources Engineering
Faculty of Engineering, Chulalongkorn University
Bangkok, Thailand

[a]bounhomekmn@gmail.com
[b]supattra.vi@chula.ac.th
[c]piyatida.h@chula.ac.th

Introduction

Reservoir operation is one of the essential and challenging problems in water resources planning and management. Reservoir operation mainly involves determining the water release to serve the purposes of the reservoir. One of the solutions to determine optimal water release can be derived using optimization techniques to solve the best solution for specific objective function [1]. To develop the optimal reservoir operations under limitation of available resources, Reference [2] demonstrated that defining the constrain, objective function and optimization technique is very important and challenging. The complexity of the problem deals with many complicated variables including reservoir inflow, volume of storage, water demand and water supply as well as climate uncertainty associated with the operational problem that must be addressed [3].

The Nam Ngum River basin (NNRB) in Lao PDR has faced several operational problems caused by natural variability such as the flood and drought and management of water supply such as lacking cooperation between stakeholders in the upper and lower stream. In addition, almost all the reservoirs in the NNRB have been operated based on outdated operation rule together with experience of the operators[4]. Traditionally, reservoir operations are based on heuristic procedures in which an optimal solution cannot be guaranteed because the operations sometime based on embracing rule curves and subjective judgments by the operator [5].Furthermore, the uncertainty in reservoir operations such as change in climate and economic activities has complicated the operations. Reference[6]discussed that the conventional reservoir operation methods are often not adequate for establishing optimal operation decisionsReference[6] applied the Water Evaluation and Planning System (WEAP) model to simulatewater distribution at the watershedscale, incorporating the climate change driven hydrologic cycle and water infrastructure operations.The results from study of [6] showed that the uncertainty affectsreservoir inflow and water allocation. This confirms the complexity in reservoir operation. Many optimization and simulation models, such as dynamic programming (DP) model, system dynamic (SD) model, have been developed and applied over the past several decades. However, the reservoir simulation method does not guarantee to yield the optimal operation because the operation is sometime based on idea and experience of

engineers[7]. In a single reservoir operation, the operation is often required balancing among objectives including water supply reliability, hydropower generation, environmental flows, flood control, etc. [8]. To achieve the optimal multipurpose of reservoir operation, Reference[1] illustrated that it is a very difficult task due to conflicting multiple objectives, dimensionalities and nonlinearities [9].

According to the background and problems of reservoir operations, the optimization model possibly provides necessary information to improve operational water release for NNRB. Nam Ngum 1 (NN1) hydropower plant is chosen as a case study for this research. This study aims to optimize water release to meet domestic demand, irrigation demand and maximize the hydropower production. However, domestic demand and irrigation demand of NN1 are small, water release through the turbine is enough for them. Therefore, this research focuses only on determining water release that maximize hydropower production for NN1. The Mixed Integer Nonlinear Programing (MINLP) [10] technique used to optimize the reservoir operation under different inflow scenariosofforecasted inflow from time series model [11]and observed inflow would be investigated in this study.The framework and methodology for developing an optimal reservoir operation for the NN1 are presented in this study and expected to be extendable to other reservoirs in the NNRB.

Study Area

The Nam Ngum River is one of the main tributaries contributing to the Mekong River. The Nam Ngum River basin (see Fig. 1) is the fourth largest basins in Laos based on the area size.

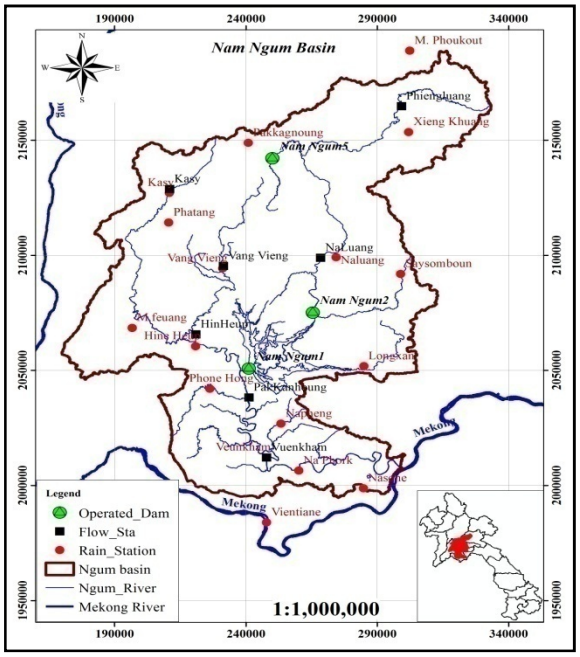

Fig. 1. Nam Ngum River basin system

The total area of the river basin is 16,931 km^2, accounting for 7.3% of Laos. Major land use in the basin is forest covering approximately 81% of the entire basin area [4]. The NNRB is characterized by tropical climate with a distinct wet season and dry season. The annual average amount of rainfall over basin is 2,472 mm and ranges from more than 3,500 mm in the central region of basin near VangVieng district to below 1,400 mm in XiengKhouang province in the north part of basin. The annual average outflow from the NNRB flow to Mekong River is 2.16 billion m^3[4].

Reservoir condition

A. Hydropower plant

The Government of Lao PDR has persistently projected to find the approach to obtain the maximum benefit from the hydropower generation, which is expected to increase significantly in the future, through the reservoir operations [12]. There are three existing cascade reservoirs on the main stream of the NNRB including the Nam Ngum 1 (NN1), Nam Ngum 2 (NN2), and Nam Ngum 5 (NN5) hydropower plants(see Fig. 1) used for hydropower generation.

The NN1 is a reservoir operated by EDL-Generation Public Company (EDL-GEN). It is located approximately 90km northof Vientiane Capital.The main features of NN1 hydropower plant are summarized in TABLEI.

Table I. Key features of NN1 hydropower plant

Category	Data	Unit
Catchment Area	8,460	km^2
Active Storage Capacity	4,700	MCM
Max. Flood Level	215	m
Full Supply Level (FSL)	212	m
Minimum supply Level (MSL)	196	m
Maximum Tailwater Level	178	m
Rated Flow per turbine	155	m^3/s

B. Reservoir operations

The decision on reservoir operations activity using rigid approach or rule often leads to ineffective energy production. Operation of reservoirs is a complex problem that involves many decision variables, multiple objectives as well as considerable risk and uncertainty. Reservoir operating rules provide general operation strategies for reservoir releases according to the current reservoir level, hydrological conditions, water demands and the time of the year. In order to obtain optimal operating rules, a large number of optimization and simulation models have been developed and applied.

C. Description of data and tool

There are 14 years (2002–2015) of historical inflow time series data used in this study. The entire time series data was divided into two sets. The first set from 2002 to 2011 was used for calibration and the second set from 2012 to 2015 was used for validation.The simulated inflow time series were developed using time series models (AR and ARIMA).

Autoregressive model (AR) is a process developed to predict value of stationary data from autoregressive time series in previous time period[13]. The AR model can be given in following form:

$$Y_t(p) = \alpha_0 + \phi_1 Y_{t-1} + \phi_2 Y_{t-2} + \ldots + \phi_p Y_{t-p} + \varepsilon_t \quad (1)$$

A Moving Average model is similar to an Autoregressive model, except that instead of being a linear combination of past time series values, it is a linear combination of the past white noise terms [13]. The AR model can be given in following form:

$$Y_t(q) = \beta_0 + \theta_1 \varepsilon_{t-1} + \theta_2 \varepsilon_{t-2} + \ldots + \theta_p \varepsilon_{t-p} + \varepsilon_t \quad (2)$$

ARIMA was developed byBox and Jenkins (1970) [13].It can be used to forecast non-stationary time series because the behavior of the data recorded in the past is assumed to be sufficient to define pattern in the present and explain the trend of itself in the future. ARIMA model is the integration between AR and MA processes. The general formulation of ARIMA model is represented as:

$$Y_t(p,d,q) = \alpha_0 + \sum_{i=1}^{p} \phi_i \Delta Y_{t-p} + \sum_{j=1}^{q} \theta_j \varepsilon_{t-q} + \varepsilon_t \quad (3)$$

where: Y is variable at time t, α and β are constant for AR and MA, $\phi$and $\theta$are coefficients for AR and MA, p and $q$are the number of lagged forecast errors in the prediction equation for AR and MA, d is the number of non-seasonal differences needed for stationarity, Δ is difference operator and ε is error.

Optimal operation model for the reservoir system was developed using mixed integer nonlinear programming (MINLP) which is solved using LINDOGlobal solver through General Algebraic Modelling (GAMS) language. The description and details of the GAMS model is omitted here and referred to [14] for more details.

According to the study of [15], the MINLP is referred to mathematical programming with continuous and discrete variables and nonlinearities in the objective function and constraints. Reference [16] also explained that MINLP problems are difficult to solve, because they combine all the difficulties of both of their subclasses: the combinatorial nature of mixed integer programs (MIP) and the difficulty in solving nonlinear programs (NLP). The MINLP can be written in following forms:

$$\begin{aligned} &Maximize && f(x,y) \\ &Subject\ to && g(x,y) > 0 \\ & && L \le x,\ y \le U \end{aligned} \quad (4)$$

where: $f(x, y)$ is nonlinear objective function
$g(x, y)$ is nonlinear constraint function
x, y are the decision variables
L, U are Lower and Upper bounds

The time series of hydrological observations data used in this study were supported from Department of Meteorology and Hydrology (DMH), Lao PDR. The total data requirements for develop optimization model are listed below:

- Inflow to the reservoirs
- Water release through spillway
- Water release through turbine
- Reservoir characteristics (see TABLE I)
- Evaporation rate
- Surface area – Volume – Elevation Curve
- Observed power generation.

Methodology

A. Inflow forecasting

Time series models were applied for simulating reservoir inflow. One time step forward forecasting technique is used. The results of average monthly inflow from AR and ARIMA models are compared with the observed inflow. The procedure of developing time series model is shown in Fig. 2 which involves four main steps of 1) collect data and perform initial check through visualization, 2) stationarizes the time series data, 3) estimate the time series model order and parameters and 4) develop time series model and simulate inflow.

The time series models were built using MATLAB toolbox. The simulated inflows from AR and ARIMAtime series models were compared with observed inflow. The accuracy of the time series modelswas evaluated using Coefficient of Determination (R^2), Root Mean Square Error (RMSE), and Mean Absolute Error (MAE). Selected inflow time series simulated from the model with relatively higher accuracy wasthen input to optimization model.

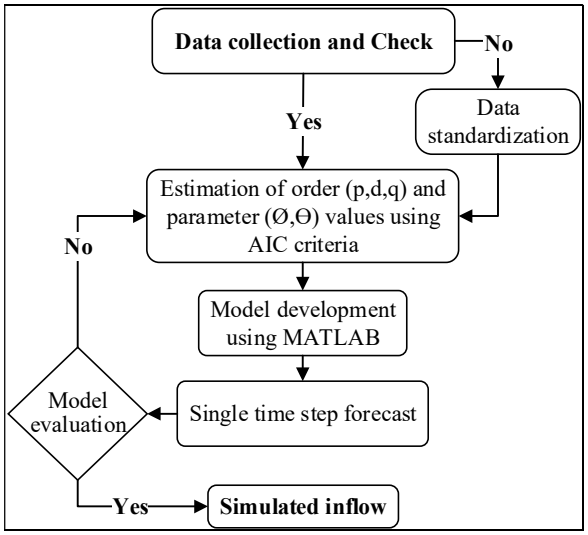

Fig. 2. Schematic of time series model

B. Reservoir operations

Reservoir operations of NN1 is optimized under two different inflow scenarios. First scenario is optimized under observed inflow. Second scenario is optimized under simulated inflow from ARIMA. The procedure of developing the optimal reservoir operation model is illustrated in the Fig. 3.

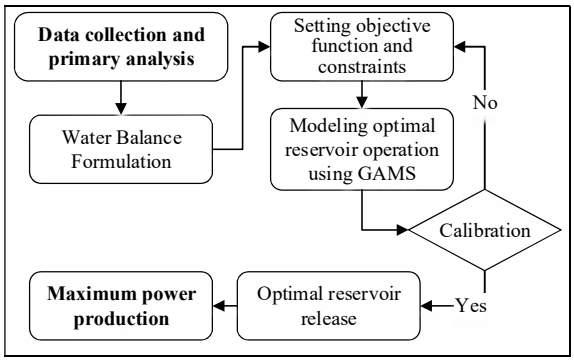

Fig. 3. Shcematic of the optimal reservoir operations.

1) Reservoir water balance

The water balance equation is used to define water inflow and outflow of each reservoir. In this study, seepage is considered negligible and omitted from the water balance equation. Based on cascade reservoir system (series reservoir), the water balance equation is defined in the following form.

$$S_{t+1} = S_t + In_t - E_t - R_t - Spill_t \qquad (5)$$

where: S_{t+1} is final storage at time t, S_t is initial storage at time t, In_t is reservoir inflow at time t, E_t is evaporation loss at time t, R_t is water release from reservoir through turbine at time t, and $Spill_t$ is water over spillway at time t.

2) Objective function

Hydropower generation is of high importance to Laos due to its positioning to be the battery of Asia. The goal of hydropower generation is to achieve domestic hydropower demand and to boost economic growth. Therefore, maximizing the monthly power generation capacity is treated as the objective function in this study. Mathematically the objective function is given by:

$$Maximize: \quad P_{Total} = \sum_{t=1}^{n} (\eta \times \gamma \times R_t \times H_t \times T) \qquad (6)$$
$$n = 1,2,3\ldots.$$

where P_{Total} is total electricity production (MWh), η is dimensionless efficiency of the turbine, γ is specific weight of water ($\approx 9.81\ KN/m^3$), R_t is water release through the turbine (m^3/s), H_t is height difference between inlet and outlet (m) and T is time for generate power in a day (hr).

3) Constraints

The propose of mathematical optimization model for NN1 reservoir considers constraints which involve release through turbine and spillway, storage volume and river capacity. The hydrologic, physical and operational characteristics of the reservoir are also considered.

Result and Discussion

The study was aimed to optimize water release for maximizing hydropower production using MINLP technique under observed inflow and simulated inflow from time series model scenarios. The results of the developed MINLP under two different inflow scenarios were discussed in the following section.

A. Inflow prediction

1) Model selection

For the calibration data sets (2002 - 2011), the performance of 11 candidate time series models including AR(1) to AR(5) and ARIMA(1,1,1) to ARIMA(4,1,3) were assessed based on the AIC value as shown in TABLE II. The best candidate model from AR and ARIMA processes was selected based on the minimum value of AIC. The AR (4) and ARIMA (2,1,3) models with the AIC value of 189.555 and 183.810, respectively were selected.

Table II. AIC values for time series model

No.	Model candidate	AIC value
1	AR(1)	245.120
2	AR(2)	195.878
3	AR(3)	194.441
4	**AR(4)**	**189.555**
5	AR(5)	196.421
6	ARIMA(1,1,1)	235.881
7	ARIMA(2,1,1)	198.212
8	ARIMA(2,1,2)	228.304
9	**ARIMA(2,1,3)**	**183.810**
10	ARIMA(3,1,3)	196.261
11	ARIMA(4,1,3)	211.426

The difference of AIC value between AR (4) and ARIMA (2,1,3) models is very small. Therefore, both AR (4) and ARIMA (2,1,3) models are tentatively selected for monthly reservoir inflow forecasting for NN1. The parameter values of the AR (4) and ARIMA (2,1,3) models shown in TABLE III. suggest that the first order of AR and ARIMA is more significant than the other orders. This means that the events of short lag time have higher correlation than the events of long lag time.

Table III. Parameter estimates

Parameter	AR(4)	ARIMA(2,1,3)
Ø1	0.9159	1.4322
Ø2	0.0197	-0.6505
Ø3	-0.2161	-0.6821
Ø4	-0.0576	-
Ø5	-0.0082	-
Θ1	-	-0.1053
Θ2	-	-0.154
Θ3	-	-0.3223
Θ4	-	-0.5216

2) Inflow forecasting

The simulated inflow is validated using the independent data set (2012-2015) and the results are shown in Fig 4 and Fig 5. In the Fig 4, it is clear that the AR (4) model can acceptably capture the overall pattern of inflow but not high flow events. The AR (4) underestimates peak and detects peak too early. When compared to AR (4), the ARIMA (2,1,3) model can capture better low flow and high flow characteristics (see Fig 5). The performance of the time series models based on RMSE, R2 and MAE, are shown in TABLE IV.

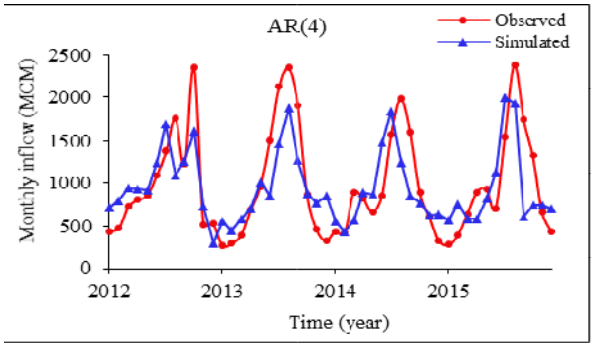

Fig. 4. Comparision between inflow from AR (4) and observed inflow

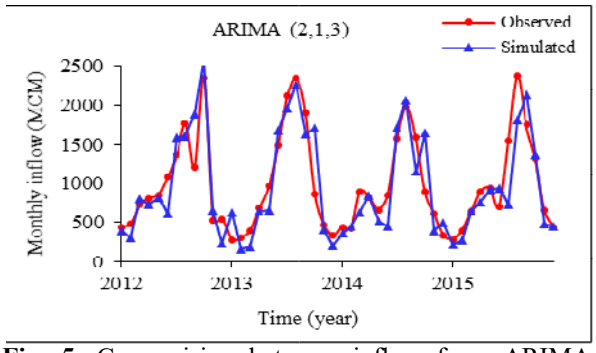

Fig. 5. Comparision between inflow from ARIMA (2,1,3) and observed inflow

Table IV. Statistical performance indices of time series model

Model	R^2	RMSE (MCM)	MAE (MCM)
AR(4)	0.54	154.26	121.45
ARIMA(2,1,3)	0.78	115.41	84.27

From TABLE IV, it is clear that the ARIMA (2,1,3) model outperformed AR (4) in terms of all performance indices. According to the better performance, the simulated inflow from ARIMA (2,1,3) will be used as input to MINLP. The results of optimal reservoir operations under two different inflow scenarios including observed inflow and ARIMA inflow are discussed in the following section.

B. Optimal reservoir operations under different inflow scenarios

The results of monthly and annual hydropower productions under different inflow scenarios were analyzed in the following section.

1) Monthly hydropower production

The optimal average monthly power production under the different inflow scenarios compared with the actual production is shown in Fig 6. It shows that the average monthly power production varies from 58,310 MW to 151,165 MW for the ARIMA inflow. The average monthly power production ranging from 78,886 MW to 120,592 MW

was also obtained from observed inflow. In all periods, the optimum hydropower under observed inflow scenario (Opt_power (Obs_inflow)) were greater than that of the ARIMA scenario (Opt_power (ARIMA_inflow)) especially, for wet season (May - Oct). This maybe because during the wet season (Jun - Sep), the reservoir was filled, and the optimal reservoir operations model kept the maximum hydropower production up to October. This difference demonstrated that the inflow forecasting from time series model affected to the reservoir operations. However, the power production in dry months of December through April slightly decreased compared with the observed power production.

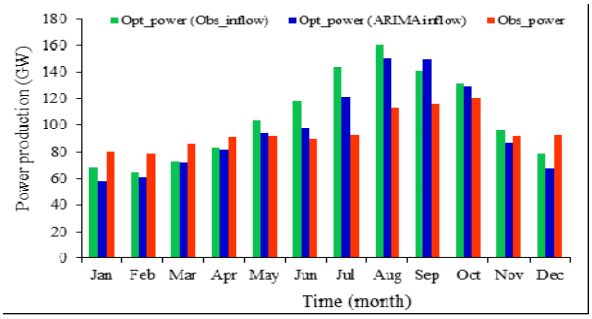

Fig. 6. Monthly hydropower production from MINLP compared with observed data.

2) Annual hydropower production

The results of optimal annual hydropower production under the different inflow scenarios are shown in TABLE V and Fig. 7.

Table V. Annual hydropower production simulated by MINLP

Year	Observed power (MWh)	Optimized power (MWh)	
		ARIMA_inflow	*Obs_inflow*
2012	1,040,707	1,312,074	1,230,977
2013	1,180,196	1,218,496	1,312,170
2014	1,141,816	1,185,843	1,324,773
2015	1,209,683	1,159,911	1,230,811
Average increase (%)		**2.22**	**12.25**

The result in TABLE V shows that the annual hydropower production optimized under the two inflow scenarios is higher than the observed power. The increase of 12.25% in power obtained from optimization under observed inflow scenario suggests that the application of the optimization model proposed here can contribute to better control of release. However, it needs to be noted that this increase may be because all the monthly inflow were input into the optimization model, while in the observed (actual) operation case, the operator has the inflow records only up until a previous month. For the optimization under ARIMA inflow, the hydropower production was slightly increased up to 2.22 % when compared with the observed power. However, the hydropower production was less than the optimization under observed inflow case because the simulated inflow from ARIMA were generally lower than the observed inflow (see Fig. 5).

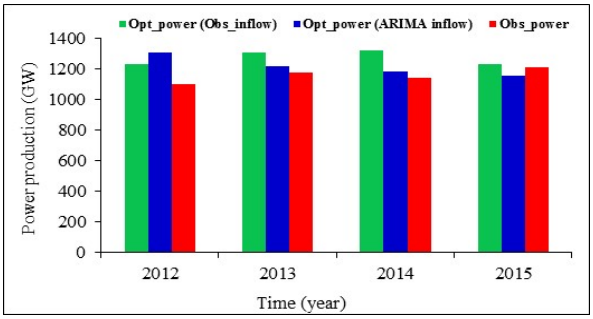

Fig. 7. Annual hydropower production from MINLP compared with observed data

Conclusions and Future study

In this study the NN1 operations were optimized for maximizing the hydropower production through MINLP technique under two different reservoir inflow scenarios. In the first scenario, the hydropower was optimized under the observed inflow and in the second scenario, the hydropower was optimized under ARIMA simulated inflow. The optimization model was developed and solved using LINDOGlobal solver through GAMS software. The entire series of data for NN1 reservoir inflow of 14 years (2002 - 2015) was divided in to two sets for time series model: calibration (2002 - 2011) and validation (2012 - 2015). The time series model, ARIMA (2,1,3) was selected for simulating monthly reservoir inflow because it outperformed other time series model in capturing low flow and high flow characteristics and yielded the best values for all statistical indices used in this study.

The optimization model was found to increase the hydropower production in both inflow scenarios. However, in some months the optimum hydropower generated under the observed inflow scenario was greater than that of the ARIMA (2,1,3) scenario. Optimization under both inflow scenarios improved existing reservoir operation as an increase in hydropower generation was achieved.When comparing between the two inflow scenarios, the optimization under observed inflow scenario yielded higher increase in hydropower compared to that of the ARIMA inflow.

Research for simulating inflow with uncertainty e.g. from climate change should be investigated further to better capture future conditions. For the optimal reservoir operation model, it is needed to improve objective functions and constraints to more explicitly address the flood at the downstream. The initial results obtained from this study should be extended to be applied for multiple multipurpose reservoir operations.

Acknowledgement

Authors would like to acknowledge the AUN (ASEAN University Network) and SEED-Net (Southeast Asia Engineering Education Development Network) who provide a PhD scholarship for the first author of this study. We extend our thanks to the Department of Meteorology and Hydrology, Ministry of Energy and Mines of Lao PDR for data support. We wish to thank the reviewersfor their thoughtful comments which were very helpful for improving this research.

References

[1] K. Taesoon, H. Jun-Haeng, B. Deg-Hyo and K. Jin-Hoon, Single-reservoir operating rules for a year using multiobjective genetic algorithm. IWA, p. 17, 2008,.

[2] Z. Liudong, G. Ping, F. Shiqi, and L. Mo, "Monthly Optimal Reservoirs Operation for Multicrop Deficit Irrigation under Fuzzy Stochastic Uncertainties," Journal of Applied Mathematics, p. 11, 2014.

[3] Pritchard and Geoffrey, "Stochastic inflow modeling for hydropower scheduling problems," European Journal of Operational Research, vol. 246, no. 2, pp. 496-504, 2015.

[4] Water Resources and Enviroment Administration (WREA), "Nam Ngum River Basin Integrateed water resources management Plan," 2009.

[5] V. Vudhivanich and A. Rittima, "Development of Probability Based Rule Curves for a Reservoir," Nat. Sci, vol. 2, no. 37, pp. 234-242, 2003.

[6] D. Jayasekera, J. Kaluarachchi, and C. Hoanh, Climate change adaptation strategies for the Nam Ngum River basin, Laos. 2016.

[7] S. K. Jain, V. P. Singh., "Reservoir Operation," vol. 51: Elsevier, pp. 615-679, 2003.

[8] R. V. Losvany, M. R. José Bienvenido, M. Jose-Luis and P. T. Julio, "Multiobjective Optimization Modeling Approach for Multipurpose Single Reservoir Operation," Water, vol. 10, no. 10, p. 3390, 2016.

[9] N. M. Lin and M. Rutten, "Optimal Operation of a Network of Multipurpose Reservoir: A Review," Procedia Engineering, vol. 154, pp. 1376-1384, 2016.

[10] P. Perawongsakul, "Multi-reservoir operations under economic development in Mae Klong River Basin," Master, Department of Water Resources Engineering, Chulalongkorn University, Thailand, 2017.

[11] M. K. Hamidi, H. Sedghi, A. Telvari, and H. Babazadeh, "Forecasting by Stochastic Models to Inflow of Karkheh Dam at Iran," Civil Engineering Journal, vol. 3, no. 5, pp. 304-350, 2017.

[12] T. Piman, T. A. Cochrane, M. E. Arias, N. D. Dat, and O. Vonnarart, "Managing Hydropower Under Climate Change Uncertainty in the Mekong Tributaries: Examples from Asia, Europe, Latin America, and Australia," S. Shrestha, A. K. Anal, P. A. Salam, and M. van der Valk, Eds.: Springer International Publishing, pp. 223-248, 2015

[13] Z. A. Saleh, "Forecasting by Box-Jenkins (ARIMA) Models to Inflow of Haditha Dam," Journal of Babylon University, vol. 21, no. 5, 2013. College of Eng., Babylon Univ., Babil, Iraq

[14] R. E. Rosenthal, "A GAMS User's guide," W. GAMS Development Corporation, DC, USA, Ed., ed, 2017.

[15] B. Pietro and K. Christian, "Mixed-Integer Nonlinear Optimization," Mathematics and Computer Science Division2012.

[16] J. A. E. Schl , and J. R. Banga, "Extended Ant Colony Optimization for non-convex Mixed Integer Nonlinear Programming," Computers & Operations Research, vol. 36, no. 7, pp. 2217-2229, 2008.

Evaluation of Economic Damages on Rice Production under Extreme Climate and Agricultural Insurance for Adaptation Measures in Northeast Thailand

Koshi Yoshida[1,a], Supranee Sritumboon[2], Mallika Srisutham[3], Desell Suanburi[4], Naruekamon Janjirauttikul[2] and Weerakaset Suanpaga[4]

Abstract

In northeast Thailand, the ratio of irrigated agricultural land was only 7.6% (in 2012) and others were rain-fed so that climate change makes agricultural production more unstable and also makes crucial damage to the societies and economics in rural area. To mitigate these issues, it is desirable to develop and disseminate enhanced adaptation systems. In this study, we focused on weather induced economic damages and effectiveness of index-based insurance system in northeast Thailand. Firstly, we evaluated how affect the seasonal rainfall amount and patterns on rice yield and production through correlation analysis by using the meteorological and agricultural statistic data. Wet-season rice had significant positive relationship with 3 months accumulated rainfall. 8 province had positive correlation R>0.3 with Jul-Sep accumulated rainfall which was employed for insurance index. And then, probability analysis was applied to monthly rainfall. As a result, setting amount and periods of index value was suitable. Secondly, household survey was conducted to grasp farmer's conditions of water use, cultivation, income balance. According to the 60 famers interview, average household income was 341,160 Baht /year, consisting of 122,433 Baht/year from agriculture and 218,727 Baht/year from non-agriculture. In recent year, some province had 600 million Baht economic loss. In 2000, total production value of wet-season rice in each province were ranged from 460 million Baht (Mukdahan) to 4,160 million Baht (Surin) so that 600 million Baht economic loss was enough large in provincial level. However, recent agricultural damage was not so large (less than 5%), because most part of farmers income relied on non-agricultural sector.

Keywords *agricultural damage, household survey, risk assessment, climate change adaptation*

[1]College of Agriculture
Ibaraki University
Ibaraki, Japan
[2]Land Development Department
Thailand
[3]Khon Kaen University
Thailand
[4]Kasetsart University
Thailand

[a]koshi.yoshida.agri@vc.ibaraki.ac.jp

Assessment of near-real-time satellite-based precipitation over Thailand

Narongthat THANYAWET[1,a] and Piyatida RUANGRASSAMEE[1,b,*]

Abstract Satellite-based precipitation products are publicly available and provide continuous series of high temporal and spatial resolution data especially for regions with limited rain gauge. However, satellite-based precipitation is derived from microwave, near infrared and radar signals thus they normally contain bias. Thailand located in the tropical zone and has been affected by floods and droughts frequently. Precipitation data are very important in assessment of water-related disasters. Although there is a good rain gauge network in Thailand, in many parts of the country, there is still quite limited number of rain gauge, for example mountainous areas in the norther part and east coast area. This study aims to statistically evaluate two near-real-time satellites-based precipitation products, namely GSMaP_NRT and PERSIANN-CCS during 2009-2013. GSMaP_NRT is hourly product with 0.1 x 0.1 degree and 4-hour latency while PERSIANN-CCS is hourly product with 0.04 x 0.04 degree with 1-hour latency. Compared to the Thai Meteorological Department rain gauge data (TMD), the two satellite-based precipitation products depict the spatial distribution well, with underestimation in monthly and annual rainfall especially in the east coast river basin and the southern parts of Thailand. The daily comparison depicts different trends in each river basin. Further adjustment to reduce bias of the satellite-based precipitation should be implemented.

Keywords *satellite-based precipitation, GSMaP_NRT, PERSIANN-CCS*

[1]Department of Water Resources Engineering
Faculty of Engineering, Chulalongkorn University
Bangkok, Thailand

[a]Narongthat.t@outlook.co.th
[b]Piyatida.H@Chula.ac.th

Introduction

Rainfall is a primary data for hydrological simulations and assessment of water-related disasters [10 ,11]. However, there is still quite limited number of rain gauge, especially in mountainous area.

Thailand, located in Southeast Asia, has experienced frequent floods and droughts. Rainfall in Thailand is influenced by monsoons and tropical storms. There is a good network of rain gauge covering all over the country by several agencies including Thai Meteorological Department (TMD), Royal Irrigation Department (RID), Department of Water Resources (DWR), and Hydro and Argo Informatics Institute (HAII). However, in some area such as the northern part and east coast area of Thailand, they are mountainous regions which make it difficult to install and maintain rain gauge. Satellite-based precipitation products are publicly available and provide continuous series of high temporal and spatial resolution data especially for regions with limited rain gauge. However, satellite-based precipitation is derived from microwave, near infrared and radar signals thus they normally contain bias. Furthermore, the satellite-based rainfall products have bias due to the estimation algorithm [4]. These products need the rain gauge data for improving the bias by bias correction [5].

This study aims to evaluate the precipitation data from two near real time satellite-based products namely, Global Satellite Mapping of Precipitation – Near Real Time (GSMaP_NRT) [8] and Remotely Sensed Information using Artificial Neural-Network – Cloud Classification System (PERSIANN-CCS) [6][9] over Thailand. The two near real time satellite-based rainfall products are compared with the observed rainfalls from TMD by analyzing statistics such as root mean squared error (RMSE), Pearson correlation coefficient (r), bias of estimation, hit rate (HR) and false alarm rate (FAR) [7, 10].

Data

A. Thai Meteorological Department (TMD) precipitation

The observed rainfall used in this study is from the 124 rain gauges of Thai Meteorological Department (TMD) as shown in Fig. 1. The rain gauge is manual, and the rainfall data are collected every three hours. The rainfall data used are from 2009-2013

B. Global Rainfall Map in Near-Real-Time (GSMaP_NRT)

GSMaP_NRT is a satellite-based rainfall productand the data are available from https://sharaku.eorc.jaxa.jp/GSMaP/ with latency time of four hours. This system uses the remotesensing data from microwave and infrared. GSMaP_NRT developed by TRMM Precipitation Radar (PR) which used to collect the data.GSMaP_NRT covers from 60 degrees Northern to 60 degrees Southern, and the time zone reference is Coordinated Universal Time (UTC) to indicate time of data by HIMAWARI satellite. The temporal resolution is 1 hour, and the spatial resolution is 0.1 degree. [3]

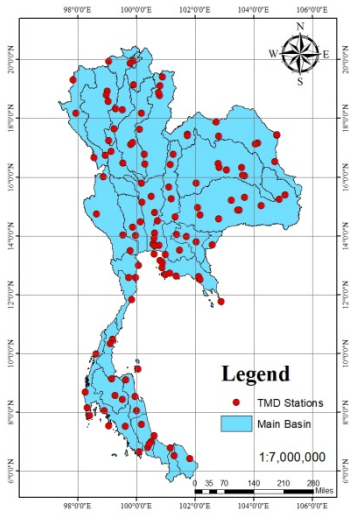

Fig. 1. Map of Thai Meteorological Department's 124 rain gauges in Thailand

C. Precipitation Estimation from Remotely Sensed Information using Artificial Neural Networks Cloud Classification System (PERSIANN-CCS)

PERSIANN-CCS covers from 60 degrees Northern to 60 degrees Southern. The temporal resolution is 1 hour, and the spatial resolution is 0.04 degree. [2] PERSIANN-CCS uses the cluster technique to classify the type of cloud by using image processing from satellite geo-station infrared. The rainfall data can be downloaded from http://chrsdata.eng.uci.edu/

Methodology

The performance of satellite-based rainfall is evaluated in this study by two aspects. The first aspect is the estimated rainfall amount, the correlation, the bias of estimation between the satellite-based rainfall and the observed rainfall. The second aspect investigated is the potential of the satellite-based rainfall in detecting the rain and bias of detection using the contingency table.

A. Exploratory Indices

The estimated near real time rainfall from GSMaP_NRT and PERSIANN-CCS were compared with the observed rainfall from TMD by calculating the RMSE and correlation coefficient. The equation to calculate the root mean squared error (RMSE) is shown in equation (1). RMSE measures the averaged difference between rainfall estimated by a satellite-based precipitation product (X_{sat}) and the rainfall observed by a rain-gauge data from TMD (X_{obs}). [1]

$$RMSE = \sqrt{\frac{\sum(X_{obs}-X_{sat})^2}{N}} \quad (1)$$

Where N is a number of total data

The Pearson correlation coefficient (r) indicates the strength and direction of a linear relationship between two variables, which are the satellite based-rainfall data and observed data in this study as shown in equation (2). The Pearson correlation coefficient is +1 in the case of a perfect increasing linear relationship, and -1 in case of a decreasing linear relationship. When the correlation coefficient is equal to 0, it means there is no linear relationship between two variables.

$$r = \frac{\sum(X_{obs}-\overline{X_{obs}})(X_{sat}-\overline{X_{sat}})}{\sqrt{\sum(X_{obs}-\overline{X_{obs}})^2\sum(X_{sat}-\overline{X_{sat}})^2}} \quad (2)$$

Bias of estimation is an averaged difference between the observation data and satellite-based rainfall data. The bias of estimation is calculated as shown in equation (3). When the bias of estimation less than zero, it means the satellite data overestimate the observed data, and when the bias is more than zero, it means the satellite data underestimate the observed rainfall.

$$Bias\ of\ estimation = \frac{1}{N}\sum(X_{obs} - X_{sat}) \quad (3)$$

B. Contingency Table

The contingency table as shown in Fig. 2 displays the relationship of rainfall detection between rain gauge and satellite-based algorithm. [1]

		Observation: Yes	Observation: No	
Satellite	Yes	a	b	a+b
	No	c	d	c+d
		a+c	b+d	n = a+b+c+d

Fig. 2. Relationship between counts (letters a – d) of satellite-based data pairs for the dichotomous nonprobability verification situation as displayed in a 2x2 contingency table.

Hit (a) is a number of days that both rain gauge and satellite data report rainfall, , false alarm (b) is a number of days that rain gauge do not report rainfall but satellite data do, miss (c) is a number of days that rain gauge reports rainfall but satellite data do not, and correct negative (d) is a number of days that both rain gauge and satellite data do not report rainfall.

Hit rate (HR) is a proportion of hit to a number of days that rain gauge reports rainfall (a and c) as shown in equation (4). This index indicates the accuracy of satellite data in detecting rainfall.

$$HR = \frac{a}{a+c} \quad (4)$$

False alarm rate (FR) is a proportion of false alarm (b) to a number of days that rain gauge does not report rainfall (b and d) as shown in equation (5).

$$FR = \frac{b}{b+d} \quad (5)$$

Results and Discussion

The scatter plots of daily, monthly, and annual rainfall over Thailand comparing between rain gauge and the two near-real-time satellites-based rainfall products, GSMaP_NRT and PERSIANN-CCS, are shown in Fig. 3, 4, and 5, respectively. The statistical indices are summarized in Table I. For daily rainfall, the correlation coefficients of GSMaP_NRT and PERSIANN-CCS are 0.46 and 0.43, respectively. The satellite-based rainfall both underestimates and overestimates rain gauge measurement on the daily time scale. The bias of GSMaP_NRT is 0.74 while that of PERSIANN-CCS is -0.15 mm/day. The RMSE of GSMaP_NRT is 12.6 mm/day which is lower than that of PERSIANN-CCS.

For monthly time scale, the correlation coefficient is much improved compare to the daily data. This is because the satellite-based rainfall products both under and overestimate resulting in less errors when summing to the monthly time scale. The correlation coefficients of GSMaP_NRT and PERSIANN-CCS are 0.75 and 0.66, respectively. The bias of GSMaP_NRT is positive indicating underestimation while the bias of PERSIANN-CCS is negative indicating overestimation. The RMSE of GSMaP_NRT is lower than PERSIANN-CCS.

For annual time scale, the correlation coefficient is lower than the monthly scale for PERSIANN-CCS. For the annual rainfall greater than 1000 mm, both satellite-based rainfall products underestimate rain gauge measurement. The bias of GSMaP_NRT is positive indicating underestimation while PERSIANN-CCS is overestimating. The RMSE of annual rainfall of GSMaP_NRT is lower than PERSIANN-CCS.

Table I. Summary of exploratory indices

	GSMaP_NRT			PERSIANN-CCS		
	R	**RMSE**	**Bias**	**R**	**RMSE**	**Bias**
Daily	0.46	0.74 mm./d.	12.63 mm./d.	0.43	-0.15 mm./d.	13.04 mm./d.
Monthly	0.75	18.40 mm./m.	105.82 mm./m	0.66	-8.63 mm./m.	125.86 mm./m.
Annual	0.74	225.78 mm./y.	556.27 mm./y.	0.45	-99.13 mm./y.	680.30 mm./y.

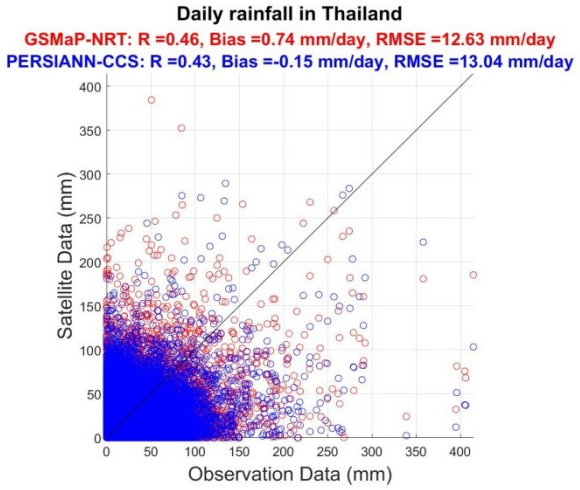

Fig. 3. Scatter plot of daily rainfall over Thailand.

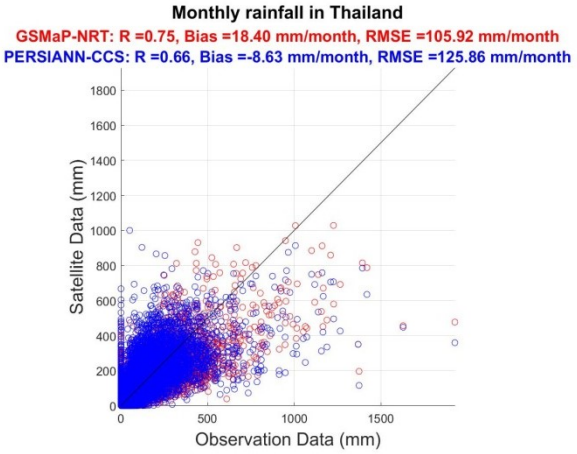

Fig. 4. Scatter plot of monthly rainfall over Thailand.

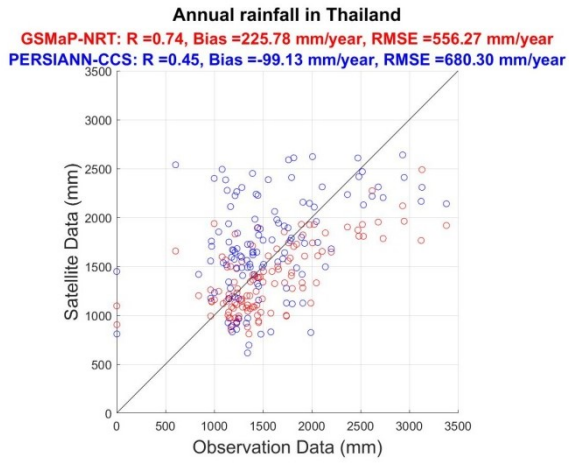

Fig. 5. Scatter plot of annual rainfall over Thailand.

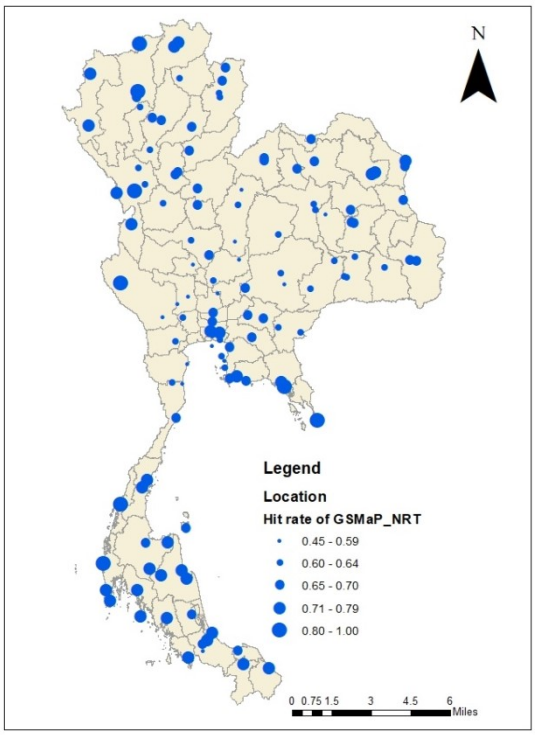

(a) Hit rate of GSMaP_NRT over Thailand

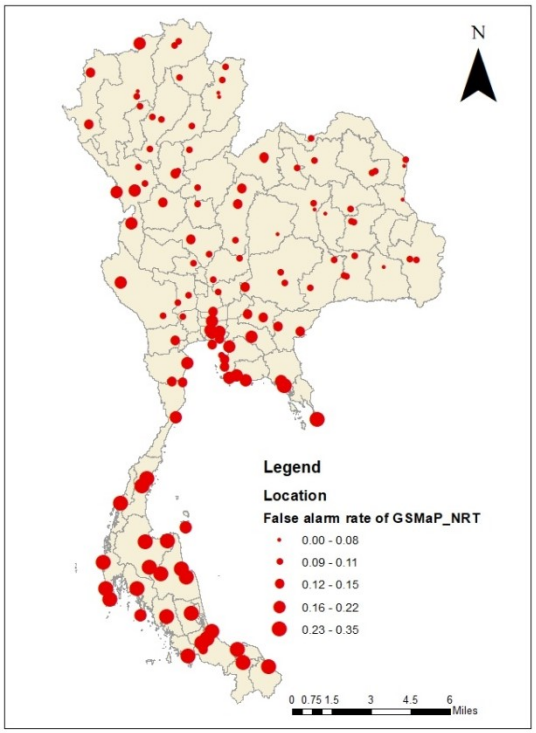

(b) False alarm rate of GSMaP_NRT over Thailand.

Fig. 6. Hit rate and false alarm rate of GSMaP_NRT over Thailand.

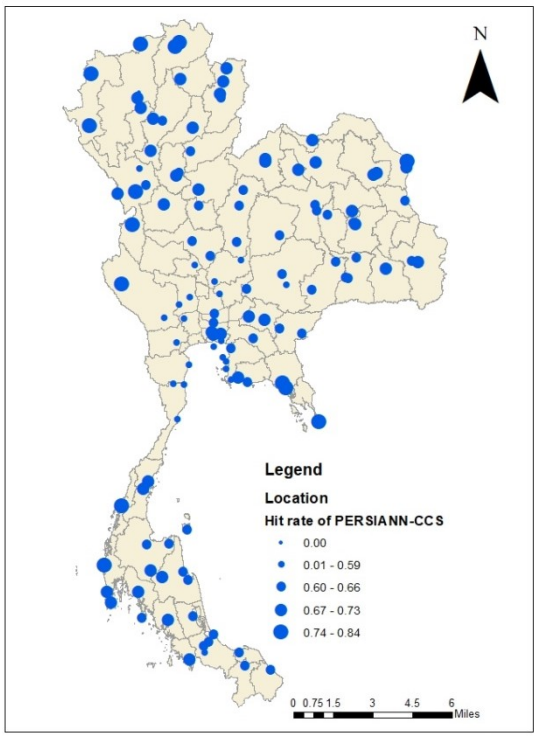

(a) Hit rate of PERSIANN-CCS over Thailand

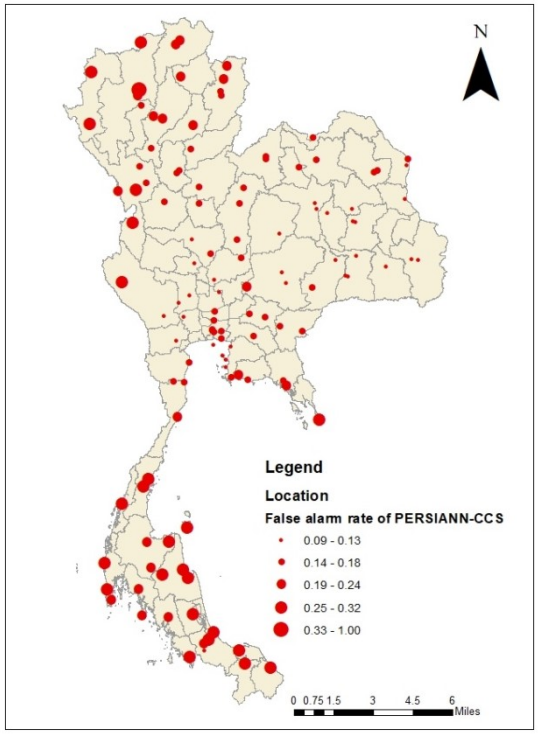

(b) False alarm rate of PERSIANN-CCS over Thailand.

Fig. 7. Hit rate and false alarm rate of PERSIANN-CCS over Thailand.

Fig 6 (a) and (b) shows the hit rate and false alarm rate of GSMaP_NRT of grids that are corresponding with the TMD rain gauges. Similarly, Fig 7 (a) and (b) shows the hit rate and false alarm rate of PERSIANN-CCS. The maps show the non-uniform distribution of the hit rate and false alarm rate over Thailand. The hit rate in the central part is relatively low. The false alarm rate of GSMaP_NRT in the eastern and southern parts are high. For PERSIANN-CCS, the false alarm rate is high in the norther and southern parts. The results show that the performance of satellite-based rainfall products depends on area. The overall hit rate and false alarm rate is shown in Table II. The hit rate and false alarm rate are very close between the two products and they show a good potential in using the near-real-time satellite-based rainfall together with rain gauge measurement in hydrologic forecasting and simulations.

Table II. The average hit rate and false alarm rate of satellite-based rainfall products.

	HR	**FR**
GSMaP_NRT	0.65	0.18
PERSIANN-CCS	0.67	0.15

Conclusions

Satellite-based precipitation products are publicly available and provide continuous series of high temporal and spatial resolution data especially for regions with limited rain gauge. It can be used complimentarily with rain gauge in the assessment of water-related disasters. In this study, two near-real-time satellites-based precipitation products, namely, GSMaP_NRT and PERSIANN-CCS during 2009-2013 are evaluated. GSMaP_NRT is hourly product with 0.1 x 0.1 degree and 4-hour latency while PERSIANN-CCS is hourly product with 0.04 x 0.04 degree with 1-hour latency. The satellite-based rainfalls are compared with daily rainfall from TMD rain gauge over Thailand.

The results show a good potential of the two satellite-based rainfall products with the hit rate of 65-67% and the false alarm rate of 15-18%. For the overall performance, GSMaP_NRT is relatively better than PERSIANN-CCS. Comparison at the daily time scale showing the correlation coefficient of 0.43-0.46 while the correlation coefficients of the monthly and annual time scales increase to 0.45-0.75. This is a result from the under and overestimation on the daily time scale. For annual rainfall greater than 1000 mm, both satellite-based rainfall products underestimate the rain gauge. It should be noted that the performance of the satellite-based rainfall products significantly varies spatially. Further adjustment to reduce bias of the satellite-based precipitation should be implemented.

Acknowledgment

The authors would like to express their gratitude to the Thai Meteorological Department for the observed rainfall data, JAXA and NASA for GSMaP_NRT, the CHRS center at University of California Irvine for PERSIANN-CCS. We acknowledge the partial funding from Department of Water Resources Engineering, Faculty of Engineering, Chulalongkorn University and Hydro and Agro Informatics Institute (HAII).

References

[1] D.S. Wils, "Statistical Methods in the Atmospheric Sciences," Theobald's Road, Lndon, Elsevier Academic Press Publications, 2006.

[2] K.Hsu, X. Gao, S. Srooshian, and H.V. Gupta, "Precipitation Estimation from Remotely Sensed Information using Artificial Neural Network," December 1996.

[3] T. Kubota, S. Shige, H. Hashizume, K. Aonashi, N. Takahashi, S. Seto, M. Hirose, Y.N. Takayabu, T. Ushino, K. Nakagawa, K. Iwanami, M. Kachi, and K. Oakamoto, "Global Precipitation Map Using Satellite-Borne Microwave Radiometers by the GSMaP Project: Production and Validation," July 2007.

[4] K. pakoksung and M. Takagi, "Effect of satellite-based rainfall products on river basin responses of runoff simulation on flood event," July 2016.

[5] T. Ram-Indra, A. Sriariyawat, and P. Hoisungwan, "Rainfall-Runoff-Inundation Simulation with Bias-corrected Satellite Based Rainfall: Case Study Yom River Basin," January 2015.

[6] T.G. Romily and M. Gebremichael, "Evaluation of satellite rainfall estimates over Ethiopia river basins," May 2011.

[7] S. Kirtsaeng and P. Sukthawee, "Heavy Rainfall Warning System in Southern Thailand," July 2015.

[8] G. Ozawa, H. Inomata, Y. Shiraishi, and K. Fukami, "Applicability of GSMaP Correction Method to Typhoon 'Morakot' in Taiwan," in Journal of Japan Society of Civil Engineering, 2011.

[9] S.B. Gebere, T. Alamirew, B.J. Merkel, and A.M. Melesse, "Performance of High Resolution Satellite Rainfall Product over Data Scarce Parts of Eastern Ethiopia," September 2015.

[10] S. Prakash, A.K. Mitra, D.S. Pai, and A. AghaKouchak, "From TRMM to GPM: How well can heavy rainfall be detected from space?," in Advance in Water Resources, December 2015.

[11] S. Ariyawat, K. Pakoksung, T. Sayama, S. Tanaka, and S. Koontanakulwaong, "Approach to Estimate the Flood Damage in Sukhothai Province Using Flood Simulation," in Journal of Disaster Research, 2013.

Reconstruction of the great famine of Western India using historical rainfall and global reanalysis datasets: challenges and uncertainties

Seemanta Sharma Bhagabati[1,a], Akiyuki Kawasaki[1] and Michihiro Ogawa[2]

Abstract The Deccan Plateau in Western India has a semi-arid climate. Historically, the region has experienced multiple hydrological disasters, affecting the agriculture and thereby the peasants' life. The region suffered extensive water scarcity during the Great Famines between 1876 and 1878. According to the British India's Famine Commission, the total fatality crossed the 5 million mark, however the actual numbers are supposed to be way more than that. Although there has been some statistical analysis of the event, spatial analysis including the extent and severity has not been conducted. The final goal of this research is to reconstruct the hydrological conditions of the great famine, using hydrological modelling as a tool. In this paper, we show the different challenges involved in doing so along with the uncertainty of the input data required for such analysis.

Keywords *19th century, Drought, Historical analysis*

[1]Department of Civil Engineering
The University of Tokyo
Tokyo, Japan
[2]International Education Center
Kanazawa University
Ishikawa, Japan

[a]seemanta@hydra.t.u-tokyo.ac.jp

Introduction

Droughts are natural disasters that affect agriculture, flora and fauna, natural resources as well as disrupt human livelihood. Natural disasters such as floods and droughts are seen throughout the globe and are more often than one might think. They affect millions of people globally every year [1]. Although, floods last from a few days to a couple of weeks, droughts on the other hand are widespread long-term persistent phenomenon. Over a million people had died globally as a result of droughts since 1974 [2].

Droughts are quite common natural disaster in India, with one drought in every three years in some part of India [3]. In India, around 94 million hectares are drought prone regions which affects over 400 million people. Figure 1 lists the monsoon rainfall anomaly for India during 1871-2003. A total of 19 major floods and 23 major droughts occurred in some parts of India.

Recently many researchers have tried to do short-term and long-term studies on droughts in the mid to late 20th century and early 21st century [4-6]. However, no study has been conducted specifically for the great famine. The final goal of this research is to understand the great famine from the hydrological perspective. In order to achieve this goal, an attempt has been made to reconstruct the historical meteorological event (Great Famine) in the Indian sub-continent.

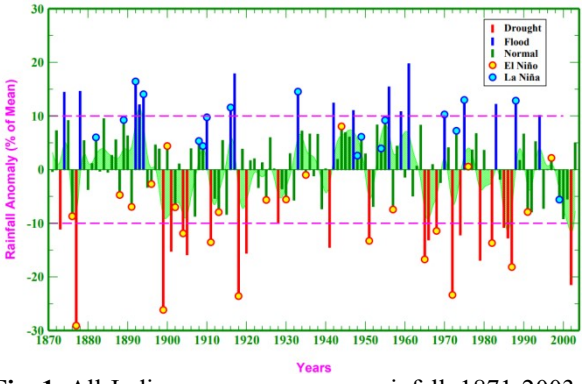

Fig. 1. All-India summer monsoon rainfall, 1871-2003 (source: Rupa Kuman Kolli, IITM, Pune, India)

The great famine

The most severe drought happened in the year 1876, the effects of which lasted until the year 1878. Figure 2 shows a historical map of the great famine,

which hit large part of the Deccan plateau. Just following the great famine was a malaria epidemic (shown in light red color, fig.2). The famine commission at the all British India level, which was set up in 1878, reported the total number of deaths amounted to around 5 million. Finally, Famine Code was enacted in 1883, on which famine policies in the British India were established based.

Fig. 2. Extent of the Great Famine

Mortality during the great famine in the Bombay Presidency

One of the most severely affected regions was the Bombay presidency. Figure 3 shows the district-wise mortality of the region in 1876 and 1877. The patterns of mortality became explicit in 1877. Districts of Dharwar, Belgaum, Bijapur (Kaladgi) and Satara had much higher mortality than other districts. Interestingly, Dharwar, Bijapur (Kaladgi), and Belgaum were in the Bombay Karnatak, namely the southern part of the Bombay Presidency. Satara District was located north of the Bombay Karnatak. These four districts were contiguous to one another, and Satara District was in the border between the Bombay Deccan and the Bombay Karnatak. The northern half of the district was less effected compared to the southern half. It indicates mortality rose as areas went near the southern part of the Bombay Presidency even at the sub-district level. Moreover, Khandesh, the northernmost district among the above nine districts, had the lowest mortality in June 1877. From the figure it can be clearly seen that the mortality kept on increasing as we move towards the southern direction.

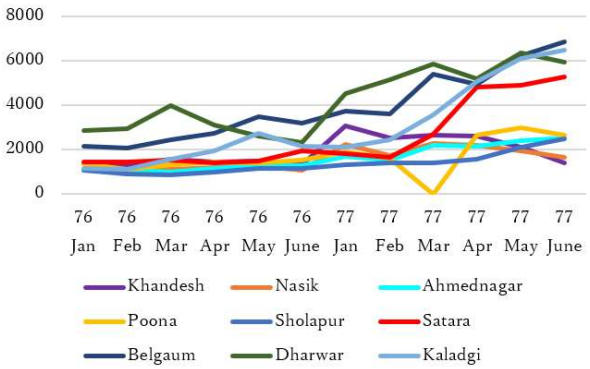

Fig 3. Death registration in the Bombay presidency

Hydrological modelling

Since this complete extent of the great famine is huge, as a pilot study, the Bhima river; a tributary river of the Krishna river, has been selected (figure 4). The Bhima river is 861 km long, with a total catchment area of around 70,614 km^2.

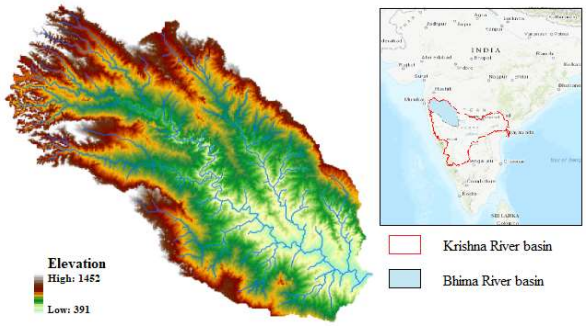

Fig. 4. The study area: Bhima River basin.

In this research we used the Water and Energy Budget-based Distributed Hydrological Model (WEB-DHM) [7,8]. This model was developed by coupling a simple biosphere scheme (SiB2) with a geomorphology-based hydrological model to describe water, energy and CO_2 fluxes at a basin scale. It calculates evapotranspiration based on both water and energy balances in each model grid and therefore has a more solid physical foundation relative to the traditional hydrological models.

The overall structure of WEB-DHM is shown in figure 5. The figure 5 (a) shows the sub-basin; (b) shows the sub-division from sub-basin to flow intervals; (c) shows the discretization from a model grid to several geometrically symmetrical hillslopes; and (d) shows the detailed process descriptions of the water moisture transfer from atmosphere to river.

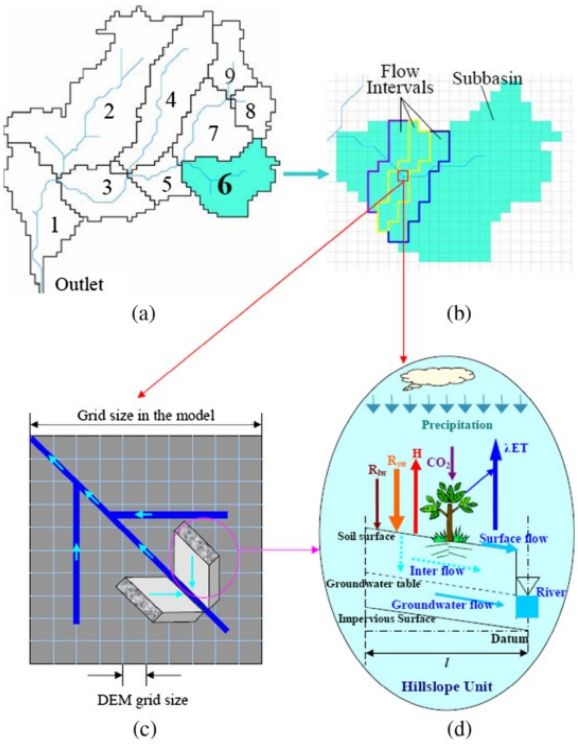

Fig. 5. Overall structure of WEB-DHM model

A. Input data

Like most other models WEB-DHM uses two kinds of data, (a) static physical data such as topography data (DEM), landuse data, soil data, etc. and (b) variable meteorological data such as precipitation, humidity, wind speed, air pressure, air temperature and downward solar radiation (short wave radiation, long wave radiation).

B. Data availibility

The target time period for this analysis is set as 1872-1878. The static datasets usually don't change even over many decades. Therefore, these data can be assumed to have not changed drastically. However, that is not the case for the meteorological data.

Even though the great famine happened during 1874-1876 (and effects lasted until 1878), daily recorded precipitation data is available from 1878 onwards. These daily data were obtained from the British library at the London School of Economics and Political Science (in form of pdf files). There are however some hand-written data for the years prior to 1878. Figure 6 shows one such example. If you look closely, the precipitation values of some days are mentioned. Upon further investigation of hundreds of such pages, it was found that there are many missing days. The data thus is incomplete. This makes the data unusable at its current status for any modelling purposes.

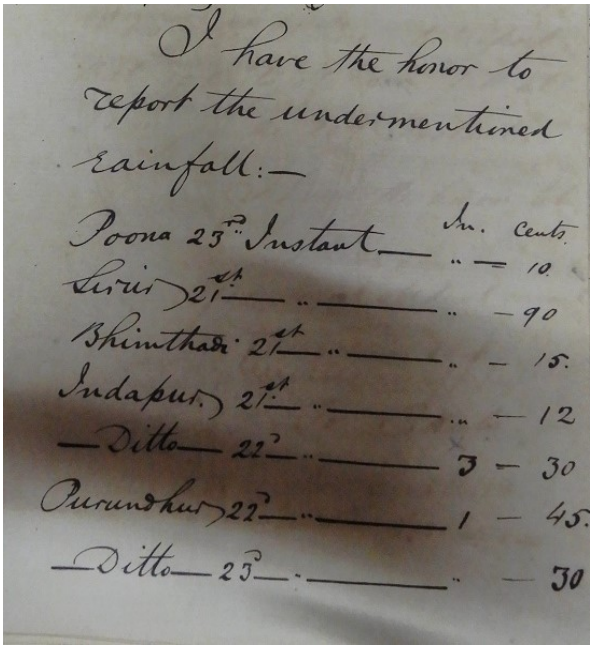

Fig. 6. Old hand-written precipitation data

But apart from the precipitation data, no other meteorological data is available. Although there are no observed data, some GCM outputs and reanalysis dataset are available during 1870s on a global scale. One such dataset is the 20th century Reanalysis datasets provided by the National Oceanic and Atmospheric Administration (NOAA) (https://www.esrl.noaa.gov/psd/data/ 20thC_Rean/). It contains all the meteorological needed to setup the WEB-DHM model.

C. Data uncertainity

As introduced in the previous section, the NOAA 20th century Reanalysis can be a viable option to be used as the input data for the model. Figure 67shows the mean monthly average temperatures (1871-1890) for June and July months and the corresponding values for 1876 and the differences.

As seen from those figures, there is not much change in temperature in the Deccan plateau of the Indian sub-continent. Very interestingly the major differences can be seen in the north India, near the Himalayas.

Figure 8 shows similar figures for relative humidity values. In this case however, a large difference in relative humidity can be seen in the deccan plateau along with a higher difference in the North India along the Himalayas.

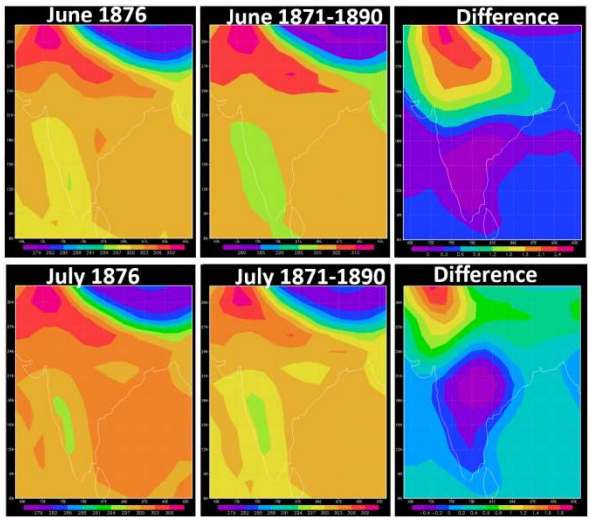

Fig. 7. Comparison of temperature during June and July 1876 with mean values for 1871-1890

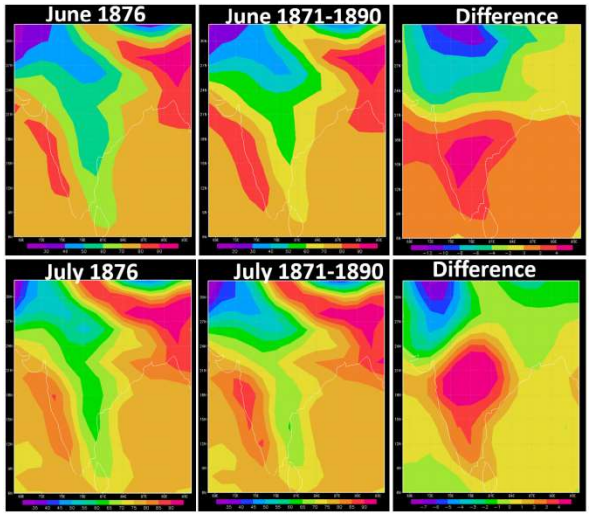

Fig. 8. Comparison of relative humidity during June and July 1876 with mean values for 1871-1890

D. Initial model setup

In order to develop a hydrological model, available discharge data at some points along the river channel is needed for initial set-up, calibration and validation. Since the available data is limited for the 19th century, with no observed/measured river discharge data, it is almost impossible to set-up and calibrate the model at that time. The model has to be setup for such a period where these conditions are met. Since, the study area also experienced a drought period during 1998-2004 and all the required data are available, an initial model has been setup for the period. Figure 9 shows the hydrographs are two locations along the Bhima river.

The model has been calibrated for 1997 and validated for the years 1998-1999, with NSE values of 0.87 & 0.89 and R^2 values of 0.82 & 0.85 respectively. These values mean that the model is applicable for the study area.

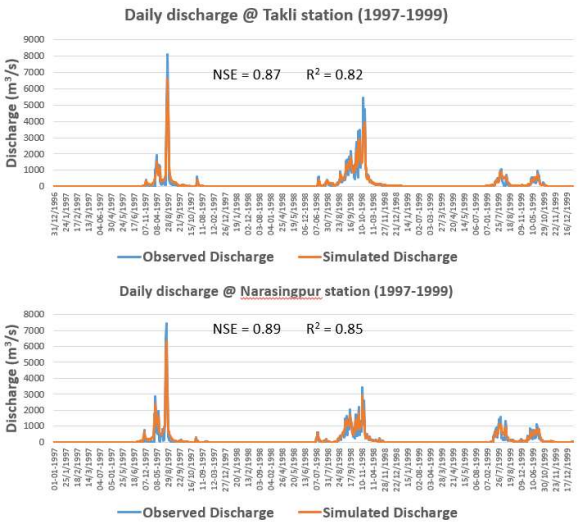

Fig. 9. Initial model setup; calibration year – 1997; validation years – 1988-1999

Disccusions

From the figures 7 and 8, although we can see some difference in temperature and relative humidity in the target region during the great famine period, the difference is rather small. The main reason is due the inabilityof the reanalysis dataset to capture the drought/famine period. Based on this analysis, it seems that the NOAA 20th century reanalysis data is not well suited to be used as the input data for setting up the WEB-DHM model to analyze the great famine in 1876.

There however, are many other Global Circulation Models (GCM) which have historical dataset, especially the CMIP5 experiments. It has global GCM outputs since 1850s. There are many sub-experiments which consider different climatic and physical conditions. Choosing an appropriate GCM output would be the next step of this research.

The observed hand-written precipitation data is also found to be incomplete. Some method must be developed either interpolation or duplication to fill-up the missing values, to be able to use the data as an input for hydrological models.

The initial hydrological model for the study area has been developed. Next step of the research is to use this same model and run it for the time period of 1875-1879. As mentioned earlier, a better alternative for meteorological data is also required.

References

[1] D. Wilhite Drought: A Global Assessment, Natural Hazards and Disasters Series, Routledge Publishers, UK (2000), pp. 213-230

[2] United nations (UN): Trends in Sustainable Development 2008–2009. United Nations publication, United Nations Division for Sustainable Development (2008)

[3] Goyal, M.K., Gupta, V., Eslamian, S., 2017. Hydrological Drought: Water Surface and Duration Curve Indices. Handbook of Drought and Water Scarcity: Principles of Drought and Water Scarcity.

[4] Singh, V., Yadav, R. R., Gupta, A. K., Kotlia, B. S., Singh, J., Yadava, A. K., Singh, A. K., and Misra, K. G., 2017. Tree ring drought records from Kishtwar, Jammu and Kashmir, northwest Himalaya, India. Quaternary International, 444(A), 53-64.

[5] Kumar, K. N., Rajeevan, M., Pai, D. S., Srivastava, A. K., and Preethi, B. 2013. On the observed variability of monsoon droughts over India. Weather and Climate Extremes, 1, 42-50.

[6] Dhorde, A. G., and Patel, N. R. 2016. Spatio-temporal variation in terminal drought over western India using dryness index derived from long-term MODIS data. 2016, 32, 28-38.

[7] Wang, L., Koike, T., Yang, D.W. and Yang, K., 2009a. Improving the hydrology of the simple biosphere model 2 and its evaluation within the framework of a distributed hydrological model. Hydrol. Sci. J.-J. Des Sci. Hydrol., 54 (6), 989–1006.

[8] Wang, L., Koike, T., Yang, K., Jackson, T.J., Bindlish, R. and Yang, D., 2009b. Development of a distributed biosphere hydrological model and its evaluation with the southern great plains experiments (SGP97 and SGP99). J. Geophys. Res., 114 (D8).

Interesting StatisticalCharacteristics of Precipitation Extremes in Major River Basins of Japan using a Large Ensemble of Climate Simulations "d4PDF"

Shigenobu Tanaka[1,a]

Abstract Climate change impact has recently attracted strong public attention whenever severe water-related disaster occurs. Generally, very infrequent events such as the ones which occur once in 100 years are estimated based on the extreme value theory with the sample of annual maximum series(AMS) or peaks over threshold (POT). In this study,the relationship between basic statistical characteristics of extremes and probability distribution functionis focused. Usually AMS of extremeshave wide range of variety and one has to conduct frequency analysis on each data set for estimating extrapolating extremes. The Gumbel distribution is a two-parameter distribution and the parameters are closely related with the basic statistics; mean and variance. The characteristics of mean and variance are examined for the past and the future experiments of "Database for Policy Decision-Making for Future Climate Change" (d4PDF) in major six river basins in Japan. The d4PDF is a large ensemble of climate simulations with 20 km grid size. The past experiment consists of 50 ensembles of 60 years and the future of 90 ensembles of 60 years. As a result, it is found that the 100-year return level and ensemble mean of AMS in the investigated river basins are distributed along a regression line with errors of a rather limited range.Then, we can use this relationship in estimation of return levels without conducting frequency analysis. Further, this relationships between return level and the mean of AMS for different durations are on the same regression line. This relationship also provides a hint of bias correction of "ensemble climatic data" such as d4PDF.

Keywords *climate change, d4PDF, precipitation extreme*

[1]Water Resources Research Center
DPRI, Kyoto University
Uji-City, Japan

[a]tanaka.shigenobu.4m@kyoto-u.ac.jp

Introduction

There have been recently occurred many flood and sediment disasters which have caused people pain long after hazards settled. And also few media have reported without "record breaking" and relationship with climate change impact. Since IPCC AR5 [1] has warned as "Extreme precipitation events over most of the mid-latitude land masses and over wet tropical regions will very likely become more intense and more frequent," it has been getting more concern than ever and many reports on the possibility of huge disaster occurrence.

Floods and debris flow disasters are caused by extreme rainfall. A large ensemble of climate simulations with a 60 km atmospheric general circulation model and dynamical downscaling with a 20 km regional climate model have been performed to obtain probabilistic future projections of low-frequency local-scale events. The simulation outputs are available as "Database for Policy Decision-Making for Future Climate Change" (d4PDF) [2], which is intended to be utilized for impact assessment studies and adaptation planning for global warming. In this study, extreme precipitations in the major six river basins are investigated in terms of statistic characteristics and rare events such as 100 year return levels as well as future change.

Used data

The d4PDF consists of two kind of grid spacing, that is , 60km and 20km. The latter is regional downscaling simulations covering the Japan area by a regional climate model (RCM). The RCM used in this study are historical climate simulation: (1951-2010, 50 ensemble members) and future climate simulation: (2051-2110, 90 ensemble members). The future 90 ensemble members consists of 6 kinds 15 members simulations corresponding to different climatological SST warming patterns such as CCSM4, GFDL-CM3, HadGEM2-AO, MIROC5, MPI-ESM-MR, MRI-CGCM3 (CC, GF, HA, MI, MP, MR, respectively). With daily precipitation of 99 grids in the major six river basins; Tone, Ara, Kiso, Nagara, Shonai and Yodo in Fig. 1, daily, 2-day and 3-day annual maximum precipitations are extracted.

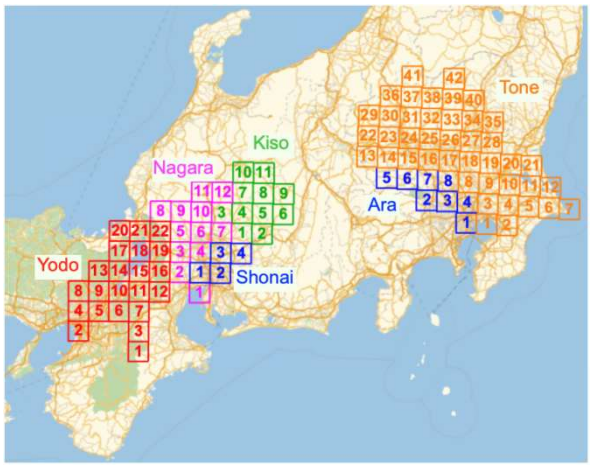

Fig. 1. Locations of Target six Major River Basins in Japan

Method of Frequency Analysis

In estimating very infrequent extreme events, it has been applied extreme value distributions [3], [4]. Generalized Extreme Value distribution (GEV) is used for block maxima while Generalized Pareto distribution (GP) for Peaks Over Threshold. Both GEV and GP are three-parameter distributions but become two-parameter distributions, Gumbel and Exponential distributions when their shape parameter are zero, respectively. When dealing with block maxima, the simplest one is Gumbel distribution which has two parameters closely related to the statistics of block maxima.

When the cumulative distribution function $F(x)$ of Gumbel distribution is expressed by (1) with variable x,

$$F(x) = \exp\{-\exp\left(-\frac{x-\xi}{\alpha}\right)\} \quad (1)$$

the location parameter ξ and shape parameter α have following relationships (2) with the mean μ and standard deviation σ of the block maxima sample.

$$\alpha = \frac{\sqrt{6}}{\pi}\sigma, \xi = \mu - 0.5772\alpha \quad (2)$$

After α and ξ determined, one can estimate nonexceedanceprobability$F$ and return period, or return level with (3).

$$x = \xi - \alpha\log\{-\log(F)\} \quad (3)$$

A. Block Size of Block Maxima

While one has to select block size in applying block maxima, AMS which is a kind of block maxima with a year as a block, has been conventionally used widely without careful examination. The d4PDF is a huge database which has 50 or 15 ensemble members of 60 years simulations. If we deal with the database as a serial simulation, we have 3,000 years AMS for the historical climate simulation and 900 years AMS for the future one. On the other hand, if we take a 60-year period as a block, we have 50 "60-year maxima." Anyway, if a sample come from a population of Gumbel distribution, the probability plots fall on a straight line on the Gumbel probability paper. Further, different block sizes yield different location parameters but the same scale parameters. Fig. 2 compares AMS plot and 60-year maxima one. In the AMS plot, the lower part looks different from upper part. At the height of 100-year return period, plotted points show different return level from both of Gumbel distribution and GEV. In this AMS, that data less than 90 mm occupy a half of the whole sample and show different tendency with upper part might be a reason of the disagreement. On the other hand, the 60-year maxima plot at which F=0.4 corresponds to 100-year return period agrees with both distributions well. In this example, the scale parameters are different from each other. Based on this difference, 60-year maxima is used for estimating 100 year return level in this study. Still, AMS is important in practical situation, the relationship between AMS and 60-year maxima will be prepared.

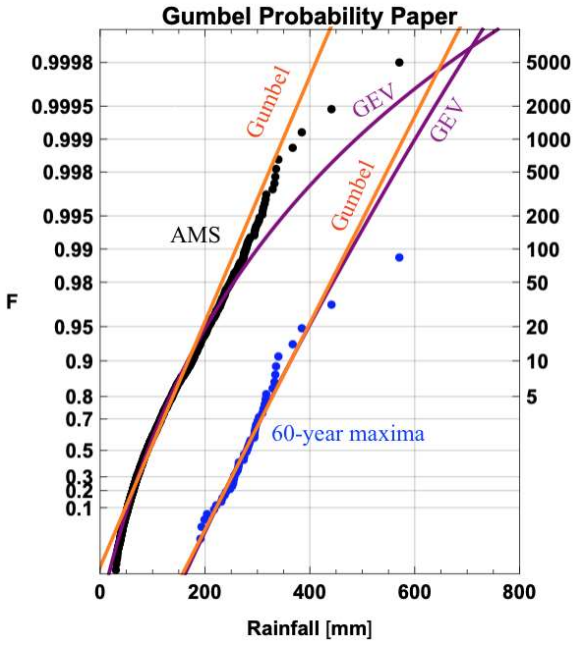

Fig. 2. Comparison of Probability plots and fits of AMS (Black) with 60-year maxima (Blue)

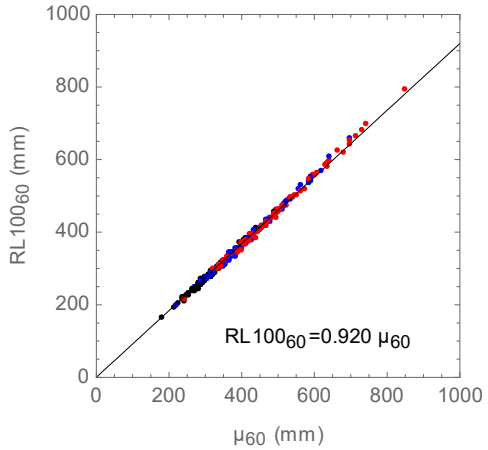

Fig. 3. Relationship between 100-year Return Level and Ensemble Mean of 60-year Maxima for 1(Black),2(Blue) and 3(Red) day Precipitation at 6 River Basins

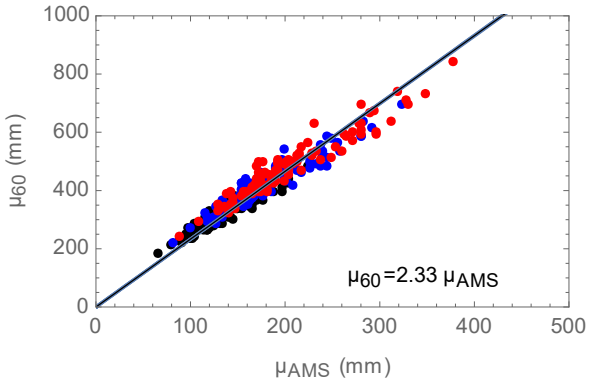

Fig. 4. Relationship between Ensemble Mean of 60-year Maximum Series and that of AMS for 1(Black),2(Blue) and 3(Red) day Precipitation at 6 River Basins

Result

In this section, the result with the historical climate simulations(past) is shown first, and then that of the future one, finally, bridge information between past and future.

A. Relationship between 100-year Return Level and Ensemble Mean of 60-year Maxima (Past)

Fig. 3 shows the relationship between 100-year return level and ensemble mean of 60-year maxima precipitation. It includes plots for each grid of six river basins and durations such as 1, 2 and 3 day. It is very interesting that all plots are almost on a single straight line. It shows that we can tell a 100-year return level of any duration at any grid in any river basin examined here with just ensemble mean of 60-year maxima regardless of grid location and duration.

B. Relationship between Ensemble Mean of 60-year Maxima and that of AMS(Past)

Fig. 4 shows the relationship between ensemble mean of 60-year maxima and that of AMS including plots for each grid of six river basins and durations. The plots are almost distributed around the regression line but rather fluctuating. However, it shows very solid relationship tendency. Using Fig. 3 and 4, you can tell 100-year return level with just ensemble mean of AMS regardless of grid location and precipitation duration. If necessary, it is possible to prepare it for each location against each river basin with each detailed information. Fig.5 shows the same relationship for respective basin. In Ara, Shounai and Yodo river basins, fluctuations are relatively small. But Tone river basin which is the largest one and showing rather wide fluctuations needs further investigation.

C. Relationship between Ensemble Mean of 2-day and daily Annual Maximum Precipitation at each River Basin(Past)

In above results, plots of 1-, 2- and 3-day precipitation always combined in to a diagram. It is valuable if there are some good relationship between daily and 2-day precipitation. Fig. 6 shows this relationship using ensemble mean for each river basin. While regression lines are different from basins, they fit very well. Fig. 7 shows the relationship between the ratio of 2-day precipitation to daily and the ratio of 3-day precipitation to daily. Using above mentioned relationships, once get the information of AMS daily precipitation, one can reach to 100-year return level of any of daily, 2-day and 3-day precipitations by way of estimating 60-year maxima.

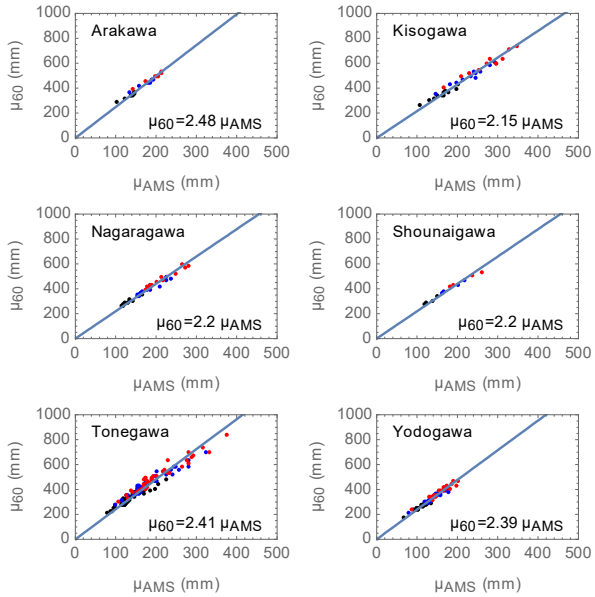

Fig. 5. Relationship between Ensemble Mean of 60-year Maximum Series and that of AMS for 1(Black),2(Blue) and 3(Red) day Precipitation at 6 River Basins

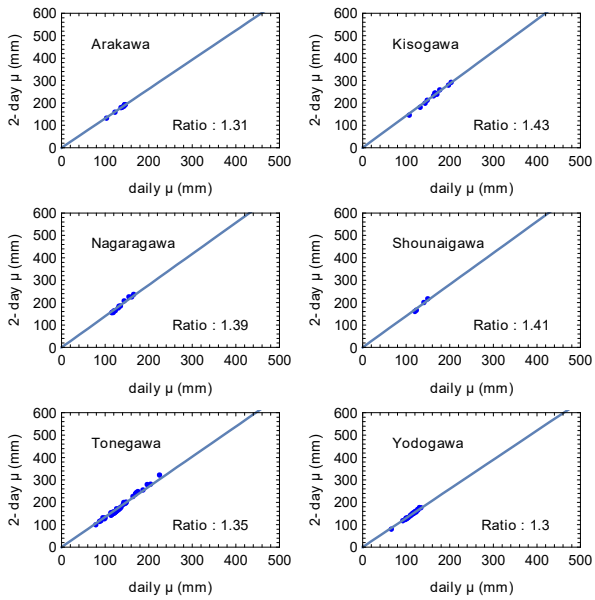

Fig. 6. Relationship between Ensemble Mean of 60-year Maximum Series and that of AMS for 1-(Black),2-(Blue) and 3-day(Red) Precipitation at 6 River Basins

Next, the relationship in the future climate simulations is investigated.

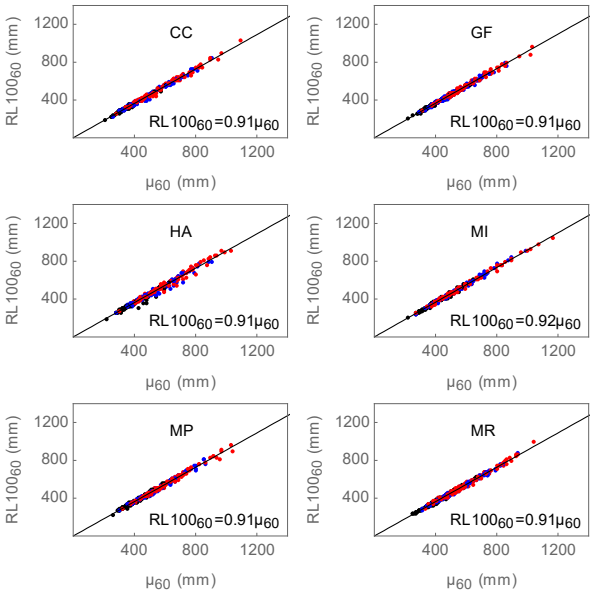

Fig. 7. Relationship between 100-year Return Level and Ensemble Mean of 60-year Maxima for 1(Black),2(Blue) and 3(Red) day Precipitation at 6 River Basins for each SST Pattern

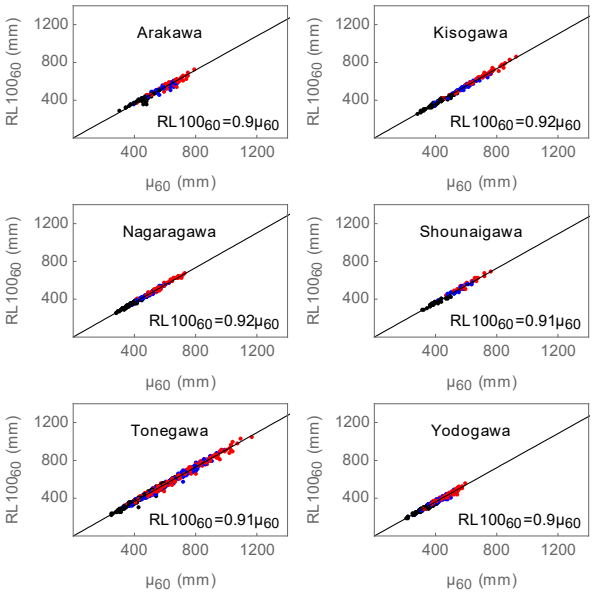

Fig. 8. Relationship between 100-year Return Level and Ensemble Mean of 60-year Maxima for 1(Black),2(Blue) and 3(Red) day Precipitation of all SST Pattern for each River Basins

D. Relationship of 100-year Return Level with Ensemble Mean of 60-year Maxima(Future)

Fig. 8 shows the relationship of 100-year return level with ensemble mean of 60-year maxima. The future climate simulations consist of six kinds SST patterns. In this figure, all result of six SST patterns are joined altogether. The most scattering are in Tone river basin. While the plots become rather scattered, plot tendency is similar to the past experimentand the slope of regression line is very similar to the past one.In order to examine this

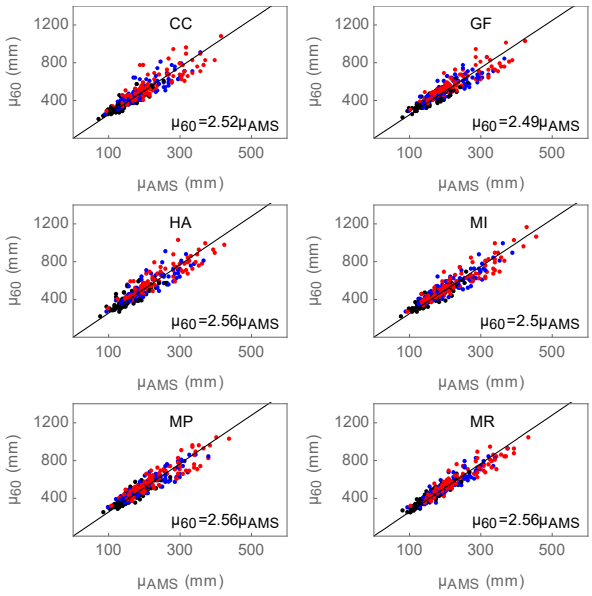

Fig. 9. Relationship between Ensemble Mean of 60-year Maxima and that of AMS of 1(Black),2(Blue) and 3(Red) day Precipitation in 6 River Basins for each SST pattern (Future)

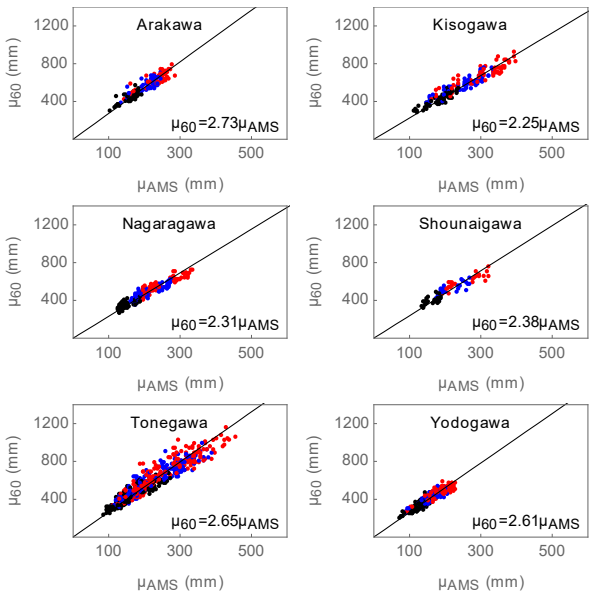

Fig. 10. Relationship between Ensemble Mean of 60-year Maxima and that of AMS of 1(Black),2(Blue) and 3(Red) day Precipitation of all SST Pattern for each River Basins (Future)

relationship for each SST pattern, see Fig. 9. Among six SST patterns, MI has the least error while it includes the deepest 3-day precipitation. On the other hand, HA has the largest error. The extent of scattering depends on the SST pattern but the regression lines have similar slopes. Fig. 10 shows similar diagram to Fig. 9 basin by basin. You can see Tone has many plots ranging widely. However, Ara has fewer plots than Tone but scattering situation is similar to Tone. The regression slope at each basin depends on river basin.

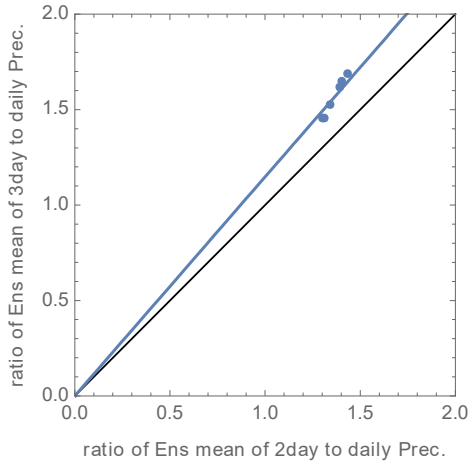

Fig. 11. Relationship between Ensemble Mean of 60-year Maximum Series and that of AMS for 1-(Black),2-(Blue) and 3-day(Red) Precipitation at 6 River Basins

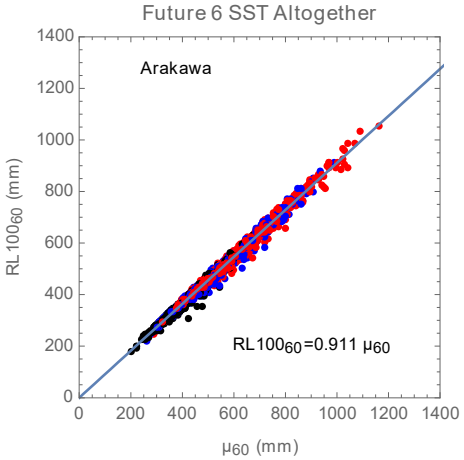

Fig. 12. Relationship between 100-year Return Level and Ensemble Mean of 60-year Maxima for 1-(Black),2-(Blue) and 3-day(Red) Precipitation at 6 River Basins for 6 SST Pattern Altogether

E. Relationship between Ensemble Mean of 60-year Maxima and mean of AMS(Future)

Fig. 11 shows relationship between ensemble mean of 60-year maxima and mean of AMS of 1-(Black), 2- (Blue) and 3-day (Red) precipitation in 6 River Basins for each SST pattern. All SST patterns shows slope of regression line of about 2.5 but with large errors. MI has the least errors among six SST patterns.

Fig. 12 shows the same data as Fig. 11 basin by basin. You can see each river basin has rather different regression slope and in Nagara, Shonai and Yodo, plots are relatively close to the regression line but the other basins have rather large errors especially in Tones river basin. These diagrams are enough to grasp overall characteristics but seem not sufficient to know the value corresponding to the ensemble mean of 60-year maxima. In order to do so, we have to prepare translation tables.

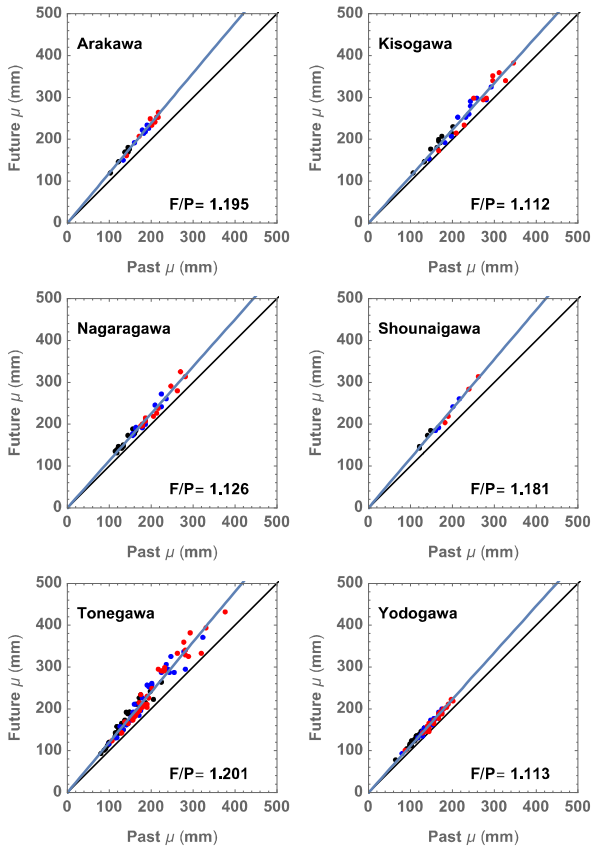

Fig. 13. Relationship between Ensemble Mean of AMS in Future and that of Past of 1(Black), 2(Blue) and 3(Red) day Precipitation (Mean of all SST Pattern for each River Basins)

F. Relationship between Ensemble Mean of AMS in Future and that of Past of 1(Black), 2(Blue) and 3(Red) day Precipitation (Mean of all SST Pattern for each River Basins)

After looking at the characteristics of the past climate simulations and the future climate simulations, finally, we need a bridge between the past climate and the future climate. While the 60-year maxima have solid relationship with 100-year return level, the 60-year maxima are not so popular and the characteristics not well-known. In contrast, AMS is widely used and people has common knowledge about AMS including magnitude of it. Fig. 13 shows the relationship between ensemble mean of AMS in future and that of the past for each River Basins. The ratios of the future to the past of them are different from river basins and range from 1.1 to 1.2 with the average at 1.16. In Kiso, Nagara and Tone, you may need more detailed translation information.

Discussion

In the previous section, various statistics relating to 100-year return level are investigated. Fig. 14 shows relationships connecting them each other. Suppose that you have a mean value of AMS of some location of this area in the past and wants to know 100-year return level of 2-day precipitation, you can proceed with Fig. 6, then Fig. 4 and 5, finally Fig. 3. If you happen to know 60-year maxima, then use just Fig. 3 which has very solid relationship to 100-year return level. For the future climate, Fig. 13 can be a bridge between the past and the future, then just same manner needed. When you want to know about the future extremes, you have to recognize there are rather large uncertainty, especially, in relationship between 100-year return level and AMS.

It is amazing that the relationships between 100-year return level and ensemble mean of 60-year maxima in the past (Fig. 3) and the future (Fig.8) are very close even their range is much different. It impliesthat the structure of extremes might be kept even in the future.

Facing recent huge water-related disasters one after another, increasing magnitude of possible hazard has been worried about. For the future risk management, frequency analysis with just observed data is not useful. The extremes from the future projections such the ones used in this study are important. However, most projections usually contain "bias" which is necessary to be removed. When the simulation is just one case, the result can be compared to the observation. With many simulation ensemble members, however, it is difficult to compare them with the observation. Fig. 3 indicates mean 60-year maxima and 100-year return level have very close connection with a single simple formula over rather large area. Hence, it is important to prepare statistics of observed extremes similar to Fig. 3. It can be a weak but robust backbone of bias correction.

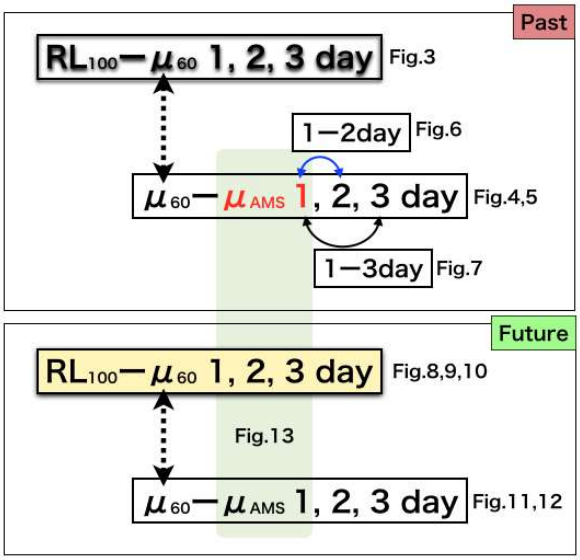

Fig. 14. Relationship among statistic characteristics connecting 100-year return level

Conclusions

The author has interested in frequency analysis and trend analysis of recent precipitation which cause water-related disasters. Many researchersin the field of climate change impact assessment have been tackled with bias correction [5], [6]. With the advent of huge ensemble database such as d4PDF, condition of bias recognition is so much different. Before that, such as quantile mapping correction method had been widely applied in bias correction. However, after the advent, it looks as if we lost the compass of this field. In this situation, the information as Fig. 3 might be a new light on this problem.

Acknowledgment

This research is supported by the "Integrated Research Program for Advancing Climate Models (TOUGOU program)" from the Ministry of Education, Culture, Sports, Science and Technology (MEXT), Japan.

References

[1] IPCC,"Climate Change 2014 Synthesis Report Fifth Assessment Report", Intergovernmental Panel on Climate Change, 2015.

[2] Mizuta, R., A. Murata, M. Ishii, H. Shiogama, K. Hibino, N. Mori, O. Arakawa, Y. Imada, K. Yoshida, T. Aoyagi, H. Kawase, M. Mori, Y. Okada, T. Shimura, T. Nagatomo, M. Ikeda, H. Endo, M. Nosaka, M. Arai, C. Takahashi, K. Tanaka, T. Takemi, Y. Tachikawa, K. Temur, Y. Kamae, M. Watanabe, H. Sasaki, A. Kitoh, I. Takayabu, E. Nakakita, and M. Kimoto, 2017, "Over 5000 years of ensemble future climate simulations by 60 km global and 20 km regional atmospheric models." Bull. Amer. Meteor. Soc. July 2017, 1383-1398.

[3] Stedinger, J.R., R.M. Vogel, and E. Foufoula-Georgiou, "Frequency Analysis of Extreme Events, Chap. 18, Handbook of Hydrology," (Ed.) D. R. Maidment, McGraw-Hill, New York, pp.18.1-18.66, 1993.

[4] Coles, S. G.,"An introduction to statistical modeling of extreme values," Springer-Verlag, 2001.

[5] Seneviratne, S. I., et al., "Changes in climate extremes and their impacts on the natural physical environment, in Managing the Risks of Extreme Events and Disasters to Advance Climate Change Adaptation: A Special Report of Working Groups I and II of the Intergovernmental Panel on Climate Change (IPCC), edited by C. B. Field et al., pp. 109–230, Cambridge Univ. Press, Cambridge, U. K., 2012.

[6] Watanabe, S. et al.,"Intercomparison of bias correction methods for monthly temperature and precipitation simulated by multiple climate models," J. Geophys. Res., 117, D23114, 2012.

Spatial Correlation for Flood Risk Assessment in Yom River Basin

Cholticha ARSSIRI[1,a] and Piyatida RUANGRASSAMEE[1,b,*]

Abstract In consideration of appropriate measures for flood mitigation, annual maximum flow data are one of the important data to be considered. Yom River Basin in Thailand has experienced floods frequently due to its topography of mountainous area in the upper basin and low-lying area in the lower basin as well as lack of largereservoirs in the basin. In flood risk assessment using flood frequency analysis, distribution function of annual maximum flow and estimated parameters of the distribution need to be determined. Additionally, a stochastic simulation of annual peak flow from multisite streamflow stations could provide valuable information for flood risk assessment. This study aims to develop a spatial correlation of peak flows in sub-basins ofYom River Basin as a step towards stochastic simulation. The methods are consisted of four parts: (1) standardization of peak flow data, (2) parameter estimation using method of L-moments, (3) goodness-of-fit test using L-moment ratio diagram, and (4) estimation of spatial correlation using semi-variogram models. The semi-variogram is fitted to three models: exponential, Gaussian, and spherical models using an ordinary least squares method. It was found that peak flow data from all four streamflow stations follow the Gumbel distribution. For the semi-variogram, the exponentialmodel is best fit. Furthermore, a stochastic simulation of annual maximum flow among stations can be developed using the obtained semi-variogram to estimate a covariance function. The stochastic simulation is a useful tool for quantifying probability of flooding in order to compare risk reduction of proposed flood mitigation measures.

Keywords *flood, Yom River Basin, Gumbel distribution, L-momets method, semi-variogram*

[1]Department of Water Resources Engineering
Faculty of Engineering, Chulalongkorn University
Bangkok, Thailand

[a]Cholticha.arssiri@gmail.com
[b]Piyatida.H@chula.ac.th

Introduction

Flow data are one of the most essential data for flood mitigation and flood risk management. Yom River Basin has experienced floods frequently due to its topography of mountainous area in the upper basin and low-lying area in the lower basin as shown in the topographic map in Fig 1. Yom River is the main river of the basin. The capacity of Yom River varies from 2,000 m^3/s in the upstream section to 300 m^3/s in the downstream section around Sukhothai province. For this reason, Sukhothai province is often flooded due to overflow.Furthermore, Yom River Basin lacks of large reservoirs for flood mitigation and water supply. Average annual flow in the basin is 4,720.7 million cubic meters but the existing reservoirs in the basin are medium and small sizes with the total capacity of only 406 million cubic meters and their main use is for irrigation (Royal Irrigation Department). The largest reservoir of the basin Mae Mok reservoir has a capacity of 96 million cubic meters and is located in Lampang province. There have been several development plans to increase water supply and mitigate floods in the basin including large, medium, and small reservoirs. However, there is still a lack of coordinated planning for the entire basin due to separate planning and management of each province in the basin. Considering spatial correlation of peak flows of multisite would provide useful information for flood risk analysis [1,2,3]. This study aims to develop a spatial correlation of peak flows in sub-basins of Yom River Basin.

Study Area and Data

Yom River Basin is one of the major upstreams of the Chao Phraya River. The average annual flows from the Yom River Basin contributes about 20 percent of the average annual flows of the Chao Phraya River (Royal Irrigation Department) at C.2 station in Nakhon Sawan. It is located in the northern part of Thailand. Heavy rainfall causesflash flood in the Upper Yom River Basin. In the Lower Yom River Basin where there is low lying area as well as narrowing river cross section in urban areas, floods frequently occurs and results in high economic and social loss [3,4]. The area of the basin is 23,616 km2and it consists of eleven sub-basins. The basin boundary includes partial areas of eleven provinces, i.e. Nan, Phayao, Lampang, Phrae, Uttaradit, Sukhothai, Tak, Phitsanulok, KampaengPhet, Phichit, and Nakhon Sawanprovinces.There are twenty-five flow stations in Yom River BasinbyRoyal Irrigation Department.

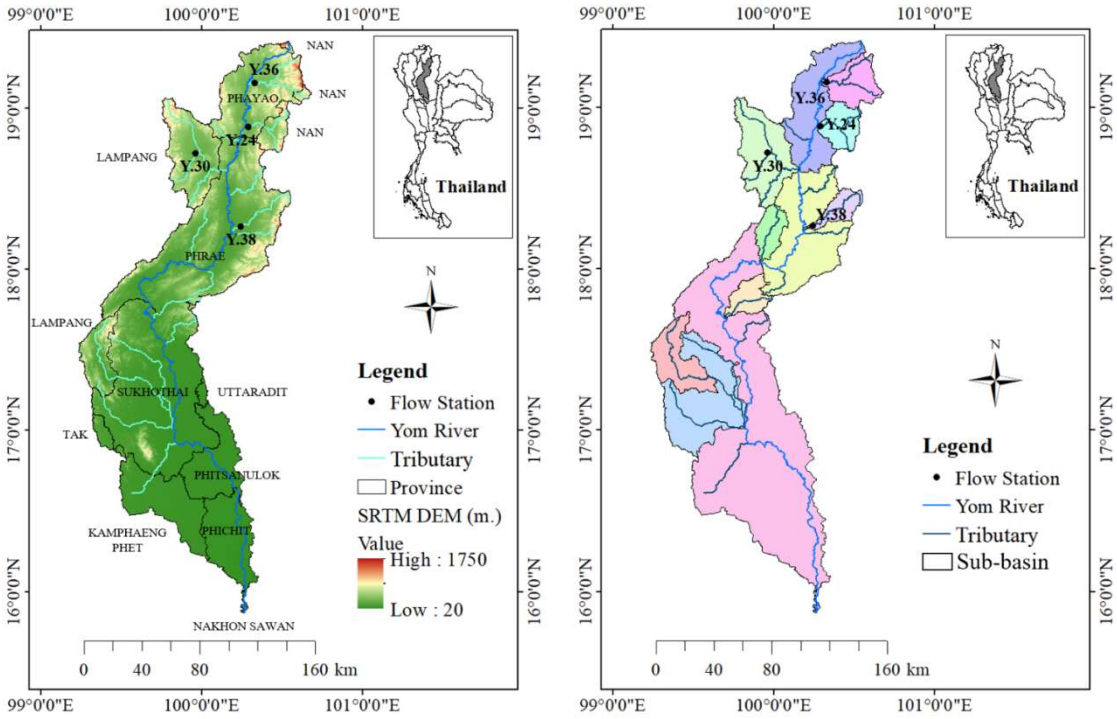

(a) (b)

Fig. 1. Map of Yom River Basin and Locations of Selected Flow Stations. (a) Topography of the basin and (b) Sub-basins of the Yom RiverBasin

Four flow stations were selected in this study area as shown in Fig 1. These four stations Y.36, Y.24, Y.30, and Y.38are located in the four sub-basins in the Upper Yom River basin. These stations are not affected by regulating infrastructure and have long historical records.In this study, we focus on the analysis of the variation in peak flows at different locations of the basin. Annual maximum flow data of four stations were collected from Royal Irrigation Department within the period of 1999-2017 as shown in Table I. Annual maximum flow usually occurs in September duringmonsoon season (May-October). The four flow stations are located on the separated tributaries. The highest annual maximum flow and the highest annual flow among the four stations arefromflow and the lowest annual flow among the four stations are from station Y.30 even though the drainage area of station Y.30 is largest. Station Y.30 is located on the right side of the main Yom River while the other three stations are located on the left side where tropical storms pass through from the South China Sea.

According to the land use data from Land Development Department in 2015-2016, the forest area and agriculture areaare major part of the basin. The upper part of the basin is mountain terrain and the lower part is flood plain. There is nolarge reservoir to reduce peak flow and store water for dry season use.

Methodology

This study is consisted of four parts:(A) standardization of peak flow data, (B) parameter estimation using method of L-moments, (C) goodness-of-fit test usingL-moment ratio diagram, and (D) estimation of spatial correlation using semi-variogram models.

Table I. List of annual peak flow stations

No.	Station	River	Province	Sub-Basin	Drainage Area (km^2)	Average Annual Flow (MCM)	Maximum Annual Peak Flow (m^3/s)	Year
1.	Y.36	Khuan	Phayao	Mae Nam Khuan	870.74	397.03	525.92	2011
2.	Y.24	Pi	Phayao	Nam Pi	656.66	146.06	312.40	2008
3.	Y.30	Huai Pong	Lampang	Mae Nam Ngao	1,753.86	41.24	78.27	2011
4.	Y.38	Mae Kham Mi	Phrae	Nam Mae Kham Mi	456.18	174.46	500.00	2004

A. Standardization of Peak Flow Data

The peak flow data from 1999 – 2017 at each station were first standardized to study the spatial correlation of the variation of the peak flows among different stations in different sub-basins. The goodness-of-test was carried out to find appropriate distribution for developing a stochastic simulation using a semi-variogram.

B. Parameter Estimation using Method of L-moments

The Extreme Value Type I or Gumbel distribution was developed in 1941. It played an important role in flood frequency analysis by Natural Environment Research Council (NERC) in 1975.In this study, the Gumbel distribution isselected based on several studies of peak flow in Thailand that was found to fit with this distribution. There are several methods of parameter estimation. One of the simplest and general approaches for estimating parameter is the method of moments [5]. For small sample size, the method of maximum likelihood sometimes gives more accurate than the method of moments. The alternative approach that was developed to reduce bias in parameter estimation is the method of L-moments. This method is more robust to outliers in the sample data and occasionally give more accurate than the method of maximum likelihood in small sample size [6].

For this reason, two parameters of the Gumbel distribution were estimated using L-moments method. The probability density function for the Gumbel distribution is given as follows [7]

$$f(x)=\frac{1}{\alpha}\exp\left[-\frac{x-u}{\alpha}-\exp\left(-\frac{x-u}{\alpha}\right)\right],-\infty<x<\infty \quad (1)$$

where u and α are the location and scale parameters respectively.

The probability weighted moments was developed by J. A. Greenwood et al. in 1979. Then L-moments were defined by J. R. Hosking in 1990 and they are linear combinations of probability weighted moments. They are similar to the ordinary moments that characterize measures of location, spread, and shape of the sample data and probability distributions [6,8].

L-moments for probability distributions (λ_r) are defined in terms of probability weighted moments (β_r , r = 0, 1, 2, 3,…).

$$\beta_r=\int_0^1 x(F)\{F(x)\}^r\,dF(x) \quad (2)$$

where $F(x)$ and $x(F)$ are respectively cumulative distribution function and quantile function.

$$\lambda_1=\beta_0 \quad (3)$$

$$\lambda_2=2\beta_1-\beta_0 \quad (4)$$

$$\lambda_3=6\beta_2-6\beta_1+\beta_0 \quad (5)$$

$$\lambda_4=20\beta_3-30\beta_2+12\beta_1-\beta_0 \quad (6)$$

$$\tau_r=\lambda_r/\lambda_2 \quad (7)$$

where τ_r is L-moment ratios (r = 3, 4,…). L-skewness (τ_3) and L-kurtosis (τ_4) have range of values between -1 to 1.

L-moments for the random sample (X) are similar to L-moments for probability distributions. Let $X_1, X_2, X_3, ..., X_n$ be the sample data that have sample of size n and arrange value in ascending order [6]. The sample probability weighted moments (b_r , r = 1, 2, 3,…) are defined as [8]

$$b_0=\frac{1}{n}\sum_{j=1}^{n}X_j \quad (8)$$

$$b_r=\frac{1}{n}\sum_{j=r+1}^{n}\frac{(j-1)(j-2)...(j-r)}{(n-1)(n-2)...(n-r)}X_j \quad (9)$$

The sample L-moments (l_r) and sample L-moment ratios (t_r , r = 3, 4,…) are given by

$$l_1=b_0 \quad (10)$$

$$l_2=2b_1-b_0 \quad (11)$$

$$l_3=6b_2-6b_1+b_0 \quad (12)$$

$$l_4=20b_3-30b_2+12b_1-b_0 \quad (13)$$

$$t_r=l_r/l_2 \quad (14)$$

where t_3 and t_4 are respectively the sample L-skewness and sample L-kurtosis. L-moment ratios are dimensionless and have range of values between -1 to 1.

Parameter estimators of the Gumbel distribution using the method of L-moments can be expressed by [6]

$$\hat{\alpha}=\frac{l_2}{\ln 2} \quad (15)$$

$$\hat{u}=l_1-\gamma\hat{\alpha} \quad (16)$$

where γ is Euler's constant with approximate value 0.5772.

C. Goodness-of-Fit Test using L-moment Ratio Diagram

The goodness-of-fit test is used to decide whether sample data resembles a particular kind of population [9]. L-skewness and L-kurtosis are characteristic of each distribution. They are less biased

than the ordinary skewness and kurtosis [10]. The Gumbel distribution has constant values of L-skewness (τ_3 = 0.1699) and L-kurtosis (τ_4 = 0.1504).

The relationship between L-skewness and L-kurtosis is performed in L-moment ratio diagram which can be used to identify an appropriate distribution. The null hypothesis of this method of goodness-of-fit test is the sample data follows the Gumbel distribution if and only if L-skewness and L-kurtosis are inside the acceptance region of the Gumbel distribution. The acceptance region with 95% confident intervals of L-moment ratio diagram for the Gumbel distribution that depend on the sample size n was established [11].

D. Estimation of Spatial Correlation using Semi-Variogram Models

Let $Z(x_i)$ be a random variable located at $x_i, i = 1,2,3,...,n$ and $\{Z(x_i), x_i \in D\}$ be random function in spatial domain (D). Under the second-order stationarity assumption is defined as

$$\mathrm{E}[\mathrm{Z}(x_i)] = \mu, \forall x_i \in D \quad (17)$$

$$\mathrm{Var}[\mathrm{Z}(x_i)] = \sigma^2, \forall x_i \in D \quad (18)$$

$$\mathrm{Cov}(\mathrm{Z}(x_i), \mathrm{Z}(x_i)) = \mathrm{Cov}(|x_i - x_j|) = \mathrm{C}(|x_i - x_j|), \forall x_i, x_j \in D \quad (19)$$

where Cov(□) and C(□) are covariance function of random variables. Spatial correlation structure does not depend on special location but it depends only on distance vector between random variables. For isotropic, covariance function is a function only of magnitude between two random variables, $\|x_i - x_j\|$ [12]. The spatial correlation structure is often characterized as a semi-variogram, $\gamma(|x_i - x_j|)$. The semi-variogram describes about dissimilarity of the data that are separated by distance $(h = |x_i - x_j|)$ but covariance function describes about similarity.

$$\gamma(h) = \gamma(|x_i - x_j|) = \frac{1}{2}\mathrm{Var}[\mathrm{Z}(x_i) - \mathrm{Z}(x_j)] = \frac{1}{2}\mathrm{E}[\mathrm{Z}(x_i) - \mathrm{Z}(x_j)]^2, \forall x_i, x_j \in D \quad (20)$$

The conditions of the basic semi-variogram are used under the standardization of the data, second-order stationary, and isotropic. The basic semi-variogram models that commonly used are exponential, Gaussian, and spherical model are used in this study. The three models can be expressed by [13]

Exponential model: $$\gamma(h) = 1 - \exp\left(-\frac{3h}{a}\right) \quad (21)$$

Gaussian model: $$\gamma(h) = 1 - \exp\left(-\frac{3h^2}{a^2}\right) \quad (22)$$

Spherical model: $$\gamma(h) = \begin{cases} 1.5\left(\frac{h}{a}\right) - 0.5\left(\frac{h}{a}\right)^3, & h \le a \\ 1, & h > a \end{cases} \quad (23)$$

where h and a are distance between two random variables and range respectively.

Results and Discussion

The annual maximum flow of four flow stations in Yom River Basin was first standardized to study the spatial correlation of the variation of peak flow. The goodness-of-fit test usingL-moment ratio diagram was carried out in each station.All flow stations fit to the Gumbel distribution with 95% confidence interval as shown in Fig 2. However, L-moment ratios of two flow stationsY.30 and Y.38 are around the edge of the 95% acceptance region. Station Y.30 is located in the city of Lampang province and station Y.38 is located in Phrae province.

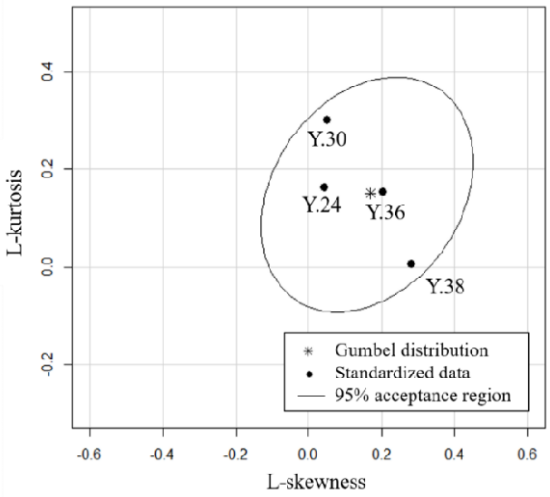

Fig. 2. L-moment ratio diagram with 95% confident intervals for the Gumbel distribution corresponds to the sample size ( ) at four flow stations in Yom River Basin

The two parameters of the Gumbel distribution of standardized annual maximum flow are estimated by the method of L-moments as shown in Table II.

Table II. Estimated parameters of the Gumbel distribution with the method of L-moments

Station	Parameter estimators	
	α	u
Y.36	0.81	-0.47
Y.24	0.83	-0.48
Y.30	0.80	-0.46
Y.38	0.80	-0.46

Under the second-order stationary and isotropic, the spatial correlation was constructed using a semi-variogram. The experimental semi-variogram was fitted to three theoretical models, i.e. exponential, Gaussian, spherical models. The ordinary least squares method was applied to determine the optimal model for spatial correlation as shown in Fig 3. The minimum sum of square errors between the experimental and theoretical semi-variogram models are criteria for the best fit. The sum of square errors from fitting to exponential, Gaussian, and spherical models are 0.070, 0.208, and 0.106 respectively. The result showed that the exponential model is the best fit. The parameter estimation of three theoretical models using the ordinary least squares method can be represented by the following equations:

Exponential model: $$\gamma(h)=1-\exp\left(-\frac{3h}{214.29}\right) \quad (21)$$

Gaussian model: $$\gamma(h)=1-\exp\left(-\frac{3h^2}{122.47^2}\right) \quad (22)$$

Spherical model:

$$\gamma(h)=\begin{cases}1.5\left(\frac{h}{155.48}\right)-0.5\left(\frac{h}{155.48}\right)^3, & h\le 155.48\\ 1, & h>155.48\end{cases} \quad (23)$$

The range of exponential model is 214.29 km indicating independency of peak flows between stations beyond this range. Station Y.36 and Y.24 are both located in Phayao province and 30 km apart. They have low semi-variance indicating strong spatial correlation. The sub-basins of station Y.36 and Y.24 contribute significantly to the flow in the main Yom River on average 397 and 146 million cubic meters annually. The maximum annual peak flow at station Y.36 is 525.92 m^3/s and at station Y.24 is 312.40 m^3/s. The semi-variance of stations Y.36 and Y.38 is 0.71 indicating weaker spatial correlation. Stations Y.36 and Y.38 are 100 km apart. Station Y.38 also contributes a large amount of annual flow of 174 million cubic meters on average to the main Yom River. The maximum annual peak flow of station Y.38 is 500 m^3/s. The obtained semi-variogram can be used to estimate a covariance function for developing a stochastic simulation to be used for risk assessment of flood mitigation measures.

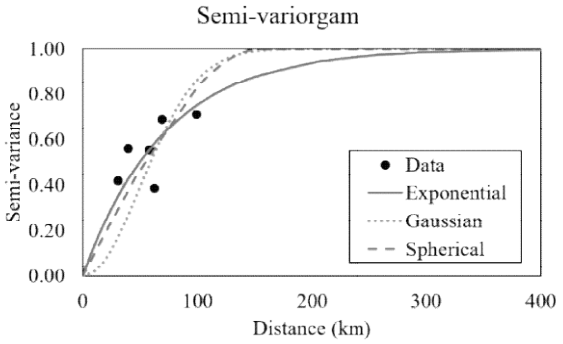

Fig. 3. The experimental semi-variogram model is fitted to the theorectical semi-variogram models (exponential, Gaussian, and spherical models)

Conclusions

Yom River Basin has experienced floods frequently due to its topography of mountainous area in the upper basin and low-lying area in the lower basin. Yom River Basin lacks oflarge reservoirs for flood mitigation and water supply. This study aims to develop a spatial correlation of peak flows in sub-basins of Yom River Basin to be used for building a stochastic simulation for risk assessment. Annual maximum flow at the selected four flow stations, namely Y.36, Y.24, Y.30, and Y.38 located in different sub-basins in the Upper Yom River Basin was fitted to the Gumbel distribution.The two-parameter Gumbel distribution is estimated by the method of L-moments. The goodness-of-test was carried out using L-moment ratio diagram. The annual maximum flow at the four stations fit with the Gumbel distribution with 95% confidence interval.

Spatial correlation structure for annual maximum flow in Yom River Basin is constructed using the semi-variogram under the second-order stationary and isotropic assumption. The sample semi-variogram of the annual maximum flows was best fitted to the exponential model with the range of 214.29 km. It was found that stations Y.36 and Y.24 has strong spatial correlation while stations Y.36 and Y.38 has weaker spatial correlation. The obtained semi-variogram can be used to estimate a covariance function for developing a stochastic simulation to be used for risk assessment of flood mitigation measures. It could be very challenging to construct a large reservoir in Yom River Basin nowadays but options of multiple medium sized reservoirs might be feasible. Understanding the spatial as well as temporal correlation of flows from each tributary would be very useful in quantifying risk reduction of each flood mitigation option or measure.

Acknowledgment

The authors gratefully acknowledge the data support provided by Royal Irrigation Department, Department of Water Resource, Department of Provincial Administration, and Land Development Department. The authors would also like to thank Prof. Ke-Sheng Cheng from National Taiwan University for his advice. The first author would like to acknowledge a partial funding from Department of Water Resources Engineering, Faculty of Engineering, Chulalongkorn University. The authors also would like to thank the reviewers for their constructive comments.

References

[1] H. Hsin-I, S. Ming-Daw and C. Ke-Sheng, "Multisite spatiotemporal streamflow simulation with an application to irrigation water shortage risk assessment". Terrestrial, Atmospheric & Oceanic Sciences, vol. 2, pp. 25, 2014.

[2] H. Hsin-I, S. Ming-Daw and C. Ke-Sheng, "Water shortage risk assessment using spatiotemporal flow simulation" Geoscience Letters, vol. 3, 2016.

[3] Committee on Agriculture and Cooperatives. "Mornitoring the development of the Yom River Basin", 2012

[4] Department of Water Resources. "Exploration and implementation of river monitoring telemetry system in Yom and Nan Basins project", 2012.

[5] S. Allan and S. Kannan. "Investigation and comparison of sampling properties of L-moments and conventional moments". Journal of Hydrology, vol. 1-2, pp. 13-34, 1999.

[6] H. Jonathan. "L-moments: analysis and estimation of distributions using linear combinations of order statistics". Journal of the royal statistical society. Series B (Methodological), pp. 105-124, 1990.

[7] V.T Chow, M. David R and M. Larry. "Applied hydrology". New York : McGraw-Hill, 1988.

[8] G. Arthur, L. Maciunas, N. Matalas, J.R Wallis. "Probability weighted moments: definition and relation to parameters of several distributions expressable in inverse form". Water resources research, vol. 15, pp. 1049-1054, 1979.

Adaptation Strategies for Rainfed Rice Production under Climate Change Scenarios in the Songkhram River Basin, Thailand

Siriwat Boonwichai[1,a] and Sangam Shrestha[1,b]

Abstract This study investigates the potential impacts and adaptation strategies on rainfed rice production under climate change scenarios in the Songkhram River Basin, Thailand. DSSAT crop simulation model was used to project the future rice production (KDML105 rice variety) based on an ensemble of four Regional Circulation Models (RCMs) for 2020-2044 under RCP4.5 and RCP8.5 scenarios. The projection of future climatic conditions shows an increasing trend in both maximum and minimum temperatures. Maximum and minimum temperatures are expected to rise by 0.9 °C under RCP4.5 scenario, and 1.0 and 1.1 °C under RCP8.5 scenario, respectively. Crop water requirement may be higher by 16 and 17% under RCP4.5 and RCP8.5 scenarios respectively. Temperature rise combined with uncertainties in rainfall may result in water deficits which may increase by 4 and 5% under RCP4.5 and RCP8.5 scenarios, respectively. A pond capacity (600 m^3) is enough to store water for one ha of rice field to meet the potential rice yield during rainfed rice season. The results of this study are helpful to policymakers in understanding the potential impacts of climate change, and the application of adaptation strategies for water and rice sectors in the basin.

Keywords *Adaptation, Climate change, Rice yield*

[1]Water Engineering and Management
Asian Institute of Technology
Pathumthani, Thailand

[a]siriwatboonwichai@gmail.com
[b]sangam@ait.asia

Introduction

Climate change has negative impacts on crop growth and production throughout the world, including many areas in Thailand. Temperature is expected to rise, and rainfall more variable at both global and local scales [6]. Changes in magnitude and patterns of temperature and rainfall could significantly reduce rice production [1][9].

Climate change refers to a change in the weather over a long period of time, including higher surface temperature, floods, droughts, storms, and sea level rise. The global mean surface temperature is expected to rise by 4.8 °C in the twenty-first century [6]. Thailand's temperature is expected to rise by approximately 2–3 ºC during the middle of the century and continue increasing until the end [4].Climate change affects humanity and the environment, causing higher temperature, changing rainfall patterns, etc. The change in temperature and rainfall affects both the quantity of available water and crops produced. Climate change can be defined as a trend in one or more climatic variables characterized by a fairly smooth continuous increase or decrease of the average value during the long period of record. This trend analysis will aid the assessment of hazard and risk of area and natural disaster by hydro-meteorological extremes such as floods, droughts and cyclones due to the change in climate extremes.

Climate is one of the most important factors in agricultural productivity and could directly influence it since it is linked to physiological processes [5]. This issue could affect global food security, especially in developing countries [1]. Climate change mayhave both positive and negative impacts on the quantity and quality of agricultural productions, depending on location, climate zone, and crops [5]. Rice is one of the most important agricultural products in the world. Reference [2][3][9]studied the potential climate change impact on rice production in Thailand and concluded that changes in the magnitude and patterns of temperature and rainfall could alter the crop growth period, water availability, photosynthesis process, etc. Temperatures above 35 ºC create high vulnerability of crops and could affect the ripening stage, significantly reducing rice production [10]. Similarly, climate change has influence on rice production and irrigation water requirement in other countries [2].

Uncertainty in future climate projection stem from several sources [5][12][13] and can be minimized by an ensemble of different RCMs [9]. The Decision

Support System for Agrotechnology Transfer (DSSAT) model has been used to simulate the impact of CC in many places in Thailand [1][2][3][9] with good model calibration and validation results.

The degree of impact from climate change on rice production depends on the adaptability of each community. Adaptation strategies can greatly reduce the magnitude of impacts on rice production under climate change conditions. Reference [1] suggested that planting dates alteration and proper nutrient management can mitigate the effect of climate change on rice production in northeast Thailand. The changing planting date, reduction in fertility stress and supplementary irrigation were evaluated in the lower Mekong basin [7].

The study aims to investigate the impact of climate change on rice yield, crop water requirement (CWR) and water availability, and evaluate adaptation strategies for farm water management on rice fields for the period 2020-2044 under RCP4.5 and RCP8.5 scenarios in the upper Songkhram river basin of Thailand.

Study area

The Songkhram River Basin is the second largest catchment in Northeast Thailand with an area of approximately 12,700 km^2 (Fig. 1). The Songkhram River which drains the basin is approximately 420 km long and originates at the Phu Phan mountainsin the Song Dao District of Sakon Nakhon Province and the Nong Han District in Udon Thani Province. It flows through the Mekong River at Chai Buri Sub-district and ThaUthen District in Nakhon Phanom.

The basin has a tropical, semi-arid climate with three seasons: summer (March to May), rainy (June to October), and winter (November to February), and receives more annual rainfall than other parts of Thailand [8]. The Thai Meteorological Department (TMD) reported variations in annual rainfall of between 1200 mm and 2000 mm, peaking during the months of July and August. The average mean temperature varies from 21 to 34 ºC. The minimum temperature falls below 10 ºC in the winter season during the months of December and January and rises to over 40 ºC during April in the summer season.

The basin is a floodplain, making it suitable for paddy fields. The Land Development Department (LDD) reported that the majority of land use in the basin is agriculture, covering approximately 68% of the land area. Most of the area consists of paddy fields, Pará rubber, and eucalyptus trees, taking up more than 90% of the agricultural land area in 2010. Household income is mainly reliant on agriculture [8].

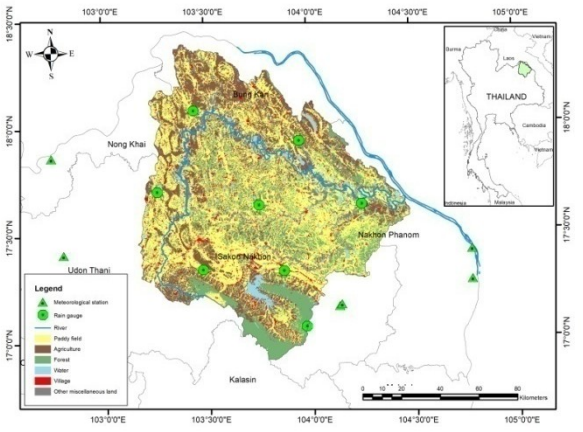

Fig. 1. Location of the meteorological stations, Sakon Nakhon Rice Research Center, and paddy fields in the Songkhram River Basin, Northeast Thailand.

Methodology

The selected Four RCMs (ACCESS1.0-CSIRO-CCAM, CNRM-CM5-CSIRO-CCAM, ICHEC-EC-EARTH-SMHI-RCA4, and MPI-ESM-LR-CSIRO-CCAM) were used to project future climate under RCP4.5 and RCP8.5 scenarios in the basin during the period 2020-2044 based on the observed climate data (1980-2004) from Thai Meteorological Department (TMD). The quantile mapping technique was applied for bias correction (Fig. 2). Missing data can have significant effects on the results, hence the best option is to fill the missing values. In this study, the missing temperature data was estimated using the linear interpolation method and rainfall estimated using APHRODITE's gridded dataset (http://www.chikyu.ac.jp/precip/).

The DSSAT model was used to simulate the future CWR and rice yield (Fig. 2). Rice experiment data from Sakon Nakhon Rice Research Center is used for calibrating and validating the DSSAT model. Calibration was conducted for period 2009-2012, and the period of 2013-2014 was used for validation. The study considered only KDML105 rice variety which is suitable for growth during wet season (June to November). The coefficient of determination (R^2), mean, and standard deviation (SD) were considered for evaluating the model performance. The ensemble of future climate model was used to project the future rice production under climate change scenarios for 2020-2044.

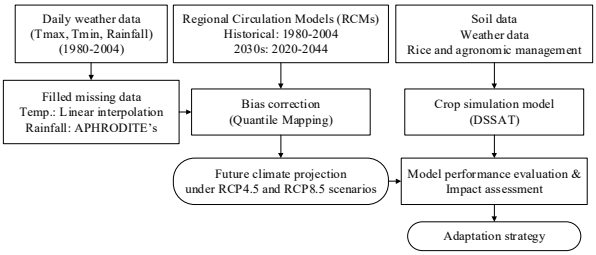

Fig. 2. Methodological framework for assessing the future rice yield and evaluating the adaptation strategy under future climate change scenarios for 2020-2044 in the Songkhram River Basin, Thailand.

Results and conclusions

A. Future climate projection

Historical maximum and minimum temperatures show increasing trends. Thai Meteorological Department presented that the maximum and minimum temperatures increased 1.0°C and 0.8°C respectively from 1980 to 2004 in the basin. The average annual maximum temperature is expected to increase by up to 0.9°C and 1.0°C, and minimum temperature expected to increase by up to 0.9°C and 1.1°C for RCP4.5 and RCP8.5 scenarios respectively during 2020-2044, as shown in Fig. 3. Previous studies indicate similar results. The maximum and minimum temperature in Thailand are expected to increase up to 0.95°C and 1.26°C under RCP8.5 scenario for 2016-2043 [9], and 1.47°C and 2.21°C under 437 CO_2 concentration for 2020-2029 [1].

Historical annual rainfall (1980-2004) was varied from 1122 mm to 1705. The peak was in 2002. The average annual rainfall was 1391 mm. The projected rainfall may not much change under climate change scenarios. Future rainfall may increase by 1394 mm and 1458 mm under RCP4.5 and RCP8.5 scenarios respectively. However, the future rainfall will be more variability that can vary from 800 mm to 2300 mm. Past studies have reported that future rainfall may be both increased and decreased in many parts of Thailand. The future rainfall may increase by 19.2% under 437 CO_2 concentration for 2020-2029 in Northeast Thailand [1], may both increase and decrease in the Nam Oon Irrigation Project [9]. This indicates that rainfall varies depending on several variables, including latitude, location, and topography.

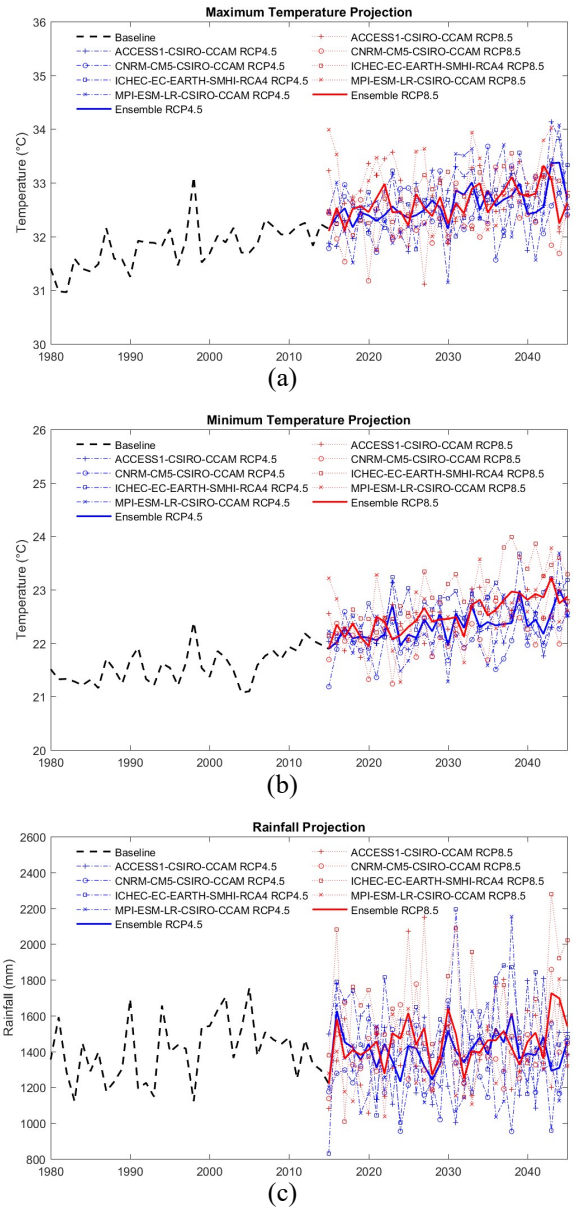

(a)

(b)

(c)

Fig. 3. Historical and projected (a) maximum temperature, (b) minimum temperature, and (c) rainfall of observation (1980-2004, baseline) and projected (2020-2044) under RCP4.5 and RCP8.5 scenarios.

B. DSSAT model calibration and validation

The DSSAT v4.6 crop simulation model was used to investigate the effect of climate change on rice yield and evaluate the potential adaptation strategies on rice production in the basin. The rice experiments data from Sakon Nakhon Rice research center of year 2009-2012 were used for model calibration. As farmers did not follow the cropping calendar suggested by the rice department (www.ricethailand.go.th), the 9 July was selected to represent the planting date for KDML105 rice variety in the basin for this study. The errors are acceptable with a coefficient of determination of 0.84. The data for year 2013-2014 was used for model validation. The average observed

rice production is 2.08 t/ha, and simulated rice production is 2.07 t/ha. Therefore, the model is suitable for simulating the future rice production under climate change conditions.

Table I Performance evaluation of the DSSAT model for the KDML105.

Year	Mean rice yield (t/ha)		RMSE (t/ha)	R^2
	Observation	Simulation		
2009-2012	1.96	1.92	0.009	0.84
2013-2014	2.08	2.07		

C. Climate change impact on rice yield

The crop water requirement (CWR) may increase by 16% and 17% under RCP4.5 and RCP8.5scenarios, respectively, as shown in Fig. 4. Increased CWR combined with unchanged rainfall may cause future water deficit. Although future rice yield may not change much (2.06 and 1.90 t/ha under RCP4.5 and RCP 8.5 scenarios, respectively) compared with baseline (1.93 t/ha), it is still lower than the potential rice yield of Jasmine rice variety (2.27 t/ha)(www.ricethailand.go.th). Results suggest that supplying water to fulfill CWR can meet the potential rice yield.

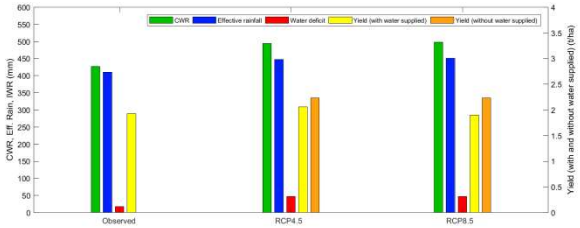

Fig. 4. Impact of climate change on crop water requirement (CWR), effective rainfall, water deficit, rice yield (with and without water supplied).

D. Adapatation stratigy for rainfed rice production

This study provides the adaptation option of on farm water management for farmers. The possible option for storing water for paddy fields is pond. Farmers should have their own pond to store the water for one rice season. The assumption is that farmers would have one ha (10,000 m^2) of paddy fields and grow only in the rainfed season. The farmers would have to store about 47 mm/season of extra water plus 20% to allow for losses from evaporation and infiltration. Thus, the pond would be required to store around 564 m^3 of water for one ha of rice field. Therefore, the pond should measure 20 m in width, 15 m in length, and 2 m in depth to store 600 m^3 of water (Fig. 5).

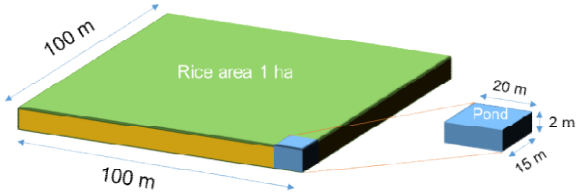

Fig. 5. Adaptation strategy on water management for one ha of rice field.

Conclusions

The future crop water requirement (CWR) and yield were investigated under climate change and a possible measure for on-farm water management in the upper Songkhram river basin was evaluated. Future climate projections during rainfed rice season indicate that maximum and minimum temperatures are expected to rise, while rainfall unchanged under both RCP4.5 and RCP8.5 scenarios for 2020-2044. CWR is expected to increase due to increased temperature and evaporation. Although variations in the future rice yield may not be significant, it is still below potential yield. The future water availability is sufficient to meet the CWR with proper management. It is suggested to have a storage pond (600 m^3) to store water for each ha of rice to overcome water deficit and reach the potential rice yield.

Acknowledgment

The authors would like to thank Thai Meteorological Department (TMD), Royal Irrigation Department (RID) and Sakon Nakhon Rice Research Center for providing the data.

References

[1] Babel, M. S., Agarwal, A., Swain, D. K., Herath, S. (2011). Evaluation of climate change impacts and adaptation measures for rice cultivation in Northeast Thailand. Climate Research, 46(2), 137-146.

[2] Boonwichai, S., Shrestha, S., Babel, M. S., Weesakul, S., Datta, A. (2018). Climate change impacts on irrigation water requirement, crop water productivity and rice yield in the Songkhram River Basin, Thailand. Journal of Cleaner Production, 198, 1157-1164.

[3] Boonwichai, S., Shrestha, S., Babel, M. S., Weesakul, S., Datta, A. (2019). Evaluation of climate change impacts and adaptation strategies on rainfed rice production in Songkhram River Basin, Thailand. Science of The Total Environment, 652, 189-201.

[4] Chinvanno, S., Southeast Asia START Regional Center, S. A. S. R. (2009). Future Climate Projection for Thailand and Surrounding Countries: Climate change scenario of 21st century. Regional Assessments and Profiles of

Climate Change Impacts and Adaptation in PRC, Thailand and Viet Nam: Biodiversity, Food Security, Water Resources and Rural Livelihoods in the GMS, 4.

[5] Deb, P., Shrestha, S., Babel, M. S. (2015). Forecasting climate change impacts and evaluation of adaptation options for maize cropping in the hilly terrain of Himalayas: Sikkim, India. Theoretical and Applied Climatology,121(3-4), 649-667.

[6] IPCC. (2014). Climate Change 2014: Synthesis Report. Contribution of Working Groups I, II and III to the Fifth Assessment Report of the Intergovernmental Panel on Climate Change [Core Writing Team, R.K. Pachauri and L.A. Meyer (eds.)]. IPCC, Geneva, Switzerland, 151 pp.

[7] Mainuddin, M., Kirby, M., & Hoanh, C. T. (2013). Impact of climate change on rainfed rice and options for adaptation in the lower Mekong Basin. Natural hazards, 66(2), 905-938.

[8] Satrawaha, R. and Wongpakam, K. (2012). Monitoring trends in the extent of major floods in the lower reach of Songkhram River Basin, Northeastern Thailand. Limnology, 13(1), 163-170.

[9] Shrestha, S., Chapagain, R., Babel, M. S. (2017). Quantifying the impact of climate change on crop yield and water footprint of rice in the Nam Oon Irrigation Project, Thailand. Science of The Total Environment, 599, 689-699.

[10] Tipparak, S., Aroonrungsikul, C. (2011). Effect of plant supplement on seed germination and seed vigor of KDML 105 rice variety. Warasan Witthayasat Kaset.

[11] Wang, W., Sun, F., Luo, Y., Xu, J. (2012). Changes of rice water demand and irrigation water requirement in Southeast China under future climate change. Procedia Engineering, 28, 341-345.

[12] Hawkins, E., and Sutton, R. 2009. The potential to narrow uncertainty in regional climate predictions. Bull. Am. Meteorol. Soc., 90: 1095–1107. doi:10.1175/2009BAMS2607.1.

[13] Hawkins, E., and Sutton, R. 2011. The potential to narrow uncertainty in projections of regional precipitation change. Clim. Dyn., 37: 407–418.

Merged Satellite And Ground-Based Precipitation Products For Evaluation Of Very High-Resolution RCM Simulations Over Cambodia

Theara Tha[1,a] and Piyatida Ruangrassame[1,b,*]

Abstract Rainfall data area crucial input for hydrological modelling and water resource planning and management studies. The need for dense and long time series data is, however, a challenging issue. In this case, merged satellite and ground-based rainfall products play a significant role as the alternative rainfall data sources. Numerous rainfall products are available, and their accuracy and performance are different over various regions. This study aims to investigate the performance of two high-resolution grid-based merged rainfall products, the Asian Precipitation–HighlyResolved Observational Data Integration Towards Evaluation of Water Resources(APHRODITE) and the Precipitation Estimation from Remotely Sensed Information using Artificial Neural Networks - Climate Data Record (PERSIANN-CDR). The rainfall products are compared with rain gauge data acquired between 2001 and 2007 on a pixel-to-pixel basis at monthly and annual timescales. Statistical indicators (CC, RMSE, BIAS), scatter plot analysis, and descriptive statistics are used as the evaluation methods. This study also tests the capability of the rainfall products in capturing extreme rainfalls through extreme rainfall indices including R99p, Rx1d, and Rx5d, which are the annual total rainfallwhen rainfall isgreater than the 99th percentile, maximum 1-day, and maximum 5-day rainfall, respectively. Furthermore, rainfall simulations from a 5-km-meshRegional Climate Model (NHRCM), which is developed atthe Meteorological Research Institute (MRI) of the Japan Meteorological Agency (JMA), are compared with the two merged rainfall products over Cambodia. Compared with the rain gauge data, APHRODITE shows slightly overestimation trend while PERSIANN-CDR shows high overestimation.Both rainfall products capture monthly and annual rainfall quite well; however,they capture the extreme rainfall events inaccurately.NHRCM performs well in capturing the average monthly rainfall over the selected study area although itunderestimates PERSIANN-CDR and overestimates APHRODITE.

Keywords *extreme rainfalls, merged satellite-gauge, RCM*

[1]Department of Water Resources Engineering
Faculty of Engineering, Chulalongkorn University
Bangkok, Thailand

[a]thatheara@gmail.com
[b]Piyatida.H@chula.ac.th

Introduction

Rainfall is a main forcing variable of the global, regional, and local water and energy cycle [1]. Rainfall data with good temporal and spatial coverage are significant to weather forecasters, climate scientists and a wide range of decision makers including hydrologists, as it is the key input in hydrological models [2]. However, the reliable observed rainfall is always scarce in many regions in the world making the estimation of spatially distributed rainfall difficult and imprecise [3]. Due to these challenges, satellite techniques have been widely applied globally as a means of supplementing rainfall records [4].

In Cambodia, rainfall data are essential as the country relies mainly on agriculture sector, especially rice production. Despite theirimportance, the number of rain gauges in Cambodia is still small, and they are unevenly distributed. Moreover, missing rainfall data at some stations and the lack of long-term rainfalldata are challenging issues, mainly for water resource management and climate change studies. In this case, satellite and ground-based rainfall products play a significant role as the alternativerainfall data sources in providing dense and long-term rainfall data.

Recently, several satellite and ground-based rainfall products are available with different spatial and temporal resolution. Moreover, the accuracy of these rainfall products is also different based on the algorithm applied for estimating the rainfall. Thus, it is important to evaluate these rainfall products before using them in any studies. Phoeurn and Ly [5] compared two high-resolution rainfall products (TRMM 3B42V7 and CHIRPS V.2) over Cambodia and suggested that both rainfall products have the capacity to capture the rainfall pattern over the study area spatially and temporally well although TRMM 3B42V7 seems to perform better compared to CHIRPS V.2. However, TRMM 3B42V7 provides short-term rainfall data (less than 30 years) only, and thus it is not suitable for the studies concerning with climate change. So, in this study, we selected two rainfall products that provide high resolution and long-term rainfall data,namely APHRODITE and PERSIANN-CDR.

This study is carried out to (1) evaluate the accuracy and performance of APHRODITE and PERSIANN-CDR over Cambodia and (2) to compare these rainfall products with simulated rainfall from a very high-resolution regional climate model (NHRCM)

which is developed by the Meteorological Research Institute (MRI) of the Japan Meteorological Agency (JMA).

Study Area

Cambodia is located in Southeast Asia and lies completely within the tropics, between latitudes 10° and 15°N, and longitudes 102° and 108°E (**Error! Reference source not found.**). The country is bordered by Thailand and the Gulf of Thailand to the north and west, Vietnam to the east and southeast, and Laos to the northeast. The total land of Cambodia is 181 035 km^2, of which the major part is a rolling plain. About 75% of the total area of Cambodia consists of the Tonle Sap Basin and the Mekong Lowlands [6]. Ministry of Water Resources and Meteorology (MOWRAM) has classified basins in Cambodia into 5 groups as the following [7]:

Basin Group 1 is the coastal zone which is located in the south-western part of the country. This basin group is rimmed with mountain ranges (the Elephant and the Cardamom Mountains ranges) to the northeast and the Gulf of Thailand to the southwest. The total area of this basin group is 18,046 km^2. The elevation highly varies throughout the basin. Rainfall stations in this basin group are very scarce.

Basin Group 2 is the 3S River Basin. This basinconsists of three rivers known as Se Kong, Se San and SrePokwhich drain the water to the Mekong River at Stung Treng. The total area of 3S Basin is 78,645 km^2, of which 25,965 km^2 is located in Cambodia. The north-eastern part of this basin are the mountains which characterized by rugged terrain with peaks of over 1,546 m.

Basin Group 3 is the Upper Mekong Basin which coversa total area of 19,522 km^2. This Basin Group is characterized by a braided channel with sand islands. In the upper part, the landscape ranges from the mountains of north-eastern Cambodia with the peaks of over 769m to valleys at about only 0-24m elevation. A major part of the area located downstream of Stung Treng (3S outlet) is occupied by the Mekong River floodplain with elevations up to 100m.

Basin Group 4 is the Tonle Sap Basin which has a total area of 81,663 km^2. Basin Group 4 is bordered by the ElephantandCardamom Mountains in the west and south-west and theDangrek mountains in the north. The major parts of Basin Group 4 are low lands with elevations generally of less than 100m above mean sea level and with very small slopes.

Basin Group 5 covers the lower Mekong River basin with a total area is 35,839 km^2. The major part of this basin is the Mekong River floodplain which is suitable for agriculture. The elevation throughout the basin is generally very low with very gentle slopes except for only the upper reach in the western part of the basin.

Cambodia is dominated by monsoons which characterized by two seasons with equal length. The rainy season starts from May to October and the remaining period isthedry season. The average rainfall in Cambodia vary from about 1400 mm in the central low land regions and may reach up to 4000 mm in the coastal zone and highland areas [8]. The annual average temperature over Cambodia is 28°C, with an average maximum temperature of 38°C in April and an average minimum temperature of 17°C in January [8].

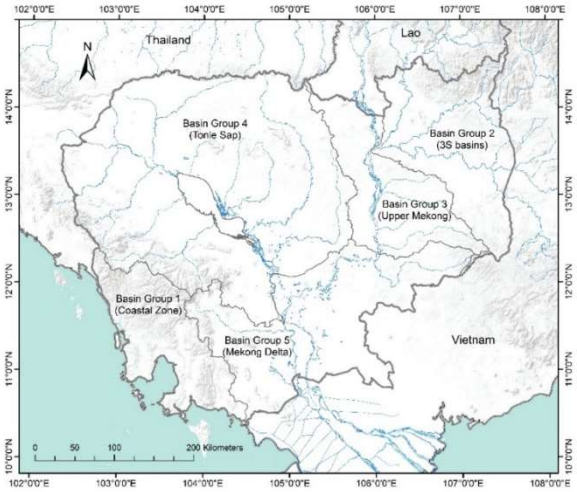

Fig. 1. Map of Cambodia and its basin groups.

Rainfall Datasets

A. Gauged Rainfall

The observed rainfall data from 174 stations located over Cambodia (Fig. 2) are obtained from the MOWRAM. Due to the missing rainfall data in some years at some stations, the numbers of stations used in this study are different from year to year. The number of rainfall stations are 144, 149, 102, 95, 95, 97, 97 for the year of 2001, 2002, 2003, 2004, 2005, 2006, and 2007, respectively. As demonstrated in Fig. 2, rainfall stations mainly located in the central plain of Cambodia (Tonle Sap and Cambodia Upper and Lower Mekong Basin). Rainfall stations in the Coastal zone and the 3S Basin are very sparse.

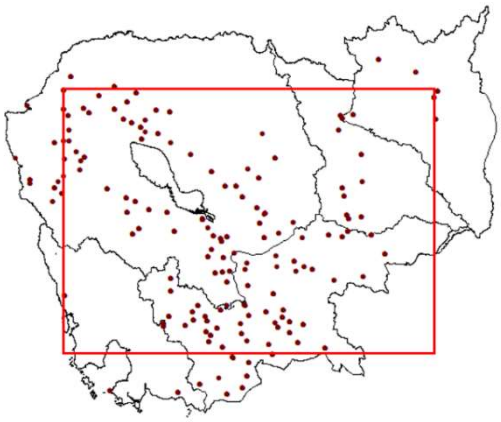

Fig. 2. Rainfall stations in Cambodiaand the area selected for rainfall comparison.

B. APHRODITE

Asian Precipitation–HighlyResolved Observational Data Integration Towards Evaluation (APHRODITE) of Water Resource project is startedin 2006 in order to develop high-resolution daily precipitation datasets covering the whole of Asia [9]. APHRODITE gridded precipitation is produced from 1) GTS-based data (the global summary of the day), 2) data precompiled by other projects or organizations, and 3) APHRODITE's own collection throughquality check and interpolation technic [9]. APHRODITE rainfalls are available in various versions for specific regions with different spatial resolution. In this study, we use APRODITE_MA_v1101 which provides 57 years daily rainfall data (1951 to 2007) at a spatial resolution of 0.25° over Monsoon Asia (60°E–150°E, 15°S–55°N). More details about the algorithm of APHRODITE precipitation is available in Yatagai, et al. [9] and Xie, et al. [10]. The dataset used in this study is available at http://aphrodite.st.hirosaki-u.ac.jp/download/.

C. PERSIANN-CDR

The Precipitation Estimation from Remotely Sensed Information using Artificial Neural Networks - Climate Data Record (PERSIANN-CDR) is a product of the Center for Hydrometeorology and Remote Sensing (CHRS) which provide a long-term near-global (60°S–60°N) daily precipitation estimates at 0.25° spatial resolution over the period of more than 30 years (1983–present) [11]. PERSIANN-CDR is developed under the concept of addressing issues in the need for a consistent, long-term, and high-resolution precipitation dataset which is suitable for global climate studies [11]. PERSIANN-CDR is produced using the Gridded satellite (GridSat-B1) [12] infrared data as the input to PERSIANN [13] algorithm. The biases of PERSIANN-CDR is removed using the Global Precipitation Climatology Project (GPCP) monthly product to preserve the consistency of the two datasets[11]. PERSIANN-CDR product is openly available at http://chrsdata.eng.uci.edu/.

D. NHRCM 5km

NHRCM rainfall used in this study is developed bythe Meteorological Research Institute (MRI) of the Japan Meteorological Agency (JMA). The rainfall is simulated with a very fine spatial resolution (5 km) and cover the area between latitudes 4.6° and 22.1°N, and longitudes 93.7° and 107.7°E.

Methods

Observed rainfall data over Cambodia is collected and qualitycheckshave been done to reduce error in the comparison. The data period selected for this study is between 2001 and 2007 for the comparison of rainfall products. The starting year of 2001 is considered because there are fewer rainfalls stations in the year before that. The ending year, 2007, is selected to match with the latest rainfall data in APHRODITE dataset.

To compare the performance between APHRODITE and PERSIANN-CDR, the observed rainfall is firstly interpolated using Inverse Distance Weighting (IDW) method with grid size and centre point in accordance to each gridded rainfall product. The area covered by rainfall stations (204 pixels), located mainly on the Tonle Sap and Mekong floodplain is then selected for the comparison (See **Error! Reference source not found.**). Statistical indicators such as Correlation Coefficient (CC), Root Mean Square Error (RMSE), and Relative Bias (BIAS) are calculated between interpolated observed rainfall and the rainfall estimates in monthly and annual timescales. Scatter plotsare constructed to demonstrate the relationship of the observed rainfall and gridded rainfall products. Cumulative Distribution Function (CDF) curves of the selected rainfall estimates against gauge-based observations are also constructed.In addition, we test the capability of the rainfall products in capturing extreme rainfalls through extreme rainfall indices includingthe annual total rainfall when rainfallis greater than the 99th percentile (R99p), maximum 1-day (Rx1d), and maximum 5-day rainfall (Rx5d).

After that, we apply both rainfall products for evaluating the performance of simulated rainfall from a very high-resolution RCM (NHRCM). The period for the comparison is between 1983 and 1992.

A. Data Quality Check

Before being used for the comparison, the data quality check is needed to be carried out. Outliers from all dataset are removed. In this study, the APHRODITE rainfall in 2002 is excluded from the comparison after being found that rainfall in that year equal to zero in almost all months in the wet season. These errors cause the annual rainfall to fall between 200 to 400 mm in most grids and that is absolutely not happening in Cambodia.

B. Statistical Indicators

Pearson correlation coefficient (CC) indicates the direction and strength of a linear relationship between two variables, for example, the simulated and observed values. CC is calculated by dividing the covariance of the two variables by the product of their standard deviation. The value of CC ranges from -1 to +1. The value of +1 shows the perfect increasing linear relationship between the two variables. When CC equal to 0, there is no linear relationship between the two variables.

$$CC = \frac{\sum_{i=1}^{n}(x_i - \bar{x}).(y_i - \bar{y})}{\sqrt{\sum_{i=1}^{n}(x_i - \bar{x})^2 . \sum_{i=1}^{n}(y_i - \bar{y})^2}} \quad (1)$$

The Root Mean Square Error (RMSE) is an indicator used to measure the differences between predicted and observed values. RMSE has the same unit as the comparing variables. The smaller the RMSE value the better the performance of the model in predicting. The formula of RMSE is given by:

$$RMSE = \sqrt{\frac{\sum_{i=1}^{n}(X_{obs,i} - X_{model,i})^2}{n}} \quad (2)$$

Where $X_{obs,i}$is the observed value and $X_{model,i}$is the predicted value at time *i*, n is the total number of data.

The Relative Bias (BIAS) is used to measure the average tendency of predicted value. The optimal value of BIAS is 0. The positive value shows overestimation, and the negative value shows the underestimation bias of the model. The Bias formula is given by:

$$BIAS = \frac{\sum_{i=1}^{n}(X_{model,i} - X_{obs,i})}{\sum_{i=1}^{n} X_{obs,i}} \times 100 \quad (3)$$

C. Extreme Rainfall Indices

To assess the performance of the two rainfall products in capturing the behaviour of extreme rainfall over Cambodia, we use 3 extreme rainfall indices namelythe annual total rainfall when rainfall is greater than the 99th percentile (R99p), maximum 1-day (Rx1d), and maximum 5-day rainfall (Rx5d).Each extreme rainfall index is described in TABLE I.Theseindices are calculated based on Zhang and Yang [14].

Table I. Extreme rainfall indices used in this analysis.

Indices	Name	Definition	Unit
R99p	Extreme wet day	Annual total rainfall when rainfall> 99th percentile	mm
Rx1d	Daily maximum rainfall amount	Annual maximum 1-day rainfall	mm
Rx5d	5-day maximum rainfall amount	Annual maximum 5-day rainfall	mm

Results and discussions

A. Accuracy of Rainfall Products

The CC, RMSE and BIASof the two rainfall products are calculated using rainfall values of all pixels located in the selected area over the 2001–2007 period and are shown in **Error! Reference source not found.**. At monthly timescale, both rainfall products have a high correlation to the observed rainfall (CC= 0.87). However, APHRODITE tends to estimate monthly rainfall better than PERSIANN-CDR based on the RMSE and BIAS values and it is clearly indicated in **Error! Reference source not found.**and**Error! Reference source not found.**. PERSIANN-CDR overestimates monthly rainfall by 52% while APHRODITE overestimatesmonthly rainfall onlyby 2.7%.

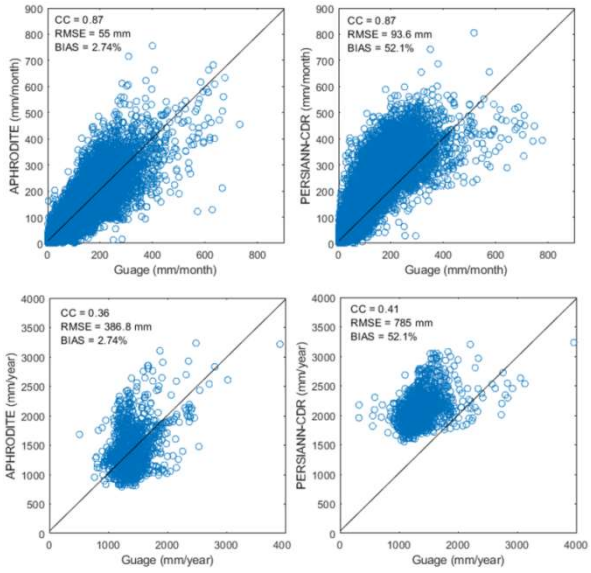

Fig. 3. Scatter plots of rainfall products versus observed rainfall for monthly and annual timescales.

Table II Evaluation statistics comparing monthly and annualrainfall of aphrodite and persiann-cdr with gauged rainfall over cambodia during 2001–2007.

Statistical Indicators	Monthly		Annual	
	PERSIANN-CDR	APHRODITE	PERSIANN-CDR	APHRODITE
CC	0.87	0.87	0.41	0.36
RMSE (mm)	93.6	55.0	785.0	386.8
BIAS (%)	52.05	2.74	52.05	2.74

At annual timescale, the correlation coefficient for APHRODITE and PERSIAN-CDR are 0.36 and 0.41, respectively. This indicates a small relationship between the annual rainfall of both rainfall products and the observed rainfall. The RMSE of PERSIANN-CDR is 785 mm (two times higher than that of APHRODITE). So, APHRODITE also predicts

the annual rainfall more accurately than PERSIANN-CDR for the selected study area.

Fig. 4 shows the CDF of monthly rainfall of both rainfall products compared with observed data. It can be clearly seen that APHRODITE fits very well with the observed rainfall. Conversely, the CDF of PERSIANN-CDRand observed rainfall are significantly different. With the same probability, the rainfall intensity of PERSIANN-CDR is higher than that of the observed rainfall.

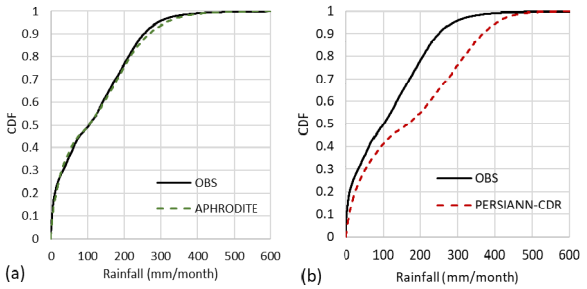

Fig. 4.CDF curves for (a) observed rainfall and APHRODITE and (b) observed rainfall and PERSIANN-CDR.

B. Extreme Rainfall Events Comparison

Fig. 5. shows the performance of APHRODITE and PERSIANN-CDR in capturing the R99p, Rx1d, and Rx5d. Both rainfall products perform poorly in capturing R99p. The CC of APHRODITE and PERSIANN-CDR are only 0.11 and 0.05, respectively. RMSE of PERSIAN-CDR is slightly higher that of APHRODITE. It is noteworthy that APHRODITE underestimates R99p with a small negative bias of -5.27% while PERSIANN-CDR overestimates R99p by 31.9%.

Similarly, correlations of the Rx1d captured by both rainfall products and observed rainfall are also small (CC = 0.07 for APHRODITE and 0.06 for PERSIANN-CDR). The CC and RMSE of both products are very close. However, there is almost no bias for APHRODITE while PERSIANN overestimates Rx1d by 26.4%.

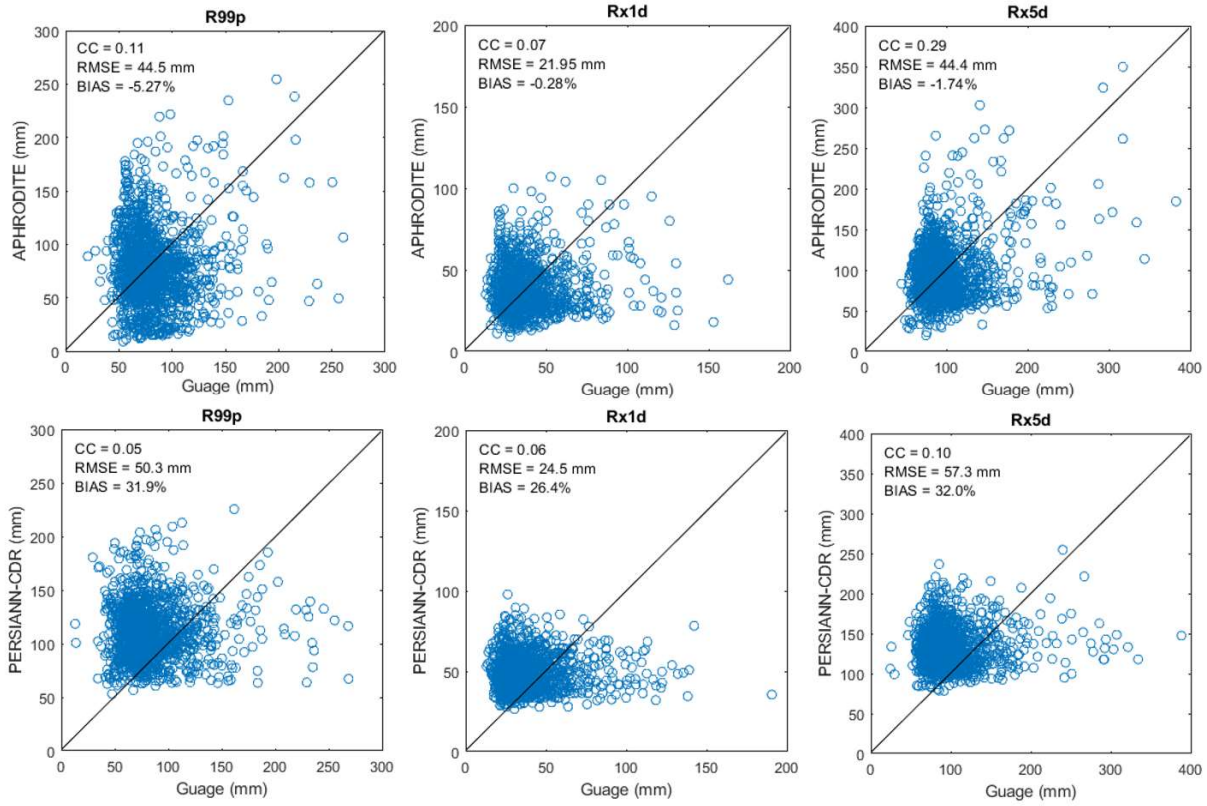

Fig. 5. Scatter plots of rainfall extreme indices for both rainfall products.

The correlation of Rx5d of APHRODITE is a bit higher thanthat of Rx1d while the correlation of Rx5d of PERSIANN-CDR remains low comparing to that of Rx1d. The RMSE of APHRODITE and PERSIANN-CDR are 44.4 mm and 57.3 mm, respectively. Again, APHRODITE has a very small negative bias while PERSIANN-CDR has a high positive bias of 32%.

Overall, APHRODITE performs slightly better than PERSIANN-CDR in capturing the extreme rainfall events. The RMSEs of all indices detected by APHRODITE are slightly smaller than those detected

by PERSIANN-CDR.The significant differencebetween these two rainfall products is the bias. The biasesof all extreme rainfall indices detected byAPHRODITE are very small and negative. Conversely, PERSIANN-CDR overestimates all extreme rainfall indices by approximately 30%.

C. Performance of NHRCM Rainfall

Average monthly rainfall data from 1983 to 1992 are extracted from NHRCM dataset and then compared with APHRODITE and PERSIANN-CDR.Fig. 6 shows the comparison of theaverage monthly rainfall between NHRCM and APHRODITE. Overall, NHRCM is able to capture the monthly rainfall pattern over the selected area well. It is observed that NHRCM slightly overestimates APHRODITE in all months except in March, April and May (transition period between dry and rainy season), and in September (peak period) where it highly overestimates APHRODITE. Compared to PERSIANN-CDR, NHRCM underestimates the average rainfall in most months(see Fig. 7). Although PERSIANN-CDR is found to be overestimating observed rainfall, its average monthly rainfall is still lower than that of NHRCM in some months such as March, April and September.

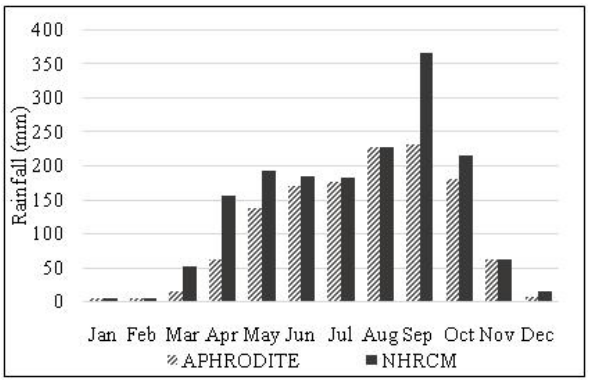

Fig. 6. Average monthly rainfall betweenNHRCM and APHRODITE(1983–1992).

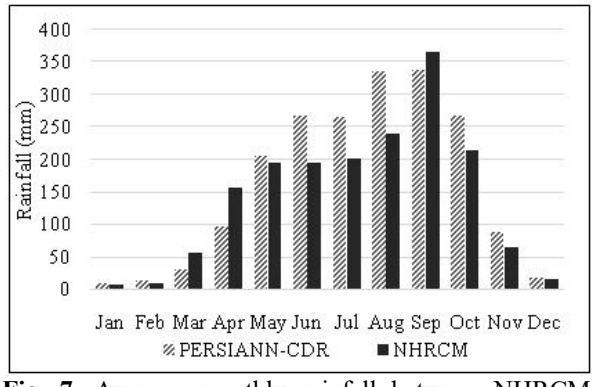

Fig. 7. Average monthly rainfall between NHRCM and PERSIANN-CDR (1983–1992).

Based on cumulative distribution function curves shown in Fig. 8a, the frequency of low rainfall of NHRCM is close to that of APHRODITE. However, When the probability ofexceedance exceeds 0.7, NHRCM tends to overestimate APHRODITE.From Fig. 8b,NHRCM underestimates PERSIANN-CDRbut it overestimates high rainfall intensity. It should be noticed that NHRCM dataset consists of monthly rainfall with the intensity up to more than 2000 mm per month.These high values come from high rainfall in the grids located in the southwestern part of Cambodia which is the Coastal Zone (Basin Group 1).

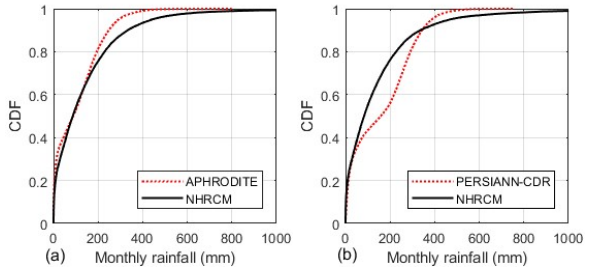

Fig. 8. CDF curves of (a) NHRCM and APHRODITE and (b) NHRCM and PERSIANN-CDR.

Conclusions

This study compares two gridded rainfall products, APHRODITE and PERSIANN-CDR over Cambodia for the period between 2001 and 2007. The performance of rainfall simulations from a very high-resolution RCM known as NHRCM have also been evaluated by comparing with these two rainfall products during the period of 1983–1992.

Overall, PERSIANN and APHRODITE have a good monthly correlation with observed rainfall. However, APHRODITE seems to perform better for both Monthly and annual timescales based on RMSE and BIAS values. The poor performance of PERSIANN-CDR is a result of overestimation,probably by the satellite technique, especially at a high rainfall intensity. APHRODITE and PERSIANN-CDR are unable to capture the extreme rainfall accurately as indicated by poor correlation and high RMSE, butAPHRODITE performs slightly better than PERSIANN-CDR.

The overall performance of the simulated rainfall from NHRCM is good over the selected study area. However,the model highly overestimates rainfall in March, April and September. Moreover, itproducesvery high monthly rainfall values in some grids which could possibly caused by the boundary condition of the model.

Thisstudy implies that APHRODITE can be used over the selected study area when monthly and annual rainfalls are required for example in the assessment of water balance/water budget. For PERSIANN-CDR, biased correction is needed sinceithighly overestimates observed rainfall. Simulated rainfall from NHRCM comprises high error

in some grids in the southeastern regions, and thus it requires more investigations.

References

[1] H. Wheater, S. Sorooshian, and K. D. Sharma, *Hydrological modelling in arid and semi-arid areas*. Cambridge University Press, 2007.

[2] M. Lekula, M. W. Lubczynski, E. M. Shemang, and W. Verhoef, "Validation of satellite-based rainfall in Kalahari," *Physics and Chemistry of the Earth, Parts A/B/C,* vol. 105, pp. 84-97, 2018.

[3] W. Abera, L. Brocca, and R. Rigon, "Comparative evaluation of different satellite rainfall estimation products and bias correction in the Upper Blue Nile (UBN) basin," *Atmospheric Research,* vol. 178, pp. 471-483, 2016.

[4] S. Janjai, P. Nimnuan, M. Nunez, S. Buntoung, and J. Cao, "An assessment of three satellite-based precipitation data sets as applied to the Thailand region," *Physical Geography,* vol. 36, no. 4, pp. 282-304, 2015.

[5] C. Phoeurn and S. Ly, "Assessment of Satellite Rainfall Estimates as a Pre-Analysis for Water Environment Analytical Tools: A Case Study for Tonle Sap Lake in Cambodia," *Engineering Journal,* vol. 22, no. 1, pp. 229-241, 2018.

[6] R. R. Ross, "Cambodia: A country study," 1987: Federal Research Division, Library of Congress.

[7] S. Tes, J.-M. Roussel, S. I. Sok, D. Cleary, and N. Hayball, "Cambodian Water Resources Profile," 2014, issue 2014.

[8] H. C. Thoeun, "Observed and projected changes in temperature and rainfall in Cambodia," *Weather and Climate Extremes,* vol. 7, pp. 61-71, 2015.

[9] A. Yatagai, K. Kamiguchi, O. Arakawa, A. Hamada, N. Yasutomi, and A. Kitoh, "APHRODITE: Constructing a long-term daily gridded precipitation dataset for Asia based on a dense network of rain gauges," *Bulletin of the American Meteorological Society,* vol. 93, no. 9, pp. 1401-1415, 2012.

[10] P. Xie *et al.*, "A gauge-based analysis of daily precipitation over East Asia," *Journal of Hydrometeorology,* vol. 8, no. 3, pp. 607-626, 2007.

[11] H. Ashouri *et al.*, "PERSIANN-CDR: Daily precipitation climate data record from multisatellite observations for hydrological and climate studies," *Bulletin of the American Meteorological Society,* vol. 96, no. 1, pp. 69-83, 2015.

[12] K. R. Knapp, "Scientific data stewardship of International Satellite Cloud Climatology Project B1 global geostationary observations," *Journal of Applied Remote Sensing,* vol. 2, no. 1, p. 023548, 2008.

[13] K.-l. Hsu, X. Gao, S. Sorooshian, and H. V. Gupta, "Precipitation estimation from remotely sensed information using artificial neural networks," *Journal of Applied Meteorology,* vol. 36, no. 9, pp. 1176-1190, 1997.

14] X. Zhang and F. Yang, "RClimDex (1.0) user manual," *Climate Research Branch Environment Canada,* vol. 22, 2004.

The assessment of climate change impact on extreme flood and drought in Yom and Nan River basin, Thailand

Chanchai Petpongpan[1,a], Chaiwat Ekkawatpanit[1,b],Duangrudee Kositgittiwong[1],Naota Hanasaki[2], Adisorn Champathong[3], Somkid Saphaokham[3], Thada Sukkapan[3], Jaray Thongduang[3] and Weerayuth Pratoomchai[4]

Abstract The climate change effects will be intensified continuously and become a severe problem in the future. The majority of people are anxious about the damage caused by this problem. Thailand always has been suffered from flood and drought disasters which are likely to be intensified by climate change especially in Yom and Nan River basin. Damages to the local people and also country income loss are concerned because this region is the important agriculture area. This study aims to assess the impacts of climate change on extreme natural hazard events consist of flood and drought in the Yom and the Nan River basins. The climate change are considered from rainfall and temperature predicted by Global Climate Model (GCM). These variable are adjusted by using a bias correction method namely the shifting and scaling method. In addition, the hydrological model is used for river runoff simulation with climate data and topography data. The model is validated by comparing the simulated results with observation data and using the efficiency coefficient. As for analysis of extreme events, we calculated the Standardized Precipitation Index and (SPI) and Standardized Runoff Index (SRI) of each subbasin.

Keywords *Climate change, Extreme flood, Extreme drought, Standardized Precipitation Index, Standardized Runoff Index, Yom River basin, Nan River basin*

[1]King Mongkut's University of Technology Thonburi
Department of Civil Engineering
Bangkok, Thailand
[2]National Institute for Environmental Studies
Tsukuba, Japan
[3]Royal Irrigation Department
Bangkok, Thailand
[4]Naresuan University
Department of Civil Engineering
Phitsanulok, Thailand

[a]Chanchai_Petchpongpan@outlook.co.th
[b]chaiwat.ekk@kmutt.ac.th

Introduction

Over the past few decades, the heat waves and bushfire weather are intensified continuously due to the climate change. The change of climate condition cause more intense extreme weather events and devastation around the world such as intense cyclones and heavy rainfall events [1]. These have directly impact to the occurrence of various natural extreme events. To prepare for several severe impacts, many researchers have attempted to study in this issue.

In Thailand, flood and drought disaster have always occurred and caused a widely damaged to lives and property especially at the northern part. Moreover, there is a tendency to intensify in this issue in the future, according to several study. For example, there was a high risk of water deficit in several basins due to the water demand increase while the rainfall are decreased. This is suitable for severe drought conditions and water shortages especially in the upper part of Thailand where the water demand tends to increase more than lower part [2]. Next, when the availability of irrigation water in the main supply area of irrigation water for the hill tribes is declined, it influences to the inhabitant of local people because their livelihoods have related with the irrigation water and cause a limitation of agricultural adaptations especially in dry season [3]. The increasing trend of water availability in wet season indicates more flood frequency and intensity [4]. In the southern part of Thailand, there was an upward trend in annual rainfall and mean annual maximum temperature. It effects to the increase of discharge especially in southwest monsoon season then the flood disaster can occur easily [5]. Moreover, the difficulties in water management of reservoir which are formed by the fluctuation between rainfalls from spatial uncertainties and averaged has a direct impact on the agricultural sector [6]

Hence, it is necessary to study in the future phenomena of extreme flood and drought for a sustainable management and protection. This study aim to assess the probability of extreme flood and drought in Yom and Nan River basins by considering on change of river runoff due to the climate change.

Hydrological Model

The Soil and Water Assessment Tool (SWAT) model is the conceptual model. Watershed is divided into a subdivision by considering a direction of main stream channels. The features of land use activities and soil properties are defined in Hydrologic Response Units (HRUs) of each sub-watersheds. The HRUs is represented in term of four storage volumes which are snow, soil profile (0–2 m), shallow aquifer (2–20 m) and deep aquifer (>20 m). For river routing, the direction of streamflow is controlled by the river path in order to flow through a channel, reservoirs and outlet of the watershed, respectively. This model uses the principle of SCS curve number or Green-Ampt infiltration equation (layered storage routing technique combined with a crack flow model) to simulate the Hydrology processes. In addition, the storage routing technique is applied to predict the water that flow through each soil layer. When the field capacity of the soil layer is exceeded and the lower soil layer was not saturated at that time, the flow had been dropped. On the other hand, if the field capacity of the next lower layer is over, the upward flow may be occurring. The ratio between soil water content and field capacity of both layers is the variable that control the movement of lower layer to an adjoining upper layer. The groundwater flow contribution to total streamflow and flow rate are simulated by routing a shallow aquifer storage component to the stream and saturated hydraulic conductivity of the soil layer respectively [7].

Study area

Yom and Nan River basin, two important basins of Thailand, are almost half of Chao Phraya River basin. Both basin locating in the north of Thailand as show in Fig. 1 cover 58,728.93 sq.km of 11 provinces.

Yom River basin has the area of 24,046.89 sq.km from the north to the south between lat. 14°50′ long. 99°16′ and lat.18°25′long. 100°40′. Upstream area begins at DoiKhunYuam in Phayao province and confluent with Nan river at Nakhon Sawan province. The large majority of rainfall are occurred during wet season (May to October) approximately 1,260.4 mm. per year on average. Main water demand is used for agriculture about 80%. In addition, there is no dam in Yom River basin. That is one of the reason that flood and drought disaster always occur in this basin [8].

Nan River basin locating between lat. 15°42′ long. 99°51′ and lat.18°37′long. 101°21′ from the north to the south cover the area of 34,682.04 sq.km. Watershed started at Luang Prabang Mountains which is the boundary between Thailand and Laos. There was a similar pattern of average annual rainfall with Yom River basin that occur in rainy season (May to October) around 1,287 mm. and also the trend of water use as the most of water is used for agriculture. However, there was Sirikit dam located at the central of basin for water management so when compare with Yom River basin, the problem of flood and draught hazard are not severe [8].

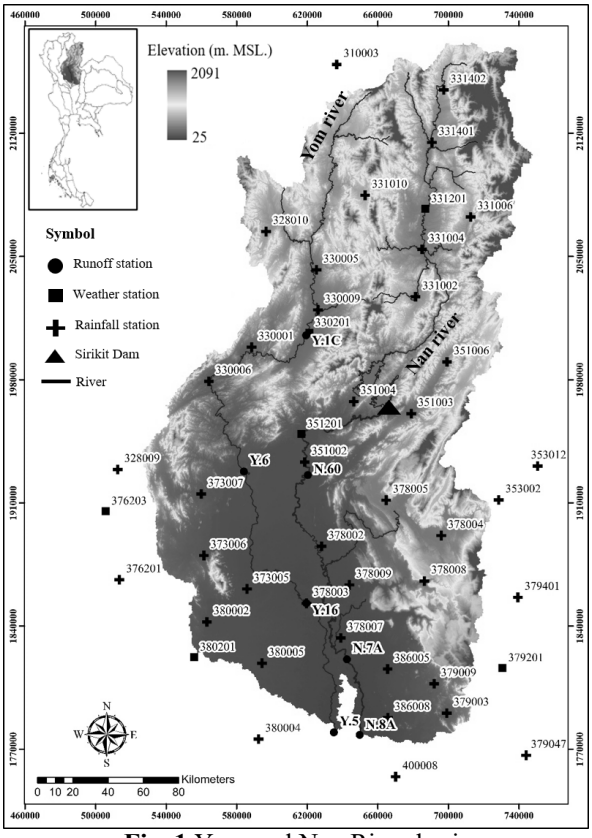

Fig. 1. Yom and Nan River basin

GCMs data and Bias-Correction method

The GCMs data which is a predicted climate data such as precipitation and temperature can be downloaded via data server of H08 model collected by National Institute for Environmental Studies, Japan (NIES). There are many GCMs data provided in this server but the most complete of information available for study area are 10 GCMs listed in Table 1.

However, it is almost impossible to use these GCMs output directly due to a systematic distributional biases from grid sizes in several scale of area [9]. To remove this bias, these GCMs output are compared with observation data and use the Bias-correction method for adjustment. The Bias-correction method is statistical technique that have been profusely developed and used so there are several type of them in recently. The shifting and scaling method is one of the bias correction method that widely use due to its simplicity and straightforward application [10]. In this method, biases is adjusted base on the observation data.

Table I. List of CMIP5 GCMs used [11]

Model	Institution
bcc-csm1-1-m	Beijing Climate Center(BCC),China Meteorological Administration,China
CNRM-CM5	Centre National de RecherchesMétéorologiques / Centre Européen de Recherche et Formation AvancéeenCalculScientifique
CSIRO-Mk3-6-0	Commonwealth Scientific and Industrial Research Organization in collaboration with Queensland Climate Change Centre of Excellence
GFDL-ESM2M	Geophysical Fluid Dynamics Laboratory, National Oceanic and Atmospheric Administration (NOAA)
HadGEM2-ES	Met Office Hadley Centre (additional HadGEM2-ES realizations contributed by Instituto Nacional de PesquisasEspaciais)
IPSL-CM5A-MR	Institut Pierre-Simon Laplace
MIROC5	Atmosphere and Ocean Research Institute (The University of Tokyo), National Institute for Environmental Studies and Japan Agency for Marine-Earth Science and Technology
MPI-ESM-MR	Max Planck Institute for Meteorology Earth System Model MR.
MRI-CGCM3	Meteorological Research Institute
NorESM1-M	Norwegian Earth System Model, Norwegian Climate Centre

Methodology

A. Model simulation and calibration

Initially, the watershed is divided into several sub-basins and then classified into a number of Hydrological Response Units (HRUs) with specific land use and soil type. The geological data define a characteristic of watershed consist of Digital Elevation Model (DEM), land use and soil properties data. DEM has 90 m. resolution created from Shuttle Radar Topography Mission (SRTM) by The National Aeronautics and Space Administration (NASA). Meanwhile, the land use and soil properties data can be received from Land Development Department (LDD). The meteorological data are precipitation, maximum and minimum air temperature, dew point temperature and wind speed. This determine a weather condition that directly relate to the hydrological regime in watershed. In this study, the precipitation data is daily rainfall intensity, but the other are monthly. It is interpolated by using Thiessen Polygon method for distribution. These observation weather data are collected from 38 rainfall stations and 10 weather stations of Thai Meteorological Department (TMD) as show in Fig.1.

Model are investigated by compared a results with hydrological observation data. The hydrological data used for calibration consist of daily river discharge and information of Sirikit dam from Royal Irrigation Department (RID) and Electricity Generating Authority of Thailand (EGAT), respectively.

B. Climate change effect and extreme event assessment

The GCMs output (precipitation) are compared with observation data during reference period from 1981-2005 to select the most three appropriate GCMs. Then, after adjusted the bias by using shifting and scaling method, these predicting data are simulated by SWAT model to assess the future situation of hydrological regime between 2021 and 2095. It is considered on scenarios RCP 2.6 and 8.5 which are and the minimum and maximum issues of global annual GHG emissions, respectively and separated into 3 phases, namely near future (2021-2045), immediate future (2046-2070) and far future (2071-2095). The comparison regarding every future scenario and reference period

For extreme flood and drought analysis, The Standardized Precipitation Index (SPI) and Standardized Runoff Index (SRI) are widely used. Both index are estimated by considering on the probability of precipitation and runoff for any time scale. The rainfall from bias correction method and runoff from SWAT model simulation are transformed into index by fitting to a probability distribution and transforming into a normal distribution, respectively. The timescales of SPI and SRI used for extreme event consideration is 6 months because this time scales is effective to represent the precipitation over distinct seasons and related with unusual stream flows and reservoir levels. The violence of flood and drought based on SPI and SRI is shown in Table 2 [12]. In addition, Peak discharge value and Flow Duration Curve (FDC) of each predicting cases are compared with observation data for extreme event analysis also.

Table II. The classification of SPI and SRI

Index value	Category
Higher than 2.0	Extremely wet
1.5 -1.99	Very wet
1.0 -1.49	Moderately wet
-0.99 -0.99	Near normal
-1.0 - -1.49	Moderately dry
-1.5 – 1.99	Very dry
Less than -2.0	Extremely dry

Result and discussion

A. Model evaluation and GCM selection

Table 3 provide the information concerning the NSE and RMSE [13] value computed for model evaluation. It can be seen that SWAT model has a high performance of river runoff simulation in every station. The whole stations provide a high value of NSE that totally higher than higher than 0.75 [14]. The second highest value of NSE are Station Y.16 and N.8A which located at the lower part of Yom and Nan River basin, accounting for 0.908 and 0.878,

accordingly. Meanwhile, the RMSE value of them are lower than 20% of average discharge that are good criteria. Station Y.1C has the minimum value of RMSE amounting to 53.871 m3/s., while the maximum value is 117.187 m3/s at inlet flow of Sirikit Dam.

Fig.2 show the comparison of precipitation from GCMs output and observation data during the reference period (1981-2005). CNRM-CM5, MPI-ESM-ES and MIROC5 are the most 3 GCMs which overall are consistent with observation data even the result in some month are dissimilar. While, CSIRO-Mk-3-6-0 and bcc-csm1-1-m are overestimated. Whereas, HadGEM2-ES is underestimated

Table III. *NSE* and *RMSE* value of runoff stations

Station	*NSE*	*RMSE*
Y.1C	0.820	53.871
Y.6	0.809	82.905
Y.16	0.908	68.335
Y.5	0.873	96.313
Inlet of Sirikit Dam	0.802	117.187
N.60	0.759	83.618
N.7A	0.858	108.613
N.8A	0.878	106.773

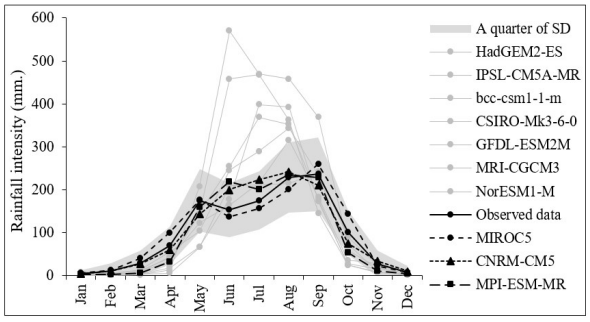

Fig. 2. Rainfall intensity from observation and GCMs during the reference period (1981-2005)

B. Impact of climate change assessment

Fig.3 provide the information about the average air temperature in the future compared with reference period in Box plot graph to show a distribution of results in several statistical index. The center line and box limits indicate a value of median, 1st and 3rd quartiles, respectively. Meanwhile, the maximum and minimum values are indicated at top and bottom bar, respectively. This can see that the air temperature max and min in the future both scenarios RCP 2.6 and 8.5 are totally higher than reference period in every statistical index. However, under scenario RCP 2.6, trend of air temperature are slightly increase, but there is a dramatic increase under RCP 8.5.

Considering on the annual runoff and rainfall change, the amount of rainfall has an increasing trend from reference period in the future especially under RCP 8.5 which are a significant trend since near until far future. While, under RCP 2.6, it remains constant after increase at near future. In addition, there are similar number in amount of runoff at Yom River basin throughout every future period under RCP 2.6 including near future under RCP 8.5 as shown in Fig.4. This is because most of rainfall rise is in a high evapotranspiration duration of the year (March-June). It effect to the amount of annual runoff value that are not different from reference period. However, there are an obviously upward trend in amount of runoff in almost case at Nan River basin including immediate and far future under RCP 8.5 at Yom River basin.

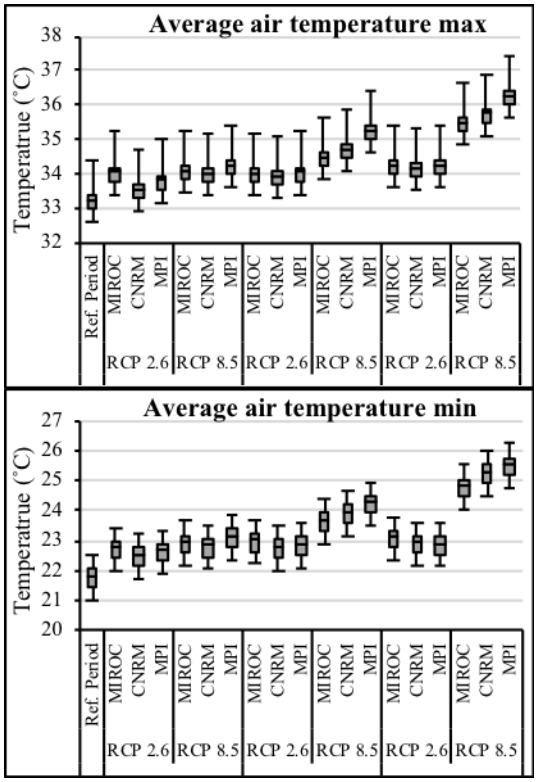

Fig. 3. Box plot of average air temperature max and min in reference period, near, immediate and far future under scenario RCP 2.6 and 8.5

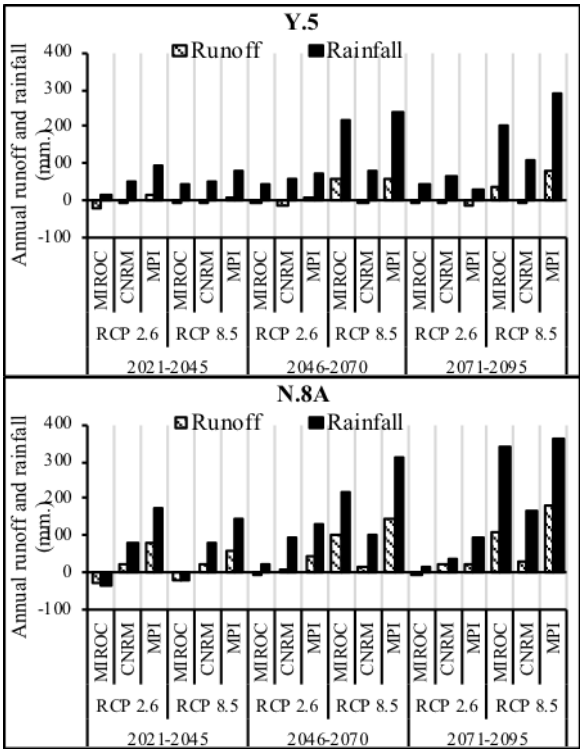

Fig. 4. Annual runoff and rainfall change in reference period, near, immediate and far future under scenario RCP 2.6 and 8.5

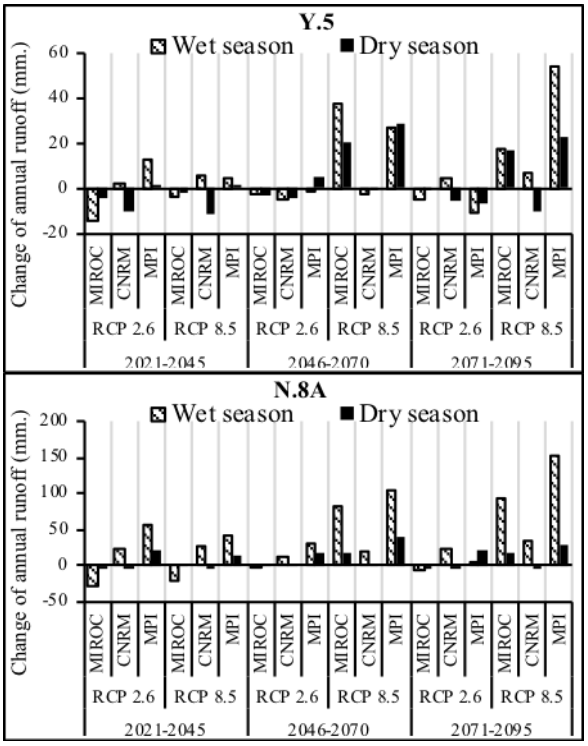

Fig. 5. The runoff change during wet and dry season in reference period, near, immediate and far future under scenario RCP 2.6 and 8.5

C. Extreme flood and drought analysis

When focusing on the average runoff during wet season (May-October) and dry season (November-April) shown in Fig. 5, it can see that most of runoff are increased in wet season. The large majority in runoff increased during wet season are occurred since immediate future onward under RCP 8.5. While, under RCP 2.6, a change of annual rainfall are stay the same from reference period. This mean that the magnitude and frequency of flood disaster are become severe in the future under RCP8.5. Interestingly, upper Nan River basin which is the area over the Sirikit dam has an increase of wet season runoff completely throughout every future period. Moreover, it can also be noted that there are a downward trend in runoff during dry season in some case. This can be simply explained that magnitude and frequency of drought disaster can be greater in some region or some period.

Fig.6-9 provide the information concerning SPI and SRI of each runoff station, respectively. In practically, SPI are generally used to analyze extreme flood and drought than SRI because SPI present the amount of runoff from rainfall directly without external factors. However, at the area located below the dam, the behavior of streamflow are controlled by reservoir operation so it is necessary to consider SRI couple with SPI. When compare with SPI during reference period, it found that the possibility of extreme flood and drought in most area of both basins are remain constant from reference period under scenario RCP 2.6. However, there still are a slight upward trend in the number of extreme drought at upper Yom River basin and downstream area below Sirikit dam. Meanwhile, under scenario RCP 8.5, the extreme flood probability rise dramatically since immediate future onward. For extreme drought, there are a slightly upward trend in near future. Next, it decrease at immediate future and increase again in far future except the area over the dam which has a declining in proportion of extreme drought event since near to far future. Furthermore, SRI represent a similar trend in the extreme flood and drought probability to that of SPI. Scenarios RCP 8.5 provide a dramatic increasing trend of extreme flood in Yom and Nan River basin, while trend of extreme drought are similar. However, under RCP 2.6, the upper Yom River basin and downstream area below Sirikit dam have not only a rising trend of extreme drought but also there are the extreme flood.

One noticed that, The Shifting and Scaling method, used for bias-correction, removed only the mean annual/monthly biases. The biases for over/under-estimation of the interannual/diurnal range might still exist in Extreme event analysis. This mean that the possibility of extreme flood and drought in the future are more likely to occur than analyze.

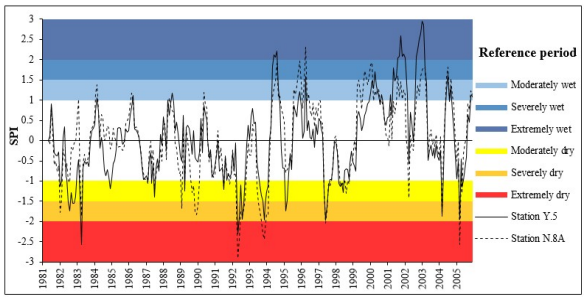

Fig. 6. The Standardized Precipitation Index in reference period of station Y.5 and N.8A

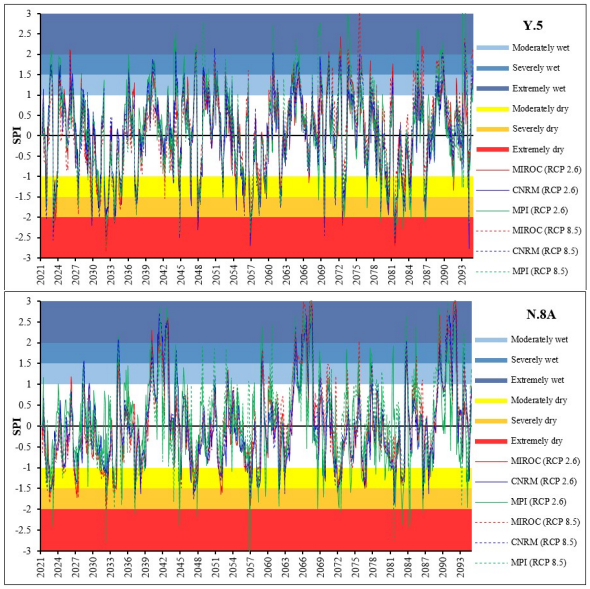

Fig. 7. The Standardized Precipitation Index in predicting period of station Y.5 and N.8A under scenario RCP 2.6 and 8.5

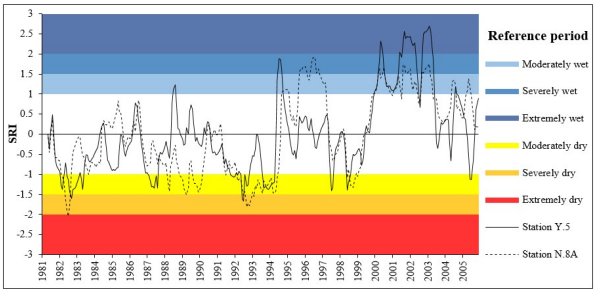

Fig. 8. The Standardized Runoff Index in reference period of station Y.5 and N.8A

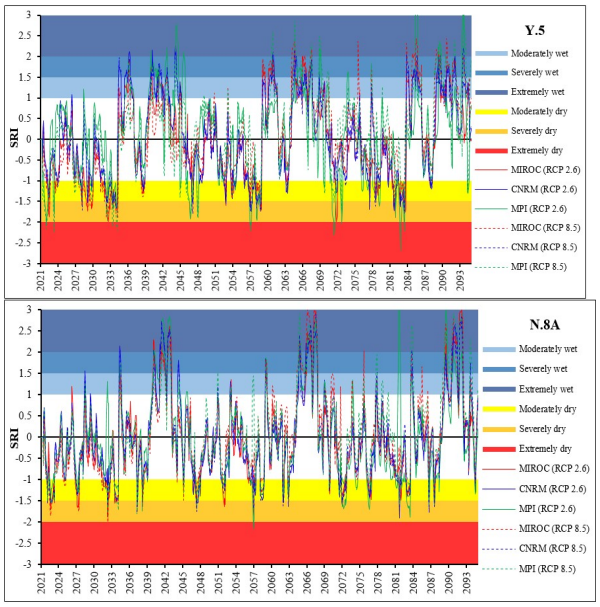

Fig. 9. The Standardized Runoff Index in predicting period of station Y.5 and N.8A under scenario RCP 2.6 and 8.5

Conclusions

According to the results, it can be summarized that there is a slow and fluctuated increasing trend in air temperature, annual rainfall and runoff under RCP 2.6. However, scenario RCP 8.5 provide a significant rising trend of them in Yom and Nan River basins during immediate and far future.

Based on the change in rainfall and runoff including SPI and SRI. Under RCP 2.6, the extreme flood and drought in almost area of Yom and Nan River basin are remain constant from reference period. However, there still are a slight upward trend in extreme drought in some period at upper Yom River basin and Lower Nan River basin. Whereas, under RCP 8.5, there are a significant upward trend in the frequency and violence of extreme flood since immediate future onward in both Yom and Nan River basins. While, extreme drought shows a slightly upward trend in near future, then decrease at immediate future and increase again in far future except the area over the dam.

Acknowledgment

This research was supported by "Advancing Co-design of Integrated Strategies with Adaptation to Climate Change in Thailand (ADAP-T)" supported by the Science and Technology Research Partnership for Sustainable Development (SATREPS), JST-JICA. The authors are grateful to the Thai Meteorological Department, the Royal Irrigation Department, Thailand, National Institute for Environmental (NIES) and Electricity Generating Authority of Thailand (EGAT) for providing us with meteorological, hydrological and GCMs data.

References

[1] Climate Counci, "The Link between Climate Change and Extreme Weather Events," Cranking up the intensity: Climate Change and Extreme weather events, Climate Council of Australia Limited, Sydney, Australia, 2017.

[2] W. Chaowiwat, S. Boonya-aroonate, and S. Weesakul, "Impact of Climate Change Assessment on Agriculture Water Demand in Thailand," IEEE Sarnoff Symposium, New Jersey, United states, 26-27 April 2004.

[3] E. Kraak, "Effects of land use change and climate change on irrigation water availability in the Mea Pheam catchment, Thailand," M.S. thesis of Utrecht University, Utrecht, Netherland, 2014.

[4] S. Shrestha, "Assessment of Water Availability under Climate Change Scenarios in Thailand," Journal of Earth Science & Climatic Change, vol. 5(3), 2014, pp. 184-190.

[5] C. Sangmanee, S. Chinvanno, J. Tanakitmethavut, S. Bunsomboonsakul, and J. Thitiwate, "Impact of Climate Change on Hydrological Regime of Khlong Krabi Yai Watershed, Krabi Province, Thailand," Technical Report No.22. Report. Southeast Asia START Regional Centre, Bangkok, Thailand, 2014.

[6] S. Chantip, P. Srisomporn, and S. Boonya-aroonate, "Effect of Climate Change on the Assessment of Water Budget of Chao Phraya River Basin,"19th National Convention on Civil Engineering, Khon Kaen, Thailand, 14-16 May 2014.

[7] P. Reungsang, "Application of SWAT model in predicting water quantity and quality for U.S. and Thailand watersheds," Retrospective Theses and Dissertations of Iowa State University, Iowa, United states, 2007.

[8] Asdecon corporation company limited, "Report of Nan River basin," Information of 25 main basins in Thailand, Hydro and Agro Informatics Institute, Bangkok, Thailand, 2017.

[9] N. Hanasaki, S. Fujimori, T. Yamamoto, S. Yoshikawa, Y. Masaki, Y. Hijioka, and M. Kainuma, "A global water scarcity assessment under Shared Socio-economic Pathways – Part 2: Water availability and scarcity,"Hydrology and Earth System Sciences, vol. 17, 2013, pp. 2393-2413.

[10] J. Alcamo, M. Florke, and M. Marker, "Future long-term changes in global water resources driven by socio-economic and climatic changes," Hydrological Sciences Journal, vol. 52, 2007, pp. 247-275.

[11] Climatology lab, "Model Name and Model Agency," CLIMATE MODELS, University of idaho, Idaho, United states, 2018.

[12] World Meteorological Organization, "Standardized Precipitation Index User Guide," WMO-No. 1090. Report, World Meteorological Organization, Geneva, Switzerland, 2012.

[13] GISGeography, "Root Mean Square Error RMSE in GIS," GIS Analysis, GISGeography, 2018

[14] J.E. Nash and J.V.Sutcliffe, "River Flow Forecasting Through Conceptual Models, Part 1: A Discussion of Principles," Journal of hydrology, vol. 10(3), 1970, pp. 282-290.

Impact of climate and land use changes on soil erosion and sediment yield in Nan river basin, northern Thailand

Studyoffuturesoilerosionandsediment yield

Patchares Chacuttrikul[1], Masashi Kiguchi[1], Taikan Oki[1], Naota Hanasaki[2], Koichiro Kuraji[3] and Koji Ikeuchi[4]

Abstract

The impacts of climate and land use changes on soil erosion and sediment in Nan river basin in north of Thailand were assessed using RUSLE, SDR and sediment transportation model. The results suggested that the changes in both climate and land use have significant impacts on both soil erosion and sediment. The increase of rainfall in near future directly affects surface runoff which is important factor related to soil erosion, and river discharge that controls the sediment flow in river. Land use change from forest to agriculture has a greater effect on soil erosion and sediment than that from one type of agriculture to another due to the reduction in plant cover. Furthermore, the severe scenarios in Nam Wa river basin which is branch of Nan river basin, illustrate how land use changes tend to affect soil erosion more than climate change, while climate change has a greater impact on sediment than land use change.This analysis can be useful in designing optimal land use that is effective for reducing soil erosion damages and decreasing sediment accumulation in the river including planning to mitigate the impact of climate change in the future.

Keywords *Climate change, land use change, soil erosion, sediment yield*

[1]Institute of Industrial Science,
The University of Tokyo Meguro-ku,
Japan.
[2]National Institute for Environmental studies, Tsukuba,
Japan.
[3]Ecohydrology Research Institute,
The University of Tokyo,
Japan.
[4]Department of Civil Engineering,
The University of Tokyo,
Japan.

Development of future climate scenario based on multi GCMs of CMIP5 and rain gridded data observed by multi-agencies in Thailand

Masashi KIGUCHI[1,a], Ruthaikarn BUAPHEAN[2], Aphantree YUTTAPHAN[3], Boonlert ARCHEVARAHUPROK[4], Eiji IKOMA[5] and Taikan OKI[6]

Abstract A bias-corrected future climate scenario is developed using multiple General Circulation Models (GCMs) outputs of CMIP5 (Coupled Model Intercomparison Project Phase 5) and rain gridded data observed by Thai Meteorological Department (TMD), Royal Irrigation Department (RID), and Department of National Parks, Wildlife and Plant Conservation (DNP) in Thailand during the period from 2080 to 2099. This dataset enabled us to conduct a projection considered spread in projections derived from multiple GCMs. Multiple performance-based projections were obtained using the correlation of monsoon rainfall between GCMs and several agencies observations. Because these three agencies (TMD, RID, and DNP) observation network covered mainly plain, area of along river, and mountainous region, respectively, it could avoid underestimating when we use only TMD and RID dataset as usual. Our results will highlight the importance of appropriate evaluation for the performance of GCMs, and the impact assessment on climate change.

Keywords *climate change, general circulation model (GCM), driving dataset*

[1]Institute of Industrial Science,
The University of Tokyo,
Meguro-ku, Tokyo, Japan
[2]Meteorological Development Division,
Thai Meteorological Department,
Bangkok, Thailand
[3]Agrometeorological Subdivision,
Meteorological Development Division,
Thai Meteorological Department,
Bangkok, Thailand
[4]Thai Meteorological Department,
Bangkok, Thailand
[5]Earth Observation Data Integration & Fusion Research Initiative,
The University of Tokyo,
Meguro-ku, Tokyo, Japan
[6]Rector's Office,
United Nations University,
Shibuya-ku, Tokyo, Japan
And,
Integrated Research System for Sustainability Science,
The University of Tokyo,
Bunkyo-ku, Tokyo, Japan

[a]kiguchi@iis.u-tokyo.ac.jp

Introduction

Climate change is one of the global issues, and might be one of elements what affects global water circulation including monsoon circulation. The DGDWGW (dry gets drier, wet gets wetter" is well known in global moisture change as one of effects of climate change. IPCC (2013) [1] shown that there is slightly increase trend in Thailand in future. Spatial resolution is, however, not fine, so that there is few research related to risk assessment and adaptation to climate change in Thailand. Finer information of rainfall as one of main factors of water related issues is necessary.

In Thailand, Asian monsoon strongly affects rainfall phenomena which is important for agriculture especially. More than 60 % of annual rainfall in Thailand is delivered by monsoon rainfall (e.g., Zhang et al., 2002 [2]). Kiguchi et al. 2015 [3] estimated high water stressed population in global, and indicated that some area newly face to water scarcity in future. Also seasonal march might affect crop calendar in agriculture. In central part of Thailand, there is pre-monsoon rainfall usually (e.g., Matsumoto, 1997 [4]). This kind of earlier rainfall prior to monsoon is important for decision making of crop calendar. Understanding of changes of rainfall in future is necessary for impact/risk assessment of climate change on water related sectors.

As above, rainfall and other elements in finer resolution is necessary but limited now. Watanabe et al. (2014) [5] developed a bias-corrected future climate dataset for projection of future river discharge in the Chao Phraya River basin, located in the center of Thailand. This research shown the importance of appropriate evaluation for the performance of GCMs. Due to only the development of dataset in the Chao Phraya River Basin region, there is no suitable dataset for impact/risk assessment in whole Thailand. Because the northeastern part of Thailand is famous region for drought and flood, the impact/risk assessments on climate change are required by society.

Now, we are conducting the project entitled "Advancing co-design of integrated strategies with adaptation to climate change in Thailand (ADAP-T)" with international collaboration between Thailand and Japan was proposed, approved, and implemented since 2016, supported by JICA (Japan International Cooperation Agency) for Thai side and JST (Japan

Science and Technology Agency) for Japanese side under the framework of SATREPS (Science and Technology Research Partnership for Sustainable Development). ADAP-T has three piers of research, namely i) Knowledgebase of climate change, ii) Adaptation measures to climate change, and iii) Co-designing adaptation measures. Because adaptation measures should be considered in context in local, it is necessary to impact/risk assessment in regional scale for estimation of adaptation measures. Purpose of this study is to develop data set for impact/risk assessments in whole Thailand. Under ADAP-T, we are firstly correcting the historical rainfall data in whole Thailand and are preparing the GCMs (Global Circulation Models) data set. Here, this activities are introduced.

Data and method

A. Data

First, we collect observational rainfall data set of Thai Meteorological Department (TMD)'s synoptic stations, which number is more than 120 during 1981-2017.

Second, we collect observational rainfall data set of TMD's district level stations. Number of stations is increasing, so number during this period is difference in each year. Before using these data, it is necessary to do quality control. Now we are doing this process.

In parallel, we collect observational rainfall data set of Royal Irrigation Department (RID) during 1981-2017. Also, we are trying to correct observational rainfall data set of Department of National Park, Wildlife and Plant Conservation (DNP). Reason we collect the observational rainfall data of multi-agencies is that most of rainfall observatory of TMD are located near city, town, and so on. According to Kuraji et al. (2009) [6], there is altitudinal increase in rainfall over small river basin, northern Thailand. When we use only TMD data set, the results of estimation of runoff and river discharge might be underestimated. Kotsuki et al. (2014) [7] and Watanabe et al. (2014) [5] discussed about the underestimation of runoff and river discharge in Chao Phraya River basin.

On the other hand, 10 GCMs of CMIP5 (Coupled Model Intercomparison Project Phase 5; Taylor et al., 2012 [8]) are utilized. Also, the d4PDF (Database for Policy Decision-Making for Future Climate Change; Mizuta et al., 2017 [9]) data set are also utilized. This data set consists of outputs from global warming simulations by a global atmospheric model, and is intended to be utilized for impact assessment studies and adaptation planning for global warming.

B. Method

A hydrological simulation will be conducted using H08 model (Hanasaki et al., 2008 [10]). This model consists of six modules, and we use only the land surface hydrology and river routing modules for projection. Bias correction of GCM output is necessary for development of forcing data sets from GCM output because correction method applied has a large impact on the results (Watanabe et al., 2012 [11]). We used the bias correction method developed by Watanabe et al., 2014 [5].

Expected results

We expect the developed data set for impact/risk assessments of global warming in future. In this study, we try to develop the rainfall grid data using not only TMD but also RID and DNP. Watanabe et al. (2014) [5] used rainfall data observed by TMD only for bias correction. We expect that underestimate of results of hydrological simulation will be avoided.

In this study, we use CMIP5 and d4PDF data sets for future projection. d4PDF is a 4K warmer simulation, and has 100 ensemble. This data set is intended to be utilized for impact assessment studies and adaptation planning for global warming. We expect this data set will contribute higher reliability results for helping policy decision making.

Closing remarks

One of ADAP-T's target is to estimate cost and benefit of adaptation measures in six sectors; 1) freshwater, 2) sediment, 3) coast, 4) forest, 5) rural planning, and 6) urban. These information is useful for evaluation of adaptation measures to contribute policy decision making about climate change measures and establishment national plan related to climate change. This study is to develop data sets as knowledge basement of climate change in Thailand and to contribute to planning of climate change counter measures by central and local governments.

Acknowledgment

This research was supported by "Advancing Co-design of Integrated Strategies with Adaptation to Climate Change in Thailand (ADAP-T)" supported by the Science and Technology Research Partnership for Sustainable Development (SATREPS), JST-JICA. We thank Ms. SpindaWattanakarn, Mr. SomkidSapaokum, Mr. AdisornChampatong, and Mr. ThadaSukhapunnaphan, who are officer of Royal Irrigation Department to provide us the data set of stations.

References

[1] IPCC, "Climate change 2013: The physical science basis", Contribution of Working Group I to the Fifth Assessment Report of the Intergovernmental Panel on Climate Change. Cambridge: Canbridge University Press, 2013.

[2] Y. Zhang, T. Li, B. Wang, and G. Wu, "Onset of the summer monsoon over the Indochina Peninsula: Climatology and interannual variations", Journal of Climate, 15, 3206-3221, 2002.

[3] M. Kiguchi, Y. Shen, S. Kanae, and T. Oki, "Re-evaluation of future water stress due to socio-economic and climate factors under a warming climate", Hydrological Sciences Journal, 60:1, 14-29, 2015. DOI: 10/1080/02626667.2014.888067

[4] J. Matsumoto, "Seasonal transition of summer rainy season ober Indochina and adjacent monsoon region", Advances in Atmospheric Sciences, 14, 2311-245, 1997.

[5] S. Watanabe, Y. Hirabayashi, S. Kotsuki, N. Hanasaki, K. Tanaka, C. M. R. Mateo, M. Kiguchi, E. Ikoma, S. Kanae, and T. Oki, "Application of performance metrics to climate models for projecting future river discharge in the Chao Phraya River basin", Hydrological Research Letters, 8, 33-38, 2014. DOI: 10/3178/hrl.8.33

[6] K. Kuraji, M. Gomyo, and K. Punyatrong, "Inter-annual and spatial variation of altitudinal increase in rainfall over Mount Inthanon and Mae Chaem Watershed, Northern Thailand", Hydrological Research Letters, 3, 18-21, 2009. DOI: 10/3178/hrl.3.18

[7] S. Kotsuki, K. Tanaka, and S. Watanabe, "Projected hydrological changes and their consistency under future climate in the Chao Phraya River Basin using multi-model and multi-scenario of CMIP5 dataset", Hydrological Research Letters, 8, 27-32, 2014. DOI: 10/3178/hrl.8.27

[8] K. Taylor, R. Stouffer, and G. Meehl, "An overview of CMIP5 and the experiment design", Bulletin of the American Meteorological Society, 93, 485-498, 2012. DOI: 10.1175/BAMS-D-11-00094.1

[9] R. Mizuta, A. Murata, M. Ishii, H. Shiogama, K. Hibino, N. Mori, O. Arakawa, Y. Imada, K. Yoshida, T. Aoyagi, H. Kawase, M. Mori, Y. Okada, T. Shimura, T. Nagatomo, M. Ikeda, H. Endo, M. Nosaka, M. Arai, C. Takahashi, K. Tanaka, T. Takemi, Y. Tachikawa, K. Temur, Y. Kamae, M. Watanabe, H. Sasaki, A. Kitoh, I. Takayabu, E. Nakakita, and M. Kimoto, "Over 5000 years of ensemble future climate simulations by 60 km global and 20 km regional atmospheric models", Bulletin of the American Meteorological Society, 98, 1383-1398, 2017. DOI: 10.1175/BAMS-D-16-0099.1

[10] N. Hanasaki, S. Kanae, T. Oki, K. Masuda, K. Motoya, N. Shirakawa, Y. Shen, and K. Tanaka, "An integrated model for the assessment of global water resources – Part 1: Model description and input meteorological forcing", Hydrology and Earth System Sciences, 12, 1007-1025, 2008. DOI: 10.5194/hess-12-1007-2008

[11] S. Watanabe, S. Kanae, S. Seto, P. J. F. Yeh, Y. Hirabayashi, and T. Oki, "Intercomparison of bias-correction methods for monthly temperature and precipitation simulated by multiple climate models", Journal of Geophysical Research, 117, D23114, 2012. DOI: 10.1029/2012JD018192

Climate Change and Land Use Change Effect on Water Accounting in Upper Nan Watershed

Sujira SORNSUNGNEAN[1,a], Venus TUANKRUA[1,b] and Piyapong TONGDEENOK[1]

Abstract This study assessed the effect of climate change and land use change on water accounting in the upper Nan watershed, Thailand, using the representative concentration pathway (RCP)4.5 scenario (SC1) and the RCP8.5 scenarios (SC2) of the fifth Assessment Report (AR5) of the Intergovernmental Panel on Climate Change (IPCC). Two additional scenarios were based on the national park policy in Nan province, Thailand which aimed to increases forest area by 3% (SC3) and 10% (SC4). The soil and water assessment tool (SWAT) model was applied to simulate the streamflow using meteorological data over a 20 year period from 1998 to 2017. The results showed that the SWAT model produced an acceptable performance for calibration and validation, yielding Nash-Sutcliffe efficiency (NSE) and coefficient of determination (R2) values greater than 0.5. Under the extreme climate change scenario (SC2) water accounting decreased annually in both the wet and dry periods. Water accounting in the land use change scenarios in which forest area increased (3% and 10%) showed increases annually and in the dry period, but there was a decrease in the wet period. This result indicated that climate change and land use change influenced water accounting in the upper Nan watershed.

Keywords *water accounting, climate change, land use change, upper Nan watershed*

Capacity Building Program for New Researcher 2019 from National Research Council of Thailand (NRCT)

[1]Department of Conservation, Faculty of Forestry
Kasetsart University
Bangkok, Thailand
[2]Department of Conservation, Faculty of Forestry
Kasetsart University
Bangkok, Thailand

[a]sujira.so@ku.th
[b]ffor.venus@gmail.com

Introduction

Climate change has caused the air temperature and rainfall intensity to change which in turn has affected the amount of rainfall and total streamflow [1] [2]. Many previous studies have assessed the impact of climate change on streamflow in watershed. These studies found that streamflow variability is closely associated with climate change. Moreover, land cover/land use (LULC) change has a continuous effect on the environment especially in the head water of a watershed with regard to quantity and timing. Therefore, many previous studies have investigated the combined effect of climate change and LULC change on hydrological [3] [4]. The two driving forces of climate change and land use change affect hydrological change in the watershed [5] [6].

The upper Nan watershed is an important head water area in the northern Thailand. It consists of steep mountains and hillsides making it extremely sensitive to change. Over an 8 years period (2009-2016), highland agricultural area increased 13.09% affecting the normal hydrological process that effect to bulk density has compacted, decreased soil infiltration andcontinuous effect on streamflow. These are the reason that hydrological has imbalanced by LULC and climate change. For example, Nan province experienced extreme flooding in August 2018.

Capacity Building Program for New Researcher 2019 from National Research Council of Thailand (NRCT)
Thus, it is crucial to assess the potential effect of climate change and land use change on water accounting spatially and temporally using the water accounting complement of Inflow, Outflow, and Depleted water [7] based on water balance to understand and drive adaptation in the future.

The Fifth Assessment Report (AR5) of the IPCC [8] is based on the Representative Concentration Pathway scenarios (RCPs; RCP8.5, RCPC6.0, RCP4.5, and RCP2.6 W/m2 radiative forcing scenarios), which range from worse to optimistic emission scenarios, respectively. The RCPs impact on climate change is considered to include impacts caused by LULC.

The current study assessed the potential effect of climate change and LULC change on water accounting in the upper Nan watershed, Thailand. Factor considered in this study are summarized as follows:

1. LULC in the watershed as developed under the Doiphukha National Park policy, which increased the forest area by expropriating cleared land from formerly forested areas.

2. The soil and water assessment tool (SWAT), a distributed hydrological model was calibrated and validated automatically to simulate the streamflow in the watershed

Study area

The upper Nan watershed has an area of 3,459 km^2 in Nan province, Thailand (Fig.1), having elevation range from 220 to 1,923 m above sea level and an average slope of 32.3º. Most precipitation occurs from July to October in the watershed and the dry period extends from December to April. The annual average precipitation is approximately 1,500 mm with an annual average temperature of 25.9ºC.

Method

A. Data preapation

The following were used

1) Digital elevation model (DEM) with a 20 m grid interval
2) Soil group map at a scale of 1: 100,000
3) Land use map scale 1: 50,000 at 2016 provided by Land Development department.
4) Daily climate data (1998 to 2017) consisting of rainfall (mm), maximum temperature (ºC), minimum temperature (ºC), humidity (%), wind speed (m/s), and solar radiation (MJ/m^2)
5) Daily runoff data (1998 to 2017) at station N64 located in Thawangpha district, Nan province, Thailand.

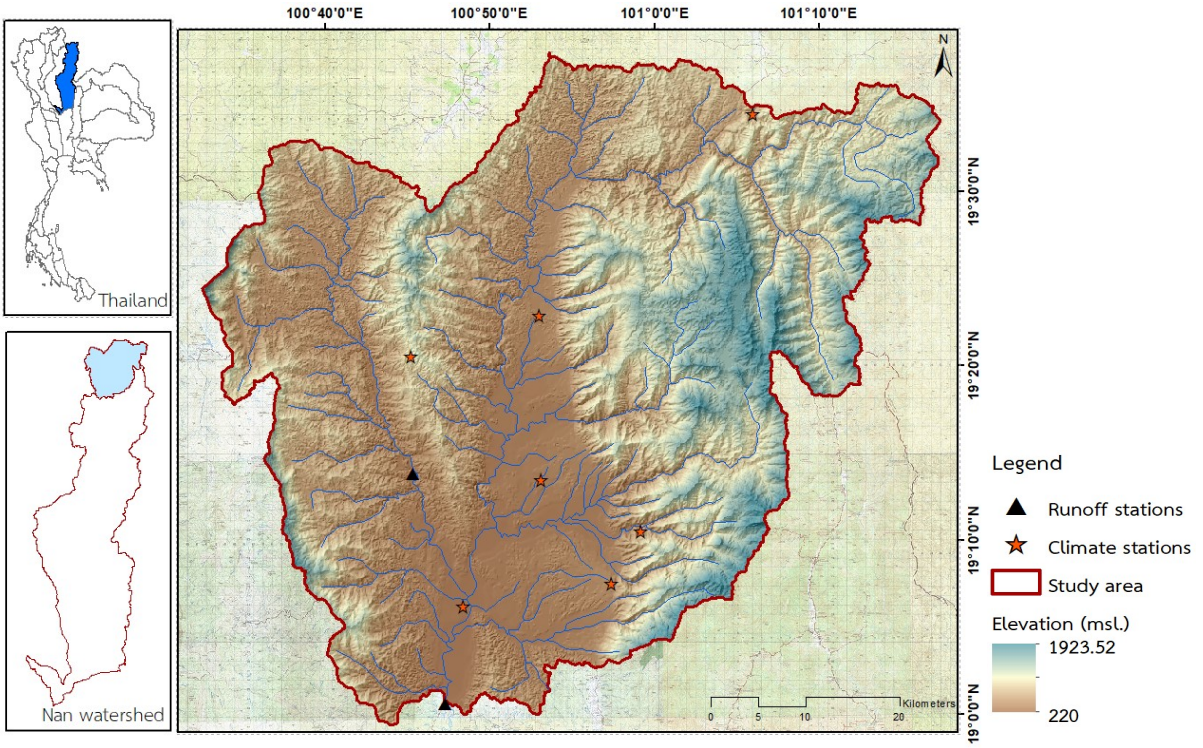

Fig. 1 Digital elevation model and location of upper Nan watershed and associated, runoff-climate stations

B. Assessment of streamflow using the SWAT model

The steps in this section were:

1) Prepare input data to SWAT model (DEM, land use map, soil group map, and daily climate data 1998 to 2017)
2) Watershed delineation was determined using the DEM to analyze the physical aspects of the watershed area
3) Hydrologic response unit (HRU) analysis was based on land use map, soil group map, and slope with multiple HRUs
4) Prepare input table of climate data and SWAT model setup and run.
5) Calibration of SWAT model including adjustment of hydrological characteristic parameter using the Nash-Sutcliffe efficient (NSE) as in (1) and coefficient of determination (R^2) as in (2)

$$R^2 = \left[\frac{\sum_{i=1}^{n}(o_i - \bar{o})(P_i - \bar{P})}{\sqrt{\sum_{i=1}^{n}(o_i - \bar{o})^2 \sqrt{\sum_{i=1}^{n}(P_i - \bar{P})^2}} \right]^2 \quad (1)$$

$$NSE = \frac{\sum_{i=1}^{n}(o_i - P_i)^2}{\sum_{i=1}^{n}(o_i - \bar{o})^2} \quad (2)$$

Where O_i =Observed data
P_i = Simulated data
$\bar{o}$ = Average of observed data
$\bar{P}$ = Average of simulation data

Satisfactory performance is indicated by tgeR^2 and NSE valuesbeing close 1 which indicates the simulation and observe data were very similar. Table I presents the performance rating for NSE, as suggested by [9]

Table I. Performance rating for the recommended statistics.

Performance rating	NSE
Very good	0.75 < NSE ≤ 1.00
Good	0.65 < NSE ≤ 0.75
Satisfactory	0.50 < NSE ≤ 0.65
Unsatisfactory	NSE ≤ 0.5

C. Assessment of water accounting

Water accounting was assessed using the model and theory as follows:

1) Inflow (I) = precipitation from the SWAT model
2) Depleted water (DP) was separated into two processes:
   a) Agricultural evapotranspiration using CROPWAT 8.0
   b) Evapotranspiration of forest area base on the SWAT model
3) Outflow (O) = streamflow as assessed using SWAT model
4) Assessment of water accounting as in (3), where a negative value indicates a deficit and a surplus is indicated by a positive value.

$$\text{Water accounting} = I - O - DP \quad (3)$$

The resultant classification is shown in Table II

Table II. Water accounting classification of upper Nan watershed

Class	Value
Extreme deficit	<-170.0
Deficit	-170.0 to -50.1
Balance	-50 to 60.0
Surplus	60.1 to 200.0
Extreme surplus	> 200.0

5) Assessment of spatial water accounting using a Geographic Information System (GIS).
   a) Combined the temporal water accounting and watershed map by join field tool.
   b) Using feature to raster tool for create component of water accounting (inflow outflow and depleted water)
   c) Calculated water accounting by Map algebra tool
   d) Classification water accounting by reclassify tool followed Table II

D. Predicted water accounting under climate change and land use change in upper Nan watershed based on four different scenarios

1) Scenario 1 (SC1) involved moderate change in climate based on RCP4.5 which increased the average air temperature by 1.4 ºC.
2) Scenario 2 (SC2) involved extreme change in climate base on RCP8.5 which increased the average air temperature by 2 ºC.
3) Scenario 3 (SC3) involved increased forest area (3%) based on the Doiphukha National Park policy which relied on expropriating cleared land from formerly forested areas during 2002 to 2014
4) Scenario 4 (SC4) involved increased forest area (10%) based on the Doiphukha National Park policy which relied on expropriating cleared land from formerly forested areas before 2002.

Results and Discussion

A. Calibration and validation model

Daily values of simulated streamflow were compared with actual observations to calibrate the SWAT model. The parameters used for the SWAT model simulation are given in Table III. The simulation values were slightly higher than the observed values (Fig. 2). In the calibration, the R^2 and NSE values were 0.86 and 0.74, respectively, while for validation, the R^2 and NSE values were 0.85 and 0.72, respectively. These results showed the calibration and validation models could describe streamflow in upper Nan watershed, as the R^2 and NSE were greater than 0.5 [7].

Table III. Sensitivity analysis parameters.

Rank	Name	Definition	Sensitivity	Process
1	CN2	SCS runoff curve number for moisture condition 2	-2	Runoff
2	ESCO	Soil evaporation compensation factor	0.7	Evaporation
3	SOL_AWC	Available water capacity of the soil layer (mm/mm soil)	1.35	Soil

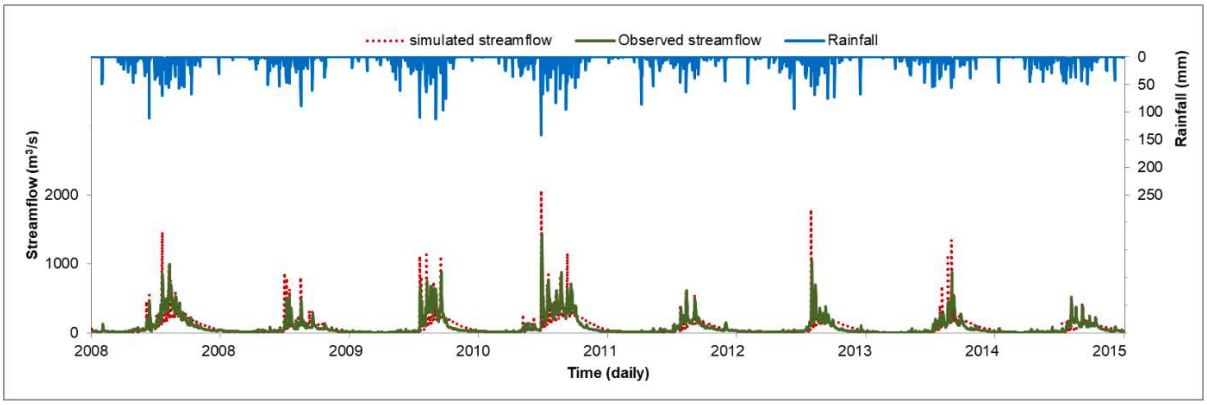

Fig. 2. Observed and simulated streamflow and corresponding daily rainfall in upper Nan watershed

B. The component of water accounting

1) The only Inflow (I) was precipitation in this area. In 2017 the total rainfall was with 1,358.6 mm which was higher than predicted under SC1 by about 4.6% due to the weak La Nina effect in 2017 [10]. In contrast, the SC2 predicted rainfall was 1,519.1 mm which was an increase of 11.8% over the actual 2017 amount (Table IV). SC3 and SC4 both had equivalent values for the rainfall as these scenarios were based on the average climate data (1998-2017).

Table IV. Annual rainfall and variability (%) of average Inflow under climate and land use scenarios for the upper Nan watershed

complement	Inflow under each scenarios				
	2017	SC1	SC2	SC3	SC4
Annual rainfall (mm)	1,358.6	1,295.9	1,519.1	1,290.0	1,290.0
Variability (%)	-	-4.6	11.8	-5.1	-5.1

2) Depleted water (DP) was analyzed as either agricultural evapotranspiration or forest evapotranspiration (Table V)

The results showed that depleted water was highest due to swidden cultivation (308.9 mm) in 2017 and was maximum from August to September. Maize had the least evapotranspiration in 2017 (38.2 mm) with the maximum during the same period as for swidden cultivation. Paddy field (120.8 mm) maximum from September to November. On the other hand, perennial land (159.6 mm) was about the same each month. Forest evapotranspiration in deciduous forest was higher than in evergreen forest (191.3 and 106.5 mm, respectively)

Both agricultural and forest evapotranspiration under SC3 and SC4 showed similar trends in 2017 though maize was lower and swidden cultivation was higher. SC1 and SC2 had lower values in all of land use types.

3) Outflow (O) consisted only of streamflow in this area. The trend was similar to that for rainfall because streamflow was influenced by rainfall [11][12] so that SC1 was the least in 2017, While streamflow was highest in SC2 (Fig. 3). Under SC1 and SC2, in the dry period from January to April there was no streamflow due to the increased temperature (2ºC). In contrast, SC3 and SC4 had increased streamflow in the dry period (January to April) and decreased streamflow from September to November (Fig. 3). The extreme climate change resulted in the highest streamflow [13] and increased forest area increased the streamflow [14].

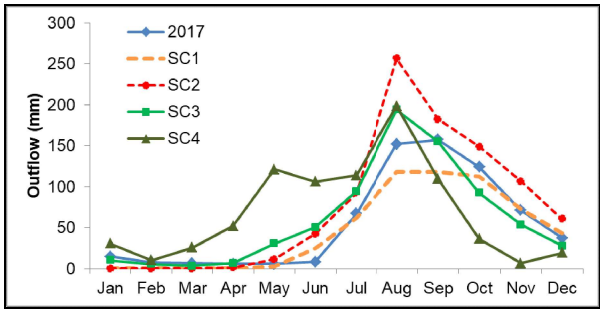

Fig. 3. Monthly Outflow under different land use change and climate change scenarios.

Table V. Annual average depleted water under different climate and land use scenarios in the upper Nan sub-watershed

Land use	Depleted water (mm)							
	Area (km^2)	2017	SC1	SC2	Area (km^2)	SC3	Area (km^2)	SC4
Maize	140.4	38.2	53.7	53.1	125.2	34.1	111.5	30.3
Paddy field	151.9	120.8	115.8	119.4	147.2	117.1	139.1	110.7
Perennial land	212.0	159.6	143.1	144.6	202.4	152.4	84.2	63.4
Swidden cultivation	744.9	308.9	348.4	341.1	698.0	300.1	592.2	281.2
Deciduous forest	1,361.4	191.3	177.8	180.9	1,439.4	191.6	1,690.6	128.1
Evergreen forest	769.9	106.5	95.9	97.3	769.9	105.0	769.9	58.9

C. Water accounting assessment

Water accounting in 2017 indicated a deficit (Fig. 4) of -134 mm (Table VI). During the dry and wet periods, there was an extreme deficit and surplus of -273.4 and 139.2 mm, respectively. However, while there was high streamflow, the depleted water was higher so that water accounting was in deficit

Climate change affect annual water accounting resulting in an extreme deficit as in Table VI and Fig.4, in the dry and wet periods there was a deficit and balance, respectively in SC2. Annual water accounting in SC1 showed a deficit, but in the dry and wet periods there was a deficit and surplus, respectively.

Forest area under the policy resulted in decreased water accounting in SC3 and SC4 (-94.1 and -68.5 mm, respectively) as show in Table VI. These were both in deficit on an annual basis (Fig.4), though both SC3 and SC4 had a deficit in dry period and a surplus in the wet period.

The classification of the water accounting was a specific class that could be used to explain water accounting in the upper Nan watershed only. These classifications will change depending on the complement of water accounting factor and each characteristic of the watershed but can be applied to determine present land use planning or in the future. If water accounting shows an extreme deficit then there will be a drought. In addition, an extreme surplus indicates flood.

Table VI. Annual, wet period and dry period water accounting under climate change and land use change scenarios.

Period	Water accounting (mm)				
	2017	SC1	SC2	SC3	SC4
Dry	-273.4	-175.5	-271.2	-184.6	-119.5
Wet	139.2	73.2	33.8	90.5	50.9
Annual	-134.2	-102.4	-237.4	-94.1	-68.5

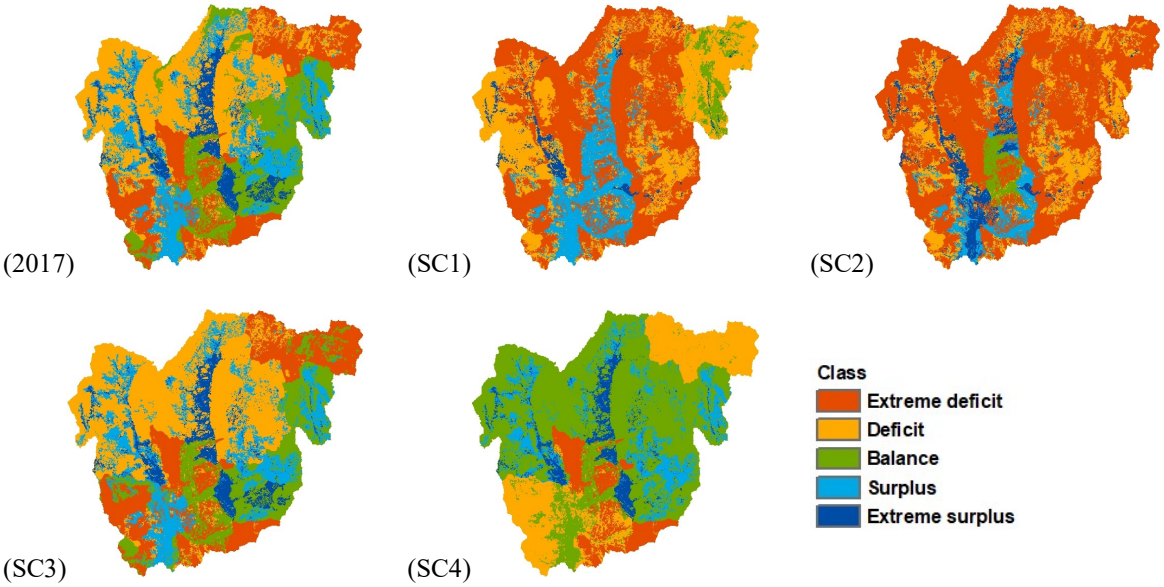

Fig. 4. Spatial distributions of water accounting under climate change and land use change.

Conclusions

The extreme climate change (SC2) scenario resulted in the baseline year of 2017 having a decreased water accounting on an annual basis and also for the wet and dry periods. Hence, increasing the uncertainty of climate change resulted in a corresponding severe drought.

Water accounting in forest land use change scenarios which (both 3% and 10%) base on 2017, produced an increase in annually and in the dry period, but a decreased in the wet period.

Thus, climate change had a negative effect on water accounting in all time periods studies, while land use had a positive effect on annually and in the dry period. In summary, climate change and land use change influenced to determining water accounting in the upper Nan watershed.

Acknowledgment

I would like to express my sincere appreciation to Dr. Venus Tuankrua and Assist. Prof. Dr. PiyapongTongdeenok for their advice.

References

[1] Wang H., Chaen L., and Yu X. Distinguishing human and climate influences on streamflow changes in Luan river basin in China. CATENA 2005, in press

[2] Wang S., Wang Y., Ran L., and Su T. Climatic and anthropogenic impact on runoff to changes in Songhua river basin over the last 56 year (1995-2010). Northeastern China. CATENA 2005,127

[3] Tomer M.D., Schilling K.E. A sinple approach to distinguish land-use and climate-change effect on watershed hydrology. J Hydrol 2007;376:24-33

[4] Tong STY, Sun Y., Ranatunga T., He J., Yang Y.J. Predicting plausible impacts of sets of climate and land use change scenarios on water resource. Appl Geogr 2012;32:477-89

[5] Chang H., and Franczyk F. Climate change, land use change, and flood; toward an integrated assessment. Geogr Compass 2008;2:1549-79

[6] Qi S., Sun G., Wang Y., McNulty SG., and Moore Myers JA. Streamflow response to climate and land use changes in a coastal watershed in North Carolina. Trans ASABE 2009;101:249-71

[7] Molden, D. Accounting for water use and productivity. SWIM Paper 1. International Irrigation Management Institute (IIMI), Columbo., 1997.

[8] IPCC. Climate Change The Physical Science Basis. Contribution of Working Group I to the Fifth Assessment Report of the Intergovernmental Panel on Climate Change. 2013:

[9] Moriasi, D.N.; Arnold, J.G.; Van Liew, M.W.; Bingner, R.L.; Harmel, R.D.; Veith, T.L. Model evaluation guidelines for systematic quantification of accuracy in watershed simulation. *Trans*. *Asabe* 2007, 50/ 885-900.

[10] NOAA. Available source: http://ggweather.com/enso/oni.htm, September 25, 2018.

[11] Chow, V.T. Handbook of Applied Hydrology. New York: McGraw-Hill Book Company, Inc. 1964.

[12] Wisler, C.O. and E.F. Brater. Hydrology. John Wiley&Son, Inc., New York. 1959.

[13] Kim. Jinsoo., Choi. Jisun., Choi. Chuluong., and Park. Soyoung. Impacts of change in climate and land use/land cover under IPCC RCP scenarios on streamflow in the Hoeya River Basin, Korea. Journal of Science of the Total Environment. 2013.

[14] Wang. H., Sun. F., Xia. J., and Liu. W. Impact of LUCC on streamflow base on the SWAT model over the Wei River basin on the Loess Plateau in Chaina. Hydrology and Earth System Sciences. 2017.

Evaluating the Impact of Land Use Change and Climate Change on Hydrological Services in Na Luang Sub-watershed, Nan Province, THAILAND

(Climate Change and Uncertainty in Hydrology and Meteorology)

Teerawach PHETCHARABURANIN[1,a] and Venus TUANKRUA[1,b]

Abstract Nowadays, deforestation under climate change of headwater in Nan province has been a big problem of land use change and encroachment area to expand the maize production area and contract farming such as rubber plantation. There were reducing the ability of soil water storage and affecting to increase runoff and sediment yield in a stream which is hydrological services from the watershed. Hence, hydrological services should be evaluating and forecast using SWAT model in forest and maize sub-watershed. This study divided into six scenarios including SC1: land use in 2016, SC2: Trend scenario, SC3: Sandbox scenario, and SC4–SC6 are land use change with RCP8.5. The results show the total forest area was 20% decreased during 2013–2016 and the maize area has been 40% increase. Water and sediment yield in sub-watershed show significant (NSE = 0.72) when compared with observed data. Both land use changes have a greater impact on annual runoff than sediment yield. Nevertheless, land use which has mostly forest cover still provide water use for agriculture in dry season rather than maize cover area. And this research it was cleared that the climate change had been affecting to hydrological services which provide from the watershed, especially the water timing. The results were obtained in this study can provide information for land use and water resource planning in small sub-watershed as well as soil and water conservation on highland.

Keywords *Land use change, climate change, hydrological services, Nan province, SWAT model*

[1]Watershed and Environmental Management field,
Faculty of Forestry, Kasetsart University,
Bangkok, Thailand

[a]P.teerawach@gmail.com
[b]ffor.venus@gmail.com

Introduction

Ecosystem services are the values and functions of ecosystems that conducive to human living and happiness were divided into 4 part i.e. provisioning service, regulating service, supporting service, and culture and recreation service. Nan province is the one of the head watersheds which provides water in Nan River. Nowadays, deforestation of the headwater in Nan province has been a big problem of land use change and encroachment area to expand the maize production area with contract farming such as para rubber plantation. Maize cropping area is the one of influenced leading cause to environmental degradation due to unsuitable land use planning. Their activities are affecting soil erosion, which is a worldwide problem directly to environmental sustainability [1]. Raindrop impact makes a large contribution to soil erosion by enhancing soil detachment and runoff disturbance [2]. When raindrops impact to the soil surface, the energy of it used to overcome the bonds holding particles in the soil surface. [3] Then, there were reducing the ability of soil water storage and affecting to increase runoff and sediment yield in the stream which is hydrological services from the watershed. Moreover, the environmental conditions are more drastically deteriorate due to the effect of climate change, there are affecting to flood in wet season and water shortage for agriculture activities during dry season. Therefore, this research has aim to evaluate and forecast the effect of land use change and climate change on hydrological services for determining land use guideline in Naluang sub-watershed using SWAT model.

Methodology

A. Study area

Naluang sub-watershed (Fig. 1) was located in Wiang Sa district, which area has 12.45 square kilometer. This research was conducted in two sub-watersheds, which was 2.51 square kilometer of forest sub-watershed and 4.27 square kilometer of maize sub-watershed. Geographic of Naluang sub-watershed most of the complex mountain and a little lowland. The average slope is more than 35%. The elevation between 210 to 1,980 meters. This area has one village

is Pang mon which their uses water for consumption and agricultural activities from Naluang stream.

B. SWAT model input data

1) GIS data
   1.1) DEM (resolution 20 x 20 m) from topographic map, map scale is 1:50,000 of The Royal Thai Survey Department.
   1.2) Land use and soil series map and statistical data (scale of 1: 50,000) [4].

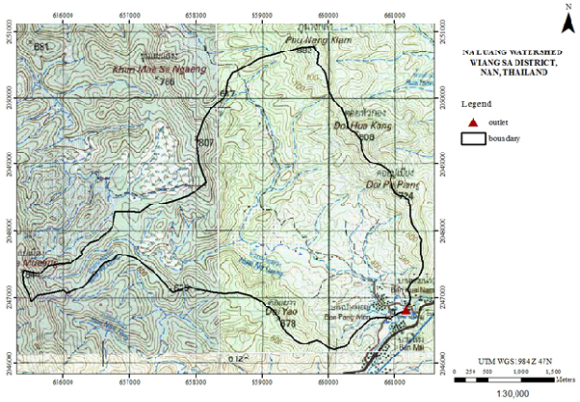

Fig. 1. Naluang sub-watershed, Wiang Sa district, Nan.

2) Statistical data
   2.1) Daily and monthly climatic data i.e. rainfall amount, maximum and minimum temperature since 1994 to 2017 [5].
   2.2) Daily runoff data of Naluang sub-watershed from the automatic water level station in two representative sub-watersheds, which is different land use patterns as deciduous forest and maize area.

C. Data analysis

1) SWAT model setup and run model

The first step of SWAT is generating sub-watershed by DEM of watershed. The streamline and outlet were created in the next step. The hydrological functions were determined based on hydrological response unit (HRUs), which represent the homogeneous combinations of soil types, land use types, and slope. The streamflow and water balance were calculated in warm-up period from 2010 to 2017. The sediment yield was calculated with MUSLE [6].

2) Model calibration and validation

This research using Sequential Uncertainty Fitting Program (SUFI-2) in the SWAT-CUP (SWAT calibration uncertainty procedures), this algorithm was used for calibration and sensitivity analysis for discharge outflow and sediment yield between observed daily and monthly data with output data from SWAT model. Streamflow will be calibrated at a daily time-step from January 2016 to December 2016. The model validation was set to run in 2017. Calibration SWAT model was adjusted parameter by Nash-Sutcliffe Efficient (NSE) and Coefficient of Determination (R2), their values were closing 1 that shown simulation and observed data were satisfactory performance. The table I present the performance rating for NSE, as suggested by [7].

Table I. Performance rating for the recommended statistics.

Performance rating	NSE
Very good	$0.75 < NSE \leq 1.00$
Good	$0.65 < NSE \leq 0.75$
Satisfactory	$0.50 < NSE \leq 0.65$
Unsatisfactory	$NSE \leq 0.5$

3) Determining land use scenarios

According to land use analysis using overlay technique on GIS, which was considered in environmental impact from land use change and climate change. Six scenarios (Fig. 2) have been contributed for the hydrological services assessment in the watershed likely to exposed floods and soil erosion risk as followed,

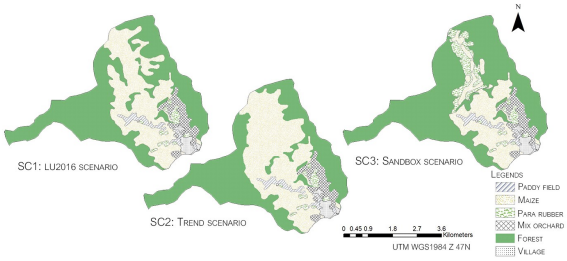

Fig. 2. Land use scenario in Naluang sub-watershed.

(SC1) LU2016 scenario; land use in year 2016 without soil and water conservation methods. There are 9 land use types i.e. dense deciduous forest, disturbed deciduous forest, teak plantation, para rubber, maize, paddy field, mix orchard, abandoned field crop and village. The highest proportion of deciduous forest was 53.69%, followed by maize was 34.52%.

(SC2) Trend scenario; land use land cover change from forest to maize was 40% (2013-2016) using transition matrix.

(SC3) Sandbox scenario; land use development in 72-18-10, which is a pilot project based on conserved forest area 100%. That's mean, to change the agricultural area which located in the conserved forest back to natural forest 72%, agro-forestry or economic forest was 18% and agricultural cropping was 10%.

(SC4) LU2016 with RCP 8.5 [8]

(SC5) Trend scenario with RCP 8.5

(SC6) Sandbox scenario with RCP 8.5

4) Forecasting water and sediment yield in each scenario

The simulation of runoff and sediment yield in the future were forecasted using SWAT model.

5) Determining the land use planning guideline

To determine the guideline of suitable and reasonable management approach in each scenario for supporting decision making of local people in land use planning as a land use map with hydrological information.

Results and discussion

Evaluating the impact of land use change and climate change on hydrological services, the results are as follows.

1) Model calibration

The different land use scenario reflects the hydrological service, including runoff and soil erosion, which come in water and sediment yield. Fig. 3 was illustrated the runoff calculated using the calibrated parameters (Table II) and the results from the SWAT model after calibrating the accuracy with measured runoff data in 2016 and 2017, showed the R2 and NSE were 0.72 and 0.71 in the calibration period, the PBIAS was 6.2% in the calibration period. [7] suggested that model predictions having NSE values larger than 0.65 and 0.50, respectively are good or satisfactory. They also suggested that model predictions have PBIAS values ±10% and ±15% respectively, are very good or good. Therefore, based on these NSE and PBIAS values, it was concluded that the modified SWAT model can accurately simulate water and sediment yield as a significant part of the watershed.

2) Influence of land use change on water and sediment yield.

LU2016 scenario had has the capacity to provided water yield from the watershed was 11 million cubic meter per year and the sediment yield was 365.50 ton per hectare per year, which was higher than the Trend scenario of 6 million cubic meters per year and 40.52 tons per hectare per year of sediment yield. The soil loss that was occurred every scenario is at a level where soil capability for agriculture is changing, which will effect on soil quality and crop yields over timeas [9] has determined a very severe level could not exceed 3.2 tons per hectare per year. Sandbox scenario that was provided the water yield nearly Trend scenario, however, the sediment yields more than 2 times as table III and Fig. 4.

The monthly hydrology change (Fig. 4), it is found that the trend of water and sediment yield of LU2016 scenario depended on the rainfall influenced while the seasonal change has less influence to water yield in Trend scenario and was provide it less than LU2016 scenario because the maize cropping activity lasts 4 months per year.

Table II. Selected calibration parameter for daily streamflow calibration in swat model.

Parameters	Description	Fitted value
CN2	Initial SCS runoff curve number	-1.88
Alpha_bf	Baseflow alpha factor	0.23
GW_Delay	Groundwater delay time	536.82
GWqmn	Threshold depth of water in the shallow	1.94
Sol_Z	Soil depth	2.49
Sol_AWC	Available water capacity of the soil layer	3.11
OV_N	Manning"n" value for overland flow	55

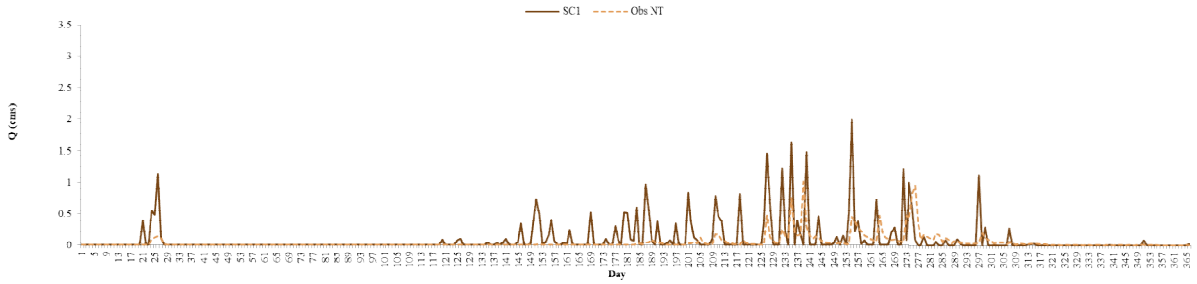

Fig. 3. Comparison of the observed and the calculated daily runoff of the Naluang sub-watershed.

Sediment yield was changed depending on the influence of rainfall. Trend scenario has a relatively low seasonal flow. It is lower than the LU2016 scenario because since the planting activity of maize is 4 months per year, after harvesting from November to December every year, farmers will abandon the crop area. During this period, the evapotranspiration from January to May was increased. Thus, the soil has a slightly absorbed rainfall capacity into the soil layer and the most of it will be evaporated back to the atmosphere that is affecting to less level of streamflow as the result of [10].The sediment yield is reduced by the amount of water yield flowing into a stream. The Sandbox scenario was similar to the LU2016 scenario, as it has the forest which more efficiently to provide water yield and soil erosion control, however in rainy season. Sandbox scenario was provided more sediment yield than Trend scenario due to the rubber plantation, there is a gap between the canopies that is a cause of rainwater directly drop to the soil surface rather than the maize. So, soil erosion was transportation into the stream become more sediment yield.

Considering the water regulation of natural forest, it was provided 42-48% of rainfall and has been soil erosion control was 19-25% of the watershed as [11], which watershed with rainfall more than 500 millimeters per year and forest cover more than 36%, the function of the forest is a constantly rate. Hence, Sandbox scenario is the best preliminary land use planning that is suitable for land management to control the environmental impact effectively on highland.

3) Influence of land use and climate change on hydrological services.

According to the first result, this part was furthered the climate change with land use scenario and the results were shown as following,

Influence of RCP8.5 was affecting to temperature and rainfall will increase in the future. Fig. 4 was illustrated the water yield in SC4, SC5, and SC6 were similar trends. During dry season, it was found that no water in the stream since January to April because the land is very dry, when the raindrop to soil surface, rain is absorbed into the soil layer immediatelymeanwhile the water in soil cannot flow into the stream due to the adhesion bond between soil particles and water in the gap is more than gravity force. Subsequently, the soil is gradually saturation from below then it will begin to release water into stream since May and raising to peak in September before become below in October and also affecting to sediment yield which was occurred due to the flow rate in the stream. Consequently, climate change was non-significant (p-value = 0.1) effect on water and sediment yield, however, the flow period in SC4, SC5, and SC6 was 4 months lag time in dry season when compare with a normal year.

Table III. Comparison water yield and sediment yield in each scenario

Month	Rainfall (millimeters)		Water yield (million cubic meters)						Sediment yield (tons per hectare)					
	Normally	RCP 8.5	SC1	SC2	SC3	SC4	SC5	SC6	SC1	SC2	SC3	SC4	SC5	SC6
1	59.4	9.3	0.6	0.5	0.2	0.0	0.0	0.0	14.0	1.1	3.3	0.0	0.0	0.0
2	2.6	11.6	0.0	0.5	0.1	0.0	0.0	0.0	0.6	0.0	0.0	0.0	0.0	0.0
3	25.0	37.2	0.2	0.5	0.1	0.0	0.0	0.0	7.2	0.0	0.1	0.0	0.0	0.0
4	66.0	129.0	0.6	0.4	0.0	0.0	0.0	0.0	7.4	0.0	0.2	0.0	0.0	0.0
5	143.3	198.4	1.3	0.5	0.3	0.1	0.1	0.1	15.5	0.3	1.8	0.3	0.4	0.2
6	134.1	135.0	1.1	0.4	0.2	0.5	0.5	0.5	29.7	0.0	2.7	0.0	0.0	0.0
7	198.7	238.7	1.8	0.5	0.6	0.9	1.0	0.9	53.7	2.7	10.5	4.0	5.6	2.0
8	267.7	282.1	2.7	0.7	1.4	1.6	1.6	1.6	121.1	21.8	35.8	8.6	12.0	4.6
9	184.0	243.0	1.7	0.8	1.4	1.8	1.8	1.8	64.9	12.7	17.2	6.2	8.6	3.3
10	95.1	120.9	0.9	0.6	1.0	1.7	1.7	1.7	38.6	0.8	7.2	0.0	0.0	0.0
11	25.6	12.0	0.2	0.6	0.6	1.3	1.3	1.3	5.8	1.1	0.9	0.0	0.0	0.0
12	32.9	6.2	0.3	0.6	0.3	0.7	0.7	0.7	7.1	0.0	0.7	0.0	0.0	0.0
Total	1,234.5	1,423.4	11.4	6.6	6.2	8.6	8.7	8.6	365.5	40.5	80.1	19.2	26.6	10.0

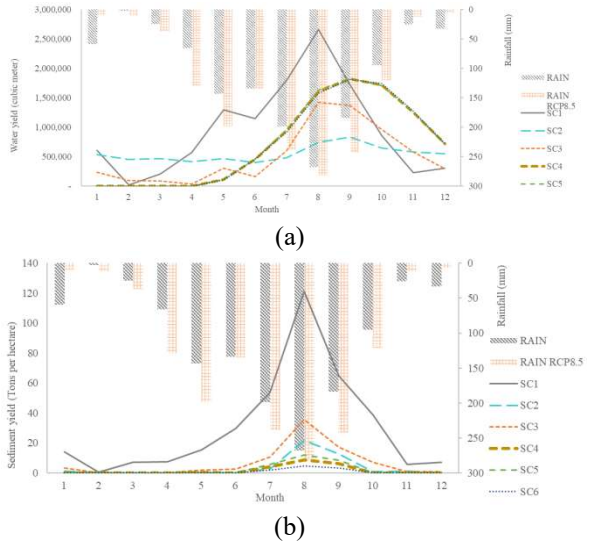

Fig. 4. Water (a) and sediment yield (b) in SC1–SC6.

4) Water management guideline for highland watersheds under land use change and climate change

SC1 and SC3, the results were explained land use change had more influenced on water amount than timing because in SC3 that was 18% increased in the para rubber plantation, which was used water to grow more than another plant. Therefore, the problem of soil erosion should be considered rather than water management. This can be done as one sees by planting shrubs in the para rubber plantation to reduce the impact of soil detachment from a raindrop. And SC2 was shown the risk's opportunity to water shortage in dry season, as a hydrological characteristic in Fig. 4, soil and water conservation is must consider e.g. terracing for decrease the surface runoff in wet season, that can reduce the opportunities in water shortage during dry season.

For SC4, SC5, and SC6, the results are shown that there is no water flow in the stream during dry period. So, it is necessary to collect water at the end of the wet season e.g. to build a small pond nearly the agricultural area such as mix orchard and paddy field and so on. On the other hand, the crop calendar will be adjusted to a suitable time period with the water flow in the stream. Even though, maize cropping activities in this area are still largely unaffected by climate change, as the cropping period from June to December, which is enough water for growth and maintenance.

Conclusions

A study of hydrological services was founded the natural forest still provided the water yield and had effectively soil erosion controlled, which was as close as possible to natural conditions. However, the overall scenario was shown trend scenario was likely to water shortage during dry season if there are no measures which reduce the surface runoff for increase the water retention. While the sandbox scenario is a land use planning that was supported the ecosystem to provided the hydrological services at an appropriate level for crop activities. Finally, this research is clear that climate change had been affecting to hydrological services, which provides from the watershed, especially the water timing.

Acknowledgment

I would like to give vastly appreciative thanks for comments and support to Dr. Venus Tuankrua and my family.

References

[1] Liu, S., Costanza, R., Troy, A., D'Asgostino, J., Mates, W., "Valuing new jersey's ecosystem services and natural capital: a spatial explicit benefit transfer approach," Environmantal Management, vol.45, pp.1271–1285, 2010.

[2] Gao, B., Walter, M.T., Steenhuis, T.S., Parlange, J.-Y., Richards, B.K., Hogarth, W.L., Rose, C.W., Sander, G., "Investigating raindrop effects on the transport of sediment and non-sorbed chemicals from soil to surface runoff," J. Hydrol., vol.308, pp.313–320, 2005.

[3] Ma, R.M., Li, Z.X., Cai, C.F., Wang, J.G., "The dynamic response of splash erosion to aggregate mechanical breakdown through rainfall simulation events in Ultisols", Catena, vol.121, pp.279–287, 2014.

[4] The Land Development Department, "Land use map in Nan province", Ministry of Agriculture and Cooperatives, 2016, unpublished.

[5] Nan Head Watershed Research Station, "Climatic data of Nan Head Watershed Station", Ministry of Natural Resources and Environment, 2017, unpublished.

[6] Williams, J.R. and H.D. Berndt, "Sediment yield prediction based on watershed hydrology", Transactions of the American Society of Agricultural and Biological Engineers, vol.20, pp.1100–1104, 1977.

[7] Moriasi, D.N., J.G. Arnold, M.W. Van Liew, R.L. Bingner, R.D. Harmel and T.L. Veith, "Model evaluation guidelines for systematic quantification of accuracy in watershed simulations", Trans. Asabe vol.50, pp. 885–900, 2007.

[8] IPCC., "Contribution of working group i to the fifth assessment report of the intergovernment panel on climate change", Climate Change the physical science basis, Cambridge University Press, Cambridge, United Kingdom, 2013.
[9] The Land Development Department, "Soil serie map in Nan province", Ministry of Agriculture and Cooperatives, 2000, unpublished.
[10] Lin, B.Q., X.W. Chen, H.X. Yao, Y. Chen, M.B. Liu, L. Gao and A. James, "Analyses of land use change impacts on catchment runoff using different time indicators based on SWAT model", Ecological Indicators, vol.58, pp.55-63, 2015.
[11] Yu, S.X., Shang, J.C., Zhao, J.S., Guo, H.C., "Factor analysis and dynamics of water quality of the songhua river northeast china", Water Air Soil Pollut., vol.144, pp.159–169, 2003.

NATURE-BASED SOLUTION FOR FLOOD MANAGEMENT AT NONG SUA DISTRICT,RANGSIT CANAL, THAILAND

Sirapee Ditthabumrung[1,a] and Sutat Weesakul[2,b]

Abstract The Nature-based Solution is inspired and supported by nature and use, or mimic, natural processes to contribute benefit back to ecological process and water cycle by improved management of water. A concept of "Room for a river" is one of nature-based solution for water management to be examined at a Nong Sua district, Rangsit area with 1,738 Rai. The study area existed for 100 year with irrigation canal systems in order to distribute water for farmer. In addition, this area has traditional furrow for orange farm and changed to palm oil instead due to plant phytopathy. In 2011, the great flood occurred in Thailand; the Rangsit area had not much damage. The objective of present study is to quantify the effectiveness of a high water channel concept for flood management for crisis water operation and management in the area.

High water level concept is applied can control amount of diverged water in furrow while traditional flood pain cannot. The Nature-based Solution for high water channel was quantified by conducting modeling approach with MIKE 11. The hydrodynamic flow and effectiveness of the capacity of the furrow area for water storage is determined in Western Raphipat canal during peak crisis water level in October 2016. The storage capacity of furrow was computed and estimated to be 753 m^3/Rai or 1.3 MCM. The computational results showed that diverting water from Western Raphipat canal into Rangsit community area reduced peak water level 34 cm same as recorded one. The model is then used to optimize nature base solution extending concept to nearby area and increases inflow. It is proved that the nature-based solution for high water channel can be applied in district without any new construction of flood control structures.

Keywords *nature-based solution, high water channel concept, flood management ; acidity soil.*

[1]Graduate Student AIT, Panya Consultant Co.ltd
[2]Hydro and Agro Informatics Institute (HAII) and Asian Institute of Technology (AIT), Thailand

[a]sirapee.dtbr@gmail.com
[b]sutat@haii.or.th

Introduction

Nature-Based solution (NBS) for water is natural processes to cost effectively contributes to improved water management. Natural ecosystem can be used and proactive in term of rehabilitation, conservation or even creation of natural processes in modified ecosystem, even mimic the natural process [1]. NBS can address and improve water availability, water for agriculture, urban water, water quality and reduce risks to water related extreme events. Netherlands initiated their "Room for the River" (RFR) programme to restore natural floodplains of river along certain non-vulnerable stretches, and creating water storage area. The concept of co-benefit of NBS is introduced to substantial value in social, economic and environment. NBS for water management have also high potential to contribute to the achievement of SDGs.

When the amounts of water come over the capacity of the stream or river, the overflow occur and lead to inundation. The goal of the room for river concept is to provide the space to be able to carry and manage high water level (roomfortheriver.nl,n.d.). According to Reference [2] in Netherlands, the concept room for the river was planned with the goal to protect the 4 million inhabitants of the river catchments from high water level. The program was considered a national and international example for integrated flood risk management and multi-level governance. However, every river has the different and requires a proper solution to apply the concept. Fig.1 shows the ways how to make room for the river. Nevertheless, the room for the river concept can be the non-structural measures to reduce and mitigate the damages from flood hazard.

A high-water channel as shown in Fig. 2 which a type of RFR, is a diked area that branches off from the main river to discharge some of the water via a separate route (roomfortheriver.nl, n.d.). The channel is not excavated below the water table but rather formed by building two dykes in the landscape. According to Reference [3], the project of the Flood Channel Veessen-Wapenveld in Netherlands, the project is one of the measures, which provides better flood protection for areas near the country's rivers. The high-water channel is located between Veessen and Wapenveld, 15 km to the south of Zwolle. It is used only when water levels reach extreme highs, water level in the IJssel River is reduced by 71 cm (ruimtevoorderivier.nl, n.d.). This is a once in a

lifetime event. The rest of the time, as now, the area can be used for farming. The channel will not be dug out, but formed by building two dikes measuring approximately 8 km. Fig. 3 shows example of high water concept. The retention area or basin is used to manage storm water runoff to prevent and collect flooding in order to protect downstream from inundation and erosion, and improve water quality in an adjacent river, stream, lake or bay.

Concept of RFR is quantified to reduce flood risk in Rhine and Meuse rivers under extreme events [4]. By increase of width of river, results in reduce exposure of flood by less economic damage and casualties. The degree of reduced flood risk by lowering water level in river not only depends on reduced consequences, but also probability of flooding. It is recommended that flood protection (embankments) combined with flood mitigation (lowering flood level) is thus the more flood risk management strategy.

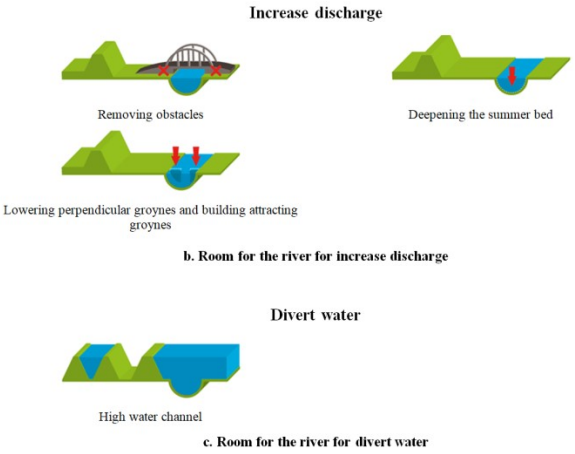

Fig. 1. How area will make room for the river, Source: (roomfortheriver.nl, n.d.)

Fig. 2. Operation of high water channel Source: (roomfortheriver.nl, n.d.)

Fig. 3. The project of the Flood Channel Veessen-Wapenveld in Netherlands, Source : [3]

Flood management in California have showed that setting levees back from river in several locations provides the most effective method of reducing local flood risk. It restores large land for floodplain habitat. The US Army Corps of Engineers found that acquiring and protecting floodplain wetlands can reduce Boston's flood risk from that Charles river for 1/10 cost of plan that introduce new engineered infrastructures [5]. Evaluating of flooding to ecosystems can be conducted through framework for both benefits and losses [6]. Flood can work as nutrient cycling function i.e. transfers of nutrients and organic matter between floodplain and rivers. Indicators for assessing change in ecological conditions are proposed.

The studies or projects of the retention or detention areas often concentrate for applying the area to store water for the same purposes. The main objective of them is to enhance and manage the area to keep the amount of water in order to protect or prevent downstream areas from flood risk and also to solve the drought. To mitigate floods in the lower Chao Phraya River Basin (CPRB) in Thailand, the setup of flood retarding areas in paddy cropping areas is one of the control options [7]. Their hydrological effect and economic impact are explored. The results show that the rice flood retarding area can reduce water level in the river at the storage and the downstream points. Moreover, the frequency of flood volume distribution shows that the existing retarding volume (1,738 MCM) is enough to store flood volume occured 12 in 24 times during 1952 – 2011 period. Cost effectiveness analysis shows that overall increased storage in retarding area reduces damage cost downstream. The guideline for floodplain management is studied for water depth in floodplain (0.40, 0.80, 1.00 m) and effective in reduced water level in Chao Phraya river [8].

In addition, Rangsit canal as the main line which feeds inhabitants, it is a valuable water resource for cultivation, transportation covering consumption, even if the function as irrigation canal is decreased by industrial; in fact, Rangsit canal is continuously supporting the people as a proficient drainage and irrigation canal from the past until now [9]. Rangsit field is an agricultural area for a century before it is adapted to water diversion area without the pre-evaluation of the impact assessment, but the area has the satisfactory potential to perform its duties. Plan to reduce flood risk in Bangkok is to divert the amount of water through the northern and eastern field of metropolis toward the sea in the southern part. The water is diverted in the northern and eastern field come from Pasak river and flow along the Raphiphat canal. This will divert water into the downstream area via Rangsit field and Rangsit canal. This plan was conducted in 2011. Due to large discharge in Raphiphat canal, the flood occurs .The Rangsit community protect the disaster of the huge flood by allowing for the amount of water pass through the area and build dikes along the canal to protect the

agricultural area [10]. Another achievement is in October 2016, the communities open the regulators to turn the area into retention area and high water channel concept, which substantially reduce the water level in Raphipat canal because of the effect from the storm.

The objective of present work is to study of a Nature-based Solution for water management for high water channel concept in Rangsit area, Nong Sua district in Phatum Thani, Thailand.

Methodology

The study area is one part of the Northern Rangsit Irrigation project of the main project in the Southern Pasak covers 3 provinces Ayutthaya, Saraburi and Phatum Thani. The Southern Pasak project locate in Lower Eastern Chao Phraya river basin. The flow regime of the Southern Pasak and study area show as Figs.4 and 5. Flow direction is from north to south and then distribute in Northen Rangsit Irrigation project. Table 1 summarized capacity of canals and regulators.

As the purpose study is focused on the application of agricultural areas to store the amount of water by cooperation in the community to encounter the flood. Hence, the sub-district namely Bueng Cham Or in Nong sua district, Phatum Thani province, Thailand is selected as study area. Rangsit canal community is located in Nong Sua district, Pathum Thani province by the Chao Phraya river basin with a total area of 54.48 km^2. Figs. 6 and 7 shows study area While 44.16 km2 have been used for agricultural production. The population is 8,926 people. Land use is summarized as follows: 19.63 km2 (44.5%) of agricultural land for fruit crops - perennial plants, 18.30 km2 (41.44%) for rice fields, 5.20 km^2 (11.8%) for vegetable crops and only 1.03 km^2 (2.33%) for farm crops [10].

Table 1 Capacity of canals and hydraulic structures (Northern Rangsit Irrigation project, 2017)

No.	Name	Type of structure	Maximum Discharge (m^3/s)
1.	Phra Narai	Gate	210.00
2.	Raphipat	Canal	170.00 - 215.00
3.	Phramahin	Gate	200.00
4.	Phraekathodsarod	Gate	190.00
5.	Phrasrisin	Gate	85.00
6.	Phratresoawapak	Gate	95.00
7.	Western Raphipat	Canal	40.00
8.	Southern Raphipat	Canal	80.00
9.	Klong 1	Canal	30.00
10.	Klong 2	Canal	20.00
11.	Klong 3	Canal	12.00
12.	Klong 4	Canal	12.00
13.	Klong 5	Canal	12.00
14.	Klong6	Canal	20.00
15.	Klong7	Canal	15.00
16.	Klong 8	Canal	15.00
17.	Klong 9	Canal	15.00
18.	Klong 10	Canal	30.00
19.	Klong 11	Canal	15.00
20.	Klong 12	Canal	15.00
21.	Rangsit Prayurasuk	Canal	45.00

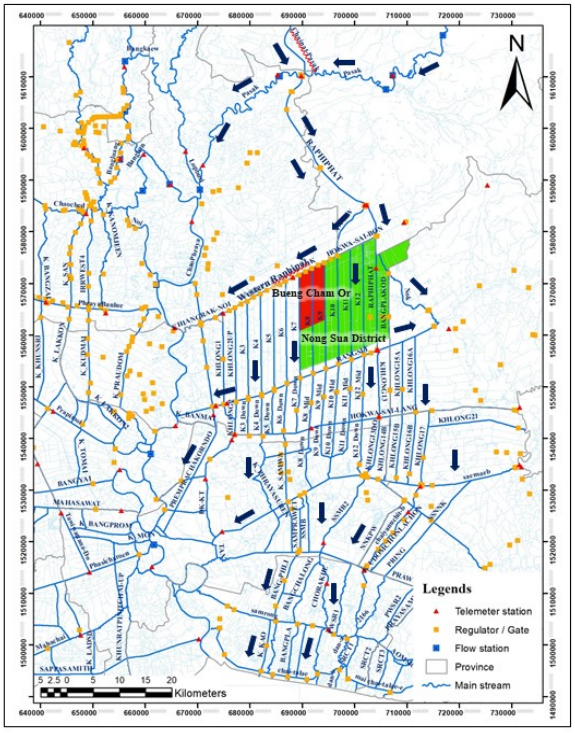

Fig. 4. Flow regime of Southern Pasak project

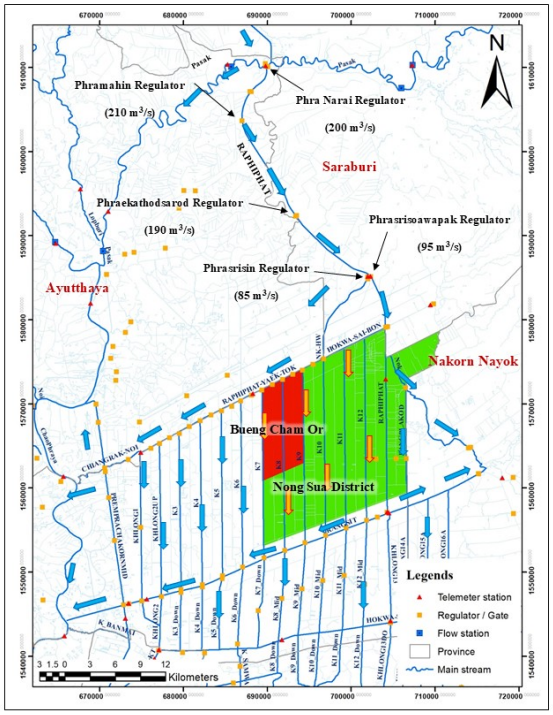

Fig. 5. Flow regime of study area

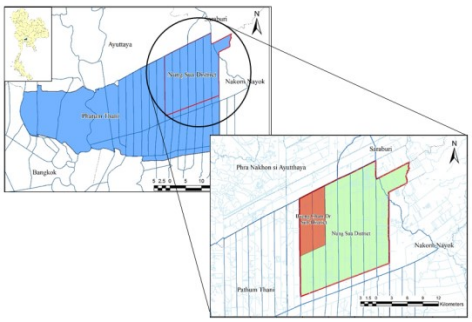

Fig. 6. Location of study area

Fig. 7. Existing canal system in study area, source: (HAII, 2017)

Rangsit canal is used for supporting the agriculture for a century since 1980 and continuously improve the potential of distribution water for irrigation until present time. For decades, communities living along Rangsit canal searched for ways to improve their livelihoods. In 1984, the communities change their farmland into the orange orchard, but an outbreak of the citrus disease and acid soil put the farmer into debt [10]. Thus, farmers turn to cultivate oil palm. The plant has a good resistance for acid soil and inundated area, which started to boost income to them. However, a lack of water due to the poorly maintained and shallow canal challenged palm oil cultivation. In addition, the severe flood of 2011 also revealed other challenges including canal bank erosion. Fig. 8 shows photographs of canals in the study area. HAII encouraged Rangsit communities to establish a CWRM committee to apply the use of science and technology (S&T). Analysis of the water balance and the design and implementation of a new water resource management system to provide water for palm oil cultivation area were conducted.

In addition, the NBS are applied in the area which is the concept for the mutual benefit of retention area and room for the canals. The main canals and sub-canals are dredged and linked with improved floodgates to maximize the water reservoir and drainage system. The water reservoir area is improved by vegetable patches around palm oil groves. A Suction Dredger Vessel, bought by Community Oil Palm Funds, diverts flood water to monkey cheeks (retention ponds) or furrows in palm oil patches and opens new waterways to agricultural areas in the dry season [10]. However, during the rainy season in August to October, the full bank flow occurs in Western Raphipat canal since it works as a diversion to bypass water from the Pasak river. One dimensional model is developed to simulate diverting water in Western Raphipat canal into the provided area using MIKE 11 model. However, the model which obtained from HAII is the model for the Lower Eastern Chao Phraya river basin which is quite big domain. Thus, the domain in this study is deducted to simplify the model and make the model domain suitable for the study area. Furthermore, a model from HAII has only the components in flow river network then the model need to add the storage component for use to simulate the diverting water to flood retention area. The model simulates flow in the river from Raphipat canal which receive water from Chainat-Pasak and Pasak river into the study area in North Rangsit operation and maintenance project. The boundary conditions consist of:

(1) Upstream boundary condition use the historical discharge data from Phrasrisin regulator and Phrasrisoawapak regulator in Raphapat canal,

(2) Downstream boundary condition use the water level data from Phra Intraracha regulator, Middle Rangsit regulator and Chulalongkorn regulator, and the discharge from Phra Thamaracha regulator, and Q/h relationship for downstream of Klong 1 to Klong 12 as shown in Fig.9.

Fig. 8. Canals in study area

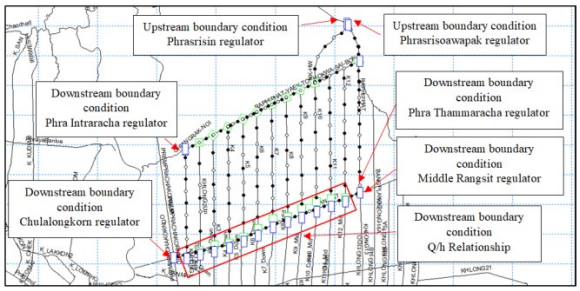

Fig. 9. Model domain and boundary conditions

Results and discussions

Furrows systems in study area are shown in Fig 10. Its connection to sub-canals, drainage canals and Western Raphipat canal is shown in Fig.11. Their function is similar to retention storage. The furrow storage capacity in Rangsit area is estimated by using furrow cross-section multiply with total length of furrow in the study area to be 753 m^3/Rai or 1.3 Million Cubic Meter (MCM). The model simulation has two conditions. First, the condition that simulates the river system in normal operation to show the stage of the canal in the normal situation. This is calibration and verification conditions. The second condition is the crisis operation which is the regulators gate opening were increased to receive water into area, and the artificial storage was added into model to be a flood retention. Results of model calibration using data in 2014 and verification in 2015 are shown in Figs 12 and 13. Correlation Coefficients for both results are 0.910 and 0.810 respectively. Bed resistance roughnesses are from 0.0035 to 0.025. Detail can be found in [11]. The crisis situation on October 2016 make the Western Raphipat had high water level more than 90% of maximum level of the canal on 13th October 2016. Therefore, HAII collaborated with Rangsit operation and maintenance project and Rangsit community to increase gate opening of Klong 7 to Klong 10 drainage canal head regulator. Water level at Western Raphipat canal reduced 34 cm within half a Day in Fig.14. The water diversion can protect water overflow due to dike repairing in Bueng cham Or area during that time. The concept of the crisis operation on 13th October 2016 is to receive water from Western Raphipat canal into drainage canal 7 – 10 and then water level in drainage canal will rise and flow into furrow by opening the farm turnout. Model results are shown in Fig.15. Computed results show that discharge flow into the storage 4 times on 14th, 18th, 22nd and 26th October with the value around 0.35, 0.22, 0.43 and 0.51 m^3/s respectively.

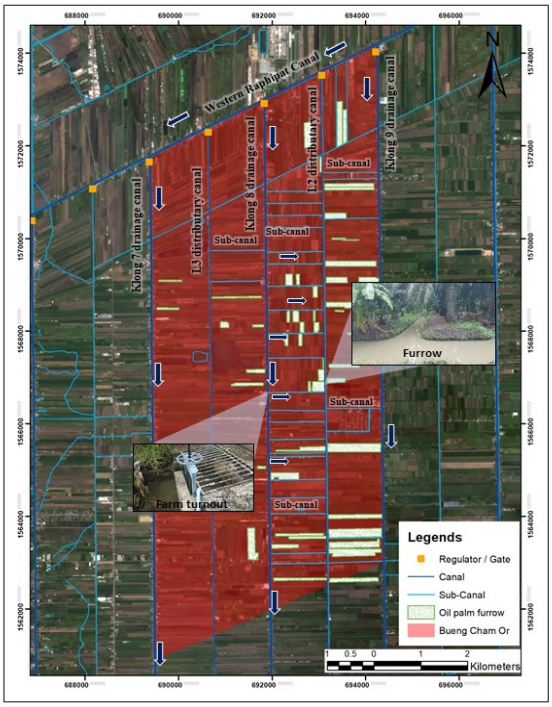

Fig. 10. Water diversion on 13th October 2016

Furthermore, the inflow that flow into the storage are kept and made the water level rise from +1.75 m.MSL in the beginning to +1.771, +1.783, +1.799 and +1.818 m.MSL respectively which increase the water depth from 50 cm to 68 cm, or the volume from 509,000 m^3 to 577,000 m^3. In order to assess the maximum capacity of storage, furrow capacity is increased in the nearby area, i.e. Bueng Ka Sam. The present storage at Bueng Cham Or, 1.3 MCM can be increased 1.0 MCM to have total furrow capacity as 2.3 MCM. Results show that increased in the water depth in furrows from 50 cm to 55 cm, and the volume from 848,333 m^3 to 940,000 m^3. Crisis operation can be improved to store more water in furrows by increasing inflow in Klong 8. The discharge is increased by 5%, 20%, 50% and 80% of discharge after 13th Oct 2016 in Fig. 16. Water level in West Raphipat canal is reduced and storage in furrows system increase as shown in Fig. 17 and 18. Water level can be reduced from 34 cm to 52 cm and storage can be increased as high as 1.1 MCM. Therefore, furrow areas are adapted to be the retention storage to keep the water which has no damage occurs in the area.

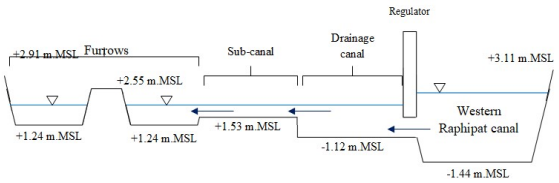

Fig. 11 Typical cross section of connection between furrows and canal

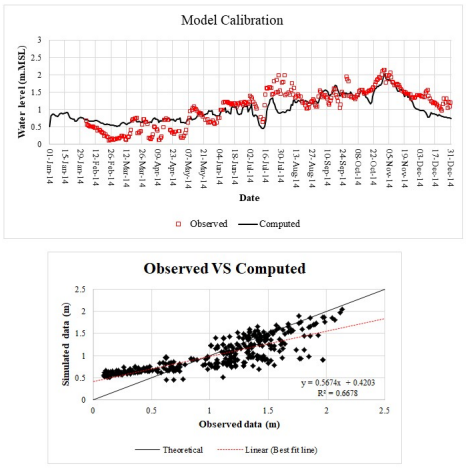

Fig. 12 Water level at Western Raphipat canal station in 2014

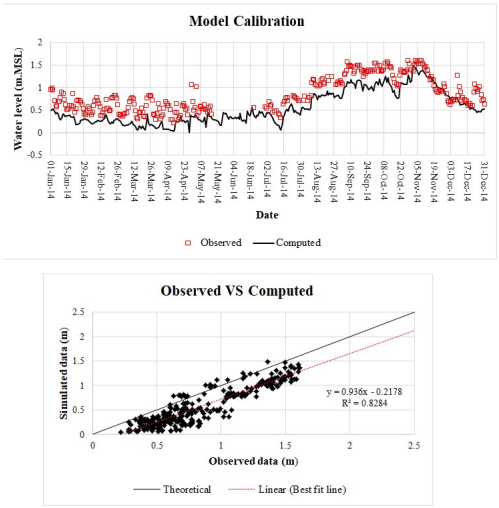

Fig. 13 Water level at Future Park station in 2015

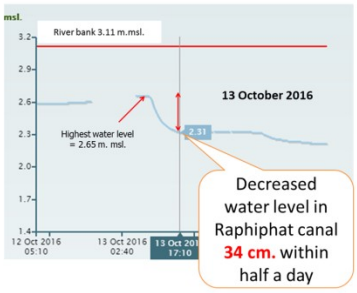

Fig. 14 Reducing water level in Western Raphipat canal on 13 October 2016,
Source: (HAII, 2017)

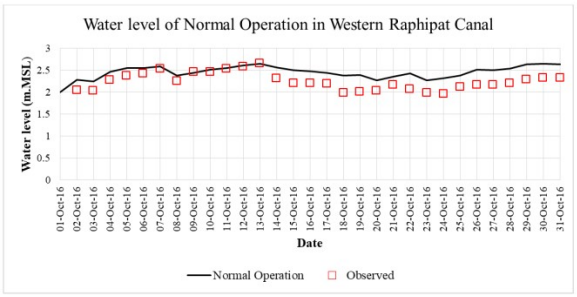

Fig. 15. Water level of Crisis operation in Western Raphipat canal

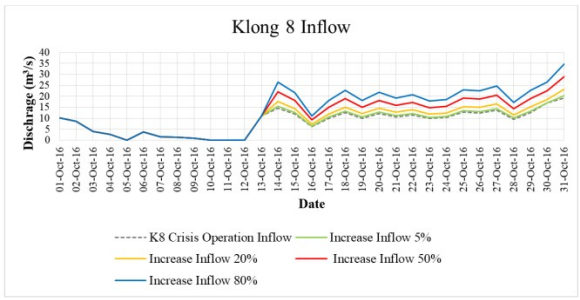

Fig. 16. Increasing inflow discharge of Klong 8 drainage canal

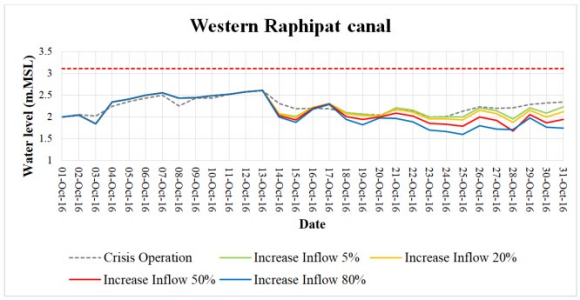

Fig. 17. Water level each scenarios in Western Raphipat canal

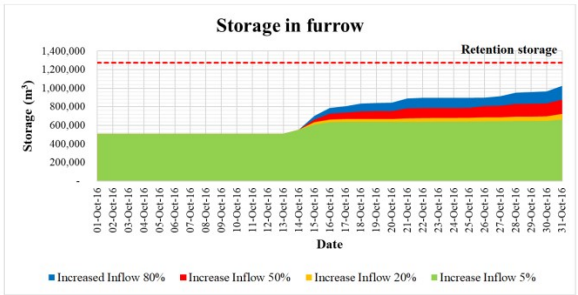

Fig. 18. Storage of furrow in each scenarios

Conclusions

The application of a Nature-based Solution (NBS) for water management is successfully implemented in the Rangsit area to adapt the existing environment, and enhance the potential use of furrows system. Storage in furrows and irrigation canal, contributes for crisis management to reduce water level from main canal, Western Paohipat, so that the present flood diversion for Bangkok can be operated as its planned. Maximum operation can be achieved by extend furrow concept to nearby area and to increase utilization of furrows storage.

Acknowledgment

This work is partially supported by the European Comission under Program HORIZON 2020, funding scheme "Innovation Action". Project Number is 776866, for the research project RECONNECT (Regenerating ECOsystems with Nature-based solutions for hydro-meteorological risk rEduCTion).

References

[1] UNWater, "Nature-Based Solutions for Water", The united nations world water development report , 2018.

[2] C. Zevenbergen, and E. Meurs, E. , "International relevance Room for the River", Programme. Retrieved from IHE Delft: https://www.un-ihe.org/stories/international-relevance-room-river-programme, June 6, 2014.

[3] V. Waterschap Vallei en , "High Water Channel Veessen-Wapenveld (Room for the River)", Retrieved from https://www.youtube.com/channel/UC7DCaBkc3IccGEYZDzA6jmw, March 29, 2013.

[4] N.E.M. Asselman and F. Klijn, "Making Room for Rivers : Quantification of Benefits from a Flood Risk Perspective", FLOODrisk2016 3rd European conference on flood risk management, 6p., 2016.

[5] US Army Corps of Engineers, " Massachusetts Natural Valley Storage Investigation ", US Army Corps of Engineers, New England Division, Waltham, MA., 1993.

[6] J. Annand, "Evaluating the Environmental Losses and Benefits from Flooding", 25 pages, 25 November, 2015.

[7] S. Kwansirinapa ,"Flood Alleviation in Chao Phraya River Basin", WM 07-13, 2007.

[8] C. Kaewsaentip , "Hydrological and Economic Effects of Rice Flood Retarding Area in Lower Chao Phraya River Basin in Thailand" , WM 12-10, 2012.

[9] Chulalongkorn university, "100 years of Rangsit canal ", 1996.

[10] HAII, & Foundation, " Application of Science and Technology for Community Water-Related Disaster Risk Reduction: Thailand Good Practices following His Majesty the King's Initiative towards Sustainable Development", Utokapat Foundation under Royal Patronage of H.M. the King and Hydro and Agro Informatics Institute (HAII), Ministry of Science and Technology, 2016.

[11] S. Ditthabumrung, "Nature-Based Solution for the Water management : A Case Study in the Rangsit Area, Thailand", Master Thesis, Asian Institute of Technology, May 2018.

EVALUATION OF SEMIVARIOGRAM MODELS IN THE STUDY OF SPATIAL INTERPOLATION OF SOIL SALINITY

A CASE STUDY OF CHAO PHRAYA AND THA CHIN LOWER BASINS, THAILAND

Kanoksuk Chankon[1,*], Sanwit Iabchoon[1], Pariwate Varnakovida[1] and Amnat Chidthaisong[2]

Abstract Sea level rise accelerated by climate change is one of the concerns in causing sea water intrusionand salt contamination in surface and ground water as well as soil.Data compilation and synthesis in the past have indicated that the sea levels in the Gulf of Thailand have been rising at 3-5 mm/year. This study evaluated several semivariogram models for the study of spatial distribution of soil salinity in the main central basins of Thailand. Soil salinity tests were carried out in Chao Phraya and Tha Chin lower basins alongside of the Gulf of Thailand. Study area is approximately 4,900 km^2. Soil salinity measurements were performed in 2018 at two levels of depth at 30 and 100 cm. Line transect sampling method was used to determine the location of measuring points. Each of measuring points was about 10 km apart. Totally 40 sampling points across the basins were selected. Suitable semivariogram model was selected from a comparison result of geostatistical analysis. Four models of semivariogram were compared: circular, spherical, exponential and Gaussian. Kriging interpolation method was used to estimating soil salinity values of unknow point. Soil salinity as measured by electrical conductivity (EC) in these areas ranges between 0.02-3.83 dS/m at 30 cm depth and 0.08-4.00 dS/m at 100 cm depth, respectively. There is a clear gradient of soil salinity at both depths; higher along the shore (>2.00 dS/m) and gradually decreases towards inland (0.08-2.01 dS/m at 50-100 km from the coastline). Evaluation of semivariogram model performance reveals that the Gaussian model and exponential model were the best models for estimating the value of soil salinity at 30 cm and 100 cm with root mean square error (RMSE) is 0.92 and 1.10, respectively.

Keywords *soil salinity, kriging, spatial interpolation, Chao Phraya and Tha Chin river basin, sea level rise*

[1]KMUTT Geospatial Engineering and Innovation Center,
King Mongkut's University of Technology Thonburi,Thailand
[2]The Joint Graduate School of Energy and Environment,
King Mongkut's University of Technology Thonburi, Thailand

sming.gt@gmail.com

Introduction

Climate change is an urgent issue that affected many aspects of human life such as public health, diseases, fresh water scarcity, and especially agricultural areas. Importantly, climate change causes an increase of global temperature resulting extreme weather and sea level rise [1]. Sea level rise is one of theconcerns that causing seawater intrusionin land and salt contamination in surface and groundwater as well as soil.

Thailand faces salinity problems in many regions including the northeastern and the central plain, especially salinity in the soil. Soil salinity is the salt content in the soil. Soil salination in Thailand causes by natural processes of the environment such as sea level rise and saltwater encroachment as well as human activity such as salinity intrusion in land from agriculture activities in upstream areas and unsuitable irrigation. Saltwater encroachment is most common in coastal areas, where the freshwater is displaced by the inland movement of saltwater from the sea [2], which also happens in coastal areas along the Gulf of Thailand. The increased of salinity in soil and water (both surface and ground water) would impacts the quality of water for drinking and irrigation with serious economic, social and environmental consequences for both rural and urban communities. [3] [4]

The study of soil salinity in the central regions of Thailand has been limited. Two studies were performed by Arunin (1996) and Takaya (1987) [5][6]. Additionally, there is not enough information about the phenomenon of temporal and spatial change of salinity in the land. To be able to closely monitor a real-time situation of soil salinity, it is necessary to have accurate, standardized and up-to-date supported data. Thus, there is the urgent need for the studies of soil salinity to guide a more efficient soil and water management. One of the common methods used for assessing spatial distribution of soil salinity is geostatistical method. Geostatistics is a class of statistics used to analyze and predict the values associated with spatial or spatiotemporal phenomena. This method describes spatial patterns and interpolates values for locations where samples were not collected [7]. The major key behind geostatistical method is called semivariogram. It is an important process, but also a difficult step of geostatistical analysis. Semivariogram used to determine a suitable model for

experimental values and useful to identify the prediction errors after the process of spatial interpolation for locations where unmeasured.

The propose of this study is to evaluate the appropriate semivariogram model for spatial interpolation of soil salinity in the lower basinof Chao Phraya and Tha Chin river basins where located in the central of Thailand.

Material and methods

A. Study Area

The study was performed in the lower part of Chao Phraya and Tha Chin river basins, located alongside of the Gulf of Thailand.This study area covering eight provinces including Bangkok, Nonthaburi, Nakhon Pathom, PathumThani, Phra Nakhon Si Ayutthaya,SamutPrakan, SamutSakhon and SuphanBuri. It is extended between 13°30'N-14°25'N and 99°40'E-101°5'E covering an area of approximately 4,900 km^2 (Fig.1) andthe distance from shoreline across to the north is around 100 km.The average height in the area is about 9.4 m with a relative height difference is 19 m. This is an important economics area in the central of country, which is dominated by agricultural land and various industries.The location of study areais illustrated in Fig. 1.

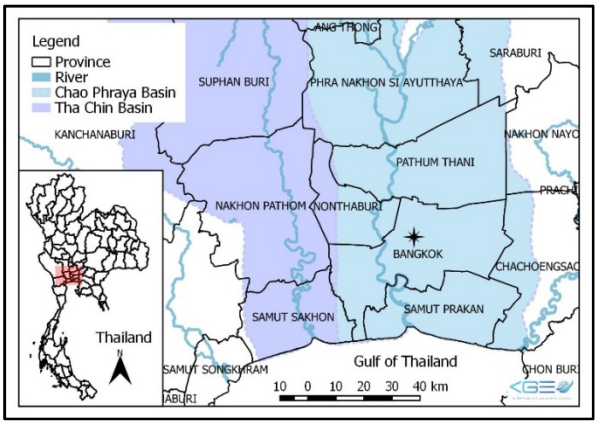

Fig. 1. Location of study area.

B. Data Collection

Soil salinity was assessed by measuring electrical conductivity (EC) in which a high EC value indicates a high salinity level [8] [9]. The EC data were collected in June 2018 at the two levels of depth which are 30 and 100 cm. Reconnaissance soil survey was carried out using LULC data during 2010-2012 and road network as base map. The sampling point were determined using Line transect sampling method [10][11]. Totally 40 soil sampling sites were selected. Each of points is located along the transect line with 10 km apart spreading over the basins as shown in Fig. 2. A handheld global positioning system (GPS) was used to record the location of each sample site. Undisturbed soilsamples at two depths (30 and 100 cm) were collected with 4 soil cores from each site and mixed well into a composite soil sample. Soil electrical conductivity values were measured by using EC meter type Hanna HI98331 and expressed as deci-Siemens per meter (dS/m).

Two series of soil test were carried out in two level of depth. For each series,statistical analyses were preceded by the calculation of basically statistical: mean, standard deviation, kurtosis, skewness, minimum value, median and maximum value.

C. Spatial Interpolation

There are many types of spatial interpolation method, for example, inverse distance weighting (IDW), spline, kriging and trend. However, in the field of soil science and geology, the often and widely used method is kriging interpolation. There are various comparative studies about surface modeling of soil properties, especially electrical conductivity. The results showed clearly that the kriging method is the most efficient to EC estimating [12] [13] [14]. Kriging is a geostatistical interpolation technique that considers both the distance and the degree of variation between known data points when estimating values in unknown areas.Spatial variability in soilsalinity was assessedusing semivariogram model, which is the basic and widely used geostatisticalfunction. This model is given by theformula [15] [16] [17]:

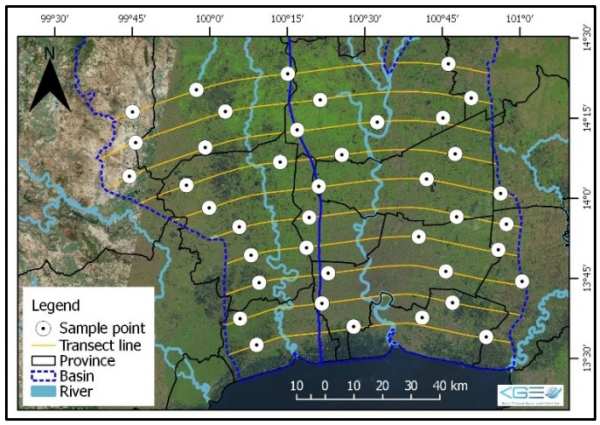

Fig. 2. Transect linesand sample points

$$\gamma(h) = \frac{1}{2N_h}\sum_{i=1}^{N_h}[z(x_i) - z(x_i + h)]^2 \quad (1)$$

where: $\gamma(h)$ is the empirical semivariogram; $z(x_i)$, $z(x_i + h)$ = soil moisture values at sample points x_i and $x_i + h$, spaced apart at distance h; N_h = number of pairs (x_i, $x_i + h$) of soil salinity values at points spaced at distance.These were used for calculating the semivariogram function.

In this study, four functions were compared to model the empirical semivariogram as follows: circular, exponential, spherical and Gaussian. Because some good results have appeared in several kinds of

soil salinity research [17]. Next step, mathematical models which given the best fit for each empirical semivariograms were selected and compared with one another.

The prediction of an unknown point was interpolated using the kriging method[10]. Kriging is a spatial interpolation method of good statistical properties. The initial equation of kriging is given by the formula [18]:

$$\hat{z} = \sum_{i=1}^{n} w_i z_i \qquad (2)$$

where: $\hat{z}$ = predicted value;z_i = sample value at location i; w_i = weight; n = number of sample data.

Assessment of prediction error is an important step used to evaluate interpolation efficiency. The following prediction errors were analyzed: mean, root mean square, mean standardized, root mean square standardized, average standard error. These parameters will help to distinguish the suitable model for this study area.

Results and discussion

Soil salinity were assessed using an electrical conductivity or EC value, unit in this study is deci-Siemens per meter or dS/m. A high EC value indicates a high salinity level. Results of basic descriptive statistics of the EC measurements are shown in Table 1.

Table I. Statistic of electrical conductivity for each series of tests.

Parameter	Series / Depth (cm)	
	1st Series / 30	*2nd Series / 100*
Count	40	40
Mean	1.01	1.49
Standard Error	0.16	0.19
Median	0.70	1.17
Mode	2.62	4.00
Standard Deviation	0.99	1.19
Sample Variance	0.99	1.42
Kurtosis	1.31	-0.08
Skewness	1.38	0.92
Minimum	0.02	0.08
Maximum	3.83	4.00
Sum	40.38	59.73

Statistical analysis presented that the EC values in the first series (30 cmdepth) of soil tests were low salinity than those values found in the second series (100 cmdepth). In addition to the first series of measurements, EC ranged from 0.02 to 3.83 dS/m. The mean of EC values for the first series was 1.01 dS/m. In the second series of soil tests, EC ranged between 0.08 to 4.00 dS/m. Also, the mean value was shifted to 1.49 dS/m higher than the first series of soil tests.The standard deviation calculated for the second series was 1.19 which is higher than the values obtained in the first series (0.99). Accordingly, the sample variance of second series were more varied than the first series of measurements, value is 1.42 and 0.99 respectively. The median of the calculated parameter of both series was similar lower than the arithmetic meanof each series, which is represents that EC values measured were asymmetrically distributed. This is related to the coefficient of skewness. Furthermore, both series of EC measurements had positively skewed data distribution (skewness > 0).

According to the study of semivariogram, spatial relationshipswere studied. This tool describesthe variationbetween measured pointsdepending on the distance between them. Prior thesemivariogram was generated, the trends which appeared in both EC data series were removed. The followingfunctions were used to model the semivariograms: circular exponential, spherical and Gaussian.

The semivariograms obtained for the first series of EC measurements and the estimate of semivariograms using theoretical models were illustrated in Fig.3. Table 2 presented the semivariogram properties of each model.

In the first series, analysis of the semivariogram graphs showed that the range of spatial autocorrelation was similar for all models. On the other hand, nugget and sill are different. The nugget was lowest in the exponential model but highest in the Gaussian model. The sill was lowest in the exponential model but highest in the circular model.

In the second series,the semivariogram were shown in Fig. 4 and the properties of the semivariogram models were shown in table 2. The properties of the spatial autocorrelation range were between 40,383 and 47,437.04 m. The lowest range was found in the circular model,but the highest range was found in the exponential model. The lowest nuggetappeared in the exponential model, whereas the highest nugget appeared in the Gaussian model. The sill was lowest in the Gaussian model but highest in the exponential model.

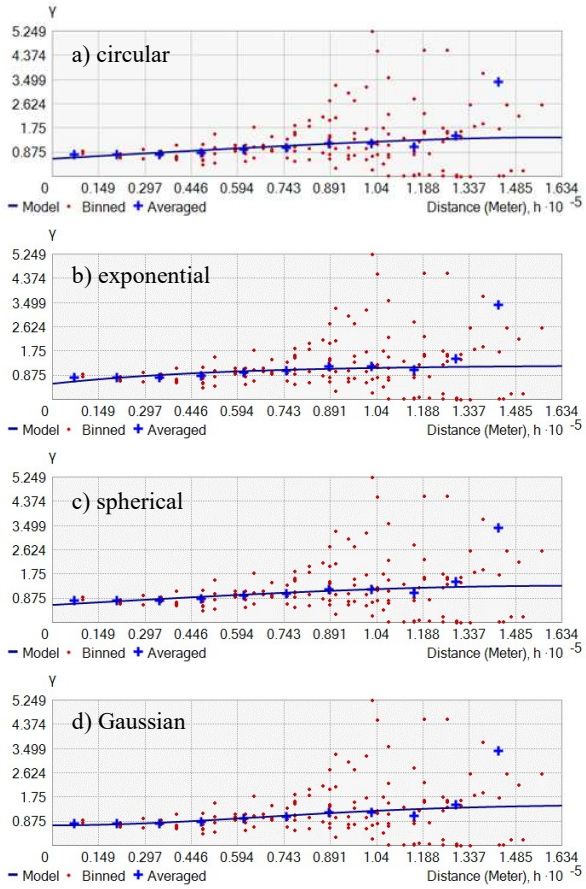

Fig. 3. Semivariogram of electrical conductivity assigned for the first series (depth, 30 cm) of soil tests and their approximate theoretical models: a) circular, b) exponential, c) spherical and d) Gaussian.

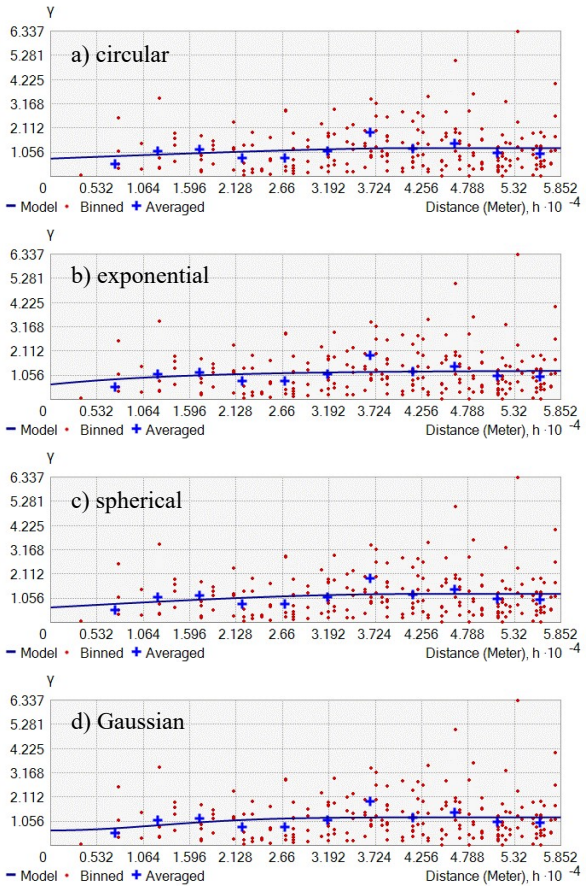

Fig. 4. Semivariogram of electrical conductivityassigned for the second series (depth, 100 cm) of soil tests and their approximate theoretical models: a) circular, b) exponential,c) spherical and d) Gaussian.

Table II. Properties of the semivariogram models of EC withboth levels of depth.

Series / Depth	Model	Nugget	Sill	Range
1st series / 30 cm	Circular	0.64	0.76	163,371.19
	Exponential	0.57	0.67	163,371.19
	Spherical	0.63	0.69	163,371.19
	Gaussian	0.73	0.74	163,371.19
2nd series / 100 cm	Circular	0.78	0.46	40,383.17
	Exponential	0.66	0.60	47,437.04
	Spherical	0.77	0.47	43,921.68
	Gaussian	0.89	0.35	43,008.99

Table III. Prediction errors for selected semivariograms models.

Depth	Prediction error	Semivariogram Model			
		Cir	*Sph*	*Exp*	*Gau*
30 cm.	Mean	-0.008	-0.008	-0.007	-0.010
	Root Mean Square	0.935	0.937	0.955	0.917
	Mean Standardized	-0.007	-0.007	-0.006	-0.009
	RMS Standardized	1.029	1.032	1.044	1.008
	Average Standard Error	0.907	0.907	0.913	0.908
100 cm.	Mean	-0.004	-0.006	-0.001	0.002
	Root Mean Square	1.118	1.108	1.099	1.101
	Mean Standardized	0.001	-0.001	0.002	0.005
	RMS Standardized	1.037	1.026	1.013	1.017
	Average Standard Error	1.074	1.076	1.083	1.079

[a.] Cir = circular, Sph = spherical, Exp = exponential, Gau = Gaussian

The calculation results of the prediction error for those two series of EC measurements were shown in Table 3.In the first series, the distinguishes of smallest values of root mean square error (RMSE) and root mean square standardized error (RMSD) at the measurement points were observed for the Gaussian model (RMSE = 0.917, RMSD= 1.008).The biggest of RMSE was found in the exponential model (0.955). These results suggested that the Gaussian model is a suitable choice for data interpolation in this case.

For the second series, the exponential model provided the lowest values of RMSE and RMSD which were 1.099 and 1.013,respectively. These results suggested that the exponential model is the most suitable model for studying soil salinity study at the 100 cm depth.

The spatial distribution of salinity level in soil was studied by EC data as explained before. Electrical conductivity in the unmeasured area was estimated using the widely employed geostatistical method called kriging interpolation [7][13]. Those two measured data series were used to generate the distribution of EC for each selected semivariogram model.

The spatial interpolation results of both series are illustrated in Fig. 5 and Fig. 6.There is a clear gradient of soil salinity at both depths; higher along the shore (EC >2.00 dS/m) and gradually decreases towards inland (EC 0.08-2.01 dS/m at 50-100 km from the coastline).When the salinity distributions from those two series of measurements are compared (Fig. 7),some similar spread trends of salinity were observed.

The salinity in soil at 30 cm depth gradually decreases from south to north (coastline to land).In 30 cm depth, the EC value in Tha Chin river mount is higher than Chao Phraya river mount. This value is the same trend withsalinity in the river from the report of water quality by Pollution Control Department that measured at the same time [15]. And of course, it might be the effect by the location of field survey points. Because of, this study focus on collect the soil samples on crop areas. That means no information from the sample location in Bangkok city center.

As shown in Fig. 2 (study area and sample points),those space that has no sample points and either the influence of longer distance between sample points in the left side and right side of Chao Phraya river. On the other hand, there are extremely increases of salinity intrusion towards in the land at 100 cm depth level.Especially in the area between the two rivers. The result shows hotspot in the border between Nonthaburi and Pathum Thani provinces, which is the rice paddy field growing areas. As shown in Fig.7, kriging result for each series which is lowest errors were compared.

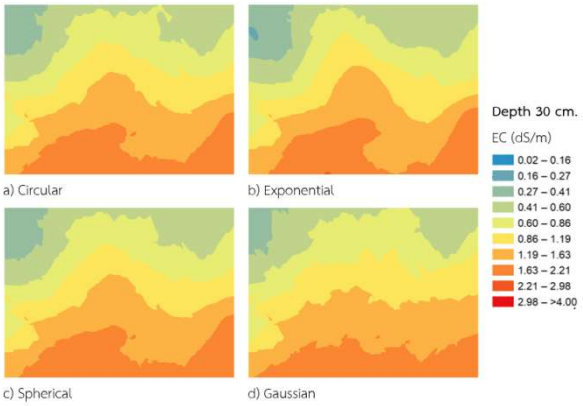

Fig. 5. The distributions of electrical conductivity in the first series of measurements (30 cm - depth), interpolated by ordinary kriging base on semivariogram models: a) circular, b) exponential, c) spherical and d) Gaussian

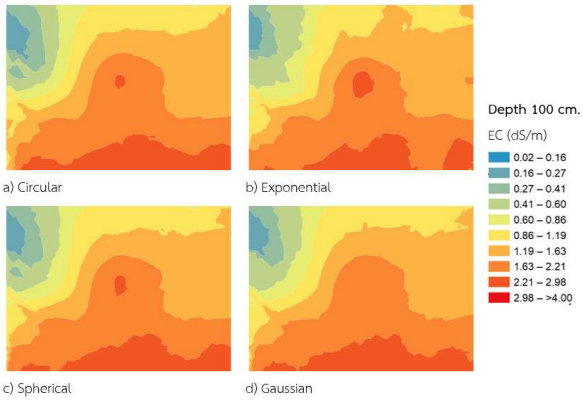

Fig. 6. The distributions of electrical conductivity in the second series of measurements (100 cm - depth), interpolated by ordinary kriging base on semivariogram models: a) circular, b) exponential, c) spherical and d) Gaussian

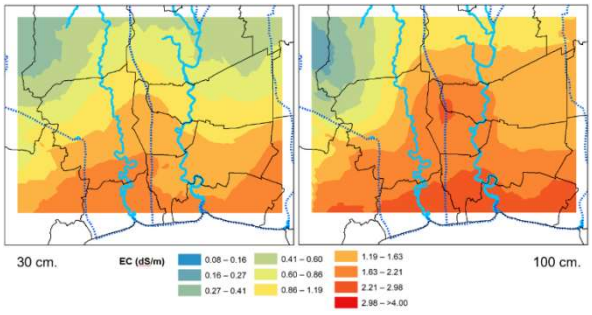

Fig. 7.A comparison of kriging results with the lowest errors model per series of EC measurements: a) Gaussian model at 30 cm. depth, and b) exponential model at 100 cm. depth.

Conclusions

This study is one part of our soil salinity research project that purpose to assessing the spatial and temporal changes of soil salinity in Chao Phraya and Tha Chin lower basins using geostatistical method. The results in thisstudy are the preliminary process to study the spatial variation of soil salinity in this study area. Aims to select the appropriate equation or model for spatial interpolation for all datasets.

Among the four models of semivariogram analyzed in this study, Gaussian and exponential models provided the lowest errors in estimating the unknown values of soil salinity relative to the empirical data. In should be noted that soil is a non-homogeneous object and diverse mixture with many particles. In the fieldwork, we found different EC values from nearby points, which highlight the important of selected location for data collection. These criteria could influence the samples data variance. Taking together, there is no perfect model for any datasets. The suitable model should have minimized differences in residuals between experimental and theoretical semivariograms.

Acknowledgment

This research was undertaken as part of the research programentitled "Evaluating salinity in river water and soil associated with climate change in Chao Phraya and Tha Chin river basins." Funding support for this study was provided by Biodiversity-Based Economy Development Office (Public Organization) (BEDO) and National Research Council of Thailand(NRCT). We are grateful to the Faculty of Science, King Mongkut's University of Technology Thonburi (KMUTT)for their place and equipmentsupport during the realization of this project.The opinions expressed here belong to the authors, and do not necessarily reflect those of BEDO, NRCT or KMUTT.

References

[1] S. Naruchaikusol, "Climate change and its impact in thailand. a short overview on actual and potential impacts of the changing climate in southeast asia," TransRe Fact Sheet, no. 2, Department of Geography, University of Bonn, Bonn, June 2016.

[2] B. D. Hoyle, "Saltwater Encroachment." Climate Change: In Context, Encyclopedia.com, November 3, 2018. [https://www.encyclopedia.com/environment/energy-government-and-defense-magazines/saltwater-encroachment]

[3] Department of Groundwater Resources, Project report of the groundwater observation network to groundwater monitoring, Department of Groundwater Resources, Bangkok, Thailand, 2015.

[4] Queensland Government, "Impacts of salinity," December 8, 2016. [https://www.qld.gov.au/environment/land/management/soil/salinity/impacts]

[5] S. Arunin, Salt affected soil in Thailand, Land Development Department (LDD), Bangkok, 1996.

[6] Y. Takaya, Agricultural Development of a Tropical Delta: A Study of Chao Phraya Delta, Univ. of Hawaii Press, Honolulu, 1987.

[7] ESRI, "Introduction to Geostatistical Analyst," Pro.arcgis.com, November 3, 2018. [http://pro.arcgis.com/en/pro-app/help/analysis/geostatistical-analyst/what-is-geostatistics-.htm]

[8] Y. Shirokova, I. Forkutsa and N. Sharafutdinova, "Use of electrical conductivity instead of soluble salts for soil salinity monitoring in Central Asia." Irrigation and Drainage Systems, 14, 2000, pp.199–205.

[9] J.D. Rhoades, F. Chanduvi and S. Lesch, Soil Salinity Assessment: Methods and interpretation of electrical conductivity measurements, Food and Agriculture Organaization of the United Nations (FAO), Rome, Italy, 1999.

[10] Zheng, Zhong, F. Zhang, F. Ma, X. Chai, Z. Zhu, J. Shi, and S. Zhang, "Spatiotemporal Changes in Soil Salinity in a Drip-Irrigated Field," Geoderma, 2009. [Doi:10.1016/j.geoderma.2008.12.002]

[11] S. Miyamoto and A. Chacon, "Soil Salinity of Urban Turf Areas Irrigated with Saline Water II Soil Factors," Landscape and Urban Planning, 2006. [Doi:10.1016/j.landurbplan.2004.12.011]

[12] G. S. Bhunia, P. K. Shit and R. Maiti, "Comparison of gis-based interpolation methods for spatial distribution of soil organic carbon (soc)," Journal of the Saudi Society of Agricultural Sciences, 17, pp.114-126, 2018.

[13] W.J. Shi, T.X. Yue and Z.M. Fan, "An overview of high accuracy surface modeling of soil,"

Procedia Environmental Sciences, 13, pp.2304-2309. 2012.

[14] H. K. Poshtmasari, Z. T. Sarvestani, B. Kamkar, S. Shataei and S. Sadeghi, "Comparison of interpolation methods for estimating pH and EC in agricultural fields of Golestan province," Intl J Agri Crop Sci., vol. 4 (4), pp.157-167, 2012.

[15] R.A. Olea, Geostatistics for engineers and earth scientists, Boston. Springer, 1999, pp. 303. [ISBN 978-0-7923-8523-3]

[16] R. Webster , M. A. Oliver, Geostatistics for environmental scientists, 2nd Ed., John Wiley & Sons, 2007, pp. 271. [ISBN 978-0-470-02858-2]

[17] R. Obrośląk and O. Dorozhynskyy, "Selection of a semivariogram model in the study of spatial distribution of soil moisture," Journal of Water and Land Development, no. 35, pp. 161-166, 2017. [DOI: 10.1515/jwld-2017-0080].

[18] P. J. Diggle, J. A. Tawn and R. A. Moyeed, "Model-based geostatistics," Appl. Statist., 47, Part 3, 1998, pp. 299-350.

[19] Polution Control Department, Weekly Water Quality Report (June 2018),Ministry of Natural Resources and Environment, Bangkok, Thailand, 2018.

Distribution of Polycyclic Aromatic Hydrocarbons (PAHs) in Soils from King George Island, Antarctica

Woranuch Deelaman[1,a], Siwatt Pongpiachan[2,b], Natthapong Iadtem[1,c], Danai Tipmanee[3,d] and Oramas Suttinun[1,e]

Abstract Polycyclic aromatic hydrocarbons (PAHs) are categorized as POPs and have been globally characterized in different terrestrial soils. PAHs in soils have been widely concerned because of its carcinogenicity and mutagenicity. PAHs have high hydrophobic property and strong partitioning with particle surfaces and thus can be accumulated in soils for comparatively long period. To date, the numbers of publication associated with PAHs in terrestrial soils collected from Antarctica are strictly limited. This study aimed to conduct both qualitative and quantitative analysis of 15 PAHs which include Phenanthrene, Anthracene, Flouoranthene, Pyrene, 11HBenzo[a] Fluoranthene, 11HBenzo[b]Fluoranthene, Benzo[a]Anthracene, Chrysene, Benzo[b]Fluoranthene, Benzo[k]Fluoranthene, Benzo[a]Pyrene, Benzo[e]Pyrene, Benzo[g,h,i]Perylene, Dibenzo[a,h]Anthracene, and Indeno[1,2,3-cd]Pyrene in soil samples from King George Island, Antarctica. The samples were extracted by using soxhlet extractor with dichloromethane (DCM) and then fractionized by using solvents of different polarities. In this study, Gas Chromatograph-Mass Spectrophotometer (GC-MS Shimadzu QP2010) was carefully selected for determination of PAHs. The total concentrations of 15 PAHs (∑15PAHs: a sum of Phe, An, Fluo, Pyr, 11H-B[a]F, 11H-B[b]F, B[a]A, Chry, B[b]F, B[k]F, B[e]P, B[a]P, Ind, D[a,h]A, B[g,h,i]P) ranged from 1.88 to 195.53 ng g^{-1} with an average of 37.37± 62.47 ng g^{-1}. PAH concentrations detected in King George Terrestrial Soils (KGS) were appreciably lower than those of World Terrestrial Soils (WTS) due to the fact that Antarctica is one of the most pristine continents in the world.

Keywords *Polycyclic Aromatic Hydrocarbons (PAHs), Soils, King George Island*

[1]Faculty of Environmental Management,
Prince of Songkla University
Hatyai, Songkhla
[2]Faculty of Social and Environmental Development
National Institute of Development Administration (NIDA)
Bangkapi, Bangkok
[3]Faculty of Technology and Environment, Prince of Songkla University
Kathu, Phuket

[a]Woranuch.dpm@gmail.com
[b]pongpiajun@gmail.com
[c]Natthapongiadtem@hotmail.com
[d]dtipmanee@hotmail.com
[e]oramas.s@psu.ac.th

Introduction

Over the past few decades, the impact of industrialization on dispersions of persistent organic pollutants (POPs) has been globally investigated in different continents. In 2001, Stockholm Convention on POPs was officially agreed as an international environmental treaty and signed by 128 countries. Polycyclic aromatic hydrocarbons (PAHs) belong to a group of persistent organic pollutants (POPs). These are a large group of organic compounds that are white or pale yellow solids, mostly colorless, and highly lipophilic [1, 2, 3]. PAHs are composed of hydrogen and carbon atoms in the form of fused benzene rings. Chemically, the PAHs are comprised of two or more benzene rings bonded in linear, cluster, or angular arrangements. Some well-known PAHs such as carcinogens, mutagens, and teratogens have toxic effect on organisms through various actions; therefore, they have been classified as priority pollutants by the US Environmental Protection Agency (US EPA) and by the European community.

PAHs are released into the environment from both natural and anthropogenic sources. They can be formed through biological processes or are the products of naturally-occurring incomplete combustion such as volcanic eruption or forest fires. Anthropogenically, they can derive from the combustion of materials for energy such as wood, gas, oil, or coal. In industrial and urban environments, PAHs are mostly released from anthropogenic sources such as smoking, thermal power stations, traffics, domestic heating, industrial emissions, etc. [3, 4, 5]

Over the past century, industrial development caused a significant increase of PAHs concentration in the environment. The results of PAHs analysis in the ice core's content from Greenland indicate that the present levels of these compounds are about 50 times higher than in pre-industrial periods [9]. PAHs can be transported over long distances when emitted into the atmosphere before they are deposited by atmospheric precipitation onto soils (major source for deposited PAHs), vegetation, rivers, and oceans. The removal of PAHs in the atmosphere is by the wet and dry deposition processes. Over the past decades, there have been very few studies of the PAHs concentration in Antarctica due to the continent's difficult accessibility. Their results only indicate that the major sources of PAHs were from the incomplete combustion of gasoline used in passenger cars [6]. Therefore, the aim

of this research is to further study the PAHs concentration in Antarctica by conducting both qualitative and quantitative analysis of 15 PAHs in soil samples from King George Island.

Materials and methods

A. Study Areas

Terrestrial soil samples were collected from 22sampling stations in the Southwestern part of King Gorge Island in Antarctica during January to February 2016 (Fig.1) from the depth of 0-10 cm. The coordinates of sampling sites are given in Table 1.King Gorge Islandis the largest of the South Shetland Islands (62°02'00.0"S- 58°21'00.0"W) with the area of 1150 km^2

B. Sample Collection and Storage

Terrestrial soil samples were wrapped in pre-cleaned aluminum foil, placed in glass bottles, and kept frozen (−20 ° C) until analysis to avoid sample degradation caused by heat, ozone, NO_2, and ultraviolet (UV) during transportation.They were then freeze-dried prior to being grounded to homogenize the samples.

C. PAHs Analysis

PAHs sample extraction, purification, analysis, and quality control were conducted according to the method described by Pongpiachan et al. (2017) [6]. In brief, 30 grams of terrestrial soil samples were extracted using organic solvents (DCM) of HPLC grade, and then performed by using 250ml of soxhlet extractors for 8 hours. The fractionation/clean-up technique was done by solid-phased extraction on to a silica gel column and finally concentrated to exactly 0.1 mL by a gentle stream of N_2 at room temperature (25°C). The samples were sealed in vials and stored at 4°C prior to analysis for the individual PAH, and quantified by Gas Chromatography with the optimization of mass spectrometric setting for both qualitative and quantitative identification of PAHs. All procedures followed the methods of Pongpiachan et al. (2009) [7].

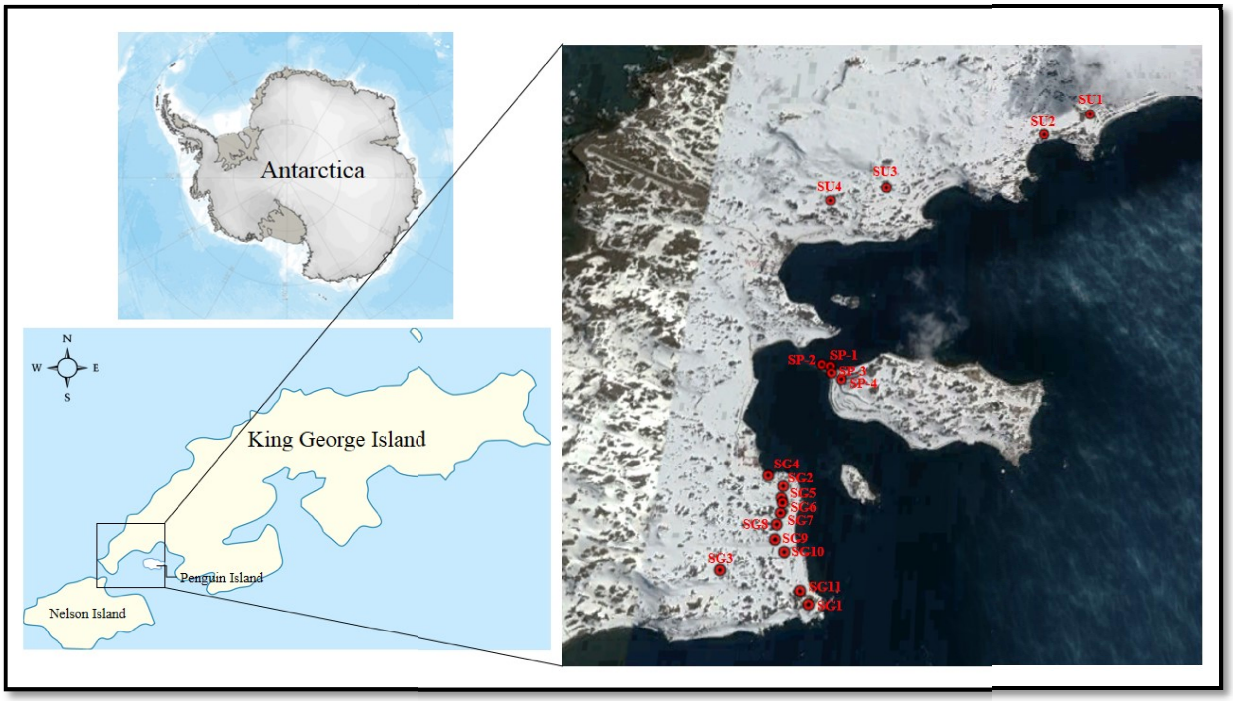

Fig. 1. Sampling sites of the King Gorge Island in Antarctica.

Table 1. Study areas and sampling sites description.

Sample Point	Site Name	Latitude	Longitude
SU1	Close to Uruguai Station	62°11'06.4"S	58°54'22.4"W
SU2	Close to Uruguai Station	62°11'14.5"S	58°54'53.0"W
SU3	Close to Uruguai Station	62°11'34.9"S	58°56'34.4"W
SU4	Close to Uruguai Station	62°11'39.7"S	58°57'09.3"W
SP1	Around Penguin Island	62°12'36.3"S	58°56'59.1"W
SP2	Around Penguin Island	62°12'35.7"S	58°57'04.2"W
SP3	Around Penguin Island	62°12'38.4"S	58°56'58.0"W
SP4	Around Penguin Island	62°12'40.4"S	58°56'52.0"W
SG1	Around Great Wall Station	62°13'43.1"S	58°56'58.3"W
SG2	Around Great Wall Station	62°13'11.9"S	58°57'18.5"W
SG3	Around Great Wall Station	62°13'34.3"S	58°57'47.1"W
SG4	Around Great Wall Station	62°13'08.9"S	58°57'27.6"W
SG5	Around Great Wall Station	62°13'15.1"S	58°57'18.9"W
SG6	Around Great Wall Station	62°13'16.5"S	58°57'17.9"W
SG7	Around Great Wall Station	62°13'19.3"S	58°57'18.4"W
SG8	Around Great Wall Station	62°13'22.4"S	58°57'19.8"W
SG9	Around Great Wall Station	62°13'26.4"S	58°57'19.8"W
SG10	Around Great Wall Station	62°13'29.7"S	58°57'14.0"W
SG11	Around Great Wall Station	62°13'39.7"S	58°57'03.5"W

Results and discussion

A. Occurrence of PAHs in terrestrial soils.

The concentrations of PAHs obtained from terrestrial soil samples from King Gorge Island are reported in Table 2. A total concentration of 15 PAHs (∑15PAHs: a sum of Phe, An, Fluo, Pyr, 11H-B[a]F, 11H-B[b]F, B[a]A, Chry, B[b]F, B[k]F, B[e]P, B[a]P, Ind, D[a,h]A, B[g,h,i]P) in terrestrial soil samples were identified and quantified. The total concentration of PAHs (∑15PAH) ranged from 1.88 to 195.53 ng g^{-1} with an average of 37.37± 62.47 ng g^{-1}. Considering only the twelve probable carcinogenic PAHs (∑PAHs: a sum of Phe, An, Fluo, Pyr, B[a]A, Chry, B[b]F, B[k]F, B[a]P, Ind, D[a,h]A and B[g,h,i]P), the total concentration were 1.86 to 193.69 ng g^{-1}or 36.96± 61.89 ng g^{-1} on average. Overall, the sample points SU2, SG2, SG3, SU3, SG4, and SU1 had higher ∑15PAH concentration with values 193.69, 181.86, 134.16, 65.18, 34.56, and 19.32 ng g^{-1} respectively, while others had concentration valuesthat are less than or equal to 10 ng g^{-1}.

Table 2.PAHs concentration in the sediment of the King Gorge Island in Antarctica expressed in ng g^{-1}

Compound	SU1	SU2	SU3	SU4	SP1	SP2	SP3	SP4	SG1	SG2	SG3	SG4	SG5	SG6	SG7	SG8	SG9	SG10	SG11
Phe	4.33	1.06	5.45	0.58	1.02	1.61	1.55	2.36	1.29	0.91	9.17	4.25	1.09	1.49	1.72	1.42	1.78	1.06	0.65
An	0.13	0.12	0.28	0.04	0.03	0.09	0.07	0.12	0.06	0.07	0.20	0.45	0.05	0.09	0.08	0.06	0.09	0.06	0.03
Fluo	0.61	0.45	1.77	0.20	0.26	0.29	0.38	0.39	0.51	0.47	4.12	3.85	0.49	0.54	0.54	0.48	0.53	0.41	0.14
Pyr	0.45	0.54	1.62	0.15	0.27	0.33	0.32	0.32	0.81	0.67	3.29	4.20	0.40	0.47	0.45	0.47	0.50	0.37	0.13
11H-B[a]F	0.10	0.67	0.17	0.02	0.06	0.14	0.02	0.01	0.11	0.51	0.98	0.61	0.04	0.08	0.06	0.08	0.03	0.07	0.01
11H-B[b]F	0.05	1.16	0.10	0.05	0.01	0.03	0.02	0.04	0.09	0.87	0.87	0.47	0.01	0.03	0.02	0.02	0.02	0.01	0.01
B[a]A	0.03	0.10	0.43	0.03	0.01	0.04	0.03	0.01	0.04	0.08	0.26	1.75	0.08	0.06	0.05	0.07	0.05	0.04	0.01
Chry	0.95	122.96	4.78	5.44	0.08	0.21	0.21	0.04	6.00	90.13	102.26	5.53	0.20	0.21	0.85	0.35	0.33	0.15	0.06
B[b]F	2.29	28.90	7.81	0.74	1.34	0.01	0.98	1.59	0.44	15.40	4.72	3.06	0.31	0.06	0.47	0.06	0.42	0.06	0.12
B[k]F	1.00	0.82	1.73	0.16	0.16	0.08	0.64	0.00	0.35	12.19	1.52	0.82	0.23	0.20	0.31	0.18	0.34	0.09	0.04
B[e]P	0.70	1.70	4.21	0.55	0.08	0.05	0.31	1.06	0.09	3.14	0.67	3.74	0.15	0.12	0.38	0.12	0.27	0.05	0.04
B[a]P	7.61	35.85	31.68	2.70	3.65	0.04	2.13	1.12	0.59	56.02	7.18	2.14	1.23	0.22	1.09	0.17	0.85	0.15	0.58
Ind	0.61	N.D.	2.48	0.16	0.08	0.02	0.20	N.D.	0.06	1.46	0.36	1.55	0.11	0.06	0.05	0.04	0.07	0.02	0.02
D[a,h]A	0.08	N.D.	0.94	0.04	0.15	N.D.	0.19	N.D.	N.D.	N.D.	N.D.	0.68	0.03	0.02	0.01	0.01	0.03	0.01	N.D.
B[g,h,i]P	0.53	1.19	2.01	0.12	0.11	0.06	0.41	N.D.	0.07	1.33	0.43	2.53	0.16	0.11	0.18	0.14	0.27	0.04	0.04
Σ15PAHs	19.48	195.53	65.45	10.97	7.30	2.99	7.46	7.06	10.52	183.25	136.02	35.64	4.58	3.75	6.27	3.67	5.58	2.58	1.88

*N.D. = not detected

The PAHs can be classified according to their molecular structure, characterized by the number of rings. There are PAHs with three rings (Phe and An), four rings (Fluo, Pyr, 11H-B[a]F, 11H-B[b]F, B[a]A, Chry), five rings (B[b]F, B[k]F, B[e]P, B[a]P, D[a,h]A) and six rings (Ind, B[g,h,i]P). The results showed that the four-ring and five-ring PAHs are the most abundant in terrestrial soils of the King Gorge Island, as shown in Fig.2. The abundance of four ring compounds ranged from 9.5 to 82.17% and five rings from 6.06 to 73.55%. Sample points SG3 and SG1 exhibited the greatest levels of four ring compounds, with 82% and 72% of total PAHs respectively. Among the low molecular weight PAHs (LMV PAHs, having 3-4 aromatic rings) found, the highest concentrations were observed for Chry, Phe, Fluo and Pyr with average concentrations of 17.93, 2.25, 0.86 and 0.83 ng g^{-1} respectively. These LMW PAHs are derived from burning of coal and other biomass at low temperatures. Materials like oil or gasoline which burn at high temperatures produce high molecular weight PAHs (HMW PAHs, having 5 and 6 aromatic rings). In the

terrestrial soil of the studied areas, the average percentage of LMW PAHs to total PAHs ranged from 23.62% to 35.95%, while HMW PAHs had the average percentages of 36.49% and 3.91%, for five and six aromatic rings respectively.

B. PAH Sources

The main sources of PAHs contamination in terrestrial soil of the King Gorge Island can be classified into pyrolytic or petrogenic processes. A pyrolytic process is an incomplete combustion of biomass or fossil fuels, while a petrogenic process involves the slow maturation of organic substances as a result of a leakage of crude oil.

The PAHs sources can be identified by using the diagnostic ratios for pairs of the same molecular mass. To ascertain the sources of PAHs in King Gorge Island, diagnostic ratios of the isomer pairs were used. Ratios An/ (An + Phe) versus Fluo/ (Fluo + Pyr) and B[a]A/ (B[a]A + chry) versus Fluo/ (Fluo + Pyr) were then plotted (Fig. 3). The An/ (An + Phe) and B[a]A/ (B[a]A + chry) relationship allowed characterizing samples into three sources: petroleum, mixed, and combustion, as shown in Fig. 3a and b. The horizontal axis with the ratio Fluo/ (Fluo + Pyr) allowed characterizing samples into three classes: underburned petroleum, petroleum and the combustion of grass, wood and coal.

The relations of An/ (An + Phe) and B[a]A/ (B[a]A + chry) also allowed characterizing samples into three sources: petroleum, mixed, and combustion, as shown in Fig. 3a and b. The horizontal axis with the ratio Fluo/ (Fluo + Pyr) also allowed characterizing samples into three classes, underburned petroleum, petroleum and the combustion of grass, wood and coal. The sample SU2 whose PAHs source arisen from the pyrolytic process is shown in the Fig. 3a and b. Samples SG2, SG4, SP1, SP2 and SU2 contained PAHs from petroleum combustion, while SU1, SU3, SU4, SP3, SP4, SG3, SG4, SG5, SG6, SG7, SG8, SG9, SG10 and SG11 contained PAHs from biomass combustion processes (wood/grass). Finally, the PAH from sample SG1 had a source that originated from oil spills. This proved that there were a variety of pollution sources which affected the samples. Overall, the results indicated that PAHs in almost all stations have their sources mainly from pyrolytic process. The samples arising from this process (SP1, SP2, SU1, SU2, SU3, SU4, SP3, SP4, SG2, SG3, SG4, SG5, SG6, SG7, SG8, SG9, SG10 and SG11) were the ones that had the highest total content of PAHs, while the sample affected bypetrogenic source (SU2) presented the highest total levels of PAHs.The origin of pyrolytic process is due to incomplete combustion of grass, wood, coal and fossil fuels. The surrounding area of King George Island has research stations from several countries. On February 25th, 2012, a fire occurred at the Brazilian Antarctic Station (The Comandante Ferraz Antarctic Station Fire: 62°100 S; 58°240 W) located in Admiralty Bay [8]. Since then, several other studies have indicated Chry, a major component of biomass and fossil fuels including diesel exhaust particles (DEP), as the major PAH.

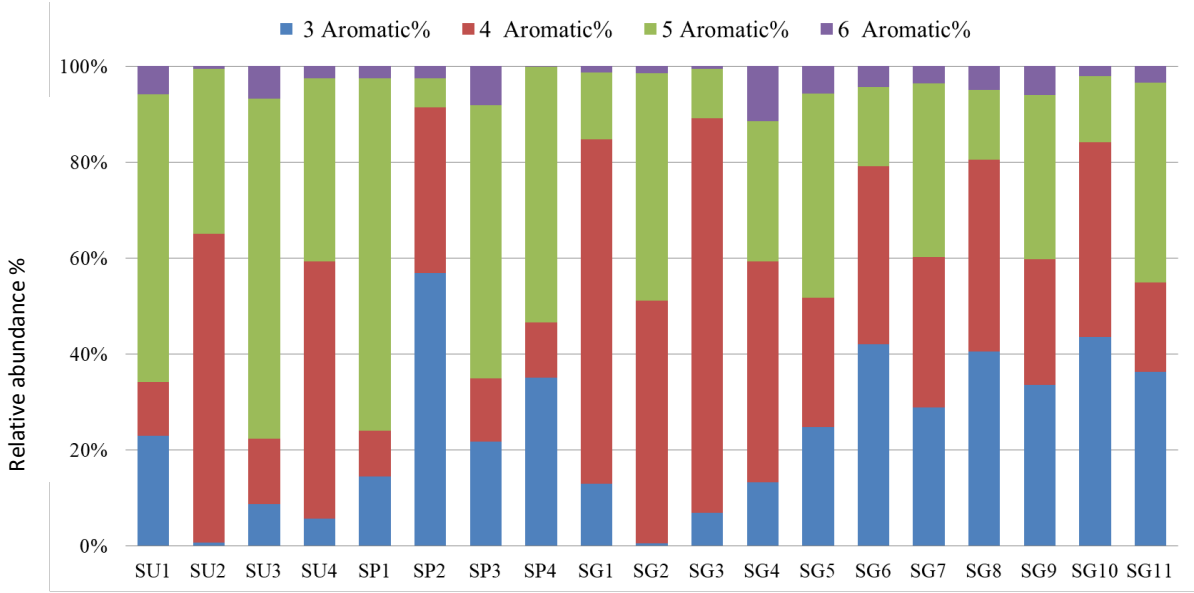

Fig. 2. Distribution patterns (%) and classification of 3-6 ring PAHs in the Terrestrial soil of soil in King Gorge Island

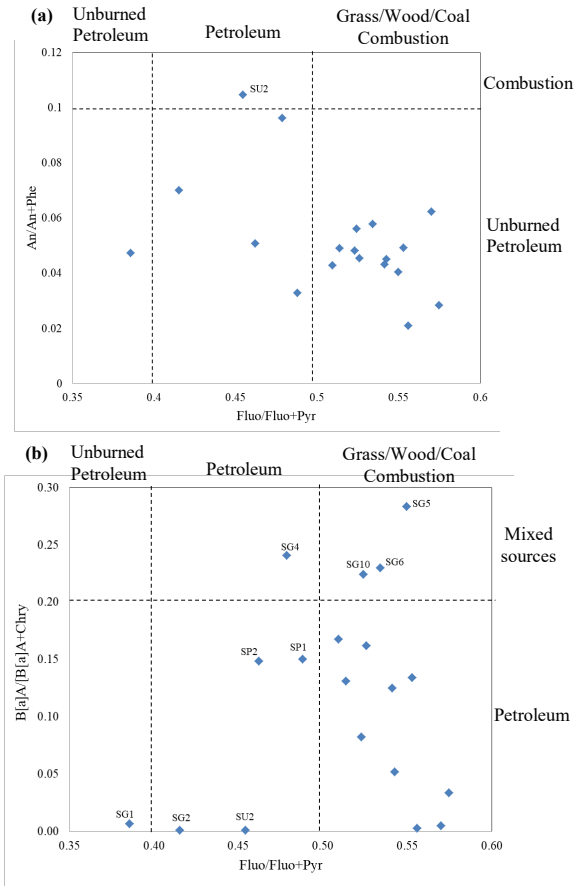

Fig. 3. Cross-plots for the ratios: (a) An/ (An + Phe) versus Fluo/ (Fluo + Pyr), (b) (B[a]A (B[a]A + chry) versus Fluo/ (Fluo + Pyr) Terrestrial soil samples from soil in King Gorge Island.

Of all the sample points except for SU2, the comparatively high percentage contribution of Chry, Phe and B[a]P observed in KGS can be attributed to the virtualization of diesel fuel and the use of biomass and oil fuels of the research station, and the use of fuels for power plants on King George Island. In addition, PAHs can also be transported by long-range atmospheric transport (LRAT) from nearby areas and continents.

The sample point SG1 is near the coast, being more susceptible to contamination from oil spill (unburned fuel). The Antarctica is gaining more attention, resulting in an increase of Antarctic tourism over the past three decades. This caused many scientists to become more concerned about the impact of tourism to the area.The increase of vehicles and boats from recreational activities is the main cause of contamination.So, it is reasonable to determine the source of PAHs to the spill of petroleum products such as gasoline, diesel fuel, lubricating oil, in their raw/unburned forms.

Conclusions

The total 15 PAHs in terrestrial soil samples from King George Island have been determined. The concentration ranged from 1.88 to 195.53 ng g^{-1}. The compounds with four and five rings were the prevalent, representing an average of 36% of all the detected PAHs. The PAHs diagnostic ratios of pollution emission indicated the coexistence of petrogenic and pyrolytic processes. However, the sources of most pollutants were pyrolytic, resulting from the combustion processes of biomass and refined oil products, with negligible contributions from petrogenic sources.

Acknowledgments

The authors acknowledge the Information Technology Foundation under the Initiative of Her Royal Highness Princess Maha Chakri Sirindhorn, Polar Research Project under the Initiatives of Her Royal Highness Princess Maha Chakri Sirindhorn, National Science and Technology Development Agency, Chinese Arctic and Antarctic Administration, and Division of Environmental Science and Technology, Faculty of Science and Technology, Rajamangala University of Technology Phra Nakhon for supporting this study.

References

[1] B.G. Armstrong, E. Hutchinson, J. Unwin, T. Fletcher, "Lung Cancer Risk after Exposure to Polycyclic Aromatic Hydrocarbons: A Review and Meta-Analysis," Environ Health Perspect, vol. 112 (9), pp. 970–978, June 2004.

[2] CCME (Canadian Council of Ministers of the Environment), "Canadian soil quality guidelines for potentially carcinogenic and other PAHs," scientific criteria document, CCME:Winnipeg, 2010.

[3] HI. Abdel-Shafy, MS.M.Mansour, "A review on polycyclic aromatic hydrocarbons: Source, environmental impact, effect on human health and remediation," Egyptian Journal of Petroleum, vol.25, pp. 107–123, March 2016.

[4] B. Maliszewska-Kordybach, "Sources, Concentrations, Fate, and Effects of Polycyclic Aromatic Hydrocarbons (PAHs) in the Environment. Part A: PAHs in Air," Polish Journal of Environmental Studies. Vol. 8, No. 3, pp 131-136. February 1999.

[5] S. Pongpiachan, D. Tipmanee, C. Khumsup, I. Kittikoon, P. Hirunyatraku, "Assessing risks to adults and preschool children posed by PM2.5-bound polycyclic aromatic hydrocarbons (PAHs) during a biomass burning episode in Northern Thailand". Sci. Total Environ. Vol.508, pp. 435–444. March 2015.

[6] S. Pongpiachan, M. Hattayanone, O. Pinyakong, V. Viyakarn, S.A. Chavanich, C. Bo, C. Khumsup, I. Kittikoon, P. Hirunyatrakul, "Quantitative ecological risk assessment of inhabitants exposed to polycyclic aromatic hydrocarbons in terrestrial soils of King George Island, Antarctica," Polar Science, Vol.11, pp. 19-29, 2017.

[7] S. Pongpiachan, S. Bualert, P. Sompongchaiyakul, C. Kositanont, "Factors affecting sensitivity and stability of polycyclic aromatic hydrocarbons," Anal.Lett, Vol.42 (13), pp. 2106-2130. September 2009.

[8] F.I. Colabuono, S. Taniguchi, C.V.Z. Cipro, J. da Silva, M.C. Bícego, R.C. Montone, "Persistent organic pollutants and polycyclic aromatic hydrocarbons in mosses after fire at the Brazilian Antarctic Station," Mar. Pollut. Bull, Vol. 93, pp. 266-269, April 2015.

[9] K. Kawamura, I. Suzuki, Y. Fuji, O. Watanabe, "Ice core record of polycyclic aromatic hydrocarbons over past 400 years," Naturwissenschaften, Vol. 81, pp. 502–505, November 1994.

Accumulation of Polycyclic Aromatic Hydrocarbons (PAHs) and Carbon Compositions in Lake Sediment Cores ofThaleNoi, Phatthalung

Natthapong Iadtem[1,a], Siwatt Pongpiachan[2,b], Woranuch Deelaman[1,c], Danai Tipmanee[3,d] and Oramas Suttinun[1,e]

Abstract This research aims to study the accumulation of 15 PAHs (∑PAHs15) and to measure OC/EC in the sediment from ThaleNoi, Phatthalung, Thailand.By analyzing the relationships of elementsdeposited in the sediment through time at different depths, the sources of PAHs can be determined. The sediment extraction process was carried out by the soxhlet method using dichloromethane (DCM) as solvent, and then took to intensity measurement by GC/MS, before OC/EC analysis was conducted by thermaloptical method. The total concentration of PAHs)∑PAHs15 (in ThaleNoi sediment ranged from 169-1217, 20-169, and 19-167 ng/g (dry weight) for station core 1, 2 and 3 respectively.Itwas found that the accumulation of PAHs showed lower contaminationcompared to those found in many other lakes, and the intensity of TC, OC, and EC hasvalues of [632,590],[368,290], and [264,300] ng g^{-1}respectively. The diagnostic ratio plots Ind/Ind+B[g,h,i]P, B[a]A/B[a]A+Chry(, OC/EC,and Char-EC/Soot-EC indicated that most of the potential sources of PAHs may be originated from the incomplete combustion of petroleum products and biomass.

Keywords *Polycyclic Aromatic Hydrocarbons (PAHs), OrganicCarbon (OC), Elemental Carbon (EC)*

[1]Facultyof Environmental Management,
Prince of Songkla University
Hatyai, Songkhla
[2]Faculty ofSocial and Environmental Development
National Institute of Development Administration (NIDA)Univercity
Bangkapi, Bangkok
[3]Faculty of Technology and Environment,
Prince of Songkla University
Kathu, Phuket

[a]natthapongiadtem@hotmail.com
[b]pongpiajun@gmail.com
[c]woranuch.dpm@hotmail.com
[d]dtipmanee@hotmail.com
[e]oramas.s@psu.ac.th

Introdution

The combustion of fossil fuels,coupled with the burning of agricultural wastes, are the major causes of carbonaceous compositions emission, whichgreatly affect the global climate system,resulting in the increase of environmental contamination. During the past few decades, both positive and negativeeffects of organic carbon (OC), elemental carbon (EC), and polycyclic aromatic hydrocarbons (PAHs) have been consistently studied in various places [1], especially on health, environment, and the accumulation in human and animal food chains. In many studies of sediment cores, the OC, EC, and PAHs relationships display strong correlations with local socioeconomic factors, such as human industrial production, consumption, occupation, and population growth [2][3][4][5][6][7][8]. Eventually, these pollutants are accumulated as sediments in lakes through adsorption process. Therefore, the examination of the contamination history of OC, EC, and PAHs inor around the lakes, released from or related to anthropogenic sources and surface run-off erosion, can be used to infer past human activities that caused such pollution.

In this study, we examined the vertical profile of OC, EC and PAHs in sediment cores from ThaleNoiLake in Phatthalung province, Thailand to better understand activities that are anthropogenically-driven leading to environmental changes. The sources of the pollutants found would provide valuable information that leads to the better and sustainable management of the lake area.

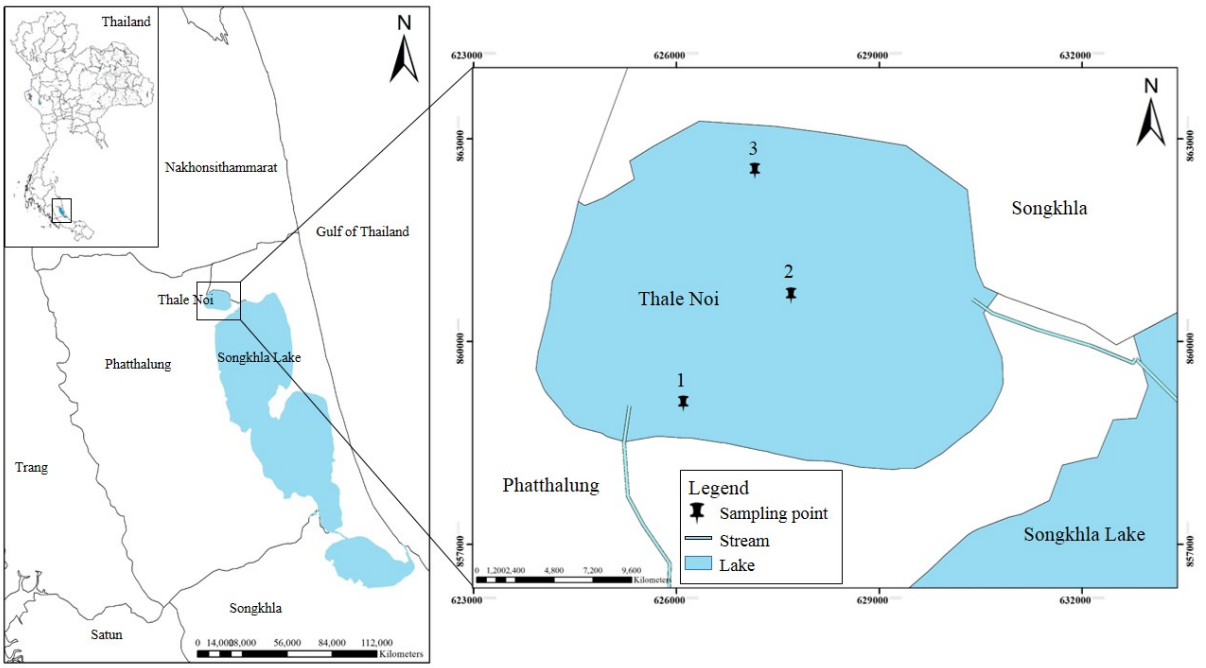

Fig. 1. Location of Studied Area

Materials and methods

A. Studied Sites and Sampling Methods

ThaleNoi(Lat. 7°46'41.7520''N, Long.100°7' 22.0296''E), located in Phatthalung, Thailand (Fig. 1), is a small and shallow eutrophic lake connected to the north of the larger Songkhla Lake. It has a surface area of 28 km^2,6 km long and 5 km wide,with an average depth of 1.5m .The sediment accumulated within the Quaternary period, with an age of about 1.8 million years,arising from the meeting of rivers and coastal waters. The line originates fromBanthadand Sankalakhiri Ranges.The totals of 73 samples, from 3 sediment core stations, werecollected on August, 12017 at depths using extractors with diameter of 10 cm and length of 150 cm. The core was cut longitudinally and divided into 2 cm pieces which were then preserved by freezing at around -20 °C in the aluminum foil.

B. PAHs Analysis

All solvents and reagents used were of HPLC grade for PAHs trace analysis obtained from Norwegian Standard. The 15 PAHs ∑)PAHs15) includePhenanthrene (Phe), Anthracene (An), Fluoranthene(Fluo),11H-Benzo[a]Fluorene (11H-B[a]F), 11H-Benzo[b]Fluorene (11H-B[b]F), Pyrene (Pyr), Benz[a]Anthracene (B[a]A), Chrysene (Chry), Benzo[b] Fluoranthene (B[b]F), Benzo[k]Fluoranthene (B[k]F), Benzo [a]Pyrene (B[a]P), Benzo[e]Pyrene (B[e]P), Indeno[1,2,3-c,d] pyrene (Ind), Dibenz[a,h]Anthracene (D[a,h]A) and Benzo [g,h,i]Perylene (B[g,h,i]P)], and a mix of recovery deuterated PAHs internal standard solutions [d12-Perylene (d12-Per) and d10-Fluorene (d10-Fl)].

The samples were prepared via soxhlet using dichloromethane by accelerated solvent extraction and 1 g of copper powder for 8 h. The extracts were concentrated with a rotary evaporator)Buchi R-100(. The fractionation chromatography and the clean-up process followed the conventional method using solvent exchanged to hexane would yield low molecular weight PAHs, andhexane:toluene (1:0.6) would yield high molecular weight PAHs.

The extracts collected were purified by Colum Chromatography using silica gel. The elution was evaporated and concentrated to 100 µL under a gentle stream of nitrogen. More details of analytical methods were clearly explained in previous literature [9][10][11][12]. Analyses of PAHs were performed on a gas chromatography–mass spectrometry (GC-MS) using a Shimadzu GCMS-QP2010 Ultra.The GCMS system was operated in splitless liner mode of both the injection liner, and transfer line were maintained at 280 °C temperature. The mobile phase used helium (He) of 99.999% purity with 1.0 ml/min flow rate. The extracts were injected into an autosamplerusing a capillary column (30 m length x 0.25 mm i.d. 0.5 µm. film thickness). The splitless injection of 1.0 µl was held for about 48 min. [13][14].

C. Organic Carbon (OC) & Elemental Carbon (EC) Analysis

All sediment samples were analyzed for OC and EC using a Thermal/Optical Carbon Analyzer. The thermal/optical reflectance (TOR) protocol [15] was used for the carbon analysis. The sampleswere tested at various temperatures:OC1 (120 °C), OC2 (250 °C), OC3 (450 °C), OC4 (550 °C),EC1 (550 °C), EC2 (700 °C), and EC3 (800 °C). OC1-OC4 were texted in a non-oxidizing helium (He) atmosphere, while EC1-EC3 were tested in an oxidizing atmosphere of 2% oxygen in a balance of helium [16]. As oxygen was added to the system, the reflection of light was optically-detectedby pyrolyzed carbon (OP). Then,the ion was analyzedwith flame ionization detector at the absorbance of 663 nm [17].

Results and discussion

A. PAHs Analysis

The highest concentration of 15 PAHs ($\sum PAHs_{15}$) was found in core 1 which ranged from 169to 1,217 ng g^{-1}(dry weight), with the mean concentration value of 344.85±296.10 ng g^{-1}. The second highest was of core 2 which ranged from 20 to 169 ng g^{-1} with the mean concentration value of 85±61 ng g^{-1}. For core 3, the results ranged from 19 to 167 ng g^{-1} with the mean concentration value of 60±51 ng g^{-1}.Overall, the PAHs concentration levels in sediment of ThaleNoi Lake were found to be similar or lower than those of the other lake areas may be of activities that occur around different lake such as Kaohsiung Harbor in Taiwan (472 to 16,201 ng g^{-1})[18], Lake Baiyangdian in China (97 to 2,402 ng g^{-1}) [19], Lake Hongfengin southwestern China (2,934 to 5,282 ng g^{-1}) [20], and Lake Kitaura in Japan (380 to 520 ng g^{-1}) [21], as shown in Fig. 2.

Considering the composition of the PAHs found in ThaleNoi Lake's sediments, the most common are B[a]P, Chry, Pyr, Fluo, and Ind, having 4-6predominant aromatic rings. This result suggested that the PAHs contamination in the sediment came from biomass and vehicle's fuel combustions [22][23][24][25].

B. Sources of PAHs

Sources of PAHs in the environment, including lake sediments, belong to two categories: petrogenic (from petrochemicals) and pyrogenic (from combustion). The feature of different PAHs and their possible sources are assessed by the diagnostic double/binary ratios plot of Ind/(Ind + B[g,h,i]P) and B[a]A/(B[a]A + Chry).If Ind/(Ind + B[g,h,i]P) is greater than to 0.2, the PAHs must have been originated from grass, wood, and coal combustion. If the diagnostic binary ratio is less than 0.2, the PAHs are most likely petrogenicin origin.In the case of B[a]A/(B[a]A + Chry), if the result is greater than to 0.35, the PAHs were originated from grass, wood, or coal ignitions. The interval between0.2-0.35 suggests that the PAHs are the product of petroleum combustion. If the ratio's result is less than 0.2, this indicated that the PAHs are of petrogenic sources [24].

PAH ratios were calculated for each sample shown in Fig.3. The results suggested that that lake sediment were contaminated by the incomplete combustion of petroleum product and biomass burning, which wereconsistent with human activities. There are many possible pyrogenic sourcesin the area such as agriculture and residence, combustion of biomass, open burning of agricultural wastes, forest fires, tourism activities, and fishery.However, the most possible sources may be from vehicles exhaust, oil spill, or discharge of lubricant oil.

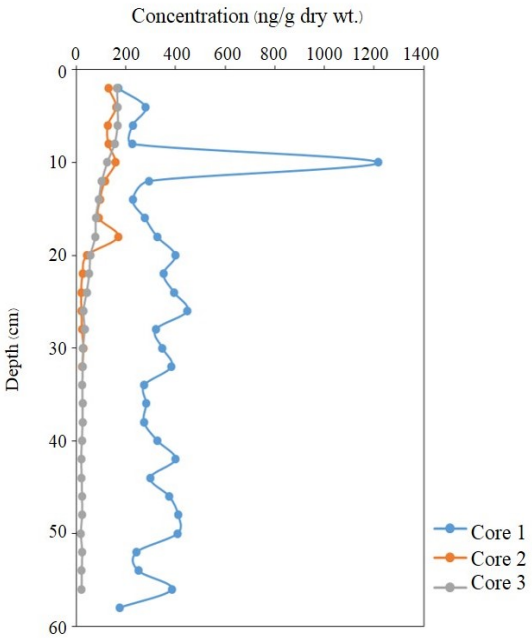

Fig. 2. Concentrations of $\sum PAHs_{15}$ in Sediment Cores: (A) Core 1, (B) Core 2, and (C) Core 3in ThaleNoi, Phatthalung

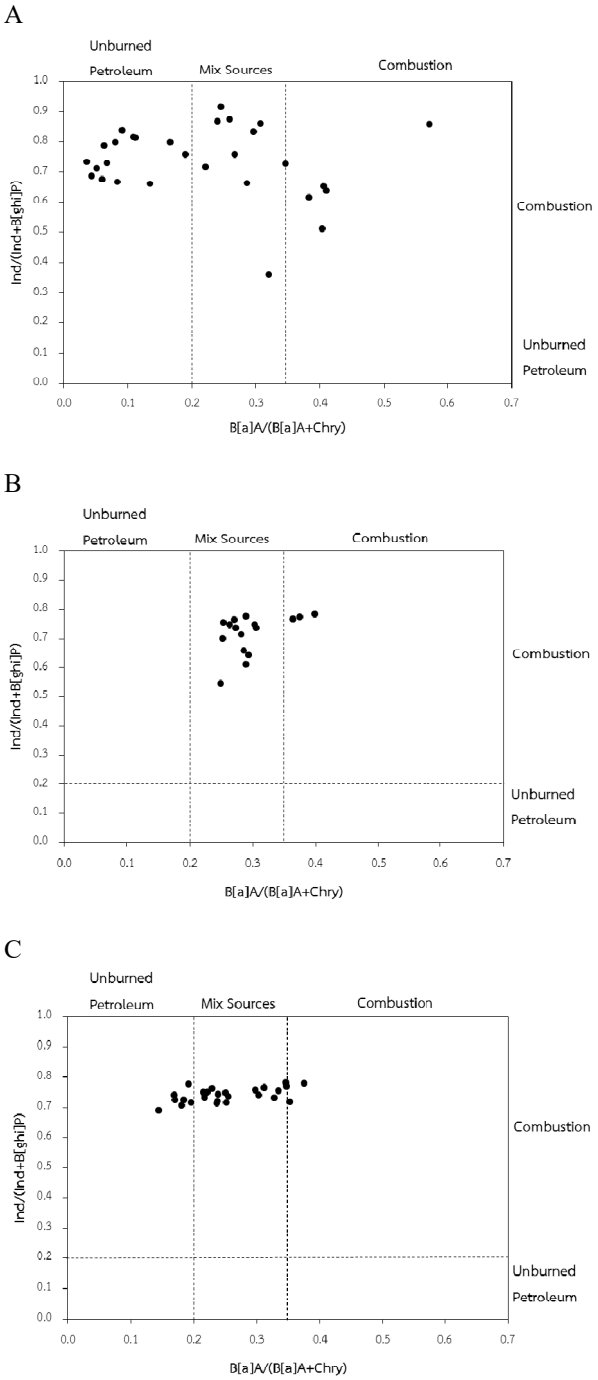

Fig. 3. Diagnostic ratios Ind/(Ind + B[g,h,i]P) versus B[a]A/(B[a]A + Chry) identifying sources of PAHs in sediments from (A) Core 1 (B) Core 2 and(C) Core 3 in ThaleNoi, Phatthalung

C. OC/EC Analysis

The carbon composition in sediment consists of total carbon (TC), organic carbon (OC), and elemental carbon (EC). The analysis yielded that average concentrations of TC, OC, and EC values of [632-590],[290-368], and [264-300] ng g^{-1} respectively, as shown in Fig. 4.Of all the 8 types of carbon concentration (OC1, OC2, OC3, OC4, EC1, EC2, EC3, and OP) in of sediments collected from the lake, the most common were EC1, OC3, and OP, withvalues of [230-349],[190-810], and [162-760] ng g^{-1} respectively.This suggested vehicular exhaust emission from all types,incomplete combustion of fossil fuels and biomass fuels, as the sources [17].

D. Sources of OC/EC

Sources of OC/EC in the environment in the lake sediments were assessed by the ratio plot of OC/EC. Inaddition, the EC could explain the origin of different burning periods belonging to two categories: Char-EC (EC1-OP) and Soot-EC (EC2+EC3) by the ratio plot of Char-EC/Soot-EC.

The OC/EC ratio concentration value of 1.39, belonging to the interval of 1.0 to 4.0, suggested vehicular exhaust emission as the source [26]. The Char-EC/Soot-EC ratio concentration value of 26.20, belonging to the interval of 20.0 to 30.0, suggested biomass combustion as the source [27].

OC/EC and Char-EC/Soot-EC ratios were calculated for each sample. They all suggested that the lake sediments were contaminated by the incomplete combustion of vehicular exhaust emission and biomass combustion. These wereconsistent with the PAHs analysis.

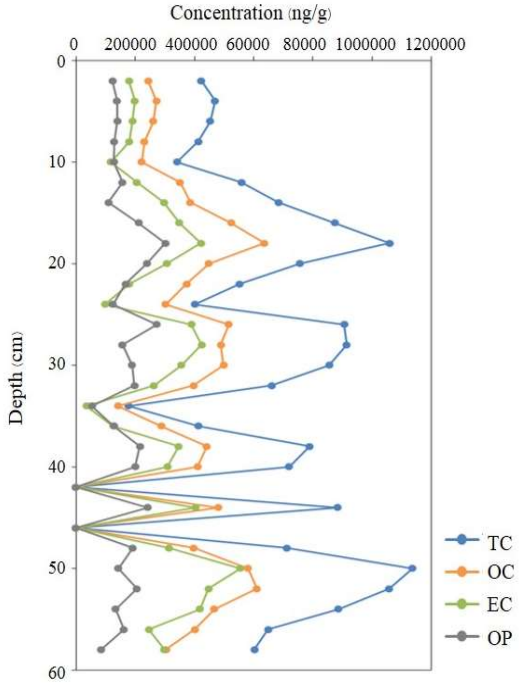

Fig. 4. Concentrations of Total Carbon (TC), Organic Carbon (OC), and Elemental Carbon (EC) in Sediment Cores from ThaleNoi, Phatthalung

Conclusions

The concentrations of total PAHs in the studied sediment samples were substantially lower than those found in many other lakes, consistentwith the OC/EC ratios. For the PAHs found in lake, the most common/predominant had 4-6 aromatic

rings.This study also provided information on the source apportionment of lake sediments with the application of different methods. The main sources of PAHs found in this study werefrom hydrocarbons derived by incomplete combustion of petroleum products, forest fires, or biomass combustion. These included oil spill, vehicle's exhaust, discharge of lubricant oil, and other waste discharge that had adversely affected the study area.

Acknowledgments

This work was supported by Distribution and characteristics of black carbon from biomass burning in the middle-and-low-latitude Asian and its impact on regional climate and monsoon precipitation from The Thailand Research Fund)TRF(,Division of Environmental Science and Technology, Faculty of Science and Technology, Rajamangala University of Technology,PhraNakhon.The authors would like to thank all the professors and relevant persons for their support throughout this project.

References

[1] P Schmid, C Bogdal, N Blüthgen, FS Anselmetti, A Zwyssig and K Hungerbuhler, "The missing piece: sediment records in remote mountain lakes confirm glaciers being secondary sources of persistent organic pollutants," Environ. Sci. Technol, 2010, pp.45:203-208.

[2] GQ Liu, G Zhang, XD Li, J Li, XZ Peng and SH Qi, "Sedimentary record of polycyclic aromatic hydrocarbons in a sediment core from the Pearl River Estuary, South China," Pollut. Bull, pp. 51:912-921, Mar 2005.

[3] W Wilcke, "Global patterns of polycyclic aromatic hydrocarbons (PAHs) in soil," Geoderma, 2007, pp. 141:157-166.

[4] Y Liu, N Yu, Z Li, Y Wei, L Ma and J Zhao, "Sedimentary record of PAHs in the Liangtan River and its relation to socioeconomic development of Chongqing, Southwest China," Chemosphere, 2012, pp. 89:893-899.

[5] KS Machado, RC Figueira, LC Côcco, S Froehner, CV Fernandes and PA Ferreira, "Sedimentary record of PAHs in the Barigui River and its relation to the socioeconomic development of Curitiba, Brazil," Sci. Total Environ, 2014, pp. 482: 2-52.

[6] G Zhang, A Parker, A House, B Mai, X Li, Y Kang and Z Wang, "Sedimentary records of DDT and HCH in the Pearl River Delta, south China," Environ. Sci. Technol, 2002, pp. 36:3671-3677.

[7] G Liu, G Zhang, Z Jin and J Li, "Sedimentary record of hydrophobic organic compounds in relation to regional economic development: a study of Taihu Lake, East China," Environ Pollut, 2009, pp.157:2994-3000.

[8] P Bigus, M Tobiszewski and J Namieśnik, "Historical records of organic pollutants in sediment cores," Pollut. Bull, pp. 78:26-42, Mar 2014.

[9] Pongpiachan, S., "Vertical distribution and potential risk of particulate polycyclic aromatic hydrocarbons in high buildings of Bangkok, Thailand," Asian Pac. J. Cancer Prev, 2013a, 14 (3), pp. 1865–1877

[10] Pongpiachan, S., "Diurnal variation, vertical distribution and source apportionment of carcinogenic polycyclic aromatic hydrocarbons (PAHs) in Chiang-Mai, Thailand," Asian Pac. J. Cancer Prev, 2013b, 14 (3), pp. 1851–1863.

[11] Pongpiachan, S., "Assessment of reliability when using diagnostic binary ratios of polycyclic aromatic hydrocarbons in ambient air PM10," Asian Pac. J. Cancer Prev, 2015a, 16 (18), pp. 8605-8611.

[12] Pongpiachan, S., "Incremental lifetime cancer risk of PM2. 5 bound polycyclic aromatic hydrocarbons (PAHs) before and after the wildland fire episode," Aerosol Air Qual. Res, 2016, 16, pp. 2907-2919

[13] Pongpiachan, S., Bualert, S., Sompongchaiyakul, P. and Kositanont, C., "Factors affecting sensitivity and stability of polycyclic aromatic hydrocarbons," Anal. Lett, 2009, 42 (13), pp. 2106–2130.

[14] Pongpiachan, S., Hirunyatrakul, P., Kittikoon, I. and Khumsup, C., "Parameters influencing on sensitivities of polycyclic aromatic hydrocarbons measured by Shimadzu GCMS-QP2010 Ultra," Gas Chromatography/Book 3 Intech Open Access Publisher, 2011, pp. 978-953-51-0298-4.

[15] Chow, J.C., Watson, J.G., Crow, D., Lowenthal, D.H. and Merrifield, T.M., "Comparison of IMPROVE and NIOSH carbon measurements," Aerosp. Sci. Technol, 2001, 34 (1), pp. 23–34.

[16] Ho, S.Y., Thorpe, J.L., Deng, Y., Santana, E., DeRose, R.A., and Farber, S.A., "Lipid metabolism in zebrafish. The Zebrafish: Cellular and Developmental Biology 2nd Ed," Methods Cell Biol, 2004, 76, pp. 87-108.

[17] Cao, J.J., Chow. J.C., Lee, S.C., Li, Y., Chen, S.W., an, Z.S., Fung, K., Watson, J.G., Zhu, C.s. and Liu, S.X., "Characterization and Source Apportionment of Atmospheric Organic and Elemental Carbon during fall and winter of 2003 in Xi'an, China," Atmos. Chem. Phys, 2005, 5, pp. 3127-3137.

[18] Chiu-Wen Chen andChih-Feng Chen, "Distribution, origin, and potential toxicological significance of polycyclic aromatic hydrocarbons (PAHs) in sediments of Kaohsiung Harbor, Taiwan," Marine Pollution Bulletin 63, 2011, pp. 417–423.

[19] Wei Guo, Yuansheng Pei, Zhifeng Yang and He Chen, "Historical changes in polycyclic aromatic hydrocarbons (PAHs) input in Lake Baiyangdian

related to regional socio-economic development," Journal of Hazardous Materials, 15 March 2011, pp. 441-449.

[20] Jian-Yang Guo, Feng-Chang Wu, Liang Zhang, Hai-Qing Liao, Run-Yu Zhang, Wei Li, Xiao-Li Zhao, She-Jun Chen and Bi-Xian Mai, "Screening Level of PAHs in Sediment Core from Lake Hongfeng, Southwest China," Arch Environ ContamToxicol, 2011, pp. 60:590–596.

[21] NobuyasuItoh, ShujiTamamura and MichioKumagai, "Distributions of polycyclic aromatic hydrocarbons in a sediment core from the north basin of Lake Biwa, Japan," Organic Geochemistry, 2010, pp. 845–852.

[22] Page, D.S., Boehm, P.D., Douglas G.S., Bence, W.A., Burn, W.A. and Mankiewicz, P.J., "Pyrogenic Polyclic Aromatic Hydrocarbon in Sediment Record Past Human Activity: A case Atudy in Prince William Sound, Alaska," Pollut. Bull, Mar 1999, pp. 4: 247-260.

[23] Wang Z. and Fingas M., "Use of methyldibenzothiophenes as markers for differentiation and source identification of crude and weathered oils," Environ. Sci. Technol, 1995, pp. 29. 2842-2849.

[24] Yunker, M.B., Macdonald, R.W., Vingarzan, R., Mitchell, R.H., Goyette, D., and Sylvestre, S., "PAHs in the Fraser River basin: a critical appraisal of PAH ratios as indicators of PAH source and composition," Org. Geochem, 2002, pp. 33: 489–515.

[25] Zeng, E.Y. and Vista, C.L., "Organic pollutants in the coastal environment off San Diego, California. 1. Source identification and assessment by compositional indices of polycyclic aromatic hydrocarbon," Environ. Toxicol. Chem, 1997, pp. 16:179-188.

[26] Schauer, J.J., Kleeman, M.J., Cass, G.R. and Simoneit, B.R.T., Measurement of emissions from air pollution sources," Environmental Science and Technology, 1999, pp. 33:1578-1587.

[27] Chen, L., W.A., Moosmuller, H., Arnott, W.P., Chow, J.C., Watson, J.G., Susott, R. A., Babbitt, R. E., Wold, C. E., Lincoln, E. N., and Hao, W. M., "Emissions from laboratory combustion of wildland fuels: Emission factors and source profiles," Envion. Sci. Technol, 2007, pp. 41: 4317-4325.

Session B

Participatory Management for Water and Irrigation Project

Guested Paper

PARTICIPATORY APPROARCH IN ADAPTIVE WATER MANAGEMENT AND RURAL DISASTER PLANNING BY IRRIGATION GATE OPERATION

Takao MASUMOTO*

Abstract

Taking the Nam Cheng River basin as an instance of flood-prone areas during rainy seasons, the relation between irrigation gates management specifically for water supply during dry seasons and floods during water-rich seasons is examined by modeling runoff, flooding processes and gate operations through the DWCM-AgWU Model (a Distributed Water Circulation Model incorporating Agricultural Water Use). In particular, technological transfer stages in trials there lead to the products of adaptive water management and rural disaster planning evoking local managers of irrigation facility control and relevant farmers and inhabitants.

The target basin (457 km2) covers one of the tributary in the Nam Ngum River system and low-lying paddies extends where the Chim and Ping Rivers join and annually repeated floods occur. Irrigation gates are situated at the end of the river basin to secure water for rice cultivation during dry seasons. In addition, they have the function to prevent the reverse flow from the Nam Ngum River, but they eventually have caused frequent floods in low-lying areas. This direction was obtained by the analyses; namely, 1) stage of field surveys and a model development, 2) Specification stage of flood causes, 3) Introduction stage of new observation facilities and modified gate operations,
4) Development stage of flood prevention guidelines. As a result, the utilization of models turns out to be very effective means for several analyses in areas with the lack of fundamental data as shown in the target area, in that the estimated values through the models would be utilized as quasi-observation data, such as temporal and spatial estimates of river discharges and water levels.

In conclusion, based on our studies progress of the 4 years term, due in part to our 7 visits to the site and 4 seminars, the proposals for adaptive water management and rural disaster planning resulted in mutually ones deepened by local managers as well as experts, not a one-sided technological transfer just from experts.

Keywords *DWCM-AgWU model, Irrigation gate, Adaptive water management*

*Akita Prefectural University, 2-2 Minami, Ogata, Akita, 010-0443, Japan.
E-mail: masumoto@akita-pu.ac.jp.

Migration and Collective Action: Evidence from China

Eduardo Araral*

Abstract

Over the past three decades, scholars have studied the effects of more than three dozen factors on collective action in the commons but little is known about the effects of rural to urban migration. We examine this question with the case of China, which has the world's most extensive levels of rural to urban migration. Using OLS, Logit and Probit models and data from a survey of 1,780 households from 18 provinces, we find that migration has a statistically significant adverse effect on collective irrigation controlling for a large number of theoretically relevant variables. The effects of migration on collective action in the commons are possibly mediated by a number of factors frequently identified in the literature, including leadership, social capital, sense of community, economic heterogeneity, and dependence on resources. We speculate that massive out migration partly explains the significant drop in the use of collective canal irrigation and exacerbated the significant increase in groundwater irrigation since the start of reforms in 1980s. These findings have important policy implications for commons governance in China given that massive rural to urban migration will continue in the next decade. Because of the increasing rural to urban migration worldwide especially in developing countries, the findings could also partly explain the deteriorating state of rural village infrastructure, natural common pool resources and ecological systems in many developing countries.

*Director of the Institute of Water Policy, NUS Lee Kuan Yew School of Public Policy

Disaster Irrigation and Water Management towards Nexus (WEF) and Sustainable Development Goals

Leong Ching*

Abstract

Flood models predict that people who experience small andmedium sized floods cope better than those who have experienced no floods at all (e.g., those who havethe benefit of infrastructure that shield them from such floods.)

These communities will then be highlyvulnerable when large floods strike because they have little adaptive power. This paper shows that this binary effect need not be true—by conducting a micro-level narrative analysis in flood prone communities in Assam, India, we find that while the ''memory effect'' of floods does decrease vulnerability in some instances,such memory effects do not always obtain.

The paper therefore suggests four distinct groups of flood responses: Aside from thewell-established ''memory'' and ''levee'' effects, there are two other groups which may resist either effect.Our analysis finds four distinct narrative types: theHardened Preparer, the Engineer, Discontent, and the Pessimist.

This paper put forward an explicitly socio-hydrological conception of resilience which takes into account the role of sociological indicators such asnarrative types and perceptions. Such contextual understandings and narrative types can form the basis ofgeneric resilience indicators which complement the anticipated outcomes of socio-hydrologic modelsgenerally. The session will also touch more generally on the irrationalities of collective environmental behaviors.

*National University of Singapore, Lee Kuan Yew School of Public Policy
Institute of Water Policy
ching@nus.edu.sg

Technical Paper

FLOODING MONITORING AND FLOOD INUNDATION ANALYSIS UGING UAV

Mikyoung Choi[1], Geunsang Lee[2] and Kwansue Jung[3]

Abstract

The prompt flood monitoring could provide fast response and damage assessment. In this study, topographical data is constructed using UAV in order to estimate area or depth in flooding in advance. And flooding monitoring was conducted in flood season. And, the topographical data was used as basic input data for the flood inundation simulation. This study presents a series of processes for creating topographical data through UAV, monitoring floods, and verifying comparisons with the results of numerical models.

Keywords *UAV; DSM; flooding monitoring; FLUMEN*

[1]International Water Resources Research Institute
Chungnam National University, Daejeon, Korea
[2]Department of Cadastre and Civil Engineering
Vision college of Jeonju, Jeonju, Korea
[3]Department of Civil Engineering
Chungnam National University, Daejeon, Korea

Knowledge gap between technical experts and reflective practitioners regarding flood sufferers' lives back in order

Cases in japan

Yoko Matsuda[1,a]

Abstract Even though well-considered flood management is installed, flood disasters may happen. In the past decade, Japan has experienced either of flash floods, landslides, and dike breaks every year in different parts of the country. Especially in 2018, the western Japan was suffered by the record-breaking heavy rain disaster which killed 224 people, in 15 prefectures. However, the basic procedures for individuals who suffered from floods to live their lives back in order are not officially documented ever, probably because it needs to cover multiple expertise including residential structure, local administration, insurance and sanitation, which experts can hardly bridge this knowledge gap in a bureaucratic social system.The paper discusses reasons and appropriate policies from detailed and prolonged observation as a field worker of a disaster-relief non-profit organizations. In addition, a challenge of collaboration between technical experts and field workers to conquer the knowledge gap.

Keywords *build back in order, knowledge gap, case studies*

This research is granted by JSPS Kakenhi JP17K06594.

[1]Department Environmental and Civil Engineering
Nagaoka University of Technology
Nagaoka, Japan

[a]ymatsuda@vos.nagaokaut.ac.jp

Introduction

In the last decade, Japan has experienced numerous flood disasters in different parts of the country. In 2015, Kinu River, a major river managed by the national government, was flooded, and in some observatories in Kyushu in 2017, a daily precipitation exceeded the average volume of their monthly precipitation.

Regarding such a situation in the country, it is apparently necessary to develop countermeasure to rebuild survivors' lives back after flood disasters, particularly focusing on individual recovering process. However in the fact, there are very few examples to instruct the procedure.The reasons might be assumed that there is a lack of "integration of expertise knowledge", and it is also assumed that the special type of professionals (reflective practitioners) can play a role to tie these disperse knowledge.

In this paper, two cases observed in a process to create manuals and posters by these stakeholders to verify this assumption.

Assumptions

Among different discussions on typology of professionals, reflective practice by Schön [1]. He called conventional professionals "technical experts" who apply their knowledge in their expertise to solve problems based on their technical rationality, whereas defined "reflective practitioners" as a different (and modern) type of professionals. Reflective practitioners try to learn in action and set a problem through dialogue with stakeholders. Figure 1 shows the comparison of these two types of professionals in that the relationship between citizens. The relative position between citizens and technical experts are vertical. Professionals are to observe what is happened, said, done among citizens. On the other hand, the relation between reflective practitioners and citizens are horizontal, or surrounding the same round table, to have a conversation on a situation to learn each other.

Apparently both types of experts need to serve in our society, however, importance of reflective practitioners has become more increased in the era that the society faces with various uncertainty including flood risks.

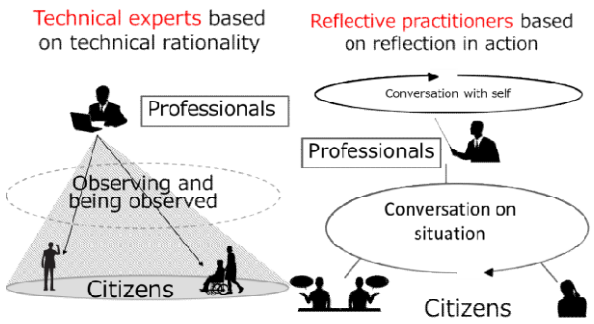

Fig. 1. Comparison between technical experts and reflective practitioners

When a disaster occurs, different professionals are dispatched to the affected area to support victims and survivors.In the following observations in this paper, we assume that all the professionals including doctors, nurses, lawyers, carpenters, civil engineers and city workers in a local administration are technical experts. They are all there to solve problems occurred around victims based on their technical rationality.

On the other hand, we also assume *aid workers* who serve in the affected sites as reflective practitioners who proactively try to have a conversation between victims. Aid workers means those who works in civil (non-governmental) sectors, and are specialized in supporting disaster survivors. The term aid workers can be contrasting against volunteers, who are active in Japan after Kobe Earthquake in 1995. Aid workers are distinguished from volunteers in that abundant experience at disaster sites.

The following observations will respond the question that what is a role of reflective practitioners in disaster responses. Remind that the assumptions above are very strict, but in many cases, professionals other than aid workers can be reflective practitioners.

Observation 1: Publishing process of a guidebook "recovering from flood disasters"

In March 2017, a network organization of disaster relief groups called Shintsuna published a guidebook for individual flood sufferers to recover their lives. Shintsuna, or Shinsai-ga-Tsunagu-Zenkoku-Network in Japanese, literally means "nationwide network of organizations connected by the earthquake". The earthquake here refers not to 2011 Tohoku Earthquake but to 1995 Kobe Earthquake.

This guidebook to recover their lives from flooding damageconsists of necessary matters of [2] (Figure 2 and Figures 3 for the English version) was issued. Since there did not exist a similar document before this guidebook, it spread rapidly after the flood in July 2017. 5,600 copies were delivered in Fukuoka Prefecture, and so did 2,800 copies in Oita Prefecture.

Here our observation is on the production process of this guidebook.

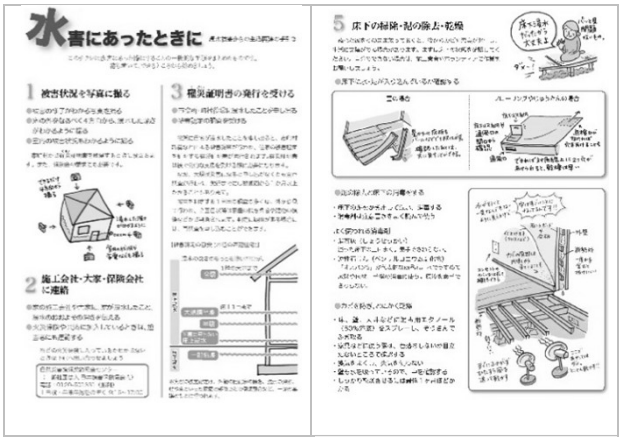

Fig. 2. Recovering from flood disasters (original flyer version in Japanese)

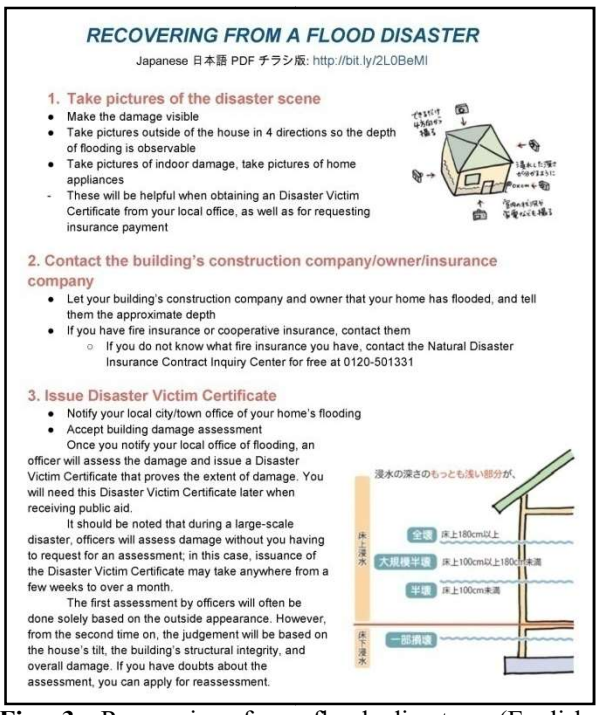

Fig. 3. Recovering from flood disasters (English translated version)

As stated above, Japan experiences flood every year. Though the total damage and damage per area (called flood damage density) are increasing [3], official documentation for disaster sufferers to learn steps ahead to recover their lives is not existed. Each necessary information for victims, including about issue of victims' certificates, cleaning up of their houses and disinfection of buildings, is delivered through radio or flyers to them. Though the bundle of flyers can be handed over to a victim, they are individual unintegrated information, therefore it was not easy for them to find an outlook to recover their lives back in order.

This fact is actually stored as experimental knowledge in aid workers, since they often had direct conversation with disaster survivors repeatedly. They

had already found that disaster victims often obtain information after a disaster only piece by piece.

To solve this very practical problem, aid workers who are also members of Shintsuna, organized all the procedure through receiving public support which occupies an important element of the living rebuilding process, and the procedure necessary up to the repair of the house. They draw the procedure in a flowchart (Figure 4).

As indicated by a thick (red) arrow in Fig.4, there are several procedures related to both administrative affairs and house repairing. For example, there led some rules such as "Report the damage to a city office AFTER taking picture of your suffered house", and "Start cleaning up houses AFTER receiving survey on damage on residence".

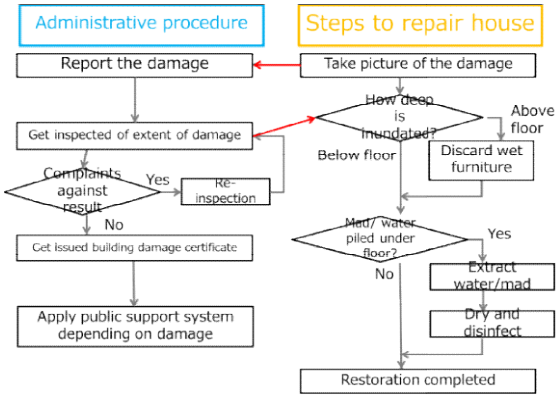

Fig. 4. Flowchart on rebuilding the lives of flood victims.

If a survivor did not know this tip to take a picture before heading to a city office, or start cleaning without receiving damage assessment, it would lead losing of opportunity to receive sufficient support.

Therefore, based on this flowchart, victims' support organizations rearrange the procedures in the order that the general victims face, and then, for individual work contents, experts in each field (administrative officials, damage insurance companies, lawyers, disinfectant makers and so on) and a completed guidebook.

Observation 2: Production of educational posters to prevent disaster-related deaths

In 2016, Shintsuna issued an educational poster and its supplementary booklet called "disaster-related deaths prevention poster" [4] (Figure 5), and distributed it to local offices of social welfare.

Disaster-related death is defined as a loss of life during and after evacuating indirectly caused by a disaster. If a loss of life is recognized as disaster-related death, his/her bereaved families are paid based on the Disaster Relief Act. In the Great East Japan (Tohoku) Earthquake in 2011, the number of deaths related to disasters was 3,591 compared to 15,894 deaths as of March 2017. Approximately 50% of disaster-related deaths are diagnosed as being caused by mental stress [5].

The observation in this section is also on the production process of this poster and booklet. After the Great East Japan Earthquake disaster-related death became a social issue as "death that could be prevented", whereas aid workers continued supporting survivors in many evacuation centers. Through these activities, aid workers experimentally found that, as far as health condition of evacuees stay away from the worst state, caring by volunteers, neighbors and other evacuees, can prevent disaster-related death in a neighborhood community.

Based on the fact, they started organizing its own concept of "potentially high-risk evacuee" (Figure 6): To prevent from their loss, aid workers found that volunteers and local citizens are the target to be advertised.

Fig. 5. Poster by Shintsuna: "Is that person okay?" [4]

Type	Condition	Assisted by
General Evacuees	• are others than below	Public service

Potential High-risk Evacuees	• are not in emergency, but have a disadvantage for well living
	  • cannot eat provided food
	  • show awkward movements (walk, sit)
	  • cannot understand information
	• seem normal but cannot adjust to accommodate in a shelter
	  • do not communicate
	  • do not move around
		Neighbors
		Volunteers
		Aid workers
		Medical or welfare experts
		(doctors or nurses)

High-risk Evacuees	• need medical or welfare care immediately
	  • Serious handicap
	  • Very bad in health condition (diabetes, high blood pressure)
	  • Difficulty in egestion	

Fig. 6. Potentially high-risk evacuees

Disucussions

A. Findings

This paper summarized the production processes of two types of printed works done by aid workers. There can be pointed out two issues in

common that: 1) Basic idea of the works is based on their practical knowledge obtained from aid workers' thick experiences, and 2) both of the works have prescriptive aim to prevent disadvantage of survivors and serve to their well-being.

In any of these cases, aid workers do not provide their own expertise knowledge. Housing repair procedure, or mental and physical symptoms indicated by evacuees are apparently basic expert knowledge shared by technical experts. A role of aid workers, or reflective practitioners, can be inferred, that just binding these dispersed knowledge into one and something with context to help citizens to understand. The result of expertise re-integration can be observed at the first case, our creation of a flowchart in the guidebook, and at the second case, a conceptualization of "Potentially high-risk evacuees" and dissemination of the awareness message.

Therefore, we got a hypothesis by abduction reasoning. One of the roles of reflective practitioners such as aid workers, is a re-integration, or re-organization of expertise knowledge provided by technical experts.

Here let us show another case toimplythe limitation of unilateral activities of technical experts. Figure 7 shows a poster to prevent from the disaster-related death by"disuse syndrome" (the whole body of mental and physical function symptoms) An educating poster published by the Ministry of Health, Labor and Welfare [6]. The stated key message of the poster is "Be aware of 'disuse syndrome'", directly to the vulnerable survivors, not to their supporters.

Fig. 7. Enlightenment poster at evacuation center by Ministry of Health, Labor and Welfare [6] Be aware of "disuse syndrome"! Consult a doctor nearby.

Of course, there is absolutely no reason to send a message to those who facing with risk of disaster-related deaths. However, in the shelter after a disaster with limited access by patrol of doctors and nurses, but they are not sufficiently performed There is nothing you can see. Here, it implies one of the important roles of aid workers as "knowledge re-integrator", not merely as supporter.

B. Suggestion for future research

In this research, the author presented the hypothesisthat a role of reflective practitioners is "re-integration of expertise knowledge". Regarding this hypothesis, it is possible to proceed deductive reasoning whether this can be supported in other contexts, or it is unique to disaster affected sites. It will be possible to make reasoning.

By using the results of this research, it will be possible to explore whether aid workers will be aware of their own role as "reorganization of expertise", thereby causing a change in future conscientious practice. This is also a future task to be left.

References

[1] Schön, Donald A, The reflective practitioner: How professionals think in action. Routledge, 2017.
[2] Shinsai-ga-Tsunagu-Zenkoku-Network, *Suigai ni atta tokini* (Recovering from flood disasters) , in Japanese, http://blog.canpan.info/shintsuna/archive/1420, 2017.
[3] Cabinet Office, *Heisei 22 nendobosai hakusho* (2010 Disaster Prevention White Paper), Saeki printing, 2010.
[4] Shinsai-ga-Tsunagu-Zenkoku-Network, *Saigai kanrenshi boshi poster,* "Is that person okay?", http://blog.Canpan.info/shintsuna/archive/, 2016. (1395 accessed in February 2018)
[5] ReconstructionAgency: *Shinsai kanren shi ni kansuru hokoku* (Report on the earthquake related death in the Great East Japan Earthquake), http://www.reconstruction.go.jp/topics/main-cat2/sub-cat2-6/20140526131634.html,2012. (Accessed in January 2018)
[6] Ministry of Health, Labor and Welfare: About the prevention of deterioration of the physical and mental functions accompanying the evacuation life by a series of earthquake of Kumamoto prefecture Kumamoto district, http://www.mhlw.go.jp/stf/seisakunitsuite/bunya/0000122332.html, 2016. (Accessed in February 2018)

Session C

Emerging/Digital Technologies in Water Management and Environment Towards Nexus (WEF) and SDGs (Big Data, IoT)

Guested Paper

Treating water to appropriate standards for different uses at the WEF Nexus

Andrew Dansie*

Abstract

Real-time water quality monitoring data is being increasingly used for real-time responses to water management and has applications for potable, agricultural and environmental water uses. Application of such automated technologies offers opportunity to create efficiencies in water management as part of the water treatment cycle. In Australia researchers from UNSW-GWI were part of the innovative Western Sydney Recycled Water Initiative (replacement flows) to deliver highly treated wastewater to the Hawkesbury-Nepean River.The river catchment surrounds Sydney, a city of over 5 million people,withnatural vegetation in the catchment significantly cleared for housing, agriculture and industry.With an expanding Sydney population and impacts of climate change, the problems facing the Hawkesbury-Nepean are escalating. The replacement flows initiative allowed drinking-quality reservoir water upstream to be reserved for urban use rather than released as environmental flows. The automated water monitoring that informed real-time water management responses allowed for efficient and suitable allocation of water for different end-users. Competing water uses at the WEF nexus can be more efficiently managed by allocating water of varying qualities that is suitable for human, agricultural, industrial or environmental use. Real-time automated monitoring can assist this management as well as proactively account for monsoon and flood storage needs within catchment-wide management of WEF water resources.The lessons learned in the Hawkesbury-Nepean River Catchment are highly suited to Asia similarly highly-populated and climate change-impacted river basins.

*University of New South Wales Global Water Institute (UNSW-GWI)

New technologies and design of future urban water systems

Katharine Cross

Abstract

The demand for water worldwide has increased substantially over the past decades. Increasing prosperity comes with the challenge to provide a growingurban population with safe quality freshwater. At the same time, the global market for wastewater recycling and reuse reached nearly US$12.2 billion in 2016 and is estimated to reach US$22.3 billion by 2021. This market expansion is in response to a growing demand from cities and industry for water against a backdrop of increased urbanisation, population growth and climate variability. To address these challenges and opportunities requires advanced treatment technologies, a focus on innovation and advancing technology.

The water industry, and in particular urban water utilities, needs to adapt to meet the emerging demands of a dynamic, highly deregulated and competitive environment with the context of a changing climate. Water 4.0 is the era of cyber-physical systems, digitalisation and big data where software, sensors, processors, communication and control technologies are increasingly integrated, to deliver sustainable and resilient water management in an increasingly changing, complex and uncertain world.

The opportunity for digital water technologies is especially promising for water professionals in emerging economies. The cost of centralised water and wastewater systems in rapidly expanding cities can be prohibitive and as a result, emerging economies can develop and manage off grid and localised water systems from scratch, much as the competitive mobile (and now smart) phone access allowed billions of isolated individuals to "leapfrog" the old world of monopoly controlled fixed landlines. Dynamic and data-driven (as opposed to mechanistic) models can help integrate and optimise smart pumps, valves, sensors and actuators; each device can "talk" to each other, or for that matter to a customer's iPhone, and send real-time information to be accessed and shared via the cloud.

Digital water technology adoption requires the engagement and commitment of incumbents, start-ups and entrants from other sectors. Water professionals often lack information technology skill sets and the perspective to appreciate what is possible, while technology entrepreneurs may not understand the nuances of complex water systems affected by multiple factors. By collaborating, urban resilience will emerge faster and smoother.

Urbanization and its impact on flood responses

Yangbo Chen*

Abstract

Urbanization is the world development trend for the past century, and the developing countries have been experiencing much rapider urbanization in the past decades. In the Pearl River Delta area of southern China, the rapidest urbanization in china has been observed for the past four decades, and dozens of highly urbanized watersheds have been appeared. Urbanization brings many benefits to human beings, but also causes negative impacts, such as increasing flood risk. Impact of urbanization on flood response has long been observed, but quantitatively studying this effect still faces great challenges. For example, deriving the urbanization pattern in the past, setting up an appropriate hydrological model representing the changed flood responses and determining accurate model parameters are very difficult in the urbanized or urbanizing watershed. In this study, a multiple classifier system (MCS) for estimating land use/cover(LUC) changes by utilizing satellite remote sensing images is proposed first, which combines advantages of different learning algorithms. With this algorithm, the LUC of the central area of Pearl River Delta area, including Guangzhou, Shenzhen and Dongguan from 1987 to 2015 at roughly every 3 years was estimated by using the Landsat satellite images, and the urbanization pattern is analyzed. Then, a physically based distributed hydrological model, the Liuxihe Model is developed for simulating the hydrological processes of the urbanized watershed. A model parameter optimization and updating strategy is proposed based on the remotely sensed LUC types, which optimizes model parameters with PSO algorithm and updates them based on the changed LUC types. Several watersheds in the highly urbanized area of the Pearl River Delta area were studied for this purpose. The LUC changes in these watersheds was first analyzed, and then the Liuxihe model was set up in these watersheds with parameters optimized and updated with the changed LUCs. Hydrological processes was simulated with the established model and parameters in different time periods, and the flood response changes was derived. The results show urbanization has big impact on the watershed flood responses, the peak flow increased a few times after urbanization which is much higher than previous studies in western countries.

*Sun Yat-sen University, Guangzhou, China
eescyb@mail.sysu.edu.cn

Multi-scale water-energy-food nexus in Asia

Makoto Taniguchi*

Abstract

Water, energy, and food are the most fundamental resources for human beings and sustainable society, and tease resources are interlinked each other. Therefore, we need integrated management and governance for the water-energy-food (WEF) nexus by increasing synergies andreducing trade-offs among the three resources. In addition to these, three resources are connected in multi-spatial scale, such as local, national, regional and global, through food and energy trades, therefore we need multiscale analyses for sustainable resources management. Water footprint and energy footprints though food trade are one of the tool for understanding how each area is inter- and intra- connected on WEF nexus. Belmont Forum SUGI project "METABOLIC" are going to establish three databases of resources, interlinkage, and scenario in multi-spatial scale including Kyoto city, Kyoto prefecture, Kansai area with 7 prefecture, Japan, and Asia. A nexus model to analyze the change of the nexus structure has been made, and assessment of the changes in three resources, carbon emission, environmental and economic impacts are analyzed.

* Research Institute for Humanity and Nature, Kyoto Japan

Conservation, Protection and Augmenting Water Resources in Peri-Urban and Rural areas – Towards better governance and management at local level using modern digital technologies.

Lawrence Surendra*

Abstract

Management of Water resources in terms of managing scarcity and over-abundance as in flood situations that can lead to disasters poses multi-dimensional challenges to planners, policy makers and local government officials. Equally so, for researchers and academics who wish to contribute to shaping public policy for better water management and in handling the Water-Energy Food Nexus in Asia. Water is not just quality or quantity. Water has many dimensions, not only as a public good and private good but as public water, private water and as common property resources. Managing this complexity of water as a resource and more so when it is entangled with social and political systems at the local level makes it even more difficult to achieve efficient water resources management. Technology and its applications, especially the use of ICT, satellite data and IOT technologies have great potential to make a significant contribution.

According to UN-ESCAP sources and estimates of the Asian Development Bank (ADB), the Asia and Pacific region requires $800 billion, or $53 billion annually, in investment over the period 2016–2030 to meet water and sanitation infrastructure needs. This includes the costs of climate proofing to ensure that infrastructure is resilient to the projected impacts of climate change. from a Water-Food- Energy (WEF) nexus, ensuring water for food security, supply of clean drinking water to all, managing water and sanitation in a manner so that critical water sources and resources are not threatened is vital. Equally critical is ensuring that improper and inadequate sanitation does not damage and destroy water sources especially in peri-urban and rural areas not only during normal times but also in times of disasters such as droughts and flooding.

This requires critically good governance and promoting good practices and accountability mechanisms at the local level. Shaping public policy especially for local governments is necessary since national level and state level policy alone cannot address specific ecosystem conditions and local characteristics of water resources, its supply and management. Post-disaster situations be it droughts or flood clearly show that if disaster prevention and risk reduction approaches at national level had been built up bottom up, both disasters and their after effects could be minimised.

For all these dimensions technology and use of technology, especially combining remote sensing technology with modern drone technologies ICT, satellite data and IOT can make a major contribution by providing a cloud based decision support system which can utilizes a framework of microwave satellite observations. Such technology will be used in two peri-urban areas that are situated in dry land farming areas and one rural area in a water abundant area, in the state of Karnataka to demonstrate how integration of such approaches using technology for policy development and management of water governance and management, can enhance efficient water use management and contribute to disaster preparedness as well. Our paper will elaborate on the field level applications of ICT, satellite image and IOT to be undertaken as well as how our work can benefit from partnerships with rich knowledge resources that have been accumulated in the work of the Water Resources System Research Unit of Chulalongkorn University and the contributions to Water Resources management made by UN-ESCAP and UNESCO.

*Chairman, The Sustainability Platform Asia and Dr.J.Jayanth, Dept. of Electronics and Communication, GSSS Institute of Engineering & Technology for Women, Mysore.

Spatio-Temporal Mapping of Water Consumption at Public Institutions: Case of United Arab Emirates (UAE) University

M. M. Yagoub and TareefaAlSumaiti, LatifaEbrahim, Yaqein Ahmed, Rauda Abdulla

Abstract

Large portion of human activities take place within buildings. Therefore, if energy and water consumption are minimized in buildings this will help in reducing climate change. UAE demarcated water in its vision 2021 as one of the areas that need more researches. This is because water is one of the basic human needs and the country spends millions of dollars every year in desalinating and transporting water to various cities and villages across UAE. Therefore, efforts could be done at individual and institutional level to optimize water usage and consequently save money and environment.

In this study, indoor water consumption at UAE university, as one of the biggest public institute in Al Ain is assessed for the period 2016-2017. The study will fill a gap in literature about water consumption at public institutes in arid environment. It utilizes Geographic Information System (GIS) to answer where water is highly consumed within the university (hot spots), when (time), who consume it, why (causes), and how to minimize consumption. It assembles diverse data reside at various departments to gain a better knowledge about the broad patterns of water consumption in the university campus. The assumption made here is that water consumption is directly proportional to population density (students/faculty/staff) and less during winter. The highest water consumption is found at the College of Information Technology (CIT) and this is due to its size and heterogeneity of its activities (lectures, workshops, conferences, book distribution, restaurants). The relationship between water consumption and number of students is modeled using least square. The coefficient of determination (R^2) is found ranged between 0.13 and 0.47. These values indicate low correlation between water consumption and number of students. This may be due to the centralized usage of buildings and movement of students between buildings during lectures.

Temporal variation showed sharp decrease during July of 2016 and 2017 irrespective of the building type/size and this is associated with summer holidays. The hypothesis of activity-driven consumption showed that the highest water consumption (67.8%) is found at residential buildings (hostels). This is due to many reasons such as longer stay time at the hostels and use of water for showering, flushing, ablution, and washing machines. The library showed consistent low water consumption. It is very interesting to deduce the library usage while investigating water consumption, but it is a lesson that water consumption could be used as a proxy to reveal number of users at buildings. The water consumption at UAEU is benchmarked with the university of Bordeaux in France and other public institutes in Al Ain. On average the water costs the university annually around two million dirhams (AED 2,030,429 = EUR 474,399 = USD 553,250). The result from this study identified sites with the highest water consumption and this could be used to adapt water conservation techniques and campaigns at these sites.

Keywords *Water consumption, public institutes, UAE University, GIS, public awareness*

Assoc. Prof. of Remote Sensing and GIS
Department of Geography and Urban Planning, College of Humanities and Social Sciences
United Arab Emirates University, P. O. Box 15551, Al-Ain
E-mail: myagoub@uaeu.ac.ae
URL: http://faculty.uaeu.ac.ae/myagoub

Use artificial intelligence and IoT technologies to build smart irrigation system.

Richard Huang*

Abstract

Taoyuan Irrigation Association (TIA) is responsible for managing irrigation water resource in Taoyuan area, Taiwan. The major water source of Taoyuan canal is from Shi-Men reservoir. Taoyuan canal transports the water to 12 branch cannels and their subsidiary ponds. All the farmland in this area is watered through these ponds. A so-called traditional irrigation policy is to supply a fixed quantity of flow for irrigation during a whole crop season. Staffs of TIA calculate required daily quantity of flow based on the factors of field size, type of crop and the period of crop growth cycle. In a crop growth cycle, water is supplied 7days x 24hours from reservoir to canals, ponds and end up to farmland.
However, the traditional irrigation policy is inefficient. The water may be over supplied in raining days and may be under supplied in hot summer. To improve the efficiency of water management, we build a system to predict the quantity of flow variation in next 3 hours of Taoyuan Canal. Base on the prediction, staffs of TIA fine tune gate of ponds to reserve extra water in advance.
All the staffs of TIA review prediction results and gate tuning suggestions from web site and mobile application.

In this project, we employ artificial intelligence model, linear planning model and IoT technologies to provide high-quality decision-making support system mentioned previously. First, we apply NNR (neural network regression) to build a prediction model. We collect over ten thousand of precipitation and water level historical data pairs as training vectors. In each vector pairs, output vector is composed by water level data and an input vector is composed by precipitation data. CC (correlation coefficient) and MAE (mean absolute error) are chosen to be the performance indices of the trained model.
The average correlation coefficient of the trained model between the predication results and on-line monitoring data from sensors is over 92%. The average mean absolute error is less than 3 centimeters.
Second, we use linear-planning model to rank the ponds which need to irrigate. The factors of the model include current volume of pond, the economic factor of pond, the length of canal between pond and main canal and the irrigation area of the pond.
The data of current volume of pond are gotten from AnaSystem's IoT system, the Senslink and SensMini A4. The SensMini A4 is an innovative compact front-end remote data acquisition device, which provides complete functions that a front-end IoT device needs. Those functions include solar charging, data logging, IP68 protection, auto data addendum, LPWAN communication (4G, LoRaWAN and NB-IoT) and universal industrial I/O.
The Senslink provides hundreds of open API for users to develop their own user interface and applications. The Senslink kernel collects, dispatch and store massive data from IoT front-end device very efficiently. In this project, our system provides gate operation suggestions for each pond every 10 minutes base on the infrastructure of Senslink.

*Chief of Operation Officer
Synergy Technology Co.,Ltd.

Technical Paper

WHAT INFORMATION ABOUT THAI LAKES DOES A WEB APPLICATION, CLIMATES OF LAKE BASINS, CONTAINS?
CLIMATES OF LAKE BASINS: CGLB

Tosiyuki NAKAEGAWA[1] and Shinichro Horiuchi[2]

Abstract Lakes are very important for multi-sectors including water sector in Thai because of a long dry season from December to April. Thai researchers know lakes in Thailand very well but foreign researchers do not always so. It is interesting to know how much information we can obtain information about lakes in Thai on the Internet. This study investigates what information and how much about lakes in Thai are accessible for preliminary scientific investigations through the Internet.

A web application, Climates of Global Lake Basins (CGLB) have been developed for providing lake information from the view point of hydrological and water resources by the combination of existing data sets. The distinction of CGLB from other web applications is that CGLB has a drawing functions of climatological information on demand. CGLB also provides landscape photographs provided by Global Confluence Project as well as quasi-real time monitoring of lake water levels using satellite altimetry provided by U.S. Department of Agriculture. The first version of CGLB contained about 600 lakes or more in the world. Recently, CGLB has been upgraded by changing a lake information database from the World Lake Database (WLDB; http://wldb.ilec.or.jp/) to the HydroLAKES following a new development of the source code due to introduction of a free database module to treat more than more than 1 million of lakes.

Lake database targeting the entire world contains some lakes only due to the coverage of the whole globe. For example, WLDB contains only 5 lakes in Thai: Boraped Reservoir (Bung Boraphet), Lam Ta Khong Reservoir, Luang Sea, Lake Songkhla, and Ubolratana Reservoir. Nobody knows the rationale of these selections. On the other hand, CGLB based on HydroLAKES contains 2004 lakes in Thailand. As an example, we demonstrate what information and how much data of Lake Thale Sap Songkhla or Thale Luang are available from CGLB.

Keywords *globa, lake, climate, Thai, web application, database*

This work was supported by Grant-in-Aid for Specially promoted Research 16H06291 from JSPS.

[1]Department of Climate Research Department
[2]Computer Management Office
Meteorological Research Institute
Tsukuba, Japan

tnakaega@mri-jma.go.jp

Introduction

Lakes has roughly 0.5% of the global land area [1] and hold more than 90% of the world's liquid freshwater in readily accessible bodies. Lakes are also one of the important components of hydrological cycles and at the same time have biogeochemical and ecological processes. In a changing climate under greenhouse gas emissions, these aspects will be affected by the global warming and will impact on human societies as well as on readily accessible water bodies.

Future projections of climates require the biogeo-chemical and ecological processes in lakes since they are embedded in the Earth system and interact with each other. Future projections of lakes require the lake information about their hydrological properties of distribution, volume and residence time. Therefore, global lake databases have been developed. Such databases are usually based on only the lake information because of their objectives. Public may want to know a climate in a target lake.

Then, we developed web application, Climates of Global Lake Basins (CGLB; http://hydro.iis.u-tokyo.ac.jp/CGLB/), combines existing datasets and interactively displays geographical, hydrological, and climatological information for hundreds of lakes around the world in 2015 [2]. The lake information in CGLB is based on the World Lake database (WLDB) [3]. Unique features of WLDB is comprehensive information about lakes from geographical information to biogeochemical one but lists only about 650 lakes. The number of the lakes in WLDB for each country is distinctly biased since they are selected as important order for people.

Recently, a new lake database, HydroLAKES has been developed with more than 1 million entry [4]. We upgraded CGLB based on HydroLAKES.

This study investigates what information and how much about lakes in Thai are accessible for preliminary scientific investigations through the Internet.

Structure of Web Application

We designed CGLB as provision of climatological information for a target lake basin so that one who want to look into the lake basin can obtain the information interactively for each own purpose.

SQLite is employed to deal with more than 1 million entry. SQLite is a relational database management system and often embedded into the end program but not client-server database engine.

New features of the CGLB are summarized below:

- replace of base lake geo-spatial information: HydroLAKES; more than 1 million lakes are listed in CGLB and other components such pouring points are newly included in CGLB,
- figures of lake shapes with either elevation or land cover type can be drawn interactively,
- Lake surface temperature can be drawn in one- or two-dimensional time series,
- link to submonthly climatology in ClimatView developed by Japan Meteorological Agency: daily data can be seen but the number of the stations are small, and
- SQLite is embedded into the end program, allowing more than 1 million entry and search by keywords.

Information on Thai Lakes

Lake database targeting the entire world contains some lakes only due to the coverage of the whole globe. For example, WLDB contains only 5 lakes in Thai: Boraped Reservoir (Bung Boraphet), Lam Ta Khong Reservoir, Luang Sea, Lake Songkhla, and Ubolratana Reservoir. Nobody knows the rationale of these selections. On the other hand, CGLB based on HydroLAKES contains 2004 lakes in Thailand. As an example, we demonstrate what information and how much data of Lake Thale Sap Songkhla or Thale Luang are available from CGLB.

Lake Songkhla Lake is the natural largest lake in Thailand. It is on the Thai Bay side or the Pacific Ocean side of the Malay Peninsula in the southern part of the country. The surface water area is 1,040 $km^2$and borders the provinces of Songkhla and Phatthalung.

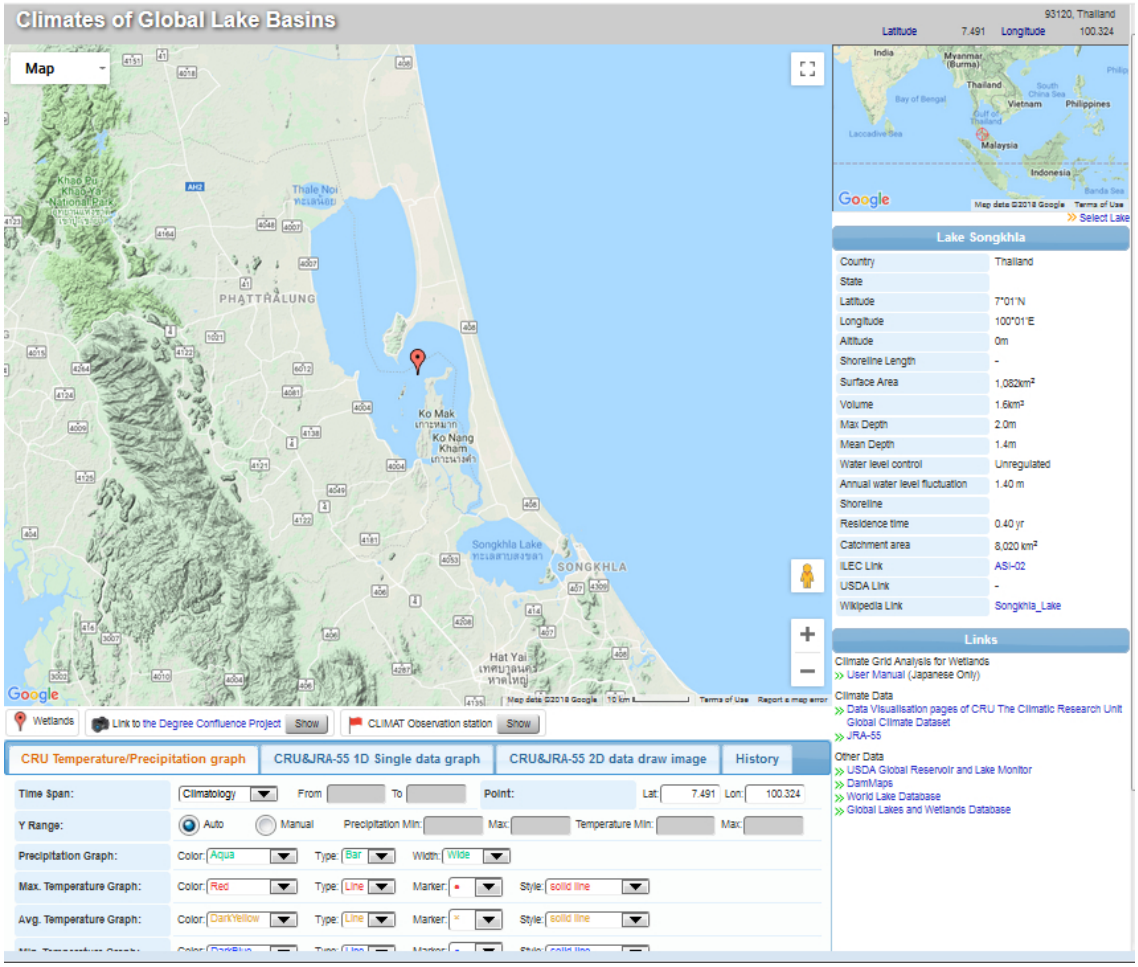

Fig. 1. Screenshot of CGLB for Lake Songkhla.

(a)

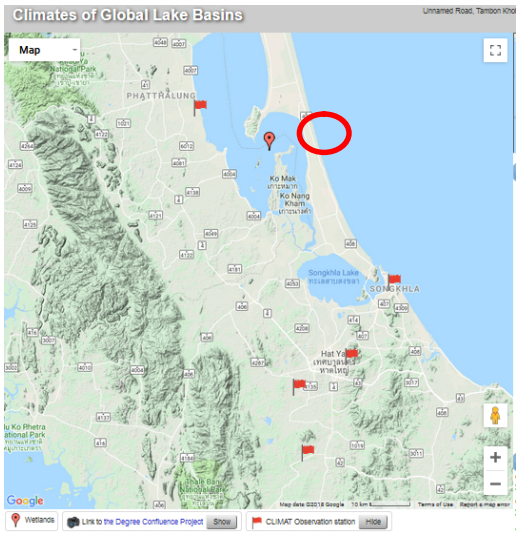

(b)

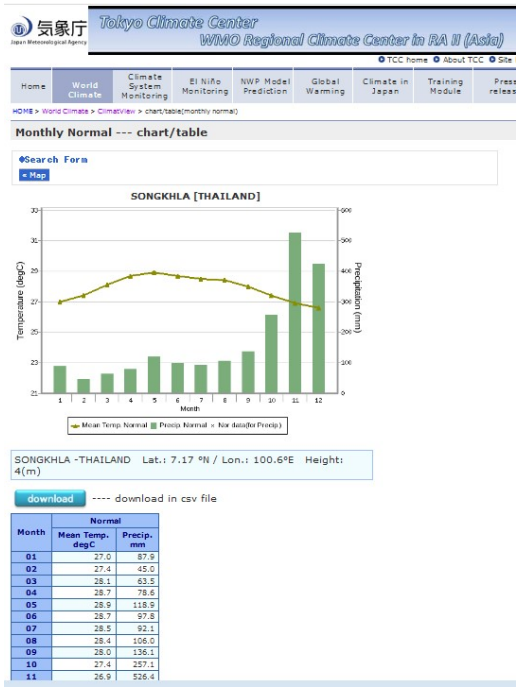

Month	Normal	
	Mean Temp. degC	Precip. mm
01	27.0	87.9
02	27.4	45.0
03	28.1	63.5
04	28.7	78.6
05	28.9	118.9
06	28.7	97.8
07	28.5	92.1
08	28.4	106.0
09	28.0	136.1
10	27.4	257.1
11	26.9	526.4

Fig. 2. (a) Screenshot of location of observation stations operated by National Meteorological and Hydrological Service, Thai Meteorological Department. Red flags denote the location of the observation station and a red circle denotes the station at Songkhla near the mouth to the Ocean and on the eastern shore of Lake Songkhla. (b) Screenshot of climatological monthly mean surface air temperature and precipitation at the station marked with the circle in (a). http://ds.data.jma.go.jp/gmd/tcc/tcc/products/climate/climatview/

Fig. 1 shows a screenshot of CGLB for Lake Songkhla. Geographical area of Lake Songkhla are shown on the Google Maps on the left-hand side and lake information based on WLDB and HydroLAKES are displayed on the right-hand side. Left-bottom below the Google Maps provides interactive draw of figures: 1-dimensional time series and 2-dimensional geographical distribution of land surface meteorological variables.

Observation stations operated by National Meteorological and Hydrological Services appear on this Google Map by one click and climatological monthly mean surface air temperature and precipitation can be seen on ClimatView developed by Japan Meteorological Agency (Fig. 2). These data are called as CLMAT and provided through World Meteorological Organization (WMO) [5]. CLIMAT is the names of the codes for reporting monthly values of meteorological parameters from weather stations and for reporting monthly aerological means from weather stations. These stations in Fig. 2a is operated by Thai Meteorological Department. Climatological annual mean temperature at Songkhla is about 28ºC in annual range of 27ºC to 28ºC. Climatological annual rainfall total is 2031.5 mm/year and climatological monthly mean rainfall reaches a peak in November. This climatological features are different from those of Bangkok.

Figure 3 shows the climatological means of monthly average, maximum, and minimum surface air temperature and the climatological mean monthly precipitation around Lake Songkhla for each month. The monthly surface air temperature and precipitation provides almost the same information in both Figures 2b and 3. Figure 3 uses gridded global data set of CRU TS3.2, while Figure 2b uses observation point dataset. The merit of gridded global dataset have no missing values which is very useful for global database like CGLB.

Figure 4 show the climatological mean monthly precipitation around Lake Songkhla for each month in two-dimensional form or geographical one. The area drawn in each panel is completely same area as in Fig.1. This figure is drawn interactively on CGLB based on your request.

Global Framework for Climate Service (GFCS) led by WMO is a global partnership of governments and organizations that produce and use climate information and services. It seeks to enable researchers and the producers and users of information to join forces to improve the quality and quantity of climate services worldwide, particularly in developing countries. CGLB may contribute to GFCS by bridging dialogues between lake-relevant communities and climate ones. Since CGLB is developed by climatologists and/or producers, more ideas by limnologists and/or lake-relevant users must be required for further developments.

Although CGLB provides figures on demand, but not even simple analysis. This implementation may depend on users' request. CGLB contains comprehensive information, and therefore would provide an opportunities in a variety of unique research on global lakes.

Concluding Summary

We upgraded a web application of CGLB by introducing a new lake database, HydroLAKES with more than 1 million entry of lakes by combining existing datasets and interactively displays geographical, hydrological, and climatological information around the world. These functions are useful for education, expedition planning, and scientific research.

For an integrated lake basin managements, socio-economic information is also required. The information will be implemented in a next updates. Another upgrade may be an implementation of a numerical simulation together using the information in CGLB. Dialogue with the users may help us with considering further developments of CGLB.

Acknowledgment

This paper is prepared based on my article in a proceeding of [6] and the contents are almost the same but for Lake Songkhla.

The Author thanks Ms. M. Morichika for preparing materials of my papers and presentations about this study. The contents of Introduction and Web application Sections are almost the same as in the author's article in the Proceedings of the 17th World Lake Conference held in Tsukuba, Japan in 2018.

References

[1] Nakaegawa T: Comparison of water-related land cover types in six 1-km global land cover datasets, Journal of Hydrometeorology, Vol. 13, pp. 649–664, 2012. DOI: 10.1175/JHM-D-10-05036.1.

[2] International Lake Environmental Committee: World Lake Database, 1999. http://wldb.ilec.or.jp. Last access April 11, 2018.

[3] Nakaegawa T, S. Horiuchi, and H. Kim: Development of a web application for examining climate data of global lake basins: CGLB, Vol. 9, pp.125-132, 2015. DOI: 10.3178/ hrl.9.125

[4] Messager M.L., Lehner B., Grill G., Nedeva I., Schmitt O: Estimating the volume and age of water stored in global lakes using a geo-statistical approach. Nature Communications: pp.13603. 2016. DOI: 10.1038/ncomms13603

[5] World Meteorological Organization: Handbook on CLIMAT and CLIMAT TEMP Reporting, WMO Technical Document, No.1188, pp.115, 2009.

[6] Nakaegwa, T. Web Application for Examining Hydroclimate Information of Global Lake Basins: CGLB Using a latest world lake database. The Proceedings of The 17th World Lake Conferences 2018.

[7] Nakaegawa T, S. Horiuchi, and H. Kim: Development of a web application for examining climate data of global lake basins: CGLB, Vol. 9, pp.125-132, 2015. DOI: 10.3178/ hrl.9.125

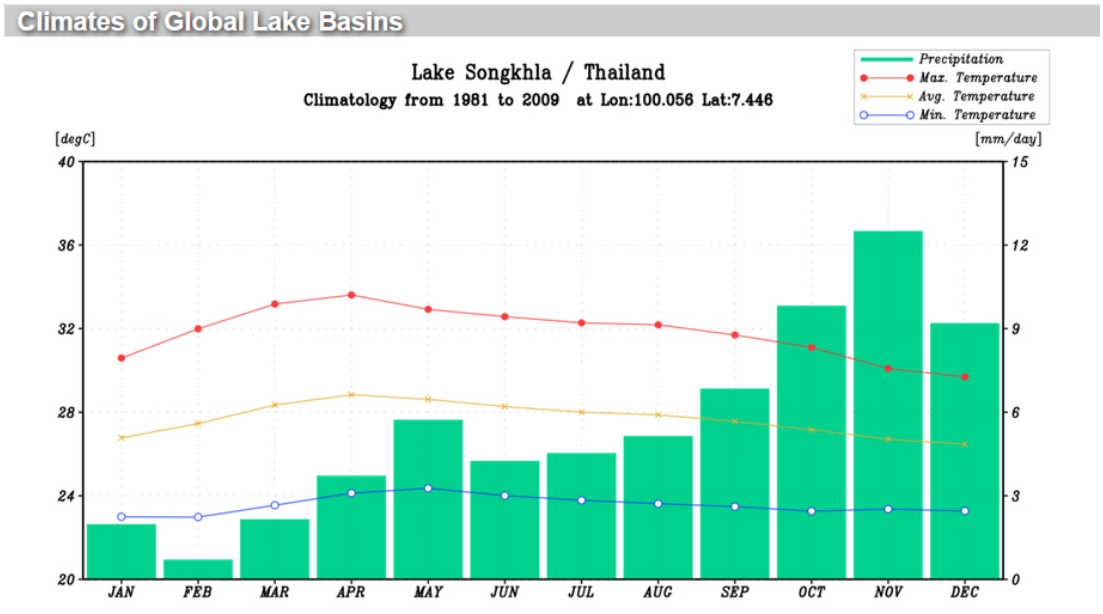

	Jan	Feb	Mar	Apr	May	Jun	Jul	Aug	Sep	Oct	Nov	Dec
Precipitation [mm/day]	1.980	0.710	2.156	3.725	5.732	4.250	4.532	5.144	6.850	9.822	12.502	9.198
Max. Temperature [degC]	30.593	31.990	33.176	33.614	32.924	32.572	32.279	32.183	31.697	31.100	30.090	29.693
Avg. Temperature [degC]	26.766	27.459	28.341	28.838	28.617	28.269	28.000	27.876	27.559	27.159	26.703	26.466
Min. Temperature [degC]	22.993	22.979	23.548	24.124	24.355	24.007	23.783	23.621	23.479	23.262	23.359	23.272

Fig. 2. Climatological monthly mean, maximum, and minimum surface air temperature and precipitation around Lake Songkhla for each month at the center point of the map. This figure is drawn interactively on CGLB. The data used is gridded global dataset of CRU TS3.2.

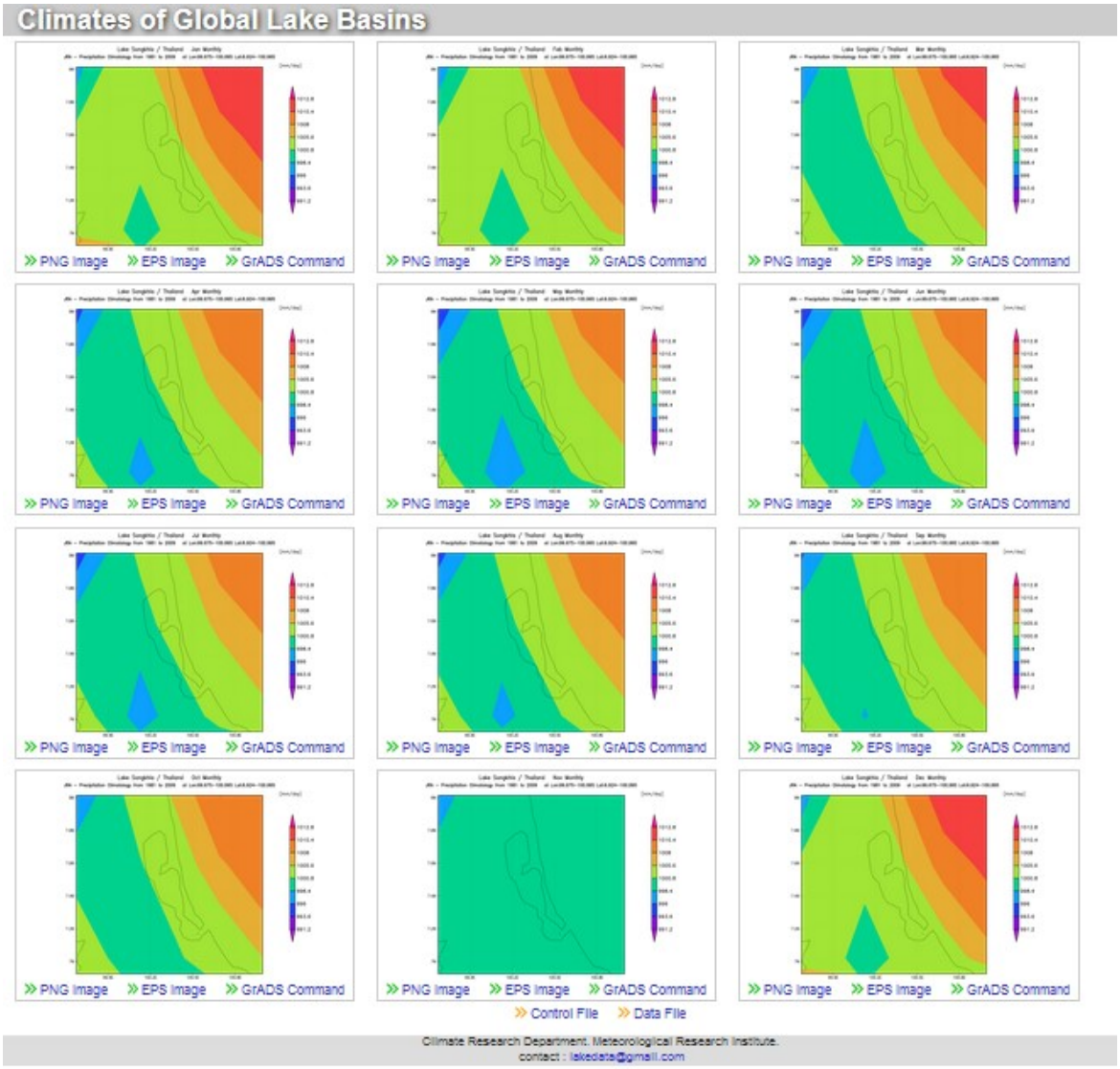

Fig. 4. Climatological mean monthly precipitation around Lake Songkhla each month in two-dimensional form or geographical one. The area drawn in each panel is completely same area as in Fig.1. This figure is drawn interactively on CGLB.

Evaluation of Satellite Precipitation from Google Earth Engine in Tonle Sap Basin, Cambodia

Phanit Mab[1], Steven Ly[2], Chuphan Chompuchan[1], Ekasit Kositsakulchai[1,3,a,*]

Abstract Precipitation is important to life on Earth. It is a predominant process in the global hydrologic cycle and is an indispensable component of water balance analysis. However, in some area like the Tonle Sap basin in Cambodia, the information on precipitation is deficient and sometimes difficult to access. In this case, satellite remote sensing coupled with GIS techniques have been applied and considered as a powerful and effective tool in handing precipitation analysis tasks. Recently, the Google Earth Engine (GEE) platform provides satellite datasets and collection of the tool for analysis of data using JavaScript without downloading huge data from the Internet. In this study, we aimed to evaluate the application of GEE platform for retrieving and analyzing precipitation data of the Tropical Rainfall Measuring Mission (TRMM) in Tonle Sap basin (TLS). The methods included: (1) to collect the satellite precipitation data (3B43V7) by manual download and by retrieving them from GEE platform; (2) to analyze monthly precipitation over the study area by GIS analysis functions and by JavaScript on the GEE platform, data in 2010 was sampling as a case study; and (3) to compare results from both GIS and GEE with observation data from ground stations. The results showed the good correlations between the precipitations from manual download and those from a GEE platform, with R greater than 0.9. In short, the application of GEE platform is very effective; it provides a comprehensive tool for managing time-consuming tasks, like precipitation data collection and analysis, and results in reliable outputs.

Keywords *Satellite precipitation, Mekong River, Google Earth Engine*

[1]Research Laboratory for Intelligent system in Agro-hydrological Monitoring and Management (INAMM)
Faculty of Engineering
at Kamphaeng Sean, Kasetsart University,
Nakhon Pathom, 73140 Thailand.
[2]Department of Civil and Earth Resources Engineering, Kyoto University, Japan.
[3]Water Engineering and Management Program,
Asian Institute of Technology,
Pathumthani, 12120 Thailand.

[a]ekasit.k@ku.th (corresponding author)

Introduction

Precipitation is a critical variable in the global hydrologic cycle, and it influences our daily lives (drought, floods, agricultural, irrigation, outdoor activities, etc.)[1]. However, the accessibility of precipitation data in the Tonle Sap Lake region is one of limitations to conduct a comprehensive hydrological analysis.

In this case, the techniques of satellite remote sensing have been widely used and been considered as a powerful and effective tool in perceiving precipitation. However, a massive datasets have to be downloaded; satellite image processing with geographic information system (GIS) analysis function is the prerequisite before retrieval ofrainfall information.

Recently, the Google Earth Engine (GEE) leverages cloud computing services to provide analysis capabilities on over 40 years of Landsat data[2], and others satellites. As a remote sensing platform, its ability to analyze global data rapidly lends itself to being an useful tool on data visualization [3]. Additionally, dataset is processing of geospatial datasets an online for rapid visualization of complex spatial analyses using the Javascript Application Programming Interface (API). This API allows us to develop a code in order to get datasets of publicly available remotely sensed imagery and other data.

This study aimed to apply the GEE platform for automatically retrieving and analyzing precipitation data of the Tropical Rainfall Measuring Mission (TRMM) in Tonle Sap Lake basin (TLS), Cambodia. The methods included: (1) to collect the monthly precipitation data (3B43V7) by manually download and to retrieve from GEE platform; and (2) to compare a selected precipitation data of whole TLS basin in 2010, derived by GIS analysis functions and by JavaScript on a GEE platform, and (3) to compare both GIS and GEE with observation data from ground stations.

Material and Method

A. Study Area

The Tonle Sap Lakeis the largest permanent freshwater lake, locating in Cambodia at the Lower Mekong River basin [4]. During the dry season, the lake is about 120 km long and 35 km widewith an area of about 2500 km^2. A bathymetrical survey of the lake

proper, conducted between 1997 and 1999, revealed a relatively flat bottom, with a maximum depth of about 3.3 m[5].During the flood period the Lakeexpands to 250 km long and 100 km wide with an area of about 17,500 km^2, and the depth reaches 8-10 m. The floodplain surrounding the lake extends 20-40 km and is dominated by seasonally inundated forest and rice field [5, 6]. The Tonle Sap basin, extends over 44% of Cambodia's total area 80,000 km^2. 32% of Cambodia's total populationdepend on this lake in living [7].

There arefiveprovinces bordering Tonle Sap Lake namely: Siem Reap, Battambang, Pusat, Kampong Cham, and Kampong Thom. Tonle Sap Basin consists of 11 sub-basins: namely (1) Stung Sreng, (2) Stung Chikreng, (3) Tonle Sap, (4) Stung Pursat, (5) Stung Dauntri, (6) Stung Boribo, (7) Stung Sangker, (8) Stung Monkong Borey, (9) Stung Staung, (10) Stung Sen, (11) Stung Chinit and (12) Stung Sieamreap (Fig. 1).

Tonle Sap basin climate influences from the tropical monsoon seasons. Dry season runs from December to April and rainy season comes when the winds shift into the southwestmonsoonfrom May to November. The monsoon returns south during August and October when the rainfall is usually heavier, with the highestrainfall in October.

B. Satellite Precipitation-TRMM 3B43V7

Many studies have been conducted on detecting diurnal cycles of precipitation over different parts of the world usingsatellite data, especially the Tropical Rainfall Measuring Mission (TRMM)[8].

Recently, data 3B43 is monthly executed to produce the precipitation rate field (3B43). These were combining the 3-hourly merged high-quality/IR estimates (3B42) with the monthly accumulated Global Precipitation Climatology Centre (GPCC) rain gauge analysis. Data are available from 1998 to presentat https://pmm.nasa.gov/data-access/downloads/trmm.

C. Precipitation Processing by GEE Platform

Google Earth Engine (GEE)platform facilitates a fast analysis by using Google's cloud-computing infrastructure(https://earthengine.google.org/).The pre-processed monthly data of Tropical Rainfall Measuring Mission data, or TRMM3B43V7, available through GEE was used to assess precipitation data across the study area. The spatial resolution of the above datasets are all equal to $0.25° \times 0.25°$ with monthly gridded rainfall data [9, 10].

This process is using JavaScript coding in GEE platform screen. TRMM 3B43V7 datasets could be specified location of boundary of Tonle Sap basins in coding. At the end, the amount of precipitation data had retrieved each sub-basins in CSV which can open with MS Excel to interpret data in number.

D. Thiessen Polygon Method

The Thiessen polygon methodallows for areal weighting of rainfall from each gauge. A_i is polygon area, P_i is average precipitation and A is total area [11].

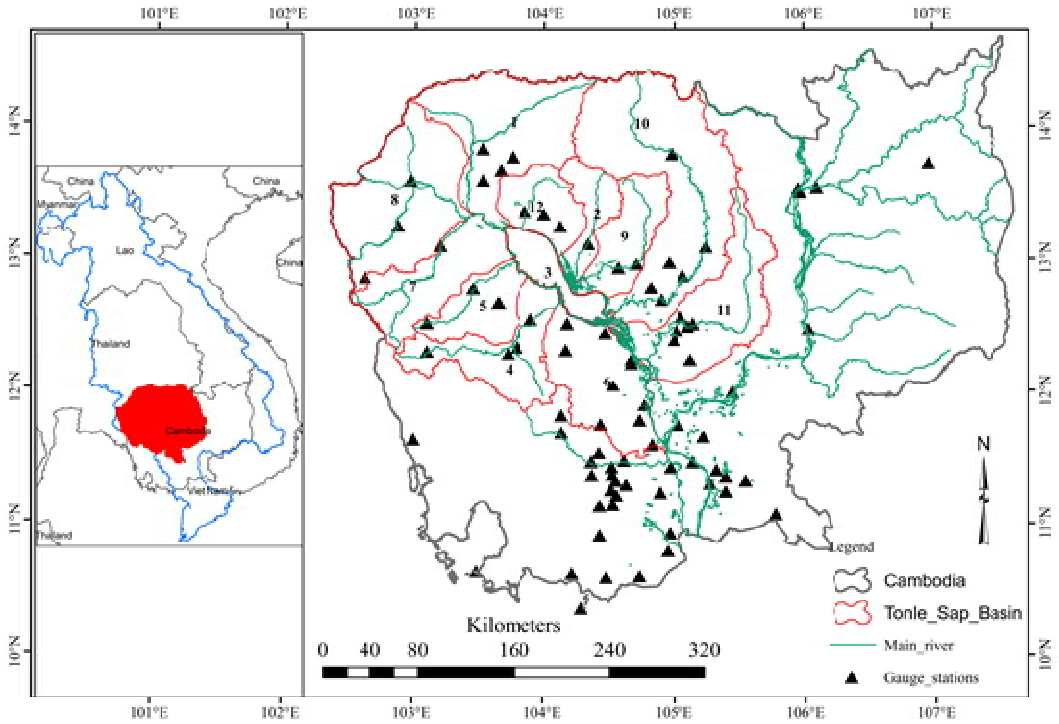

Fig. 1. Boundary of Tonle Sap Basin and location raingauge stations

E. Statistical Indicators

Correlation coefficient (r) is measured on a scale between -1 and +1 to determine the extent to which two sets of paired values are related in a linear fashion. The number closer to -1 and +1 are -1 is a perfect negative linear correlation, whereas the number closer to +1 is a perfect positive linear correlation, and 0 is no correlation.

$$r = \frac{\sum_{j=1}^{N}(X_j - \bar{X})(Y_j - \bar{Y})}{\sqrt{\sum_{j=1}^{N}(X_j - \bar{X})^2 \sum_{j=1}^{N}(Y_j - \bar{Y})^2}} \quad (2)$$

Root mean square error (RMSE) is the square root of the mean of the summation of squared differences between two sets of values where there are n number of paired values x and y. This statistic provides an absolute (neither positive nor negative) value of differences between two sets of values. A smaller value signifies less error.

$$RMSE = \sqrt{\frac{1}{N}\sum_{j-1}^{N}(x_j - y_j)^2} \quad (3)$$

F. Methodology

In this study, 94 rainfall stations from Mekong River Commission (MRC) and Cambodia's Ministry of WaterResources and Meteorology (MoWRAM) were selected which covered almost the entire of Tonle Sap basin.

To achieve the research objectives, data processing methods were divided into three main parts (Fig. 2), including manual data acquisition and GIS processing, GEE-based data processing and gauge observation using Thiessen Polygon method.

The first part is to download monthly precipitation in 2010 (TRMM 3B43v7) in raster format (HDF), and use GIS analysis functions to interpret data, change coordinate system to the same area. Using the function "Zonal statistic as table" in order to get the amount of precipitation with "shape file of boundary".

The second part is to develop the JavaScript code on the GEE platform (https://code.earthengine.google.com).The code included: importing the TRMM image dataset; specifying the boundary of study area by uploading shape file into GEE data script; extracting the mean monthly precipitation of the basin by writing code on script (see example in Fig. 3). After having execute the code, the precipitation data were retrieved on sub-basins automatically.

Lastly, the areal precipitation from gauge station were estimated by Thiessen Polygon method. Precipitation of basin was summarized using "Zonal statistic as table" with boundary of basin. The precipitation data retrieved from the first and second methods were finally compared with the observed data from gauge stations for the entire basin and each sub-basin. Statistical indicators, correlation coefficient (r) and RMSE, were estimated.

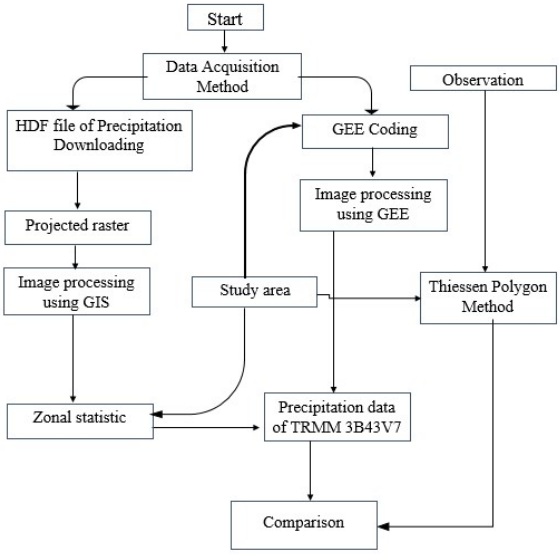

Fig. 2. Research framework

Results and discussions

A. Monthly Precipitaion Depth

Fig. 4 shows monthly precipitation of the Tonle Sap Basin in 2010, derived from 3 methods: GIS analysis of downloaded TRMM data (GIS), GEE processing (GEE) and observed rainfall with Thiessen Polygon estimation (OBS).

1) TRMM Precipitation from GIS vs. GEE Processings

The amount of precipitation from TRMM 3B43V7 using both GIS analysis of downloaded data (GIS) and Google Earth Engine processing (GEE) methods were well matched with almost identical rainfall depths from January to December on 2010. In dry season from November to April, rainfall varied from 8 to 70 mm, while in wet season from May to October, rainfall varied from 100 to 300 mm. The highest precipitation can be observed in October around 300 mm. GEE provided an almost similar the amount of rainfall compared to manually download rainfall. There are somewhat difference between 0.005 to 1.8 mm due to round-off errors during data processing.

2) Precipitation from GEE Processings vs. Observation

From Fig. 4, TRMM precipitation from GEE processing and basin rainfall estimation from gauge

station (OBS) were well captured the amount of monthly rainfall. By comparing GEE rainfall with rain gauge data, we can observed an over-estimated rainfall by GEE mostly during dry period from January to June (4 to 20 mm), in October and in December. Rainfall by GEE were under-estimated during wet period from July to September 30 to 49 mm. However, these values were observed as less error between rainfall from GEE and observation. Fig. 5 showed the spatial data on the monthly average rainfall in millimeters from the GEE platform.

3) Precipitation from GIS Processing vs. Observation

Based on result shown in Fig.4, the differences of rainfall depths between GIS processing (GIS) and the gauged observation (OBS) are comparable to those between GEE and OBS. The identical months of over- or under-estimation were observed. The GIS rainfall were over-estimated from the lowest of 4 mm on December to the highest of 20 mm on June.

B. Statistical Indicators

Statistical indicators of the whole basin were shown in Table I, the amount of precipitations from manual download and those from a GEE platform provided an almost similar monthly rainfall depth with r greater than 0.99 whole basin. Finally, both methods GEE and GIS provided a good correlation with the gauge which showed the r value greater than 0.97 and the highest RMSE of basin about 16 mm.

Statistical indicators of each sub-basins were presented in Table II, the indicators demonstrated the good correlations of rainfall between GIS *vs.* GEE, GEE *vs.* observation, and GIS *vs.* observation. The correlation coefficient, r, are 0.99, 0.81 and 0.80 respectively.

Table I. Statistical Indicators of Basin

Method	***r***	***RMSE***
GIS vs. GEE	0.999	0.70
GEE vs. OBS	0.975	16.40
GIS vs. OBS	0.977	15.88

Table II. Statistical Indicator of each Sub-basins

Sub basin	**GIS *vs.* GEE**		**GIS *vs.* OBS**		**GEE *vs.* OBS**	
	r	***RMSE***	***r***	***RMSE***	***r***	***RMSE***
1	0.9898	1.20	0.8713	23.56	0.8818	23.97
2	0.9997	1.13	0.8719	27.21	0.8259	27.73
3	0.9998	1.73	0.9611	17.72	0.9347	17.94
4	0.9998	2.15	0.9723	24.81	0.9424	25.80
5	0.9905	1.39	0.8437	23.49	0.8824	23.62
6	0.9996	2.36	0.8089	20.73	0.8984	21.46
7	0.9991	2.36	0.9032	39.27	0.8010	38.77
8	0.9997	7.26	0.8864	29.70	0.8725	26.18
9	0.9997	0.86	0.9392	19.51	0.9697	19.82
10	0.9994	1.30	0.9393	19.99	0.9638	20.14
11	0.9997	1.00	0.8326	24.96	0.8757	24.64
12	0.9997	6.59	0.8872	28.41	0.8897	27.94

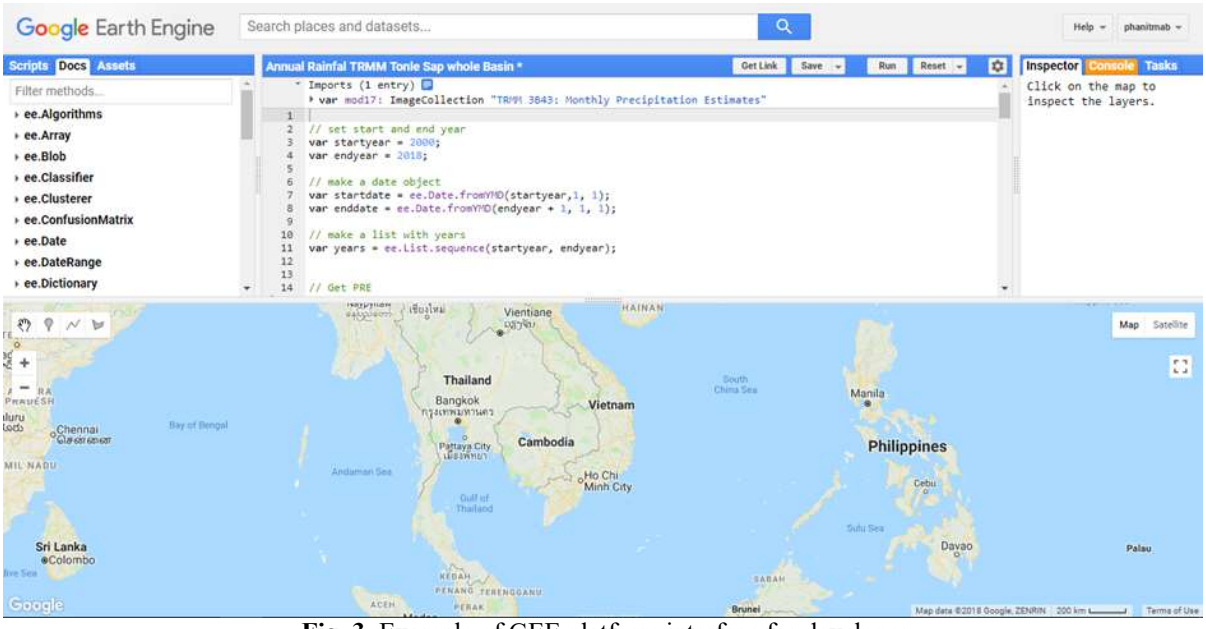

Fig. 3. Example of GEE platform interface for developer

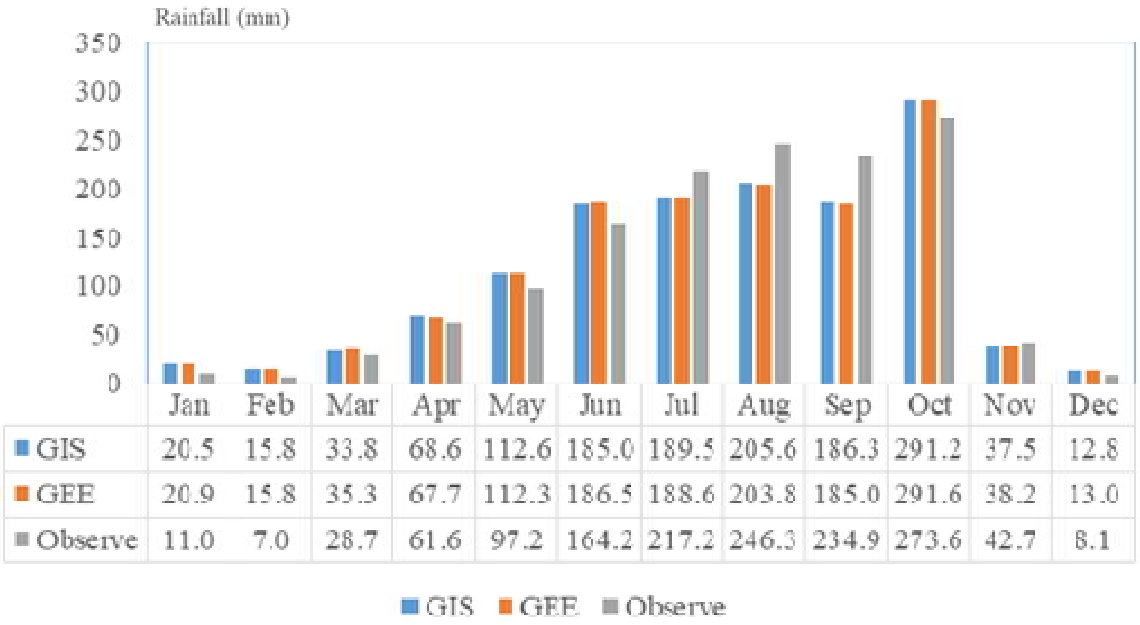

	Jan	Feb	Mar	Apr	May	Jun	Jul	Aug	Sep	Oct	Nov	Dec
GIS	20.5	15.8	33.8	68.6	112.6	185.0	189.5	205.6	186.3	291.2	37.5	12.8
GEE	20.9	15.8	35.3	67.7	112.3	186.5	188.6	203.8	185.0	291.6	38.2	13.0
Observe	11.0	7.0	28.7	61.6	97.2	164.2	217.2	246.3	234.9	273.6	42.7	8.1

Fig. 4. Montly rainfall in 2010 estimated by three methods: GIS analysis of downloaded data (GIS), GEE processing (GEE) and observed rainfall with Thiessen Polygon estimation (OBS)

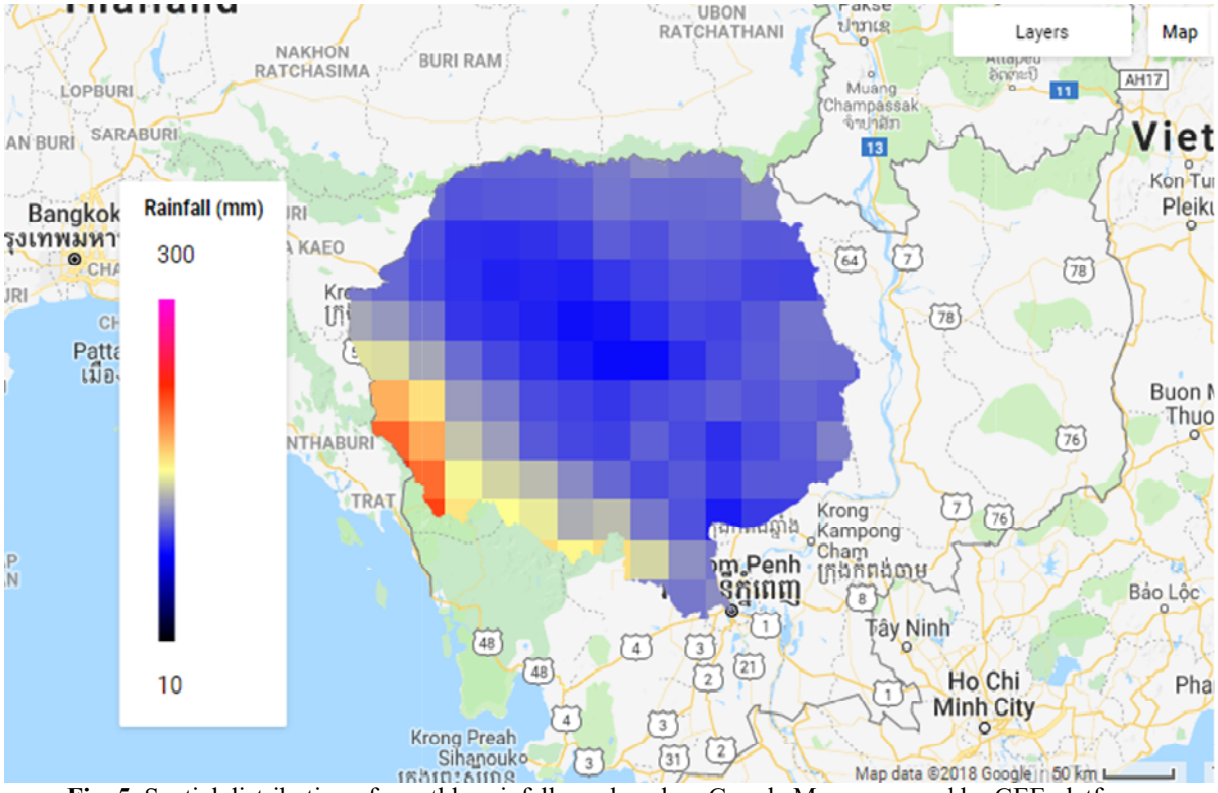

Fig. 5. Spatial distribution of monthly rainfall overlayed on Google Map processed by GEE platform

Conclusions

Both precipitations from manually download and those froma GEE platform provided an almost similar rainfall depth for each sub-basins and the entire basin. However, the amount of precipitation of each sub-basins had some error because of uncertainty and location of the gauges in basins. TRMM 3B43V7 dataset provided high correlation when compared with the gauge stations. In short, the GEE platform is an effective tool which provides a comprehensive for managing time-consuming tasks, namely precipitation data collection and analysis. It is a new concept of remote sensing platform on how to get satellite datasets easily and quickly with results in reliable outputs.

Acknowledgment

This paper was supported by the Kasetsart University Scholarships for ASEAN for Commemoration of the 60th Birthday Anniversary of Professor Dr. Her Royal Highness Princess Chulabhorn Mahidol. Moreover, the authors would also like to express their gratitude to the Google Earth Engine (GEE) developers for providing a registration during this research on retrieval datasets.

References

[1] G. Langella, A. Basile, A. Bonfante, and F. Terribile, "High-resolution space–time rainfall analysis using integrated ANN inference systems," Journal of hydrology, vol. 387, no. 3-4, pp. 328-342, 2010.

[2] J. Dong, X. Xiao, M. A. Menarguez, G. Zhang, Y. Qin, D. Thau, C. Biradar, and B. Moore III, "Mapping paddy rice planting area in northeastern Asia with Landsat 8 images, phenology-based algorithm and Google Earth Engine," Remote sensing of environment, vol. 185, pp. 142-154, 2016.

[3] N. N. Patel, E. Angiuli, P. Gamba, A. Gaughan, G. Lisini, F. R. Stevens, A. J. Tatem, and G. Trianni, "Multitemporal settlement and population mapping from Landsat using Google Earth Engine," International Journal of Applied Earth Observation and Geoinformation, vol. 35, pp. 199-208, 2015.

[4] I. Campbell, S. Say, and J. Beardall, "Tonle Sap Lake, the heart of the lower Mekong," in The Mekong: Elsevier, 2009, pp. 251-272.

[5] I. C. Campbell, C. Poole, W. Giesen, and J. Valbo-Jorgensen, "Species diversity and ecology of Tonle Sap Great Lake, Cambodia," Aquatic Sciences, vol. 68, no. 3, pp. 355-373, 2006.

[6] W. J. Junk, M. Brown, I. C. Campbell, M. Finlayson, B. Gopal, L. Ramberg, and B. G. Warner, "The comparative biodiversity of seven globally important wetlands: a synthesis," Aquatic Sciences, vol. 68, no. 3, pp. 400-414, 2006.

[7] ADB, "The Tonle Sap Basin Strategy," 2005, p. 9.

[8] M. S. K. Kiany, R. C. Balling Jr, R. S. Cerveny, and D. S. Krahenbuhl, "Diurnal variations in seasonal precipitation in Iran from TRMM measurements," Advances in Space Research, 2018.

[9] Z. Duan and W. Bastiaanssen, "First results from Version 7 TRMM 3B43 precipitation product in combination with a new downscaling–calibration procedure," Remote Sensing of Environment, vol. 131, pp. 1-13, 2013.

[10] G. J. Huffman, D. T. Bolvin, E. J. Nelkin, D. B. Wolff, R. F. Adler, G. Gu, Y. Hong, K. P. Bowman, and E. F. Stocker, "The TRMM multisatellite precipitation analysis (TMPA): Quasi-global, multiyear, combined-sensor precipitation estimates at fine scales," Journal of hydrometeorology, vol. 8, no. 1, pp. 38-55, 2007.

[11] P. B. Bedient, W. C. Huber, and B. E. Vieux, Hydrology and floodplain analysis. 2008.

Impact of Water Losses on Pressure and Energy in MWA Trunk Main Network, Thailand

Surachai Lipiwattanakarn[1,a], Adichai Pornprommin[1,b] and Sutthisak Lapprasert[2,c]

Abstract Awater distribution system simulation model using the EPANET software was built to study the impact of water losses on pressure and energy in the Metropolitan Waterworks Authority(MWA) Trunk Main Network. The model was based on the MWA data in March 2013, where the percentage of water losses (%WL) = 27.45% with the average pressure of 8.66 m, and the electricity energy consumption for water distribution system was 369 MW-h/day. The MWA is suffering from high water losses and low pressure. Thus, the MWA has set the targets to reduce %WL to 19% and raise the pressure to 10.8 m in 2021. From our model results, if the MWA open the existing 130 throttled valves on its trunk mains, the pressure may increase to 9.24 m, but it impacts %WL and the energy consumption to increase as well. If the MWA couldreduce the volume of water losses, it would benefit both higher pressure and smaller energy consumption. Also, the relationships between water losses, pressure and energy were linear. Keeping the pressure provided from pumping stations and other sources constant, we found that if the MWA could reduce %WL to 19% as its target, the pressure wouldraise to 10.7 m very close to the pressure target, and it could save the electricity energy consumption of 23 MW-h/day (~30 million baht/year). Thus, water loss control and reduction programs are an effective approach when pressure improvement and energy saving are considered.

Keywords *Water-energy nexus, Water losses, Pressure*

[1]Department of Water Resources Engineering
Faculty of Engineering, Kasetsart University
Bangkok, Thailand
[2]Waterworks Improvement Project Department
Metropolitan Waterworks Authority
Bangkok, Thailand

[a]fengsuli@ku.ac.th
[b]fengacp@ku.ac.th
[c]sutthisak@mwa.co.th

Introduction

The expansion of urban area due to population and economic growth has induced an increase in urban water demands. According to [1], at present,55% of the world's population lives in urban areas (4.2 billion in 2018), and it is expected to increase to 68% by 2050 (6.7 billion). Thus, many water utilities have to cope with the rapid growth of water demand. Also, they may experience high water losses due to their old and deteriorated infrastructures, especially leakage. Since water losses cause higher discharges in water distribution systems than water demands, energy losses will increase,andthe distribution system pressure decreases. Thus, moreinput energy is necessary to provide to maintain acceptable pressure levels in the systems. A new systematic methodology to assess energy has been proposed [2]-[3].It shows that water losses impact energy losses in two ways: an additional friction energy and an outgoing energy through water losses.Theenergy assessment (sometimes called "energy audit" or "energy matrix") of water distribution systems has been studied in some countries recently [4]-[6].

The Metropolitan Waterworks Authority (MWA) of Thailand, providing potable water for Bangkok and its two neighboring provinces (Nonthaburi and Samutprakarn) is one of many utilities in developing countries that suffer from high water losses and low pressure. To deal with water losses, in 2006, MWA has redesigned its looped water distribution system to a District Metering Area (DMA) system by partitioning the existing network into subsystems with specifically defined and permanent boundaries. Thus, the volume of water lost within DMAs can be calculated, and it can guide leak detection deployment decisions to fix leaks.Other benefits from the DMA system for water loss control can be found in [7]. As a result, the percentages of water losses (%WL) reduced from 31.00% in 2006 to 24.58% in 2013 [8].

According to [6] based on the trunk main model for March 2013, the MWA had supplied the input energy to the network (excluding pumping losses) was 277 MW-h/day under %WL of 25.8%, and its 15% of the input energy was lost through leaks, and 21% was dissipated as a result of leaks by means of the additional friction. Thus, leakage is an important parameter to be considered when energy efficiency is a concern.In addition, the distribution system

pressurewas 8.08 m.Recently, the MWA has set the targets to reduce %WL to 19% and raisethe pressure to 10.8 m in 2021. These targets are very challenging because water losses and pressure are interrelated. Increasing pressure means higher leakage flow, and leakage is the largest portion of water losses. On the other hand, if the MWA can reduce its water losses, its pressure will raise by itself without increasing the pressure at the pumping stations. Thus, this study aims to investigate the relationship between water losses, pressure and energy of the MWA distribution system and suggest how MWA can accomplish its goal.

Methodology

A. MWA water distribution system

The MWA produces around 5 million m^3 per day and covers the total area of 3,195 km^2[8]. Its water distribution system consists of 4 water treatment plants, 11 distribution pumping stations, 191 km of transmission tunnels (D = 2000-3400 mm), 1,727 km of trunk mains (D = 500-1800 mm), 31,832 km of distribution pipes (D = 100-400 mm) and about 2 million service connections.

Fig. 1. Metropolitan Waterworks Authority (MWA) trunk main network [6].

Fig. 1 shows the MWA trunk main network using in the analysis of [6] using the EPANET software.The sources are from the water treatment plants, the pumping stations andthe valve chambers, while the district meters (DMs) are the downstream ends of thisMWA trunk main network before water flowing into distribution pipe networks in DMAs. In this study, we extend this pipe network model of [6] to study the impact of water losses on pressure and energy in more details.

B. Energy balance

Table 1 shows the conceptual energy balance and components using in this study. E_{Input} is the input energy from sources. E_{Input} then turns into the output energy (E_{Output}) andthe dissipatedenergy in the network ($E_{Dissipated}$). E_{output}gets out of the network via the energy delivered to DMs ($E_{U,DM}$), the outgoing energy through water loss in DMAs ($E_{L,DM}$) or the outgoing energy through water loss on trunk mains ($E_{L,T}$). For $E_{Dissipated}$, the energy losses are due to the frictions at the DM feed lines ($E_{F,DM}$), on the trunk mains ($E_{F,T}$) and at throttledvalves on the trunk mains ($E_{F,V}$). In this study, we investigated a change of the input energy (E_{Input}) due to water losses reduction. Thus, E_{Input} can be computed as follows:

$$E_{Input} = \gamma \cdot \sum_{i=1}^{n_{Input}} \left[\sum_{k=1}^{n_t} Q_{Input_{i,k}} \cdot H_{Input_{i,k}}\right] \cdot \Delta t \qquad (1)$$

where i and k are indices, γ is specific weight of water, n_{Input} and n_t are the numbers of input energy feeders and time steps, respectively, $Q_{Input_{i,k}}$ and $H_{Input_{i,k}}$ are flow rate and energy head supplies by sources, respectively.

Table I. Conceptual energy balance and components of MWA trunk main network.

E_{Input} Input energy	E_{Output} Output energy	$E_{U,DM}$ Energy delivered to DMs
		$E_{L,DM}$ Outgoing energy through water loss in DMAs
		$E_{L,T}$ Outgoing energy through water loss on trunk mains
	$E_{Dissipated}$ Dissipated energy	$E_{F,DM}$ Friction at the DM feed lines
		$E_{F,T}$ Friction on the trunk mains
		$E_{F,V}$ Friction at throttled valves

C. Simulation scenarios

As leakage is the largest portion of water losses and dependent to pressure at leaks, we assume water loss flow (q_L) in the network as

$$q_{L,j} = C_{L,j} P_j^{N_1} \qquad (2)$$

where j is index representing junctions having leaks on the network, $C_{L,j}$ and P_j are the water loss parameter and pressure at the junction j, respectively, and N_1 is an exponent of the relationship function between leakage rate and pressure according to the concept of fixed and variable area discharge paths (FAVAD) [9].

Table 2 shows the simulation scenarios in this study to investigate the effects of valve throttling and water loss reduction. The scenario no. 0 is our base trunk main model using the data in March 2013.

According to [6], the energy loss by the friction at throttled valves ($E_{F,V}$) in the MWA trunk main network was around 13 MW-h/day (5% of E_{Input}). Throttling valves is known as an unsatisfactory practice for pressure management because it causes high energy loss and pressure drop during peak flows. But the MWA has throttled around 130 valves on its trunk mains. Since the MWA targets to increase its distribution system pressure, thus, we introduced the first scenario in which all throttled valves were fully open while all pressures at the sources and the water loss parameter (C_L) were kept at their original values. Then, the following scenarios were the reduction of water losses from the scenario no. 1 by decreasing C_L by 20% for each step.

Table II. Simulation scenarios.

Scenario	Scenario Explanation	Throttling valves	Water loss parameters
0	Base model from [6]	Yes	$C_{L,j}$
1	Remove all throttled valves	No	$C_{L,j}$
2	1st step of leak reduction	No	0.8*C_L
3	2nd step of leak reduction	No	0.6*C_L
4	3rd step of leak reduction	No	0.4*C_L

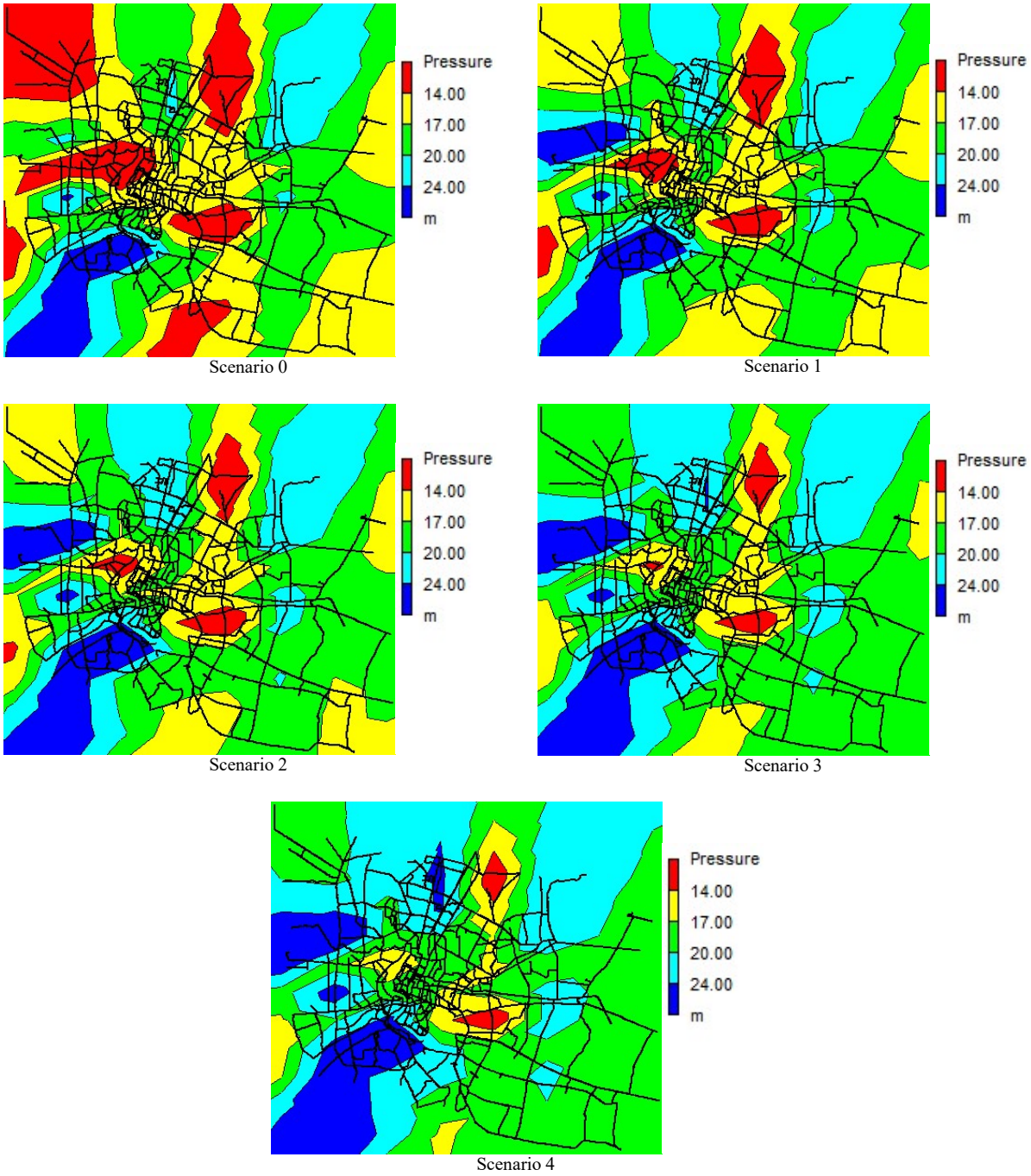

Fig. 2. Pressure distribution during peak time (7:00 am) for each simulation scenario

Table III. Results of water losses, pressure and energy.

Scenario	Volume of water losses, WL (MCM/day)	Percentage of water loses, %WL (%)	Average Pressure (m)	Range of Pressure (m)	Input Energy, E_{input} (MW-hr/day)
0	1.422	27.45	8.66	4.25 - 10.70	270
1	1.526	28.89	9.24	4.40 - 11.73	289
2	1.295	25.63	9.74	4.55 - 12.49	277
3	1.036	21.61	10.33	4.72 - 13.39	264
4	0.741	16.48	11.02	4.92 - 14.49	249

Results and discussion

A. Pressure distribution

According to the United States recommended standards for water works [10], the normal working pressure should be at least 35 psi (~24 m), and the minimum pressure in a distribution system should not be less than 20 psi (~14 m) under all conditions of flow. Fig. 2 show the pressure distribution results of the MWA trunk main network during peak time (7:00 am) for all scenarios. It can be found that the MWA normal working pressure is lower than the US recommended standard. In addition, there are some areas that the pressure is lower than 14 m (the minimum requirement under the US recommended standards). However, this range of pressure is quite common in developing countries. For example, the Manila standard recommends the minimum pressure of 7 psig (~5 m) [11].

Comparing the pressure distributions between the scenarios 0 and 1 in Fig.2, we can see that the pressure raises significantly if the throttled valves are open. The pressure in the southern and northwestern service areas turn to be higher than 14 m, and the western area that has pressure less than 14m shrinks considerably. As the water losses reduce in the scenarios 2, 3 and 4, the pressure distribution improves gradually, and, finally, there are only the northern and central areas that have the pressure less than 14 m. For the northern area, it is due to that there is no pumping station close to the area, so a high energy loss occurs during the delivery. For the central area, one pumping station operates with pressure lower than 20 m causing low pressure in its corresponding area.Also, there were only 7 pumping stations from all the distribution system sources that operate with pressure higher than 24 m (the US recommended normal working pressure).In conclusion, opening the throttled valves and reducing water losses both help to improve the pressure distribution.

B. Water losses vs. pressure and energy

The results of water losses, pressure and energy for each scenario are shownin Table 3. An average of the 24 hourly pressure in every scenario was lower than the pressure during peak time, and it was also less than 14 m. It is because the MWA has applied the pressure management, in which the pressure at the sources reduces during off-peak time. Moreover, in some areas, the pressure was even lower than 5 m. According to [12], "Loss of Pressure Boil Water Advisory" (boiling tap water before drinking) are commonly issued in the US when system pressure drops below 20 psi(~14 m).It is because microbial contaminants can enter the distribution system's water supply if a drinking water pipe is hydraulically connected to a contaminant source, and the pressure in the pipe drops to a level below that of the contaminant source including backflow, groundwater, water in repair trenches, and water in below-grade air-valve vaults [12].In addition, Michigan Department of Environmental Quality (DEQ) [14] advised that after a low pressure event (5-20 psi) is over and normal pressure is restored, the impacted area should be thoroughly flushed and coliform samples should be taken throughout the area to determine if the distribution system is free of any bacteriological contamination. However, if pressure drops below 5 psi (~3.5 m), DEQ defines it as a complete loss of pressure or negative pressure in the distribution system.After pressure is restored and the system recovers (tanks are filling, and enough sources are operating to ensure pressures do not drop again), the affected area should be thoroughly flushed and coliform samples must be taken throughout the area to determine if the distribution system remains free of coliform contamination.From our results, there are some points on the trunk mains that have pressure below 5 m. Thus, it is possible that pressure is sometimes below 5 psi (~3.5 m) in some areas on the MWA distribution pipes. As a result, the MWA distribution system is operating pressure lower than the US and other developed countries practices [13] that might cause potential contamination risk.

Comparing the scenarios 0 and 1 for the case that the throttled valves on the trunk mains were open, the volume of water losses (WL) increased 0.104 MCM/day,and the percentage of water losses (%WL) increases slightly from 27.45% to 28.89%because the system pressure raised. Also, the input energy increased around 20 MW-hr/day due to higher system flow from an increase in water losses. The FAVAD equation in (2) actually imitates an orifice flow equation under pressure. So, the water loss parameter $C_L$in (2) is a function of leakage area.Reducing C_L by 20% for each stepfrom the scenarios 1 to 4 implies

leakage area in a pipe network system decreased by 20%. However, the results show that the volume of leakage dropped less than 20% for each step because system pressure increased due to less energy losses and affected water loss flow in (2). Unlike the case of opening the throttled valves, the benefits on both pressure and energy can be clearly seen if the MWA can reduce water losses. These results are just another example to support any utilities to concentrate on controlling and reducing water losses especially leaks if they want to save energy effectively and economically [15].

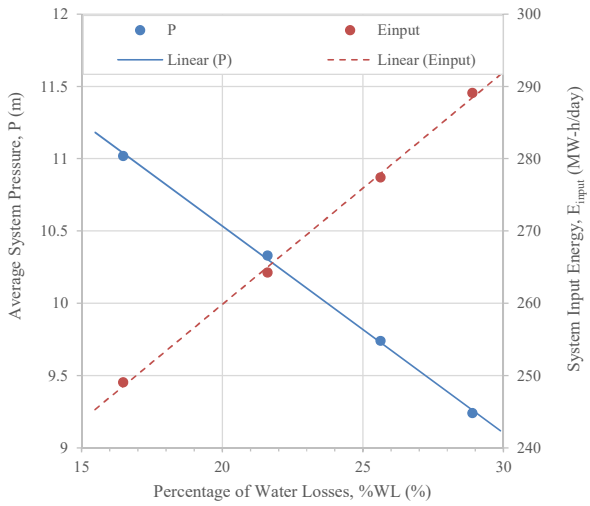

Fig. 3. Relationships between percentage of water losses, average system pressure and system input energy

C. MWA targets of presure and water loss

Fig. 3 shows two linear relationships between the percentage of water losses (%WL), the average system pressure (P) and the system input energy(E_{input}) for the MWA trunk main network. As described earlier, the MWA has set the targets to reduce %WL to 19% and raisethe pressure to 10.8 m in 2021.Although our simulation results were originally based on the MWA data in March 2013, it might provide some important information on how the MWA could approach the targets. If we set %WL of 19% and estimate P and $E_{input}$from the figure, we will get P = 10.68 m and E_{input} = 253.8MW-hr/day. Thisresult implies that if the MWA could reduce %WL to 19%, the pressure may raise to almost 10.8 m by itself without a need to increase the pressure at the sources such as pumping stations. In addition, E_{input} reduced 16.1MW-hr/day. According to [6], the electricity energy consumption for water distribution system was 369 MWh/day in March 2013, and the ratio between the input energy and the electricity consumption was estimated to be 0.70. Thus, if the 2021 targets were met, the MWA could save the electricity consumption of approximately 23 MW-h/day (= 16.1/0.7). However, when we back-calculated the value of the water loss parameter that matched %WL of 19%. We found that it equals to $0.50C_L$. It can be said that the MWA might have to fix its leaking pipes and other types of water losses to achieve the reduction of leak area by around 50% of the total leak area based on the situation in March 2013. Thus, these targets are very challenging.

Conclusions

The Metropolitan Waterworks Authority (MWA) is responsible for providing potable water for three provinces in Thailand: Bangkok, Nonthaburi andSamutprakarn. Its trunk mains network is comprised of 1,700 km of 500-1800 mm trunk mains, 4 water treatment plants and 11 distribution pumping stations. In March 2013, the system input volume (SIV) was 5.18 MCM/day, the water losses (WL) was 1.34 MCM/day (%WL = 27.45%) with the average pressure of 8.66 m, and the electricity energy consumption for water distribution system was 369 MWh/day. Using these data, the MWA trunk main network model was built and calibrated. The MWA has set the targets to reduce %WL to 19% and raise the pressure to 10.8 m in 2021. Since the MWA water losses are mainly leakage, directly depending on pressure, the achievement of both targets is rather difficult. The MWA has throttled 130 valves on its trunk main network to reduce WL and control flow, however, causing an adverse effect on pressure and energy during peak demands. Our analysis (based on the March 2013 data)found that if the input pressure at all sources remains the same but all throttled valves are open, %WL and the pressure may increase to 28.9% and 9.24 m, respectively. Then, if MWA can find and fix leaks and reduce %WL to 19% as its WL target, the pressure will raise to 10.7 m almost equal to its pressure target without increasing its pressure at the sources. The other benefits are that SIV will reduce 0.434 MCM/day, and the electricity energy consumption may reduce around 23 MW-h/day. According to the Metropolitan Electricity Authority [16], there are two types of tariffs for the large general service type including MWA: Time of Day Tariff (TOD) and Time of Use (TOU) Tariff. The energy chargeranges from 2.6107 to 4.3555 baht/kW-hdepending on the type of tariffs and the usage time (off peak and on peak times). Using the average value of 3.5 baht/kW-h, the reduction of energy consumption could be worth roughly 30 million baht per year (900,000 USD/year) for MWA.

Acknowledgment

The authors would like to thank Prof. Dr. SuwatanaChittaladakorn for his constructive comments and suggestions that helped to improve the research greatly.This research was supported by MWA Waterworks Institute of Thailand.

References

[1] WUP U. World Urbanization Prospects: the 2018 Revision. United Nations, Department of Economic and Social Affairs, New York, USA. (2018).

[2] Cabrera, Enrique, Miguel A. Pardo, Ricardo Cobacho, and Enrique Cabrera Jr. "Energy audit of water networks." Journal of Water Resources Planning and Management 136, no. 6 (2010): 669-677.

[3] Gómez, Elena, Roberto del Teso, Enrique Cabrera, and Javier Soriano. "Labeling Water Transport Efficiencies." Water 10, no. 7 (2018): 935.

[4] Dziedzic, Rebecca, and Bryan W. Karney. "Energy metrics for water distribution system assessment: case study of the Toronto network." Journal of Water Resources Planning and Management 141, no. 11 (2015): 04015032.

[5] Mamade, Aisha, Dália Loureiro, Helena Alegre, and Dídia Covas. "A comprehensive and well tested energy balance for water supply systems." Urban Water Journal 14, no. 8 (2017): 853-861.

[6] Lapprasert, Sutthisak, Adichai Pornprommin, Surachai Lipiwattanakarn, and Suwatana Chittaladakorn. "Energy balance of a trunk main network in Bangkok, Thailand." Journal-American Water Works Association 110, no. 7 (2018): E18-E27.

[7] American Water Works Association. Water Audits and Loss Control Programs: M36. Vol. 36. American Water Works Association, 2008.

[8] MWA's Annual Report Fiscal Year 2013, p. 138.

[9] May, J., "Leakage, pressure, and control," In BICS International Conference on Leakage Control Investigation in Underground Assets. London: BICS, 1994.

[10] Great Lakes--Upper Mississippi River Board of State Public Health & Environmental Managers, and Great Lakes--Upper Mississippi River Board of State Public Health & Environmental Managers. Water Supply Committee. Recommended standards for water works. The Board, 1992.

[11] Rivera Jr. V. "Tap Secrets: The Manila Water Story," Asian Development Bank, 2014.

[12] Erickson, John, J. Alan Roberson, Melinda Friedman, and Charlotte Smith. "Low-Pressure Events: Variation in State Regulations and Utility Practices." Journal-American Water Works Association 107, no. 3 (2015): E120-E129.

[13] Ghorbanian, Vali, Bryan Karney, and Yiping Guo. "Pressure standards in water distribution systems: reflection on current practice with consideration of some unresolved issues." Journal of Water Resources Planning and Management 142, no. 8 (2016): 04016023.

[14] Michigan Department of Environmental Quality (DEQ), Guidelines for Issuing Boil Water Advisories to Address Microbial Contamination of Community Water Supplies (Policy and Procedure Number ODWMA-399-022) reformatted 1/24/2013.

[15] CPUC (California Public Utilities Commission), Embedded Energy in Water Pilot Programs Impact Evaluation. Final Report Study ID CPU0053.01, ECONorthwest, Portland, Ore. Prepared for the California Public Utilities Commission Energy Division, March 9, 2011.

[16] Metropolitan Electricity Authority,"Electricity Tariff for Large General Service Type (Type 4)," https://www.mea.or.th/en/profile/109/114 (accessed Oct. 25, 2018

RESILIENCE INDEX FOR CHLORINE ANALYSIS IN WATER DISTRIBUTION NETWORKS

Suparak Kaewsang[1,a], Adichai Pornprommin[1,b], Surachai Lipiwattanakarn[1,c] and Thunchanit Wongwiset[2,d]

Abstract Reducing water losses in water distribution systems can benefit in many ways varying from a reduction of water production and distribution to energy efficiency and hydraulic reliability. In this study, we investigated an impact of water losses on chlorine distribution in a district metering area (DMA) of the Metropolitan Waterworks Authority (MWA) network. The major factor that causes the decay of chlorine is water age (time used to be transported). The longer water age isthe more reactions of chlorine in bulk water and at pipe walls, and, consequently, the more decay. Using the EPANET 2.0 software, we simulated the DMA network for two cases, the present situation with water losses and the situation without water losses. A measure of the reliability of chlorine distribution was proposed by modifying the resilience index that has been used for hydraulic reliability [1]. We found that as water losses decrease the total amount of input chlorine mass to the DMA reduces. Surprisingly, however, the reliability of chlorine distribution decreases as well. It implies that without water losses, velocities in pipes decrease and cause an increase in water age in the network. Subsequently, customers receive lower free residual chlorine concentrations. The result contrasts with what we found in the investigation of hydraulic reliability.

Keywords *Chlorine, Water distribution, Water losses, Reliability*

[1]Department of Water Resources Engineering
Faculty of Engineering, Kasetsart University
Bangkok, Thailand
[2]Bang Bua Thong Branch Office
Metropolitan Waterworks Authority
Bangkok, Thailand

[a]kaewsang_s@yahoo.com
[b]fengacp@ku.ac.th
[c]fengsuli@ku.ac.th
[d]thunchanit.w@mwa.co.th

Introduction

Free chlorine is the most common disinfectant used around the world. Chlorination has been used to meet primary disinfection requirements and provide a residual disinfectant in distribution system. According to the World Health Organization [2], free chlorine should be present in drinking-water distribution networks at a minimum concentrations of 0.2 mg/liter. Since chlorine can decay in networks by the reactions in bulk water and at pipe walls, the travel time from DMA inlet points to customer points(water age)is one of the most important factors causing the losses of chlorine in distribution networks.

The residual chlorine concentration is reduced by the flow in water pipes mainly due to the water's reaction in terms of the water's natural organic matter (NOM) (bulk decay) and with the pipe walls (wall decay) [3]-[4]. Overall water quality did not change following DMA implementation. However,water quality (chlorine residuals, turbidity, and metals) was degraded at locations with elevated water residence times such as created dead ends[5].

Recently, the analysis of water age has become more important especially for the design of water distribution systems. As the traditional way, the design was based on a hydraulic capacity-based approach to meet future demand and fire and emergency demands. Under this consideration alone, sometimes systems are oversized and cause low velocities in pipes, longer water age and, finally, negative impacts on water quality [6]. With this awareness of water quality degradation in water distribution systems, the design has been shifted toward a new approach that balances hydraulic capacity and water age.

It has been known that water lossesnot only cause an increase in water production, but also they lead to lower pressure and more energy consumption [7]-[8]. Although leakage as a major factor of water losses can result in backflow through leaks and water-borne contamination, it also causes an increase in flow velocity and, thus, water age becomes shorter.Decreasing water age is good for chlorine concentration. However, to the best of the authors' knowledge, there is no study on the impact of water losses on chlorine distribution in pipe networks. Thus, this study aims to investigate the relationship between water losses and chlorine distribution as a key

parameter to evaluate water quality by modifying the resilience index usedin hydraulic reliability.

Reliability of chlorine distribution

Hydraulic reliability in water distribution systems generally means the capability of the systems to satisfy water demands and pressure in both normal and critical situations such as pipe burst, fire and emergency demands, etc. A measure of hydraulic reliability often used in water distribution systems is a resilience index (I_r) [1]. Many studies are useI_r for investigation and optimization [9]-[12]. According to Todini's approach [1], resilience implies the intrinsic hydraulic capacity of a system to overcome failures in relation to pressure head surplus in normal operating conditions. This surplus allows a network to overcome critical operating conditions. The higher I_r value can show the higher hydraulic reliability in a system.

In terms of water quality, a concept of resilience index was implemented to investigate the reliability of chlorine distribution in this study. First, the mass of total free residual chlorine at inlet points (Cl_{tot}) can be computed by

$$Cl_{tot} = \sum_{i_t=1}^{n_t} Q_{inlet,i_t} C_{inlet,i_t} \Delta t \quad (1)$$

Wherei_t is an time index, n_t is total time step, Q_{inlet,i_t} and C_{inlet,i_t} is inflow and free residual chlorine concentration, respectively, and Δt is time interval.

Then, the mass of free residual chlorine received by water users (Cl_{ext}) can be estimated by

$$Cl_{ext} = \sum_{i_t=1}^{n_t} \sum_{i=1}^{n} q_{i,i_t} C_{i,i_t} \Delta t \quad (2)$$

Where$i$ is a user index, n is the total number of users, and q_{i,i_t} and C_{i,i_t} are water demand and concentration at a user, respectively.

In this study, the minimum free residual chlorine mass for users ($Cl_{ext,min}$) used the minimum concentration according to the WHO standard ($C_{i,\min}$ = 0.2 mg/liter). Thus, $Cl_{ext,min}$ can be written as follows:

$$Cl_{ext,min} = \sum_{i_t=1}^{n_t} \sum_{i=1}^{n} q_{i,i_t} C_{i,\min} \Delta t \quad (3)$$

Therefore, we can estimate the real free residual chlorine lost in water distribution system (Cl_{int}) can be expressed as

$$Cl_{int} = Cl_{tot} - Cl_{ext} \quad (4)$$

And, the maximum free residual chlorine lost in the system that still satisfies the constraints regarding demand and concentration at users ($Cl_{int,\max}$) is

$$Cl_{int,\max} = Cl_{tot} - Cl_{ext,\min} \quad (5)$$

Finally, the resilience index for chlorine ($I_{r,Cl}$) can be computed as follows:

$$I_{r,Cl} = 1 - (Cl_{int}/Cl_{int,\max}) \quad (6)$$

Similar to the original resilience index (I_r) by [1], $I_{r,Cl}$ implies the intrinsic water quality capacity of a system to overcome failures in relation to chlorine mass surplus in normal operating conditions. This surplus allows a network to overcome critical operating conditions. For example, the critical operating conditions regarding to water quality are an increase in water age or chlorine decay or microbial waterborne pathogens in a network.

In this study, the distribution of free residual chlorine concentration in a water distribution network was modeled using the first order decay model of the EPANET 2.0 software. Thus, the reaction rate (R) can be written as:

$$R = K_b C + \frac{A}{V} K_w C \quad (7)$$

Where$C$ is free residual chlorine concentration, A/V is the surface area per unit volume within the pipe, K_b and K_w are the bulk and wall reaction coefficients, respectively.

Study area

Our study area is DMA 54-09-03 in the Bang Bua Thong branch office (BBT) service area, the Metropolitan Waterworks Authority (MWA) as shown in Fig. 1. The BBT has a service area of around 340.23 square kilometers with 124,324 of water users. The area is divided into 123,191 small water users, 636 large users and 497 government users. The water distribution system consists of 80.3-km trunk mains and 2,059-km distribution pipes. The daily water demand is around 150,000 to 170,000 cubic meters per day, and the average pressure is approximately 6.8 meter. The BBT area is separatedinto 41 District Metering Areas (DMAs) for pressure and water loss management.

Table Ishows the hydraulic and pipe network information of our study area (DMA 54-09-03). It is a residential area with very low pressure but a high percentage of water losses.We installed three pressure loggers (P1-P3) on fire hydrants in the DMA during the period of our investigation and measured free residual chlorine concentration at three locations (C1-C3) as shown in Fig.2. At the inlet, there was a district meter where pressure and flow were automatically recorded, but we had to measure chlorine by ourselves manually (C1).

Table I. Detail of study area (DMA 54-09-03)

Data	Detail
Service area	2.10 square kilometers
Number of customer meters	2,457
Total pipe length	26.13 kilometers
Average pressure head	6.8 meters
Water loss	35.01%
Type of distribution pipe	PVC (80%), AC (20%)

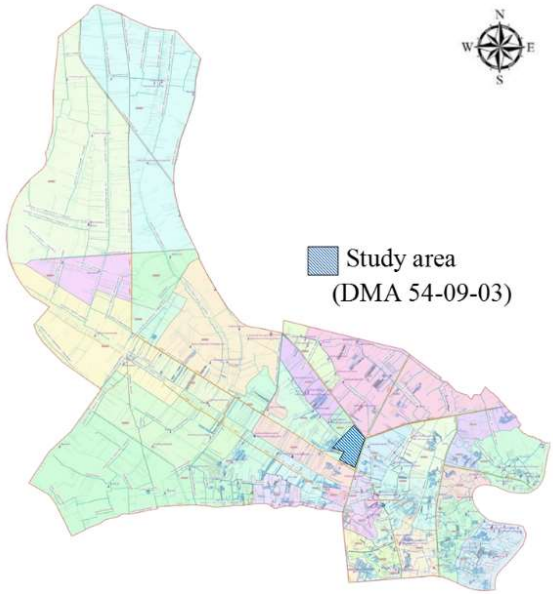

Fig. 1. DMA 54-09-03 in the Bang Bua Thong branch office service area

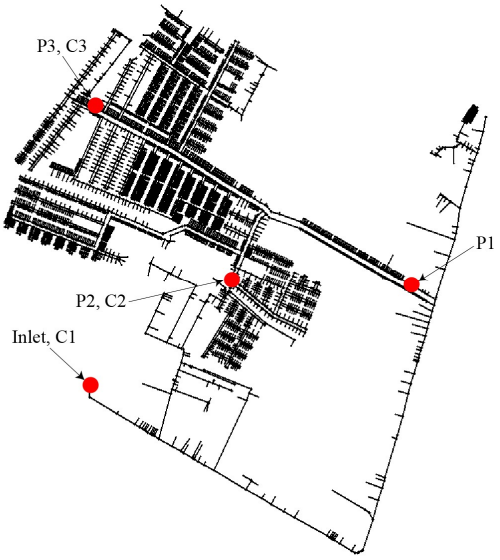

Fig. 2. Locations of the inlet, the pressure loggers (P1-P3) and the chlorine measurements (C1-C3) in DMA 54-09-03

Methodology

The methodology in this study can be described as follows.

A. necessary data were collected for model simulation and calibration such as data at observation point (DM), field data of water demand and pressure head. The model uses free residual chlorine data for the calibration.
B. Hydraulic model (EPANET 2.0) was performed the water distribution system in DMA 54-09-03
C. The model calibration was performed by using base demand andloss in the study area. Base demand input into the model to be the observed data, and water loss data input into the model using Emitter function

$$Q_{leak} = CP^N \quad (8)$$

whereQ_{leak} is a leakage rate, C is an emitter coefficient, P is pressure at any junction and N is an emitter exponent. In this study, water loss that occurs in the system was assumed to be pressure-dependent flow because pipe leakage should be a main portion of water losses [6].We used pressure variation at N = 1 and then varied C value to calibrate the water discharge at DM between the model and actual data.
D. The model calibration was executed by adjusting demand pattern for the real pattern and Hazen-Williams pipe roughness coefficient (C_{HW}) to achieve pressure in the model conform to observed pressure at 3 loggers in the field (P1-P3).
E. K_b equals -3.384 day^{-1} taken from the MWA bulk FRC test report, and $K_w$was used as our calibration parameter for chlorine distribution at C2 and C3.
F. Our water quality model after calibration was implemented.The reliability measurement of the chlorine distribution was proposed by modifying the resilience index used for hydraulic reliability and simulate2cases, the situation with water losses and the situation without water losses.

Model calibration and validation

A. Hydraulic model

1) Water inlet calibration

The result of the calibration shows that 0.1211 meter^2/day of the C value reflects flow inlet with best correlation at DM point between simulated and observed data. The data that used for the calibration is on November 11st 2017, and the case without water lossesuses the parameters and coefficients as same as the case with water losses.Only water losses dropped, so the emitter coefficient (C) is set to be zero.

2) Pressure validation

Use three loggers in the study area were used to be the observed data for model validation in November 11st 2017. The result of the validation is that the roughness coefficient (CHW) equals 138. Moreover, a comparison between observed data and

simulated data indicate a good result of model validation, the consistency of the pressure data.

B. Water quality model

This research uses free residual chlorine data from MahaSawat water treatment plant to be the missing data representative of field measurement since the pattern of free residual chlorine between the water treatment plant and the inlet point of the study area (logger C1) have been related. Thus, the pattern of free residual chlorine was expanded by substituting the missing observed data with the water treatment plant's data, but the average of free residual chlorine is smaller than the treatment plant 0.05 mg/liter as shown in Fig. 3.

From the model calibration, thevalue of $K_b$was defined as -3.384 day^{-1} and used $K_w$equal 0.00 and -0.02 meters/day. From the result, after modified K_w to -0.02 meters/day,the modelcalibration expresses a correlation better than K_w 0.00 meters/day.

It is found that the average the concentration of free residual chlorine at the inlet point is 0.85 mg/liter results the average concentration of free residual chlorine as 0.60 mg/liter (0.25 mg/liter dropped) at the farthest point from the inlet (logger C3) on the case of unconcern global wall reaction (K_w = 0.00 meters/day) and the case of concern global wall reaction (Kw = -0.02 meters/day) results the average concentration of free residual chlorine equals 0.41 mg/liter (0.44 mg/liter dropped) at the farthest point from the inlet.

It shows that the wall reaction affects chlorine decay in a similar scale as a mass reaction in water. Likewise, using the first-order reaction for K_b and K_w as equation (7) leads the equation to be the linear first-order differential equation which makes the decay rate of free residual chlorine rely on the concentration at that time.

Fig. 4showthe temporal variations of water age and free residual chlorine.From ourresult, the inverse relationship between water age and free residual chlorine can be seen. During minimum nightflow (01:00am), the water age increased, and it reached the maximum at 4:00 am while the chlorine concentration was minimum.Themeasurement point (C3) is a maximum of 53 hours,and the amount of chlorine at the measurement point (C3) in the range of 0.30-0.55 mg/L, higher than the minimum recommendation of 0.20 mg/L by WHO [1].

Result and discussion

Fig. 5 shows the contour of free residual chlorine at the shortest water age (8:00 am) and the longest water age (04:00 am) for the situations with water losses and without water losses. It was found that the chlorine concentration in DMA 54-09-03 was always higher than 0.20 mg/L (the minimum recommended value) with the average around 0.5

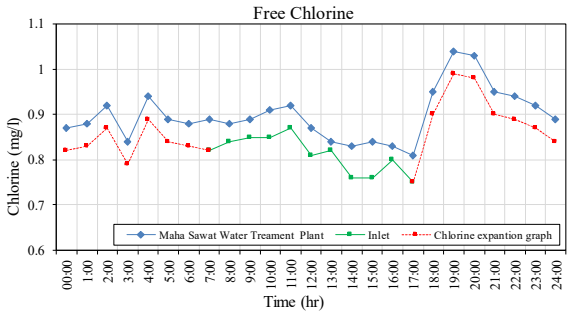

Fig. 3. The relationship of free residual chlorine between Maha Sawat water treatment plant and the inlet of DMA 54-09-03

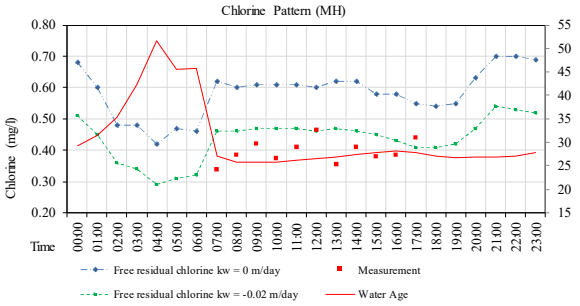

Fig. 4. Temporal variation of water age and simulated and measured free residual chlorine at point C3 in DMA 54-09-03

mg/L. From our results, the chlorine distribution at the time of the shortest and longest water ages showed a similar pattern. This is due to that the chlorine concentration at the inlet was not uniform (Fig. 3). The highest concentration at the inlet was at 19:00 pm, and it helps to increase the concentration during night time. Comparing the situationswith and without water losses, the chlorine concentration in the case without water losses is lower than that with water losses both at the time of the shortest and longest water ages.

After calculating chlorine mass for 24 hours in the cases with and without water losses, we summarized our results in Table II. The total free residual chlorine mass (Cl_{tot}) in the system reduced by -28.15% when water losseswere not considered.This means that reducing water losses can reduce the chlorine input. The chlorine concentration at the inlet was assumed to be unchanged in this study. It showedthat both free residual chlorine at customer point (Cl_{ext}) and chlorine losses in the system (Cl_{int}) reducedat almost the same rate (-28%).A smaller value of Cl_{int} implies that the losses and decay in the system reduces. This is good for the system. But a smaller value of Cl_{ext}means that users are receiving less chlorine concentration. This is due to a decreaseof flow velocity in the system when there was no water loss. It leads to an increasing of water age in the system. So, the users will receive less free residual chlorine, and finally, it drops from 0.559 to 0.515.Thisresult indicatedthat the reliability in the area became lower.

Table II. Results of free residual chlorine for 24 hours in cases with and without water losses

Free Residual Chlorine	%WL = 25% Grams (%)	%WL = 0% Grams (%)	Change (%)
Cl_{tot} Cl_{ext} Cl_{int}	2,996 (100%) 1,887 (63%) 1109 (37%)	2,153 (100%) 1,342 (62%) 811 (38%)	-28 -29 -27
$Cl_{ext,min}$ $Cl_{int,max}$	482 2,514	482 1,671	0 -34
I_r	0.559	0.515	-7.9

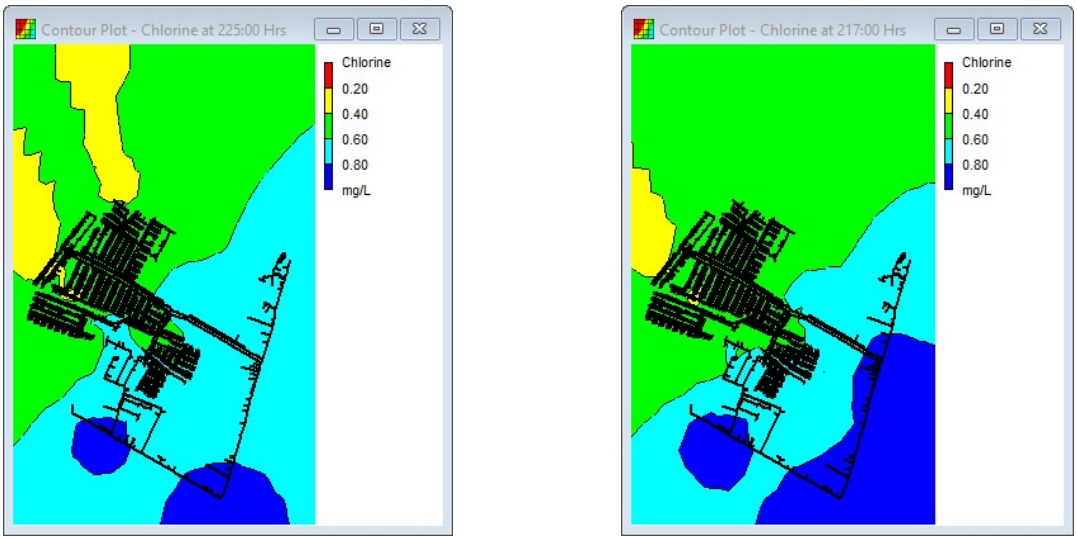

Time8:00 am. Time 04:00 am.

Contour of free residual chlorine of the situation with water losses

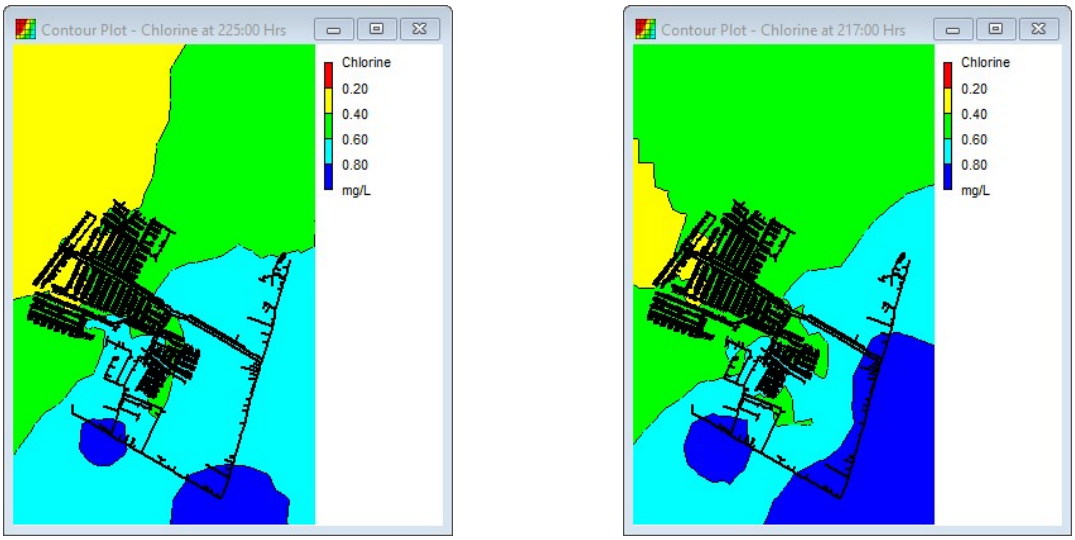

Time8:00 am. Time 04:00 am.

Contour of free residual chlorine of the situation without water losses

Fig. 5. Countour of free residual chlorine in DMA 54-09-03.

Conclusions

We have performed a pipe network model to investigate the reliability of chlorine distribution in a water distribution system of the Metropolitan Waterworks Authority (MWA), Thailand. We proposed a new indicator, the resilience index for chlorine ($I_{r,Cl}$), to assess how the system overcome the critical condition related to water quality. $I_{r,Cl}$ implies the intrinsic water quality capacity of a system to overcome failures in relation to chlorine mass surplus in normal operating conditions. This surplus allows the network to overcome critical operating conditions regarding to water quality, for example, an increase in water age or a higher chlorine decay rate or microbial waterborne pathogens in a network. It is found that the model can represent the actual hydraulic and chlorine situation of our study area very well. The inverse relationship between water age and chlorine concentration havebe found.

The result shows that reducing water losses can help to decrease the input chlorine mass into the system. However, when flows and velocities in pipes decrease due to no water losses, water age increases, and, consequently, chlorine concentration decreases. Thus, unlike the energy concept that reducing water losses, users may receive higher pressure and energy, in the case of chlorine, users receive less chlorine, and this may lead to poorer water quality if the chlorine concentration becomes lower than the recommended value of 0.2 mg/L. This discussion is clearly shown in the form of $I_{r,Cl}$ that it was lower in the case of no water losses.

In conclusion, when water losses in the system decrease significantly, the reliability of chlorine distribution can be smaller. We recommend that water companies should reanalyze their chlorine distribution and may increase chlorine concentration at inlets or feeders to maintain chlorine concentration at users and the reliability similar to the situation before reducing water losses.

Acknowledgment

The researchers would like to express the sincere thanks to Bang Bua Thong waterworks office of Metropolis Waterworks Authority for the data of this research.

Reference

[1] Todini E. Looped water distribution networks design using a resilience index based heuristic approach. Urban water. 2000 Jun 1;2(2):115-122.
[2] World Health Organization (WHO) 2011 Guidelines for Drinking-water Quality, 4th Edition.
[3] Konstantinos Gonelas, Apostolos Chondronasios, Vasilis Kanakoudis, Menelaos Patelis, Panagiota Korkana. "Forming DMAs in a water distribution network considering the operating pressure and the chlorine residual concentration as the design parameters." Journal of Hydroinformatics. 2017.
[4] Yingying Zhao, Y. Jeffrey Yang, Yu Shao, Jill Neal, Tuqiao Zhang. "The dependence of chlorine decay and DBP formation kinetics on pipe flow properties in drinking water distribution." Water Research 141 (2018): 32-45.
[5] Vanessa C.F. Dias, Marie-Claude Besner, Michèle Prévost, Predicting "Water Quality Impact After District Metered Area Implementation in a Full-Scale Drinking Water Distribution System." Journal-American Water Works Association 109, no. 9 (2017): E363-E380.
[6] American Water Works Association (AWWA). Water Quality in Distribution Systems: M68. American Water Works Association, 2017.
[7] Lapprasert, Sutthisak, Adichai Pornprommin, Surachai Lipiwattanakarn, and Suwatana Chittaladakorn. "Energy balance of a trunk main network in Bangkok, Thailand." Journal-American Water Works Association 110, no. 7 (2018): E18-E27.
[8] Gómez E, del Teso R, Cabrera E, Soriano J. Labeling Water Transport Efficiencies. Water. 2018 Jul 13;10(7):935.
[9] Prasad TD, Park NS. Multiobjective genetic algorithms for design of water distribution networks. Journal of Water Resources Planning and Management. 2004 Jan;130(1):73-82.
[10] Di Nardo A, Di Natale M, Giudicianni C, Greco R, Santonastaso GF. Complex network and fractal theory for the assessment of water distribution network resilience to pipe failures. Water Science and Technology: Water Supply. 2018 Jun 1;18(3):767-77.
[11] Maiolo M, Pantusa D, Carini M, Capano G, Chiaravalloti F, Procopio A. A New Vulnerability Measure for Water Distribution Network. Water. 2018 Jul 30;10(8):1005.
[12] Di Nardo A, Di Natale M, Gargano R, Giudicianni C, Greco R, Santonastaso GF. Performance of partitioned water distribution networks under spatial-temporal variability of water demand. Environmental Modelling & Software. 2018 Mar 31;101:128-36.

Lagrangian analysis of the Chao Phraya River estuarine circulation

Siriwat Kongkulsiri[1,a] and Sirod Sirisup[1,b]

Abstract Bangkok metropolis and its vicinity mainly rely on the Chao Phraya River in supplying the freshwater. Salinity in the freshwater is one of the critical water quality parameters. The saltwater intrusion intensifies in the dry season when the demand for fresh water is excessively high affecting various sectors including agriculture, industry and waterworks. The situation further deteriorates in the face of climate change and sea-level rise. The ocean tides and river discharge primarily control the salinity in the Chao Phraya River. Thus the interplay between these two factors is crucial in determining the availability of freshwater. As brackish water moves, each fluid particle carries tracers such as salt, nutrients as well as other particulate matters. The transport of brackish water and its tracer content, as well as the pathways and timescales for that transport, are main facets of how the ocean tides and river discharge play a role in estuarine ecology. To this end, we perform the Lagrangian analysis to analyze the outputs of the validated estuarine circulation model, Semi-implicit Cross-scale Hydroscience Integrated System Model (SCHISM). In this Lagrangian approach, large sets of virtual particles are integrated within the three-dimensional, time-evolving velocity fields. In the paper, we demonstrate and discuss the use of analysis of Lagrangian particle trajectories to improve the understanding of the Chao Phraya River estuarine circulation and dynamics.

Keywords *Lagrangian analysis, Estuary, Tracers*

[1]Data-Driven Simulation and Systems Research Team
National Electronics and Computer Technology Center
112 Klong Neung, Klong Luang, Pathumthani, Thailand

[a]siriwat.kongkulsiri@nectec.or.th
[b]sirod.sirisup@nectec.or.th

Introduction

The United Nation Sustainable development goal (SDG) 6 and 14 of the 2030 Agenda for Sustainable Development aims for conservation and sustainable use of management of water and sanitation and the oceans, seas, and marine resources. The SDG 6 and 14 explicitly considering the improvement of water quality in one of its target 6.2 as well as the sustainable management of coastal areas in two of its targets (14.2 and 14.5), respectively. The estuarine and coastal cities can benefit from interpreting and implementing the principles and guidelines set out under SDG 6 and 14.

In the estuarine region, the salinity gradient plays a significant role in determining the distribution of fresh water as well as communities of, plants, animals, and microorganisms within the estuary.

The ocean tides and river discharge primarily control the salinity in the estuary. Thus the interplay between these two factors is crucial in determining the availability of freshwater needed by the estuarine and coastal cities especially in the dry season when the freshwater is even more scarce. As brackish water moves, each fluid particle carries tracers such as salt, nutrients as well as other particulate matters. The transport of brackish water and its tracer content, as well as the pathways and timescales for that transport, are main facets of how the ocean tides and river discharge play a role in coastal and marine ecology.

In the literature, there are two main methods for estimating pathways in large-scale fluid flows. The first method makes use of tracers, such as the multitude of age tracers, see [1]. It is also noted that tracer studies are better suited for Eulerian methods, which make direct use of velocity fields on their native grids.

The other approach makes exclusive use of the Lagrangian perspective of fluid dynamics instead, see [2]. This method employs an ensemble of virtual Lagrangian particles with no spatial extent whose trajectories are determined by the velocity field. The velocity fields that are used to move the particles can either come from model based velocities such as hydrological/ocean/entuarine models or observational based velocities such as surface velocities based on satellites or measured by high frequency radars.

Statistics of the trajectoriesfor these virtual particles then define particle pathways and their associated time scales. By following the flow of virtual particles and applying further analysis to conceive the effects of subgrid scale diffusion, questions about pathways and flow connectivity can be addressed. See [3] for a recent review of this technique.

This paper extends our previous study, see [4] by thoroughly applying the Lagrangian analysis on the Chao Phraya River estuarine circulation though the similar approach can be well applied in other estuaries. Section 2 explains the material and methods in detail including the hydrodynamic model and the Lagrangian particle tracking techniques. Result and discussion of the Lagrangian analysis and connection to biological and environmental connectivity are given later in section 3, followed by conclusion in section 4.

Material and Methods

In this study, in order to thoroughly investigate the dynamic of the brackish water in the Chao Phraya River estuary, we create various scenarios according to real situations in Chao Phraya River estuary by simulating various seasonal events ofthe estuary. A validated hydrodynamic model called Semi-implicit Cross-scale Hydroscience Integrated System Model(SCHISM) has been used for this purpose. The particle tracking analysis is carried out.

A. The model and study domain

SCHISM or Semi-implicit Cross-scale Hydroscience Integrated System Model [5] is an open-source three-dimensional hydrodynamic model that used semi-implicit Finite-Element and Finite-Volume method for solving governing equations on an unstructured grid. The equations used in SCHISM are based on Naiver-Stokes equations as shown below:

$$\nabla \cdot \mathbf{u} + \frac{\partial w}{\partial z} = 0, \ (\mathbf{u} = (u, v)) \tag{1}$$

$$\frac{D\mathbf{u}}{Dt} = \mathbf{f} - g\nabla\eta + \frac{\partial}{\partial z}\left(\nu \frac{\partial \mathbf{u}}{\partial z}\right) \tag{2}$$

Where D/Dt is material derivative, t is time, $\mathbf{u}$ and w represent horizontal and vertical velocity respectively, g is an acceleration of gravity, η mean free-surface elevation and $\mathbf{f}$ stand for other forcing terms in momentum such as Coriolis, atmospheric pressure, baroclinic gradient, horizontal viscosity.

The study domain covers the lower Chao Phraya River basin following along the Chao Phraya River starting from Amphoe Phra Nakhon Si Ayutthaya in Phra Nakhon Si Ayutthaya province following along the river down to Chao Phraya River mouth withsome extension of 20 km into the upper Gulf of Thailand. The corresponding bathymetry mesh of the area is unstructured grid contain only triangular elements in a total of 176,959 elements and 97,401 nodes with the wet and dry area as shown in Figure 1.

The scenario will be created according to the actual discharges throughout the year consists of 8 cases in total. Seven of which focus on the quantity of water discharge from upstream while the other one emphasizes the effect of water pumping. The details of

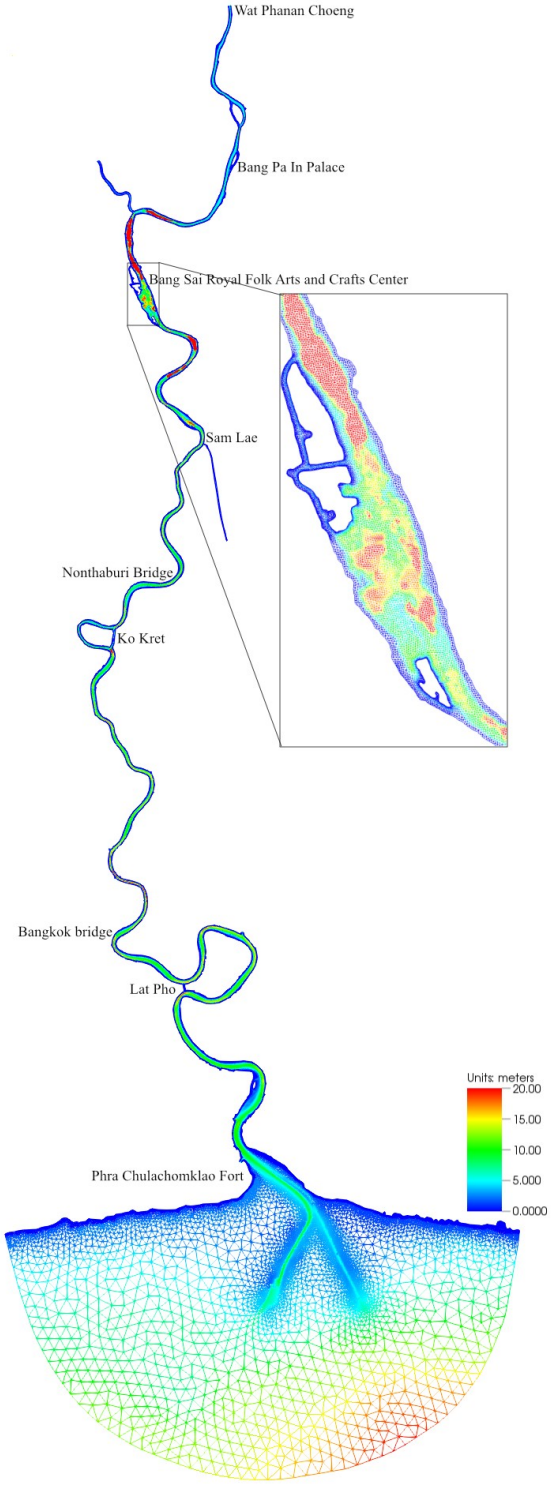

Fig. 1. The study area and the corresponding mesh

each case are described in Table I. The cases of 80 and 90 cms water discharge are the dry season scenarios while 100 cms water discharge case is a typical amount of water discharge release from the dams in these past few years. Meanwhile, the cases of 800 and 1,500 cms water discharge are usually the situation in the onset of the rainy season. 2,840 cms is the maximum carrying capacity of the Chao Phraya River and 3,700 cms is the highest amount of water discharge recorded in 2011.

The difference between the two 100 cms water discharge cases is that the case with a closed water supply canal corresponds to the closed water supply canal (as shown in figure 2) for Metropolis Waterworks Authority (MWA) which normally pumps some amount of fresh water into their waterworks plant.

Table I. Scenario setting

Scenario No.	Scenario	
	Upstream water discharge (cms)	*Water supply canal*
1	80	Open
2	90	Open
3	100	Open
4	800	Open
5	1,500	Open
6	2,840	Open
7	3,700	Open
8	100	Closed

All of the scenario cases are run for 95 days in the model time to obtained water velocity field outputs for the particle tracking analysis. The spin-up time for all cases is 15 days.

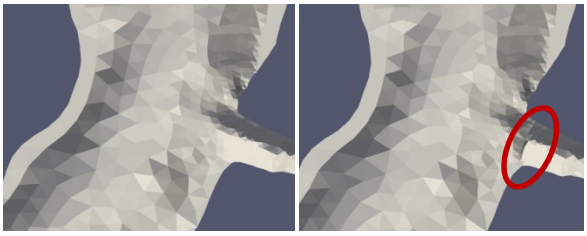

Fig. 2. Left: normal domain, Right: closed water supply canal domain

B. Lagrangian Particle Tracking

The Lagrangian particle tracking (LPT) is a technique to trace virtual particles that put into velocity field of any fluid, in this case is the velocity output of the Chao Phraya River obtained from scenarios above. The LPT method used in the current study is the off-line type, meaning that the model and LPT are not running at the same time. Instead, one can perform simulations first to obtain the velocity field data from each simulation scenario and later apply LPT algorithm to calculate the path and location of virtual particles at each time step by solving the following system of equations:

$$\frac{d\boldsymbol{X}}{dt} = \boldsymbol{v}(\boldsymbol{X}(t), t) \tag{3}$$

Where $\boldsymbol{X}$ represents the trajectory of the particle in *x, y* and*z* direction, *t* is time and$\boldsymbol{v}$ is velocity field in three dimensions.

The virtual particle has no mass nor dimension to represent a parcel of water that moves along the river. We start by releasing a total of 8,000 particles spreading into a rectangular shape with the distance between each particle of one meter at the start location near the upstream area as shown in figure 3. The particles are set to be released at midnight of the 15th day in model time simultaneously. After that, the new location of the particles is recorded in every 10 minutes for further analysis. In this study, we will focus on two main topics:

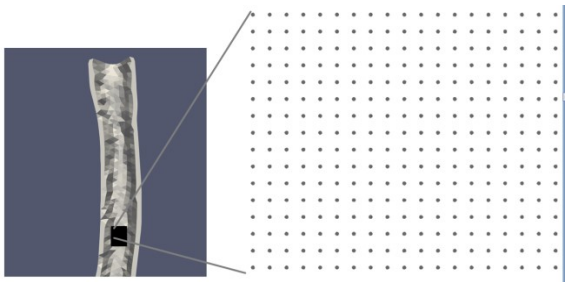

Fig. 3. Particle releasing area and placement

- Transit times – The total time particle spend between the release point and sea.
- Dispersion and Diffusivity – The particle dispersion and its rate of change, the diffusivity, are the fundamental Lagrangian diagnostics of use for understanding tracer transport in flows. Here, we interest in single-particle diffusivity and double-particle diffusivity which can be written as the following equations:

$$\kappa(t) \equiv \frac{1}{2}\frac{d}{dt}\langle \boldsymbol{X}^2(t)\rangle \tag{4}$$

$$\kappa_R(t) \equiv \tfrac{1}{2}\tfrac{d}{dt}\langle \boldsymbol{r}^2(t)\rangle = \tfrac{1}{2}\tfrac{d}{dt}\left\langle \textstyle\sum_{m\neq n}\left[\boldsymbol{X}^{(m)}(t) - \boldsymbol{X}^{(n)}(t)\right]^2\right\rangle \tag{5}$$

Where $\boldsymbol{X(t)}$ is the trajectory of particle and <> represents the ensemble mean. Specifically, single-particle diffusivity quantifies the ensemble-mean rate of particle dispersion from an initial location and double-particle diffusivity is considered as relative diffusivity which the time rate of the mean square pair separation.

Results and discussion

A. Model validation

We employ the hydrodynamic model called Semi-implicit Cross-scale Hydroscience Integrated System Model (SCHISM) in in this study. The model has been validated against the observation data. Figure 4 shows the validation results of the water level from the model and observed water level at CPY015 (Bangkok bridge) and CPY014 (Nonthaburi Bridge) stations for the year 2017. The results show good agreement between the model output and the observed data for both dry and wet season. Thus, the model output can be used for further analysis.

B. Transit times

The time taken for water to transit between defined regions is a property of the flow that provides a useful understanding of the estuary circulation. By considering the entry and exit of particles from an enclosed region in our case is the lower Choa Phraya River, transit times can also be interpreted as a residence timescale as well. In this study, we are primarily interested in the transit between the releasing point, i.e.,Amphoe Phra Nakhon Si Ayutthaya and the river mouth.

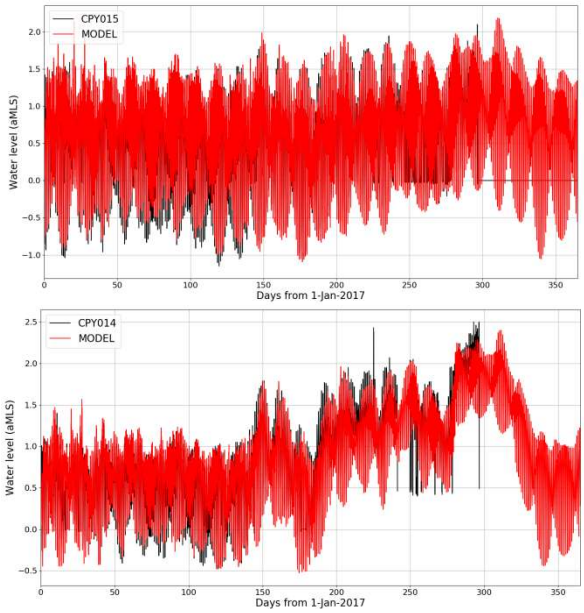

Fig. 4. Validation results at CPY015 (Bangkok bridge) and CPY014 (Nonthaburi Bridge) for the year 2017.

The transit time can be directly derived in a Lagrangian framework by determining the transit time of particles. The results of the transit times for all of the scenario are presented in Table II. Table II shows that for the dry period the transit times can be as much as two months however in the wet period the transit time is significantly reduced to around two days. We also find that as fresh water is drawn out of the river the overall transit times are indeed increased. Interestingly, the transit times for Sam Lae are slightly decreased as fresh water is drained out from the river.

Table II. Transit times

Scenario No.	Transit times (days)			
	Sam Lae	***Pak Kred***	***Lat Pho***	***River mouth***
1	14	19.7	32.5	61
2	13	16.2	31	49
3	11.8	15.9	28.9	45
8	12	15.1	23.8	32
4	1.9	2.5	3.9	6
5	1.15	1.5	2.3	3.8
6	0.76	0.98	1.4	1.8
7	0.63	0.85	1.1	1.6

Lagrangian particle tracking can also be used to assess the total distance travelled by the particle in the lower Chao Phraya River. Figure 5 depicts the total distance travelled by the particle from the releasing point, i.e., Amphoe Phra Nakhon Si Ayutthaya to the river mouth. Interestingly, the distance travelled by the particles in the dry period is almost four times more than that in the wet period where the travelled distance is approximately 130 km similar to the actual river following distance from the releasing point to the river mouth. This finding indicates that the tracers are mainly moved back and forth due to the tidal effects in the dry period while the tracers are instead directly flushed out in the wet period.

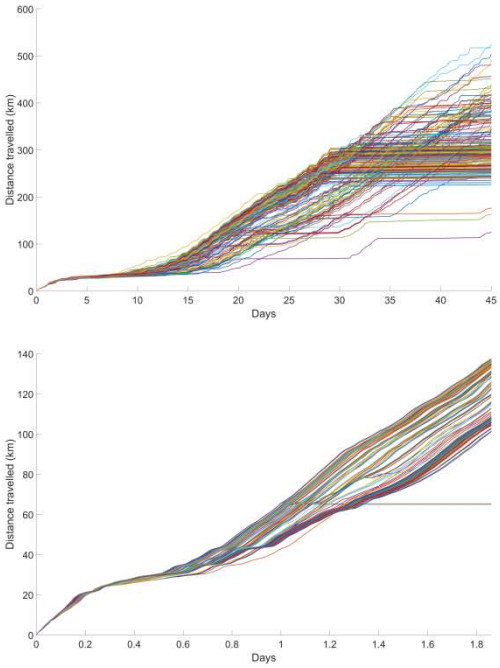

Fig. 4. Validation results at CPY015 (Bangkok bridge) and CPY014 (Nonthaburi Bridge) for the year 2017.

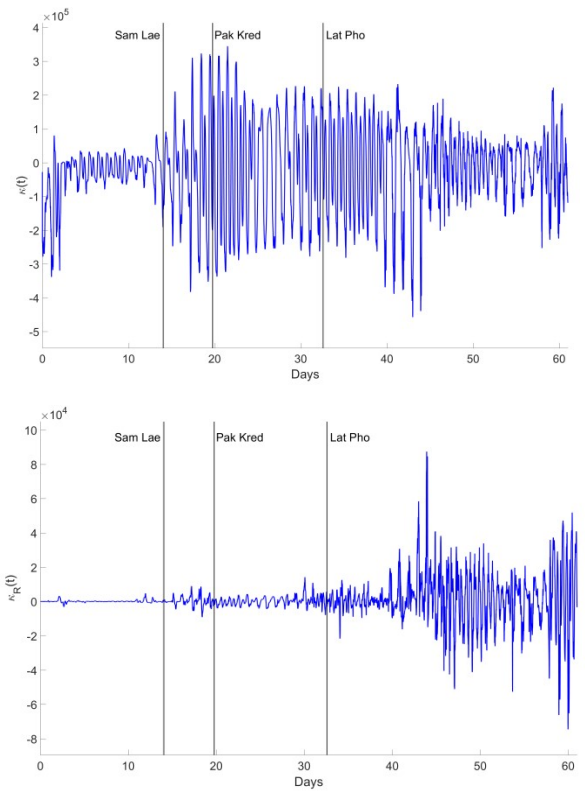

Fig. 6. Top: single- and double-particle diffusivity, bottom, for the case 80 cms upstream discharge.

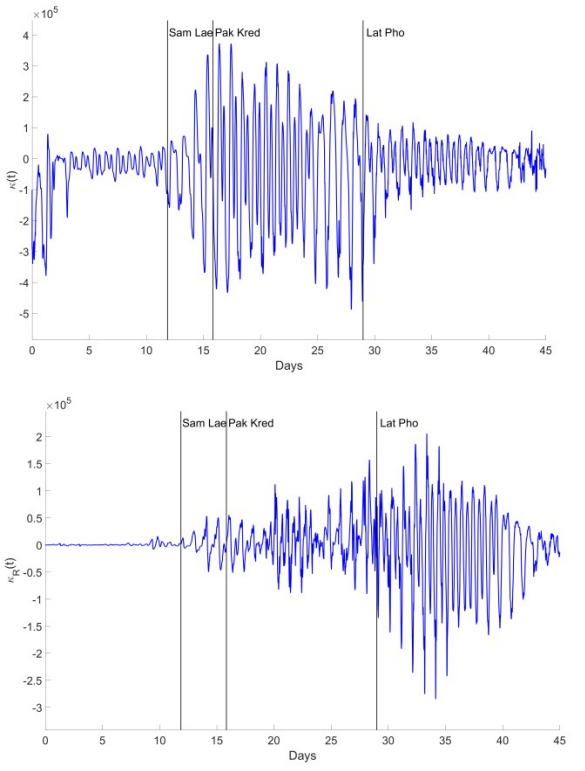

Fig. 7. Top: single- and double-particle diffusivity, bottom, for the case 100 cms upstream discharge.

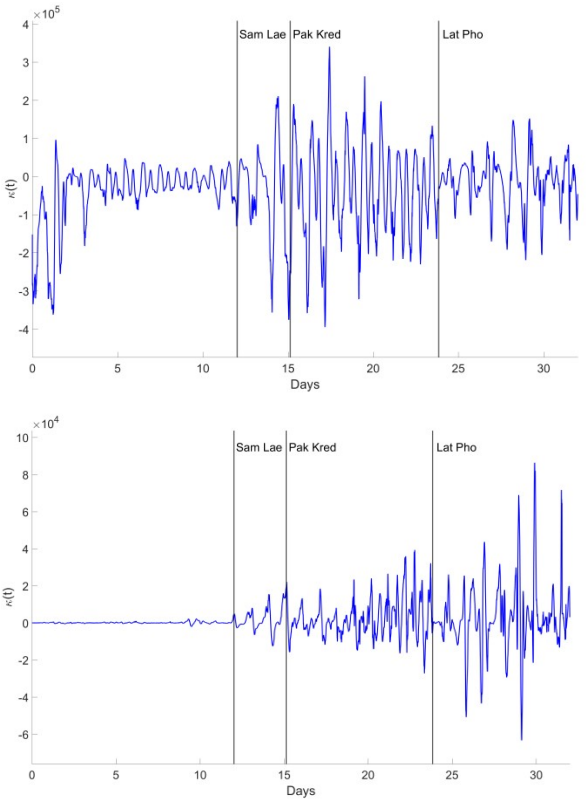

Fig. 8. Top: single- and double-particle diffusivity, bottom, for the case 100 cms upstream discharge with closed water supply canal.

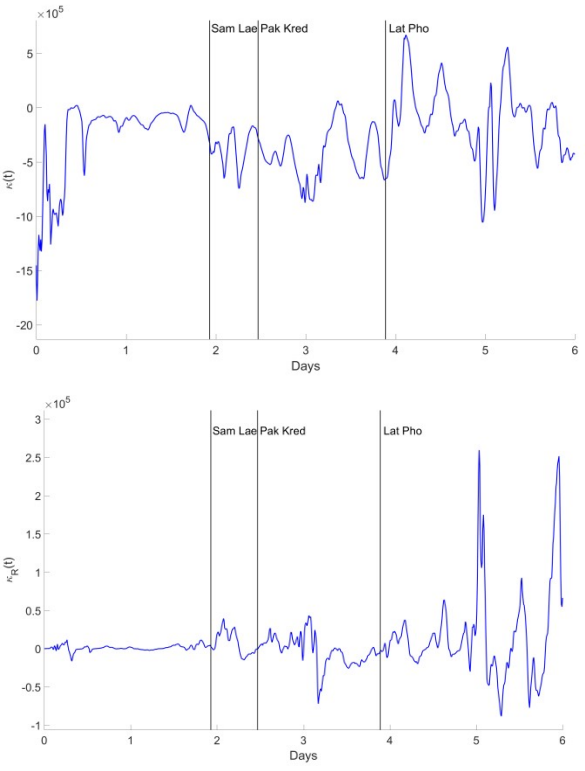

Fig. 9. Top: single- and double-particle diffusivity, bottom, for the case 800 cms upstream discharge.

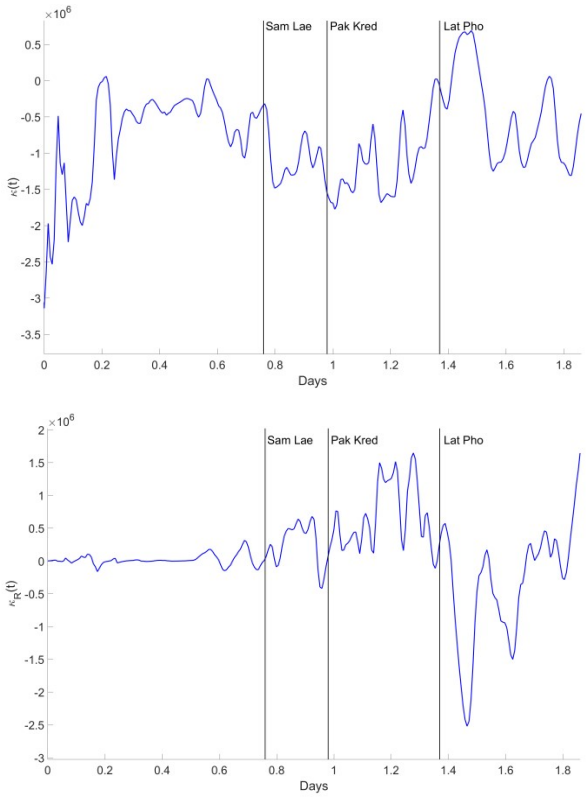

Fig. 10. Top: single- and double-particle diffusivity, bottom, for the case 2840 cms upstream discharge.

C. Dispersion and diffusivity of the Chao Phraya River estuarine circulation

The single- and double-particle diagnostics as indicated in equations 4 and 5 for all simulated trajectories are presented in Figure 6 to Figure 10. For the dry season the results from the scenarios with the upstream discharge of 80, 100 cms are presented in Figure 6 and 7 and the results from the scenarios with the upstream discharge of 800 and 2840 cms are presented in Figure 9 and 10. The scenario with a closed water supply canal is also present in Figure 8.

In order to fully understand the diffusivity, we need to clarify further what single-particle diffusivity measures. As mentioned earlier the single-particle diffusivity quantifies the ensemble-mean rate of particle dispersion from an initial location.

Thus, the lower magnitude of single-particle diffusivity should refer to a stationary or no-moving particle at that instant. For the larger magnitude, since the river is mainly aligned in the north south direction, we can infer directly that a more substantial positive magnitude of single-particle diffusivity is associated with flow tide while a larger positive magnitude of single-particle diffusivity is associated with the ebb tide. For the double-particle diffusivity, we can see directly from equation five that the lower magnitude of this number indicates that the two particles move in sync with each other. The larger magnitude of such number is, however, indicates that the pair particles instead move independently from one another in the way that particles move away for positive value or toward each other for negative one, respectively.

The results in the dry season show that the particles are transported down to the river mouth while experiencing the tidal effects the particles are still able to move in sync with each other until Sam Lae. The closer to the river mouth the more particles move independently from one another which can be the results from the tidal effects.

For the wet season, particles, however, are mainly moving directly along with each other. This should be the effect from the high discharge volume carrying out the particles to the river mouth more directly.

There is no significant difference in results from the case of 100 cms with and without a closed water supply canal. However, for the dry season, the results from the scenario with the upstream discharge of 80 cms and 100 cms suggest an interesting finding. In the case of 80 cms upstream discharge, the lower number of double-particle diffusivity can be observed from the releasing point to Lat Pho indicates that the particles are mainly packed together while transported down to the river mouth. That number for the case of 100 cms upstream discharge is much greater indicating a better mixing in this case. Here, Lagrangian particle trajectories can be used to study how water moves around in the estuary. Additionally, Lagrangian particles can also be interpreted as passively drifting (biological) or pollutant particulates. Thus, the diffusivity can be used to measure the dispersion of larvae of a marine organism or pollutants at the whim of the currents.

Thus, in the dry season, the amount of upstream discharge to the lower Chao Phraya River can also be important in both pushing the level of salinity down and enhancing the dispersion in the river. This is important as an incident of pollution leak into the river that polluted parcel of water can travel into the water supply canal and causes trouble to water supply system and riverside communities and business.

Conclusions

This study, we focus on using the Lagrangian Particle Tracking technique to investigate the tracer transport of the Chao Phraya River in a various situation when the amount of upstream discharge is conforming to seasonal variation. The hydrodynamic model, SCHISM have made simulated scenario outputs for the LPT technique. The analysis shows that transit time increment is directly related to decrement of the amount of upstream discharge. Besides, the distance travelled by the particles in the dry period is almost four times more than that in the wet period. The further analysis reveals the influence of tides on particle movements in every scenario; flow tide pushes particles up north and ebb tide pulls particles seaward. The double-particle analysis reveals that the closer to

the river mouth the more particles move independently from one another resulting from the tidal effects. The study also finds from the diffusivity analysis that in the dry season, the amount of upstream discharge to the lower Chao Phraya River can also be essential to the enhancement of the dispersion in the lower Chao Phraya River.

References

[1] Mouchet, A., Cornaton, F., Deleersnijder, E., Delhez, E., 2016. Partial ages: diagnosing transport processes by means of multiple clocks. Ocean Dynamic, 66, 2016, pp. 367–386.
[2] Bennett, A.F., Lagrangian Fluid Dynamics. Cambridge University Press, Cambridge. 2006.
[3] Erik van Sebille, *et. al.* , Lagrangian ocean analysis: Fundamentals and practices, Ocean Modelling, 121, 2018, pp. 49-75.
[4] Sirisup, S., Saengnil, N., Tomkratoke, S., Simulation of estuarine hydrological characteristic: A case study of the lower Chao Phraya River, Research and Development Journal, 25, 2015, pp. 21-30.
[5] Y. Zhang, F. Ye, E.V. Stanev, Grashorn, S., Seamless cross-scale modeling with SCHISM, Ocean Modelling, 102, 2016, pp. 64-81.

Quantification of the Nexus impact of Urbanization on Food-Water-Energy Allocation

Chun-Yueh Lin[1] and Chihhao Fan[1,*]

Abstract

Over the years, climate change results in extreme weather events of droughts, floods and heat stress, whichsignificantly threaten the utilization food, water and energy (FWE) resources. Such a disturbed FEW nexus becomes even worse under the stress of urbanization. In addition, the consumptions of FWE resources in urban and rural areas may vary significantly, due to the apparent differences in lifestyles, industrial structures and consumers' behaviors. Therefore, this study aimed to construct a sustainable FWE index to quantify the nexus among FWE resources under the influence of urbanization.In the simultaneous equations model of FWE resources developed from the present study, the rural area demonstrates higher sustainability than the urban one. The negative correlation with the population density showed that the massive consumption of FWE resources can decrease the level of sustainability. For both the urban and rural areas, the sustainability exhibits a high dependency on the water resource, which has a great influence to agriculture and industry. Due to the frequent trading and transporting, the food resource demonstrated a limited impact on sustainability in the urban area of Taiwan, and the food supply remains stable even in urban areaswith a weak agricultural productivity. Moreover, the required resources assurance and potential environmental impact reduction are the primary measures to achieve a sustainable FWE development. This research provides an overall quantification of FWE nexus and prioritizes the FWE conflicts to be solved under the stress of urbanization.

Keywords *FEW nexus, simultaneous equations model, urbanization*

Department of Bioenvironmental Systems Engineering,
National Taiwan University, Taipei, Taiwan

CLASSIFICATION OF THE RAINFED AREAS FOR THE WATER DEVELOPMENT PROJECTS IN THAILAND

Supapap Patsinghasanee[1,a], Jeerapong Laonamsai[1,b], Kalyanee Suwanprasert[1,c], Mongkol Lakmuang[1,d], Ronnaklit Parasirisakul[2,e] and Ratda Patsinghasanee[3,f]

Abstract The water resources management in Thailand is currently managed by area-based consideration composed of irrigation and rainfed areas. However, the water supplies in the rainfed areas are mainly related to rainfall, small-waterbodies and ground water resources. Therefore, the rainfed agriculture is under the water deficit risk due to the climate variability and uncertainty. For this reason, the main propose of this work is to analyze and classify the potential of rainfed areas based on land-uses, household incomes, water resources risks and household locations. The classification results showed that the rainfed areas were classified into 7 types by prioritizing the water resources risk levels (severe, moderate-low or normal levels), special economic zone, household income (higher or lower than poverty line) and revenue structures (agriculture sector or other sectors). Additionally, the rainfed classification results can be applied to support the decision maker for allocating the water resources development projects in the critical rainfed areas. Therefore, the Department of Water Resources, Thailand, was applied the rainfed classification to implement the water distribution projects by using solar-powered irrigation systems in the critical rainfed areas to provide environmentally sustainable, and reliable access to energy, and water resources, to create the agricultural innovation, and to alleviate small and medium farmer's income and livelihood.

Keywords *Rainfed areas,Water Management,Solar-Powered Irrigation System*

[1]Water Crisis Prevention Center
Department of Water Resources, DWR
Bangkok, Thailand
[2]Delta Academy
HZ University of Applied Sciences
Vlissingen, The Netherlands
[3]Thai National Mekong Committee Secretariat
Department of Water Resources, DWR
Bangkok, Thailand

[a]supapap.p@dwr.mail.go.th
[b]teeyoon100@gmail.com
[c]Kalyanee.s@gmail.com
[d]lukmuang@gmail.com
[e]man_para@hotmail.com
[f]ratdas@gmail.com

Introduction

Water is the essential natural resources for contributing human living included domestic, agriculture, industry, transportation, tourist uses and environmental flow for conservation. However, water demand is significantly increased because of the population growth and economic expansion. According to this reason, the Royal Thai's Government had established and lunched the Strategic Plan on Thailand's Water Resources Management 2015 (hereinafter referenced to as "the Strategic Plan") for managing and utilizing the water resources development projects consisted of domestic use, water security for agriculture and industry, flood management, water quality, forest rehabilitation and administrative management. The main objectives of the Strategic Plan are related to solve the water resources problems effected to the socio-economic and water utilization in terms of river basin potential [1].

Currently, the water resources management in Thailand is managed by area-based consideration on irrigation and rainfed agriculture areas. Therefore, the agriculture areas in Thailand approximately are 238,720 km^2 consisted of the 2 types of agriculture areas. The first type of agriculture area is irrigation area which is about 48,350 km^2 or 20% of the agriculture area in Thailand whereas the other 80% or the main proportion is the rainfed agriculture area covered around 190,440 km^2 [1]. The agriculture area details [2] are illustrated in Fig. 1.

However, the main water supplies are in the irrigation area which are approximately 77,680 MCM in terms of storage capacity in the large and medium reservoirs. On the other hand, the main water supplies in the rainfed agriculture are related to rainfall, waterbodies and ground water resources. Therefore, the rainfed agriculture is under the risk due to uncertainty and limitation of water from the climate variability and increase domestic, industrial, and environmental water demands, respectively.

For the above reasons, the main propose of this work is to analyze, classify and prioritize the potential of rainfed agriculture based on land-use, household income, revenue structures, water resources risk areas, specific economic zones and household locations. Furthermore, the water distribution projects by solar-powered irrigation system (hereinafter referenced to as "SIS") are planned for implementing by the Department of Water Resources (hereinafter

referenced to as "DWR") in the severe areas to provide environmentally sustainable and reliable access to water and to alleviate farmer's income and livelihood.

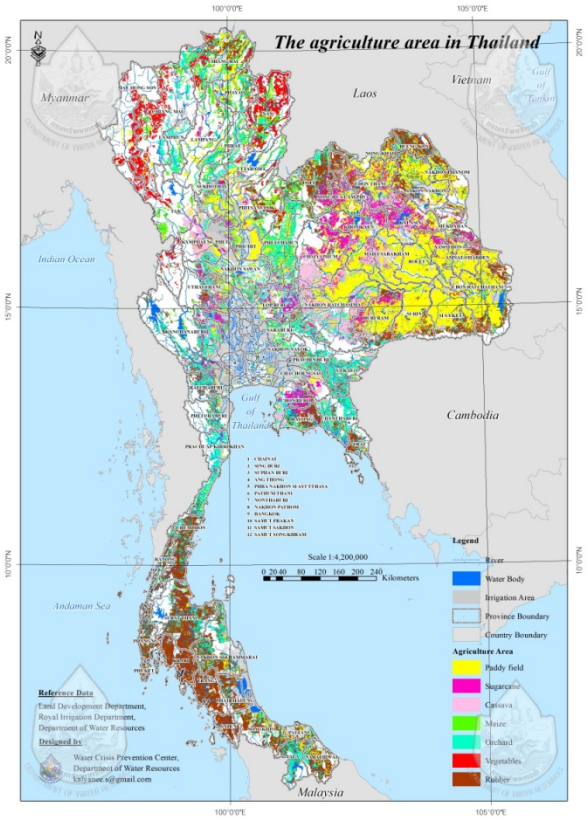

Fig. 1. The agriculture area in Thailand

Methodology

This section provides the overviews of data collection, spatial analysis and rainfed agriculture classification.

A. Data collection

Data of land-use, flood and drought risk areas, special economic zones, household incomes and revenue structures from the Royal's Thai Government was collected for this work. The details of data sources are as following;

- Land-use from Land Development Department [2]
- Irrigation areas from Royal Irrigation Department [3]
- Water resources area-based management from Department of Water Resources and Office of National Water Resources [4,5]
- Personal income in the village level from Community Development Department [6]
- Personal income in the provincial level from Office of the National Economic and Social Development Board [7]
- Number of households, National Statistical Office [8]
- Households location, The Geo-Informatics and Space Technology Development Agency (Public Organization) [9]

B. Spatial analysis

Based on the dataset in the previous section, the data were analyzed by spatial analysis. The Geographic Information System was employed to classify the rainfed agriculture areas. Additionally, the concept of spatial analysis was expressed as the following processes (Fig. 2.);

1) Define the rainfed agriculture by eliminating catchment area with irrigation area, forest, urban area, gesture, waterbody and transportation, etc.

2) Classify the rainfed agriculture using the risk level, personal annual income and revenue structure. Therefore, the rainfed agriculture was defined into 7 types as following;

a) Type 1: the server areas or special economic zones, which the majority income of the local people come from the agriculture sector while the annual personal income is less than the poverty line (1,000 USD per year) [7].

b) Type 2: the server areas or special economic zones, which the majority income of the local people come from the agriculture sector while the annual personal income is higher than the poverty line.

c) Type 3: the moderate and low risk areas, which the majority income of the local people come from the agriculture sector while the annual personal income is less than the poverty line.

d) Type 4: the moderate and low risk areas, which the majority income of the local people come from the agriculture sector while the annual personal income is higher than the poverty line.

e) Type 5: the normal areas, which the majority income of the local people come from the agriculture sector and the annual personal income is less than the poverty line.

f) Type 6: the normal areas, which the majority income of the local people come from the agriculture sector while the annual personal income is higher than the poverty line.

g) Type 7: the other areas in the rainfed agriculture, which the majority income of the local people come from the industrial and service sectors.

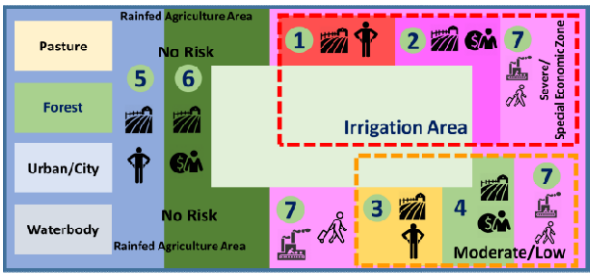

Fig. 2. The concept of spatial analysis for rainfed agriculture area.

Results

The rainfed agriculture, personal income distribution and rainfed agriculture risk classification are expressed in this section.

A. Rainfed agriculture

The water resources risk classification in the rainfed agriculture was determined by the area-based management [4, 5]. The analysis result showed that, the rainfed agriculture was classified into 4 risk levels. The first level is the severe areas and special economic zones with approximately 53,760 km^2 or 28%, the second level is the moderate area with approximately 39,810 km^2 or 21%, the third level is the low risk area with approximately 30,640 km^2 or 16%, and the last level is the no risk area or the largest proportion of the rainfed agriculture with approximately 66,230 km^2 or 35%, respectively. Details are shown in Fig. 3.

For the land-use information, this study showed that the majority vegetation area is the paddy field with approximately 79,000 km^2 or 41% following by rubber and palm trees with 41,180 km^2 or 22%. The other 37% of areas were shared by planting economic vegetation, fruits and vegetables composed of sugarcane 18,300 km^2 or 10%, cassava 17,300 km^2 or 9%, fruits 17,780 km^2 or 9%, corn 10,200 km^2 or 5%, and vegetables 6,680 km^2 or 4%, consecutively. Details were exhibited in Fig. 1.

B. Personal income distribution

The personal income in the sub-district level, number of households and the household locations were applied to analyze and determined the personal income distribution.

The results presented that the 19.20 million households or 90% have the personal income higher than the poverty line. On the other hand, 2.12 million households or 10% of national households have personal incomes lower than the poverty line. The personal income distribution is expressed in Fig. 4. The DWR analysis results in terms of the number of households and people, which are lower than the poverty line are around 2.12 million households and 5.85 million people are consistent with the Office of the National Economic and Social Development Board Report [7].

C. Rainfed agriculture classification

The rainfed agriculture is defined by the 7 classifications mentioned in the section 2.2. The classification results in each regional are illustrated in TABLE I. and Fig. 5. For the results, Type 1, 3 and 5 are approximately 3,264 km^2 or 2%, 4,848 km^2 or 3%, and 5,568 km^2 or 3%, respectively. Additionally, Type 2, 4 and 6 are roughly 45,616 km^2 or 24%, 62,032 km^2 or 33%, and 56,896 km^2 or 29%, consecutively. Furthermore, Type 7 is about 12,208 km^2 or 6%.

Discussion

After the rainfed agriculture was classified by spatial analysis as mentioned in the previous sector. The DWR applied the rainfed classification area to implement the SIS for distributing water to small farm land and increasing the annual household income in the rainfed agriculture.

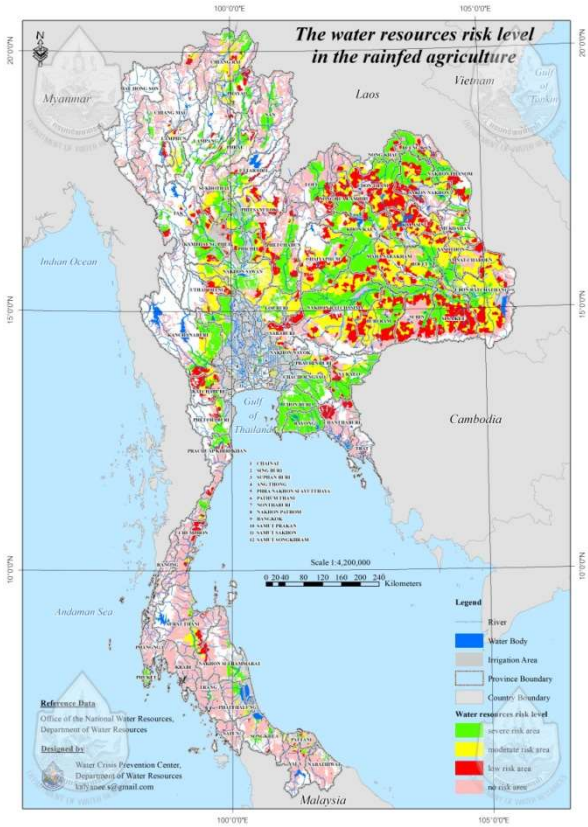

Fig. 3. The water resources risk level in the rainfed agriculture

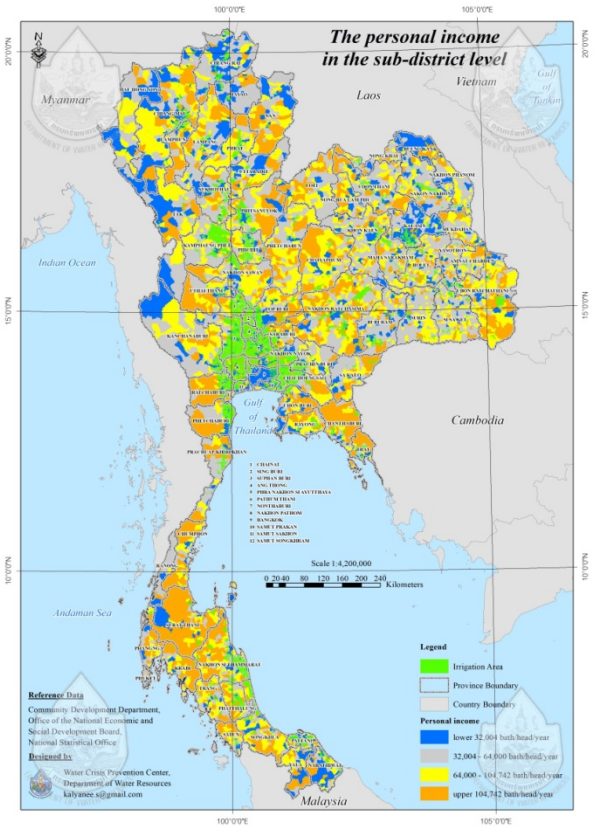

Fig. 4. The personal income in the sub-district level

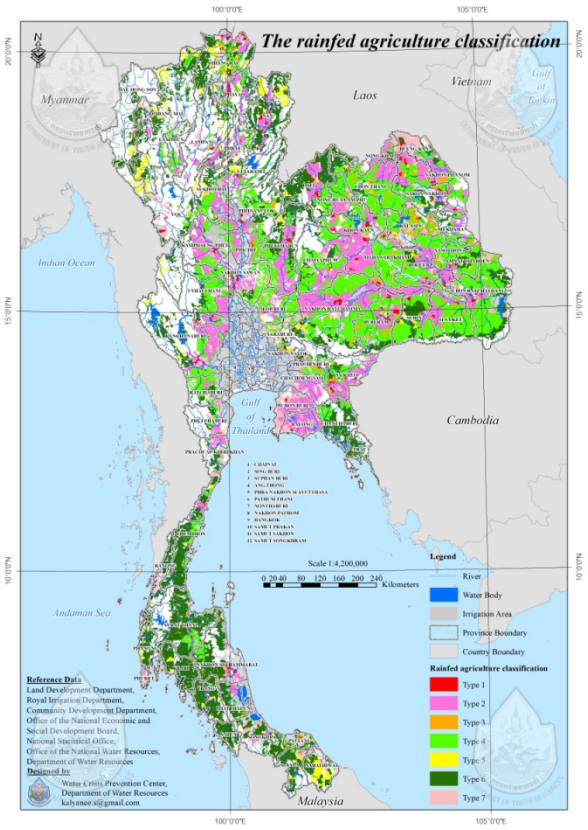

Fig. 5. The rainfed agriculture classification

Table I. The rainfed classifications in the each

Regionals	Area (km^2)						
	Type 1	Type 2	Type 3	Type 4	Type 5	Type 6	Type 7
North	896	9,920	912	10,736	2,048	11,776	1,184
Central	512	6,272	480	6,208	480	3,856	2,176
East	64	5,088	16	640	128	3,088	2,112
Northeastern	1,664	23,088	3,328	42,624	1,040	14,848	5,088
South	112	896	64	1,600	656	17,568	800
Deep South	16	352	48	224	1,216	5,760	848
Total	3,264	45,616	4,848	62,032	5,568	56,896	12,208

The overview for specification of SIS are as following:

- The coverage area approximately 60,000 m^2/system covered 25 households
- The water body with capacity larger than 30,000 m^3
- The water pump with capacity 100 m^3/day and 5 horse power or 4 k Watt
- The solar power with capacity 300 watts

As a result, the system can increase household annual income around 1,560 US dollar/year according to the previous survey from existing project in Nakhon Ratchasima and Kanchanaburi by DWR.

To solve water shortage in rainfed agriculture risk and alleviate income for the household that have income lower than the poverty line, the DWR and the Local Administrative Department are cooperated to set the urgent plan to implement 3,482 projects of SIS from 2017-2021. The expect outcomes are to apply SIS to cover 224 km^2, which will benefit 85,600 households and to increase water capacity in the rainfed agriculture approximately 122 million m^3.

According to the strategic plan on Thailand Water Resources Management, one of the main strategies is focused on the water security for production sector, which is related to increase the water storage and agriculture area. For this reason, the DWR planned to implement the SIS for the long-term plan in 20 years (2017-2037), which is expected to support the people in the rainfed agriculture areas who have the annual income lower than the poverty line as mention in previous section. Therefore, the 18,100 projects of the SIS are planned to implement in the rainfed agriculture area to improve the quality of life of 2.12 million households who have income lower than poverty line.

Conclusions

The classification of the rainfed areas for the water development projects was classified and prioritized by land-use, household income, revenue structures, water resources risk areas, special economic zones and household locations. For the classification results, the potential rainfed agriculture areas were defined into 7 classifications. Type 1, 3 and 5 are the key areas for Thailand to carry out target poverty alleviation. Therefore, the technology and innovation are needed to boost rural revitalization and modernization. Currently, Thailand is transforming its traditional agriculture sector, using science and technology by considering ecological restoration and protection to drive rural revitalization and

modernization. Consequently, the solar-powered irrigation system has played an important role in ensuring national food security, high-quality crop varieties, automate machines, water efficiency, pollution control and agriculture waste recycling.

For the potential rainfed agriculture areas, the Royal's Thai Government by Department of Water Resources, Ministry of Natural Resources and Environment and Local Administration Department, Ministry of Interior was planned to implement the solar-powered irrigation system in the urgent plan in 3,482 projects with a planned investment approximately $218 million, which will take 5 years to complete from 2017 to 2021. Moreover, the projects are expected to help boost the local economy and support the other alleviation projects. In addition, the other 18,100 projects of the solar-powered irrigation system were planned in the 20 years plan to implement in the rainfed agriculture areas to improve well-being of 2.12 million households who have income lower than the poverty line in Thailand.

References

[1] The Policy Committee for Water Resources, The Strategic Plan on Thailand's Water Resources Management, 2015
[2] Land Development Department, Landuse, 2015
[3] Royal Irrigation Department, Irrigation area, 2016
[4] Department of Water Resources, Water resources area-based management [Online], 2017, Available from: http://mekhala.dwr.go.th/download-cate.php?txtdoccate=29 [2017,September 01]
[5] Office of National Water Resources, Water resources area-based management [Online], 2018, Available from: http://www.onwr.go.th/download/AreaBase_THAI.zip [2018,August 15]
[6] Community Development Department, Report of Village Basic Information, 2015.
[7] Office of the National Economic and Social Development Board, Personal income in the provincial level, 2017
[8] National Statistical Office, Number of households, 2017
[9] The Geo-Informatics and Space Technology Development Agency (Public Organization), Household location, 2017

Water and Food Relationship Evaluation on WEF Nexus in greenhouse with water stress and soil condition

Pureun Yoon[1,a] and Jin-Yong Choi[1,b,†],Kwihoon Kim[1] and Yoonhee Lee[1]

Abstract Due to the population growth, food production demands and water use increase, there is a wide variety of global discussions on resource management in terms of securing resources such as water and food considering sustainability. The concept of "Water-Food-Energy Nexus" has emerged to interpret the linkage of water, energy and food resources and to suggest an integrated management plan. There is a trade-off relationship among input resources such as energy, water and cost, for increasing food productivity, therefore, it is necessary to analyze the relationships comprehensively rather than single resource analysis. This study was conducted to evaluate the relationship between water and food among the water-food-energy nexus of upland crops in greenhouse. Because the growing the upland crops in greenhouse could control the environmental condition such as the temperature, humidity, and wind speed, the analysis based on the scenarios according to the environmental conditions could be conducted. Also, the upland crops are more vulnerable to water stress than paddy rice which cultivated by flooding method. And water stress has a significant influence on the upland crop growth and production. Thus, this study included simulating the response of the upland crops in greenhouse to water and to evaluate the relationship between water and food resources, using AquaCrop model which estimate water productivity of the upland crop. The AquaCrop model developed by FAO analyzes the effects of water environment, fertilizer and irrigation method on the production of various crops. Input data includes weather, crop, soil data and farm management data including irrigation and fertilizer. Then, the upland crop yield and water productivity based on the irrigation method, fertilizer, weather condition are simulated in terms of water stress. From the results, it was demonstrated that the water and food relationships for Nexus water-food bridge could be quantified using AquaCrop model.

Keywords *Water-Food-Energy Nexus, Upland crop, Water stress, Soil condition, AquaCrop*

[1]Department of Rural Systems Engineering, College of Agriculture and Life Sciences, Seoul National University
Seoul, Republic of Korea

[a]vnfms3259@snu.ac.kr
[b]iamchoi@snu.ac.kr

Introduction

Four of the 10 most likely and influential global risk factors presented by Global Risks 2015 are related to climate change, water security and food security. In order to cope with such changes in the future environment, it is necessary to secure and utilize limited resources sustainably. Water-Energy-Food Nexus interprets water-energy-food interrelations to achieve efficient use of resources and ultimately to sustainability of agriculture. Sustainable water resource management using WEF Nexus can increase the sustainability of available water resources by using balanced water resources between water, food and energy. There is a trade-off relationship among input resources such as energy, water and cost, for increasing food productivity, therefore, it is necessary to analyze the relationships comprehensively rather than single resource analysis.

The purpose of this study is to evaluate the relationship between water and food among the water-food-energy nexus of the upland crops in greenhouse. Because the water stress and soil fertility have a significant influence on the upland crop growth and production, estimating the crop growth and production need to be analyzed considering the irrigation method. Thus, this study included simulating the response of the crops in greenhouse to water, soil fertility and evaluating the relationship between water and food resources, using AquaCrop model which estimate water productivity.

Materials & Methodology

A. Protected cultivation (Greenhouse)

One of the best examples of water-energy-food nexus is protected cultivation. Protected cultivation is to cut off outdoor environmental conditions such as temperature, precipitation, and wind speed, and resources such as water and energy are put in order to provide an appropriate growth environment for crops. Therefore, water-food-energy nexus was applied to the protected cultivation area as a test bed for analyzing the trade-off between water, energy and food resources according to the environmental conditions in the greenhouse.

B. Crop water requirement and production simulation using AquaCrop model

In this study, using AquaCrop model, crop yield, evapotranspiration and the amount of the irrigation water use are estimated. AquaCrop model is designed to simulate the crop growth, biomass production, yield and evapotranspiration of herbaceous crop types (FAO, 2017). AquaCrop model concept represents yield response to water as a linear, crop-specific function of the ratio of actual to potential evapotranspiration over a growing season. AquaCrop model accounts for the dynamic effects of water and temperature stress on crop growth, and the impact of evaluated atmospheric CO2 concentrations on crop water productivity.

Results & discussion

A. Total yield, total irrigation water and water productivity simulation results

Total crop yield, the amount of the irrigation water and water productivity simulation results by the temperature conditions were estimated using the AquaCrop model. Simulation scenarios were set according to the crop environmental temperature conditions from 14℃ to 30℃ to evaluate the crop response to the cold and heat stresses. 1-year total yield and irrigation water were calculated by multiplying the unit yield and irrigation water per day by the growing period to consider that the growing period varies depending on the temperature conditions. In addition, water productivity is a concept that links crop yield and agricultural water use, and is an indicator of agricultural water use efficiency. Water productivity was estimated by dividing crop yield (ton/ha) by the amount of irrigation water (mm).

Table I. Total yield of 1-year and water productivity results by the temperature scenarios

Case	Minimum Temperature (℃)	Maximum Temperature (℃)	Total yield (ton/ha/year)
Case 1	13	17	80.2
Case 2	14	18	82.9
Case 3	15	19	88.3
Case 4	16	20	92.0
Case 5	17	21	96.2
Case 6	18	22	100.9
Case 7	19	23	106.5
Case 8	20	24	109.0
Case 9	21	25	111.0
Case 10	22	26	118.4
Case 11	23	27	115.6
Case 12	24	28	123.9
Case 13	25	29	126.7
Case 14	26	30	123.6

Table II. Irrigation water requirement and water productivity of 1-year and water productivity results by the temperature scenarios

Case	Minimum Temperature (℃)	Maximum Temperature (℃)	Total irrigation water requirement (mm)	Water productivity (ton/ha/mm)
Case 1	13	17	636.9	0.126
Case 2	14	18	654.1	0.127
Case 3	15	19	669.4	0.132
Case 4	16	20	686.3	0.134
Case 5	17	21	700.5	0.137
Case 6	18	22	737.1	0.137
Case 7	19	23	759.7	0.140
Case 8	20	24	775.8	0.140
Case 9	21	25	803.1	0.138
Case 10	22	26	829.6	0.143
Case 11	23	27	868.4	0.133
Case 12	24	28	900.8	0.138
Case 13	25	29	934.5	0.136
Case 14	26	30	959.3	0.129

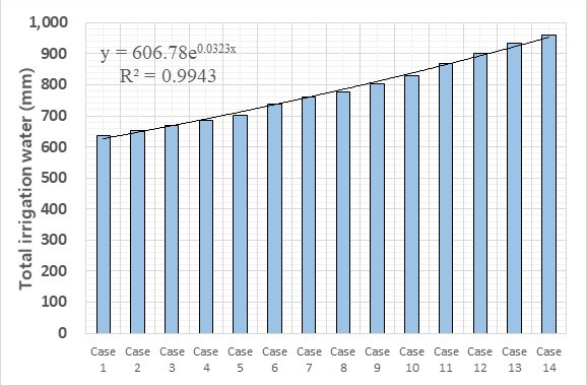

(a)

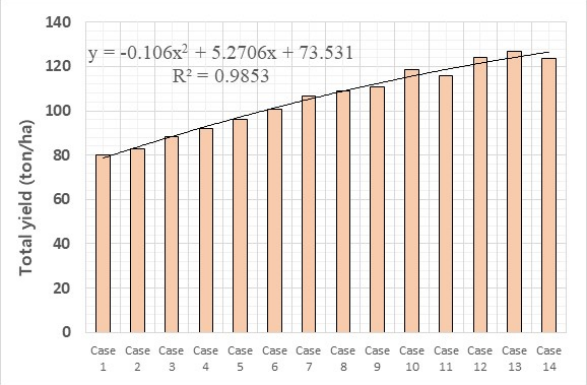

(b)

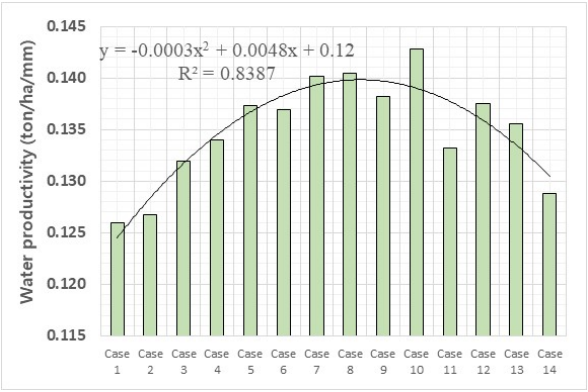

(c)

Fig. 1. Total yield, irrigation water requirement of 1-year and water productivity results by the temperature scenarios ((a): Total irrigation water requirement (mm), (b): Total yield (ton/ha), (c): Water productivity (ton/ha/mm))

The total annual crop yield, irrigation water requirement and water productivity results for each temperature scenarios are as above. As the temperature increased, both crop yield and irrigation water requirement tended to increase. However, in the case of crop yield, the increasing slope gradually decreased, and it is considered that the high temperature stress acts as the temperature continuously increases. On the other hand, in the case of irrigation water requirement, it continuously increased to show the form of exponential function. Water productivity, which is the ratio of crop yield (ton/ha) to irrigation water requirement (mm), can be used as an indicator of water use efficiency and can be used to select the most efficient scenarios and the environmental conditions in policy or decision making.

B. Crop growth simulation results by water stress

For the simulating the crop growth response to water stress and, the biomass, crop yield and the amount of the irrigation water were estimated under the water stress conditions by the irrigation method. The study crop was tomato and the growing period was from January/10 to August/7 which is the 1 growing cycle of tomato. The irrigation method was adjusted to evaluate the crop growth response to water stress, and the conditions were four (Not irrigated, irrigated at the point of 10% RAW remained (Readily available soil water), irrigated at the point of the 50% RAW remained, irrigated at the point of 10% RAW remained (potentially irrigated)).

Table III. Boimass, yield, amount of the irrigation water results by the irrigation method

Irrigation method scenario	Biomass (ton/ha)	Yield (ton/ha)	Irrigation water requirement (mm)
Not irrigated	6.04	3.41	0
Irrigated at 10% RAW remained	12.97	8.17	135.8
Irrigated at 50% RAW remained	13.42	8.47	191.4
Irrigated at 100% RAW remained (potential)	13.48	8.50	307.7

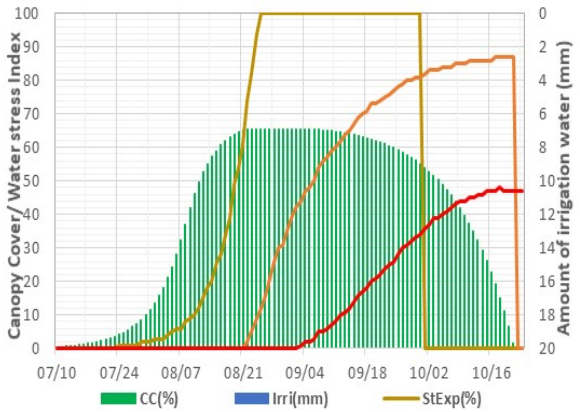

(a)

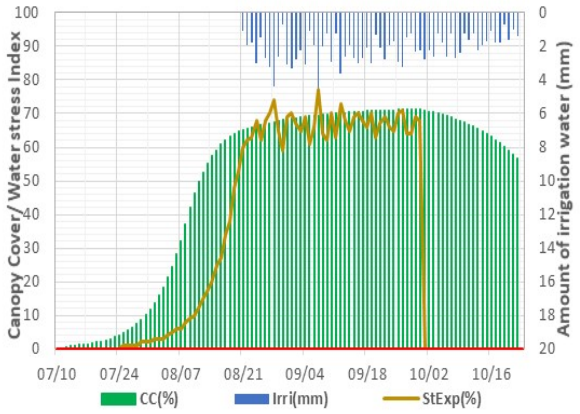

(b)

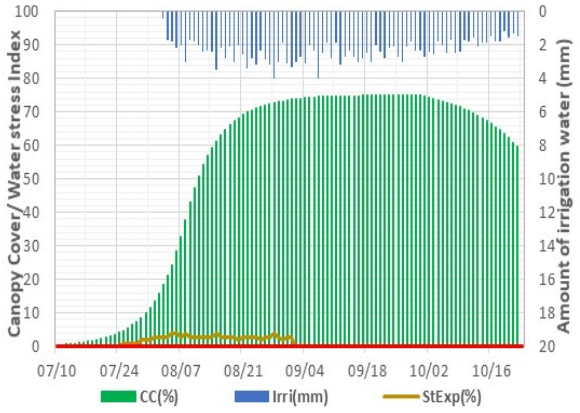

(c)

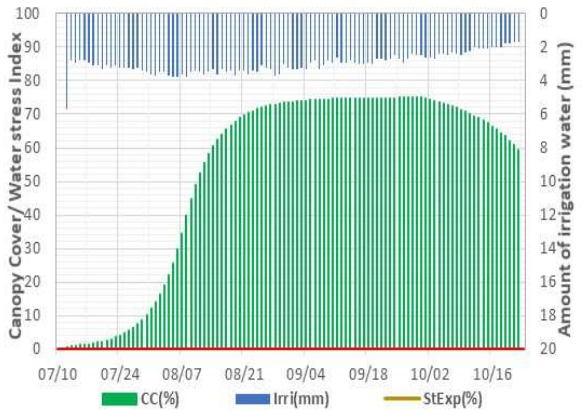

(d)

Fig. 2. Canopy cover, the amount of the irrigation water, water stress by the irrigation method ((a): Not irrigated, (b): Irrigated at 10% RAW remained (Readily available soil water), (c): Irrigated at 50% RAW remained, (d): Irrigated at 100% RAW remained (potentially irrigated))

(※ CC: Canopy cover (%), Irri: The amount of the irrigation water (mm), StExp: Percent water stress reducing leaf expansion (%), StSto: Percent water stress inducing stomatal closure (%), StSen: Percent water stress triggering early canopy senescence (%))

The crop yield, irrigation water requirement and water stress results of the one crop growing cycle according to the irrigation method are as above. Yellow, orange, and red lines indicate growth inhibition water stress, stomatal closure water stress and early canopy senescence water stress, respectively. First, without irrigation, yields were significantly lower and all three water stresses were found to occur. In the case of irrigation when the soil moisture content remained 10%, growth inhibition water stress only occurred and the yield was estimated to be 8 tons per one crop growing cycle. Secondly, when irrigation is carried out when the soil moisture content is 50%, there is a slight growth inhibition water stress, but there is no significant difference in the total yield compared to the case of irrigated potentially (Irrigated at 100% RAW remained), and the amount of irrigation water requirement is about 1.5 times.

C. Crop growth simulation results by soil fertility

For the simulating the crop growth response to soil fertility condition, the biomass, crop yield, the amount of the irrigation water and water productivity were estimated under the soil fertility stress condition. The soil fertility stress conditions were six (Potential (soil fertility stress 0%), Optimal (23%), Moderate (42%), Half (51%), Poor (59%), Very poor (69%)).

Table IV. Boimass, yield, amount of the irrigation water, water productivity results by the soil fertility condition

Soil condition (Soil fertility stress)	Biomass (ton/ha)	Yield (ton/ha)	Irrigation water (mm)	Water productivity
Potential (0%)	13.42	8.45	191.4	4.42
Optimal (23%)	10.77	6.79	174.1	3.90
Moderate (42%)	8.09	5.10	150.8	3.38
Half (51%)	6.70	4.22	136.9	3.08
Poor (59%)	5.43	3.42	122.3	2.80
Very poor (69%)	3.90	2.45	101.5	2.42

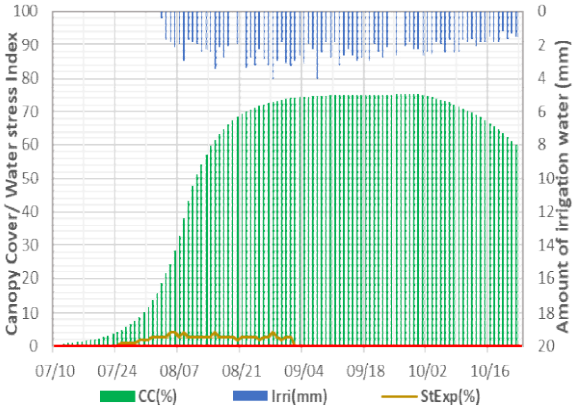

(a)

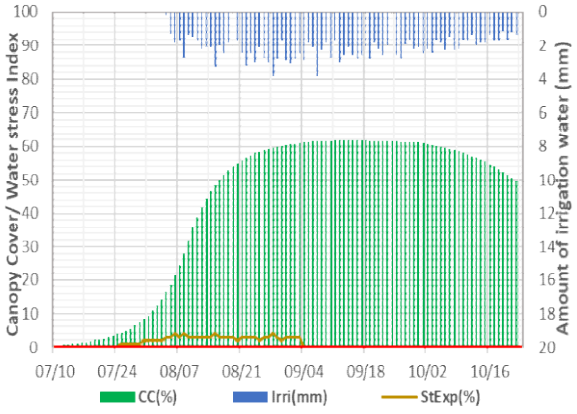

(b)

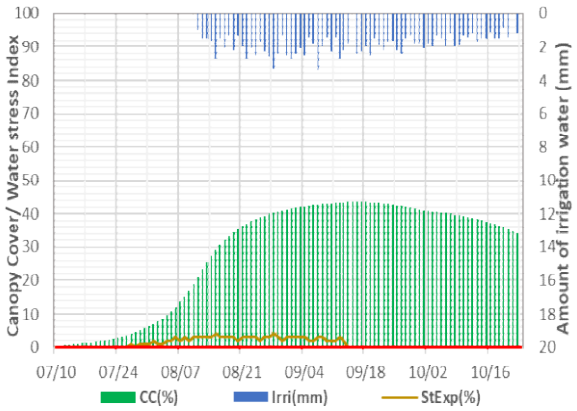

(c)

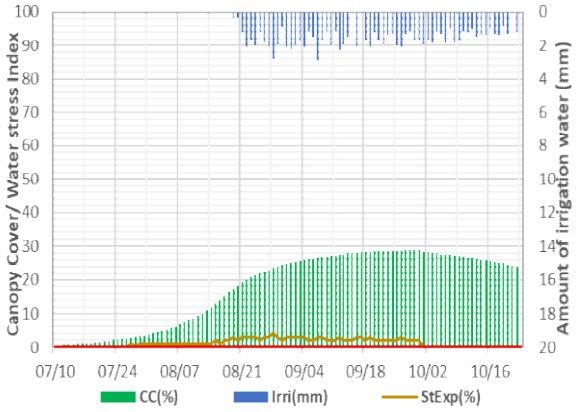

(d)

Fig. 3. Canopy cover, the amount of the irrigation water, water stress by the soil fertility stress condition ((a): Potential (soil fertility stress 0%), (b): Optimal (soil fertility stress 23%), (c): Half (soil fertility stress 51%), (d): Very poor (soil fertility stress 69%))

(※ CC: Canopy cover (%), Irri: The amount of the irrigation water (mm), StExp: Percent water stress reducing leaf expansion (%), StSto: Percent water stress inducing stomatal closure (%), StSen: Percent water stress triggering early canopy senescence (%))

Acknowledgment

This work was carried out with the support of "Cooperative Research Program for Agriculture Science and Technology Development (Project No. PJ01343502)" Rural Development Administration, Republic of Korea.

References

[1] FAO, AquaCrop training handbooks: Understanding AquaCrop, 2017

Outlier Detection of Reservoir Water Level Data Using Artificial Neural Network Model

Maga Kim[1] and Jin-Yong Choi[1,a,†]

Abstract The agricultural reservoirs determine the amount of water supply of irrigation according to water and environmental conditions of the reservoir. The reservoir water level data estimate the current water storage of the reservoir by capacity curve, to figure out the ability for irrigation and to manage agricultural water reasonably. In Korea, pieces of reservoir water level measuring equipment are installed for agricultural reservoirs having 100,000 tons storage capacity or more, and reservoir water levels are measured every 10 minutes. In spite of vast amount of available reservoir water level data, outlier detection systems for measured data is not properly equipped. The manual outlier detection and quality control requires time and labor consuming, and outliers and missing values create problematic causes in utilization of the reservoir water level data for irrigation planning appropriately. Therefore, it is necessary to detect outlier and improve the quality of reservoir water level data. This study was conducted to detect outliers of reservoir water level data using artificial neural network model. The artificial neural network model was trained with prepared training dataset as normal data (T) and outlier or missing data (F), and the artificial neural network model operated for identifying the outlier. The models are evaluated with reference reservoir water level data which were collected in daily by Korea Rural Community Corporation (KRC).

Keywords *outlier detection, artificial neural network; reservoir water level*

[1]Department of Rural Systems Engineering, College of Agriculture and Life Sciences, Seoul National University
Seoul, Republic of Korea

[a]iamchoi@snu.ac.kr

Introduction

Reservoirs are artificial irrigation facilities which store the water stream (river, flowing water). It can be possible to supply water to where requiring water at when requiring water by efficient management of reservoirs (Jung and Kim, 2007). In particular, the reservoir water level data can be used to check the reservoir storage, and the reservoir water level data is used as a criterion for determining the reservoir storage according to purpose. In addition, reservoir water level data are used for various research fields such as optimization of hydrological model (Song et al., 2017) and groundwater flow analysis (Ji, 2014). In Korea, about 1,600 reservoir water level measurement equipment are installed for agricultural reservoirs with a capacity of 100,000 tons or more, and the water level data are collected and utilized for reservoir operation and research.

The water level measurement method uses a pressure type sensor and an ultrasonic type sensor and the reservoir water level are measured at intervals of 10 minutes (Bang et al., 2017). However, in the case of the pressure type sensor, the incorrectly measured values may occur due to the inflow of the internal sludge in inclined conduit or the accumulation of the deposit near the sensor. In the case of the ultrasonic sensor, the incorrectly measured values may occur due to the temperature and humidity, wave of water and plants near the sensor. In addition, there are causes that may occur the incorrectly measured values such as equipment error, calibration error, and so on. Although the incorrectly measured values are existed, there is not proper outlier detection method yet. The administrator of reservoir conduct outlier detection in subjective and manual way at present. Because manual outlier detection method takes a lot of time and labor, it is difficult to detect the incorrectly measured values and it makes utilization of reservoir water level to decrease.

Therefore in this study, we try to apply outlier detect algorithm to make automatic outlier detect possible and evaluate applicability. The methods employing in this study is artificial neural network (ANN) model. The ANN model make training data set with statistical method and train the model with training data set. Then ANN model detect the incorrectly measured values. The results of the models were evaluated with reference data which are daily reservoir water level offered from Korea Rural Community Corporation (KRC).

Materials & Methodology

In this study, the reservoir water level data measured at 10-minute interval are used as raw data for outlier detection and daily reservoir water level data from KRC are used as reference data. The ANN model is applied to detect the incorrectly measured values. The results of the models are evaluated by comparison with the daily reservoir water level data from KRC. The reservoir water level data from KRC are measured daily and the administrator check the value. If there is problem with values, the administrator can change the value to correct value by eye observation. Fig. 1 is flow chart of this study.

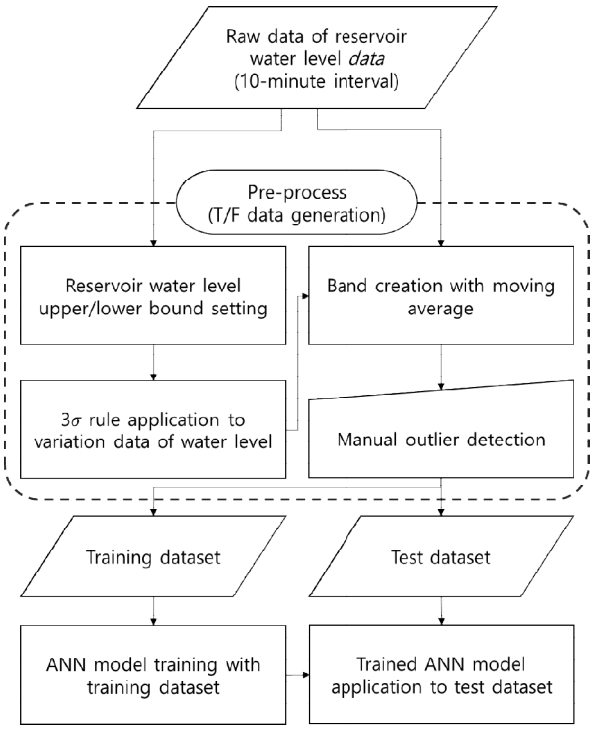

Fig. 1. Flow chart of the study

A. Subject reservoir and water level data

The subject reservoir of this study is the Gaeun reservoir which is in Gaeun-ri, Dong-myeon, Hongcheon-gun, Gangwon-do, Korea. The Gaeun reservoir has 474 ha of basin area and 1,636 thousand ton of effective storage. Table 1 is the properties of the Gaeun reservoir.

Table I. Properties of the Gaeun reservoir

Dam properties	Contents	Dam properties	Contents
Dam type	fill dam	Intake works	main facility
Dam length (m)	224	Water-intake type	intake tower
Dam height (m)	39.7	Total storage(㎥)	1,649,375
Dead storage water level (m)	22.50	Effective storage (㎥)	1,636,475
Full water level (m)	245.80	Benefitted area (㎢)	103
Flood water level (m)	246.80	Basin area (ha)	474

The reservoir water level data of the Gaeun reservoir are used as raw data for outlier detection model, and daily reservoir water level data from KRC are us ed as reference data. The reservoir water level data of the Gaeun reservoir are measured by pressure type sensor in 10 minute interval and the period of data is 2011. 01. 01. 0:00~2018. 06. 12. 11:40. The reference data are measured by sensor first, and then adjusted by manager of the reservoir with eye measurement. The interval of measuring the reference data is a day and the period of the reference data is 2009. 08. 19.~2018. 05. 23. Fig. 2 is the reservoir water level data of the Gaeun reservoir.

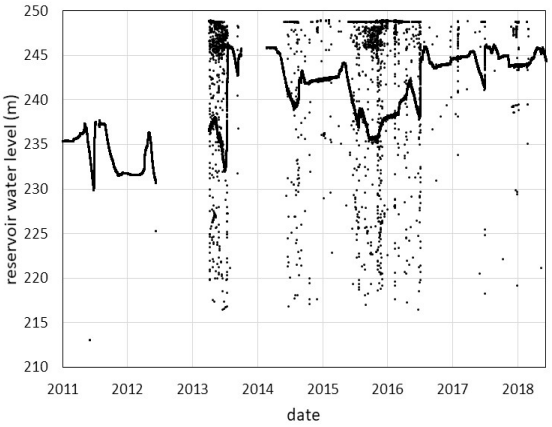

Fig. 2. 10-minute interval raw water level data of the Gaeun reservoir

B. Artificial neural network (ANN) model

The ANN model make the T/F dataset first, and then divide the dataset to training dataset for model training and test data for testing the model. T/F means normal water level data (T) and outlier or missing data (F). After the training, ANN model classify the reservoir water level data by using test data. Making the dataset is divided into four steps which are establishing upper/lower bound of reservoir water level, applying 3-sigma rule of thumb to variation data of water level, creating a band from reference value with moving average, and manual outlier detecting. When the reservoir water level value is classified as the outlier in the process of making training data set, the model exclude the value at the time and apply the result to next step.

1) Setting upper/lower bound of reservoir water level (step 1)

In first step, the reservoir water level data which are outside the bound are classified as the incorrectly measures values. The bound of reservoir water level data is determined with reservoir specification. The upper bound is established same as flood water level and the lower bound is established same as dead water level. When the reservoir water level value is classified as the incorrectly measured values in the process of making training data set, the

model exclude the value at the time and the result are employed in second step.

2) Applying 3-sigam rule to variation data of water level (step 2)

In second step, the reservoir water level data are classified by applying 3-sigma rule of thumb to variation data of water level. 3-sigma rule of thumb establish the bound using mean(m) and standard deviation(σ). If the variation data of water level is out of bounds(m ±3 σ), the reservoir water level data at the time are classified as the incorrectly measured values. In this step, if the reservoir water level value of previous point is missing value, the variation value of water level at the time is considered as zero. When the reservoir water level value is classified as the incorrectly measured values in this step, the model exclude the value at the time and the result are employed in third step.

3) Creating a band with reference vaule from moving average (step 3)

In third step, the reference value is determined by moving average from result of second step and then the raw reservoir water level data which are outside the band are classified as the incorrectly measured values. The moving average is calculated by using the previous 10 reservoir water level data including the value at the time and the constant width of band is 0.05 m.

4) Manual outlier detecting (step 4)

In fourth step, the misclassified data are reclassified as normal data or outlier. When there is sharp changes in variation data of water level, the normal data can have been misclassified as outlier (F). Thus, if there are F values for over 4 hours in a row, the classifications of reservoir water data were modified manually after checking. Also, some of the outlier can have been misclassified as normal data. They were appeared like spike noise in the graph. In that case, the misclassified outlier are reclassified manually. Fig. 3 is the dataset for ANN model which is eliminating the outliers (F).

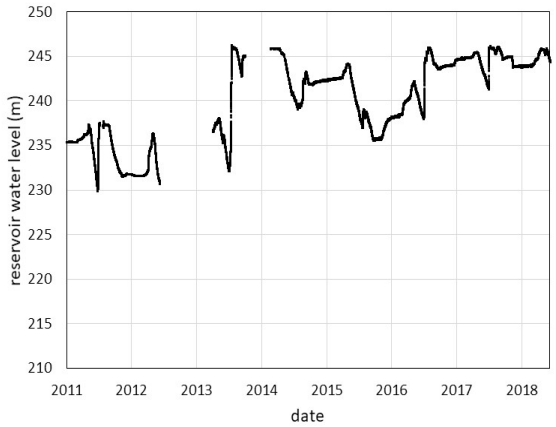

Fig. 3. T dataset after data pre-process

The ANN model is constructed with an input layer, one hidden layer, and an output layer. It applies sigmoid function as activation function for hidden layer, softmax function as activation function for output layer. The ANN model calculates error at output layer with cross entropy error function and adjusts the weights with the gradient descent method which is one of the back-propagation algorithm. The performance of the ANN model is affected by input data type which are demonstrated in Table 2.

Table II. Input data of the artificial neural network model for outlier detection

Data type	Contents
water level (wl_t)	wl_t
variation (v_t)	$v_t = wl_t - wl_{t-1}$
reservoir regularization (rr_t)	$rr_t = (wl_t - dl) / (fl - dl)$
limited regularization (lr_t)	lr_t = 1(if $rr_t > 1$) rr (if $0 < rr_t < 1$) -1 (if $rr_t < 0$)
regularization (r_t)	$r_t = (wl_t - \min(wl)) / (\max(wl) - \min(wl))$
variationregularization (vr_t)	$vr_t = (v_t - \min(v)) / (\max(v) - \min(v))$

*wl: measured reservoir water level, v: variation of reservoir water level, rr: regularized reservoir water level with dead water level (dl) and flood water level (fl), lr: regularized reservoir water level with dead water level (dl) and flood water level (fl) within range of -1 to 1, r: regularized reservoir water level, vr: regularized variation of reservoir water level

The hyper-parameters of the ANN model such as number of past-time input data, number of hidden layer nodes, and learning rate are determined by trial and error method. According to results of the trial and error method, number of past-time input data is 13, number of hidden layer nodes is 15, and learning rate is 0.005. Fig. 4 is the structure of the ANN model.

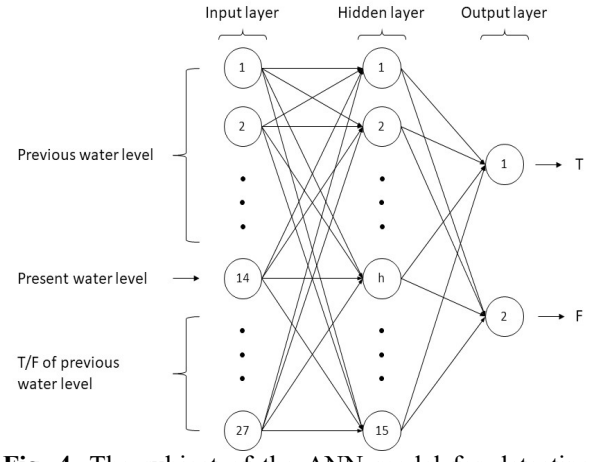

Fig. 4. The subject of the ANN model for detecting outlier

Results

The ANN model applied 6 input data type such as water level (wl), variation (v), reservoir regularization (rr), limited regularization (lr), regularization (r), variation regularization (vr) and the result of the case of applying variation (v) as input data showed the best performance among the 6 input data type. Therefore, in this study, variation (v) data is used as input data. Daily mean data are used to compare the result of the model and reference data. Fig 5 is the graph of the (a) raw data, (b) target data of the ANN model, (c) result of the ANN model, (d) reference data.

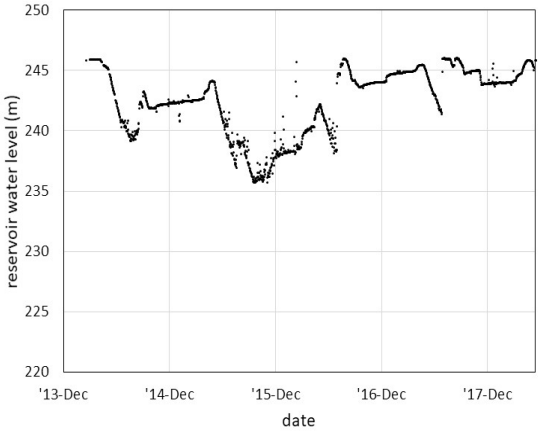

(a) raw data

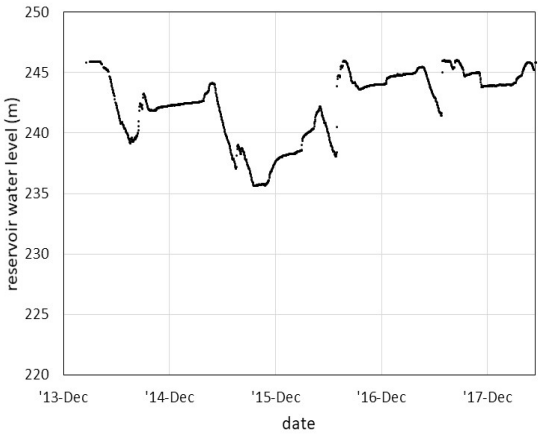

(b) target data

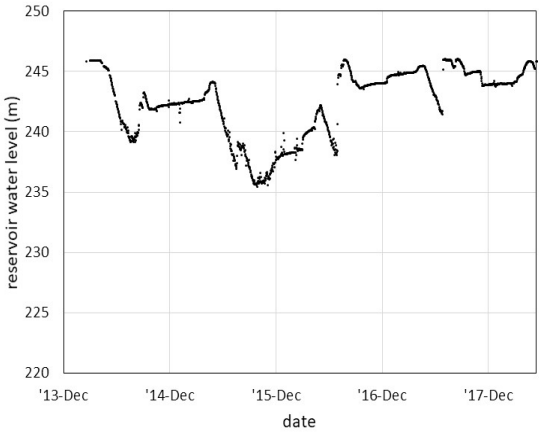

(c) ANN model result data

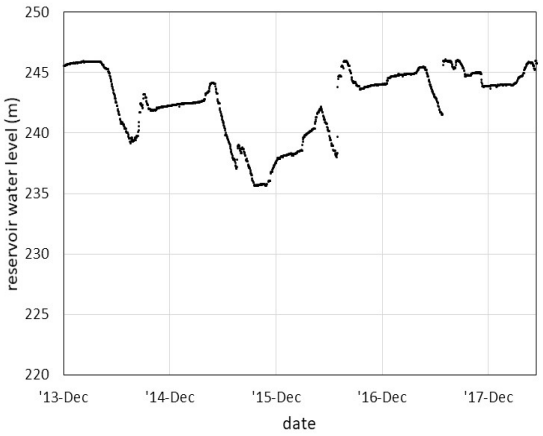

(d) reference data

Fig. 5. Daily mean value of (a) raw data, (b) target data, (c) ANN model result data, (d) reference data after ANN model application

R^2, MAE, RMSE compared to reference data are in Table 3. R^2 of target data is 0.999 while R^2 of ANN data is 0.997. It means the ANN model detect the outlier and provide improved result over raw data, but it fall short of target data which has 0.999 of R^2.

Table III. The statistical parameters (R^2, MAE, RMSE) compared to reference data

Statistical parameters	Raw data	Target data	ANN data
R^2	0.982	0.999	0.997
MAE	0.126	0.034	0.065
RMSE	0.396	0.067	0.149

Fig. 6 is the scatter plot of the result compared with reference data.

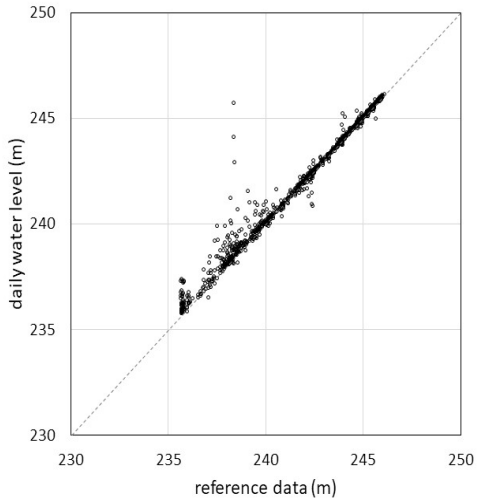

(a) raw data

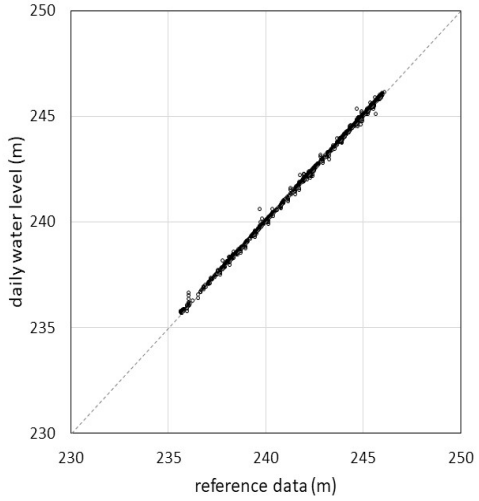

(b) target data

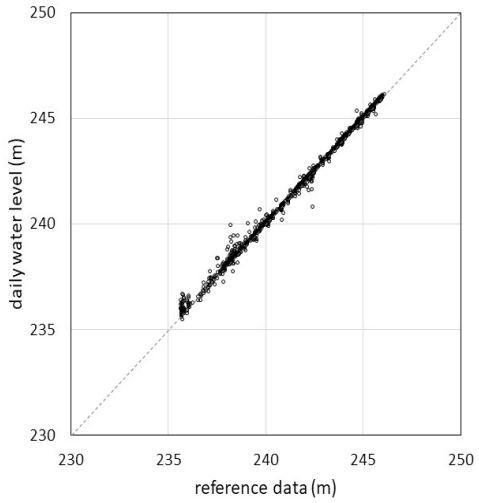

(c) ANN model result data

Fig. 6. The scatter plot of (a) raw data, (b) target data, (c) ANN model result data compared with reference data

References

[1] J. Bang, Y. Lee, S. Jung, and J. Choi, "A study of outlier detection on time series of water level in agricultural reservoir", Korean Society of Agricultural Engineers Annual Conference, October 2017.

[2] W. Ji, "Analysis of groundwater flow in the reservoir water elevation" Keimyung University.

[3] G. Jung and T. Kim, "Comparison of water distribution model through reservoir and water system operation", Water for Future, vol. 41, pp. 38-43.

[4] J. Song, M. Kang, K. Kim and J. Ryu, "Estimation of daily reservoir inflow from water level observation using a hydrological model and an optimization method", Korean Society of Agricultural Engineers Annual conference, October 2017.

Evaluation of the Relationship between Electric Conductivity and Spectral Index for Soil Salinity Mapping of Rice Paddy Field in Khon Kaen Province

Masayasu MAKI[1,a], Mallika SRISUTHAM[2], Koki HOMMA[3], Supranee SRITUMBOON[4] and Koshi YOSHIDA[5]

Abstract Geospatial information about salt injury is required for rice growth management in Khon Kaen. However, the soil salinity map which is effective for rice growth management in Khon Kaen does not exist. As the first step, evaluation of the relationship between electric conductivity (ECe) which is the indicators of salt injury before planting and leaf area index (LAI) during growth period was conducted in this study. Soil samplings for measuring ECe before planting were conducted in Khon Kaen on 6th and 7th April 2016. To generate geospatial map of rice growth condition during growth period, Spectral measurement using drone and field measurement of LAI were conducted in the same area on 7th September 2016. As the results, it was confirmed that LAI during growth period and ECe before planting had negative correlation. Secondly, evaluation of the relationship between ECe and spectral index was performed for mapping the spatial distributions of ECe in the study area. Soil samplings for measuring ECe in the study area were conducted on 22nd December 2016 and 11th May 2017. Spectral measurements using drone for calculating normalized difference salinity index (NDSI) were executed on the same days. As the result, EC and NDSI obtained on 11th May 2017 had strong positive correlation compared to the one obtained on 22nd December 2016. These above mentioned results indicate that soil salinity map derived from NDSI image on the end of dry season has the potential to give the effective information for rice growth management.

Keywords *salt affected soil, soil salinity mapping, remote sensing*

This work is supported by Japan International Cooperation Agency (JICA) under the Advancing co-design of integrated strategies with adaptation to climate change in Thailand (ADAP-T) Project.

[1]Faculty of Engineering
Tohoku Institute of Technology
Sendai, Japan
[2]Faculty of Agriculture
Khon Kaen University
Khon Kaen, Thailand
[3]Graduate School of Agricultural Science
Tohoku University
Sendai, Japan
[4]Land Development Department Regional Office 5
Land Development Department
Khon Kaen, Thailand
[5]Faculty of Agriculture
Ibaraki University
Ami, Japan

[a]makimasa@tohtech.ac.jp

Introduction

Salt affected soil is widely distributed in Northeast Thailand. Salt affected soil causes low rice productivity. There is salinity map in this region. In the map, the degree of salt injury is classified into 4 classes based on percentage of salt crust on soil surface (class 1: salt crust > 50%, class 2: 50% > salt crust > 10%, class 3: 10% > salt crust > 1%, class 4: 1% > salt crust > 0%). This map does not directly indicate the degree of salt injury because the one is not based on physical factors for evaluating salt injury. Therefore, in order to manage rice growth in Northeast Thailand, geospatial distribution map that is based on physical factors for evaluating salt injury is required. Electric conductivity (ECe) is very important indices for evaluating crop growth. However, the methodology to create the map of ECe in the study area does not exist

In this study, as the first step to develop the methodology, evaluation of relationship between ECe before planting and amount of rice body above ground surface during growth period was conducted to confirm the influence of ECe before planting on the rice growth. And then evaluation of relationship between ECe and major soil salinity index obtained from spectral information was conducted to confirm the availability of spectral index for geospatial distribution mapping.

Methodology

In order to evaluate the relationship between ECe before planting and rice growth during growth period, soil sampling for ECe measurement (6 points) was conducted in Ban Phai in Khon Kaen province (Fig. 1) during 6-7 Apr. 2016 (before planting). The study area is categorized to class 2 in existing salinity map. Landscape of the study area is shown in Fig. 2. It

can be confirmed that vegetation and salt crust are mixed. Measurement of the amount of rice above ground surface (36 points) was conducted in same region during 6-8 Sep. 2016 (during growth period). In this study, Leaf Area Index (LAI) was used as the indicator of amount of rice above ground surface. At the same time, multi-spectral images were obtained by multi-spectral camera (Sequoia, Parrot) attached to drone (Solo, 3DR). Spatial resolution of multi-spectral image was 5cm by 5cm per pixel. LAI of rice was measured by canopy analyzer (LAI-2200, Li-Cor).

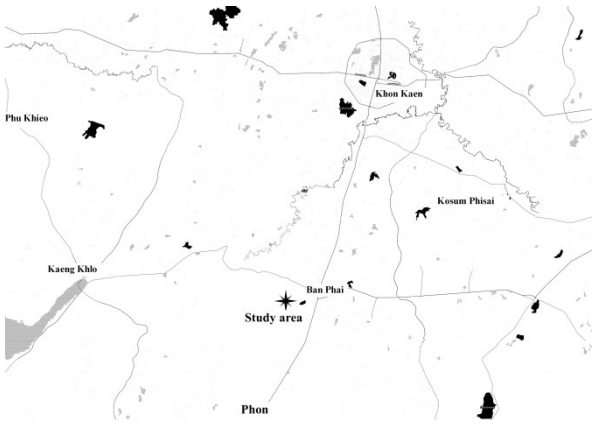

Fig. 1. Location of study area.

Fig. 2. Landscape of study area.

In this study, Green-Red ratio Vegetation Index (GRVI) [1], [2] was used for estimating rice LAI because the one was the best index for estimating LAI compare to other vegetation indices (Simple Ratio (SR), Normalized Difference Vegetation Index (NDVI), Enhanced Vegetation Index 2 (EVI 2), Red edge Chlorophyll Index), and NDRE (Normalized Difference Red Edge (CIred_edge)) in the study area. These vegetation indices were derived from multi-spectral camera data during Sep. 6-8 2016. GRVI is calculated using the following formula.

$$GRVI = (\text{GREEN} - \text{RED}) / (\text{GREEN} + \text{RED}) \quad (1)$$

where GREEN and RED in (1) indicate reflectances of wavelength in green and red, respectively. Then LAI values at the soil sampling points for ECe measurement were estimated by using the regression equation between LAI and GRVI obtained from field survey. And the relationships between ECe before planting and LAI during growth period were evaluated.

In order to estimate ECe by using spectral index, multi-spectral images were obtained on 22Dec. 2016 and 11 May 2017. Spatial resolution of these images were also 5cm by 5cm per pixel. Soil sampling for ECe that were used for comparing to spectral index were conducted on the same day. Furthermore, Soil Moisture Content (SMC) measurements was conducted at the same points on the same day because it is considered that soil water also affect to spectral information. Normalized Difference Salinity Index (NDSI) [3] was selected for estimating ECe in this study. This spectral index has been used as the one of major index for estimating degree of salinity injury in the world [3], [4]. NDSI is calculated using the following formula.

$$NDSI = (\text{RED} - \text{NIR}) / (\text{RED}+\text{NIR}) \quad (2)$$

where RED is the same one in (1). NIR is reflectance of wavelength in near-infrared. After obtaining NDSI images from multi-spectral images, the relationships between ECe and NDSI on 22 Dec. 2016 and 11 May 2017 were evaluated. And then the relationships between SMC and NDSI, and the one between ECe and SMC on the same days were evaluated for understanding the difference of the relationships between ECe and NDSI on each day. Field survey for ECe and SMC measurements for evaluating the above-mentioned relationships was conducted at 8 points on each day.

Result and Discussion

A. Evaluation of the relationship between ECe before planting and LAI during growth period

As the results of evaluation of the relationships between LAI derived from GRVI image and ECe, it is confirmed that LAI and ECe had negative correlation (Fig. 3). This means that ECe concentration before planting affect to the rice growth. Therefore, it is considered that geospatial distribution map of ECe before planting (in dry season) is very useful for suitable rice growth management.

B. Evaluation of ECe and NDSI in dry season

To generate geospatial distribution map of ECe, the relationships between NDSI derived from multi-spectral images and ECe on 22 Dec. 2016 and 11 May 2017 were evaluated. As the results, both of the relationships between ECe and NDSI on 22 Dec. 2016 and the one on 11 May 2017 had positive correlation (Fig. 4 and Fig. 5). Correlation coefficients on 22 Dec. 2016 and 11 May 2017 were 0.76 and 0.83, respectively. Although the correlation coefficient on

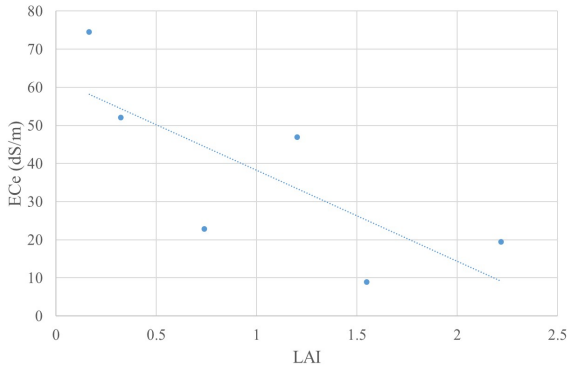

Fig. 3. Relationship between ECe before planting and LAI during growth period.

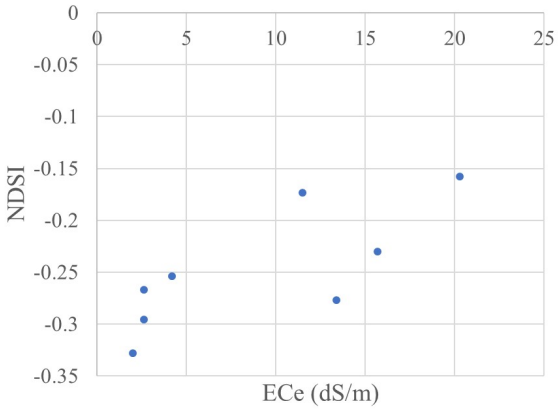

Fig. 4. Relationship between ECe and NDSI on 22 Dec. 2016.

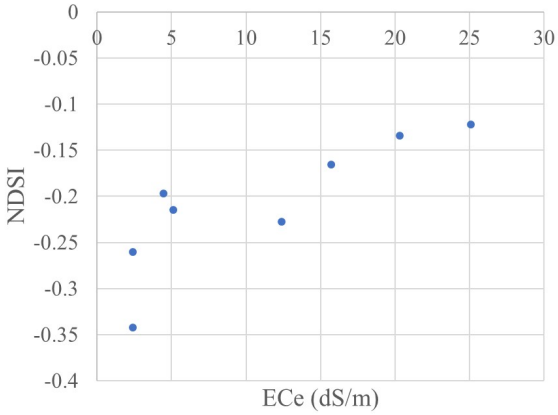

Fig. 5. Relationship between ECe and NSDI on 11 May 2017.

each day had positive value, the one on 11 May 2017 had stronger correlation than the one on 22 Dec. 2016. To understand the difference in these correlation coefficients, firstly SMC on each day was compared. And then both of relationships between NDSI and SMC on 22 Dec. 2016 and 11 May 2017 were evaluated. And relationships between ECe and SMC on each day were also evaluated.

Average values of SMC on 22 Dec. 2016 and 11 May 2017 were 15.9% and 10.7%, respectively. SMC value on 22 Dec. 2016 was higher than the one on 11 May. The correlation coefficients between SMC and ECe on each day was -0.36 and 0.71, respectively. It seems that the difference in SMC value affect to the relationship between SMC and ECe. In other word, relationship between SMC and ECe has positive correlation when SMC value is high. However, the one has negative or no correlation when SMC value is low. Figure 6 and 7 show the relationships between NDSI and SMC on 22 Dec. 2016 and 11 May 2017, respectively. Correlation coefficients on 22 Dec. 2016 and 11 May 2017 were -0.01 and 0.37, respectively. From above-mentioned results, the following findings were obtained at the study area.

- There is no correlation between NDSI and SMC when SMC value is relatively high and there is negative correlation between ECe and SMC.
- However, there is positive correlation between NDSI and SMC when SMC value is quite low and there is strong positive correlation between ECe and SMC.
- There is positive correlation between ECe and SMC when SMC value is quite low.

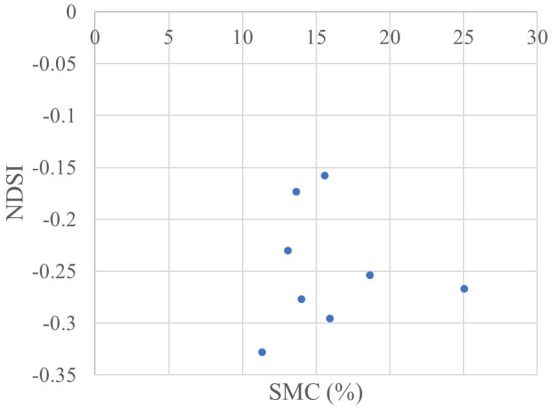

Fig. 6. Relationship between SMC and NDSI on 22 Dec. 2016.

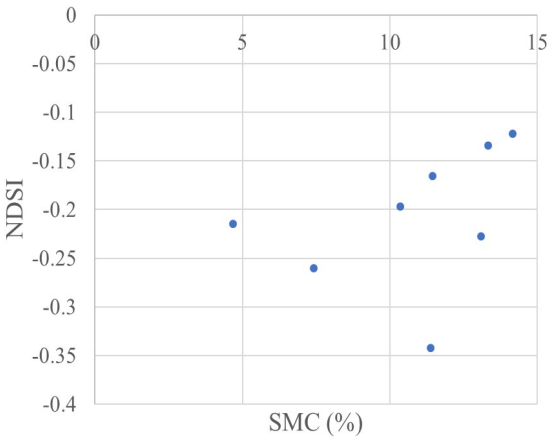

Fig. 7. Relationship between SMC and NDSI on 11 May 2017.

- There is weak negative correlation between ECe and SMC when SMC value is relatively high.
- NDSI has the potential to estimate ECe when SMC value is quite low and there is positive correlation between ECe and SMC.

Conclusions

In this study, in order to develop the methodology of mapping the spatial distribution of salt injury, evaluation of relationship between ECe before planting and amount of rice body above ground surface during growth period was firstly conducted. And the influence of ECe before planting on the rice growth was confirmed. As the result, it is confirmed that ECe before planting (in dry season) affects to the rice growth at the study area. And then evaluation of relationship between ECe measured by field survey and NDSI obtained from spectral information was conducted to confirm the availability of NDSI for geospatial distribution mapping of salt injury using remotely sensed data. In this study, it was confirmed that NDSI could estimate ECe value. However, the result was obtained when SMC value was low and SMC had strong positive correlation with ECe. And it was also confirmed that the relationship between SMC and NDSI changed when the relationship between SMC and ECe changed. Influence of SMC to estimate ECe using NDSI was small in this study. However, it is considered that SMC will affect to NDSI value for estimating ECe depends on the situation. Therefore, to develop the robust estimation method of ECe value using spectral index such as NDSI, the influence of soil moisture condition will be evaluated under several areas and conditions in the future study.

Acknowledgment

The authors thanks to the staff of ADAP-T office and LDD regional office 5 for management of field survey.

References

[1] C. J. Tucker, "Red and photographic infrared linear combinations for monitoring vegetation", Remote Sens. Environ, vol. 8, pp. 127-150, 1979.
[2] M. J. Falkowski, P. E. Gessler, P. Morgan, "Characterizing and mapping forest fire fuels using ASTER imagery and gradient modeling", Forest Ecol. Manage, vol. 217, pp. 129-146, 2005.
[3] N. M. Khan, V. V. Rastoskuev, E. V. Shalina and Y. Sato, "Mapping salt-affected soils using remote sensing indicators-a simple approach with the use of GIS IDRISI", 22nd Asian Conference on Remote Sensing, vol. 5(9), 2001.
[4] A. Dehni, M. Lounis, "Remote sensing techniques for salt affected soil mapping application to the Oran Region of Algeria" Procedia Engineering, vol. 33, pp. 188-198, 2012.
[5] E. Asfaw, K. V. Suryabhagavan, M. Argaw, "Soil salinity modeling and mapping using remote sensing and GIS: The case of Wonji sugar cane irrigation farm, Ethiopia", Journal of the Saudi Society of Agricultural Sciences, vol. 17, pp. 250-258, 2016

Monitoring landscape changes in catchment areas using remote sensing technique

Wen-Sheng Lin[1], Chihhao Fan[2], Chih-Renn Chen[3], Cheng-Jui Hsu[3] and Jia-Yu Lin[3]

Abstract This study established a monitoring process for the relationship between vegetation and satellite spectral images. Through a conversion relationship, satellite spectral values can be converted into monitoring data. According to calculation of the normalized difference vegetation index (NDVI), vegetation location can be determined. The threshold of the NDVI was found to be 0.05 for green and non-green cover. This value was further used to automatically generate a green or non-green cover image with a NDVI greater or less than the threshold respectively. In this study, the green parts of the generated image indicated vegetation area and the dark gray parts of the image indicated landscape change areas. After image transformation, the algorithm could automatically compare the pre- and postimages and select the landscape variation from the original green to non-green area. These findings reveal the effectiveness and advantages of using the NDVI to judge landscape change. Patrol personnel may be unable to identify illegal use of a catchment area. Therefore, using hyperspectral remote sensing data to judge illegal development is beneficial for conservation of catchment areas. Future development of smart image interpretation technology, image data collection, and interpretation of illegal development data could assist water resource conservation and land use management.

Keywords *remote sensing data, normalized difference vegetation index (NDVI), landscape changes*

[1]Hydrotech Research Institute,
National Taiwan University,
Taipei, Taiwan
[2]Department of Bioenvironmental Systems Engineering,
National Taiwan University,
Taipei, Taipei, Taiwan
[3]Geographic Information Technology Co., Ltd.,
Taipei, Taipei, Taiwan

Introduction

Due to frequent incidents of over development and illegal use of catchment areas, land use management must be strengthened by regularly checkingfor illegal use. Such checks serve to maintain ecological conservation within a catchment area and prevent overutilization and illegal development. Conventionally, patrol personnel conduct routine inspections onsite by using digital cameras, GPS device, and paper records. However, such manual inspection methods are timeconsuming and laborintensive, resulting in low inspection frequency and varying inspection standards due to personnel differences. Remote sensing imagescan help monitor large areas and be analyzed algorithmically to find suspicious locations. Remote sensing techniques can provide instant, low-cost, and long-term observation and monitoring of a catchment area. These advantages are especially useful for monitoring overall landscape change trends in catchments encompassing water sources and thus help in the management of these sources.Literature reviews pointed out that China monitored land use with satellite imagery to understand land changes or abnormal development practices. Other countries in the world mainly focused on the basic data survey and research of remote sensing technology and development of land geographic information system.[1-4]

This study evaluated the normalized difference vegetation index (NDVI) using hyperspectral remote sensing data for Taiwan fromthe FORMOSAT-2 satellite with 8-m spatial resolution. FORMOSAT-2 can provide red spectral band (0.630–0.690μm) and near-infrared band (0.760–0.900μm) images that can be used to estimate the NDVI. Chlorophyll in leaves has strong absorption at 0.45 and 0.67 μmand high reflectivity at near infrared (0.7–1.1 μm). In short-wave infrared spectroscopy, vegetation exhibits three absorption characteristics, which can be directly related to the water contained in the absorbed leaves[5].Because of chlorophyll absorption, plants usually have low reflectivity in the blue and red parts of the spectrum, but they have slightly higher reflectivity in the green part, which is why plants look green to human eyes. Near-infrared radiation energy is strongly reflected from plant surfaces. The amount of reflection depends on the characteristics of the leaf tissue. Contrast between vegetation and soil is largest in the red and near-infrared regions. Therefore, spectral reflectance data can be used to calculate various

nutritional indices, which are closely related to agronomic and biophysical plant parameters related to photosynthetic activity and plant productivity [6-8].

Satellite imagery has been widely used for monitoring and researching large-scale water conservation in catchment areas. Using various analytical methods, the relationship between spectral data and land use can be established to distinguish abnormal land use in catchment areas. In the present study, the relationship between vegetation cover and satellite spectral images was established. The location of vegetation cover was selected by calculating the NDVI, and then the empirical coefficient of the output threshold was calculated through statistical regression. The NDVI was employed to interpret the actual application of landform change in the catchment area.The NDVI is given as follows[9-10]:

$$NDVI = (NIR - RED) / (NIR + RED) \quad (1)$$

where NIR is reflectance in the near-infrared band and RED is reflectance in the visible red band.

Using past satellite remote sensing image data, the location for analysis was selected as the upper reaches of the Xindian Rivercatchment area. Landform variation in the water area was interpreted intelligently. Using pre- and postimages, NDVI interpretation was employed to effectively identify the landform variation points (i.e., the threshold of green and non-green covered landforms in the selected catchment area).By comparing the earlyimages with later images, the variation points could be determined interms of green to non-green coverage. The NDVI was used to interpret the geomorphological variation.

According to the transformation relationship,satellite spectral values can be converted into the information of land use. Therefore, the distribution of the overall use of the catchment area can be obtained quickly so that the correct management strategies for water conservation can be adopted. The following is a description of the monitoring process.

Methodology

A. Satellite image data collection

Selected satellite images were based on the frequency of the satellite passing through the target area and the requirements of the patrol service. In addition, satellite images are affected by cloud occlusion; therefore, reasonable frequency and period were determined according to requirements.

B. Satellite image geometry correction

Satellite image data could not be used to determine the spatial geometric distribution of images in different periods. To ensure that the spatial geometric distribution between multitemporal images corresponded correctly, geometric correction of multitemporal satellite images was conducted.

C. Satellite image correction

The purpose of this step was to correct images under different geometric or irradiation conditions at different times. Analysis and comparison of images taken in different seasons and from different positions requires consideration of varying angles of solar irradiation and different intensities of reflection. Therefore, the follow-up analysis could be conducted for images taken at different times.

D. Establishment of the regression model

According to calculation of the NDVI, the location of plants can be screened, but the threshold of each regional index differs, and therefore, a regression equation was generated by referring to the literature and empirical coefficientsof statistical regression output thresholds.

E. Mode verification and amendment

If new satellite imagery is used, the old regression relationship can be validated and corrected, and a new threshold can be established. When the validation is completed, it becomes a new regression model of catchment area, and can be used for long-term monitoring, and can build a good implementation step.

F. Conversion of spectral values to land variation points and establishing a theme map

By changing the spectral values of other satellite images into the regression formula, a land variation map was obtained.

In this study, an automatic conversion module was built.Only after the satellite images and radiometric correction processwere completed could the automatic conversion mode be brought into the system and the land variation points generated.

Case Analysis of a Satellite Image

To grasp the practical applications and advantages of using the NDVI to interpret landscape changes in catchment areas, especially when using past remote sensing image data, intelligent interpretation of landscape variations in the catchment area in the upper reaches of the Xindian River was conducted, and the pre- and postimages were used together with the aforementioned processes to effectively identify landform and landscape changes. The case analysis is further explained as follows.

A. Study location

The upper reaches of the Xindian River catchment area were used as the study site (Fig. 1).

Fig. 1. Site map of the case study in the upper reaches of the Xindian River catchment area. (Red square area is selected as study area)

B. Satellite telemetry image data

The satellite telemetry images used were multispectral images from FORMOSAT-2, providing blue, green, and red visible light bands and near-infrared light bands. The image-to-ground resolution was 8 m. The preimage data were from November 13, 2015, and the postimage data were from April 19, 2016.

C. Interpretation of images using the NDVI

According to the selected pre- and postimage data, andafter image correction, each band of image data was converted to the NDVI (Fig. 2), where every pixel from dark to light represented its NDVI from small to large (ranging from −1 to 1). If the NDVI is greater than 0, it means that the land is covered with green. If the NDVI is less than 0, it means that the land is not covered with green.

D. Converting images into green and non-green coverage

The empirical formula was estimated by coefficient calculation, and the threshold of the NDVI for green and non-green covered land in the upper reaches of the Xindian River was determined as 0.05. The image was transformed into an image with a NDVI greater or less than the threshold (Fig. 3). The green parts indicate green coverage, and the dark gray parts indicate non-green coverage.

Fig. 2. NDVI in the upper reaches of the Xindian River catchment area.

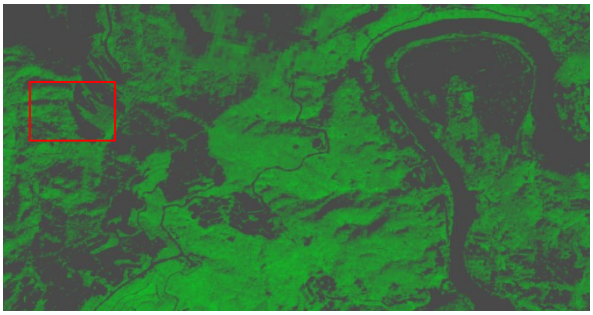

Fig. 3. Image conversion using the threshold.

E. Pre- and postimage interpretation and comparison

After image transformation, the pre- and postimages were compared using the algorithm to locate variation points in the landscape from original green coverage to non-green coverage, thereby establishing the variation areas (Figs. 4–7).

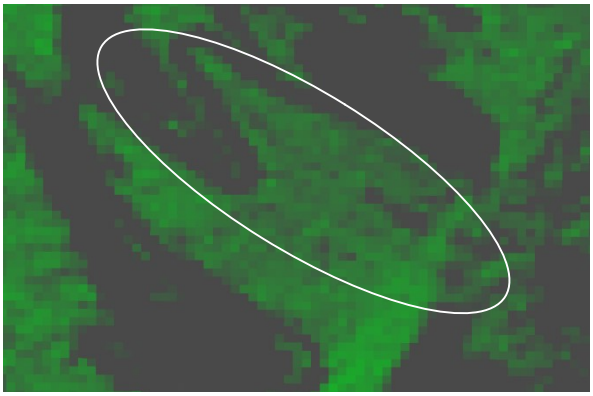

Fig. 4. Preimage green coverage in the variation area.

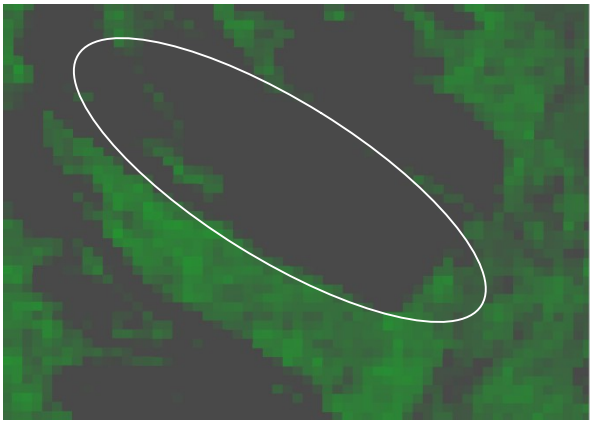

Fig. 5. Postimage non-green coverage in the variation area.

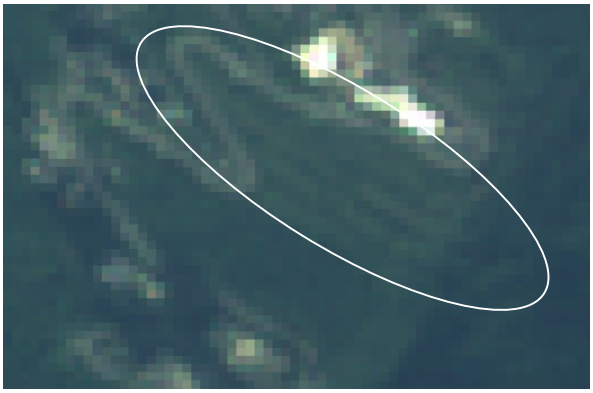

Fig. 6. Satellite preimage in the variation area.

Result and discussion

From Fig. 4, in the preimage, most water conservation areas in the catchment area were covered in green, but, from Fig. 5, green cover was reduced or even eliminated in the postimage dueto land development. The satellite imagery confirmed these findings. In Fig. 6 (the preimage), green cover is clearly visible, but the illegal use of land in the later stage leads to a decrease in green coverage, which can be viewed as surface soil in Fig. 7 (the postimage).

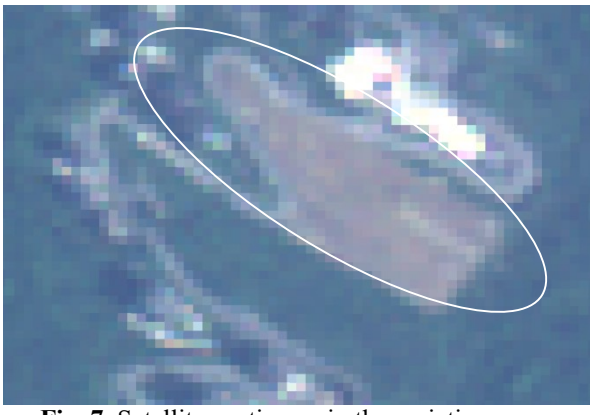

Fig. 7. Satellite postimage in the variation area.

According to the preliminary case analysis results, the NDVI can be effectively applied to interpretation of landform variation in a target catchment area. In addition to using satellite telemetry image data to calculate the NDVI of surface topography, multispectral cameras and lenses on unmanned aerial vehicles will be used in a follow-up experiment to take detailed photographs of the selected variation points for automatic interpretation. In addition to recording the variation points, multispectral images will also be recorded. Multispectral images can be used to calculate a more detailed NDVI for the site, which could enhance the reliability of the data and help in monitoring and tracking the degree of restoration in the region.

Previously, automatic interpretation technology often required manual intervention to help confirm interpretation results. Moreover, these technologies required more manpower to confirm landformvariation, which made them impractical for frequent use. Therefore, the introduction of artificial intelligenceto assist in land use interpretation will enhance the ability to search for variation points. Recent developments in computing power have led to the expansion of deep learning technology and application of neural networks, especially in terms of image recognition based on convolutional neural networks.

Conclusions

Application of satellite imagery to large-scale water conservation in catchment areas has become increasingly common, and it is now feasible to monitor and manage water resources using satellite remote sensing. By applying various analytical methods, the relationship between spectral data and land use can be established to evaluate abnormal land use in water resource conservation areas. This study established a monitoring process for the relationship between vegetation and satellite spectra. The satellite spectral values were converted to monitoring data according to the transformation relationship. With the calculated NDVI, the vegetation location can be determined. In this study, the threshold of the NDVI for green and non-green coverage was 0.05. This value was further used to automatically generate images with a NDVI greater or less than the threshold. The green parts of the image were vegetation areas and the dark gray parts were places where the landscape changed. Through image transformation, the algorithm automatically compared the pre- and postimages and selected the landscape variation points based on the change from the original green space to non-green space. The algorithm employed in this paper demonstrates that the NDVI can be used to judge the scale of landscape change. Patrol personnel may be unable to judge illegal use of catchment areas, and therefore, the use of hyperspectral remote sensing data to judge illegal development zones can further

protection and management of water resources. Intelligent image interpretation technology combined with image data acquisition and interpretation can help water resources protection and land use management in catchment areas by revealing illegal exploitation.

Acknowledgment

The authors are grateful to the WaterResourcesAgency of the Ministry of EconomicAffairs, Republic of China, for its financial support of this research under contract No. MOEAWRA1070426.

References

[1] Z. Liu,The land illegal found system based on remote sensing technology research and development, Master Dissertation, Chang'an University, Xi'an, China, 2013. (in Chinese)

[2] M. Govender, K. Chetty, and H. Bulcock, "A review of hyperspectral remote sensing and its application in vegetation and water resource studies," Water SA., vol. 33, No. 2, pp145–152, 2007.

[3] F. Nex, and F. Remondino, "UAV for 3D mapping applications: a review," Appl. Geomatics., vol. 6, No. 1, pp1–15, 2014.

[4] J. Rogan, J. Miller, D. Stow, J. Franklin, L. Levien and C. Fischer, "Land cover change mapping in California using classification trees with Landsat TM and ancillary data," Photogrammetric Engineering andRemote Sensing, vol. 69, No. 7, pp793–804, 2003.

[5] C.J. Tucker and M.W. Garratt, "Leaf optical system modelled as a stochastic process," Applied Optics, vol. 16, No. 3, pp 635-642, March 1977.

[6] B. Govaerts, N. Verhulst, The Normalized Difference Vegetation Index (NDVI) GreenSeekerTM Handheld Sensor: Toward the Integrated Evaluation of Crop Management. Part A: Concepts and Case Studies, CIMMYT: El Batan, Mexico, 2010.

[7] B.L. Ma, L.M. Dwyer, C. Costa, E.R. Cober and M.J. Morrison, "Early prediction of soybean yield from canopy reflectance measurements," Agron. J., vol. 93, pp 1227-1234, 2001.

[8] F.J. Adamsen, P.J. Pinter, E.M. Barnes, R.L. Lamorte, G.W. Wall, S.W. Leavitt and B.A. Kimball, "Measuring wheat senescence with a digital camera," Crop Sci., vol 39, pp 719-724, 1999.

[9] J.W. Rouse, R. H. Haas, J.A. Schell, D.W. Deering and J.C. Harlan, "Monitoring vegetation systems in the Great Plains with ERTS," NASA Spec Publ. 351 , pp 309-317, 1974.

[10] G.T. Yengoh, D. Dent, L. Olsson, A.E. Tengberg and C.J. Tucker, Use of the Normalized Difference Vegetation Index (NDVI) to Assess Land Degradation at Multiple Scales: Current Status, Future Trends, and Practical Considerations, Springer: New York, NY, USA, 2015, p. 100.

DTM GENERATION WITH UAV BASED PHOTOGRAMMETRIC POINT CLOUD IN LAMPHACHI RIVER

Kitipong Thongchua[1,a] and Wisuwat Taesombat[1,b]

Abstract This research aims to evaluate the efficiency of terrain digital terrain model (DTM) with aerial photo and photogrammetric point cloud. The study area is located at Lamphachi river in Kanchanaburi province of Thailand. The DJI PHANTOM 4 PRO flight was conducted with 559 aerial photographs at 120 m altitude. The ground control points were set at 8 points. Agisoft Photoscan software is used to create point cloud and CSF (Cloth Simulation Filtering) algorithms for point cloud modification.The parameters are CR (Cloth resolution), maximum iteration and classification threshold that the values were 1.0, 500 and 1.0 respectively. The results of this study were as follows: Root Mean Square Error (RMSE) was compared with 407 checkpoints, including in channel sandbars and river banks is 135 points, 119 points and 153 points respectively. The result of study found that RMSE of the channel sand bars and river embankment is 1.24 meters, 2.18 meters and 1.56 meters respectively. Outcomes of the study show that it is possible to use the UAV Photogrammetry data as map producing, surveying, and some other engineering applications with the advantages of low-cost, time conservation, and minimum field work

Keywords *UAV, Point cloud, DTM*

[1]Department of Irrigation Engineering
Kasetsart University Kamphaeng Saen Campus
Bangkok, Thailand

[a]kitipong_tc@yahoo.com
[b]fengwwt@ku.ac.th

Introduction

The Digital Terrain Model (DTM) is an important topographic product and essential demand for many applications. Traditional methods for creating DTM are very costly and time consuming because of land surveying. In time, Photogrammetry has become one of the major methods to generate DTM. Recently, airborne Light Detection and Ranging (LiDAR) system has become a powerful way to produce a DTM due to advantage of collecting three-dimensional information very effectively over a large area by means of precision and time (Polat and Uysal, 2015). However, the main disadvantage of aerial manned platforms such as airplanes is being expensive, especially for small study areas. During the last decades, low-cost Unmanned Aerial Vehicles (UAVs) are used to pass this handicap. Nowadays, the use of UAVs is increasing day by day due to its advantages at cost, inspection, surveillance, reconnaissance, and mapping (Remondino et.al., 2011).

DTMcan be described as a three – dimensionalrepresentation of a terrain surface consisting of X, Y, Z coordinates stored in digital form. It includes not only heights and elevations but other geographical elements and natural features such as rivers, ridge lines, etc. A DTM is effectively a DEM that has been augmented by elements such as breaklines and observationsother than the original data to correct for artifacts produced by using only the original data. With the increasing use of computers in engineering and the development of fast three-dimensional computer graphics the DTM is becoming a powerful tool for a great number of applications in the earth and the engineering sciences.

In this study the generation of DTM with UAV based photogrammetric point cloud and its accuracy analysis is presented.

Study area and data

A. Study area

The study area is 0.638 km^2.(Figure 1) The area adopted for this study is lower part of the Lamphachi river in Kanchanaburi province of Thailand. The terrain is flat, flooded and the river is bent. The riverbank area is covered with bamboo and is planted with sugarcane and vegetable crops.

Fig. 1. study area, lower part of Lamphachi river

B. Data

The methods concerning data acquisition comprised aerial photogrammetry and surveying techniques. In concrete terms aerial photogrammetry using a quadcopter UAV (DJI PHANTOM 4 PRO) flight was conducted with 559 aerial photographs. Flights altitude over terrain was 120 m above ground level.

For georeferencing purposes, we used ground control points (GCPs) measured with Real-Time Kinematic (RTK) (Figure 2 (a)) which used to find coordinates and elevation data for 8 ground control points (GCPs) (Figure 2(b)).

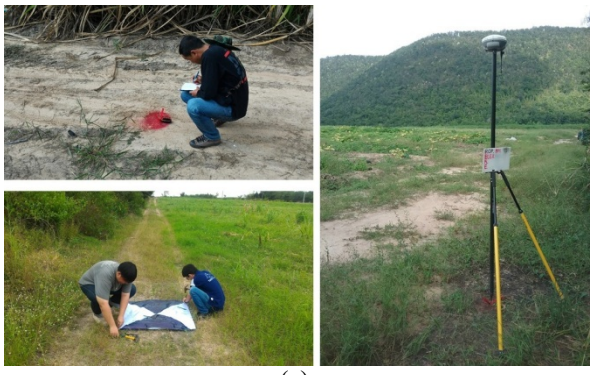

(a)

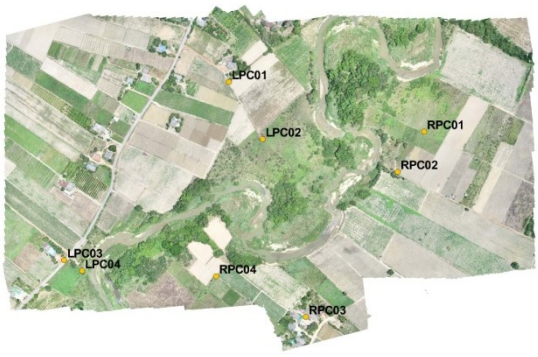

(b)

Fig. 2. Real-Time Kinematic (RTK) surveying (a), position of 8 ground control points (GCPs) (b)

Methodology

A. Image Processing

The image processing procedures involves photo alignment, create markers and point cloud generation. These processing were performed using the Agisoft PhotoScan software, which is a 3D scanner software based on digital photogrammetry, which uses photos from multiple digital cameras to rearrange. And then the image is a 2D map and then processed to create a 3D point cloud.The GCPs were used for georeferencing and adjust for mapping error.

The final result of processing get 11,666,340 for 3D point clouds and point density is 14.1189 points/m^2 (Figure 3)

Fig. 3. Image of 3D point clouds (11,666,340 points)

B. Cloth Simulation Filtering (CSF)

Separating point clouds into ground and non-ground measurements is an essential step to generate digital terrain models (DTM). Many filtering algorithms have been developed. However, even state-of-the-art filtering algorithms need to set upa number of complicated parameters.The cloth simulation filtering (CSF) algorithmimplementedto produce DTM from 3D point clouds (Zhang et al., 2016).The assumption of CSF algorithms that the cloth is soft enough to stick to the surface, the final shape of the cloth is the DSM (digital surface model). However, if the terrain is firstly turned upside down and the cloth is defined with rigidness, then the final shape of the cloth is the DTM (Figure 4).

The advance parameterthat has been used in this study for point cloud modification are 3 parameters:

- CR (Cloth resolution) refers to the grid size (the unit is same as the unit of point clouds) of cloth which is used to cover the terrain. The bigger cloth resolution you have set, the coarser DTM you will get.
- Max iterations refers to the maximum iteration times of terrain simulation. 500 is enough for most of scenes.
- Classification threshold refers to a threshold (the unit is same as the unit of point clouds) to classify the point clouds into ground and non-ground parts based on the distances between points and the simulated terrain. 0.5 is adapted to most of scenes

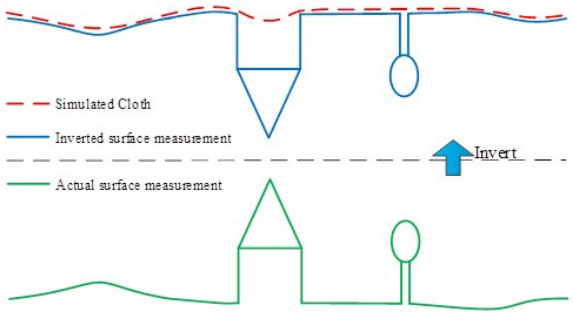

Fig. 4. Overview of the cloth simulation algorithm (Zhang et al. 2016)

The parameters are cloth resolution (CR), maximum iteration and classification threshold that the values were 1.0, 500 and 1.0 respectively. As the result, CSF algorithms can be separated 9,079,298 points as ground points (Figure 5(a)) and 2,586,986 points as non – ground points (Figure 5(b))

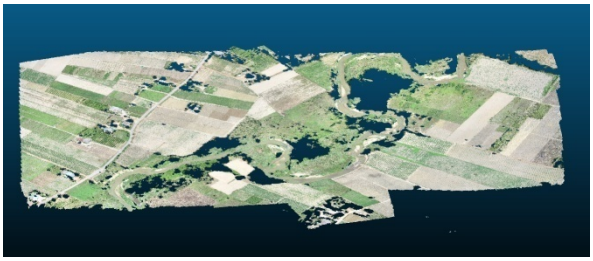

(a)

(b)

Fig. 5. 3D point cloud as ground points (a), 3D point cloud as non-ground points

Result and analysis

The obtained ground points are used to generate a 0.3 m resolution DTM. In order to get root mean square error (RMSE) of elevation data was compared with 407 checkpoints (Figure 6), including in channel sandbars and river banks is 135 points, 119 points and 153 points respectively. The equation of RMSE following equation (1)

$$RMSE = \sqrt{\frac{\sum(Elev_{DTM} - Elev_{checkpoints})^2}{N}} \quad (1)$$

Where $Elev_{DTM}$ is the elevation value from the generated DTM, and $Elev_{checkpoints}$ is the elevation value from check points .N is the number of check points.

The result of study found that RMSE of the channel sand bars and river embankment is 1.24 meters, 2.18 meters and 1.56 meters respectively.

Conclusions

This paper indicates the capability of UAVs, which is an alternative data collection technology, in a geomatic application in a small area by means of DTM generation with. Comparing with traditional manned airborne platforms, they reduce the working costs and minimize the danger of reaching to risky study sites, with sufficient accuracy. In fact, the UAVsystems have lots of advantages (low-cost, real time, high temporal and spatial resolution data, etc.) which are very important for not only geomatic but also various disciplines. The application indicates that the UAV combined digital camera systems can allow to collect usable data for geomatic applications. The study shows that UAV based data can be used for DTM generation by photogrammetric techniques with a vertical accuracy. It can be stated that the UAV Photogrammetry can be used in engineering applications with the advantages of low-cost, time conservation, minimum field work, and competence accuracy. Moreover the created 3D model is satisfactory to realize topography with texture. On the other hand, except GCP some parameters such as weather, vibrations, lens distortions, and software directly affects the process and model accuracy. Beyond all these, the UAVs system is not fully automated and still needs a user decision. Future studies may offer an automated approach for UAVs that minimizes the user attraction.

Fig. 6. DTM and the position of 407 check points

Acknowledgment

This study is supported by department of irrigation engineering at Kasetsart university Kamphaeng Saen campus.

References

[1] Polat, N., M. Uysal, 2015. Investigating performance of airborne lidar data filtering algorithms for DTM generation. Measurement,61–68.

[2] Remondino, F., Barazzetti, L., Nex, F .M . Scaioni, D .Sarazzi, 2011 .ISPRS ICWG I/V UAV-g Conference "UAV Photogrammetry for mapping and 3D modeling current status and future perspectives "Zurich, Switzerland.

[3] Zhang, W., Qi, J., Wan, P., Wang, H., Xie, D., Wang, X., and Yan, G. 2016. An easy-to-use airborne lidar data filtering method based on cloth simulation. Remote Sensing, 8(6).

Land use classification of small agricultural parcels using multiple synthetic aperture radar images

Takanori Nagano[1,a], Abudukeremu Ainalibanua[1], Yoichi Fujihara[2] and Natsuki Yoshikwa[3]

Abstract The aim of this research is to develop a robust and cost-effective methodology to monitor agricultural land use on a broad scale. Two different types of Synthetic Aperture Radar (SAR) images were compared to identify agricultural land use of small parcels in the middle and mountainous parts of Japan. Three study sites in Japan were chosen, with different geography and crop calendar. Main land use such as paddies, soybean fields and abandoned fields were assessed for their temporal backscattering coefficient (BC) change. It was relatively easier to identify paddies from other land use due to the sharp decrease in BC during the ponding period, typically between DOY (day of year) 130 and 170. Paddies and non-paddies were identified with Sentinel-1 single polarization VV data with a ground spatial resolution of 5×20 m down to parcels of 10-15 a when 5 images during the possible ponding periods were used for decision-tree classifications. Alos-2 spotlight mode 1 (single polarization HH) with a spatial resolution of 3×3 m exhibited a higher accuracy in the same identification, using only three images. Identification was possible down to parcels of 5-10 a. Ponding conditions however could not provide accurate enough identification for practical use. For soybean and abandoned fields, there was no clear signature to distinguish between the two since the state of the abandoned fields varied significantly.

Keywords *Remote sensing, SAR, Midori-net, abandoned field, paddy*

[1]Graduate School of Agricultural Science
Kobe University
Kobe, Japan
[2]Graduate School of Bioresources and Environmental Sciences
Ishikawa Prefectural University,
Kanazawa, Japan
[3]Faculty of Agriculture
Niigata University
Niigata, Japan

[a]naganot@ruby.kobe-u.ac.jp

Introduction

The agricultural land use in Japan is now facing a critical change. Aging of farmers and depopulation in rural areas are causing severe workforce shortage. The profit margin of rice is becoming marginal as the increasing import and declining domestic consumption dampen the market price. It is thought that the abandoned agricultural parcels amounting to 420,000 ha in 2015, would rise further in the coming years (MAFF, 2015 [1]). Under such circumstances, it is increasingly important to monitor the dynamics of agricultural land use frequently enough to prepare countermeasures. However in Japan, agricultural land use survey is carried out at national scale only once in every 5 years based on questionnaires (MAFF, 2015 [2]).

Countries like USA and Canada produce national crop maps every year using remote sensing (e.g. USDA, 2018 [3]). Typically, mid-resolution imageries like Landsat are used for such purposes. There are many technical and financial challenges to carry out similar missions in Japan. First Japanese agricultural parcels are small, typically less than 30 a (3,000 m2) which cannot be correctly captured with mid-resolution imageries. High-resolution images however are too costly to cover a large area. Second, the main agricultural season in Japan is March through to November with many cloudy and rainy days in summer due to monsoon. This limits the availability of cloud-free optical images. Third, signature detection of crops is difficult as the climate and crop calendar vary by region.

The purpose of this study is to develop a robust and cost-effective methodology for agricultural land use classifications on a broad scale in Japan. We focus on using mid-resolution satellite images which have recently been made available to the public for access. Synthetic aperture radar (SAR) images have proven effective in crop land detection in Japan because of regular data availability, unaffected by clouds. Takeuchi et al. (2000) [4] compared C-band and L-band SAR for crop land classifications including paddies and concluded that C-band SAR images have an advantage over L-band SAR which is often affected by Bragg Scattering. They also reported that paddy can be detected by detecting a decline of backscattering coefficient (BC) with ponding in paddies. Mukai et al. (2002) [5] proposed a combined use of SAR and optical images to increase signature for more accurate paddy detection. Takahashi et al.

(2003) [6] proposed use of parcel outline data for object-based classification. For ASTER data with a spatial resolution of 15 m, they reported an increase of accuracy by 9%. Land use identification at parcel scale was proposed by Suzuki et al. (2009) [7] with a combined use of high-resolution SAR imageries (COSMO-SkyMed) and parcel outline data. Osawa et al. (2010) [8] proposed use of time-series ASTER data and sequential classification for more accurate parcel land use detection. In 2011, parcel outline data became available on Midorinet, a union of land improvement districts in each prefecture of Japan [9].

We aim to classify three important land uses in a country that are rice, soybean and abandoned fields. We started the study in 2016 using time-series C-band SAR and regularly available and accessible Sentinel-1 images. Parcel outline data from Midorinet was used to raise accuracy of the classification. The classification had a fair accuracy for parcels larger than 16 a, but not for smaller parcels (Nagano et al., 2017) [10]. Therefore, in this study we used L-band SAR, Alos-2 in addition and compared accuracy.

Materials and methods

A. Study Area

Agricultural land use survey was carried out visually in September 2016, using aerial photos taken by a drone in two different locations. Sasayama city, Hyogo Prefecture (hereafter referred to as "Sasayama"), is situated on a plateau (altitude: 205 m). Farms are spread along rivers, sometimes reaching to the foot of mountains. Yoshikawa Land Improvement District in Joetsu, Niigata Prefecture (hereafter referred to as "Yoshikawa") is situated not far from the coast of the Sea of Japan. The district stretches from the coastal plain to the narrow valleys in mountains. In September 2017, Yabu city, Hyogo Prefecture, was added to the two study areas above (hereafter referred as "Yabu"). It is a mountainous region with small agricultural parcels situated along rivers, sometimes terraced on the hills. The main land use in Sasayama and Yoshikawa are rice soybean and abandoned fields. In Yabu, rice, abandoned fields and vegetable fields are three major land uses. There are many abandoned fields in Yabu because the parcel size is very small. The locations and characteristics of the three areas are shown in Figure 1 and Table 1.

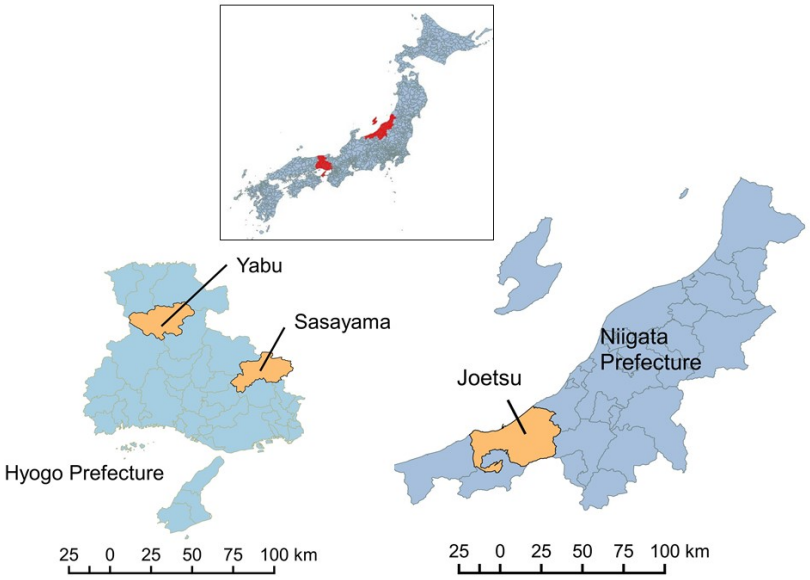

Fig. 1. Study Areas

Table I. Land uses and areas of agricultural parcels in 3 different study sites in Japan

		Sasyama		Yoshikawa		Yabu	
		Parcels	Percentage	Parcels	Percentage	Parcels	Percentage
Land use	Paddy	1,063	62%	1,916	67%	1,369	47%
	Soybean	409	24%	167	6%	5	0%
	Abandoned	123	7%	550	19%	1,012	35%
	Other	126	7%	223	8%	524	18%
	Total	**1,721**		**2,856**		**2,910**	
Area	0-5a	220	13%	442	15%	1,194	41%
	5-10a	293	17%	502	18%	719	25%
	10-15a	305	18%	431	15%	444	15%
	15-25a	457	27%	715	25%	353	12%
	25-80a	446	26%	766	27%	200	7%

B. Data

In this study, C-band SAR, Sentinel-1 images (European Space Agency) with a ground spatial resolution of 5×20 m (single polarization VV) and L-band SAR, Alos-2 (JAXA) images with a spatial resolution of 3×3 m (mode SM1, single polarization HH) were used for comparison. Sentinel-1 has a revisit time of 12 days (6 days since 2017 due to the constellation) and Alos-2 14 days. For Alos-2, observations are performed in various modes, therefore there is a much longer interval than 14 days in between image acquisitions in the same mode. Analysis

C. Analysis

For SAR images, raw images were preprocessed (geometrically corrected with Alos AW3D30 (JAXA) as the DEM and geocoded) using ENVI Sarscape (Harris Geospatial) Ver. 5.4. Refined Lee filtering was applied once before geocoding. Obtained images with backscattering coefficients (BC) were superimposed on the agricultural parcel vector data of each area, Midorinet, and the representative value of each parcel was obtained using ArcGIS (ESRI).

For classification, decision-tree library (rpart) of the statistical software (R) was used to determine threshold values of BC. Kappa coefficient (□) were calculated to evaluate the accuracy of classification.

$$\kappa = \frac{p_0 - P_e}{1 - P_e} \quad (1)$$

where p_o: the relative observed agreement among raters, p_e: the hypothetical probability of chance agreement, using the observed data to calculate the probabilities of each observer randomly seeing each category.

Results and discussions

A. Backward scattering coefficient signature of paddy

Figure 2 and 3 show temporal change of BC from Sasayama's paddies of different sizes detected by Sentinel-1 and Alos-2 in 2016. For Sentinel-1, BC takes value of -8 to -10 dB in the field raising period (around 100 cumulative days from January 1). When ponding initiated BC decreased by about 5 dB because of smoother surface of ponded water. The extent of this decrease differs according to the size of parcels. This is probably due to mixed land use occurring in pixels as target parcels get smaller. For Alos-2, a similar decrease in BC from ponding was observed. The difference due to parcel size also occurred despite of finer resolution of the imagery. For L-band, the radar wave reflected on water surface can scatter at different locations (e.g. ridges and surrounding forests) and contribute to backscatter. The sharp contrast in the ponding and non-ponding period was not observed in Yoshikawa in the early spring. L-band seems to be more sensitive to soil moisture and BC tends to be small even when paddy is not ponded.

B. Backward scattering coefficient signature of soybean

Figure 4 and 5 show temporal change of BC for soybean in Sasayama observed by Sentinel-1 and Alos-2 respectively in 2016. For Sentinel-1 BC dropped from DOY 100 to DOY 125 then increased toward DOY 200. Even on agricultural parcels of 5-10a, signatures similar to larger agricultural parcels were detected (Figure 5). With Alos-2, BC reached the lowest value at DOY 150 and then gradually increased to the maximum value obtained at around DOY 270 (Figure 6). The signatures of smaller parcels were relatively well captured. DOY 150 happens to be a transplanting period of seedlings and thus soil is tilled, furrowed and bare. DOY 270 is the harvesting period. L-band SAR seems to capture biomass increase on the ground. The difference caused by parcel size is attributed to loss of land-use-specific signature as parcel size gets smaller and occurrence of mixed cells increases.

C. Backward scattering coefficient signatures of abandoned fields

Figure 6 shows a comparison of BC from soybean and abandoned fields for Sasayama and Yoshikawa observed by Sentinel-1. BC of the abandoned field showed a similar signature to soybean, and there was no obvious signature to distinguish one from the other. The obvious difference between Sasayama and Yoshikawa was the low tendency of BC in the early spring in Yoshikawa due to snow coverage. For abandoned fields, the level of weed growth and management varies (some fields near households are mowed or tilled once a year whereas others are left untouched) thus it is difficult to distinguish abandoned fields from soy or other land usages with simple rules.

D. Appropriate period for paddy detection

From the results above, it seems reasonable to detect paddy fields first among different land use. Figure 7 shows a BC change of paddy fields at different sites detected by two different SAR images. Even among different sites, it is highly probable that paddy fields have ponded water between DOY 130 and DOY 170. Therefore, images available within this period are most eligible for accurate paddy detection.

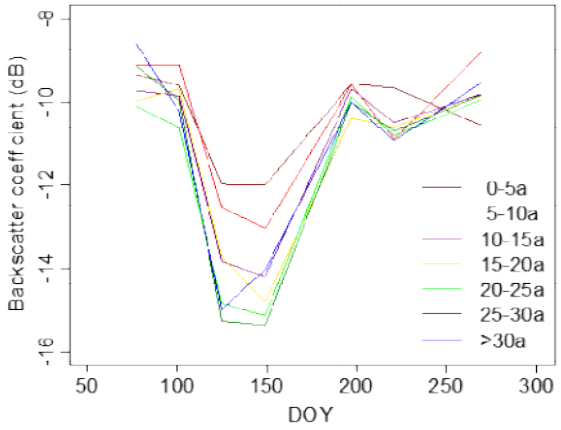

Fig. 2. Backscatter coefficients of paddy fields observed by Sentinel-1in Sasayama, 2016.

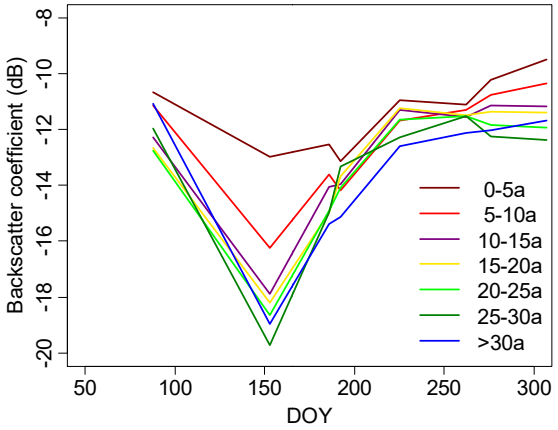

Fig. 3. Backscatter coefficients of paddy fields observed by Alos-2 in Sasayama, 2016.

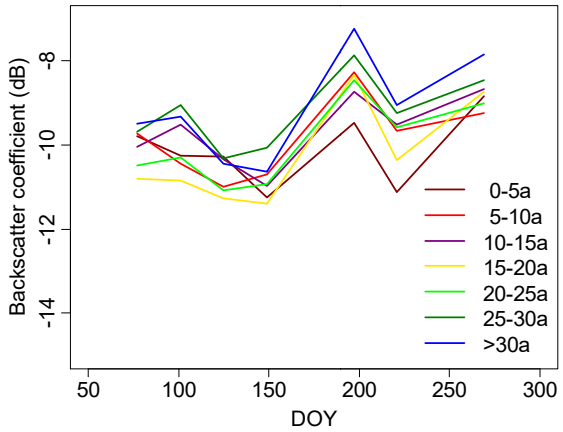

Fig. 4. Backscatter coefficients of soybean fields observed by Sentinel-1in Sasayama, 2016.

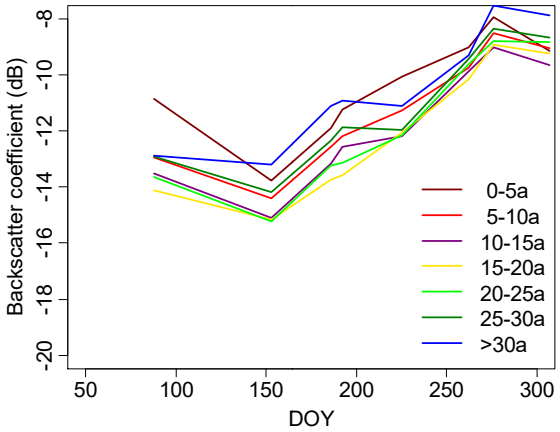

Fig. 5. Backscatter coefficients of soybean fields observed by Alos-2 in Sasayama, 2016.

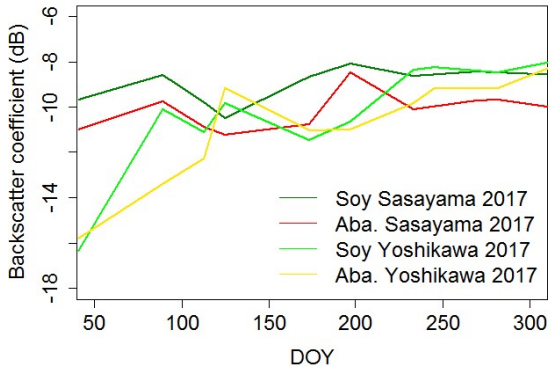

Fig. 6. Backscatter coefficients of soybean and abandoned fields observed by Sentinel-1 in Sasayama, 2016.

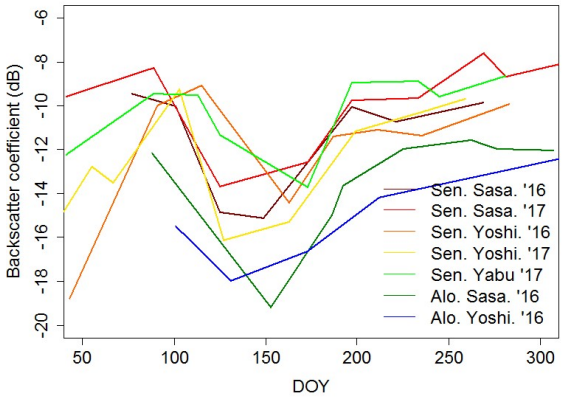

Fig. 7. Backscatter coefficients of soybean and abandoned fields observed by Sentinel-1 in Sasayama, 2016.

E. Accuracy of paddy detection

Figure 8 shows a comparison of reproducibility of paddy and non-paddy classifications. For Sentinel-1, 5 images from late April to late June with 12-day intervals were used. The decision-tree algorithm picked the best 3 thresholds which are statically significant from these dates. For Alos-2, images were much less available and 3 images available for each study site between late February and late June were all fed to decision-tree classification (For Yoshikawa classification was not possible due to availability of only two images). Table 2 shows the images used for classification at each site. Thresholds vary according to the grouping of parcel size, namely 0-5a, 5-10a, 10-15a, 15-25a and 25-80a. This means that they can be the best value for reducibility of classification of any single group. For 25-80a, both Sentinel-1 and Alos-2 offerκaround 0.8 which is considered excellent for classification. In this case, it was equivalent to a total accuracy of more than 0.9. For 15-25 a,$\kappa$is between 0.6 and 0.7 but for Yoshikawa with Sentinel-1. κislow in Yoshikawa as non-paddy fields accounted for only 4.6%of 715 parcels. Value of κ between 0.6 and 0.8 is considered good but not reliable enough for operational use. As parcel size gets smaller than 15 a, Alos-2 results in better classification although not all images capture ponding period. With Alos-2, parcels between 5 and 10 a are classified with κ close to 0.6. These higher accuracies are attributed to the finer resolution of the imagery. However, for fields between 0 and 5 a classification is no longer reliable even with Alos-2. Alos-2 is expected to exhibit better classification accuracy if more images are available between DOY 130 and DOY 170. For Sentinel-1 classification down to 15 a seems to be the limit in terms of reliability.

These results revealed that paddy detection solely relying on detection of ponding is effective but not accurate enough for operational use. This is reasonable since ponding could occur in non-paddy fields after heavy rainfall or due to water logging in the low-lying area and some paddies run dry due to erratic water management. Signature addition from BC later in the season or NDVI [5],[6] seems necessary.

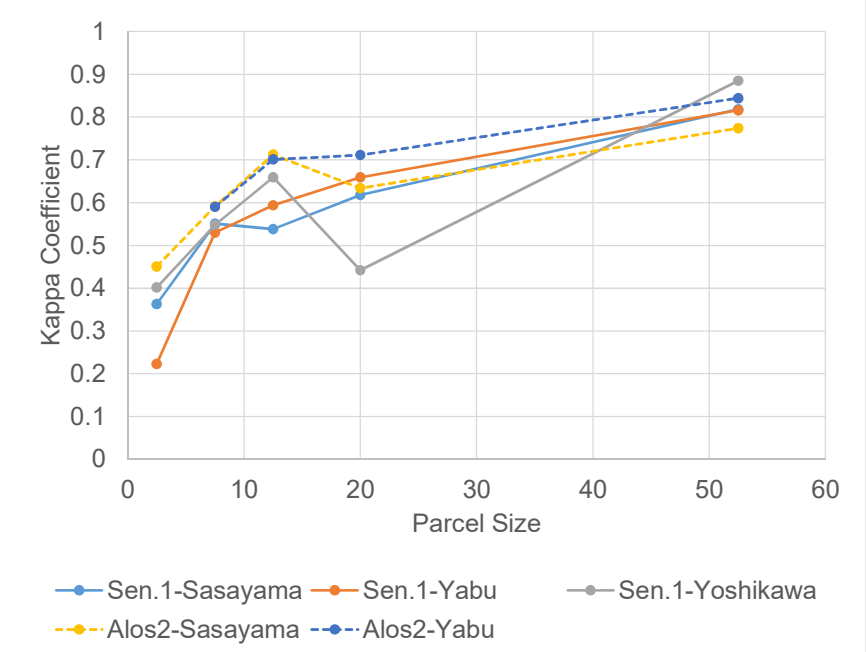

Fig. 8. Comparison of reproducibility of classification of paddy and non-paddy in 2017

Table II. Images used for paddy and non-paddy classification

Sensor	Site	Day of image acquisition in 2017	
Sentinel-1	Sasayama	May 5, May 17, May 29, June 10, June 22	
	Yabu	May 5, May 17, May 29, June 10, June 22	
	Yoshikawa	May 7, May 19, May 31, June 12, June 24	
Alos-2	Sasayama	March 13, May 17, June 19	
	Yabu	Feb 27, Apr. 24, June 5	
	Yoshikawa	Mar. 17, June 20 (only 2 data were available)	

Conclusions

Temporal images captured with C-band and L-band SAR were compared to identify rice, soybean and abandoned fields at parcel level. Sentinel-1 single polarization VV data with a ground spatial resolution of 5×20 m identified paddies and non-paddies down to parcel size of 15 a with Kappa coefficient of more than 0.6 when 5 images during the possible ponding period were used for decision-tree classifications. Alos-2 spotlight mode 1 (single polarization HH) with a spatial resolution of 3×3 m performed identification down to parcel size of 5a. For soybean and abandoned fields, there was no clear signature to distinguish between the two possibly because there was a large variation in the state of abandoned fields.

Acknowledgment

This research was carried out under Grant-in-Aid No. 16K 07942 and JAXA 1st Earth Observation Research Announcement (RA 1 R 701). Midori-net provided us parcel vector data.

References

[1] Ministry of Agriculture, Forestry and Fisheries, Kouhainouchi no genjou to taisaku ni tsuite (The state of devastated agricultural land and countermeasures), http://www.maff.go.jp/j/nousin/tikei/houkiti/pdf/2804_genjo.pdf, last viewed on Sep. 8, 2018, (2015).

[2] Ministry of Agriculture, Forestry and Fisheries, Census, http://www.maff.go.jp/e/data/stat/index.html, last viewed on Oct. 22, 2018, (2015).

[3] USDA National Agricultural Statistic Service, CropScape, https://nassgeodata.gmu.edu/CropScape/, last viewed on Aug. 29, 2018 (2018).

[4] Takeuchi S., Konishi T., Suga Y. and Oguro Y., Rice planted area estimation in early stage using Space-borne SAR data, Journal of the Japan Society of Photogrammetry, 39 (4), (2000), pp 25-30.

[5] Mukai Y., Rikimaru A., Takahashi K. and Sugawara, K., Estimation of rice acreage by satellite borne Synthetic Aperture Radar and optical sensor data, Technical report of the Technological University of Nagaoka, Vol. 24, (2002), pp 23-28.

[6] Takahashi K., Rikimaru A. and Mukai Y., Verification of high precise estimation method of the rice planted fields acreage with outline data reference using ASTER/VNIR Image, Journal of the Japan Society of Photogrammetry, Vol. 42, No. 4, (2003), pp 18-26.

[7] Suzuki K. and Shibata J., Detection of rice planted plots using COSMO-SkyMed imageries. Journal of the Japanese Agricultural Systems Society, Vol. 25, No. 4, (2009), pp 215-220.

[8] Osawa K., Kunii D. and Saito G., Classification of arable land using multi-temporal Terra/ASTER data. Journal of the Japanese Agricultural Systems Society, Vol. 26, No. 2, (2010), pp 67-77.

[9] Midorinet, National federation of Land Improvement districts, http://www.inakajin.or.jp/jigyou/tabid/185/Default.aspx, last viewed on 31 Aug. 2018, (2014).

[10] Nagano T., Asano T., Kotera A., Fujihara Y. and Yoshikawa, N., Plot-by-plot classification of agricultural land use by mid-resolution satellite imageries, proceedings of annual meeting of JSIDRE (2017).

Session D

Disaster Management/Groundwater Management

Guested Paper

Sustainable groundwater management in Anthropocene

Makoto Taniguchi*

Abstract

Global sustainability during the Anthropocene depends on the groundwater governance in Asia, this is not only because of large water footprints through global trade of agricultural/industrial materials, but also due to carbon emissions through human activities using groundwater in Asia. Challenges for the future of groundwater hydrology towards global sustainability are discussed from the viewpoints of system knowledge, target knowledge, and transformation knowledge. Regarding system knowledge, interactions between groundwater-food-energy nexus and environmental/economical impacts, and groundwater footprints with sustainability indices are essential as the center of information among nature, society and humanity. Back cast scenarios and future designs are important for target knowledge. Transformation knowledges are related to human behavioral changes and technological innovations. Natural and social tipping points, regime shifts, and resilience are keys for the future of hydrogeology and a sustainable society. Sustainable groundwater governance has cultural dependency because of differences in hydroclimate, hydrogeology, water management, and water culture in each area. Therefore, an interaction between humanity and nature is important for finding solutions towards sustainability for the current complicated and wicked global environmental problems.

*Research Institute for Humanity and Nature

Delivering Big Data and the Changing Landscape of Mobile andWeb-based Technologies to AddressGroundwater Security Challenges

Sachin Shah*

Abstract

Water security challenges require an understanding of how the primary drivers of groundwater stress—overuse and drought—affect the management of groundwater issues. Major progress has been made in the use of traditional water management tools such as remote sensing and groundwater modeling. In developing and middle-income countries, augmenting traditional water management tools with web-based applications for disseminating large data sets (big data) vital to solving water security challenges is essential. Compiling and disseminating big data by using digital solutions such as mobile and web applications provides water-resource managers with the tools they need to act swiftly and confidently when making water management decisions. For example, unprecedented economic expansion, land development, and climate variability in regions such as Southeast Asia have increased the frequency and intensity of urban and rural groundwater usage. Leveraging new technological solutions has helped the U.S. Geological Survey (USGS) to work with collaborators and stakeholders to track changing groundwater levels and management scenarios over time. In addition to addressing groundwater-level changes and simulating aquifer conditions , emerging technology helps areas that have under gone rapid environmental changes to address other issues such as land-subsidence, and changes in water quality. Tran boundary aquifers are inevitably linked to water-related conflicts, creating the need for faster access to water data for water use and regional allocation decisions. To help alleviate conflict, water-data infrastructure and governance serves as the backbone for efficient data delivery. To enable and sustain a high level of efficiency, rigorous data management processes can facilitate communication among agencies and NGOs to foster collaboration—a key to effective trans boundary water data sharing and delivery. As applications are modernized and new data are included, the public's understanding of groundwater hydrology and how the data benefit their daily lives can also grow. Open access to transparent data on mobile and web-based applications can increase the public's confidence in water management institutions, and data-driven decisions can drive investment in groundwater-resource solutions to meet challenging and continually changing groundwater issues.

*U.S. Geological Survey, Geospatial Science and Cyber Innovation Branch

ThamLuang Cave Systems in the view of Hydrogeology and related issues

Chaiporn Siripornpibul*

Abstract

ThamLuang Cave system in Chiang Rai Province, Thailand, is located in thevery thick carbonate rocks, mainly consists of limestone and some parts of marble, which created unique aquifers andaccommodating complex hydrogeological conditions in 3 different cave systems; dry caves,stream caves and phreatic caves in the same area. Besides, it is the 4th longest caves in Thailand with a total length of about 10.3 km.Rainfall pattern in this area is the main factor controlling changes of water levels in the main cave and causes flooding passages during the rainy season.Another factor is the complexity of the cave system, especially the variety of cave passages in term of dimensions and elevations.OnJune 23, 2018,the heavy rainfall caused flooding that trapped a soccer team of 12 boys and their coachinside the cave. To rescue the team, the author and staffs from the Department of Mineral Resources, together with the experts from the Royal Irrigation Department, Department of National Parks, Wildlife and Plant Conservation, Thai Royal Army and several hundreds of local peoplewerecollaborating to search for locations of stream sinks where water from streams flow into the upper part of the cave system. Also, they constructed small weirs to divert water from the northern and southern parts of the main cave. These actions ledsignificantwater-level decline, therefore the decision maker began the unbelievable rescue operation that successfully saved the football team out from the cave. ThamLuang cave area is the outstanding place and attractive for adventure tourismbecauseofitsastonishing karst features. In addition, there are pieces ofhydrogeological evidence that we can investigate and further studysuch as Karst Biodiversity, Paleontology, Paleo-climate, Carbon sink and Neo-tectonic.

*Department of Mineral Resources,
Ministry of Natural Resources and Environment, Thailand.
e-mail: alekchaiporn@gmail.com

GROUNDWATER PROTECTION IN LARGE CITIES

Vuong Bui Tran

Abstract

Currently there are 795 cities in Việtnam, of which, 2 cities (Hanoi and Ho Chi Minh City) are the special cities; 3 cities (Hai Phong, Da Nang and Hue) are Class I citiesdirectly under the central government;14 cities are Class I cities; 25 cities are Class II cities; 41 cities are Class III cities; 84 cities are class IV cities and 626 cities are Class V cities.

The volume of water used for the cities in Vietnam is from several hundred to thousand millions of m3 per year, of which, about 50% of water supply amount is from groundwater. The abstraction of groundwater has contributed significantly to the socio-economic development of the country, improving the quality of people life. However, groundwater abstraction and urbanization have created many adverse impacts to groundwater resources such as: depletion, increased pollution , salt water intrusion of groundwater resources and land surface subsidence.

Recognizing the importance of groundwater resources for socio-economic development in our country's cities now and for many years to come, the Prime Minister issued Decision No. 323 / QD-TTg dated 18/02/2013 approving the project "Groundwater protection in large cities". Following the decision of the Prime Minister, the Ministry of Natural Resources and Environment issued Decision No. 1557 / QD-BTNMT dated 30 August 2013 approving the content and budgetfor the groundwater protection project. Phase I will be implemented in 09 key cities: Ha Noi, Thai Nguyen, Hai Duong, Quy Nhon, Vung Tau, Buon Me Thuot, Ho Chi Minh City, Can Tho and My Tho.

The project wasimplemented by the National Center for Water Resources Planning and Investigation with the participation of the following organizations: Division of Water Resources Planning and Investigation for the North of Vietnam, Division of Water Resources Planning and Investigation for the Central of Vietnam; Divisiong of Water Resources Planning and Investigation for the South of Vietnam; Center for Quality and Protection of Water Resources; Water Resources Data Center; Center for Water Resources Technology and Department of Water Resources Management. The project was implemented from 2013 to 2017, basically completed in 2018.

The presentation will present the main results and several recommendation of and from the above-mentioned project.

ADAP-T for Water Disaster Risk Management and Sustainable Development

Taikan Oki[1], Kiatiwat Thanya[2], Hiroaki Shirakawa[3], Weerakaset Suanpaga[2], Taichi Tebakari[4], Sompratana Ritphring[2], Masashi Kiguchi[1], and Kyoko Matsumoto[1]

Abstract

The anthropogenic climate change is increasing water-related disaster risks such as flood and drought, in particular, because most of the adverse impacts of climate change is delivered to society through water. The global mean temperature has risen by more than 1.0 degree Celsius increase compared to pre-industrial era and it is predicted that it will likely reach 1.5 degree Celsius between 2030 and 2052 if it continues to increase at the current rate, according to the latest IPCC Special Report on the impacts of global warming of 1.5 degree Celsius. Mitigation efforts to reduce the greenhouse gas, e.g., CO2, emission and to reduce the speed of climate change is essentially important, and at the same time, adaptation measures to reduce the vulnerability and exposure of human lives and properties from risks exacerbated by climate change are also relevant.

After the Paris Agreement of UNFCCC in 2015, all the member states are encouraged to set their National Adaptation Plan, and a new research project entitled "Advancing co-design of integrated strategies with adaptation to climate change in Thailand (ADAP-T)" with international collaboration between Thailand and Japan was proposed, approved, and implemented since 2016, supported by JICA for Thai side and JST for Japanese side under the framework of SATREPS. ADAP-T has three piers of research, namely i) Knowledgebase of climate change, ii) Adaptation measures to climate change, and iii) Co-designing adaptation measures. Major sectors prone to climate change, such as riverine hydrology, forest hydrology, sediment erosion, coastal erosion, urban hydrology, and agricultural hydrology are considered in ADAP-T, and Kasetsart University, Thai Meteorological Department, Royal Irrigation Department, and ONEP (Office of Natural Resources and Environmental Policy and Planning) are managing the ADAP-T project in Thailand with close communication with The University of Tokyo and member researchers. Latest research achievements will be introduced in the THA2019.

[1]The University of Tokyo
[2]Kasetsart University
[3]Nagoya University
[4]Toyama Prefectural University

Flood Computations for Changing River Environment in Korea

KYUNG SOO JUN*

Abstract

The primary objective of the Four Major Rivers Restoration Project, the largest pan-national river project in Korean history in terms of its spatial coverage and budget, is to secure water in river channels. This is achieved by large-scale channel dredging and constructing a number of weirsin low flow channels. Among the four major rivers, the Nakdong River is the focus of the project. The weirs and estuary barrage in the Nakdong River are partially gated. The gates are to be opened when a flood occurs to prevent water level rise. On the other hand, the water level of the weirs and estuary barrage should not fall far below the normal pool level at the end of the flood because it is required to secure water in the low flow channel. Gate operation strategies for weirs and estuary barrage are needed to satisfy those two conflicting objectives, and appropriate simulation models are essential for developing them. A numerical model was developed that can simulate gate openings of estuary barrage and a series of weirs as well as the unsteady flow in the Nakdong River, Korea. The computational model can appropriately simulate composite flows at multi-functional weirs including weir overflow, orifice-type flow, and fluvial-type flow. Operation strategies for weirs were established such that gates are closed for water level below a certain reference level and gate openings increase as the water level rises. The prescribed operation conditions were well simulated by the model, and sensitivities to the parameters of the gate operation strategy were analyzed. The computational model developed herein has been utilized in establishing operational strategies during flood periods for a series of the weirs and the Nakdong Estuary Barrage.

Keywords *Flood computation, Gate operation, Unsteady river flow, Nakdong River*

*Graduate School of Water Resources, Sungkyunkwan University,
2066, Seobu-ro, Jangan-gu, Suwon, Republic of Korea

FUTURE DROUGHT RISK ASSESSMENT IN CHANGING CLIMATE USING HYDRO-METEOROLOGICAL AND SOCIO-ECONOMIC INDICATORS

Joo-Heon Lee*, Hyun-Pyo Hong, Seo-Yeon Park, Chanyang Sur

Abstract

Climate change is a major crisis facing the world and future generations, and the frequent occurrence of extreme weather phenomena can lead to changes in the stabilized hydrologic cycle. In addition, the extreme drought caused by climate change should be prepared not only for natural disasters but also for the level of catastrophic that have enormous socio-economic impacts. For sustainable management of water resources, it is very important to understand the frequency and severity of the extreme climate and the impacts and vulnerabilities of the climate damage to the economy.

In this study, 26 GCMs of CMIP5 based on the RCP scenario were evaluated for the extreme drought risk assessment considering future climate change (2011 ~ 2099). Through analyzing the annual average rainfall, the number of rainless days, the drought frequency, and the average drought severity, we selected the GCMs that predict the future drought most severely. In order to evaluate the historic drought using observed meteorological data, KMA(Korean Meteorological Administration) ASOS(automated synoptic observation system) data (1976 ~ 2005) were used to quantitatively assess past and future Korean drought to predict changes in drought risk.

In this study, Drought Hazard Index (DHI) was calculated for the future period (2012 ~ 2040, 2041 ~ 2070, 2071 ~ 2099) divided into three time windows based on RCP 4.5 and RCP 8.5 scenarios considering meteorological drought occurrence characteristics. For calculating the drought hazard index, the frequency of drought, average drought severity, and probable drought severity were used.

The Drought Vulnerability Index(DVI) was calculated using socioeconomic indicators including population, agricultural land area, and municipal, industrial, agricultural water use. The calculated indicators were transformed into dimensionless variables through the re-scaling method, which is a standardization method, and the DHI and the DVI were calculated by applying the weighting factors for each indicators with use of Analytic Hierarchy Process(AHP).

The Drought Risk Index(DRI) was calculated as the product of DHI and DVI. According to the results of this study, the risk of future extreme drought calculated through Hazard and Vulnerability changes in time and space in the future. Based on the results of this study, it will be possible to predict the future extreme drought risk and to develop customized drought countermeasures.

Keywords *drought risk, climate change, vulnerability, hazard*

*Joongbu University Gyeunggi-do, 10279, Republic of Korea
leejh@joongbu.ac.kr

Technical Paper

Relationship between groundwater, hydrology and water use in lower north region of Thailand

Tuantan Kitpaisalsakul[1,a] and Athit Laphimsing[2,b]

Abstract Groundwater is an alternative water resource in addition to the widely used surface water. If the groundwater is used excessively more than the groundwater safe yield, it will cause the groundwater to decline continuously and increase the cost of groundwater pumping. This study was carried out to investigate the status of groundwater in the lower north region of Thailand covering three provinces such as Sukhothai, Phitsanulok and Phichit, located in Yom and Nan river basins. The provinces are important agricultural areas of rice production and often pump the groundwater for conjunctive use along with the surface water. The study was done to determine the trend of groundwater and the relationships between the groundwater levels and the related factors such as the river water levels and the water uses in the areas. It is found that the trend of groundwater levels was to decline on the average of 0.69m./year in Sukhothai, 0.37m./year in Phitsanulok and 0.46m./year in Phichit, indicating the excessive groundwater uses. The groundwater levels were found to be closely related to the rainfall amounts and Yom and Nan river water levels, showing the role of recharging the groundwater. Also, the groundwater levels were related to the groundwater uses. The water demands, water uses and water resources within the three provinces were studied. The total average annual water demand was 3,765 million cum., dividing into Sukhothai as 30.9%, Phitsanulok as 43.1% and Phichit 26%. The water demand was classified according to the different uses such as the agriculture as 75.4%, the ecology as 17%, the consumption as 7% and the industry as 0.6%. The water resources to meet the water demands were obtained from the effective rainfall as 43.6%, the surface water resource as 42.7% and the groundwater resource as 13.7%.

Keywords *groundwater levels, Yom and Nan river water levels, groundwater uses*

[1]Department of Water Resources Engineering
Chulalongkorn University
Bangkok, Thailand
[2]Office of the National Water Resources
The Prime Minister's Office
Bangkok, Thailand

[a]tuantan.k@chula.ac.th
[b]athit@onwr.go.th

Introduction

Groundwater is a natural water resource in addition to the surface water such as surface runoff, reservoirs, ponds including rainfall. In general, the surface water is used as the primary water resource while the groundwater is used as a supplementary one.The lower north region of Thailand covering three provinces such as Sukhothai, Phitsanulok and Phichit, located in Yom and Nan river basins is the location of important agricultural areas of rice production. The water uses are supplied from both surface water and groundwater. The surface water depends on the runoff in Yom and Nan rivers. However, about the availability of large storage reservoir in the upstream of the two river basins, there is only one large reservoir, namely Sirikit reservoir, in the Nan river basin but none in the Yom river basin. This causes the limitation of surface water frequently in the dry seasons. Tuantanstudied and found that in the central plain basin covering the three provinces, the water deficit has occurred in the past (1979-2006) and expected to occur continuously in the near future(2015-2039) and far future(2075-2099) due to the excessive water demand and the impact of climate change [1]. Accordingly, there has been often the withdrawal of groundwater particularly for rice cropping requiring a large amount of water. The withdrawal of groundwater may exceed the potential or safe groundwater yield, causing the groundwaterto decline continuously for many years. From the study result by the Department of Groundwater Resources of Thailand [2], it was found that in the lower north region covering Sukhothai, Phitsanulok and Phichitprovinces during the recent decade, the groundwater levels decline continuously on the average of 0.10 – 0.25 m./year, causing the groundwater levels in the critical areas to be the depth of more than 8 m. below the ground surface and then affecting the cost of pumping groundwater. Also, Tuantan and Athit found the trend of groundwater level decline in Sukhothai [3] andPhitsanulok[4]. Therefore, this study was carried out to investigate the trend of groundwater levels, the relationship between the groundwater levels and Yom and Nan river levels and the groundwater uses. The study result can be utilized to find the appropriate mitigation measures to alleviate and solve the problem of the groundwater decline in the future.

Objectives

The objectives of this study are to determine

1) the statistics and trend of groundwater levels
2) the relationship between the groundwater levels and Yom and Nan river levels
3) the relationship between the groundwater levels and the groundwater uses

Study area

The study area is located in the lower north region of Thailand covering three provinces such as Sukhothai, Phitsanulok and Phichit, located in Yom and Nan river basins as shown in Fig. 1. Figure 1 also shows the location of groundwater observation wells and Yom and Nan rivers.

Methodology

1) The water uses were determined in four sections such as agriculture, ecology, industry and consumption.
2) The water resources were determined in three sources such as effective rainfall, surface water resource andgroundwater resource.
3) The data wereanalyzed in monthly time scale during the years 2007 - 2014.
4) The statistical analysis was applied to determine the average, drawdown, recovery and trend of the groundwater levels.
5) The graphs of plotting the related parameters were developed to determine the relationships.
6) The groundwater level data were obtained from the observation wells of the Department of Groundwater Resources [5].
7) The Yom and Nan river leveldata were obtained from the Royal Irrigation Department [6].
8) The rainfall data were obtained from the Meteorological Department [7].
9) The agricultural cropping area data were obtained from theDepartment of Agricultural Extension [8].
10) The industrial water use data were obtained from theHydro and Agro Informatics Institute [9].
11) The household water consumptiondata were obtained from the Provincial Waterworks Authority [10].

Result and discussion

A. *Statistic and trend of groundwater levels*

Fig.2 shows the time series of groundwater levels, Yom andNan river levelsin Phitsanulokprovince.The groundwater levels varied with time throughout each year, increasing in the rainy seasons and decreasing in the dry seasons. In addition, the groundwater levels varied according to the Yom and Nan river levels. Table 1 shows the summary of groundwater depthbelow the ground surfacein the year 2013, annual groundwater drawdown,annual groundwater recoveryand the rate of groundwater level decline in the observation wells in Sukhothai, Phitsanulok and Phichit provinces during the years 2007-2014. It is found that

a) The groundwater depth was maximum in Sukhothai as 18.27 m. while the groundwater depths inPhitsanulok and Phichitprovinceswere 9.90 m. and 12.17 m. respectively. This result indicates that Sukhothai encountered the most cost of pumping groundwater while Phitsanulokhad the most shallow groundwater depth due to gaining more water from the two rivers to supply surface water and recharge the groundwater.
b) The groundwater drawdown was due to groundwater withdrawal while the groundwater recovery was due to groundwater recharge. The annual groundwater drawdown and recovery depths were maximum in Phichit, indicating the most vulnerability of groundwater due to the limitation of groundwater storage.
c) The rate of groundwater level decline was maximum Sukhothai as 0.69m./year, indicating the groundwater use much exceeding the safe yield of groundwater storage.

B. *Relationship between the groundwater levels and Yom and Nan river levels*

Fig. 2 shows the variation of the monthly groundwater levels compared to Yom and Nan river levels in Phitsanulokprovince. It is found that the groundwater levelsvaried according to the Yom and Nan river levels in the dry and rainy seasons in each year. In addition, the groundwater levels were more affected by the Nan river levels thanthe Yom river levels due to the reason that the Nan river is larger and has more runoff thanthe Yom river.

C. *Relationship between the groundwater levels, groundwater drawdown, and groundwater uses*

1) Water demands

Table 2 shows the annual water demands for various water use sections in Sukhothai, Phitsanulok and Phichitprovinces. Also, the water demands were determined in term of proportions as the percentage of the total water demand in each province and each water use section. It is found that

a) The total average annual water demand was 3,765 million cum., dividing into Sukhothai as 30.9%, Phitsanulok as 43.1% and Phichit as 26%. The result shows that Phitsanulok had the most water demand, considerably more than those of Sukhothai and Phichit.

b) The water demand was classified according to the different sections of water uses such as the agriculture as 75.4%, the ecology as 17%, the consumption as 7% and the industry as 0.6%. The result shows that the agriculture was the section requiring the most water demand as much as 3/4 of the total water demand, significantly much more than those of the other sections as summed up as 1/4 of the total water demand.

2) Water resources

Fig.3 shows the time series of annual water uses from rainfall, surface water and groundwater in Phitsanulok province.It is found that

a) The water resources from the rainfall significantly affected the total water use in each year. The total water use varied according to the rainfall amount. The water use was large as occurred in the wet year 2011 and decreased as occurred in the dry year 2014.
b) The rainfall and the surface water were the major and fundamental water resources for the water uses and significantly much more than the groundwater.
c) The groundwater resource was used as the supplementary water to the rainfall and the surface water when the available surface water resource was insufficient.

3) Relationship between the groundwater level and groundwater use

Fig.2 shows the monthly groundwater levels whileFig.3 shows the annual groundwater uses in Phitsanulok province. It is found that the groundwater levelsvaried inversely with the groundwater uses such that the low groundwater levels occurred in the same years as the large groundwater uses. As occurred in the dry year 2013, the large groundwater use lowered the groundwater level significantly. Oppositely, as occurred in the wet year 2011, much less groundwater use little lowered the groundwater level. This result shows that the groundwater use affected the groundwater level.

4) Relationship between the groundwater drawdown and groundwater use

Fig.2 shows the monthly groundwater drawdown depths while Fig.3 shows the annual groundwater uses in Phitsanulok province. The groundwater drawdown depth is defined as the lowering depth of the groundwater level from maximum level to minimum level in each year cycle before changing to recover or increase. It is found that the groundwater drawdown depths varied along with the groundwater uses such that the more groundwater use, the more groundwater drawdown.The large groundwater drawdown depths occurred in the same years as the large groundwater uses, as occurred in the dry year 2013.Oppositely, as occurred in the wet year 2011, little groundwater use caused little groundwater drawdown. This result shows that the groundwater use affected the groundwater drawdown.

Conclusions

a) The groundwater levels in the three provinces had trends to decline continuously, causing the increase of depths of groundwater levels in the wells and the cost of pumping the groundwater for use.
b) The groundwater levels varied according to the Yom and Nan river levels.
c) The total average annual water demand was 3,765 million cum., dividing into Sukhothai as 30.9%, Phitsanulok as 43.1% and Phichit 26%. The water demand was classified according to the different uses such as the agriculture as 75.4%, the ecology as 17%, the consumption as 7% and the industry as 0.6%.
d) The water resources to meet the water demands were obtained from the different sources such as the effective rainfall as 43.6%, the surface water resource as 42.7% and the groundwater resource as 13.7%.
e) The groundwater levels varied inversely with the groundwater uses. The large groundwater uses caused the groundwater levels to decline. The continuous decline of groundwater levels indicated that the groundwater uses in the past exceeded the potential or safe yield of the groundwater resources in the areas.

References

[1] Tuantan Kitpaisalsakul, Sucharit Koontanakulvong and Winai Chaowiwat, "Impact of climate change on reservoir operation in Central Plain Basin of Thailand", Journal of Thai Interdisciplinary Research. Vol.11 No.2 March - April 2016.
[2] Department of Groundwater Resources, "Pilot Study and Experiment on Managed Aquifer Recharge Using Ponding System in the Lower North Region River Basin", Department of Groundwater Resources, Ministry of Natural Resources & Environment, 2011.
[3] Tuantan Kitpaisalsakul and Athit Laphimsing, "Relationship between groundwater, hydrology and water use in Sukhothai Province", Journal of Thai Interdisciplinary Research. Vol.10 No.2 September – October 2015.
[4] Athit Laphimsing and Tuantan Kitpaisalsakul, " Relationship between groundwater, hydrology and water use in Phitsanulok Province", Proceedings of the

Conference of the 21st National Convention on Civil Engineering, Songkhla, Thailand, 28-30 June 2016.
[5] Department of Groundwater Resources, Groundwater well data. Ministry of Natural Resources and Environment, Thailand, 2014.
[6] Royal Irrigation Department, Yom and Nan river level data. Ministry of Agriculture and Cooperatives, Thailand, 2014.
[7] Meteorological Department, Monthly rainfall data. Ministry of Information and Communication Technology, Thailand, 2014.
[8] Department of Agricultural Extension, Agricultural cropping area data. Ministry of Agriculture and Cooperatives, Thailand, 2014.
[9] Hydro and Agro Informatics Institute, Industrial water use data. Ministry of Science and Technology, Thailand, 2014.
[10] Provincial Waterworks Authority, Provincial waterworks data. Ministry of Interior, Thailand, 2014.

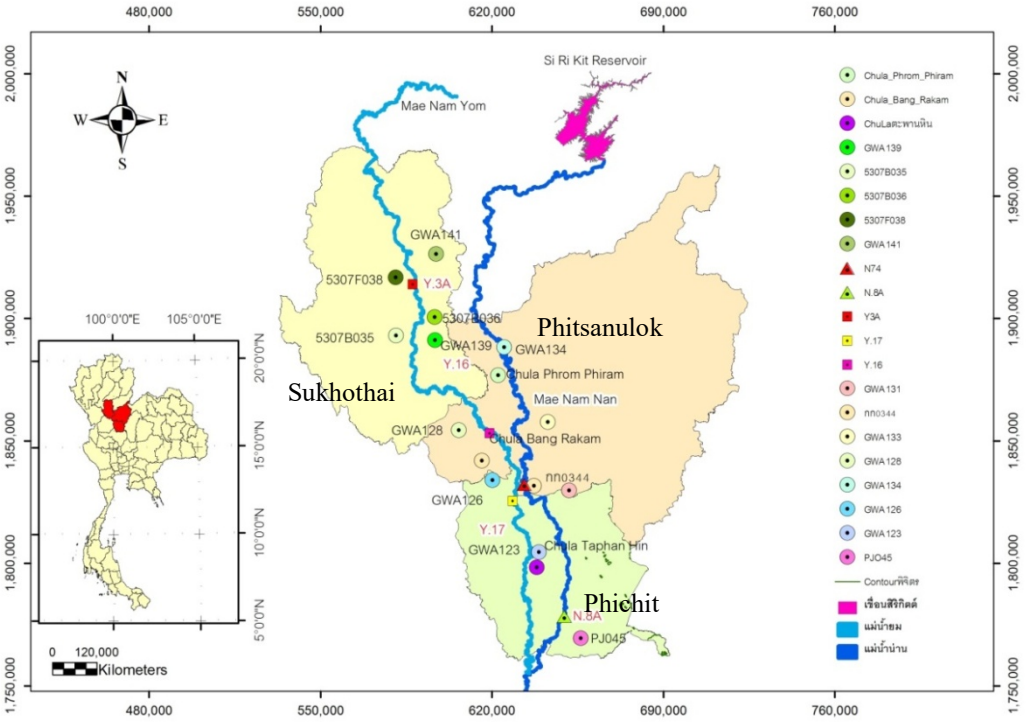

Fig 1. Map of three provinces, two rivers and groundwater observation wells

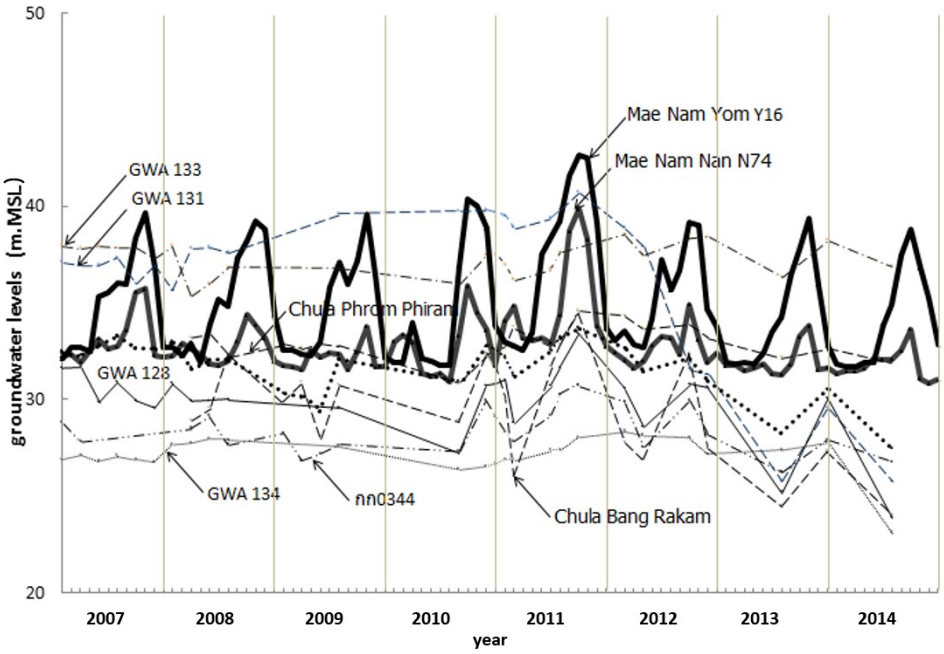

Fig. 2. Time series of groundwater levels and river water levels in Phitsanulok province

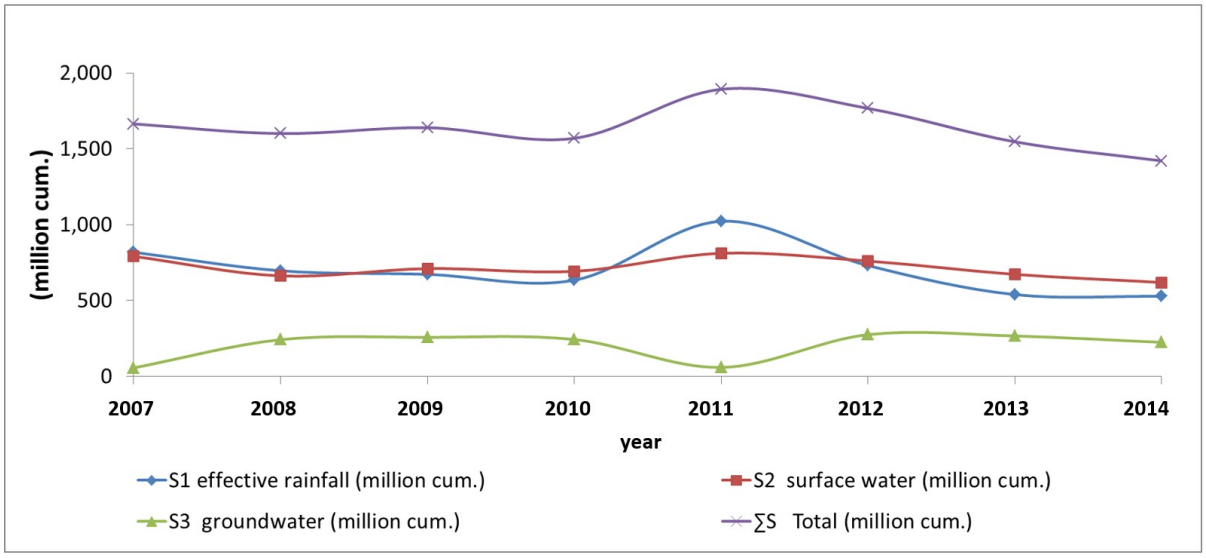

Fig. 3. Time series of water uses from rainfall, surface water and groundwater in Phitsanulok province

Table I. Groundwater depth, drawdown depth, recovery depth, rate of groundwater level decline

No	item	Sukhothai	Phitsanulok	Phichit
1	groundwater depth below ground surface in year 2013(m)	18.27	9.90	12.17
2	annual groundwater drawdown(m/year)	2.95	2.64	3.37
3	annual groundwater recovery(m/year)	2.14	1.77	3.06
4	rate of groundwater leveldecline (m/year)	-0.69	-0.37	-0.46

Table II. Annual water demands for water use sections in Sukhothai, Phitsanulok and Phichit

Section Province	agriculture (million cum.)	ecology (million cum.)	consumption (million cum.)	industry (million cum.)	Total (million cum.)
Sukhothai	869	198	85	11	1,163
Phitsanulok	1224	276	114	8	1,622
Phichit	743	167	66	4	980
Total	2836	641	265	23	3765
proportion(%)	75.4	17	7	0.6	100

Table III. Annual water uses from rainfall, surface water and groundwater

Water source Province	effective rainfall (million cum.)	surface water (million cum.)	groundwater (million cum.)	Total (million cum.)	proportion(%)
Sukhothai	507	482	174	1,163	30.9
Phitsanulok	704	715	203	1,622	43.1
Phichit	430	412	138	980	26
Total	1641	1609	515	3765	100
proportion(%)	43.6	42.7	13.7	100	

EFFECTIVENESS OF THE LEVEE AGAINST FLOODING AT DIFFERENT RAINFALL RETURN PERIODS IN MANDULOG RIVER, ILIGAN CITY, PHILIPPINES

Alan E. Milano[1,a], Sheila N. Frias[1,b], Peter D. Suson[1,c] and Daniel S. Mostrales[1,d]

Abstract The Mandulog river levee located in Hinaplanon, Iligan City, Philippines is one of the engineering mitigating measures undertaken by the national government in order to prevent another devastating flood, like the one brought by TS Washi (locally known as Typhoon Sendong) that badly hit Iligan City and Cagayan de Oro City in December, 2011 resulting to thousands of death toll. The study determines the effectiveness of the levee against possible flood overtopping using a 50-year and 100-year rainfall return periods. Hydrologic simulation and 2D flood modelling were done using HEC-HMS 4.1 and HEC-RAS 5.0.3. The LiDAR dataset and bathymetric river survey in 2012 was used in river and floodplain geometric data generation. Results of the 2D flood model shows that the levee can prevent river flooding for the two rainfall scenarios. However, it blocks the runoff from the land side outside the levee, thereby causing flooding in densely populated areas. It is imperative to provide a device that will overcome the blockage. Otherwise it nullifies the usefulness of the levee, squander substantial resources and above all put to risk densely populated communities.

Keywords *levee, rainfall return period, flooding*

[1]MSU-IliganInstitute of Technology,
GeoSAFER Mindanao Project,
Tibanga, Iligan City, Lanao del Norte, Philippines, 9200

[a]aemilano1960@yahoo.com
[b]frias.sheila123@gmail.com
[c]peter.suson@g.msuiit.edu.ph
[d]dsmostrales@gmail.com

Introduction

The plan to construct a flood control structure in particular a flood levee along the banks of the Mandulog River was a source of great joy and relief among the inhabitants of Iligan City as it was in that basin where the Mandulog River flows through that were worst hit during the tropical storm Washi (Sendong) December 17, 2011 where a substantial number of people died, perished, injured and displaced and a vast amount of properties and infrastructure were either lost or damaged[1].

However to these authors, the euphoric response led to a sobering concern during the public hearing of the flood levee project where it was revealed that tributaries that drain to the Mandulog River will be blocked by the levee[2] (Figure 1).

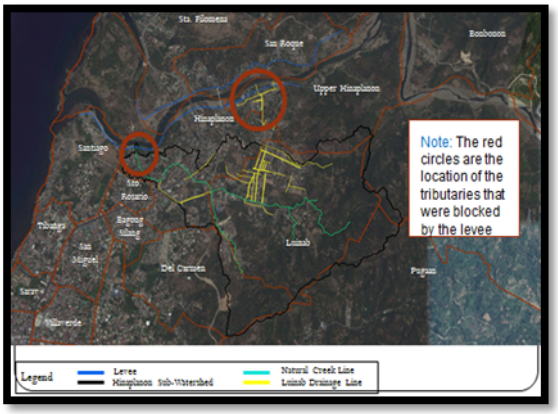

Fig. 1. Blocked Tributaries

Based from the original plan of the government construction agency, no pump is provided to drain water from the tributaries to hurdle the levee but rather only a sluice gate is provided. However, the sluice gate will open only if the depth of the main river is lower than the depth of the tributary that drains to it[3]. But in a storm event, it is most likely that the depth of the main river is higher than the depth of the tributary that drains to it. So when such event occurs, it is expected that drained water from the tributary will be blocked, accumulate and thereby rise up causing

flooding. The risk for flooding disaster is high as the affected area is densely populated.

So for decision makers to see the authors' grave foreboding and to act upon it, the authors have embarked on this study to simulate the scenario where drained water from the tributary is blocked by the flood levee and the resulting flood magnitude. Furthermore this study will also assess the effectiveness of the flood levee to control flooding that emanates from the river.

Methodology

A. Levee Condition, Cross Section and the Flood Model

Currently, both the left and right bank levees are not fully completed. For simulation purposes, the levee was assumed to be fully completed in the model. Annex1 shows the GIS representation of the levee alignment with respect to its centreline. It is composed of the right and left bank levees referenced facing downstream. The plans acquired only showed the levees in green and blue lines. The levee in red line was already constructed before the study was made. Hence, it was included in the simulation using the elevation of the downstream portion of the left levee in blue line. The culverts along the levee were not considered in this study. The hydraulic model uses the LiDAR DEM integrated with levee. The roadway width of 6.7 m and additional 2 m on both sides for the shoulder were raised along its alignment with reference to the elevations. Annexes 2 and 3 shows the typical cross-section of the levee, its crown is designed to be a roadway.

The boundary conditions used were the inflows identified in the hydrologic model with respect to the defined floodplain area. Another boundary conditions used were the storage area represented by the floodplain and the portion of theMandulog River from the upstream todownstream of the study area. The tidal data is part of the limitation. Hence, there was no tidal condition set for the model.

B. Flood Modelling

The flood magnitude which is in terms of flood extent and flood depth was compared between the presence of the levee (with levee) and the absence of the levee (without levee) at two rainfall scenarios (50 and 100 year rainfall return period). To do it; a flood simulation study was conducted using the softwares: HEC-HMS 4.1,HEC-RAS 5.03 and ArcMap 10.2 and GIS datasets such as raster files (IFSAR-DEM and LiDAR-DTM) and shape files (watershed, flood plain and levee polyline).

The flood magnitude which is in terms of flood extent and flood depth was compared between the presence of the levee (with levee) and the absence of the levee (without levee) at two rainfall scenarios (50 and 100 year rainfall return period). To do it; a flood simulation study was conducted using the softwares: HEC-HMS 4.1,HEC-RAS 5.03 and ArcMap 10.2 and GIS datasets such as raster files (IFSAR-DEM and LiDAR-DTM) and shape files (watershed, flood plain and levee polyline).

To determine the flood depth, there are four (4) major steps involve. First determine the run-off in terms of peak run-off, total run-off volume and lag time using the HEC-HMS 4.1, IFSAR-DEM. For the second step, a geometric data was prepared where the flood plain and flood extent in cross section intervals were defined/ The output of the first and second step becomes the input of the third step which is the generation of the flood depth raster file. The third step makes use of the HEC-RAS 5.03, LiDAR-DTM and flood plain). The fourth and the last step was to define and convert the flood depth raster file into a shape file. This makes use of ArcMap 10.2. This is done by reclassifying the flood depth raster file into three new classes or values with corresponding values of 0.5, 1.5 and the next highest value with respect to the highest value of the raster. After reclassification, the reclassified flood depth raster file is converted into shape file. This procedure is true for the condition where there is no flood levee.

However for the condition where there is flood levee, the preparation of a geometric data is more tedious. As this involve the integration of the newly generated Levee DTM with the LiDAR-DTM and to mark it as the Levee- LiDAR-DTM to distinguish it from the natural terrain. This process interchangeably uses ArcMap 10.2 and HEC-RAS 5.03 softwares and the GIS dataset: LiDAR-DTM and the levee polyline shape file. Once the process in preparing geometric data is finished, the step in generating a flood depth raster file now proceeds.

Finally for the flood extent, the flood depth result in shape file is used as an input using ArcMap 10.2. In the attribute table of the flood depth, another field was added naming that field as Area. The area was computed using Hectares as the unit for area. This will populate the Area attribute of the corresponding flood extent polygon for the selected rainfall scenario and according to flood depth classification which is low (≤ 0.5 m), medium (0.5 – 1.50 m) and high (> 1.5 m).

Results and discussion

A. Flooding with and without levee

The simulation results show that when the water from the tributary cannot drain to the Main or the Mandulog River due to levee blockage then there is flooding and that the depth and extent has very narrow differences at both rainfall scenarios (Figures 2 and 3). Furthermore at high flood depth under the 100

year rainfall return period (RRP) the extent of flooding is higher when there is levee (Figure 4).

In the absence of a device that guarantees drainage of tributary waters to the main river, the presence of a levee might even make flood disaster more risky compared in the absence of a levee that is because the location where the tributary water is blocked is located in a highly densely populated areas (Figure 1). Also because the extent of flooding is higher when there is levee at high flood depth level at 100 year rainfall return period (Figure 4).

During the public hearing discussion, the provision for a pump to drain water from the tributary was mentioned by one among the participants, however the agency responsible for the project mentioned that in a storm event an electrically powered pump will be useless due to brownouts. But another participant said why not a fuel fed pump. The same agency countered that the person responsible to start the pump might be the first to flee. Such concern can be resolved by using sensors to automate the pump to start and to use renewablesource of energy as additional power source to run the pump.

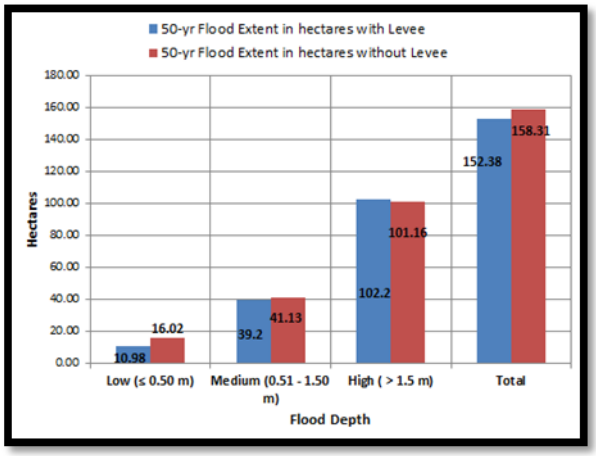

Fig. 2. Flood extent at 50 year Rainfall Return Period

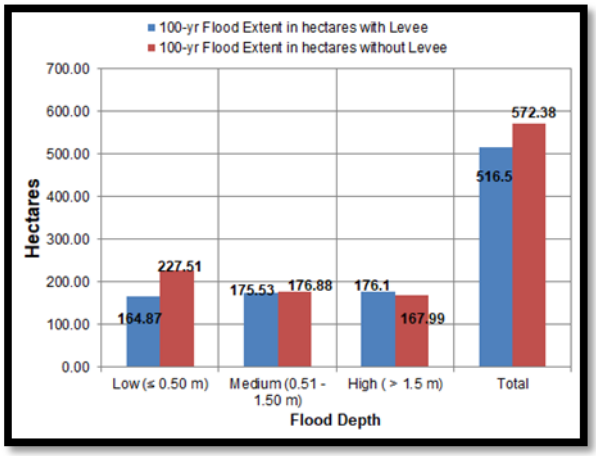

Fig. 3. Flood extent at 100 year RRP

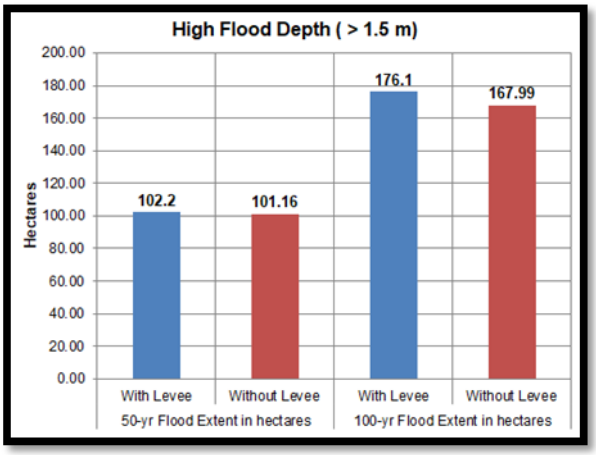

Fig. 4. High Flood Depth at 50 year and 100 yearRainfall Return Period

B. Flooding emanating from the Main River

The flood levee is very effective in controlling river flooding in both 50 year and 100 year rainfall return period (Table 1 and Figure 5). For 50 year RRP there's still remaining clearance of 3.582 m and 3.182 m for 100 year RRP. However its effectiveness is nullified by flooding from the landward side due to the blockage of tributary water to drain into the main river.

Table I. Levee height and water surface elevation for 50 year and 100 year Rainfall Return Period

	(m)				
Average Levee Height at Right Bank facing downstream	8.084	Average Maximum Water Surface Elevation for 50-yr RRP	Difference (m)	Average Maximum Water Surface Elevation for 100-yr RRP (m)	Difference (m)
Average Levee Height at Left Bank facing downstream	9.420				
Average	8.752	5.17	3.582	5.57	3.182

Note: Left and right bank levee naming convention is referenced facing downstream.

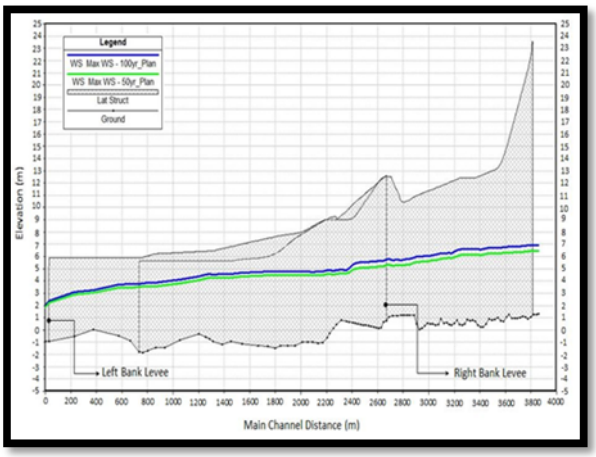

Fig. 5. Levee height and water surface elevation

Conclusions and recommendation

The effectiveness of the flood levee is nullified by flooding from the landward side due to tributary blockage. It is imperative that a device should be provided to guarantee drainage of water from the tributary to the main river. That device could be a form of a pump[3] powered by renewable energy and programmed to pump once tributary blockage commenced or the construction of retention ponds[4]. In the absence of any device to drain water from the tributary will render the flood levee project as a waste of substantial resources and put to risk a large portion of Iligan residents to flood especially in an age when extreme weather conditions is becoming a norm.

Acknowledgement

We are very grateful for the research funding and support given to us by DOST–PCIEERD; to UP–Diliman LiDAR Team, GeoSAFER Program, MSU–Iligan Institute of Technology, NAMRIA, and DPWH, Region 10, Philippines for making this study a success.

References

[1] Iligan City Disaster Risk Reduction Management Council. (2013). Final Report on Typhoon Sendong (Washi). Iligan City, Philippines.
[2] Milano, Alan E., Suson, Peter D. and Frias, Sheila. (2016). Revisiting the Disaster brought by Tropical Storm (TS) Washi in Iligan City: the case of the Mandulog River, Causes, Current Major Mitigation Measure, Evaluation and Recommendations. Unpublished
[3] A.V. Shivapur M.ISH & M.N. Shesha Prakash F. ISH. (2005). Inclined Sluice Gate for Flow Measurement. ISH Journal of Hydraulic Engineering. Volume 11, 2005. Issue 1.
[4] Machajski, Jerzy and Kostecki, Stanislaw. (2018). Hydrological Analysis of a Dyke Pumping Station for the Purpose of Improving Its Functioning Conditions. Water 2018,10.737;doi:10.3390/w10060737
[5] Yping Guo, (2001). Hydrologic Design of Urban Flood Control Detention Pond. Journal of Hydrologic Engineering. December 2001.

ANNEXES

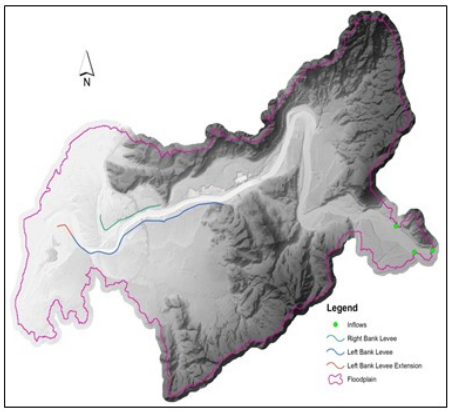

Annex 1

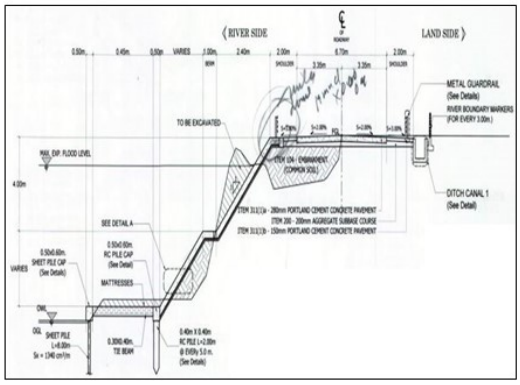

Annex 2

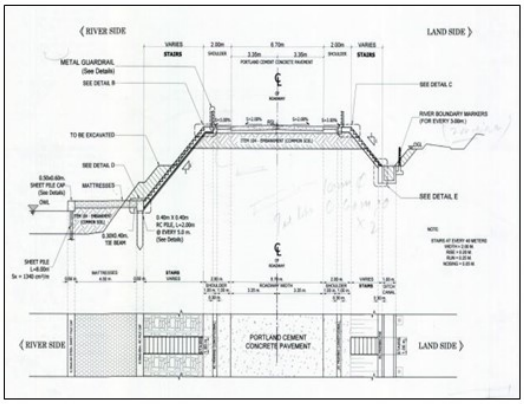

Annex 3

Comparison of Two Land Cover Scenarios and its Effect on the Runoff and Flooding inside the Mandulog River Basin, Philippines

Alan E. Milano, Peter D. Suson, Stephanie Mae B. Salcedo and Jennifer G. Blasco

Abstract This study aims to determine the effect on runoff and flooding when no proper land use management is done and another is when sound land use management is adopted. Hence, two (2) land cover/use scenarios were created. The first is the Projected Land Cover, where land cover was projected 10 years after the latest available landcover dataset. The second is the Proposed Land Use wherein it makes use of slope, elevation and distance from the river as the basis in assigning the different land uses. Hydrologic and hydraulic modelling was done at different rainfall conditions. The Projected Land Cover has a higher total runoff volume, peak flow and shorter Lag time as compared to the Proposed Land Use in four (4) Rainfall scenarios.The results also shows that the effect on flooding by Projected Land Cover shows more areas have been flooded with more areas inundated with higher flood depth level as compared to the Proposed Land Use in the same rainfall scenarios. The study shows when land cover conditions are left by itself without any intervention to stop land conversion, flooding is more likely to be magnified. The study also shows that flood can be mitigated if the Proposed Land Use scenario will be adopted.

Keywords *flooding, runoff, land cover, land use*

Introduction

The Mandulog River Basin is located in Northern Mindanao, Philippines with coordinates at 8°00'N to 8°20'N Latitude and 124°15' E to 124°35'E Longitude. The downstream of the basin is Iligan City; a highly urbanized city. In December 17, 2011 Tropical Storm Washi struck the city. An updated assessment shows that 1,278 died, 28,730 families displaced, 35 out of the 44 villages were affected and initial structural damage assessment was about USD 81.4 Million[1]. It is because of that fateful event that there has been an interest in studying the flooding behavior of the watersheds traversing Iligan City .

This study aims to determine what happens to runoff and flooding after some given time in the absence of any intervening land use management wherein deforestation is on-going and compare it when sound land use management is adopted. In that light, two (2) scenarios were created. One is the Land Cover projected 10 years from the available 2010 land cover dataset which is termed here as the 2020 Projected Land Cover and the other scenario is the Proposed Land Use, where it matches land uses with the slope.The ultimate goal of this simulation study is to provide information and persuade the local planning and decision making bodies to seriously adopt and implement sound land use management plan and practices. Currently there is no deliberate measure to design land use planning inside the basin to mitigate flood.

Methodology

The Projected Land Cover scenario in 2020 was created using a Trend Analysis function from MS Excel derived from available geospatial vector data of 1998, 2004 and 2010 land cover scenarios to get the area in hectares of the different land cover classes and edited the 2010 land cover shape file in a GIS software in accordance to the area of the different land cover classes at year 2020. On the other hand, the Proposed Land Use makes use of slope as the basis in assigning the different land uses. Specifically, agriculture and built-up were assigned to 0-18% slope, 18-30% slope for agroforestry, 30-50% for production forest and >50% for protection forest. A slope vector file was created from a slope raster file. The slope raster file in turn was derived from an integrated Digital Elevation Model (DEM). The DEM is mostly of the Interferometric Synthetic Aperture Radar (IFSAR) has a resolution of 5m but it was integrated

with the limitedly available Light Detection and Ranging Digital Elevation Model (LiDAR DEM) which has a resolution of 1m to produce a more detailed slope geospatial data. Furthermore, a river buffer zone was assigned and which consist of three (3) buffer zones. These were the Protection Forest Riparian zone (0-20 m from the river), the Production Forest Riparian zone (20-60 m from the river) and the Urban River Buffer Zone (0-2 m from the river). Also a Protected Area was assigned to areas with more than 1,000 masl. Finally for the Built-up area, it was based on the current extent using the Google Earth Image.The difference between the Projected Land Cover and the Proposed Land use is that the projected land cover shows what happens to the land cover after 10 years based on the latest available land cover data which is 2010. The underlying assumption of which is that land cover conditions are left by itself without any intervention to stop land conversion. On the other hand, the Proposed Land Use makes use of land conservation principles and environmental policies that will promote soil and water conservation via the enhancement of forest vegetation cover on critical slopes.

Determining the Runoff behavior revolves around the concept and equation postulated by the Soil Conservation Service (SCS) method. The SCS method can be selected as a function or a modeling method in the HEC-HMS (Hydrologic Engineering Center-Hydrologic Modeling System) software. To make the two (2) scenarios SCS ready, these were intersected with another available geospatial vector file called Soil Hydrological Group. After which these two (2) scenarios together with the integrated DEM were fed into the HEC-GeoHMS (Hydrologic Engineering Center-Geospatial Hydrologic Modeling System) software for basin model and initial preparation of the parameters. Once the preparations have been made, the HEC-HMS was used for simulating the runoff of the Projected Land Cover and the Proposed Land Use. These two (2) scenarios were compared in terms of Runoff volume, Peak Flow and Lag Time for four (4) Rainfall Return Period (RRP) scenarios. These are 5 years, 25 years, 50 years and 100 years. Details on the use of the HEC-GeoHMS and HEC-HMS are well described by a previous study[2].

The output on the impact of the Projected Land Cover and the Proposed Land Use to runoff in the previous study was used as an input to determine the impact of the aforementioned land cover scenarios to flooding. The software that was used to determine flooding was the Hydrologic Engineering Center's-River Analysis System (HEC-RAS) 2D model and a GIS extension application called HEC-Geo-RAS. The LiDAR-DTM (Light Detection and Ranging-Digital Terrain Model) bathymetrically burned geospatial raster dataset was the input used for the software processing of the flood. The flood parameters that were determined was flood depth/level and extent for the different rainfall return periods (RRP) in particular the 5 year, 10 year, 25 year, 50 year and 100 year. There were three flood depth or level that were determined, this was low, medium and high with corresponding values in range namely: 0-0.5 m, 0.5-1.5 m and >1.5 m.Geometric data was prepared in HEC-RAS by manually delineating the 2D area and generating a 50x50 mesh.

Unsteady flow was simulated for 5,10,25,50 and 100yr RRP in 10min flow data interval with an EG Slope of 1 and a minimum flow of 27 m3/s. Animation and visualisation was done in RAS Mapper which is also capable in exporting flood map results in files readable to GIS.

Results and discussion

A. RUNOFF

1. Projected Land Cover

Table 1.1 shows the land cover classification and area of the 2020 Projected Land Cover which was derived using the trend analysis function of MS Excel based on the temporal land cover of 1973, 1989, 1998, 2008 and 2010. Based on that table, there has been an increase in the area for agriculture, built-up, open forest, open space and shrubs while there has been a decrease in the area for coconut and grassland. Closed Canopy Forest will disappear. Table 1.2 shows the land cover proportion of the 2020 Projected Land Cover wherein forest cover constitutes only 25.03% of the whole river basin area. More over the quality of the forest is not that good in so far as reducing surface runoff is concern since the dominant type of forest cover is classified as Open Canopy Forest. This means that the presence of tree vegetation does not completely protect the soil from rainfall impact.

Table 1.1. Land cover classification and area of the 2020 Projected Land Cover

Landcover (hectares)	1998	2004	2010	2020
1. Brushland	10,324.05	19,343.13	14,793.24	0.00
2. Built-Up	722.91	291.67	496.80	1,754.32
3. Closed Canopy Forest	39,974.93	31,810.12	23,691.29	7,796.97
4. Cultivated Area	5,012.63	4,411.56	5,377.04	8,186.81
5. Grassland	5,578.60	2,381.06	7,234.48	25,817.55
6. Open Canopy Forest	11,660.44	17,786.07	20,044.71	11,695.45
7. Perennials	4,588.73	1,838.69	6,224.72	22,611.20
TOTAL	77,862.30	77,862.30	77,862.30	77,862.30

Table 1.2. Land cover proportion of the 2020 Projected Land Cover

2020 Projected Land Cover	Hectares	%
1. Brushland	0.00	0.00
1. Built-up	1,754.32	2.25
2. Closed Canopy Forest	7,796.97	10.01
3. Cultivated Area	8,186.81	10.51
4. Grassland	25,817.55	33.16
5. Open Canopy Forest	11,695.45	15.02
6. Perennials	22,611.20	29.04
Total	77,862.30	100.00

2. Proposed Land Use

Table 2 shows the land use area and proportion of the Proposed Land Use. As can be gleaned from the table the total forest cover is 70.13% this is thrice as much as that of the projected land cover scenario. Moreover the percentage of forest that maintained solely for protection (Protection Forest, Protected Area and Protection Riparian Forest) is 40.82 %. Forest vegetation is known to improve soil infiltration by improving and/or maintaining soil macropores. Macroporosity is a good predictor of infiltration capacity[3]. In addition, the agroforestry land use which is about 15.24% of the total river basin area is known to sufficiently prevent rain induced erosion and conserve water via improved infiltration[4].

Table 2. Land use area and proportion of the Proposed Land Use

Proposed Landuse	Land Features	Area (hectares)	%
1. Agriculture	0-18% slope	10,881.81	13.98
2. Agroforestry	18-30% slope	11,869.55	15.24
3. Production Forest	30-50% slope	17,575.90	22.57
4. Protection Forest	>50% slope	18,067.90	23.20
5. Protected Area	>1000 masl	11,096.86	14.25
6. Built-up	Derived from the current Google image	493.84	0.63
7. Protection Riparian Forest	0-20 m from the river	2,622.13	3.37
8. Production Riparian Forest	20-60 m from the river	5,244.27	6.74
9. Urban River Buffer Zone	2 m from the river	10.04	0.01
TOTAL		77,862.30	100.00

3. Projected Land Cover scenario versus Proposed Land Use scenario

To meaningfully compare the Projected Land Cover with the Proposed Land Use in relation to mitigating flood it is important to compare these two land cover scenarios in terms of their total forest vegetation. Table 3.1 shows that the Proposed Land Use has a lot more forest cover (70.13%) than the 2020 Projected Land Cover which is 25.03%.

Table 3.1. Total Forest Cover of the 2020 Projected Land Cover and the Proposed Land Use

2020 Projected Land Cover	%	Proposed Landuse	%
1. Closed Canopy Forest	10.01	1. Production Forest	22.57
2. Open Canopy Forest	15.02	2. Protection Forest	23.20
		3. Protected Area	14.25
		4. Protection Riparian Forest	3.37
		5. Production Riparian Forest	6.74
TOTAL	25.03		70.13

Tables 3.2 to 3.6 graphically illustrates that the Proposed Land Use scenario has lower peak outflow of runoff and total runoff volume and longer lag time between peak rainfall and peak runoff outflow than the 2020 Projected Land Cover in the 5 year, 10 year, 25 year, 50 year and 100 year Rainfall Return Period. The numerical values for the differences are shown in Tables 3.1 to 3.5. The reason for the results is that the Proposed Land Use scenario has more than twice the amount of forest vegetation as compared to the 2020 Projected Land Cover, it has better forest cover quality in the presence of the protection forest wherein degree of cover is similar to that of a Close Canopy Forest. In addition, the Proposed Land Use scenario has a 19% agroforestry land use which is known to promote soil and water conservation.

Table 3.2. Five (5) Year Rainfall Return Period (RRP); Proposed Land Use vs. 2020 Projected Land Cover

Parameters	Proposed Land Use	2020 Projected Land Cover	Difference
Total Rainfall (mm/day)	141.89	141.89	
Peak Rainfall (mm)	24.50	24.50	
Peak outflow (m3/s)	907.10	2,049.50	-1160.5
Total Runoff Volume (m3)	57,634.50	110,146.70	-63644.5
Time to Peak	17 hours and 50 minutes	17 hours	50 minutes
Lag Time	5 hours and 50 minutes	5 hours	50 minutes

Table 3.3. Ten (10) Year RRP; Proposed Land Use vs. 2020 Projected Land Cover

Parameters	Proposed Land Use	2020 Projected Land Cover	Difference
Total Rainfall (mm/day)	300.49	300.49	
Peak Rainfall (mm)	37.00	37.00	
Peak outflow (m3/s)	2,753.20	5,118.10	-1160.5
Total Runoff Volume (m3)	157,245.80	269,210.00	-63644.5
Time to Peak	18 hours	16 hours and 40 minutes	1 hour and20 minutes
Lag Time	6 hours	4 hours and 40 minutes	1 hour and20 minutes

Table 3.4. Twenty- Five (25) Year RRP; Proposed Land Use vs. 2020 Projected Land Cover

Parameters	Proposed Land Use	2020 Projected Land Cover	Difference
Total Rainfall (mm/day)	373.89	373.89	
Peak Rainfall (mm)	44.00	44.00	
Peak outflow (m3/s)	907.10	6,588.80	-1160.5
Total Runoff Volume (m3)	210,865.20	348,119.50	-63644.5
Time to Peak	17 hours and 50 minutes	16 hours and 30 minutes	1 hour and20 minutes
Lag Time	5 hours and 50 minutes	4 hours and 30 minutes	1 hour and20 minutes

Table 3.5. Fifty (50) Year RRP; Proposed Land Use vs. 2020 Projected Land Cover

Parameters	Proposed Land Use	2020 Projected Land Cover	Difference
Total Rainfall (mm/day)	427.59	427.59	
Peak Rainfall (mm)	49.20	49.20	
Peak outflow (m3/s)	4,462.90	7,680.30	-1160.5
Total Runoff Volume (m3)	252,122.40	406,818.20	-63644.5
Time to Peak	17 hours and 50 minutes	16 hours and 30 minutes	1 hour and20 minutes
Lag Time	5 hours and 50 minutes	4 hours and 30 minutes	1 hour and20 minutes

Table 3.6. One Hundred (100) Year RRP; Proposed Land Use vs. 2020 Projected Land Cover

Parameters	Proposed Land Use	2020 Projected Land Cover	Difference
Total Rainfall (mm/day)	481.16	481.16	
Peak Rainfall (mm)	54.40	54.40	
Peak outflow (m3/s)	5,206.80	8,760.70	-1160.5
Total Runoff Volume (m3)	293,939.60	465,682.70	-63644.5
Time to Peak	17 hours and 40 mins	16 hours and 20 mins	1 hour and20 minutes
Lag Time	5 hours and 40 mins	4 hours and 20 mins	1 hour and20 minutes

B. FLOOD

Flood depth or level is lower in the Proposed Land Use than the 2020 Projected Land Cover and this is much pronounced at higher flood level or depth in all of the rainfall return period events (Figures 2.1 to 4.5). Likewise the total extent of flooding is much lower in the Proposed Land Use than the 2020 Projected Land Cover as also shown in Figures 2.1 to 4.5.

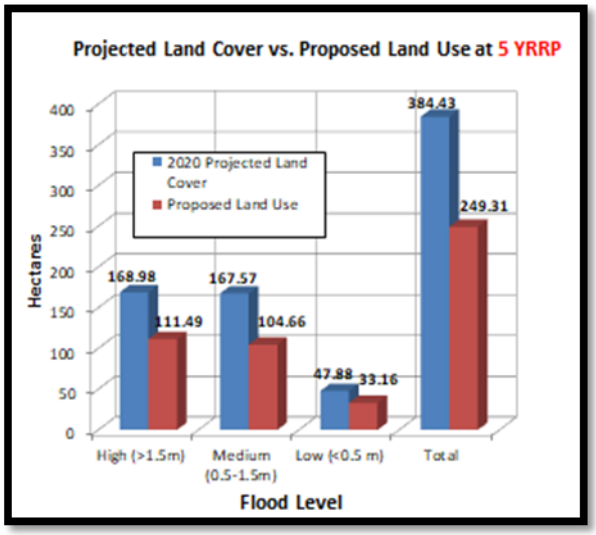

Fig. 2.1. Extent of Flood Level at 5 Year Rainfall Return Period

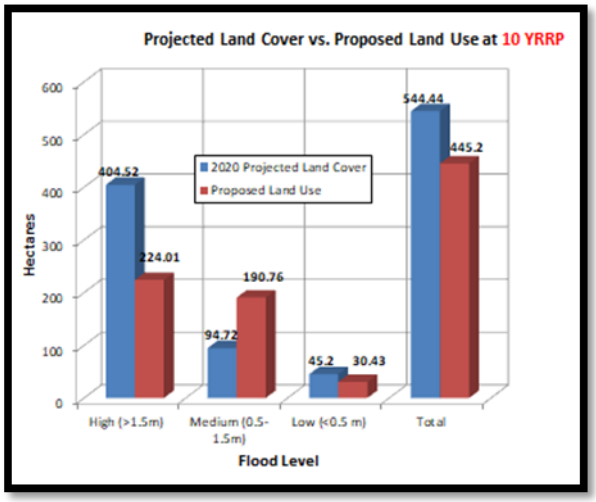

Fig. 2.2. Extent of Flood Level at 10 Year Rainfall Return Period

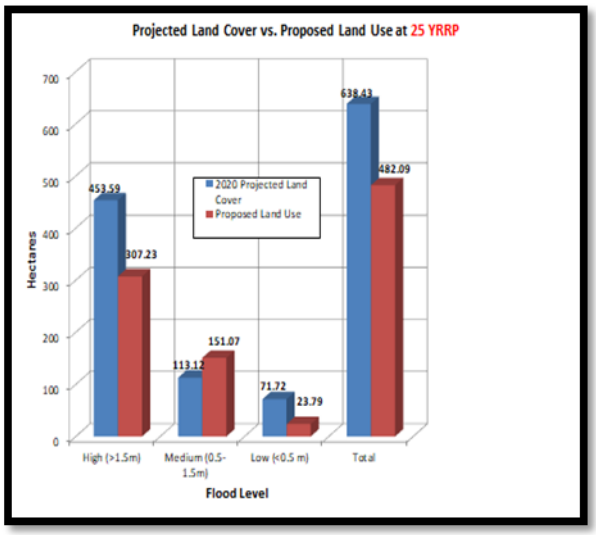

Fig. 2.3. Extent of Flood Level at 25 Year Rainfall Return Period

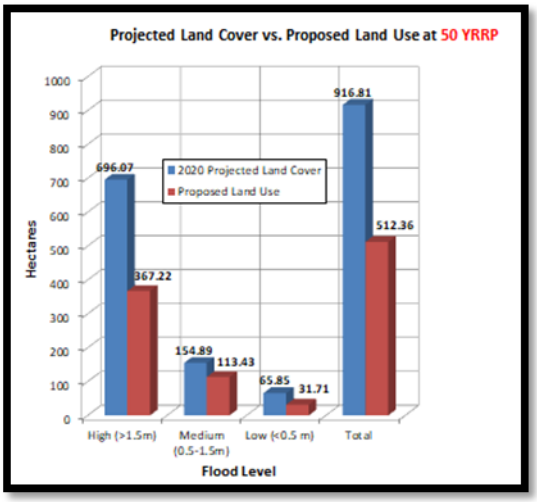

Fig. 2.4. Extent of Flood Level at 50 Year Rainfall Return Period

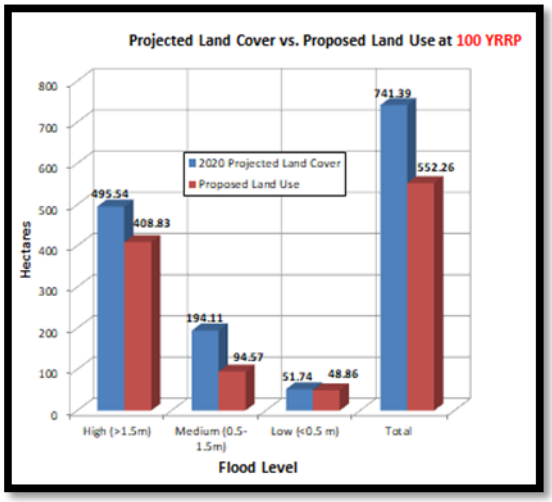

Fig. 2.5. Extent of Flood Level at 100 Year Rainfall Return Period

The reason for a lower flood depth and extent for the Proposed Land Use than the 2020 Projected Land Cover is because as what has been aforementioned in the Runoff discussion section, the Projected Land Cover has higher runoff values in terms of discharge volume, peak discharge and Lag Time as against the Proposed Land Use scenario. This is in view of the fact that runoff is the major source for flood waters.

Conclusions

The study shows when land cover conditions are left by itself without any intervention as represented by the 2020 Projected Land Cover scenario, the impact of flood disaster is more likely to be magnified due to higher peak runoff flow and total runoff volume and shorter lag time The study also shows that flood disaster can be mitigated if the Proposed Land Use scenario will be adopted as one of the course of action in flood disaster risk reduction management since it has lower peak runoff flow and total runoff volume and longer lag time. Hence this study lends credence the significant role of adopting sound land use management in mitigating flood hazard.

Acknowledgement

We are very grateful for the research funding and support given to us by DOST–PCIEERD; as well as to UP–Diliman LiDAR Team, GeoSAFER Program, MSU–Iligan Institute of Technology, NAMRIA, DENR and DPWH, Region 10, Philippines for making this study a success.

References

[1] Iligan City Disaster Risk Reduction Management Council, 2013. Final Report on Typhoon Sendong (Washi), Iligan City, Philippines.
[2] Salcedo, Stephanie Mae B., Suson, Peter D. ,Milano, Alan E. and Ignacio, Ma. Teresa T. Impact of dynamically changing land cover on runoff process: The case of Iligan river basin. Unpublished.
[3] Taylor, Matthew, Mulbolland, Murray and Thomburrow, Danny, "Infiltration Characteristics of Soils Under Forestry and Agriculture in the Upper Waikato Catchment", 12 September 2008, http://www.waikatoregion.govt.nz/PageFiles/13347/Tr0918.pdf.
[4] Noordwijk, Meine Van and Verbist, Bruno, "Overstory # 104-Soil and Water Conservation", http://www.agroforestry.net/the-overstory/165-overstory-104-soil-and-water-conservation

Groundwater and surface water interaction patterns via groundwater model - case study in Plaicumphol Irrigation Project

Pwint Phyu Aye[1,a] and Sucharit Koontanakulvong[1,b]

Abstract In the last decades, water demand has increased due to the rapid development in economy in Thailand. Because of the spatial and temporal distribution of rainfall and insufficient water storage, groundwater has played an important role for agricultural productivity in Plaichumphol Irrigation Project area. In order to better groundwater management in this area, the study aimed to understand the groundwater and surface water interaction patterns via local groundwater model with the grid size of 400 x 400 square meters. Boundary conditions were determined based on the geology, hydrogeology and piezometry of the aquifer of the calibrated regional groundwater model. River water level, pumping wells and recharge rates are also used from regional groundwater model with grid size of 2 x 2 sq.km. Recharge parameter were carried out to estimate land recharge rate and river hydraulic conductance to analysis interaction mechanism and to compare with the developed local groundwater model (flux) results. It is found that in this area, the main factors for groundwater flow budget are land recharge in rainy season and river recharge in dry season. The interaction volume and patterns between surface water and groundwater were analyzed from water balance via developed local groundwater model. Based on the change in water year, the aquifer gains water as land recharge is 2.72MCM/day in wet year and 2.18MCM/day in drought year of the total inflow. River recharge (river loss) to the aquifer is 2.25MCM/day in wet year and 1.82MCM/day in drought year.

Keywords *sw-gw interaction, field measurement, seepage, flow budget, Plaiumphol Irrigation Project*

[1]Department of Water Resources Engineering
Faculty of Engineering, Chulalongkorn University
Bangkok, Thailand

[a]Pwint.P@student.chula.ac.th
[b]Sucharit.k@chula.ac.th

Introduction

There were several studies in this area such as groundwater modelling for conjunctive use patterns [1], groundwater and surface water dynamic interaction model [2], groundwater model to mitigate the climate change [3], and conjunctive used management [4]. Because of the spatial and temporal distribution of rainfall and insufficient mount of water storage, groundwater is an important role of agricultural productivity in Plaichumphol Irrigation Project area. The farmer used groundwater 1.43MCM/year [4]. However, these amounts are not enough for their cultivation. In this area, groundwater discharge occurs where groundwater level is hydrographically higher than the surface water level. Depending on the structure of the hydrogeological cross-section and the profile of groundwater table, the groundwater discharge varies by hydraulic connection between aquifer and river. Therefore, an understanding of the interaction between groundwater and surface water is need for effective management of water management.

A. Purpose of study

The main purpose of this study is to understand the groundwater and surface water interaction mechanism (volume and patterns) via development of local groundwater model. For this purpose, soil moisture sensor system and seepage meter measurements were carried out in Plaichumphol Irrigation Project area (PIP). The field soil moisture sensor system was developed to monitor soil moisture to understand land recharge for developing groundwater model. The seepage measurement was conduct to estimate discharge and recharge from river seepage to analyse interaction and to compare and check the calibrated values from local groundwater model (flux).

B. Study area conditions

The study adopted the Plaichumphol Irrigation Project (PIP), as a case study for the groundwater and surface water interaction. This area located in Phitsanulok Province, the lower northern region of Thailand. The irrigated area is 338sq.km of total project area (436sq.km) is shown in Fig.1 [4]. Main Surface water basin is dissected by Yom river in the west and Nan river in the east which drain from

north to sourth. The elevation of topography is 40-60m.MSL.

Materials and methods

A. Aquifer characteristics

There are mainly three types of hydrogeological characteristics in this study area, namely high terrace deposits, low terrace deposits and recent flood plain deposits. The aquifer system in this study was defined as semi-confined layer and confined layer with three deposit types whereby the thickness is 40-100m and 100-200m. The groundwater aquifer has formed the geological basis as a depositional flood plain, flow from north to south-east.

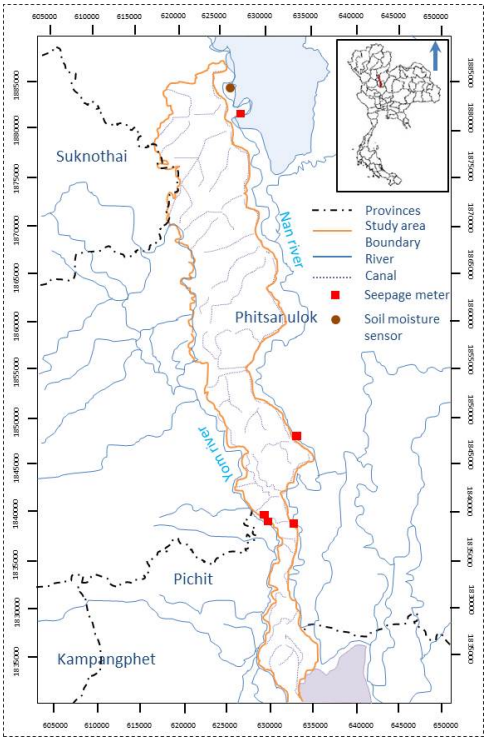

Fig. 1. Boundary of the study area

B. Method of study

To develop the local groundwater model, the required ground surface elevations, well locations, groundwater level, surface water elevation and boundary condition were used from the previous study [5]. It was developed with smaller grid size 400x 400 sq.meter. The proper recharge parameters; land and river recharge were measured in the site as shown in Fig. 1. The field measurements of soil moisture via sensor system and seepage meter were done to investigate land recharge and river conductance [6]. The values of these interaction parameters were used to compare with calibrated interaction parameters between groundwater and surface water from the developed local groundwater model.

C. Equations used

1) Groundwater flow model

Groundwater flow model was accomplished using MODFLOW within the Groundwater Modeling System (GMS) version 10.1. MODFLOW is the U.S. Geological Survey modular finite-difference flow model, which is a computer code that solves the groundwater flow equation. The program is used to simulate the flow of groundwater through aquifers and to predict aquifer fluxes into and out of an aquifer. The three-dimensional movement of groundwater of constant density through porous earth material may be described by the partial differential equation.

$$\frac{\partial}{\partial x}\left[Kxx\frac{\partial h}{\partial x}\right]+\frac{\partial}{\partial y}\left[Kyy\frac{\partial h}{\partial y}\right]+\frac{\partial}{\partial z}\left[Kzz\frac{\partial h}{\partial z}\right]+W=S_s\frac{\partial h}{\partial t} \quad (1)$$

Where, K_{xx}, K_{yy} and K_{zz} are the values of hydraulic conductivity in the x, y and z directions along coordinate axes, h is hydraulic head, W is a volumetric flux per unit volume and represents sinks and/or sources S_s is the specific storage of the porous material and t is time.

2) Land recharge

Recharge rate is estimated using daily soil moisture balance on a single soil water store in Phitsanulok Province [6]. HYDRUS-1D software package [7] was used to simulate one dimensional vertical flow with the standard Richards equation for unsaturated flow as follow:

$$\frac{\partial\theta}{\partial t}=\frac{\partial}{\partial z}\left[K(h)\left(\frac{\partial h}{\partial z}+1\right)-S(h)\right] \quad (2)$$

Where θ is the volumetric water content by time (t), vertical ordinate (z) assumed to be zero at the soil surface directed upward. K represents the unsaturated hydraulic conductivity, h is the pressure head and S is a sink term to account for root water uptake.

To solve this equation (2), Genuchetn-Mualem model [8] was used to describe the soil water retention θ(h), hydraulic conductivity K(h) and effective saturation as follow:

$$\theta(h)=\begin{cases}\theta_r+\frac{\theta-\theta_s}{[1+|\alpha h|^n]^m} & h<0\ (m=1-\frac{1}{n})\\ \theta_s & h\geq 0\end{cases} \quad (3)$$

3) River hydraulic conductance

Calculating the flow between river and aquifer is done using a coefficient that represents the streambed conductance. This coefficient, termed C estimated from streambed deposits properties.

$$C=(KWL)/M \quad (4)$$

Where, K is the hydraulic conductivity of the bed material, L defines the length and the river cell for the

calculation node, W is the total width of interaction layer and M is the thickness of aquifer. This equation is used to find the conductance C from seepage and the flow rate of river loss and gain.

4) River recharge

In groundwater modelling, the flow across river bed is represented as follow [9]

$$Q = C\,(h_i - h) \qquad (5)$$

Where, Q is the flow between the river and aquifer, taken as positive if it is directed into the aquifer; C is the hydraulic conductance of the river-aquifer interconnection: h_i is the water level (stage) in the river; and h is the head of groundwater.

5) River loss and gain

Interaction between surface and groundwater is determined by the relation between surface water and groundwater levels

$$\Sigma^{n}_{i=1}Q = \Sigma^{n}_{i=1}\,(Q_{up} - Q_{down}) \qquad (6)$$

Where, Q is the river loss or gain; Q_{up} is river discharge in upstream and Q_{down} is river discharge in downstream.

Field methods and model development

A. Land recharge

Soil moisture sensor system designed with Arduino was developed and installed (1-4m) depth in the soil at an agricultural field (spacing 1m), for land recharge analysis (Fig. 3). There are two probes in the soil moisture sensor and there is circuitry inside the sensor for measuring the resistance and converting it into voltage as output. HYDRUS-1D was applied to simulated water movement with soil hydraulic parameter estimates using field data. The daily rainfall, evaporation and transpiration data were also measured. The soil sample in the field was taken and is classified as well-drained sandy clay loam. The shallow groundwater table was constant at 5 meter from the ground surface during the study period (rainy season). The effects of rainfall and evaporation can be seen from the soil moisture fluctuations with time lag at each depth except at the depth of 4 meter which was wetted all the time and affected from the shallow groundwater level. The daily maximum recharge rate in this area is 4.43cm/day at 2m depth when the soil moisture is saturated [6].

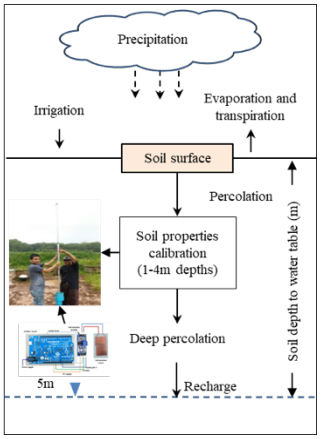

Fig. 2. Schematic of soil moisture sensor installation

B. River recharge

Seepage meter was constructed inexpensively in the Plaichumphol Irrigation Project area. The seepage meter used in this study was modified to measure the flow of surface water and groundwater along the river from those described by [10] and consisted of a pan and a collection bag (Fig.4). The seepage meter is made by cutting 15cm long, end sections from a 0.208cm (55gallon) metal drum. Rubber stopper (rubber band) with a single hole drilled in the center to accept tubing and clear flexible tubing that will fit tightly into the hole in the rubber stopper. The plastic collection bag is connected with the vent tube which insert into the rubber stopper compactly. The size of the plastic collection bag depends on the rate of seepage and the period that measurements are made. A large bag is needed for longer measurement periods and location with larger rates of seepage. In water over 20cm depth, a single tube through the top of the seepage meter works both as a vent for any gas released from the sediment and as a connecting for the measuring bag. A known volume of water is filled into the collection bag using the graduated cylinder. Install the collection bag assembly on the seepage meter with the rubber stopper fits in the vent hole that was drilled in the seepage meter.

The results of seepage measurement are in the range of 7.8 to 6.3 m/day for upstream (sand), 5.7 to 5.5m/day for midstream (silt) and 4.8m/day for downstream (clay) and were used to compare with calibrated river recharge parameter from the local groundwater model.

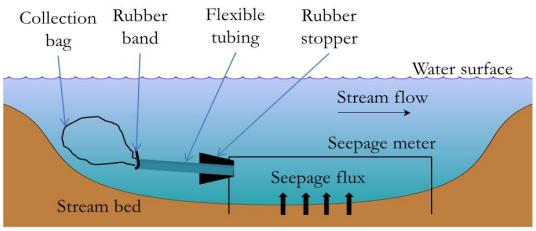

Fig. 3. Cross-section showing a typically installation of a seepage meter

C. Local groundwater flow model development

The 3D block-centred grid model represented the groundwater basin which has a finer grid size 400x400 sq.m. The thickness of aquifer system for this study defined unconfined layer between 40-100m. Hydrological features adjacent to and within the model domain represented in the model by mathematical boundary conditions. It was determined based on the geology, hydrogeology and piezometric heads of the previous regional groundwater model [5] were used as boundaries in this local groundwater model. River water level, pumping wells and recharge rates are initially used as input data.

Recharge parameters; land and river recharge values are adjusted and defined to provide the best match between measured and simulated values of hydraulic heads. And pumping rates are also adjusted by seasonal and zoning. The final results of the calibrated model were used for a sensitivity analysis in order to evaluate the model sensitivity to any changes in the model input parameters. The procedure used in this analysis depends on changing only one input parameter and keeping the rest fixed. The purpose was to assess the groundwater response to any change in the hydraulic parameter and which of them have the highest effect on the hydraulic heads.

Results of model application

A. Interaction parameter adjustments

1) Land recharge

Land recharge is defined as the downward flow of water reaching the water table. In this study area, groundwater is mainly recharged by vertically infiltration of precipitation where it falls on the ground surface. Recharge rates were defined by percent of rainfall in each soil group zone. In this study, recharge zones were defined by soil type such as zone 1 is sand; zone 3 is sandy clay; zone 4 is sandy clay loam; and zone 5 is clay (Fig. 4). The initial recharger rate from previous model for sandy clay loam is 6.2cm./day which is higher than the field measurement data (4.43cm/day)[6] for same soil type as shown in Table 1. Therefore groundwater recharge was adjusted and calibrated values. The Mean Error (ME) of calibrated value in the range 0.5 shows the less error (0.12) then other range of initial recharge rate (Fig.5). The calibrated value from the error was noted and used this range to calibrate the initial recharge rate in the local model. As shown in Table 1, the calibrated recharge rate for sandy clay loam is 3.7cm/day and sandy clay is 4.9cm/day which is closed to the field measured data and is also in the range with the past study [11, 12].

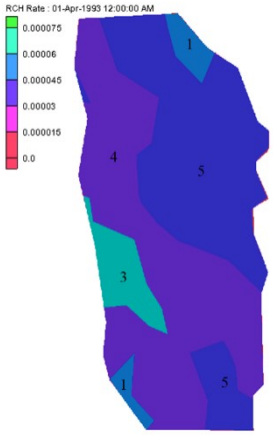

Fig. 4. Recharge rate calibration zoning by each soil zone

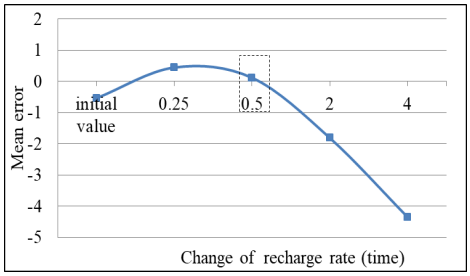

Fig. 5. Recharge rate calibration zoning by each soil zone

Table I. Recharge rates by each soil types

Soil zone	Soil type	Initial recharge rate (previous study)	Calibrated recharge rate (After adjustment)
3	Sand	12	6.14
1	Sandy clay	9.8	4.9
5	Sandy clay loam	6.2	3.7
4	Clay	7.3	3.1

2) River conductance

Seepage flux was measured along the rivers (Nan and Yom rivers) to know discharge and recharge from the river seepage. The seepage values are different from upstream to downstream base on bed materials. The bed materials of upstream, mid-stream and downstream are sand, sandy clay and clay [13]. From the previous model calibration with monitored well records near rivers, the conductivity value range from 2.2 to 2.0m/day in Nan River and 1.2 to 1.9m/day in Yom River. From the field measurement, seepage flux varies from 7.8 to 4.8 m/day. The field measured conductance values shows higher values than those previous model values. Since the upstream is sand, there was a good interaction to the aquifer from upstream to downstream. Therefore, the conductance values along the river were adjusted and calibrated (Fig. 6). The less error of the calibrated conductance values is noted. The calibrated values range from 1.0 to 5.5m/day in Nan River and 1.0 to 1.5m/d in Yom River (Table 2). The calibrated values

are also higher than field measurement data. However, these values are close to the other study (0.1 to 4.9m/d) in Saigon River [14] and used in local groundwater model development.

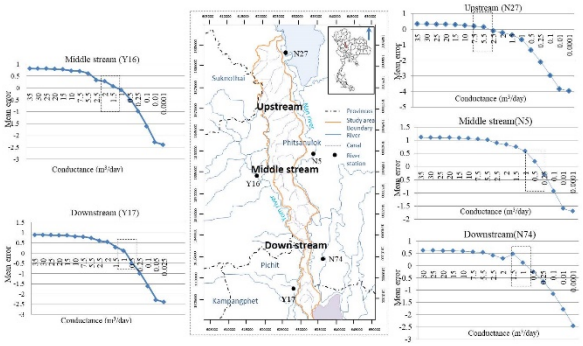

Fig. 6. River conductance rate by river bed materials

Table II. River conductance values

Stream	Bed material	Previous study		Calibrated	
		Nan	Yom	Nan	Yom
Upstream	Sand	2.2	-	5.5	-
Midstream	Sandy clay	2.1	1.5	0.5	1.5
Downstream	Clay	2.0	2.0	1.0	1.0

B. Local model calibration

First, boundary conditions are defined from peizometric heads of previous region model (Fig.7) and adjusted recharge parameters; land recharge and river conductance values were used and calibrated during the period 1993 to 2003 in both steady and transient states. Recharge parameters were provided the best match with the nearby observed data.

A steady-state model was then calibrated with data from development time and the transient model was constructed using the calculated heads from a steady-state model as initial head conditions. The time period for simulation is divided into two stress period. A steady-state period is 1993 and the transient period is from 1993 to 2003. The computed peizometric head values of a steady-state and transient state gave the good performance when compared with the observed data (Fig. 8) and the total error summary in both states are shown in Table 3.

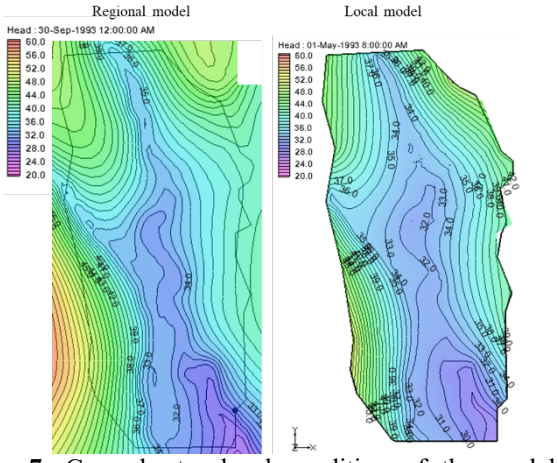

Fig. 7. Groundwater level condition of the model (Right: previous regional model, Left: local model)

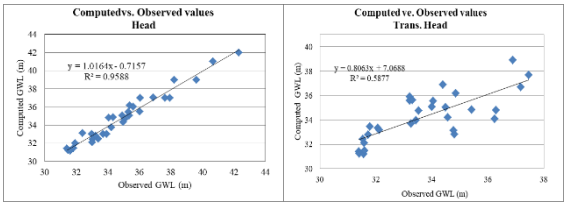

Fig. 8. Comparison of computed and observed peizometeric heads in both states

Table III. Error summary of calibration resluts in both states

Error (unit: m)	Steadystate	Transient
Minimum	-0.92	-2.18
Maximum	0.96	2.68
Mean error (ME)	-0.14	0.53
Mean absolute error (MAE)	0.50	1.16
Root mean squared error (RMSE)	0.58	1.39
Nash-Sutcliffe coefficient (NSE)	0.92	0.69

C. Groundwater flow budget

Flow budget of Groundwater was analysed to present exchange flow volume of all components of groundwater budget including gw-sw interactions. The flow budget tools in groundwater model provide the inflow and outflow volume at each cell such as river recharge, land recharge, pumping discharge, storage and net of inflow and outflow. The groundwater flow budget is analyzed in seasonal: rainy (April to September) and dry (October to March) and water year patterns (very dry, dry, normal, wet based on dam storage volume) [15] from well calibrated groundwater model results. The annual average rainfall is about 1243mm/year [13]. From the analysis, the groundwater flow budget can be described as follows (Fig. 9).

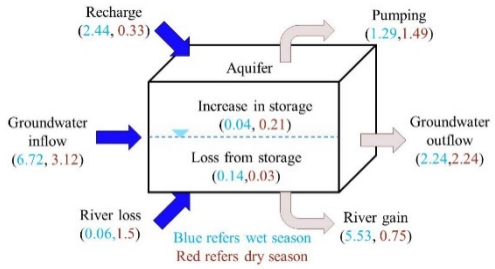

Fig. 9. The conditions of groundwater flow budget

D. Interaction volume and patterns

1) Land recharge

According to flow budget analysis from local groundwater model (Table 5). Water year is definde the reservoir storage of Bumhipol and Sirikit Dam [15]. In wet year, groundwater flow from the baoundary into the aquifer is 6.34 MCM/day (rainy) and 2.81MCM/day (dry). Land recharge to the aquifer 1.92MCM/day (rainy) and 0.26MCM/day (dry). River loss to the aquifer 0.42MCM/day (rainy) and 1.83MCM/day (dry). Meanwhile, river gains 4.73MCM/day (rainy) and 0.59MCM/day (dry) from the groundwater. In dry year, well pump 1.36MCM/day(rainy) and 1.65MCM/day which is higher that wet year. In this area, the main factor for groundwater flow budget is land rechage in rainy season and river recharge in dry seaon.

Table IV. Water budget by season and water year; unit: MCM/day

Water Year	*Groundwater inflow*		*River loss*		*Land recharge*		*Storage in*	
	Wet	*Dry*	*Wet*	*Dry*	*Wet*	*Dry*	*Wet*	*Dry*
Very Dry	6.77	3.84	0.00	1.82	1.92	0.26	0.01	0.2
Dry	6.95	3.28	0.04	1.83	2.09	0.32	0.00	0.18
Normal	6.22	2.74	0.15	1.91	2.32	0.27	0.07	0.14
Wet	6.34	2.81	0.42	1.83	2.45	0.27	0.01	0.22
Water Year	*Groundwater outflow*		*River gain*		*Well pumping*		*Storage out*	
	Wet	*Dry*	*Wet*	*Dry*	*Wet*	*Dry*	*Wet*	*Dry*
Very Dry	2.39	2.34	5.9	1.21	0.76	1.70	0.17	0.00
Dry	2.38	2.43	5.3	0.62	1.36	1.65	0.00	0.06
Normal	2.21	2.30	4.58	0.52	1.40	1.43	0.02	0.01
Wet	2.07	2.18	4.73	0.59	1.35	1.49	0.03	0.04

2) River loss and gain

There are two main aspects of interaction between surface water and groundwater. Firstly, the flow of groundwater support rivers flow and secondly the flow from rivers to groundwater. The rate of flow between river and aquifer is calculated from the different in hydraulic heads in the river and the adjacent aquifer using equation (5). There are mainly three river stations along Nan River and two stations at Yom River.

The condition of river loss and gain during the study period (1993-2003) is shown in (Fig.10). Groundwater loss water 1.2 MCM/day (rainy) and 1.19MCM/day (dry). River gave to the aquifer 0.93MCM/day (rainy) and 0.95MCM/day (dry) in upstream (N27). Water stored in middle stream (N5A) and goes down into downstream (N74) on Nan River. In Yom river, aquifer gave to the river 0.7MCM/day (rainy) and 2.62MCM/day (dry). It means that the river store the water in the upstream and flow to the downstream.

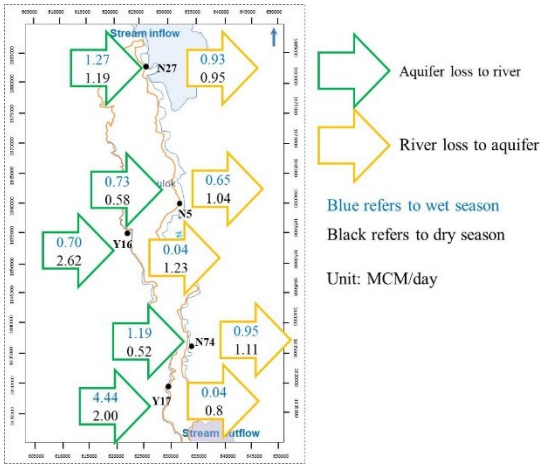

Fig. 10. The conditions of river gain and loss along river reach

Conclustions

In summary, the local groundwater model was developed by boundary condition from the previous regional groundwater model. Recharge parameters; land and river were adjusted and compared with field measurement data. Land recharge and river recharge were measured in the field measurement. The calibrated land recharge rates are 4.9, 6.1, 3.1 and 3.6cm/day for each soil zone and the average recharge rate of the field measured value is 4.43cm/day. It can be used in the local groundwater model development. The adjusted river conductance values are 5.5m/day for upstream, 0.5m/day for midstream and 1.0m/day for downstream which showed small value than field data.

The interaction volume and patterns between surface water and groundwater was analysed from water balance via developed local groundwater model. Based on the change in water year, the aquifer gains water as land recharge are 2.72MCM/day in wet year and 2.18MCM/day in drought year of the total inflow. River recharge (river loss) to the aquifer is 2.25MCM/day in wet year and 1.82MCM/day in drought year. River recharge to aquifer is higher than land recharge in wet yea. However, river recharge is higher in drought year than land recharge. The river loss and gain is also main affect to the groundwater balance of the study area. River loss water from upstream and water store in middle stream and goes down into downstream. The value of river loss and gain in the rivers were estimated from river conductance and the values are smaller than the field measurement which needs more detail field survey. These findings can be used for future groundwater planning and management in the area.

Acknowledgment

The authors wish to thank the staff at the Rice Water Use Experiment Station2 of Royal Irrigation Department and the staff from Civil Engineering Department at Narasuan University, Thailand for data collection and field experiments. We also value the support of our colleagues form the Department of Water Resources Engineering, Chulalongkorn University. We would like to acknowledge the financially support of Doctoral Degree Sandwich program scholarship from AUN/SEED-Net (JICA).

References

[1] W.Bejranonda, S. Koontanakulvong, and C. Suthidhummajit, "Groundwater modelling for conjunctive use patterns investigation in the upper Central Plain of Thailand," in *International smposium-Aquifers Systems Management-30th May-1st June 206*Dijon, France, 2006, pp. 161--174.

[2] W. Bejranonda, M. Koch, and S. Koontanakulvong, "Surface water and groundwater dynamic interaction models as guiding tools for optimal conjunctive water use policies in the central plain of Thailand," *Environmental earth sciences,* vol. 70, no. 5, pp. 2079-2086, 2013.

[3] C. Suthidhummajit, S.. Koontanakulvong, "The Role of Groundwater to Mitigate the Drought and as an Adaptation to Climate Change in the Phitsanulok Irrigation Projrct, in the Nan Basin,Thailnd," *jurnalteknologi,utm.my,* vol. 76, no. 15, pp. 89-95, 2015.

[4] W.Bejranonda, S. Koontanakulvong, and C. Suthidhummajit, "Study of the Interaction between Streamflow and Groundwater toward the Conjunctive use Management: a Case Study in an Irrigation Project," 1st NPRU Academic Conference, Oct. Annals, 2008, pp. 59-67

[5] P. P. Aye and S. Koontanalulvong, " Hydrogeological parameter distribution estimation by Geostatistical methods in Regional Groundwater Modeling in the Upper Central Plain, Thailand", IJCIET, vol 9, no. 3, March 2018, pp. 313-322.

[6] P. P. Aye, S. Koontanakulvong and T.T. Long, " Deep percolation characterisitcs via field soil moisture sensors: case study in Phitsanulok, Thailand", Taiwan Water Conservancy, in press.

[7] J. Šimůnek, M. T. van Genuchten, and a. M. Šejna, "The HYDRUS-1D software package for simulating the one-dimensional movement of water, heat, and multiple solutes in variable-saturated media," in HYDRUS softeare series 1, University of California Riversitd, USA, 2005.

[8] Y. Mualem, "A new model for predicting the hydraulic conductivity of unsaturated porous media," *Water Resources Research,* vol. 12, no. 3, pp. 513-522, June, 1976.

[9] M.G. McDonald and W.A. Harbaugh, "A modular three-dimensional finite difference groundwater flow model," U.S.Geological Survey, Open file report, pp. 83-875, 1988.

[10] D.R Lee and J.A. Cherry, A field exercise on groundwater flow using seepage meters and mini-piexometers,Journal of Geological Education, vol. 27,no1, pp. 6-10, 1978.

[11] M. J. Xiaohui Lu, Martinus Th. van Genuchten, Binggo Wang, "Groundwater Recharge at FIve Representative Sites in the Hebei Plain, China," *National Ground Water Association,* vol. 49, no. 2, pp. 286-294, 2010 2010.

[12] R. A. Schincariol and J. D. McNeil, "Errors with small volume elastic seepage meter bags," *Ground water,* vol. 40, no. 6, pp. 649-651, 2002.

[13] W. R. S. R. Unit, "The impact of Climate Change on Irrigation Systems and Adaptation Measuers (Plaichumphol Irrigation Project case study),"pp. 301, 2010.

[14] T.V.Pham and S. Koontanakulvong "Groundwater and River Interaction Parameter Estimation in Saigon River, Vietnam," *Engineering Journal,* vol. 22, no. 1, pp. 257-267, 31/Jan/2018 2018.

[15] S. Koontanakulvong, C. Suthidhummajit, "Flow budget and conjunctive use pattern of groundwater system under climate change in Upper Central Plain, Thailand," in *THA 2017 International Conference on ―Water Management and Climate Change Towards Asia's Water-Energy-Food Nexus*, Bangkok, Thailand, 2017, pp. 186-191.

DETERMINATION OF DEEP PERCOLATIONS via SOIL MOISTURE APPROACH IN SAIGON RIVER BASIN, VIETNAM

Tran Thanh Long[1,a] and Sucharit Koontanakulvong[1,b]

Abstract As a critical factor of the groundwater balance, the groundwater recharge rate plays an essential role in determining sustainable yields for groundwater resources, especially in overexploited aquifers. The paper focused on describing deep percolation flow using Richard's function (Hydrus 1D). First, the field measurement was designed, and moisture sensors were installed in three locations in Saigon River Basin, Vietnam. Second, the daily deep percolation of 3 soil types is simulated using the Hydrus 1D model. The water retention parameters are calibrated and verified by field experimental data in the study area. Third, relationship of effective rainfall and land recharge is analyzed to detect the deep percolation functions for 3 soil types in the study area. Finally, the assessment water balance provides a better understanding of the deep percolation flow mechanism. The investigation gives an insight on deeper percolation as well as potential land recharge from rainfall utilizing soil moisture approach for developing groundwater modeling. The percolation ratio of sand clay loam, sand clay, and clay are estimated 0.33, 0.22, and 0.18, respectively. Henceforth, the deeper percolation procedure and results will be useful for further determining groundwater yields and disaster management as in the consecutive drought years.

Keywords *Deep percolation; Hydrus 1D; Soil moisture approach, Saigon River basin*

[1]Department of Water Resources Engineering
Faculty of Engineering, Chulalongkorn University
Bangkok, Thailand

[a]ttlongdcbk@yahoo.com
[b]sucharit.k@chula.ac.th

Introduction

Since 1990s, under the pressure of social economic growth in the Ho Chi Minh City, the water resources are facing a critical shortage during current drought years. To meet rising water demand, the groundwater extraction is exploited excessive which cause dramatically drawdown to aquifers. In order to have well planned for sustainable socio development, groundwater recharge mechanism needs to be explored more intensively under transient condition. Although land recharge is one of important factor [1], investigation of land recharge somehow remains a challenging task.

Since 1960s, there are varied commonly methods applied to estimate natural groundwater recharge, e.g., i) soil water balance method [2-7], ii) zero flux plane method [8-12], iii) one-dimensional soil water flow model [13-17]; iv) infiltration test using single ring, double rings, the well permeameter [18, 19], v) inverse modeling technique [20-22], vi) groundwater level fluctuation method [6, 23, 24], vii) Chemical/ radioactive method[25-28]. However, these methods sometimes are difficult and expensive in the field test. Moreover, the water balance in unsaturated zone cannot be evaluated easily and lead incorrectly equated with the sustainable yield of an aquifer.

Along the development of technology, soil water content can be monitored via Arduino soil moisture sensor [29, 30]. This approach shows potential useful to validate soil profile under water movement process. Hence, the paper focused on describing deep percolation flow using Richard's function (Hydrus 1D) and observed soil moisture via field sensors. First, the field measurement system was designed and installed three locations in the Saigon Basin. Second, the daily deep percolation of 3 soil types (sand clay loam, sand clay, and clay) are simulated using the Hydrus 1D model. The water retention parameters are calibrated and verified by field experimental data from Oct 2017 to August 2018 in the study area. Third, relationship effective rainfall and land recharge are analyzed to detect the deep percolation function for 3 soil types in the study area. Final, the assessment water balance provides a better understanding of the deep percolation flow mechanism.

These investigations gave an insight on deeper percolation as well as potential land recharge from rainfall utilizing soil moisture approach for developing groundwater modeling. Henceforth, the

deeper percolation procedure and results will be useful for further determining groundwater yields and disaster management as in the consecutive drought years.

Study area

Study area stretches from latitude 10.320 E to 11.201 Eand from longitude 106.215 N to 107.024 N with anarea of 6,640 km2. It covers all area of Ho Chi MinhCity and some districts of Dong Nai, Binh Phuoc, Binh Duong, Long An and Tay Ninh Province (Fig. 1). The area has a tropical climate, specifically a tropical wet and dry climate, with an average humidity of 75%. The year is divided into two distinct seasons. Mean annual rainfall is at 1,612 mm and mean annual temperature is at 27°C. Terraced plain mainly characterizes the topography of the area with elevation varies from 0 MSL to 70 MSL. In the area, there are 3 major rivers as Sai Gon River, Vam Co Dong River, and Dong Nai River. Regarding soil type, the monitor soil sensors were set up in 3 locations, i.e., B1 is sand clay loam, B2 is sand clay, B3 and B3 is clay.

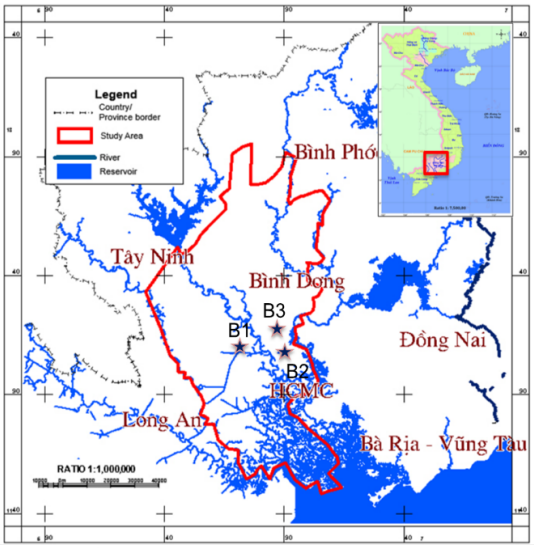

FIELD TEST
B1- Sand clay loam, B2- Sand clay, B3- Clay

Fig. 1. Study area

Theories and Procedures used

The study began by installing soil moisture sensors in 3 field sites with automatic data collection. There soil samples were collected to calibrate soil moisture sensors in the lab. Then, the percolation flows are simulated using Richard's function (Hydrus 1D). The water retention parameters are calibrated and verified by observed soil moisture in the field. The performance of soil moisture simulation is justified due to statistic parameters and the regression. The water balance was accessed to give better understanding on percolation movement. Finally, the percolation is analyzed to find the ratio between land recharge and effective rainfall. The procedures of study are shown as Fig. 2.

A. Field measurements

At field sites, the Arduino sensors were installed every meter in 5 meters depth. The soil moisture sensor monitored every 1-meter depth daily. The soil moisture of each soil type is calibrated with moisture measurement in the lab. Then, the measurements in three field sites are converted to soil moisture. The circuit includes Arduino board, soil moisture module, and soil moisture sensor (copper plate), automatic data transmit. The study approach is summarized and shown in Fig. 3.

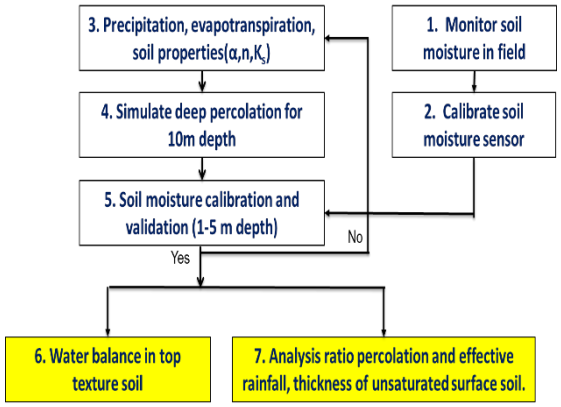

Fig. 2. Study procedures

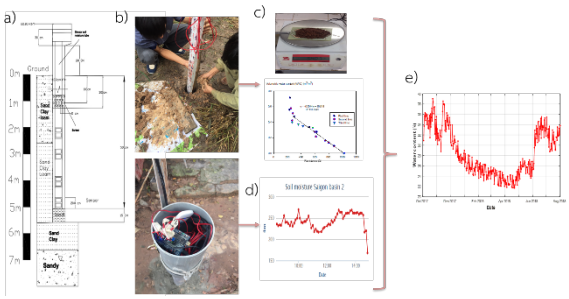

Fig. 3. Approch of field measurement (a: borelog design; b: inject sensor into soil; c: calibration soil moisture; d: field measurement data; e: monitor soil moisture)

B. Percolation simulation theories

The governing flow equation for the uniform Darcian flow of water in a porous medium is adopted by the following modified form of the Richards' equation: (Simunek, Van Genuchten, and Sejna 2005)

$$\frac{\delta\theta}{\delta t} = \frac{\delta}{\delta x_i}\left[K\left(K_{ij}^{A}\frac{\delta h}{\delta x_j} + K_{iz}^{A}\right)\right] - S \quad (1)$$

θ is the volumetric water content, (L^3L^{-3})
K is the hydraulic conductivity (LT^{-1}),
h is the pressures head (L)
S is a sink term [T^{-1}]
x_i (i-1,2) is the spatial coordinates [L],

t is the time (T) and

z is the vertical ordinate (L)

K^A_{ij} are components of a dimensionless anisotropy tensor K^A

K is the unsaturated hydraulic conductivity function [LT^{-1}] given by

$$K(h) = K_s S_e^{1/2}\left[1-(1-S_e^{1/m})^m\right]^2 \quad (2)$$

$$\theta(h) = \begin{cases} \theta_r + \dfrac{\theta_s-\theta_r}{[1+|\alpha h|^n]^m} & h<0 \\ \theta_s & h \geq 0 \end{cases} \quad (3)$$

$$S_e = \frac{\theta-\theta_r}{\theta_s-\theta_r} \quad (4)$$

$$m=1-1/n, n>1 \quad (5)$$

S_e is the effective water content

θ_r denote the residual water content

θ_s denote the saturated water content

K_s is the saturated hydraulic conductivity

α is the inverse of the air-entry value (or bubbling pressure)

n is a pore-size distribution index

The percolation simulation applied rainfall and evaporation of study area from Oct 2017 to August 2018. The upper boundary condition is set as atmosphere condition. The bottom boundary condition is set as seepage condition. The initial retentions parameters (θ_r, θ_s, α , n, K_s)are referred from Rosetta program [31].

Results and discussions

A. Field measurement

In this experiment, the percolation rates at each depth were compared with effective rainfall. The effective rainfall defines as rainfall minus evaporation. Fig. 4 shows sample of field observed water content and effective rainfall (rainfall-evaporation) during Oct 2017- August 2018 at sand clay loam field site. The observed water content corresponded with effective rainfall. The soil moistures at 1 m depth are sensitive with rainfall event. The lower soil depth has less sensitive with rainfall events.

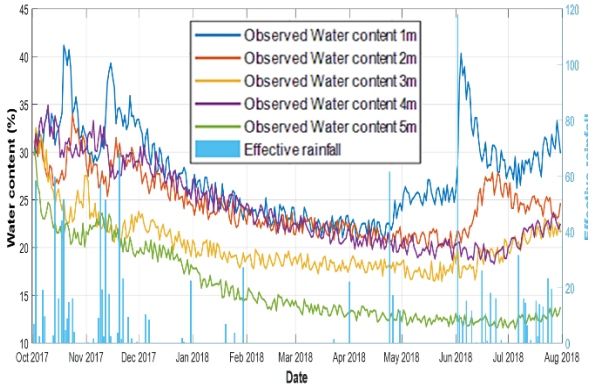

Fig. 4. Observed water content and effective rainfall during Oct 2017- August 2018 at sand clay loam field site

Fig. 5 shows soil moistures of 3 soil types at rainy season 2017 and dry season 2017. The difference of soil moisture in sand clay loam is the highest. The difference of soil moisture in clay is the lowest. The soil moisture increases after rainy season and decreases after dry season. The measurement data show that modified soil moisture sensors give reliable value under natural condition. Then, the percolation and water balance analyses can apply the field soil moisture data via installed sensors.

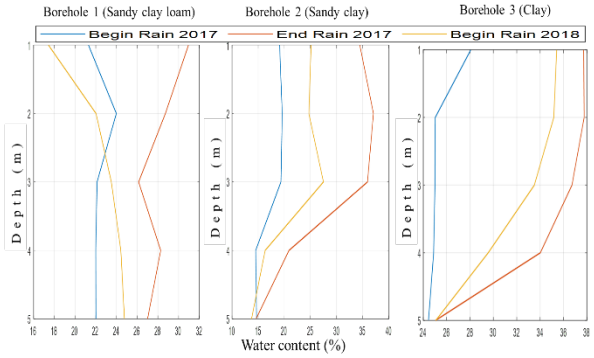

Fig. 5. Soil moistures of 3 soil types in rainy season 2017 and dry season 2017

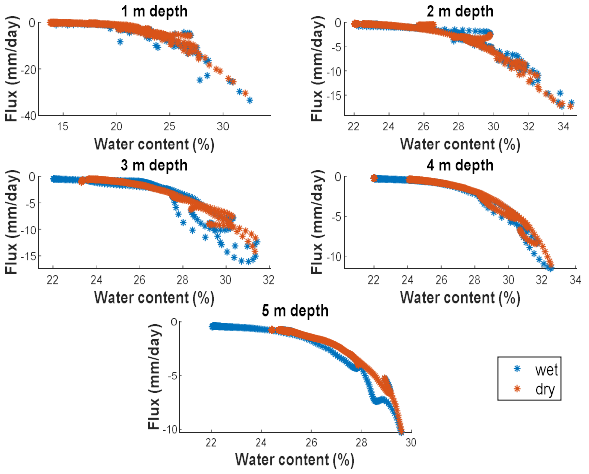

Fig. 6. The relationship between fluxes in filed test and water contents of sandy clay loam

Fig. 6 demonstrates the relationship between fluxes in filed test and water contents. The flux and soil moisture show closed relationship, especially in seasonal. The fluxes in wet season are higher than in dry season.

B. Calibration and verification of percolation simulation

Retention parameter calibrations relied on performance statistics of observed soil moisture. In calibration step, the calculated soil moistures of three soil type match well with observed data. The maximum error (%) is 2.98 to 1.45. The minimum error (%) is 0. The mean error (%) is 0.66 to 1.16. The RMSE is 0.67 to 1.37. The R-square is 0.7 to 0.88.

The Nash coefficient is 0.65 to 0.8. In verification step, the calculated soil moistures of three soil type are similar with observed data. The maximum error (%) is 4.68 to 1.35. The minimum error (%) is 0. The mean error (%) is 0.8 to 1.8. The RMSE is 0.83 to 1.81. The R-square is 0.65 to 0.8. The Nash coefficient is 0.62 to 0.8.

TABLE I shows the soil retention parameter values after calibration and verification. The soil retention parameters are proportional with percentage of sand. The α, n, K parameters decrease in deeper depths. The sand clay loam has highest hydraulic conductivity. The lowest hydraulic conductivity is clay.

Table I. Soil retention parameters after calibration and verification

	Depth	Sand (%)	Silt (%)	Clay (%)	Soil type	θ_r	θ_S	α (1/mm)	n (-)	K (mm/day)
Borehole 1	1m	71.4	14.6	13.9	Sandy loam	0.065	0.41	0.0075	1.89	361
	2m	67.5	8.5	24	Sandy clay loam	0.0605	0.3807	0.0029	1.6	124.4
	3m	65.5	6.5	28	Sandy clay loam	0.0605	0.3807	0.00277	1.64	120.3
	4m	63.2	16.4	20.4	Sandy clay loam	0.0644	0.3919	0.0029	1.48	114
	5m	64.1	12.8	23.1	Sandy clay loam	0.0629	0.3807	0.0015	1.7	120
Borehole 2	1m	50.2	10.4	39.4	Sandy clay	0.1	0.38	0.0035	1.65	55.8
	2m	53	9.6	37.4	Sandy clay	0.1	0.38	0.0032	1.62	51
	3m	54.5	7.5	38	Sandy clay	0.1	0.38	0.0031	1.65	45
	4m	56	5.7	38.3	Sandy clay	0.1	0.38	0.0027	2.2	60
	5m	61.3	4.6	34.1	Sandy clay	0.1	0.38	0.00025	2.1	65
Borehole 3	1m	17.2	3.4	79.4	Clay	0.068	0.391	0.0015	1.29	15.6
	2m	16.7	7	76.3	Clay	0.068	0.391	0.0012	1.25	17.6
	3m	10.8	2	87.4	Clay	0.068	0.389	0.0008	1.25	18.1
	4m	23.6	5.4	71	Clay	0.068	0.385	0.0006	1.26	24
	5m	23.5	4.5	73	Clay	0.068	0.385	0.0004	1.75	27

C. Water balance analysis

TABLE II shows total fluxes at three field sites from Oct 2017-August 2018. The fluxes in deeper depth are lower than in topsoil. The fluxes in lower depth also give a lag time compared with flux in upper depth (Fig. 7 as a sample). The percolation amount of sandy clay loam is the highest. In contrast, the clay has the lowest percolation. The gap between fluxes of two soil depth can be explained by the fluctuation water content in its depth.

Table II. total fluxes at three field sites from Oct 2017-August 2018.

Soil type	Sand clay loam	Sand clay	Clay
Total. Effective rainfall (mm)	2285.4	2285.4	2285.4
Total flux 1m (mm)	1849.09	1545.91	1174.2
Total flux 2m(mm)	1600.96	1328.26	964.38
Total flux 3m (mm)	1420.21	1218.19	809.21
Total flux 4m (mm)	1112.36	1176.35	577.81
Total flux 5m (mm)	988.17	525.47	421.58

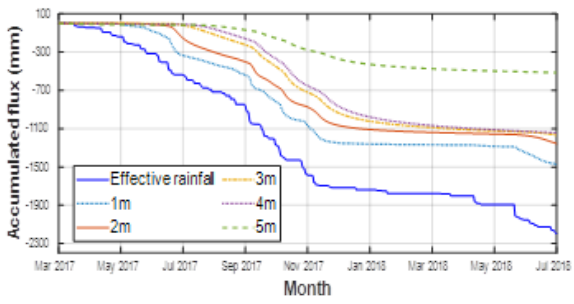

Fig. 7. Accumulated flux at the field site of sandy clay loam

Fig. 8 shows water balance of 3 soil types during wet season. The difference of water content in clay during rainy season is the highest. Therefore, water was captured in upper soil layer and cannot reach to bottom layer at the same rate. While the delta water content in sand-clay loam and sand-clay are lower than clays. Thus, deep percolation amount of sand clay loam and sand-clay are higher than clay's. This experiment also reveals that grain size of soil and percentage of sand has strong relationship with percolation flux.

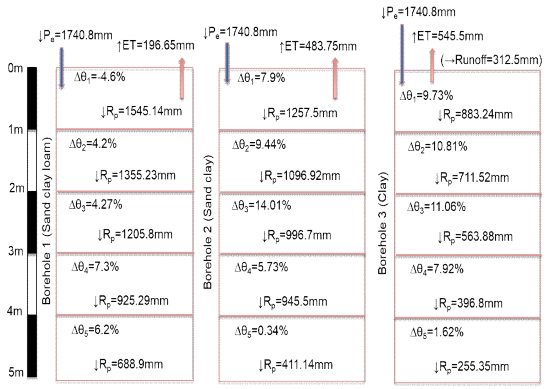

Fig. 8. Water balance of 3 soil types during wet season

Fig. 9 shows water balance of 3 soil types during dry season. The difference of water contents in upper soil depth is low. Hence, the rainfall did not infiltrate in dry season. While, the difference of water contents in lower soil depth is high. These phenomena can help to explain the lag time of fluxes in lower depth. The sandy clay loam shows the highest amount of percolation after lag time. In other side, sand clay and clay have similar amount of percolation after lag time.

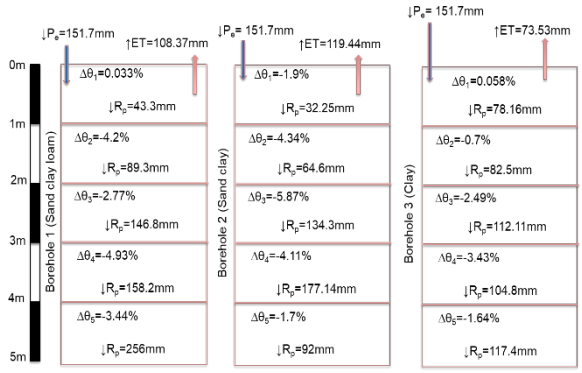

Fig. 9. Water balance of 3 soil types during dry season

D. Percolation rate ratio

The percolation fluxes were compared with effective rainfall to find the percolation rate ratio in study area. The percolation rate ratios of three soil types decrease from top to bottom depth. The highest ratio is sand clay loam. The second ratio is sand clay. The lowest is clay. The ratio of sand clay loam from top to bottom is 0.8 to 0.33. The ratio of sand clay from top to bottom is 0.67 to 0.22. The ratio of clay from top to bottom rate is 0.5 to 0.18.

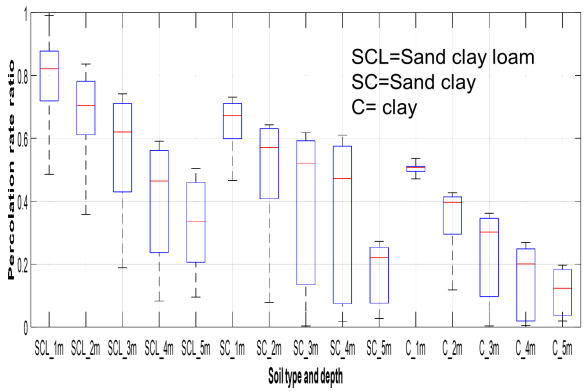

Fig. 10. Percolation rate ratios of 3 soil types

Conclusions

The percolation ratio is proportional with percentage of sand in soil (Fig. 11). The water was captured in upper clay layer and reach difficultly to bottom layer. While the water pass through sand clay loam and sandy clay more than clay. Under high evaporation, rainfall in dry season cannot infiltrate to soil. Hence, the percolation rate in dry season at 5 meter is from water of upper soil which absorbed during wet season.

The percolation ratio of sand clay loam, sand clay, and clay are 0.33, 0.22, and 0.18, respectively (Fig.12). The experiments are in concordance with the results of previous study [32], which also pointed out land recharge is limited to 27.6% of rainfall.

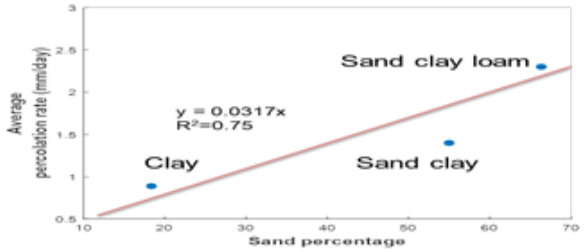

Fig. 11. Relationship between percolation rate and percentage of sand

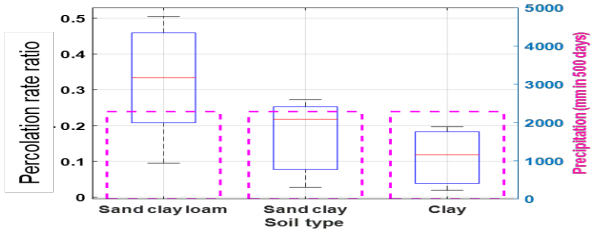

Fig. 12. Percolation rate at 5 meters of 3 soil types

These experiments presented an insights approach to estimate better deep percolation from effective rainfall via field soil moisture sensor. The approach gives better understanding mechanism of deep percolation. The approach has potential to help planning the water resources and disaster management more efficient in the consecutive drought years.

Acknowledgment

This paper could not be accomplished without thesupport of Ph. D sandwich program scholarship from AUN – Seed net and the Water Resources System Research Unit of Faculty of Engineering, Chulalongkorn University. The authors also thank to the staff at Division for Water Resources Planning and Investigation for the South of Vietnam, Southern Regional Hydrometeorology Center Department of Resources and Environmental for data collection.

References

[1] S. Koontanakulvong and P. Siriputtichaikul, "Groundwater Modeling In the North Part of the Lower Central Plain, Thailand," in International Conference On Water and Environment, Bhopal, India, Vol. Ground Water Pollution, 2003, no. 19, pp. 180-187.

[2] S. J. Reddy, "A simple method of estimating the soil water balance," Agricultural Meteorology, vol. 28, no. 1, pp. 1-17, 1983.

[3] J. Lloyd, "A review of aridity and groundwater," Hydrological processes, vol. 1, no. 1, pp. 63-78, 1986.

[4] G. W. Gee and D. Hillel, "Groundwater recharge in arid regions: review and critique of estimation methods," Hydrological Processes, vol. 2, no. 3, pp. 255-266, 1988.

[5] R. Lal, "Current research on crop water balance and implications for the future," in Proceedings of the International Workshop of the Soil Water Balance in the Sudano-Sahelian Zone, Niamey, Niger, 1991, pp. 31-44.
[6] C. Kumar, "Estimation of natural ground water recharge," ISH Journal of hydraulic Engineering, vol. 3, no. 1, pp. 61-74, 1997.
[7] R. M. Feltrin, J. B. D. de Paiva, E. M. C. D. de Paiva, and F. A. Beling, "Lysimeter soil water balance evaluation for an experiment developed in the Southern Brazilian Atlantic Forest region," Hydrological Processes, vol. 25, no. 15, pp. 2321-2328, 2011.
[8] S. Wellings, "Recharge of the Upper Chalk aquifer at a site in Hampshire, England: 1. Water balance and unsaturated flow," Journal of Hydrology, vol. 69, no. 1-4, pp. 259-273, 1984.
[9] J. Cooper, C. Gardner, and N. Mackenzie, "Soil controls on recharge to aquifers," European Journal of Soil Science, vol. 41, no. 4, pp. 613-630, 1990.
[10]C. Tang, "Interception and recharge processes beneath a Pinus elliotii forest," Hydrological processes, vol. 10, no. 11, pp. 1427-1434, 1996.
[11]M. Tsujimura, A. Numaguti, L. Tian, S. Hashimoto, A. Sugimoto, and M. Nakawo, "Behavior of subsurface water revealed by stable isotope and tensiometric observation in the Tibetan Plateau," Journal of the Meteorological Society of Japan. Ser. II, vol. 79, no. 1B, pp. 599-605, 2001.
[12] M. Khalil, K. Seki, T. Miyazaki, M. Mizoguchi, and M. Sakai, "Analysis of zero flux plane behavior under periodical water supply," Transactions of the Japanese Society of Irrigation, Drainage and Reclamation Engineering (Japan), 2006.
[13] D. Nielsen and J. Biggar, "Water flow and solute transport processes in the unsaturated zone," Water resources research, vol. 22, no. 9S, 1986.
[14] V. Z. Antonopoulos and Z. G. Papazafiriou, "Solutions of one-dimensional water flow and mass transport equations in variably saturated porous media by the finite element method," Journal of hydrology, vol. 119, no. 1, pp. 151-167, 1990.
[15] H.-F. Yeh, C.-H. Lee, J.-F. Chen, and W.-P. Chen, "Estimation of groundwater recharge using water balance model," Water Resources, vol. 34, no. 2, pp. 153-162, 2007.
[16] G. Cao, Recharge estimation and sustainability assessment of groundwater resources in the North China Plain. The University of Alabama, 2011.
[17] S. Feiznia, M. Kholghi, and A. Malekian, "Groundwater recharge simulation using a coupled saturated-unsaturated flow model," Journal of Applied Hydrology, vol. 1, no. 2, pp. 1-9, 2014.
[18] J. Wu and R. Zhang, "Analysis of rainfall infiltration recharge to groundwater.," in Proceedings of Fourteenth Annual American Geophysical Union: Hydrology Days, 1994.
[19] W. Sangbun, S. Sangchan, and P. Mekpruksawong, "Groundwater Recharge in the Irrigated Upstream Area of the Regulating Gate in the Lower Nam Kam River, Thailand," The 9th International Symposium on Social Management Systems SSMS2013, 2-4 December 2013, Sydney, Australia, vol. Vol.1, no. Issue 9, 2014.
[20] H. Q. Khai and S. Koontanakulvong, "Impact of Climate Change on groundwater recharge in Ho Chi Minh City Area, Vietnam," in Int. Conf. on Climate Change and Water & Environment Management in Monsoon Asia, Bangkok, Thailand, 2015.
[21] S. Koontanakulvong and C. Suthidhummajit, "The role of groundwater to mitigate the drought and as an adaptation to climate change in the Phitsanulok irrigation project, in the Nan basin, Thailand," 2015.
[22] P. V. Tuan and S. Koontanakulvong, "Groundwater and River Interaction Parameter Estimation in Saigon River, Vietnam," Engineering Journal, vol. 22, no. 1, pp. 257-267, 2018.
[23] A. Lutz, S. Minyila, B. Saga, S. Diarra, B. Apambire, and J. Thomas, "Fluctuation of groundwater levels and recharge patterns in Northern Ghana," Climate, vol. 3, no. 1, pp. 1-15, 2014.
[24] V. Hung Vu and B. J. Merkel, "Estimating groundwater recharge for Hanoi, Vietnam," Science of The Total Environment, vol. 651, pp. 1047-1057, 2019/02/15/ 2019.
[25] P. Sharma and S. Gupta, "Soil water movement in semi-arid climate. An isotopic investigation," 1985.
[26] W. Drost, "Single-well and multi-well nuclear tracer techniques: A critical review," in International Hydrological Programme, vol. 3: Unesco, 1989.
[27] K. Seiler, "Isotope studies of the hydrological impact of large scale agriculture," in Isotope techniques in the study of environmental change, 1998.
[28] H. Moser and W. Rauert, "Isotopic tracers for obtaining hydrologic parameters," in Isotopes in the Water Cycle: Springer, 2005, pp. 11-24.
[29] Y. Kojima et al., "Low-Cost Soil Moisture Profile Probe Using Thin-Film Capacitors and a Capacitive Touch Sensor," Sensors, vol. 16, no. 8, p. 1292, 2016.
[30] T. T. Long, S. Koontanakulvong, and P. P. Aye, "Examination of land recharges using soil moisture approach: Case study in Thailand," presented at the Internet Journal of Society for Social Management Systems 2017.
[31] M. G. Schaap, F. J. Leij, and M. T. Van Genuchten, "Rosetta: A computer program for estimating soil hydraulic parameters with hierarchical pedotransfer functions," Journal of hydrology, vol. 251, no. 3-4, pp. 163-176, 2001.
[32] B. T. Vuong and P. N. Long, "Groundwater Environment in Ho Chi Minh City, Vietnam," in Groundwater Environment in Asian Cities: Elsevier, 2016, pp. 287-315.

Review and Future Direction of Research on Delta at Risk and Resilience to Water-Related Disasters

Alvin Yesaya[1,a] and Akiyuki KAWASAKI[b]

Abstract The number of population living in the delta cities are increasing year by year due to abundant natural resources and accessibility. However, this condition is not equivalent with the capabilities of the cities against natural disasters. The inclination toward global climate change will increase the risk of water-related disasters. Assessing the delta city resilience on infrastructure, social-ecology, and policy is necessary to reduce damage and loss. This paper aims to review the current research trend on the vulnerability of delta cities toward the water-related disasters. These disasters which define as a natural event such as flood, tsunami, storm, climate change effects cause great damage and loss in delta region. Reviewing current achievement and methodology, finding the missing gaps from previous literature, and providing the future recommendation for researcher are important for future outlook in this subject. Using Scopus database and some private institutions as a complement to sort particular papers in this topic, the results show that many studies are still centralized in Asian and European countries. Mostly, the articles focus on climate change effect and the lack of policy on disaster resilience. Adding new scenario framework, integrating with policy sector, and shifting study location to Africa or Oceania to evaluate the resilience status in delta cities against water-related disasters can be a breakthrough in this field.

Keywords *water-related disasters, delta city resilience, climate change*

[1]Department of Civil Engineering
University of Tokyo
Tokyo, Japan

[a]alvin.yesaya@coastal.t.u-tokyo.ac.jp
[b]kawasaki@hydra.t.u-tokyo.ac.jp

Introduction

Coastal zones have attracted human due to the abundant resources and accessibility of logistic for trading and transport. The development in the coastal areas is snowballing in the past decades. Moreover, the increasing number of population along with urbanization growth will affect the seaside regions in the future. Sixty percent of the 31 megacities based on United Nations data 2016, which have more than 10 million populations, are located in seashore regions. The majority of big cities are located in the coastal zone and in the large delta. Based on the study, in 2000, 10.9% of the 6.1 billion global population lived in the coastal zone, and the number is projected to increase to 12% of 11.3 billion global population in 2060 [40].

These circumstances create high tension within coastal environment and natural resources. Beside the fragility due to geography condition, the urbanization growth will aggravate the risk and vulnerability. Moreover, devastating conditions of the delta cities are mostly led by water-related disasters, such as the Indian Ocean tsunami in 2004, Hurricane Katrina in the United States in 2005, the earthquake and tsunami in the northern coast of Japan in 2011, Typhoon Haiyan in the Philippines in 2013 [19]. Based on those reasons, measuring the capability of the delta cities against disaster is essential. For example, in Indian Ocean tsunami disaster, the recovery of damaged cities focused on long-term social and ecological effects [56]. In the past, post-disaster conditions developed awareness to build the structure to protect the residential area. However, the concept of resilience nowadays has shifted to the anticipation efforts before disasters. Integrating environmental and human behaviour factors to understand the risk will improve the response to the hazard [19].

Evaluating and assessing the delta cities resistance against water-related disasters are exceptionally necessary. This paper sets out to examine the current situation of research regarding the connection between water-related disaster and delta cities. The objectives of this study are: **Providing information on delta at risk against water disaster**, collecting and analysing papers related to resilience against water-related disasters in delta regions around the world; **Reviewing recent studies outlook**, discussing and criticizing the current trend of methodologies, approaches, and limitation of previous

research; **Creating future path**, finding the missing gaps and giving suggestion to researchers for future trajectories in this topic.

Background

A. Vulnerability of delta cities toward disaster

Besides of the benefits dwelling in a delta city, numerous disasters might haunt the occupants anytime. The hazard to the residents is quite high due to the increasing rate of population. Recently, research showed that 24 deltas have been sinking gradually and 85% of which experienced severe flooding in the past decades (International Geosphere-Biosphere 2014). Moreover, the threat of climate change is perceived nowadays, and it may cause sea level rise. Intergovernmental Panel on Climate Change (IPCC) mentioned that the global mean sea level has already increased by 20 mm from 2005 to 2012 and been projected to increase by around 150 mm to 239 mm due to the RCP (Representative Concentration Pathways) scenarios in 2100 [34]. Combining sea level rise and land subsidence will escalate the exposure toward the catastrophe. Grayman (2011) classified the major natural cataclysm related to water as [23]: Flood such as coastal flood, riverine flooding, flash flood, dam failure; Storm likes typhoon, hurricane, tropical cyclone, tornado, local storm; Climate change such as global sea water level, changing rainfall pattern; Drought; tidal wave and tsunami; Contamination; water-borne epidemics; Slides such as landslide, avalanche, mudflow

This paper will focus on four water-related disasters: flood, storm, tsunami, and climate change. These disasters are common occurrence in the delta regions. Flood is described as the inundation due to heavy rainfall in the short term and harms the people and infrastructure directly. Storm and tsunami which generally occur in the offshore can induce massive damage in the delta regions. Climate change is defined as a phenomenon which causes floods/subsidence in a long-term duration as a result of extreme weather and sea level rise.

B. Resilience to water-related disaster

Resilience, according to Holling [25], is "the endurance of a system to absorb the disruption and changes of circumstances or variables and still persist". Resilience combines the environment and society ability to deal with hazard in various ways such as learning, adapting, and reorganizing the impact [10]. Discovering the resilience capability in delta cities can be a guide to evaluate the system dealing with hazard holistically. For instance, private institutions such as C40 cities or Delta Alliance have measured the vulnerability index to develop awareness about disasters.

Many types of resilience can be assessed for looking the resistance of city. The resilience of disaster that are used in this study are [12, 19]:

1. Engineering resilience
2. Social & Ecology resilience
3. Governance resilience

we approach engineering resilience as a concept in engineering terms to build hard infrastructures which can reduce damage. Social and ecology resilience is interpreted as the system that can absorb the disturbance and build the capacity for adaption. To make it convenient, we imply social and ecological resilience as a system which can be adapted toward disaster, which is applicable for both human and the environment. Meanwhile, governance resilience is critical to avoid the governance failure when institution decision-making processes create a barrier for learning [12]. We interpret this resilience by looking at the rule and policy that create an integrated system to foster public awareness toward disaster. Therefore, Government plays an important role in this terminology.

The resilience of water-related disasters means the ability of the system in the city to recover from and stand firm against water catastrophe. Revealing the capability and readiness of individual city to face the danger of water-related disasters is essential for the residents by increasing the public perception to minimize the damage.

Method

The methods in this study focus on the extend of the research on water-related disasters and resilience that are addressed in journals, companies' documents, or in academic theses in the last 20 years. Figure 1 shows the flowchart of the method to sort the number of the papers which are related with resilience against delta city. Using the Scopus database and the keywords ("WATER DISASTER") AND ("DELTA RESILIENCE") in the abstract section, 3103 papers from various journal types were identified. After that, 1516 papers were filtered by using the same keywords but restricted to the fields of ecology, economy, geography, geology, engineering, environmental science. It is deemed necessary to limit the scope of the research only to those specific fields so that we could concentrate on the various kinds of resilience in those subjects.

The final set up was to screen the papers by adding more details as filters. We divided the water disasters to six specific categories, namely "Water Disasters", "Storm", "Flood", "Tsunami", "Climate Change", and "Extreme Weather" and combined them with the keywords "Delta Resilience". Next, the results were read carefully and the articles which were not suitable for delta region or irrelevant with the topic were discarded. This selection process produced 70 journal papers.

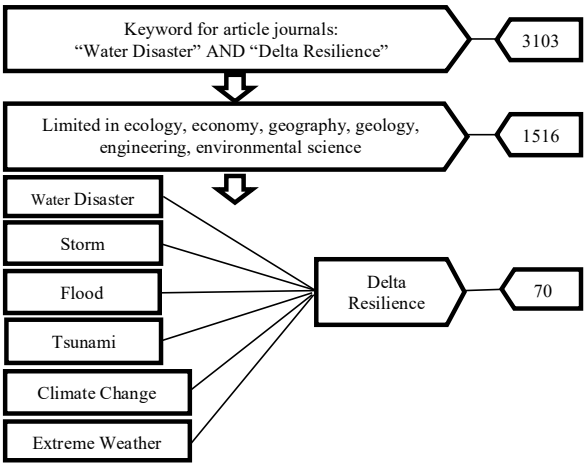

Fig. 1. Sorting articles of water disaster and resilience in delta city

We also added some other documents from international organizations, NGOs, or private sectors related with this topic. Generally, they conducted the worldwide scope survey and measuring with the same criteria. In total with combining all the documents, this study used 83 documents for creating a review paper with detail 70 journal papers, 10 NGO or company documents, 3 books/theses. Nexus understanding of delta resilience against water disaster from the current research trend will be covered by these documents.

Result and Discussion

Among of 83 articles related to resilience against water-related disaster, we distributed the number of papers based on the region which has already studied by researcher. The distribution of papers is mainly concentrated in the Asian and European regions with the amount of 50 papers and 29 papers respectively. Meanwhile, North America and Africa are intermediate with numbers 21 and 17. There were few of researches in the Oceanian and South American, only 11 and 12 respectively. Though the research in Asian is abundant, mostly only focus on Vietnam and Bangladesh. The position of Bangladesh was in the downstream of Ganges-Brahmaputra river with 100 million people live there [7]. Similar condition occurred in Mekong delta, Vietnam, which had contributed to the agriculture crop production by almost 70% and, at the same time, constitutes the most vulnerable area to flood caused by typhoon and climate change. Similar to the Asian region, the research in European region was mostly concerned on the Netherlands, especially Rotterdam city [55]. It typifies the well advanced in urban resilience planning regarding the hard structure (dyke) and soft infrastructure (social and community awareness [59]. also the policy, the Delta Program, which was introduced by Dutch Government to guarantee safety in the present and future [49].

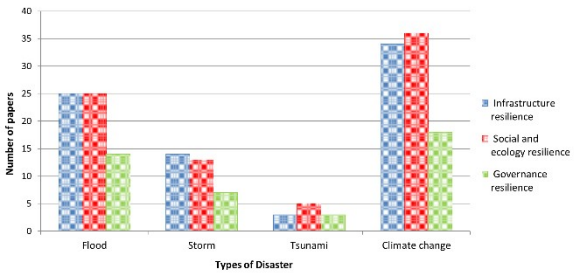

Fig. 2. Papers amount of water-disasters and types of resilience

However, the types of water-related disasters in the literature recently do not distribute smoothly. As represented in figure 2, the number of research on floods and climate change dominated than the others. Regarding to resilience type, not so many papers focused on policy against disaster. However, recently the number of research on social-ecology resilience is almost equal to the number of research on infrastructure resilience. This trend brings proper development of resilience by combining social and infrastructure solution. There has been an increasing trend of integrating science and society today due to the rising interest in comprehensive study. For instance, the study by Renaud et al. 2013 [48] mentioned that human activities could increase the risk of reaching tipping points of the environmental change in Rhine-Meuse delta in European regions and in Ganges River in India because of the constructions of drainage systems and excessive use of groundwater for fresh water.

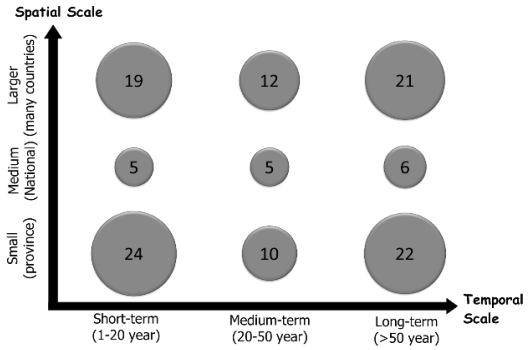

Fig. 3. Study methods in terms of spatial and temporal scale

Moreover, in terms of time and spatial scale, most studies are conducted within a short-term period and small region. The temporal scale is defined as the duration of disaster or resilience in the articles. In y-axis, we divided the spatial scale into three categories, namely small for specific province or district, medium for national scope, and larger ones for the papers covering many countries. For example, the study of adapting planning of climate change in four deltas [28] is categorized as a larger scale. As shown in figure 3, many studies were conducted in a short-term period and in small area. Though, the number of studies conducted in a long-term period covering small and larger area is

Table 1 Summarized of idea about reviewing some papers

Author	Methods	Result/Conclusion	Spatial Scope			Type of Resilience		
			S	M	L	Infra	Social	Gov
Syvitski,2009	Using High resolution Shuttle Radar Topography in delta related to mean sea level to see delta sinking and Moderate Resolution Imaging Spectroradiometer images to set the recent flooding from storm surge or river run-off	Most of the deltas are sinking faster than global sea level rising and below sea level, so during the storm surge it will easy to inundated.			✓	✓		
Jeuken,2015	Comparing 4 deltas (Dutch Delta Program, Thames estuary 2100, PlaNYC2013, Jakarta Coastal Defence) with approaching of adaptation planning framework and find the most adequate actions	Adaptations planning in deltas should prepare for future scenarios of climate, subsidence, socioeconomic with a robust and flexible actions			✓	✓	✓	✓
Nguyen KV,2013	Qualitative and quantitative approaches to conceptualize household resilience to floods in Mekong delta, Vietnam by forum group discussions, questionnaire, and interview.	characteristics of household resilience are capable of self-organizations (supply food during flood season), cope the disturbance in terms housing sector, doing creative things (create jobs for local labor in flood seasons)	✓				✓	
Verschuur, J., Kolen, B., & van Veelen, P. C, 2017	Doing flood risk assessment combining from economic risk (GDP) and fatal risk (population) based on inundation simulation of global hydrological model (PCR-GLOBWB) with climate change projections in 2030 RCP8.5 (worst scenario)	38 deltas cities has been assessed with measuring flood index every city and Risk in million Euro anually. The highest rank of total list in 2015 is Buenos Aires, Argentina and in 2030 is Tianjin, China. The lowest ranks in 2015 and 2030 is Port Elizabeth, South Africa		✓	✓	✓	✓	

almost the same with the short-term ones, the condition is different once we are looking at the number of studies conducted in a national scale or medium-term period. The number of articles which have criticized the resilience delta in national scope are limited.

Table 1 shows the summarized of reviewing some papers in this study. Current results showed many researcher has been studied in the world-wide scope and combining infrastructure and social together in terms to evaluate cities resilience. People are doing adaptation to do

A. Recent achievement and reviewing current methodology

The result has indicated that the flood that frequently occurred in the Asia region created an opportunity for the researchers to conduct the study. It is evident that the highest delta regions population growth is located in Asia especially in South Asia (Bangladesh, India, and Pakistan) [40]. Less developed region and dense population compose the fragile circumstances against water-disaster. For instances, several flood incidents in Dhaka, Bangladesh in 1988, 1998, and 2004 have caused huge damaged [30]. In the early 20th century, China experienced the deadliest natural disaster in Yangzi-Huai River because of the single flood incident [23]. Even now, in the Pearl River Basin, the flood risk is increasing due to the booming of socio-economy and growing population [65]

The cutting edge in Geographic Information System (GIS) using satellite images is enhancing the global scope of the study, for example, the subsidence cities and increasing sea level because of climate change [57]. Merging with IPCC fifth Assessment Report (AR5) in 2014, the prediction of the inundation caused by climate change mainly based on the RCP projection in 2100. In terms of the study based on time scale, IPCC provides the study that can be used as a global standard parameter to project the carbon concentration in the future. For example, the studies on the inundation in Nile River, Egypt [8], Mekong Delta, Vietnam [51,53,58], Beas River Basin, India [54] or the assessment of the mangrove vulnerability in Fiji [16] mentioned and used the results from IPCC documents to analyse and forecast disasters. Not only IPCC, but some of the documents from World Bank related to population or GDP in every country also contribute to the assessment of the vulnerability index in delta cities [62].

Using technology with social impact are required to get the holistic approach about resilience toward disaster. Vulnerability is not just registered by exposure to hazard but also by how people deal with the system in experiencing the hazard [9]. Furthermore, the human activities have had an interior growing risk of coastal flooding, wetland loss, and subsidence [57]. Scholars realized that the connection between social-economy and climate change factors should be accounted for in order to get more reliable outcomes. If the residents still have the normalcy bias towards disasters, the exposure degree to such disasters is still high regardless of how advanced the infrastructure against the disaster is built. The study of 2004 Indian Ocean Tsunami post-disaster revealed that building infrastructure and developing cultural awareness towards disasters can increase the resilience [56]

The importance of mutual assistance among delta cities around the world has been realized. The establishment of C40 Cities Climate Leadership Group in 2005 proves the benefit of collaboration. This group connects 90 world greatest cities, two-thirds of which are located in coastal delta regions [10]. Another institution, Deltares, has developed a method for assessing flood risk of the cities worldwide based on open data. They released the index to measure the vulnerability of 38 cities against flood disaster. Creating a global parameter to measure the capability of the city is required to evaluate delta city in the same manner [62]

B. Missing Gaps

There are missing gaps in recent publications, especially in Oceanian. Oceania will experience directly the impact from rising sea water level because consists of small islands and are prone to storm disaster. Because of the GDP and population are not as high and dense as in Asian countries, it makes lack

of research. Omitting this region from vulnerability assessment will create colossal shock later on.

The number of papers on a national scale and within a medium-term period is limited. Mostly the research scope only emphasizes on one particular place. Improving and evaluating the national resilience outlook in the delta regions might give an insight to the residents to increase their awareness and sensibility against disaster. Medium-term scale should also be considered while creating plan in the society because both environment and climate are dynamic. Merely focusing on long-term plan is too risky. The larger number of articles on Asia does not mean that all the places in Asia have been covered. Many research papers only concentrate on one country for study location. For example, in Asia and Europe, the studies mostly focus on Bangladesh/Vietnam and the Netherlands respectively, accounting for more than ten papers. Though those places are prone to disasters, conducting some studies equally on other regions is essential to get the better outcome.

The current literature has yet to encompass the entire delta cities in the world. The big delta covers 75 places based on the Department of Geology & Geophysics at Louisiana State University data, the research recently just discussed 70% of the total delta locations. Whereas, the global climate change should be anticipated as soon as possible in whole deltas. The academic contributions are necessary for stakeholders as a reference to establish resilience. Another missing gap in this study is the absence of paper on the tsunami resilience assessment. Most tsunami evaluations are only based on historical data such as from Indian Ocean tsunami 2004 or Japan tsunami 2011. Tsunami regularly causes enormous impact and traumatic memory to the society. Giving an account of tsunami will be useful to measure the vulnerability or resilience city.

C. The Future Path of Research Development

There are several future paths for academia to develop research related with disaster resilience in delta cities:

1. Integrate the policy sector to reassess the delta vulnerability index. The policy from the city or national government is crucial to fortify the people reliance which can decrease the vulnerability percentage. The index should also be covered for all the water-related disaster, not only flood.
2. Conduct the research about tsunami prediction in worldwide scope and apply profiling the risk assessment for a tsunami in delta city due to tsunami impact is really devastated. Creating initial research for worldwide tsunami forecast will be a breakthrough.
3. Use the new scenario framework for climate change research with shared socioeconomic pathways (SSP) and share climate policy assumption (SPA) [41,59]/
4. Investigate some other deltas, such as Limpopo in Mozambique, Volta in Ghana, or Mahakam in Indonesia. These places are decided by referring the risk trends for delta worldwide which was published by Tessler et al. (2015) [60] on Science. Mostly in Africa region, many big delta cities have not been addressed in scientific analysis report by the researchers. Moreover, the countries in the Oceanian region are needed to calculate the vulnerable index to prevent lousy havoc in the future due to sea level rise.

Conclusions

Population growth in delta regions boosts the risk toward water-related disasters. Resilience against hazard is introduced in three ways, infrastructure resilience, social and ecological resilience, and governance resilience. Reviewing papers gives the result that latest studies mostly concentrates in Asian and European regions especiallyon flood and climate change. Current trend methods are shifting from pure science to integrating social aspect and the scope becoming broadens due to the cutting edge of geospatial technology. IPCC documents with RCP scenario influence the study on climate change issue. However, more studies in tsunami resilience, introducing a standard parameter, and enhancing research in other deltas are highly recommended to fill the gaps in this study.

We acknowledge the limitation because the method only covers the keywords in abstract section. It is possible that there are some studies related to this topic that does not mention the words "resilience" and "disaster" in their abstracts. The water-related disasters that we discussed do not include the drought, landslide or avalanche, and water-borne disease. Nevertheless, we believe that the information in this study is sufficiently enough to review the current situation and to give an insight for researchers to conduct further study.

Acknowledgment

This research was supported by Civil Engineering, University of Tokyo and Indonesian Endowment Fund for Education (LPDP) for funding the study of the first author.

References

[1] Aerts, Jeroen, David C. Major, Malcolm J. Bowman, Piet Dircke, and M. Aris Marfai. "Connecting delta cities: coastal cities, flood risk management and adaptation to climate change". 2009.

[2] Alongi DM. "Mangrove forests: resilience, protection from tsunamis, and responses to global climate change. Estuarine, Coastal and Shelf ",Science, vol 76 no 1, January 2008, pp.1-13.
[3] Amer R, Kolker AS, Muscietta A. "Propensity for erosion and deposition in a deltaic wetland complex: Implications for river management and coastal restoration," Remote Sensing of Environment, vol 199, September 2017,pp.39-50.
[4] Armaş I, Avram E. "Perception of flood risk in Danube Delta, Romania," Natural hazards,vol 50 no 2, August 2009, pp.269-287.
[5] Arnold, Margaret, Robin Mearns, Kaori Oshima, and Vivek Prasad. "Climate and disaster resilience: The role for community-driven development," 2014.
[6] Aung, Toe Toe, Yukira Mochida, and Maung Maung Than. "Prediction of recovery pathways of cyclone-disturbed mangroves in the mega delta of Myanmar," Forest ecology and management, vol 293, April 2013, pp.103-113.
[7] Aung TT, Mochida Y, Than MM. "Prediction of recovery pathways of cyclone-disturbed mangroves in the mega delta of Myanmar," Forest ecology and management, vol 293, April 2013, pp.103-13.
[8] Batisha AF. "Implementing fuzzy decision making technique in analyzing the Nile Delta resilience to climate change," Alexandria Engineering Journal, vol 54 no 4, December 2015, pp.1043-1056.
[9] Berkes F."Understanding uncertainty and reducing vulnerability: lessons from resilience thinking," Natural hazards, vol 41 no 2, May 2007 pp.283-295.
[10] C40 Cities. "Climate change adaptation in delta city," 2016.
[11] Carle MV, Sasser CE."Productivity and resilience: long-term trends and storm-driven fluctuations in the plant community of the accreting Wax Lake Delta," Estuaries and coasts, vol 39 no 2, March 2016 pp.406-22.
[12] Chandler D."Beyond neoliberalism: resilience, the new art of governing complexity," Resilience, vol 2 no 1, January 2014, pp.47-63.
[13] Darby SE, Dunn FE, Nicholls RJ, Rahman M, Riddy L. "A first look at the influence of anthropogenic climate change on the future delivery of fluvial sediment to the Ganges–Brahmaputra–Meghna delta,"Environmental Science: Processes & Impacts, vol 17 no 9, 2015, pp.1587-1600.
[14] Dewulf A, Termeer C. "Governing the future? The potential of adaptive delta management to contribute to governance capabilities for dealing with the wicked problem of climate change adaptation," Journal of Water and Climate Change, vol 14, July 2015.
[15] Elias EP, van der Spek AJ. "Dynamic preservation of Texel Inlet, the Netherlands: understanding the interaction of an ebb-tidal delta with its adjacent coast," Netherlands Journal of Geosciences, vol 96 no 4, December 2017, pp.293-317.
[16] Ellison JC. "Vulnerability assessment of mangroves to climate change and sea-level rise impacts." Wetlands Ecology and Management, vol 23 no 2, April 2015, pp.115-137.
[17] Ewing L. "Community resilience to coastal disasters," University of Southern California, 2014.
[18] Field CB, Barros V, Stocker TF, Dahe Q, editors. "Managing the risks of extreme events and disasters to advance climate change adaptation: special report of the intergovernmental panel on climate change," May 2012,Cambridge University Press.
[19] Folke C. "Resilience: The emergence of a perspective for social–ecological systems analyses," Global environmental change vol 16 no 3, August 2006, pp.253-267.
[20] Francesch Huidobro MD. "The Governance of Climate Adaptation in Flood-Prone Delta Cities: Issues on Spatial Planning and Flood Risk Management," InNUS-Energy Studies Institute Seminar, 2015.
[21] Gersonius B, Rijke J, Ashley R, Bloemen P, Kelder E, Zevenbergen C. "Adaptive Delta Management for flood risk and resilience in Dordrecht, The Netherlands," Natural Hazards, vol 82 no 2, June 2016, pp.201-216.
[22] Ghosh A, Mukhopadhyay S. "Vulnerability assessment through index modeling: a case study in Muriganga–Saptamukhi estuarine interfluve, Sundarban, India," Arabian Journal of Geosciences,vol 10 no 18, September 2017,pp.408.
[23] Grayman WM. "Water-related disasters: A review and commentary," Frontiers of Earth Science, vol 5 no 4, December 2011, pp.371-377.
[24] Hajra R, Szabo S, Tessler Z, Ghosh T, Matthews Z, Foufoula-Georgiou E. "Unravelling the association between the impact of natural hazards and household poverty: evidence from the Indian Sundarban delta," Sustainability Science, vol 12 no 3, May 2017, pp.453-464.
[25] Holling CS. "Resilience and stability of ecological systems," Annual review of ecology and systematics, vol 4, November 1973,pp.1-23.
[26] Ibáñez C, Day JW, Reyes E. "The response of deltas to sea-level rise: natural mechanisms and management options to adapt to high-end scenarios," Ecological engineering, vol 65, April 2014, pp.122-130.
[27] Pachauri RK, Allen MR, Barros VR, Broome J, Cramer W, Christ R, Church JA, Clarke L, Dahe Q, Dasgupta P, Dubash NK. "Climate change 2014: synthesis report. Contribution of Working Groups I, II and III to the fifth assessment report

of the Intergovernmental Panel on Climate Change," IPCC; 2014.

[28] Jeuken A, Haasnoot M, Reeder T, Ward P. "Lessons learnt from adaptation planning in four deltas and coastal cities," Journal of Water and Climate Change, vol 6 no 4, December 2015, pp.711-728.

[29] Karanja JM, Saito O. "Cost–benefit analysis of mangrove ecosystems in flood risk reduction: a case study of the Tana Delta, Kenya," Sustainability Science, vol 13 no 2, March 2018, pp.503-516.

[30] Khan DM, Veerbeek W, Chen AS, Hammond MJ, Islam F, Pervin I, Djordjević S, Butler D. "Back to the future: assessing the damage of 2004 DHAKA FLOOD in the 2050 urban environment," Journal of Flood Risk Management, vol 11, January 2018, pp.S43-54.

[31] Klijn F, van Buuren M, van Rooij SA. "Flood-risk management strategies for an uncertain future: living with Rhine River floods in the Netherlands?," AMBIO: A Journal of the Human Environment, vol 33 no 3, May 2004, pp.141-147.

[32] Kriegler E, Edmonds J, Hallegatte S, Ebi KL, Kram T, Riahi K, Winkler H, Van Vuuren DP. "A new scenario framework for climate change research: the concept of shared climate policy assumptions," Climatic Change, vol 122, February 2014, pp.401-414.

[33] Larsen RK, Calgaro E, Thomalla F. "Governing resilience building in Thailand's tourism-dependent coastal communities: Conceptualising stakeholder agency in social–ecological systems," Global Environmental Change, vol 21 no 2, May, pp.481-491.

[34] Leal Filho W, Modesto F, Nagy GJ, Saroar M, YannickToamukum N, Ha'apio M. "Fostering coastal resilience to climate change vulnerability in Bangladesh, Brazil, Cameroon and Uruguay: a cross-country comparison," Mitigation and Adaptation Strategies for Global Change., vol 23 no 4, April 2018, pp.579-602.

[35] Liao KH, Le TA, Van Nguyen K. "Urban design principles for flood resilience: Learning from the ecological wisdom of living with floods in the Vietnamese Mekong Delta," Landscape and Urban Planning, vol 155, November 2016, pp.69-78.

[36] Moffett KB, Nardin W, Silvestri S, Wang C, Temmerman S. "Multiple stable states and catastrophic shifts in coastal wetlands: Progress, challenges, and opportunities in validating theory using remote sensing and other methods.," Remote Sensing, vol 7 no 8, August 2015, pp.10184-10226.

[37] Morita A. "Infrastructuring amphibious space: the interplay of aquatic and terrestrial infrastructures in the Chao Phraya Delta in Thailand," Science as Culture, vol 25, January 2016, pp.117-140.

[38] Morrison A, Westbrook CJ, Noble BF. "A review of the flood risk management governance and resilience literature," Journal of Flood Risk Management, vol 11, September 2018, pp.291-304.

[39] Musa ZN, Popescu I, Mynett A. "The Niger Delta's vulnerability to river floods due to sea level rise," Natural Hazards and Earth System Sciences vol 14 no 12, December 2014, pp.3317-3329.

[40] Neumann B, Vafeidis AT, Zimmermann J, Nicholls RJ. "Future coastal population growth and exposure to sea-level rise and coastal flooding-a global assessment," PloS one, vol 10 2015,p.e0118571.

[41] Ng ST, Xu FJ, Yang Y, Lu M, Li J. "Necessities and challenges to strengthen the regional infrastructure resilience within city clusters," Procedia engineering, vol 121, January 2018, pp.198-205.

[42] Nguyen KV, James H. "Measuring household resilience to floods: a case study in the Vietnamese Mekong River Delta," Ecology and Society, vol 18, September 2013.

[43] O'Neill BC, Kriegler E, Riahi K, Ebi KL, Hallegatte S, Carter TR, Mathur R, van Vuuren DP. "A new scenario framework for climate change research: the concept of shared socioeconomic pathways. Climatic Change," vol 122 no 3, February 2014, pp.387-400.

[44] Owrangi AM, Lannigan R, Simonovic SP. "Mapping climate change-caused health risk for integrated city resilience modeling," Natural Hazards, vol 77, May 2015, pp.67-88.

[45] Pelling M, Blackburn S, editors. "Megacities and the coast: risk, resilience and transformation," Routledge, January 2014.

[46] R. Haitsma. "An explorative research on monitoring flood resilience in Delta Cities," Master thesis land use planning, 2016, LUP-80436.

[47] Renaud FG, Le TT, Lindener C, Guong VT, Sebesvari Z. "Resilience and shifts in agro-ecosystems facing increasing sea-level rise and salinity intrusion in Ben Tre Province, Mekong Delta.," Climatic change, vol 133, November 2015, pp.69-84.

[48] Renaud FG, Syvitski JP, Sebesvari Z, Werners SE, Kremer H, Kuenzer C, Ramesh R, Jeuken A, Friedrich J. "Tipping from the Holocene to the Anthropocene: How threatened are major world deltas?,"Current Opinion in Environmental Sustainability, vol 5, December 2013, pp.644-654.

[49] Restemeyer B, van den Brink M, Woltjer J. "Between adaptability and the urge to control: making long-term water policies in the Netherlands," Journal of environmental planning and management, vol 60, May 2017, pp.920-940.

[50] Schiermeier Q. "Floods: holding back the tide," Nature News, vol 508, April 2014; pp.164.
[51] Schmitt K, Albers T, Pham TT, Dinh SC. "Site-specific and integrated adaptation to climate change in the coastal mangrove zone of Soc Trang Province, Viet Nam," Journal of Coastal Conservation, vol 17, September, pp.545-558.
[52] Seddon AW, Froyd CA, Leng MJ, Milne GA, Willis KJ. "Ecosystem resilience and threshold response in the Galápagos coastal zone," PloS one, vol 6, July 201,pp.e22376.
[53] Smith TF, Thomsen DC, Gould S, Schmitt K, Schlegel B. "Cumulative pressures on sustainable livelihoods: coastal adaptation in the Mekong Delta," Sustainability, vol 5, January 2013, pp.228-241.
[54] Soundharajan BS, Adeloye AJ, Remesan R. "Evaluating the variability in surface water reservoir planning characteristics during climate change impacts assessment," Journal of Hydrology, vol 538, July 2016,pp.625-639.
[55] Stead D. "Urban planning, water management and climate change strategies: adaptation, mitigation and resilience narratives in the Netherlands," International Journal of Sustainable Development & World Ecology, vol 21, January 2014, pp.15-27.
[56] Stephan C, Norf C, Fekete A. "How "Sustainable" are Post-disaster Measures? Lessons to Be Learned a Decade After the 2004 Tsunami in the Indian Ocean," International Journal of Disaster Risk Science, vol 8, March 2017, pp.33-45.
[57] Syvitski JP, Kettner AJ, Overeem I, Hutton EW, Hannon MT, Brakenridge GR, Day J, Vörösmarty C, Saito Y, Giosan L, Nicholls RJ. "Sinking deltas due to human activities," Nature Geoscience, vol 2, 209, pp.681–686.
[58] Takagi H, Thao ND, Anh LT. "Sea-level rise and land subsidence: Impacts on flood projections for the Mekong delta's largest city," Sustainability, vol 8, September 2016, pp.959.
[59] Termeer CJ, Dewulf A, Karlsson-Vinkhuyzen SI, Vink M, van Vliet M. "Coping with the wicked problem of climate adaptation across scales: The Five R Governance Capabilities," Landscape and Urban Planning, vol 154, October 2016, pp.11-19.
[60] Tessler ZD, Vörösmarty CJ, Grossberg M, Gladkova I, Aizenman H, Syvitski JP, Foufoula-Georgiou E. "Profiling risk and sustainability in coastal deltas of the world," Science, vol 6248,August 2015,pp.638-643.
[61] Thomalla F, Lebel L, Boyland M, Marks D, Kimkong H, Tan SB, Nugroho A. "Long-term recovery narratives following major disasters in Southeast Asia," Regional Environmental Change vol 18, April 2018 pp.1211-1222.
[62] United Nations, Department of Economic and Social Affairs, Population Division. "The world Cities in 2016," 2016.
[63] Verschuur, J., Kolen, B., & van Veelen, P. C. "Flood Delta City Index: Drivers to Support Adaptation of Cities,' 2017.
[64] Wolters ML, Kuenzer C. "Vulnerability assessments of coastal river deltas-categorization and review," Journal of coastal conservation, vol 19, June 2015, pp.345-368.
[65] Zhang Q, Gu X, Singh VP, Xiao M. "Flood frequency analysis with consideration of hydrological alterations: Changing properties, causes and implications," Journal of hydrology vol 519, November. 2014, pp.803-813.

Assessments of Groundwater–Surface Water Connectivity for the Lower Yom and Nan Rivers

Soonthornnonda, P.[1,*], Chuenchooklin, S.[1], Pratoomchai, W.[1], Saraphirom, P.[2] and Saenchai, P.[2]

Abstract This study outlined the first-time assessments of groundwater–surface water connectivity for the Lower Yom and Nan Rivers. The direct measurements of exchange fluxes using seepage meters were carried out. The diurnal flow directions between groundwater and surface water were then investigated based on thermal conditions in streambeds (8-m depth within the sediment). The study's findings exhibited seasonal influxes and effluxes (-4.32 to 163 cm/day for the Lower Nan and -1.90 to 198 cm/day for the Lower Yom) of surface water associated with groundwater. In addition, the rapid thermal responses (approximately 1.5 degree Celsius) in the streambed due to high rates of infiltration were diurnally evident. The groundwater–surface water interactions are essential for laying the foundations of conjunctive water management approach. Better understandings of the groundwater–surface water connectivity would help enhancing integrated water resource planning and management at the river basin level in order to achieve the efficiency of agricultural production, economic equality, and environmental sustainability.

Keywords *groundwater connectivity, exchange fluxes, seepage meters, infiltration, conjunctive water management.*

[1]Department of Civil Engineering and Water Resources Research Center, Faculty of Engineering, Naresuan University, Phitsanulok 65000, Thailand.
[2]Groundwater Resources Research Institute, Khon Kaen University, Khon Kaen 40002, Thailand.

Introduction

This study illustrated the first-time assessments of groundwater–surface water connectivity for the Lower Yom and Nan Rivers. The direct measurements of exchange fluxes using seepage meters were carried out. The diurnal flow directions between groundwater and surface water were then investigated based on thermal conditions in streambeds at 8-m depth within the sediment. The groundwater-surface water interactions are essential for laying the foundations of conjunctive water management approach. Better understandings of the groundwater-surface water connectivity would help enhancing integrated water resource planning and management at the river basin level in order to achieve the efficiency of agricultural production, economic equality, and environmental sustainability.

Materials and Methods

A. Monitoring sites

Ten monitoring sites of seepage fluxes were chosen from the total Lower Yom and Nan River Basin areas (Figure 1). The Y6-L (Gravelly Sandy Clay) and DR2.8Y-L (Sand Bar) were located at the left side of Yom River in Si Satchanalai District (Sukhothai Province) and Bangkratum District (Phitsanulok). The DR2.8Y-R (Sand Bar) was located at the right side of Yom River in Bangkratum District (Phitsanulok). The N60-L (Sand Bar) and N67-L (Loamy Sand) were located at the left side of Nan River in Tron District (Uttaradit Province) and Chum Saeng District (Nakhon Sawan Province). The N60-R (Loamy Sand), N27A-R (Clay), WTRN-R (Clay), DR2.8N-R (Clay), and N67-R (Clay) were located at the right side of Nan River in Tron District (Uttaradit Province), Phrom Phiram District (Phitsanulok), Mueang Phitsanulok District (Phitsanulok), Bangkratum District (Phitsanulok), and Chum Saeng District (Nakhon Sawan Province), respectively. These 262 exchange flux measurements were conducted during October 2017 to April 2018.

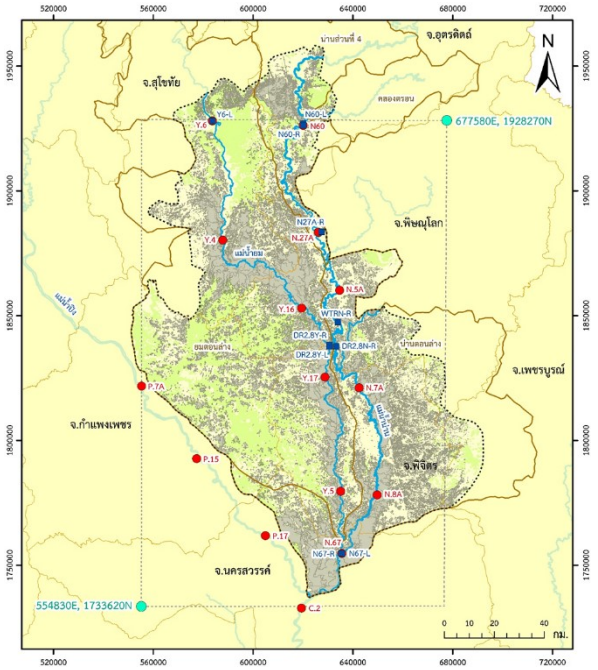

Fig. 1. Monitoring sites of seepage fluxes.

B. Seepage meters

This cylindrical seepage meter was developed based on [1 & 2]. The seepage meter was made from the stainless steel with the 30-cm height, and its diameter is 57 cm. There are two valves in the meter. The first valve is for releasing air inside the meter, and the second valve is for letting the water out (Figure 2). The black hose (1-cm diameter and 1-m length) is used to connect the second valve with the plastic box. This plastic box contains the plastic bag for storing the water which comes out of the second valve. In addition, the box will not allow the flowing river water to directly contact with the plastic bag. This would prevent the excessive stored water in the plastic bag. The seepage meter is normally placed on the riverbed with 10-cm depth. After getting rid of the air inside the meter, each measurement then begins [3].

Fig. 2. Seepage meter components.

C. Exchange Flux Determination

By recording the water volume contained in the bag at the times of emplacement and removal, the volumetric seepage flux is computed by

$$Q=\frac{V_{t2}-V_{t1}}{t_2-t_1} \quad (1)$$

where V_{t1} is the volume contained in the bag at the start of the measurement period (cm^3), V_{t2} is the volume in the bag at the end of the measurement period, and t_1 and t_2 are the times at the start and end of the measurement period (day). Dividing the volumetric seepage flux by the area of seepage cylinder (0.25 x π x 57^2 = 2,553 cm^2) gives seepage flux in length per time (cm/day) [3] as

$$q=\frac{Q}{A} \quad (2)$$

D. Streamflow Information

There are relevant 3 hydrological monitoring sites for the Yom River (i.e., Y6, Y16, and Y17), and 5 hydrological monitoring sites for the Nan River (i.e., N5A, N7A, N27A, N60, and N67) from Thai Royal Irrigation Department [hydro-2.rid.go.th and hydro-5.rid.go.th]. Selected monthly streamflow during the year 2017-2018 (based on seepage monitoring months in Figure 1) are exhibited in Table 1. One example of cross-sectional schematic for Y6 is illustrated in Figure 3.

Table 1. Selected monthly streamflow during the year 2017-2018 based on seepage monitoring months.

Monitoring Months	Hydrological Monitoring Sites							
	Y6	**Y16**	**Y17**	**N5A**	**N7A**	**N27A**	**N60**	**N67**
October 2017	860							
November 2017							139	
December 2017		58.0	236					
January 2018				662	708	634		770
February 2018	27.1							
April 2018	7.33							

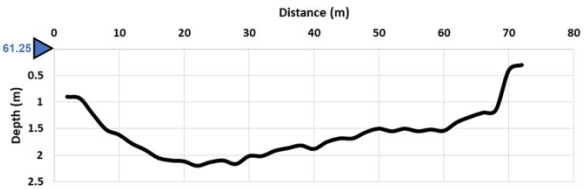

Fig. 3. A cross-sectional schematic of Y6 (April 2018).

E. Streambed thermal measurements

The DR2.8Y-L and DR2.8N-R were selected to install the 8-m and 6-inch PVC wells, and Lutron (TM-1947SD) Temperature Data Loggers (Figure 4 and Table 2). Both thermocouple probes were then placed at the riverbed surface outside the well and 8-m depth inside the well. The temperature measurements were carried out during July 2018.

Fig. 4. Streambed thermal measurement sites.

Table 2. Riverbed information for thermal measurement sites

Site Code	Well Depth (m)									
	1	2	3	4	5	6	7	8	9	10
DR2.8Y-L	Sand					Clay		Sand		
DR2.8N-R	Clay								Sand	

Results and Discussion

A. Exchange fluxes

Most observed exchange fluxes had positive values, and there were decreasing tendencies towards the drier season (-4.32-163 cm/day for the Lower Nan and -1.90-198 cm/day for the Lower Yom) (Figures 5 and 6). These would indicate the flow direction from the groundwater into the river. The higher fluxes were observed while the seepage meter were placed closer to the river bank. Sometimes when a rice farmer pumped the groundwater from the well next to the river for irrigating the paddy field, negative flux with fluctuated values were evident. Exchange fluxes, obtained from the monitoring site closed to the municipal area, were fluctuated.

The median influx (Groundwater Discharge) for the Lower Yom River were generally found to be ~1.5 times higher than that for the Lower Nan River. Upper areas of the Lower Yom River had the greater amount of groundwater discharge than lower areas. Upper areas of the Lower Nan River had the lesser amount of groundwater discharge than lower areas.

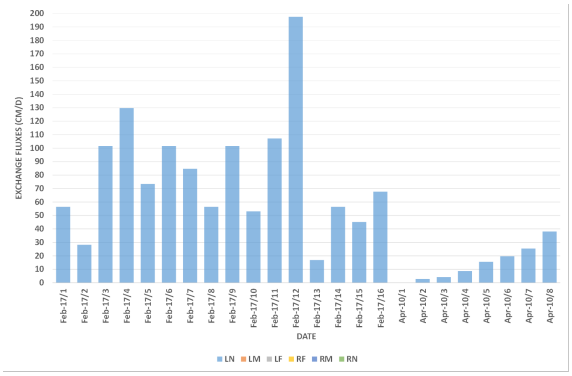

Fig. 5. Exchange fluxes observed from Y6 (February and April, 2018).

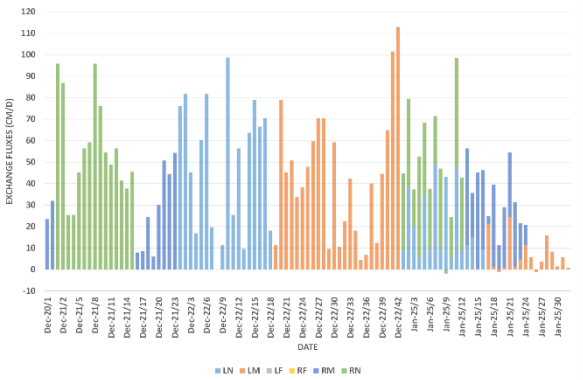

Fig. 6. Exchange fluxes observed from DR2.8Y (December 2017 and January 2018).

B. Streambed thermal conditions

Higher streambed thermal variations at the 8-m depth and sediment surface were found at site DR2.8N-R. The clay layer of riverbed at the 8-m depth could be able to maintain the water temperature, while the sand layer could not. Both temperatures (Figures 7 and 8) were higher from 7 am to 3 pm (peaks). The temperatures then decreased and returned to the original stage around 8-10 pm.

There were possibilities that the losing river occurs from 7 am to 3 pm, and the gaining river occurs from 3 pm to the equilibrium state around 8-10 pm at night. In addition, the rapid thermal responses (approximately 1.5 degree Celsius) in the streambed due to high rates of infiltration [4 & 5] during 7-10 am were diurnally evident.

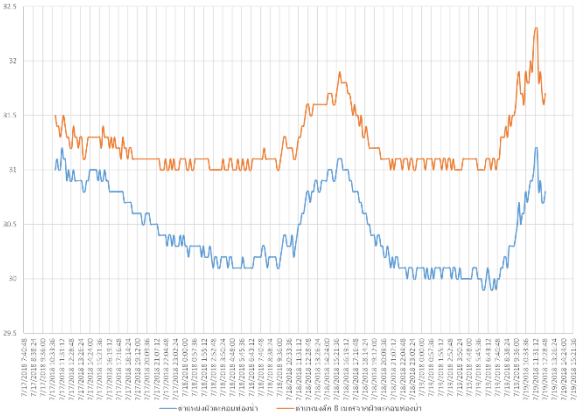

Fig. 7. Riverbed thermal conditions at DR2.8Y-L.

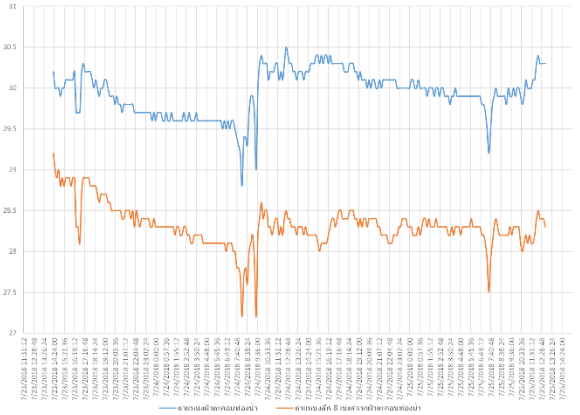

Fig. 8. Riverbed thermal conditions at DR2.8N-R.

C. Conjunctive Water Management

Inquires to the local farmers indicate that the shallow groundwater is conjunctively used for irrigating their paddy fields. Due to the lower groundwater table, wells with lowering pumping machines are normally evident in the area. These wells are also dangerous for routine maintenance. The major reason for the lower groundwater table is that the groundwater use has exceeded the natural replenishment of groundwater. The conjunctive water management with new and/or exiting recharge facilities (e.g., dug wells and irrigated canals) could be an option.

Conclusions

On the basis of this work, we draw the following conclusions:

1. The cylindrical seepage meter is well applied for direct measurement of exchange flux. This is demonstrated for the Lower Yom and Nan Rivers during October 2017 to April 2018.
2. Exchange fluxes of -4.32 to 163 cm/day for the Lower Nan and -1.90 to 198 cm/day for the Lower Yom exhibit similar decreasing tendencies towards the drier season.
3. The groundwater has discharged into the Lower Yom River ~1.5 times higher than the Lower Nan River.
4. The rapid thermal responses in the streambed are due to high rates of infiltration (High Groundwater Recharge in the Morning). The exchange direction could then vary throughout the day (Groundwater Discharge in the Late Afternoon and Evening).
5. The conjunctive water management approach may be taken into consideration in the use of new and/or existing facilities for recharging the groundwater due to imbalance of groundwater use and natural replenishment.

Acknowledgment

This work is supported by the Groundwater Development Fund (พ5/2560), Thai Department of Groundwater Resources (DGR). We thank Banjong Promchan, Jittrakorn Suwanlert, Tussanee Nettasana, and other relevant Thai DGR staffs for providing all data and helpful discussions.

References

[1] C. Zamora, Estimating Water Fluxes Across the Sediment-Water Interface in the Lower Merced River, California, Scientific Investigations Report 2007–5216, U.S. Geological Survey: Reston, Virginia, 2008.
[2] D. O. Rosenberry, "A seepage meter designed for use in flowing water," J. Hydrol., vol.359, pp.118-130, June 2008.
[3] J. T. Anderson, C.A. Davis, Wetland Techniques, Voume 1 Foundation, Springer: New York, 2013.
[4] J. Constantz, "Heat as a tracer to determine streambed water exchanges," Water Resour. Res., vol.44, pp.1-20, December 2008.
[5] U.S. Geological Survey (USGS), Heat as a Tool for Studying the Movement of Ground Water Near Streams, Circular 1260, U.S. Geological Survey: Reston, Virginia, 2003.

Grid-based Socioeconomic Database For Exposure Estimation in Flooding Risk Analysis

Ling Feng Chang[1,a], Wen-Tsun Feng[2,b] and MingDaw Su[3,c,*]

Abstract Floods are among the most frequent and costly natural disasters in terms of human hardship and economic loss. Most of the governments invest heavy resources to provide information for impact mitigation of this natural disaster. Flood Risk Maps are vital information in regional planning for flood disaster mitigation. This precious information about flooding disaster characteristics cannot be established with the absences of socioeconomic data and vulnerability models for damage assessment.

This paper will present a grid-based spatial database to capture the regional variations in socioeconomic data for better loss and risk assessments in risk analysis for flooding disaster mitigation. A 40m by 40m digital terrain model (DTM) available in Taiwan was commonly used in flood simulation. Although a new version DTM with 5m by 5m resolution has been established for better capture of terrain variations, a grid framework with 40m resolution will be used for this database construction considering the necessity for spatial variation representation in socioeconomic data.

Multiple sources were used for this database establishment including: Population Census, Agriculture Census, Commercial & Industrial Census, Building Administrations, Land use survey, Address Coordinate database, Manufactory and Business Registration, etc. Data from the above sources were spatially disaggregated from their original spatial units into the grid framework with 40m resolution.

Keywords *Flood risk, Socioeconomic, Exposure, Flood loss assessment, Census*

[1]Associate Research Fellow,
Agricultural Engineering Research Center,
TaoYuan, Taiwan
[2]Research Fellow and Acting Director,
Agricultural Engineering Research Center, Taiwan
TaoYuan, Taiwan
[3]Dept. of Bioenvironmental Systems Engineering,
National Taiwan University,
Taipei, Taiwan.

[a]changlf@aerc.org.tw
[b]wtfang@aerc.org.tw
[c]sumd@ntu.edu.tw

Introduction

A natural disaster is caused by major adverse events in natural (hydrological, geological, or metrological) processes. An adverse event will not rise to the disaster level if it occurs in an area without vulnerable population or economic activities. In a vulnerable area, it can have disastrous consequences causing loss of life, property, and lasting damage, requiring years to repair.

According to review on last 20-year records, the UNISDR shows that 90% of disasters are weather-related (floods, storms, droughts, etc.) and the rate of weather-related disasters is growing. Although the casualty from flood is reduced but it still affected more people than most of the other natural disasters (UNISDR,2015).

There is a growing importance and understanding that data collection, analysis, and management can help to identify disaster risks and make disaster management more efficient and effective. The need for systematic data for disaster mitigation and prevention is an increasing concern of both development and response agencies. According to Margareta Wahlström, UN Special Representative of the Secretary-General for Disaster: "Access to information is critical to successful disaster risk management. You cannot manage what you cannot measure." This paper proposed a grid-based socio-economic database for exposure estimations in the flood risk analysis and mitigation and even in emergency responses.

Risk Management Framework

In the process of handling the natural disaster impact to the society, a risk management framework as shown in figure 1 is usually followed. Risk must be identified and evaluated so that impact mitigation may be planned. A monitoring system may be established for early warning as the hazardous event occurs to reduce the impacts or damages. The recovery stage will follow the event and eventually into the risk analysis stage for reinvestigate the risk for better future events. The risk analysis and mitigation planning will be referred as "risk management" and the preparedness and recovery as the "emergency response". Risk management is much more important as it may reduce the panic and the severity of damages as the event hits.

Risk analysis is the key component in the risk management process and the analysis results will become vital basis for selection and implementation of disaster prevention and mitigation measures. The risk analysis of natural hazard composed of four components as hazard, exposure, vulnerability and resilience.

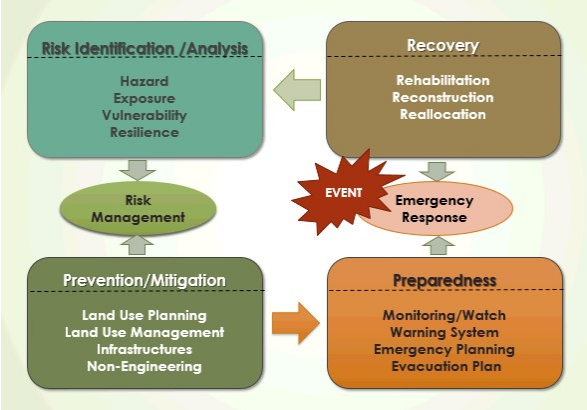

Fig. 1. The Risk Management Framework

The hazard may be defined as source of potential harm (ISO 31000, 2009). In flooding disaster, the hazard can be expressed as the inundation depths. The exposure is the extent to which an organization and/or stakeholder is subject to an event (ISO31000, 2009). In the case of flood disaster, the exposure is the population, housing, and other economic activities such as industry, commercial and agriculture that are inundated in the event. Vulnerability is the intrinsic properties of something resulting in susceptibility to a risk source that can lead to an event with a consequence. So it will be the relationship of the loss versus flooding depth for each categories of the above exposures. At last, resilience is the adaptive capacity of an organization in a complex and changing environment. In case of flood, resilience will be the capacity of the risk receptor to adapt to the disaster. The resilience can be viewed as the social vulnerability of the risk receptors because this will more related for socio-economical characteristics of the receptors (Martin, 2015).

The risk of natural disaster (take flood as an example) can be defined as the summation of the total damage under a single event (H*E*V) multiple by its occurrence probability for all the probable evens in a specific period (e.g. a year).

$$Risk=SUM(H*E*V*Pr.) \quad (1)$$

Where:
Risk: Expected annual loss (in $)
H: Hazard potential (inundation depth in flood)
E: Exposure (number of household, or acreage)
V: Vulnerability (Loss/Depth/unit household)
Pr: occurrence probability of the event

The above equation may be applied to a designated spatial unit, e.g. county, township, or unit grid in a mesh system, and the results from each unit in the region collectively produce a map showing the spatial distribution of the flood risk.

Exposures

As shown in equation (1), the flood risks are estimated from hazard (flood depth), exposure (socio-economic activities) with the loss functions (vulnerability). The flood hazard maps, generated from hydraulic model with hydrological and morphological data, are the most available data in most of the countries. The exposure data are another vital data for risk analysis. As stated in the talk of Rohini Swaminathan, she said "There is nothing natural about disaster."(Swaminathan,2016) Nature causes extreme events (usually called "hazards" when they threaten people), but people create disasters. So the exposure can be identified as the most important data in the process of risk analysis, since there will be no harm from a huge hazard if there is not any socio-economic activities at the site.

The "exposure" is defined by ISO as "the extent to which an organization and/or stakeholder is subject to an event". This includes all kind of socio-economic activities, and most of them can usually be linked with different land use: such as residential, commercial, industry, agriculture, husbandry, also life lines and public work (infrastructures).

Residential

All the socio-economic activities are developed by human and demographic data will be the most basic ones. Residential data of different living styles need to be established as the first batch in the exposure database. The residential data were separated into two major categories: Single Family and Multiple Family. As shown in Figure 2(a), single household in a single building is Single Family. A building used by multiple households as shown in Figure 2(b) is multiple family. These two living styles have very different characteristics. The single family may suffer to less loss than multiple family under same flooding depth, because valuables or people may be moved to higher floor.

Fig. 2. Residential Styles

Commercial

The commercial activities may be classified into three categories according to their loss characteristics from flooding: Retail, Wholesale, and Service. As shown in Figure 3, the wholesalers will pile their goods up to the ceiling while the retailers

won't. And the service stores, like banks have no merchandizes other than office equipment.

Fig. 3 Wholesaler, Retailer and Services

Industry

This category includes all the factories and manufacturing activities. The flooding loss features are the most complicated ones for modeling. The flooding losses may be dependent on the time of flooding and the kinds of the manufacturing activities. Even the same industry may be different from each other due to their manufacturing technology and equipment. There may be raw material, semi-finished products or products ready for shipping at the time of flooding.

Agriculture

The agriculture land use can be diversifies and have frequent variations from time to time. The flooding losses of perennial orchard and short term crops may be quite different. Some crops (e.g. peanuts) may be more sensitive to inundation than the others (e.g. sugarcane).

Husbandry/*Aquaculture*

Husbandry and aquaculture may be important activities in rural area. Different Livestock and poultry breeds, growth stages, and feeing methods may also have different loss features from flooding. Facilities like barn and stable may also be considered in damage assessments.

Infrastructures

Public work including transportations, life lines, schools and parks may be suffered from flooding loss and need to be considers as exposures in flooding risk analysis.

Data availability

From above discussions, it is complicated for an exposure database establishment. Many assumptions or approximations may have to be made depending on the data availability. This paper reports the Taiwanese experiences in constructing the exposure database for natural disaster risk management.

Census

The Directorate-General of Budget, Accounting and Statistics, Executive Yuan, Taiwan conducts three major censuses periodically, i.e. Population and housing Census (every 10 years); Agriculture, Forestry, Fishery and Animal Husbandry Census (every 5 years); and Industry and Service Census(every 5 years). The data are published aggregately based on spatial unit with different levels of aggregation for privacy concern.

Registries

The government kept a very efficient registry system for different kind of socioeconomic activities for management and taxes collection purposed. These include household and residence (for registered population), real estate properties, cars, business, and manufactories. All these registries linked with street addresses or cadastral IDs'. A geocoding system has been implemented for every single street addresses in Taiwan, so all the registered socioeconomic activities are GIS ready for further spatial analysis. Figure 4 shows a map of Taichung City at the central part of the Island with all the street addresses. The points shown in Fig.4 may have more than one point stacked together at a x-y coordinate since there maybe more than one street address in an apartment or high-rise building.

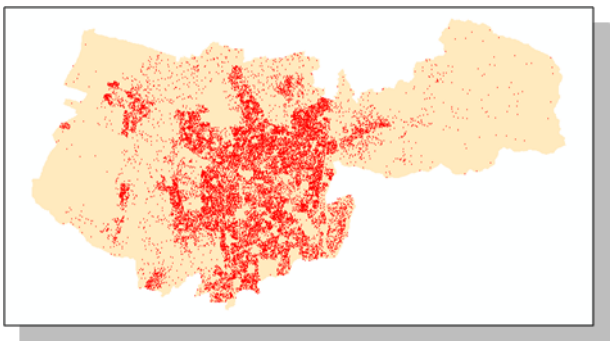

Fig. 4. Street Address Geocoding in Taichung City, Taiwan

Land use survey

A land use survey was also done for the whole country and was corrected/ adjusted as necessary from time to time. A sample map is shown in Figure 5. The Land Uses are categorized into three hierarchical levels. For example:

01: Agriculture;
0101: Crop;
010101: Paddy; 010103: Orchard;
0102: Aquaculture;
0103: Livestock;.

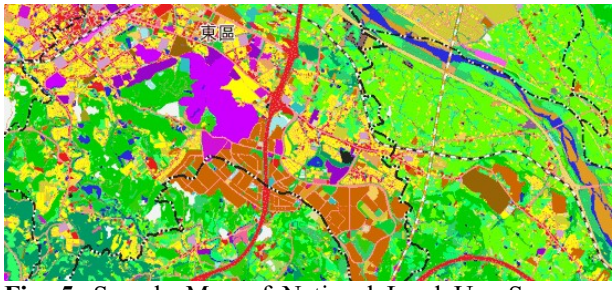

Fig. 5. Sample Map of National Land Use Survey, Taiwan

Data Statistical System

The socioeconomic data are related to persons and have privacy concerns. Most of the socioeconomic data usually disseminate after aggregation to some specific spatial administration units (e.g. city, county) for privacy protection. But this spatial aggregation may create problems distorting the spatial distribution patterns known as Modifiable Areal Unit Problem (MAUP). The spatial distribution pattern distortions may create problems of inequity or under/over designs in regional planning for public work, public health and safety. A Geographical Statistical Classification System, as shown in Fig. 6, was established for mitigation of MAUP in spatial aggregation for socioeconomic data disseminations.

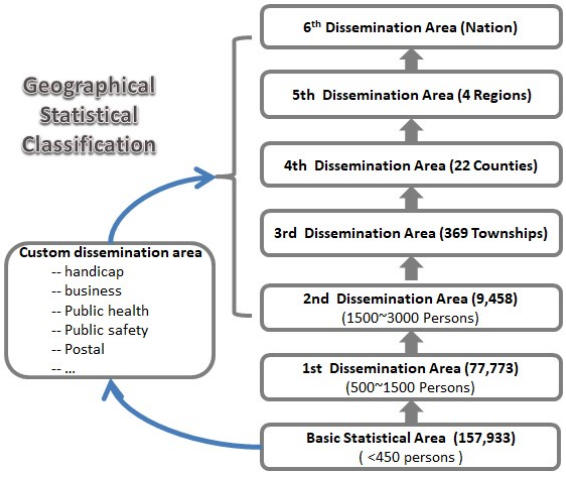

Fig. 6. Geographical Statistical Classification System

Grid-based database

All these exposure data will be overlaid with the hazard maps in flood risk analysis as shown in Figure 7. Since most of the flood simulation models are grid-based, the grid-base spatial data model is used for this exposure database implementation. A grid system with resolution of 40 meters is used to host all the related socioeconomic data in the exposure database system.

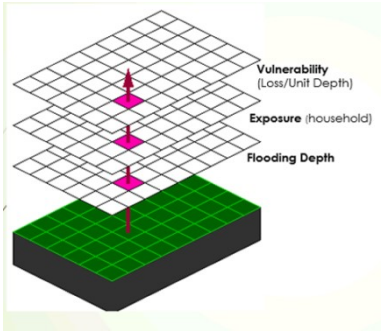

Fig. 7. Grid-based Flood Risk Estimations

Most of the socioeconomic data available in Taiwan are spatially aggregated to the selected level in Geographical Statistical System that is usually much larger than the 40m by 40m cell-system used in this paper, The multi-layer and multi-class Dasymetric model, as shown in eq.(1) (Su, et.al., 2010) and Figure 8. was used to redistribute the published aggregated socioeconomic data into the grid cell in our database, as shown in Figure 9.

$$D_{ij} = \frac{P_i \times (A_{ij} W_j)}{\sum_{j=1}^{m} A_{ij} W_j} \qquad (1)$$

Where i and j are the subscripts for areal unit and subclasses respectively, m is the number of the subclasse, Dij are the population density, Pi is the population in areal unit i, Wj is the weighting factor for subclass j and Aij is the area of subclass j in unit i.

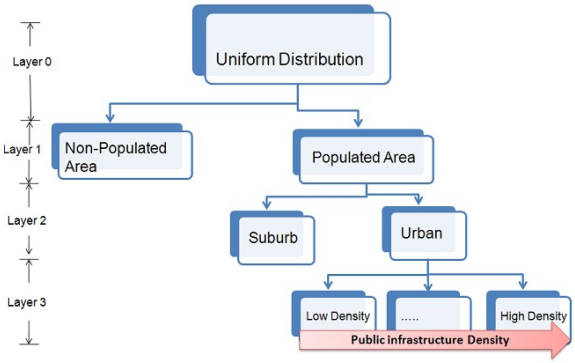

Fig. 8. Multi-layer multi-case dasymetric framework for population desegregation. (Lin and Su, 2009)

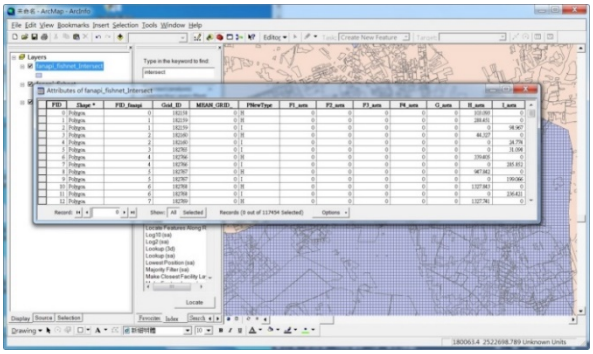

Fig. 9. Grid-based Socioeconomic Database

Summary

Exposure data are one of the most important data for flood risk management. Exposure is the extent to which an organization and/or stakeholder is subject to an event. This includes all kind of socio-economic activities. This paper presents a grid-based GIS database with a resolution of 40m by 40m integrating necessary socioeconomic data that are vital for flood risk analysis.

References

[1] ISO 31000, 2009, Guide 73:Risk management-Vocabulary, ISO GUIDE 73:2009

[2] Lin, M.C. and Su, M.D. (2009), "A Grid-Based Multi-layer and Multi-Class Dasymetric Model for Reconstructing Spatial Population Distribution.", GIS in Humanities and Social Sciences 2009, Section 6: Spatial Statistical Analysis in the Humanities

[3] Martin, S.A., 2015, A framework to understand the relationship between social factors that reduce resilience in cities: Application to the City of Boston, I. J. of Disaster Risk Reduction 12(2015):53-80

[4] Su,MD, Lin,MC, Hsieh,HI, Tsai,BW, Lin,CH (2010), Multi-layer multi-class dasymetric mapping to estimate population distribution, The Science of the Total Environment, 408: 48767-4816 (SCI)

[5] Swaminathan, R; 2016 "There is nothing natural about disaster", https://www.youtube.com/watch?v=h7fbfZxoWlY)

[6] UNISDR, 2015, Disasters in Numbers, http://www.unisdr.org/files/47804_2015disastertrendsinfographic.pdf

THE CHARACTERISTICS OF SEDIMENT TRANSPORT IN THE UPPER AND MIDDLE YOM RIVER, THAILAND

Matharit Namsai[1,a], Suphakorn Sirapojanakul[2,b], Nathamon Phanomphongphaisarn[1,c], Ruetaitip Mama[3,d], Seree Chanyotha[1,e] and Butsawan Bidorn[1,f,*]

Abstract The objectives of this study were aimed at investigating and evaluating sediment transport characteristics and annual total sediment loads in the upper and middle river reaches of the Yom River. River survey data including river cross-sections, flow velocities, river discharges, suspended sediment concentration samples, bed load samples, and bed material samples, were collected during the wet and dry seasons in 2018. Additionally, historical river flow and sediment data during the period 1964-2014 were obtained from Royal Irrigation Department (RID). Based on the observed river survey data in conjunction with RID historical river and sediment data, long-term sediment loads in the study area were assessed. Results from the study revealed that the mountainous reach of the Yom River was characterized by coarse sand to very coarse sand with d50 ranging from 0.70 mm to 1.75 mm. The sediment loads of this river were mainly in suspension. The daily suspended sediment loads along the Yom River showed good correlation with the daily river discharges (R2>0.8). The bed-to-suspended sediment loads ratio along the mountainous river reach varied from less than 1:100 to 1:20. Moreover, the total sediment loads had a tendency to increase in the downstream direction of the river. The average estimated annual total sediment load of upper and middle Yom River basins varied from 0.57 Mt to 0.79 Mt.

Keywords *bed load, suspended sediment load, mountainous river basin*

[1]Department of Water Resources Engineering
Chulalongkorn University
Bangkok, Thailand
[2]Department of Civil Engineering
Rajamangala University of Technology Thanyaburi
Pathum Thani, Thailand
[3]Bureau of Water Management and Hydrology
Royal Irrigation Department
Bangkok, Thailand

[a]Matharit.Na@student.chula.ac.th
[b]ong_rit@yahoo.com
[c]nathamon.p@student.chula.ac.th
[d]ruetaitip.mama@gmail.com
[e]seree.c@chula.ac.th
[f]butsawan.p@chula.ac.th

Introduction

Knowledge of sediment transport in a river is typically required in planning, designing, and operation of water resources development projects, especially for designing the size of dam, barrage and water supply system [1]. However, sediment data are limited due to cost and time consuming and the difficulty of sediment measurement, especially bedload sampling. In general, suspended sediment load is sampled at hydrologic stations on regular basis, but measurement of bedload transport is rare [2]. Therefore, the transport of total river sediment, which comprises of suspended and bed loads, is typically evaluated based on observed suspended sediment data, while bed load data are commonly estimated by several methods such as Maddock and Borland [3], Lane and Borland [4], Einstein's function [5], and bed-to-suspended ratio from field observation.

The Yom River is one of the major tributaries of the Chao Phraya River, which is the largest river in Thailand. The flood and drought disasters have frequently occurred in the Yom River Basin. Severe flood events in 1981, 1995, 2001-2002, 2006, and 2011, took place in the floodplain of the lower portion of the basin [6]. As the gradient of the Yom's lower reach is much less than that in the upper and middle reach, located in mountainous area, the sedimentation may occur in the lower reach causing the reduction in flow capacity of the lower portion of the Yom River. Without large water regulationsystem to regulate flash flood from the upper and middle river basin combined with the poor natural drainage of the basin outlet, the lower portion of the Yom River basin is vulnerary to severe flood disasters. To prevent and mitigate damage not only from flooding but also from drought in this region, several water management projects were planned to be developed in the upper and middle basins. As sediment data, which are area specific, are the key parameters for designing water regulation structures and systems, the information on sediment characteristics and sediment processes are needed.

Sediment data in the Yom River is rarely available, especially bed load. Few previous studies reported that measured bed loads in the lower portion of the Yom River basin ranged 0-5 percent of suspended load [7]. Meanwhile, the Royal Irrigation Department (RID), which is the major government agency responsible for water resources management of the country, suggested using bed load of 35-70

percent of suspended load in order to design hydraulic structures in the Yom River Basin [8], [9], [10]. RID generally estimates bed load as 30 percent of suspended load for each basin in Thailand [11]. However, previous studies showed that bed-to-suspended ratios of several rivers were different such as 0-202 percent for the Ping River [12], 0-6 percent for the Wang River [7], and 0-16 percent for the Nan River [13], [14]. Consequently, bed loads of the Yom River in the mountainous area may be different from previous studies.

The objectives of this study were to 1) study sediment transport characteristics along the mountainous river reach located in the upper and middle portions of the Yom River, and 2) evaluate annual total sediment loads transported along the mountainous river reach of the Yom River. These data are the crucial information for determining dimension of the hydraulic structures and for operating water regulation system in order to prevent water related disasters in the Yom River basin.

Study Area

The Yom River, the tributaries of the Chao Phraya River, is located in the northern part of Thailand (Fig. 1). The total length of the river is 735 km with the drainage area of 24,074 km^2. The Yom River basin is bounded by latitudes 15° 50′ and 19° 25′ North, and longitude from 99° 16′ to 100° 40′ East (Fig. 1). The basin can be divided into three distinct terrain systems: the upper, middle, and lower portions. The upper and middle basins cover 12,130 km^2 of the mountainous area with river gradient of 1:700 for the upper reach and of 1:2,300 for the middle reach. The lower portion of the river basin is a floodplain area, and the river gradient varied between 1:9,000 and 1:35,000. The climate of the basin is dominated by two seasonal monsoon winds. The Southwest monsoon brings a warm moist air from Indian Ocean toward the country during mid-May to mid-October causing abundant rain (wet season). The Northeast monsoon brings dry air from China mainland over the central and northern part of the country during October to mid-February (dry season)(https://www.tmd.go.th/en/archive/thailand_climate.pdf). The annual rainfall ranged between 800 and 1,600 mm with the mean annual rainfall of about 1,250 mm. Almost 90% of the annual rainfall occurs during the rainy or wet season. The mean annual discharge of the river is approximately 4,960 MCM [15]. In this study, sediment characteristics and sediment loads along the mountainous river section of the Yom River were assessed.

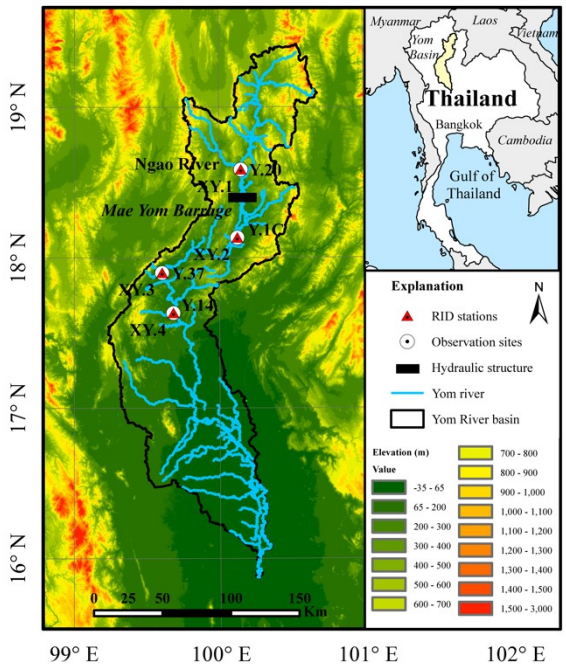

Fig. 1. Yom River Basin area, observation sites, and RID stations.

Methods

To study the sediment transport characteristics along the study area, river surveys were carried out in 2018 at four observation sites (XY.1, XY.2, XY.3, and XY.4 in Fig. 1). The XY.1, XY.2, and XY.3 were located near the RID's hydrological stations, Y.20, Y.1C, and Y.37, respectively. The location of XY.4 was at 7 km upstream of Station Y.14. River data including river cross-sections, flow velocities, suspended sediment concentrations, bed loads, and bed materials were collected at each site during the wet and dry seasons.

The river discharge and current velocity were measured using the Sontek River Surveyor M9. The M9 was also used to measure the water depth along traverse distance for assessing the river cross-section. Suspended sediment load was collected using the depth-integrated sediment sampler US DH-49 at 7 sub-strips of each river cross section. Suspended sediment was filtered from the water samples using GIF filter paper, which retained particles larger than 0.5 µm. The sediment contained on the filters was dried and weighed. Then, suspended sediment concentration was calculated using weight difference method.

The bed loads were sampled at 7 sub-strips across the river flow section using Helley-Smith sampler, which is a medium-weight sampler containing a polyester sampling bag. The sampler operation was limited to flow velocity less than 2.5 m/s, and the sample bag allowed the collection of gravel and sand with a diameter greater than 0.25 mm. Each bed load sampling was taken over 3 to 5 minutes for each sub-strip. The samples were analyzed using a

standard test method of particle-size analysis of soil (ASTM D422). The bed materials were sampled using the Van Veen grab sampler at the left, middle, and right of each river cross-section. The samples were analyzed using the same method as the bedload analysis.

In order to evaluate the annual total sediment loads in mountainous area of the Yom River, historical river flow and suspended sediment data, which have been recorded at RID's hydrological stations (Y.1C, Y.14, Y.20, and Y.37), were collected. The daily river flow and suspended sediment data has been recorded since 1964 and 1975, respectively. Unlike river flow data, the RID did not collected suspended sediment data on a regular basis. Therefore, the suspended loads were estimated from sediment rating curve for each station. The sediment rating curves were obtained from the analysis of historical sediment transport characteristics. By knowing the daily discharge, the daily suspended load was estimated. As bed load information did not available in Thailand, annual bed loads in the Yom River were estimated using bed-to-suspended sediment load ratios analyzed from field data in this study. By combining annual suspended load and annual bed load, the annual total sediment loads were assessed.

In this study, Mann-Kendall (MK) test was used for testing statistical trends of long-term annual runoff and annual suspended sediment load. This test is non-parametric statistical test that has been widely used to identify a monotonic trends in series of environmental data, climate data or hydrological data, even though the series contain non-normally distributed, censored and missing data [16], [17].

Results and discussion

A. River flow and sediment transport characteristics in 2018

River flow and sediment transport characteristics data observed at Stations XY.1, XY.2, XY.3, and XY.4 during the dry and wet seasons in 2018 are summarized in Table 1. Based on the observed river flow (Q_w) data along the Yom River in the mountainous area, the river discharges increased from 2.3 m^3/s (XY.1) to 6 m^3/s (XY.4) during the dry season and from 233 to 275 m^3/s during the wet season. The river flow tended to increase towards downstream as a result of the expansion of drainage area in the direction of river flow.

The analysis of bed material samples revealed that the river reach in the upper and middle portions of the Yom River Basin was characterized by coarse sand to very coarse sand with median grain size (d_{50}) ranging between 0.70 and 1.75 mm (Table 1). In the upper river reach of the study area (XY.1 and XY.2) was characterized by coarse sand with 0.70 to 0.96 mm. The middle river reach between XY.2 and XY.3 was characterized by coarse sand to very coarse sand with 0.77 to 1.67 mm. Meanwhile, the lower reach (between XY.3 and XY.4) was a mainly coarse-sand river with d_{50} of 1.67-1.75 mm. The seasonal variation in river bed materials was found at XY.1 and XY.4. At XY.1, the median size of bed materials observed during the wet season was greater than that observed during the dry season probably due to the deposition of coarser sediment near the confluence of the Yom River and its tributary, Ngao River, located 1.5 km upstream. In contrast, the size of bed material collected at XY.4 during the wet season was smaller than that taken in dry season. It probably occurred because the deposited coarser sediment during the dry season was moved away by a stronger river flow during the wet season. Anomaly of bed material gradation found along the mountainous river reach was possibly due to the irregular river bed slope, difference in geologic features along the river reach, and changes in hydraulic conditions by human activities such as bridges, barrage, check dams, etc.

Based on observed sediment data (Table 1), the suspended sediment loads (Q_s) observed during the dry season slightly increased from 4.2 tonnes/day (t/d) (XY.1) to 4.9 t/d (XY.4). Regarding the low flow condition during the dry season, the suspended sediment loads observed at all sites were low, and the rates of sediment transport were slightly different from each other's (Fig. 2). The greatest rate of suspended sediment transport during the dry season was observed at XY.2 (9.5 t/d) (Table 1). As the sub-catchment areas along this river section were agricultural, the water drained to the river possibly contained higher suspended sediment concentration compared to other locations. For the wet season, the rate of suspended sediment transport significantly declined from 11,470 t/d at XY.1 to 5,424 t/d at XY.3 and then grew to 8,425 t/d at XY.4 (Table 1). The highest suspended sediment transport rate during the wet season was observed at XY.1 (the uppermost observation site) with the rate of 11,470 t/d as a result of high rate of soil erosion on the mountain slopes.

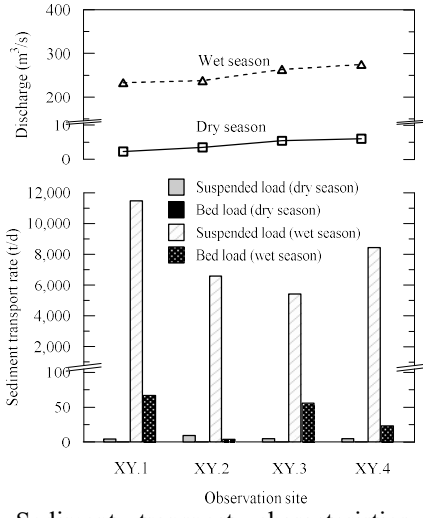

Fig. 2. Sediment transport characteristics at the observation sites in 2018.

The suspended sediment loads significantly decreased at the middle portion of river reach (XY.2 and XY.3) as illustrated in Fig. 2. The sediment reduction likely related to sedimentation in Mae Yom Barrage situated upstream of the XY.2 (Fig. 1). In contrast, the rate of suspended sediment transport rose again at the lower portion of the river reach (XY.4). The sediment augmentation found in this river reach was possibly affected by the finer sediment size, the faster current velocity compared to other sites. Results from sediment data analysis indicated that more than 99 percent of Yom River's sediment was transported in suspension form.

Based on observed bed load data in Table 1, the bed loads (Q_b) along the river varied between 4 and 67 t/d during the wet season with mean current velocity at the observation sites of more than 0.85 m/s. The highest bed load transport was found at XY.1 (Fig. 2). The bed loads tended to decrease towards downstream except at XY.2, where bed load transport rate was significantly lower than that observed in other site. The amount of bed load transport seemed to relate with the river gradient. However, the bed load observed at the XY.2 was significant low possibly as a result of scouring protection near the observation site. During the dry season, as the mean current velocities at all observation sites were less than 0.15 m/s, the bed sediment transport along the river reach of the study area was under detectable.

B. Historical river flow and sediment transport characteristics

The raw data of daily river flow and suspended sediment load between 1978 and 2014 at four RID's stations were used to study historical sediment transport characteristics. Suspended sediment data available at Stations Y.20, Y.1C, Y.37, and Y.14 started from 1984, 1997, 2007, and 1978, respectively. However, these data had not been measured on a regular basis.

The relationship between river discharge and suspended sediment transport rate were plotted as shown in Fig. 3. The result shows that the daily suspended sediment load had a strong correlation with daily river discharge for all stations with the coefficient of determination (R^2) more than 0.8. The regression equations for Stations Y.20, Y.1C, Y.37, and Y.14 are shown in Eqs. (1)-(4), respectively. The suspended sediment loads rose when the river discharge increased (Fig. 3). As a high river discharge induced more bed material motion, the movement of suspended sediment load increased.

$$Q_s = 0.87Q_W^{1.681} \quad (1)$$

$$Q_s = 1.745Q_W^{1.497} \quad (2)$$

$$Q_s = 1.056Q_W^{1.514} \quad (3)$$

$$Q_s = 0.926Q_W^{1.546} \quad (4)$$

Where Q_s was a daily suspended load (t/d), and Q_w was a daily discharge (m^3/s).

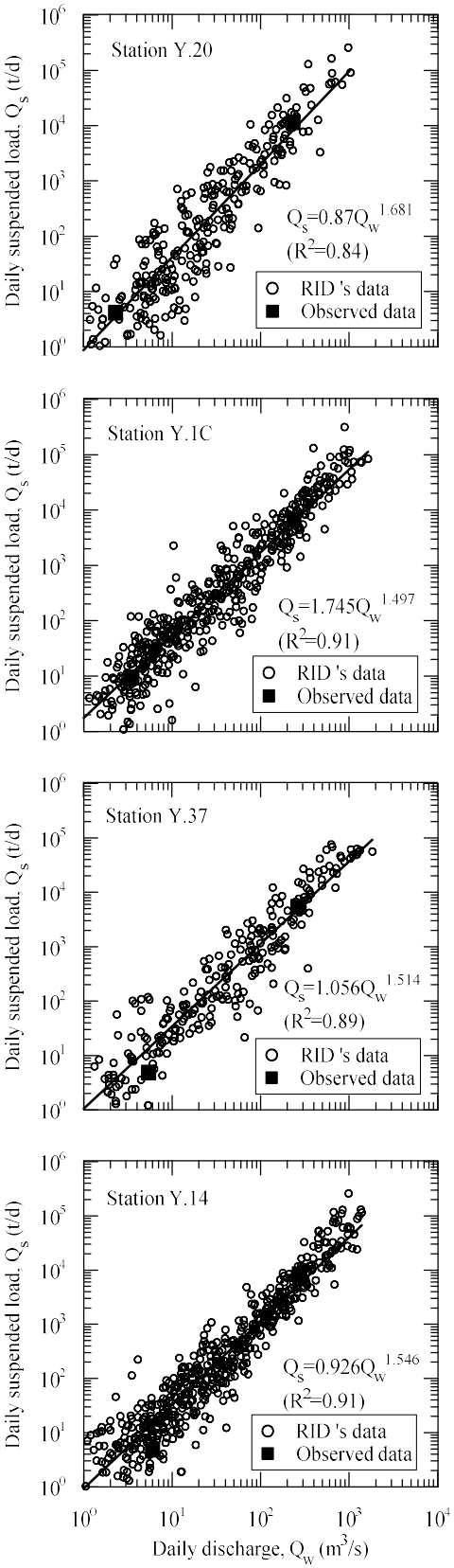

Fig. 3. Relationship between daily suspended load and daily river discharge at Stations Y.20, Y.1C, Y.37, and Y.14.

C. Sediment loads of the river in mountainous river basin

The daily hydrologic data between 1964 and 2014, river survey analysis data, and suspended sediment rating curves were used to assess annual sediment discharges of mountainous river basin. Annual total sediment loads comprises of annual suspended loads and annual bed loads. However, observation data indicated that less than 1 percent of the total sediment loads transported as the bed loads. Therefore, annual total sediment discharge along the mountainous river reach of the Yom River can be roughly estimated from suspended sediment load data. The daily suspended sediment loads at Staions Y.20, Y.1C, Y.37, and Y.14 were calculated by substituting daily river discharge data in to the Eqs. (1)-(4), respectively. Time series of the measured annual runoff (Q_w) and estimated annual suspended sediment load (Q_s) are illustrated in Fig. 4.

Regarding the time series of annual river discharge data, it was found that that the annual streamflows at Station Y.20 during the period 1975-2014 ranged from 590 to 3,330 million cubic meters (MCM) with an average discharge of 1,420 MCM. The annual runoff at Y.1C located downstream Y.20 averaged between 1979 and 2014 was 1,750 MCM. The highest and lowest river discharges at this station were 547 and 4,870 MCM, respectively. For Station Y.37 located downstream Y.1C, the average river discharge from 1979 to 2014 was 2,970 MCM with the maximum of 7,030 MCM and minimum of 1,670 MCM. Meanwhile, Station Y.14 located at the lowermost of the study area had an average river discharge of 2,720 MCM. The range of annual river runoff at Y.14 over 1964-2014 was 840 to 8,780 MCM. By considering the annual runoff along the river during the same time period (1999-2014), the average streamflows were 1,610, 2,160, 2,970, and 3,390 MCM at Stations Y.20, Y.1C, Y.37, and Y.14, respectively. Similar to the observed river data, the river discharges along the study area tended to increase towards downstream due to the increase of catchment area. Moreover, based on Mann-Kendal test, statistically significant increasing trend of long-term annual river discharge was found at Station Y.1C and Y.14.

Based on results from annual suspended sediment estimation (Fig. 4), the annual suspended sediment discharges at Station Y.20 during the period 1975-2014 ranged from 0.08 to 1.68 million tonnes (Mt) with an average of 0.57 Mt. The average annual suspended sediment load transported along this river portion was haft of that estimated by previous study (1.04 Mt) [10]. The annual suspended loads at Y.1C averaged between 1979 and 2014 was 0.58 Mt. The highest and lowest suspended sediment discharges at this station were 0.084 and 2.627 Mt, respectively. Meanwhile, at Station Y.37 had an average annual sediment load of 0.76 Mt. The range of annual suspended sediment discharge at Y.37 over 1999-2014

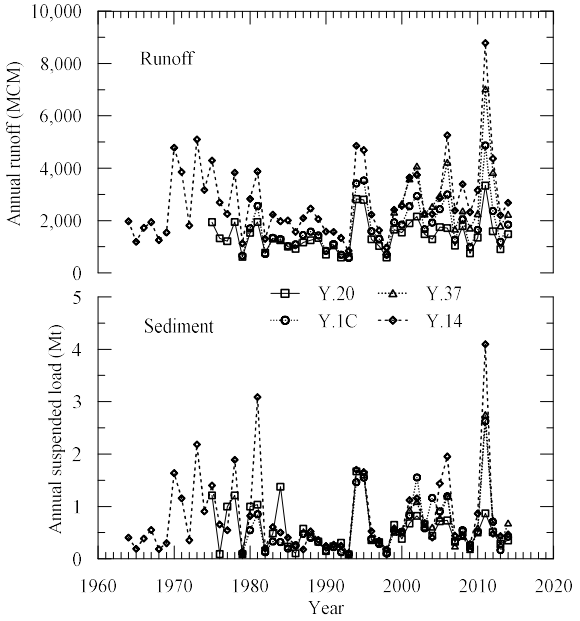

Fig. 4. Annual runoff and annual suspended load at RID stations.

was 0.18 to 2.76 Mt. For Station Y.14, the annual suspended sediment load from 1964 to 2014 averaged 0.79 Mt with the maximum and minimum annual sediment discharges of 0.11 and 4.10 Mt, respectively.

Regarding the average estimated annual suspended sediment load data during 1999-2014, the average sediment discharges of Station Y.20, Y.1C, Y.37, and Y.14 were approximately 0.54, 0.80, 0.76, and 0.96 Mt, respectively. Similarly to the river discharge, the average annual suspended sediment discharge tended to increase towards downstream likely due to the increase of catchment area and river runoff. The reduction of sediment transport between upper and lower reach observed at Station Y.37. It reflected some other factors influencing sediment transport characteristics along the mountainous river reach of the Yom River such as geological condition or human activities along the river reach. Based on MK test, no statistical significant trend has been found in sediment transport along the Yom River's mountainous river reach.

Conclusions

Based on river flow and sediment data observed in 2018, it was evident that the Yom River reach located in the mountainous area was a sandy bed river. This mountain stream of the Yom River was characterized by coarse sand to very coarse sand with the median grain size (d_{50}) in the range of 0.70 to 1.75 mm. The results from this study also revealed that sediment along the mountain river reach mainly transported as suspended sediment load. The bed load

transport accounted for less than 1 percent of the total sediment load along the study area.

Results from the analyses of historical river flow and sediment data measured by RID during the period 1978-2014, indicated that the daily suspended loads along the river strongly correlated with the their corresponding daily river discharges (R^2> 0.8). As more than 99 percent of total sediment transported in suspension form, therefore, the sediment rating curves developed from suspended sediment data at each station can be roughly used for estimating daily total sediment discharges of the mountainous river reach of the Yom River.

Regarding the estimated annual sediment load over the past four decades, it was found that the sediment transport of the upper Yom River reach (Station Y.20) varied between 0.08 and 1.67 Mt with an average sediment load of 0.57 Mt. For the lowest mountainous portion of the Yom River (Station Y.14), the average suspended load was 0.79 Mt with range of sediment transport between 0.11 and 4.10 Mt. By the considering average 15-year annual sediment load (1999-2014) along the study area, the sediment discharges tended to increase towards downstream. No significant trends of long-term sediment load had found at any section along the Yom River.

Due to the lack of sediment transport observation data, especially bed load transport in the Yom River, up to 70 percent of suspended sediment was recommended by RID for estimating the bed load for the Yom River basin's water development projects. However, results from river observations in this study combined with the previous studies suggested that about bed load transport was responsible for 1-5 percent of the total sediment transported along the mountainous river reach of the Yom River.

Acknowledgments

The authors acknowledge the support of the 100th Anniversary Chulalongkorn University Fund for Doctoral Scholarship, the 90th Anniversary Chulalongkorn University Fund (Ratchadaphiseksomphot Endowment Fund), and Chulalongkorn University; Government Budget (GB-B_61_078_21_10). The authors also thank the Royal Irrigation Department and Department of Water Resources Engineering, Chulalongkorn University for providing historical and observed river dataset in this study.

Table I. River flow and sediment transport characteristics data at observation sites in 2018

Sites	Date	Flow area, A (m^2)	Mean velocity, V (m/s)	Discharge, Q_w (m^3/s)	Suspended load, Q_s (t/d)	Bed load, Q_b (t/d)	Q_b/Q_s	Bed load size, d_{50} (mm)	Bed material size, d_{50} (mm)
Dry season									
XY.1	27-Mar-2018	80	0.029	2.3	4.2	~0	0	-	0.70
XY.2	27-Mar-2018	28	0.125	3.5	9.5	~0	0	-	0.77
XY.3	28-Mar-2018	81	0.067	5.4	4.9	~0	0	-	1.67
XY.4	28-Mar-2018	40	0.150	6.0	4.9	~0	0	-	1.75
Wet season									
XY.1	23-Jul-2018	274	0.850	232.8	11,469.8	66.7	0.006	0.80	0.96
XY.2	23-Jul-2018	259	0.918	237.7	6,592.0	4.0	0.001	0.19	0.77
XY.3	24-Jul-2018	296	0.889	263.2	5,424.4	55.8	0.010	1.65	1.67
XY.4	24-Jul-2018	293	0.937	274.6	8,425.2	23.4	0.003	0.90	0.92

References

[1] P. Wuttichaikitcharoen, and M. Babel, "Principal Component and Multiple Regression Analyses for the Estimation of Suspended Sediment Yield in Ungauged Basins of Northern Thailand," *Water*, vol. 6, no. 8, pp. 2412-2435, August 2014.

[2] J. M. Turowski, D. Rickenmann, and S. J. Dadson, "The partitioning of the total sediment load of a river into suspended load and bedload : a review of empirical data. Sedimentology," *Sedimentology*, vol. 57, no. 4, pp. 1126-1146, June 2010.

[3] T. Maddock, and W. M. Borland, "Sedimentation studies for the planning of reservoirs by the Bureau of Reclamation," United States Department of Interior, Bureau of Reclamation, Branch of Project Planing, 1950.

[4] E. W. Lane, and W. M. Borland, "Estimating bed load," *Transactions American Geophysical Union*, vol. 32, no. 1, pp. 121-123, Febuary 1951.

[5] H. A. Einstein, "The bed load function for sediment transportation in open channel flow," United States Department of Agricuture, Soil Conservation Service, Technical bulletin 1026, 1950.

[6] P. Hanittinan, "The impact assessment on flood at the Sukhothai province due to global climate change," M.S. thesis, Department of Water Resources Engineering, Chulalongkorn University, Bangkok, Thailand, 2013. (in Thai)

[7] B. Bidorn, S. Chanyotha, S. A. Kish, J. F. Donoghue, K. Bidorn, and R. Mama, "The effects of Thailand 's Great Flood of 2011 on river sediment discharge in the upper Chao Phraya River Basin, Thailand," *International Journal of Sediment Research*, vol. 30, no. 4, pp. 328-337, December 2015.

[8] Royal Irrigation Department (RID), "Yom basin development project ," Haward Humphreys & Partners, Reading, England, 1980.
[9] Royal Irrigation Department (RID), "Kaeng Sue Ten project in Prae province," Panya consultant and partners, Bangkok, Thailand, 2001. (in Thai)
[10] Royal Irrigation Department (RID), "Intergrated development of special area in the Yom River Basin (Mae Yom Dam)," Panya consultant and partners, Bangkok, Thailand, 2010. (in Thai)
[11] Royal Irrigation Department (RID), "The relation between suspended sediment and drainage area in 25 river basins," Office of Water Management and Hydrology, Royal Irrigation Department, Bangkok, Thailand, 2012. (in Thai)
[12] B. Bidorn, S. A. Kish, J. F. Donoghue, K. Bidorn, and R. Mama, "Sediment transport characteristic of the Ping River basin," *Procedia Engineering*, vol. 154, pp. 557-564, 2016.
[13] P. Kitisuntorn, "Sediment transport and navigation problem in lower Nan River," Doctoral dissertation, Department of Civil Enginering, Chulalongkorn University, Bangkok, Thailand, 1994.
[14] B. Bidorn, S. A. Kish, J. F. Donoghue, K. Bidorn, and R. Mama, "Change in sediment characteristics and sediment load of the Nan River due to large dam construction," *Proceeding of the 37th IAHR World Congress*, Kuala Lumpur, Malaysia, August 13-18, 2017, pp. 403-412.
[15] Hydro and Agro Informatics Institute (HAII), "Report on data collection and analysis : Database development project and flood and drought modeling of 25 river basins (Yom River Basin)," Asdecon Co-operation Co. Ltd., Bangkok, Thailand, 2012. (in Thai)
[16] H. Shi, C. Hu, Y. Wang, C. Liu, and H. Li, "Analyses of trends and causes for variations in runoff and sediment load of the Yellow River," *International Journal of Sediment Research*, vol. 32, no. 2, pp. 171-179, June 2017.
[17] J. Zhang, X. Zhang, R. Li, L. Chen, and P. Lin, "Did streamflow or suspended sediment concentration changes reduce sediment load in the middle reaches of the Yellow River?," *Journal of Hydrology*, vol. 546, pp. 357-369, March 2017.

HISTORICAL SHORELINE CHANGE OF THAP SAKAE COAST, PRACHUAP KHIRI KAN, THAILAND

Nathamon Phanomphongphaisarn[1,a], Butsawan Bidorn[1,b,*] and Anurak Sriariyawat[1,c]

Abstract Coastal erosion is a critical problem in Thailand significantly affecting the coastal development and economy of the country. This paper presents the situation of shoreline change along the Thap Sakae coast, which is one of the highest potential areas for Thailand's coastal development. To evaluate the coastal erosion situation of the study area, ten shoreline positions were extracted from the aerial photographs and satellite images taken between 1966 and 2017 using the Geographic Information System (ArcGIS). The rates of shoreline change were analyzed by the Digital Shoreline Analysis System (DSAS). Additionally, field surveys was carried out in 2018 to observe the current coastal environment. Based on the results from shoreline analyzes, the long-term (1966-2003) and short-term (2003-2017) average rates of shoreline change along the Thap Sakae coast were -0.14 and 0.3 m/y, respectively. As the average rate of shoreline change was less than ±1 m/y, the Thap Sakae coast seemed to be a stable coastal area. However, local coastal erosion was found during the past 15 years due to land development mainly for tourism purpose. Coastal protection structures were found in many locations along the study area. Those coastal developments and coastal protection measures have likely been driving the negative effects on their adjacent shoreline. As Thap Sakae coast has a high economic value, an erosion rate with a small degree can cause significant damages to the local and regional economy.

Keywords *coastal erosion, sandy beach, human activities, coastal protection*

[1]Department of Water Resources Engineering, Chulalongkorn University
Bangkok, Thailand

[a]nathamon.p@student.chula.ac.th
[b]butsawan.p@chula.ac.th
[c]Anurak.S@chula.ac.th

Introduction

A coast is a place that landinteracts with the sea,and it is one of the most dynamic earth features. There are several natural factors such as wind, wave, tide, and nearshore current affecting shape of a coastline by either moving it landward or seaward [1]. Human activities are also the major causes of shoreline change, for example, coastal developments for tourism, fishery, shipping, transportation, and energy production, and they can significantly alter coastal processes and shoreline movement patterns [2][3][4]. Due to increasing population growth in modern society, many cities and infrastructures have been developed along the coasts worldwide [5][6]. Two-third of the world's megacities are situated on the coastal areas, however, they are vulnerable to shoreline retreat and natural hazards [4]. A construction of the coastal or marine structure typically disturbs the long-term equilibrium of the shoreline resulting in shoreline migration [7][8][9]. As an investment in coastal zone is normally immense, the study of historical shoreline changes including the observation of the existing coastal structures along the coast is necessary for a coastal project planning and development. Meanwhile, post-construction monitoring is a crucial process in order to evaluate the function and effectiveness of the structures and/or the project [4].

In Thailand, Prachuap Khiri Khan Coast situated on the west side of the Gulf of Thailandhas about 250 km long [10]. The coast comprises of several different coastal features such as rocky coast, sandy coast, cliff, lagoon, mangrove forest, and tidal flat, which have been continuously developed since the past. However, the Department of Marine and Coastal Resources, Thailand, reported that a critical coastal erosion with the rate of more than -5 m/y was recently found in some locations such as Khlong Wan, and Ban Thung Pradu villages [10][11].

The aim of this paper is to document the historical shoreline changes along the Thap Sakae coastline (Fig. 1), a part of the Prachuap Khiri Khan Coast, which is a potential site for several coastal development projects. The paper summarized the long- and short-term shoreline change rates including the current situation of shoreline change along the Thap Sakae coast. The information provided a more comprehensive view of the coastal change in this area and key references that can be used for coastal planning and management in a regional context.

Study area

The Thap Sakae coast is located in Prachuap Khiri Khan Province in the southern part of Thailand, bounded by 11° 22' to 11° 45' N and 99° 34' to 99° 47' 00" E. The study area covered about 50 km of the sandy coastline extending from Khlong Wan Mountain (the meaning of "Khlong" is channel) to Thong Chai Mountain as shown in Fig. 1. The coastline is characterized by sand, gravel, silt, shell fragment, and organic matter [12].

The climate of the study area is dominated by two major monsoons. The Southwest monsoon generates southwestward wind during May to Septembercausing moderate wave with an average wave height of about 0.1-0.5 m. The Northeast monsoon, which starts from December through March, brings northeastwardly strong wind of 4-8 knots and intense wave of 0.5-2.0 m high [13] [14].

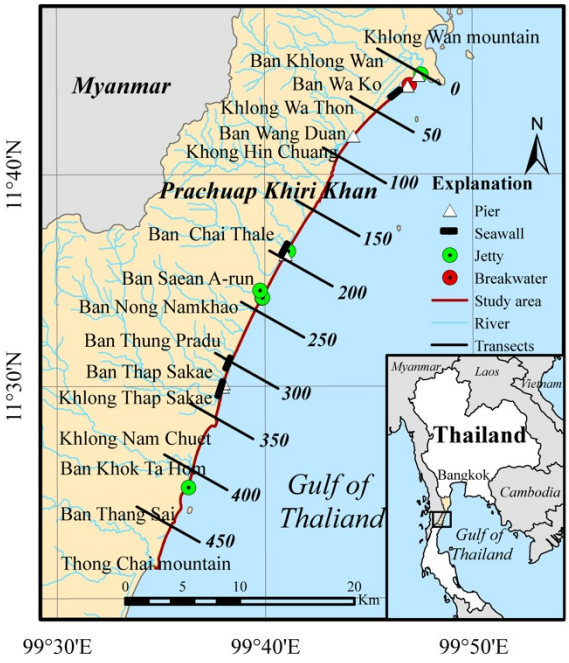

Fig. 1. Location of Thap Sakae coast.

Materials and methods

A. Compilation of historical shoreline

Historical shoreline positions along the Thap Sakae coast were derived from aerial photographs and satellite imagery taken in 1966, 1976, 1994, 1997, 2002, 2003, 2013, 2014, 2015, and 2017. The TIF images of scanned aerial photographs and satellite data were rectified using the Geographic Information System (ArcGIS) software version 10.4 by placing at least 8 well-spaced ground control points to remove distortions from aerial photographs with root mean square errors (RMSE) of less than 1.0 m. All images were projected to Universal Transverse Mercator with reference to the World Geodetic System 1983 (WGS1983), and then shorelines were digitized. Even though the High Water Level (HWL) has been typically used as the shoreline proxy for more than 150 years because it could be visually detected in the field [15][16][17], different proxies can be used to define the shoreline positions depending on coastal location, data sources and scientific preference [15]. In this study, the vegetation line, boundary of coastal structure, and cliff base were used for representing shoreline positions. Shorelines from all sources were merged to produce a single shoreline shapefile for calculating shoreline change rates.

The rates of shoreline changes in the study area were evaluated in ArcGIS with the Digital Shoreline Analysis System (DSAS) version 4.3 [18] developed by United States Geological Survey in cooperation with TPMC Environment Service [15][18]. In order to analyze the shoreline change using DSAS, baselines were constructed parallel to the general trend of the Thap Sakae shorelines. The 482 transects were generated perpendicular to the baseline with the spacing of 100 m (Fig. 1). The long-term rates of shoreline change (between 1966 and 2003) were calculated at each transect using linear regression (LRR) method, which is the most statistically robust quantitative method when the number of shorelines is limited [16][18]. Meanwhile, the endpoint rate method (EPR) is used to calculate the short-term shoreline change rates which are calculated with 90 percent of the confident interval to compare the 2003 and 2017 (most recent) shoreline positions.

The movement of shoreline was also calculated by DSAS. Statistic methodcalled Net Shoreline Movement (NSM) was used to calculate the distance of net shoreline change. This method measures the distance of shoreline from oldest to youngest.

B. Field observation

As Thap Sakae coast composes of a wide range of coastal landforms and has been developed during the past decades. A field survey was carried out on 5th -7thJune 2018 to observe the existing coastal characteristics including human activities along the Thap Sakae coast. Eight survey locations, Ban Khlong Wan (transect 7), Ban Wa Ko (transect 28), Ban Wang Duan (transect 76), Ban Chai Thale (transect 192), Ban Sang A-run (transect 238), Ban Thung Pradu (transect 303), Ban Thapsakae (transect 321), and Ban Khok Ta Hom (transect 414), where the major development can be recognized from the remote sensing data, are illustrated in Fig. 1.

Results and discussion

Regarding the shoreline change analyzes in this study, long-term and short-term shoreline change rates along the Thap Sakae coast are shown in Fig. 2a and Fig. 2b, respectively. A positive value of the

shoreline change rates denotes the distance of shoreline moving seaward per year (shoreline accretion rate). Meanwhile, the negative value represents the distance of shoreline migrating landward per year (shoreline retreat rate). The substantial erosion/accretion trends including human-induced change within the Thap Sakae coastal system are discussed below.

A. Long-term shoreline change along the Thap Sakae coast

Based on the results from long-term shoreline change analysis, approximately 65 percent of the Thap Sakae coastline was eroding. The net long-term shoreline change rate averaged over 482 transects was -0.14 m/y with an erosional trend. The recession of the shoreline was mainly found between Khlong Hin Chuang and Thong Chai mountain (transect 27-428) (Fig. 2a) with the net land loss of 0.42 km^2. The highest erosion rate of -1.3 m/y was measured on the south of Khlong Thap Sakae inlet (Fig. 2a). Long-term accretion occurred along the remaining 25 percent of the Tap Sakae coastline. The significant accretional trend was mainly found at Ban Sang A-run and Ban Thang Sai (transects 238-460). However, the maximum long-term accretion rate of 2 m/y was measured at the inlet of Khlong Ang Thong (Fig. 2a). The net long-term land accretion was about 0.17 km^2.

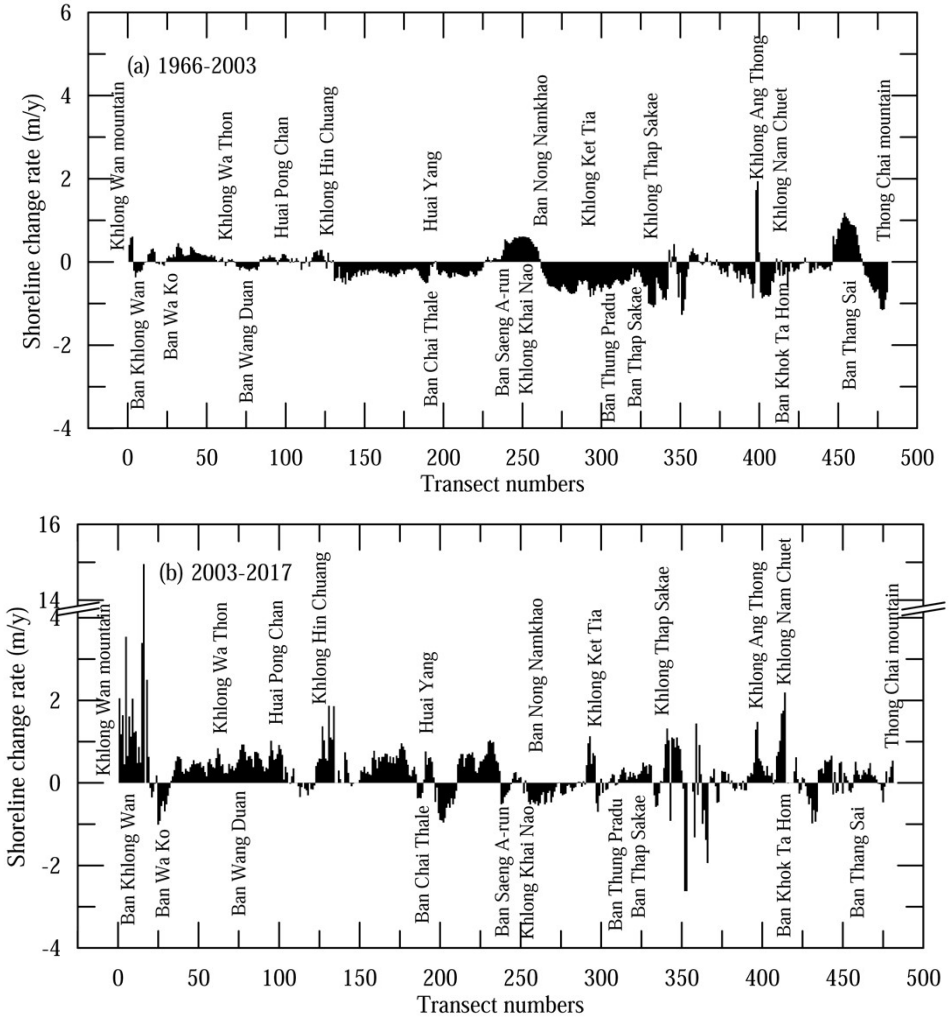

Fig. 2. Shoreline change rates along the Thap Sakae coast (a) Long-term change rates during 1966-2003 (b) Short-term change rates during 2003-2017.

B. Short-term shoreline change along the Thap Sakae coast

Results from short-term shoreline change analysis revealed that the average short-term shoreline change rate throughout the Thap Sakae shoreline during the past fourteen yearswas 0.3 m/y. Along the 70 percent of the total coastline had a short-term accretional trend with the average rate of 0.56 m/y. The maximum shoreline accretion rate of 15 m/y occurred at the upcoast of Ban Khlong Wan (Fig. 1) fishery pier (Pier 2 in Fig. 3)constructed in 2005. The total land accretion was 0.24 km^2 during the period 2003-2017.

The shoreline change trends of more than half of the eroded areas have shifted from long-term erosional to short-term accretional trends. About one-third of the Thap Sakae coastline was still experiencing erosion during the period 2003-2017. However, the average rate of short-term shoreline retreat in this area was less than -1 m/y. The highest shoreline recession rate of -2.6 m/y taking place at 2.3 km from the Khlong Thap Sakae (transect 353) southward seemly related to natural changes in beach features and riverine system.Total land loss between 2003 and 2017 was 0.05 km^2. Decreasing of the shoreline erosion rate seemed to relate with coastal development and protections during the recent year.

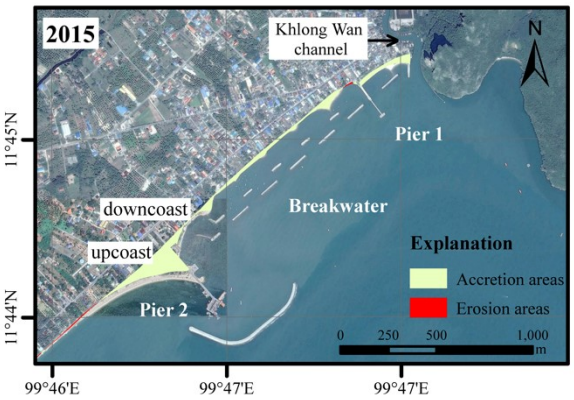

Fig. 3. Shoreline change during 2003-2015 at Ban Khlong Wan (transects 1-22).

C. Comparison between long- and short-term shoreline changes.

Based on satellite imagery and field survey data, many coastal projects have been developed along the Thap Sakae coastsas shown in Fig. 1, and the shoreline has responded to those coastal developments in different degrees.

For example, Ban Khlong Wan coast located between transects 1 and 22 had a significant shoreline erosion up to -20 m during the period 1966-1976. Pier 1 (Fig. 3) was built in 1989 for fishery purposes. The pier has trapped sediment from the Khlong Wan, which transported southwardly, resulting in sediment deposition along the previously eroded coast.In 2005, a new fishery pier (Pier 2 in Fig. 3) was constructed causing a significant sand deposition on the southern side of the new pier (Fig. 3) with the maximum distance of 220 m. Series of the offshore breakwater was built as a part of new fishery project to mitigate sediment starvation on the northern side of the pier (Fig. 3). Even though Pier 2 has caused land accretion on the upcoast of the structure, the coast along Ban Wa Ko located on the south of the Pier 2 has experienced a significant shoreline retreat (Fig. 4) response to the changes in coastal processes due to the Pier 2. Between Khlong Wa Ko and Khlong Hin Chuang (transects 35-135), the rate of accretion obviouslyincreased recently resulting in increasing of shoreline accretion of about 1.5 times (Fig. 2). As this section is located between two major channels, the significant shoreline advance in this region seemed to reflect the increase of sediment supply from the Khlong Wa Thon and/or Khlong Hin Chuang channels.

Along Ban Chai Thale coast (between transects 135 and 215), the rate of shoreline change in this section has shifted from insignificant erosional rate of less than -1 m/y to accretion rate of 1 m/y after the constructions of two jetties at the Huai Kok Ma and Rong Nong Kok Channel mouths in 2005 and 2008, respectively. However, the jetties at Rong Nong Kok Channel mouths caused erosion along the Ban Saeng A-run coast due to the deficit in sediment transporting southward. Between Ban Thung Pradu and Ban Thap Sakae (transects 303 and 321), where the long-term shoreline retreat rate was about -1 m/y, the shoreline has shifted seaward during the past 14 years as a result of land reclamation and coastal protection using seawalls.

The dramatic shifts in erosional long-term trend to depositional short-term trends were found near the coast adjacent to the major channel mouths such as the Khlong Thap Sakae (transect 331), Khlong Ang Thong (transect 399), and Khlong Nam Chuet (transect 413). The maximum short-term erosion rate occurred at a port (transect 353) operated between 1997 and 2007. Since the port has been removed in 2008, the shoreline was readjusting to reach its new equilibrium.

D. Historical of shoreline movement and existing coastal environment along the Thap Sakae coast.

Evolution of the shoreline along the study area compared to the shoreline in 1966 is illustrated in Fig 4. Between 1966 and 1976, most coastal areas had experienced shoreline erosion probably related to three tropical depressions directly hitting Prachuap Khiri Khan coast in 1975 [19]. After that shoreline change pattern along the Thap Sakae coast was mostly steady. The maximum distance of shoreline accretion was 200 m occurred at the south of pier at Ban Khlong Wan (Pier 2 in Fig. 3). While the highest shoreline recession was 50 m was found at the south of Khlong Thap Sakae (transect 351). Land accretion mainly took place at river mouths, such as Khlong Wa Thon (transect 62), Khlong Khai Nao (transect 253), Khlong Thap Sakae (transect 331) and Khlong Nam Chuet (transect 413)(Fig. 4), which are the major sources of sediment supply to the coast. In contrast, land losses were found at Ban Nong Nam Khao (transect 262), the south of Khlong Thap Sakae (transect 351) and the north of Thong Chai mountain (transect 475).

From 1966 to 1976, the shoreline near the mouth of Khlong Wan retreated with the distance of about 20 m. After the construction of concrete pier (Pier 1 in Fig. 3) in 1989, it was found that shoreline between the river mouth and Pier 1 migrated seaward of about 15 m in 2002. As a result of the construction

of a new fishery pier (Pier 2) at Ban Khlong Wan in 2005, longshore sediment transported northward were trapped at the upcoast of Pier 2. Therefore, seawalls and series of offshore breakwater were constructed at downcoast of the Pier 2 in order to reduce the beach erosion affected by the pier. Based on a field survey in 2018, however, failure of those coastal protections was found on the southern coast of Pier 1as shown in Fig. 5. Ban Wa Ko coast located on the south of Pier 2 has also faced shoreline retreat because Pier 2 has trapped the longshore sediment transporting southward. Consequently, the downcoast experienced more than 15 m of shoreline retreat. Field surveys data indicated that private seawalls constructed by landowner have successfully protected the horizon changes (Fig. 6), but the vertical erosion of the beach occurred in front of those seawalls as depicted in Fig. 6.

Along 20km coastline from Khong Wa Ko to the south (between transects 31 and 225), the pattern of shorelinemigration slightly changed except the coastlines adjacent to the river mouths (Khlong Wa Thon, Huai Pong Chan, and Khlong Hin Chuang), which the shore mostly grew seawards due to sediment supply from the rivers. However, the shoreline recession was found at both upcoast and downcoast of Huai Yang river mouth (transect 192). Although, several coastal structures such as seawalls and jetties were applied to stabilize the coastline, up to -20 m of shoreline retreat was observed along the coast. It indicated that the sediment supplied from Huai Yang Channel was significantly less than longshore sediment transport in this area.

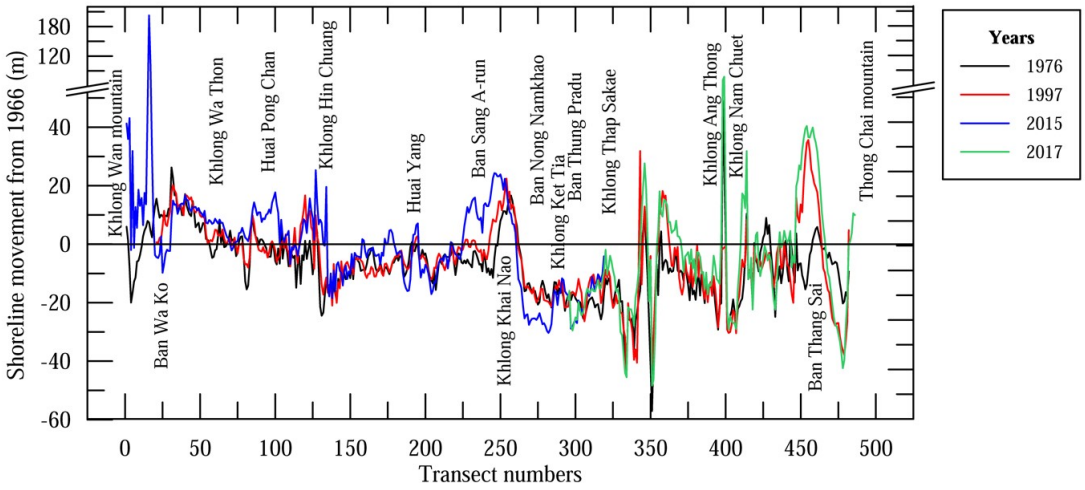

Fig. 4. Historical shoreline movement along the Thap Sakae coast during the period 1966-2017.

Fig. 5. Failure of shoreline protection at Ban Khlong Wan between transect 3 and 5.

Fig. 6. Beach erosion along Ban Wa Ko.

Along 3.5 km coastline between Rong Nong Kok (Ban Sang A-run)and Khlong Khai Nao channels (transects 225 -260), the shoreline near Khong Khai Nao inlet has migrated seaward of about 20 m during the period 1966-2015 reflecting the significant amount of sediment supply from Khlong Kai Nao. Results from shoreline analysis indicated that the net sediment transported northward and sank at the inlet of Rong Nong Kok channel to prevent sedimentation in the navigation channel in 2007. A pair of jetties with 40 and 50 m long was constructed at the southern and northern sides of the river mouth, respectively. Unfortunately, the jetty functioned as intended only several years because it was too short for trapping the large amount of sediment transporting to the south. The jetty improvement was done in 2015. The length of the south- and north- jetty structures were extended to 110 and 60 m, respectively .

The 1.5 km coastline from Ban Nong Nam Khao to Ban Thung Pradu(transects 260 to 310) has experienced shoreline retreat of more than -20 m between 1966 and 1976. Then the coast seemed to be stable during the period 1976-1997 (21 years).

However, the abrupt shoreline retreat of more than 10 m occurred between 1997 and 2017 (Fig. 2 (b)). Moreover, the beach in this area was narrow with the beach width of about 10 to 20 m. Even though the rate of shoreline change in this area may be low (less than -1 m/y) compared to other regionsof the country, it has caused severe damages to local communities living along the coast as shown in Fig. 7. Figure 8 presents the construction of coastal protection structure (seawall) to mitigate the coastal land loss in this area.

Fig. 7. Beach erosion and property damages along Ban Thung Pradu

From Ban Thap Sakae to Ban Thang Sai (transects 310-455), most of the 14.5 km long coastline in this section has undergone shoreline recession. The coast was severely eroded more than -40 m in some locations during the period 1966-1997. Concrete seawall with 500 m long was built to stabilize the eroding shoreline. Since 1976, the northern portion of the coast has been more or less stable. At the southmost of the study area, Thong Chai Mountain was situated. As it functioned as a headland of the study area, no significant shoreline change has been observed during the past five decades.

Fig. 8. The seawall was under construction along Ban Thung Pradu.

Conclusions

Historical shoreline analysis over the past five decades from this study indicated that 65 percent of the Thap Sakae coastline, Prachuap Khirikhan Province, has experienced coastal erosion with the long-term land losses and land accretion of 0.42 km^2 and 0.17 km^2, respectively. Although the average long-term rate of shoreline retreat was generally low (-0.37 m/y) , about 30 percent of the coastline was still eroding during the past 14 years with the short-term erosion rate of about -1 m/y. The highest rates of shoreline recession (-2.62 m/y) were found near a headland (2.5 km from Khlong Thap Sakae toward the south) relating to natural interaction processes among beach features, riverine system, and local wave climate. The decrease in eroded coastline was related to coastal protection measures applied along the coast recently.

The long-term shoreline accretion was found in severalplaces near the river mouths with an average rate of generally less than 1 m/y. As many coastal developments and coastal stabilization projects have been developed along the Thap Sakae coast during the past 14 years, more than 50 percent of the areas with the erosional trend has shifted to accretional trend. Up to the present, land accretion along the Thap Sakae coast has increased to 0.24 km^2. The maximum shoreline advance of 200 m was found near the new Ban Khlong Wan fishery pier.

The rates of shoreline change along Thap Sakae coast seem to be not critical compared to that found in other coasts of Thailand such as the Chao Phraya Delta coast, which the erosion rate was more than -25 m/y. However, based on field observation, severe damages on private properties were found in many locations. As the Thap Sakae coastline is characterized by narrow sandy beaches, such a low rate of shoreline change can cause significant effects on coastal development in this area.

Acknowledgment

This study was supported by Electricity Generating Authority of Thailand (EGAT), Research Assistant Scholarship, Chulalongkorn University and Department of Water Resources Engineering, Chulalongkorn University. This is one part of Pre-feasibility of Developing EGAT's LNG Hub for Thailand project.

References

[1] M. Pawlukiewicz, P. K. Gupta, and C. Koelbel, Ten principles for coastal development. Washington, D.C: Urban Land Institute, 2007.
[2] J. P. Doody, Coastal Conservation and Management An Ecological Perspective. Springer Science and Business Media New York, 2011.
[3] Life Environment, Life and Coastal management. Luxembourg: European Union, 2012.doi:10.2779/54470.
[4] C. W. Finkl, Coastal Hazards. vol. 6, New York: Springer, 2013.
[5] L. Creel, "Ripple effects: population and coastal regions," Making the Link, Washington, DC: Population Reference Bureau, 2003, pp. 2-8.
[6] E. Bird, "Coastal Geomorphology An Introduction," 2nd ed. Chichester: John Wiley & Sons, 2008, p. 1.

[7] C. Saengsupavanich, "Assessing and Mitigating Impacts of Shore Revetment on Neighboring Coastline," International Conference on Environment Science and Engieering. Singapore, vol. 32, 2012, pp. 24-28.

[8] S.C. Selvan, R. S. Kankara, V. J. Markose, B. Rajan, and K. Prabhu, "Shoreline change and impacts of coastal protection structures on Puducherry, SE coast of India. Natural Hazards," vol. 83, pp. 293-308, April 2016. doi:10.1007/s11069-016-2332-y.

[9] B. Bidorn, and C. Rukvichai, "Impacts of Coastal Development on the Shoreline Change of the Eastern Gulf of Thailand," the 5th International Conference on Coastal and Ocean Engineering. IOP Conf, 2018.

[10] Department of Marine and Coastal Resources, "Report of shoreline erosion in 23 provinces," Thailand, 2015. (in Thai)

[11] Department of Mineral Resources, "Report of coastal changing along the Gulf of Thailand," Bangkok: Department of Mineral Resources, 2002. (in Thai)

[12] Department of Mineral Resources, Geological and mineral resources management at Prachaup Khiri Khan Province. vol. 1, Bangkok, Department of Mineral Resources, 2008. (in Thai)

[13] S. Vongvisessomjai, R. Polsi, C. Manotham, D. Srisaengthong, and A.S. Charulukkana, "Coastal Erosion in the Gulf of Thailand," Springer, 1996, pp. 131-150.

[14] Marine Department, "Report of feasisbility study of the environmental impact and revise coastal structure design at Ban Thung Pradu, Thap Sakae, Prachuap Khiri Khan Province," 2015. (in Thai)

[15] C.J. Hapke, D. Reid, B.M. Richmond, P. Ruggiero, and J. List, "National assessment of shoreline change Part 3: Historical shoreline change and associated coastal land loss along sandy shorelines of the California Coast," US Geological Survey Open File Report 2006-1219, 2006.

[16] U. Natesan, A. Parthasarathy, R. Vishnunath, G. E. J. Kumar, and V. A. Ferrer, "Monitoring Longterm Shoreline Changes along Tamil Nadu, India Using Geospatial Techniques," Aquatic Procedia, vol. 4, 2015, pp. 325-332. doi:https://doi.org/10.1016/j.aqpro.2015.02.044.

[17] Y. Fan, S. Chen, B. Zhao, S. Pan, C. Jiang, and H. Ji, "Shoreline dynamics of the active Yellow River delta since the implementation of Water-Sediment Regulation Scheme: A remote-sensing and statistics-based approach," Esturine, Coastal and Shelf Science, vol. 200,2018, pp. 406-419.doi:https://doi.org/10.1016/j.ecss.2017.11.035.

[18] E. Thieler, E. Himmelstoss, J. Zichichi, and A. Ergul, "Digital Shoreline Analysis System (DSAS) Version 4.0 - An ArcGIS Extension for Calculating Shoreline Change," USA: US Geological Survey 2009.

[19] Thai Meteorological Department, "Report of monthly statistic of Tropical storm between 1951 and 2017, Thailand," 2018.(in Thai)

Delineation of Unconventional Groundwater: II. Saline Geothermal Groundwater in Krabi, Thailand

Wipada Ngansom[1,a] and Helmut Duerrast[2,b]

Abstract Common groundwater is usually of meteoric origin; rain seeps into the ground and thus forms aquifers at depth, which then can be utilized via wells for human consumption and industrial use. The quality and the amount of groundwater in such an aquifer depend on water-rock interactions and the physical properties of the sediments and rocks forming the aquifer. Groundwater aquifers are exposed to dangers of contamination and pollution from external sources as for human consumption requires a certain quality. Hence, the protection of groundwater sources is of uttermost importance. However, naturally occurring un-conventional groundwater also can be found in the subsurface, mainly originating at deeper depth from geological fluids, which often are not feasible for human consumption. Therefore, a clear delineation of the boundaries between both types of groundwater is required. The saline geothermal groundwater in Khlong Thom District of Krabi Province in Southern Thailand is one example. Here, a range of geological, geophysical, and geochemical methods and investigations have been applied in order to fully characterize the geothermal system, thus determining its boundaries from the conventional groundwater system. Parallel, this also allows a better utilization and management of the hot water itself as it can be used for human health purposes as well as for renewable energy production, either as direct use for drying food, for example, or for electricity production via geothermal power plants. A continuous monitoring of the overall system will ensure a sustainable use of the saline hot water as well as the surrounding common groundwater.

Keywords *Unconventional groundwater, saline hot spring, Krabi*

[1]Geophysics, Department of Physics,
Prince of Songkla University,
Hat Yai, Thailand
[2]Geophysics Research Center, Department of Physics,
Prince of Songkla University,
Hat Yai, Thailand

[a]p_wipada@hotmail.com
[b]helmut.j@psu.ac.th

Introduction

In Southern Thailand, altogether 30 hot springs with surface exit temperatures from 45 to 80 °C indicate active geothermal systems at depth, however in many cases heat sources have not been clearly identified [1]. Generally, hot water heated up at depth is rising towards the surface through open pathways, often provided by faults and fractures, which also allow the recharge of the geothermal system by meteoric water. Among all hot springs in Southern Thailand one with natural saline hot water can be found [2], the so called Saline Hot Spring Khlong Thom (KB4), which is located in Khlong Thom District of Krabi Province, Thailand, about 814 km south of Bangkok or about 70 km southeast of Krabi city, at latitude 7° 54.199' N and longitude 99° 6.505' (Fig. 1a and b). At the KB4 site altogether 15 natural hot springs can be found with surface exit temperatures between 41 and 47 °C (Fig. 2a-d, Fig.3, Table 1). Moreover, several hot springs have been developed for tourism with a rapid expansion of the site as a tourist attraction (Fig. 2a, b). An integrated geoscientific study was carried out combining geological fieldwork, geophysical surveys, and geochemical analysis for an understanding of the geological, hydrogeological, and hydrogeothermal boundaries.

Methodology

In order to understand the subsurface structure of the saline hot springs geological fieldwork including shallow soil borings were carried out. Geochemical analysis of hot spring water and groundwater samples were collected with temperature and salinity measured in the field. Major cation and anion as well as isotopes and REEs were measured at the Faculty of Science Laboratory of Prince of Songkla University in HatYai and at the Geoscience Centre at the University of Göttingen (GZG, Germany). Geophysical surveys were carried out:vertical electrical soundings (VES) at 30 measurement points with Schlumberger array and a maximum AB/2 of 300 m and four profiles of an electrical resistivity tomography (ERT) surveys in dipole-dipole configuration have been carried in the larger area. The ERT processing was done with RES2DINV software to produces an image of the electrical resistivity distribution of the subsurface. Moreover, two profiles of shallow seismic reflection

(SSR) surveys have been recorded in the northern and southern part of the study area.

Results and Discussion

A. Integrated geoscientific investigations

All result from geological, geochemical, and geophysical investigations allows explaining the current situation of KB4 hot spring system as followed below.

Geological surveys in the area showed different geological units belonging to Tertiary and alluvial deposits [3], Fig. 3. The shallow subsurface of alluvial deposits consists of medium to coarse grained sand with plant roots, black marine clay and clay, and covers most parts of the study area (Fig. 4).

Sandstones of Tertiary deposits cover all of the study area, and carbonate crusts can be found around the natural pools inside the mangrove area and near local wells (Fig. 2c). The carbonate crusts indicate that the hot water pathway from the depth of the reservoir likely was through a layer of the carbonate rock, e.g. limestone, which is found nearby (Fig. 3).

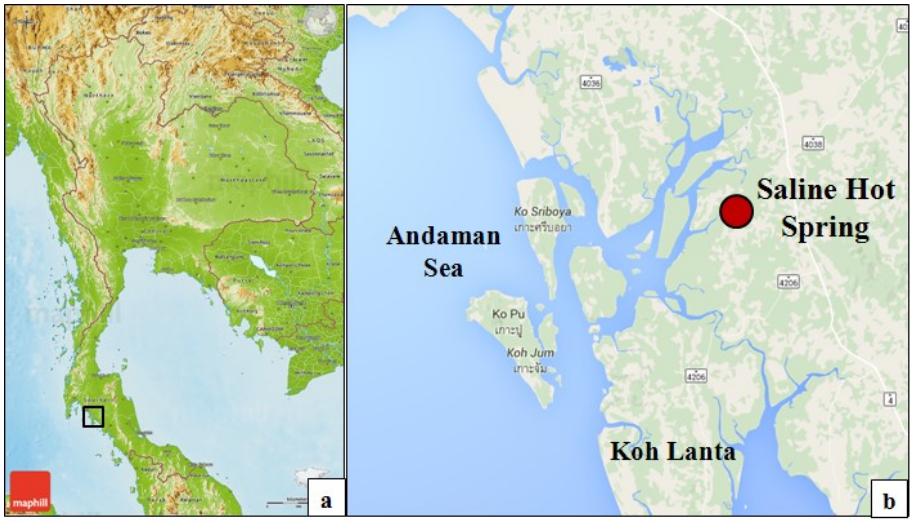

Fig. 1. Location of the study area; a) Thailand topographic map (from maphill.com), black lined square detailed in b), b) Natural saline hot spring located in southern part of Krabi Province near major estuaries connected to the Andaman Sea.

Fig. 2. Saline hot spring KB 4; a) man-made pool structures for tourism at KB 4/5, b) man-made pool structures for tourism at KB 4/1, c) natural hot spring KB4/10 used by local villagers, and d) natural hot spring sites with precipitated carbonate crust around in the area between KB 4/1 and KB 4/10 (for locations see also Fig. 3).

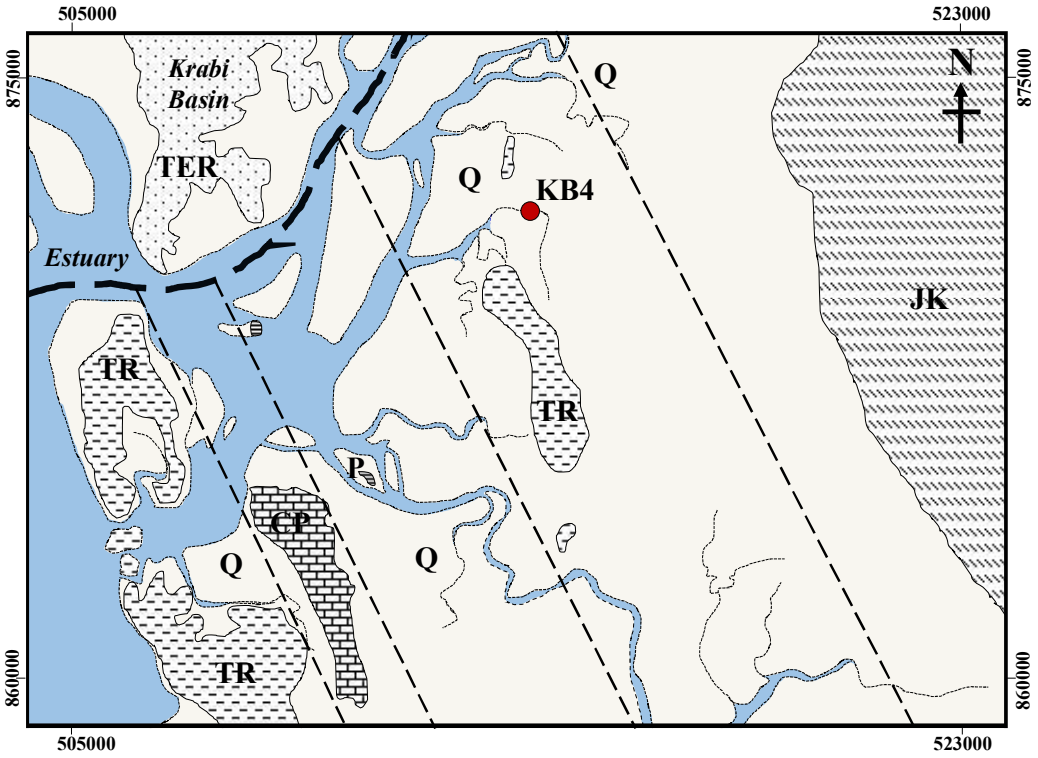

Fig. 3 Geological setting of Krabi Province: Quaternary (Q), Tertiary (TER), Triassic (TR), Cretaceous-Jurassic (JK), Permian (P), Permian-Carboniferous (CP), after DMR (2010), Saline Hot Spring Khlong Thom at KB4; dashed lined indicate faults, thinner lines = faults, thicker line = fault zone (basin boundary of Krabi basin) Grid in UTM, Zone 47, WGS-84.

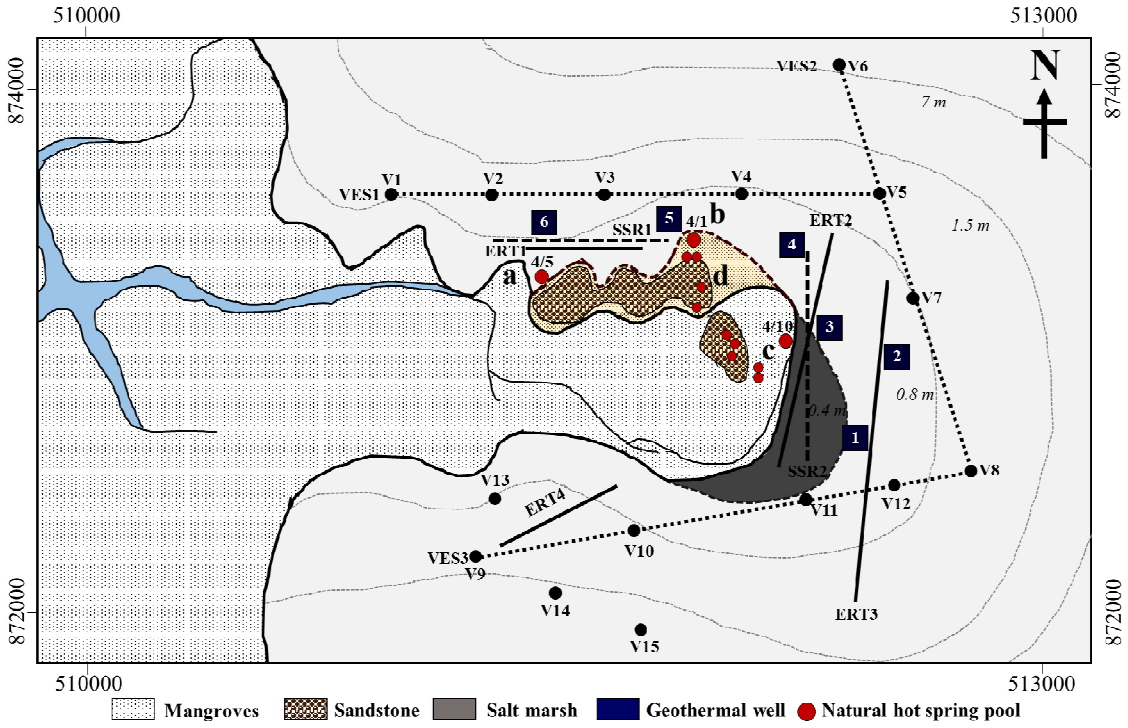

Fig. 4. Location of the study area, elevation data (dotted lines), location of salt marsh, boundary of shoreline, hot spring locations (selected with numbers), well locations and numbers (black squares), as well as VES cross sections, and ERT and SSR survey line locations. a-d indicate location of photos in Fig. 2; Grid in UTM, Zone 47, WGS-84.

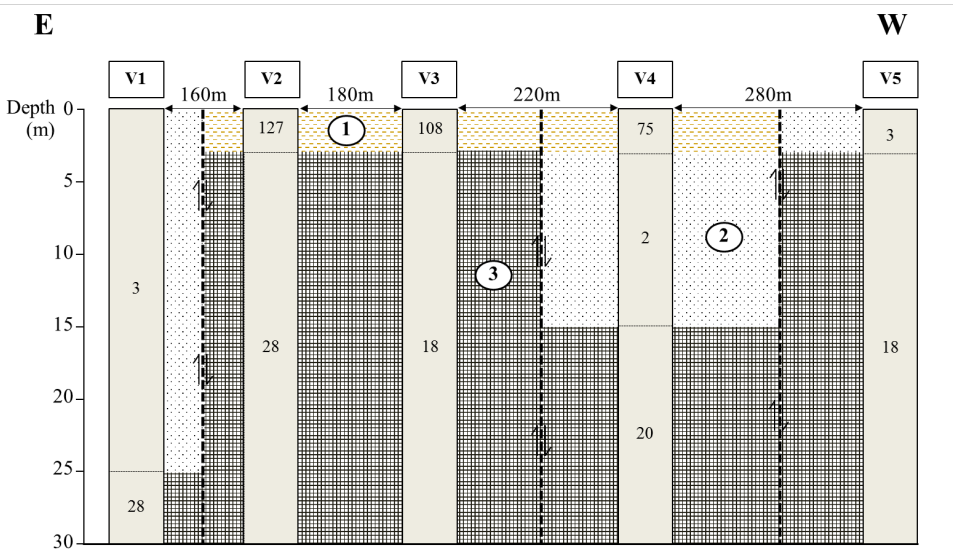

Fig. 5. Vertical electrical sounding results for station V1-V5 (see Fig. 4), with three main layers: (1) topsoil, partly more sandy, partly more clayey, (2) low resistivity second layer with (salty?) clay , and (3) sand/sandstone with saline (hot?) water; faults have been introduced to accommodate resistivity contracts at relatively short horizontal distance.

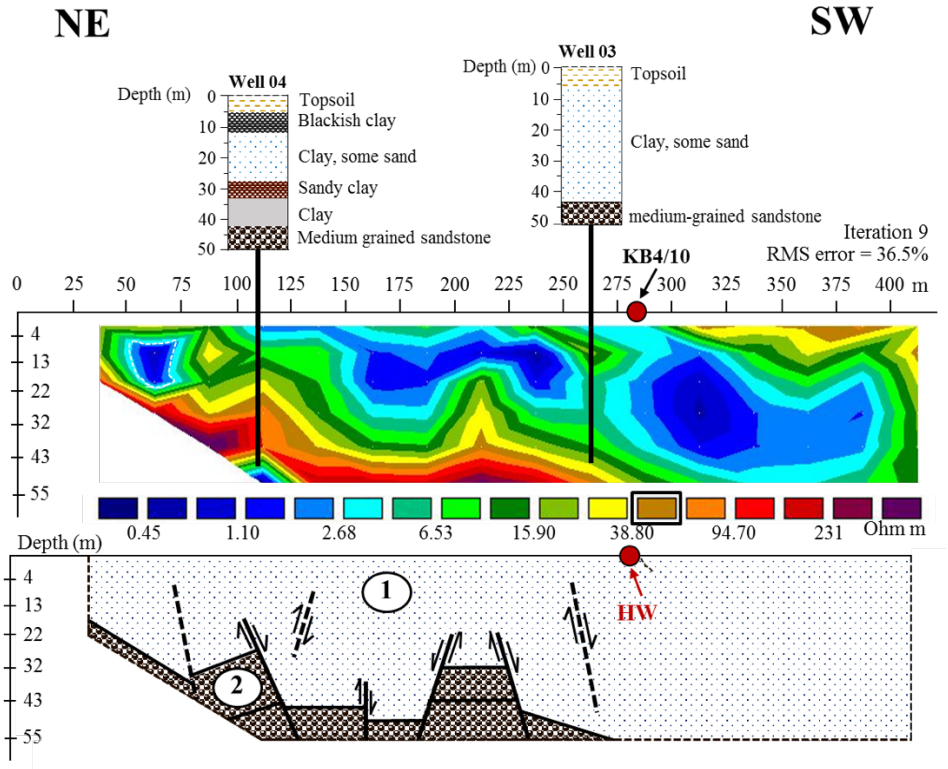

Fig. 6. ERT2 with location of natural hot spring (KB 4/10) and the Well 03 and Well 04, using dipole–dipole configuration; (1) clay/sand layers with saline (hot?) water, (2) medium-grained sandstone. HW: geothermal hot water surface exit at KB 4/10.

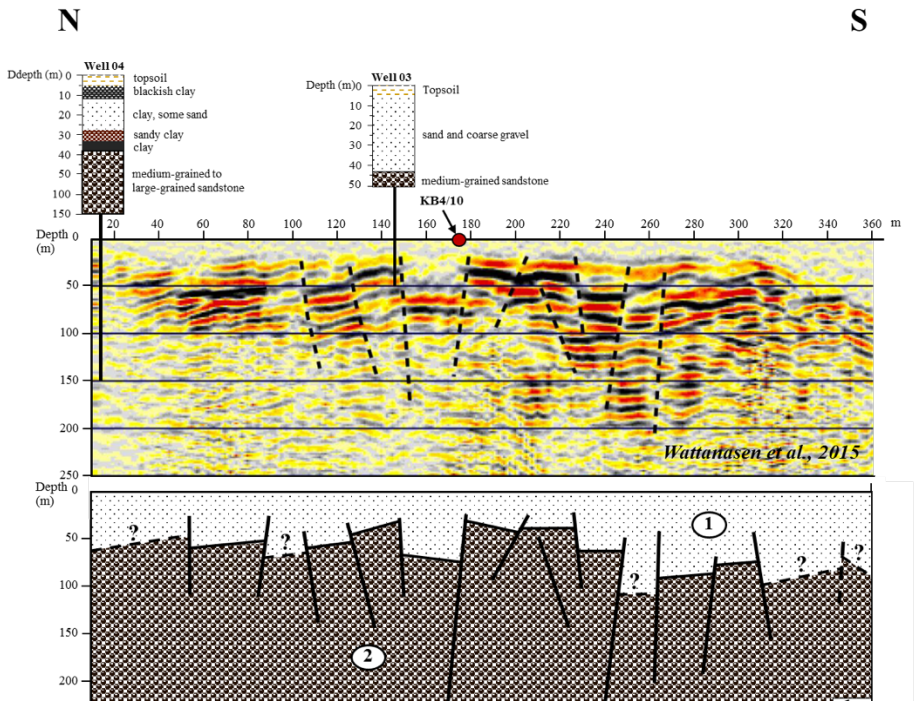

Fig. 7 Geological section based on well data along seismic reflection profiles; here interpreted North–South seismic line with location of natural hot spring (KB 4/10). A sharp seismic contrast indicates a possible vertical fault (black dashed line), Layer (1) indicate sand/clay with saline (hot?) water, (2) sandstone; after [4].

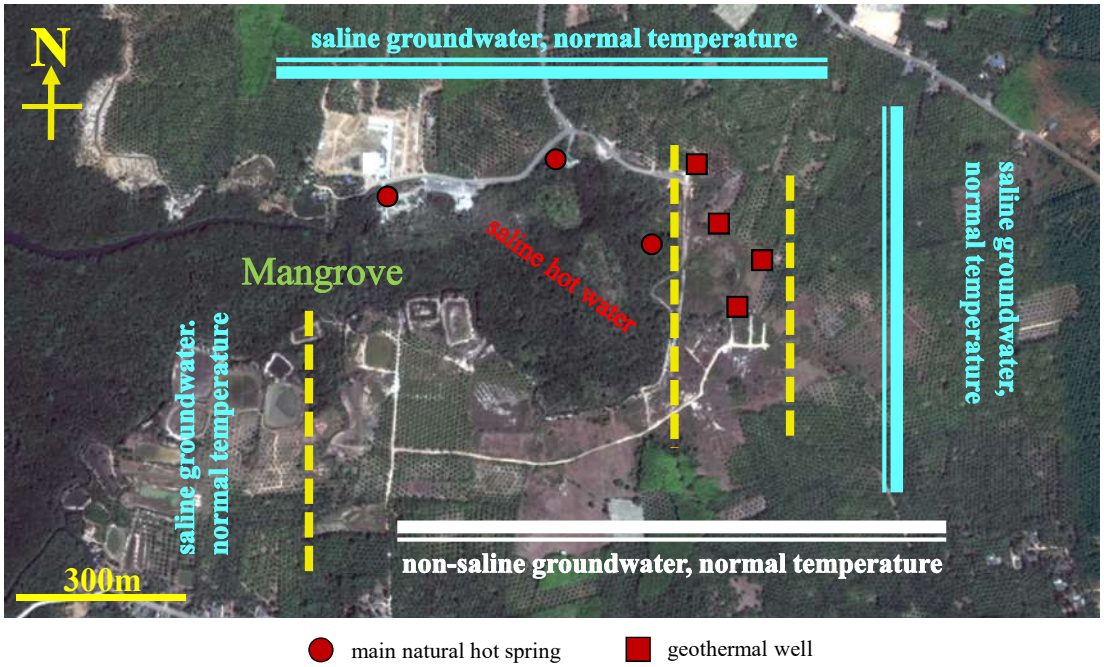

Fig. 8. Estimated boundaries of KB4 area, with possible faults (indicated by dashed yellow lines) and thinning of layers (indicated by white/blue double lines). Estimated areas of different water types are indicated. Basemap GoogleEarth™.

All the water samples from KB4 system are taste salty thus leading to the name "saline hot spring". The exit temperature, pH and concentrations of some cations and anions of all water samples in KB4 area are presented in Table 1. The salinity was measured with a refractometer at sampling points shown salinity values of about 21,000 mg/L, while estuary and sea water represented approximately 31,000 mg/L and 36,000 mg/L, respectively. TDS concentrations in the natural hot springs and geothermal wells range from 12,000 to 13,000 mg/l (Table 1). Water salinity can vary according to the TDS concentration [5] and thus can be expressed as the sum of the total dissolved concentrations of major inorganic ions (i.e. Na, Ca, Mg, K, HCO_3, SO_4, and Cl), with results for KB4 of around 17,000 mg/L and for the estuary water over 35,000 mg/L. According to the classification of saline waters both values characterize "very highly saline" water [5]. On the other hand, $^{87}Sr/^{86}Sr$ isotopes and rare-earth elements (REEs) (data not shown) indicate that KB4 hot spring samples are close to the estuary/sea water composition, thus confirming the interaction and mixing of both waters in the shallow subsurface.

Table I. pH, temperature, and major element composition (in mg/L) of KB4/5, geothermal wells (see Fig. 4), an estuary sample, and non-saline groundwater (GW). TDS: total dissolves solids.

Parameter	KB4/5	Well1	Well2	Well3	Estuary	GW
T (°C)	46	43	42	41	27	28
pH	6.76	6.54	6.51	6.8	7.8	6.98
TDS	12,663	12,669	12,673	12,671	34,483	43.00
Cl	10,361	9,086	9,237	7,710	19,345	15.52
HCO_3	289	174	192	203	145	19.22
Ca	948	838	838	253	416	2.52
SiO_2	32	35	34	34	28	1.2
K	183	158	166	88	390	0.37
Mg	339	316	317	138	1,295	0.45
Na	5,198	4,710	4,741	626	10,752	7.40
SO_4	420	582	584	512	2,701	10

Electrical resistivity surveys (ERT, VES) show very low resistivity values (below 5 ohm-m) at relatively shallow depth (Fig. 5 and 6). At profile ERT2 (Fig. 6), low resistivity values are at 5 to 20 m in the southern and at 5 to 60 m in the northern part of KB4/10 site (Fig. 4 and 6). These low values can be correlated to saline water in sandstone layers. A 150 m-deep well drilled of Well04 in the hot spring area shows only sandstone of different color, with upper layers weathered. In order to explain this, a fault has been introduced between both sites. In the western part another fault has been introduced based on significant differences in ERT2 profiles at short horizontal distances, which could not be explained by normal stratigraphy. Vertical electrical soundings (VES, Fig. 5) also present similar resistivity distributions with depth as shown in ERT2. Shallow seismic refraction (SSR, Fig. 7) surveys also indicate shallow and deeper fault, down to around 150 m depth.

B. Hydrogeological setting

Integrating all data from geological, geophysical and geochemical analysis the hydrogeological setting of the KB4 geothermal hot spring area can be drawn. Hot water coming along faults upwards to the near surface where they are mixing with the local saline groundwater from estuary water intrusion. This makes the hot water salty, which then exits naturally through hot springs. Calcium dissolved in the hot water then flowing through subsurface limestone precipitates at the surface and makes the carbonate crust around the hot springs. When the hot water exits in a surface water body, no such crust could develop. Most of the shallow subsurface is faulted and these faults also can act as seals preventing lateral flow.

C. Boundaries of KB4 hot spring area

From the topography the KB 4 hot spring site is located at the shore line of the Andaman Sea in a lower lying circle-shaped area, open towards the estuary at in the western side, sandstone hills and outcrops can be found inside (Fig. 4). Shallow layers are mainly (marine?) clay and sand weathered from the hills. Salt water from the estuary in the area contaminated these shallow aquifers. Faults related to the overall tectonics (see Fig. 3), traced down to at least 200 m depth (Fig. 7), separated the area in a small scale compartments and also allowing hot water to flow up. Towards the outer boundaries of the circle-shaped low lying area elevation increases (Fig. 4; except to the west), and the shallow sedimentary layers stratigraphically phase out as shown in the seismic and ERT sections; Fig. 6 and 7 show this towards the northern boundary (Fig. 8). VES and ERT data, which are not shown here, also confirm this towards the eastern and southern boundary (Fig. 8).

Conclusions and remark

Geophysical and geochemical investigations at the saline hot spring area in Krabi Province have shown that the hot water is coming from a deeper reservoir whereas the salty water is coming from the estuary via intrusion into shallow aquifers. The exchange might be through faults that have been delineated in the shallow subsurface. They also act as boundaries for the hot waters and by this restricting further flow into the aquifers, by this limiting the spatial extent of the hot spring area. However, the outer boundaries of saline hot water system are marked by the topography of the circle-shaped low lying area where KB 4 is located in as sedimentary layers stratigraphically phase out marked by increasing elevation at the surface. Any extensive drilling and use of any of the waters may alter the whole system.

References

[1] M. Raksaskulwong, "Geothermal direct–use in southern Thailand", in the 6th Asian Geothermal Symposium, 2004, 26–29 October.
[2] W. Ngansom and H. Durrast, "Saline hot spring in Krabi, Thailand: A unique geothermal system", in Society of Exploration Geophysicists, 2016, pp. 1949–4645
[3] DMR, Department of Mineral Resources, Geological Map of Thailand Scale 1:2,500,000, 2010.
[4] Wattanasen K, Duerrast H, Yordkayhun S, Wattanasen S Geological Characterization of the Klongtom Geothermal Saline Hot Spring, Krabi Province Using Geophysical Methods and Soil-Water Quality. Project (I) of The Sustainable Tourism Development of the Klongtom Saline Hot Spring, Krabi. National Research Council of Thailand (NRCT) and The Thailand Research Fund, 2015.
[5] A.E. Sveinbjörnsdóttir, "Composition of geothermal minerals from saline and dilute fluids Krafla and Reykjanes, Iceland", in Lithos, vol. 27,1992, pp. 301–315

Delineation of Unconventional Groundwater: I. Soda Groundwater in Songkhla, Thailand

Poonnapa Klamthim[1,a], Helmut Duerrast[1,b] and Manussawee Hengsuwan[2,c]

Abstract The majority of groundwater bodies are of conventional type, but in rare cases unconventional groundwater can be found, mainly related to fluids rising from the depth. Soda rich groundwater is a special case of groundwater, called carbon dioxide-rich groundwater or CO_2-rich groundwater. This type of water can be often found in volcanic geological settings, but it is less common in basin settings. Sources of the carbon dioxide vary from site to site. In Thailand there is one known site of soda-rich groundwater, in Khlong Hoi Khong, Songkhla Province. Various geophysical and geochemical methods have been applied to understand and characterize the occurrence and pathways of the CO_2 in this area. Initial results of this ongoing study suggest upper mantle CO_2 as the source and the carbon dioxide moved up along faults before accumulating in shallow groundwater aquifers, which were sealed by clay formations.

Keywords *carbon dioxide, soda-rich groundwater, Southern Thailand, Songkhla*

[1]Geophysics, Department of Physics,
Prince of Songkla University
Hat Yai, Thailand
[2]Department of Groundwater Resources
Ladyao, Chatuchak
Bangkok, Thailand

[a]aumaimm_pk@hotmail.com
[b]helmut.j@psu.ac.th
[c]manussawee.h@dgr.mail.go.th

Introduction

Groundwater is freshwater from rain that is stored under the Earth's surface in pore spaces. The majority of groundwater bodies are of conventional type and its utilization is important for people's livelihood as well as for agriculture and industrial production. In rare cases unconventional groundwater can be found, mainly related to fluids rising from the depth. Soda groundwater is a special case of groundwater, called carbon dioxide-rich groundwater or CO_2-rich groundwater that can occur in special tectonic settings [1]. There is no formal definition of carbon dioxide-rich groundwater, but common characteristics are: slightly acidic, relatively high content of total dissolved solids or TDS, very high partial pressure of carbon dioxide gas in equilibrium with water or $P(CO_2)$, and high concentrations of carbon dioxide fluid which compose of CO_2, HCO_3^- and CO_3^{2-} [2]. Groundwater with high carbon dioxide concentrations is globally distributed but it is not a common phenomenon. A suitable geological system for carbon dioxide storage and carbon dioxide-rich groundwater as shown in Fig. 1 includes: (1) A source of carbon dioxide gas, (2) pathways for carbon dioxide to move from the source upwards into the groundwater, (3) porosity and permeability of the formation that can provide storage volume for the carbon dioxide, and (4) the system must be covered by an impermeable layer acting as a seal to prevent carbon dioxide leakage [3]. Soda groundwater sites can be classified in different geology settings: Volcanic, metamorphic, and sedimentary basin setting. Comparing to the first two settings soda groundwater occurrence in sedimentary basins is less common and also the source of carbon dioxide is not obvious.

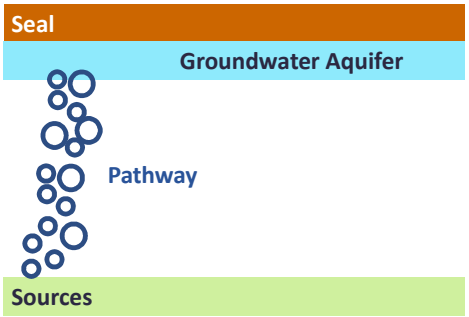

Fig. 1. Schematic drawing of the CO_2 pathway from various sources to be accumulated in groundwater becoming CO_2-rich groundwater.

There are many possible sources of CO_2 in groundwater. First is CO_2 from magmatic CO_2 which dissolved in magma as magmatic fluid rises from the upper mantle towards the crust. CO_2 rich mantle fluid moves up along faults or fracture. Second is metamorphic source. The contact metamorphism occurs around magma in high temperature area when magma rises through the rock and interacts with limestone. Third is CO_2 from a decomposition of organic matter or soil organic matter. Last is CO_2 from the weathering of carbonate rock. Carbonic acid from dissolve carbon dioxide in rain water interacts with carbonate rock and then the reaction produces CO_2 in form of calcium bicarbonate [2].

There is one report about CO_2 rich groundwater in Thailand which is located in Khlong Hoi Khong, Songkhla, in Southern Thailand. A better understanding of this soda rich groundwater, which is the objective of this ongoing study, will benefit the people living in the area and might also open opportunities to utilize this unconventional groundwater.

Study area

The study area is in Khlong Hoi Khong at a Royal Research Farm, which is located about 20 km southwest of Hat Yai City, Songkhla Province, Thailand. Many agricultural activities are carried out on this 1.28 km2 farm, e.g. cattle production, fruit tree plantations, and plant crop production. The study area is located in the central part of Hat Yai Basin (Fig. 2 and 3).

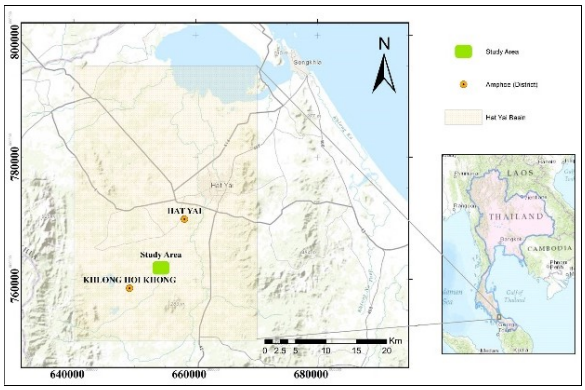

Fig. 2. Topographic map of Hat Yai Basin, Songkhla Province, Thailand (modified after ESRI world topographic map).

Hat Yai Basin is thought to be a graben which is bounded at the east and west by mountain ranges, which are part of a horst system. U-Tapao is the main river system in this area, which is about 80 km long and flows from south to north into the Songkhla Lake. Hat Yai Basin is a sedimentary basin ranging in age from Carboniferous to Quaternary (see Fig 4, next page). Granitic rocks intruded into Carboniferous and Triassic sedimentary rocks. Metamorphic rocks were found mainly at the eastern and western side of the basin, which form the basement of the basin Pegmanite, aplite, and quartz veins locally cut granites and sedimentary rocks. Carboniferous rocks are composed of sandstone, mudstone, chert, and quarzitic sandstone. Triassic rock comprises of a red bed of conglomerates, sandstones, mudstones, and limestone. Late Triassic to early Jurassic granites are mainly coarse-grained porphyritic biotite and biotite-muscovite granites with quartz veins [4].

Hat Yai basin is overlain by thick Quaternary deposits with an age from 1.6 million years to present time. The Quaternary alluvium composes of gravel, sand silt, and clay. The aquifer system comprises of unconsolidated and consolidated aquifers. There are three main aquifers in Hat Yai Basin. The upper aquifer (Hat Yai aquifer) is an unconfined to semi-confined aquifer at a depth of 20 to 40 m. This aquifer consists of moderately to well-sorted sand and gravel and is separated from the lower aquifer by a layer of low permeable clay. The lower aquifer (Khu Tao aquifer) is a confined aquifer, which consists of poorly sorted sand, gravel and several clay layers. The depth to the top of aquifer ranges from 50 to 100 m. The deepest aquifer is the Khohong aquifer, which is deeper than 100 m. It consists of unconsolidated and semi-consolidated clay, sand, and gravel [5].

Drilling encountered at two sites on the Royal Research Farm area soda rich groundwater with well D2 and D4 (see Fig. 3). Only about 500 m north of the well D2 several wells were drilled showing normal (freshwater type) groundwater; well D1 and D9 are shown in Fig. 3.

Methodology

In order to characterize the source and pathways of the soda rich groundwater mainly geophysical and geochemical methods were applied.

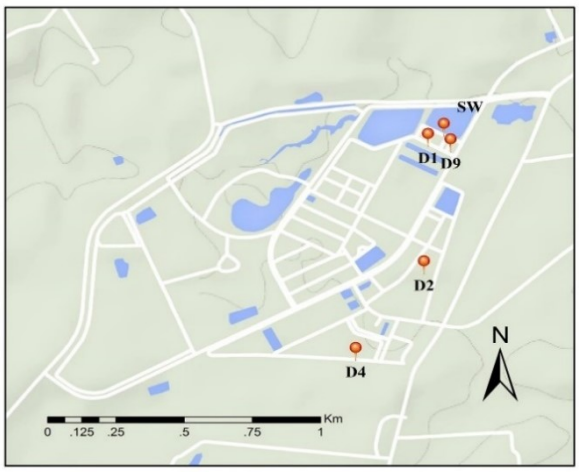

Fig. 3. Sample locations on the Royal Farm: D1 and D9 are non-CO_2-rich groundwater; D2 and D4 are CO_2-rich groundwater locations; SW is surface water. Modified after Google Maps.

Geophysical methods comprise mainly of 1D (vertical electrical sounding, VES) and 2D resistivity surveys (electrical resistivity tomography, ERT) on the farm and in the surrounding area in order to investigate lithological boundaries and fluid pathways in the upper 150 m. Schlumberger configuration was used for VES surveys with maximal AB/2 of 600 m. ERT surveys were conducted in dipole-dipole array type arrangement with maximal n=8. For all measurements ABEM terrameter SAS 1000 was utilized.

To obtain hydrochemical and isotopic data, two samples of CO2-rich groundwater (D2, D4), two samples of non CO2-rich groundwater (D1, D9), one surface water sample, and four borehole cutting samples from a newly drilled groundwater borehole (D9) were collected. D1, D2, D4, and D9 are at 108, 128, 136, and 78 meter depth, respectively (Fig. 3).

All water samples for major cations, rare earth elements and Sr-isotope measurements were filtered through a 0.45 µm membrane filter and acidified to pH 2 with concentrated double-distilled HNO3. Non-acidified water samples were collected for anion and Tritium (3H) determination. For 13C measurement, NaOH was added to water samples to pH 11. Precipitates of BaCO3 formed after adding BaCl2 to the alkaline solution. These precipitates were removed from the residual water and oven-dried at 60 °C.

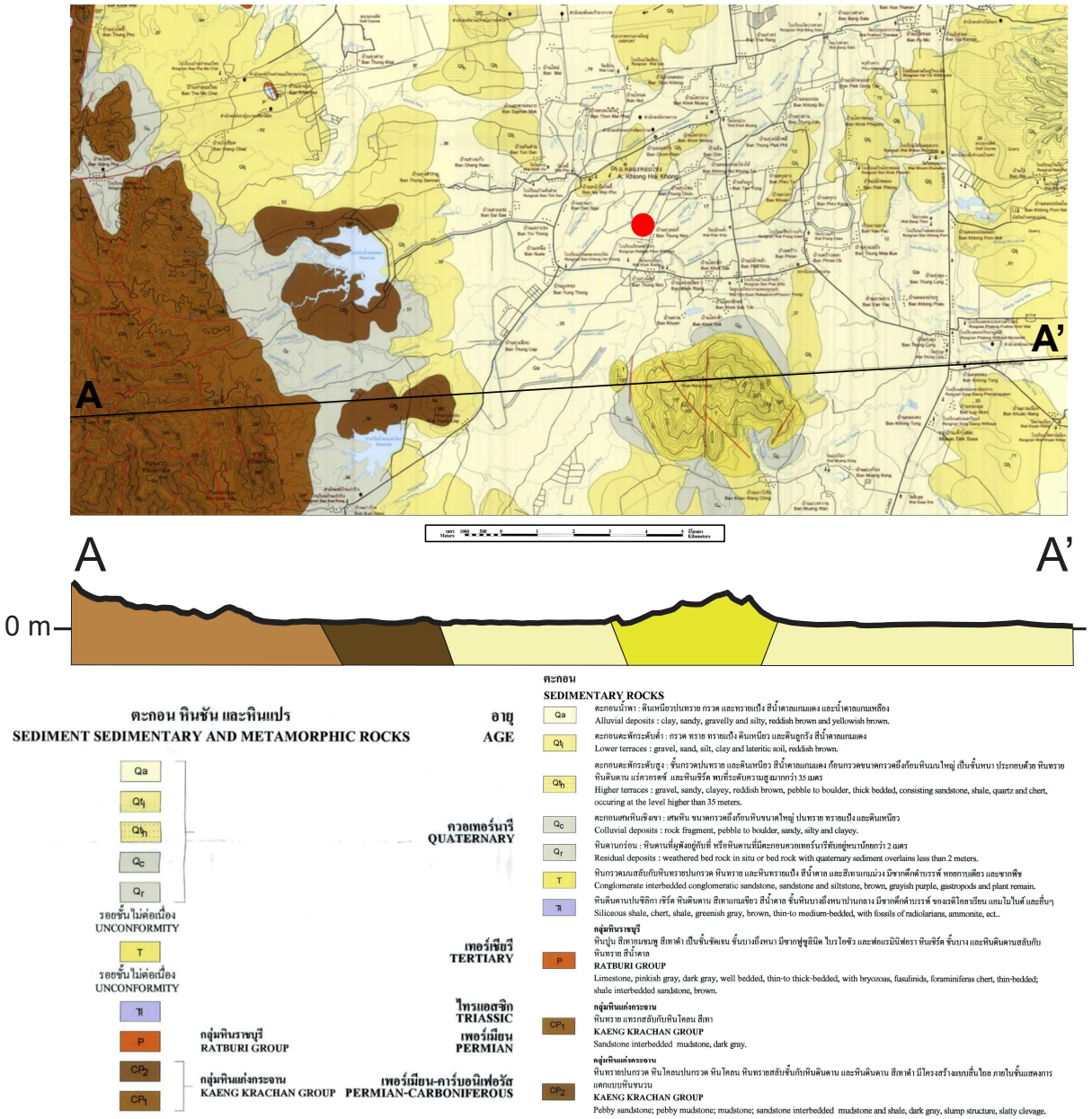

Fig. 4. Geological map of the larger study area of southern the southern part of Songkhla Province (from and modified after [6]). Red dot – location of farm.

Major cations and anions were performed at the Central Equipment Division, Faculty of Science, Prince of Songkla University (PSU, Thailand) using an ICP-OES, ion chromatography and titration method. Rare earth elements and 13C were analyzed by ICP-MS on a VG Plasma Quad II and Thermo Kiel IV with Finnigan DeltaPlus Mass Spectrometer, respectively, at the Geoscience Centre at University of Göttingen (GZG, Germany). ^{3}H contents were analyzed by Liquid Scintillation Counter (Tricarb 3180 TR/SL) after electrolytic enrichment at the Thailand Institute of Nuclear Technology (TINT). Sr analyses were performed on a Thermo-Finnigan Triton© TIMS at the Geoscience Centre at University of Göttingen (GZG, Germany). Prior to digestion, samples were mixed with a tracer solution enriched in ^{87}Rb-^{84}Sr.

Fig. 5. Vertical electrical sounding (VES, 1D) surveys in the study area and south of it: left: location of center, line direction, and max. AB/2 in meter; right: location of cross section 1 shown in Fig. 6.

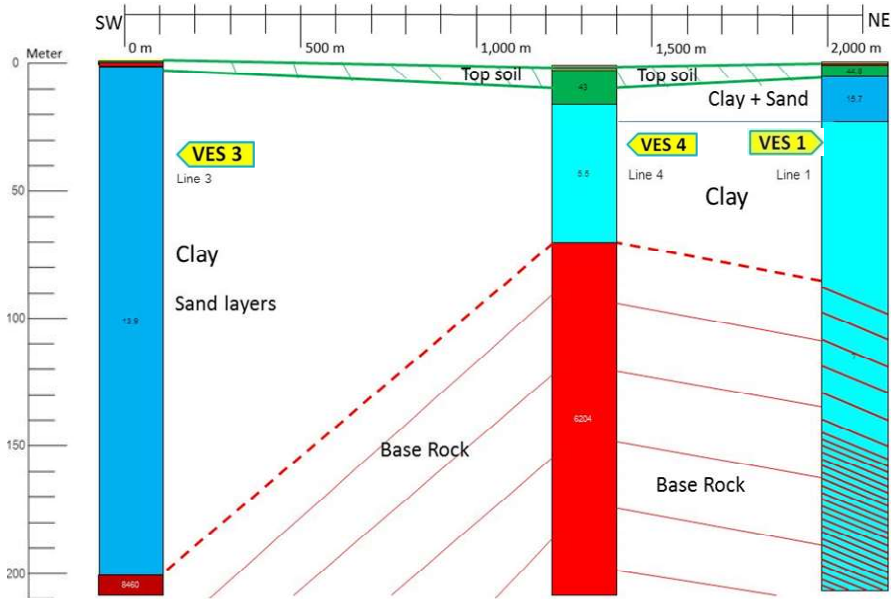

Fig. 6. Vertical electrical sounding (VES, 1D) surveys in the study area and south of it: Cross section comprising VES 3, 4, and 1 from SW to NE. Below the top soil is a low resistivity clay layer (with relatively thin sand layers). At the bottom is higher resistivity base rock (mud stone) increasing in depth from NE to SW over a short horizontal distance, thus requiring the introduction of a fault (see Fig. 7).

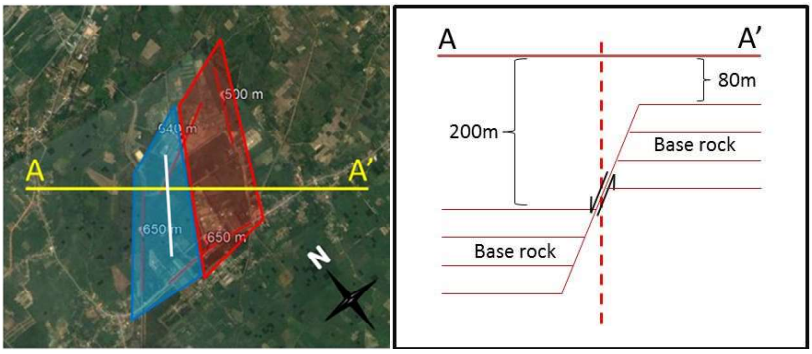

Fig. 7. Schematic cross section and possible fault orientation based on vertical electrical sounding (VES, 1D) surveys in the study area and south of it, see also Fig. 5 and 6.

Throughout this work a value of 0.710259±0.000076 (2σ) for the NBS 987 (n=4) was observed. Instrumental mass fractionation was corrected with $^{88}Sr/^{86}Sr$ of 0.1194 using exponential law.

Results and Discussion

Results show that the investigated groundwater can be classified in Na-Cl type for non-CO_2-rich groundwater (D1, D9) and in Na-Ca-HCO_3 type for CO_2-rich groundwater (D2, D4). The concentrations of the most cations (e.g. Ca, Mg, Na, K, Ba) and anions (e.g. Cl, SO4, HCO_3) including total dissolved solid (TDS) in CO_2-rich groundwater are significantly higher than that in non-CO_2-rich groundwater. In both CO_2-rich groundwater samples (D2 and D4) HCO_3 is the dominant anion (1,658 and 1,756 mg/L, respectively), followed by SO_4 (122 and 110 mg/L, respectively).

Sr concentrations in CO_2-rich groundwater were relatively high, ranging from 1.30 to 1.37 µg/g. These concentrations are about 100 times higher than in non-CO_2-rich groundwater. The $^{87}Sr/^{86}Sr$ ratio of D2 and D4 showed a specific value of 0.726, whereas the $^{87}Sr/^{86}Sr$ ratios in the other waters ranged from 0.725 to 0.731. The high concentrations of ^{3}H were found in D1, D9 and surface water. The ^{3}H amount in soda groundwater was about four times lower than in non-soda groundwater. The $\delta^{13}C$ was significantly more depleted in D1, D9 and surface water than in D2 and D4. Sr concentrations and $^{87}Sr/^{86}Sr$ from well D9 ranged from 4.6 to 60.0 µg/g and 0.74118 to 0.776916 respectively.

Eu showed a positive anomaly ranging from 1.97 to 2.95 in non-CO_2-rich groundwater and exhibited a slightly negative anomaly in surface water. In contrast, the Eu anomaly of CO_2-rich groundwater was significantly positive with values of 32.38 and 72.26.

$\delta^{13}C$ values of CO_2-rich groundwater in this area ranging from -4.8 to -4.3‰ VPDB are in good agreement with the magmatic $\delta^{13}C$ values, which are normally characterized by $\delta^{13}C$ values between -10 and -3‰ VPDB [6]. Tritium amount close to zero (0.29-0.38 TU) is an evidence of long residence time for water circulation exceeding 50 years. These hydrogeochemical and isotopic data indicate that the CO_2-rich groundwater was formed by the supply of deep-seated (magmatic) CO_2 at depth and rise along a fault system to the relatively shallow aquifers.

Geophysical VES results presented in Fig. 5-7 show higher resistivity bedrock at different depth, deeper in the SW part and shallower in the NE part south of the farm, thus indicating an extension of vertical faults under the farm. In some 2D resistivity sections (data not shown here) the resistivity distributions indicate vertical faults.

Conclusions

The CO2-rich groundwater in Khlong Hoi Khong in Songkhla Province, Thailand, can be characterized by its high HCO3, high TDS, and weak acidic to neutral pH. Based on the isotopic and hydrochemical data it can be concluded that the difference in CO2 content in the groundwater of this farm area can be interpreted to be the result of tectonic activities, probably during the basin development, with the migration of deep CO2-rich waters along fault systems up to shallower aquifers, where they accumulated as thicker clay layers acted as a seals prevented the CO2 to exit to the surface (Fig. 8; see also Fig. 1).

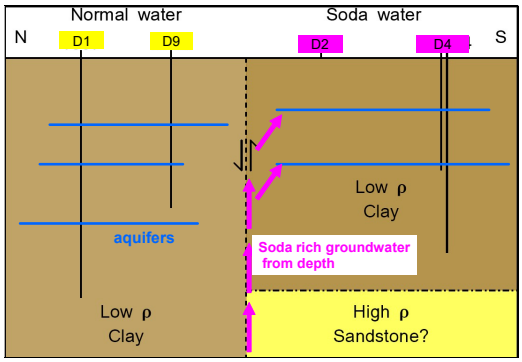

Fig. 8. Schematic drawing of the hydrogeological setting resulting in CO_2-rich groundwater occurrence in Songkhla.

Acknowledgment

Both authors thank K. Chotirat (Department of Groundwater Resources, DGR, Thailand) and B.T. Hansen (formerly GZG, University of Goettingen, Germany) for their valuable support and fruitful discussions. Support from the management and staff members of the Royal Farm is highly acknowledged, as well from the offices of DGR Trang, DGR Songkhla, and DGR Bangkok.

References

[1] D.L. Thomas, D.K. Bird, S. Arnórsson, and K. Maher, "Geochemistry of CO_2-rich waters in Iceland," Chemical Geology, 444, 158-179, 2016.

[2] Y.K. Koh, B.Y. Choi, S.T. Yun, H.S. Choi, B. Mayer and S.W. Ryoo, "Origin and evolution of two contrasting thermal groundwaters (CO_2-rich and alkaline) in the Jungwon area, South Korea," Hydrochemical and isotopic evidence. Journal of Volcanology and Geothermal Research, 178(4), 777-786, 2008.

[3] E.K. Halland. "CO_2 Storage Atlas, Norwegian North Sea, Norway," Norwegian Petroleum Directorate, 2011.

[4] W. Lohawijarn, "Potential Ground Water Resources of Hat Yai Basin in Peninsular Thailand by Gravity Study." Songkhlanakarin Journal of Science and Technology 27(3), 633-647, 2005.

[5] A. Wattanathum, T. Chalermyanont, P. Sompongchaiyakul and S. Piromlert, "Numerical groundwater flow model for Hat Yai Basin, Songkhla Province, Thailand: a conceptual model," In the Proceeding of the 3rd National Environmental Conference. Hat Yai, Songkhla, 2004.

[6] DMR, Department of Mineral Resources, Geological Map of Ban Khlong Ngae Quadrangle, 2006.

[7] I.D. Clark and P. Fritz, "Environmental Isotopes in Hydrogeology". USA, CRC Press. 328 p, 1954.

Potential impact of severe weather on hydraulic performance of a field-scale wastewater treatment plant: A case study of baffle-based pond

Saifhon Tomkratoke[1,a], Teppatat Pantuphag[1,b] and Sirod Sirisup[1,c]

Abstract Water pollution is a relevance problem in Thailand's water resources management. Overall, the current status of the surface water of Thailand is moderate to good quality except that of the central Chao Phraya watershed which deteriorates. This fact indicates that the environmental management policy and wastewater treatment infrastructure of the country may need to be improved for enhancing efficiency in wastewater and stormwater treatment. Focusing on the latter issue, despite significant wastewater contributions from domestic and industrial sectors, establishing and maintaining their wastewater treatment plants need utmost responsibilities and must be ready for challenges from climate variation influences. However, the excessive cost is still a vital issue in developing wastewater treatment infrastructure, therefore, improving and modernizing the existing structures can be more useful alternatives. On a field scale, waste stabilization ponds with baffles (WSPBs) configuration can be one of the possible solutions to the mentioned issue. However, generalizing the structure to fit various sites and finding the optimal design remains a challenge. In developing know-how for a country with different climatic regions like Thailand, the impacts of environmental factors like severe weather, unusually heavy rainfall on hydraulic performance and caring capacity of the pond should also be included. In this study, we conduct a numerical experiment of hydraulic flow of WSPBs via a sophisticated Navier-Stoke model. Several hydraulic flow scenarios associated with severe weather conditions have been used to drive the model. Finally, the optimal design of WSPBs will be evaluated. This research could help benefit the communities related to water pollution management and provide an understanding of wastewater infrastructure design.

Keywords *wastewater treatment, hydraulic performance, baffles, porous media fliter*

[1]Data-driven Simulation and Systems Research Team, National Electronics and Computer Technology Center, Pathumthani, Thailand

[a]saifhon.tomkratoke@nectec.or.th
[b]teppatat.pantuphag@nectec.or.th
[c]sirod.sirisup@nectec.or.th

Introduction

Waste stabilization ponds (WSPs) are open basins designed for removing pathogens from wastewater collected from the sewerage system of urban, agricultural and industrial units. Using natural processes such as sunlight exposure, sedimentation, hydraulic flow and physical-chemical factors (including temperature and pH) to remove pathogens is the main concept of this technology. However, controlling hydraulic efficiency of the ponds is the most suggested approach for design, operation and maintenance basis of pathogen removal in WSPs. Mostly, guidance may suggest maintaining theoretical hydraulic retention time (HRT) of the pond for receiving an optimal level of treatment performance. Systems with significantly long hydraulic retention times can contribute certainly influences on pathogen removal in WSPs. Because longer reside of wastewater in WSPs may enhance treatment performance of pathogens and pollutants by higher sedimentation and longer contact with sunlight. Consequently, discharging of slowest growing microorganisms (necessary for an anaerobic process) and spreading of helminth eggs and coliforms are disrupted. Recently, impacts of hydraulic retention times (HRTs) and pond depths on the reduction of pathogens have been reported by [1].

Controlling HRT is such beneficial guidance for operating/designing WSPs, but in reality, this may be a difficult doing. Because factors such as constantly changing flow rate, hydraulic dead space and hydraulic short-circuiting, channeling effect, sludge accumulation, inlet/outlet configurations, etc. can effect hydraulic efficiency in the ponds. As hydraulic problems of WSPs is considered, the improving scheme such as baffles is commonly used in WSPs. Therefore, waste stabilization pond with baffles (WSPBs) is also a widely used configuration in the opened-wastewatertreatment system. Because of the balance between the received treatment performance and the cost. Generally, both concrete and earthen structures are used for installing baffles in WSPs. Moreover, basins separated by baffles can be applied such a primary treatment sequentially i.e. anaerobic ponds, facultative ponds and maturation ponds. However, the function of the pond can be the sub-optimal level as some hydraulic behaviors i.e. short-circuiting and dead space occurs. The first behavior can arise when applying small baffle

geometric ratios i.e. small inlet size and overuse numbers of baffles while the second one is the result of the reversal flow cell or eddy. The increment of fluid momentum is a driver of the latter phenomena. Hence, both pond geometries and flow rates are involved in treatment inefficiency. Besides, most of WSPs are established in the opened natural areas where the influence of weather conditions (temperature, rainfall, evaporation and wind) or even the consequences of stochastically synoptic conditions (severe rain and strong wind) can be important. The latter condition can naturally induce large stormwater magnitudes flowing through the WSPs.

Draining excess wastewater to nearby hydrological system can normally be designed for combined sewer overflows (CSOs). If such approach is included in the combined sewer system, the effect of stormwater can be separated from the WSPs. However, the impact of the approach may occur such as severe contamination in the adjacent environmental system. For achieving minimal waste and contamination, the CSOs may essentially need to be discharged to the WSPs. This condition implies that the interference of the instantaneous hydrological process (severe surface runoff) of the plants can dominate over the designed hydraulic function of the WSPs. The consequences of this phenomenon may not be considered because of some reason (the treatment performance of the WSPs may partially maintain). However, if the treatment performance of the WSPs dropped by severe surface runoff, its impacts may rapidly spread to the vicinity ecologic system. If this problem cannot be overlooked, an efficient scheme solving the problem is always required. Besides, the insight physical processes and impacts of the mentioned issue should be sought.

To reduce the effects of severe weather on wastewater infrastructures efficiently, improving and modernizing existing infrastructure may need to be focused. For an open system such as WSPs, the role of baffles can be one of the possible solutions to improve their hydraulic control. However, generalizing the structure to fit various topography and finding the optimal design remains a challenge. In developing know-how for a country with different climatic regions like Thailand, the impacts of environmental factors like severe weather, unusual high rainfall amount on WSPBs hydraulic performance and caring capacity should also be included.

In this study, we conduct a numerical experiment of hydraulic flow of WSPBs via a sophisticated Navier-Stoke model. Several hydraulic flow scenarios associated with severe weather conditions have been used to drive the model. Finally, the optimal design of WSPBs will be evaluated. This research could help benefit the communities related to water pollution management and provide an understanding of wastewater infrastructure design.

Methodology

A. WSPB design

In designing WSPBs, the rectangular pond with the transversal four [2] and six baffles [3] are frequently suggested as an efficient configuration for achieving the best hydraulic performance. Expectantly, the best treatment performance may also be received. However, based on the fact that linear relationship of hydraulic performance (HP) and treatment performance (TP) is not guaranteed. Thus, higher/lesser baffle geometric ratios such as 2 and 8 may also be applied for improving/ensuring the treatment performance. However, misapplications of those configurations are also possible if the associated hydrodynamic behaviors have never been well analyzed. This may cause the inefficient design of the WSPBs.

For improving the above process, the hydrodynamic perspective given from numerical simulation can be significantly beneficial. Thus, we endeavor to make a numerical study investigating advantages and limitations and as well finding the improving approaches for the WSPBs. In the current study, the transverse 2 and eight baffles are selected to be the WSPB configurations (Fig. 1). To compare the hydraulics behaviors of those configurations to the conventional WSP, the flow solution of the unbaffled pond are also investigated. We also consider the effects of the inlet (spillway) constructed at the end of the baffles. Thus, the effect of changing the inlet sizes is to be examined. We define the hydraulic retention time (HRT) for operating the pond to be five days. Therefore, the associated incoming flow rate and volume of the pond are 29000 cubic meter/day and 150000 cubic meters, respectively.

We determine the advantage of the applied WSPBs by the minimal appearance of the dead space or the eddy cells in the pond. For testing WSPBs limitation, we consider the hydraulic response associated with mitigation of overtop or flooding during the severe flow rate. Besides, the possible way to mitigate such effect is also considered. In doing so, first, steady-state solutions driven by different flow rates would be numerically investigated. These solutions would help in determining the possible characteristic of the dead space subject to the baffle configurations and flow rates. Besides, we can provide a proper boundary condition for unsteady-state calculations. The schemes for potentially improving the hydraulic performance at the operating HRT or even in the cases under severe flow rate conditions are also determined. Details are presented in the next section.

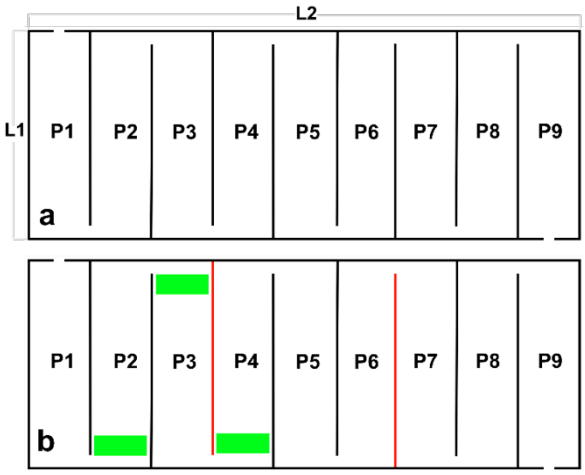

Fig. 1. a: Schematic of WSP geometry and baffle configuration. b: The same shape except for filters (green rectangular areas) applied to the sub-basin number 2, 3 and 4. Red lines indicate positions of the two elevated baffles. L1/L2=1/2.6.

B. Design for improvement schemes

Because of the impact of hydraulic dead space in the WSPBs is depended on the characteristic of the eddy cells. Hence, the practices in suppressing such phenomenon would consider being one of the efficient improving schemes. We speculate that constructing a porous-media-like filter near the jet flow of the pond may efficiently suppress the development of the eddy cells. However, calculating that flow problem cannot be easily performed. Importantly, the proprietary software (porous-shallow water solvers or CFD) is significantly expensive. We aim to investigate the cheaper approach by applying the hydrodynamic opensource software such as SCHISM [4]. Alternatively, we apply the array of circular obstacles [5] to the WSPB domain for representing the ideal porous-media-like filter effect. The placement of the filters are presented in Fig. 1b. For managing the overflow condition, the effect of baffle elevation including the filter is considered.

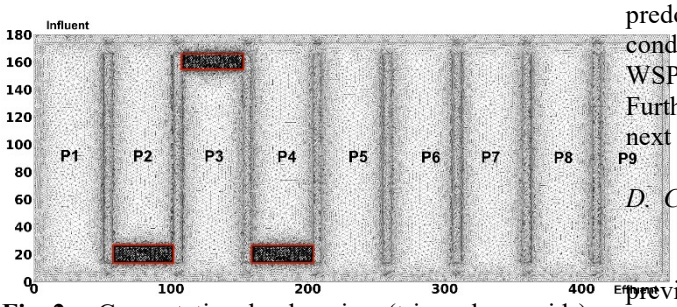

Fig. 2. Computational domain (triangular grids) designed for the SCHISM model. The porous-media-like filters are located inside in the red rectangle.

C. Effect of stormwater

Theoretically, the flow problem of the WSPBs induced by the geometric effect can be avoided during the engineering design process if the insight hydrodynamic mechanisms are understood. Instead, the effect of the uncertainty in flow rate is more difficult to manage than the geometric effect. For the tropic region, this problem would be intensified for the open WSP system. The important source of instantaneous high flow rate can naturally be surface runoff/excess rainfall originated in the watershed area adjacent to the WSPs. Under the condition of high rainfall intensity over the sufficiently large watershed area with saturated soils (or impervious land cover), high surface runoff rate can possibly discharge to the supported WSPs. If this is the case, the hydraulic retention time (HRT) supporting the biochemical process of the wastewater treatment cannot be maintained. Establishing schemes for efficiently managing this issue remains a challenge for the relevance communities. However, understanding the development of the dead space and other flow behaviors subject to the instantaneous flow rate with different WSPBs configuration would be beneficial in designing an efficient scheme. We aim to study this issue by performing the hydrodynamic simulation of the WSPBs under unsteady flow rate. Thus, the synthetic varying flow rate (Fig. 3) associated with the heavy rainfall effect is designed and applied in the simulation.

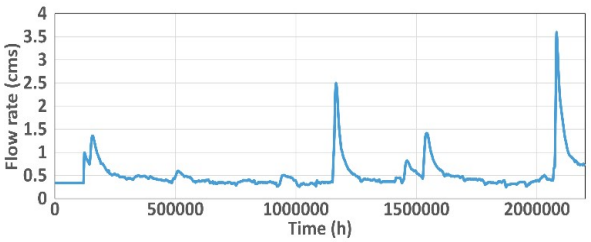

Fig. 3. Synthetic input flow designed for WSP operation and representing stormwater influence

The characteristic of the mentioned flow rate is given from long duration of rainfall with sufficient intensity (20-30 mm/hr) induced by the active intertropical convergence zone and monsoon trough predominate over Thailand. Within the saturated soil condition, even small catchment area adjacent to the WSPBs can generate the high surface runoff flow. Further details of the simulation are presented in the next section.

D. Computational details

From the WSP design schemes detailed in the previous sections, the associated computational domains can be developed and presented in Fig.2. It is noted that the vertical geometry of the sub-basin number P1 of the domain is characterized by uniform depth of 3.5 meters (referenced from the pond bank elevation) while the shallower depth of -2.5 meters is rather applied to the rest basin. The elevation of the baffle edges and the banks surrounding the pond are

0.5 and 0.0 meters, respectively. However, the effects of the higher/shorter baffle edges are also tested for the purpose mentioned in section *A*. Besides, the effect of the inlets will be examined by changing the spillway height.

For performing the steady-state calculation, the setups are prescribed by constant flow rate for both inlet and outlet positions. The considered flow rates are in the range of 0.3-2.5 cms. Interpreting the solution of these experiments would determine the associated hydraulic properties subject to the operating HRT and other considered conditions. Besides, the most efficient configuration would be suggested.For including the porous-media-like filter effect in the calculation for section *B*, we locate the geometry of the circular obstacle array (Fig. 3b) in the computational domain. It is noted that the two different sizes of the obstacle diameters (0.15 and 0.5 meters) with mostly staggered arrangement are implemented in the calculations. For differentiating the effect of the filters form the other influences, their placements are only near the inlets of the P2, P3 and P4 basins (Fig.1 b). We consider that the predominance of the phenomenon mentioned in section *C* may contribute an inefficiency of WSP operation under the severe weather condition. Thus, the simulation setups for the section *A* and *B* (Fig. 2) are duplicated but the driving force is instead the varying flow signal characterizing the magnitude for WSP operation and stormwater influence (Fig. 3). It is noted that the open boundary condition at the outlet of the domain is prescribed with the free surface (zeta) derived from flow information of the steady-state solutions. All flow problems will be solved by the SCHISM solver [4].

Result

A. Hydraulic flow structure

In Table 1 and Fig. 4, the characteristics of hydraulic flow given by different configurations are summarized and presented. The structure of plug flow seems to appear in the ponds with WSP+8Bs+Inlet1 (Fig. 4a and c) setting and unbaffled pond (Fig. 4b) while large hydraulic dead spaces occur in the two baffles pond.

Table I. Major Flow behaviors of the WSP configuration

Configuration	HRT condition	Flow behavior
WSP+8Bs+Inlet1	5 days	Mostly plug flow
WSP+8Bs+Inlet2	5 days	Small dead space
WSP+2Bs+Inlet1	5 days	Large dead space
WSP+2Bs+Inlet2	5 days	Large dead space
WSP+8Bs+Inlet1	0.7 days	Medium dead space
WSP+8B+Inlet1+filter	0.7 days	Partially plug flow
Unbaffled WSP	5 days	Mostly plug flow
Unbaffled WSP	0.7 day	Mostly plug flow

[a]Noted that WSP is stabilization pons, B is a baffle, the cross section areas for the Inlet1 and Inlet 2 are 2.5 and 1.5 square meters, respectively.

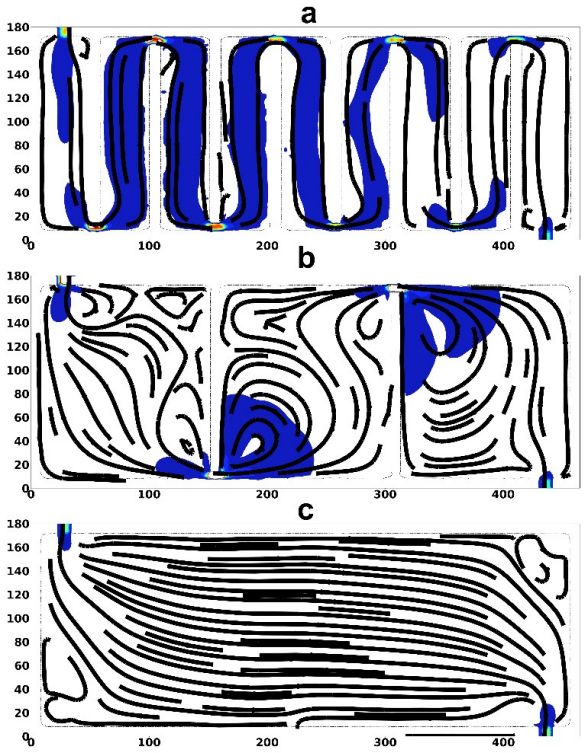

Fig. 4. Flow magnitudes and overlaid streamlines subject to the baffle configurations and the HRT condition of 5 days. a: 8 baffles. b: 2 baffles. c: Unbaffled pond. The min/max values of the contour are 0.001 and 0.25 m/s. The inlet size is 2.5 square meters.

Because plug flow is one of the most important hydraulic features for treatment performance of WSPs, hence, we suggest that the function of the pond with eight baffles is more efficient than that of the two baffles and unbaffled ponds. The importance of the latter configurations is disregarded because they potentially induce large hydraulic dead spaces and short-circuiting (Fig. 1b and c).However, the effective inlet is strictly required for effectively applying the eight baffles pond. At the operating HRT (5 days), we have found that the effect of the inlet size of 2.5 square meters can efficiently

reduce the sizeof eddy cells. By considering the mentioned results, the most advantageous configuration for the operating HRT can be assessed as the WSP+8Bs+Inlet1.

In addition, some issue for the best configuration may need to be considered as the higher flow rates become influenced. In that situation, the flow rates should directly change the HRT of the pond. Besides, the treatment processes may also be disrupted by the effect of the large dead space or large eddy cells developed in the WSP. This problem may disappear if the baffle height decrease, however, another situation such as overtopping flow on the baffle tops may occur.

The embankment over the baffles of the WSP+8Bs+Inlet1 configurationmay benefit for reducing flood level. However, the dead space problem should normally return. The practices in suppressing such phenomenon are determined.Nonetheless, we have found that a scheme related to hydrodynamic filters can help manage that problem efficiently. Besides, the suggestion for the efficient use of the filteris speculated. The corresponding details are revealed in the *C* section.

B. Stormwater effect

Previously, the flow behavior representing the function of the WSP associated with the most efficient configuration (WSP+8B+Inlet1) is presented. In this section, the response of the configuration to the severe weather is focused. It is noted that the effect of the weather condition is input to the model as the unsteady flow rate. Performing the simulation with this driving force would benefit the study for extracting the flow behaviors after the effect of the external condition decays. The corresponding results of the section are shown in Fig. 5.

As the peak flow rate (2.5 cms) of the stormwater passes through the pond with the WSP+8B+Inlet1 setting, the large eddy cells can develop near the inlet of each sub-basins of the pond (Fig. 5a). Since the stormwater flow decreases and the operating flow dominates, the eddy cell sizes turn to be smaller but it can remain in some sub-basin for 24.0 hours (the corresponding graphic is not shown).

If another configuration such the WSP+8B+Inlet2 is instead applied, the size of the remaining eddy can be wider (the corresponding graphic is not shown). This effect may turn the pond function to be inefficient. Potentially, the severe stormwater or the instantaneously high flow rate may turn the WSPBs function to be under the optimal level.

Generally, the WSPBs may be designed with a small inlet for keeping a small HRT. Since the instantaneous flow rate becomes significantly high, the overtopping flow on the baffle edges can occur. The simulation of this case is performed via the WSP+8B+Inlet2 configuration, but the lower baffle edges are instead replaced. The result of this experiment is shown in Fig. 5b.As seenin Fig. 5b, mostly, the flow across the baffle edges with higher flow magnitude.

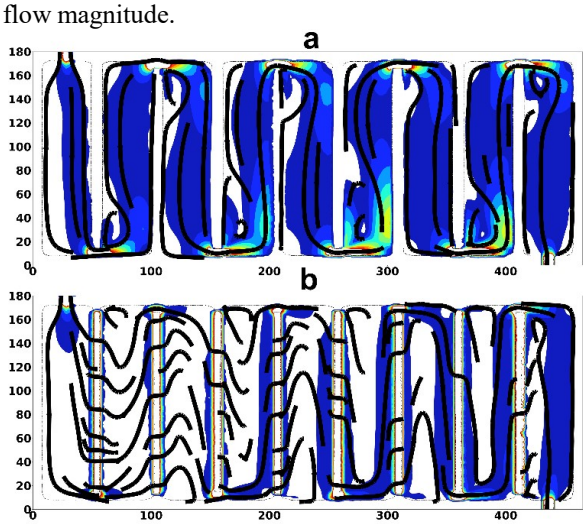

Fig. 5. Same as Fig.4 except for only the eight baffles and the HRT becomes 0.7 days. a: The most efficient configuration. b: The smaller inlets with lower baffle edges. The min/max values of the contour are 0.02 and 0.25 m/s.

Focusing on Fig. 5b, although the flow pattern in the pond (smaller inlets and lower baffle edges) tend to agree with minimal appearance of the hydraulic dead space, however, the flow path is instead shorter than that of another configuration. Such flow behavior should also potentially induce short-circuiting condition. This condition would also be an essential factor in the reduction of the WSP efficient. If this situation becomes intensified in real WSPs, some pollutant can remain high concentration at the outlet. Besides, it may induce strong erosion condition on the baffle edges. Hence, finding improvement schemes for the above issues may be needed. In the current study, some advantage of CFD knowledge such as staggered cylinder arrays is applied to be an improvement practice for the problem. The results are revealed next.

C. Effect of the improvement scheme

In this section, the results of the schemes designed for reducing the impact of the severe stormwater are presented. The interpretation mainly focuses on the effects of the filters and the baffle edges. The situations are designed to be under the HRT of 0.7 days (under the optimal level). First, the results of the WSP+8B+Inlet1 configuration on the mentioned condition is interpreted. In Fig. 6a, it is seen that the effects of the filters can significantly suppress the development of the eddy cells in the basins of P2, P3 and P4.

The hydraulic flow influenced by the filter is mainly the plug flow. Instead, the flow in the basins without the filters tend to exhibit the large dead space.

We speculate that the latter structure can disappear if the more filter structures are applied. Besides, the latter results may also indicate some advantage/disadvantage of the porous filter-like treatments such as the wetland plants which may need to be sufficiently determined for the best efficiency of the application.

We can suggest that the WSP together with the efficient baffles, effective inlet size and the porous media-like filters is the most advantageous configuration for operating the WSP with HRT of 5 days. Even in the flood situation, this structure yet shows a safer condition to operate the WSP than that of the other settings. Assume that other settings become applied for other purposes (i.e. for keeping the large HRT, performing the complete mixing flow, or even the underestimation of the stormwater effect), the alternate ways (more cheaper or easier) to deal with this situation may need to be explored.

At the end of this section, the result associated with the effect of the schemes for managing the overtopping flow and hydraulic dead space induced by flood condition is presented. It is noted that the geometry of the pond is duplicated from the WSP+8B+Inlet2 configuration. Previously, the response of such setting is presented and its response can be explained as the overtopping flow with strong current magnitude on the baffle edges. Here, the effects of the filters and embankment in that setting are seen (Fig. 6b). When particular baffle tops are sufficiently higher (the red lines in Fig.6b), the overtopping flow condition still be found. However, their associated flow magnitudes reduce.

The effect of the filter may turn the development of the eddy to be the straight flow paths (P3 and P4 basins). However, the large eddy cells and higher flow magnitude appear in the other basins without the filter treatment (P7, P8 and P9 basins). If the complete removal of the eddy cells are needed, we speculate that increasing the number of baffle and filter region or even rearrangement of these components can efficiently help. Besides, another assist such as changing the inlet design would also be beneficial.These results may suggest one of efficient approaches for managing the hydraulic flow of the WSPBs during the severe stormwater. However, the unexpected effects andoverbalancing of cost and wastewater treatment performance may be received if the related hydraulic behaviors subject to the considered configuration cannot be precisely investigated.

In summary, this study investigated the hydraulic/hydrodynamic behavior of the WSPs under the impact of baffles and the unsteady inflow rates. Wehave found that the number of baffles and drainage channels size can significantly influence the flow characteristics (eddy cell) of the ponds. Therefore, we may design an efficient wastewater treatment pond (minimal appearance of eddy cell) as revealed in the results. When applying the designed treatment pond under an unstable flow rate, the eddy cell may remain in the pond although the flow rate become weaken. We also found that properly installed porous-media-like filters could improve the hydraulic performance (suppressing the eddy cell) of the pond even in the flood condition.

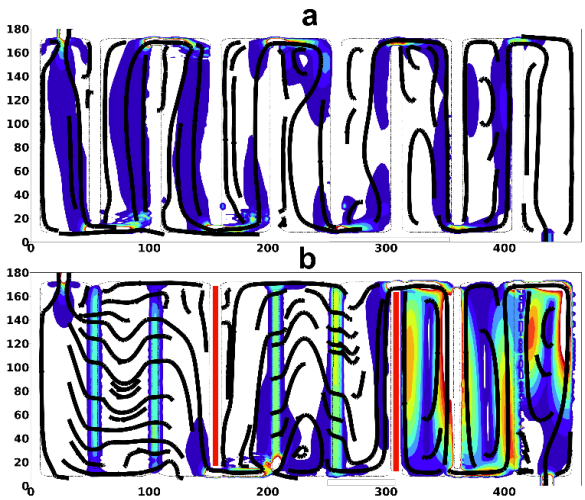

Fig. 6. Same as Fig.5 except for the effect of the filters (a) and the two elevated baffles+filters are instead applied.

In the context of worldwide water pollution, or even in Thailand, stakeholder involvement may be involved in solving problems effectively. Without this contribution, the ability of other contributors may be ineffective. However, incorrect understanding of the relevant scientific phenomena will reduce the effectiveness of such participation and overall problem resolution. In addition, there may be conflicts. From a scientific standpoint, the strength of science for investigation and adequate knowledge for all stakeholders is an important tool in addressing such issues. Finding a new high-performance wastewater infrastructure, improving efficiency and modernizing the existing system are essential, although they are considered as minor issues in the water pollution problem. Nevertheless, if they are not implemented, the severe problem will always occur. Furthermore, we recognize that awareness and understanding of hydraulic behaviors and biochemical processes of wastewater treatment can help to reduce conflicts among stakeholders. Occasionally, performance and infrastructure constraints can be important questions during the environmental assessment process for new development projects. The precise answer will suppress the origin of the conflict. Besides, in improving existing infrastructure, a real understanding of the relevant scientific phenomena is essential. One of the most effective approaches to solve these problems is the numerical simulation shown in the present study.

Conclusions

In this study, we conduct a numerical experiment of hydraulic flow of the wastewater stabilization pond with baffles (WSPBs) via a sophisticated mathematical model. Finding an optimal design of WSPBs to reduce effect of severe rainfall is our major objective. Besides, we aim to produce substantial knowledge related to the hydraulic design of WSP for the related communities. Therefore, the effects of baffle configurations, inlet sizes and porous-media-like filters have been investigated. The synthetic flow rate scenarios associated with both of the operating hydraulic retention times (HRT) and severe weather conditions have been used to drive the model. We have found that the number of baffles and inlet size can significantly influence on development of eddy cell (hydraulic dead space) in the ponds. Hypothetically, we can design the best configuration of WSPBs which produce minimal development of eddy cell (the configuration of 8 baffles with the inlet size of 2.5 square meters). However, the efficiency of the configuration become reduced as the effect of surface runoff (excess rainfall) dominates. Besides, the pond can experience flood condition. We also have found that properly installed porous-media-like filter structures could improve pond performance (suppressing the eddy cell) even in flood condition.

Water pollution is a relevance problem in Thailand's water resources management. Overall, the current status of the surface water of Thailand is moderate to good quality except that of the central Chao Phraya watershed which deteriorates. This fact indicates that the environmental management policy and wastewater treatment infrastructure of the country may need to be improved for enhancing efficiency in wastewater and stormwater treatment. Focusing on the latter issue, despite significant wastewater contributions from domestic and industrial sectors, establishing and maintaining their wastewater treatment plants need utmost responsibilities and must be ready for challenges from climate variation influences. However, the excessive cost is still a vital issue in developing wastewater treatment infrastructure, therefore, improving and modernizing the existing structures can be more useful alternatives. On a field scale, waste stabilization ponds with baffles (WSPBs) configuration can be one of the possible solutions to the mentioned issue. Furthermore, generalizing the structure to fit various sites and finding the optimal design remains a challenge. In developing know-how for a country with different climatic regions like Thailand, the impacts of environmental factors like severe weather, unusually heavy rainfall on hydraulic performance and caring capacity of the pond should also be included. Thus, our research would benefit the communities related to water pollution management and provide an understanding of wastewater infrastructure design.

References

[1] M.E. Verbyla, M. von Sperling and Y. Maiga, "Waste Stabilization Ponds". In: J.B. Rose and B. Jiménez-Cisneros, (eds) Global Water Pathogen.

[2] H. Abbas, R. Nasr and H. Seif, "Study of waste stabilization pond geometry for the wastewater treatment efficiency", J. Ecol. Eng., vol 28 (1), pp. 25-34, November 2006.

[3] M. Li, H. Zhang, C. Lemckert, A. Roiko and H. Stratton, "On the hydrodynamics and treatment efficiency of waste stabilization ponds: From a literature review to a strategic evaluation framework", J. Clean Prod., vol 183, pp. 459-514, May 2018.

[4] Y. Zhang, F. Ye, E.V. Stanev and S. Grashorn, "Seamless cross-scale modeling with SCHISM", Ocean Model., vol 102, pp. 64-81, June 2016.

[5] A. D. Araújo, J. S. Andrade, and H. J. Herrmann, "Critical role of gravity in filters", Phys. Rev. Lett., vol 97, pp.138001, September 2006.

Geographically Weighted Regression Analysis Applied to the Establishment of Paddy Field Flooding Loss Functions

Ling-Fang Chang[1,a], Wen-Tsun Fang[2,b], Ming-Daw Su[3,c] and Hsueh-Yen Shih[4,d]

Abstract

Disasters due to typhoons and heavy rainfall occur frequently in Taiwan. With the increase of social and economic development density, flood damages are becoming more and more serious. Flood risk management has thus turned into a very important task. Flood damage assessment is the basis of flood risk management. The disaster damage estimation model is often divided into residential areas, industrial and commercial areas, agricultural areas and public facilities. Previous studies have mostly focused on residential, industrial and commercial areas. Agricultural losses are due to a large number of impact factors, and the relevant literature is insufficient.

The most common methods are the loss curves for unit area and the flood depth loss curves method. Although the loss curves for unit area method is relatively simple, the differences in loss caused by various flooding depths are not considered. The flooding depth loss curve method often needs to be established through questionnaires. However, questionnaire surveys have to consume lots of manpower and material resources. Both the two methods above do not take the growth period of crops into consideration.

When disasters occur in different growth periods of crops, the losses caused by the same flooding depth are different due to the various flooding tolerances of crops in each growth period. Due to the hydrological and geographical factors, such as climate, the growth period of rice transplanting is different due to dissimilar climatic conditions. The complexity of establishing a flooding loss curve for paddy field is thus obvious.

In addition, in case the analysis of the flooding loss data is based on the traditional global regression analysis approach, there usually exists a spatial autocorrelation of the residual term with no consideration of spatial variation. This result violates the assumption of linear regression. In view of this, this study is expected to use paddy field as the research object.

At first, paddy field loss factors considered in each literature are reviewed and studied. Relevant domestic factors are also collected and it then to establish a paddy field flooding loss estimation model, and then use the geographically weighted regression model for spatial analysis and spatial grouping comparison. The selection of the research site is to consider large-scale historical disaster events. The event is selected for analysis and assessment of the disaster area o of Typhoon Morakot in Kaohsiung City in 2008.

Keywords *Paddy field flooding loss function, Paddy field flooding loss curves for growth period, Geographically weighted regression analysis*

[1]Associate Research Fellow
Agricultural Engineering Research Center
Taoyuan, Taiwan
[2]Research Fellow
Agricultural Engineering Research Center
Taoyuan, Taiwan
[3]Associate Research Fellow
Dept. of Bioenvironmental Systems Engineering National Taiwan University
Taipei, Taiwan
[4]Assistant Research Fellow
Agricultural Engineering Research Center
Taoyuan, Taiwan

[a]changlf@aerc.org.tw
[b]wtfang@aerc.org.tw
[c]sumd@ntu.et.tw
[d]isacyen@aerc.org.tw

Analysis of Erosion Hazard in Upstream Ciliwung Watershed Bogor, West Java, Indonesia

Annisa Daniswara Santoso[1], Astrid Damayanti[1,a] and Achmad Hafidz[2]

Abstract Erosion is the loss of a soil or parts of soil from a place that is transported by water or wind to another place. The growing quantity of human activity makes buildings around upstream Ciliwung watershed Bogor, West Java, Indonesia increase as well. The current condition of natural and environmental resources in the upstream Ciliwung watershed is quite apprehensive where environmental damage is already severe due to inappropriate use and use of land and urgent life needs. Therefore, mapping the spatial distribution of erosion hazards in the relevant research area needs to be done. The method that researcher use to predict erosion is the Universal Soil Loss Equation (USLE) equation. This equation is an erosion estimation model used to calculate the amount of erosion that occurs in the long term in an area. This equation can predict the average erosion rate in a plot of land at various slope steepness with a certain rain pattern for each existing cropping effort and soil management action. Variables used in this method are Rainfall Erosion, Soil Erodibility, Slope, Ground Cover Vegetation and Soil Conservation Action Factors. USLE analysis is done using Arc GIS 10.1 software.The final output of this research is the spatial hazard distribution of erosion of the upstream Ciliwung watershed Bogor.

Keywords *Analysis, Erosion, USLE, GIS*

[1]Department of Geography
Universitas Indonesia
Indonesia
[2]Department of Civil and Environment Engineering
Bogor Agricultural Institute
Indonesia

[a]astrid.damayanti@sci.ui.ac.id

Introduction

High population growth causes high human activity [1]. Therefore, land conversion occurs which causes a reduction in vegetation cover and an increase in built up land [1,2]. It was noted that the rate of land conversion and forest damage on the island of Java, Indonesia reached 0.71 hectaresper year [1].
This phenomenon of land use change and forest destruction has caused large erosion that occurred in the upper watershed [3]. Erosion is a process or event of loss of the top soil surface layer, either caused by the movement of water or wind [2]. Therefore, there are at least 16 watersheds in Java which are in critical condition [1].

Critical land can endanger hydrological functions (reduced watershed capacity to absorb water), orological (decreased soil fertility), to agricultural production (decrease in economic value of agricultural land) [4]. Upstream Ciliwung Watershed is one of 13 watersheds in very critical conditions with relatively large erosion rates [3]. The Ciliwung watershed experienced erosion rates in 2001 reaching 44 tons per hectare per month, in 2002 reaching 74 tons per hectare per month [5]. Erosion affects the formation of critical land so that the issue of critical land is closely related to the Upstream Ciliwung Watershed. The increase in critical land Upstream Ciliwung Watershed occurred along with the increase in erosion, in 2003, the critical land area amounted to 2438.18 hectares, in 2008 it increased to 4013.78 hectares [6].

Upstream Ciliwung Watershed was chosen as the research geomer because of the fact that the erosion trend that occurred increased from year to year. This phenomenon is a major problem for the management of Upstream Ciliwung Watershed. In addition, Upstream Ciliwung Watershed is important to be preserved because it is a water catchment area, while managing the water management system that supports life in the Indonesian capital, Jakarta. Upstream Ciliwung Watershed is also an ecosystem that provides landscape services to the surrounding area, namely in the form of water management, biodiversity, carbon sequestration, and landscape beauty services [7]. Therefore, this study aims to analyze the erosion hazard of Upstream Ciliwung Watershed and it is important to do it because it provides benefits, namely as a better initial step for watershed management.

Methodology

This study was conducted in Upstream Ciliwung Watershed with an area of 14.860 hectares which is geographically located at 106º 49º 40 "- 107º 00 '15" East Longitude. Administratively, Upstream Ciliwung Watershed covers 30 villages in Bogor Regency, namely 2 villages (Sukaraja District), 7 villages (Ciawi District), 10 villages (Cisarua District), 11 villages (Megamendung District) and 1 village in East Bogor District. Variables in this study are rain erosivity, soil erodibility, slope length and slope, plant and management factors, and soil conservation factors.

A. Rain Erosivity (R)

Rain Erosivity is very much related to kinetic energy, namely the parameters associated with the rate of rainfall or the volume of rain [9]. Rainfall data from Upstream Ciliwung Watershed is represented by data collection from Citeko Climatology Station and Bogor Climatology Station. Way to determine the amount of rain erosivity index using the Lenvain formula as follows (1) [8]:

$$R = 2.21\ P^{1.36} \quad (1)$$

Where:
R: Erosion Index
P: Monthly Rainfall (cm)

The calculation of rainfall erosivity uses IDW interpolation analysis. Inverse Distance Weighted (IDW) is a simple deterministic method by considering the surrounding points [10]. The assumption of this method is that the interpolation value will be more similar to the sample data i.e. closer than the farther away [11].

B. Soil Erodibility (K)

The soil erodibility index is the resistance of soil particles to erosion and soil displacement by rainwater kinetic energy [9]. Determination of the K value based on the data of the Upstream Ciliwung Watershed soil type.Source of Soil type data from BPDAS Ciliwung-Citarum. The K value for each type of soil is included in the data attribute map of the soil type. K value is referred to from Bogor Research and Development Center.

Table 1. Value of K

Soil Type	K
Reddish Dark Brown Latosol	0.121
Yellowish Brown Andosol	0.223
Chocolate Litosol	0.191
The association of chocolate andosol Association and Chocolate Regosol	0.271
The association of reddish brown latosol and brown latosol	0.293

C. Slope and Slope length (LS)

Slope can be expressed in degrees (°) or percent (%). The length and slope factors can be calculated at once as the LS value using map calculation, where LS = topographic factor, L = slope length (m), S = slope (%) [8] To find LS can be done by the equation:

$$LS = \sqrt{L}(0.0138+0.0096S+0.00138S^2 \quad (2)$$

Table 2. LS values

Slope Class	Slope (%)	LS Value
Flat	0-8	0.4
Sloping	8-15	1.4
Slightly Steep	15-25	3.1
Steep	25-40	6.8
Very Steep	>40	9.5

D. Pland and Management Factor (C) and Soil Conservation Factor (P)

C Factor (plant management factor) is the ratio of eroded soil in a type of crop management to eroded soil with the same land surface conditions but without crop management or without crop [12]. P Is the ratio of land lost when the land management effort is carried out (terrace, plants in contours, etc.) without conservation efforts. The P factor is the ratio between the average eroded soil from a land i.e.given certain conservation treatment of the average eroded soil from the land treated without conservation action [8]. Without soil conservation the value of P = 1. CP factor in this study refers to Asdak 2004 according to table 3.

Table 3. CP values

Land Use	C	P
Natural Forest	0.001	0.30
Dryland Forest	0.5	0.3
Plantation	0.5	0.15
Settlement	0.75	0.25
Rice fields	0.001	0.10
Shrubs	0.30	0.40
Open Land	1	1
Moor / fields	0.40	0.46
Body of water	0.01	1
Industry	0.75	0.25

E. Data Verification

Verification in the form of identification of land cover and soil conservation in the research area. The verification point is 62 points spread near the road access. When verification, things are done in the form of ploting coordinates, identification of land use, land management, coservation and picture location.

F. Classification of Erosion Danger Levels

This study uses the USLE method in calculating erosion rates. USLE (Universal Soil Loss Equation) is an erosion model designed to predict the average long-term soil erosion of a farming area with

certain cropping and management systems [9]. Estimation of soil erosion and depth is considered to predict Erosion Danger Level for each land unit. The Erosion Danger Level Class is given to each land unit with a matrix that Uses soil information and estimated erosion according to the USLE Formula.

USLE formula (3) according to Wischmeier and Smith (1978) [9]:

$$A = Rx\ Kx\ LSx\ CP \qquad (3)$$

A: The amount of eroded land
(tons per hectare per year)
R: Rainfall Erosion Factors
K: Soil Eroductivity Factors
L: Slope Length Factor
S: Slope Factor
C: Ground Cover Vegetation Factors
P: Soil Conservation Action Factors

This erosion hazard level classification analysis uses weighted overlay analysis. Weighted overlay is one method of modeling suitability. Data processing and analysis is done using Arc GIS 10.1 software. ArcGIS uses the following process for this analysis [13].

- Each raster layer is assigned a weight in the suitability analysis
- Values in the rasters are reclassified to a common suitability scale
- Raster layers are overlayed, multiplying each raster cell's suitability value by its layer weight and totaling the values to derive a suitability value.
- These values are written to new cells in an output layer
- The symbology in the output layer is based on these values.

Result and discussion

The output of the data processing and analysis in the form of erosion hazard maps in Upstream Ciliwung Watershed. To get the final output, this study first obtained the results of rain erosivity (R), soil erodibility (K), slope length (L), slope (S), land cover factor (C) and soil conservation (P).

Rain erosion is a driving force which causes the peeling and removal of soil particles to a lower place [8]. The calculation of R is strongly influenced by the monthly rainfall in the region. Therefore, the higher the monthly rainfall the higher the R value(Fig 1). The Ciliwung Upstream Region Watershed is classified as having a high monthly rainfall throughout the region (Fig 1).

Monthly rainfall in the Upstream Ciliwung Watershed area is 1511-2351 cm / month or 15110-23510 mm / month. The amount is included in the category of high rainfall areas. However, rainfall to the northwest is higher than the surrounding area because rainfall in the Bogor City area is higher than Bogor Regency. This is because Upstream Ciliwung Watershed is a rain shadow area. Due to this high rainfall, Upstream Ciliwung Watershed has high rainfall erosivity with an index value of 46609-570182.

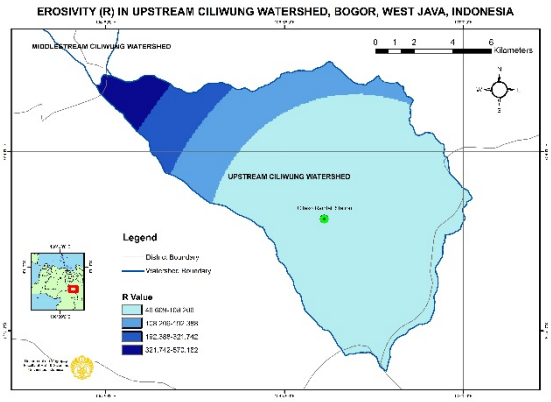

Fig 1. Erosivity

Next is the condition of Soil Erodibility (K).Soil erodibility is whether or not the soil is experiencing erosion, which is determined by various physical and chemical properties of the soil [8]. Soil accessibility is strongly related to the type of soil. The type of soil in Upstream Ciliwung Watershed is dominated by brown latosol soil, association of reddish brown latosol and brown latosol, and the association of red latosol, reddish-brown and lateric latosol of groundwater. The remainder is a small portion of gray regosol complex and lysosol, reddish brown latosol soil and yellowish brown andosol soil. These different types of soil cause differences in soil erodibility values in Upstream Ciliwung Watershed. (Fig. 2)

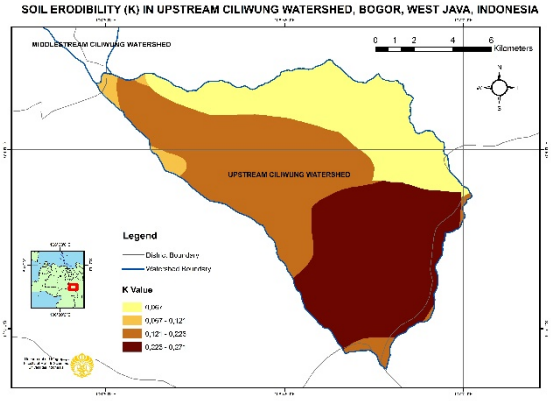

Fig. 2. Soil Erodibility

The range of K values in Upstream Ciliwung Watershed is 0.067-0.271 . The higher the erodibility value, the higher the level of danger of surface erosion. The lowest K value is in the northeast of Upstream Ciliwung Watershed because in this area the type of soil is the association of reddish brown latosol and brown latosol. This type of soil has a rounded form of soil structure and low infiltration capacity.

The value of K which is in the range from 0.067 to 0.121 is in the northwest of the Upstream Ciliwung Watershed. The K value of this terrestrial region is low because the reddish-brown latosol soil type has relatively clear horizon boundaries, clay textures, with crumbs to solid structures, consistency varies and loose (fertile) once [14] Although the clay fraction has a grain size of 0.002 mm, a high fertility rate means that it contains high organic matter. Soil organic matter is needed for the formation and stabilization of soil aggregates. Soil particles help for soil structures that contain both large and small pores and as a result improve water and air conditions [15]. Thus, better infiltration and percolation rates will reduce run-off and erosion and steady soil aggregates are not easily separated from the soil surface and carried by water [15].

The K value is moderate, extending from the northwest to the middle region of the Upstream Ciliwung Watershed. While the highest K value is in the southeast because the type of soil in this region is the association of brown andosols and brown regosols. The K value of this type of soil is higher than the others because this type of soil has rather good drainage characteristics of a rather smooth rounded soil structure and low infiltration capacity. Therefore the possibility of surface erosion is even greater.

Furthermore, the condition of LS in Upstream Ciliwung Watershed. LS factor is a combination of slope length (L) and slope (S) is the ratio of the amount of erosion of a slope with a certain length and slope to the magnitude of erosion from the land plot [2]. Slope is classified into 4 groups, namely flat (0 -8%) up to very steep (> 40%). Upstream Ciliwung Watershed is a plateau with slopes that are predominantly flat (34.90%) and wavy (25.19%), and the remainder are sloping plains (10.65%), steep (12.10%) and very steep (13.16%). (Fig 3.)

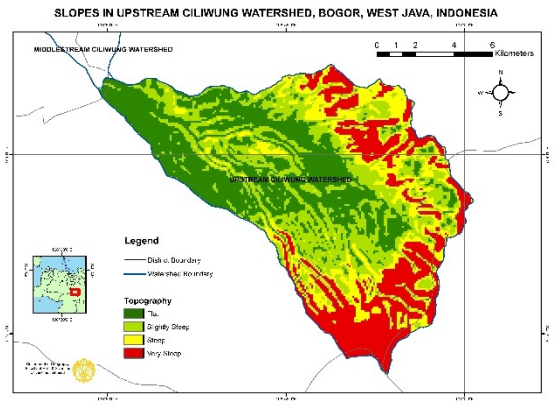

Fig. 3. Slopes

Flat topography and ramps can be found extending from southwest to southeast. A slightly steep topography is randomly scattered throughout the region. Whereas steep and very steep topography is dominated in the southeastern part of Upstream Ciliwung Watershed. This condition is caused by the position of Upstream Ciliwung Watershed whose existence is surrounded by several mountains, namely Mount Gede Pangrango, Mt. Mandalawangi, Mt. Kencong and others.

The last factor is the CP factor whose size depends on the existing land use (Fig. 4). The land uses in Upstream Ciliwung Watershed are primary dry land forest, dry land secondary forest, conservation forest, settlement, dry land agriculture, shrubs and open land. The northwest region extending to the southeast is dominated by settlements and dry land. While the forest area in the northeast is also southeast.

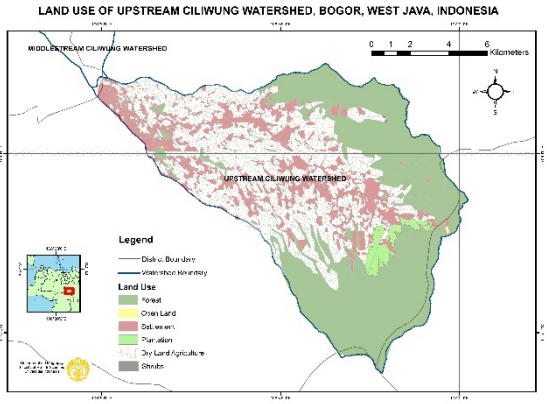

Fig. 4. Land Use

The land use in the form of forest area are 4.274 hectares (National Park conservation area of Gede Pangrango 1869 hectares, Nature Reserve / CA and Tourism Park conservation area / TW Telaga Warna 370 hectares, and production forest and protected forest area managed by Perhutani Public Corporation covering 2035 hectares) The land area of 7607 hectares is cultivated by the community by 43% for agricultural cultivation activities in residential land 23%. The remaining land is in the form of sleeping land and the left-right side of the river / tributary which generally with steep topography up to very steep. This land with heavy topography is spread along the channel and upstream of the Upper Ciliwung River.

The results of USLE's analysis produce four levels, namely very high, high, medium and low erosion hazard with each quantity> 480 tons per hectare per year, 180-480 tons per hectare per year, 60-180 tons per hectare per year and <60tons per hectare per year (Fig.5 and Table 4.)

Table 4. Extent of Erosion Hazard Areas

Level of Erosion	*Erosion Quantity (tons per hectare per year)*	*Area (Hectares)*	Percentage (%)
Low	<60	545,52	3,60
Moderate	60-180	3847,023	25,36
High	181-480	9822,18	64,74
Very High	>480	955,96	6,30

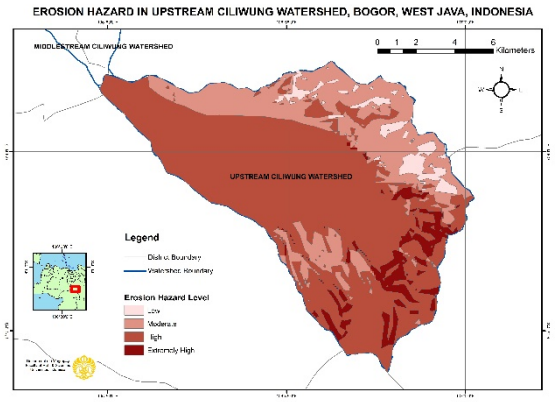

Fig. 4. Erosion Hazard

The most dominant level of erosion is the high erosion rate of 9822.18hectares with an erosion rate of 181-480 tons per hectare per year. This high erosion area extends from northwest to southeast which reaches 64.74% of the Upstream Ciliwung Watershed. This high erosion is in 4 sub-districts, namely Cisarua, Megamendung, Sukaraja and Ciawi with a total of 12 villages. High erosion in this region is because in this region there are many very residential land uses, agriculture without good land management as well as high rainfall throughout the Upstream Ciliwung Watershed area.Although the topography of the area is quite flat, the level of soil erodibility is high enough so that the soil is easily eroded.

Whereas the least erosion rate is the low erosion level, covering an area of 545.52 hectares with an erosion amount of <60 tons per hectare per year. This low erosion area is only 3.6% and is scattered randomly in the northeast region. Low erosion is due to the region's rainfall tends to be lower, flat topography and sloping, and is a forest area so that the infiltration power tends to be higher.

Other levels are moderate and very high erosion rates with an area of 3847.02 hectares and 955.96 hectares respectively. The erosion rate is scattered in the northeast and slightly in the southeast. Land use in moderate erosion and high erosion is almost the same as the absence of settlements, topographic conditions are also flat to steep. However, in moderate erosion areas, the level of soil erodibility is very low at 0.07.

Furthermore, there was a very high erosion all over the southeastern part of Upstream Ciliwung Watershed. This very high erosion is very much influenced by the existing topographic conditions which are very steep. The level of soil erodibility is also the highest compared to other regions. So even though it is a forest area, the level of erosion in this region remains very high.

Conclusions

The results of the erosion hazard distribution in the study area are influenced by the variables in Upstream Ciliwung Watershed which are rain erosivity (R), soil erodibility (K), slope length (L), slope (S), land cover factor (C) and soil conservation (P). The results of erosion hazard levels are dominated by high erosion levels covering an area of 9822.18 hectares with an erosion rate of 181-480 tons per hectare per year. This high erosion area extends from northwest to southeast. Whereas the least erosion rate is the low erosion level, covering an area of 545.52 hectares with an erosion amount of <60 tons per hectare per year. Low erosion areas are scattered in the northeast. Other levels are moderate and very high erosion rates with an area of 3847.02 hectares and 955.96 hectares respectively. The erosion rate is scattered in the northeast and slightly in the southeast. While the erosion area is very high all over in the southeast part of Upstream Ciliwung Watershed.

References

[1] Mawardi, I. (2010). Watershed Damage and Decrease in Water Resource Capacity in Java Puai and Handling Efforts. *.Indonesian Hydro Journal Vol.5 No.2*., In press.

[2] Suripin. (2002*). Preservation of soil and water resources*. Yogyakarta: Andi Press.

[3] Sobirin. (2004). *Nineteen West Java Watersheds in Critical Condition.* Bandung: Pikiran Rakyat 3rd edition November 2004.

[4] Puslittanak. (1997). *Critical Land Mapping Guide.* Bogor: Land Research Center and Agro-climate.

[5] Qodariah, L. (2004). *Application of Answers Simulation Model for Estimating Erosion and Sedimentation in the Upper Ciliwung Watershed*. Bogor: IPB Press.

[6] Nugraha, Rizky. (2008). *Remote Sensing Utilization and Geographic Information Systems in Mapping of Ciliwung Hulu Bogor Critical Land.* Bogor: IPB Press.

[7] Rewards for Use of and Shared Investment in Pro-Poor Environmental Services [RUPES]. (2009). *Policy Ideas: Concept of Environmental Services and Payment for Environmental Services in Indonesia*. Accessed from http://www.worldagroforestry.org/sea/Publications/files/leaflet/LE0160-09.PDF on 20/09/2018 at 06.23 WIB.

[8] Asdak, Chay. (2002). *Hydrology and Management of Watersheds*. Yogyakarta: Gadjah Mada University Press.

[9] Wischmeier, W.H. and J.V. Mannering. (1969). Relation of Soil Properties to Its Erodibility. *Soil Sci Proceeding 33: 131-137.*, in press.

[10] NCGIA. (2007). *Interpolation: Inverse Distance Weighting*. Accessed

fromhttp://www.ncgia.ucsb.edu/pubs/spherekit/inverse.html on 20/09/2018 at 06.23 WIB.

[11] Pramono, G. (2008). Accuracy of IDW and Kriging Methods for Interpolating Suspended Sediment Distribution. *Geography Forum, Vol. 22, No. 1*., in press.

[12] Hardjoamidjojo, S. and Sukartaatmadja, S. (1992). *Soil and Water Preservation Techniques*. Bogor: JICA IPB.

[13] ESRI. (2014). Understanding Weighted Overlay. Hands On esri.com

[14] Haryani, Nanik Suryo. (2012). Landslide Analysis in Tenjolaya Uses Remote Sensing Data. *Article Lapan Technology 29 Number 318.*

[15] Konhnke. (1968). *Soil Physics*. Minnesota: McGraw Hill Publications

Verification of ArcGIS for flood hazard mapping: A case study of Cholburi Province, Thailand

Supatchaya Chuanpongpanich[1,a] and Tawatchai Tingsanchali[1,b,*]

Abstract Flood hazard maps of a study area can be constructed by using ArcGIS. Generally, the weights of input data are assumed without verification. The objective of this study is to develop a novel method to verify the ArcGIS for flood hazard mapping given the input data, such as: rainfall, ground slope, ground terrain elevation, land use and soil types. To calibrate and verify the ArcGIS, the weight of individual input data is first assumed and adjusted systematically and iteratively to determine the best set of weights of all input data for computing the flood hazard maps. The calibration and verification of the weights are based on comparison of the computed flood inundation areas with the satellite observed data. The final weights are obtained when satisfactory agreement between the computed and observed flood hazard maps is obtained.

A case study was carried out for flood hazard mapping in Cholburi Province, Thailand. Five input data to ArcGIS are specified as mentioned above. The weights of all input data are assumed and adjusted systematically in the calibration to obtain satisfactory agreement between the computed and actual flood inundation maps in 2013 and 2010. The same weights obtained from calibration are verified by using them to compute the inundation map in 2008 and compared with the satellite observed inundation. The comparison shows satisfactory agreement on calibration and verification of ArcGIS. It is recommended to apply this method to other floods and in other areas.

Keywords *ArcGIS verification, flood hazard maps, Cholburi, Thailand*

[1]Faculty of Engineering at Sriracha,
Kasetsart University Sriracha Campus
Cholburi, Thailand

[a]supatchaya@eng.src.ku.ac.th
[b]tawatchai2593@gmail.com

Introduction

Cholburi Province in East Thailand has an area of 4,634 km^2 (Fig. 1). The topography of the province is mountainous in the east, northeast and south of the province where low lying areas are in the northwest and west. After heavy rainfalls, floods occurred and caused large damages in northern part of Cholburi. The development of the flood hazard map for the Cholburi province will be useful for planning of land use and for flood damage mitigation. Flood hazard mapping is a vital component for appropriate land use planning in flood-prone areas. It creates easily-read, rapidly-accessible charts and maps which facilitate the identification of areas at risk of flooding and also helps prioritize mitigation and response efforts [1]. A previous study [2] has been done to estimate flood hazard area in the Cholburi province based on a matching index computed from ArcGIS for overall inundation area in the 10-year period of 2008-2017. The five types of input data considered in their study were rainfall, ground slope, ground elevation, land use and soil type. But the study [2] did not calibrate and verify the weights of input data. This may lead to error as the weights of input factors control the score of the matching index for inundation area. Other previous studies such as the study by [3] on flood risk area in the upper Pasak river basin in Lomsak, Phetchabun Province and [4] on flood risk area around western sub-basins area of Songkhla Lake in Phatthalung Province using GIS did not calibrate and verify the weights of input factors. Therefore it is in doubt whether the weights of the input factors are correct or not.

Purpose of study

The purpose of this study is to calibrate and verify the ArcGIS model by searching the best set of weights of the input factors that work well for flood inundation in the considered calibration and verification years. In this study, the annual flood inundations in 2013 and 2010 were considered for calibration and in 2008 for verification. The successful calibration and verification will assure the validity and reliability of the ArcGIS in estimating flood inundation in the study area in other flood years and elsewhere.

Fig. 1. The flooded area under study, Cholburi Province

Flood hazard mapping using ArcGIS

Computing Matching Index

ArcGIS version10.5 which is a Geographic Information System application for map construction is used to analyze the related parameters and flooded areas by weighting technique [5] and [6]. The matching index M is computed and compared with the satellite observed flood inundation area. Five input factors are used namely: rainfall with assigned index number i=1, ground slope with i=2, ground elevation with i=3, land use with i=4 and soil type with i=5. Equation 1 is used to compute the matching index M based on point score analysis [7] to represent the magnitude of flood hazard inundation area.

$$M = W_1R_1 + W_2R_2 + W_3R_3 + \dots W_iR_i \dots + W_nR_n \quad (1)$$

Where W_i is the weight of i^{th} input factor; R_i is the scale value of the magnitude of the i^{th} input factor; n is the total number of input factors and n is equal to 5. The weight W is set equal to 5 for the most influential input factor. For the least influential input factor, W is set equal to1.

Each input factor is categorized into 5 classes with intervals according to the ranges of field data as shown in Table 1. Each class of input factor is designated by a scale value R, e.g. R=1 for very low significance, 2 for low, 3 for moderate, 4 for high and 5 for very high.

For example, the flood inundation is increased when the amount of rainfall increases. Therefore, the highest scale R=5 is given to the rainfall of more than 200 mm. The lowest scale R=1 is given to the lowest range of rainfall that is less than 50 mm as shown in Table 1.The scales R of the classes of the other input factors are specified according to field data range and are kept unchanged throughout this study.

Table 1. Classes and intervals of input factors and assigned scale values

Input factor and index i	Classes of input	Inputs and their intervals	Scale of input factor, R*
Rainfall, i=1	1	Class 1:Less than50 mm	1
	2	50 – 100 mm	2
	3	100 – 150 mm	3
	4	150 – 200 mm	4
	5	More than200 mm	5
Ground slope, i=2	1	More than20%	1
	2	15-20%	2
	3	10-15%	3
	4	5-10%	4
	5	Less than 5%	5
Elevation, i=3	1	High mountain	1
	2	Mountainous	2
	3	Hilly terrain or plateau	3
	4	Low land	4
	5	Flood plain	5
Land use, i=4	1	Forest	1
	2	Industrial	2
	3	Urban	3
	4	Agricultural	4
	5	Rivers or canals	5
Soil type, i=5	1	Very well drained	1
	2	Well drained	2
	3	Moderately drained	3
	4	Poorly drained	4
	5	Very poorly drained	5

*scale of 1 means lowest significance to flood inundation, and of 5 means highest significance

Spatial Rainfall Distribution over Study Area

Due to non-uniform spatial distribution of rainfall, annual rainfalls at 21 stations in Cholburi Province were interpolated to obtain spatial average

rainfall for input to ArcGIS. This was done by using Inverse Distance Weighted (IDW) method from ArcGIS as shown in Fig. 2. This method is a spatial interpolation technique that can estimate spatial average rainfall over the study area based on the distance from known rainfall values at many stations [8].

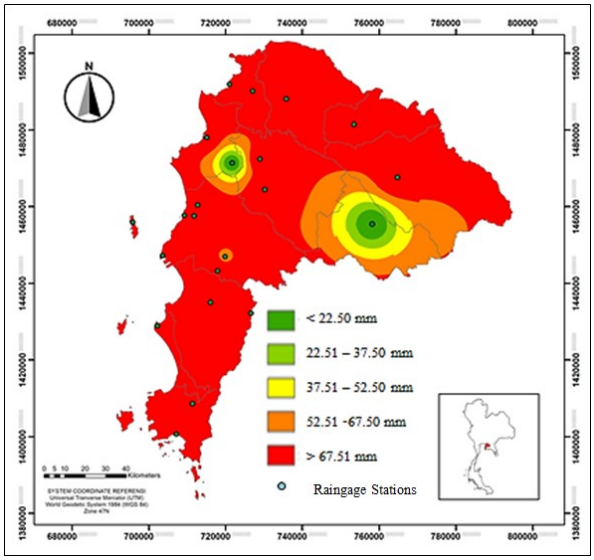

Fig. 2. Spatial average rainfall distribution by Inverse Distance Weighted Method, Cholburi Province

Calibration and Verification on Weights of Input Factors

This study attempts to determine the best values of the weights of input factors W_1 to W_5 for the study area. This is done by calibration of the weights W's of input data by comparing the computed matching index M which relates to the magnitude of flood inundation area with the satellite observed flood inundation area in the years 2013 and 2010. For the class 1 to class 5 of each input factor, the scale values R from 1 to 5 are assigned respectively. In the calibration, the weights of the input factors W_1 to W_5 are tried by changing from their assumed initial values that is W_1=5, W_2=4, W_3=3, W_4=2 and W_5=1. The number of combinations of W_1 to W_5 is equal to factorial 5 or 5x4x3x2x1=120 combinations. Based on these combinations, 120 calibration runs of the ArcGIS were done for each year to obtain 120 values of matching index M from (1). To classify the matching index M, the full range of M from maximum and minimum possible values in ArcGIS is subdivided into five classes, e.g., 0-20% for very low, 21-40 % for low, 41-60% for moderate, 61-80% for high and 81-100% for very high. These classes were shown by different color codes for visualization in the plotted figures. In the same way, the observed flood inundation areas are classified into the same five classes. In each calibration run, the class of M and the class of satellite observed inundation area are compared for each grid. The score of agreement between the class of M and the class of observed inundation is evaluated by using the following procedure.

The observed flooded area is divided into square grids each of 1 km by 1 km. By comparing the class of M and of the class of observed inundation in each grid, the score of agreement is counted as 1 if the agreement is perfect. If the agreement is not perfect, a score of agreement of less than 1 is read from the criteria in Table 2. The total score of agreement for the whole flooded area is the sum of all scores given to all grids. The overall average score of agreement of all grids in the flooded area is equal to the sum of scores of all grids divided by the total number of grids in the flooded area.

Table 2. Scores for agreement between classe of M and class of satellite observed data

Score of Agreement between M & Satellite		Classes of Calculated M				
		Very high	***High***	***Moderate***	***Low***	***Very low***
Classes of Satellite Data	***Very high***	1	0.75	0.50	0.25	0
	High	0.75	1	0.75	0.50	0.25
	Moderate	0.50	0.75	1	0.75	0.50
	Low	0.25	0.50	0.75	1	0.75
	Very low	0	0.25	0.50	0.75	1

Results of model calibration and verification

Model calibration is done for the floods in 2013 and 2010. The weights of the five input factors W_1 to W_5 obtained from their 120 combinations of W's in each year are used. The agreement between the computed matching index M of the calibration run no. 9 and the satellite observed inundation data is found to yield the best comparison with W1=5, W2=3, W3=1, W4=4 and W5=2. The score of agreement is 81% for 2013 and 72% for 2010 respectively. The comparison results for 2013 are shown in Figs. 3 and 4 respectively.

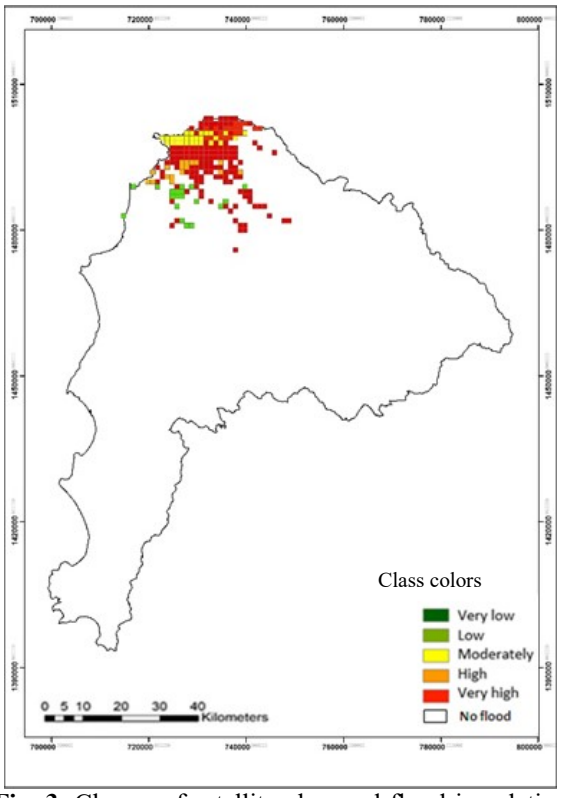

Fig. 3. Classes of satellite observed flood inundation area for model calibration in 2013

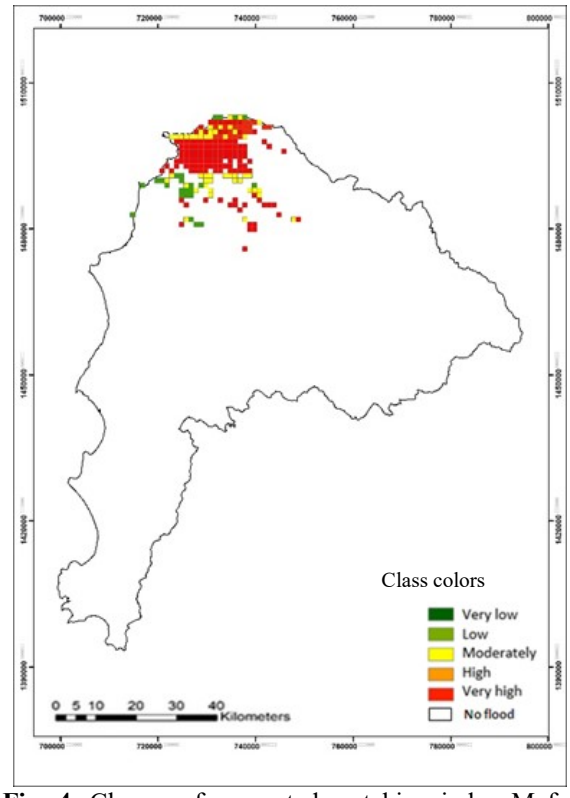

Fig. 4. Classes of computed matching index M for flood inundation area for model calibration in 2013

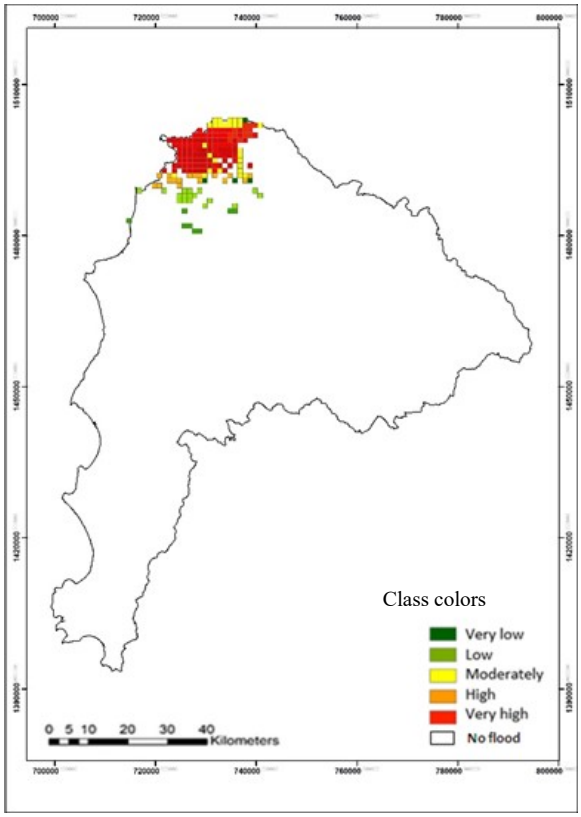

Fig. 5. Classes of satellite observed flood inundation area for model verification in 2008

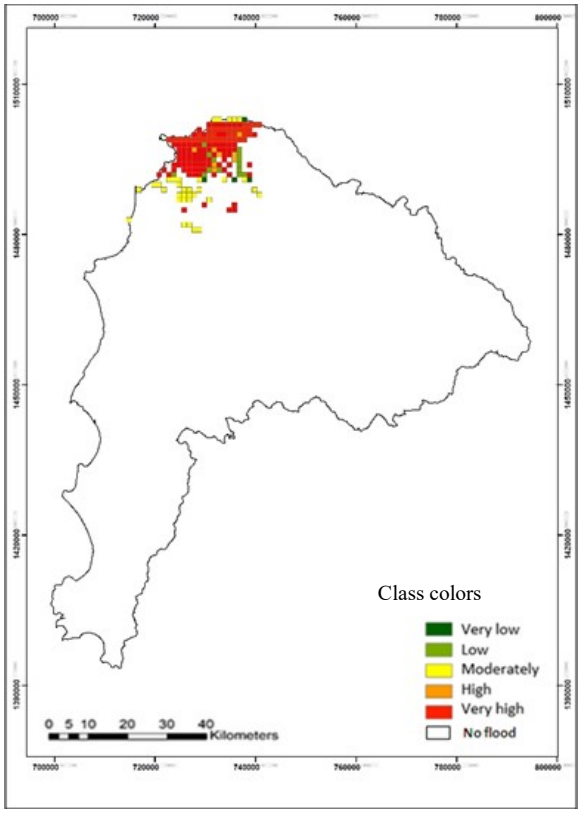

Fig. 6. Classes of computed matching index M for flood inundation area for model verification in 2008

Table 3. Weights w's of input factors in calibration runs for 2013

Calib Run No.	% Agreement	Weights of Five Input factors				
		W1 Rain	*W2 Slope*	*W3 Elev*	*W4 Land use*	*W5 Soil type*
1	68 %	1	3	2	4	5
2	81 %	1	3	4	5	2
3	75 %	2	1	5	4	3
4	68 %	2	3	1	4	5
5	72 %	3	2	1	4	5
6	76 %	3	2	4	5	1
7	78 %	4	1	5	3	2
8	65 %	4	2	1	3	5
9 Best	81 %	5	3	1	4	2
10	44 %	5	1	4	2	3

For model verification, the best set of the weight W's obtained from calibration runs for 2013 and 2010 (case 9 in Table 3) is kept unchanged and is used to run the ArcGIS model for another big flood in 2008. Fig. 5 shows the classes of satellite observed inundation area in 2008 and Fig. 6 shows the classes of computed matching index M for flood inundation in the same year. Comparing both figures, the results show a satisfactory agreement with the percentage of agreement of 66%.

Hence, the successful model calibration and verification ensure the validity and reliability of the AcrGIS model developed in this study in applying it to predict annual flood inundation areas in other years.

Discussions and conclusions

In other previous studies, the ArcGIS model was applied to determine flood hazard such as flood inundation areas by assuming the weights of various input factors that have influences on the floods. However, these weights were assumed rather intuitively without considering whether they correspond to the actual situation or not. In this study, an innovative approach is developed for the calibration and verification of the ArcGIS model for application in determining the flood inundation areas.

Usually, the flood inundation areas and flood depths depend on many input factors such as rainfall, ground slopes, ground elevation, land use types and soil types and other factors. The influence of these factors varies from one location to another location depending on the physiographical characteristics, hydro-meteorological characteristics and human activities in the study area.

The weights of these input factors in this study are assumed from 1 to 5, where 1 represents the weight for the lowest influence input factor and 5 for the highest influence. By using computer algorithm for successive iterations of weights of the inputs, the total number of iterations for the weights of the five inputs is equal to factorial 5 or 120 iterative computations. The 120 computations yielded 120 values of matching M for a selected flood. In this way, there are 120 calibration runs for each of the flood years of 2013 and 2010. Consistently a unique set of the integers W_1=5, W_2=3, W_3=1, W_4=4 and W_5= 2 are found to be the best set for 2013 and 2010 (for calibration) and 2008 (for verification). From this result, it shows that rainfall is the most important input factor, followed by land use, ground slope, soil type and ground elevation respectively. The calibrated values of W1 to W5 obtained from the model calibration is found to work satisfactorily well and also in the verification runs of the year 2008.The assigned percentage ranges for classification of matching M and the observed inundation area in five categories described in Section III, work well for both calibration and verification in this study. However, these percentage ranges should be tested for other study areas depending on the physiographical and flood characteristics as well as the development of the study areas.

Recommendations

The ArcGIS model requires calibration and verification of the weights of input data or input factors. With calibration and verification, the model output will be reliable. This is necessary to arrive at the best set of weights W's which are applicable for estimation of flood hazard condition for different floods. With the calibrated and verified set of the weights, the ArcGIS model and the developed methodology assures the validity and reliability in its application for estimation of flood hazard of other years in the study area. It is also recommended to apply this methodology for other areas.

Acknowledgment

The authors wish to express their sincere thanks to Sompop Kaewsawee of Kasetsart University, Sriracha Campus for providing useful data and information for this study.

References

[1] G.V. Bapulu, and R. Sinha, GIS in flood hazard mapping: a case study of Kosi River Basin, India. Noida: GIS Development.[ONLINE] Available from:http://home.iitk.ac.in/~rsinha/PDF's/2006_FloodGISdevelopment.pdf, 2005,[Accessed: 21/07/10].

[2] Sompop Kaewsawee and Supatchaya Chuanpongpanich, "Flood hazard map and evaluation of economic loss in Chonburi Province", 3rd Technical Conference, Kasetsart

University, Sriracha Campus, August, 2018, pp.235-243

[3] Supapon Naka, Climate Change 2007: Analysis of flood risk area in the upper Pasak river basin, Lomsak, Phetchabun Province. Thesis in Natural Resources and Environment, Naresuan University, Thailand, 2015.

[4] Nardnarade Akasuwan, Study on incidence of flood risk area factors using geographical information systems and prevention guidelines around western sub-basin area of Songkla lake in Phatthalung province. Master Thesis, Graduate School, Thaksin University, Thailand, 2009.

[5] ESRI, *How weight overlay works*. [ONLINE] available at:http://desktop.arcgis.com/en/arcmap/10.3/tools/spatial-analyst-toolbox/how-weighted-overlay-works.htm,2016, [Accessed 10 August 2018].

[6] D. A. Zimmer. 2011. "What is the Weighted Scoring Method." [ONLINE] Available at:https://pmterms.com/, 2011, [Accessed 26 July 2018].

[7] B. W. Ilbery. 1977. "Point Score Analysis: A Methodological Framework for Analysing the Decision-making Process in Agriculture". Journal of Economic and Social Geography, Vol. 68. Issue 2/ pp. 65-128.

[8] ESRI, *How Inverse Distance Weight (IDW) Interpolation works.* April 26th 2018, Retrieved from ArcGIS 9.2 Desktop Help. [ONLINE] Available at:http://webhelp.esri.com/arcgisdesktop/9.2/index.cfm?TopicName=How_Inverse_Distance_Weighted_(IDW)_interpolation_works, 2007,[Accessed 18 July 2018].

Deep Percolation Characteristics via Field Moisture Sensor Measurements in Rice Experimental Field, Phitsanulok, Thailand

Nittaya Kangboonma[1,a] and Sucharit Koontanakulvong[1,b]

Abstract Groundwater is an alternative use for the area where lack of surface water or increasing use of irrigation water. In the past studies, there were experiments of recharging water into underground by adding water through the pond or well, making weir under sand dune to help increasing water in canals or cheeks and studying infiltration rate through the soil surface depending on characteristic of soil. However, basic knowledge on deep percolation characteristics depending on soil type and rainfall pattern is still inadequate.

The objective of research is to study deep percolation characteristics and relationship with rainfall and soil type at 1-5 meters of soil depth (above shallow zone of groundwater level). The study area is in the Rice Experimental Field of Royal Irrigation Department, Phitsanulok Province, Thailand. This study designed sensor system and installed soil moisture sensor to measure soil moisture daily in the field. The period of soil moisture measurement is from July 13, 2017 tillJune 27, 2018 (twowet and two dry periods). The soil samples were collected at each depth from field for test and to determine the relative parameters ofRichards' Equation included hydrological data and hydrogeological data for simulating deep percolation by HYDRUS-1D model.

The study found that the percolation flux of sandy loam from top to bottom is 10.79 to7.46 mm/dayin wet period. The average rate of percolation to effective rainfall in each period is 0.43-0.49. The percolation rate is also affected from rainfall pattern and intensity, i.e., more intensified rainfall, more water content and more percolation, i.e., rainfall intensity of 2-11 mm/day induced percolation rate of 2-11 mm/day in exponential curve.

The results from the model help to understand the deep percolation characteristics, the relationship of deep percolation rate with soil moisture content, effects of rainfall pattern and rainfall intensity. It also helped to estimate groundwater recharge and groundwater potentials in areas where the groundwater is used to mitigate the drought.

Keywords *deep percolation, infiltration, field moisture sensor measurements, HYDRUS-1D*

[1]Department of Water Resources Engineering
Faculty of Engineering, Chulalongkorn University
Bangkok, Thailand

[a]pornittayakangboonma@gmail.com
[b]sucharit.k@chula.ac.th

Introduction

In recent several years, surface water tends to be more deficits in some areas. The insufficient surface water resources lead to increase groundwater abstraction especially in dry season. In this last ten years, the tendency of groundwater level declined in the Lower Yom and Nan River due to groundwater use mainly for irrigation use. Groundwater recharge mechanism knowledge is essential to understand groundwater movement especially in the area where groundwater use is excessive.

Deep percolation from irrigation water plays a key role in irrigation demand and groundwater supply by replenishing shallow aquifers at the local and regional scales. Percolation is accounted by vertical flow during the experiment. This phenomenon has also been widely observed and documented by many others [1]. A simple approach for determining deep percolation below the root zone is the use of the water balance method [2]. There are three main factors impacted to groundwater system in Phitsanulok Province: land recharge from precipitation, leakage from river, and groundwater pumping [3], i.e., water passed through soil performs under infiltration and percolation. These two related but different processes describing the movement of moisture through soil. Percolation rate is often equated to recharge in groundwater modeling describing water movement below the root zone. However, percolation measurement is sometime difficult and expensive in the field test. Thus, percolation used is to estimate indirectly from unsaturated zone water balance, Darcy flux, and water table fluctuation [4]. Deep percolation must be monitored below the root zone where it would be constant [5]. In the study, the soil moisture sensor module is used to detect the moisture of the soil or judge if there is water around the sensor. If more water is presented in the soil, the sensor would output resistance of soil which could covert to soil moisture. The motivation of soil moisture sensor is adapted from low-cost soil moisture profile probe [6]. Percolation identified water content in the soil flows below root zone efficiently [7]. The advantage of percolation is to induce recharge to groundwater and dilute chemicals in the soil. Hillel [8] concluded that percolation rate

relied on both soil property and water content. Soil properties, affected to percolation, are porosity, void distribution, and void shape while flow properties, affected to percolation, are density and viscosity.

This investigation aimed to understand deep percolation mechanism (soil moisture change, water balance, percolation rate) from rainfall utilizing soil moisture approach for developing groundwater modeling. Henceforth, the deeper percolation analysis procedure and results will be useful for further determining groundwater yields and groundwater recharge in the study area and in the consecutive drought years.

Study area

The experimental field site was located in the Rice Water Use Experimental Station 2 of Royal Irrigation Department at Amphoe Phrom Phiram (17º2′0″N, 100°12′7″E) in the north-western part of Phitsanulok Province, Upper Central Plain, Thailand (see Fig. 1). Due to previous studies[9, 10] ,the aquifer profile consists of poorly graded sand and fine to medium sand is 85% , is 10% and clay is 5%. From thee past study, the saturation of water content, field capacity of the soil type and the wilting point of the sandy loam is same soil type in the study area 0.420%, 0.255% and 0.175% [11].

Fig. 1. Experimental site location

Procedures and Theories used

The procedures of study was conducted in steps as follows,
First, the field measurement system was designed and installed in Rice Experimental Field, Phitsanulok Province, Thailand. Daily data of soil moisture and related hydrological data were collected. Second, the daily deep percolation was simulated by using the Hydrus 1D model. The water retention parameters were calibrated and verified by field experimental data collected from July,13 2017 to June 27, 2018 in the study area. Thirdly, relationship of effective rainfall and soil moisture are analyzed to detect the deep percolation characteristics from the simulated results. Finally, the assessment water balance provides a better understanding of the deep percolation rate from the data of two rainy and two dry periods.

A. Field measurements

At field sites, the Arduino sensors were installed at every meter in 5 meters depth as shown in Fig 2. The soil moisture sensor monitored every 1meter depth daily. The soil moisture of each soil type at each depth (shown in Table II) was calibrated with moisture measurement in the lab. Then, the measurements in the field site are converted to soil moisture. The circuit includes Arduino board, soil moisture module, and soil moisture sensor (copper plate), automatic data transmit as shown in Fig. 3.

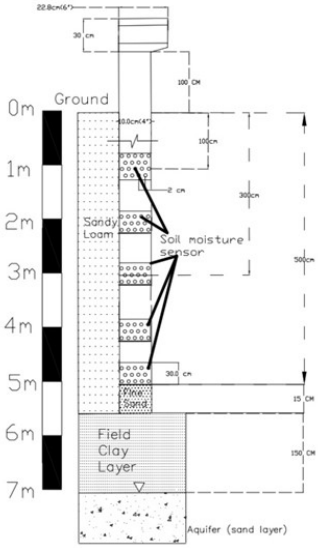

silt

Fig. 2.Field sensor installation

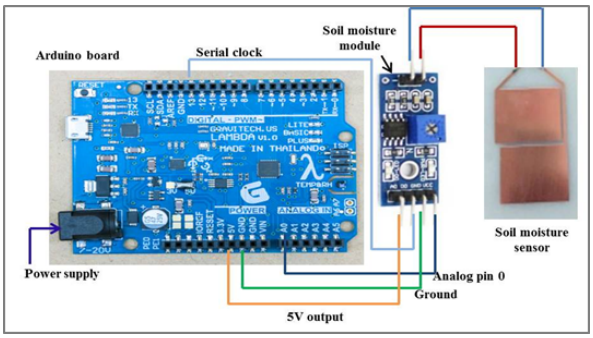

Fig. 3. The schematics of digital measurement of soil moisture by developed sensor

B. Percolation simulation theory

The governing flow equation for the uniform Darcy flow of water in a porous medium is adopted by the following modified form of the Richards' equation: [12]

$$\frac{\delta\theta}{\delta t} = \frac{\delta}{\delta x_i}\left[K\left(K_{ij}^{A}\frac{\delta h}{\delta x_j} + K_{iz}^{A}\right)\right] - S \qquad (1)$$

θ is the volumetric water content, (L^3L^{-3})

K is the hydraulic conductivity (LT^{-1}),

h is the pressures head (L)

S is a sink term [T^{-1}]

x_i (i-1,2) are the spatial coordinates [L],

t is the time (T) and

z is the vertical ordinate (L)

K^A_{ij} are components of a dimensionless anisotropy tensor

K^A

K is the unsaturated hydraulic conductivity function [LT^{-1}] given by

$$K(h) = K_s S_e^{1/2}\left[1-(1-S_e^{1/m})^m\right]^2 \quad (2)$$

$$\theta(h) = \begin{cases} \theta_r + \dfrac{\theta_s-\theta_r}{[1+|\alpha h|^n]^m} & h<0 \\ \theta_s & h \geq 0 \end{cases} \quad (3)$$

$$S_e = \frac{\theta-\theta_r}{\theta_s-\theta_r} \quad (4)$$

$$m = 1-1/n, n>1 \quad (5)$$

S_e is the effective water content

θ_r denote the residual water content

θ_s denote the saturated water content

K_s is the saturated hydraulic conductivity

α is the inverse of the air-entry value

n is a pore-size distribution index

The percolation simulation applied rainfall and evaporation of study area from July13, 2017- June 27, 2018 (350 days). The upper boundary condition set as atmosphere condition. The bottom boundary condition set as free drainage condition. The initial retention parameters (θ_r , θ_s, α, n, K_s)are referred from Rosetta program [13]. The calibrated retention parameters were validated by sensor recorded data.

Results and discussions

A. Field measurement

From the field experiment, Fig. 4 shows sample of field observed water content and daily effective rainfall (rainfall-evaporation) during July 13, 2017- June 27, 2018 at each depth with soils of sandy loam and sandy clay. The observed water content corresponded with effective rainfall. The soil moistures at 1 meter depth is located near surface and affected from root plant zone that are sensitive with rainfall and evaporation. Different soil property in each soil layer, for example sand material,has different permeability that causes water can through the inner porosity of its material to below soil layer in different speed. Water content in each soil layer also changes in wetting and drying periods. The lower soil depth has less sensitive with rainfall events. The field monitor periods were spited into Wet 1, Dry 1, Wet 2 and Dry 2 due to the change of amount of rainfall and water content patterns.

Fig.5 demonstrates relationship offlux in field test and water contents in each depth level during wetting and drying periods in 2017-2018. The flux and soil moisture show closed relationship in wetting and drying periods. The fluxes in wettingperiod are higher than in dryingperiod and decrease in each soil depth because of influence of gravity force.The percolation flux of soil moisture in sandy loam is higher and The water content of wet and dry periods are clearly different (at the depth of 1 to 4 meter) that effects available water in each soil layer. On other hand, sandy clay shows the lowest difference in soil moisture (at 5meters depth) due to low permeability of soil property that can store water in the soil. The soil moisture fluctuates more in the firstmeter depth due to rainfall and evaporation outputs.

The measurement data showed that developed soil moisture sensors gave reliable values under natural conditions. Then, the percolation and water balance analyses can apply the field soil moisture data monitored by installed sensors.

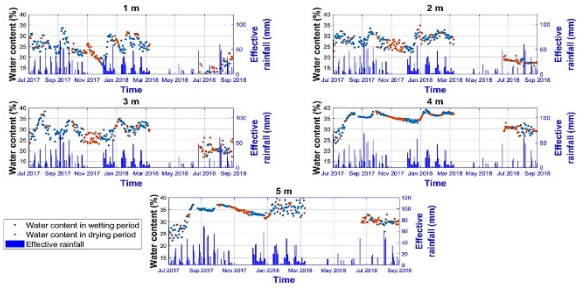

Fig. 4. Observed water content and effective rainfall during July 2017-June 2018

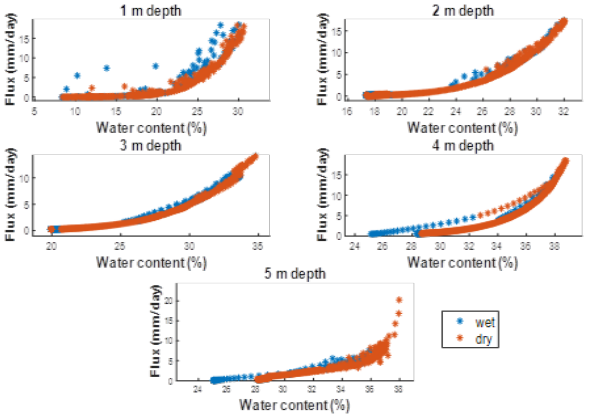

Fig. 5. Relationship of fluxs and water contents in the field test

B. Calibration and verification of percolation simulation

The HYDRUS 1-D model was applied to simulate water content in the soil and calibrated/verified with field water content as shown in Fig. 6. Retention parameter calibrations relied on performance statistics of observed soil moisture. In calibration step, the calculated soil moistures of two soil type match well with observed data. The maximum error (%) is 4.23 to 2.86. The minimum error (%) is 0. The mean error (%) is 0.30 to 1.09. The RMSE (%) is 0.56 to 1.39. The Nash coefficient is 0.62 to 0.97. In verification step, the calculated soil moistures of twosoil type are similar with observed data. The maximum error (%) is 5.72 to 2.00. The minimum error (%) is 0. The mean error (%) is 0.3 to 1.57. The RMSE (%) is 0.84 to 1.57. The Nash coefficient is 0.62 to 0.85 (as shown in Table I).

TABLE II shows the soil retention parameter values after calibration. The soil retention parameters are related with soil type. The α, n, K_s parameters have decreasing values at each depth except the residual water content that had low value at 1-4 meter because large pore-size of particle soil that caused water flow through and did not remain water in the soil layer. The sandy loam has highest hydraulic conductivity. The lowest hydraulic conductivity is sandy clay.

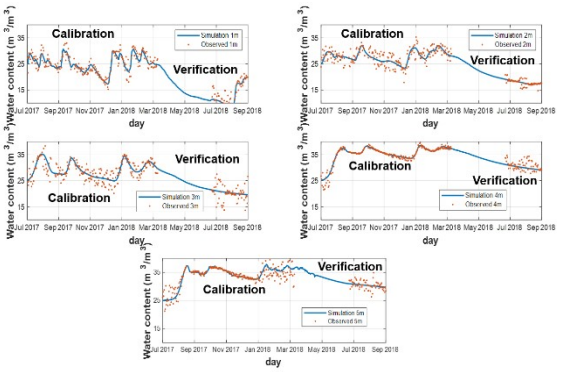

Fig. 6. Calibration and Verification results

Table I. Errors from calibration and verification

Statistical errors	Calibration					Verification				
	Soil depth					Soil depth				
	1 m	2 m	3 m	4 m	5 m	1m	2 m	3 m	4 m	5 m
Max	4.23	3.51	3.99	2.86	3.83	5.72	2.00	5.05	2.50	3.54
Min	0.00	0.00	0.00	0.00	0.00	0.00	0.00	0.02	0.00	0.00
Mean	1.06	1.06	1.09	0.30	0.77	1.01	0.30	1.57	0.56	0.73
RMSE	1.38	1.30	1.39	0.56	1.17	1.57	0.54	2.12	0.84	1.02
NASH	0.83	0.72	0.80	0.97	0.90	0.83	0.77	0.79	0.85	0.62

Table II. Soil retention parameters after calibration

Depth (m)	Soil type	θ_r	θ_s	α	η	K_s
1	Sandy Loam	0.065	0.41	0.0075	1.89	170
2	Sandy Loam	0.065	0.41	0.0065	1.75	150
3	Sandy Loam	0.065	0.41	0.0045	1.65	90
4	Sandy Loam	0.065	0.41	0.0027	1.47	30
5	Sandy Clay	0.100	0.38	0.0021	1.35	25

C. Water balance analysis

TABLE III shows total fluxes at four periods (Wet 1, Dry 1 in the first year and Wet 2, Dry 2 in the second year) from July 13, 2017- June 27, 2018. The flux rate in top layer is higher than in lower soil layer because available space for water flowed through soil. The percolation rate depends on the intensity of rainfall as shown in Fig. 7. Percolation rate in the second year has higher flux and amount of effective rainfall is also more than in the first year. Due to the permeability property of soil, the derived percolation rate is different in each soil type in the study area. The percolation rate of sandy loam is the highest. The sandy clay in bottom has the lowest amount percolation. The gap between fluxes of two soil depth can be explained by the fluctuation water content in its depth.

The percolation fluxes were compared with effective rainfall to find the effect of soil type and rainfall pattern/intensity in the study area. The percolation rate ratios decrease from top to bottom depth in both the periods of Wet 1 and Wet 2. The mean percolation flux of sandy loam from top to bottom is 10.79 to 7.46 mm/day in wet periods.

Table III. Percolation rates at each soil DEPTH and period

Soil depth	Average percolation flux rate (mm /day)					
	Wet 1	Dry 1	Wet 2	Dry 2	Mean	
	July 13 – Oct 10, 2017 (90 days)	Oct 11 Dec 18, 2017 (69 days)	Dec 19, 2017 – Mar 19 , 2018 (91 days)	Mar 20 – June 27 2018 (100 days)	Wet (mm/day)	Dry (mm/day)
1 m	10.16	2.71	11.42	0.64	10.79	1.48
2 m	8.15	2.68	11.27	2.21	9.71	2.40
3 m	7.78	2.08	7.15	1.93	7.46	1.99
Effective rainfall	969.39	306.26	1003.3	149	10.96	3.00

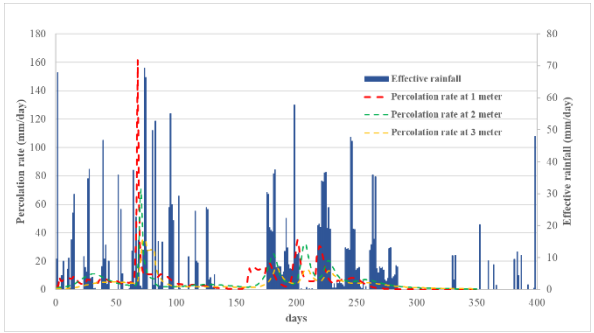

Fig. 7. The relationship between percolation rate in each depth andeffective rainfall

From Table III, the amount of rainfall in the first period (Wet 1) is 969.39 mm period in 90 days while the amount of rainfall in the third period (Wet 2) is 1003.3 mm in 91 days. The rainfall intensity in the third period is more than in the first period. The average rate of percolation to effective rainfall in each period is 0.43-0.49. Fig. 8 shows annual water balance and water content change at each soil depth and different effective rainfall intensity from the simulationsin the year 2017-2018. It is noticed that

rainfall pattern affected the percolation rate, i.e., more intensified rainfall, more water content in each soil layer and more percolation as shown in Fig. 9.

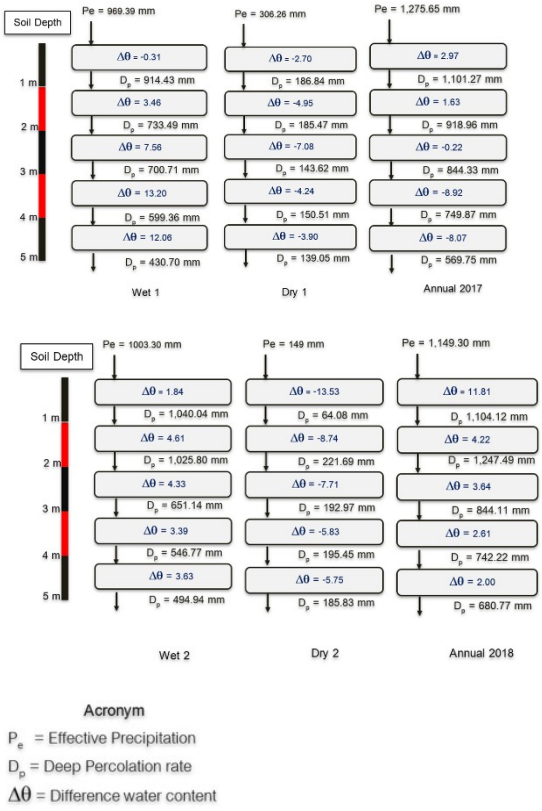

Fig. 8. Water balance and water content change in 2017-2018

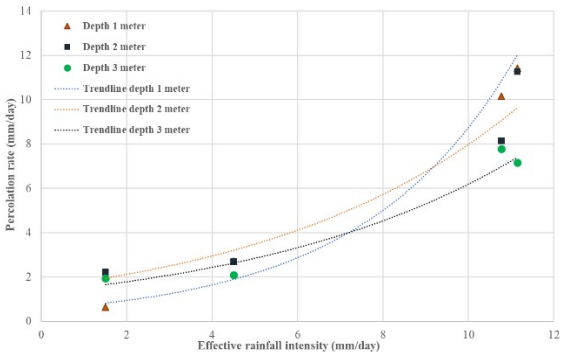

Fig. 9. The relationship percolation rate and effective rainfall intensity

Conclusions

The developed soil moisture sensor system gave reliable values of soil moisture under natural conditions. The field monitored data with the application of HYDRUS 1-D model can estimate percolation rate and analyze water balance in each soil depth in more details.

The percolation fluxes were compared with effective rainfall to find the percolation ratio in the study area. The percolation ratios decrease from top to bottom depth. The highest ratio is sandy loam. The second ratio is sandy clay. The percolation flux of sandy loam from top to bottom is 10.79 to 7.46 mm/day in wet period. It is shown that the average rate of percolation to effective rainfall in each period is 0.43-0.49. The percolation rate is also affected from rainfall pattern and intensity, i.e., more intensified rainfall, more water content and more percolation, i.e., rainfall intensity of 2-11 mm/day induced percolation rate of 2-11 mm/day in exponential curve.

The results from the model help to understand the deep percolation characteristics, the relationship of deep percolation rate with soil moisture content, effects of rainfall pattern and rainfall intensity. It also helped to estimate groundwater recharge and groundwater potentials in areas where the groundwater is used to mitigate the drought

Acknowledgment

This paper could not be accomplished without the supports from Royal Irrigation Department and the Water Resources System Research Unit of Faculty of Engineering, Chulalongkorn University. The authors also thank to the RID staff at Rice Experimental Field for field data collection.

References

[1] Steenhuis, T.S., et al., *Preferential movement of pesticides and tracers in agricultural soils.* Journal of Irrigation and Drainage Engineering, 1990. **116**(1): p. 50-66.

[2] Jaber, F.H., S. Shukla, and S. Srivastava, *Recharge, upflux and water table response for shallow water table conditions in southwest Florida.* Hydrological Processes: An International Journal, 2006. **20**(9): p. 1895-1907.

[3] Koontanakulvong, S. and P. Siriputtichaikul. *Groundwater Modeling In the North Part of the Lower Central Plain, Thailand*. in *International Conference On Water and Environment, Bhopal, India, Vol. Ground Water Pollution*. 2003.

[4] Wu, J. and R. Zhang, *Analysis of Rainfall-Infi l tration Recharge to Groundwater*, in *Proceedings of Fourteenth Annual American Geophysical Union: Hydrology Days* 1994, Hydrology days: Colorado State University.

[5] Slavich, P., G. Petterson, and D. Griffin, *The effect of gypsum on deep drainage from clay soil used for rice.* Australian sodic soils: distribution, properties and management. CSIRO, Melbourne, 1995: p. 205-210.

[6] Kojima, Y., et al., *Low-cost soil moisture profile probe using thin-film capacitors and a capacitive touch sensor.* Sensors, 2016. **16**(8): p. 1292.

[7] Irmak, S., *Simplified Forms of Deep Percolation Estimation Method below the Crop Root Zone for*

Silt-Loam Soils. Journal of Irrigation Engineering, 2017: p. 1-6.

[8] Hillel, D., *Fundamentals of soil physics*. 2013: Academic press.

[9] Kantasinee Chaengpui, W.S.-a., Sujin Charoonsak & S. P. P. Srima, *Study on Consumptive Use of Dragon Fruit (2nd year)*, in *In Irrigated Agriculture Newsletter*. 2015, Royal Irrigation Department: Royal Irrigation Department.

[10] Long, T.T., S. Koontanakulvong, and P.P. Aye, *Examination of land recharges using soil moisture approach: Case study in Thailand.* Internet Journal of Society for Social Management Systems 2017. **Vol.11**(issue1): p. 10.

[11] Lee, T.J. and R.A. Pielke, *Estimating the soil surface specific humidity.* Journal of Applied Meteorology, 1992. **31**(5): p. 480-484.

[12] Simunek, J., M.T. Van Genuchten, and M. Sejna, *The HYDRUS-1D software package for simulating the one-dimensional movement of water, heat, and multiple solutes in variably-saturated media.* University of California-Riverside Research Reports, 2005. **3**: p. 1-240.

[13] Schaap, M.G., F.J. Leij, and M.T. Van Genuchten, *Rosetta: A computer program for estimating soil hydraulic parameters with hierarchical pedotransfer functions.* Journal of hydrology, 2001. **251**(3-4): p. 163-176.

Water Quality Characteristics of Ions Originating from Seawater and Man-made in The lower Chao Phraya River, Thailand

YUSUKE HORIUCHI[1,a], TAKUYA MATSUURA[1,b], TAICHI TEBAKARI[2,c] and SANIT WONGSA[3]

Abstract The purpose of this study is to clarify seasonal and longitudinal change of electric conductivity, ions originating from seawater (Na^+, K^+, Mg^{2+}, Cl^-, Ca^{2+}, SO_4^{2-} and HCO_3^-) and man-made (NO_3^-) at the surface and the riverbed water in the lower Chao Phraya River, Thailand. The environmental water quality standard is still low and does not satisfied in Thailand. Regularly and/or continuous measurement and analysis of water quality will be important background information/data if water quality trouble will occur in the future. We have observed and analyzed water quality at the surface and the riverbed in the lower Chao Phraya River for more than two years since August 2016. Moreover, we have analyzed automatic water quality data observed by Metropolitan Waterworks Authority (MWA).As a result, the electric conductivity had seasonal characteristics caused by the dam operation throughout a year. It is clarified that the seawater intruded upstream as well-mixed type because the ions originating from sea water at the surface and the bottom were almost same values. The ions originating from man-made did not have any seasonal characteristic. However, NO_3^- which was ions originating from man-made at the surface and the bottom were shown different values at C02_T01(a distance of 26.6 km from the river mouth) and C06_S04(a distance of 90.1 km from the river mouth). Above-mentioned results had clear seasonal change caused by release water from the Chao Phraya Dam.

Keywords *electric conductivity, sea water origin, man-made origin*

[1]Graduate School of Engineering
Toyama Prefectural University
Imizu, Toyama, Japan
[2]Department of Environmental and Civil Engineering
Toyama Prefectural University
Imizu, Toyama, Japan
[3]Civil Technology Education
King Mongkut's University of Technology Thonburi
Bangkok, Thailand

[a]t857008@st.pu-toyama.ac.jp
[b]t877002@st.pu-toyama.ac.jp
[c]tebakari@pu-toyama.ac.jp

Introduction

It is costly to manage and analyze the quality of river water, in terms of both time and effort. In addition, water quality is low in many rivers in developing countries, which affects the social economy. However, improvement efforts initiated by governments and corporations tend to limited and thus citizen involvement is essential to improve the environment. InThailand, a developing country, river water quality has not improved commensurately with the social economy, and there has been little change evident since 1996. In addition, the domestic drainage settlement penetration rate in Thailand is about 20%, which is extremely low compared to that of Malaysia (approximately 65%). In fact, the quality of one of Thailand's major rivers, the Chao Phraya, is steadily declining [1]. The government of Thailand has designated this river an important basin for water quality control and water managementresource strategy development for 201 5–2026 [2].

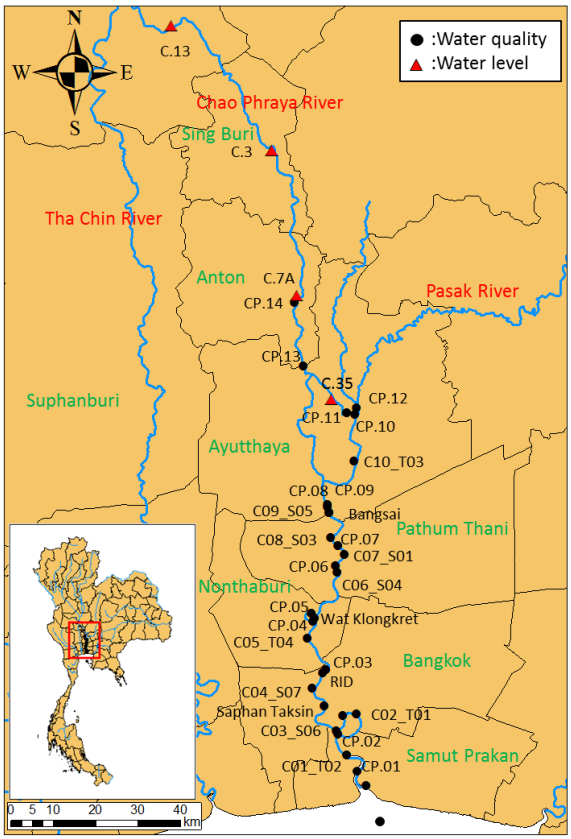

Fig. 1. Map of Thailand and the lower Chao Phraya River.

Table I. Locations and types of data collected

No	Station Name	Distance from the river mouth (km)	Water level	Month/Year						Remarks
				Nov.2016	Mar.2017	Aug.2017	Nov.2017	Apr.2018	Jun.2018	
1	Sea water	-10.0					●			TPU (Toyama Prefectural Univercity)
2	The river mouth	0.0					●			TPU (Toyama Prefectural Univercity)
3	CP.01	6.5					●			TPU (Toyama Prefectural Univercity)
4	C01_T02	11.3				○	●	●	●	MWA Obs.Station, TPU (Toyama Prefectural Univercity)
5	CP.02	17.6					●			TPU (Toyama Prefectural Univercity)
6	C02_T01	28.4				○	●	●	●	MWA Obs.Station, TPU (Toyama Prefectural Univercity)
7	C03_S06	34.2				○	●			MWA Obs.Station, TPU (Toyama Prefectural Univercity)
8	Saphan Taksin	44.2			○		○		●	TPU (Toyama Prefectural Univercity)
9	C04_S07	50.0						●	●	MWA Obs.Station, TPU (Toyama Prefectural Univercity)
10	RID	54.5			●		●	●	●	TPU (Toyama Prefectural Univercity)
11	CP.03	55.8					●			TPU (Toyama Prefectural Univercity)
12	C05_T04	64.9				○	●	●	●	MWA Obs.Station, TPU (Toyama Prefectural Univercity)
13	CP.04	69.5					●			TPU (Toyama Prefectural Univercity)
14	Wat Klangkret	69.6						●	●	TPU (Toyama Prefectural Univercity)
15	CP.05	75.1		○						TPU (Toyama Prefectural Univercity)
16	C06_S04	90.1				○	●	●	●	MWA Obs.Station, TPU (Toyama Prefectural Univercity)
17	CP.06	91.5		○						TPU (Toyama Prefectural Univercity)
18	C07_S01	95.1				○		●	●	MWA Obs.Station, TPU (Toyama Prefectural Univercity)
19	CP.07	97.8					●			TPU (Toyama Prefectural Univercity)
20	C08_S03	100.5				○	●	●	●	MWA Obs.Station, TPU (Toyama Prefectural Univercity)
21	C09_S05	109.3				○	●	●	●	MWA Obs.Station, TPU (Toyama Prefectural Univercity)
22	Bangsai	109.3			●		●			TPU (Toyama Prefectural Univercity)
23	CP.08	110.9					○			TPU (Toyama Prefectural Univercity)
24	CP.09	112.4		○						TPU (Toyama Prefectural Univercity)
25	C10_T03	131.0				○	●	●	●	MWA Obs.Station, TPU (Toyama Prefectural Univercity)
26	CP.10	143.7		○						TPU (Toyama Prefectural Univercity)
27	CP.11	144.1		○						TPU (Toyama Prefectural Univercity)
28	CP.12	144.6		○						TPU (Toyama Prefectural Univercity)
29	C.35	152.9	▲							RID
30	CP.13	164.9		○						TPU (Toyama Prefectural Univercity)
31	CP.14	183.1		○						TPU (Toyama Prefectural Univercity)
32	C.7A	185.0	▲							RID
33	C.3	229.0	▲							RID
34	C.13	278.4	▲	○						RID

○: Only Surface water ●: Surface and Riverbed water ▲:Water level

In 1956, 31 monthly water quality analyses were conducted in Thailand, constituting the most comprehensive study of the country's water quality to date [3]. In that study, vertical salinity was also measured, and the results contributed to the countermeasures taken in the Chao Phraya delta against salt damage [4]. This was followed by a period of vigorous observation and study in the 1980s, when concerns were raised regarding the very poor water quality in the lower Chao Phraya. The water quality failed to meet cleanliness criteria in several categories, including dissolved oxygen (DO), chemical oxygen demand (COD), and coliform bacteria [5]. Recently, chlorophyll content has been used as a metric for assessing river water quality in Thailand [6]. Sea level rise due to climate change will increase the intrusion of saline water into the Chao Phraya River [7], and the Intergovernmental Panel on Climate Change (IPCC) suggests that the sea level will rise by 1.16 m by 2100 and recommends the installation of pumping stations to counter upstream increases in salinity. The IPCC has also reported on regions where water will no longer be obtainable for agriculture in Thailand. Recently, waterworks have been built above the Chao Phraya River; however, the government only monitors water quality and no analyses have been performed on the resulting data.

In this study, we clarify the seasonal and longitudinal changes in the electric conductivity caused by ions originating from sea water (Na^+, K^+, Mg^{2+}, Cl^-, Ca^{2+}, SO_4^{2-}, HCO_3^-) and manmade (NO_3^-) sources in the lower Chao Phraya, based on field observations and analyses of the results over a 2-year period.

Study area

Figure 1 shows a map of Thailand and the lower Chao Phraya River. The data and locations from which they were collected are summarized in Table 1. The Chao Phraya River basin extends from the northern region of Thailand to its central plain; the catchment area is 157,925 km^2, which accounts for about 30% of the country's total area, and it is the largest river basin in the 29 prefectures of Thailand. Topographically, the upper northern region is mountainous, the middle region is a floodplain, and the lower stream region is a delta. The Ping River (36,018 km^2), Wang River (11,708 km^2), Yom River (24,720 km^2), and Nan River (34,557 km^2) join in Nakhon Sawan, located in the middle region, to become the Chao Phraya River. The Sakae Krang River flows into the Chao Phraya from the west and the Pasak River (18,200 km^2) joins in Ayutthaya from

the east; the Chao Phraya empties into the Bay of Bangkok [8].

Field observations and analysis data

A. Field observations

We measured electric conductivity, pH, and water temperature during our field observations and sampled the river water from the water sampling points and sampling times shown in Table 1. We measured the water quality in the field using a portable water quality meter (LAQUAact D-70/ES-70; HORIBA). Water samples were collected with a polyethylene bucket and transported in a cooler box to maintain the water in a cool and dark state. Samples from near the riverbed were obtained by first measuring the water depth using a DT-X (Biosonics) metrological fish finder and then using a small submersible pump (DIK-670 B-A1, Daiki Rika Ko gyo Co., Ltd.) to collect water.

B. Analysis

All samples were transported to our laboratory, where we analyzed the concentrations of 14 types of dissolved ion, namely, Na^+, NH_4^+, K^+, Mg^{2+}, Ca^{2+}, Li^+, Cl^-, NO_3^-, SO_4^{2-}, HCO_3^-, F^-, NO_2^-, Br^-, and PO_4^{3-}. The concentrations were measured using the alkalinity titration method; all remaining ions were measured using an ion chromatograph (ICS-2000; Dionex) after filtration through a 0.45 μm membrane filter. We judged the validity of the results of ion chromatography analyses by comparing them to measured values of electric conductivity.

C. MWA observation data

We obtained water level and water quality data from the metropolitan water authority (MWA), which collects data automatically every 10 min. We also downloaded electric conductivity data from the MWA website for comparison with our observational data [9].

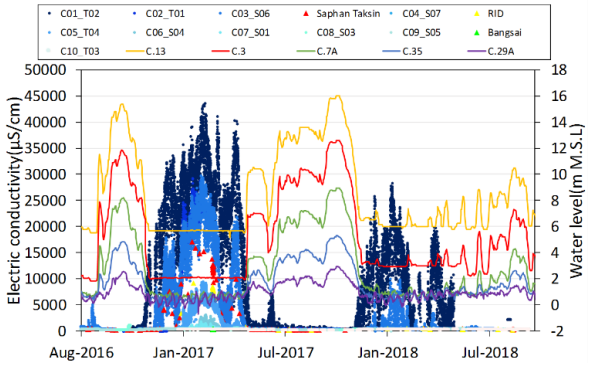

Fig. 2. Time series of electric conductivity and water levels from August2016 to October 2018 in the lower Chao Phraya River.

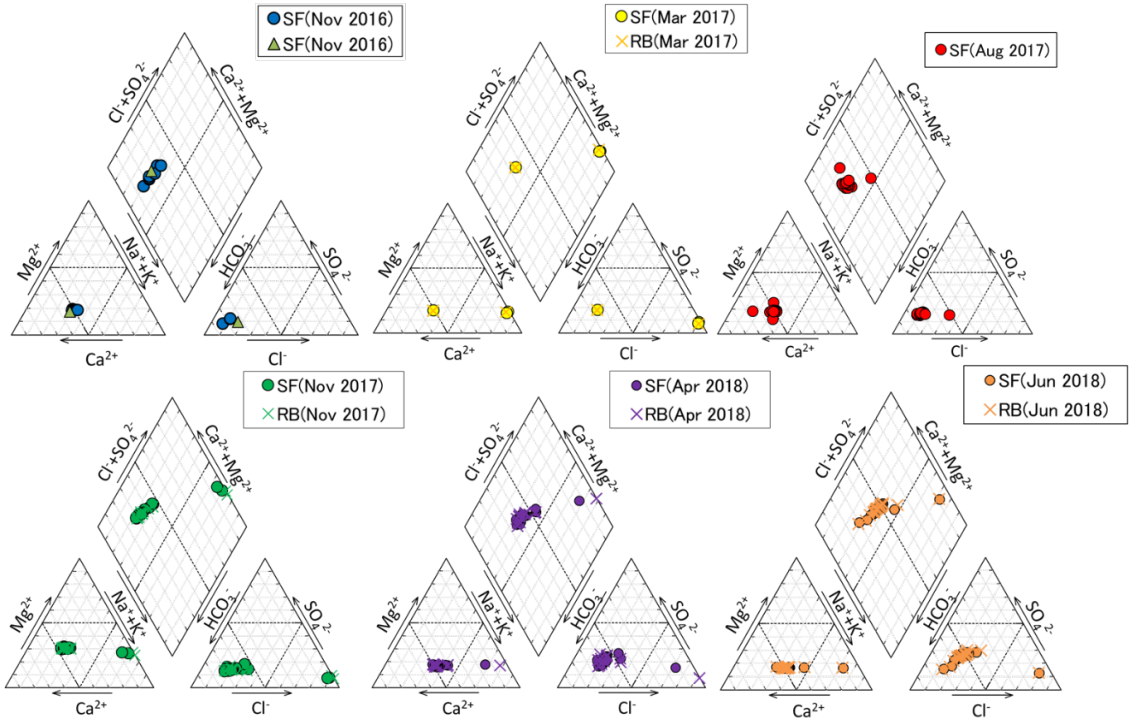

Fig. 3. Trilinear diagrams for November 2016, March 2017, August 2017, November 2017, April 2018, and Jun 2018.

Seasonal and longitudinal change of electric conductivity

We compared water quality between the rainy season (May–October) and the dry season (November–April); the Royal Irrigation Department of Thailand uses these data to devise water management strategies. Figure 2 shows a time series of the electric conductivity values and longitudinal water levels from August 2016 to October 2018. The flow conditions clearly differ between the rainy and dry seasons. In the dry season, from November 2016 to April 2017, water was released from the Chao Phraya Dam (C.13) at a rate of 70 m^3/s. In June 2017, the flow from the upstream part of the river increased due to a tropical cyclone. The discharge was temporarily decreased by the Chao Phraya Dam. The river water level decreased with this decrease in discharge and the electric conductivity increased slightly in the lower Chao Phraya River. The electric conductivity was lower across the whole Chao Phraya River in the dry season between November 2017 to April 2018 than it had been in the dry season. The decrease in electric conductivity was caused by the increase in discharge from the Chao Phraya Dam. Figure 3 shows trilinear diagrams of surface and riverbed water in November 2016, March 2017, August 2017, November 2017, April 2018, Jun 2018. In November 2016 and November 2017, at the beginning of the dry season, the characteristics of the river water mainly indicate the presence of Ca-HCO_3. However, the data from November 2017 also indicated that Na-Cl and Na-SO_4 were present. Inthe dry season months of March 2017 and April 2018, the dominant ions changed from Ca-HCO_3 to Ca-Cl and Na-SO_4, as we traversed downstream from the upstream region. This may have been due to the influence of saltwater intrusion from sea water. In the rainy season months of August 2017 and June 2018, there was a predominance of Ca–HCO_3, but Na-Cl and Na-SO_4 were also found in the downstream area. These results suggest that the downstream area was affected by saltwater incursion, even during the rainy season.

Results

Figure 4 shows the results of the longitudinal electric conductivity field measurements. At the beginning of the dry season, we found similar values in both the surface and riverbed layers. Even in the longitudinal direction, the electric conductivity did not vary significantly between the surface water and the water from the riverbed at distances over 10 km from the mouth of the estuary. We believe that the intrusion of saline water was suppressed by the amount of water discharged during the rainy season, thus the sea water was diluted by freshwater. The observed electric conductivities were much higher in March 2017 than in April 2018. This is due to the fact that the period during which the water level was increasing due to discharge from the Chao Phraya dam in the rainy season of 2016 was very short compared to that of 2017. This may have prevented the dilution of the sea water entering the river.

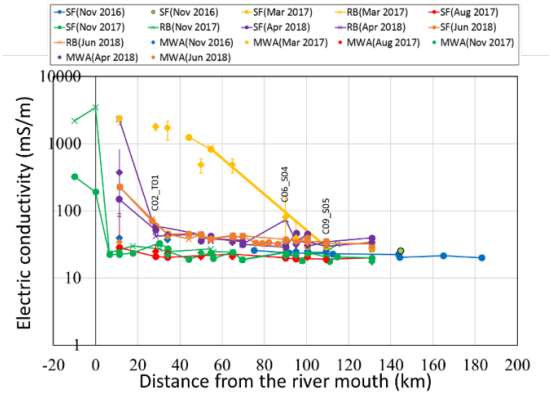

Fig. 4. Longitudinal change of electric conductivity in the lower Chao Phraya River.

A. Ions originating from sea water

Figure 5 shows the longitudinal profile of the river ions originating from sea water. According to the electric conductivity measurements of the sea water taken in August 2017, June 2018 (during the rainy season), November 2016, and November 2017 (at the beginning of the dry season), the ion concentration remained constant. We believe that the saltwater incursion was suppressed by the volume of water discharged from the Chao Phraya dam during the rainy season, so the conductivity was not influenced by ions originating from sea water. However, there were more ions originating from sea water in March 2017 and April 2018 (during the dry season) than during the rainy season. This may have been caused by the dominance of ions originating from sea water. In addition, in terms of ions originating from sea water, there were no differences between the water at the surface and the water at the riverbed in either the rainy season or the dry season. This seems to be because sea water from the ocean is incorporated throughout the entire depth of the river.

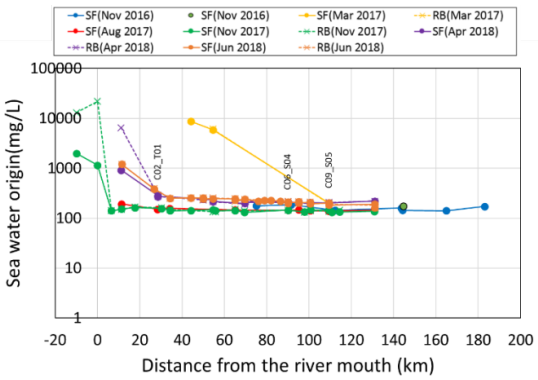

Fig. 5. Longitudinal change of ions originating from seawater in the lower Chao Phraya River.

B. Ions originating from man-made

The main sources of nitrogen compounds are natural sources: ①nitrogen oxides generated by nitrogen oxidation by lightning, ②nitrogen fixed algae, ammonia generated by reduction of nitrogen molecules by nitrogen fixing bacteria, artificial origin: ①industrial air by the harbor · Bosch method Nitrogen oxides supplied by nitrogen fixing in ② gasoline, nitrogen oxide generated by oxidation of nitrogen molecules in the atmosphere in a diesel engine[10]. The nitrates produced by these reactions are taken up by animals and plants and are mainly discharged as ammonia. This ammonia turns into nitrate through the following reaction formula in soil and water, and nitrogencirculates. The effects of NO_3^- are represented by Formulas (1) and (2), which summarize its reactions with aerobic microorganisms in the river and with anaerobic microorganisms, respectively.

$$NH_3 + 2O_2 \rightarrow NO_3^- + H_2O + H^+ \quad (1)$$

$$2NO_3^- + 5H^+ \rightarrow N_2 + 4H_2O + 2OH^- \quad (2)$$

Figure 6 shows the longitudinal river profile of ions originating from manmade sources (NO_3^-). Comparing the results from the rainy season and the dry season, we can see that, although there was no seasonal trend in the NO_3^- concentration, it was higher in the dry season than in the rainy season. We attribute this result to either the stagnation of electrolytes in the river when there was no dilution due to freshwater inflow from the Chao Phraya dam, or to the decrease in the level of rainfall in the dry season. In November 2016 (at the beginning the dry season), the NO_3^- concentration decreased significantly after the Pasak River merged into the Chao Phraya, most likely due to dilution from the influx of water of different quality. As a result, there was more NO_3^- at the riverbed during November 2017 (at the beginning the dry season) than on the surface layer slightly upstream from point C09_S05. This may have been due to nitrification caused by aerobic microorganisms found in nitrogen fertilizer, excrement, and carcasses accumulated in the sediment. There was more NO_3^- at the surface at point C02_T01 than on the riverbed. The around this area is a region where ship traverses a lot of industries, there was a possibility that nitrogen oxides have been generated and flowed in by ships use. This may have been also due to the reduction of NO_3^- to N_2 by denitrification caused by anaerobic microorganisms, or to the reaction with aerobic microorganisms. In April 2018 (during the dry season), there was more NO_3^- at the riverbed than at the surface at point C06_S04. This may have been due to nitrification by aerobic microorganisms. The water quality at point C02_T01 was similar to that at C06_S04 in November 2017, with the riverbed containing more NO_3^- than the surface layer due to the denitrification. There was also the possibility that organic matter abundantly exists in this area. It was considered that the influence of nitrogen oxides by use of their car as the transportation network was developed in Thailand.

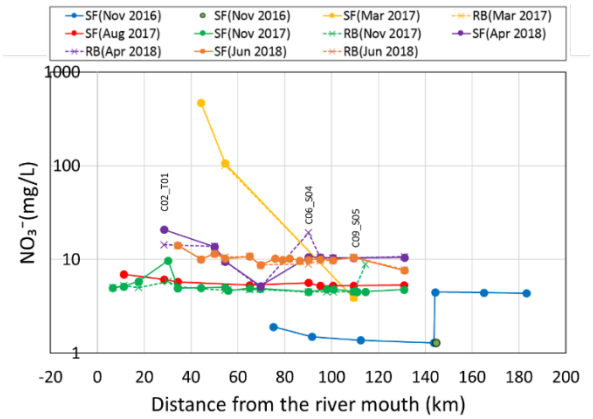

Fig. 6. Longitudinal change of ions (NO_3^-) originating from man-made in the lower Chao Phraya River.

Conclusions

We investigated the seasonal variation in the electric conductivity of the lower Chao Phraya River and found that conductivity varied between seasons in a characteristic manner, with clear water level changes between the rainy and dry seasons. Changes in the discharge volume from the Chao Phraya Dam greatly suppress intrusion by saline sea water, and has a large influence on the seasonal and longitudinal changes in the water quality. We found that sea water enters all layers of the river, as indicated by the fact that the concentrations of ions originating from sea water were the same at both the surface and the riverbed layer. The concentration of ions originating from manmade sources did not vary between the seasons. Rather, it depended on the environment around the river, as this determined the inflow from nitrogen fertilizer, excrement, atmosphere, and other sources.

Acknowledgments

This research was supported by the Japan Society for the Promotion of Science (JSPS), a Grant-in-Aid of Scientific Research (No. 15H05222), and by the Japan Science and Technology Agency//Japan International Cooperation Agency (JST/JICA) Science and Technology Research Partnership for Sustainable Development (SATREPS) program.

References

[1] WEPA "Outlook on Water Environmental Management in Asia 2015", (2015), pp98-105.
[2] Taichi Tebakari., "Current Status on Water Resources Policy in Thailand", J. Japan Soc. Hydrol. And Water Resour, Vol.30, No.4, (2017), pp 237-240.

[3] Jun Kobayashi., "Chemical study of rivers in Southeast Asian countries on the water quality of Thailand"., Agricultural research, Vol.2, No.46, (1958), pp 63-110.

[4] Isao Minami., "Hydrological and Meteorological Feature: Salinity Problems in Chao Phraya River"., Southeast Asian Studies, Vol.3, (1966), pp 77-82.

[5] Muttamara, S., Sales, C.L. "Water quality management of the Chao Phraya River (a case study)", Environmental Technology, Vol. 15, 6, (1994), pp 501-516.

[6] Yoshiaki T., Thammarat K. and MD Mafizur R., "Water Quality Profiles of the Tidal Rivers and Canal in Peri-urban Areas of Bangkok, Thailand, and Dhaka, Bangladesh, Focusing on the Water Quality Transition in Coastal Areas", Journal of Water Environmental Association, Vol.32, No.1, (2009), pp 47-52.

[7] Wongsa, S., "Impact of Climate Change on Water Resources Management in the Lower Chao Phraya Basin, Thailand", Journal of Geoscience and Environment Protection, 3, (2015), pp 53-58.

[8] Taichi T., Kentaro D., Masashi S. and Pongsthakorn S., "Heavy Rainfall and Drought Potential in the Chao Phraya River Basin, Thailand", J.JSCE,Ser.G (Environmental Research), Vol.71, No.5, (2015), pp I_269-I_276.

[9] Metropotitan Waterworks Authority: http://rwc.mwa.co.th/page/home/ (accessed October 31, 2018).

[10] Kenichi S., ''Nitrogen compounds in the global environment supplied from natural origin and human origin'', AIRIES, Vol.15, No.2, (2010), pp 97-102.

Numerical Experiment of Change in Flooded Area Using Gridded Rainfall Data During 1981-2017 in The Mun and The Chi Rivers Basin, Thailand

Shigehiko ODA[1,a], Shojun ARAI[1], Kazuya URAYAMA[2], Takuya MATSUURA[1], Taichi TEBAKARI[2,b] and Boonlert Archevarahuprok[3]

Abstract

Thailand is concerning that the effects of climate change such as strong drought during the dry season and massive flood during the rainy season and unseasonable weather may increase. Especially, there is a possibility that the occurrence frequency and scale of flood damage will be increasing. Heavy flooding caused serious damage in the eastern region in 2011 and 2017. In the large flood of 2011, extensive flooding occurred in Yasothon, Sisaket and Ubon Ratchathani Provinces, where the Mun and Chi Rivers joined. Furthermore, the river slope was very gentle and the discharge capacity was small, which was considered to have caused extensive flooding. The impact of the flood has been causing serious damage to Thailand's major industries, manufacturing, agriculture and tourism. That is an urgent task to suppress such chronic flood damage.The purpose of this study is to clarify the historical change in flooded area in the Mun and Chi Rivers basin using numerical simulation during 1981-2017. This study used the rainfall gridded data obtained by interpolating the point rainfall data observed by the Thai Meteorological Department (TMD) during 1981-2017 into 0.5 degree grid using the Kriging method. RRI (Rainfall Runoff Inundation) model, which is a rain runoff model capable of integrating analysis of river basin and river flow from rain runoff to flood, was selected for this study. Model parameters had been tuned by the rainfall event in 2011. Using these parameters, the maximum-flooded area of each year for 37 years was calculated and trend analysis was conducted.

Keywords *Numerical simulation, Flood, Thailand*

[1]Graduate School ofEnvironmental Engineering
Toyama Prefectural University
Imizu, Toyama, Japan
[2]Department of Environmental and Civil Engineering Toyama Prefectural University
Imizu, Toyama, Japan
[3]Thai Metrological Department
Bangkok, Thailand

[a]t757003@st.pu-toyama.ac.jp
[b]tebakari@pu-toyama.ac.jp

A Study of the Impacts of Cross-basin Flow Interchange on River Management

Chang-Mien Wang[1], Chih-Tsung Huang[1], Wei-Cheng Lo[1] and Meng-Hsuan Wu[1]

Abstract Taiwan is located in a region of the Pacific Ocean where typhoons frequently form. Its rainfall intensity is thus typically high over very short periods of time. The heavy rainfall from typhoons can cause floods that lead to large economic losses and loss of human life. The spatial and temporal redistribution of surface runoff produces greater levels and fewer peak times in urbanized areas. Because of the risk of flooding associated with this change, there is a need to reassess the design criteria for existing flood control measures in flood-prone areas. Research on general planning has focused on drainage basins, or catchment areas, which are defined as areas of land where precipitation collects and drains off into a common outlet, such as a river, bay, or other body of water. The water surface exchange between a basin and a river affects river management. This study uses a physiographic drainage-inundation model to simulate inundation due to flooding in different return period events and to determine the impact of cross-basin flow interchange on river management.

Keywords *physiographic drainage-inundation (PHD) model, cross-basin, basin management*

[1]Department of Hydraulic and Ocean Engineering,
National Chen Kung University
Tainan, Taiwan

Introduction

Taiwan is located in one of the most active typhoon regions in the western Pacific. Three to four typhoons hit Taiwan in summer and autumn, which are thus characterized by high-intensity rainfall. For example, Typhoon Morakot, which was over Taiwan from August 7 to August 9, 2009, caused a record rainfall of 3,060 mm in three days. Morakot's extreme torrential rains caused flooding and debris flow throughout the country, resulting in 681 deaths and a total economic loss of about NT$ 200 billion. In order to prevent severe damage to downstream alluvial plains and cities, Taiwan has adopted many structural flood control measures, such as the building of dams and flood walls and channel improvement, in recent decades. However, rapid economic growth and population growth have been accompanied by the expansion of residential, commercial, and industrial areas. This anthropogenic change in land use has led to an increase in impervious areas, removal of vegetation cover, surface formation, and many other terrain changes. These man-made changes significantly change the rainfall runoff process. The spatial and temporal redistribution of surface runoff produces greater levels and fewer peak times in urbanized areas. Because of the risk of flooding associated with this change, there is a need to reassess the design criteria for existing flood control measures in flood-prone areas.

Research on general planning has focused on drainage basins. A drainage basin or catchment area is defined as any area of land where precipitation collects and drains off into a common outlet, such as a river, bay, or other body of water. Drainage basins connect to other drainage basins at lower elevations in a hierarchical pattern, with smaller sub-drainage basins in turn draining into a common outlet. A drainage basin acts as a funnel by collecting all the water within the area covered by the basin and channeling it to a single point. Each drainage basin is separated topographically from adjacent basins by a perimeter called a drainage divide, making up a succession of higher geographical features (such as a ridge, hill, or mountain) and forming a barrier.

The water surface exchange between a basin and a river, which impacts river management, is investigated in this study. The Gaoping River and Donggang River basins in southern Taiwan, which are adjacent, are considered here. The study area for the Gaoping River is larger than that for the Donggang

River. The lower reaches of the basin are the largest alluvial plain in Taiwan and form a flourishing agricultural area. The warm climate and fertile soil associated with abundant irrigation sources allows the production of various agricultural products.

A physiographic drainage-inundation (PHD) model was established to assess the flooding conditions in the study area using a design storm to define a precipitation model for hydrological system design. The PHD model was developed to simulate flooding in Taiwan and can be adjusted to fit actual topographical situations; it was thus selected for the simulation in this study. By inputting hydrological and geographic data into the PHD model, the submerged depth of the study area can be obtained. Hydrology analysis, basin and river channel characteristics analysis, and steady flow analysis are used to revise river regulation planning and improve and modify the lines for flood prevention facilities, thereby providing a basis for flood prevention engineering and river management.

Methodology

A PHD model was developed based on the inundation theory presented by Cunge (1975) to determine the flood depth and duration in a given region for a design storm. The study area was firstly discretized into small computational cells based on 5 m × 5 m digital elevation model (DEM) data and land use data. Roads, railroads, and dikes were taken as barriers that hinder water from flowing and were selected as borders of cells during computation. The shape of a computational cell was thus irregular, but such cells were flexible enough to fit the complex topography of the study area. The flow routing among cells across various borders was governed by a continuous equation and a flow flux equation. Assuming that the i -th cell is surrounded by Ni cells, the continuous equation accounting of water balance for the i-th cell is:

$$A_{si}\frac{\partial h_i}{\partial t} = \sum_{k=1}^{N_i} Q_{i,k}(h_i, h_k) + P_{ei}A_{si}, \qquad (1)$$

where t is time; A_{si} is the area of the i-th cell; h_i and h_k are the water level of the i-th and the k-th cell, respectively; N_i is the total number of cells surrounding the i-th cell;$Q_{i,k}$ is the discharge flowing from the k-th cell into the i-th cell, and $P_{ei}$is the effective rainfall of the i-th cell, which is estimated using the SCS method (Chow et al. 1988).

$$P_e = \frac{(P-0.2S)^2}{P+0.8S},\ S = \frac{25400}{CN} - 254, \qquad (2)$$

where P_e is rainfall depth in mm; CN is dimensionless curve number ranging between 0 and 100. The values of CN for various soil types and land uses follow Chow et al. (1988). The flow fluxes $Q_{i,k}$ between the i-th and k-th cells depend both on the water stages of these two cells and the border types. If two cells are separated by hydraulic structures such as embankments or dikes, flow that crosses the border is assumed to be similar to the flow through a broad-crested weir. Thus, the flow rate between cells follows the weir formulas, which are categorized into free overfall and submerged weirs. The flow rate between two cells for a free overfall weir and a submerged weir respectively is determined by

$$Q_{i,k} = \mu_1 b\sqrt{2g}(h_k - Z_w)^{\frac{3}{2}}, \text{ when } h_i - Z_w < \frac{2}{3}(h_k - Z_w) \qquad (3)$$

$$Q_{i,k} = \mu_2 b\sqrt{2g}(h_i - Z_w)(h_k - Z_w)^{\frac{1}{2}}, \text{ when } h_i - Z_w \geq \frac{2}{3}(h_k - Z_w) \qquad (4)$$

where Z_w is the elevation of the weir crest, which represents the elevation of the border between the i-th and k-th cells; b is the effective length of the weir, which represents the length of the border, and in this study, μ_1 and μ_2 are the weir discharge coefficients of the free overfall weir and submerged weir, with values of 0.4 and 1.04, respectively.

If hydraulic structures are not present between the borders of two cells, the flow rates follow the Manning's equation, that is

$$Q_{i,k} = \frac{h_k - h_i}{|h_k - h_i|}\Phi(\bar{h}_{i,k})\sqrt{|h_k - h_i|}, \text{ when} \frac{\partial Q_{i,k}}{\partial h_i} \leq 0 \qquad (5)$$

$$Q_{i,k} = \Phi(h_k)\sqrt{|h_k - h_i|}, \text{ when } \frac{\partial Q_{i,k}}{\partial h_i} > 0, \qquad (6)$$

where $\bar{h}_{i,k}$is the water level at the border of the i-th and k-th cells, and $\Phi(h)$ is defined as

$$\Phi(h) = \frac{A(h)R^{\frac{2}{3}}(h)}{n\sqrt{\Delta x}}, \qquad (7)$$

where$\Delta x$is the distance between the centers of the i-th and k-th cells; A and R are the cross-section area and hydraulic radius of the border between the i-th and k-th cells, and n is the Manning's roughness coefficient, which is determined by land uses.

A finite difference scheme is adopted to solve the above equations and determine the water stage for each cell. A detailed description of the computation scheme can be found in Chen et al. (2007). The water depth at the i-th cell is then determined by

$$d_i = h_i - z_i, \qquad (8)$$

where d_i is the water depth of the i-th cell, an z_i is the land surface elevation of the i-th cell. Inputs to this PHD model include the digital elevation model (DEM) and the GIS topography, landform, and vegetation layers used to discretize the computational cells. Additionally, a recorded or design rainfall hyetograph is required to estimate the effective rainfall in each cell, which initiates the surface runoff processes. In this study, a design hyetograph with a

specific recurrence interval is employed to evaluate flooding vulnerability in the study area.

Numerical Simulation

The Gaoping River and Donggang River basins in southern Taiwan, shown in Fig. 1, are considered in this study. The Gaoping River is a major river in southern Taiwan. It is the largest river in Taiwan based on drainage area. The river is 171 km long, and drains a rugged area on the western side of the Central Mountain Range. With an average annual discharge of 8.45 km3, the Gaoping River is the second largest river in Taiwan by volume. About 90% of the precipitation, and consequently about 70–90 percent of the total flow, occurs during the rainy season, from May to October. The Gaoping River carries large amounts of silt, ranging from 36 to 49 million tons per year; it is the second largest river in Taiwan in terms of suspended sediment load. Almost half of the total basin has an elevation greater than 1,000 metres. Only about 20 percent of the basin is lower than 100 metres in elevation. The Gaoping River valley is generally considered to be the boundary between the Alishan Range on the west and the higher Yushan Range to the east. For its prevention criteria, the planned flood discharge of the Gaoping River is set on the basis of a 100-year return period, where the values are those bulletined in 1984, this time through the result of a hydrology analysis.

The Donggang River is located in Pingtung County. Officially, the river system covers an area of about 767.07 km2, with agriculture being the most common industry. The river flood plains are usually used for agriculture and fisheries. The upper reaches of the Donggang River system are of the mountain river type, with many picturesque waterfalls and giant boulders. The middle and lower reaches used to be part of the Ailiao River, which in ancient times created a network of crisscrossing waterways. During wet periods, the Donggang River system has an annual runoff volume of about 956.98 million m3. For its prevention criteria, the planned flood discharge of the Donggang River is set on the basis of a 50-year return period, where the values are those bulletined in 1984 this time through the results of a hydrology analysis.

The digital elevation data for the study area was adopted from the "High Precision, High-Resolution Digital Topographic Measurement and Production" (Ministry of the Interior, Taiwan, 2013). The DEM map, whose ground resolution is 5 m × 5 m, is shown in Fig. 2. As shown, the elevation in the study area ranges from -12.8 m to 3,950 m. By combining the DEM map with aerial photographs, the boundary of the study area can be further defined by analyzing the elevation.

Every watershed has its own unique topography, landform, land use, and vegetation. In order to verify the accuracy of the cells, a 1/25,000-scale topographical map of Taiwan and an aerial photograph of the study area were referenced. Based on this information, narrow cells were merged and large cells were divided to suit the topography. The study area was divided into 12,336 cells, as shown in Fig. 3. The area of the smallest cells is 306 m2, and that of the largest cells is 5.98 km2. The boundary of this study area is the surface watershed. The west side boundaries are the coast and sea dikes. After constructing the cells, the DEM and slope map were used to generate the cell items, i.e., area, average elevation, average slope, center coordinate, number of neighboring cells, interface elevation, length of the interface from cells, types of interface (flow or weir), and orientation. These data were input into the PHD model to simulate the flood process, inundation depth, and area.

There are 53 rainfall gauge stations in the study area. To control the rainfall within the cells, Thiessen's polygon method was used to distribute the study area. Furthermore, there is one tide station near the study area, namely the Donggang tide station of the Central Weather Bureau, Taiwan. The highest astronomical tide (HAT) is 0.932 m, the mean high water level (MHWL) is 0.616 m, the mean sea level (MSL) is 0.326 m, the mean low water level (MLWL) is 0.015 m, and the lowest astronomical tide (LAT) is 0.367 m.

There are some limits and conditions related to the cells used in the PHD model. All water exchange between cells should follow the formula and function delineated in the PHD model. The embankment in the study area was assumed to be impermeable, and thus the water in the cells was released only through the downstream river channel. The rainfall data input were controlled using Thiessen's polygon method. The downstream boundary conditions were set using tide data from a nearby tide gauge station. The flood potential maps show only the most serious flood situations. Typhoon Soudelor in 2015 and Typhoon Megi in 2016 were selected to verify the validity of the PHD model in the study area.

Typhoon Soudelor hit Taiwan between 8/6/2015 and 8/9/2015; Typhoon Megi hit Taiwan between 9/26/2016 and 9/28/2016. The simulation times were set from 8/8/2015 00:00 to 8/10/2015 24:00 and from 9/27/2016 00:00 to 9/29/2016 24:00, for a total of 72 hours.

Water level can be used to verify this model. In this study, Liugui and Chaozhou were selected to conduct a comparison for Typhoon Soudelor and Typhoon Megi. The results are shown in Figs. 4 and 5. The observed times of the peaks and the shapes of the hydrographs are similar to those in the simulation. The PHD model was therefore able to simulate the flooding process due to a heavy-rainfall-event flood in the study area within a reasonable range.

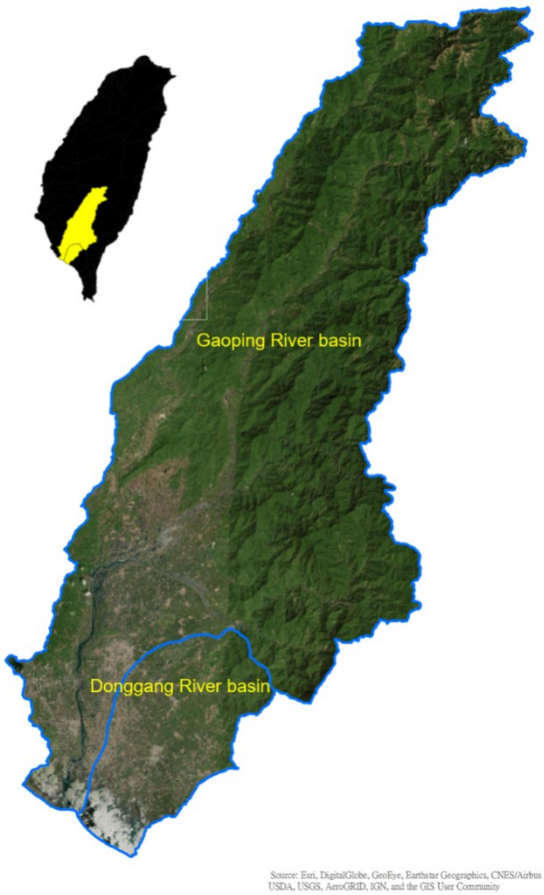

Fig. 1. Location of the study area

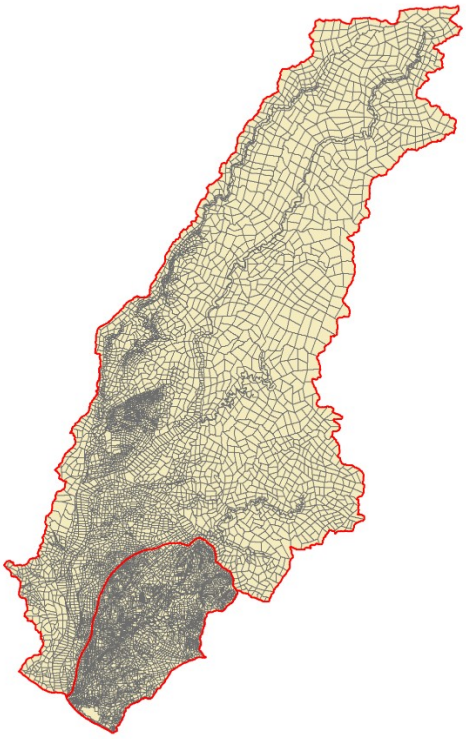

Fig. 3. The cells in the study area

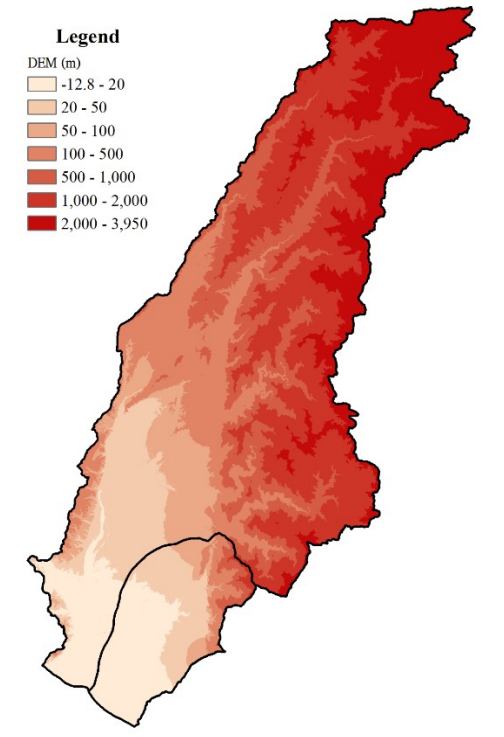

Fig. 2. The digital elevation model in the study area

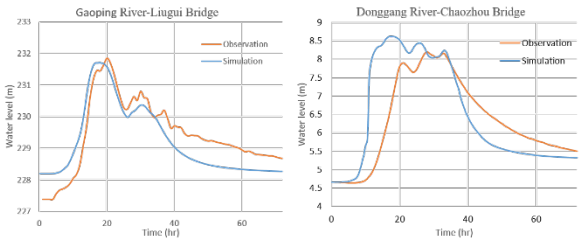

Fig. 4. Observation and simulation water level during Typhoon Soudelor

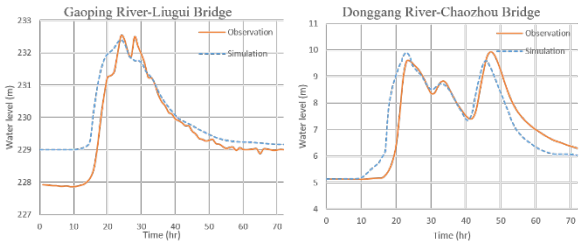

Fig. 5. Observation and simulation water level during Typhoon Megi

Achievement and Results

In order to study the hydrological effect of cross-basin flow on flood depth, 50-, 100-, and 200-year periods were used in the simulation. The hyetograph for the study area, obtained from the Water Resources Agency, Ministry of Economic Affairs, Taiwan, is shown in Table 1. The results of the inundation simulation for various recurrence intervals of rainfall and scenarios are discussed below. The inundation results from the PHD model can be shown on an ArcGIS map.

The 50-, 100-, and 200-year design rainfalls were used in the PHD model for the study area. The simulation results of flooding with and without considering cross-basin flow are obtained shown on ArcGIS maps in Figs. 6, 7, 9, 10, 12, and 13. As shown, the flooded area is concentrated downstream. The impact of cross-basin flow can be seen in Figs. 8, 11, and 14. The difference between the largest 50-, 100-, and 200-year flood depths obtained with and without cross-basin flow are 0.901, 1.049, and 0.956 m, respectively. The results show that flood depths obtained without considering cross-basin flow in some areas are underestimated. But cross-basin flow interchange on flood-prevention facilities is not as expected.

Table I. Design rainfall in the study area

Gaoping River	50-year	100-year	200-year
48-hour total rainfall (mm)	758	826	890
Donggang River	50-year	100-year	200-year
48-hour total rainfall (mm)	786	875	964

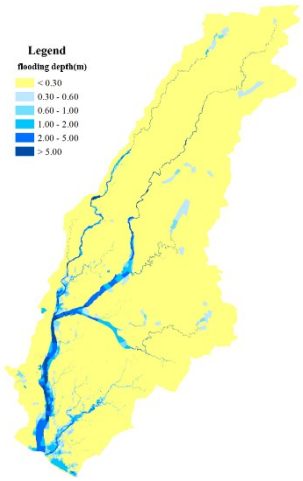

Fig. 6. Flood of 50-year return period in considering cross-basin

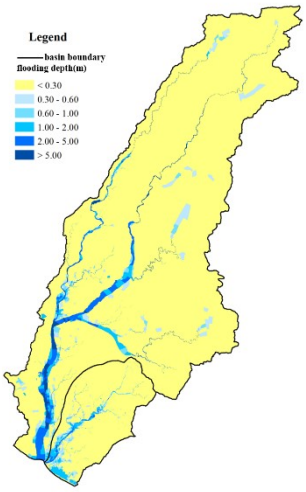

Fig. 7. Flood of 50-year return period without considering cross-basin

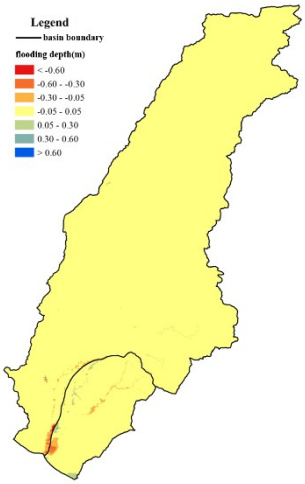

Fig. 8. Flood difference of 50-year return period in or without considering cross-basin

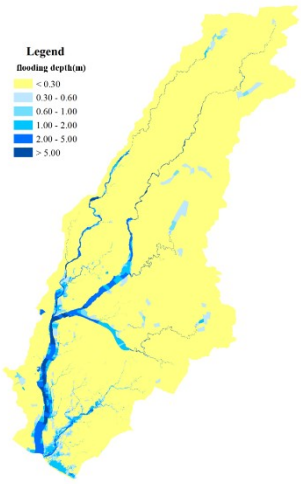

Fig. 9. Flood of 100-year return period in considering cross-basin

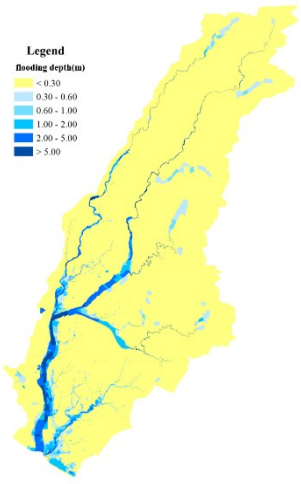

Fig. 12. Flood of 200-year return period in considering cross-basin

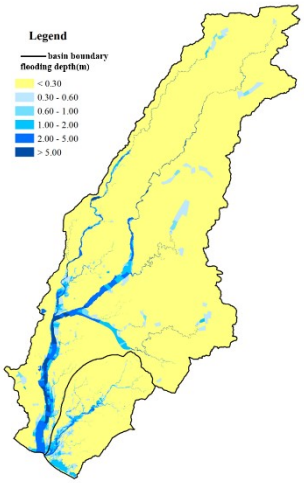

Fig. 10. Flood of 100-year return period without considering cross-basin

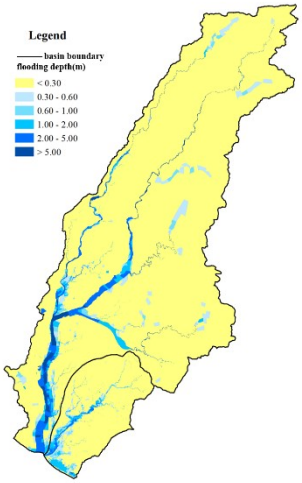

Fig. 13. Flood of 200-year return period without considering cross-basin

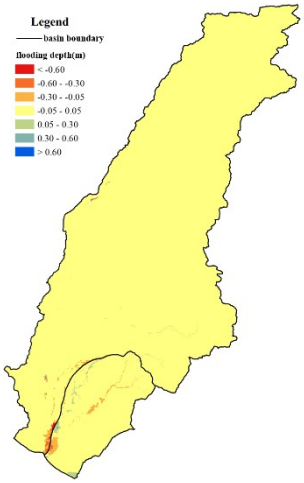

Fig. 11 Flood difference of 100-year return period in or without considering cross-basin

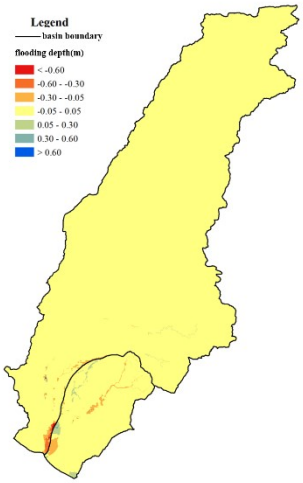

Fig. 14. Flood difference of 200-year return period in or without considering cross-basin

References

[1] Chao, Y. C., Li, H. C., Liou, J. J., & Chen, Y. M. (2016). Extreme bed changes in the Gaoping River under climate change. Terrestrial, Atmospheric and Oceanic Sciences, 27(5), 717-727.

[2] Chen, C. N., Tsai, C. H., & Tsai, C. T. (2006). Simulation of sediment yield from watershed by physiographic soil erosion–deposition model. *Journal of hydrology*, *327*(3), 293-303.

[3] Chen, C. N., Tsai, C. H., & Tsai, C. T. (2007). Reduction of discharge hydrograph and flood stage resulted from upstream detention ponds. *Hydrological processes*, *21*(25), 3492-3506.

[4] Harrington, L., Cook, S. E., Lemoalle, J., Kirby, M., Taylor, C., & Woolley, J. (2009). Cross-basin comparisons of water use, water scarcity and their impact on livelihoods: present and future. Water International, 34(1), 144-154.

[5] Hayashi, M., & Rosenberry, D. O. (2002). Effects of ground water exchange on the hydrology and ecology of surface water. Groundwater, 40(3), 309-316.

[6] Inoue, K., Iwasa, Y., & Matsuo, N. (1987, March). Numerical analysis of two-dimensional free surface flow by means of finite difference method and its application to practical problems. In *Proceedings of ROC-Japan Joint Seminar on Water Resources Engineering, Taipei*.

[7] IWasa, Y., & InOue, K. (1982). Mathematical simulations of channel and overland flood flows in view of flood disaster engineering. *Natural disaster science*, *4*(1), 1-30.

[8] Kitheka, J. U., Obiero, M., & Nthenge, P. (2005). River discharge, sediment transport and exchange in the Tana Estuary, Kenya. Estuarine, Coastal and Shelf Science, 63(3), 455-468.

[9] Li, M. H., Hsu, M. H., Hsieh, L. S., & Teng, W. H. (2002). Inundation potentials analysis for Tsao-Ling landslide lake formed by Chi-Chi earthquake in Taiwan. *Natural Hazards*, *25*(3), 289-303.

[10] McDonald, R. I., Weber, K., Padowski, J., Flörke, M., Schneider, C., Green, P. A., ... & Boucher, T. (2014). Water on an urban planet: Urbanization and the reach of urban water infrastructure. Global Environmental Change, 27, 96-105.

[11] Nickolas, L. B., Segura, C., & Brooks, J. R. (2017). The influence of lithology on surface water sources. Hydrological Processes, 31(10), 1913-1925.

[12] O'brien, J. S., Julien, P. Y., & Fullerton, W. T. (1993). Two-dimensional water flood and mudflow simulation. *Journal of hydraulic engineering*, *119*(2), 244-261.

[13] Teng, W. H., Hsu, M. H., Wu, C. H., & Chen, A. S. (2006). Impact of flood disasters on Taiwan in the last quarter century. Natural Hazards, 37(1), 191-207.

[14] Todini, E., & Venutelli, M. (1991). Overland flow: a two-dimensional modeling approach. In *Recent Advances in the Modeling of Hydrologic Systems* (pp. 153-166). Springer Netherlands.

[15] Woessner, W. W. (2000). Stream and fluvial plain ground water interactions: rescaling hydrogeologic thought. Groundwater, 38(3), 423-429.

Flooding in Oda river basin during torrential rainfall event in July 2018

Shakti P.C.[1,a] and Hideyuki Kamimera[1,b]

Abstract

Extreme rainfall events cause severe flooding and/or landslides almost every summer in Japan. It seems that the frequency of such events and induced human/economic losses has increased in recent years. A torrential rainfall event in early July 2018 caused severe flooding in many river basins over Hiroshima and Okayama Prefectures of western Japan and resulted a number of fatalities and serious damage to property. One of them is the Oda river basin (about 498 km2), which was severely affected by the flood during the event. Different types of observation systems were used to measure or estimate rainfall for this event. Comparison of radar and satellite-based rainfall shows a good agreement with the rain gauge observations of the entire period. Basin-mean total rainfall from Japan Meteorological Agency's analyzed radar rainfall (RADJ), Water and Disaster Management Bureau's radar rainfall (RADW), Automated Meteorological Data Acquisition System (AMeDAS), and satellite-based rainfall data (GSMaP) were about 314, 322, 357 and 304 mm, respectively during July 5–7 2018.

In this study, we applied Rainfall–Runoff–Inundation (RRI) to acquire a detailed understanding of flood processes in the Oda river basin. All the available rainfall data including different spatial resolution of hydrographic features were considered as the main input data in the model separately. In the preliminary simulation, gridded flow and map of the possible maximum flood depth across the basins were generated and validated. Simulated discharge based on high resolution topographic data at the Yakage gauging station of the basin are more closely aligned with observed data. It is also found that the maximum flood inundation areas estimated by the RRI model using radar rainfall data appeared somewhat closer with the extent of flood-affected areas from the model with data of the Japanese Geospatial Information Authority (GSI) over the Mabi city. It is believed that modelled results of the basin can be used an important reference in the disaster mitigation and that they may be useful for further studies.

Keywords *floods, torrential rainfall, RRI model, discharge, inundation*

[1]Storm, Flood and Landslide Research Division
National Research Institute for Earth Science and Disaster Resilience (NIED),
Tsukuba, Japan

[a]shakti@bosai.go.jp
[b]kamimera@bosai.go.jp

Assessment of Satellite-based Rainfall Estimates over Japan

Hideyuki Kamimera[1,a]

Abstract

This study investigated the performance of the Global Satellite Mapping of Precipitation (GSMaP) products of satellite-based rainfall estimates (SRE) over Central and Eastern Japan for the period from 7 to 11 in September 2015. Before detailed investigations of the GSMaP performance, five products of radar-based rainfall estimates (RRE) and three GSMaP SRE products were compared with rain gauge data at 4,713 stations on hourly, daily and five-day bases. All the five RRE products basically agreed with the rain gauge data at every time scale. In particular, the R2 product (based on C-band radars of the Water and Disaster Management Bureau) had best performance in the five RRE products. The three GSMaP SRE products did not show high performance. To search causes of the low performance of the GSMaP SRE products revealed, only over land, instantaneous rainfall rate values of passive microwave radiometers (PMWRs) extracted from the GSMaP near real-time (NRT) product were compared strictly with their corresponding instantaneous values from the R2 product aggregated spatially in each GSMaP grid box. The PMWRs tended to underestimate rainfall rate more, when mean or standard deviation of the R2 rainfall rate was larger in a GSMaP grid box. However the PMWRs provided more accurate rainfall rate, when geographical pattern (the shape of probability density function, PDF) of the R2 rainfall rate was more homogeneous (pointed) in a GSMaP grid box. Thus, subgrid-scale geographical pattern (PDF) of rainfall rate may be a key index to correct rainfall rate values from the PMWRs. Making scatterplots individually for rainfall rate values from each PMWR and the R2 product, it can be recognized that larger variances existed in the scatterplots for sounders than the scatterplots for imagers and imaging/sounding sensors. Thus, the type of PMWR should be clearly considered in further assessments of the GSMaP SRE products.

Keywords *rainfall, satellite, GSMaP*

[1]Storm, Flood and Landslide Research Division
National Research Institute for Earth Science and Disaster Resilience (NIED)
Tsukuba, Japan

[a]kamimera@bosai.go.jp

Cross Validation of Spatial Interpolated Rain Gage and Satellite-Based Rainfall over Chao Phraya River Basin Thailand

Nelson Stephen L. Ventura[1,a] and Piyatida Ruangrassamee[1,b,*]

Abstract The availability of satellite-based precipitation products has greatly improved as more organizations and institutions produce these data. However, these datasets contain some bias because it is not a direct measurement of rainfall. Before satellite precipitation data can be bias corrected using rain gage data, the local rain gage data should be able to accurately represent its spatial distribution. Using spatial interpolation techniques on these point data would estimate the values where there gaps are found. The study analyzes the results of different spatial interpolation methods namely Inverse Distance Weighting (IDW), Kriging with a Spherical Semivariogram, Kriging with an Exponential Semivariogram, and Kriging with a Gaussian Semivariogram over Chao Phraya River Basin in Thailand with daily rain gage data from 2000 to 2010 from Thai Meteorological Department (TMD) and Royal Irrigation Department (RID). Subsequently, the correlation coefficient (CORR) of each interpolated dataset to the satellite precipitation estimate of Precipitation Estimation from Remotely Sensed Information using Artificial Neural Network - Cloud Classification System (PERSIANN-CCS) in 2010 would be determined. The cross-validation results show that Kriging generally has a lower root-mean-square-error (RSME) than IDW interpolation. As for the case in Thailand, Kriging with Spherical Semivariogram has the lowest RSME and CORR with respect to the daily rain gage data. The interpolation method with the highest correlation coefficient when compared to the PERSIANN-CCS dataset varied with each month. Overall, the Kriging with Spherical Semivariogram provides a better representative to the rain gage data due to its stochastic characteristic which allows probability and uncertainty in the computation. Applying this technique in adjusting satellite data could improve the correction results.

Keywords *precipitation data estimation, spatial interpolation, kriging, satellite-based precipitation*

[1]Department of Water Resources Engineering,
Faculty of Engineering
Chulalongkorn University
Bangkok, Thailand

[a]nelsonstephenventura@gmail.com,
[b]Piyatida.H@chula.ac.th

Introduction

In recent years, the availability of satellite-based precipitation products has greatly improved as more organizations and institutions produce these data. However, these datasets contain some bias when compared to the actual precipitation occurring on the surface of the earth. Therefore, the discrepancies must be corrected using ground-based recordings to improve the accuracy of satellite rainfall [1]. Some literatures used spatially interpolated precipitation estimates from rain gages for the correction of satellite rainfall products [2][3].

Spatial interpolation may show rainfall patterns that could be correlated with the satellite precipitation data. Moreover, the results of these interpolations can be used in various ways. Examples of these are for hydrologic modeling [4][5], estimation of average daily precipitation [6], rainfall network design [7], and others.

However, one interpolation methods may not best represent the rainfall over a certain vicinity in all cases. There are different approaches to conducting spatial interpolation. Deterministic approaches such as Inverse Distance Weighting (IDW) interpolation are simple and do not require elaborate computations but it may not be a good representative if there are only limited number of points. As such, this method has been utilized for its simplicity [8][9][10]. On the contrary, applying geostatistical methods such as Kriging objectively predicts values using parameters relating to the spatial characteristics of the data but the computations are more complex and may require more resources than its counterpart [11][12]. In addition, incorporating more factors complex in the procedures, such as using the elevation, can be used in estimation of the precipitation through stochastic spatial interpolation [13][14][15][16]. Cross validation of the interpolation methods is one of the numerous ways to determine the accuracy of a certain approach.

The aim of this study is to identify the most adequate spatial interpolation method for the Chao Phraya river basin and determine the correlation of the satellite-based precipitation to the interpolation output. Similar comparisons in determining which interpolation approach have been conducted by numerous studies [17][18][19]. The purpose of determining the correlation of the output interpolation data with the satellite date is to identify how significant the bias for correction.

Study Area and Data

In this study, the rain gage datasets from the Thai Meteorological Department (TMD) and Royal Irrigation Department (RID) in Thailand are tested for consistency and used for the cross validation of the spatial interpolation methods and for comparison with the satellite precipitation data.

A. Study Area

The selected area in this study is the Chao Phraya river basin in Central Thailand as shown in Fig. 1. The country has 25 defined river basins with Chao Phraya being the 9th largest, having an area of 20526.37 km^2. Majority of the country's main productivity are situated in this river basin, which include the agriculture, industry, and service sectors. Moreover, the main water body in the Chao Phraya river basin is the Chao Phraya River, which flows through Bangkok, the capital of Thailand.

B. Rainfall Data

The rain gage datasets used in this study were from TMD and RID. The daily rain gage data used in this study is a collection of multiple rain gage data from 2000 to 2010. The first dataset has 381 stations in Chao Phraya river basin. The second dataset has 12 stations within the study area but only 6 stations have rainfall records.

The satellite-based rainfall dataset were from the Precipitation Estimation from Remotely Sensed Information using Artificial Neural Networks - Cloud Classification System (PERSIANN-CCS) developed by the Center of Hydrometeorology and Remote Sensing (CHRS) of University of California, Irvine [1]. The satellite product has a resolution of 0.04 degree by 0.04 degree (approximately 4km by 4km). The satellite data used for the study were all days of the year 2010.

Methodology

The study evaluated the spatial interpolation methods through cross validation. The areal rainfall outputs of each method were then correlated with the satellite precipitation products of PERSIANN-CCS. The interpolation methods were chosen based on the common approaches used in the literatures.

A. Spatial Interpolation

Spatial interpolation can be categorized into two approaches: deterministic and stochastic. These different methods have been mainly used in the estimation of the precipitation [20]. For the deterministic method, the Inverse Distance Weighting (IDW) method would be used. On the other hand, Kriging would be used for the stochastic approach.

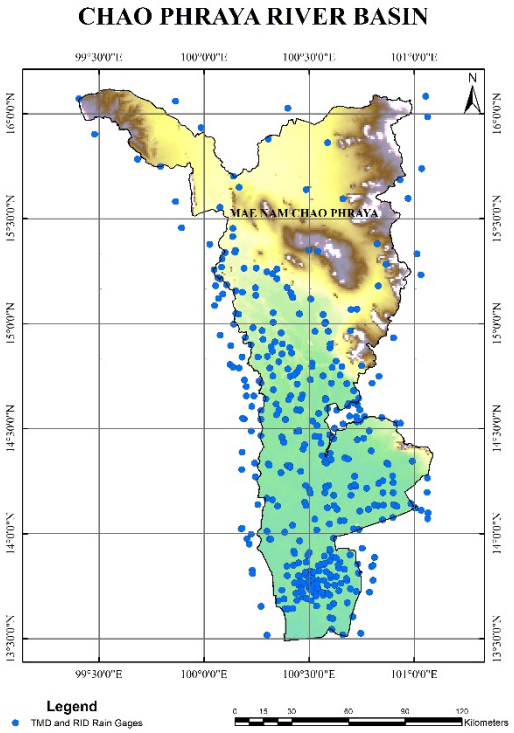

Fig. 1. Chao Phraya River Basin and the Rain Gage Stations within

1) Inverse Distance Weighing (IDW)

In this approach, values at specific location is computed through weighted average. The weights used in the computation is the inverse of the distance of the target point to each known point. As shown in (1), the prediction value is

$$z^*(u)=\frac{\sum_{i=1}^{n}\frac{z(u_i)}{d(u_i)^k}}{\sum_{i=1}^{n}\frac{1}{d(u_i)^k}} \quad (1)$$

where $z^*(u)$ is the predicted value at the location, u, $z(u_i)$ are the actual values at each known location, u, $d(u_i)$ is the distance of the each known location, u, from the predicated value location, and k is the exponent of the distance. The exponent for the method carry the significance of the known values to the predicted value.

In this study, two IDW interpolations were computed. The difference between the two computations were the value of the exponent, where the first calculation used an exponent value, k, equal to 1, while the second calculation used squared weights where the exponent value of 2.

2) Kriging

This method is similar to IDW to which the weights are defined by the distance of the target point to the known points. However, each weight is determined by a function called a semivariogram.

A semivariogram is the representation of the spatial correlation of every point in a given dataset to

each other. With (2), the semivariogram value binned at a specific distance is the mean of the variance of pairs of each data point to every other points,

$$\gamma(h) = \frac{1}{2n(h)} \sum_{i=1}^{n(h)} [z(u_i) \quad (2)$$

where γ(h) is the variogram at the lag distance, h, n(h) is the number of data pairs falling in the same lag distance, h, and z(u) is the value at location, u. The semivariogram values would be plotted against the distance. This empirical semivariogram plot would then be fitted in a theoretical semivariogram model in order to have a continuous function to be used for the Kriging weights.

In this study, data values within the same month were binned together in one semivariogram to give consideration to the temporal dimension of the datasets.

Different semivariogram models have been used for Kriging. In this study, the models used were the following:

- Spherical Semivariogram Model

$$\gamma(h) = \begin{cases} c\left(\frac{3h}{2a} - \frac{1h^3}{2a^2}\right), & h \le a \\ c, & h > a \end{cases} \quad (3)$$

- Exponential Semivariogram Model

$$\gamma(h) = \left\{ c\left[1 - e^{-\left(\frac{h}{a}\right)}\right], \; h > 0 \right. \quad (4)$$

- Gaussian Semivariogram Model

$$\gamma(h) = \left\{ c\left[1 - e^{-\left(\frac{h}{a}\right)^2}\right], \; h > 0 \right. \quad (5)$$

where c is the sill and a is the range. In some studies, parameters and characteristics of different semivariograms have been assessed in order to find the best model to be used in Kriging precipitation interpolation [21][22].

Once the theoretical semivariogram has been prepared, the prediction value can be computed by (6),

$$z^*(u) = \sum_{i=1}^{n} \lambda_i \cdot z(u_i) \quad (6)$$

where λ_i is the Kriging weight for each known value determined from the semivariogram model.

Due to the computational constraints that would arise from large matrices, the study only considered the five nearest points in computing the prediction value.

B. Cross Validation

This study used the leave-one-out cross validation method in the evaluation of the spatial interpolation methods. This cross validation approach removes one point from the dataset and computes the value at the removed point with all the remaining data in the set. This value would then be compared to the actual value. The process continues until every data entry has a corresponding computed value.

The statistical analysis used in the cross validation of the spatial interpolation methods were Mean Absolute Error (MAE) as in (7), Root-Mean-Square Error (RMSE) as in (8), and Correlation Coefficient (CORR) as in (9)

$$MAE = \frac{1}{n} \sum_{i=1}^{n} \left| z(u_i) - z^*(u_i) \right| \quad (7)$$

$$RMSE = \sqrt{\frac{1}{n} \sum_{i=1}^{n} [z(u_i) - z^*(u_i)]^2} \quad (8)$$

$$CORR = \frac{\sum_{i=1}^{n} \left[z^*(u_i) - \bar{z}^*\right][z(u_i) - \bar{z}]}{\sqrt{\sum_{i=1}^{n} \left[z^*(u_i) - \bar{z}^*\right]^2} \times \sqrt{\sum_{i=1}^{n} [z(u_i) - \bar{z}]^2}} \quad (9)$$

where $\bar{z}^*$ is mean of the predicted values and $\bar{z}$ is the mean of the actual values. Because there would be large numbers of zero values in the dataset, only days with occurrence of rainfall for both observed and predicted would be considered.

C. Satellite Data Analysis

It is crucial to determine how well the interpolation outputs would be related to the satellite-based precipitation data. Similar to the cross validation, MAE, RSME, and CORR would be computed for each month where the interpolated values would be considered as the known data while the satellite data would be the predicted data.

Results and Discussion

A. Monthly Semivariogram Parameters

The monthly theoretical semivariogram sill and range resulted from the binning of data pairs at the temporal dimension. From January to December, each day of every month was collected into one empirical semivariogram where the theoretical semivariogram parameters was fitted into the model functions. The results of this process for each theoretical semivariogram model is shown in Table 1.

Compared to the usual way of computing the theoretical semivariogram parameters, combining the data pairs of each day into each month produced faster computation. Since the typical manner of Kriging interpolation considers only the currently observed data pairs, theoretical semivariogram parameters would be computed for each day. This would use more resources than simply using one semivariogram model for the whole month

Table I. Monthly Semivariogram Parameters

MON	2000 - 2009					
	SPHERICAL		EXPONENTIAL		GAUSSIAN	
	RANGE	SILL	RANGE	SILL	RANGE	SILL
JAN	0.02033	2.56	0.00662	2.56	0.00877	2.56
FEB	0.12217	8.10	0.04941	8.12	0.04867	8.09
MAR	0.20371	20.46	0.10798	20.72	0.06924	20.35
APR	0.08366	38.18	0.05352	38.47	0.02984	38.10
MAY	0.14748	59.27	0.12965	60.72	0.05586	59.11
JUN	0.32412	61.89	0.95885	84.74	0.10901	61.32
JUL	0.17929	47.79	0.09810	48.36	0.06445	47.60
AUG	0.26584	54.26	0.14834	55.29	0.09059	53.87
SEP	0.22198	108.11	0.32225	117.20	0.06145	107.12
OCT	0.05289	62.95	0.77177	81.79	0.01868	62.88
NOV	0.02484	12.77	0.01074	12.78	0.00921	12.77
DEC	0.00658	2.54	0.00138	2.54	0.00313	2.54

B. Cross Validation for 2000 to 2009 Dataset

The dataset from the year 2000 to 2009 was cross validated using the interpolation methods considered in this study. Each month was evaluated using the statistical parameters MAE, RMSE, and CORR as shown in Table 2. It can be observed that Kriging with daily Spherical semivariogram model has the highest correlation to the actual rainfall data and the lowest errors out of all the interpolation method. This is followed by Kriging with monthly Spherical and Exponential semivariogram which did not vary too much in comparison to the previous method. Subsequently, both IDW interpolation methods resulted in correlation coefficient and errors lower than the stated Kriging method but were not the worst interpolation for the dataset. The approach with the lowest correlation coefficient and error values is monthly Kriging with Gaussian semivariogram which reach very low CORR values especially in months with higher occurrence of rainfall.

In terms of complexity of computation, IDW interpolation methods were the simplest and the fastest. Kriging using the monthly semivariogram was more complicated than IDW but since there were already defined semivariogram parameters, the computation did not take a significant number of resources to accomplish. On the other hand, Kriging using the daily semivariogram took twice as long as using the monthly semivariogram since the parameters would be computed for each day.

C. Cross Validation for 2010 Dataset

In addition to the 10 year data of 2000 to 2009, the data from year 2010 were also interpolated and cross validated. These two datasets share the same stations. However, in this computation, three different semivariogram parameters were used. These parameters were from the daily semivariogram of dataset 2010, the monthly semivariogram of dataset 2010, and the monthly semivariogram of dataset 2000 to 2009.

Similar to the previous case, all cases of Kriging with Spherical semivariogram overall provided the higher correlation coefficient and relatively lower error values than other Kriging methods. Comparing the results of using these three different semivariogram, the outcome did not vary much. Although the CORR and RMSE values were less favorable during months with less rainfall, Kriging using monthly Spherical semivariogram of 2000 to 2009 had better results than the other interpolation approaches. In this regard, using the semivariogram parameter of a dataset with the same stations as the one being evaluated may be used for the interpolation approach. Fig. 2a to Fig. 2e visually represent the result of the interpolation.

Table II. Cross Validation Results for Dataset 2000 to 2009

MONTH	IDW			IDW (2nd Power)			Daily Semivariogram from 2000 - 2009									Monthly Semivariogram from 2000 - 2009								
							Kriging (Spherical)			Kriging (Exponential)			Kriging (Gaussian)			Kriging (Spherical)			Kriging (Exponential)			Kriging (Gaussian)		
	MAE	RMSE	CORR	MAE	RMSE	CORR	MAE	RMSE	CORR	MAE	RMSE	CORR	MAE	RMSE	CORR	MAE	RMSE	CORR	MAE	RMSE	CORR	MAE	RMSE	CORR
JAN	9.2	16.9	0.41	8.6	15.9	0.47	8.5	13.3	0.59	12.1	18.2	0.35	12.6	19.0	0.33	8.7	13.7	0.56	8.6	13.6	0.56	8.7	13.7	0.56
FEB	10.4	17.9	0.57	10.0	16.7	0.61	10.2	16.0	0.66	13.9	22.2	0.43	13.5	21.4	0.44	10.2	16.1	0.66	10.3	16.3	0.65	12.7	23.3	0.49
MAR	10.4	17.6	0.42	9.9	16.5	0.49	10.2	16.5	0.51	13.6	20.7	0.36	13.7	20.6	0.36	10.3	16.5	0.51	10.2	16.5	0.51	20.1	72.3	0.19
APR	12.3	20.0	0.49	11.7	19.0	0.53	12.3	19.5	0.53	17.1	25.7	0.32	16.9	25.5	0.33	12.4	19.6	0.53	12.3	19.4	0.53	16.2	42.3	0.26
MAY	9.4	15.3	0.46	8.9	14.6	0.51	9.4	15.0	0.51	13.0	20.0	0.31	12.9	19.7	0.32	9.4	15.0	0.51	9.4	15.0	0.51	18.1	103.0	0.09
JUN	8.9	14.9	0.45	8.5	14.3	0.51	8.9	14.6	0.51	12.0	19.2	0.31	12.1	19.4	0.31	9.0	15.0	0.49	9.0	14.9	0.50	28.0	214.7	0.06
JUL	8.3	14.6	0.47	7.8	13.8	0.53	8.2	13.8	0.54	11.1	17.5	0.36	11.1	17.7	0.36	8.3	13.8	0.54	8.2	13.7	0.55	13.1	41.9	0.20
AUG	8.9	14.8	0.50	8.4	14.1	0.54	8.9	14.6	0.54	12.4	19.3	0.35	12.4	19.3	0.35	9.0	14.7	0.53	8.9	14.5	0.54	17.5	66.2	0.16
SEP	10.9	18.9	0.53	10.4	18.2	0.57	10.9	18.2	0.58	15.0	25.2	0.38	15.0	25.4	0.38	11.0	19.0	0.56	11.0	19.0	0.56	25.8	150.6	0.11
OCT	10.3	16.9	0.46	9.7	16.0	0.52	10.2	16.4	0.53	14.1	21.6	0.35	14.1	21.6	0.35	10.2	16.3	0.53	10.4	16.8	0.52	34.6	232.8	0.07
NOV	10.5	17.0	0.51	9.9	16.1	0.55	10.2	16.2	0.55	14.3	21.7	0.38	14.4	21.9	0.38	10.2	16.1	0.56	10.1	16.0	0.56	10.2	16.5	0.54
DEC	9.1	15.7	0.38	8.7	14.7	0.43	8.2	13.8	0.50	10.7	16.4	0.35	11.0	17.1	0.32	8.5	14.2	0.47	8.5	14.2	0.47	8.5	14.2	0.47

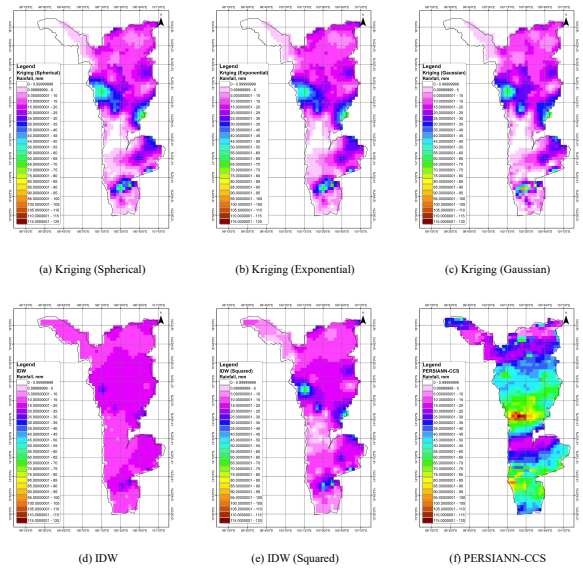

Fig. 2. Interpolation Results for day of August 10, 2010; (a) Kriging with Spherical Semivariogram, (b) Kriging with Exponential Semivariogram, (c) Kriging with Gaussian Semivariogram, (d) IDW Interpolation, (e) IDW (Squared) Interpolation, and (f) PERSIANN-CCS data.

Table III. Correlation of Satellite Data to Each Interpolation Method Output

MONTH	IDW	IDW (2nd Power)	Monthly Semivariogram from 2000 - 2009		
			Kriging (Spherical)	Kriging (Exponential)	Kriging (Gaussian)
	CORR	CORR	CORR	CORR	CORR
JAN	0.11	-0.10	-0.03	0.11	-0.11
FEB	0.21	0.05	0.30	-0.04	0.12
MAR	0.44	0.45	0.32	0.43	0.44
APR	0.21	0.15	0.05	0.26	0.23
MAY	0.20	0.34	0.15	0.27	0.16
JUN	0.18	0.16	0.10	0.13	0.08
JUL	0.22	0.19	0.06	0.10	0.06
AUG	0.25	0.16	0.15	0.04	0.01
SEP	0.30	0.36	0.24	0.06	0.21
OCT	0.20	0.12	0.05	0.08	0.04
NOV	0.60	-0.03	-0.35	-0.19	0.15
DEC	0.37	0.32	0.16	0.11	-0.06

D. Comparison of PERSIANN-CCS Data with Interpolated Data

As shown in Table 3, the interpolation data with the highest correlation to the satellite data of PERSIANN-CCS differed with each month. However, the IDW interpolation had the most consistent correlation coefficient and did not have any negative values. It might depend on each month whether an interpolation method would be suitable for correcting the satellite data. Moreover, since PERSIANN-CCS utilizes a cloud classification system for its estimation of precipitation, there might be some discrepancies with the interpolated data as the methods used in this study did not consider factors such as wind direction and ground elevation which affects the actual precipitation on the surface of the earth. As such, this result has shown the need for the correction of the PERSIANN-CCS data in order to fully utilize its potential in hydraulic and hydrologic analyses.

Conclusions and Recommendations

Overall, Kriging with Spherical semivariogram showed the best performance among the interpolation methods for this study. The approach resulted with the highest correlation coefficient and lowest error values. The IDW interpolation methods provided better and more consistent results than the other two Kriging methods.

Among the three semivariogram models, the Spherical model gave the best results. On the other hand, the Gaussian model showed the worst results with correlation coefficients reaching almost zero values.

Moreover, the results showed that using the monthly semivariogram could improve the interpolation in some ways. Comparing the computational resources, the Kriging monthly computation took less than half the time it would for the daily semivariograms. The results also showed that the monthly semivariogram can only be used for datasets sharing the same stations.

As for the comparison of the PERSIANN-CCS data with the interpolation output, the correlation is quite low. The correlations during dry season (Nov – Mar) are generally higher than wet season. The highest correlation of 0.60 is in November with the IDW interpolation. The IDW interpolation had the most consistent correlation coefficient. The results demonstrate the needs of bias correction of the satellite data before applying them and also the improvement in developing the near-real-time satellite rainfall.

Further study of the concept of spatial interpolation would improve the areal representation of precipitation. Furthermore, accounting the temporal characteristic of rainfall in the interpolation would be recommended. As such, these improvements may also lead to more accurate bias correction of satellite precipitation products.

Acknowledgment

The authors would like to express their gratitude to the Thai Meteorological Department (TMD) and Royal Irrigation Department (RID) for generously sharing their data to the researchers of this study. Moreover, N.S.V extends his gratefulness to ASEAN University Network / Southeast Asia Engineering Education Development Network (AUN/SEED-Net) for supporting his study in the university through the organization's Graduate Degree Program Scholarship.

References

[1] Z. Yang, K. Hsu, S. Sorooshian, X. Xu, D. Braithwaite, & K. M. J. Verbist (2016), Bias adjustment of satellite based precipitation estimation using gauge observations: A case study in Chile, Journal of Geophysical Research: Atmospheres, vol. 121, 3790–3806

[2] D. Caracciolo, A. Francipanec, F. Viola, L.V. Noto, & R. Deidda, "Performances of GPM satellite precipitation over the two major Mediterranean islands"Atmospheric Research, vol. 213, 2018, pp 309-322

[3] PengxinDeng, et al.,"Error analysis and correction of the daily GSMaP products over Hanjiang River Basin of China", Atmospheric Research, vol. 214, 2018, pp 121-134

[4] M. Mendez, & L. Calvo-Valverde, "Assessing the performance of several rainfall interpolation methods as evaluated by a conceptual hydrological model", Procedia Engineering, vol. 154, 2016, pp 1050-1057

[5] S. Louvet, J. E. Paturel, G. Mahé, N. Rouché, & M. Koité, "Comparison of the spatiotemporal variability of rainfall from four different interpolation methods and impact on the result of GR2M hydrological modeling—case of Bani River in Mali, West Africa", Theoretical and Applied Climatology, vol. 123, 2016, pp 303-319

[6] S. Kohnová, K. Hlavcova, J. Szolgay, & J. Parajka, "On the choice of spatial interpolation method for the estimation of 1-to 5- day basin average design precipitation", Flood Risk Management: Hazards, Vulnerability and Mitigation Measures, 2006, pp 77-89

[7] D. A. Mooley & P.M.M. Ismail, "Correlation functions of rainfall field and their application in network design in the tropics", Pure and Applied Geophysics, vol. 120, 1982, pp. 249-260

[8] G. Bastos, L.T.P. Correia, J.F. Oliveira Jr., & M. Zeri, "Evaluation of methods of spatial interpolation for monthly rainfall data over the state of Rio de Janeiro, Brazil", Theoretical and Applied Climatology, vol. 134, 2018, 955-965

[9] F.W. Chen & C.W. Liu, "Estimation of the spatial rainfall distribution using inverse distance weighting (IDW) in the middle of Taiwan", Paddy and Water Environment, vol. 10, 2012, pp 209-222

[10] K.N. Dirks, J.E. Hay, C.D. Stow, & D. Harris, "High-resolution studies of rainfall on Norfolk Island: Part II: Interpolation of rainfall data", Journal of Hydrology, vol. 208, 1998, pp 187-193

[11] D. Béal, G. Guillot, D. Courault, & C. Bruchou, "Interpolation of rainfall at small scale in a Mediterranean region", geoENV IV — Geostatistics for Environmental Applications, 2004, pp 379-389

[12] M. Li, Q. Shao, & L. Renzullo, "Estimation and spatial interpolation of rainfall intensity distribution from the effective rate of precipitation", Stochastic Environmental Research and Risk Assessment, vol. 24, 2010, pp 117-130

[13] M. Kumari, C.K. Singh, O. Bakimchandra, & A. Basistha, "DEM-based delineation for improving geostatistical interpolation of rainfall in mountainous region of Central Himalayas, India", Theoretical and Applied Climatology, vol. 130, 2017, pp 51-58

[14] C.C.F. Plouffe, C. Robertson, & L. Chandrapala, "Comparing interpolation techniques for monthly rainfall mapping using multiple evaluation criteria and auxiliary data sources: A case study of Sri Lanka" Environmental Modelling & Software, vol. 67, 2015, pp 57-71

[15] M. Kumari, C.K. Singh, & A. Basistha, "Clustering data and incorporating topographical variables for improving spatial interpolation of rainfall in mountainous region", Water Resources Management, vol. 31, 2017, pp 425-442

[16] M. Gentilucci, C. Bisci, P. Burt, M. Fazzini, & C. Vaccaro, "Interpolation of rainfall through polynomial regression in the marche region (Central Italy)", The Annual International Conference on Geographic Information Science, 2018, pp 53-73

[17] C. Berndt, & U. Haberlandt, "Spatial interpolation of climate variables in Northern Germany—Influence of temporal resolution and network density", Journal of Hydrology: Regional Studies, vol. 15, 2018, pp 184-202

[18] M. Kumari, A. Basistha, O. Bakimchandra, & C. K. Singh, "Comparison of spatial interpolation methods for mapping rainfall in Indian Himalayas of Uttarakhand region", Geostatistical and Geospatial Approaches for the Characterization of Natural Resources in the Environment, 2016, pp 159-168

[19] M.O. Kisaka, et al, "Potential of deterministic and geostatistical rainfall interpolation under high rainfall variability and dry spells: case of Kenya's Central Highlands", Theoretical and Applied Climatology, vol. 124, 2016, pp 349-364

[20] U. Haberlandt, "Interpolation of precipitation for flood modelling", Flood Risk Assessment and Management, 2011, pp 35-52

[21] Z.K. Bargaoui, & A. Chebbi, "Comparison of two kriging interpolation methods applied to spatiotemporal rainfall", Journal of Hydrology, vol. 365, 2009, pp 56-73

[22] T. Yan-bing, "Comparison of semivariogram models for Kriging monthly rainfall in eastern China" Journal of Zhejiang University-SCIENCE A, vol. 3, 2002, pp 584-590

Method to assess Water Scarcity of Product based on ISO14046 for Thailand : A case study of 44 products in Thailand

Natworapol Rachsiriwatcharabul[1] and Jirawatr Jirajariyavech[1,a]

Abstract Water and Environment Institute for Sustainability (WEIS) under The Federation of Thai Industries (F.T.I.) cooperated withGroundwater Development Fund of Department of Groundwater Resources (DGR) conduct the project to assess groundwater use throughout the product life cycle or water footprint of product. The objective is to promote the water footprint in accordance with ISO 14046 and Life Cycle Assessment (LCA) for industrial sector and develop Thai experts of water footprint. As well as developing the appropriate certification system of water footprint for Thailand.

There are 15 pilot industries (companies) participating in this project and the experts join the consultation with the pilot industries to evaluate the water footprint of products and also to study the ways to reduce groundwater use (including surface water) from the manufacturing process. In addition, the technical committee has been appointed to develop the appropriate water footprint assessment and verification guideline for Thailand (in accordance with ISO 14046) and also appointed the water footprint certification committee to certify water footprint of product.

Outcomes of the project, we can develop a appropriate guideline of water footprint assessment and verification, water footprint certification system that suitable for Thailand and there are 44 products (15 products from 15 companies under the project and 29 products from 13 companies outside the project) from 12 product groups (corrugating medium, drinking water, soft drink, alcoholic beverages, portland cement, rubber, sugar, fresh chicken and products processed from chicken meat, polymer car accessories, electricity and steam, industrial water, aromatics) that have been certified for Water Scarcity Footprint (WSF).

Keywords *ISO 14046, Water Scarcity Footprint (WSF)*

[1]Water and Environment Institute for Sustainability (WEIS)
The Federation of Thai Industries (F.T.I.)
Bangkok, Thailand

[a]jirawatrj@off.fti.or.th

Water and Environment Institute for Sustainability (WEIS) has adopted and applied the Water Footprint Assessment Tool, an environmental tool to assess the amount of direct and indirect water use and degradation water (considering only fresh water) to assess the amount of water demand in the industrial process. Also include the hot spot of water use to determine the best ways to maximize water efficiency and to find ways to reduce the amount of water used in the production process. This is to prepare the waterproof footprint certification system for Thailand. WEIS got funding from the Groundwater Development Fund, Department of Groundwater Resources (DGR) to implementing the project to assess groundwater use throughout the product life cycle (or Water Footprint of Product). The project has the following main objectives:

1) To promote Water Footprint Assessment in accordance with ISO 14046 to be concrete in the industry.
2) To develop water footprint specialists and establish the Water Footprint network in Thailand.

This project covers the activities scope of work as follows:

1) To appoint Project director committee, Working committee and Technical committee
2) Public relation of the project and pilot industries recruitment.
3) Pilot industries selection.
4) Training and workshop on Water Footprint Assessment.
5) In-depth consultation to pilot industries.
6) Preparation of Water Footprint Assessment Report and guidelines of water use reduction.
7) Verification of data from third party.
8) Water Footprint Certification.
9) Evaluating the value of the project. (environment, economic and social)
10) Seminar to public the success of the project.

There are 34 industries apply to participate,including sugar industry, petrochemical industry, cement industry, ethanol production industry, textile and dyeing industry, electrical and electronic industry, rubber industry, automotive parts industry, pulp and paper industry, food and beverage industry, feed industry and broiler farms. Finally, it was selected as a pilot industry from 15 companies.

In-depth consultation with pilot industries to assess Water Footprint

Project implementation, there will be experts in depth consultation with the pilot industries and also study on ways to reduce groundwater use (Including surface water) from the manufacturing process or form use phase of product. The project experts consulted with each pilot industry for 4 times, as well as WEIS established the technical committee meeting to develop a guideline of Water Footprint Assessment in accordance with ISO 14046 for Thailand. The Water Footprint Assessment guideline will be used for consulting the pilot industries.

1) Technical Committee Meeting

WEIS organizes the Technical Committee meetings to develop guideline of Water Footprint Assessment and Water Footprint certification system in accordance with ISO 14046 for Thailand. Also discuss for the technical comments and suggestions about the Water Footprint Assessment. The Technical Committee consists of 21 members, representatives from industry sectors, academics, educational institution and related organizations.

2) Development of Water Footprint Assessment Guideline

This project, Water Footprint Assessment is implemented in accordance with ISO 14046 which consists of 4 main steps, similar to Life Cycle Assessment (LCA).

- Step 1 Goal and Scope Definition: The assessor must determine Functional Unit, Product Unit and form of assessment before proceeding to collect data and process the water footprint inventory.
- Step 2 Water Footprint Inventory Analysis: It is a step to establish Water Footprint Inventory by collecting quantitative and qualitative data. Water Balance of the whole organization is required.
- Step 3 Water Footprint Impact Assessment: Assessment is related to the amount or shortage of water (Water Scarcity Footprint)in the unit of H_2Oeq. In the case of direct water use from nature, Water Footprint is calculated by multiplying the amount of water use by the factor called Water Stress Index (WSI). In the case of indirect water through technological processes or water integrated to raw materials or water used for the acquisition of raw materials, Water footprints is calculated from the activity data multiplied by a factor called Water Scarcity Footprint (WSF).
- Step 4 Interpretation of the Results

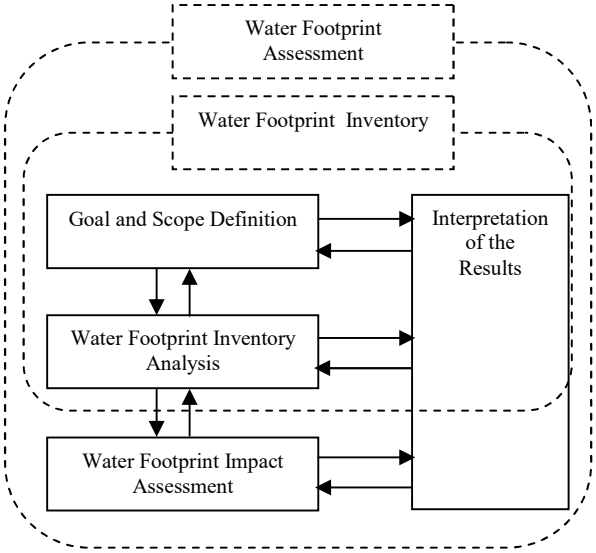

Fig. 1. Main steps of Water Footprint Assessment

3) Product Category Rule (PCR)

WEIS has developed Product Category Rule for Water Footprint Assessment. PCR include following details such as specific product details, scope of assessment, data collection in the life cycle of the product, display of Water Scarcity Footprint (WSF) and Water Stress Index (WSI). WEIS has developed a PCR, divided into 9 groups of product that covering pilot products.

- Group 1: Corrugating medium products
- Group 2: Drinking water products
- Group 3: Soft drink products
- Group 4: Alcoholic beverages products
- Group 5: Portland cement products
- Group 6: Rubber products
- Group 7: Sugar products
- Group 8: Fresh chicken meat and processed chicken meatproducts
- Group 9: Polymer Car Accessories

4) In-depth consultation

The 1st in-depth consultation, to clarify the project details,visiting the production process, determining the scope of Water Footprint Assessment in accordance with ISO 14046, as well as identifying the information to be collected from various activities such as input-output material,determining the extent assessment which depends on the type of product (Business-to-Business (B2B) or Business-to-Consumer (B2C) based on the principles of Life Cycle Inventory)and Water Balance (water consumption mapping of surface water and groundwater) for use in calculating the Water Footprint of Product.

The 2nd in-depth consultation,to provide technical advisory and technical support to collect non-collectable information or data that may require a calculation method. Also study ways to reduce water use from activities or production processes.

The 3rd in-depth consultation,to inquire and understand the details of the information received. Describe the assumption that will be used to assess Water Footprint. Including the draft measures of water reduction in the production process

The 4th in-depth consultation,to summarize the Water Footprint Assessments of product and measures to reduce the use of water from the production process or from the use phase of products.

Data Verification of Water Footprint Assessment

Under this project,the data verification ofWater Footprint Assessment is required and focus on transparency, relevance, completeness, consistency accuracy and comprehensivenessforWater Footprint Assessmentof product is accurate according to academic principles, respectful and acceptable The procedure of Water Footprint Verification is as follows.

- The Water Footprint Assessor delivers the documents and information of Water Footprint Assessment to the verifier.
- The verifier takes into consideration the information from the documents that sent by the assessor.
- The verifier checks the information from the site visit.
- The assessor corrected the information as notified by the verifier.
- The verifier considers the modified information that sent by assessor.
- The verifier certified the result of Water Footprint Assessment and prepare documents for certification.
- The verifier informs and sends the certificate of Water Footprint Assessment to WEIS.

Water Footprint Certification

WEIS appointed Water Footprint certification committee to certify Water Footprint Assessment and set up a committee meeting to consider the methods of Water Footprint of Product Certification and to certify Water Footprint of Product. In summary, the results of the WaterFootprint of Product certification are as follows.

- To obtain a Certification of Water Footprint of Product, The industry must conduct a thorough assessment of the water footprint of product and through the verification of water footprint of product. The industry will provide the documents of Water Footprint Assessment include presentation, PCR and Verification Sheet. After that, the Water Footprint certification committee will consider the information and inquire further questions. The secretary will provide additional information or ask more questions to the verifier on matters that still have doubts. If considered and approved, the Water Footprint certification committee then certify the Water Footprint of Product. However, if not passed the certification the industry will need to correct the Water Footprint Assessment data.
- Currently, Thailand has Water Stress Index (WSI) of the 25 basins (average monthly and annual) that were provided by The Joint Graduate School of Energy and Environment (JGSEE), and also has Water Scarcity Footprint (WSF) of 8 groups (129 databases) were provided by the National Metal and Materials Technology Center (MTEC). WSI and WSF were used to supportWater Footprint Assessment of Product in Thailand.
- The Verification scope of the Water Footprint of Product (under certification by WEIS)is according to ISO 14001: 2006, Environmental Management - Life Cycle Assessment - Requirements and Guidelines based on the Life Cycle Assessment (LCA).
- Currently,WEIS will certify only Water Scarcity Footprint because of the limitations of water database in Thailand that used for Water Footprint Assessment. It will broaden the coverage of certification in the future. Under this project there are 15 products from 15 pilot industries were certificated Water Footprint of Product and there are 29 products from 13 industries (outside this project) were certified. Water Scarcity Footprint of 44 products as follows

Table I. Result of Water Scarcity Footprint of 44 products

No	Product	Scope (B2B/B2C)	Water Scarcity Footprint (H_2Oeq)
Group 1: Corrugating medium products			
1	Corrugated Medium (CA 105 gsm.)	B2B	10.8 m^3 H_2O eq
2	Corrugated Medium (KI 125 gsm.)	B2B	11.4 m^3 H_2O eq
Group 2: Drinking water products			
3	Drinking Water (Crystal) PET bottle 1,500 ml.)	B2C	2.49 L H_2O eq
4	Drinking Water (Crystal) (PET bottle 1,000 ml.)	B2C	1.76 L H_2O eq
5	Drinking Water (Crystal) (PET bottle 600 ml.)	B2C	1.10 L H_2O eq
Group 3: Soft drink products			
6	Coca-Cola (PET bottle 1.25 l.)	B2C	25.8 L H_2O eq
7	Coca-Cola (PET bottle 590 ml.)	B2C	29.1 L H_2O eq
Group 4: Alcoholic beverages products			
8	Chang Beer Classic (bottle 620 ml.)	B2C	8.16 L H_2O eq
9	Blend 285 (bottle 700 ml.)	B2C	64.4 L H_2O eq
10	Sangsom Gold Medallion (bottle 700 ml.)	B2C	55.7 L H_2O eq
11	Monsoon Valley Signature Red Wine (bottle 750 ml.)	B2C	250 L H_2O eq
12	HONG THONG (bottle 700 ml.)	B2C	44.4 L H_2O eq

No	Product	Scope (B2B/B2C)	Water Scarcity Footprint (H_2Oeq)
Group 5: Portland cement products			
13	Portland Cement Type I (INSEE Petch) (Bulk)	B2B	329 L H_2O eq
14	SCG Portland Cement Type I (Bulk 1 ton)	B2B	341 L H_2O eq
Group 6: Rubber products			
15	Standard Thai Rubber 20 (STR20)	B2B	4.85 m^3 H_2O eq
Group 7: Sugar products			
16	Mitr Phol Refined Sugar 50 kg. (1 ton)	B2B	6.76 m^3 H_2O eq
Group 8: Fresh chicken meat and processed chicken meatproducts			
17	Fresh Chicken (fillet bag 1,000 g.)	B2C	91.8 L H_2O eq
18	Tender Chicken Breast (CP Delight) (fillet bag 90 g.)	B2C	12.9 L H_2O eq
19	Jumbo Chicken Sausage (Betagro) 1 pack (13 pieces)	B2C	87.5 L H_2O eq
Group 9: Polymer Car accessoriesproducts			
20	Fog Lamp GARNISH COVER, Toyota Hilux Revo	B2B	221 L H_2O eq
Group 10: Electricity, steam and chillerproducts			
21	Electricity (1 MWh)	B2B	126 L H_2O eq
22	Electricity 500 kV (1 kWh)	B2B	0.20 L H_2O eq
23	Electricity 115 kV (1 kWh)	B2B	0.81 L H_2O eq
24	Electricity 115 kV (1 kWh)	B2B	0.66 L H_2O eq
25	Electricity 115 kV (1 kWh)	B2B	0.63 L H_2O eq
26	Electricity 115 kV (1 kWh)	B2B	0.30 L H_2O eq
27	Electricity 115 kV (1 kWh)	B2B	0.29 L H_2O eq
28	Electricity 115 kV (1 kWh)	B2B	1.33 L H_2O eq
29	Electricity 22 kV (1 kWh)	B2B	0.81 L H_2O eq
30	Electricity 22 kV (1 kWh)	B2B	0.66 L H_2O eq
31	Electricity 22 kV (1 kWh)	B2B	0.63 L H_2O eq
32	Electricity 22 kV (1 kWh)	B2B	0.30 L H_2O eq
33	Electricity 22 kV (1 kWh)	B2B	0.29 L H_2O eq
34	Steam (1 GJ)	B2B	27.3 L H_2O eq
35	Steam (1 GJ)	B2B	67.8 L H_2O eq
36	Steam (1 GJ)	B2B	55.0 L H_2O eq
37	Steam (1 GJ)	B2B	52.1 L H_2O eq
38	Steam (1 GJ)	B2B	25.2 L H_2O eq
39	Steam (1 GJ)	B2B	23.7 L H_2O eq
Group 11: Industrial waterproducts			
40	Service water 1 m^3	B2B	71.0 L H_2O eq
41	Demin water 1 m^3	B2B	145 L H_2O eq
Group 12: Aromaticsproducts			
42	Benzene 1 kg	B2B	0.61 L H_2O eq
43	Paraxylene 1 kg	B2B	1.03 L H_2O eq
44	Orthoxylene 1 kg	B2B	1.03 L H_2O eq

Remark : B2B = Business to Business B2C = Business to Customer

Assessing value of project implementation (environmental, economic and social)

WEIS has conducted a cost-effective evaluation to project implementation that promote and support sustainable water management in the environmental, economic and social. The results are as follows.

1) Worthiness of environmental

The implementation of this project can reduce the environmental impact because the industry has a way to reduce the use of groundwater (Including surface water) in the production, which if implemented will help to conserve groundwater. It can reduce the pollution of wastewater and discharge into public water source. It also increases the potential for groundwater to be used in areas where industrial plants are located.

2) Worthiness of economic

At present, Thailand lacks appropriate Water Footprint Assessment methods, which require expensive international experts. The results of this project will help to build the Water Footprint Assessment expert in Thailand and reduce the cost of the foreign experts in the assessment. It encourages and support the industry to conduct a more thorough assessment of water use throughout the product lifecycle.

In addition, the results of the project make the pilot industries can consider production units that use high volume (hot spot) of groundwater (including surface water) and have ways to reduce water use. This will help the industry to improve water efficiency and reduce production costs. In addition, it can enhance both domestic and international competitiveness.

3) Worthiness of social

This project is part of the showcase of social responsibility for water use. If the industry adopts the guidelines to reduce water use, it will reduce the water consumption from the industry and can bring the water which reduced to use for other areas such as consumption, agricultural and can help to reduce social conflict between industry and community, including agriculture. Encourage the sustainable coexistence.

In addition, groundwater which preserved can also be used as a reservoir for the community and agricultural sector during the drought crisis to reduce the impact on living and society.

The benefits that Department of Groundwater Resources receives from this project

This project is in addition to the benefits to the industry, there are also benefits that Department of Groundwater Resources receives.

- Network of industries that comply with the regulations of Department of Groundwater Resources. It also focuses on reducing the use of groundwater and improving the efficiency of groundwater use that help to regulate the responsibilities of Department of Groundwater Resources.
- There is a preliminary reference (benchmark) on the water use of each industrial sector (but may not be representative). This can be used as a baseline for determining the demand of water and the proportion of groundwater use in various industrial sectors for use as groundwater management information.
- Pilot industries have ways to reduce water consumption and improve water efficiency. If the industry takes the approach to practice, this will help to conserve groundwater and

increase the potential of groundwater to be used in the area where the plant is located. It can also be used groundwater which reduced as a source of water in case of a drought crisis.

Problems, barriers and limitations for Water Footprint Assessment in Thailand.

1) Water Footprint is relatively new to Thailand. And the water database for the calculation is quite small.
2) Some products, such as wine, have a long production period. The wine must be fermented for a period of 20 months, so it is hard to keep track of all the information.
3) Restrictions on access to data, such as ingredients of beverages or alcoholic drink. This information is only formulated and confidential.
4) The industry has a lot of information to gather. Some have to gather information from the upstream factory in the supply chain.
5) Water Footprint Assessment must be established the water balance of the entire facility. Many industrial plants do not have fully equipped water meters wherever they are used. Most industries also give priority to energy usage data rather than water use data. The reason is that energy costs are significantly higher than water, it causes of no complete information to support the establish of water balance.

The approach that should continue.

Water and Environment Institute for Sustainability (WEIS) has commented and suggested to promote Water Footprint Assessment because of the benefits and achievements from this project.

1) Water and Environment Institute for Sustainability (WEIS) will be the main organization to certificate Water Footprint of Thailand. WEIS will encourage and expand the Water Footprint Assessments to cover all industrial sectors and continuity, so thatthe industry can consider the use of water in the production process thoroughly and use waterefficiently.
2) (2) Extend the water footprint assessment to a greater area or industrial sectors. If there are enough industrial data and examples. It can be benchmarked for specific industrial sector and used as a reliable representative data. The Department of Groundwater Resources (DGR) can be used as groundwater management information to determine the demand ofgroundwater and the proportion of groundwater use for specific industries and also used as surface water management information, leading to overall water management in the country.

References

[1] ISO 14001: 2006, Environmental Management - Life Cycle Assessment - Requirements and Guidelines based on the Life Cycle Assessment (LCA)
[2] ISO 14046 : 2014, Environmental management - Water footprint - Principles, requirements and guidelines

Micro-Scale Flood Hazard Assessment in Phnom Penh City, Cambodia

Naichy Sea[1,a], Supattra Visessri[1,b,*] and Sokchhay Heng[2,c]

Abstract Water-related disasters in urban area, especially urban floods have become more frequent and severe. This leads to loss of life, infrastructure damage, business interruption as well as time delay for traveling to any destinations. Phnom Penh, the capital city of Cambodia, has frequently experienced significant rainfall-flood events during rainy season. Without proper mitigation and management of urban drainage system, Phnom Penh is expected to face with the current and future challenge of water-related disaster. To address this urban flood inundation, flood modeling can make a visual representation of the urban flood hazard as basic information for land-use planning and limit development in flood-prone areas. This study, therefore, aims to simulate inundation situation in a downtown area with the complex storm drainage system in Phnom Penh using FLO-2D model. An independent catchment covering an area of 12.5 km^2 is chosen as study area since it is strategically important and frequently affected by rainfall-flood events. The simulated result is delineated into flood hazard map defined by three categories, ranging from low to high, based on flood depth and flood duration. The result shows that the area under low, medium, and high hazard are 25.60%, 8.24%, and 2.72%, respectively of the total area.

Keywords *Urban flood, flood hazard, FLO-2D, Phnom Penh.*

[1]Department of Water Resources Engineering
Faculty of Engineering, Chulalongkorn University
Bangkok, Thailand
[2]Faculty of Hydrology and Water Resources Engineering
Institute of Technology of Cambodia
Phnom Penh, Cambodia

[a]Naichy.a2@gmail.com
[b]Supattra.vi@chula.ac.th
[c]Heng_sokchhay@yahoo.com

Introduction

Flooding is one of the most serious natural disasters in the world in terms of its frequency and severity. Due to the severe effect of climate change, it is expected that flooding will occur more often and increase in magnitude in the future [1]. In the world index, Cambodia ranked 9th among the most 15 disaster prone countries in the world [2]. Furthermore, the rate of urbanization of Cambodia was the highest one in the region, averaging about 3.5% per year between 1990 and 2013. This rapid urbanization over the past two decades has brought severe water-related disaster to Cambodia's population. Phnom Penh capital, located at the confluence of the Mekong River, Tonle Sap River, and Bassac River, is the political, economic and cultural center of Cambodia. Recent studies of Phnom Penh showed that 42% of urban poor residents were affected by flooding from polluted water bodies [3], and 23% lived on the banks of rivers [4]. Poor quality housing, lack of sanitation facilities and high rates of poverty are also characteristics of urban poor areas that increase their vulnerability to disasters. More importantly, a network of wetlands, streams, and ponds in Phnom Penh which are the temporary flood storage, are currently being filled with earth to create developable land [5]. Without proper mitigation and management of urban drainage system, Phnom Penh is expected to face with the current and future challenge of water-related disaster. In such context, Molyvann [6] stated that the development with little planning or control resulted in flooding problems, informal settlement along drainage ways, increased landfill and poor urban infrastructure.

There are two significant cases of flood events in Phnom Penh – daily rainy season flood events and episodic larger scale flood plain events. During rainy season, some low-lying streets are flooded with water level around 1.5 m deep adversely affecting normal daily lives, society, and environment. To deal with such problem, the Government of Cambodia (GOC) made an urgent request to the Government of Japan (GOJ) to formulate an integrated plan for urban drainage and flood control. Later, the Japan International Cooperation Agency (JICA) dispatched by GOJ has conducted over $325 million of infrastructure upgrades in Phnom Penh including drinking water supply facilities, flood protection, drainage improvements and the rehabilitation of the Phnom Penh port. As a result of JICA's work, flooding in some area of Phnom Penh has been

decreased. However, it cannot be relied upon JICA's project outcome to eliminate all of Phnom Penh's drainage problems or to prevent future flooding in the areas developed without flood protection. To address this urban flood inundation, the spatial description of the flood hazard plays an important role in the decision-making process about improving flood management and response planning. Meanwhile, flood modeling can make a visual representation of the urban flood hazard which is fundamental to land-use planning, limiting development in flood-prone areas. This study therefore aims to simulate inundation situation in a downtown area with the complex storm drainage system in Phnom Penh using FLO-2D model.

Methodoloy

A. FLO-2D Model review

FLO-2D was developed in 1988 and first known as MUDFLOW. It was first used to simulate an urbanized alluvial flood in Colorado for Federal Emergency Management Agency (FEMA). It is a grid-based physical process model that routes rainfall-runoff and flood hydrographs. It is specifically initiated for delineating flood hazards, regulating floodplain zoning or designing flood mitigation of river overbanks flows and unconventional flooding problems such as unconfined flows and channel flow. The main utility of the model is for urban flood simulation with building, streets, walls, and storm drains. Two main constitutive fluid motion equations: the continuity equation (1) and the momentum equation (2) are used as governing equations in FLO-2D:

$$\frac{\partial h}{\partial t} + \frac{\partial hV}{\partial x} = i \tag{1}$$

$$S_f = S_0 - \frac{\partial h}{\partial x} - \frac{V}{g}\frac{\partial V}{\partial x} - \frac{1}{g}\frac{\partial V}{\partial t} \tag{2}$$

where h is the flow depth, V is the depth-averaged velocity and i is the excess rainfall intensity. S_f and S_0 are the friction slope and bed slope respectively based on Manning's equation.

FLO-2D flood routing model is used along with the Environmental Protection Agency (EPA) Storm Water Management Model (SWMM). At runtime, FLO-2D is linked to the EPA-SWMM model to exchange overland flow and storm drain. Infiltration is simulated using either the Green-Ampt infiltration model or Soil Conservation Service curve number. In this study, the Green-Ampt infiltration was applied.

B. Description of study area

The capital city of Cambodia, Phnom Penh, covers an area of 678 km^2 and is home of population of 2.2 million [7]. It is spread out over a flat alluvial floodplain where an intersection of the Mekong River, Tonle Sap River and Bassac River crosses each other. This intersection is called "Four Faces or Chaktomuk". The gradient feature of Phnom Penh is slightly inclined from north to south and from west to east. The overall elevation difference of the city is around 10 m where the relatively high land area with elevation of 14 m is situated at Pochentong Airport and the low land with elevation 4 m is at Tumpun area. Phnom Penh capital city is governed by tropical monsoon climate. The annual average rainfall from 1985 to 2013 is around 1,414 mm. Fig.1 presents the annual rainfall from 1985 to 2013 and 5-year moving average, indicating a slight increasing trend of annual rainfall in Phnom Penh city.

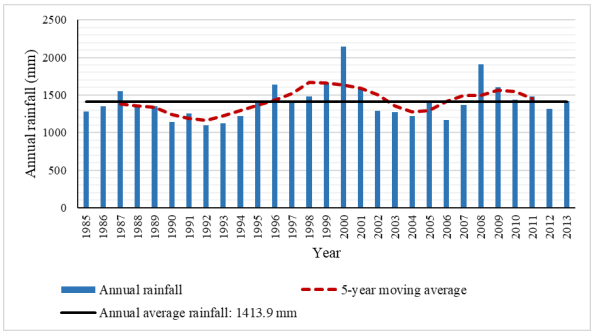

Fig. 1. Annual rainfall (1985-2013) and 5-year moving average

An independent catchment in Phnom Penh city covering an area of 12.5 km^2 is selected as the study area (Fig.2).This area consists of residences, commercial companies, busy roads and many municipal administrations such as Royal Palace, Olympic Stadium and embassies and it is surrounded by the Tonle Sap River at the east. The land use for the study area is divided into road, building, and open spaces. Water is drained from the north to south (Beoung Trabek Station, P1). Since the elevation at the outfall is higher, water is pumped out by four pumping stations located as shown in Fig.2.

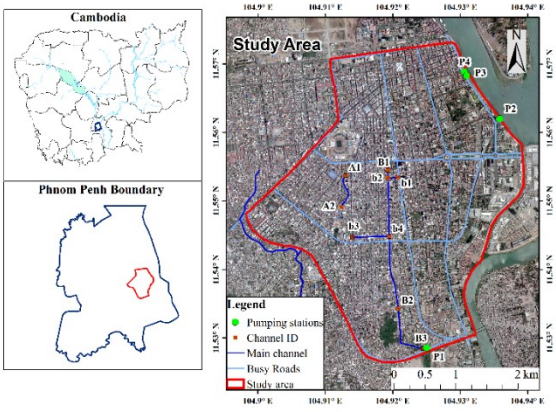

Fig. 2. Map of study area

C. Model set up

The size of the developed grid element should reflect the resolution of the terrain elevation data and provide an acceptable number of grid elements. There should be equitable between the grid element size, resolution of the desired FLO-2D result and the model computer runtime. Therefore, in this study, the grid system was created with the grid size of 10 m x 10 m and a satellite image with a resolution of 2 m x 2 m was also employed to visualize the computational domain. The grid elevation was obtained from the surveyed interpolation DTM elevation point.

The computer modeling is commonly comprised of three main components: input, simulation, and output. To get acceptable output, reliable data is required as the input. The important input data of FLO-2D to generate flood map in this study are summarized in Error! Reference source not found.. An overall flowchart of the methodology used in this study is shown in Fig. 3.

Table I. Available input data

No	Data type	Period	Frequency	Source
1	Rainfall	2010-2016	5 min	ITC
2	IDF curve	-	-	JICA
3	DEM	2016	2 m x 2 m	MRC
4	Drainage system	2010 & 2015	-	Phnom Penh Capital Hall
5	Phnom Penh Image	2016	2 m x 2 m	MRC

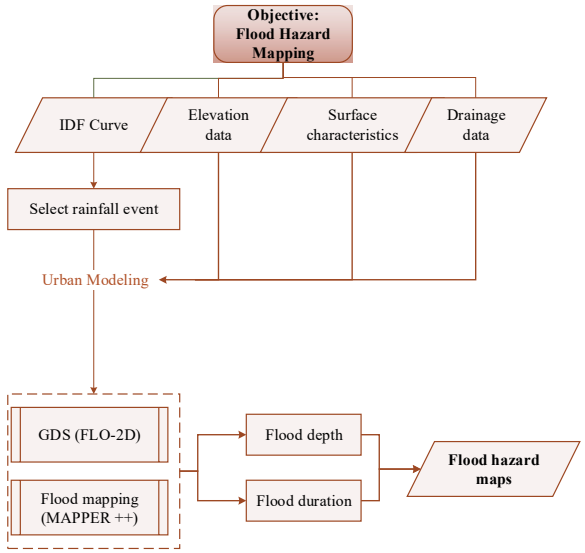

Fig. 1. Overall flowchart

D. Design rainfall

Rainfall is the main driving element attributing to urban floods and the severity of flooding is depended on rainfall intensity, duration, and frequency. Thus, selecting extreme events for flood mapping is very important. In this study, an event-based rainfall with accumulated depth 103.4 mm for duration of 2 hours occurred on 23 April 2011 is considered as heavy rainfall and selected to represent the flood situation corresponding to 50 years return period. This event is selected from five minutes time-scale rainfall based-event of ITC station installed near to the study area.

E. Flood simulation

The depth of flooding of each 10 m x 10 m grid is calculated and classified into three depth categories: low, medium, and high based on two critical depths 0.30 m, and 0.60 m. The basis of the selected critical depth is in reference to the data analysis from questionnaire surveys of public perceptions on the urban flood in Phnom Penh conduced in 2016 [8]. It was reported that when the water level was less than 0.30 m, it is very common for citizens. Hence, the damage was estimated to be minor since citizens can adapt to this condition. In case the flood depth varied between 0.30 m and 0.60 m, the damage is considered moderate which would contribute to negative effects on business, traveling, and health. Besides, such damage will be huge as the flood depth increases to over 0.60 m.

The duration of flooding is a crucial factor for the hazard assessment that was agreed by many reaseachers [9, 10]; however, there is very limited literature to quantify this parameter. Keokhumcheng, et al. [10] determined the duration of flooding by using three inundation maps of flood for rising flood, peak flood, and receding flood from the model simulation. On the other hand, only areas belonging to the flood-affected area with flood depth higher than 0.10 m were used to determine flood duration. The duration of flooding in this study is determined by overlapping the three inundation maps of rising, peak flood, and receding flood. The duration of flooding is subdivided into three categories: short, medium, and long. The areas shown as flooded in all inundation maps are considered to have a long duration of flooding. Areas shown as flooded in any two flooded maps are considered to have a medium duration of flooding. Areas shown as flooded in only one or free of flooding in all inundation maps are considered to have a short duration of flooding.

F. Hazard assessment

From flow simulation results, two parameters of flood depth and flood duration estimated for each grid and maps of each individual parameter have been prepared. The hazard index developed for this study for the flood depth is classified as 1, 2, 3 representing as low, medium, and high, accordingly as shown in Error! Reference source not found.. The hazard index for flood duration is classified as 1, 2, 3 representing short, medium, and long as shown in Error! Reference source not found..

Table II. Hazard of flood depth

Depth of flooding (m)	Flood depth category	Hazard index
$D \leq 0.3$	Low	1
$0.3 < D \leq 0.6$	Medium	2
$D > 0.6$	High	3

Table III. Hazard of flood duration

Duration of flooding	Flood duration category	Hazard index
Areas flooded in one or free of flooding in three inundation maps	Short	1
Area flooded in two maps of three inundation maps	Medium	2
Area flooded in three inundation maps	Long	3

The combined effect of two parameters, namely the depth of flooding and duration of flooding has been considered while classifying the hazard at the grid point. Various combinations of these parameters are classified into 9 groups as shown in Error! Reference source not found.. These hazard criteria are assigned index on 1-3 scale.

Table IV. Hazard index for combination of two parameters

No. Scenario	Function of flood depth and duration	Hazard index	Hazard category
1	Low and short	1	Low
2	Low and medium	1	Low
3	Low and long	2	Medium
4	Medium and short	1	Low
5	Medium and Medium	2	Medium
6	Medium and long	3	High
7	High and short	2	Medium
8	High and medium	3	High
9	High and high	3	High

Results and discussions

A. Hazard of flood depth

From the simulation of flood inundation, the floodplains in the study area are 69.10%, 7.50%, and 3.40% for low, medium and high flood depth hazard category, respectively (Error! Reference source not found.). Error! Reference source not found. shows the result of maximum flood depth from Mapper++ (FLO-2D). At the northern part of the selected study area, there are four locations (A, B, C and D) which are affected by flood within the category of medium and high hazard during the rainfall event of 50-year return period. The location A is along Kampuchea Krom Boulevard. The location B is in Kandal market area. The location C and D are area around the Royal Palace. On the other hand, the hazard which affected to area around National Assembly of Cambodia (E) and Beoung Keng Kang high school (F) have been classified into the medium category. Moreover, there are other three locations (G, H, and I) which are found at the southern part of the study area have serious flood. The locations are around Khmer-Soviet Friendship Hospital (G), along Mao Tse Toung Boulevard (H), and in Beoung Trabek area (I). Meanwhile, Boeung Trabeck Lake Muy and Boeung Trabeck Lake Pir having a role as flood storages are represented by point K and L, respectively.

It is observed that the locations of A, E, G, and I have serious flood due to low elevation and deficiency of storm drain system. Meanwhile, flooding of other areas such as B, C, D, F, and H is caused by low elevation comparing to elevation of neighboring areas. In addition, it is noticed that almost the whole of the study area is suffering from flood.

Table V. Inundation area of flood depth hazard

Flood depth category	Inundation area (km^2)	Percentage of flooded area (%)
Low	8.64	69.10
Medium	0.93	7.50
High	0.43	3.40

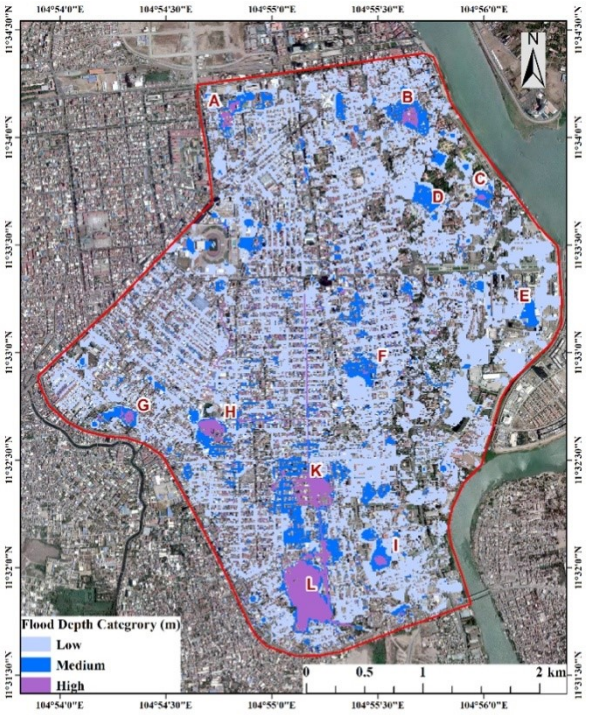

Fig. 4. Hazard map of flood depth

B. Hazard of flood duration

For the classification of flood duration, the floodplains in the study area are 26.24%, 18.56%, and 1.12% for short, medium, and long flood duration of hazard category, respectively (Error! Reference source not found.). Error! Reference source not found. illustrates the result of the spatial flood duration. It is noticed that the whole floodplain area affected by flood is fallen into the category of the short and medium hazard only. The map of flood duration shown in Error! Reference source not found. is produced with the receding flood map with 6 hours after rainfall has stopped. Thus, it means that the water

of areas belonging to short category is completely drained within no longer than 6 hours after rain has stopped while flood of areas belonging to medium category is longer than 6 hours after rain has stopped.

Table VI. Inundation area of flood duration hazard

Flood duration category	Inundation area (km^2)	Percentage of flooded area (%)
Short	3.28	26.24
Medium	2.32	18.56
Long	0.14	1.12

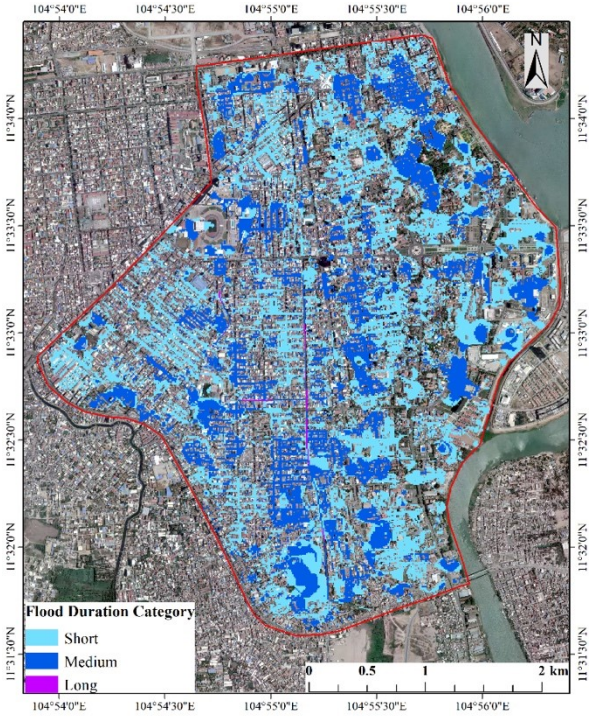

Fig. 5. Hazard map of flood duration

C. Hazard mapping

The result in Error! Reference source not found. shows that the area under low, medium, and high hazard are 25.60%, 8.24%, and 2.72%, respectively of the total area. The high hazard areas are seen in Kampuchea Krom Boulevard, Kandal market, around the Royal Palace, Olympic stadium, and the area in Beoung Trabek district (Error! Reference source not found.).

Table VII. Inundation area of flood hazard

Flood hazard category	Hazard area (km^2)	Percentage of hazard area (%)
Low	3.20	25.60
Medium	1.03	8.24
High	0.34	2.72

D. Model cabribration process for future study

The results above were analyzed based on the simulation result without model calibration which leads to some uncertainty. However, the parameters input for the model were obtained from previous study of [7] which the model overall performance was evaluated by comparing with the results of JICA survey and flood photo analysis. Thus, it is imperative to access model calibration and validation for future study. In order to do model calibration and validation in this study,observed flood depths in the channels and on the streetscorresponding to any heavy rainfall events need to be

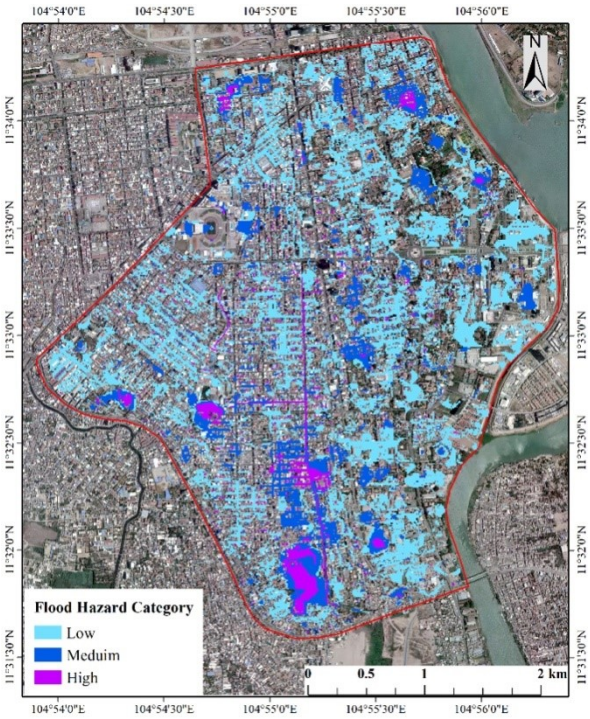

Fig. 6. Hazard map of two parameter combination

collected. Then, rainfall event corresponding to observed data are employed as input in the model. The model calibration can be done by comparing the simulation result with the observed data of flood depths using some statistical error or goodness-of-fit indicators [11] such as Root Mean Square Error (RMSE), Nash-Sutcliff Efficiency (NSE), Percent Bias (PBIAS), coefficient of determination (R^2), and so on and so forth.

Conclusions

FLO-2D model is applied to compute the flow in the complex storm drainage in Phnom Penh City. However, there is some uncertainty since there is no enough observed flood data to do the calibration to confirm the model performance. Thus, the required data need to be collected in further study to evaluate the performance of model and clarify the results.

Based on the results, there are some main locations in the study area which confront to the high hazard with the depth higher than 0.6m. Regarding to duration of flooding, the water of most study area can be completely drained within 6 hours after rainfall has stopped while flooding areas around 11% of total area encounter flooding longer than 6 hours.

This result is beneficial to the policy maker and the urban planner to consider on renewal and maintenance of drainage system in some inundation areas. Moreover, investing in structural measures such as constructing more detention basin or ground storage are able to reduce the water level in the inundation area.

Acknowledgment

We would like to express our sincere thanks to Scholarship Program for ASEAN Countries of Chulalongkorn University for financial support to the first author.

References

[1] D. Kvočka, R. A. Falconer, and M. Bray, "Flood hazard assessment for extreme flood events," *Natural Hazards,* vol. 84, no. 3, pp. 1569-1599, 2016.

[2] J. Birkmann *et al.*, "World risk report 2014," Alliance Development Works, United Nations University3981449541, 2014.

[3] F. Meg, "The Phnom Penh survey," in "A Study on Urban Poor Settlements in Phnom Penh," Sahmakum Teang Tnaut February 2014.

[4] P. P. Capital, "Urban poor assessment," in "A Baseline Survey on the Social and Economic Situations and Capacity of Existing Services in Urban Poor Communities," Phnom Penh CapitalDecember 2012.

[5] D. Shelby, "Phnom Penh, city of water," Sahmakum Teang Tnaut December, 2012.

[6] V. Molyvann, *Modern Khmer Cities*. Reyum, 2003.

[7] H. Sokchhay, K. Kimleng, C. Kong, L. Sarann, and K. Tsuyoshi, "Urban flood modeling in Phnom Penh using Flo-2D," presented at the Energy connectivity, environment, and development, Asian Institute of Technology, 28-30 November, 2017.

[8] H. Sokchhay, L. Sarann, C. Sochittra, and P. Kruy, "Analysis of public perceptions on urban flood in Phnom Penh, Cambodia," presented at the Water Security and Climate Change: Chanllenges and Opportunities in Asia, Asian Institute of Technology, Bangkok, Thailand, 2016.

[9] D. R. O. United Nations, "Mitigating natural disasters: phenomena, effects, and options," *Manual for Policy Makers and Planners,* pp. 34-40, 1991.

[10] Y. Keokhumcheng, T. Tingsanchali, and R. S. Clemente, "Flood risk assessment in the region surrounding the Bangkok Suvarnabhumi Airport," *Water International,* vol. 37, no. 3, pp. 201-217, 2012.

[11] A. Ritter and R. Muñoz-Carpena, "Performance evaluation of hydrological models: Statistical significance for reducing subjectivity in goodness-of-fit assessments," *Journal of Hydrology,* vol. 480, pp. 33-45, 2013/02/14/ 2013.

Estimation of groundwater use pattern and distribution in the coastal Mekong Delta, Vietnam via socio-economical survey and groundwater modeling

Tuan Pham Van[1,a,*] and Sucharit Koontanakulvong[1,b]

Abstract

Surface water resources in the Mekong Delta are under increasing strain due to unplanned extraction, pollution, salinization and climate change effects. In many provinces of Mekong delta, excessive groundwater extraction has resulted in many serious groundwater-related problems. The increase in demands and the aforementioned negative effects of groundwater depletion raise the urgent question: at what time in future are the limits to local groundwater use reached? Hence, there is a need to know groundwater use (GWU) pattern and distribution in the study area for future groundwater management.

In this study, firstly, the study used socio-economic data of Tra Vinh Province to classify group of revenue, potential of water resources and population distributed in each district to design and conduct the socio-economic survey to explore information relevant to groundwater use (GWU) for each purpose. Secondly, the data set of 419 survey questionnaires per 9 survey communes were analyzed by SPSS tool to estimate ratio of household using groundwater (RHHUG) for each purpose as well as average pumping rate (APR) per household and per ha for domestic use agriculture use, respectively. Thirdly, the APRs were extended to propose the total groundwater use pattern and distribution during 2007-2016 by using socio-economic data of the province and expand to spatial distribution by using correlation with land surface temperature (LST) which was estimated from Landsat 8. Besides, the groundwater flow model of the study area was developed to verify and correct amount of groundwater pumping (pattern and distribution proposed) from 2007 to 2016.

The study found that the annual GWU of Tra Vinh Province in 2016 was 347,793 m^3/d in which both Duyen Hai district and Tra Cu district occupied more than 50 percentages, i.e., about 188,551 m^3/d. In those two districts, RHHUG increased from 2 to 3 times during the period of 2007 and 2016. LST distribution performed a good correlation (R^2 = 0.646) with GWU distribution in Tra Cu district. Results of groundwater modeling shown that the discharge from aquifer (mainly pumping) was always higher than the recharge to aquifer. It explained why the observed groundwater level declined about 0.1 m per year of the period from 2007 to 2016.

Keywords *groundwater use, pattern, distribution, groundwater modeling, land surface temperature, field survey*

[1]Department of Water Resources Engineering
Faculty of Engineering, Chulalongkorn University
Bangkok 10330, Thailand

[a]phamtuanld8@gmail.com
[b]sucharit.k@chula.ac.th

A study on local knowledge in adaptation to landslide disasters in Sri Lanka

Uditha Dasanayaka[1,a] and Yoko Matsuda[1,b]

Abstract

Natural disasters are unforeseen events which occur at hydrologic, geologic, and atmospheric origins. The Policy-makers still rely on mitigation strategies based on scientific approaches. However, many scholars had emphasized the importance of incorporating local knowledge and related practices for disaster risk management. In that context, this study investigates the local knowledge in adaptation to mitigate the landslides disaster situations by studying a village in Sri Lanka which is located at the central region of Sri Lanka which is vulnerable for landslide disasters. Landslides is one of the severe types of disasters in hilly terrains and which cause to loss of lives and property damages especially in Asia region. This study employed the field surveys, questionnaire surveys and semi structured interviews for data collection. The findings of the research indicate how the local knowledge-based practices in settlement layout & planning, landscaping had enhanced disaster adaptation level of the community. Further the local knowledge-based value systems act as a strong mechanism in identifying early signs of landslide disasters. Finally, the paper discusses the possibilities of upscaling such local practices for mainstream disaster management practices.

Keywords *Landslides, local knowledge, adaptation, semi structured interviews.*

[1]Department of Civil & Environmental Engineering
Nagaoka University of Technology
Japan

[a]uditha05@gmail.com
[b]ymatsuda@vos.nagaokaut.ac.jp

POLICY GUIDELINES ON DISASTER RISK REDUCTION FOR FLOOD PREVENTIONAT KLONG YAN SUB-WATERSHED, SURATTHANI PROVINCE, THAILAND

Siwaporn Promdaen[1,a] and Sangchan Limjirakan[2,b]

Abstract The Fifth Assessment Report of the Intergovernmental Panel on Climate Change stated that observed and statistical data in long-term trends since the 20th century showed the average globally surface warming due to an increasing of greenhouse gas emissions into the atmosphere (IPCC AR5, 2013). It also reported that water is a vulnerable resource to the impacts of climate change. Thailand is one of South-east Asian countries that have been suffered from several extreme events resulting from climate change (UNESCAP, 2012). One consequence of changes is the severity and frequency of extreme events leading to flooding in all regions of Thailand. This research is aimed to study policy guidelines on disaster risk reduction for flood prevention at Klong Yan Sub-Watershed, Suratthani province of Thailand. The purposive sampling method was used to select stakeholder's involvement, which included local governmental officers, local community leaders, local wisdom scholars, non-profit organization and the network of watershed group. These groups were in-depth interviewed using a set of questionnaires. Data collection included both desk study of secondary data and in-depth interviews of primary data and data obtained were analyzed using descriptive method. The research results found that about 31 % of the respondents were familiar to the policy guidelines on disaster risk reduction such as a master plan of disaster prevention and mitigation. They viewed that the policy guidelines on disaster risk reduction is important to reduce losses and damages from floods. However, about 69 % of respondents did not familiar to the policy guidelines on disaster risk reduction. They viewed that effective policy implemented requires knowledge training and awareness raising, improving law and regulations, supportive infrastructures, building the communication system and early warning system, financial supports and creating collaboration among relevant stakeholders.

Keywords *Policy guidelines, Disaster risk reduction, Flood prevention, Klong Yan Sub-Watershed*

[1]The Environment, Development and Sustainability Program
Graduated School,Chulalongkorn University
Bangkok, Thailand
[2]The Environmental Research Institute
Chulalongkorn University
Bangkok, Thailand

[a]spromdaen@yahoo.com
[b]sangchan.l@chula.ac.th

Introduction

According to the Fifth Assessment Report of the Intergovernmental Panel on Climate Change (IPCC AR5), the rising of the average surface temperature was a result from human activity where greenhouse gas emissions is increasing into the atmosphere [1]. It is likely projected to be increasing temperature on the earth's surface in the range from 2^0 C to 4.5 ^{0} C over the next 100 years. Additionally, evidences from the IPCC AR5 also reported that climate change is expected to dramatically impacts on environment, societies and economic activities in terms of natural disasters or extreme events. Therefore, increasing temperature causes to change in the climate system, leading to the frequency and severity of adverse disasters. Moreover, the United Nations Economic and Social Commission for Asia and the Pacific (UNESCAP) pointed thaturban expansion problems and increasing population led to unsuitable settlements in the floodplain land areas, making people vulnerable to the impact of flooding. [2]

Thailand is one of South-east Asian countries that have experienced from the impact of natural disaster. Floods still remain the top priority of severe disaster due to the impact of climate change [3]. In 2011, Thailand faced to severe flood which 64 out of 77 provinces were affected; the number of death toll raised to 1,026 people and the total economic damage loss of about 1.44 billion Bath or US$ 45.7 billion. [4] Surat Thani Province is located in the southern region of Thailand, facing with floods, and still continue facing such problems due to the impact of climate change. In 2018, the Department of Disaster Prevention and Mitigation reported that there were approximately affected 80,267 households and economic damage was around 900 million Baht in Surat Thani Province [5]. Meanwhile, the Klong Yan Sub-Watershed which is at Surat Thani Province was one of the severely affected areas.

The research is aimed to study the policy guideline on disaster risk reduction in the area of Klong Yan Sub-Watershed, Surath Thani Province in order to reduce the risk to floods.

Materials and methods

A. The study area

The study areas as shown in Figure 1, were Vibhavadee District and Kirirat Nikom District, Surat Thani Province, Thailand because these areas are the most affected from floods in Klong Yan Sub-Watershed. [6]

Vibhavadee District is located in the mid-area of the Klong Yan Sub-Watershed at the latitude 9^0 14'20" N and the longitude 98^0 58' 44" E. This district is covered 5435.30 square kilometer andcomprising of 2 sub-district, namely Takuk Nuea and Takuk Yai. While Kirirat Nikom Districtis located in the downstream of the Klong Yan Sub-Watershed at the latitude 9^0 1'48" N and the longitudes 98^0 57' 12" E of the total area 13473.70 square kilometer that composed of 8 sub-district, including Tha Khoanon, Ban Yong, Nam Hak, Kapao, Tha Kradan, Yan Yoo, Tham Singkhon and Ban Thamniap [7][8]. The topography of Vibhavadee District and Kirirat Nikom District is high plains and isolated hills. There is the Klong YanRiver flowing from the north to the south. It joins with the Phum Duang River and then flows to the sea at the Pak Nam Tapee. (Figure. 1).

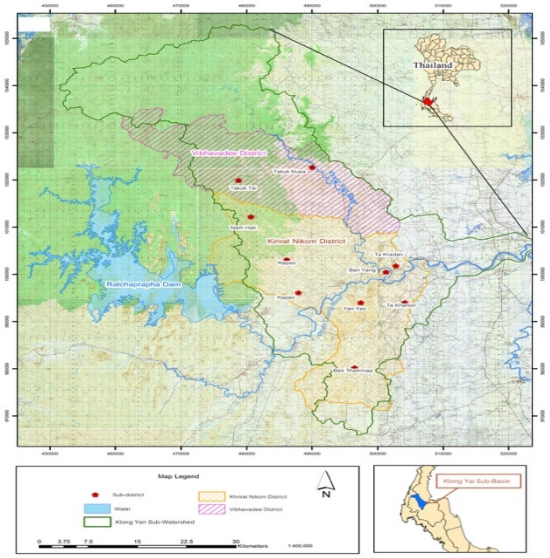

Fig. 1. The geography of Kirirat Nikom andVibhavadee Districts
Source: The Royal Thai Survey Department, 2015

B. Research methodology

The quantitative and qualitative methods were conducted by this research. Respondents of the study were applied by using the purposive sampling method in order to select stakeholder's involvement. The number of respondents were 29 including governmental officials, local leaders, local wisdom scholars, non-profit organization, the network of watershed groups. Data were collected by using a set of questionnaires for an in-depth interviews and were analyzed by using descriptive research method.

Results and discussion

Based on the National Disaster Prevention and Mitigation Plan in 2015, there have been guidelines to develop system of disaster prevention, preparation and potential formation to manage the remaining disaster through educating activities and some measures. In this regard, this plan has embraced the relevant global frameworks for action based on the Sendai Framework for Disaster Risk Reduction 2015 – 2030. [4]

The strategies for guidelines consist of disaster risk reduction, emergency management, build back better and safer, and international cooperation on disaster management as shown in Figure 2. The details are as follows;

1. Disaster risk reduction is the action to respond before disaster occurrence in order to avoid or reduce negative effects from related disasters through the analysis of the factors and impacts of the disaster under measures or actions. Therefore, this action is the guidelines to avoid the impact of the disaster through disaster prevention, mitigation and strengthening preparedness on disaster risk reduction which include:

1.1. Guidelines for Disaster Prevention and Mitigation

Preventions and mitigations are actions to avoid the disaster impacts through the implementation of structural and non-structural measures. These guidelines consist of infrastructure building, land-use planning, reinforcing laws and regulations, planning the collaboration with stakeholders, training and educating on disaster preventions and mitigations and financial supports.

1.2 Guidelines for Disaster Preparedness

Preparedness actions are measures to reduce the disaster risks prior disaster occurrence through activities in communities. These actions include increasing educations, strengthening the volunteer group and the network, exchanging knowledge, setting warning systems and communication systems, practicing the evacuation plans, raising awareness, and reviewing laws and regulations.

2. Emergency management is action to respond during-disaster occurrence through organizational structure, decision-making processes and command system in order to reduce the impact from the disaster. This phase includes the setting of the incident command center, the emergency operations, the communication systems, the data center and the emergency medical service system. Therefore, the emergency action has provided the

response of the incident situation in a rapid, efficient and timely manner.

3. Build back better and safer is the action to respond after disaster occurrences. This step composes the restoration of damaged public utilities and facilities, infrastructures, environmental system and people who are affected to be back to normal situation. Therefore, the rehabilitation and reconstruction has contributed the opportunity for disaster relief, leading normal livelihood.
4. International cooperation on disaster management is action in the post-disaster process. This action provides development and coordination with international agencies in order to request for disaster rehabilitation. Thereby, developing collaboration with national organization will provide the strengthening for addressing disasters.

In this regard, it can be concluded that the strategy of policy guidelines ondisaster risk management aims to increase the efficiency of disaster management that includes disaster prevention and mitigation, preparedness, along with emergency management as well as recovery to build back better under international cooperation.

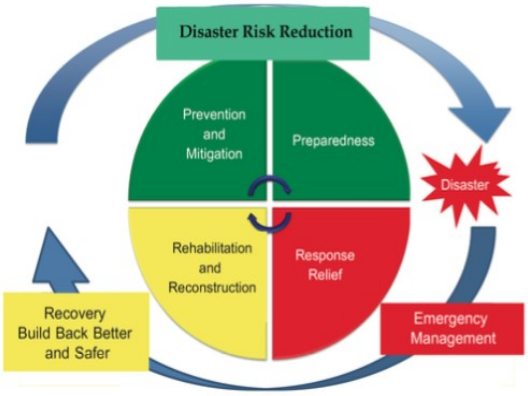

Fig. 2. Disaster Risk Management Cycle
Source: The National Disaster Risk Management Plan, Department of Disaster Prevention and Mitigation, 2015

According to policy guidelines on disaster risk reduction, the study found that 31.03 % of the respondents knew about the policy guidelines. They explained that the policy guidelines on disaster risk reduction are integrated with the community planning and multiple sectors such as governmental sector, private sector, and the network group through knowledge and training activities. In addition, respondents viewed that policy guidelines are the ways to practice pre-disaster steps, during-disaster steps and post-disaster steps in order to decrease the disaster risks. Moreover, the respondents mentioned that policy guidelines are the access information for planning before, during and after disaster. Finally, respondents noted that policy guidelines on disaster risk reduction are measure to lay down for disaster risk reduction.

Another point of views from the respondents was that policy guidelines on disaster risk reduction are necessary because it would help preventing and coping with the disaster impacts in a long term. They also indicated that the policy's achievements on disaster risk reduction are important due to the reduction of losses and damages from the disasters. The policy guidelines would ensure people in the communities to be ready to cope with the upcoming disasters in a long term. The policy actions can provide communities to response and recover the managing of the remaining disaster risk. The policy actions are also advantaged to provide the communities with well-timed disaster preparedness and capacity building on disaster occurrence.

In terms of disaster prevention and mitigation, this study reviewed that physical structures, namely concrete weirs, small dam, rock embankment were indicated by 77.78% of respondents. Meanwhile, 88.89 % of them indicated that laws and regulations are needed for the construction control in the community. Also, 100 % of the respondents unanimously agreed with stakeholder collaboration through the meeting in the community. For example, the monthly meetings among the network of Klong Yan groups should be conducted. The network of Klong Yan groups consists of the community leader, local wisdom scholars, the network of friend-warning groups, and the Forest and Sea Foundation members. This activity provides the opportunities for people to exchange knowledge and discuss the existing problems together within the community. Additionally, 77.78 % of the respondent's opinions revealed that the improvement and revision of law on disaster risk managementwill help reducing risk disaster. In local organization, there was an improvement of the action plan of disaster prevention and mitigation for sub-district administration organization every year. Besides, all respondents (100%) pointed that the educating on disaster prevention and mitigation will help people realize the necessity of the disaster management such as the methods of preparation, and evacuation practices. There was also supportive disaster management with technology of warning system such as emergency communication system, radio system, and emergency alert. There is also a usage of local wisdom in order to monitor the adverse disaster in the communities, namely the changes of the water level, the changes of colors in the river, the frequency of rainfall rates.

For a financial issue, all the respondents (100%) agreed that there should be more organizations to budget them for disaster risk management. At present, such budgets come from sub-district administration organization, Department of Disaster Prevention and Mitigation on the emergency and recovery, the Forest and Sea Foundation on agricultural development, the Coca-Cola Foundation

on reforestation and check dam and the Utokapat Foundation on mountain plumbing.

Regarding preparedness measures, all respondents (100%) are well-educated of preparedness before, during and after disaster. Those respondents stated that there is a training by using local knowledge for preparation such as the observation of the nature and surroundings such as monitoring the frequency of the rainfall, the rising level of the river, and the changing color of the river. Furthermore, there is a training on pre-evacuated preparation, for instance, the food, the medicine, the fuel supplies, and the vehicles as well as the primary and secondary routes for the emergency situation. Also, raising awareness ofthe disaster effects in the community are all agreed by 100 % of the respondents. They noted that holding a meeting on 14th day of every month makes them aware of the dangerous effects among members of Klong Yan network groups. They have exchanged information and experiences about the effects of the flood which lead others to conserve the forest in the community. Besides, the respondents also said that they try to encourage others to join the reforestation, building more weirs, and planting perennial trees in order to reduce flash floods and soil erosion as a way of raising awareness among the people.

The study found that there are many groups in the community such as the network of friend-warning groups, the network of Klong Yan groups, Klong Yan Youth Group, the network of warning friends, Mr.warning groups, the member of civil protection volunteers, and the member of health volunteers. Those groups were supported by government sectors and non-profit organizations to participate on disaster risk management in community. All the respondents (100%) also exchanged their knowledge inside and outside their community. For example, the Forest and Sea Foundation has shared their information about the sufficiency economy philosophy, organic planting, and organic agriculture to the communities, the Utokapat Foundation has shared information about water management by using local wisdom and Department of Disaster Prevention and Mitigation has shared information about disaster management.

The annual evacuation practice, based on emergency situation, was held by all the respondents (100%). This study reviewed that there is an annual evacuation practice with all sectors in the community in order to ensure enhancing capacities of preparedness for disaster risk reduction. There is also a yearly revision of the working plan of disaster prevention and mitigation by sub-district administration organization.

Furthermore, the study found that the implementation on monitoring and early warning systems in the questionnaire was chosen by all the respondents (100%). The method of monitoring would include a following-up the weather situation from television, radio, facsimile, mobile-phone, broadcast tower, broadcast mobile-car and social media as known as Line groups, and Facebook of Thai Meteorological Department. Moreover, there is a real-time monitoring the situation from the network of friend-warning groups at the upstream area by using radio system. Setting the communication system or channel to respond for warning disaster, including backup community system was also chosen by all the respondents (100%). Additionally, the result further found that there are the warning towers to broadcast the situation and activate emergency alert around the community as well as a daily morning radio communication system test by the network of radio communication groups.

On the other hand, the majority of respondents accounted for 68.97% were not familiar with the policy guidelines. They viewed that they relied on their experiences to deal with floods and other related ones such as encouraging knowledge through preparedness training for people in communities, practicing yearly evacuation plan, setting the network group for disaster warning and building check dams at the upstream.

Acknowledgment

I would like to express my sincere gratitude to my research advisor, Dr. Sangchan Limjirakan for her guidance and encouragement on my research work.

References

[1] The Intergovermental Panel on Climate Change(IPCC)(2013).Climate change: Impacts, adaptation, and vulnerability; Working Group II contribution to the fifth assessment report of the Intergovernmental Panel on Climate Change. n.d . Cambridge :Cambridge University Press.

[2] The United Nations Economic and Social Commission for Asia and the Pacific (UNESCAP). (2012).Climate Change Adaptation for Water Management in a Green Economy . United Nations publication .

[3] Nakasu, T. (2017). Natural Disasters and Disaster Management in Thailand. Natural Disasters and Disaster: Status, Risks, and Trends. Online Retrieved from: https://www.researchgate.net/publication/318446964.

[4] The Department of Disaster Prevention and Mitigation (DDPM). National Disaster Prevention and Mitigation Plan. [Online]. 2015. Retrieved from: http://www.disaster.go.th/th/dwn-download-7-1/.

[5] The Department of Disaster Prevention and Mitigation (DDPM). Incident Action Plan of Flood, Storm and Landslide at Surat Thani Province. [Online]. 2018. Retrieved

from:http:///122.155.1.141 cmsdetail.directing-/28057/6.191menu_/3897.2/4469.

[6] The Department of Disaster Prevention and Mitigation (DDPM). National Disaster Prevention and Mitigation Plan. [Online].2018. Retrieved from: http://122.155.1.141/inner.directing-6.191/cms/menu_4469/4143.1/.

[7] Tangsripong, P. (1998). Effect of Land Cover and Land Use Change on Water Qulity and Regime Flow in Klong Yan Basin. Master's Thesis, Major of Evironmental Science, Interdisciplinary, Graduate Program, Kasetsat University, pp 13-29.

[8] The Royal Thai Survey Department (RTSD). Map Topography at Kirirat Nikom and Vibhavadee Districts. [Online]. 2015. Retrieved from: https://www.rtsd.mi.th/main.

Estimation of Groundwater Recharge from GRACE Satellite and Land Surface Model

Daiya Shiojiri[1,a], Kenji Tanaka[2,b] and Shigenobu Tanaka[2,c]

Abstract Due to the dramatic growths of global population and world economy, water use is increasing. Groundwater availability is decreasing in some areas by too much groundwater abstraction. To prevent groundwater depletion, we should develop a tool to evaluate the sustainability of the groundwater use. This study aims to improve a global water cycle model in-land developed by a previous study [1] to simulate groundwater resources storage. To define appropriate amount of groundwater recharge, we compare the seasonal variations of terrestrial water storage (TWS) observed by GRACE satellite. Land surface model SiBUC is used to simulate TWS. There is a strong correlation between time series of simulated and observed TWS in many areas even if we do not include groundwater and river water storage into TWS calculation. The reason why river water storage is not considered is to exclude human activity which strongly affects natural condition. There are no data which indicates how much water is withdrawn from river water, and TWS can change significantly depending on the amount of water withdrawal from river water. By taking groundwater into account, correlation coefficient between the time series of simulated and observed TWS should be improved if the quality of meteorological forcing data is good enough. Therefore, appropriate groundwater recharge can be determined when correlation coefficient becomes highest value. The amount of groundwater recharge is regarded as the proportion of base flow (q3) simulated by SiBUC, and determining the ratio of groundwater recharge to base flow in the area where ground water withdrawal is negligible is the aim of this research.

Keywords *land surface model, terrestrial water storage, GRACE, groundwater recharge*

[1]Kyoto University
Graduate School of Engineering
Uji, Kyoto, Japan
[2]Kyoto University
Disaster Prevention Research Institute
Uji, Kyoto, Japan

[a]shiojiri.daiya.66w@st.kyoto-u.ac.jp
[b]tanaka.kenji.6u@kyoto-u.ac.jp
[c]tanaka.shigenobu.4m@kyoto-u.ac.jp

Introduction

Historically, the amount of global water use have increased twice as fast as population growth [2]. United Nations reported the world population will be 8.6 billion in 2030, and 9.7 billion in 2050 when current population is about 7.3 billion. Such rapid population growth may cause serious water shortage around the world in the future. To prevent such situation, we need to know the accurate amount of water resources in global scale to maintain sustainable water use. Especially, considering the sustainability of groundwater resources is essential because it is threaten in some areas. Groundwater depletion occurs when the amount of groundwater abstraction excesses groundwater recharge through the year [3].

For this purpose, a lot of global hydrological models were developed, and some models enable to simulate groundwater resources sustainability, for example PCR-GLOBWB [4], WaterGAP [5], HiGW-MAT [6] or H08 [7]. Shiojiri et al. [8] also simulated global water cycle in-land. In this research, the model developed by Kotsuki et al. [1] is improved to simulate groundwater resources storage. The characteristic of the model is physical representation of the irrigation water requirement in the water balance calculation. Furthermore, normalized difference vegetation index (NDVI) derived from satellite observation is used to determine the crop calendar. By using satellite data, sowing date can be identified more accurately with higher resolution compared to agricultural statistics based data Shiojiri et al. [8] visualized the non-sustainable groundwater use areas using this model. However, the result is not verified, and groundwater recharge is assumed to be 20 % of base flow. This assumption is insufficient to achieve accurate evaluation. Therefore, this research aims to simulate more accurate groundwater recharge.

To obtain better groundwater recharge, simulated terrestrial water storage (TWS) is compared with GRACE (Gravity Recovery and Climate Experiment) satellite data. Terrestrial water storage is the total amount of water in and on the ground. GRACE does not observe groundwater directly, but it is an only satellite which can observe the mass change of groundwater resources. Other models which can simulate the volume of groundwater resources (WaterGAP , HiGW-MAT and H08) do not use satellite data to simulate groundwater recharge, but use the method originally derived from field observation in most of cases. It will be difficult to

acquire accurate evaluation of groundwater resources sustainability by applying the method developed in local scale to the simulation in global scale. PCR-GLOBWB3) calculates groundwater recharge using only global elevation dataset, and this may be too simple to simulate groundwater recharge precisely. On the other hand, by analyzing the result of spatial pattern given from satellite, the groundwater recharge rate can be parameterized reflecting the diverse characteristics of each grid cell.

Methods

A. Model

Our model developed by Kotsuki et al. [1] is a distributed model consisting of land surface model SiBUC (Simple Biosphere Model including Urban Canopy) [9] and river routing model (kinematic-wave theory), but we improve only land surface model SiBUC in this research. Fig. 1 shows a schematic diagram of SiBUC. This model simulates water balance in a vertical direction by giving meteorological forcing data and land surface parameters as input data. Not only water balance but also heat and radiation balance are solved, and it makes the water balance simulation highly accurate

In SiBUC, soil layer consists of three layers and water balance is calculated between those layers. The equations indicating water exchange between those layers are derived from Darcy's low. First soil layer is surface layer and evaporation occurs from this layer. Second soil layer is root zone where transpiration occurs. Third soil layer is recharge zone, and base flow (q3) is obtained as drainage water from this layer. The volume of base flow is determined based on the sine component of mean topographic slope.

$$q_3 = k_s W_3^{2B+3} \sin\theta \tag{1}$$

Where is saturated hydraulic conductivity, is soil wetness in third soil layer, B is a parameter depending on soil type, and θ is mean topographic slope. In this equation, the excess water in the third soil layer is drained along the slope. However, a proportion of drainage water from recharge zone should infiltrate to the deep groundwater layer. Therefore, we assume groundwater recharge to be some proportion of base flow

$$rech = \alpha(q_3 - \overline{q_3}) \tag{2}$$

Where is annual mean base flow, and is an undetermined coefficient. To reflect seasonal variation of groundwater resources storage, we estimate groundwater recharge by this equation. Identifying α appears in this equation is the objective of this research.

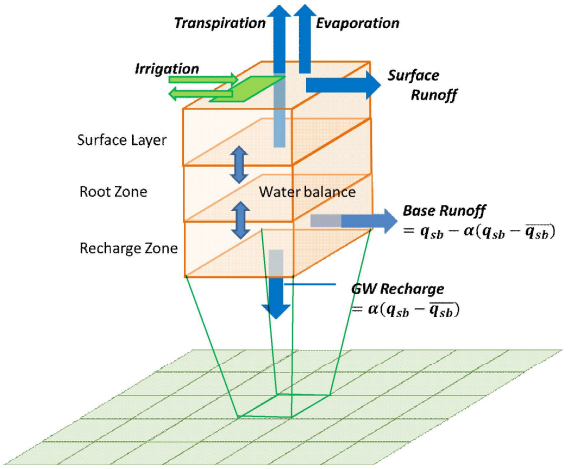

Fig. 1. Schematic diagram of SiBUC

B. Land surface and vegitation parameters

As soil and vegetation input, Ecoclimap offered by METEO France. For 1km elevation and land use, GTOPO30 and GLCC v2.0 offered by USGS (U.S. Geological Survey) are used. At the same time, MIRCA2000 [10] is used for the distribution of irrigated crop area, global rain-fed agricultural area, and crop type data. After making land cover ratio of irrigated and non-irrigated crop land using GLCC v2, it is modified to be same as MIRCA2000.

C. Meteorological forcing data

In this research, we conduct the simulation at the period of 2002 to 2017. Meteorological forcing data is required to run the model. We used Japanese 55-years reanalysis (JRA55) in this research. However, global total of yearly precipitation is much larger than other product or the datasets used other researches shown in TABLE 1. Therefore, we corrected precipitation using GPCC v6 and APHRODITE v1101. Both products are made based on field observation data. GPCC covers all over the world and APHROSITE covers Eurasian continent but mainly Asia. More observation data is used to make APHRODITE than GPCC. Thus, we used APHRODITE if there is data, or we used GPCC. However, these datasets are available only until 2006. We calculated whole period average of monthly precipitation from 2002 to 2006 and corrected JRA55 precipitation by following equation.

$$P_{corrected}^{JRA} = P_{raw}^{JRA} \times \frac{P_{mon,ave}^{GPCC+APHRO}}{P_{mon,ave}^{JRA}} \tag{3}$$

Table I. Globaltotalofyearly precipitation in-land [Gt/yr]

JRA55	144,840
GPCC_v6 and APHRODITE v1101	110,518
Kotsuki et al. (2012)[8]	99,863
Baumgartner and Reichel (1975)[11]	111,000
Hanasaki et al. (2007)[12]	108,000

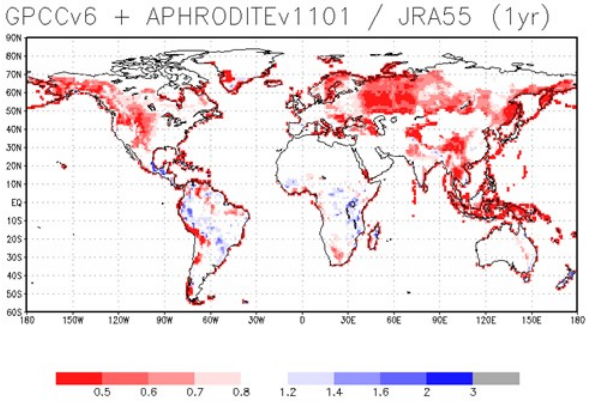

Fig. 2. Yearly average of multiplied ratio used for precipitation correction

This correction is applied only when monthly precipitation exceeds 10mm. In *Fig. 2*, yearly average of multiplied ratio is shown, but the grids whose monthly precipitation is less than 500mm are not displayed. In this figure, large difference is contained between these products. Overestimation is seen especially in Southeast Asia, and there are a lot of grids whose precipitation is 1000mm ~ 2000mm in APHRODITE but more than 3000mm in JRA55.

Results

A. Method of TWS simulation

We simulate TWS using SiBUC with following equation.

$$TWS = SM + SWE \quad (4)$$

Where SM is soil moisture and SWE is snow water equivalent. On the other hand, GRACE measures the change of total volume of water on and in the ground, and groundwater storage, river water storage and reservoir water storage are also included. However, they are not considered in our simulation. The reason why groundwater storage is not considered is that it is not modeled yet and modeling of this part from the comparison of TWS is the goal of this research. Regarding river and reservoir water storage, we exclude them to eliminate the impact of human activities. There are no data which indicates how much water is withdrawn from river water, and it depends on how water withdrawal is expressed in the model. Therefore, the distribution of the amount of river water withdrawal varies from model to model. If river and reservoir water storage are considered for TWS simulation, groundwater recharge derived from TWS comparison will differ from actual one. Thus, we consider only variables outputted by SiBUC and reproduce groundwater recharge in the area where groundwater withdrawal is negligible. By finding out the relationship between the ratio and the characteristic of the grid, we will be able to parameterize the ratio in the area human activities affect TWS variation.

This simulation is conducted from 2002 to 2017 at 1 degree spatial resolution. GRACE data is offered monthly from April 2002 to January 2017 at 1 degree after smoothed when original resolution is 300km. We selected the same resolution as offered GRACE data for this simulation. When we compare simulated TWS with measured one, we use average of three solutions (CSR, GFZ and JPL) as observed TWS to reduce the noise [13].

B. Comparison of time series of TWS

We compared the time series of observed and simulated TWS. Here, we introduce the results of some peculiar grids. Simulated TWS shown in the graphs is adjusted for the average of whole period to be the same as the one of GRACE. This is because measured TWS is not the absolute quantity but the variation.

Fig. 3 shows the time series of TWS in the center of Brasil. In this figure, both TWS time series overlap clearly and our simulation reproduces TWS in this region very well. This is because there is much precipitation in this area and main factor of TWS change is soil water. The impact of soil water against TWS variation is too large for groundwater or other factors to affect.

Fig. 4 shows the result at a grid in Thailand. These two lines fit well. *Fig. 5* shows the result without correcting precipitation at the same grid as *Fig. 4*. Simulated TWS changed significantly, and correlation coefficient decreased. Therefore, we could confirm precipitation correction is necessary.

Fig. 6 shows the result at the center of Greenland. In the GRACE variation, decreasing trend is seen. This is caused by glacier melting. [14] However, our simulation cannot reflect the effect. We have to improve our model to simulate glacier melting. When the decreasing trend seen in GRACE is removed, the influence of glacier melting should be smaller, and the time series changed to *Fig.7*. By removing trend, correlation coefficient increased a little and RMSE decreased. This means our model could simulate TWS without glacier well.

In *Fig. 8*, the result at a grid including New Delhi is shown. Groundwater depletion occurs in New Delhi [15], and we can see the decreasing trend caused by it in GRACE time series. We do not consider groundwater for TWS calculation, this decreasing trend is not seen in simulated TWS. However, when the decreasing trend is removed, correlation coefficient increased and RMSE decreased (*Fig. 8*). Therefore, we can confirm that our simulation can reproduce TWS without human activities well.

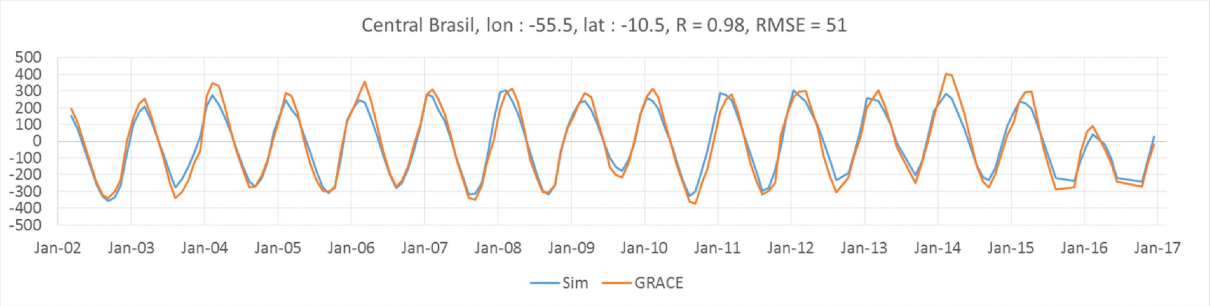

Fig. 3. Time series of TWS in the center of Brasil

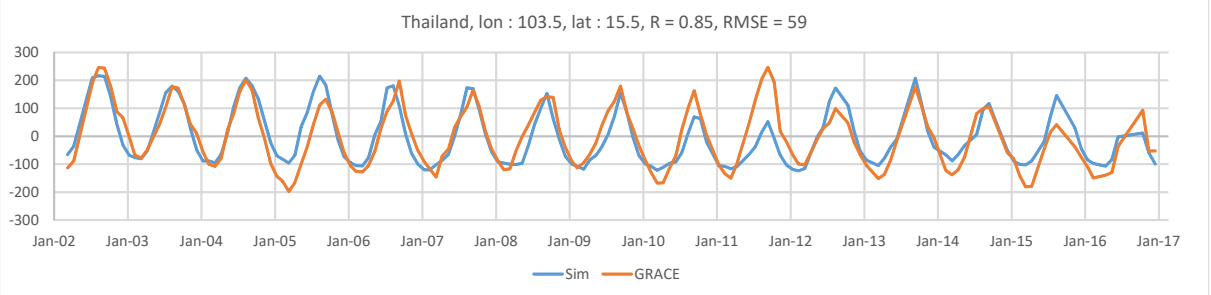

Fig. 4. Time series of TWS at northeast part of Thailand

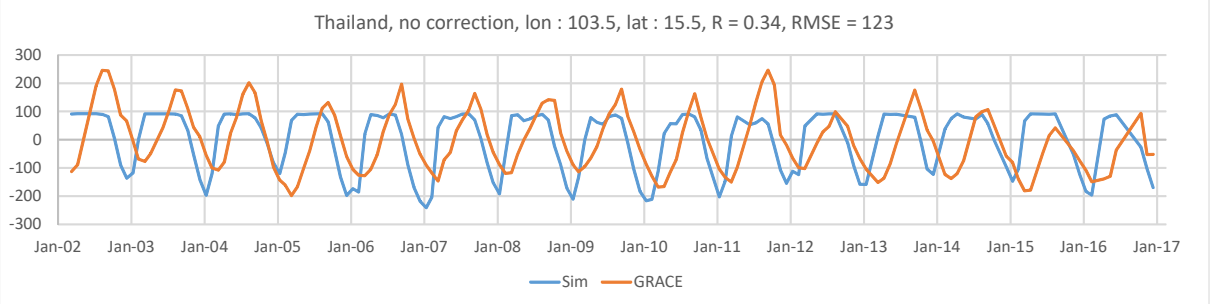

Fig. 5. Time series of TWS without precipitation correction at the same grid as Fig. 4

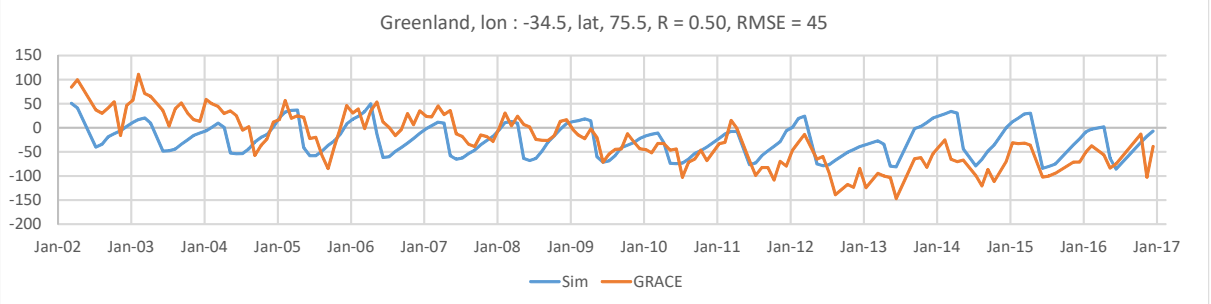

Fig. 6. Time series of TWS at the center of Greenland

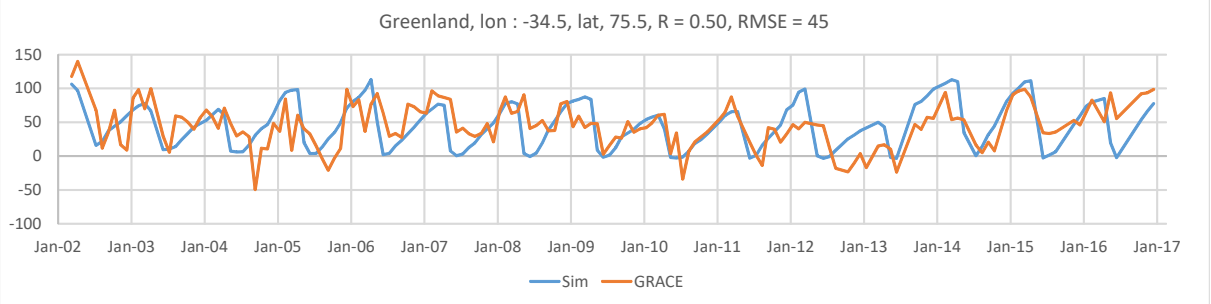

Fig. 7. Time series of TWS removed trend from GRACE at the same grid as Fig.6

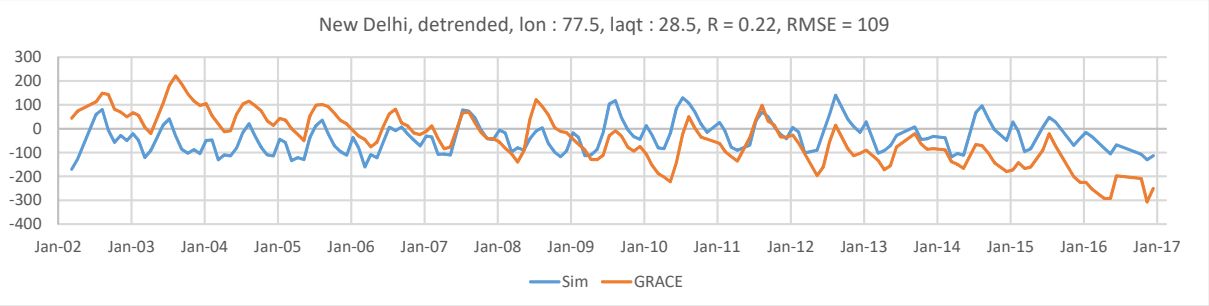

Fig. 8. Time series of TWS at a grid including New Delhi, India

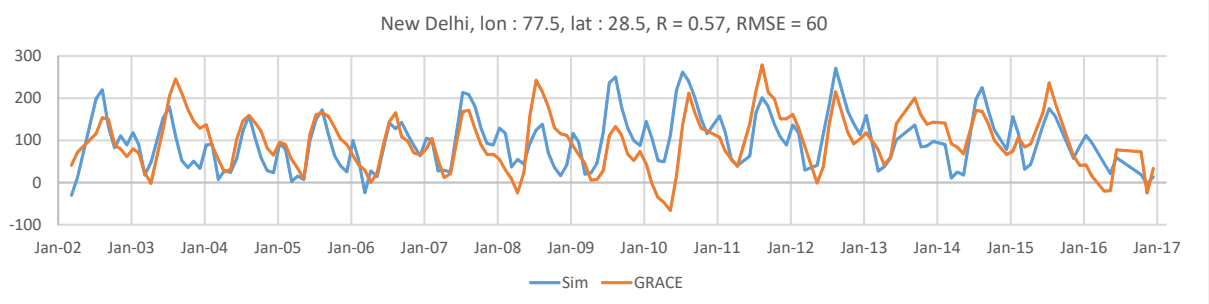

Fig. 9. Time series of TWS removed trend from GRACE at the same grid as Fig. 8

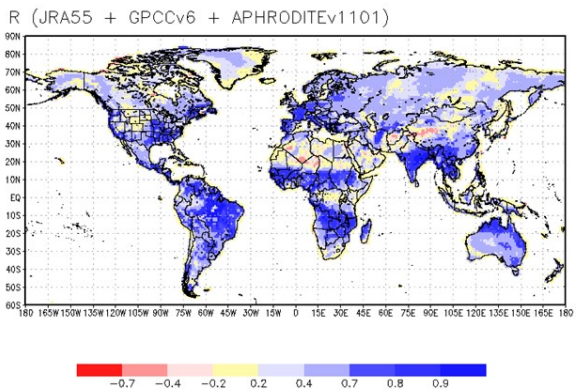

Fig. 10. Correlation coefficient of time series of simulated and observed TWS

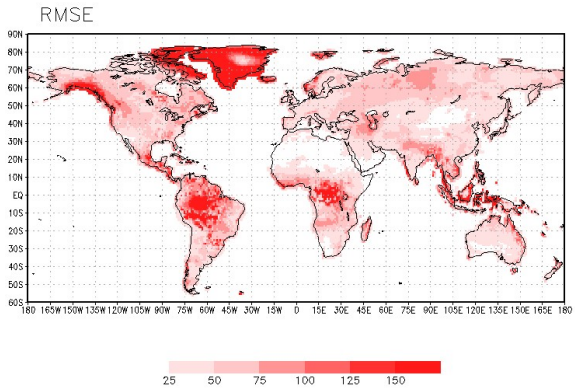

Fig. 11. RMSE between simulation and observation

C. Evaluation of simulation accuracy

We compared the time series of simulated and observed TWS representatively shown in *Fig. 3~9* at all grids. To evaluate the simulation accuracy, we calculate correlation coefficient and root mean square error (RMSE). *Fig.10* shows correlation coefficient and *Fig. 11* shows RMSE. In *Fig. 10*, strong correlation is seen at a lot of grids. However, correlation coefficient becomes low in some areas, for example north of Africa. This is because variation range of TWS is too small. In *Fig. 11*, RMSE is small in north of Africa or other grids where correlation coefficient is low, and this means the average of the difference between simulated and observed value is small. Although seasonal variation seen in measured TWS is not reproduced, the absolute quantity is reproduced well. Therefore, the accuracy of the simulation is confirmed at almost all grids.

D. Estimation of groundwater recharge

It is confirmed that TWS simulation is accurate enough without considering groundwater, river water storage or reservoir water storage. When accurate groundwater is added to TWS, correlation coefficient should be improved. We try to estimate groundwater recharge by this comparison of correlation coefficient.

Groundwater recharge is assumed to be the proportion of base flow. We estimated α appears in (2) which is necessary to calculate groundwater recharge from the comparison. At first, we added groundwater to TWS with various α value. Next, we calculate the correlation coefficient between GRACE data and the TWS including groundwater. When the correlation coefficient became maximum, we assumed the ratio as appropriate value. Estimated α is shown in *Fig. 12*. In this figure, there are many grids whose value is 0 or 1. When α is 0, it means the variation of

simulated SM and SWE is too large. On the contrary, when the ratio is 1, simulated SM and SWE are small or the influence of river water storage or human activity is large. However, we do not validate the accuracy of α. To confirm the accuracy, we have to examine whether there are the relationships between the ratio and the characteristic of the grid, for example slope, soil type, elevation, and so on. If we can find out the relationship, parameterization of α in global scale becomes possible, and we can evaluate the influence of human activities by comparing GRACE data and simulated TWS including groundwater and human activities.

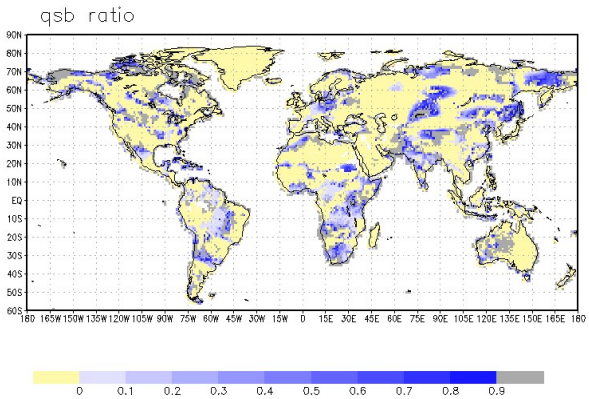

Fig. 12. Estimated α in (2)

Conclusions

We simulated TWS as sum of SM (soil moisture) and SWE (snow water equivalent) to estimate groundwater recharge from the comparison with GRACE satellite data. At that time, we did not consider groundwater, river water storage and reservoir water storage in order to eliminate the influence of human activities. Therefore, we could not reproduce the decreasing trend measured by GRACE whose cause is too much extraction of groundwater. This will be reproduced after we can estimate groundwater recharge appropriately. Long term decreasing trend caused by glacier melting was not reproduced either because we did not incorporate that module. Evaluation of glacier melting will be possible by putting a lot of snow as initial condition on the ground in a land surface model.

By comparison with GRACE satellite data, we could confirm our simulation reproduced TWS well. If groundwater is included into TWS calculation, correlation coefficient should be higher. Therefore, we added groundwater to TWS with various α which appears in (2), and we assumed α to be the appropriate value when correlation coefficient becomes maximum. By this method, we could estimate α and groundwater recharge. To find out the relationship between the ratio and the characteristics of the land is a future work. Using other satellite datasets is also a future work in order to separate each component of TWS. For example, we can separate soil moisture by using SMAP, or SMMR enables to separate SWE. More accurate groundwater recharge will be obtained by these satellite datasets.

References

[1] S. Kotsuki, K. Tanaka, T. Kojiri, T. Hamaguchi, "Simulation of global water cycle in land using a crop calendar specified by phenological analysis of NDVI," J. Japan Soc. Hydrol. and Water Resour., Vol. 25, No.6, 373 – 388, 2012.

[2] I. A. Shiklomanov, "World water resources and their use," a joint SHI/UNESCO product, 1999

[3] Gleeson, T., J. VanderSteen, A. A. Sophocleous, M. Taniguchi, W. M. Alley, D. M. Allen, and Y. Zhou, "Groundwater sustainability strategies," Nat. Geosci., 3, Commentary, 378–379, 2010

[4] P. Döll, H. Hoffmann-Dobrev, F. T. Portmann, S. Siebert, A. Eicker, M. Rodell, G. Strassberg, , and B. R. Scanlon, "Impact of water withdrawals from groundwate r and surface water on continental water storage variations," J. Geodyn., 59–60, 143–156, 2012.

[5] Y. Wada, L. P. H. van Beek, C. M. van Kempen, J.W. T. M. Reckman, S. Vasak, , and M. F. P. Bierkens, "Global depletion of groundwater resources," Geophys. Res. Lett., 37, L20402, 2010

[6] Y. Pokhrel, N. Hanasaki, S. Koirala, J. Cho, P. J. F. Yeh, H. Kim, S. Kanae, and T. Oki, "Incorporating Anthropogenic Water Regulation Modules into a Land Surface Model," J. Hydrometeorol., 13, 255–269, 2012.

[7] N. Hanasaki, S. Yoshikawa, T. Pokhrel, and S. Kanae, "A global hydrological simulation to specify the sources of water used by humans," Hydrol. Earth Syst. Sci., 22, 789-817, 2018.

[8] D. Shiojiri, K. Tanaka, S. Tanaka, T. Hamaguchi, "Estimation of global distribution of water stress considering groundwater withdrawal," Global Env. –JSCE, Vol. 72, No. 5, 265-270, 2016.

[9] K. Tanaka, "Development of the new land surface scheme SiBUC commonly applicable to basin water management and numerical weather prediction model," doctoral dissertation, Kyoto University, 2004.

[10] F. T. Portmann, S. Siebert, P. Doll, "MIRCA2000 －global monthly irrigated and rainfed crop areas around the year 2000: a new high-resolution data set for agricultural and hydrological modeling," Global Biogeochemical Cycles 24: 1-24, 2010.

[11] A. Baumgartner, E. Reichel, "The world water balance－mean annual global, continental and maritime precipitation, evapotranspiration and run-off," Elsevier, Scientific, 210, 1975.

[12] N. Hanasaki, N. Utsumi, T. Yamada, Y. Shen, M. Bengtsson, S. Kanae, M. Otaki, T. Oki, "Development of a global integrated water resources model for water resources assessments

under climate change," J. Hydraul. Eng.-JSCE, 51, 229-234, 2007.

[13] C. Sakumura , S. Bettadpur, S. Bruinsma, "Ensemble prediction and intercomparison analysis of GRACE time - variable gravity field models," Geophys. Res. Lett., 41, 1389-1397, 2010.

[14] J. L. Chen, C. R. Wilson, B. D. Tapley, "Satellite gravity measurements confirm accelerated melting of Greenland ice sheet," Science 29, Vol. 313, Issue 5795, pp. 1958-1960, 2006.

[15] M. Rodell, I. Velicogna, J. S. Famiglietti, "Satellite-based estimates of groundwater depletion in India," Nature vol-ume 460, 999–1002, 2009

Perception of climate change and adaptation in rural area in Thailand

Kyoko MATSUMOTO[1,a], Sompratana RITPHRING[2], Masashi KIGUCHI[1] and Taikan OKI[3,4]

Abstract This research was conducted to clarify to 1) understand local people's perception of climate change and adaptation, and 2) figure out climate information collection and sharing in vulnerable rural area in Thailand. Data were collected using semi-structured interview and questionnaire survey from a total sample of 297 households in Songkhla province. As a result, it was found that natural disaster which link to life directly such as storm, high tide, stream erosion, typhoon, land slide, flash flood is considered to become more serious in future. 95.6% of respondents they perceived local climate change, and 79.6% of respondents answered that their life styles were affected by climate change. Nevertheless, 53.6% of respondents answered that "I do not have willingness to adapt to climate change" and "I cannot decide whether I will take adaptation measures or not" from a long-term perspective. The proportion of respondents who perceive that their lifestyles have been changed by climate change or natural disaster is high. However, even if the frequency of natural disaster increase, those who have willingness to do adaptation is less than half of respondents. Moreover, it is recommended that to make climate information spread from various sources. Especially local government is considered to have higher reliability. It is also to be noted that "local wisdom" namely their own experiences such as observation changes of cloud, moon, sky and ocean also has high reliability. It is worthwhile to dispatch adaptation information incorporating local wisdom. In addition, to construct system to share the information among the community residents is effective.

Keywords *Perception of climate change, adaptation to climate change, climate information collection*

[1]Institute of Industrial Science,
The University of Tokyo,
Meguro-ku, Tokyo, Japan
[2]Faculty of Engineering,
Kasetsart University,
Bangkok, Thailand
[3]Rector's Office,
United Nations University,
Shibuya-ku, Tokyo, Japan
[4]Integrated Research System for Sustainability Science,
The University of Tokyo,
Bunkyo-ku, Tokyo, Japan

[a]matsumoto@rainbow.iis.u-tokyo.ac.jp

Introduction

Rural area is dependent on natural resources that are prone to be affected by climate changes, especially serious effect on those who live in vulnerability areas. Local adaptation strategies are necessary to mitigate the impact of climate change. Thailand ranked number 10 of 180 nations most affected in the period from 1996 to 2015 (annual average) by "The Long-Term Climate Risk Index (CRI)" [1]. Thailand is vulnerable to extreme weather events such as tropical storms, floods and drought. For tackling these issues, Thai government formulated "Climate Change Master Plan 2015-2050" in 2015. The vision is to achieve climate resilience and low carbon growth in accordance with sustainable development agenda. This master plan has 3 key approaches such as adaptation, mitigation and capacity building. "Thailand's National Adaptation Plan" has been projected and the implementation process will be started from 2018 to 2021. They concerning information on gaps and needs of local level is necessary, however limited [2].

In previous research on people's perception of climate change in Thailand, Manandhara, Pratoomchaia, Ono, Kazama and Komori found that nearly 45% of households have personally perceived climate change. More than 70% of households have perceived droughts and floods impacts on their livelihoods but have not completely understood their causes [3]. Pratoomchai, Kazama, Manandhar, Ekkawatpanit, Saphaokham, Komori and Thongduang clarified that examining the people's perception of different generations, people who are≥41 years old shared almost the same people's perception, and the people who are≤40 years old showed more awareness of climate change impacts. From an optimistic point of view, the younger generation realized potential climate change impacts [4]. According to earlier study by Henry, Kawasaki and Meguro, the most socially vulnerable with low-income, middle school graduate and below, 60 years of age or more face to difficulty to access to information on climate [5]. The coastal vulnerability to erosion considering a disaster leading to land loss in Songkhla province in the Lower Gulf of Thailand was evaluated by Ritphring and Sungngam. The vulnerability level of coastal area of Songkhla province is categorized into very high, high, moderate, low and very low by coastal characteristic, coastal forcing and socio-economic [6].

As far as we know, there have been few reports about people's perception of climate change and adaptation, information collection and sharing in vulnerability rural area in Thailand. This research aimed to 1) understand local people's perception of climate change and adaptation, and 2) figure out climate information collection and sharing in vulnerability rural area in Thailand.

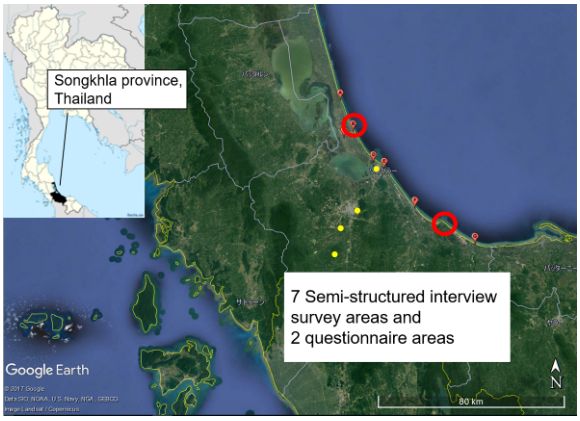

Fig. 1. Location of study area

Materials and methods

A. Study area

This study focuses on vulnerable rural area to climate impact. 2 villages in coastal areas where categorized the coastal vulnerability level is high were selected as study areas in Songkhla province. Songkhla province is located southern part of Thailand, occupies an area of 7393 square kilometers with the coastline length about 158 kilometers [7]. The coastal area in Songkhla province are potentially vulnerable to erosional hazard [6]. According to census in 2000, Songkhla has 1,255,700 total population consisting 76.6% of Buddhism and 23.2% of Muslims. The average years of education attainment aged 15 years and over is 7.5 years, and population aged 6-24 years not attending school is 36.5%. The ration of occupations are employers is 2.0%, own account workers is 33.1%, employees is 41.4% and unpaid family workers is 23.4% [8].

B. Data collection

Data were collected using semi-structured interview and face to face questionnaire survey from a total sample of 297 households in Songkhla province. The semi-structured interview was conducted in 7 coastal areas in Songkhla province to extract components of questionnaire about perception, information collection and sharing of climate change and adaptation using previous studies as references (TABLE I.) [5, 9, 10, 11]. The questionnaire was developed based on the semi-structured interview and distributed to 300 households in 2 villages where were categorized coastal vulnerability level is high [6]. The data from questionnaires were collected in 2018. Fig.1. shows location of study area. TABLE I. shows outline of questionnaire survey.

Table I. Research outline

Topic	Question	Scale
Climate change	Perceive of climate change[9, 10]	Multiple-choice
	Long-term view on climate change	Multiple-choice
Adaptation	Adaptation to climate change	Multiple-choice
	Behavioral intention towards adaptation	Single-choice
Climate information	Access to climate information	Single-choice
	Climate information sources [5]	Multiple-choice
	Reliability of information sources	4 scales
	Climate information sharing [11]	Single-choice
Personal attribute	Age, gender, occupation, income, educational level, religion, disaster experience	-

Result and discussion

298 questionnaires were returned with a response rate of 99.0%. The attributes of questionnaire responses are shown in Fig. 2. The attributes of respondents were fifties (29.9%) and forties (24.8%), office worker/organization staff (25.7%), independent business (25.0%), Islam (95.3%) and natives of the study area (78.3%) have higher proportions.

Topic	Item	Number of responses	Ratio of responses for each item
Age	Under 20 years old	2	0.7
	Twenties	7	2.4
	Thirties	35	11.9
	Forties	73	24.8
	Fifties	88	29.9
	Sixties	61	20.7
	Seventies	22	7.5
	Over 80 years old	6	2.0
Gender	Male	226	77.9
	Female	64	22.1
Occupation	Office worker/ organization staff	76	25.7
	Independent business	74	25.0
	Forestry	47	15.9
	Government employee	31	10.5
	NPO/NGO	29	9.8
	Fishery	21	7.1
	Agriculture	10	3.4
	Part time job	4	1.4
	Housewife	1	0.3
	Student	1	0.3
	Middle of job hunting	1	0.3
	Without occupation	1	0.3
Religion	Buddhism	11	3.7
	Islam	286	96.3
Hometown	This village	235	79.9
	Other places	59	20.1

Fig. 2. Attribute of the questionnaire responses

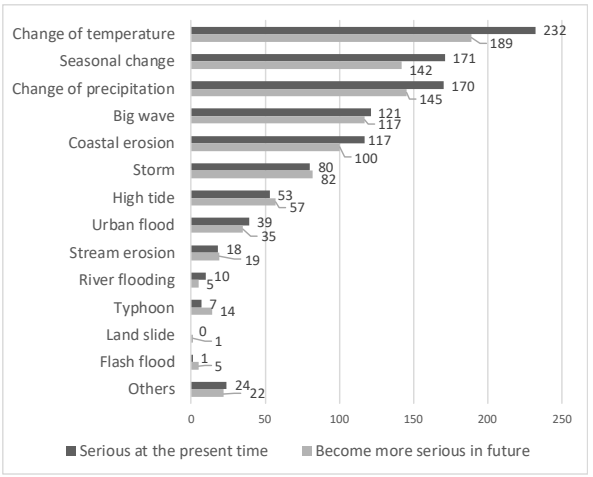

Fig. 3. Perception of climate change (Multiple-answer)[a]

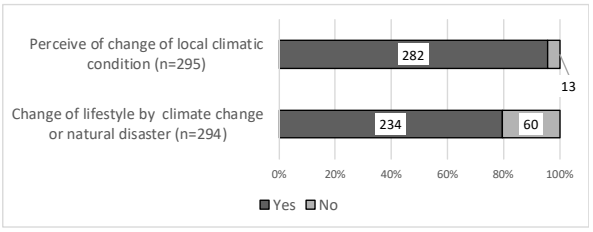

Fig. 4. Perceive of change of local climatic condition and lifestyle[a]

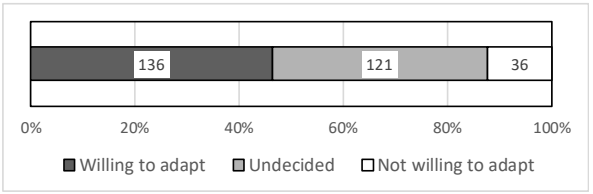

Fig. 5. Perception of adaptation implementation (n=293) [a]

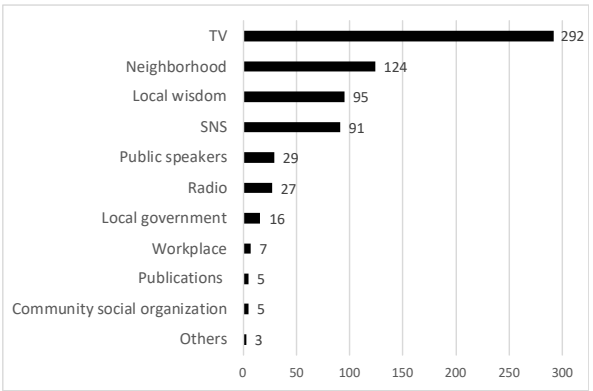

Fig. 6. Sources of climate information (Multiple-answer) (n=292) [a]

[a.]The numbers in fig. 3.4.5. 6. show the number of respondents.

A. Perception of climate change and adaptation

It was found that 81.4% of respondents of questionnaire survey answered that "Change of temperature is serious at the present time". Next to change of temperature, the percentage of respondents are high in the order of seasonal change (60.0%), change of precipitation (59.6%), big wave (42.5%), coastal erosion (41.1%), storm (28.1%). On the other hand, 65.2% of respondents answered that "Change of temperature will become more serious in future" from a long-term perspective. Next to change of temperature, the percentage of respondents are high in the order of change of precipitation (50.0%), seasonal change (49.0%), big wave (40.3%), coastal erosion (34.5%) and storm (28.3%) (Fig. 3.). Natural disasters which link to life directly such as storm, high tide, stream erosion, typhoon, land slide, flash flood is considered to become more serious in future was found.

Fig. 4. shows perceive of change of local climatic condition in the past decade and change of lifestyle by climate change or natural disaster. It was found that 95.6% of respondents answered that they perceived local climate change, and 79.6% of respondents answered that their life styles were affected by climate change. Nevertheless, as shown in Fig. 5., 53.6% of respondents answered that "I do not have willingness to adapt to climate change" and "I cannot decide whether I will take adaptation measures or not" from a long-term perspective. The proportion of respondents who perceive that lifestyles have been changed by climate change or natural disaster is high. However, even if the frequency of natural disaster increase, those who have willingness to do adaptation is less than half of respondents.

B. Climate information collection and sharing

We found that 99.3% of respondents got climate information from TV. Next to TV, the percentage of respondents are high in the order of neighborhood (46.2%), SNS (Social Network Services) (33.9%), local wisdom namely their own experiences such as observation changes of cloud, moon, sky and ocean (33.6%) (Fig.6.). Regarding reliability of information resources, the highest percentage of "very reliable" information source is local government (77.8%) (n=18). Next to local government, the percentage of respondents are high in the order of local wisdom (59.2%) (n=98), radio (56.1%) (n=41) and TV (53.8%) (n=290) (Fig.7.). Fig.8. reveals information sharing. 93.5% of respondents share the climate information with neighborhood directly. Next to neighborhood, the percentage of respondents are high in the order of "no one" (3.6%), "with coworkers directly" (2.5 %), "community social organization" (0.4%), "SNS" (0%) and "others" (0%). Here it can be seen that it is necessary to spread information from various sources, especially local government and local wisdom have higher reliability.

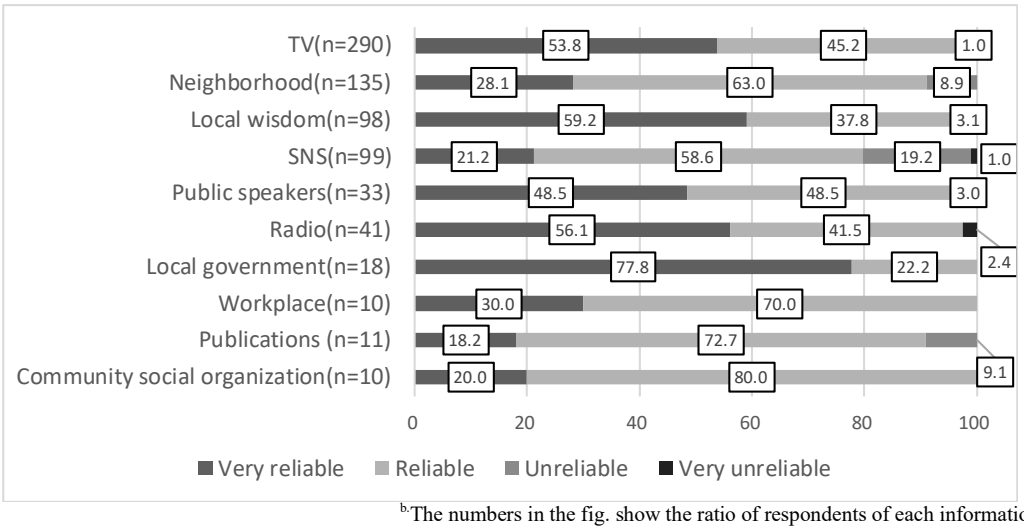

[b] The numbers in the fig. show the ratio of respondents of each information sources.

Fig. 7. Reliability of each information sources [b]

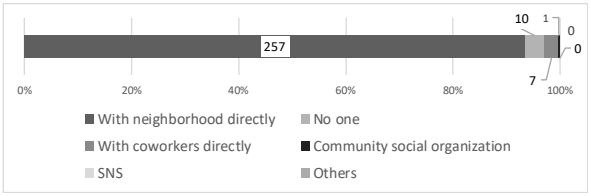

[c] The numbers in the fig. show the number of respondents.

Fig. 8. Climate information sharing (n=275) [c]

Conclusions

We can deduce the following: 1) It is shown that natural disasters which link to life directly are considered to become more serious in future was found. The proportion of respondents who perceive their lifestyle have been changed by climate change is high, however, raising awareness of implementation of adaptation to climate change is still necessary. 2) It is recommended that to make climate information spread from various sources, especially local government. It is also to be noted that "local wisdom" also has high reliability. Therefore, it is worthwhile to dispatch adaptation information incorporating local wisdom. Moreover, the system to share information among the community residents is effective.

Acknowledgment

This research was supported by "Advancing Co-design of Integrated Strategies with Adaptation to Climate Change in Thailand (ADAP-T)" supported by the Science and Technology Research Partnership for Sustainable Development (SATREPS), JST-JICA.

References

[1] Sönke Kreft, David Eckstein and Inga Melchior, "GLOBAL CLIMATE RISK INDEX 2017" Eds. Joanne Chapman-Rose, Daniela Baum, Germany: Germanwatch e.V., November 2016. https://reliefweb.int/sites/reliefweb.int/files/resources/16411.pdf.

[2] Kollawat Sakhakara, "Thailand's National Adaptation Plan (NAP)Processes", United Nations Development Programme, 2017. https://adaptation-undp.org/resources/presentation/thailand%E2%80%99s-national-adaptation-plan-nap-processes.

[3] Sujata Manandhara, Weerayuth Pratoomchaia, Keisuke Ono, So Kazamaand Daisuke Komori "Local people's perceptions of climate change and related hazards in mountainous areas of northern Thailand", International Journal of Disaster Risk Reduction, Volume 11, March 2015, pp. 47-59.

[4] Weerayuth Pratoomchai, So Kazama, Sujata Manandhar, Chaiwat Ekkawatpanit, Somkid Saphaokham, Daisuke Komori and Jaray Thongduang "Sharing of people's Perceptions of Past and Future Hydro-Meteorological Changes in the Groundwater Use Area", Water Resour Manage, 29, May 2015, pp. 3807-3821.

[5] Michael Henry, Akiyuki Kawasaki and Kimiro Meguro, "Information collection of disadvantaged populations during the 2011 Thai flood", Journal of social safety science, No.21, November 2013, pp. 241-250. (In Japanese)

[6] Sompratana Ritphring and Sarawut Sungngam "The Assessment for Coastal Erosion Vulnerability : A Case Study of Songkhla, Thailand", The 11th Regional Conference on Environmental Engineering 2018 (RCEnvE-2018)Jointly held with The 3rd International Symposium on Conservation and Management of Tropical Lakes "Enhancing

Sustainability and Resilience under Anthropogenic Pressure and Climate Change", Cambodia, September 2018, pp. 251-253.

[7] Department of Marine and Coastal Resources "Marine and coastal resources: Songkhla", Thailand, 2018. http://www.dmcr.go.th/detailLib/3756. (In Thai)

[8] National Statistical Office, Ministry of Information and Communication Techonlogy "(SONGKHLA) Key indicators of the population and households, Population and Housing Census 1990 and 2000", Thailand, http://web.nso.go.th/census/poph/finalrep/songkhlafn.pdf.

[9] Byron Zamasiya MSC, Kefasi Nyikahadzoi and Billy Billiard Mukamuri, "Factors influencing smallholder farmers' behavioural intention toward adaptation to climate change in transitional climatic zones: A case study of Hwedza District in Zimbabwe", Journal of Environmental Management , August 2017, pp. 233-239.

[10] Uttam Khanal, Clevo Wilson, Viet-Ngu Hoang and Boon Lee, "Farmers' Adaptation to Climate Change, Its Determinants and Impacts on Rice Yield in Nepal", Ecological Economics, February 2018, pp. 139-147.

[11] Kenichirou Onitsuka and Satoshi Hoshino, "The Actual Situation of Information Sharing by Word of Mouth and Challenges for the Improvement in Rural Areas: Quantitative Study through Social Network Analysis by Utilizing 2-mode Data focusing on Receiving Organization Affi liations", Journal of Rural Planning Association, 34, 1, 2015, pp. 67-76. (In Japanese)

Enhancing the Roles of Groundwater in the Context of the Sustainable Development Goals via Aquifer Vulnerability Assessment

Sasin Jirasirirak[1,a], Aksara Putthividhya[1,b] and Aranya Fuangsawasdi[2,c]

Abstract Groundwater resources in Thailand have become central to socio-economic development over the course of decades, including providing water for domestic use, enabling food production, and sustaining critical ecosystems function. In some parts of the country, groundwater is often preferred over surface water because of its relative stability in terms of both quality and quantity. Sustainable and equitable groundwater use plays a critical role in the context of SDGs as follows: groundwater is most explicitly linked to ensuring availability and sustainable management of water and sanitation for all (SDG 6); and groundwater can also directly contribute to poverty eradication (SDG 1), food security (SDG 2), gender equality (SDG 5), sustainability of cities and human settlement (SDG 11), combating climate change (SDG 13), as well as protecting terrestrial ecosystems (SDG 15). Overall sustainable groundwater use can only be achieved through policy recommendation and implementation related to proper monitoring, management and governance that uses integrated and precautionary approaches while giving appropriate attention to the potential boundary nature of groundwater. For such implementation of the SDGs at the strategic policy making-level, assessing groundwater quality at the larger scale is particularly important for designing efficient monitoring strategies in sustainable water resources management plans. For our nation's groundwater resource, there is also evidence to suggest that the quality of groundwater is also under threats as a result of high concentrations of human/economic activities (e.g., industrial, agricultural and household). Numerous groundwater contaminated sites have been reported from both natural and anthropogenic activities with extent of plume migration, leading to a degrading quality of groundwater which is unacceptable for safe human consumption. Therefore, this paper attempts to assess vulnerability and pollution risk of groundwater by compilation of the most recent local- to regional-scale information on all major soil, land use, geology, hydrogeology, surface pollution sources, and climate conditions in Geographical Information System (GIS)-based environment in the Central and Northern parts of Thailand where groundwater resources are overexploited and an unknown number are experiencing pollution problems and/or degradation of groundwater dependent ecosystems. Groundwater vulnerability maps are constructed by means of DRASTIC method involving overlaying the DRASTIC vulnerability map with land use and potential pollution sources. Linear regression statistical analysis between rainfall-groundwater depth and adjusted hydraulic conductivity (K) are applied to modify some parameters in the original DRASTIC model. Some area in the central Chao Phraya region is dominated by high pollution risk classes and this is very strongly related to shallow groundwater systems and the development of agricultural activities. DRASTIC mapping models are validated using observed nitrate data in groundwater as a proxy of pollution risk. The original DRASTIC model provides a conservative estimate of low risk while the advanced DRASTIC model shows better regression coefficient between the vulnerability index and nitrate concentration.

Keywords *SDG, groundwater vulnerability, GIS, remote sensing, DRASTIC, risk map*

[1]Department of Water Resources Engineering
Chulalongkorn University
Bangkok, Thailand
[2]Department of Groundwater Resources Thailand
Bangkok, Thailand

[a]Sasin_sk@gmail.com
[b]Dr.aksara.putthividhya@gmail.com
[c]faranya@gmail.com

Introduction

Groundwater is one of the most valuable natural resources, which supports human health, economic development and ecological diversity [**1-3**]. It has been recognized as the major and sometimes the preferred source of drinking water in rural as well as urban areas due to its relative stability in terms of both quality and quantity as it caters up to 80% and 50% of the total drinking water and agricultural water requirement in many parts of Thailand, respectively. The occurrence of drought and heavy rainfall are the most important climatic extremes having both short- and long-term impacts on the groundwater availability. Besides the natural forces creating pressure on water resources, ever-increasing human water demand have become the primary drivers of the pressure affecting our water systems.

Sustainable and equitable groundwater use plays a critical role in the context of SDGs as follows: groundwater is most explicitly linked to ensuring availability and sustainable management of water and sanitation for all (SDG 6); and groundwater can also directly contribute to poverty eradication (SDG 1), food security (SDG 2), gender equality (SDG 5), sustainability of cities and human settlement (SDG 11), combating climate change (SDG 13), as well as protecting terrestrial ecosystems (SDG 15). Overall sustainable groundwater use can be achieved through policy recommendation and implementation related to proper monitoring, management and governance that uses integrated and precautionary approaches while giving appropriate attention to the potential boundary nature of groundwater. For such implementation of SDGs at the strategic policy making-level and defining sustainable water resources management plans at the national scale, assessments of groundwater resources quantitatively and qualitatively as well as other associated pressures are strongly needed [**4**] for designing efficient monitoring strategies in sustainable water resources management plans.

Several efforts have been undertaken by academic researcher along with Department of Groundwater Resources Thailand (DGR) to improve the knowledge of groundwater systems in Thailand both at local- and national-scales. Studies have confirmed that groundwater in Thailand is abundant and subjected to different pollution pressure exerted by several sources as a results of high concentrations of human/economic activities from industrial, agricultural, and household, such as leaking sewage systems, solid waste dumpsites, household waste pits, surface water infiltration spots, agricultural activities, petrol service stations (i.e., underground storage tanks), and abandoned wells. Numerous groundwater contaminated sites have been reported from both natural and anthropogenic activities with extent of plume migration, leading to a degrading quality of groundwater which is unacceptable for safe human consumption. According to our evaluation, the major issues of surface water/groundwater quality in Thailand may be listed as follows: i) nitrate pollution; ii) heavy metal pollution; iii) pathogenic agents; iv) organic pollution (e.g., hydrocarbons and volatile organic compounds; v) salinization; and vi) acid mine drainage. At the national- and regional-scales, studies include the development of Thai National groundwater maps, the assessment of groundwater potential, the assessment of basin yield, storage capacity, flow types and saturated thickness, drought vulnerability, and groundwater quality baseline mapping. Assessing groundwater vulnerability and pollution risk at the large scale is necessary and particularly important for monitoring progress in sustainable development and the implementation of the UN SDGs for water.

In this context, assessing the groundwater vulnerability for pollution is important for designing efficient regional scale groundwater management and protection strategies. When dealing with groundwater vulnerability, a difference can be made between ***specific vulnerability*** and ***intrinsic vulnerability*** [**5**]. Intrinsic vulnerability of an aquifer can be defined as the capacity with which a contaminant introduced at the ground surface can reach and diffuse in groundwater [**6**]. Specific vulnerability, on the other hand, is used to define the vulnerability of groundwater to a particular contaminant or a group of contaminants. For specific vulnerability, specific physic-chemical properties from contaminants should be considered [**7**]. Groundwater pollution risk can be defined as the process of estimating the possibility that a particular event may occur under a given set of circumstances [**8**] and the assessment is achieved by overlaying hazard and vulnerability [**7, 9]**. Several approaches exist for assessing groundwater vulnerability as they can be grouped into methods based on the use of i) process-based simulation models; ii) statistical models; and iii) overlay and index methods [**7, 10, 11, 12**]. Alternatively, they can be classified according to the degree of integration of monitoring data in the vulnerability assessment **[13]**. Hence, distinction can be made between vulnerability assessment methods based on generic data, based on groundwater monitoring data, or hybrid methods based both on monitoring and generic data.

Within the class of generic data based methods, the most established method worldwide is the DRASTIC method [**14, 15]**. The method has been widely used for regional vulnerability assessments in many parts of the world, including USA **[16, 17]**, China **[18]**, Canada **[19**], India **[20]**, Turkey [**21]**, Tunisia [**22, 23**], and South Africa [**24]**. The DRASTIC method, as like similar index models, has many advantages: i) the method has a low cost of application and can be applied at the regional scale, because it is based on often easily available generic data [**14]**); and ii) the use of a high number of input data layers is believed to limit the support of errors or uncertainties of the individual data layer in the final output [**25; 26]**. Despite its popularity, the DRASTIC method has as well some disadvantages [**27]**. First, many variables are factored into the vulnerability index. All these factors are not necessarily sensitive for groundwater vulnerability for a particular setting [**6]**. Hence, in many cases vulnerability can be explained with a subset of DRASTIC factors. Second, studies based on DRASTIC method tend to overestimate the vulnerability of porous media aquifers compared to aquifers of fractured media [**26**]. Third, only a few studies have been performed to validate the DRASTIC vulnerability method at the regional scale. Despite these disadvantages, the DRASTIC method can easily be deployed to make continental scale assessment of groundwater vulnerability.

The major attempts in this study are therefore to assess the groundwater vulnerability using the DRASTIC indicator methodology by compilation of the most recent local- to regional-scale information on all major soil, land use, geology, hydrogeology, surface pollution sources, and climate conditions in Geographical Information System (GIS)-based environment in the Central and Northern parts of Thailand where groundwater resources are overexploited and an unknown numbers are experiencing pollution problems and/or degradation of groundwater dependent ecosystems. As some area in the central Chao Phraya region is dominated by high pollution risk classes and this is believed to be strongly related to shallow groundwater systems and the development of agricultural activities. Linear regression statistical analysis between rainfall-groundwater depth and adjusted hydraulic conductivity (***K***) are applied to modify some parameters in the original DRASTIC model. The final original and modified DRASTIC mapping models are validated using observed nitrate data in groundwater as a proxy of vulnerability and pollution risk.

Materials and Methods

A. Study Area

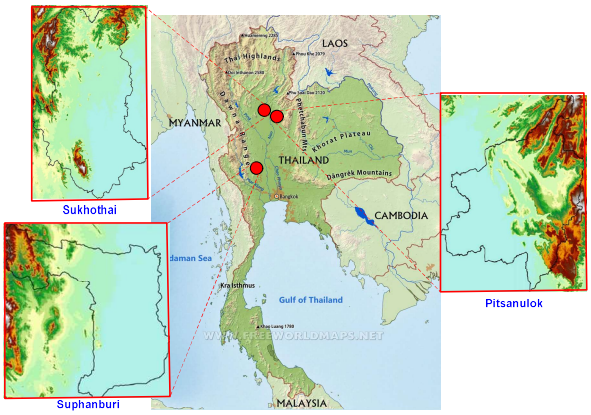

Fig.1 Study Area.

Pitsanulok, Sukhothai, Suphanburi, and Chanchoengsao are the focusing areas selected for this study as illustrated in **Fig. 1**. Sukhothai and Pitsanulok provinces are located in the upper central plain of Thailand covering approximately 18,000 km^2. The main landuse is 63% agricultural, out of which 21% is irrigated and 24% forest. The basin is surrounded in the East and West by volcanic rocks. The average elevation of the basin is 40-60 m above mean sea level. The basin drains into the lower basin in the South where some free discharge is partially obstructed by crystalline rocks. The 900-1,450 mm annual rainfall within the study region is apportioned to 81% in the wet season (April-September) and 19% in the dry season (October-March).

Suphanburi province is approximately 100 km west of Bangkok, the Capital city of Thailand. Topography is mainly flood plain in the east and mountainous areas in the west. Agricultural land covered much of the flood plain in the eastern and southeastern parts of the study area. Approximately 42% of the study area is occupied by forest, 35% by agricultural land, and 23% by others (such as urban areas and water bodies). The major field crops are rice and sugarcane (cover more than 50% of the total agricultural area). Average annual rainfall of 976 mm was reported for the entire province based on 30 years period of data (between 1989-2008) with the peak rainfall in September. **Ramnarong (1993)** [**28**] described that the study area has been hydrologically divided into highland and lowland areas, in which groundwater occurs in several consolidated and unconsolidated aquifers, underlying most of the agricultural lowland. These aquifers consisted of gravel, sand, and clay of deltaic plains, recent alluvial plains, and rolling terraces. Yields of all aquifers in the study area range from 1-50 m^3/yr.

B. DRASTIC Model

In the present study, DRASTIC method is employed for evaluating groundwater vulnerability for pollution. The acronym DRASTIC corresponds to the initials of the seven variables that drives vulnerability as defined according to **Aller et al. (1987)** [**14**] and shown in **Table 1**.

The DRASTIC vulnerability index was carried out by the addition of the different products (rating × weight of the corresponding parameter), using the following equation:

$$D_i = D_w D_{r,i} + R_w R_{r,i} + A_w A_{r,i} + S_w S_{r,i} + T_w T_{r,i} + I_w I_{r,i} + C_w C_{r,i} \quad (1)$$

Table 1 Weight setting for DRASTIC parameters [**14**]

Symbol	Parameter	Weight
D_w	Depth to Water	5
R_w	Net Recharge	4
A_w	Aquifer Media	3
S_w	Soil Type	2
T_w	Topography	1
I_w	Impact of Vadose Zone	5
C_w	Hydraulic Conductivity	3

Table 2 Five Classes/Degrees of DRASTIC Vulnerability [**29**]

DRASTIC Index	Vulnerability Class
> 176	Very High
146-175	High
115-145	Moderate
84-114	Low
< 84	Very Low

where D_i, is the DRASTIC index; ***D***, ***R***, ***A***, ***S***, ***T***, ***I***, and ***C*** are the seven parameters as defined in **Table 1**; and the subscripts ***r***, ***i*** are ***w*** are the corresponding rating for grid cell ***i*** and weights.

Table 3 Data Sources for DRASTIC 7-Layer Generation

Raw Data	Sources	Format	Resolution/Scale	Date	Output
Groundwater Depths	DGR	Shapefile	1 km	2008	Depth of Water (***D***)
Recharge Data	DGR	Point Measurement	-	2008	Recharge (***R***)
	University of Frankfurt	Shapefile	0.5°× 0.5°		
GLiM	Hamburg University	Geodatabase	1: 3,750,000	2012	Aquifer Media (***A***) and Impact of Vadose Zone (***I***)
Aquifer Media	DGR	Shapefile	1 km × 1 km	2009	
Soil Data	LDD	Shapefile	1 km × 1 km	2009	Soil Type (***S***)
	ISRIC, World Soil Information	Raster	1 km × 1 km	2014	
SRTM90	UCL/Elle-Geometrucs (Belgium) and CGIAR/CSI	Raster	90 m × 90 m	2000	Topography (***T***) or Slope (%)

The weights indicate the relative importance of each DRASTIC parameter with respect to the other parameters. These weights are constant [**30**]. Also, for each DRASTIC parameter, the designated rating varies from 1 o 10. The rating ranges were determined depending on the properties at the specific area of interest. A good knowledge of geology and hydrogeology of the research area is a pre-requisite to determine the ratings assigned in this study were similar to the typical ratings suggested in the original DRASTIC study [**14**]. Finally, for purposes of interpretation, we subdivided the possible values of the DRASTIC index calculated into 5 classes/degrees of vulnerability as shown in **Table 2**.

C. Data Acquisition and Database Compilation

We constructed a GIS database for hydrogeology, geology, soil, groundwater recharge, and topography of the study area. **Table 3** shows the data of the constructed GIS database. We processed all data with ArcGIS 10.2™, QGIS ™, and Matlab ™.

Data came in various spatial resolutions. We re-sampled data layers to be suitable with the proposed resolution of the GIS model. We proposed a 1 km × 1 km (for area with local data) and 15 km × 15 km (for area with global meta data only) resolutions for this study, based on the fact that this resolution was reasonable compromising between different resolutions of the datasets, computing constraints, and regional extent. We obtained the vulnerability maps, after classifying and assigning relative ratings and weights, then overlaying the individual maps in a GIS environment. **Fig. 2** gives an overview of the methodology used to develop the intrinsic groundwater vulnerability map. Each parameter processes in the GIS described below.

D. Development of the DRASTIC Parameters

Depth to Groundwater (D)

The 'Depth to Water Table' (***D***), is the vertical distance from the land surface to the top of the saturated zone in the aquifer. It represents the distance that a potential contaminant must travel before reaching the aquifer. Consequently, ***D*** will have an impact on the degree of interaction between the percolating contaminant and the subsurface materials (air, minerals, water) and, therefore on the degree and extent of the physical and chemical attenuation and the degradation process [**31**]. In general, the vulnerability for pollution should decrease with ***D***. For our study, ***D*** was calculated from the data as presented by 1:50,000 groundwater maps provided by DGR (2008). Some extra groundwater depth data was not continuous and originally obtained from other local studies in a categorical data format.

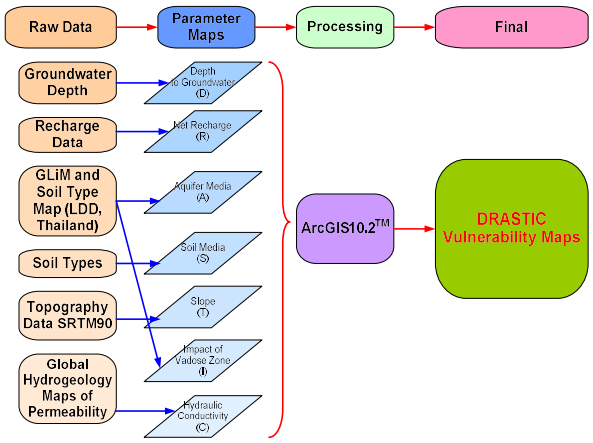

Fig.2 Methodology Flowchart to Develop Groundwater Vulnerability Map with DRASTIC Index Model in GIS Environment.

Table 4 Rate and Weight of 7 DRASTIC Parameters (Modified from **Aller et al. 1987 [14]**)

Depth to Groundwater (m)		Net Recharge (mm)		Topography (%)		Hydraulic Conductivity (m/d)		Soil Media	
Interval	Rating	Interval	Rating	Interval	Rating	Interval	Rating	Soil Classes	Rating
0-7	10	0-45	1	0-2	10	0.0 - 5.00	1	Clay	1
7-25	8	45-123	3	2-4	9	5.01 – 15.00	2	Clay Loam	3
25-50	5	123-224	6	4-8	8	15.01 – 35.00	3	Loam	5
50-100	3	224-355	8	8-12	5	35.01 – 75.00	4	Loamy Sand	7
100-250	2	>355	9	12-18	3	75.01 – 155.00	6	Sandy Clay	2
> 250	1			> 18	1	155.01 – 315.00	8	Sandy Clay Loam	4
								Sandy Loam	6
						> 315.01	10	Silty Clay Loam	3
								Sand	9
Weight = 5		Weight = 4		Weight = 1		Weight = 3		Weight = 2	

Table 5 Rate and Weights (***A***=3 and ***I***=5) of Aquifer Media (***A***) and Impact of Vadose Zone (***I***) (Modified from **Aller et al. 1987 [14]**)

Lithology Classes[32]	Hydrolithology Classes[33]	Bedrock Materials	***A*** and ***I*** Ratings
Unconsolidated Sediments	Unconsolidated		8
	c.g. unconsolidate	Alluvial Deposits, Dune Sands	
	f.g. unconsolidate	Loess (Aeolian Sediment), Organic Sediment	
Siliciclastic Sediments	Siliciclastic Sedimentary	Limestone, Sandstone	6
	c.g. siliciclastic sedimentary	Dolomite, Siltstone, Salt	
	f.g. sedimentary	Conglomerate, Shale	
Mixed Sedimentary Rocks	Carbonate	Karst Limestone	10
Carbonate Sedimentary Rocks			
Evaporites			
Acid Volcanic Rocks	Volcanic	Permeable Basalt	9
Intermediate Volcanic Rocks			
Acid Plutonic Rocks	Crystalline	Igneous/Metamorphic Rocks	A(3) and I(4)
Intermediate Plutonic Rocks			
Basic Plutonic Rocks			
Metamorphic Rocks			
Water Bodies	*Other Rock*	-	8

*Net Recharge (**R**)*

The 'Net Recharge' (***R***) represents the amount of water per unit area of land penetrating the ground surface and reaching the water table. It is thus influenced by the amount of surface cover, the slope of the land surface, the permeability of the soil and the amount of water that recharge the aquifer. The dispersion and dilution of contaminants are known to greatly depend on the volume of water available in the vadose zone as well as in the saturated zone and thus on the net recharge. High recharge areas are definitely more vulnerable than low recharge areas. Net recharge values were mainly derived from the global-scale modeling of groundwater recharge (**34**) assimilated with some local observation data from Department of Groundwater Resources Thailand (DGR).

*Aquifer Media (**A**)*

The 'Aquifer media' (***A***), refers to a type of consolidated or unconsolidated material which hosts the aquifer [**21**]. ***A*** was referred from three main data sources: (1) the high resolution global lithological database (GLiM) [**32**]; (2) the global permeability estimates of **Gleeson et al. (2011) [33]**; and (3) DGR. The analysis of the global permeability has permitted to identify parent material for each hydrolithologic unit. The GLiM databases encompass 16 lithological classes, which we then assumed to represent geology. Aquifer media were determined of each hydrolithology with similar hydrological characteristics **[33]**, e.g., unconsolidated sediments, siliciclastic sediments, carbonate rocks, crystalline rocks, and volcanic rocks. The vulnerability of the aquifer will increase of the grain size and the fractures or openings within the aquifer will increase **[35]**.

*Impact of the Vadose Zone (**I**)*

The role of the unsaturated zone above the water table is integrated in the ***I*** parameter. It is an important parameter in the estimation of vulnerability, because it influences the residence time of pollutants in the unsaturated zone, and hence the attenuation probability. Similar to the ***A*** parameter, the method used to identify the vadose zone material depend on GLiM data and the DGR hydrogeological map. The weights and ratings for ***I***are tabulated in **Table 5**.

*Topography (**T**)*

The 'Topography' (***T***), determines the runoff and infiltration capacity of the surface water into the soil, and hence the capacity to introduce pollutants into the soil. If the slope is important, more runoff will be generated and hence groundwater contamination risk will be low. However, flat areas tend to retain water for a longer period, therefore increasing the potential for migration of contaminants. The ***T*** was inferred from the 90 m Shuttle Radar Topography Mission (SRTM90) database. The slope values were generated with the SRTM 90 by using the Spatial Analyst software of ArcGIS10.2™. The slope layers were re-sampled and re-classified with the ratings into 6 classes.

Soil Media (S)

Soil is the first media the contaminant passes through when it percolates into the ground, and thus has a significant impact on the amount of recharge that can infiltrate and the ability of a contaminant to vertically penetrate into the vadose zone [**36]**. For this study, the soil map of Thailand was inferred from the data officially collected by Land Development Department in 2009

*Hydraulic Conductivity (**C**)*

The 'Hydraulic Conductivity' (***C***), is a measure of the ability of the aquifer to transmit water when submitted to a hydraulic gradient. It determines the migration velocity of pollutants, and hence the residence time and attenuation potential. High conductivity values usually are associated to higher contamination risks **[31]**). We inferred the hydraulic conductivity map generated from the global hydrogeolgical map of permeability and porosity [**33]** and 1:50,000 hydrogeological map of parts of Thailand (DGR). The global permeability map is generally given in log values of permeability (***k***). The hydraulic conductivity (***K***) can be calculated from the **Equation 2** below.

$$K = \frac{k\rho g}{\mu} \quad (2)$$

where ***K*** (m/s) is hydraulic conductivity which depends on fluid viscosity and density; $\boldsymbol{\rho}$ (kg/m^3) is the fluid density (= 999.97 kg/m3 for water), $\boldsymbol{g}$ (m/s^2) is the acceleration due to gravity (= 9.8 m/s^2); and $\boldsymbol{\mu}$ (kg/m-s or Pa-s) is the viscosity of the fluid.

E. Validation using Local Spatially Distribution Patterns of Observed Nitrate

DRASTIC indicator model proposed above is an indirect way for evaluating vulnerability and pollution potential of groundwater systems at a regional scale. This method heavily relies on accessible generic data and should therefore be validated. Indeed, the use of methods that are not validated can result in erroneous conclusions and subjective vulnerability assessment [**37]**. However, since intrinsic and vulnerabilities only measure the likelihood that groundwater systems may be degraded, or become degraded in the future, it cannot

be measured directly ***in-situ***. This challenges the empirical validation of vulnerability mapping (**38**).

In this study, we compare the vulnerability patterns with proxies of vulnerability that can be measured ***in-situ*** using the degradation of groundwater quality by nitrates from agriculture activities and urban development. Also, main groundwater monitoring programs in Thailand always include nitrate as a monitoring parameter, and therefore nitrate contamination are commonly available at the regional scale. The spatial distribution patterns of nitrate in groundwater are therefore presumably closely related to the spatial patterns of anthropogenic activities and are thus reasonable proxies for the spatial patterns of overall vulnerability. Existing groundwater nitrate contamination data in Suphanburi province were collected from more than 160 groundwater samples, most of which surrounding heavily fertilization crop lands. The validation of the groundwater vulnerability map was accomplished through the nitrate distribution analysis and the vulnerability classes. ArcGIS10.2^{TM} was employed to distribute spatially and compared with the various degrees of DRASTIC vulnerability maps.

Results and Discussions

A. Rating of DRASTIC Parameters and Aquifer Vulnerability

Ratings and weights of each parameter of DRASTIC are illustrated in **Tables 4 and 5**, with scales varying from 1 to 10. The higher the number, the greater the pollution we should expect.

The ***D*** map is show in **Fig.3** generated with values ranged from 0 to shallow groundwater depth and deeper groundwater depth. The shallow groundwater depth areas are more susceptible to contamination according to DRASTIC assumptions. The high values of ***D*** are located in large sedimentary aquifer which contains a considerable proportion of Thailand's groundwater. The assigned ***D*** ratings vary between 1 and 10, according to the classification of **Aller et al. (1987) [14]**. The highest scores of 9 and 10 are assigned where the depths are in the class 0-7 m and 7-25 m, respectively. The lowest depths are assigned with a rating of 1.

The ***R*** map is illustrated in **Fig. 4** which was generated and later layered up to construct the final DRASTIC map. Pitsanulok, Sukhothai, and Suphanburi have areas with low net recharge rate (< 50 mm/year) for which a rating of 1 is assigned, and other areas with high recharge ranges (> 225 mm/year), for which a rating of 9 is assigned,

The ***A*** map is also shown in **Fig. 5**. The ratings in **Table 5** are assigned as commonly found in previous studies. A rating of 10 is assigned to high permeable rock/porous media. The major aquifer media in the study area is unconsolidated sediments (i.e., clay, sand, and gravel), which is assigned a rating of 8 (**39**). A low rating of 3 is assigned to crystalline rocks, fractured igneous and other metamorphic rocks in the area.

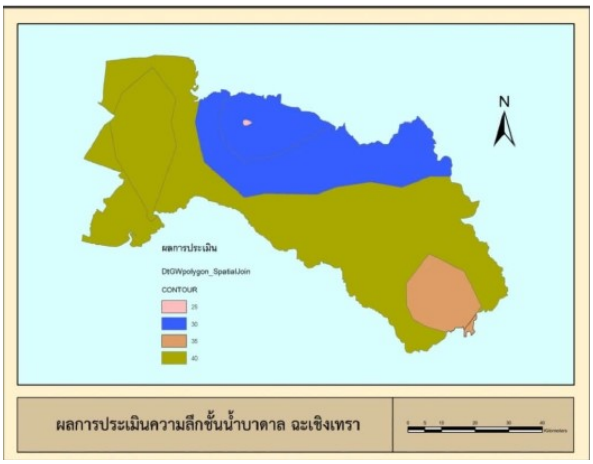

Fig. 3 DRASTIC Rating of the Depth to Groundwater (***D***) in Chachoengsao Province of Thauiland

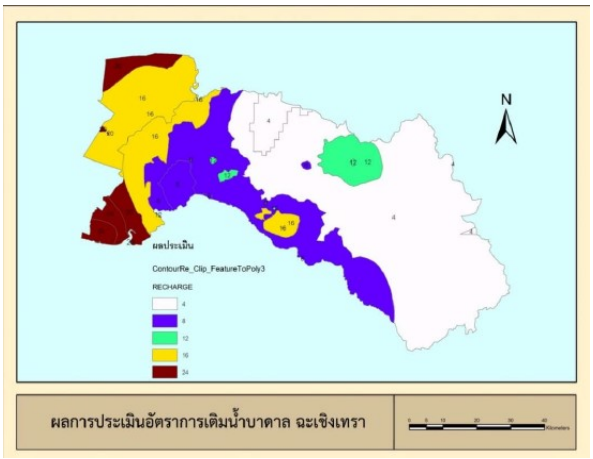

Fig. 4 DRASTIC Rating of the Recharge (***R***) in Chachoengsao Province of Thailand

Fig. 5 DRASTIC Rating of the Aquifer Media (***A***) in Chachoengsao Province of Thailand

The texture based ***S*** map is represented in **Fig. 6**. Soils are mapped in 7 different classes. The dominant textures at the representative sites are sandy clay, loam and clay loam. The silty clay and sandy soil types appear in a lower proportion. The highest rating of 9 is assigned to the sandy soil and the lowest rating of 1 to the clayey soil. There is no information available on soils in some parts of the study areas, thus these parts were left 0.

The ***T*** map representing the surface slope is shown in **Fig. 7**. A gentle slope of 0-4% is dominating the largest portion of Pitsanulok and Sukhothai, and therefore a rating score of 9 and 10 is assigned to this class, indicating that there is a large susceptibility of pollution infiltration. The highest slopes are located in the mountainous proximity in Suphanburi area where larger slopes of 18% can be found, leading to the minimal potential effects on the groundwater vulnerability.

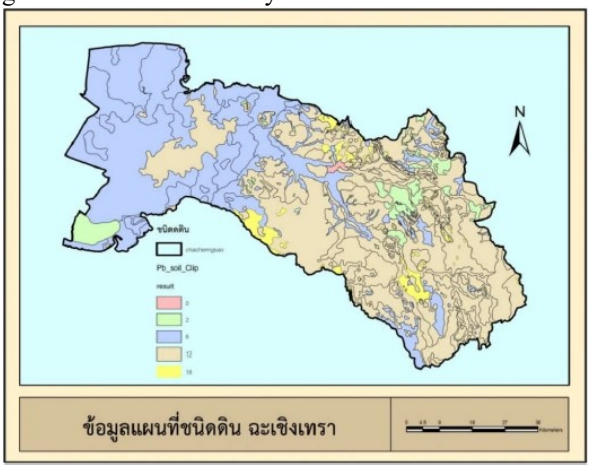

Fig. 6 DRASTIC Rating of the Soil Type (***S***) in Chachoengsao Province of Thailand

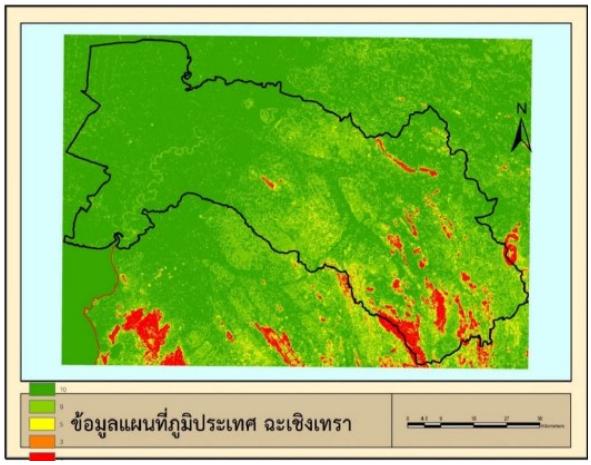

Fig. 7 DRASTIC Rating of the Topography/Slope (***S***) in Chachoengsao Province of Thailand

The ***I*** map is presented in **Fig. 8**. The data used for this purpose is basically the same set of data for generating the ***A*** map. Although the same hydrolithology is employed for both ***A*** and ***I*** parameters, the final maps turned out differently because the crystalline rocks (igneous/metamorphic rocks) of the vadose zone are assigned a rating of 4 for ***I*****[14]**. Weights and ratings for ***I*** are shown in **Table 4**.

The ***C*** map is shown in **Fig. 9**. The hydraulic conductivity calculated is inferred both from global permeability database and local permeability measurements and has been classified into 6 classes. In general, the variability of C parameter is not high. Lowe hydraulic conductivity values, as low as 0.01 m/d, can be commonly found in the study area. The averaged hydraulic conductivity range is between 0.04 to 0.13 m/d.

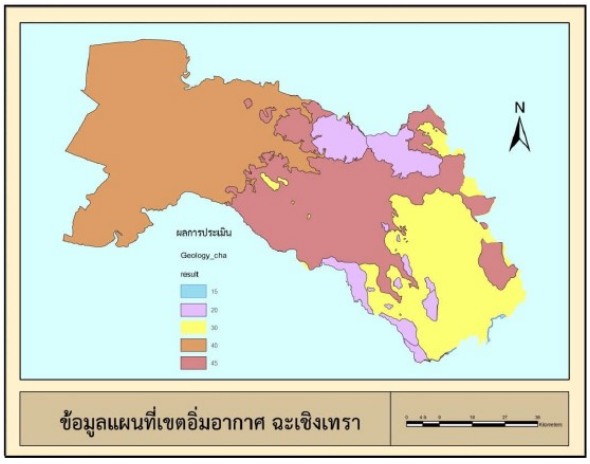

Fig. 8 DRASTIC Rating of the Impact of Vadose Zone (***I***) in Chachoengsao Province of Thailand

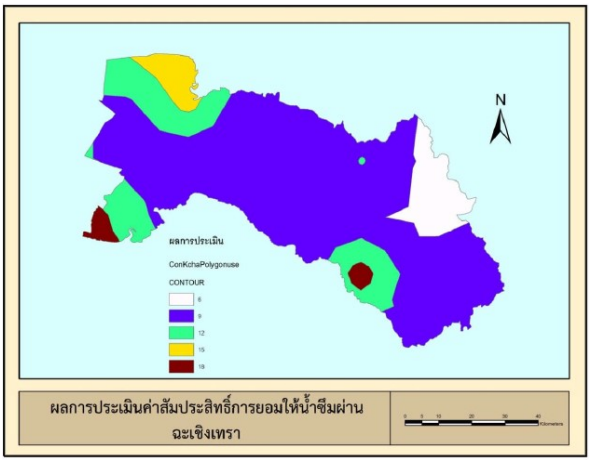

Fig. 9 DRASTIC Rating of the Hydraulic Conductivity (***C***) in Chachoengsao Province of Thailand

The resultant DRASTIC map is shown now in **Fig. 10**. DRASTIC classes have been grouped into very low, low, moderate, high, and very high vulnerability intervals. We observed a very low and low vulnerability in the Western part of the province where large sedimentary basins are found with high recharge rates. Indeed, the absence of important anthropogenic activities should be in combination with very low and low contamination risks. In

general, high vulnerability areas are lower-land where intensive agricultural activities and urban development are concentrated. On the other hands, a region with low vulnerability degree does not really mean that it is free from groundwater contamination, but it rather represents relatively less susceptible to contamination compared with other regions.

The intrinsic vulnerability map in **Fig. 10** indicated that the representative study areas are dominated by very high and high intrinsic vulnerabilities. The shallow groundwater depths in these regions along with high recharge rate explain this high intrinsic vulnerability. In the northeastern part of Chachoengsao has been characterized as low intrinsic vulnerability due to its deeper groundwater depth and very low recharge rates. The topography parameter had the highest impact for assessing the intrinsic vulnerability of our study area. The impact of vadose zone, the aquifer media, and depth to groundwater had a moderate mean rating value. The soil media, net recharge, and hydraulic conductivity play the least important roles in quantifying vulnerability based on DRASTIC indexing method.

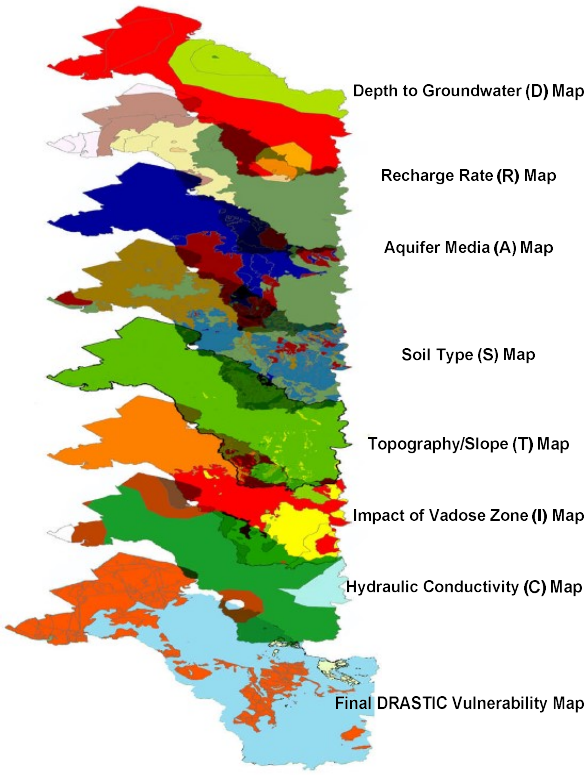

Fig. 10 Final DRASTIC Vulnerability Map in Chachoengsao Province of Thailand

B. Validation of the Groundwater Vulnerability Map

Spatial Concentrations of Nitrate

The spatial distribution of nitrate in groundwater in Suphanburi province is illustrated in **Fig. 11**. More than 160 long-term groundwater samples were collected from domestic and monitoring wells at various depths (100 samples from < 30 m deep, and 60 samples from > 30 m deep) and analyzed. Samples were carefully preserved and transported back for further chemical parameter analyses at a certified analytical laboratory in Bangkok. The environmental parameters include: total hardness as $CaCO_3$, non-carbonated hardness as $CaCO_3$, total dissolved solid, BOD, alkalinity, Fe, Mn, Cu, Zn, SO_4, Cl, F, nitrate (NO_3^-), As, CN^-, Pb, Hg, Cd, Se, Hexavalent Cr, and Ni. Nitrate spatial distribution patterns were processes in ArcGIS environment.

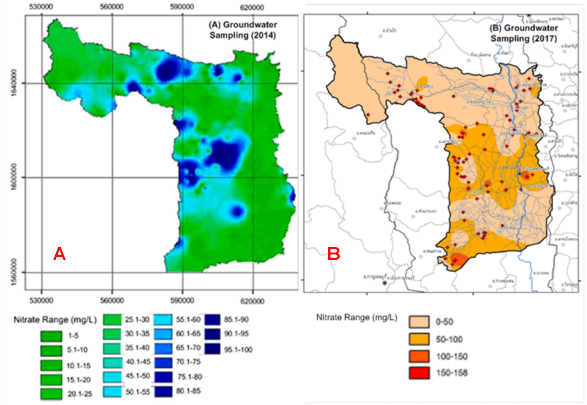

Fig. 11 Extent of the Spatial Soluble Nitrate Contamination in Groundwater in Suphanburi Province: (A) Data from Groundwater Sampling in 2014; and (B) Data from Recent Groundwater Sampling in 2017.

The distribution of nitrate in groundwater in Suphanburi province indicated that there were abundant of soluble nitrate detected in aquifer systems underneath Suphanburi. Areas that were subjected to the most severe contamination are U-Thong (central part of Suphanburi) and Song-Pee-Nong (southern part of Suphanburi). Also in this work, groundwater samples were taken to evaluate the extent of nitrate contamination in Suphanburi (from the same municipal wells and monitoring wells previously sampled). The current spatial distribution of nitrate in groundwater is compared with the results previously examined as shown in **Fig. 11**.

Since naturally occurring concentration of nitrate are generally less than 2 mg/L nitrate N, nitrate concentration detected in the environment greater than 2 mg/L should ne consider anthropogenic-origin. Using the nitrate MCL at 45 mg/L, the results in **Fig. 11** indicate that the extent of nitrate contamination in groundwater has actually been expanding in 3 years time span from 2014 to 2017. Some nitrate hotspots, particularly in Song-Pee-Nong (southern part of Suphanburi), Nong-Ya-Sai (north part of Suphanburi), and Dan-Chang (north western of Suphanburi), are disappeared and nitrate concentration detected in groundwater is below 45 mg/L. However, the majority of nitrate former hot spots still noticeably exist with nitrate concentrations as high as 100 mg/L, i.e., in Derm-Baang-Nang-Buad

and U-Thong. To make the story worse, the new nitrate hot spots with extremely high concentrations up to 158 mg/L are observed based on the investigation in this work as can be seen in Muang and Southern Song-Pee-Nong districts shown in **Fig. 11**.

Regression of Aggregated Nitrate Concentration Data with Intrinsic Vulnerability of Groundwater in Suphanburi

The authors also further aggregated the observed maximum nitrate concentration for each vulnerability class and compared it with vulnerability degree. In this approach, DRASTIC index has been used as surrogate of the vulnerability map and regressed against the extracted nitrate concentration. **Fig. 12** illustrates that the aggregated maximum nitrate concentration data are positively correlated to the intrinsic vulnerability (R^2 = 0.89), suggesting that the generic model for mapping vulnerability in groundwater is consistent with observed nitrate inferred from the literature. We chose the maximum nitrate concentrations as aggregate values in order to show the performance of groundwater vulnerability model because the sample size may not be large enough for single measurement validation. The aforementioned results suggest that further validation using more extensive data set is recommended.

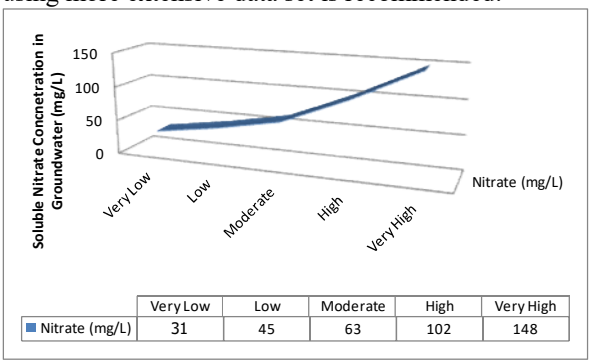

	Very Low	Low	Moderate	High	Very High
Nitrate (mg/L)	31	45	63	102	148

Fig. 12 Correlation between Maximum Nitrate Concentration and DRASTIC Vulnerability Level with R^2= 0.89.

Conclusions

We assessed the intrinsic vulnerability of Thailand's groundwater vulnerability to pollutions. The empirical index model DRASTIC was employed in GIS environment to provide an effective analysis environment and a strong capacity for handling large amounts of spatial data. We identified 7 environmental DRSTIC parameters: Depth to Groundwater (***D***), net recharge (***R***), aquifer media (***A***), soil media (***S***), topography (***T***), impact of vadose zone (***I***), and hydraulic conductivity (***C***) from available generic global data assimilated with sparse local observations. We classified and coded these main geo database to create an intrinsic groundwater vulnerability map, resulting in DRASTIC index varies between 66 and 213. DRASTIC index were further classified into 5 classes/degrees, ranging from very low; low; moderate, high, and very high.

Despite the lack or very limited groundwater contamination data in Thailand, we attempted to validate our intrinsic vulnerability assessment using soluble nitrate concentration data as proxies for groundwater vulnerability. Potential effects of nitrate on the quality of surface water and groundwater as well as the implications of such effects on human health (especially to children), pose issues of international concern that require science-based assessment and response. Suphanburi is selected as our tested area due to the previous reports on surface and subsurface nitrate contamination. Recent evidence from this study indicates that nitrate levels exceed the maximum contaminant level (MCL) of 45 mg/L in aquifer systems that underlie agriculture-dominated area with the maximum soluble nitrate concentration up to 158 mg/L near Muang and Southern Song-Pee-Nong districts. Nitrate hotspots have been re-identified based on the more recent discovery. 30% of shallow groundwater samples (< 30 m) are detected with higher nitrate concentration than MCL whereas only 23% of groundwater samples taken from > 30 m deep are found contaminated, suggesting the direct association major nitrate contamination in groundwater aquifer with potential source on the ground surface. High nitrate concentrations detected from our investigations coincide with high intrinsic vulnerability based on the vulnerability map of Suphanburi generated from empirical DRASTIC index method, illustrating the consistency between the calculated vulnerability using generic data and real observation. DRASTIC vulnerability assessment procedures and vulnerability maps generated as outputs from this work can improve effectiveness and efficiency of potential national groundwater management and monitoring programs. The vulnerability map at the national-scale is necessary to achieve SDGs in the context of SDG 6, SDG 1, SDG 2, SDG 5, SDG 11, SDG 13, and SDG 15 as it can serve as a general guideline for sustainable groundwater use through policy recommendation and implementation related to proper monitoring, management and governance that employs integrated and precautionary approaches while giving appropriate attention to the potential boundary nature of groundwater.

Acknowledgment

The authors thank Asahi Glass Foundation for their financial support. In addition, this study was partially supported by Department of Groundwater Resources Thailand and the Science and Technology Research Partnership for Sustainable Development, JST_JICA, Japan.

References

[1] Zekster, I.S., Groundwater and the Environment: Applications for the Global Community. Lewis Publishers, Boca Raton, Florida, USA (2000).

[2] Humphreys, W.F., Hydrogeology and groundwater ecology: does each inform other?. Hydrogeology Journal, 17(1): 5-21 (2009).

[3] Steube, C., S. Richter, and C. Griebler, First attempts towards an integrative concept for the ecological assessment of groundwater ecosystems. Hydrogeology Journal, 17(1): 23-25 (2009).

[4] Hasiniaina, F., Zhou, J., Guoyi, Z.L., 2010. Regional assessment of groundwater vulnerability in tamtsag basin, Mongolia using drastic model. Journal of American Science 6(11), 65–78.

[5] National Research Council, 1993. Groundwater Vulnerability Assessment, ContaminantPotential Under Conditions of Uncertainty. National Academy Press, Washington DC.

[6] Vrba, J., Zaporozec, A., 1994. Guidebook on Mapping Groundwater Vulnerability. 16. International Association of Hydrogeologists, Hannover, Germany 131pp.

[7] Gogu, R.C., Dassargues, A., 2000. Current and future trends in groundwater vulnerabilityassessment. Environ. Geol. 39 (6), 549–559.

[8] Voudouris, K., 2009. Assessing groundwater pollution risk in sarigkiol basin, NW Greece. In: Gallo, M., Herrari, M. (Eds.), River Pollution Research Progress. Nova Science Publishers Inc., pp. 265–281 Chapter 7.

[9] Uricchio, V.F., Giordano, R., Lopez, N., 2004. A fuzzy knowledge-based decision support system for groundwater pollution risk evaluation. J. Environ. Manage. 73, 189–197.

[10] Al-Hanbali, A., Kondoh, A., 2008. Groundwater vulnerability assessment and evaluation of human activity impact (HAI) within the Dead Sea groundwater basin, Jordan. Hydro-geology Journal 16 (3), 499–510.

[11] Farjad, B., Mohamed, T.A., Wijesekara, N., Pirasteh, S., Shafri, H.Z.B.M., 2012. Groundwater intrinsic vulnerability and risk mapping. Proceedings of the ICE — Water Management 165 (8), 441–450.

[12] Mimi, Z.A., Mahmoud, N., Madi, M.A., 2011. Modified DRASTIC assessment for intrinsic vulnerability mapping of karst aquifers: a case study. Environmental Earth Sciences 66 (2), 447–456.

[13] Vanclooster, M., Mfumu, K.A., Ouedraogo, I., 2014. L'union fait la force or how different approaches should be combined to assess groundwater vulnerability at the regional scale. IAH (Marrakech, Maroc, du 15/09/2014 au 19/09/2014).

[14] Aller L, Bennet, T., Leher, J.H, Petty, R.J & Hackett G. (1987). DRASTIC: A Standardized System for Evaluating Ground Water Pollution Potential Using Hydrogeological Settings.U.S. Environmental Proctection Agency, Ada Oklahoma 74820, EPA 600/2-87-035, 662 pp.

[15] Aller, L., Bennet, T., Lehr, J. H., and Petty, R. J., (1985). DRASTIC: A Standardized System for Evaluating Groundwater Pollution Using Hydrological Settings. Ada, OK, USA: Prepared by the National Water Well Association for the US EPA Office of Research and Development. EPA/600/2-85-018, 163pp.

[16] Fritch, T.G., McKnight, C.L., Yelderman Jr, J.C., Arnold, J.G., 2000. An aquifer vulnerability assessment of the Paluxy aquifer, central Texas, USA, using GIS and a modified DRASTIC approach. Environ. Manag. 25 (3), 337–345.

[17] Shukla, S., Mostaghimi, S., Shanholt, V.O., Collins, M.C., Ross, B.B., 2000. A county-level assessment of ground water contamination by pesticides. Groundwater Monitoring & Remediation 20 (1), 104–119.

[18] Mao, Yuan-yuan, Zhang, Xue-gang, Wang, Lian-sheng, 2006. Fuzzy pattern recognitionmethod for assessing groundwater vulnerability to pollution in the Zhangji area. J. Zhejiang Univ. Sci. B. 7 (11), 1917–1922.

[19] Liggett, J., Gilchrist, A., 2010. Technical summary of intrinsic vulnerability mapping methods in the regional districts of Nanaimo and Cowichan valley. Geological Survey of Canada, Open File 6168 64p.

[20] Senthilkumar, P., Nithya, J., Babu, S.S., 2014. Assessment of Groundwater Vulnerability in Krishnagiri District, Tamil Nadu, India Using DRASTIC Approach. International Journal of Innovative Research in Science, Engineering and Technology 3 (3).

[21] Ersoy, A.F., Gültekin, F., 2013. DRASTIC-based methodology for assessing groundwater vulnerability in the Gümüşhacıköy and Merzifon basin (Amasya, Turkey). Earth sciences research journal 17 (1), 33–40.

[22] Saidi, S., Bouri, S., Ben Dhia, H., 2010. Groundwater vulnerability and risk mapping of the Hajeb-jelma aquifer (Central Tunisia) using a GIS-based DRASTIC model. Environmental Earth Sciences 59 (7), 1579–1588.

[23] Saidi, S., Bouri, S., Ben Dhia, H., 2011. Sensitivity analysis in groundwater vulnerability assessment based on GIS in the Mahdia-Ksour Essaf aquifer, Tunisia: a validation study. Hydrol. Sci. J. 56 (2), 288–304.

[24] Musekiwa, C., Majola, K., 2013. Groundwater vulnerability map for South Africa. South African Journal of Geomatics 2 (2), 152–163.

[25] Evans, B.M., Myers, L.W., 1990. A GIS-based approach to evaluating regional groundwater

pollution potential with DRASTIC. J. Soil Water Conserv. 45 (2), 242–245.

[26] Rosen, L., 1994. A study of the DRASTIC methodology with emphasis on Swedish conditions. Groundwater 32 (2), 278–285.

[27] Neshat, A., Pradhan, B., Pirasteh, S., Shafri, H.Z.M., 2014. Estimating groundwater vulnerability to pollution using a modified DRASTIC model in the Kerman agricultural area. Iran. Environ. Earth Sci. 71 (7), 3119–3131.

[28] Ramnarong V., Groundwater Resources in Mae Klong Basin, Bangkok, Thailand, Report by Department of Mineral Resources, Ministry of Industry, Thailand, 1993.

[29] Jourda J. P., Kouame K. J., Adja M.G., Deh S. K., Anani A. T., Effini A. T., Biemi J. (2007). Evaluation du degré de protection des eaux souterraines : vulnérabilité à la pollution de lanappe de Bonoua (Sud-Est de la Côte d'Ivoire) par la méthode DRASTIC, Conférence Francophone ESRI, 10–11 Octobre-Versailles, 8pp.

[30] Ehteshami, M., Peralta, R.C., Eisele, H., Deer, H., Tindall, T., 1991. Assessing pesticide contamination to groundwater: a rapid approach. Journal of Ground Water 29 (6), 939–944.

[31] Rahman, A., 2008. A GIS based DRASTIC model for assessing groundwater vulnerability inshallow aquifer in Aligarh, India. Appl. Geogr. 28, 32–53.

[32] Hartmann, J., Moosdorf, N., 2012. The new global lithological map database GLiM: a representation of rock properties at the Earth surface. Geochem. Geophys. Geosyst. 13 (12), Q12004. http://dx.doi.org/10.29/2012GC004370.

[33] Gleeson, T., Moosdorf, N., Hartmann, J., Beek, L., 2014. A glimpse beneath earth's surface: GLobal HYdrogeology MaPS (GLHYMPS) of permeability and porosity. Geophys. Res. Lett. 41 (11), 3891–3898.

[34] Döll, P., Fiedler, K., 2008. Global-scale modeling of groundwater recharge. Hydrol. Earth Syst. Sci. 12, 863–885.

[35] Alwathaf, Y., 2011. Assessment of Aquifer Vulnerability Based on GIS and ARCGIS Methods: A Case Study of the Sana'a Basin (Yemen). Journal of Water Resource and Protection 03 (12), 845–855.

[36] Lee, S., 2003. Evaluation of waste disposal site using the DRASTIC system in Southern Korea. Environ. Geol. 44 (6), 654–664.

[37] Leal, J.A.R., Castillo, R.R., 2003. Aquifer vulnerability mapping in the turbio river valley, Mexico: a validation study. Geofísica Internacional 42 (1), 141–156.

[38] Andreo, B., et al., 2006. Karst groundwater protection: First application of a Pan-European Approach to vulnerability, hazard and risk mapping in the Sierra de Libar (Southern Spain). Sci. Total Environ. 357 (1–3), 54–73.

[39] MacDonald, A., Davies, J., Callow, R.C., 2008. African hydrogeology and rural water supply. In: Adelana, S., MacDonald, A. (Eds.), Applied Groundwater Studies in Africa. CRC Press, Leiden, The Netherlands, pp. 127–148 (IAH selected papers on hydrogeology, 13).

Modified Critical Antecedent Precipitation Index (MCAPI) for Flood Warnings in Upper Nan Watershed, Nan Province, Thailand

Venus Tuankrua[1,a], Wanchai Arunpraparat[2], Kuraji Koichiro[3] and Wipaporn Baiya[4]

Abstract Recently, the high land of northern Thailand became to be disturbs forest area and farmers usually plant mono crop like a maize or para rubber tree. It generates imbalance in head watershed that alter hydrological services. Nan province had experienced extreme flood on August, 2018 recently.The critical antecedent precipitation index (CAPI) is an index of maximum water storage in soil depend on soil depth, bulk density and saturated soil water. It act as a flood threshold. The modified CAPI was calculated and mapped using GIS technique and clustering MCAPI by soil properties for forecasting MCAPI. CAPI and modified CAPI were compared with extreme rainfall and flood event in 2017–2018. The results was noticed that the modified critical API in Upper Nan watershed were changed range from 206.355 to 415.609 mm. Modified CAPI showed highest changing (increase) in forest area around Phua district. The CAPI and API_t can possible apply to use real time flood warning in upper Nan watershed. It was indicated that CAPI were significant positive relationship with Soil moisture content (SM) but was shown significant negative relationship with slope percent. Finally, There are three models of forecasting MCAPI from bulk density and soil moisture as the 1st pattern (A) was low MCAPI (0-250 mm) was clustered by low bulk density (0-1 g/cm3) and low soil moisture (0-30 % by vol.) and the 2rd pattern (B) was clustered by low soil moisture (0-30 % by vol.) and high bulk density (1-1.8 g/cm3) and the last pattern (C) was clustered by high bulk density (1-1.8 g/cm3) and high soil moisture (0-30 % by vol.).

Keywords *API, Antecedent Precipitation Index, Soil properties, Flood warnings, Upper Nan watershed*

[1]Department of Conservation, Faculty of Forestry
Kasetsart University, Bangkok, Thailand
[2]Department of Forest Engineering, Faculty of Forestry
Kasetsart University, Bangkok, Thailand
[3]University of Tokyo, JAPAN
[4]Doiphukha national park, DNP, Thailand

[a]ffor.venus@gmail.com

Introduction

In northern Thailand is the mountainous area and steep slope. So, there were high frequency of flash flood and landslide. They damaged not only asset but also loss people life. The main causes of flashflood are heavy rainfall and potential of soil storage. In present, the high land of northern Thailand became to be disturbs forest area and farmers usually plant mono crop like a maize or para rubber tree. It generates imbalance in head watershed that alter hydrological services. Nan province had experienced extreme floodon August, 2018 recently.

Kohler first defined antecedent precipitation index (API) in the 1940s [1].During that period, various techniques which tried to conceptualize soil characteristics, through infiltration theory and etc. were complex, especially when trying to apply them to a very large basin [2]. The API has been used as a reasonable way to estimate the soil water status [3], and it contained effective antecedent precipitation, the consumption by surface and groundwater runoff, also the evaporation consumption. A very simple deterministic model was developed based on the "API" [4]. Soil moisture initialization program was provided by Peng based on the API method and the water equilibrium theory, which solved the soil moisture interpolation difficulties over the climatic humid zone. Based on the API model and the soil relative moisture (SRM) data, an empirical formula was established to supplement and predict the SRM in the regions lacking of monitoring data. Soil moisture data was positively correlated with subsequent precipitation by analyzing a 14year soil moisture data set from the state of Illinois. It was necessary to reduce the uncertainties related to the initial moisture conditions estimation prior to a flood event. The antecedent wetness conditions were found highly correlated with the soil wetness index for the three investigated catchments [5].A daily APIindex was computed on the whole precipitation series before the beginning of each flood event using an optimized K value (K stands for the attenuation factor). The estimation of antecedent soil water content was important in storm rainfall-runoff modeling [5], also essential in controlling runoff during medium and low intensity storms,and effective antecedent rainfall was considered significantly related to the debris flow.

The antecedent rainfall plays a significant role in a situation of the soil slope. Reference [6] proposed that the antecedent rainfall during the five-

day was significant in causing landslide. Reference [7] proposed the landslide warning criteria for northern Thailand, which used relationship the three-day antecedent rainfall and the rainfall in a day. Therefore, the hydrology model for this study is the antecedent precipitation index (API). The antecedent precipitation index is an index of moisture stored within a soil mass which considers the previous and present rainfall. The critical antecedent precipitation index (CAPI) is an index of maximum water storage in soil depend on soil depth, bulk density and saturated soil water. It act as a flood threshold. If there are rainfall greater than CAPI value, rainfall excess will possible occur and risk to flood. Additional, influence of climate change or extreme weather are important driving factors cause more extreme flood often.

Hence, the aims of this study were to assess the Modified Critical Antecedent Precipitation (MCAPI) in upper Nan watershed, to find correlation among MCAPI and various factors, and to apply MCAPI for flood warning in different climate conditions.

Study area

Upper Nan watershed has an area of 2,220.14 km^2 in Nan province, Thailand (Fig.1). It has the elevation ranges from 205.77 to 1926.22 meters above sea level and average slope of 34 percent. Most precipitation occurs from July to October in the watershed and dry period extends from December to April. The annual average precipitation is approximately 2,000 mm with an annual average temperature of 25.9 ºC

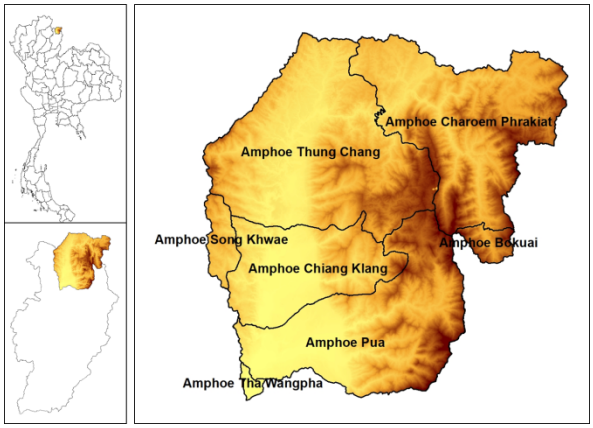

Fig.1 Location of the upper Nan watershed, Nan province.

Method

The main methodology were calculation MCAPI and analysis correlation among MCAPI and various factors. Finally, comparing MCAPI and API_t for flood warning under different climate conditions.

A. Data preapation and data fields collection

1) Digital Elevation Model (DEM) with 20 m grid interval
2) Soil group map scale 1: 100,000 provided by Land Development department.
3) 3) Land use map scale 1: 50,000 in 2016 provided by Land Development department.
4) 4) Soil properties database from previous research papers
5) 5) Soil properties data collection from fields; Bulk density (BD), Soil moisture (SM), Water holding capacity (WHC), slope percent, soil depth and land use type (ground based checking) in 2018 (Fig.2).

Fig. 2 Gather field soil sample and analysis soil properties data in different land use types and different elevations.

B. Calculation of Modified Critical Antecedent Precipitation (MCAPI)

The critical antecedent precipitation index (CAPI) is an index of maximum water storage in soil use (1) to calculate in each sites as;

CAPI = Saturated soil water x Soil depth

When saturated soil water is maximums soil moisture content (percent by volume) and Soil depth (mm) as show in Fig.3

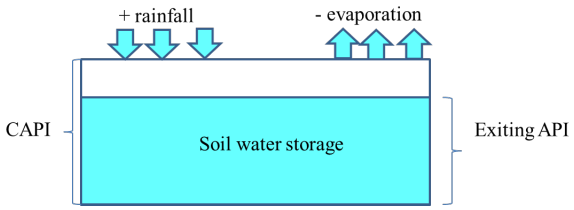

Fig. 3 The critical antecedent precipitation index (CAPI) and soil water storage

Then, interpolation MCAPI was generated by IDW method for spatial MCAPI maps (cell size = 20 x 20 m).

C. Correlation analysis among MCAPI and various factors

MCAPI and various factors were analyzed correlation among as Bulk density (BD), Soil moisture

(SM), Water holding capacity (WHC), slope percent, soil depth. The matrix will demonstate the positive/negative relationships among variables.

D. Application of MCAPI for flood warning in different climate conditions

The MCAPI could be shown the threshold of soil water storage in each area but the existing API (API_t) was required for confirm the present status and use for flood warning.

The antecedent precipitation index (API_t), The API_t is an index of moisture stored within a drainage basin before a storm. It is a weighted summation of daily precipitation amounts, used as an index of soil moisture. This index is intended to reproduce the saturation state of the basin by calculating the cumulative rainfall of previous days. Equation (2) defined API [3] as;

$$API_t = kAPI_{t-1} + P_t \quad (1)$$

The index of one day j is the index of the previous day t −1 multiplied by the factor k. If rainfalls occur on day t, it is added to the index.

The previous flood events in upper Nan watershed were selected to use in case study for flood warning simulation;

Event I: Flood and landslide event in Boklua district, Nan province during 27−29th July, 2018.

Event II: During July to September in 2011 (Strong Lanina)

Result and Discussion

After Modified Critical Antecedent Precipitation (MCAPI) has been completed, the spatial MCAPI was interpolated to create map. The details as follows;

A. Modified Critical Antecedent Precipitation (MCAPI)

The result was shown the mean, maximum and minimum Modified CAPI were 257.74, 106.82 and 425.61 mm, respectively. It was higher than the old CAPI (Table 1).

Table 1 Old CAPI and Modified CAPI of upper Nan watershed

	Old CAPI (mm)	Modify CAPI (mm)
mean	204.04	257.74
minimum	142.12	106.82
maximum	323.18	425.61
N	21.00	54.00

The maps in Fig.4 was shown Critical Antecedent Precipitation (CAPI) of Old CAPI (left) and Modified CAPI (right). It was indicated that high CAPI in Pua district but less CAPI in other districts. The area has high CAPI, it could be said that this area has deep soil profile and high potential of soil storage. On the other hand, if it has less CAPI that mean low potential of soil storage. These area will be risk for flood if heavy rainfall continuing 2-3 days.

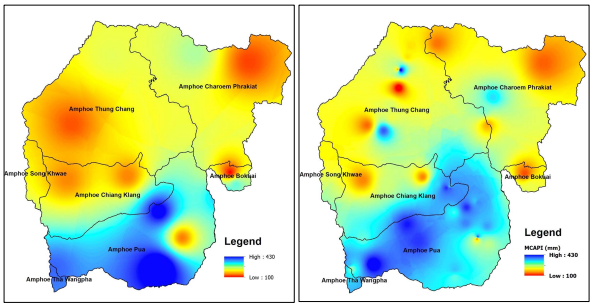

Fig. 4 Critical Antecedent Precipitation (CAPI) of Old CAPI (left) and Modified CAPI (right)

When considering MCAPI in different land use types, it was shown that the highest average CAPI was showed in orchard area as 312.713 mm and following by rubber plantation because average soil depth was quietly high (>80 cm or 0.8 m). In forest plantation, there was lowest CAPI because high bulk density. It could be said that less soil pore that influent with soil water storage capacity (Fig.5).

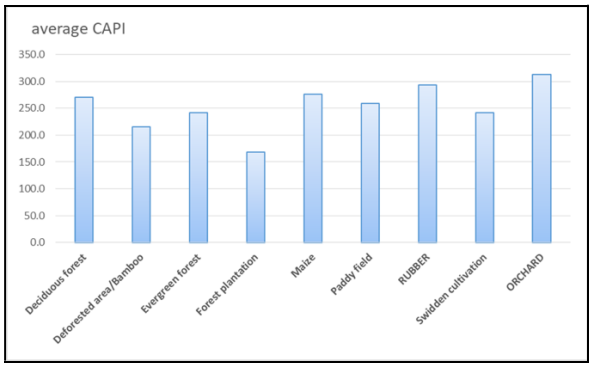

Fig. 5 MCAPI in different land use types.

B. Correlation analysis among MCAPI and various factors

For correlation coefficients (r) in Table 2, it was indicated that CAPI were significant positive relationship with Soil moisture (SM) but significant negative relationship with slope percent. So, Soil moisture (SM) was significant negative relationship with bulk density (BD) and soil depth. If any area have more bulk density (BD), it will have less space for water storage in soil.

It was indicated that CAPI were significant positive relationship with Soil moisture content (SM) but was shown significant negative relationship with slope percent. So, Soil moisture (SM) was significant negative relationship with bulk density (BD) and soil depth. If any area have more bulk density (BD), it will have less space for water storage in soil.

Table 2 Correlation coefficients in each factors

	LU_ID	Slope	BD	SM	soil_depth	CAPI
LU_ID	1	.268*	-.284*	.059	.049	-.144
Slope	.268*	1	-.403**	.012	.056	-.231*
BD	-.284*	-.403**	1	-.566**	.367**	.080
Sm	.059	.012	-.566**	1	-.504**	.569**
soil_depth	.049	.056	.367**	-.504**	1	.155
CAPI	-.144	-.231*	.080	.569**	.155	1

Remarks: ** = significant at 0.01
* = significant at 0.05

It can observed that bulk density (BD) was high negative relationship with Soil moisture content (SM) but high positive relationship with Water holding capacity (WHC) because high bulk density will have high capillary force as show in Fig.6.

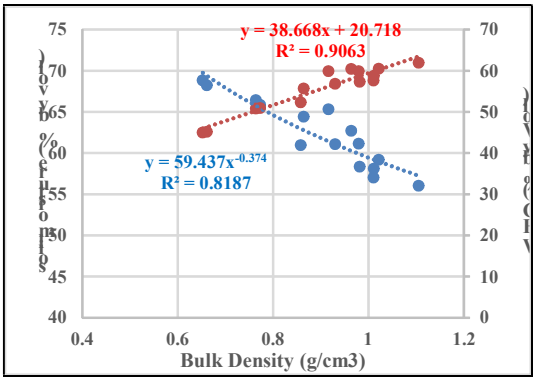

Fig. 6 Relationship among bulk density (BD), Soil moisture content (SM) and Water holding capacity (WHC)

The 3 patterns of MCAPI forecasting model were determined using multi-criteria analysis and clustering analysis based on wet soil moisture content (SM) and bulk density (BD).

In Fig. 7, the 1st pattern (A) was low MCAPI (0-250 mm) was clustered by low bulk density (0-1 g/cm^3) and low soil moisture (0-30 % by vol.) and the 2rd pattern (B) was clustered by low soil moisture (0-30 % by vol.) and high bulk density (1-1.8 g/cm^3) and the last pattern (C) was clustered by high bulk density (1-1.8 g/cm^3) and high soil moisture (0-30 % by vol.).

C. Application of MCAPI for flood warning in different climate conditions

Event I: Flood and landslide event in Boklua district, Nan province during 27–29th July, 2018 (heavy rainfall).

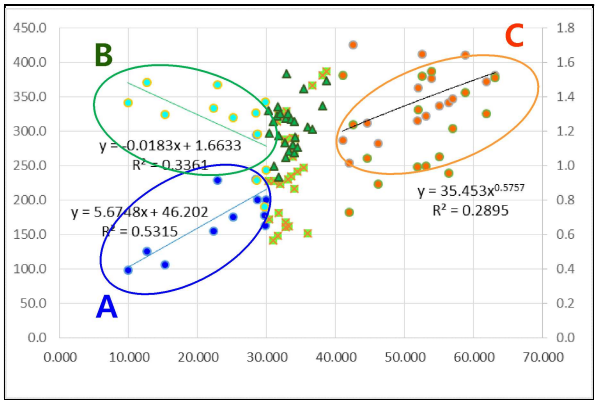

Fig. 7 The 3 patterns of MCAPI clustering model

The existing API (API$_t$) was shown that it was not greater than CAPI. So, CAPI in Doi phuka national park is 313.3 mm. On 28 July, rainfall continue increase and it was highest API$_t$ and quite near CAPI. The landslide event occur in this time (Table 3).

Table 3 Application of MCAPI for flood event in extreme rainfall, Nan province during 27–29th July, 2018

	24-Jul	25-Jul	26-Jul	27-Jul	28-Jul	29-Jul	30-Jul
rainfall	41.7	94.8	56.9	25.4	91	45.2	30.5
rainfall accumulation	41.7	136.5	193.4	218.8	309.8	355	385.5
APIt (k= 0.89 , APIt-1 = 239.8 mm)	255.1	308.2	270.3	238.8	304.4	258.6	243.9

The existing API (APIt) was shown that it was not greater than CAPI. So, CAPI in Doi phuka national park was approximately 266 mm. On 28 July, rainfall continue increaseand API$_t$ were more than or quite near CAPI. Flood and landslide events occurred as projected (Fig. 8). From this event, the organizer that concern about early warning especially local organizer have to closely investigate and observe daily rainfall.

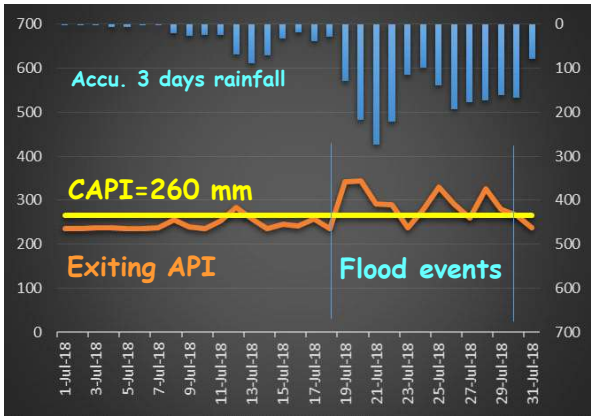

Fig 8. Application of MCAPI for flood event in extreme rainfall, Nan province during 27–29th July, 2018

When compare APIt with CAPI, other stations did not occurred flood because APIt less than CAPI (Fig.9).

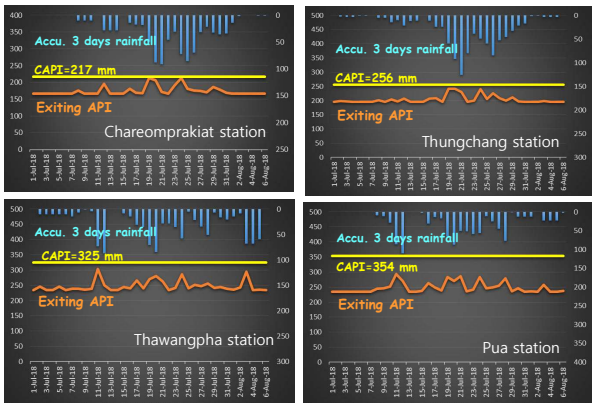

Fig. 9 Comparing API_t with CAPI in other stations

Event II: During July to September in 2011 (Strong Lanina)

When compare API_t with CAPI in 2011, accumulate rainfall at Doi phuka national park high increase and API_t were more than or quite near CAPI. Flood events occurred as projected on 20-26 August 2011 (Fig10).

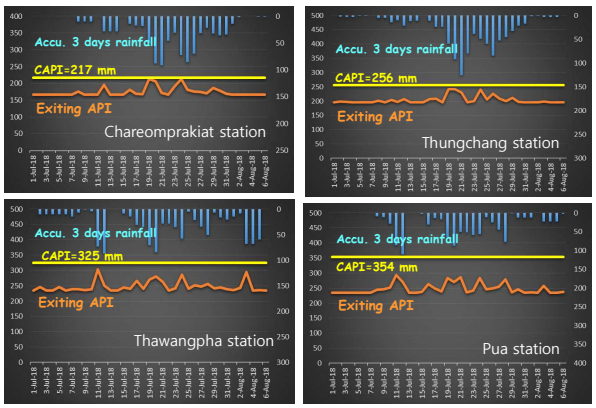

Fig.10 Comparing API_t with CAPI during July to September in 2011 (Strong Lanina)

Conclusions and Recommendation

Average Modified Critical Antecedent Precipitation (MCAPI) was approximately 257.74 mm. It could be said that quite low moderate soil storage capacity because average bulk density was showed quite high (1.22 g/cm^3) and average saturated soil moisture was quite low (36.6% by vol.)

The 3 patterns of MCAPI forecasting model were determined using multi-criteria analysis and clustering analysis based on saturated soil moisture and bulk density.

When compare API_t with CAPI in 2018, accumulate rainfall at Doi phuka national park continued increase and API_t were more than or quite near CAPI. Landslide events occurred as projected. Other stations did not occurred flood because API_t less than CAPI.

Acknowledgment

I would like to thank you ADAPT project for research funding. In addition, this research would not have succeeded if the lack of assistance from local officials of Doi Phukha national park, Nan province, Department of National Parks, Wildlife and Plant Conservation for field survey and data collection.

References

[1] Koehler, M. A. & Linsley, R. K. Predicting the runoff from storm rainfall. Research Paper no. 34, Weather Bureau, US Dept of Commerce, Washington, USA., 1951

[2] Benkhaled A, Remini B, Mhaiguene M. 2004. Influence of antecedent precipitation index on the hydrograph shape. Paper presented at the hydrology: science and practice for the 21st century. In: Proceedings of the British Hydrological Society International Conference. Imperial College, London, July 2004. British Hydrological Society, London, UK.

[3] Walter T. SittnerCharles E. SchaussJohn C. Monro. 1969. Continuous Hydrograph Synthesis with an API-Type Hydrologic Model.

[4] Luc Descroix, Jose L. Gonzalez Barrios, J.P Vandervaere, David Viramontes, and A Bollery. 2002. An experimental analysis of hydrodynamic behaviour on soils and hillslopes in a subtropical mountainous environment (Western Sierra Madre, Mexico). Journal of Hydrology 266(1-2):1-14.

[5] Luca BroccaF., MeloneF., MeloneT., MoramarcoT., and Moramarco. 2008. On the estimation of antecedent wetness condition in rainfall-runoff modeling. Hydrological Processes 22(5):629-642.

[6] Rahardjo, H., Li, X. W., Toll, D. G., & Leong, E. C. The Effect of Antecedent Rainfall on Slope Stability. Geotechnical and Geological Engineering, Vol. 19, 2001, pp. 371-399.

[7] Soralump, S., & Thowiwat, W. Dynamics Landslide Susceptibility Model. Proceedings the 15th National Convention on Civil Engineering, Thailand, 2010

Aanalysis of Local Community Awareness on Climate Hazards in Pursat Province, Cambodia

Chhunleang Rorm[1,a,*], Pongsak Suttinon[1,b], Sokchhay Heng[2,c] and Sophea Chhim[3,d]

Abstract Pursat province, a potential province for agricultural development in Cambodia, is prone to climate hazards such as flood and drought. Almost every year, flooding and flash flood happen during the monsoon season while drought frequently occurs all year round, resulted in damages to agriculture, housing, and infrastructure. To propose a proper mitigation measure for such natural disasters, understanding the characteristics of the climate hazards and local community awareness on those hazards are considered as one of the essential steps to implement. This study is aimed to identify ways and means for rural and indigenous communities, as well as to local institutions, to prepare and to mitigate and respond to natural disasters. Structured and semi-structured questionnaire survey on 750 peoples out of 47,880 people in 45 villages of Bakan and Phnom Kravanh district in Pursat province was conducted. Seventeen samples on average in each village were randomly selected for the interview. Major findings of the survey are: (1) the area, mainly relying on agriculture, is high vulnerability to climate hazard especially drought and flood; (2) drought is the major climate hazard confronting by communities whose main assets confronting to drought are agricultural land, water supply, livelihood, livestock, and natural resources; (3) flood occurred was flashflood that takes shorter time to finish. Flood hazard is not really a major problem at the present but in the future, it would be; (4) the capacity response to drought and flood is low and also limit to response climate hazards in the future. The results provide important information for further studies in order to propose a sustainable disaster management strategy.

Keywords *Climate hazards, drought, flood, local community awareness, Pursat province*

[1]Department of Water Resource Engineering
Faculty of Engineering, Chulalongkorn University
Bangkok, Thailand
[2]Faculty of Hydrology and Water Resources Engineering
Institute of Technology of Cambodia
Phnom Penh, Cambodia
[3]Community Based Disaster Risk Management and Farmer Water Users Community Support Project
Phnom Penh, Cambodia

[a]leangchhun35@gmail.com
[b]Pongsak.Su@chula.ac.th
[c]heng_sokchhay@yahoo.com
[d]spchhim@gmail.com

Introduction

Pursat province, the potential province for agricultural development, is prone to natural disasters including flood, drought, and typhoon. Almost every year, climate hazards cause significant damages and losses to lives, injury, loss of livestock, and damages to housing, crop and community infrastructures. The most vulnerable group during the disaster occurrence includes the poor, women-headed households, children, old people, and the disables. Previously remarkable flood damages in the province were in 1996, 2000, 2011 and 2013, which normally shoved the local people into poverty, food insecurity, and health problem while drought happens almost every year, which severely affects crop productivity especially rice. Flood and drought recovery, for a developing country like Cambodia, always takes time and good budget allocation, which directly or indirectly prolongs the growth of the country economy.

The Royal Government of Cambodia (RGC) plans to develop Cambodia to be an upper-middle-income country in 2030 and a high-income country in 2050 [1]. In order to reach this target, many strategic plans have been set up including the disaster management plan both national and local level to help to improve the quality of life of local people to be resilient with the flood as well as other disasters. To implement this strategic plan, understanding about characteristics of the climate hazards and awareness of local people to respond to those hazards is very essential for flood risk management [2]. Therefore the RGC agency particularly, Ministry of Water Resources and Meteorology (MOWRAM) cooperated with Asian Development Bank (ADB) under the project of Community Based Disaster Risk Management (CBDRM) and Farmer Water Users Community (FWUC) proposed an activity called "Hazard Vulnerability and Capacity Assessment (HVCA)" to accelerate the CBDRM plan in 45 villages of Bakan and Phnom Kravanh district in Pursat province, so as to enable with provision of safer villages.

The public awareness and attitudes towards climate hazards such as flood and drought need to be understood for hazard management plan while this impact could be mitigated through the application of

both structural and non-structural measures. Therefore, the overall objective of HVCA was to identify ways and means for rural and indigenous communities, as well as to local institutions, to prepare and to mitigate and respond to natural disasters in 45 villages of Bakan and Phnom Kravanh districts in Pursat province. The key research questions are:

1. What is the characteristic of flood and drought in Bakan and Phnom Kravanh districts?
2. What are the major impacts of flood and drought on the local people in the villages?
3. What are the flood and drought responses of people living in Bakan and Phnom Kravanh district?

Materials and Methods

A. Study area

Pursat, the fourth biggest province in Cambodia, is located in the western part of country with the total area of 12,692 km^2. It is located at 12°00'N to 13°00'N North latitude and 102°55'E to 104°30'E East longitude (Fig. 1). The whole province is divided into 6 districts: Bakan, Kandieng, Krakor, Phnom Kravanh, Krong Pursat, and Veal Veng district with the total population of 397,107 heads in 2008. The climate is humid and tropical but with some variation over the period of a year. The highest monthly rainfall was about 260 mm in October while the highest temperature was in April, around 35 °C. The total annual rainfall is typically around 1,500 mm [3].

The 45 villages are located in 5 communes in Bakan and Phnom Kravanh districts as shown in Fig. 1 with the total area of around 380 km^2. The area is laid in the central part of the Pursat river catchment surrounded by Cardamon Mountain at the south-western part of the province, starting at an elevation of around 1.7 masl to 1778 masl, and flat land at the north-eastern part of the province until reaching the Tonle Sap Great Lake. The Pursat River has two main tributaries: Stung Peam (Peam river) and Stung Santre (Santre river); both rivers flow in a northerly direction and meet the Pursat river at latitude 12°20' and longitude 103°45', just above the Bac Trakoun hydrological station. This situation makes the selected villages prone to flood and flash flood during the intensive rainfall, and easily get dry without rain in just a few weeks. Moreover, storm and lightning also caused deaths, injuries, as well as properties lose to local people during the monsoon season.

B. Hazard Vulnerability and Capacity Assessment (HVCA)

The Hazard, Vulnerability and Capacity Assessment (HVCA) refers to the use of participatory rural appraisal method and tools in gathering information about past patterns of hazards, present threats and vulnerabilities at the community level and of the available resources community uses or can use to cope with the adverse effects of a disaster events. As shown in **Fig. 2**, the conduct of HVCA is not the desired end goal, yet an HVCA is conducted because of the need to obtain a disaster risk profile of the community and based on this, formulate and implement a proper-disaster preparedness and mitigation plan for the community. In this research, climate hazards mainly refer to flood and drought – the characteristic and the impact of flood and drought.

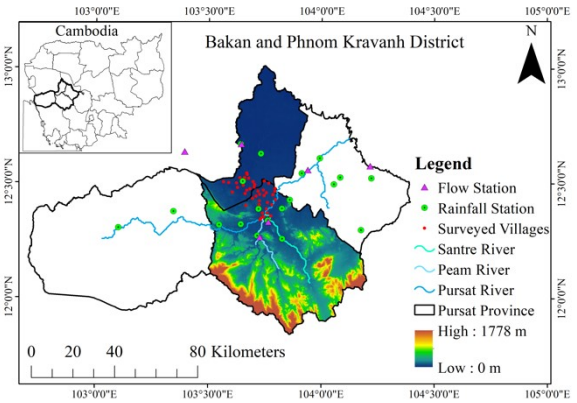

Fig. 1. Bakan and Phnom Kravanh districts, Pursat province

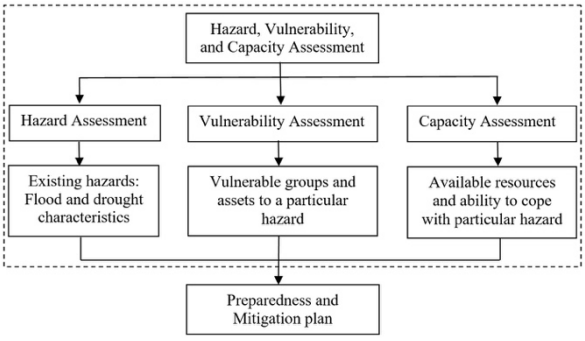

Fig. 2. Component of Hazard, Vulnerability and Capacity Assessment

C. Questionnaire survey

A set of questions was designed and developed by the HVCA group. The questionnaire is composed of 5 main sections which are general information, population data, socio-economic data, disaster events and vulnerability assessment, and disaster events response and capacity assessment.

The data collection and HVCA processing was conducted in 45 villages from 30 December 2015 to 05 April 2016 by the project team including gender staff and team, where the theme was in consonance of provincial and district administration. Prior intimation was given to all government line departments and community based stakeholders to ensure wider participation or to be on board. The process started

with direct group discussions with villagers to know some basic demographic facts of the village and commune including number of villages, demography, river network, and infrastructure. Other facts included of different hazards prevalent in the area and disaster history, livelihood of the villagers and a visit of the area for a better understanding. The processes were very interactive, giving everybody a right to participate and provided full chance to speak and ask anything from the team, about which they do not understand. After orientation, the villagers were asked to deliver facts and figures and to make it further interesting. The team spent 3 days to process HVCA for each village.It is a participatory process of 15 to 17 villagers engaged.

TABLE I. Area, population, and sample size of each village

N°	Name of village	Area (km^2)	Population (head)	Sample size	Sample density (head/km^2)
1	Trayang Sa	2.11	424	15	7.11
2	Boeng Kak	4.83	909	15	3.11
3	Serei Kunthea	3.66	830	15	4.10
4	Chhnal Moan	4.69	635	15	3.20
5	Rohal Til	31.00	1783	15	0.48
6	Ou Ruessei	2.00	1085	16	8.00
7	Chan Serei	1.02	301	14	13.73
8	Buor Chres	2.62	513	17	6.49
9	Prahal	27.31	1911	17	0.62
10	Prey Veang	8.63	1644	15	1.74
11	Prey Kantout	93.63	1907	17	0.18
12	Prek Mouy	8.99	909	15	1.67
13	Tuol Thma	3.30	488	15	4.55
14	Kandal	3.17	1207	15	4.73
15	Thmei	9.00	1551	18	2.00
16	Baos Ko	5.23	1114	16	3.06
17	Tuol Chreav	3.15	423	15	4.77
18	Prey Roung	10.50	1340	15	1.43
19	Kaoh Svay	4.27	795	17	3.98
20	Prey Tao	3.10	570	19	6.13
21	Kouk Rumlo	2.20	456	27	12.27
22	Tuol Pongro	3.09	386	15	4.85
23	Krabau Chrum	4.88	1710	15	3.08
24	Damnak Kansaeng	Missing	488	15	0.00
25	Som Sant	15.91	2242	16	1.01
26	Tang Kouk	27.88	2189	16	0.57
27	Ou Rumchang	3.80	1623	15	3.95
28	Koh Voat	4.05	849	18	4.44
29	Kaoh Svay	4.27	795	16	3.74
30	Ou Heng	3.61	989	15	4.15
31	Prek Mouy	Missing	1981	20	0.00
32	Preaek Bei	1.74	911	15	8.62
33	Samraong 1	1.51	577	15	9.93
34	Samraong Pi	6.56	1792	21	3.20
35	Ta Lou	7.50	1813	21	2.80
36	Thlok Dangkao	9.30	1669	16	1.72
37	Kranham	6.37	1459	15	2.35
38	Bak Chenhchien	5.11	1824	21	4.11
39	Stokhtom	4.69	950	16	3.41
40	Prey Kanlang	4.45	1057	15	3.37
41	Chrey Kroem	3.75	1887	15	4.00
42	Phteah Rung	10.43	1249	15	1.44
43	Bat Rumduol	Missing	2263	20	0.00
44	Ta Sas	7.70	1632	22	2.86
45	Chongruk	7.46	1750	19	2.55
	Total	378.47	54880	750	
	Average	9.01	1220	17	1.98

Results and Discussion

A. Spatial distribution of samples and general information of respondants

The HVCA team interviewed 750 persons, in which 377 respondents are female. The average age of the persons is found to be 48 years old, the less aged is 17 years old, and the most aged is 85 years old. The distribution of the age of the respondents is illustrated in Fig. 3. The statistic reflects that approximately 72% of respondents are local farmers while the rests are working as local government agencies and doing small business. However, still a part of their income comes from agriculture even though they have other positions in the government or do other small businesses.

TABLE I indicates the area, name, total population, and the sample size of each village. The average sample size is found to be 17 people per village on average varying from 27 respondents in Kouk Romlo villagae to 14 respondents in Chan Serei village. The average sample density is approximately 2 people/km^2.

B. Population data

The population data provides the basic information about the detail statistics of the respondents living in the villages, which included following important sub-details in the order of average, minimum, and maximum of male and female population as 628/160/1,164, number of households as 264/66/481, number of children (0-15 years old) as 415/10/852, number of elderly persons (> 60 years old) as 79/13/249, number of orphan as 3/0/21, number of landless families as 11/0/47, number of

people migrating per year (average last 5 years) on seasonal basis as 44/0/153, number of people migrating per year (average last 5 years) on long-term basis as 22/0/212.

The total population in the 45 villages are 54,880 people in which 51.5 % are female with 11,870 of households meaning that there are around 4 or 5 people in a family on average. The main source of income of the people is agricultural activities where typical activities are growing rice, cassava, and other vegetables as well as livestock. People migrated out for work are about 9.6 % of the total population, in which 50.2% migrated within Cambodia and 49.8% did outside Cambodia. People migrated out for work are adults who mostly finished their study in primary and secondary school.

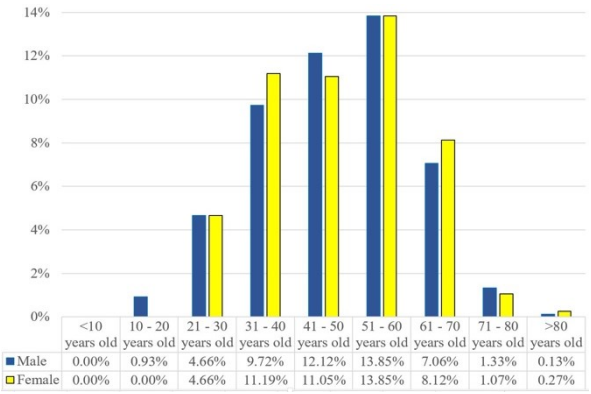

	<10 years old	10 - 20 years old	21 - 30 years old	31 - 40 years old	41 - 50 years old	51 - 60 years old	61 - 70 years old	71 - 80 years old	>80 years old
Male	0.00%	0.93%	4.66%	9.72%	12.12%	13.85%	7.06%	1.33%	0.13%
Female	0.00%	0.00%	4.66%	11.19%	11.05%	13.85%	8.12%	1.07%	0.27%

Fig. 3. Age of respondents

C. Socio-economic data

Understanding about socio-economic development in the community is very necessary for disaster risk management because the risk is different based on the level of standard of living of the people [4].

The percentage of the household having motorbike, car, 2-wheel tractor, 4-wheel tractor, livestock, poultry, concrete or brick house, water storage tank, and mobile phone is indicated in Fig. 4. All families have poultries basically referred to household chickens and ducks, while 63% of the households feeds animal such as cattle and pigs. Moreover, all households have their own water storage tanks (big concrete jar) for rainwater harvesting during the rainy season. All families own the mobile phone more than one since it is very useful and affordable. On the other hand, only 2% of the families has their own car, 4-wheel tractor, and concrete/brick house while 24% of households have the 2-wheel tractor and 68% of the households owns motorbike.

Fig. 5 indicates the challenges of the socio-economic development in the villages. The most difficult issue of the people in the villages is lacking of irrigation system. Because almost 100% of the main sources of the income of the people in the village is agriculture, lacking of irrigation system makes their agricultural activities less intense. For example, people can grow rice only once per year depending on rainwater, which is very risky and vulnerable to the impact of climate hazards such as flood and drought. Moreover, according to [5], agriculture in Cambodia is more or less affected by climate change without climate change adaptation measure. Other challenges are lack of market and low price for agricultural productions, especially the price for the rice and cassava, lack of stable employment and no factories nearby the community resulted in migration out for work, lack of infrastructure such as road, water supply and sanitation. Other difficulties are the lack of technical support for agriculture, health problems and being in debt of micro-finance (50% of the households).

D. Disaster events and vulnerability assessment

The frequent hazards over the last 20 years are indicated in TABLE II. The level of severity of the hazards are classified based on the experience of respondents in term of the impact of climate hazards on their agricultural production since agriculture is the main source of their incomes. In this case, it is assumed that people get 100% of their agricultural products without the impact of climate hazards, 3 tons/ha for paddy rice on average (major crop). Based on this baseline scenario, the order of severity of climate hazards is categorized; for instance, less than 15% of yield reduction is called Slightly with the symbol of one star in the remark (*); between 15% to 30% of yield reduction is called Moderate (**); 30% to 60% of yield reduction is called Severe (***), and more than 60% is called Extreme (****). According to National Committee for Disaster Management (NCDM), the majority of agricultural damages in Cambodia is caused by flood and drought, where 70% of damages caused by flood and other 30% caused by drought. People easily differentiate these two climate hazards by the amount of available water for their crops during the growing period in each year. Crop damages due to water scarcity is called "Drought"; on the other hand, crop damages due to too much water in the field is called "Flood".

Based on this classification, it can be summarized that slightly and moderate drought happened in 2002, 2004, 2009, 2012, 2013, and extreme drought recently happened in 2014, 2015 and 2016. The significant flood was in 2000, 2011 and 2013. Storm only occurred in 2012, 2013 and 2014. In 2013, storm and flood were the major climate hazards in the country which severely affected and destroyed crops, households and infrastructures. According to the disaster damage record from NCDM, flood rarely occurs; however, the damages caused by flood are more severe comparing with drought damage.

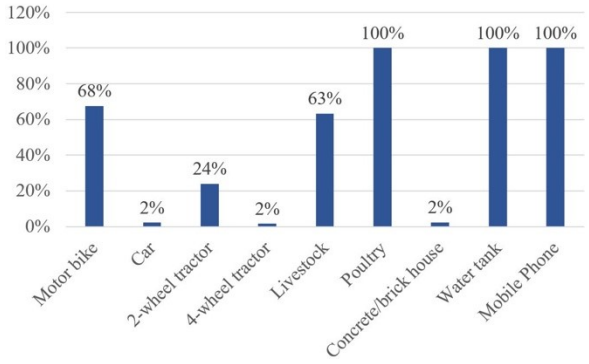

Fig. 4. Household having these assets

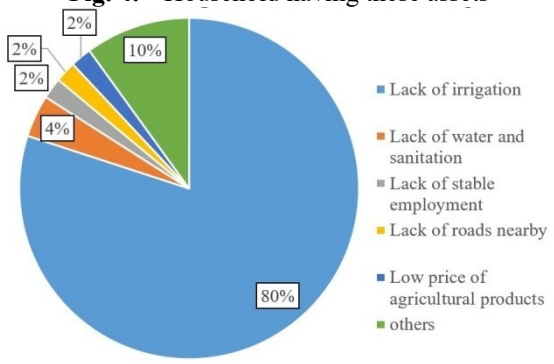

Fig. 5. Challenges of socio-economic development

TABLE II. History of occurrence climate hazards

Year	Drought	Flood	Storm	Hot temperature
1995-1999				
2000-2004	**	****		
2005-2009	**			
2010				
2011		**		
2012	*		**	*
2013	**	**	***	*
2014	****		**	**
2015	****			**
2016	****			**

* Slightly, ** Moderate, *** Severe, **** Extreme

TABLE III. Major impact by climate hazard

Rank of impact	Drought	Flood	Storm
1st	Crop	Road	Housing
2nd	Water supply	Crops	People
3rd	Livestock	Livestock	Crops
4th	People	People	Livestock

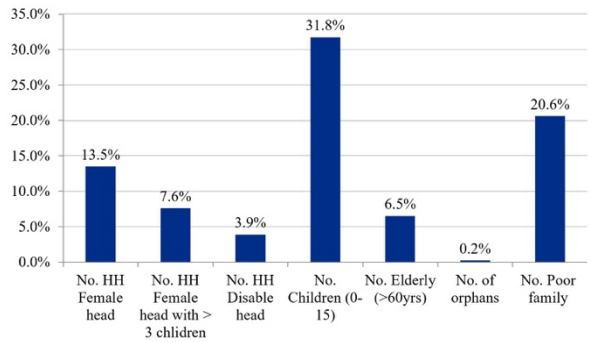

Fig. 6. Vulnerable group during the climate hazards

The major impact by climate hazard is summarized in **TABLE III**. As can be seen, crop is the most vulnerable to drought, while infrastructure and housing aresusceptible to flood and storm respectively. The most vulnerable group during the climate hazards in the villages are illustrated in **Fig. 6**. The vertical axis refers to the number of vulnerable group in percentage (%). From the survey, children are the most vulnerable group to all climate hazards (31.8%), which is similar to the record from National Committee for Disaster Management (NCDM) of Cambodia between 1996 and 2014, where the people death, missing, and injured during the climate hazards were mostly children (0-15 years old). Besides, poor family (income less than 100 US$ per month per family), women-headed family, the elder group (> 60 years old), disable people and orphans are also very vulnerable to climate hazards since they are not resilient enough to climate hazards both physical and financial condition.

E. Disaster events response and capacity assessment

The discussion in this part focuses mainly on the behavior of the local people in the villages responding to flood and drought with their existing traditional adaptation measures. Well-understood about the knowledge, behavior and resources of the local people using to cope with climate hazards leads to define the appropriate preparedness and mitigation measures for the community.

The identification of the hazard can be observed by the people. In this case, 100% of the respondents knows exactly which hazards occurred when their crops were damaged, for example, their crops destroyed by flood or affected by drought. Moreover, 24% of respondents revealed that they define the characteristic of flood or drought due to the water level in the river and based on their experiences, they can predict some climate hazards and prepare their assets from damages caused by those hazards; however, this situation is valid for only people who live near water sources. Similarly, 73% of the respondents identifies the hazards differently due to their experiences in different ways such as observing the insect behaviors, dead animals, unusually hot, heavy rainfall, strong wind, and no rainfall.

Besides hazard identification, the statistic also reflected that 42% of the total villages has the disaster response plan and preparation while 58% of the villages does not prepare any disaster response plan and preparation. People often adapt with the climate hazards by their traditional measures; for instance, seed and fertilizer preparation, reserve water (water jars, ponds…), changing crop types, animals shelters, migrate out for work to get income during the drought period. Flood adaptation measures include: paddy rice seed preparation, reserve food, medicine, and clean water, prepare stuffs and put high enough safe from level of flood water, reserve safe place for

family and animal, migrate out for work. However, it is confirmed that the traditional adaptation measures are practical as long as the climate hazards are not extreme and frequent so that they can have resources to prepare and respond to the climate events; otherwise, they are still highly vulnerable.

As can be seen in Fig. 7, the nearest safe sites for most of the villagers were school, health center, elevated place and pagoda. The average maximum distance of these places is more or less than 1000m. The furthest safe place was high way, which was around 3000 to 4000m from their houses.

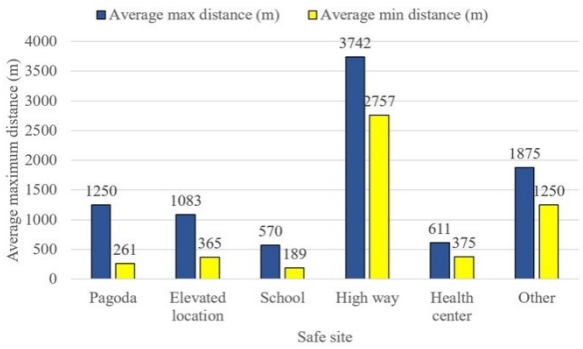

Fig. 7. Range of distance to safe site for most people

F. HVCA evaluation

The same study was conducted in district Thatta, Sinhd, Pakistan in 2014 [6]. The study area is around 17,355 km^2 with the total population 1.113 million in 1998, which is quite big comparing with the area and population of 45 villages in Bakan and Phnom Kravanh districts. According to the finding, the economy of district Thatta is based on agriculture and fishing, where the main crops are wheat, rice and sugarcane. Flood hazard is considered as the most affected to life, health, property, and natural floodplain resources comparing with drought, which is different from our study area, where flood is not really a major climate hazard. The element at risk during flooding including vulnerable groups and assets in the district Thatta are elderly people (> 65 years old), Children (< 15 years old) and pregnant women, and livestock, housing and infrastructure, which is quite the same of those in Bakan and Phnom Kravanh districts. Other hazards in district Thatta are cyclone and saline water intrusion since the area is located near the Arabian Sea. The most vulnerable groups of these hazards are people who live near the sea (fisherman), and also some assets such boats and fishing nets, as already mentioned that fishing is the second largest occupation to get the income in the area. Comparing with Bakan and Phnom Kravanh districts, both study areas are prone to climate hazards. According to the finding, it can be said that district Thatta is even more vulnerable due to the location of the area. However, the coping capacity of most of the people in district Thatta are better meaning that they can find the way to cope with those climate hazards better since they have frequently experienced many types of climate hazards, whereas the ability and resources of the people in Bakan and Phnom Kravanh districts are very limited and very traditional to adapt with the climate hazards. This situation make them more vulnerable if the extreme hazards occur in the future.

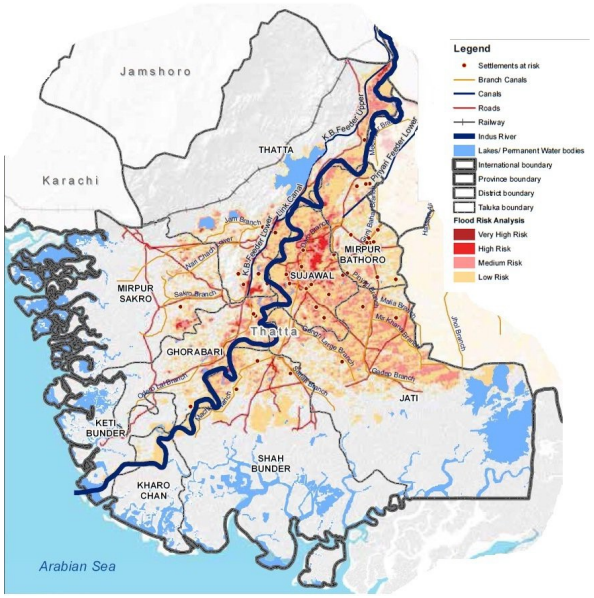

Conclusions

This study attempts to analyze ways and means for rural and indigenous communities, as well as to local institutions, to prepare and to mitigate and respond to natural disasters. A set of questions was developed and used to interview 750 people in 45 villages within two districts: Bakan and Phnom Kravanh districts in Pursat province, the most vulnerable area to climate hazards, corresponding to about 2 sample/km^2 on average. The survey was implemented by the project team. Questionnaire survey was conducted using a random method for respondents as local people together with some criteria such as local governor selection, for instance, village chief and deputy village chief. The questionnaire is composed of 5 main sections which are general information of respondents, population data, socio-economic data, disaster events and vulnerability assessment, and disaster events response and capacity assessment. The survey took place from 30 December 2015 to 05 April 2016. Major findings of the survey are: (1) the area, mainly relying on agriculture, is high vulnerability to climate hazards especially drought and flood. The major challenges for socio-economic development in the villages were lacking of irrigation system, water and sanitation, stable employment in the villages, low price of agricultural products; (2) drought is the major climate hazard confronting by communities whose main assets confronting to drought are agricultural land, water supply, livelihood, livestock, and natural resources; (3) flood occurred d was flashflood that takes shorter time to finish. Flood

hazard is not really a major problem at the present but in the future, it would be. The main assets confronting to flood are infrastructure, agricultural land, housing, and livestock; (4) the capacity response to drought and flood is low and also limit to response climate hazards in the future. The results provide important information for further studies in order to propose a sustainable disaster management strategy.

Acknowledgment

The authors would like to express high gratitude to the Community Based Disaster Risk Management (CBDRM) and Farmer Water Users Community (FWUC) Project of which the data was extracted for the analysis in this paper.

References

[1] RGC, "National Strategic Development Plan 2014-2018 of The Royal Government of Cambodia," 2014.
[2] N. S. Romali, M. S. A. K. Sulaiman, Z. Yusop, and Z. Ismail, "Flood Damage Assessment: A Review of Flood Stage–Damage Function Curve," pp. 147-159, 2015.
[3] "Cambodia Water Resources Profile, Water Resources Management Sector Development Program ADB Loan 2673-CAM and TA 7610-CAM," 2014.
[4] T. T. Vu and R. Ranzi, "Flood risk assessment and coping capacity of floods in central Vietnam," Journal of Hydro-environment Research, vol. 14, pp. 44-60, 2017.
[5] T. S. Thomas et al., "Cambodian Agriculture: Adaptation to Climate Change Impact," Environment and Production Technology Division, vol. IFPRI Discussion Paper 01285, 2013.
[6] M. Khan, "SIRAT Hazard Vulnerability and Capacity Assess (1)," Islamic Relief 2014.

Formulationof adaptation measures for flood management under the uncertainty of future projection

Hisaya Sawano[1], Katsunori Tamakawa[1], Badri Bhakta Shrestha[1], Tomoki Ushiyama[1], Maksym Gusyev[1] and Toshio Koike[1]

Abstract Climate change is anticipated to affect the conditions of precipitation, which may, in turn, increase flood and drought risks in the future. Therefore, the necessity of adaptation measures is widely recognized and advocated. However, the evaluation of climate change impacts is still in the realm of uncertainty because various future development scenarios and Global Climate Models provide different future projections. Thus, the formulation of adaptation measures requires first quantifying uncertainty in order to identify the range of probable precipitation and assessing potential disaster risk in the future with socioeconomic changes. Then, measures to reduce disaster risks should be determined by combining structural measures to mitigate the impact of hazards and non-structural measures to cope with the remaining risk that cannot be mitigated by structural measures. Essential elements of this process are past and present data of hazards, damage, and socioeconomic factors to assess current and future risks and evaluate the effectiveness of selected adaptation measuresby utilizing science and technology. Close cooperation among decision makers and practitioners is crucial in this process by sharing information and resources to formulate effective measures. To facilitate dialogue and consensus among decision makers in a country for actions to achieve disaster risk reduction, the platform on water resilience and disasters has been in place in several Asian countries and is expected to be the basis for the formulation of adaptation measures. This paper explains an effective mechanism and requirements for formulating adaptation measures for mitigating the future impact of climate change.

Keywords *climate change; adaptation measures; disaster risk reduction; platform on water resilience and disasters*

[1]International Centre for Water Hazard and Risk Management (ICHARM)
Public Works Research Institute (PWRI)
Tsukuba, Japan

Current and future water-related disasters and efforts for disaster reduction

In the recorded numbers of natural disasters in the world, water-related disasters occupy around 80% of all natural disasters, and about 40% of the water-related disasters occur in Asia alone (Fig.1) [1]. Water-related disasters are also frequent in Japan. Flood disasters, in particular, have become more destructive as torrential rainfall has become increasingly localized and intensified. In addition, more floods of larger scales have been reported in areas that have rarely experienced such events before, causing a huge loss of human lives and property and inflicting serious damage on socio-economic activities.

The Synthesis Report of the Fifth Assessment Report of the Intergovernmental Panel on Climate Change (IPCC) warns that extreme precipitation events will become more intense and frequent in many regions and cause concerns for the possibility of further intensification of flood disasters in the future. Therefore, for the formulation of adaptation measures to respond to the impact of climate change, future changes in discharge, inundation, and other aspects of a flood hazard should be analyzed first based on the assessment of future changes in rainfall. Then, the results should be used to evaluate corresponding changes in flood disaster risk as fundamental information for designing effective adaptation measures. In the formulation of adaptation measures, it is crucial to share information among organizations concerned to create a common understanding of issues to be addressed, which is a basis to formulate a strategy with the best mix of different measures under the control of different government agencies.

There are primarily four essential issues in the process of formulating a strategy. One is the identification of uncertainty arising in the prediction of future events. Such uncertainty originates in differences among Representative Concentration Pathways (RCP) scenarios and Global Climate Models (GCMs). Another is the understanding of the background of uncertainty among all stakeholders to form a consensus. The third one is the quantification of uncertainty by predicting the range of possible values in the future, and the last one is the application of uncertainty to decision making on the best mix of adaptation measures so as to cope with possible future conditions.

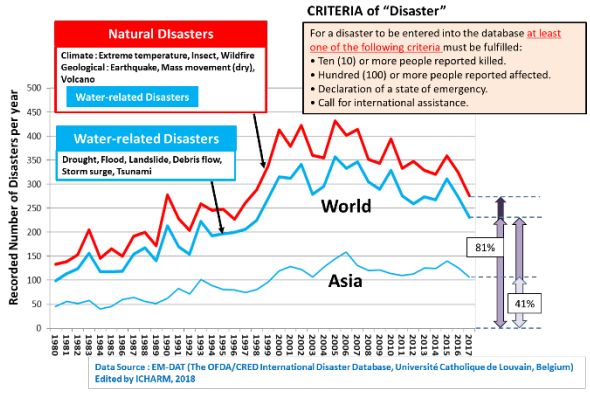

Fig. 1. Natural Disaster Trend (1980-2017)

In formulating a strategy with the best mix of adaptation measures, each measure should be evaluated for its effectiveness based on analysis using the latest science and technology. Unfortunately, since the development of the capacity needed to undertake this task is still underway in many developing countries, international cooperation and support are essential. The United Nations is working on this challenge through the promotion of disaster prevention activities at international meetings and conferences, while requesting countries to make vigorous efforts to achieve the targets adopted in such conferences as an international agreement.

In 1994, the "World Conference on Natural Disaster Reduction (WCDR)" was held in Yokohama, Japan, as the first international interdisciplinary conference to discuss natural disasters and adopted the "Yokohama Strategy and Plan of Action for a Safer World." Despite such events, the interest in natural disasters was not so high in the international society in the 1990s and 2000s since the high-risk areas of natural disasters were mainly in Asia, Africa and South America. Accordingly, when the 2nd WCDR was planned in January 2005, it did not draw much attention from many developed countries. However, it turned out to be an important event and attracted a lot of global attention because of the tsunami disaster caused by the Indian Ocean earthquake in December 2004 with more than 230,000 dead or missing including many tourists from developed countries. As a result, the 2nd WCDR was attended by participants from almost all UN member countries, and the "Hyogo Framework of Action (HFA) 2005-2015" was adopted as guidelines for the international efforts to tackle disaster reduction.

After the 2nd WCDR, though many efforts had been made for disaster risk reduction, large-scale natural disasters occurred in the world such as Hurricane Katrina of USA in 2005, Cyclone Nargis of Myanmar in 2008, a large-scale flood of Brazil in 2011, the tsunami disaster by the Tohoku Earthquake of Japan in 2011, and a large-scale flood of Thailand in 2011. In 2015, the 3rd WCDR was held in Sendai, Japan after those disasters and adopted the "Sendai Framework for Disaster Risk Reduction 2015-2030," which states four priority actions (1.Understanding disaster risk, 2.Strengthening disaster risk governance to manage disaster risk 3.Investing in disaster risk reduction for resilience, and 4. Enhancing disaster preparedness for effective response and to "Build Back Better" in recovery, rehabilitation and reconstruction) and seven global targets such as the reduction of global disaster mortality and disaster economic loss. In September 2015, the "Sustainable Development Goals (SDGs)" were adopted at the UN Sustainable Development Summit, aiming, as one of the targets, to "significantly reduce the number of deaths and the number of people affected and substantially decrease the direct economic losses caused by disasters including water-related disasters." In December 2015, the "Paris Agreement" was adopted at the UN Climate Change Conference, or COP21, in Paris, and the "enhancing adaptive capacity, strengthening resilience and reducing vulnerability to climate change" was addressed as a global goal. In December 2016, the "International Decade for Action -Water for Sustainable Development-" was adopted at the UN General Assembly, and the participants agreed with the necessity of concerted efforts to manage water-related disaster risks. Each member state is requested to make necessary efforts for the achievement of the objectives adopted at such international conferences, and the international society has reached a consensus that it will make continuous support for countries to realize the objectives.

Prediction of impact of climate change

A. Impact assessment of climate change using Global Climate Models (GCMs)

For the evaluation of climate change impacts on flood disasters and the investigation of adaptation measures, changes in flood disaster risk due to climate change should be assessed as the first step. The process of flood disaster risk assessment starts from the identification of future precipitation, which is followed by the analysis of discharge and inundation caused by the precipitation in the floodplain to evaluate possible damage to be caused by the inundation as flood disaster risk. The future condition of precipitation should be estimated with an appropriate resolution for the discharge analysis of the target rivers. Such rainfall distribution can be obtained from Global Climate Models (GCMs). Although GCMs have coarse resolutions, high-resolution rainfall distribution data can be produced using a downscaling technique. However, each GCM has its own characteristics because of different structures and approximation methods used for the models to calculate the precipitation process. Simulation results differ among GCMs, which is a cause of uncertainty in the rainfall by the GCM projections. Therefore, ICHARM developed a combined method for the

assessment of climate change impacts and applied it to the ADB project in Vietnam, "Climate Change and Flood Hazard Simulations Tools for ADB Spatial Application Facility (SC 109094REG)," for the assessment of flood disaster risk, which consists of: 1. Quantitative impact assessment applied to the formulation of adaptation measures and 2. Qualitative impact assessment for the evaluation and understanding of uncertainty.

1*) Quantitative impact assessment applied to the formulation of adaptation measures:*The Atmospheric Global Climate Model (AGCM), which is a type of GCM, is used for the calculation of atmospheric conditions with the sea surface temperature (SST) as premises. The model provides a good resolution since a load of calculation is relatively low compared to coupled GCMs,and its grid size of calculation is smaller than other models. ICHARM uses MRI-AGCM3.2S[2] constructed by the Meteorological Research Institute (MRI) with 20-km mesh as boundary conditions, and downscaling is performed using the Weather Research and Forecasting (WRF) model [3] to obtain high-resolution results (much finer horizontal and temporal resolutions), which makes it possible to examine flood risk and its changes due to climate change in the target river basin [4]. In the case of the ADB Project in Vietnam, the horizontal resolution is 18-km nationwide and 6-km for the Red and Perfume River basins. SST is collected from monthly mean observations (present) or observations plus future changes derived from the Coupled Model Intercomparison Project (CMIP) [5]. Based on the results of the downscaling, a quantitative impact assessment method is developed, in which the daily rainfall intensity is calculated for the target probability of the present and future periods and the analysis of the discharge volume and inundation area is conducted using an observed rainfall pattern when a large-scale flood occurred in the past.

*2) Qualitative impact assessment for the evaluation and understanding of uncertainty:*To compare and comprehend the characteristics of each GCM, CMIP is being undertaken and currently CMIP5 is available. Though the uncertainty caused by model differences in predicting the impact of climate change at a global scale has been decreasing as GCMs have been improved year by year, the uncertainty generated in prediction at a regional scale is still significant. The uncertainty at a regional scale originates in the ability of each model to represent the characteristics of climate at a regional level, since each model has its compatibility; some models are suitable to represent climate conditions in some specific area while other models are suitable to do so in other areas. Therefore, understanding the difference among models in representation of climate conditions in the target area is essential to understand the uncertainty caused by the model differences.

For identifying suitable models to the target area, the scoring process is adopted in which: 1) models are selected from CMIP5 if they have enough data of basic meteorological elements (e.g., monthly precipitation, outgoing long-wave radiation, pressure at sea level, air temperature 850h Pa level, zonal wind 850h Pa level, meridional wind 850h Pa level) and 2) some of them are excluded by comparing simulated and observed data in terms of the spatial correlation coefficient (CC) and the absolute values of root mean square error (RMSE) of meteorological elements [6]. Then, statistic downscaling is undertaken to the remaining models to compare the precipitation condition in high resolution using ground observed data.

In the case of the ADB project in Vietnam, four models have been selected based on scoring system and the result of downscaling shows a similar pattern to the present (1979-2003) condition. For the future (2075-2099) period, one model (Max Planck Institutes-Earth System Model-Low Resolution(MPI-ESM-LR)) shows a different pattern from the other three models (Community Earth System Model - Community Atmospheric Model version 5 (CESM1-CAM5), National Centre for Meteorological Research - Climate Model version 5 (CNRM-CM5), NOAA Geophysical Fluid Dynamics Laboratory -Climate Model version 3 (GFDL-CM3)) (Fig.2) [7]. This is because the simulation results of the three models show that the north wind is dominant while the one model shows that the south wind is dominant as a result of the simulation of north-east monsoon formulated in the seasonal climate changes. As this case demonstrates, the simulation of climate change impact may differ according to model differences, and thus it is considered as one of the reasons causing uncertainty in the prediction.

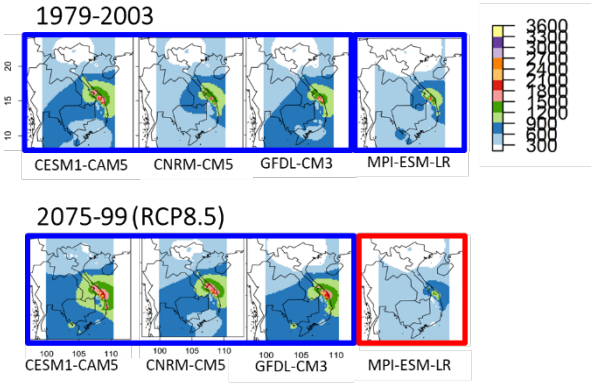

Fig. 2. Average Rainfall in October-November-December

B. Uncertainty caused by future climate scenarios

The fifth assessment report of IPCC sets four scenarios such as RCP2.6, RCP4.5, RCP6.0 and RCP8.5 in assessing the impact of future climate change. The results of future prediction for each scenario varydepending on models, and therefore the

report shows a certain range of future prediction value for each scenario. As is described in II A 2), the uncertainty caused by model differences should be well recognized, but it is not realistic to calculate all the prediction values of each model to be reflected in planning. The most practical and valid way is to use a high-resolution model of AGCM for dynamic downscaling. Even in such analysis, the uncertainty caused by the four scenarios should be noted and counted in the formulation of adaptation measures.

Disaster risk assessment

After the identification of the target precipitation, discharge and inundation analysis is conducted to simulate flood hazard conditions and then assess flood disaster damage. The damage caused by a flood is categorized into direct and indirect damage; direct damage refers to mortality, damage to agriculture, damage to houses and buildings, interruption of lifeline utilities such as water supply, gas and electricity. Indirect damage includes stagnation of socio-economic activities caused by the interruption of lifeline utilities and transportation.

For the quantification of direct damage according to the scale of a flood (area, depth and period of inundation), the correlation between damage and flood scale is indicated in the form of a damage curve. Fig.3 is an example of a damage curve [8], which shows the percentage of rice yield loss caused by the depth and duration of inundation in the rice field. By using a damage curve, the monetary value of damages can be evaluated by simulating a flood hazard.Fig.4 compares the damage to rice crop between the present and future climates for the same flood probability (return period) [9]. Since a damage curve can be established from the actual data of past floods and damage in the field, the accumulation of data is essential.

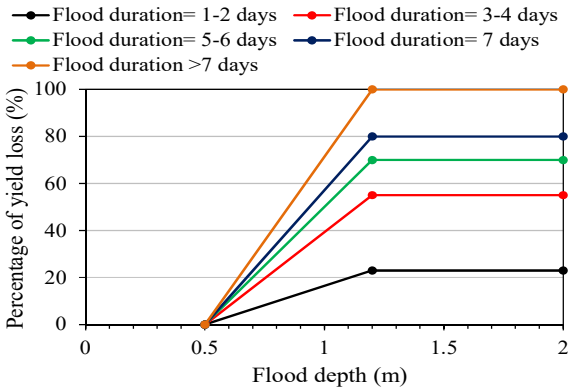

Fig. 3. Damage Curves for Maturity Stage of Rice Crops

The contents and scales of indirect damage are deduced from the condition of socio-economic activities in the area. So-called "chain-reaction damage" should be also considered, since flood damage sometimes expands to areas outside the directly affected area especially when they are connected through socio-economic activities. For example, a massive flood occurred in 2011 in the Chao Phraya River basin, Thailand, submerged a myriad of companies in its industrial estates that were producing mechanical parts for manufactures in Japan. These companies were compelled to stop operation, which affected manufactures in Japan considerably, and caused international chain-reaction damage. This incident typically teaches us that it is desirable to evaluate not only direct damage but also indirect damage in the assessment of disasters, and the differences between the two types of damage should be always kept in mind. While direct damage has a clear correlation with the scale of a flood, an indirect damage is not defined by the scale of a flood alone. Furthermore, damage evaluation requires expertise on target objects and activities for collecting information and conducting analyses. Investigation and research should be performed by employing interdisciplinary approaches under the cooperation of various fields of science and technology related to flood disasters.

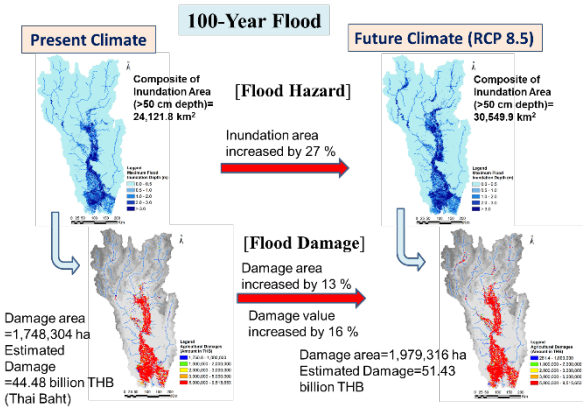

Fig. 4. Flood Damage Assessment (Rice Crops) in Chao Phraya River Basin

Formulation of adaptation measures

The basic process to formulate a strategy for flood disaster risk reduction is comprised of: 1) Identification of a target flood, 2) Assessment of flood disaster risk caused by the target flood, 3) Evaluation of the effectiveness of countermeasures to reduce disaster risk, and 4) Adoption of a strategy consisting ofdifferent measures. The formulation of adaptation measures for climate change also follows the same sequence. The elements of flood disaster risk are the scale of a hazard, the vulnerability of the target objectives and actions, and the exposure of the target objectives and actions to the flood hazard (Fig.5), and flood disaster risk is defined by these three overlapping elements [10]. A risk reduction strategy is developed by considering how each of the elements can be reduced. Hazard can be reduced by structural measures such as dams and diversion channels, vulnerability by flood-proofing buildings and basic

infrastructure and installing early warning systems, and exposure by river improvement, land use changes and evacuation. A practical strategy can be formulated by creating the best mix of these measures. For structural measures, cost effectiveness can be assessed by comparing the construction cost with the economic benefit that is estimated based on the difference in economic damage before and after the completion of structural measures.

Flood Disaster Risk = f (Hazard, Vulnerability, Exposure)

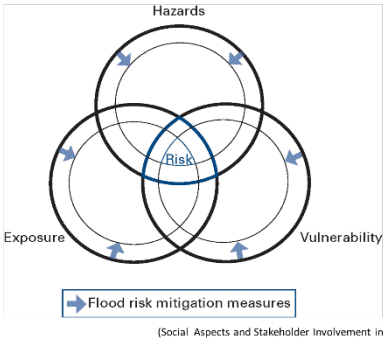

Fig. 5. The Elements of Flood Disaster Risk

As mentioned before, in the formulation of adaptation measures for climate change, the uncertainty derived from the difference among models and scenarios should be considered in the determination of a target flood. Another important point is that the consideration of the remaining risk, which refers to the possibility of a flood occurrence exceeding the probability (return period) of a target flood set to design structural measures. A contingency plan should be prepared to save lives and certain types of property by, for example, early warning and evacuation in case of a flood that exceeds the design flood defined for the structure. Flood hazard maps are a useful and effective tool for developing a contingency plan providing information on possible inundation area and depth in case of a flood exceeding the design flood scale of the structure or when structural measures are destroyed.

In an actual process of formulating a strategy for climate change, the first step is to decide the target scenario from four RCP climate change scenarios for designing structural measures. The second step is to adopt a model with a resolution high enough for the planning, which is followed by the third and fourth steps to set the design scale of a flood in terms of probability (return period) and analyze the discharge volume needed to design structural measures. The probability of occurrence of discharge exceeding the design flood volume for the structural measures that is caused by the uncertainty should also be considered as the remaining risk and incorporated in a contingency plan. In this process, although the uncertainty caused by different scenarios can be quantified, the uncertainty originating in different models can be hardly quantified since it takes a huge volume of calculation to estimate all the model-derived uncertainty, as described above. At present, therefore, it is practical and preferable to select one high-resolution model using the latest science and technology and assess uncertainty by calculating the discharge based on the four scenarios and identifying the range of future risk. It should be noted, however, that the evaluation method of uncertainty will be reexamined according to the future revisions of the scenarios or the improvement of modeling methods. In such occasions, hazard maps and contingency plans also need to be reviewed.

Conclusions and recommendations

For the formulation of adaptation measures to prepare for the impact of climate change,it is practical and rational to introduce structural measures to ensure a certain safety level and to use contingency planning to manage the remaining risk, which arisescorresponding to uncertainty derived from different future scenarios or climate models or from the possibility of occurrence of a flood that exceeds the design scale of the structure measures. A contingency plan should contain:1) Provision and supply to the public of disaster risk information produced by the governmentbased on science and technology; 2) Support and assistance provided bythe government for the public to take emergency actions (securing evacuation sites and routes, preparing communication systems, etc.);and 3) Appropriate preparedness and smooth emergency response by the public based on the information provided from the government.These actions can be effective only when the government and the public work together under a cooperative scheme. Therefore,a trans-disciplinary relationship between "science and technology" and "society" should be promoted.

Based on science and technology, the government should create and deliver disaster risk information and risk reduction measures.To facilitate such efforts, theInternational Flood Initiative (IFI), for which ICHARM has been the secretariat, assists the government and academiaentities in formulatinga "Platform on Water Resilience and Disasters (Platform)" of each country.In addition,the High-Level Panel on Water, consisting of the heads of 11 countries, submitteda report entitled "Making Every Drop Count – An Agenda for Water Action – " to the UN Secretary-General and the World Bank President on March 14, 2018, which underlines the importance of building preparedness to reduce water-related disasters and the necessity to formulate a Platform involving all stakeholders to facilitate dialogue and scale up community-based risk reduction practice. In the Global Earth Observation System of Systems (GEOSS) Asia Pacific (AP) Symposium 2018, the Platform project was highlighted in the session of the GEOSS Asian Water Cycle Initiative (AWCI) with reports from several countries where the project is

already in progress.The symposium was wrapped up, adopting the Kyoto Statement 2018,which stresses that the Platform project deserves the full-scale efforts of AWCI [11]. Since further implementation of a Platform in each country needs advice and assistance based on science and technology from the international society, IFI has been vigorously working to strengthen communication among countries and between countries and international organizations. For science and technology to contribute to socio-economic development, the global community needs to continue making concerted efforts to facilitate global dialogue, sharepractical knowledge and experience, and enhance international cooperation.

Acknowledgement

This work was conducted under the Program for Risk Information on Climate Change (SOUSEI Program) and the Integrated Research Program for Advancing Climate Models (TOUGOU Program), both of which are supported by the Ministry of Education, Culture, Sports, Science, and Technology-Japan (MEXT), and the project "SC 109094 REG : Climate Change and Flood Hazard Simulation Tools for ADB Spatial Application Facility, 2018" organized by Asian Development Bank (ADB) and UCCRTF (Urban Climate Change and Resilient Fund).

References

[1] EM-DAT (The OFDA/CRED International Disaster Database, Université Catholique de Louvain, Belgium)

[2] R. Mizuta, H. Yoshimura, H. Murakami, M. Matsueda, H. Endo, T. Ose, K. Kamiguchi, M. Hosaka, M. Sugi, S. Yukimoto, S. Kusunoki, A. Kitoh, "Climate simulations using MRI-AGCM3.2 with 20-km grid", Journal of the Meteorological Society of Japan 90A: 233–258, 2012, DOI: 10.2151/jmsj.2012-A12.

[3] W.C. Skamarock, J.B. Klemp, J. Dudhia, D.O. Gill, D.M. Barker, M.G. Duda, X.Y. Huang, W. Wang, J.G. Powers, "A description ofthe Advanced Research WRF version 3", 2008, NCAR TechnicalNote, NCAR/TN-47 + STR; 113.

[4] T. Ushiyama, A. Hasegawa, M. Miyamoto, Y. Iwami, "Dynamic downscaling and bias correction of rainfall in the Pampanga River basin, Philippines, for investigating flood risk changes due to global warming", Hydrological Research Letters 10(3), 106–112, 2016, DOI: 10.3178/hrl.10.106

[5] A. Kitoh, H. Endo, "Changes in precipitation extremes projected by a 20-km mesh global atmospheric model", Weather and Climate Extremes 11: 41–52, 2016 DOI: 10.1016/j.wace.2015.09.001.

[6] A. Kawasaki, A. Yamamoto, P. Koudelova, R. Acierto, T. Nemoto, M. Kitsuregawa, T. Koike, "Data Integration and Analysis System (DIAS) Contributing to Climate Change Analysis and Disaster Risk Reduction", Data Science Journal, 16, p.41, 2017, DOI: http://doi.org/10.5334/dsj-2017-041

[7] K. Tamakawa, A. Hasegawa, M. Gusyev, T. Ushiyama, B. Sah, H. ITO, T. KOIKE, "Climatological Understanding on Uncertainty of Precipitation by Climate Change Prediction in Vietnam", Annual Journal of Hydraulic Engineering (JSCE), Vol.74, No.5, 2018.

[8] B. B. Shrestha, T. Okazumi, M. Miyamoto, H. Sawano, "Flood damage assessment in the Pampanga river basin of the Philippines", Journal of Flood Risk Management, Vol.9, No.4, pp.355-369, 2016. DOI: 10.1111/jfr3.12174

[9] B. B. Shrestha, Y. Yamazaki, D. Kuribayashi, A. Hasegawa, H. Sawano Y. Tokunaga, "Assessment of future flood damage on agricultural areas under climate change in the Chao Phraya River basin of Thailand", Proceedings of Japan Geoscience Union Meeting 2018, HDS06-03, 2018. (https://confit.atlas.jp/guide/event-img/jpgu2018/HDS06-03/public/pdf?type=in (Accessed on 8 November 2018))

[10] World Meteorological Organization, "Social Aspects and Stakeholder Involvement in Integrated Flood Management", APFM Technical Document No.4, Flood Management Policy Series, 2006, (http://www.apfm.info/advocacy/advocacy_social.htm (Accessed on 8 November 2018)) ISBN: 92-63-11008-5

[11] The 11th GEOSS Asia-Pacific Symposium, 2018. Retrieved from: https://geoss-ap-symp11.org/_public/Kyoto_Statement_2018_Final.pdf

Flood Hazard Assessment using Hydro-geospatial Technique: A Case Study of River Chenab from Qadirabad to Trimmu in Pakistan

Tawatchai Tingsanchali[1,a] and Muhammad Asim Shoaib[2,b]

Abstract HEC-RAS flood flow model with flood inundation mapping through HEC-GeoRAS were applied to compute flood peak attenuation and mapping of flood inundation areas and flood depths in floodplains of Chenab River in Pakistan from Qadirabad to Trimmu, a reach length of 209 km. Input river cross-sections to HEC-RAS model were collected from field survey and partly extracted from DEM SRTM 30 m resolution using HEC-GeoRAS. An exceptionally high flood of 2014 and a very high flood of 2006 were considered for model calibration and verification. The results of model calibration and verification of HEC-RAS show high correlation coefficients thus assuring high model accuracy. Results of HEC-RAS model were exported to ArcGIS to perform flood inundation mapping and consequently flood hazard assessment. Flood inundation extent and depth maps were computed for floods of return periods of 25, 50, 100 and 200 years respectively. The effectiveness of the existing flood control infrastructure was evaluated in terms of flood depths and inundation areas. The novel contribution of this study is the flood hazard assessment using two different criteria: one on people safety and another on flood depths and extents. The two criteria were applied to evaluate flood hazard to people and deficiency of existing flood control embankments. Recommendations for further improvement are given.

Keywords *flood control effectiveness, hazard mapping, hazard assessment, Chenab River, Pakistan*

[1]School of Engineering and Technology
Asian Institute of Technology
Pathumthani, Thailand
[2]Punjab Irrigation Department
Pakistan

[a]tawatchai2593@gmail.com
[b]engrasimshoaib@gmail.com

Introduction

Pakistan is a flood prone country. Floods occur frequently mainly due to heavy concentrated rainfalls in monsoon season, mostly augmented by the snowmelt, in the catchment areas of major and other rivers. Floods of various magnitudes caused disorder in vast areas of almost all parts of the country [1]. The Indus basin which is the largest river basin has more than 138 million populations where irrigated agriculture is a major source of livelihood [2]. The Chenab River is the second largest river of the Indus river basin (Fig.1). It has experienced floods of various magnitudes, for example, in 1973, 1977, 1988, 1992, 1995, 1996, 1997, 2006, 2013 and 2014. In each of these floods, the overall damages to both the public and private properties were enormous. Whenever River Chenab overflowed, major cities and surrounding villages on both sides of the river were severely affected by floods.

The first objective of this study is to perform flood modeling of the 209 km reach of Chenab River using the HEC-RAS model. The river reach is from Qadirabad Barrage to Trimmu Barrage. The recent flood periods in 2006 and 2014 were considered in the model simulation. The second objective is to assess flood hazards using two different hazard assessment criteria under the conditions with and without flood control infrastructures under various flood return periods.

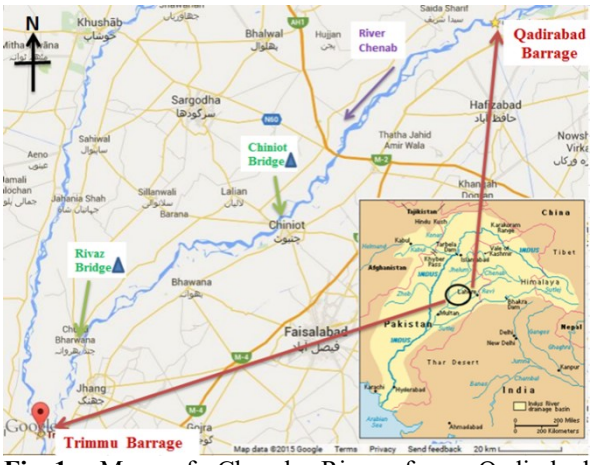

Fig. 1 Map of Chenab River from Qadirabad Barrage to Trimmu Barrage, Chiniot and Rivaz Bridges

Study area

Qadirabad and Trimmu are two barrages, located 209 km apart, on the River Chenab. Qadirabad Barrage has a design capacity of25,481 m^3/s while that of Trimmu Barrage is 18,262 m^3/s. The study area comprises of a selected river reach starting from Qadirabad Barrage to Trimmu Barrage. There are two gauging stations in the study reach, one at Chiniot Bridge and another at Rivaz Bridge. Fig. 1 shows the study area with the locations of Qadirabad Barrage, Trimmu Barrage, Chiniot Bridge and Rivaz Bridge. Nine existing flood bunds or flood control infrastructures were constructed along river sides.

Methodology

The methodology comprises of 1) data collection and analysis, 2) flood frequency analysis, 3) flood modeling, 4) assessing effectiveness of flood control infrastructure and 5) flood hazard assessment.

1) Data Collection

The following data were collected and analyzed namely:

a) historic flooding events in the study reach; b)Chenab River annual flood peaks in Qadirabad-Trimmu reach from 1983-2015; c) daily outflow data at Qadirabad Barrage for upstream model boundary condition and daily stage data at Trimmu Barrage for downstream boundary condition; d) input cross sections from field survey and that extracted from DEM SRTM 30 m resolution using digitization in HEC- GeoRAS. Field surveyed cross sections were available only for about 60% of study reach at about 4 km apart. Remaining cross sections were based on digitized verified DEM obtained by comparing field surveyed elevations with SRTM DEM elevations and applyingcorrection [4]; e) Stage-discharge rating curves at Qadirabad and Trimmu Barrages; f) locations and geometry of 9 existing flood bunds shown in Fig.2 and their lengths and heights given in Table 1.

Table 1 salient features of flood control bunds [1]

Name of Flood Bund	Length (km)	Top Width (m)	Avg. Top Level (m msl)
1.Humber Flood	25.146	6.096	198.75
2.Pindi Bhattian	44.348	6.096	218.64
3.Kot Najja Flood	40.386	6.096	218.64
4.Chiniot Flood	30.023	6.096	218.64
5.Muhammad Wala	7.62	7.62	218.64
6.Thatta Mahla- Rivaz	15.545	6.096	154.34
7.Thatta Mahla Loop	3.505	6.096	154.34
8.Jhang	19.507	7.62	154.34
9.Massan Disty	20.631	6.096	159.45

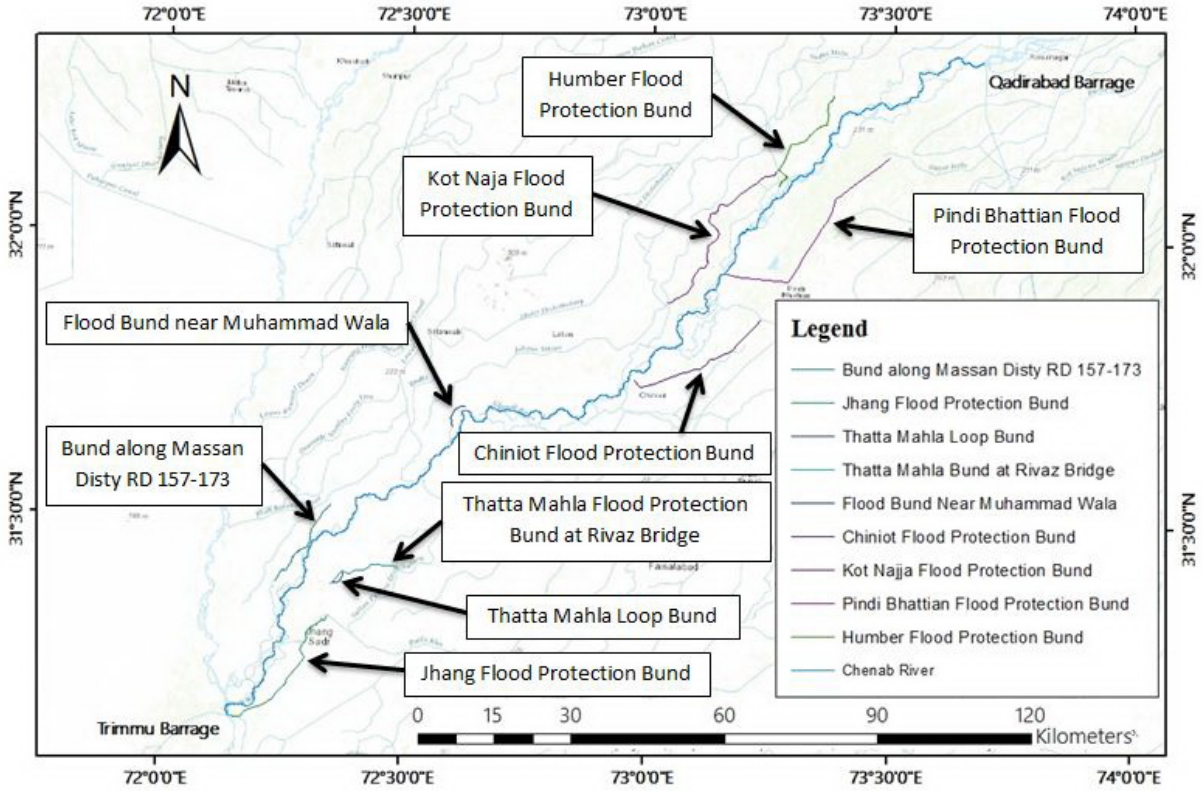

Fig. 2 Locations and names of the nine flood bunds

2) Flood Frequency Analysis

Gumbel flood frequency distribution on the observed peak discharges at the Qadirabad barrage under full gate opening from 1983-2015 was done to obtain the flood peak discharges of 25, 50, 100 and 200 year return periods. The flood hydrograph of each return period was obtained by multiplying the peak discharge from frequency analysis to the average normalized flood hydrograph which has the normalized peak equal to 1. The average normalized flood hydrograph is constructed by averaging the normalized hydrographs of many past floods. The normalized flood hydrograph is obtained by dividing the discharges by itspeak discharge. The flood hydrographs of various return periods are shown in Fig.3

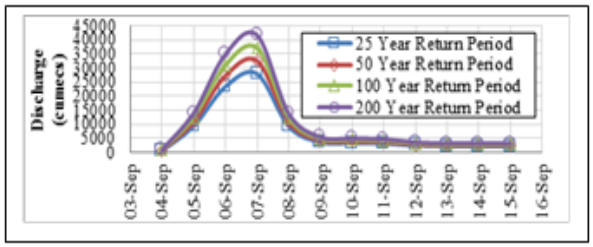

Fig. 3 Constructed flood discharge hydrographs at Qadirabad of various return periods

HEC-RAS Model Calibration and Verification

The HEC-RAS flood flow model [3] was used for modeling flow in Chenab River and its flood plains from Qadirabad Barrage to Trimmu Barrage. The river cross-section data and flood plain elevations from field measurements and DEM were input to HEC-RAS. Due to flat topography of the flood plains, the river flood level was assumed to be horizontal across the river and its flood plains on its left bank and right bank. The model configuration is shown in Fig.4.

1) Initial and Boundary conditions

The initial flow condition along the river reach was assumed to be steady flow at a constant upstream discharge at the beginning according to the Manning equation [5]. The model upstream boundary condition was the flow hydrographs of the measured discharge at Qadirabad Barrage. The downstream boundary condition was the measured stage hydrograph just upstream of the Trimmu Barrage. The lateral inflows between Qadirabad Barrage and Trimmu Barrage (Fig.4) were very small compared to very large river flood magnitudes and hence neglected.

2) Calibration of Model Results

In the calibration, the observed and simulated stage hydrographs in 2014 from 5 to 15 September at Chiniot Bridge and Rivaz Bridge were compared. The Manning's n coefficient 'n' was initially assumed based on literature [5] and the site conditions. The final values of Manning n was determined by trial and error calibration. After several trials, Manning's n was found equal to 0.029 for the main channel and 0.047 for floodplains. Fig.5 shows that the observed and simulated hydrographs agreesatisfactorily well with a correlation coefficient of 0.97 and Nash and Sutcliffe coefficient of 0.86.

3) *Verification of Model Results*

The model is verified for the 2006 flood from 3 to 14 September. The observed and computed stage hydrographs at the Chiniot Bridge and Rivaz Bridge were compared by keeping Manning n's from the model calibration unchanged. Fig. 6 shows an example of model verification at Chiniot Bridge with satisfactory agreement. The correlation coefficient was 0.97, and Nash and Sutcliff coefficient was 0.79.

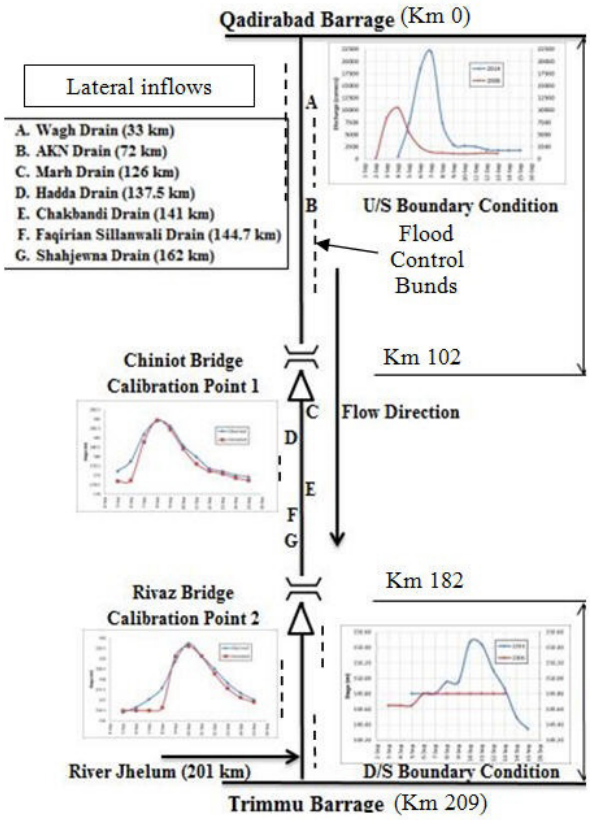

Fig. 4 Configuration of HES-RAS Model for the Chenab River Reach from Qadirabad Barrage to Trimmu Barrage

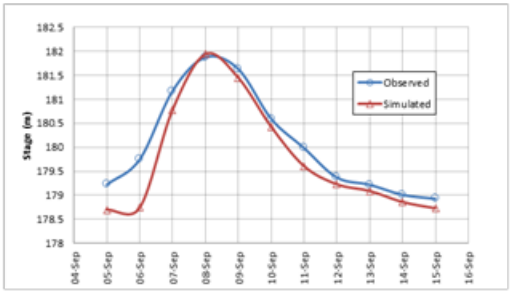

Fig. 5 Results of model calibration at Chiniot Bridge, 2014

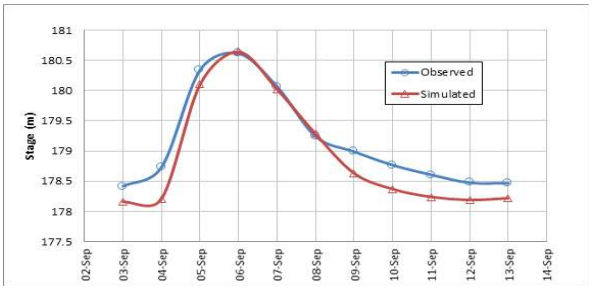

Fig. 6 Results of model verification at Chiniot Bridge, 2006

Assessing effectiveness of flood control infrastructure

In assessing the effectiveness of the existing flood control infrastructure, the HEC-RAS model simulations were performed for different scenarios with and without flood control. This was done by entering generated flow hydrographs for different return period floods as upstream boundary conditions and water levels generated through extension of the downstream stage-discharge rating curve, against the peak discharge values of different return periods as downstream boundary conditions.

Model simulations were done for the cases with and without Flood Control Infrastructure to find out their effectiveness. The results of HEC-RAS model were exported to Arc-GIS through its tool HEC-GeoRAS which were further analyzed to generate flood maps in the form of flood inundation area and depth maps. Comparisons were done to assess the effectiveness of flood control infrastructure on the basis of inundation depths and flooding areas

Flood Hazard Assessment

In assessing flood hazard assessment, two criteria are used namely ESCAP criterion [6] and DEFRA criterion [7]. The ESCAP flood hazard criterion is based on flood inundation depth only. By classifying flood depth based on the assigned critical depths of 0.8, 1.0 and 3.5 m according to ESCAP criterion, a flood hazard map was prepared in which flood depth was classified in four different intervals namely: 0.0-0.81 m as low, 0.82-1.00 as medium, 1.01-3.50 as high and from 3.51-higher as very high respectively.

The criterion of DEFRA considers flood hazard to people (FHR) as a function of depth and velocity:

$$FHR = d\,(v + 0.5) + DF \qquad (1)$$

Where d = depth of flooding (m), v = velocity of flow (m/s) and DF = debris factor (equal to 1 if d > 0.25m otherwise 0). The hazard to people was calculated and plotted as map using ArcGIS based on DEFRA criterion below (Table 2).

Table 2 DEFRA criteria for flood hazard to people [7]

Flood hazard rating = d(v+0.5)	Degree of Flood Hazard	Description
<0.75	Low	Caution (Flood zone with shallow flowing water or deep standing water)
0.75-1.25	Moderate	Dangerous for some (i.e. children, flood zone with deep or fast flowing water)
1.25-2.5	Significant	Dangerous for most people (Danger: flood zone with deep fast flowing water)
>2.5	Extreme	Dangerous for all (Extreme danger: flood zone with deep fast flowing water)

Results on Flood Control Effectiveness, Flood Hazard and Discussions

1) Assessing Effectiveness of Flood Control Infrastructure

From the model computation of flood conditions with the existing flood control infrastructure, the simulated maximum depths in the floodplains for 25, 50, 100 and 200 year return floods were 11.73, 12.58, 13.46 and 14.46 m respectively. For the case without the flood control infrastructure, the model computed results shown that there was an increase by about 8-10% in inundation depth and flooded area more than the case with flood control infrastructure for the 25, 50 and 100 year floods. For the 200 year flood, there was no significant difference in inundation area and depth for the cases with and without the flood control infrastructure. Hence the overall effectiveness of the flood control infrastructure is ensured only for the floods of 100 year return period and smaller. For the floods larger than the 100 year flood, e.g. the 200 year flood, the effectiveness of the flood control infrastructure is not ensured.

Detailed investigation was made on individual effectiveness of each component of the existing flood control infrastructure, i.e. the nine flood bunds or embankments [13]. The results shown that out of the nine existing flood embankments, four of them are not

safe against the flood larger than the 100 year flood. These embankments were Thatta Mahla, Thatta Mahla Loop, Jhang and Massan Disty respectively. The computations shown that for the 200 year flood, these bunds were overtopped by flood depths of 2.77, 2.77, 1.40 and 2.94 m respectively. These four bunds need to be raised and strengthened in order to ensure safety against the heavy floods. In assessing flood hazard assessment, two criteria were used namely ESCAP criterion [6] and DEFRA criterion [7]. The ESCAP flood hazard criterion is based on flood inundation depth only by classifying flood depth based on the assigned critical depths of 0.8, 1.0 and 3.5 m. DEFRA criterion considers both depth and velocity in assessing flood hazard to people.

2) Flood Hazard Assessment

After assessing the effectiveness of the existing flood control bund infrastructure, the HEC-RAS model simulations wereperformed for different scenarios. Figs. 7 and 8 show the flood hazard maps according to ESCAP and DEFRA criteria for the 100 year flood with the presence of the flood control infrastructure. The protected flood plain areas behind by the flood bunds are shown as geometric-shape flood free areas in both figures.The results show that for the 25-, 50-, 100- and 200-year floods, both assessment criteria give the increasing trends of hazard to people and properties and the existing flood control bunds. For the ESCAP criterion, mostly the hazard level in the flood plains was low and moderate for the 25 year flood, medium and high for the 50 and 100 year floods, high and very high for the 200 year flood. For the DEFRA criterion, the flood hazard to people was low for the 25 year flood, moderate for the 50 year flood, moderate and significant for the 100 year flood and extreme for the 200 year flood.

Conclusions and Recommendations

Flood inundation along the flood plains of 209 km reach of the Chenab River, Pakistan from Qadirabad Barrage to Trimmu Barrage was simulated by using HEC-RAS flood flow model. The novelty of this study is the application of two assessment criteria namely ESCAP and DEFRA to assess the flood hazard impacts with and without the existing flood control infrastructure. The ESCAP criterion considers flood hazard based on magnitudes of flood depth but does not consider flood velocity. While the DEFRA criterion considers both depth and velocity in assessing the flood hazard to people on their safety and their life. The ESCAP criterion is better used to assess flood hazard impacts due to inundation depth only and ignore the impact due to flood velocity. While the DEFRA criterion is better used to assess the flood impact on people only; due to both flood depth and velocity. The purposes of ESCAP and DEFRA criteria are different but when used together they provide useful assessment in estimating the effectiveness of the flood control structures in reducing flood hazard on the safety of flood control infrastructures and on the people. The effectiveness of the nine existing flood control bunds have been assessed and found that five of them were effective in controlling the flood plain inundation for the flood return periods up to 200 years. The other four bunds were not fully safe for the floods of 100 years and more. The four flood bunds are at the following locations namely; Thatta Mahla, Thatta Mahla Loop, Jhang and Massan Disty. They must be increased in heights and strengthened to ensure safety against the floods of 100 years and more.

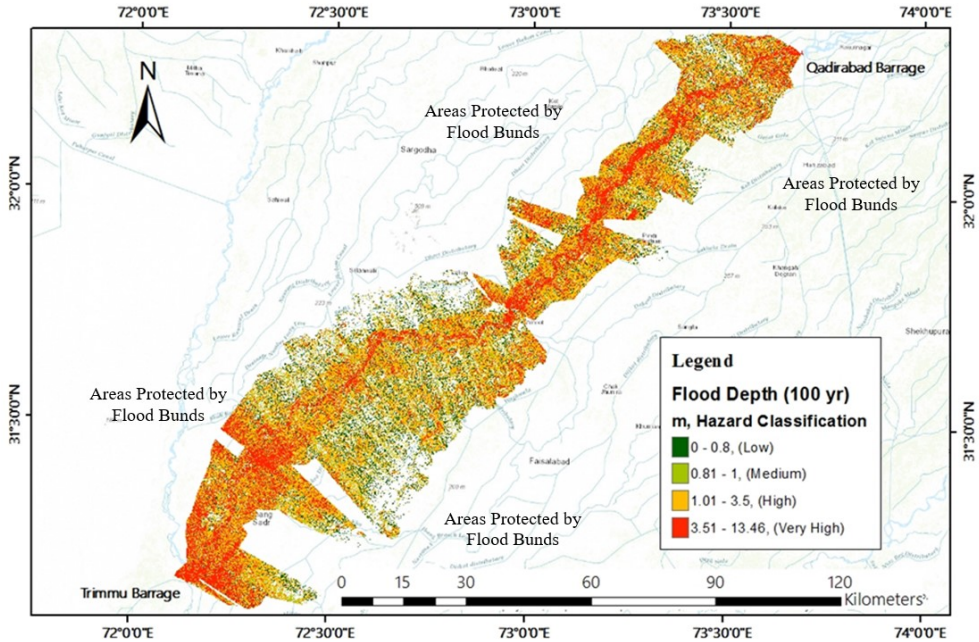

Fig. 7 Flood hazard map for 100-year return period flood using ESCAP assessment criterion

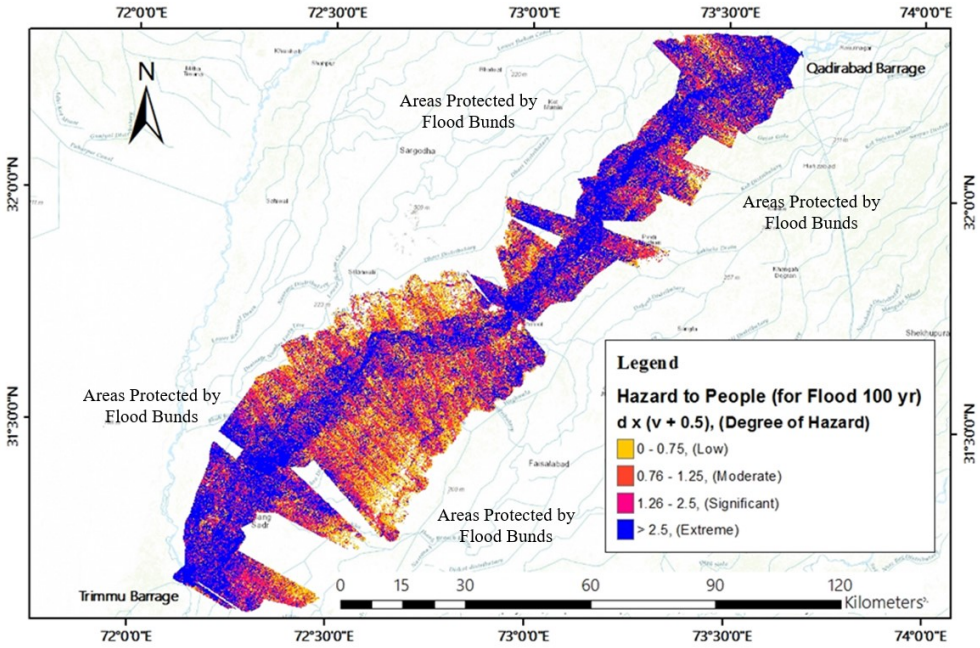

Fig. 8 Flood map of hazard to people for 100-year return period flood using DEFRA assessment criterion

The following recommendations are given:

- The missing river cross sections in the study reach should be field-surveyed in the future rather than extracting from STRM DEM data
- Flood hazard and risk assessment should be further accomplished by incorporating various land-uses, land cover, demographic data, private properties and public infrastructures, etc. [8], [9] and [10].
- Other flood hazard assessment methods should be considered, for example, multi-hazard loss estimation or HAZUS-MH of FEMA, USA[11]; and national flood-risk management guidelines of National Flood Risk Advisory Group of Australia [12].

Acknowledgments

Sincere acknowledgments are expressed to the Asian Institute of Technology, Thailand and the Punjab Irrigation Department, Pakistan in providing support in this study.

References

[1] FFC, Annual Flood Report 2014. Islamabad: Office of the Chief Engineering Advisor & Chairman Federal Flood Commission. Retrieved from http://www.ffc.gov.pk/downloads.aspx , 2014.

[2] A. Ali, Indus Basin Floods: Mechanisms, impacts, and management, Asian Development Bank, Mandaluyong City, Philippines, 2013.

[3] HEC, HEC-RAS User's manual. Davis, 609, Second Street, United States of America: US Army Corps of Engineers, Institute for Water Resources, Hydrologic Engineering Center, January, 2010.

[4] U. Khalil, N.M. Khan and H. Rehman, "Assessment of flood using geospatial technique for Indus River reach: Chashma-Taunsa," Science International (Lahore), vol. 27(3), 2015, pp.1985-1991.

[5] V.T. Chow, Open Channel Hydraulics. McGraw-Hill Book Company, New York, 1959.

[6] ESCAP, Manual and guidelines for comprehensive flood loss prevention and management. Bangkok, Thailand: Economic and Social Commission for Asia and the Pacific, 1991.

[7] DEFRA, *Flood risks to people, Phase 2, FD2321/TR2, Guidance Document.* HR Wallingford, Flood Hazard Research Centre, Middlesex University, Department for Environment Food and Rural Affairs. DEFRA /Environment Agency Flood and Coastal Defence, R & D Programme, 2006.

[8] M.M. Islam, and K. Sado, "Development of flood hazard maps of Bangladesh using NOAA-AVHRR images with GIS," Hydrological Sciences Journal, vol.3 (45), 2000, pp.337-355. doi:10.1080/02626660009492334.

[9] T. Tingsanchali, and F. Karim, "Flood-hazard assessment and risk-based zoning of a tropical flood plain: case study of the Yom River, Thailand,". Hydrological Sciences Journal, vol. 55(2), 2010, pp.145-161.

[10] Y. Keokhumcheng, T. Tingsanchali, and R. Clemente,"Flood risk assessment in the eastern region of Bangkok flood plain," Water International, vol. 37(3), 2012, pp. 201-217. doi:10.1080/02508060.2012.687868.

[11] FEMA, Multi Hazard Loss Estimation Methodology for Flood Model, Department of Homeland Security. Washington DC: Federal Emergency Management Agency, 2007.
[12] NFRAG, Flood Risk Management in Australia. Australian Journal of Emergency Management, 2008, vol. 23(4), pp. 21-23.
[13] M.A. Shoaib,Assessing flood hazard using hydro-geospatial technique:A case study of River Chenab from Qadirabad to Trimmu in Pakistan, Master Thesis, Asian Institute of Technology, Pathumthani, Thailand, 2015.

Reviewers

Full name	Organization	Country
Assoc. Prof. Dr. Bancha Kwanyuen	Kasetsart University	Thailand
Dr. Tosiyuki Nakaegawa	Meteorological Research Institute	Japan
Professor. Yasuto Tachikawa	Kyoto University	Japan
Dr. Kazuaki Yorozu	Kyoto University	Japan
Assoc. Prof. Takahiro Sayama	Kyoto University	Japan
Dr. Patinya Hanittinan	Kyoto University	Japan
Prof. Shigenobu Tanaka	Kyoto University	Japan
Prof. Tetsuya Sumi	Kyoto University	Japan
Prof. Tomoharu Hori	Kyoto University	Japan
Prof. Dr. Makoto Taniguchi	Research Institute for Humanity and Nature (RIHN)	Japan
Associate Professor, Dr. Kiguchi Masashi,	Institute of Industrial Science, the University of Tokyo	Japan
Assistant Professor, Dr. Noda Keigo	Gifu University	Japan
Associate Professor, Dr. Tebakari Taichi	Toyama Prefectural University	Japan
Professor. Lo, WeiCheng	National Cheng Kung University	Taiwan
Prof. Wu, Jianhong	National Cheng Kung University	Taiwan
Dr. Wu, Meng-Hsuan	National Cheng Kung University	Taiwan
Mr. Huang, Chi-Htsung	National Cheng Kung University	Taiwan
Ms. Chen Li-Chen	National Cheng Kung University	Taiwan
Prof. Dr. Ming-Daw Su	National Taiwan University	Taiwan
Professor C.H. Fan	National Taiwan University	Taiwan
Prof. K.S. Cheng	National Taiwan University	Taiwan
Professor M.C. Hu	National Taiwan University	Taiwan
Professor Y.L. Yeh	National Taiwan University	Taiwan
Dr. Seungsoo Lee	APEC Climate Center (APCC)	Republic of Korea
Prof. Dr. Yeonsu Kim	K-water	Republic of Korea
Prof. Dr. Wansik Yu	K-water	Republic of Korea
Prof. Dr. Joo-Cheol Kim	K-water	Republic of Korea
Prof. Dr. Kwansue Jung	Chungnam National University	Republic of Korea
Prof. Dr. Mikyoung Choi	Chungnam National University	Republic of Korea
Prof. Dr. Hyunuk An	Chungnam National University	Republic of Korea
Prof. Dr. Chang-lae Jang,	Korea National University of Transport	Republic of Korea
Assoc. Prof. Dr. Yongwon Seo	Yeungnam University	Republic of Korea
Prof. Dr. LIU Hui Zhi	Institute of Atmospheric Physics	China
Prof. Dr. Lin WANG	Institute of Atmospheric Physics	China
Prof. Dr. Chenghai Wang	Lanzhou University	China
Prof. Dr. Song YANG	SunYat-sen University	China
Prof. Dr. Alan Milano	Mindanao State University– Iligan Institute of Technology	Philippines

Reviewers

Full name	Organization	Country
Prof. Dr. Muhammad Syahril Badri Kusuma	Institut Teknologi Bandung	Indonesia
Prof. Ignas Sutapa	Indonesian Institute of Sciences	Indonesia
Prof. Dr. Vuong Bui Tran	Vietnam National University	Vietnam
Prof. Dr. Lawrence Surendra	University of Mysore	India
Dr. Jiramate Changklom	Imperial College London	UK
Dr. Priyantha Ranjan Sarukkalige	Curtin University	Australia
Asst. Prof. Dr. Somchai Donjadee	Kasetsart University	Thailand
Asst. Prof. Dr. Nitirach Sanguanduan	Kasetsart University	Thailand
Assoc. Prof. Dr. Chaisri Suksaroj	Kasetsart University	Thailand
Asst. Prof. Dr. Wisuwat Taesombat	Kasetsart University	Thailand
Assoc. Prof. Dr. Adichai Pornpromin	Kasetsart University	Thailand
Assoc. Prof. Dr. Surachai Lipiwattanakarn	Kasetsart University	Thailand
Asst. Prof. Dr. Jirawat Kanasut	Kasetsart University	Thailand
Asst. Prof. Dr. Napaporn Piamsa-nga	Kasetsart University	Thailand
Dr. Songsak Bhaddraravudthichai	Kasetsart University	Thailand
Asst . Prof. Dr. Jerasorn Santisirisomboon	Ramkhamheang University	Thailand
Assoc. Prof .Dr. Usa Humphries	King Mongkut's University of Technology Thonburi	Thailand
Assoc. Prof. Amnat Chidthaisong	King Mongkut's University of Technology Thonburi	Thailand
Asst. Prof. Dr. Chaiwat Ekkawatpanit	King Mongkut's University of Technology Thonburi	Thailand
Asst. Prof. Dr. Duangrudee Kositgittiwong	King Mongkut's University of Technology Thonburi	Thailand
Dr. Prem Rangsiwanichpong	King Mongkut's University of Technology Thonburi	Thailand
Assoc. Prof. Dr. Uma Seeboonruang	King Mongkut's Institute of Technology Ladkrabang	Thailand
Dr. Chanyut Kalakan	Burapha University	Thailand
Dr. Srisunee Wuthiwongyothin	Burapha University	Thailand
Assoc. Prof. Dr.Sombat Chuenchooklin	Naresuan University	Thailand
Dr. Tipaporn Homdee	Nakhon Phanom University	Thailand
Assoc. Prof. Dr. Sacha Sethabutra	Srinakharinwirot University	Thailand
Dr. Phayom Saraphirom	Khon Kaen University	Thailand
Assoc. Prof. Dr. Sucharit Koontanakulvong	Chulalongkorn University	Thailand
Asst. Prof. Dr. Anurak Sriariyawat	Chulalongkorn University	Thailand
Asst. Prof. Dr. Aksara Putthividhya	Chulalongkorn University	Thailand
Assoc. Prof. Dr. Tuantan Kitpaisalsakul	Chulalongkorn University	Thailand
Dr. Piyatida Ruangrassamee	Chulalongkorn University	Thailand
Dr. Pongsak Suttinon	Chulalongkorn University	Thailand
Dr. Supattra Visessri	Chulalongkorn University	Thailand
Dr. Patama Singhruck	Chulalongkorn University	Thailand
Dr. Somkiat Apipattanavis	Office of the National Water Resources	Thailand
Dr. Atsamon Limsakul	Department of Environmental Quality Promotion	Thailand
Dr. Oranuj Lophensi	Department of Groundwater Resources	Thailand

Reviewers

Full name	Organization	Country
Dr. Aranya Fuangswasdi	Department of Groundwater Resources	Thailand
Dr. Sukrit Kirtsaeng	Thai Meteorological Department, Bangkok	Thailand
Dr. Piyaman Srisomporn	Hydro and Agro Informatics Institute	Thailand
Dr. Surajate Boonya-aroonnet	Hydro and Agro Informatics Institute	Thailand

Sponsored by